An underwater photograph showing a dense forest of seaweed or kelp. The plants are tall and vertical, with large, dark green, blade-like leaves. Several fish are swimming in the water, some near the seaweed. The water is clear and blue, with sunlight filtering down from the surface, creating a bright, hazy atmosphere.

# Light and Photosynthesis

in Aquatic Ecosystems

THIRD EDITION

JOHN T. O. KIRK

CAMBRIDGE

CAMBRIDGE

[www.cambridge.org/9780521151757](http://www.cambridge.org/9780521151757)

This page intentionally left blank

## Light and Photosynthesis in Aquatic Ecosystems

Third edition

Beginning systematically with the fundamentals, the fully updated third edition of this popular graduate textbook provides an understanding of all the essential elements of marine optics. It explains the key role of light as a major factor in determining the operation and biological composition of aquatic ecosystems, and its scope ranges from the physics of light transmission within water, through the biochemistry and physiology of aquatic photosynthesis, to the ecological relationships that depend on the underwater light climate. This book also provides a valuable introduction to the remote sensing of the ocean from space, which is now recognized to be of great environmental significance due to its direct relevance to global warming.

An important resource for graduate courses on marine optics, aquatic photosynthesis, or ocean remote sensing; and for aquatic scientists, both oceanographers and limnologists.

JOHN T.O. KIRK began his research into ocean optics in the early 1970s in the Division of Plant Industry of the Commonwealth Scientific & Industrial Research Organization (CSIRO), Canberra, Australia, where he was a chief research scientist, and continued it from 1997 in Kirk Marine Optics. He was awarded the Australian Society for Limnology Medal (1981), and besides the two successful previous editions of this book, has also co-authored *The Plastids: Their Chemistry, Structure, Growth and Inheritance* (Elsevier, 1978), which became the standard text in its field.

Beyond his own scientific research interests, he has always been interested in the broader implications of science for human existence, and has published a book on this and other issues, *Science and Certainty* (CSIRO Publishing, 2007).



# Light and Photosynthesis in Aquatic Ecosystems

Third edition

JOHN T. O. KIRK

*Kirk Marine Optics*



**CAMBRIDGE**  
UNIVERSITY PRESS

CAMBRIDGE UNIVERSITY PRESS

Cambridge, New York, Melbourne, Madrid, Cape Town, Singapore,  
São Paulo, Delhi, Dubai, Tokyo, Mexico City

Cambridge University Press  
The Edinburgh Building, Cambridge CB2 8RU, UK

Published in the United States of America by Cambridge University Press, New York

[www.cambridge.org](http://www.cambridge.org)

Information on this title: [www.cambridge.org/9780521151757](http://www.cambridge.org/9780521151757)

© John T. O. Kirk 2011

This publication is in copyright. Subject to statutory exception  
and to the provisions of relevant collective licensing agreements,  
no reproduction of any part may take place without  
the written permission of Cambridge University Press.

First published 1983  
Second edition 1994

Printed in the United Kingdom at the University Press, Cambridge

*A catalogue record for this publication is available from the British Library*

*Library of Congress Cataloging-in-Publication Data*

Kirk, John T. O. (John Thomas Osmond), 1935–  
Light and photosynthesis in aquatic ecosystems / John T. O. Kirk. – 3rd ed.  
p. cm.

Includes bibliographical references and indexes.

ISBN 978-0-521-15175-7 (Hardback)

1. Photosynthesis. 2. Plants—Effect of underwater light on. 3. Aquatic plants—  
Ecophysiology. 4. Underwater light. I. Title.

QK882.K53 2010

572'.46—dc22

2010028677

ISBN 978-0-521-15175-7 Hardback

Cambridge University Press has no responsibility for the persistence or  
accuracy of URLs for external or third-party internet websites referred to  
in this publication, and does not guarantee that any content on such  
websites is, or will remain, accurate or appropriate.

# Contents

---

<i>Preface to the third edition</i>	<i>page</i> ix
<b>PART I THE UNDERWATER LIGHT FIELD</b>	<b>1</b>
<b>1 Concepts of hydrologic optics</b>	<b>3</b>
1.1 Introduction	3
1.2 The nature of light	3
1.3 The properties defining the radiation field	6
1.4 The inherent optical properties	14
1.5 Apparent and quasi-inherent optical properties	21
1.6 Optical depth	24
1.7 Radiative transfer theory	24
<b>2 Incident solar radiation</b>	<b>28</b>
2.1 Solar radiation outside the atmosphere	28
2.2 Transmission of solar radiation through the Earth's atmosphere	30
2.3 Diurnal variation of solar irradiance	38
2.4 Variation of solar irradiance and insolation with latitude and time of year	42
2.5 Transmission across the air–water interface	44
<b>3 Absorption of light within the aquatic medium</b>	<b>50</b>
3.1 The absorption process	50
3.2 The measurement of light absorption	53
3.3 The major light-absorbing components of the aquatic system	61

3.4	Optical classification of natural waters	92
3.5	Contribution of the different components of the aquatic medium to absorption of PAR	95
<b>4</b>	<b>Scattering of light within the aquatic medium</b>	<b>98</b>
4.1	The scattering process	98
4.2	Measurement of scattering	104
4.3	The scattering properties of natural waters	116
4.4	The scattering properties of phytoplankton	128
<b>5</b>	<b>Characterizing the underwater light field</b>	<b>133</b>
5.1	Irradiance	133
5.2	Scalar irradiance	143
5.3	Spectral distribution of irradiance	144
5.4	Radiance distribution	147
5.5	Modelling the underwater light field	149
<b>6</b>	<b>The nature of the underwater light field</b>	<b>153</b>
6.1	Downward irradiance – monochromatic	153
6.2	Spectral distribution of downward irradiance	159
6.3	Downward irradiance – PAR	159
6.4	Upward irradiance and radiance	168
6.5	Scalar irradiance	178
6.6	Angular distribution of the underwater light field	181
6.7	Dependence of properties of the field on optical properties of the medium	188
6.8	Partial vertical attenuation coefficients	197
<b>7</b>	<b>Remote sensing of the aquatic environment</b>	<b>199</b>
7.1	The upward flux and its measurement	200
7.2	The emergent flux	215
7.3	Correction for atmospheric scattering and solar elevation	218
7.4	Relation between remotely sensed reflectance and the scattering/absorption ratio	225
7.5	Relation between remotely sensed reflectances and water composition	228

<b>PART II PHOTOSYNTHESIS IN THE AQUATIC ENVIRONMENT</b>	<b>263</b>
<b>8 The photosynthetic apparatus of aquatic plants</b>	<b>265</b>
8.1 Chloroplasts	265
8.2 Membranes and particles	268
8.3 Photosynthetic pigment composition	275
8.4 Reaction centres and energy transfer	298
8.5 The overall photosynthetic process	300
<b>9 Light capture by aquatic plants</b>	<b>308</b>
9.1 Absorption spectra of photosynthetic systems	308
9.2 The package effect	311
9.3 Effects of variation in cell/colony size and shape	314
9.4 Rate of light absorption by aquatic plants	319
9.5 Effect of aquatic plants on the underwater light field	325
<b>10 Photosynthesis as a function of the incident light</b>	<b>330</b>
10.1 Measurement of photosynthetic rate in aquatic ecosystems	330
10.2 Photosynthesis and light intensity	339
10.3 Efficiency of utilization of incident light energy	360
10.4 Photosynthesis and wavelength of incident light	380
<b>11 Photosynthesis in the aquatic environment</b>	<b>388</b>
11.1 Circulation and depth	388
11.2 Optical characteristics of the water	397
11.3 Other limiting factors	400
11.4 Temporal variation in photosynthesis	430
11.5 Photosynthetic yield per unit area	440
<b>12 Ecological strategies</b>	<b>453</b>
12.1 Aquatic plant distribution in relation to light quality	453
12.2 Ontogenetic adaptation – intensity	469
12.3 Ontogenetic adaptation – spectral quality	479
12.4 Ontogenetic adaptation – depth	488
12.5 Significance of ontogenetic adaptation of the photosynthetic system	503
12.6 Rapid adaptation of the photosynthetic system	514

12.7	The microphytobenthos	528
12.8	Highly productive aquatic ecosystems	532
	<i>References and author index</i>	539
	<i>Index to symbols</i>	626
	<i>Index to organisms</i>	628
	<i>Index to water bodies</i>	632
	<i>Subject index</i>	638

The colour plates appear between pages 212 and 213.

## Preface to the third edition

---

Four things are required for plant growth: energy in the form of solar radiation; inorganic carbon in the form of carbon dioxide or bicarbonate ions; mineral nutrients; and water. Those plants which, in the course of evolution, have remained in, or have returned to, the aquatic environment have one major advantage over their terrestrial counterparts: namely, that water – lack of which so often limits productivity in the terrestrial biosphere – is for them present in abundance; but for this a price must be paid. The medium – air – in which terrestrial plants carry out photosynthesis offers, within the sort of depth that plant canopies occupy, no significant obstacle to the penetration of light. The medium – water – in which aquatic plants occur, in contrast, both absorbs and scatters light. For the phytoplankton and the macrophytes in lakes and rivers, coastal and oceanic waters, both the intensity and spectral quality of the light vary markedly with depth. In all but the shallowest waters, light availability is a limiting factor for primary production by the aquatic ecosystem. The aquatic plants must compete for solar radiation not only with each other (as terrestrial plants must also do), but also with all the other light-absorbing components of the aquatic medium. This has led, in the course of evolution, to the acquisition by each of the major groups of algae of characteristic arrays of light-harvesting pigments that are of great biochemical interest, and also of major significance for an understanding both of the adaptation of the algae to their ecological niche and of the phylogeny and taxonomy of the different algal groups. Nevertheless, in spite of the evolution of specialized light-harvesting systems, the aquatic medium removes so much of the incident light that aquatic ecosystems are, broadly speaking, less productive than terrestrial ones.

Thus, the nature of the light climate is a major difference between the terrestrial and the aquatic regions of the biosphere. Within the

underwater environment, light availability is of major importance in determining how much plant growth there is, which kinds of plant predominate and, indeed, which kinds of plants have evolved. It is not the whole story – biotic factors, availability of inorganic carbon and mineral nutrients, and temperature, all make their contribution – but it is a large part of that story. This book is a study of light in the underwater environment from the point of view of photosynthesis. It sets out to bring together the physics of light transmission through the medium and capture by the plants, the biochemistry of photosynthetic light-harvesting systems, the physiology of the photosynthetic response of aquatic plants to different kinds of light field, and the ecological relationships that depend on the light climate. The book does not attempt to provide as complete an account of the physical aspects of underwater light as the major works by Jerlov (1976), Preisendorfer (1976) and Mobley (1994); it is aimed at the limnologist and marine biologist rather than the physicist, although physical oceanographers should find it of interest. Its intention is to communicate a broad understanding of the significance of light as a major factor determining the operation and biological composition of aquatic ecosystems. It is hoped that it will be of value to practising aquatic scientists, to university teachers who give courses in limnology or marine science, and to postgraduate and honours students in these and related disciplines.

Certain features of the organization of the book merit comment. Although in some cases authors and dates are referred to explicitly, to minimize interruptions to the text, references to published work are in most cases indicated by the corresponding numbers in the complete alphabetical reference list at the end of the book. Accompanying each entry in the reference list is (are) the page number(s) where that paper or book is referred to in the text. Although coverage of the field is, I believe, representative, it is not intended to be encyclopaedic. The papers referred to have been selected, not only on the grounds of their scientific importance, but in large part on the basis of their usefulness as illustrative examples for particular points that need to be made. Inevitably, therefore, many equally important and relevant papers have had to be omitted from consideration, especially in the very broad field of aquatic ecology. I have therefore, where necessary, referred the reader to more specialized works in which more comprehensive treatments of particular topics can be found. Because its contribution to total aquatic primary production is usually small I have not attempted to deal with bacterial photosynthesis, complex and fascinating though it is.

The behaviour of sunlight in water, and the role that light plays in controlling the productivity, and influencing the biological composition, of aquatic ecosystems have been important areas of scientific study for more than a century, and it was to meet the perceived need for a text bringing together the physical and biological aspects of the subject, that the first, and then second, editions of *Light and Photosynthesis in Aquatic Ecosystems* were written. The book was well received, and is in use not only by research workers but also in university courses. In the 27 years since the first edition, interest in the topic has become even greater than it was before. This may be partly attributed to concern about global warming, and the realization that to understand the important role the ocean plays in the global carbon cycle, we need to improve both our understanding and our quantitative assessment of marine primary production.

An additional, but related, reason is the great interest that has been aroused in the feasibility of remote sensing of oceanic primary productivity from space. The potentialities were just becoming apparent with the early Coastal Zone Color Scanner (CZCS) pictures when the first edition was written. The continuing stream of further remote sensing information in the ensuing years, as space agencies around the world have put new and improved ocean scanners into orbit, enormously enlarging our understanding of oceanic phytoplankton distribution, have made this a particularly active and exciting field within oceanography. But the light flux that is received from the ocean by the satellite-borne radiometers, and which carries with it information about the composition of the water, originates in fact as a part of the upwelling light flux within the ocean, which has escaped through the surface into the atmosphere. To interpret the data we therefore need to understand the underwater light field, and how its characteristics are controlled by what is present within the aquatic medium.

In consequence of this sustained, even intensified, interest in underwater light, there is a continued need for a suitable text, not only for researchers, but also for use in university teaching. It is for this reason, the first and second editions being out of print, that I have prepared a completely revised version. Since marine bio-optics has been such an active field, a vast amount of literature had to be digested, but as in the earlier editions, I have tended to select specific papers mainly on the basis of their usefulness as illustrative examples, and many other equally valuable papers have had to be omitted from consideration.

In the 16 years since the second edition of this book appeared, interest in this subject has, if anything, increased. While there has been an

acceleration, rather than a slackening in the rate of publication of new research it must be said that this has been much more evident in certain areas than in others. Remote sensing of ocean colour, and its use to arrive at inferences about the composition and optical properties of, and primary production going on within, ocean waters has been the standout example of a very active field. A variety of new instruments for measuring the optical properties of the water, and the underwater light field, have been developed, and a number of these are described. So far as photosynthesis itself is concerned, the most notable change has been the development of instrumentation, together with the necessary accompanying theoretical understanding, for *in situ* measurement of photosynthetic rate, using chlorophyll *a* fluorescence. A great deal more is also now known about carbon concentrating mechanisms in aquatic plants, and these topics are discussed. The presumptive role of iron as a limiting factor for primary production in large areas of the ocean has received a great deal of attention in recent years, and current understanding is summarized. Nevertheless, quite apart from these specific areas, there has been across-the-board progress in all parts of the subject, no chapter remains unchanged, and the reference list has increased in length by about 50%.

I would like to thank Dr Susan Blackburn, Professor D. Branton, Dr M. Bristow, Mr S. Craig, Dr W. A. Hovis, Mr Ian Jameson, Dr S. Jeffrey, Dr D. Kiefer, Professor V. Klemas, Professor L. Legendre, Dr Y. Lipkin, Professor W. Nultsch, Mr D. Price, Professor R. C. Smith, Dr M. Veski; Biospherical Instruments Inc., who have provided original copies of figures for reproduction in this work; and Mr F. X. Dunin and Dr P. A. Tyler for unpublished data. I would like to thank Mr K. Lyon of Orbital Sciences Corporation for providing illustrations of the SeaWiFS scanner and spacecraft, and the SeaWiFS Project NASA/Goddard Space Flight Center, for remote sensing images of the ocean.

John Kirk  
Canberra  
April 2010

# PART I

## The underwater light field



# 1

## Concepts of hydrologic optics

### 1.1 Introduction

The purpose of the first part of this book is to describe and explain the behaviour of light in natural waters. The word ‘light’ in common parlance refers to radiation in that segment of the electromagnetic spectrum – about 400 to 700  $\mu\text{m}$  to which the human eye is sensitive. Our prime concern is not with vision but with photosynthesis. Nevertheless, by a convenient coincidence, the waveband within which plants can photosynthesize corresponds approximately to that of human vision and so we may legitimately refer to the particular kind of solar radiation with which we are concerned simply as ‘light’.

Optics is that part of physics which deals with light. Since the behaviour of light is greatly affected by the nature of the medium through which it is passing, there are different branches of optics dealing with different kinds of physical systems. The relations between the different branches of the subject and of optics to fundamental physical theory are outlined diagrammatically in [Fig. 1.1](#). Hydrologic optics is concerned with the behaviour of light in aquatic media. It can be subdivided into limnological and oceanographic optics according to whether fresh, inland or salty, marine waters are under consideration. Hydrologic optics has, however, up to now been mainly oceanographic in its orientation.

### 1.2 The nature of light

Electromagnetic energy occurs in indivisible units referred to as *quanta* or *photons*. Thus a beam of sunlight in air consists of a continual stream of photons travelling at  $3 \times 10^8 \text{ m s}^{-1}$ . The actual numbers of quanta

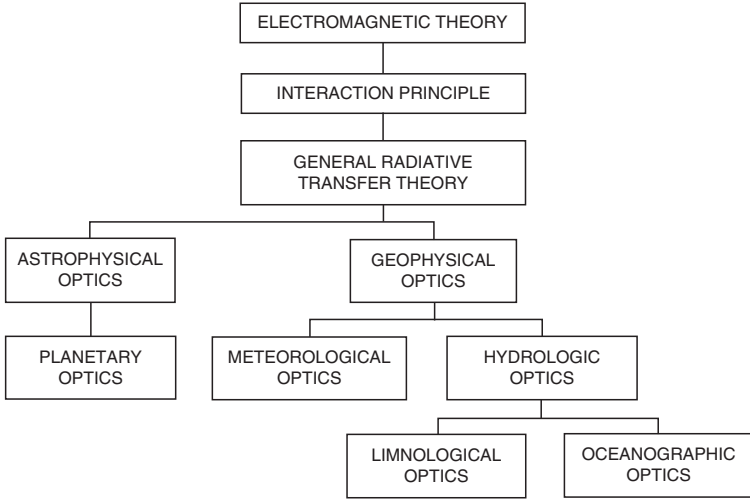


Fig. 1.1 The relationship between hydrologic optics and other branches of optics (after Preisendorfer, 1976).

involved are very large. In full summer sunlight, for example,  $1 \text{ m}^2$  of horizontal surface receives about  $10^{21}$  quanta of visible light per second. Despite its particulate nature, electromagnetic radiation behaves in some circumstances as though it has a wave nature. Every photon has a wavelength,  $\lambda$ , and a frequency,  $\nu$ . These are related in accordance with

$$\lambda = c/\nu \quad (1.1)$$

where  $c$  is the speed of light. Since  $c$  is constant in a given medium, the greater the wavelength the lower the frequency. If  $c$  is expressed in  $\text{m s}^{-1}$  and  $\nu$  in  $\text{cycles s}^{-1}$ , then the wavelength,  $\lambda$ , is expressed in metres. For convenience, however, wavelength is more commonly expressed in nanometres, a nanometre (nm) being equal to  $10^{-9} \text{ m}$ . The energy,  $\varepsilon$ , in a photon varies with the frequency, and therefore inversely with the wavelength, the relation being

$$\varepsilon = h\nu = hc/\lambda \quad (1.2)$$

where  $h$  is Planck's constant and has the value of  $6.63 \times 10^{-34} \text{ J s}$ . Thus, a photon of wavelength 700 nm from the red end of the photosynthetic spectrum contains only 57% as much energy as a photon of wavelength 400 nm from the blue end of the spectrum. The actual energy in a photon of wavelength  $\lambda \text{ nm}$  is given by the relation

$$\varepsilon = (1988/\lambda) \times 10^{-19} \text{ J} \quad (1.3)$$

A monochromatic radiation flux expressed in quanta  $\text{s}^{-1}$  can thus readily be converted to  $\text{J s}^{-1}$ , i.e. to watts (W). Conversely, a radiation flux,  $\Phi$ , expressed in W, can be converted to quanta  $\text{s}^{-1}$  using the relation

$$\text{quanta s}^{-1} = 5.03 \Phi \lambda \times 10^{15} \quad (1.4)$$

In the case of radiation covering a broad spectral band, such as for example the photosynthetic waveband, a simple conversion from quanta  $\text{s}^{-1}$  to W, or *vice versa*, cannot be carried out accurately since the value of  $\lambda$  varies across the spectral band. If the distribution of quanta or energy across the spectrum is known, then conversion can be carried out for a series of relatively narrow wavebands covering the spectral region of interest and the results summed for the whole waveband. Alternatively, an approximate conversion factor, which takes into account the spectral distribution of energy that is likely to occur, may be used. For solar radiation in the 400 to 700 nm band above the water surface, Morel and Smith (1974) found that the factor ( $Q/W$ ) required to convert W to quanta  $\text{s}^{-1}$  was  $2.77 \times 10^{18}$  quanta  $\text{s}^{-1} \text{W}^{-1}$  to an accuracy of plus or minus a few per cent, regardless of the meteorological conditions.

As we shall discuss at length in a later section (§6.2) the spectral distribution of solar radiation under water changes markedly with depth. Nevertheless, Morel and Smith found that for a wide range of marine waters the value of  $Q:W$  varied by no more than  $\pm 10\%$  from a mean of  $2.5 \times 10^{18}$  quanta  $\text{s}^{-1} \text{W}^{-1}$ . As expected from eqn 1.4, the greater the proportion of long-wavelength (red) light present, the greater the value of  $Q:W$ . For yellow inland waters with more of the underwater light in the 550 to 700 nm region (see §6.2), by extrapolating the data of Morel and Smith we arrive at a value of approximately  $2.9 \times 10^{18}$  quanta  $\text{s}^{-1} \text{W}^{-1}$  for the value of  $Q:W$ .

In any medium, light travels more slowly than it does in a vacuum. The velocity of light in a medium is equal to the velocity of light in a vacuum, divided by the refractive index of the medium. The refractive index of air is 1.00028, which for our purposes is not significantly different from that of a vacuum (exactly 1.0, by definition), and so we may take the velocity of light in air to be equal to that in a vacuum. The refractive index of water, although it varies somewhat with temperature, salt concentration and wavelength of light, may with sufficient accuracy be regarded as equal to 1.33 for all natural waters. Assuming that the velocity of light

in a vacuum is  $3 \times 10^8 \text{ m s}^{-1}$ , the velocity in water is therefore about  $2.25 \times 10^8 \text{ m s}^{-1}$ . The frequency of the radiation remains the same in water but the wavelength diminishes in proportion to the decrease in velocity. When referring to monochromatic radiation, the wavelength we shall attribute to it is that which it has in a vacuum. Because  $c$  and  $\lambda$  change in parallel, eqns 1.2, 1.3 and 1.4 are as true in water as they are in a vacuum: furthermore, when using eqns 1.3 and 1.4, it is the value of the wavelength in a vacuum which is applicable, even when the calculation is carried out for underwater light.

### 1.3 The properties defining the radiation field

If we are to understand the ways in which the prevailing light field changes with depth in a water body, then we must first consider what are the essential attributes of a light field in which changes might be anticipated. The definitions of these attributes, in part, follow the report of the Working Groups set up by the International Association for the Physical Sciences of the Ocean (1979), but are also influenced by the more fundamental analyses given by Preisendorfer (1976). A more recent account of the definitions and concepts used in hydrologic optics is that by Mobley (1994).

We shall generally express direction within the light field in terms of the *zenith angle*,  $\theta$  (the angle between a given light pencil, i.e. a thin parallel beam, and the upward vertical), and the *azimuth angle*,  $\phi$  (the angle between the vertical plane incorporating the light pencil and some other specified vertical plane such as the vertical plane of the Sun). In the case of the upwelling light stream it will sometimes be convenient to express a direction in terms of the *nadir angle*,  $\theta_n$  (the angle between a given light pencil and the downward vertical). These angular relations are illustrated in Fig. 1.2.

*Radiant flux*,  $\Phi$ , is the time rate of flow of radiant energy. It may be expressed in W ( $\text{J s}^{-1}$ ) or quanta  $\text{s}^{-1}$ .

*Radiant intensity*,  $I$ , is a measure of the radiant flux per unit solid angle in a specified direction. The radiant intensity of a source in a given direction is the radiant flux emitted by a point source, or by an element of an extended source, in an infinitesimal cone containing the given direction, divided by that element of solid angle. We can also speak of radiant intensity at a point in space. This, the *field* radiant intensity, is the radiant flux at that point in a specified direction in an infinitesimal cone

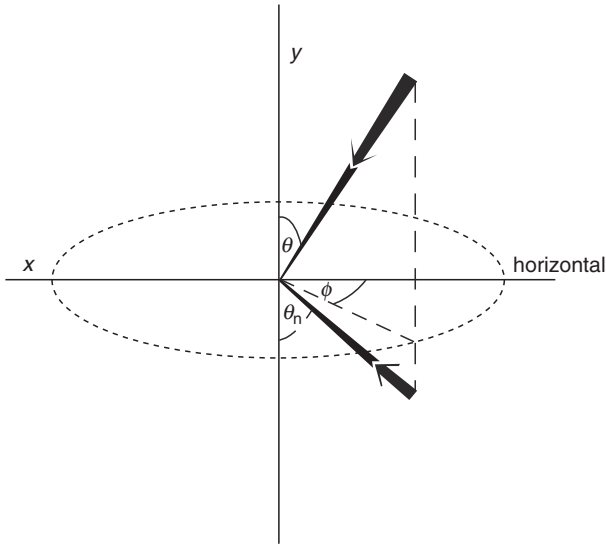


Fig. 1.2 The angles defining direction within a light field. The figure shows a downward and an upward pencil of light, both, for simplicity, in the same vertical plane. The downward pencil has zenith angle  $\theta$ ; the upward pencil has nadir angle  $\theta_n$ , which is equivalent to a zenith angle of  $(180^\circ - \theta_n)$ . Assuming the  $xy$  plane is the vertical plane of the Sun, or other reference vertical plane, then  $\phi$  is the azimuth angle for both light pencils.

containing the given direction, divided by that element of solid angle.  $I$  has the units  $\text{W (or quanta s}^{-1}\text{) steradian}^{-1}$ .

$$I = d\Phi/d\omega$$

If we consider the radiant flux not only per unit solid angle but also per unit area of a plane at right angles to the direction of flow, then we arrive at the even more useful concept of *radiance*,  $L$ . Radiance at a point in space is the radiant flux at that point in a given direction per unit solid angle per unit area at right angles to the direction of propagation. The meaning of this *field* radiance is illustrated in Figs. 1.3a and b. There is also *surface* radiance, which is the radiant flux emitted in a given direction per unit solid angle per unit projected area (apparent unit area, seen from the viewing direction) of a surface: this is illustrated in Fig. 1.3c. To indicate that it is a function of direction, i.e. of both zenith and azimuth angle, radiance is commonly written as  $L(\theta, \phi)$ . The angular structure of a light field is expressed in terms of the variation of radiance with  $\theta$  and  $\phi$ . Radiance has the units  $\text{W (or quanta s}^{-1}\text{) m}^{-2}\text{ steradian}^{-1}$ .

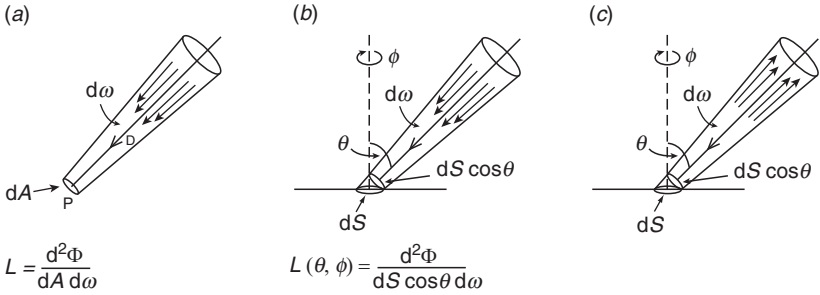


Fig. 1.3 Definition of radiance. (a) Field radiance at a point in space. The field radiance at P in the direction D is the radiant flux in the small solid angle surrounding D, passing through the infinitesimal element of area dA at right angles to D divided by the element of solid angle and the element of area. (b) Field radiance at a point in a surface. It is often necessary to consider radiance at a point on a surface, from a specified direction relative to that surface. dS is the area of a small element of surface.  $L(\theta, \phi)$  is the radiance incident on dS at zenith angle  $\theta$  (relative to the normal to the surface) and azimuth angle  $\phi$ : its value is determined by the radiant flux directed at dS within the small solid angle,  $d\omega$ , centred on the line defined by  $\theta$  and  $\phi$ . The flux passes perpendicularly across the area  $dS \cos \theta$ , which is the projected area of the element of surface, dS, seen from the direction  $\theta, \phi$ . Thus the radiance on a point in a surface, from a given direction, is the radiant flux in the specified direction per unit solid angle per unit projected area of the surface. (c) Surface radiance. In the case of a surface that emits radiation the intensity of the flux leaving the surface in a specified direction is expressed in terms of the surface radiance, which is defined in the same way as the field radiance at a point in a surface except that the radiation is considered to flow away from, rather than on to, the surface.

$$L(\theta, \phi) = d^2\Phi / dS \cos \theta d\omega$$

*Irradiance* (at a point of a surface),  $E$ , is the radiant flux incident on an infinitesimal element of a surface, containing the point under consideration, divided by the area of that element. Less rigorously, it may be defined as the radiant flux per unit area of a surface.\* It has the units  $\text{W m}^{-2}$  or quanta (or photons)  $\text{s}^{-1} \text{m}^{-2}$ , or mol quanta (or photons)  $\text{s}^{-1} \text{m}^{-2}$ , where 1.0 mol photons is  $6.02 \times 10^{23}$  (Avogadro's number) photons. One mole of photons is sometimes referred to as an *einstein*, but this term is now rarely used.

\* Terms such as 'fluence rate' or 'photon fluence rate', sometimes to be found in the plant physiological literature, are superfluous and should not be used.

$$E = d\Phi/dS$$

Downward irradiance,  $E_d$ , and upward irradiance,  $E_u$ , are the values of the irradiance on the upper and the lower faces, respectively, of a horizontal plane. Thus,  $E_d$  is the irradiance due to the downwelling light stream and  $E_u$  is that due to the upwelling light stream.

The relation between irradiance and radiance can be understood with the help of Fig. 1.3*b*. The radiance in the direction defined by  $\theta$  and  $\phi$  is  $L(\theta, \phi)$  W (or quanta  $s^{-1}$ ) per unit projected area per steradian (sr). The projected area of the element of surface is  $dS \cos \theta$  and the corresponding element of solid angle is  $d\omega$ . Therefore the radiant flux on the element of surface within the solid angle  $d\omega$  is  $L(\theta, \phi)dS \cos \theta d\omega$ . The area of the element of surface is  $dS$  and so the irradiance at that point in the surface where the element is located, due to radiant flux within  $d\omega$ , is  $L(\theta, \phi) \cos \theta d\omega$ . The total downward irradiance at that point in the surface is obtained by integrating with respect to solid angle over the whole upper hemisphere

$$E_d = \int_{2\pi} L(\theta, \phi) \cos \theta d\omega \quad (1.5)$$

The total upward irradiance is related to radiance in a similar manner except that allowance must be made for the fact that  $\cos \theta$  is negative for values of  $\theta$  between 90 and 180°

$$E_u = - \int_{-2\pi} L(\theta, \phi) \cos \theta d\omega \quad (1.6)$$

Alternatively the cosine of the nadir angle,  $\theta_n$  (see Fig. 1.2), rather than of the zenith angle, may be used

$$E_u = \int_{-2\pi} L(\theta_n, \phi) \cos \theta_n d\omega \quad (1.7)$$

The  $-2\pi$  subscript is simply to indicate that the integration is carried out over the  $2\pi$  sr solid angle in the *lower* hemisphere.

The *net downward irradiance*,  $\vec{E}$ , is the difference between the downward and the upward irradiance

$$\vec{E} = E_d - E_u \quad (1.8)$$

It is related to radiance by the eqn

$$\vec{E} = \int_{4\pi} L(\theta, \phi) \cos \theta d\omega \quad (1.9)$$

which integrates the product of radiance and  $\cos \theta$  over all directions: the fact that  $\cos \theta$  is negative between  $90$  and  $180^\circ$  ensures that the contribution of upward irradiance is negative in accordance with eqn 1.8. The net downward irradiance is a measure of the net rate of transfer of energy downwards at that point in the medium, and as we shall see later is a concept that can be used to arrive at some valuable conclusions.

The *scalar irradiance*,  $E_o$ , is the integral of the radiance distribution at a point over all directions about the point

$$E_o = \int_{4\pi} L(\theta, \phi) d\omega \quad (1.10)$$

Scalar irradiance is thus a measure of the radiant intensity at a point, which treats radiation from all directions equally. In the case of irradiance, on the other hand, the contribution of the radiation flux at different angles varies in proportion to the cosine of the zenith angle of incidence of the radiation: a phenomenon based on purely geometrical relations (Fig. 1.3, eqn 1.5), and sometimes referred to as the Cosine Law. It is useful to divide the scalar irradiance into a downward and an upward component. The *downward scalar irradiance*,  $E_{od}$ , is the integral of the radiance distribution over the upper hemisphere

$$E_{od} = \int_{2\pi} L(\theta, \phi) d\omega \quad (1.11)$$

The *upward scalar irradiance* is defined in a similar manner for the lower hemisphere

$$E_{ou} = \int_{-2\pi} L(\theta, \phi) d\omega \quad (1.12)$$

Scalar irradiance (total, upward, downward) has the same units as irradiance.

It is always the case in real-life radiation fields that irradiance and scalar irradiance vary markedly with wavelength across the photosynthetic range. This variation has a considerable bearing on the extent to which the radiation field can be used for photosynthesis. It is expressed in terms of the variation in irradiance or scalar irradiance per unit spectral distance (in units of wavelength or frequency, as appropriate) across the spectrum. Typical units would be  $\text{W}$  (or  $\text{quanta s}^{-1}$ )  $\text{m}^{-2} \text{nm}^{-1}$ .

If we know the radiance distribution over all angles at a particular point in a medium then we have a complete description of the angular structure of the light field. A complete radiance distribution, however, covering all zenith and azimuth angles at reasonably narrow intervals, represents a large amount of data: with  $5^\circ$  angular intervals, for example, the distribution will consist of 1369 separate radiance values. A simpler, but still very useful, way of specifying the angular structure of a light field is in the form of the three average cosines – for downwelling, upwelling and total light – and the irradiance reflectance.

The average cosine for downwelling light,  $\bar{\mu}_d$ , at a particular point in the radiation field, may be regarded as the average value, in an infinitesimally small volume element at that point in the field, of the cosine of the zenith angle of all the downwelling photons in the volume element. It can be calculated by summing (i.e. integrating) for all elements of solid angle ( $d\omega$ ) comprising the upper hemisphere, the product of the radiance in that element of solid angle and the value of  $\cos \theta$  (i.e.  $L(\theta, \phi) \cos \theta$ ), and then dividing by the total radiance originating in that hemisphere. By inspection of eqns 1.5 and 1.11 it can be seen that

$$\bar{\mu}_d = E_d/E_{0d} \quad (1.13)$$

i.e. the average cosine for downwelling light is equal to the downward irradiance divided by the downward scalar irradiance. The average cosine for upwelling light,  $\bar{\mu}_u$ , may be regarded as the average value of the cosine of the nadir angle of all the upwelling photons at a particular point in the field. By a similar chain of reasoning to the above, we conclude that  $\bar{\mu}_u$  is equal to the upward irradiance divided by the upward scalar irradiance

$$\bar{\mu}_u = E_u/E_{0u} \quad (1.14)$$

In the case of the downwelling light stream it is often useful to deal in terms of the reciprocal of the average downward cosine, referred to by Preisendorfer (1961) as the *distribution function* for downwelling light,  $D_d$ , which can be shown<sup>712</sup> to be equal to the mean pathlength per vertical metre traversed, of the downward flux of photons per unit horizontal area per second. Thus  $D_d = 1/\bar{\mu}_d$ . There is, of course, an analogous distribution function for the upwelling light stream, defined by  $D_u = 1/\bar{\mu}_u$ .

The average cosine,  $\bar{\mu}$ , for the total light at a particular point in the field may be regarded as the average value, in an infinitesimally small volume element at that point in the field, of the cosine of the zenith angle of all the photons in the volume element. It may be evaluated by integrating the product of radiance and  $\cos \theta$  over all directions and dividing by the total

radiance from all directions. By inspection of eqns 1.8, 1.9 and 1.10, it can be seen that the average cosine for the total light is equal to the *net* downward irradiance divided by the scalar irradiance

$$\bar{\mu} = \frac{\vec{E}}{E_0} = \frac{E_d - E_u}{E_0} \quad (1.15)$$

That  $E_d - E_u$  should be involved (rather than, say,  $E_d + E_u$ ) follows from the fact that the cosine of the zenith angle is negative for all the upwelling photons ( $90^\circ < \theta < 180^\circ$ ). Thus a radiation field consisting of equal numbers of downwelling photons at  $\theta = 45^\circ$  and upwelling photons at  $\theta = 135^\circ$  would have  $\bar{\mu} = 0$ .

Average cosine is often written as  $\bar{\mu}(z)$  to indicate that it is a function of the local radiation field at depth  $z$ . The total radiation field present in the water column also has an average cosine,  $\bar{\mu}_c$ , this being the average value of the cosine of the zenith angle of all the photons present in the water column at a given time.<sup>716</sup> In principle it could be evaluated by multiplying the value of  $\bar{\mu}(z)$  in each depth interval by the proportion of the total water column radiant energy occurring in that depth interval, and then summing to obtain the average cosine for the whole water column, i.e. we would be making use of the relationship

$$\bar{\mu}_c = \int_0^\infty \bar{\mu}(z) \left[ \frac{U(z)}{\int_0^\infty U(z) dz} \right] dz \quad (1.16)$$

where  $U(z)$  is the radiant energy density at depth  $z$ . The radiant energy density at depth  $z$  is equal to the scalar irradiance at that depth divided by the speed of light in water,  $c_w$

$$U(z) = E_0(z)/c_w \quad (1.17)$$

Making use of the fact that  $\bar{\mu}(z)$  at any depth is equal to the net downward irradiance divided by the scalar irradiance (eqn 1.15), then substituting for  $\bar{\mu}(z)$  and  $U(z)$  in eqn 1.16 and cancelling out, we obtain

$$\bar{\mu}_c = \frac{\int_0^\infty [E_d(z) - E_u(z)] dz}{\int_0^\infty E_0(z) dz} \quad (1.18)$$

Taking eqns 1.16 to 1.18 to constitute an alternative definition of  $\bar{\mu}_c$ , then an appropriate alternative name for the average cosine of all the photons in the water column would be the *integral average cosine* of the underwater light field.

The remaining parameter that provides information about the angular structure of the light field is the *irradiance reflectance* (sometimes called the *irradiance ratio*),  $R$ . It is the ratio of the upward to the downward irradiance at a given point in the field

$$R = E_u/E_d \quad (1.19)$$

In any absorbing and scattering medium, such as sea or inland water, all these properties of the light field change in value with depth (for which we use the symbol  $z$ ): the change might typically be a decrease, as in the case of irradiance, or an increase, as in the case of reflectance. It is sometimes useful to have a measure of the rate of change of any given property with depth. All the properties with which we have dealt that have the dimensions of radiant flux per unit area, diminish in value, as we shall see later, in an approximately exponential manner with depth. It is convenient with these properties to specify the rate of change of the logarithm of the value with depth since this will be approximately the same at all depths. In this way we may define the *vertical attenuation coefficient* for downward irradiance

$$K_d = -\frac{d \ln E_d}{dz} = -\frac{1}{E_d} \frac{dE_d}{dz} \quad (1.20)$$

upward irradiance

$$K_u = -\frac{d \ln E_u}{dz} = -\frac{1}{E_u} \frac{dE_u}{dz} \quad (1.21)$$

net downward irradiance

$$K_E = -\frac{d \ln(E_d - E_u)}{dz} = -\frac{1}{(E_d - E_u)} \frac{d(E_d - E_u)}{dz} \quad (1.22)$$

scalar irradiance

$$K_0 = -\frac{d \ln E_0}{dz} = -\frac{1}{E_0} \frac{dE_0}{dz} \quad (1.23)$$

radiance

$$K(\theta, \phi) = -\frac{d \ln L(\theta, \phi)}{dz} = -\frac{1}{L(\theta, \phi)} \frac{dL(\theta, \phi)}{dz} \quad (1.24)$$

In recognition of the fact that the values of these vertical attenuation coefficients are to some extent a function of depth they may sometimes be written in the form  $K(z)$ . For practical oceanographic and limnological

purposes it is often desirable to have an estimate of the average value of a vertical attenuation coefficient in that upper layer (the *euphotic zone*) where light intensity is sufficient for significant photosynthesis to take place. A commonly used procedure is to calculate the linear regression coefficient of  $\ln E(z)$  with respect to depth over the depth interval of interest (§5.1). Choice of the most appropriate depth interval is inavoidably somewhat arbitrary. An alternative approach is to use the irradiance values themselves to weight the estimates of the irradiance attenuation coefficients.<sup>717</sup> This yields  $K$  values applicable to that part of the water column where most of the energy is attenuated. If we indicate the irradiance-weighted vertical attenuation coefficient by  ${}^wK(av)$  then

$${}^wK(av) = \frac{\int_0^{\infty} K(z)E(z)dz}{\int_0^{\infty} E(z)dz} \quad (1.25)$$

where  $E(z)$  can be  $E_d(z)$ ,  $E_u(z)$ ,  $\vec{E}(z)$ , or  $E_0(z)$  and  $K(z)$  can be  $K_d(z)$ ,  $K_u(z)$ ,  $K_E(z)$  or  $K_0(z)$ , respectively. The meaning of eqn 1.25 is that when we calculate an average value of  $K$  by integrating over depth, at every depth the localized value of  $K(z)$  is weighted by the appropriate value of the relevant type of irradiance at that depth. The integrated product of  $K(z)$  and  $E(z)$  over all depths is divided by the integrated irradiance over all depths.

## 1.4 The inherent optical properties

There are only two things that can happen to photons within water: they can be absorbed or they can be scattered. Thus if we are to understand what happens to solar radiation as it passes into any given water body, we need some measure of the extent to which that water absorbs and scatters light. The absorption and scattering properties of the aquatic medium for light of any given wavelength are specified in terms of the absorption coefficient, the scattering coefficient and the volume scattering function. These have been referred to by Preisendorfer (1961) as *inherent* optical properties (IOP), because their magnitudes depend only on the substances comprising the aquatic medium and not on the geometric structure of the light fields that may pervade it. They are defined with the help of an imaginary, infinitesimally thin, plane parallel layer of medium, illuminated at right angles by a parallel beam of monochromatic light (Fig. 1.4). Some of the incident light is absorbed by the thin layer. Some is

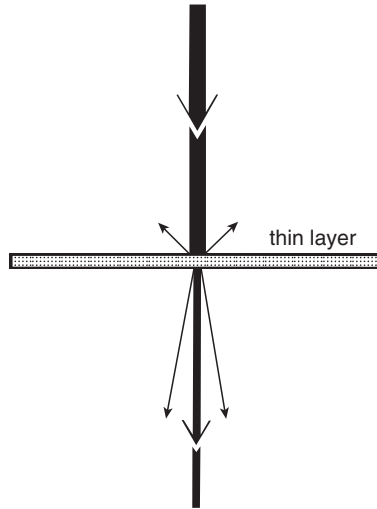


Fig. 1.4 Interaction of a beam of light with a thin layer of aquatic medium. Of the light that is not absorbed, most is transmitted without deviation from its original path: some light is scattered, mainly in a forward direction.

scattered – that is, caused to diverge from its original path. The fraction of the incident flux that is absorbed, divided by the thickness of the layer, is the *absorption coefficient*,  $a$ . The fraction of the incident flux that is scattered, divided by the thickness of the layer, is the *scattering coefficient*,  $b$ .

To express the definitions quantitatively we make use of the quantities *absorptance*,  $A$ , and *scatterance*,  $B$ . If  $\Phi_0$  is the radiant flux (energy or quanta per unit time) incident in the form of a parallel beam on some physical system,  $\Phi_a$  is the radiant flux absorbed by the system, and  $\Phi_b$  is the radiant flux scattered by the system. Then

$$A = \Phi_a / \Phi_0 \quad (1.26)$$

and

$$B = \Phi_b / \Phi_0 \quad (1.27)$$

i.e. absorptance and scatterance are the fractions of the radiant flux lost from the incident beam, by absorption and scattering, respectively. The sum of absorptance and scatterance is referred to as *attenuance*,  $C$ : it is the fraction of the radiant flux lost from the incident beam by absorption and scattering combined. In the case of the infinitesimally thin layer, thickness  $\Delta r$ , we represent the very small fractions of the incident flux that are lost by absorption and scattering as  $\Delta A$  and  $\Delta B$ , respectively. Then

$$a = \Delta A / \Delta r \quad (1.28)$$

and

$$b = \Delta B / \Delta r \quad (1.29)$$

An additional inherent optical property that we may now define is the *beam attenuation coefficient*,  $c$ . It is given by

$$c = a + b \quad (1.30)$$

and is the fraction of the incident flux that is absorbed and scattered, divided by the thickness of the layer. If the very small fraction of the incident flux that is lost by absorption and scattering combined is given the symbol  $\Delta C$  (where  $\Delta C = \Delta A + \Delta B$ ) then

$$c = \Delta C / \Delta r \quad (1.31)$$

The absorption, scattering and beam attenuation coefficients all have units of 1/length, and are normally expressed in  $\text{m}^{-1}$ .

In the real world we cannot carry out measurements on infinitesimally thin layers, and so if we are to determine the values of  $a$ ,  $b$  and  $c$  we need expressions that relate these coefficients to the absorbance, scatterance and beam attenuation of layers of finite thickness. Consider a medium illuminated perpendicularly with a thin parallel beam of radiant flux,  $\Phi_0$ . As the beam passes through, it loses intensity by absorption and scattering. Consider now an infinitesimally thin layer, thickness  $\Delta r$ , within the medium at a depth,  $r$ , where the radiant flux in the beam has diminished to  $\Phi$ . The change in radiant flux in passing through  $\Delta r$  is  $\Delta\Phi$ . The attenuation of the thin layer is

$$\Delta C = -\Delta\Phi / \Phi$$

(the negative sign is necessary since  $\Delta\Phi$  must be negative)

$$\Delta\Phi / \Phi = -c \Delta r$$

Integrating between 0 and  $r$  we obtain

$$\ln \frac{\Phi}{\Phi_0} = -cr \quad (1.32)$$

or

$$\Phi = \Phi_0 e^{-cr} \quad (1.33)$$

indicating that the radiant flux diminishes exponentially with distance along the path of the beam. Equation 1.32 may be rewritten

$$c = \frac{1}{r} \ln \frac{\Phi_0}{\Phi} \quad (1.34)$$

or

$$c = -\frac{1}{r} \ln(1 - C) \quad (1.35)$$

The value of the beam attenuation coefficient,  $c$ , can therefore, using eqn 1.34 or 1.35, be obtained from measurements of the diminution in intensity of a parallel beam passing through a known pathlength of medium,  $r$ .

The theoretical basis for the measurement of the absorption and scattering coefficients is less simple. In a medium with absorption but negligible scattering, the relation

$$a = -\frac{1}{r} \ln(1 - A) \quad (1.36)$$

holds, and in a medium with scattering but negligible absorption, the relation

$$b = -\frac{1}{r} \ln(1 - B) \quad (1.37)$$

holds, but in any medium that both absorbs and scatters light to a significant extent, neither relation is true. This can readily be seen by considering the application of these equations to such a medium.

In the case of eqn 1.37 some of the measuring beam will be removed by absorption within the pathlength  $r$  before it has had the opportunity to be scattered, and so the amount of light scattered,  $B$ , will be lower than that required to satisfy the equation. Similarly,  $A$  will have a value lower than that required to satisfy eqn 1.36 since some of the light will be removed from the measuring beam by scattering before it has had the chance to be absorbed.

In order to actually measure  $a$  or  $b$  these problems must be circumvented. In the case of the absorption coefficient, it is possible to arrange that most of the light scattered from the measuring beam still passes through approximately the same pathlength of medium and is collected by the detection system. Thus the contribution of scattering to total attenuation is made very small and eqn 1.36 may be used. In the case of the scattering coefficient there is no instrumental way of avoiding the losses due to absorption and so the absorption must be determined separately and appropriate corrections made to the scattering data. We shall consider ways of measuring  $a$  and  $b$  in more detail later (§§ 3.2 and 4.2).

The way in which scattering affects the penetration of light into the medium depends not only on the value of the scattering coefficient but also on the angular distribution of the scattered flux resulting from the primary scattering process. This angular distribution has a characteristic shape for any given medium and is specified in terms of the *volume scattering function*,  $\beta(\theta)$ . This is defined as the radiant intensity in a given direction from a volume element,  $dV$  illuminated by a parallel beam of light, per unit of irradiance on the cross-section of the volume, and per unit volume (Fig. 1.5a). The definition is usually expressed mathematically in the form

$$\beta(\theta) = dI(\theta)/E \, dV \quad (1.38)$$

Since, from the definitions in §1.3

$$dI(\theta) = d\Phi(\theta)/d\omega$$

and

$$E = \Phi_0/dS$$

where  $d\Phi(\theta)$  is the radiant flux in the element of solid angle  $d\omega$ , oriented at angle  $\theta$  to the beam, and  $\Phi_0$  is the flux incident on the cross-sectional area,  $dS$ , and since

$$dV = dS \cdot dr$$

where  $dr$  is the thickness of the volume element, then we may write

$$\beta(\theta) = \frac{d\Phi(\theta)}{\Phi_0} \frac{1}{d \, \omega dr} \quad (1.39)$$

The volume scattering function has the units  $\text{m}^{-1} \text{sr}^{-1}$ .

Light scattering from a parallel light beam passing through a thin layer of medium is radially symmetrical around the direction of the beam. Thus, the light scattered at angle  $\theta$  should be thought of as a cone with half-angle  $\theta$ , rather than as a pencil of light (Fig. 1.5b).

From eqn 1.39 we see that  $\beta(\theta)$  is the radiant flux per unit solid angle scattered in the direction  $\theta$ , per unit pathlength in the medium, expressed as a proportion of the incident flux. The angular interval  $\theta$  to  $\theta + \Delta\theta$  corresponds to an element of solid angle equal to  $2\pi \sin \theta \, \Delta\theta$  (Fig. 1.5b) and so the proportion of the incident radiant flux scattered (per unit pathlength) in this angular interval is  $\beta(\theta) \, 2\pi \sin \theta \, \Delta\theta$ . To obtain the proportion of the incident flux that is scattered in

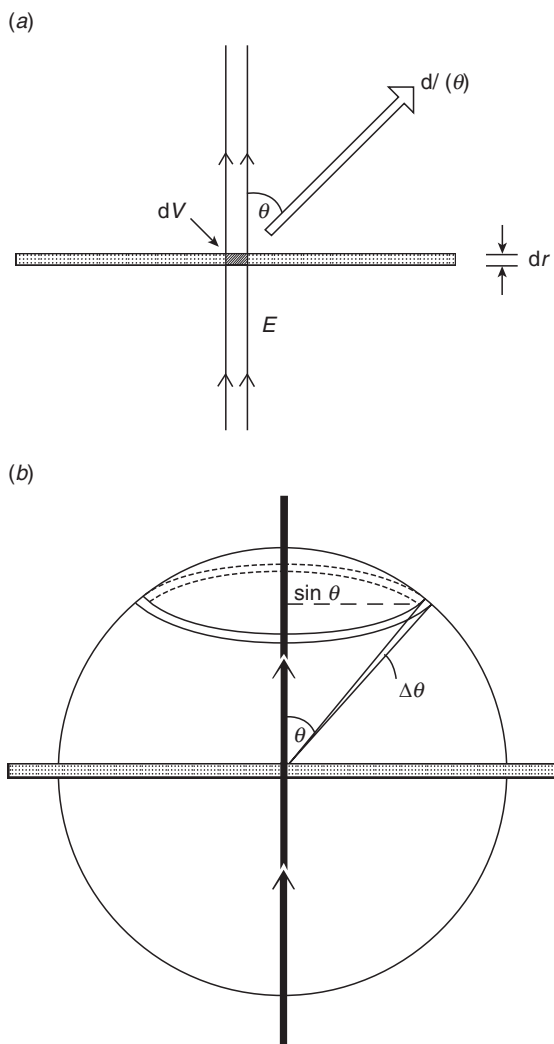


Fig. 1.5 The geometrical relations underlying the volume scattering function. (a) A parallel light beam of irradiance  $E$  and cross-sectional area  $dA$  passes through a thin layer of medium, thickness  $dr$ . The illuminated element of volume is  $dV$ .  $dI(\theta)$  is the radiant intensity due to light scattered at angle  $\theta$ . (b) The point at which the light beam passes through the thin layer of medium can be imagined as being at the centre of a sphere of unit radius. The light scattered between  $\theta$  and  $\theta + \Delta\theta$  illuminates a circular strip, radius  $\sin \theta$  and width  $\Delta\theta$ , around the surface of the sphere. The area of the strip is  $2\pi \sin \theta \Delta\theta$ , which is equivalent to the solid angle (in steradians) corresponding to the angular interval,  $\Delta\theta$ .

all directions per unit pathlength – by definition, equal to the scattering coefficient – we must integrate over the angular range  $\theta = 0^\circ$  to  $\theta = 180^\circ$

$$b = 2\pi \int_0^\pi \beta(\theta) \sin \theta d\theta = \int_{4\pi} \beta(\theta) d\omega \quad (1.40)$$

Thus an alternative definition of the scattering coefficient is the integral of the volume scattering function over all directions.

It is frequently useful to distinguish between scattering in a forward direction and that in a backward direction. We therefore partition the total scattering coefficient,  $b$ , into a *forward scattering coefficient*,  $b_f$ , relating to light scattered from the beam in a forward direction, and a *backward scattering coefficient* (or simply, *backscattering coefficient*)  $b_b$ , relating to light scattered from the beam in a backward direction

$$b = b_b + b_f \quad (1.41)$$

We may also write

$$b_f = 2\pi \int_0^{\pi/2} \beta(\theta) \sin \theta d\theta \quad (1.42)$$

$$b_b = 2\pi \int_{\pi/2}^\pi \beta(\theta) \sin \theta d\theta \quad (1.43)$$

The variation of  $\beta(\theta)$  with  $\theta$  tells us the absolute amount of scattering at different angles, per unit pathlength in a given medium. If we wish to compare the *shape* of the angular distribution of scattering in different media separately from the absolute amount of scattering that occurs, then it is convenient to use the *normalized volume scattering function*,  $\tilde{\beta}(\theta)$ , sometimes called the scattering phase function, which is that function (units  $\text{sr}^{-1}$ ) obtained by dividing the volume scattering function by the total scattering coefficient

$$\tilde{\beta}(\theta) = \beta(\theta)/b \quad (1.44)$$

The integral of  $\tilde{\beta}(\theta)$  over all solid angles is equal to 1. The integral of  $\tilde{\beta}(\theta)$  up to any given value of  $\theta$  is the proportion of the total scattering that occurs in the angular interval between  $0^\circ$  and that value of  $\theta$ . We can also define normalized forward scattering and backward scattering coefficients,  $\tilde{b}_f$  and  $\tilde{b}_b$ , as the proportions of the total scattering in forwards and backwards directions, respectively

$$\tilde{b}_f = b_f/b \quad (1.45)$$

$$\tilde{b}_b = b_b/b \quad (1.46)$$

Just as it is useful sometimes to express the angular structure of a light field in terms of a single parameter – its average cosine ( $\bar{\mu}$ ) – so it can also be useful in the case of the scattering phase function to have a single parameter that provides some indication of its shape. Such a parameter is the *average cosine of scattering*,  $\bar{\mu}_s$ , which can be thought of as the average cosine of the singly scattered light field. It is also sometimes referred to as the *asymmetry factor*, and given the symbol,  $g$ . Its value, for any given volume scattering function, may be calculated<sup>712</sup> from

$$\bar{\mu}_s = \frac{\int_{4\pi} \beta(\theta) \cos \theta d\omega}{\int_{4\pi} \beta(\theta) d\omega} \quad (1.47)$$

or (using eqn 1.44 and the fact that the integral of  $\tilde{\beta}(\theta)$  over  $4\pi$  is 1) from

$$\bar{\mu}_s = \int_{4\pi} \tilde{\beta}(\theta) \cos \theta d\omega \quad (1.48)$$

## 1.5 Apparent and quasi-inherent optical properties

The vertical attenuation coefficients for radiance, irradiance and scalar irradiance are, strictly speaking, properties of the radiation field since, by definition, each of them is the logarithmic derivative with respect to depth of the radiometric quantity in question. Nevertheless experience has shown that their values are largely determined by the inherent optical properties of the aquatic medium and are not very much altered by changes in the incident radiation field such as a change in solar elevation.<sup>59</sup> For example, if a particular water body is found to have a high value of  $K_d$  then we expect it to have approximately the same high  $K_d$  tomorrow, or next week, or at any time of the day, so long as *the composition of the water remains about the same*.

Vertical attenuation coefficients, such as  $K_d$ , are thus commonly used, and thought of, by oceanographers and limnologists as though they are optical properties belonging to the water, properties that are a direct measure of the ability of that water to bring about a diminution in the appropriate radiometric quantity with depth. Furthermore they have the same units ( $\text{m}^{-1}$ ) as the inherent optical properties  $a$ ,  $b$

and  $c$ . In recognition of these useful aspects of the various  $K$  functions, Preisendorfer (1961) suggested that they be classified as *apparent optical properties* (AOP) and we shall so treat them in this book. The reflectance,  $R$ , is also often treated as an apparent optical property of water bodies.

The two fundamental inherent optical properties – the coefficients for absorption and scattering – are, as we saw earlier, defined in terms of the behaviour of a parallel beam of light incident upon a thin layer of medium. Analogous coefficients can be defined for incident light streams having any specified angular distribution. In particular, such coefficients can be defined for incident light streams corresponding to the upwelling and downwelling streams that exist at particular depths in real water bodies. We shall refer to these as the *diffuse* absorption and scattering coefficients for the upwelling or downwelling light streams at a given depth. Although related to the normal coefficients, the values of the diffuse coefficients are a function of the local radiance distribution, and therefore of depth.

The *diffuse absorption coefficient* for the downwelling light stream at depth  $z$ ,  $a_d(z)$ , is the proportion of the incident radiant flux that would be absorbed from the downwelling stream by an infinitesimally thin horizontal plane parallel layer at that depth, divided by the thickness of the layer. The diffuse absorption coefficient for the upwelling stream,  $a_u(z)$ , is defined in a similar way. Absorption of a diffuse light stream within the thin layer will be greater than absorption of a normally incident parallel beam because the pathlengths of the photons will be in proportion to  $1/\bar{\mu}_d$  and  $1/\bar{\mu}_u$ , respectively. The diffuse absorption coefficients are therefore related to the normal absorption coefficients by

$$a_d(z) = \frac{a}{\bar{\mu}_d(z)} \quad (1.49)$$

$$a_u(z) = \frac{a}{\bar{\mu}_u(z)} \quad (1.50)$$

where  $\bar{\mu}_d(z)$  and  $\bar{\mu}_u(z)$  are the values of  $\bar{\mu}_d$  and  $\bar{\mu}_u$  that exist at depth  $z$ .

So far as scattering of the upwelling and downwelling light streams is concerned, it is mainly the backward scattering component that is of importance. The diffuse backscattering coefficient for the downwelling stream at depth  $z$ ,  $b_{bd}(z)$ , is the proportion of the incident radiant flux from the downwelling stream that would be scattered backwards (i.e. upwards) by an infinitesimally thin, horizontal plane parallel layer at that depth, divided by the thickness of the layer:  $b_{bu}(z)$ , the

corresponding coefficient for the upwelling stream is defined in the same way in terms of the light scattered downwards again from that stream. Diffuse total ( $b_d(z)$ ,  $b_u(z)$ ) and forward ( $b_{fd}(z)$ ,  $b_{fu}(z)$ ) scattering coefficients for the downwelling and upwelling streams can be defined in a similar manner. The following relations hold

$$\begin{aligned} b_d(z) &= b/\bar{\mu}_d(z), & b_u(z) &= b/\bar{\mu}_u(z) \\ b_d(z) &= b_{fd}(z) + b_{bd}(z), & b_u(z) &= b_{fu}(z) + b_{bu}(z) \end{aligned}$$

The relation between a diffuse backscattering coefficient and the normal backscattering coefficient,  $b_b$ , is not simple but may be calculated from the volume scattering function and the radiance distribution existing at depth  $z$ . The calculation procedure is discussed later (§4.2).

Preisendorfer (1961) has classified the diffuse absorption and scattering coefficients as *hybrid optical properties* on the grounds that they are derived both from the inherent optical properties and certain properties of the radiation field. I prefer the term *quasi-inherent optical properties*, on the grounds that it more clearly indicates the close relation between these properties and the inherent optical properties. Both sets of properties have precisely the same kind of definition: they differ only in the characteristics of the light flux that is imagined to be incident upon the thin layer of medium.

The important quasi-inherent optical property,  $b_{bd}(z)$ , can be linked with the two apparent optical properties,  $K_d$  and  $R$ , with the help of one more optical property,  $\kappa(z)$ , which is the average vertical attenuation coefficient in upward travel from their first point of upward scattering, of all the upwelling photons received at depth  $z$ .<sup>710</sup>  $\kappa(z)$  must not be confused with, and is in fact much greater than,  $K_u(z)$ , the vertical attenuation coefficient (with respect to depth increasing downward) of the upwelling light stream. Using  $\kappa(z)$  we link the apparent and the quasi-inherent optical properties in the relation

$$R(z) \approx \frac{b_{bd}(z)}{K_d(z) + \kappa(z)} \quad (1.51)$$

At depths where the asymptotic radiance distribution is established (see §6.6) this relationship holds exactly. Monte Carlo modelling of the underwater light field for a range of optical water types<sup>710</sup> has shown that  $\kappa$  is approximately linearly related to  $K_d$ , the relationship at  $z_m$  (a depth at which irradiance is 10% of the subsurface value) being

$$\kappa(z_m) \approx 2.5 K_d(z_m) \quad (1.52)$$

## 1.6 Optical depth

As we have already noted, but will discuss more fully later, the downward irradiance diminishes in an approximately exponential manner with depth. This may be expressed by the equation

$$E_d(z) = E_d(0)e^{-K_d z} \quad (1.53)$$

where  $E_d(z)$  and  $E_d(0)$  are the values of downward irradiance at  $z$  m depth, and just below the surface, respectively, and  $K_d$  is the average value of the vertical attenuation coefficient over the depth interval 0 to  $z$  m. We shall now define the *optical depth*,  $\zeta$ , by the eqn

$$\zeta = K_d z \quad (1.54)$$

It can be seen that a specified optical depth will correspond to different physical depths but to the same overall diminution of irradiance, in waters of differing optical properties. Thus in a coloured turbid water with a high  $K_d$ , a given optical depth will correspond to a much smaller actual depth than in a clear colourless water with a low  $K_d$ . Optical depth,  $\zeta$ , as defined here is distinct from *attenuation length*,  $\tau$  (sometimes also called optical depth or optical distance), which is the geometrical length of a path multiplied by the beam attenuation coefficient ( $c$ ) associated with the path.

Optical depths of particular interest in the context of primary production are those corresponding to attenuation of downward irradiance to 10% and 1% of the subsurface values: these are  $\zeta = 2.3$  and  $\zeta = 4.6$ , respectively. These optical depths correspond to the mid-point and the lower limit of the euphotic zone, within which significant photosynthesis occurs.

## 1.7 Radiative transfer theory

Having defined the properties of the light field and the optical properties of the medium we are now in a position to ask whether it is possible to arrive, on purely theoretical grounds, at any relations between them. Although, given a certain incident light field, the characteristics of the underwater light field are uniquely determined by the properties of the medium, it is nevertheless true that explicit, all-embracing analytical relations, expressing the characteristics of the field in terms of the inherent optical properties of the medium, have not yet been derived. Given the complexity of the shape of the volume scattering function in natural waters (see [Chapter 4](#)), it may be that this will never be achieved.

It is, however, possible to arrive at a useful expression relating the absorption coefficient to the average cosine and the vertical attenuation coefficient for net downward irradiance. In addition, relations have been derived between certain properties of the field and the diffuse optical properties. These various relations are all arrived at by making use of the equation of transfer for radiance. This describes the manner in which radiance varies with distance along any specified path at a specified point in the medium.

Assuming a horizontally stratified water body (i.e. with properties everywhere constant at a given depth), with a constant input of monochromatic unpolarized radiation at the surface, and ignoring fluorescent emission within the water, the equation may be written

$$\frac{dL(z, \theta, \phi)}{dr} = -c(z)L(z, \theta, \phi) + L^*(z, \theta, \phi) \quad (1.55)$$

The term on the left is the rate of change of radiance with distance,  $r$ , along the path specified by zenith and azimuthal angles  $\theta$  and  $\phi$ , at depth  $z$ . The net rate of change is the resultant of two opposing processes: loss by attenuation along the direction of travel ( $c(z)$  being the value of the beam attenuation coefficient at depth  $z$ ), and gain by scattering (along the path  $dr$ ) of light initially travelling in other directions ( $\theta'$ ,  $\phi'$ ) into the direction  $\theta$ ,  $\phi$  (Fig. 1.6). This latter term is determined by the volume scattering function of the medium at depth  $z$  (which we write  $\beta(z, \theta, \phi; \theta', \phi')$  to indicate that the scattering angle is the angle between the two directions  $\theta$ ,  $\phi$  and  $\theta'$ ,  $\phi'$ ) and by the distribution of radiance,  $L(z, \theta', \phi')$ . Each element of irradiance,  $L(z, \theta', \phi')d\omega(\theta', \phi')$  (where  $d\omega(\theta', \phi')$  is an element of solid angle forming an infinitesimal cone containing the direction  $\theta'$ ,  $\phi'$ ), incident on the volume element along  $dr$  gives rise to some scattered radiance in the direction  $\theta$ ,  $\phi$ . The total radiance derived in this way is given by

$$L^*(z, \theta, \phi) = \int_{2\pi} \beta(z, \theta, \phi; \theta', \phi') L(z, \theta', \phi') d\omega(\theta', \phi') \quad (1.56)$$

If we are interested in the variation of radiance in the direction  $\theta$ ,  $\phi$  as a function of depth, then since  $dr = dz/\cos \theta$ , we may rewrite eqn 1.55 as

$$\cos \theta \frac{dL(z, \theta, \phi)}{dz} = -c(z)L(z, \theta, \phi) + L^*(z, \theta, \phi) \quad (1.57)$$

By integrating each term of this equation over all angles

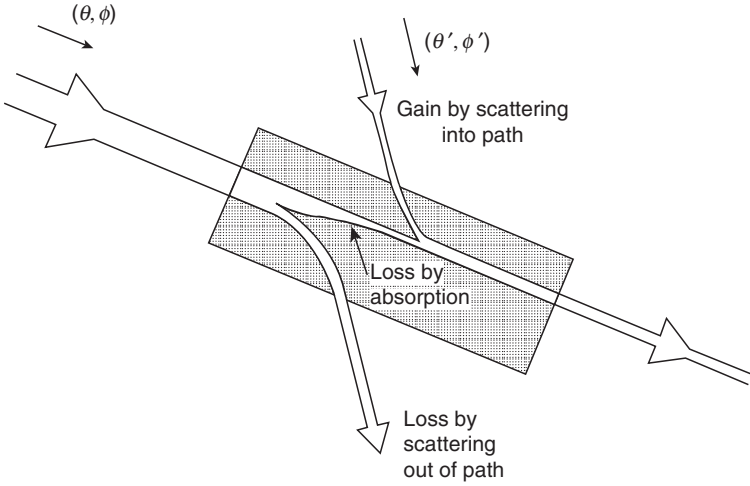


Fig. 1.6 The processes underlying the equation of transfer of radiance. A light beam passing through a distance,  $dr$ , of medium, in the direction  $\theta, \phi$ , loses some photons by scattering out of the path and some by absorption by the medium along the path, but also acquires new photons by scattering of light initially travelling in other directions  $(\theta', \phi')$  into the direction  $\theta, \phi$ .

$$\int_{4\pi} \cos \theta \frac{dL(z, \theta, \phi)}{dz} d\omega = - \int_{4\pi} c(z)L(z, \theta, \phi)d\omega + \int_{4\pi} L^*(z, \theta, \phi)d\omega$$

we arrive at the relation

$$\frac{d\vec{E}}{dz} = -cE_0 + bE_0 = -aE_0 \tag{1.58}$$

originally derived by Gershun (1936).

It follows that

$$a = K_E \frac{\vec{E}}{E_0} \tag{1.59}$$

and

$$a = K_E \bar{\mu} \tag{1.60}$$

Thus we have arrived at a relation between an inherent optical property and two of the properties of the field. Equation 1.60, as we shall see later (§ 3.2), can be used as the basis for determining the absorption coefficient of a natural water from *in situ* irradiance and scalar irradiance measurements.

Exploration of the properties of irradiance-weighted vertical attenuation coefficients (defined in §1.3, above) has shown<sup>717</sup> that the following relationships, analogous to the Gershun equation, also exist

$${}^wK_E(av) = \frac{a}{\bar{\mu}_c} \quad (1.61)$$

and

$${}^wK_0(av) = \frac{a}{\bar{\mu}(0)} \quad (1.62)$$

where  ${}^wK_E(av)$  and  ${}^wK_0(av)$  are the irradiance-weighted vertical attenuation coefficients for net downward and scalar irradiances, respectively,  $\bar{\mu}_c$  is the integral average cosine for the whole water column, and  $\bar{\mu}(0)$  is the average cosine for the light field just below the water surface.

Preisendorfer (1961) has used the equation of transfer to arrive at a set of relations between certain properties of the field and the *diffuse* absorption and scattering coefficients. One of these, an expression for the vertical attenuation coefficient for downward irradiance,

$$K_d(z) = a_d(z) + b_{bd}(z) - b_{bu}(z)R(z) \quad (1.63)$$

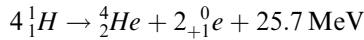
we will later (§6.7) find of assistance in understanding the relative importance of the different processes underlying the diminution of irradiance with depth.

## 2

# Incident solar radiation

### 2.1 Solar radiation outside the atmosphere

The intensity and the spectral distribution of the radiation received by the Earth are a function of the emission characteristics and the distance of the Sun. Energy is generated within the Sun by nuclear fusion. At the temperature of about  $20 \times 10^6$  K existing within the Sun, hydrogen nuclei (protons) fuse to give helium nuclei, positrons and energy. A number of steps is involved but the overall process may be represented by



The energy liberated corresponds to the slight reduction in mass that takes place in the fusion reactions. Towards its periphery the temperature of the Sun greatly diminishes and at its surface it is only about 5800 K.

For any physical system with the properties of a black body (or ‘full radiator’) the amount of radiant energy emitted per unit area of surface and the spectral distribution of that radiation are determined by the temperature of the system. The radiant flux\* emitted per unit area is proportional to the fourth power of the absolute temperature, in accordance with the Stefan–Boltzmann Law

$$M = \sigma T^4$$

where  $\sigma$  is  $5.67 \times 10^{-8} \text{ W m}^{-2} \text{ K}^{-4}$ . The Sun appears to behave approximately as a full radiator, or black body, and the radiant flux emitted per  $\text{m}^2$  of its surface is about  $63.4 \times 10^6 \text{ W}$ , corresponding (assuming a diameter of  $1.39 \times 10^6 \text{ km}$ ) to a total solar flux of about  $385 \times 10^{24} \text{ W}$ . At the

\* Throughout this chapter radiant flux and irradiance will be in energy units rather than quanta.

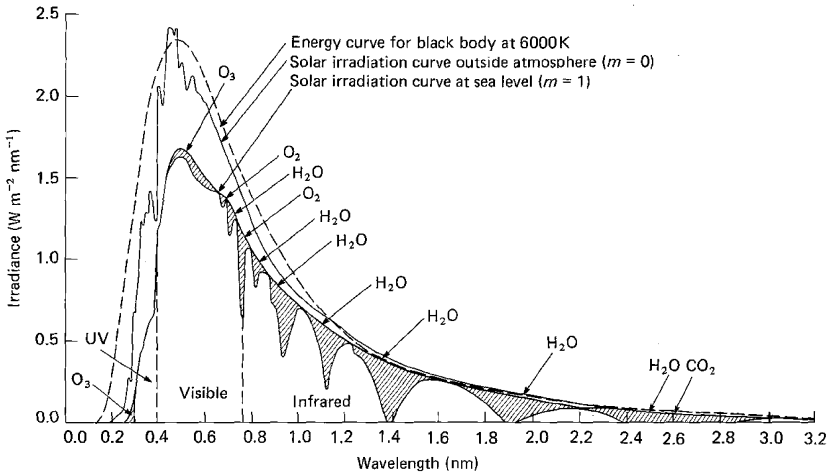


Fig. 2.1 The spectral energy distribution of solar radiation outside the atmosphere compared with that of a black body at 6000 K, and with that at sea level (zenith Sun). (By permission, from *Handbook of Geophysics*, revised edition, US Air Force, Macmillan, New York, 1960.)

distance of the Earth's orbit ( $150 \times 10^6$  km) the solar flux per unit area facing the Sun is about  $1373 \text{ W m}^{-2}$ .<sup>553</sup> This quantity, the total solar irradiance outside the Earth's atmosphere, is sometimes called the *solar constant*.

The Earth, having a diameter of 12 756 km, presents a cross-sectional area of  $1.278 \times 10^8 \text{ km}^2$  to the Sun. The solar radiation flux onto the whole of the Earth is therefore about  $1755 \times 10^{14} \text{ W}$ , and the total radiant energy received by the Earth from the Sun each year is about  $5.53 \times 10^{24} \text{ J}$ .

For a full radiator, the spectral distribution of the emitted energy has a certain characteristic shape, rising steeply from the shorter wavelengths to a peak, and diminishing more slowly towards longer wavelengths. As the temperature  $T$ , of the radiator increases, the position of the emission peak ( $\lambda_{\text{max}}$ ) moves to shorter wavelengths in accordance with Wien's Law

$$\lambda_{\text{max}} = \frac{w}{T}$$

where  $w$  (Wien's displacement constant) is equal to  $2.8978 \times 10^{-3} \text{ m K}$ . The Sun, with a surface temperature of about 5800 K has, in agreement with Wien's Law, maximum energy per unit wavelength at about 500 nm, as may be seen in the curve of solar spectral irradiance above the Earth's atmosphere in Fig. 2.1. It can be seen that the spectral distribution of the emitted solar flux is, compared to the theoretical curve for a full radiator

at 6000 K, somewhat irregular in shape at the short-wavelength end. The dips in the curve are due to the absorption bands of hydrogen in the Sun's outer atmosphere. Photosynthetically available radiation (commonly abbreviated to PAR), 400 to 700 nm, constitutes 38% of the extraterrestrial solar irradiance.

## **2.2 Transmission of solar radiation through the Earth's atmosphere**

Even when the sky is clear, the intensity of the solar beam is significantly reduced during its passage through the atmosphere. This reduction in intensity is due partly to scattering by air molecules and dust particles and partly to absorption by water vapour, oxygen, ozone and carbon dioxide in the atmosphere. With the Sun vertically overhead, the total solar irradiance on a horizontal surface at sea level is reduced by about 14% with a dry, clean atmosphere and by about 40% with a moist, dusty atmosphere, compared to the value above the atmosphere.<sup>931</sup> The proportion of the incident solar flux removed by the atmosphere increases as the solar elevation (the angle of the Sun's disc to the horizontal) decreases, in accordance with the increase in pathlength of the solar beam through the atmosphere. The atmospheric pathlength is approximately proportional to the cosecant of the solar elevation: it is, for example, twice as long with a solar elevation of 30° as with the Sun at the zenith.

### **Effect of scattering**

Since the air molecules are much smaller than the wavelengths of solar radiation, the efficiency with which they scatter light is proportional to  $1/\lambda^4$ , in accordance with Rayleigh's Law. Scattering of solar radiation is therefore much more intense at the short-wavelength end of the spectrum, and most of the radiation scattered by the atmosphere is in the visible and ultraviolet ranges.

Some of the radiation scattered from the solar beam is lost to space, and some finds its way to the Earth's surface. In the case of 'pure' Rayleigh scattering (scattering entirely due to air molecules, with a negligible contribution from dust), there is as much scattering in a forward, as in a backward, direction (Fig. 2.2; Chapter 4). Thus, ignoring for simplicity the effects of multiple scattering, half the light scattered from a

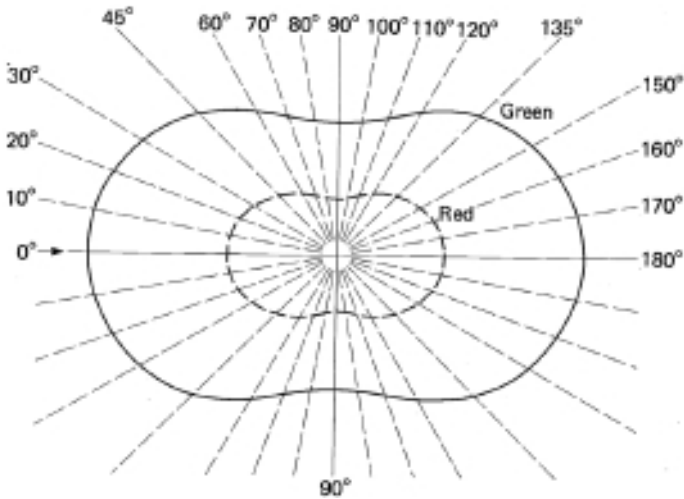


Fig. 2.2 Polar plot of intensity as a function of scattering angle for small particles ( $r \approx 0.025 \mu\text{m}$ ) for green ( $\lambda \approx 500 \text{ nm}$ ) and red ( $\lambda \approx 700 \text{ nm}$ ) light. (By permission, from *Solar Radiation*, N. Robinson, Elsevier, Amsterdam, 1966.)

sunbeam in a dust-free atmosphere will be returned to space and half will continue (at various angles) towards the Earth's surface. The total solar energy reflected (by scattering) back to space by a cloudless dust-free atmosphere alone after allowing for absorption by ozone, is about 7%.<sup>1141</sup>

The atmosphere over any part of the Earth's surface always contains a certain amount of dust, the quantity varying from place to place and with time at any given place. Dust particles scatter light, but are generally not sufficiently small relative to the wavelength of most of the solar radiation for scattering to obey the Rayleigh Law. They exhibit instead a type of scattering known as Mie scattering (see [Chapter 4](#)), which is characterized by an angular distribution predominantly in the forward direction, and a much weaker dependence on wavelength, although scattering is still more intense at shorter wavelengths. Although dust particles scatter light mainly in a forward direction, they do also scatter significantly in a backward direction; furthermore, a proportion of the light scattered forward, but at large values of scattering angle, will be directed upwards if the solar beam is not vertical. Since the particle scattering is additive to the air molecule scattering, a hazy (dusty) atmosphere reflects more solar energy to space than does a clean atmosphere.

That fraction of the solar flux which is scattered by the atmosphere in the direction of the Earth's surface constitutes skylight. Skylight appears blue because it contains a high proportion of the more intensely scattered, blue light from the short-wavelength end of the visible spectrum. In a hazy atmosphere the increased scattering increases skylight at the expense of the direct solar flux. The proportion of the total radiation received at the Earth's surface which is skylight varies also with the solar elevation. As the atmospheric pathlength of the solar beam increases with decreasing solar elevation, so more of the radiation is scattered: as a consequence the direct solar flux diminishes more rapidly than does skylight.

At very low solar elevations ( $0^{\circ}$ – $20^{\circ}$ ) in the absence of cloud, the direct solar beam and the diffuse flux (skylight) contribute approximately equally to irradiance at the Earth's surface. As solar elevation increases, the irradiance due to the direct beam rises steeply but the irradiance due to skylight levels off above about  $30^{\circ}$ . At high solar elevations under cloudless conditions, skylight commonly accounts for 15 to 25% of the irradiance and the direct solar beam for 75 to 85%:<sup>928</sup> in very clear dry air the contribution of skylight can be as low as 10%.

### **Spectral distribution of irradiance at the Earth's surface**

The scattering and absorption processes that take place within the atmosphere not only reduce the intensity, but also change the spectral distribution of the direct solar beam. The lowest curve in Fig. 2.1 shows the spectral distribution of solar irradiance at sea level for a zenith Sun and a clear sky. The shaded areas represent absorption, and so the curve forming the upper boundary of these shaded areas corresponds to the spectral distribution as it would be if there were scattering but no absorption. It is clear that the diminution of solar flux in the ultraviolet band ( $0.2$ – $0.4\ \mu\text{m}$ ) is largely due to scattering, with a contribution from absorption by ozone. In the visible/photosynthetic band ( $0.4$ – $0.7\ \mu\text{m}$ ), attenuation is mainly due to scattering, but with absorption contributions from ozone, oxygen and, at the red end of the spectrum, water vapour. In the long, infrared tail of the distribution, scattering becomes of minor importance and the various absorption bands of water vapour are mainly responsible for the diminution in radiant flux.

The proportion of infrared radiation removed from the solar beam by absorption during its passage through the atmosphere is variable since the amount of water vapour in the atmosphere is variable. Nevertheless it is generally true that a higher proportion of the infrared is removed than of the photosynthetic waveband. As a consequence, photosynthetically

available radiation (0.4–0.7  $\mu\text{m}$ ) is a higher proportion of the solar radiation that reaches the Earth's surface than of the radiation above the atmosphere. Photosynthetically available radiation constitutes about 45% of the energy in the direct solar beam at the Earth's surface when the solar elevation is more than  $30^\circ$ .<sup>930</sup> Skylight, consisting as it does of scattered and therefore mainly short-wave radiation, is predominantly in the visible/photosynthetic range.

Using the best available data for the spectral distribution of the extraterrestrial solar flux, Baker and Frouin (1987) have carried out calculations of atmospheric radiation transfer to estimate the PAR (in this case taken to be 350 to 700 nm) as a proportion of total insolation at the ocean surface, under clear skies, but with various types of atmosphere, and varying Sun angle. They found  $E_d(350\text{--}700\text{ nm})/E_d(\text{total})$  for all atmospheres to lie between 45 and 50% at solar altitudes greater than  $40^\circ$ . The ratio increased with increasing atmospheric water vapour, because of a decrease in  $E_d(\text{total})$ . It was essentially unaffected by variation in ozone content, or in the aerosol content provided the aerosol was of a maritime, not continental, type. It was little affected by solar altitude between  $40^\circ$  and  $90^\circ$ , but decreased 1 to 3% as solar elevation was lowered from  $40^\circ$  to  $10^\circ$ .

Since the efficiency with which the photosynthetic apparatus captures light energy varies with wavelength, the usefulness of a given sample of solar radiation for primary production depends on the proportion of different wavelengths of light present, i.e. on its spectral distribution. Figure 2.3 shows data for the spectral distribution of solar irradiance at the Earth's surface under clear sunny skies, within a few hours of solar noon at three different locations. As the solar elevation diminishes, the ratio of short- (blue) to long- (red) wavelength light in the direct solar beam decreases because of the intensified removal of the more readily scattered, short-wavelength light in the longer atmospheric path. On the other hand, as solar elevation diminishes, the relative contribution of skylight to total irradiance increases, and skylight is particularly rich in the shorter wavelengths: there is therefore no simple relation between solar elevation and the spectral distribution of total irradiance.

### Effect of cloud

In addition to the effects of the gaseous and particulate components of the atmosphere, the extent and type of cloud cover are of great importance in determining the amount of solar flux that penetrates to the Earth's surface. We follow here the account given by Monteith (1973).

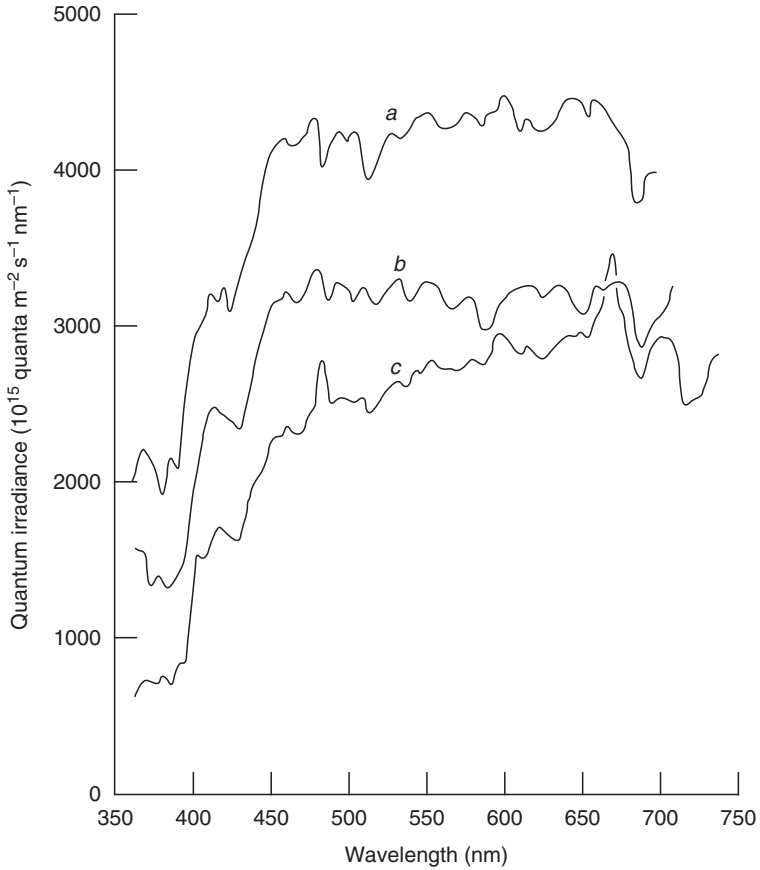


Fig. 2.3 Spectral distribution of solar quantum irradiance at the Earth's surface at three geographical locations (plotted from the data of Tyler and Smith, 1970). (a) Crater Lake, Oregon, USA ( $42^{\circ}56' \text{ N}$ ,  $122^{\circ}07' \text{ W}$ ). Elevation 1882 m. 11:00–11:25 h, 5 August 1966. (b) Gulf Stream, Bahamas, Atlantic Ocean ( $25^{\circ}45' \text{ N}$ ,  $79^{\circ}30' \text{ W}$ ). 12:07–12:23 h, 3 July 1967. (c) San Vicente reservoir, San Diego, California, USA ( $32^{\circ}58' \text{ N}$ ,  $116^{\circ}55' \text{ W}$ ). 09:37–09:58 h, 20 January 1967. All the measurements were made under clear skies.

A few isolated clouds in an otherwise clear sky increase the amount of diffuse flux received at the Earth's surface but, provided they do not obscure the Sun, they have no effect on the direct solar beam. Thus, a small amount of cloud can increase total irradiance by 5 to 10%. A continuous sheet of cloud, however, will always reduce irradiance. Under a thin sheet of cirrus, total irradiance may be about 70% of that

under a clear sky. A deep layer of stratus cloud, on the other hand, may transmit only 10% of the solar radiation, about 70% being reflected back to space by its upper surface and 20% being absorbed within it. On a day with broken cloud, the irradiance at a given point on the Earth's surface is intermittently varying from the full Sun's value to perhaps 20 to 50% of this as clouds pass over the Sun.

In desert regions there is rarely enough cloud to affect surface irradiance, but in the humid parts of the globe, cloud cover significantly reduces the average solar radiation received during the year. In much of Europe, for example, the average insolation (total radiant energy received  $\text{m}^{-2}\text{day}^{-1}$ ) in the summer is 50 to 80% of the insolation that would be obtained on cloudless days.<sup>928</sup>

In recent years, a large amount of new information on the distribution and optical characteristics of clouds around the Earth has become available from satellite remote sensing. The International Satellite Cloud Climatology Project (ISCCP) has been combining such data from geostationary and polar orbiting meteorological satellites from mid-1983 onwards. Bishop and Rossow (1991) have used the ISCCP data, together with modelling of radiation transfer through the atmosphere, to assess the effects of clouds on the spatial and temporal variability of the solar irradiance around the globe. The results show that the oceans are much cloudier than the continents, and receive a correspondingly lower solar irradiance. For example, in July 1983, approximately 9% of the ocean was perpetually cloud covered, contrasting with only 0.3% over land.

There are marked differences between regions of the ocean: the Northern and Southern ocean waters are almost perpetually cloud covered, but at an equatorial mid-Pacific location ( $1^\circ\text{N}$ ,  $140^\circ\text{W}$ ) clear skies consistently prevail. In the northern hemisphere the Atlantic Ocean receives substantially more solar radiation than the Pacific Ocean in the summer, but there is little difference between the two oceans in the southern hemisphere. The irradiance at the ocean surface, as a per cent of the clear sky value is about halved between  $30^\circ\text{S}$  and  $60^\circ\text{S}$  due to the persistent band of circumpolar cloudiness centred at  $60^\circ\text{S}$ . The Argentine Basin and Weddell Sea sectors of the western South Atlantic are, however – presumably due to proximity to land – consistently less cloudy than the rest of this circumpolar region, and are known to have greater levels of primary productivity. Bishop and Rossow suggest that solar irradiance is a major determinant of the rate of carbon fixation by phytoplankton in these nutrient-rich southern ocean waters.

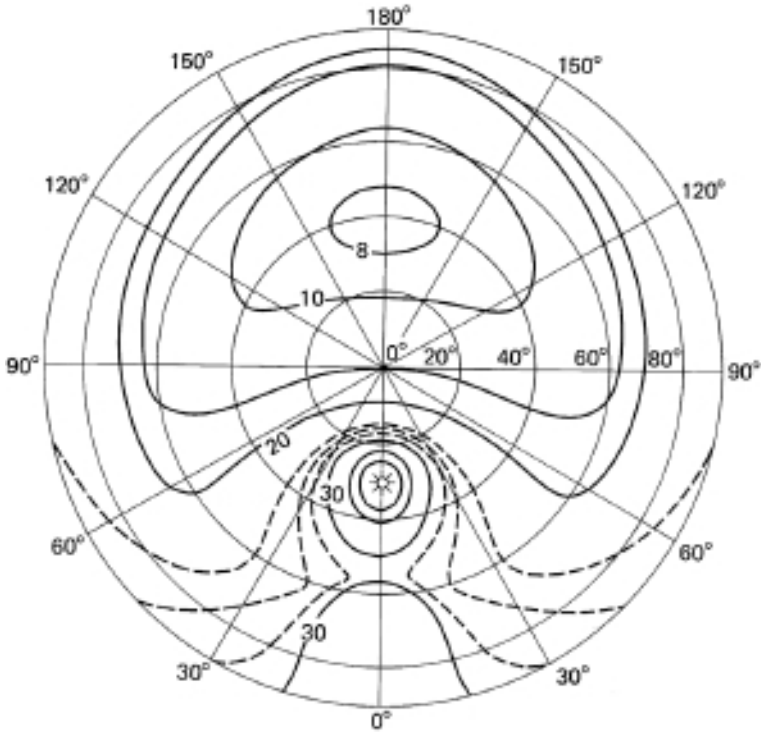


Fig. 2.4 Angular distribution of luminance (approximately proportional to radiance) in a clear sky. (By permission, from *Solar Radiation*, N. Robinson, Elsevier, Amsterdam, 1966.)

### Angular distribution of solar radiation under different atmospheric conditions

That part of the solar radiation at the Earth's surface which is the direct solar beam, of necessity consists of a parallel flux of radiation at an angle to the vertical equal to the solar zenith angle. Radiance in the direction of the solar disc is very high and falls off sharply just beyond the edge of the disc.

The angular distribution of skylight from a clear sky is complex; it is shown diagrammatically in Fig. 2.4. Because scattering by dust particles, and to a lesser extent by air molecules, is strong in a forward direction, skylight is particularly intense at angles near to the angle of the Sun.<sup>928</sup> Radiance from the sky decreases markedly with increasing angular distance from the Sun; it reaches its minimum in that region of the celestial

hemisphere approximately  $90^\circ$  from the Sun and then rises again towards the horizon. On the basis of more than 3000 scans of clear skies above Calgary, Canada, Harrison and Coombes (1988) arrived at an empirical relationship for the angular distribution of clear sky radiance: this somewhat complex relationship gives the normalized sky radiance,  $\bar{N}(\psi)$ , as a function of direction

$$\begin{aligned} \bar{N}(\psi) = & (1.63 + 53.7 e^{-5.94\psi} + 2.04 \cos^2 \psi \cos \theta^*) \\ & \times (1 - e^{-1.9 \sec \theta})(1 - e^{-0.53 \sec \theta^*}) \end{aligned} \quad (2.1)$$

where  $\theta^*$  is the solar zenith angle,  $\theta$  is the zenith angle of any given sky radiance direction, and  $\Psi$  is the scattering angle, i.e. the angle between the parallel solar beam (at zenith angle  $\theta^*$ , and azimuth angle  $\phi = 0^\circ$ ) and the sky radiance direction (at  $\theta, \phi$ ).  $\Psi$  is given by

$$\cos \psi = \cos \theta \cos \theta^* + \sin \theta \sin \theta^* \cos \phi \quad (2.2)$$

Radiance is the radiant flux in a given direction per unit solid angle per unit area at right angles to the direction of propagation, and has the units watts (or quanta  $\text{s}^{-1}$ )  $\text{m}^{-2}$  steradian $^{-1}$ . To obtain the normalized sky radiance, the actual measured radiance in a given direction,  $N(\theta, \phi)$ , is divided by  $E_{ds}$ , the diffuse sky irradiance on a horizontal surface, and then rendered dimensionless by multiplying by  $\pi$  steradians.

$$\bar{N}(\psi) = \frac{\pi N(\theta, \phi)}{E_{ds}} \quad (2.3)$$

Thus, when we want a specific sky radiance in a certain waveband,  $N(\theta, \phi, \lambda)$ , then using an appropriate value however obtained (see later) for the diffuse irradiance in that waveband on a horizontal surface,  $E_{ds}(\lambda)$ , we rearrange eqn 2.3

$$N(\theta, \phi, \lambda) = \frac{\bar{N}(\psi) E_{ds}(\lambda)}{\pi} \quad (2.4)$$

and with the help of eqns 2.1 and 2.2 to provide  $\bar{N}(\psi)$ , we obtain the desired value.

Contrary to what casual observation might suggest, the radiance distribution beneath a heavily overcast sky is not uniform. In fact, the radiance at the zenith is two to two-and-a-half times that at the horizon. To provide an approximation to the radiance distribution under these conditions, a Standard Overcast Sky has been defined<sup>929</sup> under which the radiance as a function of zenith angle,  $\theta$ , is given by

$$L(\theta) = L(0)(1 + B \cos \theta)/(1 + B) \quad (2.5)$$

where  $B$  is in the range 1.1 to 1.4. The radiance under a sky with broken cloud must necessarily vary with angle in a highly discontinuous manner, and no useful general description can be given.

### **Average transmission characteristics of the atmosphere**

A valuable summary of the effects of the atmosphere as a whole on the transmission of solar radiation from space to the Earth's surface has been provided by Gates (1962) in terms of the average fate of the radiant flux incident on the northern hemisphere. Over a year, 34% of the incoming solar radiation is reflected to space by the atmosphere; this is made up of 25% reflected by clouds and 9% scattered out to space by other constituents of the atmosphere. Another 19% of the incoming radiation is absorbed by the atmosphere: 10% within clouds, 9% by other components. This leaves 47% of the solar flux, which, on average, reaches the Earth's surface. Of this 47%, 24% consists of the direct solar beam and 23% of diffuse light scattered from clouds (17%) and from the air (6%).

In the cloudy, dirty, moist atmosphere of London, about a third of the incident solar radiation per year is scattered back to space, about a third is absorbed within the atmosphere and the remainder penetrates to the Earth's surface.<sup>928</sup> Of the 30% or so that is absorbed, 13% is by water vapour, 9% within clouds and 8% by dust and smoke.

### **2.3 Diurnal variation of solar irradiance**

For a given set of atmospheric conditions, the irradiance at any point on the Earth's surface is determined by the solar elevation,  $\beta$ . This rises during the day from zero (or its minimum value in the Arctic or Antarctic during the summer) at dawn to its maximum value at noon, and then diminishes in a precisely symmetrical manner to zero (or the minimum value) at dusk. The exact manner of the variation of  $\beta$  with time of day depends on the latitude, and on the solar declination,  $\delta$ , at the time. The declination is the angle through which a given hemisphere (north or south) is tilted towards the Sun (Fig. 2.5). In summer it has a positive value, in winter a negative one; at the spring and autumn equinoxes its value is zero. Its maximum value, positive or negative, is  $23^{\circ}27'$ . Published tables exist in which the solar declination for the northern

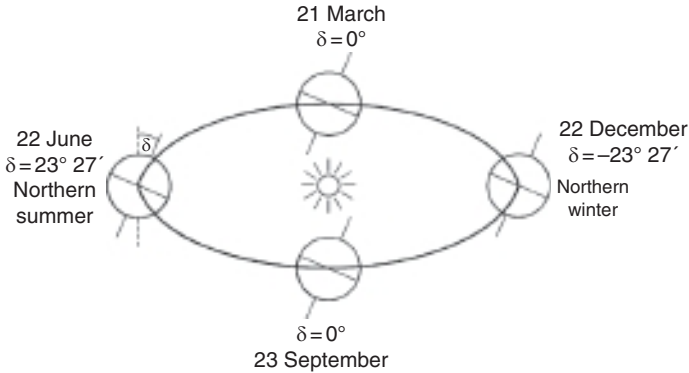


Fig. 2.5 Variation of the solar declination throughout the year.

hemisphere may be found for any day of the year. Alternatively, a relation derived by Spencer (1971) may be used

$$\delta = 0.39637 - 22.9133 \cos \psi + 4.02543 \sin \psi - 0.3872 \cos 2\psi + 0.052 \sin 2\psi \quad (2.6)$$

where  $\psi$  is the date expressed as an angle ( $\psi = 360^\circ \times d/365$ ;  $d =$  day number, ranging from 0 on 1 January to 364 on 31 December): both  $\delta$  and  $\psi$  are in degrees. The declination for the southern hemisphere on a given date has the same numerical value as that for the northern hemisphere, but the opposite sign.

The solar elevation,  $\beta$ , at any given latitude,  $\gamma$ , varies with the time of day,  $\tau$ , (expressed as an angle) in accordance with the relation

$$\sin \beta = \sin \gamma \sin \delta - \cos \gamma \cos \delta \cos \tau \quad (2.7)$$

where  $\tau$  is  $360^\circ \times t/24$  ( $t$  being the hours elapsed since 00.00 h). If we write this in the simpler form

$$\sin \beta = c_1 - c_2 \cos \tau \quad (2.8)$$

where  $c_1$  and  $c_2$  are constants for a particular latitude and date ( $c_1 = \sin \gamma \sin \delta$ ,  $c_2 = \cos \gamma \cos \delta$ ), then it becomes clear that the variation of  $\sin \beta$  with the time of day is sinusoidal. Figure 2.6 shows the variations in both  $\beta$  and  $\sin \beta$  throughout a 24-hour period corresponding to the longest summer day (21 December) and shortest winter day (21 June) at the latitude of Canberra, Australia ( $35^\circ$  S). For completeness, the values of  $\beta$  and  $\sin \beta$  during the hours of darkness are shown: these are negative and correspond to the angle of the Sun below the horizontal plane.

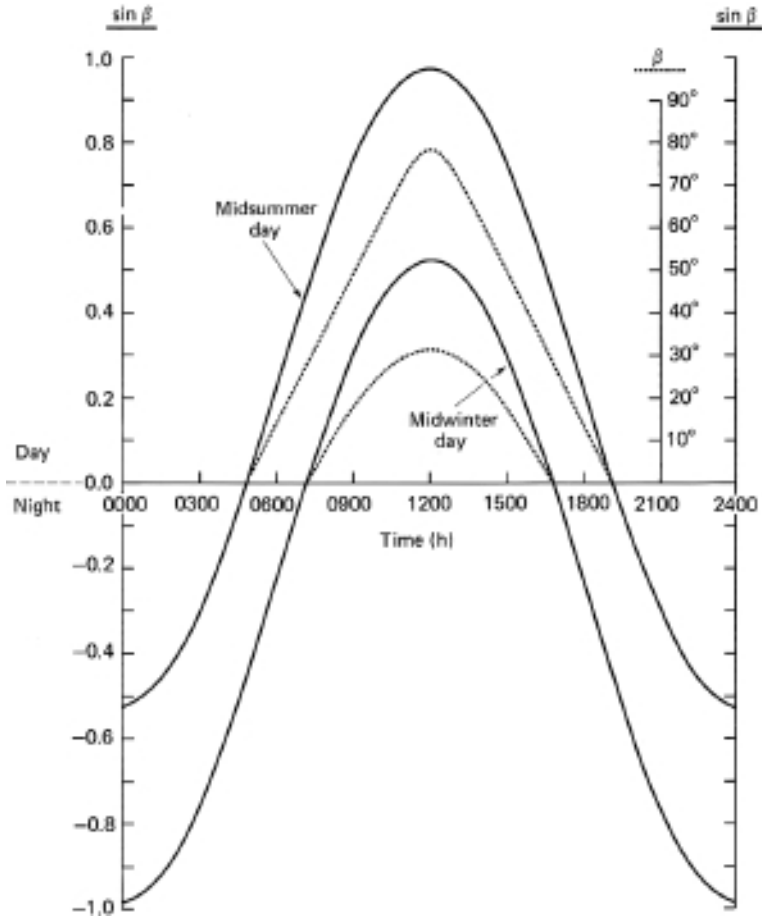


Fig. 2.6 Variation in solar elevation ( $\beta$ ) and  $\sin \beta$  during a 24-h period on the longest summer day and the shortest winter day at  $35^\circ$  latitude.

The variation of  $\sin \beta$  is sinusoidal with respect to time measured within a 24-hour cycle, but not with respect to hours of daylight.

The sine of the solar elevation  $\beta$  is equal to the cosine of the solar zenith angle  $\theta$ . Irradiance due to the direct solar beam on a horizontal surface is, in accordance with the Cosine Law, proportional to  $\cos \theta$ . We might therefore expect that in the absence of cloud, solar irradiance at the Earth's surface will vary over a 24-hour period in much the same way as  $\sin \beta$  (Fig. 2.6), except that its value will be zero during the hours of darkness. Exact conformity between the behaviour of irradiance and  $\sin \beta$  is not to be expected since, for example, the effect of the atmosphere varies with solar

elevation. The greater attenuation of the direct beam at low solar elevation due to increased atmospheric pathlength, although in part balanced by a (proportionately) greater contribution from skylight, does reduce irradiance early in the morning and towards sunset below the values that might be anticipated on the basis of eqn 2.8. This has the useful effect of making the curve of daily variation of irradiance approximately sinusoidal with respect to daylight hours, even though, as we have seen, the variation of  $\sin \beta$  is strictly speaking only sinusoidal with respect to hours since 00:00 h. Figure 2.7 gives some examples of the diurnal variation of total irradiance at different times of year and under different atmospheric conditions.

A smooth curve is of course only obtained when cloud cover is absent, or is constant throughout the day. Broken cloud imposes short-term irregularities on the underlying sinusoidal variation in irradiance (Fig. 2.7). If  $E(t)$  is the total irradiance at time  $t$  h after sunrise, then by integrating  $E(t)$  with respect to time we obtain the total solar radiant energy received per unit horizontal area during the day. This is referred to as the *daily insolation* and we shall give it the symbol,  $Q_s$

$$Q_s = \int_0^N E(t) dt \quad (2.9)$$

where  $N$  is the daylength.

If  $E(t)$  has the units  $\text{W m}^{-2}$  and  $N$  is in s, then  $Q_s$  is in  $\text{J m}^{-2}$ . On a day of no, or constant, cloud cover the diurnal variation in  $E(t)$  is expressed approximately by

$$E(t) = E_m \sin(\pi t/N) \quad (2.10)$$

where  $E_m$  is the irradiance at solar noon.<sup>928</sup> By integrating this expression in accordance with eqn 2.9, it can be shown that the daily insolation on such a day is related to the maximum (noon) irradiance by

$$Q_s = 2NE_m/\pi \quad (2.11)$$

Thus if, as for example in Fig. 2.7c (16 March), the maximum irradiance is  $940 \text{ W m}^{-2}$  in a 12-hour day, then the total energy received is about 26 MJ.

On days with broken cloud, the degree of cloud cover is varying continuously throughout any given day. Nevertheless, in many parts of the world, the cloud cover averaged over a period as long as a month is approximately constant throughout the day.<sup>1399</sup> Therefore, the diurnal variation in total irradiance averaged over a month will be approximately sinusoidal and will conform with eqn 2.10. From the average maximum irradiance, the average daily insolation can be calculated using eqn 2.11.

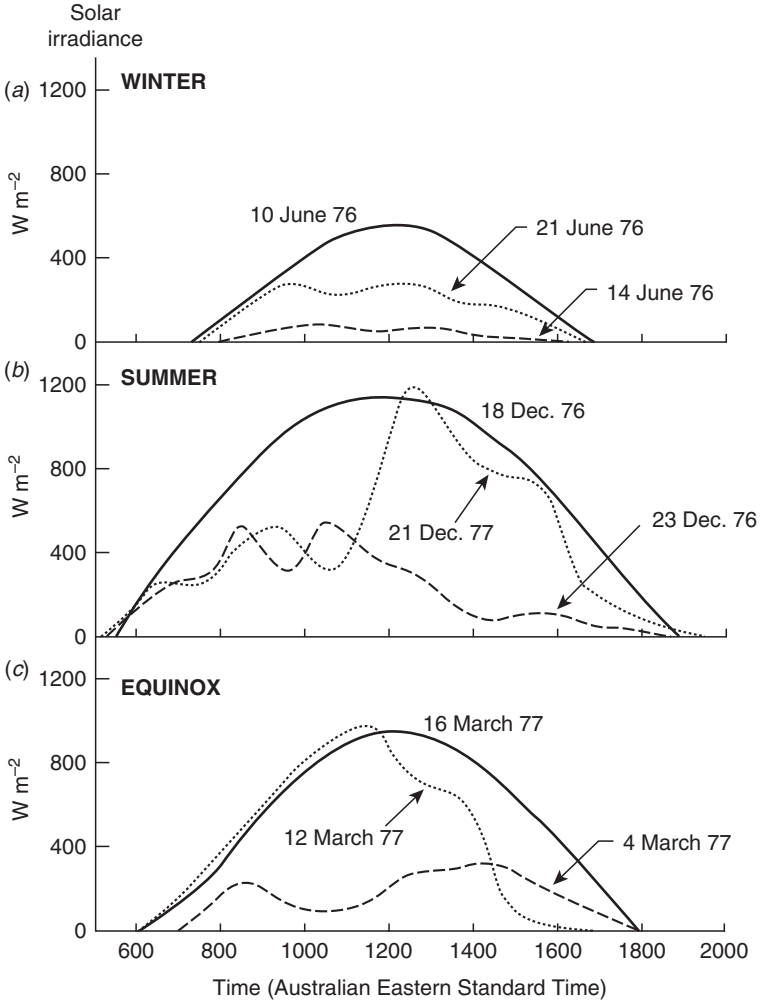


Fig. 2.7 Diurnal variation of total solar irradiance at different times of year and under different atmospheric conditions. The measurements were made at Krawaree, NSW, Australia (149°27' E, 35°49' S; 770 m above sea level) on dates close to (a) the shortest winter day, (b) the longest summer day, (c) the autumn equinox. (— clear sky; ..... intermittent cloud; ----- generally overcast). Data provided by Mr F. X. Dunin, CSIRO, Canberra.

### 2.4 Variation of solar irradiance and insolation with latitude and time of year

At any given point on the Earth's surface the daylength and the solar elevation reach their maximum values in the summer and their minimum

values in the winter. Substituting into eqn 2.7 we can obtain expressions for the noon solar elevation on the longest summer day ( $\delta = 23^\circ 27'$ )

$$\sin \beta = 0.39795 \sin \gamma + 0.91741 \cos \gamma \quad (2.12)$$

and the shortest winter day ( $\delta = -23^\circ 27'$ )

$$\sin \beta = -0.39795 \sin \gamma + 0.91741 \cos \gamma \quad (2.13)$$

as a function of latitude. At the latitude of Canberra ( $35^\circ$  S) for example, the corresponding solar elevations are  $78.5$  and  $31.5^\circ$ : at the latitude of London ( $51.5^\circ$  N) they are  $62$  and  $15^\circ$ .

Maximum and minimum daylengths can also be obtained using eqn 2.7. If the time (expressed as an angle) at sunrise is  $\tau_s$  then (since  $\sin \beta = 0$  at sunrise) at any time of year

$$\cos \tau_s = \tan \gamma \tan \delta \quad (2.14)$$

Daylength expressed as an angle is  $(360^\circ - 2\tau_s)$ , which is equal to  $2 \cos^{-1}(-\tan \gamma \tan \delta)$ . Expressed in hours, daylength is given by

$$N = 0.133 \cos^{-1}(-\tan \gamma \tan \delta) \quad (2.15)$$

The longest day is therefore  $0.133 \cos^{-1}(-0.43377 \tan \gamma)$  h and the shortest day is  $0.133 \cos^{-1}(0.43377 \tan \gamma)$  h.

With increasing latitude, the solar elevation at noon and therefore the maximum value of solar irradiance ( $E_m$ ) decrease, which in accordance with eqn 2.11, decreases the daily insolation. In the summer, however, this effect is counteracted by the increase in daylength ( $N$  in eqn 2.11) with increasing latitude, and the net result is that high-latitude regions can have a slightly greater daily insolation in midsummer than tropical regions. In the winter, of course, the high-latitude regions have shorter days (zero daylengths in the polar regions) as well as lower solar elevations, so their daily insolation is much less than at low latitudes. Throughout most of the year, in fact, the rule-of-thumb holds that the higher the latitude, the lower the daily insolation. Figure 2.8 shows the change in daily insolation throughout the year, calculated ignoring atmospheric losses, for a range of latitudes. Figure 2.9 shows the true (measured) daily insolation as a function of time of year at a southern hemisphere site, near Canberra, Australia, averaged over a three-year period, illustrating the steady rise to a peak in the summer followed by a decline to the winter minimum. These data, unlike those in Fig. 2.8, include the effects of cloud and atmospheric haze.

In oceanic regions with monsoonal climates there can be two seasonal peaks of intensity of solar radiation within the year.<sup>168a,30</sup> Figure 2.10 shows the mean monthly surface-incident PAR over a seven-year period averaged over the

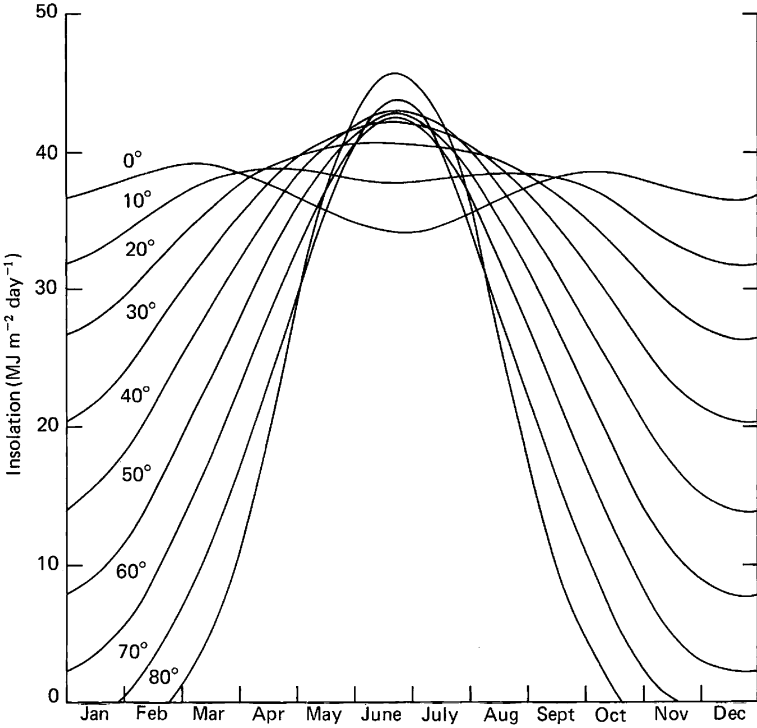


Fig. 2.8 Change in calculated daily insolation (ignoring the influence of the atmosphere) throughout the year at different latitudes in the northern hemisphere. The latitude is indicated above each curve. Plotted from data of Kondratyev (1954).

Arabian Sea. After the winter minimum in December to January,  $E_d(\text{PAR})$  rises to a spring maximum in March, April and May, and then declines to a minimum in June and July in response to increased cloud cover and aerosols associated with the onset of the southwest monsoon.<sup>30</sup> Solar irradiance then rises to a second, lower, peak in September, following which it declines once again to the winter minimum. In more typical parts of the ocean, such as the North Atlantic, there is a single irradiance maximum, in the summer.

## 2.5 Transmission across the air–water interface

To become available in the aquatic ecosystem, the solar radiation that has penetrated through the atmosphere must now find its way across the air–water interface. Some of it will be reflected back into the atmosphere.

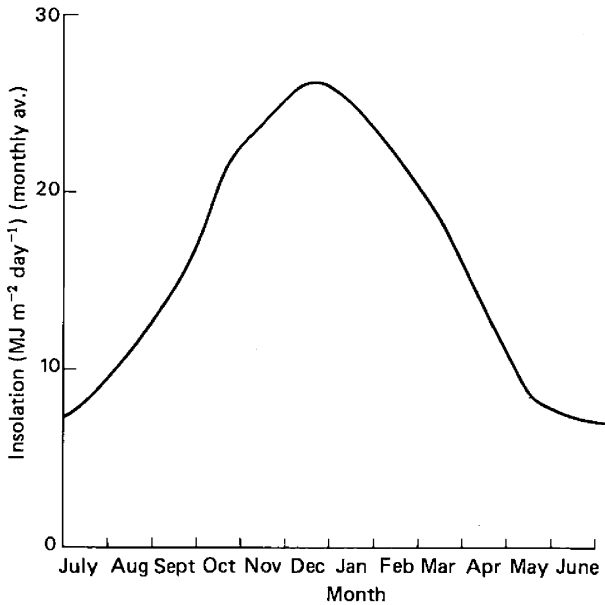


Fig. 2.9 Change in measured daily insolation throughout the year at the CSIRO Ginninderra Experiment Station, (35° S, 149° E). The curve corresponds to the daily average for each calendar month, averaged over the period 1978–80.

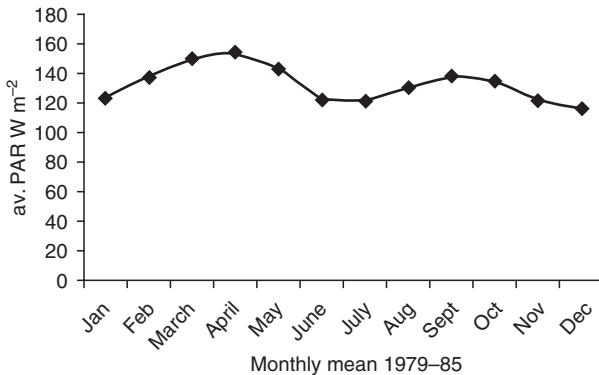


Fig. 2.10 The mean interannual irradiance of PAR ( $\text{W m}^{-2}$ ) at the sea surface for the entire Arabian Sea basin (excluding the Persian Gulf and the Red Sea) from 1979 to 1985. Plotted from data in Plate 4 of Arnone *et al.* (1998). *J. Geophys. Res.*, **103**, 7735–48.

The proportion of the incident light that is reflected by a flat water surface increases from 2% for vertically incident light towards 100% as the beam approaches grazing incidence. The dependence of reflectance,  $r$ , of

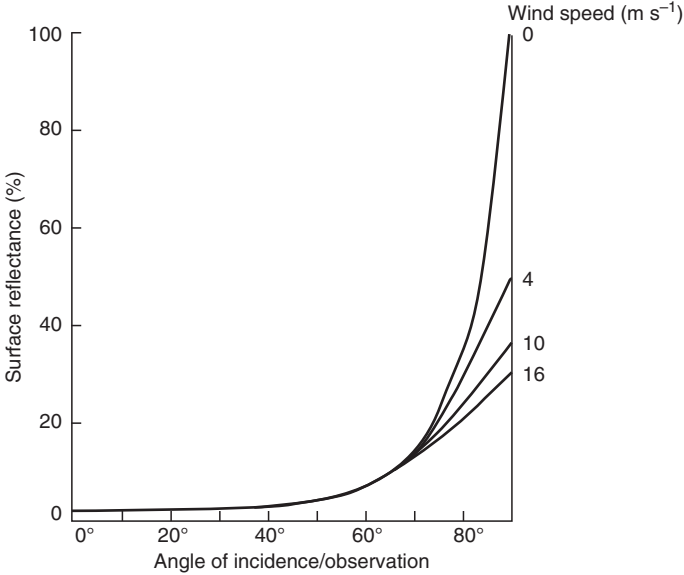


Fig. 2.11 Reflectance of water surface as a function of zenith angle of light (incident from above), at different wind speeds (data of Gordon, 1969; Austin, 1974a).

unpolarized light on the zenith angle of the incident light in air ( $\theta_a$ ), and on the angle to the downward vertical of the transmitted beam in water, ( $\theta_w$ ), is given by Fresnel’s Equation

$$r = \frac{1}{2} \frac{\sin^2(\theta_a - \theta_w)}{\sin^2(\theta_a + \theta_w)} + \frac{1}{2} \frac{\tan^2(\theta_a - \theta_w)}{\tan^2(\theta_a + \theta_w)} \tag{2.16}$$

The angle,  $\theta_w$ , in water is itself determined by  $\theta_a$ , and the refractive index, as we shall shortly see. The percentage reflectance from a flat water surface as a function of zenith angle is shown in Fig. 2.11, and in tabular form in Table 2.1. It will be noted that reflectance remains low, increasing only slowly, up to zenith angles of about 50°, but rises very rapidly thereafter.

Roughening of the water surface by wind has little effect on the reflectance of sunlight from high solar elevations. At low solar elevations, on the other hand, reflectance is significantly lowered by wind since the roughening of the surface on average increases the angle between the light direction and the surface at the point of entry. The three lower curves in Fig. 2.11 show the effect of wind at different velocities on the reflectance.<sup>494,41</sup>

Table 2.1 Reflectance of unpolarized light from a flat water surface. The values of reflectance have been calculated using eqns 2.16 and 2.19, assuming that the water has a refractive index of 1.33.

Zenith angle of incidence $\theta_a$ (degrees)	Reflectance (%)	Zenith angle of incidence $\theta_a$ (degrees)	Reflectance (%)
0.0	2.0	50.0	3.3
5.0	2.0	55.0	4.3
10.0	2.0	60.0	5.9
15.0	2.0	65.0	8.6
20.0	2.0	70.0	13.3
25.0	2.1	75.0	21.1
30.0	2.1	80.0	34.7
35.0	2.2	85.0	58.3
40.0	2.4	87.5	76.1
45.0	2.8	89.0	89.6

As wind speed increases the waves begin to break, and whitecaps are formed. The fraction of the ocean surface covered by whitecaps,  $W$ , is a function of windspeed,  $U$  ( $\text{m s}^{-1}$  at 10 m above surface), and can be represented as a power law

$$W(U) = AU^B \quad (2.17)$$

The coefficient  $A$  and the exponent  $B$  are functions of water temperature, but combining data from a range of water temperatures, Spillane and Doyle (1983) found the relationship

$$W(U) = 2.692 \times 10^{-5} U^{2.625} \quad (2.18)$$

to give the best fit. Equation 2.18 predicts, for example, that whitecaps cover about 1% of the sea surface at a wind speed of  $10 \text{ m s}^{-1}$ , and 13% at  $25 \text{ m s}^{-1}$ . Freshly formed whitecaps consist of many layers of bubbles, and have a reflectance of about 55%.<sup>1464,1284</sup> They have, however, a lifetime of only 10 to 20 s in the ocean, and Koepke (1984) found that as they decay their reflectance decreases markedly due to thinning of the foam, and he estimated the effective reflectance to be on average only about 22%, and their contribution to total oceanic reflectance to be minor. Using eqn 2.18 we can calculate the additional ocean surface reflectance due to whitecaps to be only about 0.25% at a wind speed of  $10 \text{ m s}^{-1}$ , and  $\sim 3\%$  at  $25 \text{ m s}^{-1}$ .

Because of the complex angular distribution of skylight, the extent to which it is reflected by a water surface is difficult to determine. If the very

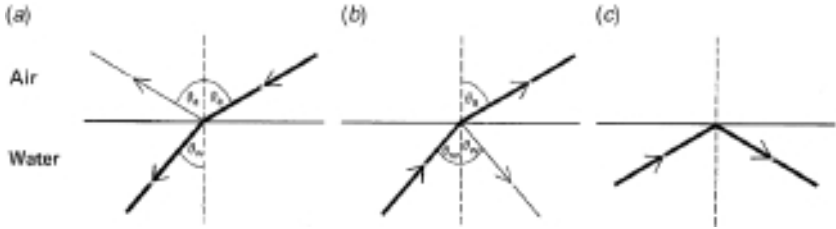


Fig. 2.12 Refraction and reflection of light at air–water boundary. (a) A light beam incident from above is refracted downwards within the water: a small part of the beam is reflected upwards at the surface. (b) A light beam incident from below at a nadir angle of  $40^\circ$  is refracted away from the vertical as it passes through into the air: a small part of the beam is reflected downwards again at the water–air boundary. (c) A light beam incident from below at a nadir angle greater than  $49^\circ$  undergoes complete internal reflection at the water–air boundary.

approximate assumption is made that the radiance is the same from all directions, then a reflectance of 6.6% for a flat water surface is obtained.<sup>636</sup> For an incident radiance distribution such as might be obtained under an overcast sky, the reflectance is calculated to be about 5.2%.<sup>1074</sup> Roughening of the surface by wind will lower reflectance for the diffuse light from a clear or an overcast sky.

As the unreflected part of a light beam passes across the air–water interface, it changes its direction to the vertical (while remaining, if the surface is flat, in the same vertical plane), due to refraction. The phenomenon of refraction is the result of the differing velocities of light in the two media, air and water. The change in angle (Fig. 2.12) is governed by Snell's Law

$$\frac{\sin \theta_a}{\sin \theta_w} = \frac{n_w}{n_a} \quad (2.19)$$

where  $n_w$  and  $n_a$  are the refractive indices of water and air, respectively. The ratio of the refractive index of water to that of air is a function of temperature, salt concentration and the wavelength of the light in question. For our purposes a value of 1.33 for  $n_w/n_a$  is close enough for both sea and fresh water at normal ambient temperatures and for light of any wavelength within the photosynthetic range. As Fig. 2.12 shows, the effect of refraction is to move the light closer to the vertical in the aquatic medium than it was in air. It will be noted that even light reaching the surface at grazing incidence ( $\theta_a$  approaching  $90^\circ$ ) is refracted downwards so that  $\theta_w$  should not be greater than about  $49^\circ$  for a calm surface.

When the water is disturbed, some of the light will be found at angles greater than  $49^\circ$  after passing through the surface: nevertheless most of the downwelling light will be at values of  $\theta_w$  between  $0^\circ$  and  $49^\circ$ . Statistical relations between the distribution of surface slopes and wind speed were derived by Cox and Munk (1954) from aerial photographs of the Sun’s glitter pattern. The Cox and Munk data are summarized by the equations

$$\sigma_u^2 = 0.00316 U \pm 0.004 \quad (2.20)$$

$$\sigma_c^2 = 0.003 + 0.00192 U \pm 0.002 \quad (2.21)$$

where  $U$  is the wind speed at 12.5 m above the water surface,  $\sigma_u^2$  is the mean square slope of the waves measured in the upwind/downwind (i.e. parallel to the wind) direction, and  $\sigma_c^2$  is the crosswind value, measured at right angles to the wind. Wave slope in this context is  $\tan \psi$ , where  $\psi$  is the angle between the vertical and the normal to the sea surface at a given point. Calculations using these relations show that, as might be expected, as wind speed increases, the underwater light becomes more diffuse.<sup>515</sup> Recent measurements of wind speed and the associated ocean sunglint intensity and pattern from space, using instruments on the ADEOS satellite, are in excellent agreement with the Cox and Munk slope distribution model.<sup>158</sup>

Snell’s Law works in reverse also. A light beam passing upward within the water at angle  $\theta_w$  to the downward vertical will emerge through the calm surface into the air at angle  $\theta_a$  to the zenith, in accordance with eqn 2.19. There is, however, a very important difference between transmission from water to air, and from air to water, namely that in the former case complete internal reflection can occur. If, in the case of the upward-directed light beam within the water,  $\theta_w$  is greater than  $49^\circ$  then all the light is reflected down again by the water–air interface. Disturbance of the surface by wind decreases water-to-air transmission for upwelling light at angles within the range  $\theta_w = 0^\circ$  to  $\theta_w = 49^\circ$  but, by ensuring that not all the light is internally reflected, it increases transmission within the range  $\theta_w = 49^\circ$  to  $\theta_w = 90^\circ$ .

# 3

## Absorption of light within the aquatic medium

Having discussed how the solar radiation gets through the water surface, we shall now consider what happens to it within the water. Sooner or later most of the photons are absorbed: how this happens, and which components of the medium are responsible, form the subjects of this chapter.

### 3.1 The absorption process

The energy of a molecule can be considered to be part rotational, part vibrational and part electronic. A molecule can only have one of a discrete series of energy values. Energy increments corresponding to changes in a molecule's electronic energy are large, those corresponding to changes in vibrational energy are intermediate in size and those corresponding to changes in rotational energy are small. This is indicated diagrammatically in Fig. 3.1. When molecules collide with each other in the liquid or gaseous state, or are in contact with each other in the solid state, there can be transfer of rotational or vibrational energy between molecules and this is accompanied by transitions from one rotational or vibrational energy level to another within each molecule.

Molecules can obtain energy from radiation as well as from other molecules. When a photon passes within the vicinity of a molecule, there is a finite probability that it will be captured by that molecule, i.e. be absorbed. If the photon is captured, then the energy of the molecule must increase by an amount corresponding to the energy of the photon. If the photon is of long wavelength ( $>20\ \mu\text{m}$ ), in the far infrared/microwave region of the spectrum, then its energy is low and its absorption can only cause a transition in the energy of the molecule from one rotational energy level to another. If the photon is in the

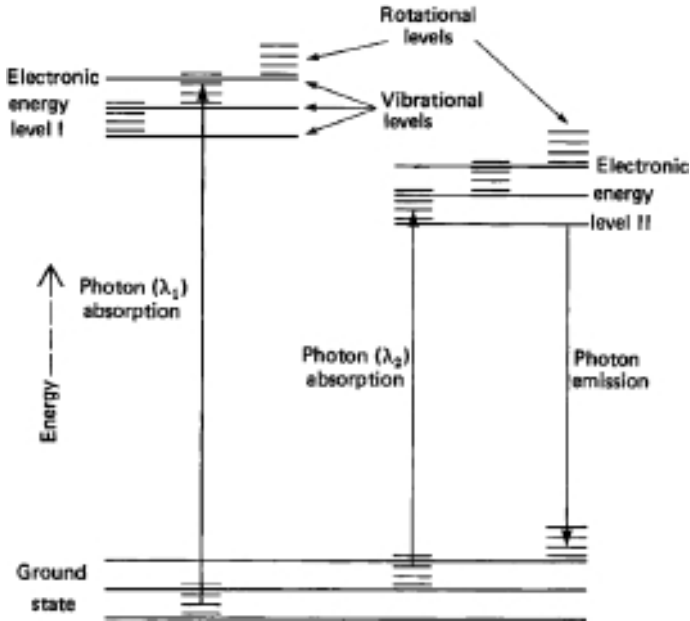


Fig. 3.1 Absorption of a photon raises an electron from the ground state to one of two possible excited singlet states, depending on the wavelength (and therefore energy) of the photon. Wavelengths  $\lambda_1$  and  $\lambda_2$  are each within a separate absorption band in the absorption spectrum of the molecule ( $\lambda_2 > \lambda_1$ ).

infrared region ( $<20 \mu\text{m}$ ), then its absorption will cause a transition from one vibrational level to another.

Photons in the visible/photosynthetic part of the spectrum have sufficient energy to bring about, when they are absorbed, transitions from one electronic energy level (usually the ground state) to another. The first event in the absorption of light by the aquatic medium is, therefore, the capture of a photon by some molecule in the medium and the simultaneous transition of an electron in that molecule from the ground state to an excited state.

Within a complex molecule such as chlorophyll or any of the other photosynthetic pigments, there is usually more than one possible electronic energy transition that can occur. For example, in Fig. 3.1 excitation can occur up to electronic energy level I or to level II: to be more precise, excitation will occur to one of the many vibrational/rotational levels belonging to the given electronic energy level. Any given electronic transition is preferentially excited by light that has an amount of energy per

photon corresponding to the energy required for the transition. Chlorophyll, as we shall see later, has two main absorption bands, in the red and in the blue regions of the spectrum. Absorption of a blue photon leads to transition to a substantially higher electronic energy level than absorption of a red photon. Because of the multiplicity of vibrational/rotational states, these two electronic energy states nevertheless overlap: i.e. the highest vibrational/rotational levels of the lower electronic state can have energies as high as the lowest level of the upper electronic state (Fig. 3.1). As a consequence, immediately after absorption of a blue photon there is a very rapid series of transitions downwards through the various rotational/vibrational levels (associated with transfer of small increments of rotational/vibrational energy to adjoining molecules) until the lower electronic energy state (referred to as the lowest excited singlet state) is reached.

It is the energy in this lowest excited singlet state that is used in photosynthesis and it is because an excited chlorophyll molecule usually ends up in this state anyway, that all *absorbed* visible quanta are equivalent, i.e. a red quantum, or even a green quantum if it succeeds in being absorbed, brings about as much photosynthesis as a blue quantum. This is also the reason why, in the context of primary production, it is more meaningful to express irradiance in quanta  $\text{m}^{-2} \text{s}^{-1}$  than in  $\text{W m}^{-2}$ .

In the case of light-absorbing molecules in the aquatic medium that are not part of the photosynthetic system, and that cannot therefore transfer their energy to a reaction centre for use in photosynthesis, there is likely to be a transition from the lowest excited singlet state to the corresponding triplet state by interaction with a paramagnetic molecule such as oxygen. In a singlet state, the two members of every pair of electrons in the molecule have opposite spin ( $+\frac{1}{2}$  and  $-\frac{1}{2}$ ) so that the resultant spin is zero: in a triplet state, the members of a pair of electrons in the molecule have the same spin so that the resultant spin is one. The excited triplet state is at a lower energy level and is also much longer lived than the excited singlet state, the average lifetime of the excited molecules being  $10^{-5}$  to  $10^{-4}$  s in the former case, compared to  $10^{-9}$  to  $10^{-8}$  s in the latter. Eventually, by interaction with a paramagnetic molecule such as oxygen, the excited molecule is returned to a singlet state by spin reversal and, by vibrational/rotational interactions with the surrounding molecules, it undergoes a downwards transition to one of the upper vibrational levels of the ground state. The electronic energy is thus dissipated as heat energy.

Excitation energy, whether in the photosynthetic system or in a molecule outside it, can be lost by re-emission of radiation. An electronically excited molecule, after undergoing the radiationless transition to the

lowest level of the lowest excited singlet state, can then undergo a transition to one of the vibrational/rotational levels of the ground state by re-emitting a photon of light. This phenomenon is referred to as *fluorescence*. In living, photosynthesizing algal cells, only a very small proportion, ~1%, of the absorbed light is lost in this way. Most of the absorbed energy, whether captured initially by chlorophyll, carotenoid or biliprotein, is transferred by inductive resonance to the reaction centres where it is used to bring about biochemical changes (see [Chapter 8](#)). If photosynthesis is inhibited, say with dichlorophenylmethylurea (DCMU), then fluorescence increases to about 3% of the absorbed light. The non-photosynthetic, light-absorbing material of the aquatic medium can also re-emit some of its absorbed energy as fluorescence, but the fluorescence yield (quanta emitted/quanta absorbed) is again very low: most of the excited molecules are converted to the triplet state (see above), and from there to the ground state before they can emit a photon.

Thus, most of the light energy absorbed by the aquatic ecosystem, after existing for a very brief period as electronic excitation energy, ends up either as heat (vibrational/rotational energy distributed among all the molecules of the system) or as chemical energy in the form of photosynthetically produced biomass. Only a tiny proportion is turned back into light again by fluorescence, and even this is for the most part re-absorbed before it can escape from the system.

### 3.2 The measurement of light absorption

We saw in [Chapter 1](#) how the light absorption properties of the aquatic medium are characterized in terms of the absorption coefficient,  $a$ . We saw also that although  $a$  is defined in terms of the behaviour of light passing through an infinitesimally thin layer of medium, its value can nevertheless be obtained from the observed absorbance,  $A$ , of a layer of medium of finite thickness, provided that the effects of scattering can be overcome. Instruments specifically designed to measure the absorption coefficients of surface water bodies, marine or inland, are referred to as *absorption meters*.

#### Laboratory methods

Commercially available equipment (spectrophotometers) used for the measurement of light absorption, do so in terms of an optical parameter known as the *absorbance* or *optical density*: although there is no standard

symbol we shall indicate it by  $D$ . Although absorbance is one of the most frequently measured parameters in biochemistry and chemistry it does not, unfortunately, appear to have a rigorous definition. It is commonly defined as the logarithm to the base 10 of the ratio of the light intensity,  $I_0$ , incident on a physical system to the light intensity,  $I$ , transmitted by the system

$$D = \log_{10} \frac{I_0}{I} \quad (3.1)$$

The meaning of the word ‘intensity’ is not usually given: we shall equate it to radiant flux,  $\Phi$ . The incident beam is generally assumed to be parallel. The exact meaning of ‘transmitted’ is also not stated. If we make the simplest assumption that any light that re-emerges from the system, in any direction, is ‘transmitted’, then  $I$  includes all scattered light as well as that neither absorbed nor scattered. Thus,  $I$  is equal to the incident flux minus the absorbed ( $\Phi_0 - \Phi_a$ ), from which, given that  $\Phi_a/\Phi_0$  is absorbance,  $A$ , it follows that

$$D = \log_{10} \frac{1}{(1 - A)} = -\log_{10} (1 - A) \quad (3.2)$$

If we can arrange that all the scattered light is included in the measured value of  $I$ , then scattering may be ignored (except in so far as it increases the pathlength of the light within the system), and so eqn 1.36 may be considered to apply. Therefore,

$$D = 0.4343ar \quad (3.3)$$

i.e. the absorbance is equal to the product of the absorption coefficient of the medium and the pathlength ( $r$ ) through the system, multiplied by the factor for converting base  $e$  to base 10 logarithms. The absorption coefficient may be obtained from the absorbance value using

$$a = 2.303 D/r \quad (3.4)$$

In a typical spectrophotometer, monochromatic light beams are passed through two transparent glass or quartz cells of known pathlengths, one (the sample cell) containing a solution or suspension of the pigmented material, the other (the blank cell) containing pure solvent or suspending medium. The intensity of the light beam after passing through each cell is measured with an appropriate photoelectric device such as a photomultiplier. The intensities of the beams that have passed through the blank cell

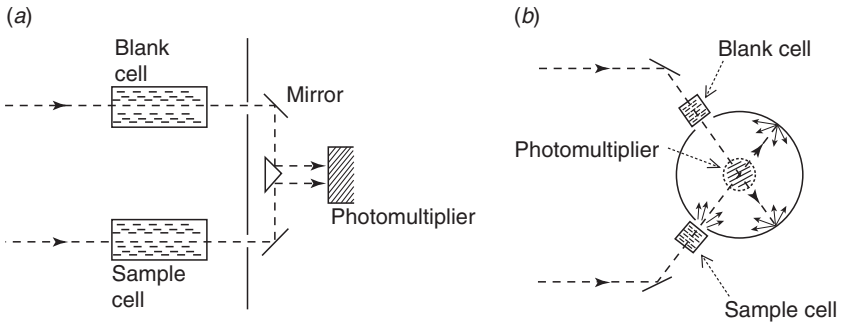


Fig. 3.2 Principles of measurement of absorption coefficient of non-scattering and scattering samples. The instrument is assumed to be of the double-beam type, in which a rotating mirror is used to direct the monochromatic beam alternately through the sample and the blank cells. (a) Operation of spectrophotometer in normal mode for samples with negligible scattering. (b) Use of integrating sphere for scattering samples.

and the sample cell are taken to be proportional to  $I_0$  and  $I$ , respectively, and so the logarithm of the ratio of these intensities is displayed as the absorbance of the sample.

When used in their normal mode (Fig. 3.2a), however, spectrophotometers have light sensors with a collection angle of only a few degrees. Thus any light scattered by the sample outside this collection angle will not be detected. Such spectrophotometers do not, therefore, measure true absorbance: indeed if their collection angle is very small, in effect they measure attenuation (absorption plus scattering, see §1.4). If, as is often the case, the sample measured consists of a clear coloured solution with negligible scattering relative to absorption, then scattering losses are trivial and the absorbance displayed by the instrument will not differ significantly from the true absorbance. If, however, the pigmented material is particulate, then a substantial proportion of the light transmitted by the sample may be scattered outside the collection angle of the photomultiplier, the value of  $I$  registered by the instrument will be too low, and the absorbance displayed will be higher than the true absorbance.

This problem may be solved by so arranging the geometry of the instrument that nearly all the scattered light is collected and measured by the photomultiplier. The simplest arrangement is to have the cells placed close to a wide photomultiplier so that the photons scattered up to quite wide angles are detected. A better solution is to place each cell at an entrance window in an integrating sphere (Fig. 3.2b): this is a spherical

cavity, coated with white, diffusely reflecting material inside. By multiple reflection, a diffuse light field is set up within the sphere from all the light that enters it, whether scattered or not. A photomultiplier at another window receives a portion of the flux from this field, which may be taken to be proportional to  $I$  or  $I_0$  in accordance with whether the beam is passing through the sample, or the blank cell. With this system virtually all the light scattered in a forward direction, and this will generally mean nearly all the scattered light, is collected.

Another procedure, which can be used with some normal spectrophotometers, is to place a layer of scattering material, such as opal glass, behind the blank and the sample cell.<sup>1211</sup> This ensures that the blank beam and the sample beam are both highly scattered after passing through the cells. As a result, the photomultiplier, despite its small collection angle, harvests about the same proportion of the light transmitted through the sample cell, as of the light transmitted through the blank cell, and so the registered values of intensity are indeed proportional to the true values of  $I$  and  $I_0$ , and thus can give rise to an approximately correct value for absorbance.

With all these procedures for measuring the absorbance of particulate materials, it is important that the suspension should not be so concentrated that, as a result of multiple scattering, there is a significant increase in the pathlength that the photons traverse in passing through the sample cell. This would have the effect of increasing the absorbance of the suspension and lead to an estimate of absorption coefficient that would be too high. Even with an integrating sphere, some of the light is scattered by the sample at angles too great for collection: a procedure for correction for this error has been described.<sup>701</sup>

An instrument based on completely different principles to any of the above is the *integrating cavity absorption meter*,<sup>357,418,419</sup> (ICAM). The water sample is contained within a cavity made of a translucent, and diffusely reflecting, material. Photons are introduced into the cavity uniformly from all round, and a completely diffuse light field is set up within it, the intensity of which can be measured. The anticipated advantages are, first, that since the light field is already highly diffuse, additional diffuseness caused by scattering will have little effect; second, because the photons undergo many multiple reflections from one part of the inner wall to another, the effective pathlength within the instrument is very long, thus solving the pathlength problem. A prototype instrument gave very satisfactory results.<sup>419</sup> In an alternative version of the ICAM – the *point source integrating cavity absorption meter* (PSICAM) – the cavity

is spherical, and a uniform light field is achieved by introducing the photons from a centrally placed point light source.<sup>715,783</sup> In this case also prototype instruments have given excellent results.<sup>1150</sup>

Most seawater, and many freshwater, samples have absorption coefficients (above those of pure water) too low to measure accurately in laboratory spectrophotometers. An approach pioneered by Yentsch (1960), applicable to the particulate fraction is to pass the water through a filter – usually glass fibre – until enough particulate matter has accumulated, and then measure the spectrum of the material on the filter itself without resuspension, using a moist filter as a blank. To correct for the additional attenuation due to scattering by the particles on the filter the value of apparent absorbance at some selected wavelength (715–750 nm) in the near infrared, where it is assumed that true absorption is negligible, is subtracted from absorbance at all other wavelengths.

Implicitly it is assumed that the substantial attenuation due to scattering by the filter itself is the same for both the sample and blank filters. This assumption is not necessarily correct. The particles collected on the sample filter, as well as adding to total scattering may change its angular distribution and thus alter the proportion of transmitted light captured by the photomultiplier. To reduce this error, Tassan and Ferrari (1995) have developed a variation on the procedure – the ‘transmittance–reflectance’ method – in which, as well as measuring absorbance in the usual manner, spectral reflectance is also measured and used to correct for backscattering. This procedure has been found to reduce the variability of the measurements of absorption coefficients of particulate matter in the somewhat turbid coastal waters of the Adriatic.<sup>1346</sup>

The most fundamental problem with the filter method, however, is that, as a consequence of multiple internal reflection within the particulate layer, there is very marked amplification of absorption, the amplification factor being commonly indicated by  $\beta$ . To calculate the true absorption coefficients that the particulate material has, when freely suspended in the ocean or lake, the absorption amplification factor must be determined reasonably accurately, and this is not easy. The approach has generally been to find correction factors by growing phytoplankton species in the laboratory and comparing optical densities measured on filters with those obtained on suspensions in cuvettes.<sup>245</sup> The most commonly used algorithm in recent years makes use of a quadratic relationship, first arrived at by Mitchell (1990)

$$\text{OD}(\lambda)_{\beta\text{-corrected}} = C_1 \text{OD}(\lambda)_{\text{measured}} + C_2 \text{OD}^2(\lambda)_{\text{measured}} \quad (3.5)$$

where  $C_1$  and  $C_2$  are empirically determined coefficients. Equation 3.5 implies that the value of  $\beta$ , the amplification factor, varies with optical density.

Roesler (1998) points out that if, as seems plausible, a completely diffuse light field is established within the glass fibre filter, then the average cosine of the forward-transmitted photons should be 0.5, which would correspond to a pathlength amplification factor of 2.0. Her investigations suggest that much of the variability encountered in using this method arises from the fact that the optical properties of the filter pad itself are markedly affected by the volume of water filtered through it, and it is typically the case that a much larger volume is passed through the sample filter than the blank filter. With the appropriate filter preparation, the assumption that  $\beta = 2.0$  gave satisfactory results in this study.

Allali *et al.* (1995) have developed a method that, while still making use of filtration to concentrate the particles, avoids the optical problems associated with the filter itself. In their *filter-transfer-freeze* method the samples are filtered through a polycarbonate filter with  $0.4 \mu\text{m}$  pores, so that the particles collect on the surface. The loaded filter is then transferred, particle side down, onto  $5 \mu\text{l}$  of sea water on a glass microscope slide and quickly frozen using liquid nitrogen. The filter is then peeled off, leaving the frozen layer of particle suspension attached to the slide, and replaced with a glass cover slip. After thawing, the absorption spectrum is measured using an integrating sphere.

A different experimental approach has been developed by Iturriaga and Siegel (1989), who use a monochromator in conjunction with a microscope to measure the absorption spectra of individual phytoplankton cells or other pigmented particles. If sufficient particles are measured, and their numbers in the water are known, then the true *in situ* absorption coefficients due to the particles can be calculated. While laborious, this does avoid the uncertainty associated with estimation of the amplification factor in the filter method.

For measurements of soluble colour, scattering problems can be largely eliminated by filtration, so that measurements over long pathlengths can be used. D'Sa *et al.* (1999) used a 0.5 m long,  $550 \mu\text{m}$  internal diameter, capillary waveguide (see reflective tube principle, below) to measure the absorption spectrum of dissolved organic matter in seawater samples.

As we shall see later, the absorption coefficients of the different constituents of the aquatic medium can be determined separately. The value of the absorption coefficient of the medium as a whole, at a given wavelength, is equal to the sum of the individual absorption coefficients of all the components present. Furthermore, providing that no changes in

molecular state or physical aggregation take place with changes in concentration, then the absorption coefficient due to any one component is proportional to the concentration of that component (Beer's Law).

### ***In situ* methods**

The total absorption coefficient of a natural water at a given wavelength can be determined from a measurement made within the water body itself. To make accurate measurements at those wavelengths where marine, and some inland, waters absorb only feebly, quite long pathlengths (~0.25 m or more) are needed. The simplest arrangement is to have, immersed in water, a light source giving a collimated beam and, at a suitable distance, a detector with a wide angle of acceptance. Most of the light scattered, but not absorbed, from the beam is detected: diminution of radiant flux between source and detector is thus mainly due to absorption and can be used to give a value for the absorption coefficient.

An alternative approach is to have, not a collimated beam, but a point source of light radiating equally in all directions.<sup>78,850</sup> The detector does not have to have a particularly wide angle of acceptance. For every photon that is initially travelling towards the detector and is scattered away from the detector, there will, on average, be another photon, initially not travelling towards the detector, which is scattered towards the detector. Thus diminution of radiant flux between source and detector is entirely due to absorption. An absorption meter based on this principle has been used to measure the absorption coefficient of water in Lake Baikal (Russia).<sup>107</sup> A problem with this and the previous type of absorption meter is that although scattering may not directly prevent photons reaching the detector, it increases the pathlength of the photons and thus increases the probability of their being absorbed, i.e. spuriously high values of absorption coefficient may be obtained. This error can be significant in waters with high ratios of scattering to absorption, but a correction can be made using the values of the scattering coefficient and average cosine of the scattering phase function if these are available for the water in question.<sup>719</sup>

To avoid the necessity of comparing readings in the water body with readings in pure water or other standard medium, a variant on the second type of absorption meter has been developed that still uses a point light source but has two detectors at different distances from the source: from the difference in radiant flux on the two detectors, the absorption coefficient may be obtained.<sup>414</sup> By means of interference

filters, this particular instrument carries out measurements of absorption coefficient at 50 nm intervals from 400 to 800 nm.

With all these absorption meters, if the light source is modulated and the detector is designed to measure only the modulated signal, then the contribution of ambient daylight to radiant flux on the detector can be eliminated.

In the case of an absorption meter using a collimated light beam, one possible solution to the problem of distinguishing between attenuation of the signal that is genuinely due to absorption from that which is due to photons in the measuring beam simply being scattered away from the detector, is to shine the beam down an internally reflecting tube<sup>235,1496</sup> containing the water under investigation. The principle is that photons that are scattered to one side will be reflected back again, and so can still be detected at the other end. In such an instrument, however, there is still some residual loss of photons by non-reflection at the silvered surface, and by backscattering, and so a correction term proportional to the scattering coefficient needs to be applied.<sup>713</sup> Current commercial instruments<sup>6</sup> have dispensed with the silvered surface and rely on the internal Fresnel reflection (100% for scattering angles up to 41°) of photons that takes place in water within a glass cylinder surrounded by air.<sup>1497</sup> The light is collected by a diffused large area detector at the far end of the flow tube. These instruments can be used for vertical profiling of absorption coefficients.<sup>163</sup>

Gray *et al.* (2006) have described an in-principle design of a cylindrical flow-through absorption meter, which makes use of the integrating cavity principle. Musser *et al.* (2009) have constructed a prototype instrument, based on this design. The sample fluid flows through a 122 cm long quartz tube, internal diameter 2.54 cm, surrounded by two cylindrical diffuse reflectors, 102 cm long, separated by an air gap. Light from light emitting diodes (LEDs) operating at six wavelengths is introduced into the air gap, leading to the establishment of a diffuse light field within the sample cylinder. The device has an operating range from 0.004 m<sup>-1</sup> to 80 m<sup>-1</sup>, and like other instruments based on the ICAM principle, is essentially unaffected by high levels of scattering within the sample.

Absorption meters and other optical instruments are sometimes attached to moorings at various depths to obtain long-term time series of optical data for periods up to several months. Unfortunately, instruments submerged for long periods will – unless preventative measures are taken – soon have their measurements compromised by fouling – the settlement and growth of marine organisms on their surfaces.

Davis *et al.* (1997) arranged for a concentrated solution of bromine to diffuse into the flow tube between sampling periods, and in this way were able to prevent biofouling for 3.5 months at 11 m and 6 months at 40 m, in the Bering Sea.

Absorption coefficients of natural waters can also be determined *in situ* from measurements of irradiance and scalar irradiance. The instrumentation for such measurements we shall discuss in a later chapter (see §5.1). Determination of absorption coefficient makes use of the relation (see §1.7)

$$a = K_E \frac{\vec{E}}{E_0}$$

where  $E_0$  is the scalar irradiance,  $\vec{E}$  is the *net* downward irradiance ( $E_d - E_u$ ) and  $K_E$  is the vertical attenuation coefficient for  $\vec{E}$ . Thus  $a$  can be obtained from measurements of net downward and scalar irradiance at two, or a series of, depths (measurements at more than one depth are required to give  $K_E$ ). Absorption meters based on these principles have been built.<sup>570,1283</sup> By making use of empirical relationships derived from numerical modelling of underwater light fields, estimates of absorption (and scattering) coefficients can be derived from *in situ* irradiance,<sup>714,145</sup> or irradiance and nadir radiance,<sup>1307,885,890</sup> measurements.

### 3.3 The major light-absorbing components of the aquatic system

Essentially all the light absorption that takes place in natural waters is attributable to four components of the aquatic ecosystem: the water itself, dissolved yellow pigments, the photosynthetic biota (phytoplankton, and macrophytes where present) and inanimate particulate matter (*tripton*). We shall now consider the spectral absorption properties of each of these, and their relative contributions to the absorption of photosynthetically available radiation.

#### Water

Pure water, although it appears colourless in the quantities we handle in everyday life, is in fact a blue liquid: the blue colour is clearly apparent under sunny conditions in oceanic waters or in coastal waters that are

infertile and have little input from rivers. The colour of pure water arises from the fact that it absorbs only very weakly in the blue and the green regions of the spectrum, but its absorption begins to rise as wavelength increases above 550 nm and is quite significant in the red region: a one-metre thick layer of pure water will absorb about 35% of incident light of wavelength 680 nm.

Because of the very weak absorption it is very difficult to measure the absorption coefficient of pure water in the blue/green spectral region, and the values reported in the literature, determined by normal spectrophotometric procedures, vary widely. I rely here predominantly on the measurements of Pope and Fry (1997) using their integrating cavity absorption meter, supplemented with those obtained by Quickenden and Irvin (1980) and Litjens *et al.* (1999) using long-pathlength cells.

The extent to which pure water absorbs light in the ultraviolet (UV), including the ecologically relevant UVB (280–320 nm) region, is a matter of some controversy. Liquid water does have an intense absorption band at 147 nm due to an electronic transition, but this, on theoretical grounds, would be expected to tail away to very low values in the 200 to 300 nm range. An anticipated exponential diminution of absorptivity with decreasing photon energy (the Urbach rule) implies, for example, an absorption coefficient of only  $\sim 0.02 \text{ m}^{-1}$  at 207 nm, and still lower values at higher wavelengths.<sup>1096</sup> While some workers over the period 1928 to 1976 found absorption coefficients (200–300 nm) that appeared to be orders of magnitude higher than this, more recent studies by Quickenden and Irvin (1980), and Boivin *et al.* (1986) using very carefully purified water, indicate that absorption is indeed very low in the near UV. The previously reported high absorption coefficients are attributable to dissolved oxygen, which does absorb UV quite strongly (and which is, of course, present in sea and lake water anyway), and to trace organic materials.

Literature values for the absorption coefficient of pure water over the range 280 to 800 nm are listed in Table 3.1, and Fig. 3.3 shows the absorption spectrum of pure water from the near ultraviolet, through the photosynthetic range, to the near infrared. It can be seen that the absorption by water at the red end of the visible spectrum is really the tail end of a series of much stronger absorption bands in the infrared: there are even more intense absorption bands beyond 1000 nm. The two shoulders in the visible spectrum – the distinct one at  $\sim 604$  nm and the weak one at  $\sim 514$  nm – have been identified as corresponding to the fifth and

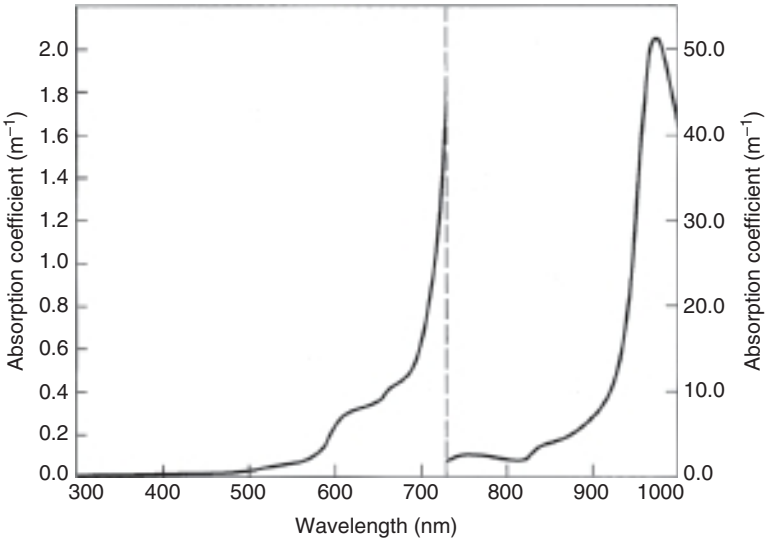


Fig. 3.3 Absorption spectrum of pure water. Absorption coefficient values have been taken from Table 3.1 for the range 310 to 790 nm, and from the data of Palmer to Williams (1974) for the range 790 to 1000 nm.

sixth harmonics, respectively, of the O-H stretch vibration of liquid water;<sup>1341</sup> the peaks at  $\sim 960$  and  $\sim 745$  nm in the infrared correspond to the third and fourth harmonics (the fundamental is at about  $3 \mu\text{m}$ ). Light absorption by pure water shows no significant temperature dependency at wavelengths below 550 nm, but does increase slightly with temperature at longer wavelengths.<sup>1324,1038</sup> A plot of  $\Psi_T$  ( $da/dT$ ,  $\text{m}^{-1} \text{ } ^\circ\text{C}^{-1}$ ) shows small peaks centred at wavelengths of  $\sim 604$  and  $662$  nm, and a large peak at  $\sim 740$  nm. The peaks in  $\Psi_T$  correspond to shoulders in the absorption spectrum of pure water. The  $\Psi_T$  maximum at 740 nm has a peak value of  $\sim 0.015 \text{ m}^{-1} \text{ } ^\circ\text{C}^{-1}$ , corresponding to an absorption coefficient change of  $0.3 \text{ m}^{-1}$  over a  $20^\circ\text{C}$  change in water temperature. Sullivan *et al.* (2006) found pure NaCl at a concentration of 10% (w/w) to have little effect on water absorption below  $\sim 600$  nm, a small positive peak between 600 and 650 nm, a negative peak between 680 and 730 nm, and a marked increase in absorption between 735 and 750 nm. They attribute these changes to effects of the salt ions on the molecular vibrations of the water molecules rather than to intrinsic absorption by NaCl itself. The implications for sea water (salinity 36) are that the additional absorption induced by salt in the 400 to 680 nm spectral range is very small, with a maximum magnitude of  $\leq 0.002 \text{ m}^{-1}$ .

Table 3.1 Absorption coefficients for pure water: 280 to 320 nm, Quickenden and Irvin (1980); 366 nm, Boivin et al. (1986); 380 to 720 nm, Pope and Fry (1997); 730 to 800 nm, Smith and Baker (1981).

$\lambda$ (nm)	$a$ ( $\text{m}^{-1}$ )	$\lambda$ (nm)	$a$ ( $\text{m}^{-1}$ )
280	0.0239 <sup>ab</sup>	560	0.0619
290	0.0140 <sup>ab</sup>	570	0.0695
300	0.0085 <sup>ab</sup>	580	0.0896
310	0.0082 <sup>ab</sup>	590	0.1351
320	0.0077 <sup>ab</sup>	600	0.2224
366	0.0055 <sup>a</sup>	610	0.2644
380	0.0114	620	0.2755
390	0.0085	630	0.2916
400	0.0066	640	0.3108
410	0.0047	650	0.340
420	0.0045	660	0.410
430	0.0050	670	0.439
440	0.0064	680	0.465
450	0.0092	690	0.516
460	0.0098	700	0.624
470	0.0106	710	0.827
480	0.0127	720	1.231
490	0.0150	730	1.799
500	0.0204	740	2.38
510	0.0325	750	2.47
520	0.0409	760	2.55
530	0.0434	770	2.51
540	0.0474	780	2.36
550	0.0565	790	2.16
		800	2.07

<sup>a</sup> Absorption coefficients derived from the published attenuation coefficients by subtracting estimated values<sup>632,832</sup> of scattering coefficients.

<sup>b</sup> These values were obtained using deoxygenated water.

The contribution of water itself to the attenuation of PAR by absorption of quanta is of importance only above about 500 nm. While the salts present in sea water appear to have no significant effect on absorption in the visible/photosynthetic range,<sup>1113,1244</sup> the nitrates and bromides do cause a marked increase in absorption below 250 nm.<sup>161,1006,1011</sup>

Understanding the optical properties of water in its frozen, solid forms – ice and snow – has taken on greater importance as ice at high altitudes and latitudes (glaciers, Arctic Ocean, the Greenland and Antarctic ice sheets) melts at increasing rates with the advent of global warming. This information is essential for an accurate assessment of the

overall energy balance of the planet, but is much harder to acquire than for liquid water. The first measurements of absorption by ice were carried out by Sauberer (1950) on blocks of ice cut from a lake in Austria. He found that absorption was high, as it is in liquid water, in the near-infrared and red regions but fell markedly with decreasing wavelength, arriving at a minimum at about 400 nm. Snow itself is so highly scattering that the light field becomes diffuse within a few centimetres of the surface, and clean, fine-grained snow reflects 97 to 99% of incident light in the 300 to 600 nm range, although reflectivity falls off, due to increasing absorption, as wavelength increases into the red and near-infrared.<sup>1440</sup> On the basis of their measurements within clean Antarctic snow, Warren *et al.* (2006) conclude that the absorption coefficient of pure ice has a minimum at ~390 nm, and is everywhere below  $0.1 \text{ m}^{-1}$  between 300 and 600 nm.

### **Coloured dissolved organic matter (CDOM, gilvin, yellow substance): chemistry and origins**

When plant tissue decomposes in the soil or in a water body, most of the organic matter is broken down by microbial actions within days or weeks to, ultimately, carbon dioxide and inorganic forms of nitrogen, sulfur and phosphorus. In the course of the decomposition process there is formed, however, a complex group of compounds loosely referred to as 'humic substances'. It is from these humic substances that the yellow-coloured dissolved organic matter in inland and marine waters is derived. The chemistry of humic substances has been reviewed by Schnitzer (1978).

Degradation and other studies indicate that these substances are polymers consisting of aromatic rings that are joined by long-chain alkyl structures to form a flexible network.<sup>1195</sup> Figure 3.4 shows some of the many different compounds produced on oxidative chemical degradation of humic substances. A humic substance sample from the water of the Okefenokee Swamp, Georgia, USA, was found to have<sup>1357</sup> an average atomic composition of  $\text{C}_{74}\text{H}_{72}\text{O}_{46}\text{N}_{0.7}$ .

Humic substances vary in size from freely soluble compounds with molecular weights (relative molecular masses) of a few hundred, to insoluble macromolecular aggregates with molecular weights in the hundreds of thousands and perhaps ranging up to the millions. Soil chemists classify humic substances into three main fractions on the basis of solubility behaviour. The soil is first extracted with dilute alkali. The humic material that does not dissolve is referred to as *humic*. Of the

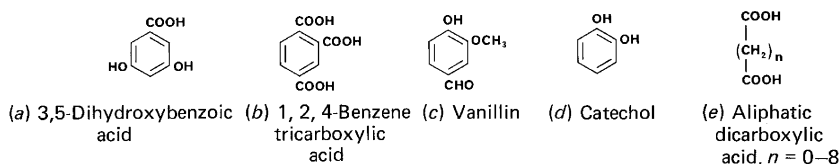


Fig. 3.4 Structures of some of the products liberated on chemical degradation of humic substances.

alkali-soluble fraction, some is precipitated on acidification: this is called *humic acid*. The humic material remaining in solution is called *fulvic acid*. In fact all three fractions are chemically very similar and differ mainly in molecular weight, humic acid molecules being larger than those of fulvic acid. They are yellow to brown in colour (the soluble ones giving rise to yellow-brown solutions), hydrophilic and acidic (due to the presence of carboxyl and phenolic groups). Fulvic acid has a higher content of oxygen-containing groups such as carboxyl and hydroxyl. The insolubility of the humin fraction may be due to its being firmly adsorbed or bonded to mineral particles and/or to its having a very high molecular weight.

While some humic material may be formed by oxidation and polymerization directly from the existing phenolic compounds (particularly lignin) in the decomposing plant tissue, it is also true that some saprophytic fungi excrete large amounts of phenolic substances when grown on carbohydrate, and these phenolic substances can undergo oxidation and polymerization to give humic-like material.<sup>292</sup> Thus it seems likely that some of the aromatic subunits of the humic materials originate in the plant and some are generated *de novo* during microbial breakdown. McKnight *et al.* (2001) compared the fluorescence properties of fulvic acids isolated from streams and rivers receiving predominantly terrestrial sources of organic material with those from lakes with microbial sources. They found that, with excitation at 370 nm, the ratio of emission intensity at 450 nm to that at 500 nm was  $\sim 1.4$  for terrestrially derived fulvic acid and  $\sim 1.9$  for the microbially derived material, and they proposed the use of this index as an additional tool for the identification of the origin of fulvic acids within inland waters. The difference in emission spectrum is attributable to the lower content of aromatic carbon (12–17%) in microbially derived fulvic acids than in plant-derived fulvic acids (25–30%).

The relative distribution of the various lignin-derived aromatic subunits of dissolved humic substances in river and lake waters reflects the botanical composition of the dominant vegetation in the catchments.

Ertel, Hedges and Perdue (1984) found that two Oregon water bodies had quite different phenolic composition in their dissolved humic acid, and these in each case corresponded closely to the phenolic composition of the lignin in the, respectively, non-woody angiosperm- and woody gymnosperm-dominated catchments from which the waters were derived. In both water bodies the humic fraction yielded (on oxidation) four to six times more lignin phenols, relative to total organic carbon, than did the fulvic acid fraction. Moran and Hodson (1994) found that lignin is the primary source (66% of total) of the dissolved humic substances exported from coastal salt marshes in the southeastern USA to adjacent marine environments. Using lignin phenols as biomarkers they concluded that 11 to 75% of the dissolved humic substances in the waters of the south-eastern US continental shelf is from vascular plant-dominated environments, about half this material being contributed by salt marshes and half by river export.

It has been shown in Canadian lakes and rivers that the coloured dissolved organic matter is substantially, but not entirely, excluded from the surface ice when it forms in the winter.<sup>93</sup> It seems that only the less complex, lower molecular weight compounds are retained within the ice.

The proportion of aromatic carbon in marine humic and fulvic acids is lower than in the corresponding freshwater substances.<sup>853</sup> Marine fulvic acid appears in fact to contain only a very small proportion of aromatic residues and is predominantly aliphatic in nature.<sup>541,853</sup> Harvey *et al.* (1983, 1984) propose that fulvic and humic acids in sea water consist mainly of polymeric compounds formed by the oxidative crosslinking of polyunsaturated lipids derived from the biota. This is unlikely, however, to be the whole story, since total dissolved humic material from the eastern equatorial Pacific Ocean has been shown to contain measurable amounts of lignin-derived phenolic residues.<sup>901</sup>

It seems likely that most of the dissolved yellow colour in inland waters is due to soluble humic substances leached from the soils in the catchment areas, and thus indirectly from the vegetation. Yellow material of the humic type can also be generated by decomposition of plant matter within the water: this could be of significance in productive water bodies. Much of the soluble humic material in river water is precipitated when it comes into contact with sea water.<sup>636,1221</sup> Nevertheless, a fraction of the material remains in solution and most of the dissolved yellow colour in coastal sea water is due to humic substances derived from the land in river discharge. For example, Monahan and Pybus (1978) found that in regions with major river discharge off the west coast of Ireland, the concentration of

soluble humic material diminished linearly with increasing salinity: the results indicated that essentially all the humic material in these coastal North Atlantic waters originated in the rivers. Since it is mainly the humic acid fraction that is lost in the estuaries,<sup>368,407</sup> the contribution of river inflow to yellow colour in the sea is mainly in the form of fulvic acid. The specific absorption (per unit mass, at 440 nm) of marine fulvic acid is much lower than that of marine humic acid,<sup>204</sup> but this is made up for by the usually much higher concentration of fulvic acid, so that the two forms of dissolved humic material make comparable contributions to the absorption of light in the ocean.

Boss *et al.* (2001) found that on the continental shelf in the Middle Atlantic Bight of the northeastern USA, variability of coloured dissolved organic matter was dominated by storms, these being associated with resuspension of sediments and accompanied by an increase in absorption by dissolved material. They concluded that bottom sediments can act as a source of dissolved organic carbon during sediment resuspension events.

As in fresh waters, some formation of dissolved yellow materials takes place within marine waters. Brown seaweeds, for example, actively excrete phenolic compounds, which, probably as a consequence of oxidation and polymerization, give rise to yellow-brown materials of the humic type within the water.<sup>1222</sup> It seems possible that this phenomenon might make a significant contribution to the amount of dissolved yellow material in the water near luxuriant brown algal beds. Hulatt *et al.* (2009) found that green and red macroalgae also excrete CDOM, but at a rate lower than that of brown algae. For brown, red and green species, exudation increased on exposure to light.

It is not certain to what extent the yellow substance (present at low concentrations but still optically significant) in oceanic waters away from the coastal zone is land-derived humic material or is generated within the sea by decomposition of the phytoplankton. Højerslev (1979), on the basis of his measurements in the Baltic and North Atlantic, considers it unlikely that significant amounts of yellow substance are formed in the sea and attributes it, even in oceanic areas, to river discharge. Jerlov (1976), however, argues that the presence of yellow substance in the upwelling region west of South America proves its immediate marine origin, as this area is practically devoid of fresh water supply from land drainage. In the East Sound estuary, Washington State, USA, there is a persistent layer, 2 to 4 m thick, of phytoplankton. On the basis of their studies, Twardowski and Donaghay (2001) concluded that there is rapid

*in situ* production of coloured dissolved organic matter associated with phytoplankton primary production in this layer, although it contributed ~10% or less of the total dissolved colour in East Sound. In the Chukchi Sea, Hill (2008) found that CDOM concentration was highest in the early spring, well before riverine input had commenced, and proposed that it originated in CDOM formed within sea ice from ice algae, and released into the Arctic Ocean as the surface ice breaks up. Calculations indicated that the energy absorbed by this CDOM has the potential to account for 48% of the springtime ice melt driven by water column heating.

Bricaud, Morel and Prieur (1981), on the basis of their measurements in a variety of waters, suggest that in the ocean away from regions of river discharge, the concentration of yellow substance is determined by biological activity averaged over a long period. Kopelevich and Burenkov (1977) observed a strong correlation between the concentration of yellow substance and the level of phytoplankton chlorophyll in productive oceanic waters. They proposed that oceanic yellow substance is of two kinds: a component resulting from the recent decomposition of phytoplankton, and a more stable component of much greater age. This latter 'conservative' component would predominate in oligotrophic waters and might, in agreement with Bricaud *et al.*, reflect average biological activity over a long time.

New evidence on the contribution of the terrestrial biosphere to the humic material in the ocean has come from measurement, in the oxidation products of humic substance from ocean water, of specific phenols derived from lignin, a structural polymer present only in land plants. Meyers-Schulte and Hedges (1986), using humic material from the Amazon River as a standard (entirely terrestrially derived), conclude on the basis of measurement of lignin-specific phenols, that about 10% of the humic material in ocean water from the eastern equatorial Pacific is terrestrially derived. Since this is the part of the world ocean least affected by direct river input, it seems likely that the percentage would be higher in other oceanic regions.

The humic material that ends up in the dissolved state in natural waters occurs in a wide range of molecular weights. Vapour-phase osmometry and small-angle X-ray scattering indicate molecular weights of 600 to 1000 for river fulvic acids and 1500 to 5000 for river humic acids.<sup>12,853</sup>

On the continental shelf the spatial and seasonal distribution of CDOM is substantially determined by river outflow. For example, along the New Jersey (eastern USA) coast a plume of low-salinity water from the Hudson River, with a content of dissolved (and particulate) colour,

periodically flows along the coast trapped in an inshore region of 5 to 15 km width and over 100 km long.<sup>647</sup> The Amazon River strongly influences the optical properties of the western tropical North Atlantic Ocean at distances over 1000 km from the river mouth in the high-flow season but has much less effect in the low-flow season.<sup>301</sup> The Orinoco River also has a major, seasonally varying, effect on the distribution of dissolved colour in this oceanic region.<sup>127</sup> At stations on the continental shelf of the US Middle Atlantic Bight along a track extending from Delaware Bay to the Sargasso Sea the concentration of dissolved colour was observed to vary two- to three-fold between seasons in the period August 1993 to April 1994.<sup>297</sup> On the continental shelf of the South Atlantic Bight (southeastern USA) the concentration of dissolved colour in the spring of 1993 at a time of high river discharge was up to ten times as high as that measured in the previous summer at a time of low discharge.<sup>980</sup>

Photobleaching (see next section) can also have major effects on the concentration of dissolved colour on a seasonal scale. In the Middle Atlantic Bight, following shallow stratification in August, photo-oxidation brought about a 70% fall in the concentration of CDOM.<sup>1417,1424</sup> In the North Atlantic Ocean and Caribbean Sea the lowest surface concentrations of CDOM are found in the central subtropical gyres, while the highest are found along the continental shelves and within the subpolar gyre.<sup>983</sup>

### **Coloured dissolved organic matter: light absorption**

From the point of view of aquatic ecology, the significance of the soil humic material is that as water, originating as rainfall, drains through soil and into rivers and lakes, and ultimately into estuaries and the sea, it extracts from the soil some of the water-soluble humic substances and these impart a yellow colour to the water, with major consequences for the absorption of light, particularly at the blue end of the spectrum. James and Birge (1938) in the USA and Sauberer (1945) in Austria carried out extensive quantitative studies on the absorption spectra of lake waters with varying degrees of yellowness. The colour of humic substances is due to the presence of multiple double bonds, many of them conjugated, some in aromatic nuclei. In any sample of humic material there are numerous different chromophores, and consequently a multitude of electronic excitation levels, which, because they overlap, give rise to a rather undifferentiated UV/visible absorption spectrum. Visser (1984) found that in surface waters derived from coniferous forest catchments in Quebec

(Canada), the colour intensity per unit mass of the humic acid was nearly four times that of the fulvic acid: its concentration, however, was only about one seventh that of the fulvic acid, implying that in these waters, humic acid contributed about one third, and fulvic acid two thirds, of the total colour. As well as absorbing light, dissolved humic material in natural waters has a broad fluorescence emission band in the blue region.

The light absorption properties of these dissolved humic materials in natural inland waters can be determined relatively easily by measuring the absorption spectrum of a water sample that has been filtered (0.2–0.4  $\mu\text{m}$  pore size) in 5 cm or 10 cm pathlength cells.<sup>696</sup> Figure 3.5 shows the absorption spectrum of this material from some Australian inland waters. These are typical humic substance absorption spectra, with absorption being very low or absent at the red end of the visible spectrum, and rising steadily with decreasing wavelength towards the blue: absorption in the ultraviolet region is higher still.

The presence of dissolved yellow material in inland waters is often easily apparent to the eye. Its presence in marine waters (where its concentration is much lower) is not so readily apparent, and the fact that it is important in these ecosystems too was pointed out by Kalle (1937, 1966). Figure 3.5 also shows the absorption spectra of soluble yellow material in estuarine and coastal waters.

The dissolved yellow material in natural waters has been variously referred to as ‘yellow substance’, ‘gelbstoff’ (the same name, in German), ‘yellow organic acids’, ‘humolimnic acid’, ‘fulvic acid’, ‘humic acid’ etc. Dissolved yellow materials from different waters vary not only in molecular size but also in chemical composition.<sup>671,1314,1315</sup> In the context of light attenuation it would be useful to have a general name, applicable to all or any of these compounds regardless of their chemical nature, which simply indicates that they preferentially absorb light at the blue end of the spectrum. ‘Yellow substance’ or ‘gelbstoff’ are too non-specific and could apply to anything from butter to ferric chloride. I have suggested the word ‘*gilvin*’, a noun derived from the Latin adjective *gilvus* meaning pale yellow.<sup>696</sup> ‘Gilvin’ would thus be defined as a general term to be applied to those soluble yellow substances, whatever their chemical structure, which occur in natural waters, fresh or marine, at concentrations sufficient to contribute significantly to the attenuation of PAR. While ‘gilvin’ is certainly to be found in the aquatic literature, it is nevertheless true that the term that is most commonly used in recent papers is the acronym *CDOM* (pronounced ‘seedom’), which is taken to stand for either *coloured dissolved organic matter*, or *chromophoric dissolved organic matter*. In recognition of

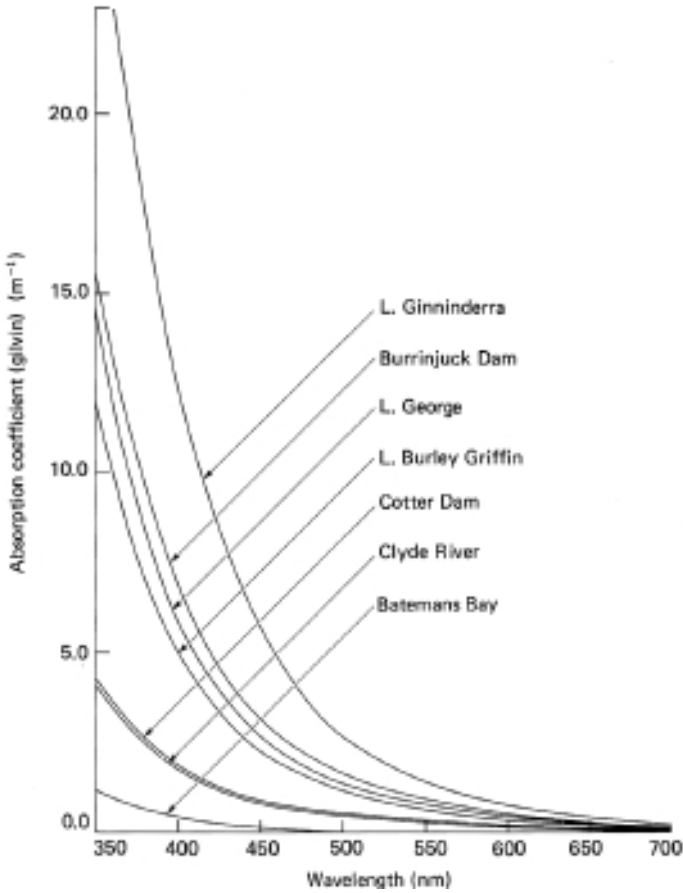


Fig. 3.5 Absorption spectra of soluble yellow material (gilvin, CDOM) in various Australian natural waters (from Kirk, 1976b). The lowest curve (Batemans Bay, NSW) is for coastal sea water near the mouth of a river; the next curve (Clyde River, NSW) is for an estuary; the remainder are for inland water bodies in the southern tablelands of New South Wales/Australian Capital Territory. The ordinate scale corresponds to the true *in situ* absorption coefficient due to gilvin.

this common usage, but without prejudice as to which interpretation is implied, I shall, in the remainder of this book, use ‘CDOM’ interchangeably with ‘gilvin’ for the dissolved yellow substances in natural waters.

As the absorption spectra in Fig. 3.5 show, the concentration of CDOM varies markedly, not only between marine and fresh waters, but also among different inland waters. A convenient parameter by means of which the concentration of CDOM may be indicated is the absorption

coefficient at 440 nm due to this material within the water: this we shall indicate by  $g_{440}$ . This wavelength is chosen because it corresponds approximately to the mid-point of the blue waveband peak that most classes of algae have in their photosynthetic action spectrum.

In many waters, certainly most inland waters, the CDOM absorption is sufficiently high for  $g_{440}$  to be measurable with reasonable accuracy, using 50 or 100 mm pathlength cells. When CDOM absorption is low, as in most marine waters, the absorption coefficient can be measured on a filtrate with an absorption meter of the ICAM, or PSICAM type (§3.2 above) with very long equivalent pathlength, or with a reflective tube absorption meter. Alternatively, measurement can be carried out in the near-ultraviolet (350–400 nm) where absorption is higher, and  $g_{440}$  determined by proportion from a typical CDOM absorption spectrum, or using the approximate relationship.<sup>161</sup>

$$a(\lambda) = a(\lambda_0)e^{-S(\lambda-\lambda_0)} \quad (3.5)$$

where  $a(\lambda)$  and  $a(\lambda_0)$  are the absorption coefficients at wavelengths  $\lambda$  and  $\lambda_0$  nm, respectively, and  $S$  is a coefficient describing the exponential slope of the absorption curve. For ~350 stations in various coastal waters around Europe (English Channel, Adriatic, Baltic, Mediterranean and North Seas) Babin *et al.* (2003b) found that  $S$  varied within a narrow range around  $0.0176 \pm 0.0020 \text{ nm}^{-1}$ . For 12 New Zealand lakes,  $S$  varied from 0.015 to  $0.020 \text{ nm}^{-1}$ , with a mean of  $0.0187 \text{ nm}^{-1}$ ,<sup>285</sup> and for 22 Australian inland waters,  $S$  varied from 0.012 to  $0.018 \text{ nm}^{-1}$ , with a mean of  $0.016 \text{ nm}^{-1}$ .<sup>720</sup> When partial photobleaching of CDOM takes place, the surviving dissolved colour has a spectrum with a somewhat higher  $S$  value.<sup>1417</sup> In agreement with this observation, Twardowski and Donaghay (2002) found surface waters to have higher  $S$  values than bottom waters in a coastal fjord: they proposed that the higher spectral slopes commonly associated with oceanic CDOM relative to coastal CDOM may be due to increased cumulative photobleaching.

When excited with near-UV light, typically ~355 nm or ~370 nm, CDOM fluoresces with a very broad peak in the blue region. The quantum yield is about 0.8%.<sup>1418</sup> The intensity of this fluorescence in natural waters is found to be highly correlated with CDOM absorption, and it can be used as an alternative way of measuring CDOM, either in the water, using a submersible fluorometer, or remotely by excitation of the fluorescence by an airborne laser (see Chapter 7).<sup>1418,94</sup>

Table 3.2 contains a selection of published data in the form of values of  $g_{440}$  for marine as well as fresh waters in various geographical regions.

Table 3.2 Value of absorption coefficient at 440 nm due to dissolved colour ( $g_{440}$ ) and particulate (phytoplankton + tripton) colour ( $p_{440}$ ) in various natural waters. Where several measurements have been taken, the mean value, the standard deviation, the range and the time period covered are in some cases indicated. For some waters only the absorption coefficient for CDOM plus particles ( $g + p$ ) was available.

Water body	$g_{440}$ ( $m^{-1}$ )	$p_{440}$ ( $m^{-1}$ )	Reference
<b>I. Oceanic waters</b>			
<i>Atlantic Ocean</i>			
Sargasso Sea	~0	0.01	760
Off Bermuda	0.01 <sup>a</sup>	–	616
Caribbean Sea	0.03 ( $g + p$ )	–	636
Gulf of Mexico – Gulf loop intrusion	0.005	–	204
Romanche Deep	0.05 ( $g + p$ )	–	636
Mauritanian upwelling	0.034–0.075 <sup>a</sup>	–	161
Gulf of Guinea	0.024–0.113	–	161
<i>Pacific Ocean</i>			
Galapagos Islands	0.02 <sup>a</sup>	–	189
Galapagos Islands	0.16 ( $g + p$ )	–	636
Central Pacific	0.04 ( $g + p$ )	–	636
Off Peru	0.05 <sup>a</sup>	–	189
<i>Indian Ocean</i>			
Oligotrophic water	0.02	–	748
Mesotrophic water	0.03	–	748
Eutrophic water	0.09	–	748
<i>Mediterranean</i>			
Western	0.0–0.03 <sup>a</sup>	–	574
<i>Arctic Ocean</i>			
Beaufort & Chukchi Seas	0.054	0.13	1439
<i>Southern Ocean</i>			
North–South transect, 42–55° S, along 142° E	0.019–0.099 <sup>b</sup>	–	242
<b>II. Shelf, coastal &amp; estuarine waters</b>			
<i>Gulf of Mexico</i>			
Yucatan Shelf	0.006	–	204
Bay of Campeche	0.022	–	204
Cape San Blas	0.054	–	204
Mississippi plume	0.028	–	204
<i>North America, Atlantic coast</i>			
New England shelf, summer	0.060	0.044	1269
Southeast USA, Georgia, 60 km offshore, spring 1993 (high river discharge)	0.200 <sup>b</sup>	0.026 <sup>b</sup>	980
Summer 1992	0.021 <sup>b</sup>	0.031 <sup>b</sup>	980
Rhode R. Estuary	0.72	8.4	428

Table 3.2 (cont.)

Water body	$g_{440}$ ( $\text{m}^{-1}$ )	$p_{440}$ ( $\text{m}^{-1}$ )	Reference
Chesapeake Bay (Rhode R. Mouth)	0.27	0.80	428
Georgia salt marsh	1.52	—	1460
<i>Arabian Sea</i>			
Cochin, India, 3 km offshore	0.24 <sup>c</sup> ( $g + p$ )		1113
30 km offshore	0.10 <sup>c</sup> ( $g + p$ )		1113
<i>Bay of Bengal</i>			
Near Ganges mouths	0.37 <sup>a</sup>	—	745
<i>Yellow Sea</i>	0.20–0.23 <sup>a</sup>	—	574
<i>Eastern Pacific</i>			
Peruvian coast	0.29 <sup>a</sup>		745
<i>South Pacific</i>			
Chatham Rise (east of New Zealand), av. of 19 stations	0.044	0.026	1218
<i>North Atlantic/North Sea/Baltic system</i>			
W. Greenland	0.004 <sup>a</sup>	—	574
North Atlantic	0.02 <sup>a</sup>	—	670
Iceland	0.016 <sup>a</sup>	—	574
Orkney–Shetland	0.016 <sup>a</sup>	—	574
North Sea (Fladen Ground)	0.03–0.06 <sup>a</sup>	—	574
Wadden Sea	~0.64 (0.0–3.0)	—	583
Skagerrak	0.05–0.12 <sup>a</sup>	—	574
Kattegat	0.12–0.27 <sup>a</sup>	—	574
Århus Bay, Denmark (Kattegat)	0.232		834
Baltic Sea	0.36–0.42 <sup>a</sup>	—	574
South Baltic Sea	0.26	—	636
Bothnian Gulf	0.41 <sup>a</sup>	—	636
Loch Etive, Scotland	0.7–1.0	—	887
<i>Mediterranean</i>			
Villefranche Bay	0.060–0.161 <sup>a</sup>	—	161
Marseilles drainage outfall	0.074–0.646 <sup>a</sup>	—	161
R. Var mouth	0.136 <sup>a</sup>	—	161
R. Rhone mouth	0.086–0.572 <sup>a</sup>	—	161
<i>Tyrrhenian Sea</i>			
Gulf of Naples	0.02–0.20 <sup>a</sup>	—	391
<i>Northern Adriatic Sea</i>			
Sacca di Goro (R. Po mouth)	0.32–3.43 <sup>a</sup>	—	391
Venice Lagoon	0.44–0.73 <sup>a</sup>	—	391
<i>Black Sea</i>			
Crimean Peninsula (coastal)	0.081–0.197 <sup>b</sup> (av. 0.13)	—	311
<i>Southeast Australia</i>			
(a) Jervis Bay			
3 stations	0.09–0.14 <sup>a</sup>	0.03–0.04	720

Table 3.2 (cont.)

Water body	$g_{440}$ ( $m^{-1}$ )	$p_{440}$ ( $m^{-1}$ )	Reference
<i>(b) Tasman Sea/Clyde R. system</i>			
Tasman Sea	0.02 <sup>a</sup>	—	697
Batemans Bay	0.18	—	696
Clyde R. Estuary	0.64	—	697
<i>(c) Gippsland (estuarine) lakes system</i>			
L. King	0.58	0.25	720
L. Victoria	0.65	0.22	720
L. Wellington	1.14	2.27	720
Latrobe R.	1.89	2.78	720
<i>(d) Tasmania</i>			
Huon R. Estuary mouth	0.16–0.30	—	241
<i>Northeast Australia/Great Barrier Reef</i>			
Great Barrier Reef, ~18° S	0.050 ± 0.028	0.010	126
Mossman-Daintree estuarine, 16° S. Dry season	0.082 ± 0.087	0.085	126
Wet season	0.246 ± 0.254	0.531	126
Fitzroy R./Keppel Bay system, 23° S. Dry season. Estuary station 2	0.471	—	1025
Offshore, 28 km	0.006	—	1025
<i>Western Australia</i>			
Swan R. Estuary:			
7 km upstream from mouth	0.66 (0.09–2.95)		749
39 km upstream	3.82 (2.21–10.6)		749
<i>New Zealand</i>			
South Island, 11 shelf stations	0.04–0.10 (av. 0.07)	—	283
North Island, 9 estuaries, mouth sites, low water	0.1–0.6	—	1401
<i>Japan, Pacific coast</i>			
17 km off Shimoda	0.024	0.133	727
5 km off Shimoda	0.011	0.095	727
Nabeta Bay	0.054	0.140	727
Funka Bay, Hokkaido	0.065	—	1171
<b>III. Inland waters</b>			
<i>Europe</i>			
Rhine R.	0.48–0.73 <sup>a</sup>	—	574
Donau R., Austria	0.85–2.02	—	574
Ybbs R., Austria	0.16 <sup>a</sup>	—	574
Neusiedlersee, Austria (8 months)	~2.0 ± 0.4 1.4–2.8	—	314
Blaxter L. (bog lake), England	9.65	—	891
<i>Ireland:</i>			
Carmean Quarry	0.23	—	643
Killea Reservoir	0.5	—	643

Table 3.2 (cont.)

Water body	$g_{440}$ ( $\text{m}^{-1}$ )	$p_{440}$ ( $\text{m}^{-1}$ )	Reference
Lough Neagh	1.9	—	643
Lough Fea	4.7	—	643
Lough Erne	5.3	—	643
Loughnagay	6.4	—	643
Lough Bradan	17.4	—	643
Lough Napeast	19.1	—	643
Lough Leven, Scotland	1.2	—	1336
Mountain lakes (Alps, Pyrenees):			
Predominantly rock catchments	0.074 av. (0.00–0.28)	—	776
Alpine meadow catchments	0.154 av. (0.09–0.21)	—	776
Forested catchments	0.232 av. (0.02–0.53)	—	776
<i>Africa</i>			
L. George, Uganda	3.7	—	1336
L. Victoria (Uganda), Murchison Bay	0.45	—	1013
<i>North America</i>			
Crystal L., Wisc., USA	0.16	—	620
Adelaide L., Wisc., USA	1.85	—	620
Otisco L., NY, USA	0.27	0.27	1446
Irondequoit Bay, L. Ontario, USA	0.90	0.65	1445
Lake Erie	0.23 (0.08–0.75)	—	116
Bluff L., N.S., Canada	0.94	—	495
Punch Bowl, N.S., Canada	6.22	—	495
<i>South America</i>			
Guri Reservoir, Venezuela	4.84	—	805
Carrao R., Venezuela	12.44	—	805
<i>China</i>			
L. Tianmuhu	0.48 $\pm$ 0.24	—	1501
<i>Japan</i>			
L. Kizaki	0.30	0.71	727
L. Fukami-ike	0.85	3.11	727
<i>Australia</i>			
(a) <i>Southern Tablelands</i>			
Cotter Dam	1.28–1.46	0.77	701, 720
Corin Dam	1.19–1.61	0.11	701, 720
L. Ginninderra	1.54 $\pm$ 0.78	0.16–0.58	696, 697, 701, 720
(3-year range)	0.67–2.81	—	
L. George	1.80 $\pm$ 1.06	3.73–4.21	696, 697, 701, 720
(5-year range)	0.69–3.04		

Table 3.2 (cont.)

Water body	$g_{440}$ ( $\text{m}^{-1}$ )	$p_{440}$ ( $\text{m}^{-1}$ )	Reference
Burrinjuck Dam	2.21 $\pm$ 1.13	0.63–1.44	696, 697, 701, 720
L. Burley Griffin (5-year range)	2.95 $\pm$ 1.70 0.99–7.00	2.91–2.96 –	696, 697, 701, 720
Googong Dam	3.42	0.83	701
Queanbeyan R.	2.42	–	720
Molonglo R.	0.44	–	720
Molonglo R. Below confluence with Queanbeyan R.	1.84	–	720
Creek from boggy catchment	11.61	–	720
<i>(b) Murray-Darling system</i>			
Murrumbidgee R., Gogeldrie Weir (10 months)	0.4–3.2	–	1014
L. Wyangan	1.13	0.38	720
Griffith Reservoir	1.34	3.73	720
Barren Box Swamp	1.59	2.55	720
Main canal, MIA	1.11	5.35	720
Main drain, MIA	2.12	10.34	720
Murray R., upstream of Darling confluence	0.81–0.85	–	1014
Darling R., above confluence with Murray	0.7–2.5	–	1014
<i>(c) Northern Territory (Magela Creek billabongs)</i>			
Mudginberri	1.11	1.13	725
Gulungul	2.28	1.68	725
Georgetown	1.99	18.00	725
<i>(d) Tasmania</i>			
Huon R.	7–14	–	241
Lakes:			
Perry	0.06	–	152
Ladies Tarn	0.40	–	152
Risdon Brook	0.98	–	152
Barrington	3.05	–	152
Gordon	8.29	–	152
<i>(e) Southeast Queensland, coastal dune lakes</i>			
L. Wabby	0.06	–	151
Basin L.	0.46	–	151
L. Boomanjin	2.59	–	151
L. Cooloomera	14.22	–	151
<i>(f) South Australia</i>			
Mount Bold Reservoir	5.40	2.25	433

Table 3.2 (cont.)

Water body	$g_{440}$ ( $\text{m}^{-1}$ )	$p_{440}$ ( $\text{m}^{-1}$ )	Reference
<i>New Zealand</i>			
Waikato R. (330 km, L. Taupo to the sea):			
L. Taupo (0 km)	0.070	0.033	282
Ohakuri (77 km)	0.22	0.32	282
Karapiro (178 km)	0.82	0.71	282
Hamilton (213 km)	0.97	0.98	282
Tuakau (295 km)	1.37	1.67	282
Lakes (mean of monthly values over 11 months):			
Rotokakahi	0.09	–	285
Rotorua	0.23	–	285
Opouri	0.86	–	285
Hakanoa	1.84	–	285
D	4.87	–	285

<sup>a</sup> Values measured at a wavelength less than 440 nm and converted to  $g_{440}$  on the basis of an appropriate CDOM absorption spectrum.

<sup>b</sup> Measurements carried out at 443 nm, to conform with the corresponding SeaWiFS band.

<sup>c</sup> Published values for  $c$  at 440 nm corrected for scattering.

This compilation gives some idea of typical gilvin concentrations that may be expected in natural waters, but the lack of measurements in what are otherwise limnologically well-characterized parts of the world is apparent. The data in Table 3.2 show that marine waters generally have much less dissolved colour than inland waters, and the greater the distance from land, the lower the concentration. The high concentration (for a marine water) within the Baltic Sea is noteworthy: it decreases from the Bothnian Gulf southwards, as the proportion of river water in the sea diminishes. The increase in concentration with distance from the sea upstream in estuarine systems can be seen in the data for Clyde River-Batemans Bay and Latrobe River-Gippsland Lakes (Australia). The Amazon River, with its massive outflow of coloured water, contributes very large quantities of CDOM to the western tropical North Atlantic Ocean, its influence on the optical properties being detectable at distances greater than 1000 km from the river mouth.<sup>301</sup>

Although gilvin is chemically rather stable – its concentration in a refrigerated stored sample usually shows only small changes over a few weeks – its concentration within any inland water body changes, in either

direction, with time, in accordance with rainfall events in different parts of the catchment and consequent changes in the concentration of gilvin in the inflowing waters. Some of the data in Table 3.2 give an indication of the extent of this variability. For example, in Lake Burley Griffin (Canberra, Australia) the value of  $g_{440}$  varied seven-fold over a five-year period. Nevertheless, for any given water body, variation does tend to be around a certain mean value and the water body can usefully be regarded as typically high, low or intermediate in gilvin concentration. The category in which a particular lake, impoundment or river falls is determined by the drainage pattern, vegetation, soils and climate in the catchment.

The factors governing the concentration of gilvin in surface waters are not well understood and in view of the great influence of this material on aquatic primary production it would be desirable to know more. One generalization that can be made is that gilvin concentration is high in drainage water from bogs or swamps: this can readily be seen, for example, in the peat bogs of northern Europe, and is shown quantitatively in the  $g_{440}$  values for an English bog lake and a creek draining boggy ground in the Australian southern tablelands (Table 3.2). Gilvin concentration is also high in the waters draining from humid tropical forests,<sup>805</sup> as the  $g_{440}$  values for two Venezuelan waters in Table 3.2 show. The lack of oxygen in the permanently, or frequently, waterlogged soil of such areas leads to a build-up of partially decomposed organic matter, and gilvin is derived from the soluble component of this. The other side of the coin is that water draining limestone-rich catchments tends to be low in gilvin. An inverse relationship between water colour and lake depth has been observed for North America.<sup>496</sup> The effects of vegetation type, soil mineralogy, agricultural practices, climate and other environmental parameters on gilvin concentration are not well understood.

Although, as we have noted, gilvin is chemically quite stable, it does undergo photochemical degradation by intense sunlight in the surface layer.<sup>685,751</sup> The breakdown products have been found to include a range of low molecular weight carbonyl compounds, such as pyruvate, formaldehyde and acetaldehyde, and lower molecular weight carboxylic acids (oxalic, malonic, formic and acetic)<sup>685,105</sup> all of which would be readily utilized by aquatic microbes. On the basis of their rate measurements, Kieber *et al.* (1990) estimate that the half-life of dissolved humic substances of riverine origin in the oceanic mixed layer is 5 to 15 years. Mopper *et al.* (1991) present evidence suggesting that the photochemical

pathway is in fact the main route for the degradation of the long-lived biologically refractory, dissolved organic carbon of the ocean. Microbial decomposition of CDOM is, however, also significant: in water from the Mississippi River plume it occurred at about 30% of the photo-oxidation rate.<sup>552</sup>

Although action spectra indicate that the UVB region is the part of the solar spectrum (280–320 nm) that is the most damaging for CDOM,<sup>685</sup> it does not follow that it is UVB that carries out most of the photo-oxidation through the water column in natural water bodies. The very high absorption of UVB by CDOM ensures that this spectral waveband is rapidly attenuated with depth, so that photo-oxidation occurring further down the water column must be due to light of longer wavelengths. For a humic lake in Finland, Vähätalo *et al.* (2000) calculated that UVB contributed 9%, UVA (320–400 nm) 68% and visible light 23% to the photochemical mineralization. For lakes in Argentina and Pennsylvania, USA, Osburn *et al.* (2001) calculated that the contribution of UVB radiation to photobleaching of CDOM was small (<20% of total decrease in the absorption coefficient) compared to that of UVA and blue light. For continental shelf waters of the South Atlantic Bight (southeastern USA), the calculations of Miller *et al.* (2002) indicate that it is the UVA region of the solar spectrum that is primarily responsible for photo-oxidation of dissolved organic matter. For the estuarine waters of Chesapeake Bay (USA), Osburn *et al.* (2009) found that the long-wave photobleaching of CDOM increased with increasing salinity.

In the case of freshwater reservoirs, the colour of the water can be a function of how long it is exposed to sunlight before use. In tropical northern Australia, Townsend *et al.* (1996) found that in two closely adjacent reservoirs with similar catchments, the average concentration of gilvin over eight years was inversely proportional to retention time. The Manton River Reservoir colour was typically two to three times that in the Darwin River Reservoir, which they attributed to the shorter retention time, and therefore shorter time for photobleaching, in the former water body.

Since the total organic matter in a water body may contain some undetermined proportion of colourless organic material, it is difficult to know what meaning to give measurements of the specific absorption coefficient (absorption per unit weight) of CDOM. For Danish coastal waters, Stedmon *et al.* (2000) found values ranging from  $0.0727 \text{ m}^2 \text{ g}^{-1} \text{ C}$  in the Skagerrak to  $0.630 \text{ m}^2 \text{ g}^{-1} \text{ C}$  in the Kattegat, with a data set mean of  $0.29 \pm 0.11 \text{ m}^2 \text{ g}^{-1} \text{ C}$ , at 375 nm. For a large number of mountain

lakes in the Alps and the Pyrenees, Laurion *et al.* (2000) found specific absorption coefficients of total dissolved organic carbon at 320 nm over the range 0.43 to 3.51 m<sup>2</sup> g<sup>-1</sup> C. Specific absorption coefficients were generally lower in surface waters than in deeper layers, an effect possibly attributable to photobleaching.

### Tripton

The inanimate particulate matter, or tripton, of natural waters is the fraction whose light absorption properties have received the least attention because they are so difficult to measure. At typical concentrations the material does not absorb light strongly but scatters quite intensely and so its absorption properties cannot be characterized by normal spectrophotometry with long-pathlength cells. One approach to overcoming these problems is to collect the particulate matter from a natural water sample on a filter and resuspend it in a much smaller volume: the absorption spectrum of the concentrated material is then measured in a short-pathlength cell, placed at the entrance port of an integrating sphere, and from the absorbance values the absorption coefficients due to the particulate matter, in the original water body, may be calculated.<sup>701</sup> Such measurements still have to be corrected for the attenuation due to backscattering. To improve the procedure, Babin and Stramski (2002) placed the sample cuvette at the centre of a large (15 cm diameter) integrating sphere: the scattering error became negligible. An alternative approach is to measure the total absorption spectrum of the water sample with an ICAM or PSICAM, taking advantage of the long equivalent pathlengths and immunity to scattering error of these instruments (§3.2, above), repeat the measurement on a filtrate and obtain the spectrum of the particulate fraction by difference.

The total particulate fraction (*seston*, in limnological parlance) will of course include phytoplankton as well as tripton. If, however, the phytoplankton concentration is low then the particulate fraction spectrum can be attributed to tripton. Figure 3.6 shows the absorption spectra of the particulate and soluble fractions of several Australian inland waters. In all cases except (c) and (f) the absorption by the particulate fraction is almost entirely due to tripton, although in two of these ((d) and (g)) a small 'shoulder' at about 670 nm due to phytoplankton chlorophyll may be seen.

To obtain a tripton spectrum uncontaminated by phytoplankton absorption, Kishino *et al.* (1985) extracted the filter on which the

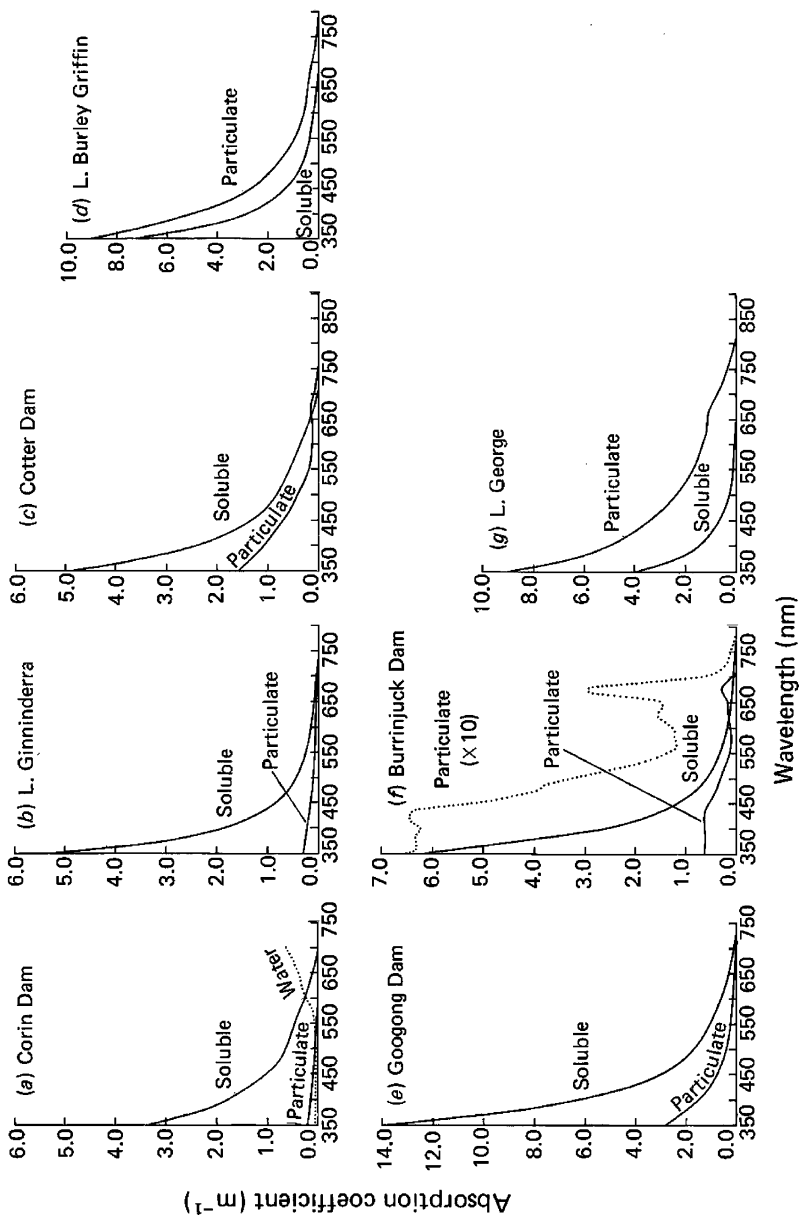


Fig. 3.6 Comparison of the spectral absorption properties of the particulate and soluble fractions of various Australian inland waters in the southern tablelands of New South Wales/Australian Capital Territory (from Kirk, 1980b). The absorption spectrum of pure water is included in (a) for comparative purposes. The phytoplankton chlorophyll *a* contents ( $C_a$ ) and nephelometric turbidities ( $T_n$ ) of the different water bodies at the time of sampling were as follows: (a) Corin Dam, 8 June 1979,  $C_a = 2.0 \text{ mg m}^{-3}$ ,  $T_n = 0.51 \text{ NTU}$ ; (b) Lake Ginninderra, 6 June 1979,  $C_a = 1.5 \text{ mg m}^{-3}$ ,  $T_n = 1.1 \text{ NTU}$ ; (c) Cotter Dam, 8 June 1979,  $C_a = 9.0 \text{ mg m}^{-3}$ ,  $T_n = 1.6 \text{ NTU}$ ; (d) Lake Burley Griffin, 6 June 1979,  $C_a = 6.3 \text{ mg m}^{-3}$ ,  $T_n = 17.0 \text{ NTU}$ ; (e) Googong Dam, 21 June 1979,  $C_a = 1.7 \text{ mg m}^{-3}$ ,  $T_n = 5.8 \text{ NTU}$ ; (f) Burrinjuck Dam, 7 June 1979,  $C_a = 16.1 \text{ mg m}^{-3}$ ,  $T_n = 1.8 \text{ NTU}$ ; (g) Lake George, 28 November 1979,  $C_a = 10.9 \text{ mg m}^{-3}$ ,  $T_n = 49 \text{ NTU}$ . The ordinate scale corresponds to the true *in*

particulate fraction had been collected, with methanol. This removes the chlorophylls and carotenoids but leaves the humic colour. Methanol does not, however, remove the biliprotein pigments that will be present in any cyanobacteria or cryptophytes algae in the sample. As an alternative, Tassan and Ferrari (1995) have developed a procedure in which the filter is treated with sodium hypochlorite. This bleaches the algal pigments, including the biliproteins.<sup>1345,392</sup> It is assumed in this procedure that the short exposure to hypochlorite does not affect the non-algal pigments.

The tripton absorption spectra all have much the same shape: absorption is low or absent at the red end of the spectrum and rises steadily as wavelength decreases into the blue and ultraviolet. These are typical humic substance absorption spectra and indeed have much the same shape as those of the dissolved yellow materials. Furthermore, typical tripton samples collected on a filter are brown in colour. The most plausible supposition is that the yellow-brown tripton colour is largely due to particulate humic material existing either bound to mineral particles or as free particles of humus. It seems likely that in inland waters it arises, together with the soluble humic material (gilvin), from the soils in the catchment. In productive waters or in oceanic waters well away from land drainage, some of the light-absorbing inanimate matter arises by decomposition of the phytoplankton. The detrital (non-living, particulate) fraction in sea water also has an absorption spectrum of the humic type (Fig. 3.7) but sometimes with shoulders due to the breakdown products of photosynthetic pigments.<sup>164,962,1146,615</sup>

The spectral slope of the spectrum of non-algal particulate matter is typically less than that observed for CDOM. For coastal waters around Europe, Babin *et al.* (2003b) found the spectral slope for non-algal particles to have an average value of  $0.0123 \pm 0.0013 \text{ nm}^{-1}$ . In coastal waters

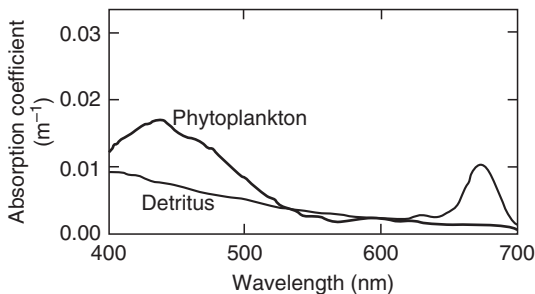


Fig. 3.7 Absorption spectra of detrital and phytoplankton particles from a mesotrophic station in the Sargasso Sea (after Iturriaga and Siegel, 1989).

in the Northern Gulf of Mexico, influenced by Mississippi River outflow, D'Sa *et al.* (2006) found an average value of  $0.011 \text{ nm}^{-1}$  for the spectral exponential slope of this fraction.

It is commonly assumed that absorption by the living and non-living particulate matter of natural waters in the near-infrared,  $\sim 720$  to  $750 \text{ nm}$ , is negligible, and on the basis of this assumption, measurements in the near-IR are commonly used to provide the scattering correction for absorbance measurements. Using their improved integrating sphere method (above), Babin and Stramski (2002) have shown that this assumption is indeed valid for a variety of particles – phytoplankton species, phytoplankton detritus and coloured mineral particles – of the type likely to be encountered in marine or inland waters.

The *in situ* absorption coefficient due to particulate matter at  $440 \text{ nm}$  is a convenient general measure of particulate colour in any water. A suitable symbol would be  $p_{440}$ , which is analogous to  $g_{440}$  previously defined as a measure of soluble colour, Table 3.2 lists some observed values of  $p_{440}$  for various natural waters. In turbid waters containing large amounts of suspended material derived from soil erosion in the catchment or (in shallow waters) wind resuspension of sediments, non-living particulate absorption can exceed absorption due to dissolved colour. The waters of the Murrumbidgee Irrigation Area (Table 3.2) are examples of the first situation (see also Fig. 3.6d) and Lake George, NSW, is an example of the second (Fig. 3.6g; Table 3.2). Rivers frequently become more turbid and coloured with increasing distance downstream, from the headwaters to the estuary. A case in point is New Zealand's longest river, the Waikato. Davies-Colley (1987) found a progressive increase in both particulate ( $p_{440}$ ) and soluble ( $g_{440}$ ) colour in this river down its  $330 \text{ km}$  path from Lake Taupo to the sea (Table 3.2): the water is clear and blue-green as it leaves the oligotrophic lake, but is yellow and turbid when it finally enters the Tasman Sea.

In some coastal waters, wind-blown dust arising from dust storms in the dry interiors of nearby continents can constitute a significant proportion of the suspended particulate matter. 'Red-rain' events, loaded with Saharan dust are, for example, common along the Mediterranean coast. Samples of Asian mineral dust were found to have mass-specific absorption coefficient values at  $440 \text{ nm}$  ranging from  $\sim 0.028 \text{ m}^2 \text{ g}^{-1}$  from a Chinese desert to  $0.15 \text{ m}^2 \text{ g}^{-1}$  for volcanic soil dust from Korea.<sup>1309</sup> In dust, or soil-derived, particles with low organic matter content, a yellow or reddish colour where present is typically due to the presence of iron oxide. Samples with high concentrations

of iron, instead of smooth, exponentially rising, spectra, have substantial shoulders in the blue-green and near-UV regions.<sup>49</sup>

It should be realized that  $p_{440}$  is not as good a general guide to particulate colour as  $g_{440}$  is to soluble colour. Whereas all gilvin spectra have approximately the same shape, the shape of the particulate fraction spectrum can change significantly in accordance with the proportion of humic material or phytoplankton (see below) in it. Nevertheless, in those waters (of common occurrence) with a substantial particulate humic component, it is a useful parameter.

### **Phytoplankton**

The absorption of light by the photosynthetic pigments – chlorophylls, carotenoids and biliproteins – of the phytoplankton contributes to the attenuation of PAR with depth. Indeed in productive waters, the algae may be present in concentrations such that by self-shading they limit their own growth.

Light absorption by algal cells grown in laboratory culture has received a great deal of attention because of the use of such cultures as experimental material in fundamental photosynthesis research. What we need, however, is information on the light absorption properties of phytoplankton populations as they occur in nature since we cannot assume that the natural populations have absorption spectra identical to those of the same species grown in culture. The total concentration of pigments and the relative amounts of the different pigments can all be affected by environmental variables such as nitrogen concentration in the medium, light intensity and spectral distribution etc. Ultimately what is required is not only the shape of the absorption spectrum, but the actual values of the absorption coefficients due to phytoplankton in the original water body. Data on phytoplankton populations consisting mainly of single known species would be particularly valuable.

Many studies of the absorption spectra of natural populations of marine phytoplankton have now been carried out (refs. [164,688,729,804,916,962,1487,52,1270,275,259,1439,353,1306,328,952,1359,241,1405,1438,563,1171,1218](#) are a representative sample). Almost invariably in recent years – because of the low concentrations of cells present in the water – collection and measurement of the spectrum on a filter has been the method of choice. To correct for non-algal absorption, the spectrum of the material remaining after decolourization of the algae with methanol or hypochlorite (see above) can be measured, and the phytoplankton spectrum obtained of by difference. The filter

method does, however, as we noted earlier, require the somewhat problematic estimation of a large absorption amplification factor. As we have noted earlier, the freeze-transfer technique of Allali *et al.* (1995), although somewhat more demanding, does avoid this problem. Also, as discussed above for total particulates, measurements with an integrating cavity or reflective tube absorption meter, on the unfiltered water sample and on the filtrate, would avoid these optical problems.

Iturriaga and Siegel (1989) have used their technique of microspectrophotometry of individual cells to determine both the shape of the spectrum, and the *in situ* absorption coefficients, for natural phytoplankton populations in the Sargasso Sea (Fig. 3.7). Neumüller *et al.* (2002) have measured the spectra of individual phytoplankton cells from laboratory cultures using an epifluorescence microscope equipped with a spectrograph and a charge-coupled device (CCD) array detector. This method could presumably, like that of Iturriaga and Siegel, be applied to natural phytoplankton populations.

In the case of productive marine or fresh waters, it is feasible to measure absorption spectra of phytoplankton populations in suspension – if necessary, after a preliminary concentration step – using an integrating sphere, or opal glass,<sup>516,701,873</sup> and calculate the *in situ* absorption coefficients directly. Figure 3.6f shows the spectrum (integrating sphere method) of the particulate fraction from Burrinjuck Dam, a eutrophic impoundment in New South Wales, Australia, at a time when it had a mixed bloom of *Melosira* sp. (a diatom) and *Anacystis cyanea* (a blue-green alga). The fraction consisted mainly of algal biomass and so the spectrum provides approximate values (somewhat too high in the blue due to the presence of some tripton) for the *in situ* absorption coefficients due to phytoplankton. Figure 3.8 shows the particulate fraction spectrum – again largely due to phytoplankton – of the estuarine water of Lake King (Gippsland Lakes, Australia).

A quite different route to the determination of *in situ* phytoplankton absorption has been taken by Bidigare *et al.* (1987) and Smith *et al.* (1989). Making the plausible assumption that essentially all the undegraded photosynthetic pigments in the water column originate in living cells, they carried out a complete pigment analysis of the total particulate fraction, using high-performance liquid chromatography (HPLC); then, using literature data on the spectral properties of pigment-protein complexes, they calculated the absorption coefficients due to phytoplankton.

It is possible to estimate the absorption coefficient of the medium at a given wavelength from the vertical attenuation coefficient for irradiance

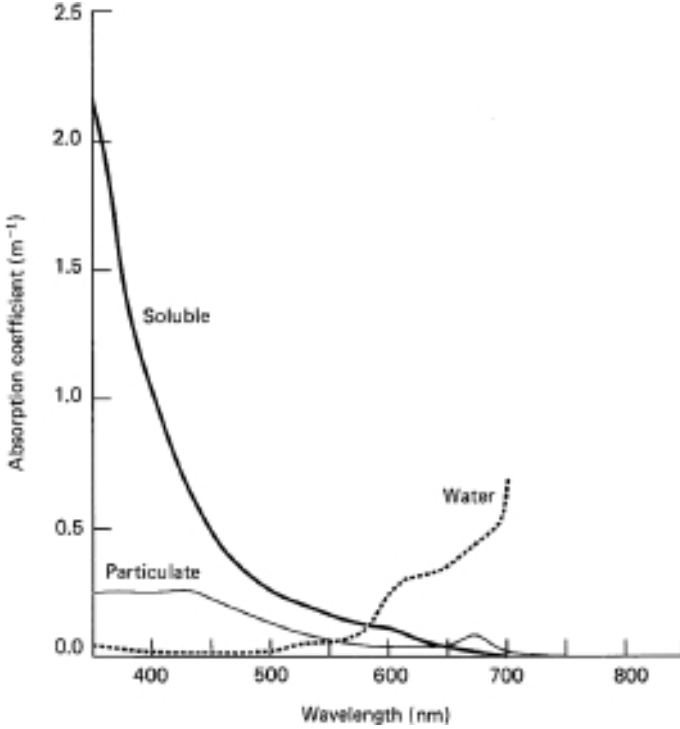


Fig. 3.8 Comparison of the spectral absorption properties of the different fractions in an estuarine water from southeast Australia – Lake King, Victoria (Kirk, unpublished data). Phytoplankton were present at a level corresponding to  $3.6 \text{ mg chlorophyll } a \text{ m}^{-3}$  and the turbidity of the water was  $\sim 1.0$  NTU.

at that wavelength. By carrying out such calculations for pairs of stations (in the Atlantic off Northwest Africa) where the scattering coefficients were about the same but the phytoplankton population varied, Morel and Prieur (1977) were able to arrive at an absorption spectrum for the natural phytoplankton population present. The absorption coefficients corresponding to  $1 \text{ mg chlorophyll } a \text{ m}^{-3}$  are plotted against wavelength in Fig. 3.9. The amount of light harvested by the phytoplankton component of the aquatic medium depends not only on the total amounts of the photosynthetic pigments present, but also on the size and shape of the algal cells or colonies within which the pigments are located. This subject is dealt with later (§9.3).

Absorption spectra of phytoplankton are normally measured only over the range corresponding to photosynthetically active radiation (PAR,

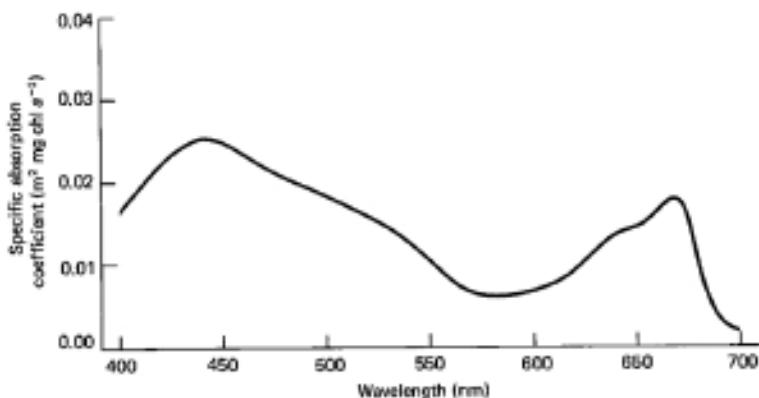


Fig. 3.9 Specific absorption coefficient (*in situ*), corresponding to 1 mg chlorophyll  $a\text{ m}^{-3}$ , for oceanic phytoplankton (after Morel and Prieur, 1977).

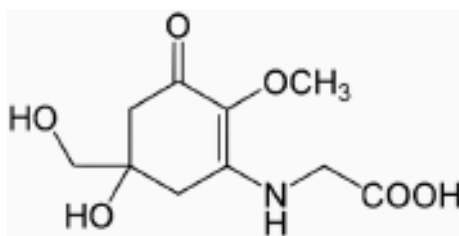


Fig. 3.10 Mycosporine-glycine structure.

~400–700 nm). Absorption in the near-UV, below 400 nm, even though it contributes little to photosynthesis, is nevertheless significant for primary production since it is energy in this waveband that is particularly effective at causing photo-inhibition (§10.1). A protective response that phytoplankton have evolved over the eons of geological time is to synthesize sunscreens in the form of UV-absorbing amino acids known as *mycosporine-like amino acids*, commonly abbreviated as MAAs. They have absorption peaks in the 300 to 400 nm range. *Shinorine* and *mycosporine-glycine* are typical examples, both found in algae: the structure of the latter compound is shown in Fig. 3.10. Figure 3.11 shows the absorption spectrum of a phytoplankton sample collected at 10 m depth over the Chatham Rise, East of New Zealand, in the South Pacific Ocean: the large peak between 300 and 360 nm is plausibly attributable to MAAs. Llewellyn and Harbour (2003) found that in phytoplankton populations in the English Channel, MAAs were present year round, but

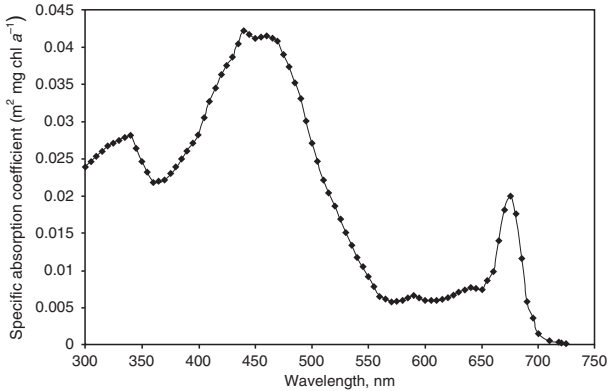


Fig. 3.11 Absorption spectrum of a natural oceanic phytoplankton population, showing a peak between 300 and 360 nm in the UV, plausibly attributable to the presence of mycosporine-like amino acids. Sample taken at 10 m depth over the Chatham Rise, South Pacific Ocean (Shooter *et al.*, 1998). The spectrum was measured on a glass fibre filter, and has been corrected for the contribution of inanimate particulate matter. The curve is for the specific absorption coefficient ( $\text{m}^2 \text{mg chl a}^{-1}$ ), assuming a value of  $0.02 \text{ m}^2 \text{mg chl a}^{-1}$  at 675 nm.

concentrations increased rapidly in the spring and summer to levels (maximum  $8.5 \text{ mg m}^{-3}$ ) exceeding those of chlorophyll *a* (maximum  $3.6 \text{ mg m}^{-3}$ ). Absorption spectra of phytoplankton from the 0 to 50 m layer in the Tropical North Atlantic off Bermuda, collected in the summer show a strong UV absorption peak centred on  $\sim 320 \text{ nm}$ , typical of MAAs, which is virtually absent in the winter population.<sup>960</sup> The spectrum of a sample of the toxic dinoflagellate, *Gymnodinium catenatum*, collected during a bloom of that species in the Huon estuary, Tasmania, had a substantial peak in the UV (300–400 nm) believed to be due to MAAs.<sup>241</sup> By contrast, a sample of the phytoplankton collected at a time when diatom species were dominant, had a much smaller peak in this region.

### Total absorption spectra

At any wavelength, the aquatic medium has a total absorption coefficient, which is the sum of the absorption coefficients of all the light-absorbing components, at that wavelength. The variation of this total absorption coefficient with wavelength is the absorption spectrum of the medium as a whole. For any given water body, the total absorption coefficient at each wavelength is obtained by adding together the known

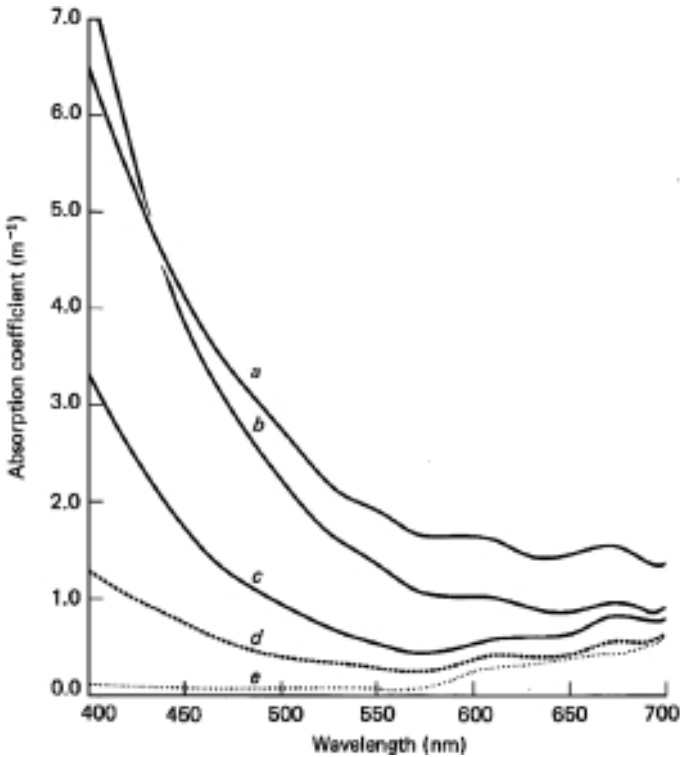


Fig. 3.12 Total absorption spectra of various natural waters in southeastern Australia (Kirk, 1981a and unpublished data). (a) Lake George, NSW. (b) Lake Burley Griffin, ACT. (c) Burrinjuck Dam, NSW. (d) Lake King, Victoria. (e) Jervis Bay, NSW. Waters *a*, *b* and *c* are inland, *d* is estuarine, *e* is marine (Tasman Sea). Chlorophyll and turbidity data for waters *a*–*d* are given in the legends to Figs. 3.6 and 3.8. The Jervis Bay water (*e*) contained  $0.2 \text{ mg phytoplankton chlorophyll } a \text{ m}^{-3}$  and was optically intermediate between Jerlov oceanic water types I and III.

absorption coefficient of pure water at that wavelength and the absorption coefficients due to dissolved and particulate colour, determined as described above. Figure 3.12 shows the total absorption spectra of five Australian waters, three inland, one estuarine and one marine. To give an approximate indication of how the total absorption spectrum might be made up, Fig. 3.13 shows, for an idealized, rather productive, ocean water, the individual absorption spectra of dissolved colour (gilvin), phytoplankton and detritus at plausible levels, and of water itself, together with the total absorption spectrum of the water due to all four components together.

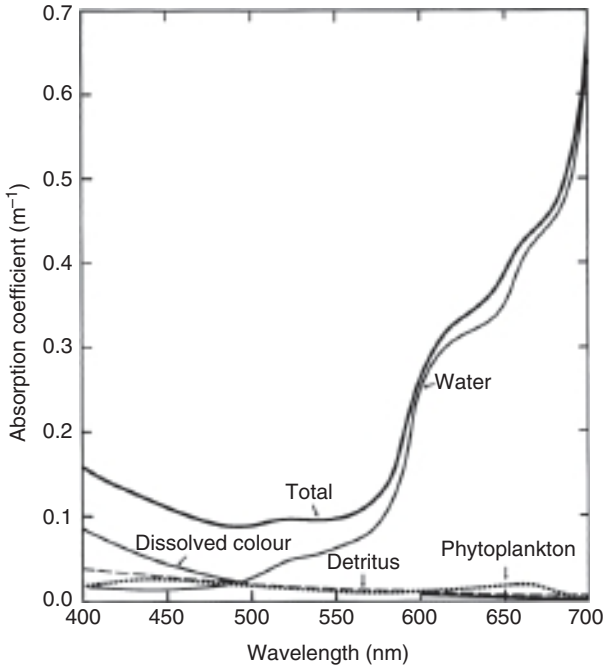


Fig. 3.13 Total absorption spectrum of an idealized, productive ( $1 \text{ mg chlorophyll } a \text{ m}^{-3}$ ) oceanic water, together with spectra of the individual absorbing components.

### 3.4 Optical classification of natural waters

Natural waters vary greatly in the extent to which they transmit solar radiation and it is useful to have some broad indication of the optical character of a water without having to fully specify all the inherent optical properties. Jerlov (1951, 1976) has classified marine waters into a number of different categories on the basis of the curve of per cent transmittance of downward irradiance against wavelength. He recognized three basic types of oceanic water (I, II and III) and nine types of coastal water (1 to 9), in order of decreasing transmittance: the spectral variation of percentage transmittance for some of these water types is shown in Fig. 3.14.

Jerlov's pioneering measurements were, however, made with broad-band colour filters, and the curves obtained with modern submersible spectroradiometers are in some cases in poor agreement with his. Pelevin and Rutkovskaya (1977) proposed that, instead, ocean waters be classified in terms of the vertical attenuation coefficient (base 10 logarithm) for

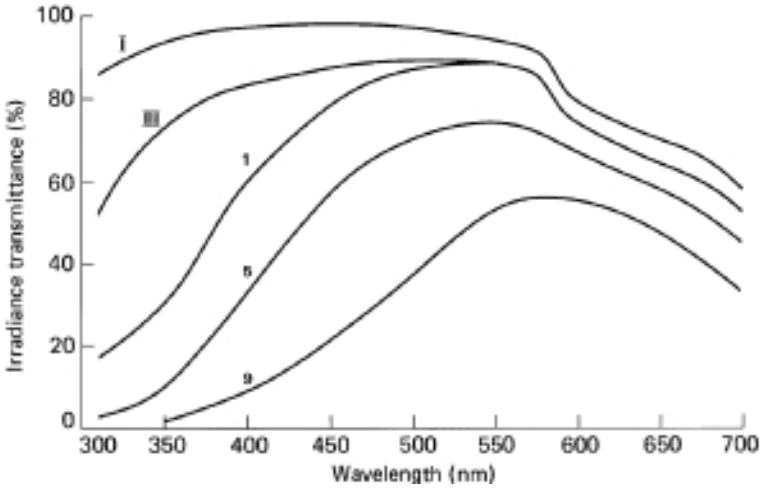


Fig. 3.14 Transmittance per metre of various optical types of marine water for downward irradiance. The waters are Jerlov's oceanic types I and III, and coastal types 1, 5 and 9 (data from Table XXVI of Jerlov, 1976).

irradiance at 500 nm, multiplied by 100. Since the  $K_d$  versus  $\lambda$  curves vary in a fairly systematic manner from one oceanic water to another, the value of  $K_d(500\text{ nm})$  would indeed convey quite a lot of information about any such water. However, given that all definitions of optical properties for natural waters are now standardized to use logarithms to the base  $e$  rather than base 10,<sup>402</sup> it would be preferable to modify Pelevin and Rutkovskaya's proposal so that the water type was specified by  $100 K_d(500\text{ nm})$ , where  $K_d$  is based on  $\log_e$ , in accordance with the definition in eqn 1.20. This has the advantage that the number obtained is approximately equal (if attenuation is not too intense) to the percentage of downwelling light that is removed. For example, Jerlov's oceanic waters I and III, with irradiance transmittance values at 500 nm of 97.3% and 89%, corresponding to irradiance diminution of 2.7% and 11%, have  $100 K_d(500\text{ nm})$  values of 2.7 and 11.6. One of the oceanic parameters that is now commonly mapped by ocean colour remote sensing is  $K_d(490)$  (Chapter 7, §7.5), which is close enough to  $K_d(500)$  for Pelevin and Rutkovskaya's classification system to be put into effect.

Smith and Baker (1978b), on the basis of their measurements of the spectral variation of the vertical attenuation coefficient ( $K_d$ ) for irradiance in various ocean waters, have concluded that in regions away from terrigenous influences, the attenuation (apart from that due to water) is mainly due to the phytoplankton and the various pigmented detrital

products that covary with it. They suggest that for such ocean waters, the total content of chlorophyll-like pigments provides a sufficient basis for optical classification, since on the basis of the pigment content, the curve of  $K_d$  against wavelength can be calculated. A classification that has been found useful in the context of remote sensing of the ocean is that into 'Case 1' and 'Case 2' waters, put forward by Morel and Prieur (1977), and further refined by Gordon and Morel (1983). Case 1 waters are those for which phytoplankton and their derivative products (organic detritus and dissolved yellow colour, arising by zooplankton grazing, or natural decay of the algal cells) play a dominant role in determining the optical properties of the ocean. Case 2 waters are those for which an important or dominant contribution to the optical properties comes from resuspended sediments from the continental shelf, or from particles and/or dissolved colour in river run-off or urban/industrial discharge. Case 1 waters can range from oligotrophic to eutrophic, provided only that the particulate and coloured materials characteristic of Case 2 waters do not play a significant role. In Case 2 waters, phytoplankton and their derivative products may or may not also be present in significant amount.

A crude optical classification applicable mainly to inland waters was proposed by Kirk (1980b) on the basis of measurements of the absorption spectra of the soluble and particulate fractions from Australian water bodies. In type G waters, the dissolved colour (gilvin), at all wavelengths in the photosynthetic range, absorbs light more strongly than the particulate fraction: examples are shown in Figs 3.6a, b and e. In type GA waters, gilvin absorbs more strongly than the particulate fraction throughout the shorter wavelength part of the spectrum, but the absorption coefficients of the particulate fraction exceed those of the soluble fraction at the red end of the spectrum due to the presence of substantial levels of algal chlorophyll: Figs 3.6c and f are examples. In type T waters, the particulate fraction, consisting mainly of inanimate material (tripton), absorbs light more strongly than the soluble fraction at all wavelengths: turbid waters with large amounts of suspended silt particles (Figs 3.6d and g) are in this category. In type GT waters, absorption by the soluble and particulate fractions is roughly comparable throughout the photosynthetic range: the waters in certain billabongs in tropical Australia have been observed to be in this category. In highly productive waters, the absorption coefficients due to algal biomass may exceed those due to dissolved colour (and water itself). Measurements by Talling (1970) of the spectral variation of the vertical attenuation coefficient of water from Loch Leven, Scotland, suggest that this eutrophic lake,

dominated by *Synechococcus* sp., was in this category (type A) at the time: the waters of the upwelling area off West Africa, studied by Morel and Prieur (1975), also appear to be of type A. Most oceanic, and some coastal, waters (Fig. 3.12e) are so non-productive, and so free of silt and dissolved colour, that water itself is the dominant light absorber: they may be categorized as type W. Such waters are rare inland: one example is Crater Lake, Oregon, USA.<sup>1253</sup> In certain estuarine and the more coloured coastal waters, the gilvin absorption at the blue end of the spectrum can be roughly similar in magnitude to the water absorption at the red end. Such waters, for example that in Fig. 3.8, may be classified as WG.

A water body can change from one optical type to another. Heavy rain in the catchment with consequent soil erosion could, for example, quickly change a type G water (gilvin dominated) to a type T water (tripton dominated); development of an algal bloom could change it to a type GA water. Nevertheless, some water bodies have water of a particular type most of the time. Bog lakes are typically type G all the time. Shallow, wind-exposed lakes with unconsolidated sediments are likely to be of type T all the time. Marine waters are, apart from the effects of the yearly phytoplankton cycle (in non-tropical areas), generally constant in their optical properties.

### **3.5 Contribution of the different components of the aquatic medium to absorption of PAR**

Apart from the small amount of light scattered back out of the water, attenuation of PAR in water bodies is due to absorption, although the extent of this absorption within a given depth may be greatly amplified by scattering, which increases the average pathlength of the photons within that depth. The relative contribution of different components of the system to this absorption at a given wavelength is in proportion to their absorption coefficients at that wavelength. Absorption coefficients for any particular component and the intensity of the incident solar radiation vary independently with wavelength throughout the photosynthetic range, and so the contribution of the different components to absorption of total PAR can be assessed by carrying out the appropriate calculations at a series of narrow wavebands and summing the results. In this way it is possible to calculate what proportion of those photosynthetic quanta that

Table 3.3 *Calculated distribution of absorbed photosynthetic quanta between the particulate fraction, soluble fraction and water in Australian water bodies. The calculations have in each case been carried out for the euphotic zone of the water body in question. Data from Kirk (1980b), Kirk and Tyler (1986) and unpublished.*

Water body	Optical type	Quanta absorbed (% of total)		
		By water	By dissolved colour (CDOM)	By particles (tripton/phytoplankton)
<i>Coastal-Oceanic</i>				
Jervis Bay <sup>a</sup>	W	68.1	23.9	8.0
<i>Estuarine</i>				
Lake King <sup>b</sup>	WG	41.9	40.4	17.7
<i>Inland impoundments</i>				
Corin Dam <sup>c</sup>	G	34.8	60.0	5.2
Lake Ginninderra <sup>c</sup>	G	39.1	50.4	10.5
Googong Dam <sup>c</sup>	G	22.0	60.4	17.6
Cotter Dam <sup>c</sup>	GA	26.2	49.8	24.0
Burrinjuck Dam <sup>a</sup>	GA	28.2	45.5	26.3
Lake Burley Griffin <sup>c</sup>	T	19.4	22.2	58.4
<i>Natural inland waters</i>				
Latrobe River <sup>b</sup>	T	17.5	28.1	54.5
Lake George <sup>a</sup>	T	12.4	8.3	79.3
Gulungul billabong <sup>d</sup>	GT	20.0	39.7	40.3
Georgetown billabong <sup>d</sup>	T	5.9	7.5	86.6

<sup>a</sup>New South Wales, <sup>b</sup>Victoria, <sup>c</sup>Australian Capital Territory, <sup>d</sup>Northern Territory.

are absorbed are captured by each of the different absorbing components of the system.<sup>696,701</sup> Table 3.3 presents the results of such calculations for 12 Australian water bodies.

It is clear that the three major components into which the light-absorbing material of the system has been divided – the water itself; the dissolved yellow substances (gilvin, CDOM); and the particulate fraction (tripton/phytoplankton) – can all be substantial light absorbers. In type W waters, most of the photosynthetic quanta are captured by water itself. In oceanic waters not affected by terrigenous material (type W, Case 1), those quanta not absorbed by water are captured mainly by the pigments of the living and dead phytoplankton.<sup>1241</sup> In coastal waters, with low but significant amounts of gilvin, the contributions of the phytoplankton and the dissolved yellow material to absorption are likely to be small and

comparable. In estuarine waters, such as Lake King (type WG), with more substantial levels of soluble yellow substances, the water and the gilvin capture most of the photosynthetic quanta. In the type G inland waters (plenty of dissolved colour, but low turbidity) described in Table 3.3, gilvin captures the most quanta, followed by water. In the type GA waters (dissolved colour, rather low turbidity, plentiful phytoplankton), gilvin is still the most important component but the particulate fraction now captures about as many quanta as does the water. In the type T waters (high turbidity due to tripton), most of the quanta are absorbed by the particulate fraction. The particulate fraction and gilvin between them take most of the quanta in type GT waters (intense soluble colour, high tripton turbidity). In highly productive, type A, waters, dominated by phytoplankton, we may assume that the algal biomass captures more photosynthetic quanta than the other components of the medium.

McKee *et al.* (2002) studied photon partitioning in the surface layer (~5 m deep, of lower salinity due to river inflow) of Loch Etive, a Scottish fjord. Despite its high colour ( $g_{440}$  1.2–1.4 m<sup>-1</sup>), due to river-borne CDOM, it is a productive system (chlorophyll *a* 3.5–8.5 mg m<sup>-3</sup>). Calculations on the basis of the absorption data indicated that ~20% of the PAR in the water column was absorbed by phytoplankton, 44% by CDOM and 36% by sea water. For a marine system, using a different approach (multiple linear regression analysis carried out on a large number of samples), Pfannkuche (2002) estimated that in the waters of the Otago Shelf (East of the South Island of New Zealand) gilvin absorbed 11%, phytoplankton 39%, inorganic particles 38% and water itself 12% of the PAR. For 13 stations in Lake Biwa (Japan), the data of Belzile *et al.* (2002a) indicate that on average 25% of the (400–700 nm) photons were captured by water, 33% by CDOM and 42% by particles.

Siegel *et al.* (2002) have used satellite imagery from SeaWiFS (Chapter 7) to characterize the global distribution of light absorption due to coloured detrital and dissolved materials (CDM, equivalent to CDOM plus tripton). They conclude that, taking the world's oceans as a whole, CDM makes roughly the same contribution to blue light absorption as phytoplankton. Field observations show that most of the CDM absorption is carried out by CDOM, the dissolved component. In a later study, using SeaWiFS data, Siegel *et al.* (2005) estimated that the contribution of CDM to total non-water absorption at 440 nm varies from 30 to 40% in the subtropical gyres to more than 60% at high latitudes.

## 4

# Scattering of light within the aquatic medium

We have seen that most of the solar photons which enter the water are absorbed. Many of these photons – most, in some waters – undergo scattering one or more times before they are absorbed. Scattering does not by itself remove light – a scattered photon is still available for photosynthesis. The effect of scattering is to impede the vertical penetration of light. It makes the photons follow a zig-zag path as they ricochet from one scattering particle to the next. This increases the total path-length that the photons must follow in traversing a certain depth, and so increases the probability of their being captured by one of the absorbing components of the medium. In addition, some of the photons are actually scattered back in an upwards direction. Thus the effect of scattering is to intensify the vertical attenuation of the light.

In this chapter we shall consider the nature of the scattering process and the scattering properties of natural waters.

### 4.1 The scattering process

What do we mean by scattering? We say that a photon is scattered when it interacts with some component of the medium in such a way that it is caused to diverge from its original path. There are two kinds of scattering to be considered – density fluctuation scattering and particle scattering.

#### Density fluctuation scattering

In understanding the basis of density fluctuation scattering in liquids, it is helpful to begin with a consideration of molecular, or Rayleigh, scattering by gases such as air. According to the Rayleigh theory, within any

particle, such as an air molecule, in a light field, a dipole is induced by the electrical vector of the field. As the dipole oscillates at the frequency of the exciting radiation, it emits radiation of the same frequency in all directions. It is this radiation that is the scattered light.

The Rayleigh molecular theory of scattering does not apply to liquids: the strong interactions between the molecules make it impermissible to consider the interaction of the radiation with molecules on an individual basis. In any liquid, however, the continual random motion of the molecules leads to localized microscopic fluctuations of density and therefore of dielectric constant and, in the Einstein–Smoluchowski theory, the interaction of the radiation field with these inhomogeneities – each of which can be regarded as a dipole – rather than with the individual molecules is considered. The predicted angular distribution of scattering is similar to that given by the Rayleigh theory for gases, i.e. it is identical in the forward and backward directions (Figs. 2.2 and 4.8). Again, as in Rayleigh scattering by gases, scattering by a pure liquid is predicted to vary inversely with the fourth power of the wavelength.

### Particle scattering

The Rayleigh and Einstein–Smoluchowski theories of scattering apply only when the scattering centres are small relative to the wavelength of light: this is true in the case of gas molecules and of the tiny density fluctuations in pure liquids. Even the most pristine natural waters, however, are not, optically speaking, pure and they invariably contain high concentrations of particles – mineral particles derived from the land or from bottom sediments, phytoplankton, bacteria, dead cells and fragments of cells etc. all of which scatter light. The particles that occur in natural waters have a continuous size distribution, which is roughly hyperbolic,<sup>54</sup> i.e. the number of particles with diameter greater than  $D$  is proportional to  $1/D^\gamma$ , where  $\gamma$  is a constant for a particular water body, but varies widely from 0.7 to 6 in different water bodies.<sup>636</sup> Although a hyperbolic distribution implies that smaller particles are more numerous than big ones, nevertheless most of the particle cross-sectional area that would be encountered by light in natural waters is due to particles of diameter greater than  $2\ \mu\text{m}$ ,<sup>636</sup> which is not small relative to the wavelengths of visible light, and so scattering behaviour different to the density fluctuation type must be anticipated. The smaller particles, although numerous, have a lower scattering efficiency.

A theoretical basis for predicting the light-scattering behaviour of spherical particles of any size was developed by Mie (1908). The physical basis of the theory is similar to that of Rayleigh in that it considers the oscillations set up within a polarizable body by the incident light field and the light re-radiated (i.e. scattered) from the body as a result of these oscillations. Instead of (as in Rayleigh theory) equating the particle to a single dipole, the Mie theory considers the additive contributions of a series of electrical and magnetic multipoles located within the particle. The advantage of the Mie theory is that it is all-embracing – for very small particles, for example, it leads to the same predictions as the Rayleigh theory; the disadvantage is that the analytical expressions are complex and do not lend themselves to easy numerical calculations. For particles larger than the wavelength of the light, Mie theory predicts that most of the scattering is in the forward direction within small angles of the beam axis (Fig. 4.1). A series of maxima and minima is predicted at increasing scattering angle, but these are smoothed out when a mixture of particle sizes is present.

In the case of particles larger than a few wavelengths of light, a reasonable understanding of the mechanism of scattering can be obtained on the basis of diffraction and geometrical optics, without recourse to electromagnetic theory. When an object is illuminated by a plane light wave, the shadow of an object on a screen placed behind it is not quite precisely defined: just outside it a series of concentric faint dark bands will be present; and lighter concentric bands, where clearly some light is falling, will be present within the area of the geometric shadow. This phenomenon – *diffraction* – is due to interference (destructive in the dark rings, constructive in the light rings) between parts of the wave coming from different points around the edge of the illuminated object, and arriving simultaneously but out of phase (because of the different distances traversed) at particular points on the screen. In the case of a round object, superimposed on the circular shadow, there is a bright spot in the centre, surrounded by alternate dark and light rings. In fact most of the light diffracted by a particle is propagated in the forward direction within a small angle of the initial direction of the beam (giving rise to the bright spot). With increasing angular distance away from the axis, the diffracted intensity goes through a series of minima and maxima (dark and light rings), which diminish progressively in height.

Applying geometrical optics to these larger particles, it can readily be appreciated that some of the light will be reflected at the external surface and some will pass through the particle and undergo refraction, or internal reflection as well as refraction (Fig. 4.2). In all cases the photons

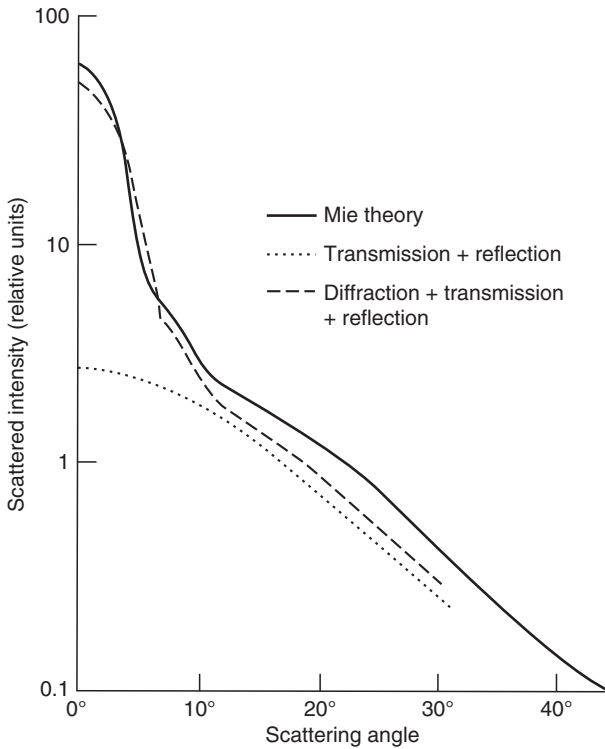


Fig. 4.1 Angular distribution of scattered intensity from transparent spheres calculated from Mie theory (Ashley and Cobb, 1958) or on the basis of transmission and reflection, or diffraction, transmission and reflection (Hodkinson and Greenleaves, 1963). The particles have a refractive index (relative to the surrounding medium) of 1.20, and have diameters 5 to 12 times the wavelength of the light. After Hodkinson and Greenleaves (1963).

involved will be made to deviate from their initial direction, i.e. will be scattered. Light scattered by these mechanisms is still predominantly in the forward direction: scattered intensity diminishes continuously with increasing angle but does not show the same degree of concentration at small angles as does scattering due to diffraction. Calculations by Hodkinson and Greenleaves (1963) for suspensions of spherical particles of mixed sizes show that most of the scattering at small angles (up to about  $10^\circ$  to  $15^\circ$ ) can be attributed to diffraction, whereas most of the scattering at larger angles is due to external reflection and transmission with refraction (Fig. 4.1). The angular variation of scattering calculated on the basis of diffraction and geometrical optics is reasonably close to

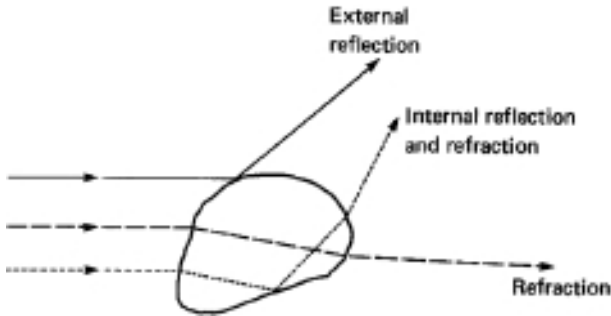


Fig. 4.2 Scattering of light by a particle: reflection and refraction processes.

that derived by the Mie electromagnetic theory. Such discrepancies as exist may be largely due to the fact that as a result of the phase change induced in the transmitted ray by passage through a medium of higher refractive index, there are additional interference effects between the diffracted and the transmitted light:<sup>1395</sup> this phenomenon is known as anomalous diffraction.

Any particle in a beam of light will scatter a certain fraction of the beam and the radiant flux scattered will be equivalent to that in a certain cross-sectional area of the incident beam. This area is the *scattering cross-section* of the particle. The efficiency factor for scattering,  $Q_{\text{scat}}$ , is the scattering cross-section divided by the geometrical cross-sectional area of the particle ( $\pi r^2$  for a spherical particle of radius  $r$ ). Similarly, in the case of an absorbing particle, the radiant flux absorbed is equivalent to that in a certain cross-sectional area of the incident beam: this area is the *absorption cross-section* of the particle. The efficiency factor for absorption,  $Q_{\text{abs}}$ , is the absorption cross-section divided by the geometrical cross-sectional area of the particle. The efficiency factor,  $Q_{\text{att}}$ , for attenuation (absorption and scattering combined) is thus given by

$$Q_{\text{att}} = Q_{\text{scat}} + Q_{\text{abs}} \quad (4.1)$$

The attenuation efficiency of a particle can be greater than unity: that is, a particle can affect the behaviour of more light in the incident beam than will be intercepted by its geometrical cross-section. This can be true of absorption and scattering separately: i.e. it is possible for a particle to absorb, or to scatter, more light than its geometrical cross-section would intercept. In terms of electromagnetic theory we may say that the particle can perturb the electromagnetic field well beyond its own physical boundary. Mie theory, based as it is upon electromagnetism, can be used to

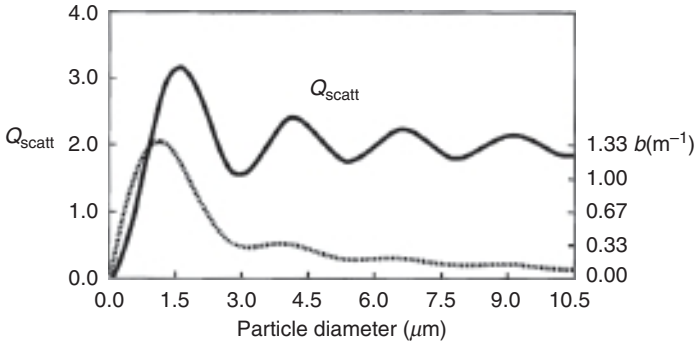


Fig. 4.3 Scattering efficiency of non-absorbing spherical particles as a function of size. The particles have a refractive index, relative to water, of 1.17. Wavelength = 550 nm. Continuous line,  $Q_{\text{scatt}}$  for a single particle, calculated using the equation of Van de Hulst (1957) – see text. Broken line, the scattering coefficient ( $b$ ) for a suspension containing 1 g of particles  $\text{m}^{-3}$ .

calculate the absorption and scattering efficiencies of particles. The simpler anomalous diffraction theory of van de Hulst (1957) can also be used to calculate the scattering efficiency of particles with refractive index up to about twice that of the surrounding medium. The relation is

$$Q_{\text{att}} = 2 - \frac{4}{\rho} \sin \rho + \frac{4}{\rho^2} (1 - \cos \rho) \quad (4.2)$$

where  $\rho = (4\pi a/\lambda)(m-1)$ ,  $m$  being the refractive index of the particle relative to that of the surrounding medium, and  $a$  being the radius of the particle. For a non-absorbing particle,  $Q_{\text{scatt}} = Q_{\text{att}}$ . Figure 4.3 shows the way in which the scattering efficiency for green light of a spherical non-absorbing particle of refractive index relative to water of 1.17 (a typical value for inorganic particles in natural waters), varies with particle size. It can be seen that scattering efficiency rises steeply from very low values for very small particles to about 3.2 at a diameter of 1.6  $\mu\text{m}$ . With increasing diameter, it first decreases and then increases again and undergoes a series of oscillations of diminishing amplitude to level off at a  $Q_{\text{scatt}}$  value of 2.0 for very large particles. A similar general pattern of variation of  $Q_{\text{scatt}}$  with size would be exhibited by any scattering particle of the types found in natural waters at any wavelength in the photosynthetic range.

As diameter decreases below the optimum for scattering (e.g. from 1.6  $\mu\text{m}$  downwards in Fig. 4.3), so efficiency for a single particle decreases. However, for a given mass of particles per unit volume, the number of

particles per unit volume must increase as particle size decreases. It is therefore of interest to determine how the scattering coefficient of a particle suspension of fixed concentration by weight varies with particle size. The results of such a calculation for particles of density in the range typical of clay minerals at a concentration of  $1 \text{ g m}^{-3}$  is shown in Fig. 4.3. As might be anticipated, because of the increase in particle number simultaneous with the decrease in diameter, total scattering by the suspension, expressed in terms of the value of  $b$ , does not decrease as precipitately with decreasing diameter below the optimum, as single particle scattering efficiency does, and the optimum particle diameter for suspension scattering ( $\sim 1.1 \mu\text{m}$ ) is lower than that for single particle scattering ( $\sim 1.6 \mu\text{m}$ ). As particle diameter increases beyond the optimum so scattering by the suspension shows a progressive decrease to very low values, with only minor, heavily damped, oscillations corresponding to the oscillations in  $Q_{\text{scatt}}$  for the individual particles.<sup>707</sup>

## 4.2 Measurement of scattering

### Beam transmissometers

In the absence of absorption, the scattering coefficient could in principle be determined by measuring the loss of intensity of a narrow parallel beam passing through a known pathlength of medium. If absorption as well as scattering occurs, then the parameter measured by the instrument would in fact be the beam attenuation coefficient,  $c$ , rather than the scattering coefficient. If it is possible also to measure the absorption coefficient,  $a$ , of the water at the appropriate wavelength, then the scattering coefficient,  $b$ , may be calculated ( $b = c - a$ ).

Beam attenuation meters – or beam transmissometers as they are more commonly called – for the *in situ* measurement of  $c$  have long been important tools in hydrologic optics. In principle all they have to do is measure the proportion,  $c$ , of the incident beam that is lost by absorption and scattering in a pathlength,  $r$ , the beam attenuation coefficient being equal to  $-\ln(1 - C)/r$  (§1.4). In practice, the construction of instruments that accurately measure  $c$  is difficult. The problem is that most of the scattering by natural waters is at small angles. Therefore, unless the acceptance angle of the detector of the transmissometer is very small ( $< 1^\circ$ ), significant amounts of scattered light remain in the beam and so attenuation is underestimated.

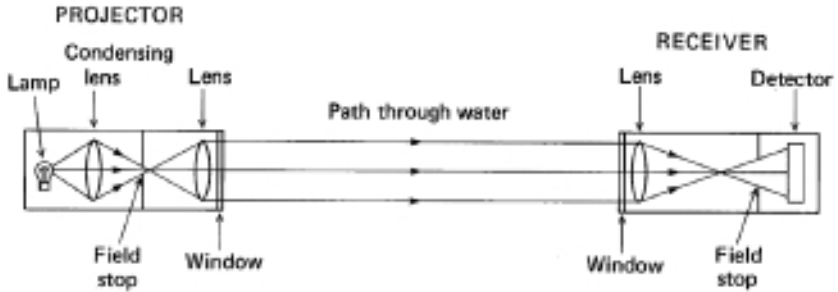


Fig. 4.4 Beam transmissometer optical system (adapted from Austin and Petzold, 1977). To confine measurements to a narrow spectral waveband, a filter can be included in the light path within the receiver.

The principles of design of beam transmissometers and the variation of the size of the error with the design parameters have been discussed by Austin and Petzold (1977). One possible optical system is shown schematically in Fig. 4.4. Most beam transmissometers are monochromatic, but spectral instruments also exist.<sup>135</sup> One of the simpler monochromatic instruments is the WET Labs C-Star, which uses an LED light source to provide a narrow bandwidth centred on 650 nm. This is focused and collimated with an aperture and a lens to produce a parallel beam, which passes through a pathlength of either 10 cm or 25 cm in the water. At the receiver end the light is brought to a focus with another lens, and its intensity measured with a silicon photodiode. The acceptance angle in water is  $1.2^\circ$ .<sup>141</sup> Laser light sources have the advantage for beam transmissometry that the beam is already highly collimated. The Sequoia Scientific LISST-100X, which is a multi-angle scattering meter used for measuring particle size distribution, and the volume scattering function (see below), uses a laser light source at 670 nm and provides values of beam attenuation coefficient in addition to the other data. Its pathlength is 5 cm and it has an acceptance angle in water of  $0.0269^\circ$ .<sup>141</sup>

The WET Labs ac-9 instrument package includes a spectral beam transmissometer, together with an absorption meter.<sup>6</sup> Both instruments operate at nine wavelengths over the range 412 to 715 nm. Light from an incandescent source passes through a 1 mm aperture, and is then collimated with a 38 mm lens followed by a 6 mm aperture. Approximate monochromaticity is achieved by passing the beam through a rotating wheel containing nine 10-nm full width half maximum (FWHM) filters. The collimated monochromatic beam passes through a flow tube 25 cm (or 10 cm) long, containing the surrounding water in which the instrument

is immersed. Whereas in the absorption meter the tube is, as discussed earlier (§3.2), a reflective quartz cylinder surrounded by an air layer which ensures that most sideways-scattered photons are not lost, in the transmissometer the tube has a blackened surface so that sideways-scattered photons are removed. At the receiving end a 30 mm lens re-focuses the light onto a detector behind a 1 mm aperture. The acceptance angle in water is  $0.93^\circ$ . Another WET Labs instrument, the ac-s, is broadly similar to the ac-9 but uses a linear variable filter to achieve spectral coverage over the range 400 to 730 nm with  $\sim 80$  wavebands of 15.5 nm FWHM.<sup>1498</sup> The acceptance angle is  $0.75^\circ$  in water.

Although *in situ* measurements of  $c$  are to be preferred, it is possible to measure the beam attenuation coefficient in the laboratory with a spectrophotometer, provided that a very small acceptance angle and long-pathlength cells are used.

If, in any water body, the vertical attenuation coefficient for downward irradiance,  $K_d$ , and the beam attenuation coefficient are both measured for the same spectral waveband, then using certain empirical relations that have been found to exist between  $K_d$ ,  $b$  and  $c$ ,<sup>1369</sup> or  $K_d$ ,  $a$  and  $c$ ,<sup>1053</sup> it is possible to estimate  $b$  and thus determine  $a$  (from  $c = a + b$ ), or estimate  $a$  and thus determine  $b$ . Gordon (1991) has described a calculation procedure by means of which, from near-surface measurements of  $c$ ,  $K_d$  and irradiance reflectance ( $R$ ), it is possible to estimate  $a$ ,  $b$  and the backscattering coefficient,  $b_b$ . This method, like the others, makes use of empirically established relationships between these quantities, but has the advantage that it makes no assumption about the shape of the scattering phase function.

### Variable-angle scattering meters

The scattering properties of natural waters are best determined by directly measuring the scattered light. The general principle is that a parallel beam of light is passed through the water, and the light scattered from a known volume at various angles is measured. In the ideal case, the volume scattering function,  $\beta(\theta)$ , is measured from  $0$  to  $180^\circ$ : this provides not only the angular distribution of scattering for that water but also, by integration, the total, forward and backward scattering coefficients (§1.4). Such measurements are in reality difficult to carry out and relatively few natural waters have been completely characterized in this way. The problem is that most of the scattering occurs at small angles (typically 50% between  $0$  and  $2-6^\circ$ ) and it is hard to measure the relatively faint

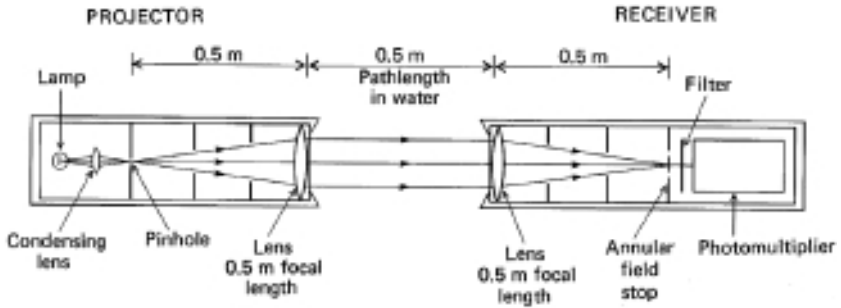


Fig. 4.5 Optical system of low-angle scattering meter (after Petzold, 1972). The vertical dimensions of the diagram are exaggerated.

scattering signal so close to the intense illuminating beam. We shall consider *in situ* scattering meters first.

An instrument developed by Petzold (1972) for very low angles (Fig. 4.5) uses a highly collimated beam of light traversing a 0.5 m pathlength in water and then being brought to a focus by a long-focal-length lens. Light that has been neither scattered nor absorbed comes to a point in this plane. Light that has been caused to deviate by scattering arrives at this plane displaced a certain distance (proportional to the scattering angle) to one side. A field stop is placed in the focal plane, opaque except for a clear annular ring that allows only light corresponding to a certain narrow (scattering) angular range to pass through and be detected by a photomultiplier behind the stop. Three such field stops are used, each with the annular ring a different radial distance from the centre: these correspond to scattering angles of 0.085, 0.17 and 0.34°. To measure the intensity of the incident beam a fourth stop is used, which has a calibrated neutral-density filter at the centre.

Kullenberg (1968) used a He-Ne laser to provide a collimated light beam traversing a pathlength of 1.3 m in water. At the receiving end of the instrument, the central part of the beam was occluded with a light trap and a system of conical mirrors and annular diaphragms was used to isolate the light that had been scattered at 1, 2.5 or 3.5°.

Bauer and Morel (1967) used a central stop to screen off the collimated incident beam and all light scattered at angles up to 1.5°. Light scattered between 1.5 and 14° was collected by a lens and brought to a focus on a photographic plate:  $\beta(\theta)$  over this angular range was determined by densitometry.

The LISST-100X particle size analyzer, referred to earlier, measures light scattering at 32 forward angles over a range depending on which

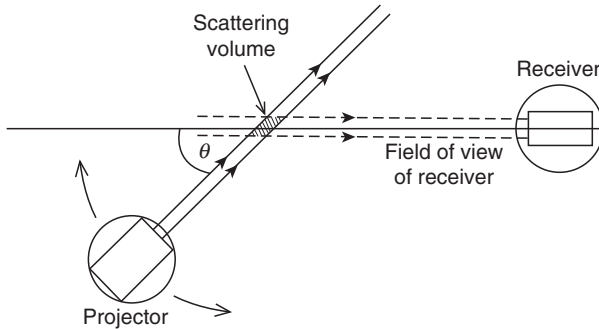


Fig. 4.6 Schematic diagram of optical system of general-angle scattering meter (after Petzold, 1972).

version of the instrument is used. In the Type B instrument the range is  $0.1$  to  $18^\circ$ . The light source is a solid-state laser operating at  $670$  nm over a  $5$  cm pathlength, and there are  $32$  ring detectors whose radii increase logarithmically.<sup>816</sup>

Instruments for measuring scattering at larger angles are constructed so that either the detector or the projector can rotate relative to the other. The general principle is illustrated in Fig. 4.6. It will be noted that the detector 'sees' only a short segment of the collimated beam of light in the water, and the length of this segment varies with the angle of view. Instruments of this type have been developed by Tyler and Richardson (1958;  $20$ – $180^\circ$ ), Jerlov (1961;  $10$ – $165^\circ$ ), Petzold (1972;  $10$ – $170^\circ$ ) and Kullenberg (1984;  $8$ – $160^\circ$ ). The recently described volume scattering meter, developed at the Marine Hydrophysical Institute at Sevastopol (Ukraine) in collaboration with Satlantic in Canada, measures the volume scattering function over the range  $0.6$  to  $177.3^\circ$ , with an angular resolution of  $0.3^\circ$ .<sup>786</sup> This instrument differs from the normal design in that the positions of the light source and detector are fixed. The measurement angle is modified by rotation of a special periscope prism. The initial version was monochromatic, but there is now a multispectral model, operating at seven wavelengths –  $443$ ,  $490$ ,  $510$ ,  $532$ ,  $555$ ,  $590$  and  $620$  nm.<sup>104</sup>

The scattering properties of natural waters can be measured in the laboratory but, at least in cases in which scattering values are low, as in many marine waters, there is a real danger that the scattering properties may change in the time between sample collection and measurement. In the case of the more turbid waters commonly found in inland, estuarine and some coastal systems, such changes are less of a problem but it is still

essential to keep the time between sampling and measurement to a minimum and to take steps to keep the particles in suspension. Commercial light scattering photometers were developed primarily for studying macromolecules and polymers in the laboratory, but have been adapted by a number of workers for the measurement of  $\beta(\theta)$ , in natural waters.<sup>83,1278</sup> The water sample is placed in a glass cell illuminated with a collimated light beam. The photomultiplier is on a calibrated turntable and can be positioned to measure the light scattered at any angle within the range of the instrument (typically 20 to 135°). Laboratory scattering photometers for very small angles have been developed<sup>40,1281</sup> and commercial instruments are available.

From the definition of volume scattering function (§1.4) it follows that to calculate the value of  $\beta(\theta)$  at each angle it is necessary to know not only the radiant intensity at the measuring angle, but also the value of the scattering volume 'seen' by the detector (this varies with angle as we noted above), and the irradiance incident upon this scattering volume. In the case of laboratory scattering meters, scattering by a water sample can be related to that from a standard scattering medium such as pure benzene.<sup>937</sup>

Once the volume scattering function has been measured over all angles, the value of the scattering coefficient can be obtained by summation (integration) of  $2\pi\beta(\theta) \sin\theta$  in accordance with eqn 1.40. The forward and backward scattering coefficients,  $b_f$  and  $b_b$ , are obtained by integration from 0 to 90°, and from 90 to 180°, respectively.

### Fixed-angle scattering meters

As an alternative to measuring the whole volume scattering function in order to determine  $b$ ,  $\beta(\theta)$  can be measured at one convenient fixed angle, and by making reasonable assumptions about the likely shape of the volume scattering function in the type of water under study (see below), an approximate value of  $b$  can be estimated by proportion. In marine waters, for example, the ratio of the volume scattering function at 45° to the total scattering coefficient ( $\beta(45^\circ)/b$ ) is commonly in the range 0.021 to 0.035 sr<sup>-1</sup>.<sup>636</sup> From an analysis of their own measurements of  $\beta(\theta)$  and  $b$  in the Pacific and Indian Oceans and in the Black Sea, Kopelevich and Burenkov (1971) concluded that the error in estimating  $b$  from single-angle measurements of  $\beta(\theta)$  is lower for angles less than 15°: 4° was considered suitable. A linear regression of the type

$$\log b = c_1 \log \beta(\theta) + c_2 \quad (4.3)$$

where  $c_1$  and  $c_2$  are constants, was found to give more accurate values for  $b$  than a simple proportionality relation such as  $b = \text{constant} \times \beta(\theta)$ . On the basis both of Mie scattering calculations, and analysis of literature data on volume scattering functions for ocean waters, Oishi (1990) concluded that there is an approximately constant ratio between the backscattering coefficient and the volume scattering function at  $120^\circ$ , so that  $b_b$  can be calculated from a scattering measurement at  $120^\circ$ , using the relationship

$$b_b \approx 7 \beta(120^\circ) \quad (4.4)$$

As a function of the volume scattering function, the backscattering coefficient can be expressed (§1.4) in the form

$$b_b = 2\pi \int_{\pi/2}^{\pi} \beta(\theta) \sin \theta \, d\theta$$

which for any given value of  $\theta$  can be replaced with

$$b_b = 2\pi \chi(\theta) \beta(\theta) \quad (4.5)$$

where  $\chi(\theta)$  is a dimensionless constant, sometimes referred to as the conversion factor, which makes this equality true at angle  $\theta$ .<sup>849</sup> Equation 4.5 can be regarded as a more general form of eqn 4.4, and so for backscattering meters using the Oishi principle (which in fact works quite well over a wide angular range) but operating at an angle other than  $120^\circ$ ,  $\chi(\theta)$  is determined empirically. Equation 4.4 corresponds to  $\chi(120^\circ) \approx 1.1$ . Single-angle estimates of  $b_b$  are often carried out at  $140^\circ$ . For coastal shelf waters off New Jersey (USA), Boss and Pegau (2001) found an average value of 1.18 for  $\chi(140^\circ)$ ; for Black Sea coastal waters Chami *et al.* (2006a) obtained an average value of 1.21.

As can readily be verified, eqn 4.4 works very well for the two volume scattering functions listed in Table 4.2. On the basis of Mie theory calculations, Oishi concluded that this relationship should be unaffected by wavelength. Field measurements of  $\beta(\theta)$  by Chami *et al.* (2006a) confirm that this is the case in coastal waters of the Black Sea.

The WET Labs ECO BB scattering meter makes use of this principle to measure  $b_b$ . The light from an LED, modulated at 1 kHz, is emitted into the water and scattered light is received by a detector positioned where the acceptance angle forms a  $117^\circ$  intersection with the source beam.<sup>1179</sup> Versions of the instrument operating at 470, 532 or 660 nm

are available; another version incorporates all three wavelengths. The HOBI Labs HydroScat-2 Backscattering Sensor<sup>849, 605</sup> also uses a modulated LED as a light source and measures light back-scattered at an angle centred on  $140^\circ$ . It operates at two wavelengths, 420 and 700 nm: versions with other pairs of wavelengths are available. The HydroScat-4 measures backscattering at four wavelengths.<sup>604</sup> These instruments also measure chlorophyll fluorescence.

If, for a given water, the beam attenuation coefficient and the absorption coefficient can both be measured, then the scattering coefficient can be obtained by difference ( $b = c - a$ ). This indirect approach is in principle less accurate since the estimate of  $b$  must combine the separate errors in the determination of  $c$  and  $a$ . To obtain  $b$  by a direct measurement of scattered light is preferable. Nevertheless, when both  $c$  and  $a$  data are available from, for example, an instrument such as the ac-9, then it is worth while collecting values of  $b$  as well.

### Turbidimeters

A specialized and simplified laboratory form of the fixed-angle scattering meter is the nephelometric turbidimeter. The word 'turbidity' is used in a general sense to indicate the extent to which a liquid lacks clarity, i.e. scatters light as perceived by the human eye. In the most common type of instrument, a beam of light is directed along the axis of a cylindrical glass cell containing the liquid sample under study. Light scattered from the beam within a rather broad angle centred on  $90^\circ$  is measured by a photomultiplier located at one side of the cell (Fig. 4.7). The 'turbidity' ( $T_n$ ) of the sample in nephelometric turbidity units (NTU) is measured relative to that of an artificial standard with reproducible light-scattering properties. The standard can be a suspension of latex particles, or of the polymer formazin, made up in a prescribed manner. Turbidimeters, as at present constituted, do not attempt to provide a direct estimate of any fundamental scattering property of the water and the nephelometric turbidity units are essentially arbitrary in nature. Nevertheless, the turbidity measured in this way should be directly related to the average volume scattering function over an angular range centred on  $90^\circ$ , and so for waters of given optical type (e.g. waters with moderate to high turbidity due to inorganic particles) should bear an approximately linear relation to the scattering coefficient. Since turbidimetric measurements are so easily made, and since there already exist a large amount of turbidimetric data on inland water bodies, comparative studies on a

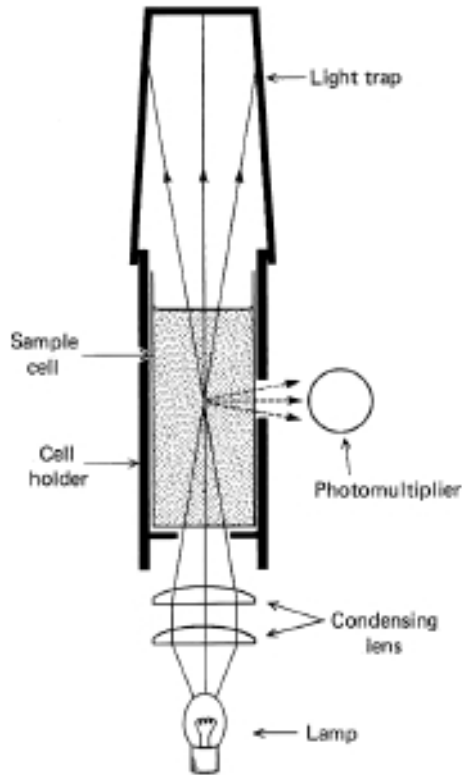


Fig. 4.7 Schematic diagram of optical system of nephelometric turbidimeter.

variety of natural waters to determine the empirical relation between nephelometric turbidity and scattering coefficient would be valuable. Some existing indirect measurements (see below) suggest that for turbid waters, by a convenient coincidence,  $b/T_n$  is about  $1 \text{ m}^{-1} \text{ NTU}^{-1}$ . Turbidimeters are, however, not well suited for characterizing waters with very low scattering values, such as the clear oceanic types.

### Indirect estimation of scattering properties

While few aquatic laboratories carry out measurements of the fundamental scattering properties of natural waters, many routinely measure underwater irradiance (§5.1). Since irradiance at any depth is in part determined by the scattering properties of the water, there is the

possibility that information on the scattering properties might be derived from the measured irradiance values. For water with a specified volume scattering function and with incident light at a given angle, then at any given optical depth (see §1.6 for definition), the irradiance reflectance,  $R$ , and the average cosine,  $\bar{\mu}$ , of the light are functions only of the ratio,  $b/a$ , of scattering coefficient to absorption coefficient. Conversely, if the value of reflectance at a certain optical depth is given, then the values of  $\bar{\mu}$  and  $b/a$  are fixed, and in principle determinable. Kirk (1981a, b) used Monte Carlo numerical modelling (§§5.5 and 6.7) to determine the relations between  $b/a$  for the medium and  $R$  and  $\bar{\mu}$  at a fixed optical depth, for water with a normalized volume scattering function identical to that determined by Petzold (1972) for the turbid water of San Diego harbour. It was considered that these relations would be approximately valid for most natural waters of moderate to high turbidity. Using the computer-derived curves it is possible, given a measured value of irradiance reflectance at a specified optical depth, such as  $\zeta = 2.3$  (irradiance reduced to 10% of the subsurface value), to read off the corresponding values of  $\bar{\mu}$  and  $b/a$ . The irradiance values are used to estimate  $K_E$ , the vertical attenuation coefficient for net downward irradiance (§1.3), and the value of  $a$  is calculated from the relation  $a = \bar{\mu} K_E$  (§1.7). Knowing  $a$  and  $b/a$ , the value of  $b$  may then be obtained.

As a test of the validity of this procedure, Weidemann and Bannister (1986) compared, for Irondequoit Bay, L. Ontario, estimates of  $a$  derived from irradiance measurements as indicated above, with estimates obtained by summing the measured absorption coefficients due to gilvin, particulate matter and water: agreement was good. Furthermore, estimates of  $\bar{\mu}$  read off from the  $\bar{\mu} = f(R)$  curve agreed with those obtained from the measured ratio of net downward, to scalar, irradiance (eqn 1.15): a similar finding was made by Oliver (1990) for a range of river and lake waters in the Murray Darling basin, Australia.

Values of scattering coefficient obtained in this way by Kirk (1981b) for various bodies in Southeastern Australia were found to correlate very closely with the values of nephelometric turbidity, ( $T_n$ ), a parameter that (see above) we might reasonably expect to be linearly related to the scattering coefficient: the average ratio of  $b$  to  $T_n$  was  $0.92 \text{ m}^{-1} \text{ NTU}^{-1}$ . Using literature data for Lake Pend Oreille in Idaho, USA,<sup>1076</sup> the method was found to give a value of  $b$  differing by only 5% from that derived from the beam attenuation and absorption coefficients.

With the help of a separately derived expression (eqn 6.11) for  $K$  as a function of  $a$ ,  $b$  and  $\mu_0$  (the cosine of the refracted solar beam beneath the surface), and another for  $b/a$  as a function of  $R$  at the 10% irradiance depth ( $z_m$ ), it is possible to replace the graphical procedure described above with an explicit expression by means of which  $a$  can be calculated from the measured irradiance profile and the solar altitude<sup>714</sup>

$$a = \mu_0 K_E(z_m) \left\{ \frac{1 - R(z_m)}{1 + R(z_m)[103 G_E(\mu_0 - 1)]} \right\}^{1/2} \quad (4.6)$$

where  $G_E(\mu_0) = 0.473 \mu_0 - 0.22$  (§6.7). To obtain  $b$ , the value of  $a$  is then multiplied by  $b/a$ .

Di Toro (1978), using radiation transfer theory with a number of simplifying assumptions, arrived at an approximate relation between the scattering coefficient and a certain function of the reflectance and vertical attenuation coefficient for irradiance. For the turbid waters of San Francisco Bay, he observed a good linear relation between the values of  $b$  calculated in this way and the nephelometric turbidity: the actual ratio of scattering coefficient to turbidity was  $1.1 \text{ m}^{-1} \text{ FTU}^{-1}$ , which is in reasonable agreement with the value of  $0.92 \text{ m}^{-1} \text{ NTU}^{-1}$  (NTU and FTU being equivalent) obtained by Kirk (1981b). Combining these results with similar findings by numerous other workers<sup>282,433,1014,1401,1402,1445,1446</sup> we arrive at the useful and convenient conclusion that, at least for waters of moderate to high turbidity, the scattering coefficient ( $\text{m}^{-1}$ ) has approximately the same numerical value as the nephelometric turbidity (NTU),

### Diffuse scattering coefficients

As we saw in our discussion of radiation transfer theory (§1.7), certain quasi-inherent optical properties of the medium – the diffuse scattering coefficients – play an essential role in our understanding of the underwater light field. These scattering coefficients have been defined previously (§1.5) in terms of the light scattered backwards or forwards by a thin layer of medium from an incident light field that is not a parallel beam at right angles (as in the case of the normal scattering coefficients) but has a radiance distribution identical to the downwelling or upwelling parts of a given underwater light field existing at a certain depth in a certain water body. There is no way at present of directly measuring the diffuse

scattering coefficients. If, however, the radiance distribution at a given depth in the water body and the volume scattering function for the water are known, then it is possible to calculate the diffuse scattering coefficients.<sup>700</sup>

To calculate, for example, the backscattering coefficient for downwelling flux, the downwelling radiance distribution is distributed into a manageable number, e.g. 15, of angular intervals. Using the volume scattering function, the proportion of the incident flux in each angular interval that is scattered in an upwards or a downwards direction by a thin layer of medium is calculated. The summed flux (for all incident angles) travelling upwards after scattering, expressed as a proportion of the total downwelling flux, divided by the thickness of the layer of medium, is  $b_{bd}(z)$ , the diffuse backscattering coefficient for downwelling flux at depth  $z$  m in that particular water body:  $b_{bd}(z)$  is commonly two- to five-fold greater than  $b_b$  in natural water bodies.<sup>700</sup> The radiance distribution data necessary for such calculations may be obtained by direct measurement (§5.1), or derived from the inherent optical properties by computer modelling (§5.2).

An approximate estimate of the diffuse backscattering coefficient can be obtained much more simply from underwater irradiance measurements. Rearranging eqn 1.51 we obtain

$$b_{bd}(z) = R(z)[K_d(z) + \kappa(z)] \quad (4.7)$$

which with help of eqn 1.52 can be rewritten

$$b_{bd}(z) \approx 3.5R(z_m)K_d(z_m) \quad (4.8)$$

where  $z_m$  is the depth at which downward irradiance is 10% of the subsurface value.  $R(z_m)$  and  $K(z_m)$  are obtained from the irradiance data, and  $b_{bd}(z_m)$  is calculated accordingly.

From the value of the diffuse backscattering coefficient derived in this way we can then go on to obtain an estimate of the normal backscattering and total scattering coefficients,  $b_b$  and  $b$ . Kirk (1989a) presents a Monte Carlo-derived curve, for optical water types covering the range  $b/a = 0.5-30$ , showing the ratio of diffuse to normal backscattering coefficient plotted against reflectance at depth  $z_m$ . From the observed value of reflectance, the ratio  $b_{bd}(z_m)/b_b$  is read off, and is then used, in conjunction with eqn 4.8 to give  $b_b$ . Assuming  $b \sim 53b_b$  (a reasonable estimate for most inland and coastal waters), the total scattering coefficient may then be obtained. Values of  $b$  calculated in this way are in good agreement with those obtained from irradiance data by the other indirect procedure, described in the previous section.

### 4.3 The scattering properties of natural waters

The scattering properties of pure water provide us with a suitable baseline from which to go on to the properties of natural waters. We shall make use here of a valuable review by Morel (1974) of the optical properties of pure water and pure sea water. For measurements of the scattering properties, water purified by distillation *in vacuo* or by repeated filtration through small-pore-size filters must be used: ordinary distilled water contains too many particles. Scattering by pure water is of the density fluctuation type, and so varies markedly with wavelength. Experimentally, scattering is found to vary in accordance with  $\lambda^{-4.32}$  rather than  $\lambda^{-4}$  as predicted by density fluctuation theory alone: this is a result of the variation of the refractive index of water with wavelength. Pure sea water (35–38‰ salinity) scatters about 30% more intensely than pure water. Table 4.1 lists values of the scattering coefficient for pure water and pure sea water at a number of wavelengths. The volume scattering function of pure water or pure sea water has, as predicted by density fluctuation theory, its minimum at  $90^\circ$  and rises symmetrically towards greater or lesser angles (Fig. 4.8).

When water molecules scatter light, most of the scattered light undergoes no change in wavelength – so-called *elastic* scattering. A small proportion of the scattered photons, however, when they interact with the scattering molecule, lose or gain a small amount of energy corresponding to a vibrational or rotational energy transition within the molecule, and so after scattering are shifted in wavelength. This is *inelastic* scattering. These photons appear in the scattered light as emission bands at wavelengths other than that of the exciting light, and are referred to as *Raman emission lines*, after the Indian physicist who discovered this phenomenon. A particularly strong Raman emission in the case of water arises from the O–H vibrational stretching mode: this shows up as an emission band roughly 100 nm on the long-wavelength side of the exciting wavelength. For an incident wavelength of 488 nm the Raman scattering coefficient of pure water is  $2.4 \times 10^{-4} \text{ m}^{-1}$ .<sup>75,307</sup> Raman scattering of water exhibits a strong inverse dependence on wavelength: over the range 250 to 500 nm, Bartlett *et al.* (1998) found this to correspond to  $\lambda^{-5.5}$  when normalized to units of energy and to  $\lambda^{-5.3}$  when normalized to units of photons. They found no significant difference between the Raman scattering coefficients of sea water and pure water.

The scattering coefficients of natural waters are invariably much higher than those of pure water. Table 4.1 lists a selection of values from the

Table 4.1 Scattering coefficient values for various waters.

Water body	Wavelength (nm)	Scattering coefficient, $b$ ( $\text{m}^{-1}$ )	Reference
Pure water	400	0.058	939
	450	0.0035	939
	500	0.0022	939
	550	0.0015	939
	600	0.0011	939
Pure sea water	450	0.0045	939
	500	0.0019	939
<b>Marine waters</b>			
<i>Atlantic Ocean</i>			
Sargasso Sea	633	0.023	758
	440	0.04	636
Caribbean Sea	655	0.06	636
3 oceanic stations	544	0.06–0.30	747
Bahama Islands	530	0.117	1051
Mauritanian upwelling <sup>a</sup>	550	0.4–1.7	942
Mauritanian coastal <sup>b</sup>	550	0.9–3.7	942
Iceland coastal	655	0.1–0.5	576
New England shelf, summer	440	0.312	1269
Coccolithophore bloom, North Atlantic	440 & 550	1–3	65
New Jersey, 2–15 km offshore	532	~3.4	1262
Great Bay Estuary (New Jersey)	532	~3.3	1262
Rhode R. Estuary (Chesapeake Bay)	720	1.7–55.3	428
Northern Gulf of Mexico: inside coastal barrier islands	532	5.08 ± 2.69	428
	10–20 km outside coastal barrier islands	532	2.02 ± 1.55
<i>Pacific Ocean</i>			
Central (Equator)	440	0.05	636
Galapagos Islands	655	0.07	636
	440	0.08	636
126 oceanic stations	544	0.18 (av.)	747
Kieta Bay (Solomon Is.)	544	0.54	747
Great Barrier Reef (Australia), ~18° S	555	0.093 ± 0.036	126
Mossman-Daintree estuarine (NE Australia) 16° S. Dry season	555	0.780 ± 0.405	126
	Wet season	555	5.005 ± 9.381
Fitzroy R./Keppel Bay system (NE Australia), 23° S. Dry season. Estuary station 2	555	>20	1025
	Offshore (28 km)	555	0.002
Lagoon, Tarawa atoll (Gilbert Is.)	544	1.04	747
Offshore, Southern California	530	0.275	1051
Monterey Bay, California	532	0.52 ± 0.31	1262

Table 4.1 (cont.)

Water body	Wavelength (nm)	Scattering coefficient, $b$ ( $m^{-1}$ )	Reference
San Diego Harbour, California	530	1.21–1.82	1051
Chatham Rise (East of New Zealand), av. of 17 stations	493	0.246	1218
<i>Indian Ocean</i>			
164 oceanic stations	544	0.18 (av.)	747
<i>Tasman Sea</i>			
<i>Australia</i>			
Jervis Bay, NSW			
Entrance, 30 m depth	450–650	0.25	1053
Inshore, 15 m depth	450–650	0.4–0.6	1053
<i>New Zealand</i>			
North Island, 9 estuaries, mouth sites, low water	400–700	1.1–4.8	1401
<i>Mediterranean Sea</i>			
Tyrrhenian Sea (1000 m depth)	546	0.016	938
Western Mediterranean	655	0.04	569
Bay of Villefranche	546	0.1	938
<i>North Sea</i>			
Fladen Ground	655	0.07–0.13	571
English Channel	546	0.65	938
<i>Baltic Sea</i>			
Kattegat	655	0.15	636
South Baltic	655	0.20	636
Bothnian Gulf	655	0.28	636
<i>Black Sea</i>			
33 stations	544	0.41 (av.)	747
<b>Inland waters</b>			
<i>North America</i>			
L. Pend Oreille	480	0.29	1076
L. Ontario, coastal	530–550	1.5–2.5	183
L. Ontario, Irondequoit Bay	400–700	1.9–5.0	1445
Otisco L., N.Y.	400–700	0.9–4.6	347,1446
Onondaga L., N.Y.	400–700	2.2–11.0	348
Owasco L., N.Y.	400–700	1.0–4.6	347
Seneca R., N.Y.	400–700	3.1–11.5	347
Woods L., N.Y.	300–770	0.13–0.20	184
Dart's L., N.Y.	300–770	0.19–0.25	184
<i>China</i>			
Lake Taihu	532	20.2 (3.3–48.1)	1325
<i>Australia</i>			
<i>(a) Southern tablelands</i>			
Corin Dam	400–700	1.5	703

Table 4.1 (cont.)

Water body	Wavelength (nm)	Scattering coefficient, $b$ ( $\text{m}^{-1}$ )	Reference
Burrinjuck Dam	400–700	2.0–5.5	703
L. Ginninderra	400–700	4.4–21.6	703
L. Burley Griffin	400–700	2.8–52.6	703
L. George	400–700	55.3, 59.8	703
<i>(b) Murray-Darling system</i>			
Murrumbidgee R., Gogeldrie Weir	400–700	9–58	1014
Murray R., upstream of Darling confluence	400–700	13.0	1014
Darling R., above confluence with Murray R.	400–700	27.8–90.8	1014
<i>(c) Northern Territory (Magela Creek billabongs)</i>			
Mudginberri	400–700	2.2	725
Gulungul	400–700	5.7	725
Georgetown	400–700	64.3	725
<i>(d) Tasmania (lakes)</i>			
Perry	400–700	0.27	152
Risdon Brook	400–700	1.8–2.7	152
Barrington	400–700	1.1–1.4	152
Pedder	400–700	0.6–1.3	152
Gordon	400–700	1.0	152
<i>(e) Southeast Queensland, coastal dune lakes</i>			
Basin	400–700	0.6	151
Boomanjin	400–700	1.1	151
Wabby	400–700	1.5	151
<i>(f) South Australia</i>			
Mount Bold Reservoir	400–700	5.7–6.8	433
<i>New Zealand</i>			
Waikato R. (330 km, L. Taupo to the sea):			
L. Taupo (0 km)	400–700	0.4	282
Ohakuri (77 km)	400–700	1.0	282
Karapiro (178 km)	400–700	1.2	282
Hamilton (213 km)	400–700	1.9	282
Tuakau (295 km)	400–700	6.3	282
Lakes:			
Rotokakahi	400–700	1.5	1402
Rotorua	400–700	2.1	1402
D	400–700	3.1	1402

<sup>a</sup> Waters rich in phytoplankton.

<sup>b</sup> High concentration of resuspended sediments.

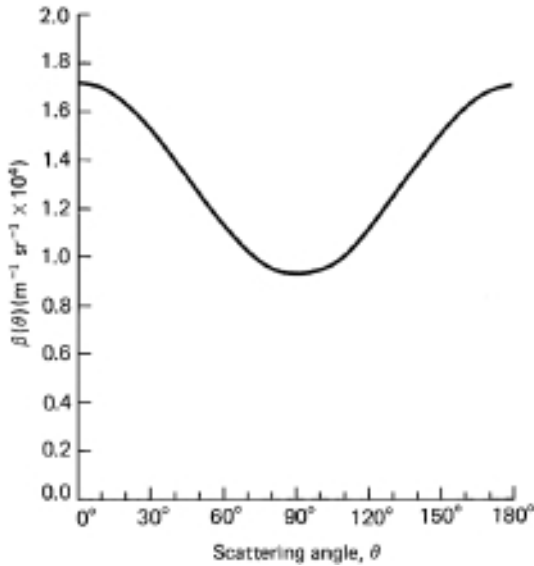


Fig. 4.8 Volume scattering function of pure water for light of wavelength 550 nm. The values are calculated on the basis of density fluctuation scattering, assuming that  $\beta(90^\circ) = 0.93 \times 10^{-4} \text{ m}^{-1} \text{ sr}^{-1}$  and that  $\beta(\theta) = \beta(90^\circ) (1 + 0.835 \cos^2\theta)$  (following Morel, 1974).

literature. Even the lowest value  $-0.016 \text{ m}^{-1}$  at 546 nm for water from 1000 m depth in the Tyrrhenian Sea<sup>938</sup> – is ten times as high as the value for pure water at that wavelength. Unproductive oceanic waters away from land have low values. Coastal and semi-enclosed marine waters have higher values due to the presence of resuspended sediments, river-borne terrigenous particulate material and phytoplankton. Resuspension of sediments is caused by wave action, tidal currents and storms. High levels of phytoplankton can give rise to quite high values of the scattering coefficient in oceanic upwelling areas, such as the Mauritanian upwelling off the west coast of Africa.<sup>942</sup> In arid regions of the continents large amounts of dust are carried up into the atmosphere by wind, and when subsequently redeposited in adjoining areas of the ocean, can substantially increase scattering in the water.<sup>746</sup> Scattering coefficient values are on average higher in inland and estuarine waters than in the open sea. Indeed the very high values that can occur in some turbid inland waters (Table 4.1) are unlikely to be equalled in the sea because high ionic strength promotes the aggregation and precipitation of colloidal clay minerals. Resuspension of sediments by wind-induced

turbulence, especially in shallow waters, can substantially increase scattering in inland water bodies.<sup>995</sup> Filter-feeding zooplankton, by packaging suspended clay particles into more rapidly settling faecal pellets, can substantially increase the rate of clearing of turbid lake water.<sup>463</sup>

Water in its solid form – snow or ice – is a highly scattering medium. On the basis of their measurements of spectral irradiance within, and transmittance through, sea ice in the Beaufort Sea (Arctic Ocean), Light *et al.* (2008) estimated that the scattering coefficient at 600 nm was 500 to 1100  $\text{m}^{-1}$  in the surface layer, and 8 to 30  $\text{m}^{-1}$  in the ice interior. Ehn *et al.* (2008) measured irradiance spectra at a series of increments within the bottom-most layers of landfast sea ice in Franklin Bay, Canada. On the basis of inverse radiative transfer modelling they estimated that for light at 400 nm,  $b$  was  $\sim 400 \text{ m}^{-1}$  in the bottom 0.1 m of the ice, decreasing to 165  $\text{m}^{-1}$  in the 0.1 to 0.2 m layer.

Volume scattering functions for natural waters differ markedly in shape from that of pure water. They are invariably characterized, even in the clearest waters, by an intense concentration of scattering at small forward angles. This, as we saw earlier, is typical of scattering by particles of diameter greater than the wavelength of light, and scattering in natural waters is primarily due to such particles. Figure 4.9 shows the volume scattering functions for a clear oceanic water and a moderately turbid, harbour water. They are quite similar in shape but there is a noticeable difference at angles greater than 90°: scattering by the oceanic water shows a greater tendency to increase between 100° and 180°. This is because at these larger angles density fluctuation scattering (which exhibits this kind of variation in this angular range – Fig. 4.8) becomes a significant proportion of the total in the case of the clear oceanic water (see below), but remains insignificant compared to particle scattering in the case of the harbour water.

A knowledge of the shape of the volume scattering function is essential for calculations on the nature of the underwater light field. Table 4.2 lists values for the normalized volume scattering function  $\tilde{\beta}(\theta) = \beta(\theta)/b$ , and the cumulative scattering (between 0° and  $\theta$ , as a proportion of the total) at a series of values of  $\theta$ , for Tongue-of-the-Ocean (Bahamas) and San Diego Harbour water.<sup>1051</sup> It will be noted that backscattering ( $\theta > 90^\circ$ ) constitutes 4.4% of total scattering in the case of the clear oceanic water but only 1.9% in the turbid harbour water. At a Crimean coastal water station, 600 m offshore in the Black Sea, Chami *et al.* (2005) from a large

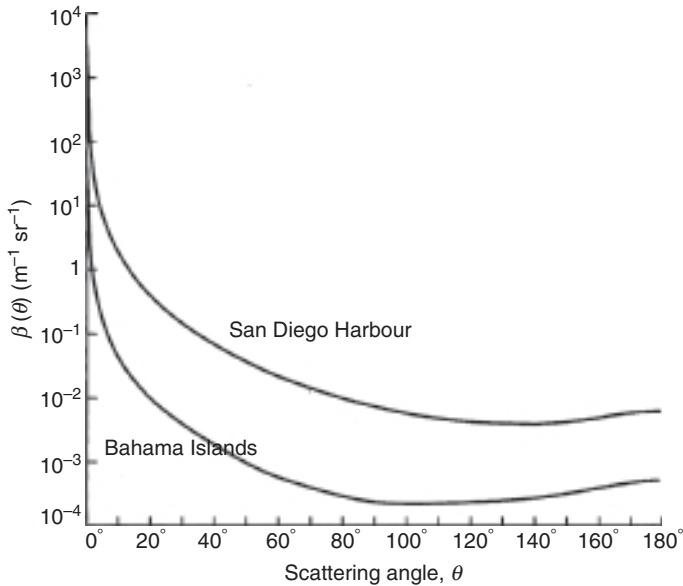


Fig. 4.9 Volume scattering functions for a clear, and a moderately turbid, natural water. The curves for the clear ocean water ( $b = 0.037 \text{ m}^{-1}$ ) of Tongue-of-the-Ocean, Bahama Islands, and the somewhat turbid water ( $b = 1.583 \text{ m}^{-1}$ ) of San Diego Harbour, have been plotted from the data of Petzold (1972).

number of measurements, found for the particulate fraction (which accounted for nearly all the scattering) an average backscattering ratio of  $\sim 1.9\%$ , at all three wavelengths used (443, 490 and 555 nm), but the results did show high intrinsic variability (1.2 to 3.2%). Waters of a given broad optical type appear, on the basis of published measurements to date, to have  $\tilde{\beta}(\theta)$  curves of rather similar shape. We may therefore take the data sets in Table 4.2 as being reasonably typical for clear oceanic, and moderately/highly turbid waters, respectively. Above a certain minimum level of turbidity, such that particle scattering is dominant at all angles, we would not expect the normalized volume scattering function to alter its shape with increasing turbidity, since the shape of the  $\tilde{\beta}(\theta)$  curve is determined by the intrinsic scattering properties of the particles, not by their concentration. This is why the San Diego Harbour data may reasonably be applied to much murkier water. Indeed the  $\tilde{\beta}(\theta)$  data in Table 4.2(b) are applicable to the majority of natural waters other than the very clear oceanic ones: Timofeeva (1971) has presented evidence that  $\tilde{\beta}(\theta)$  is virtually the same for most natural waters. However, in the specialized

Table 4.2 Volume scattering data for green (530 nm) light for a clear and a turbid natural water.  $\tilde{\beta}(\theta)$  = normalized volume scattering function ( $\beta(\theta)/b$ ). Cumulative scattering =  $2\pi \int_0^\theta \tilde{\beta}(\theta) \sin \theta d\theta$ . Data from Petzold (1972).  
 (a) Atlantic Ocean, Bahama Islands,  $b = 0.037 \text{ m}^{-1}$ .  
 (b) San Diego Harbour, California, USA,  $b = 1.583 \text{ m}^{-1}$ .

Angle $\theta$ ( $^\circ$ )	(a)		(b)	
	$\tilde{\beta}(\theta)$ ( $\text{sr}^{-1}$ )	Cumulative scattering $0^\circ \rightarrow \theta$	$\tilde{\beta}(\theta)$ ( $\text{sr}^{-1}$ )	Cumulative scattering $0^\circ \rightarrow \theta$
1.0	67.5	0.200	76.4	0.231
2.0	21.0	0.300	23.6	0.345
3.16	9.0	0.376	10.0	0.431
5.01	3.91	0.458	4.19	0.522
6.31	2.57	0.502	2.69	0.568
7.94	1.70	0.547	1.72	0.616
10.0	1.12	0.595	1.09	0.664
15.0	0.55	0.687	0.491	0.750
20.0	0.297	0.753	0.249	0.806
25.0	0.167	0.799	0.156	0.848
30.0	0.105	0.832	0.087	0.877
35.0	0.072	0.857	0.061	0.898
40.0	0.051	0.878	0.0434	0.916
50.0	0.0276	0.906	0.0234	0.940
60.0	0.0163	0.925	0.0136	0.956
75.0	0.0093	0.943	0.0073	0.971
90.0	0.0066	0.956	0.00457	0.981
105.0	0.0060	0.966	0.00323	0.987
120.0	0.0063	0.975	0.00276	0.992
135.0	0.0072	0.984	0.00250	0.995
150.0	0.0083	0.992	0.00259	0.997
165.0	0.0110	0.997	0.00323	0.999
180.0	0.0136	1.000	0.00392	1.000

situation of scattering being dominated by organic particles with a low refractive index, as might be the case in oceanic upwelling areas or eutrophic inland waters, a somewhat different set of  $\tilde{\beta}(\theta)$  data might be appropriate.

Since the scattering effects of water itself are the same for every location, it is sometimes considered useful to subtract the contribution of the water so as to more clearly reveal the characteristics of the scattering by particles. In such cases we may refer to  $b_p$  for the scattering coefficient, and  $\beta_p(\theta)$  for the volume scattering function, of the particulate fraction on its own.

Agrawal (2005) has used the LISST-100 particle size analyzer (see above) to measure the volume scattering function over the range  $0.1$  to  $20^\circ$  in shallow (15 m) water off the New Jersey (USA) coast. Time-averaged (one week duration) scattering phase functions were calculated for 2, 4, 6 and 8 m depth. Agreement with the Petzold phase function was fair at 2 m but less good at the other depths. These results suggest that, at least at small angles, scattering phase functions may be somewhat more variable in shape than earlier data have seemed to imply.

The contribution of density fluctuation scattering to total scattering varies not only with the type of water body but also with the angular range of scattering and wavelength of light under consideration. In the moderately or very turbid waters such as are typically found in inland, estuarine and some coastal water bodies, scattering at all angles and all visible wavelengths is predominantly due to the particles present. In contrast, in the very clear waters of the least fertile parts of the ocean, density fluctuation scattering can be a significant component of total scattering at short wavelengths and the major component at large scattering angles. In the Sargasso Sea, for example, Kullenberg (1968) found that density fluctuation scattering accounted for 3% of the total scattering coefficient at 655 nm and 11% at 460 nm. For scattering angles from  $60$ – $75$  to  $180^\circ$ , however, the greater part of the scattering at both wavelengths was due to density fluctuation: in the case of blue (460 nm) light it accounted for only 0.3% of the scattering at  $1^\circ$ , but contributed 89% at  $135^\circ$ . Because of its importance as a component of backscattering in oceanic waters, density fluctuation scattering makes a disproportionately large contribution to the upwelling light stream. Morel and Prieur (1977) pointed out that even for a water with a total scattering coefficient of  $0.29 \text{ m}^{-1}$  (rather turbid by oceanic standards), while density fluctuation scattering accounts for only 1% of the total scattering coefficient, it contributes about 33% of the backscattering. Thus, even in the not-so-clear oceanic waters, density fluctuation scattering initiates a substantial proportion of the upwelling light flux.

Compared with density fluctuation scattering by pure water itself, particle scattering is less sensitive to wavelength. Since, even in a very clear oceanic water, density fluctuation scattering makes up only a small proportion of the total scattering coefficient, the dependence of this scattering on  $\lambda^{-4.3}$  does not by itself bring about a marked variation of the value of  $b$  for natural waters with wavelength. There is, however, some evidence that in particle-dominated natural waters, the value of  $b$  varies

inversely with wavelength. For 63 stations in the Arabian Sea, Northern Gulf of Mexico and coastal North Carolina, Gould *et al.* (1999) obtained spectral scattering data over the range 412 to 715 nm, by difference between beam attenuation coefficient and absorption coefficient measurements made with an ac-9 instrument. Scattering coefficients at 412 nm ranged from 0.2 to 15.1 m<sup>-1</sup>. The value of  $b(\lambda)$  was found to decrease in an approximately linear manner with wavelength, but the slope of the spectral scattering relationship decreased progressively from high-scattering turbid waters dominated by suspended sediments to lower-scattering clear waters dominated by phytoplankton.

Using the same technique, Blondeau-Patissier *et al.* (2009) measured  $b(\lambda)$  at a number of locations in the Great Barrier Reef region (Australia), covering inshore, estuarine, lagoonal and reef waters. Scattering decreased with wavelength approximately in conformity with  $b(\lambda) \propto \lambda^{-\gamma_b}$  where the average values of  $\gamma_b$  for seven sites ranged from ~0.43 to 0.75, although highly variable at each site. In a variety of stations within the large (670 km<sup>2</sup>) and deep (av. 44 m) Lake Biwa in Japan, Belzile *et al.* (2002a) found, using the ac-9 difference method, that  $b$  decreased approximately linearly with wavelength. Expressed as a power law, the exponent  $\gamma_b$  varied from 0.50 to 1.06 (mean 0.78). For the turbid waters of Lake Taihu (China), dominated by inorganic suspended matter, Sun *et al.* (2009) found, using the ac-9 difference method, a decrease of  $b(\lambda)$  with wavelength, expressible as a power law with  $\gamma_b = 0.729$ .

By contrast, in shallow (10–30 m) inshore waters in Jervis Bay (SE Australia), Phillips and Kirk (1984) found little variation in scattering coefficient over the spectral range, 450 to 650 nm. A similar finding was made by Roesler and Zaneveld (1994) in the waters of East Sound, Washington. Also, for Case 2 (coastal) waters around Europe, Babin *et al.* (2003a) found only a slight tendency for  $b_p(\lambda)$  to decrease towards longer wavelengths. For Case 1 (oceanic, phytoplankton-dominated) waters they found a somewhat greater tendency for scattering to decrease towards longer wavelength, but the scattering spectra were clearly affected by absorption, with significant minima being evident in the main phytoplankton absorption bands in the blue and the red wavebands. For the specific scattering coefficient (scattering per unit mass) at 555 nm, average values of 1.0 and 0.5 m<sup>2</sup> g<sup>-1</sup> were found for Case 1 and Case 2 waters, respectively.<sup>51</sup>

The general behaviour of *total* scattering with respect to wavelength, as just described, can conceal somewhat different patterns of the wavelength variation of scattering at certain specific angles. When backscattering alone

is considered, then in oceanic waters, in which as we saw above density fluctuation scattering is a major contributor for  $\theta > 90^\circ$ , a more marked inverse dependence on wavelength is to be expected. In the Great Barrier Reef region (Australia, see above) Blondeau-Patissier *et al.* (2009) found that backscattering (determined directly) decreased with wavelength with an average value of the exponent,  $\gamma_{bb}$ , of  $\sim 2.0$  for the reef and open waters, but in the range  $\sim 0.65$  to  $0.95$  for the other locations (inshore, estuarine, lagoonal). For a large number of US near-shore coastal waters, Snyder *et al.* (2008) found that particulate backscattering varied inversely with wavelength, clustered around a power-law exponent of  $-0.94$ .

If the scattering particles have significant light absorption, this can affect the wavelength dependence of scattering. With increasing wavelength the real part of the refractive index undergoes a dip and then an increase as it passes through an absorption band,<sup>1395</sup> and associated with the dip there is a decrease in the scattering coefficient. In their studies on light scattering in coastal Crimean waters, Chami *et al.* (2006b) found that as the concentration of particles absorbing strongly in the blue region increased, the ratio of  $\beta_p(140^\circ)$  at 443 nm to that at 555 nm decreased from  $\sim 1.2$  to  $\sim 0.7$ .

McKee and Cunningham (2005) measured the backscattering ratio ( $b_b/b$ ) at 470 and 676 nm at 120 stations in the Irish Sea. If the shape of the scattering phase function in this oceanic region is the same at all wavelengths, then the backscattering ratio should everywhere be the same in the blue as it is in the red, i.e.  $(b_b/b)_{470}/(b_b/b)_{676}$  (which they indicated by  $B$ ) should be  $\sim 1.0$ . In fact in less than 5% of stations was this function between 0.9 and 1.1. At most stations the backscattering ratio was greater in the blue than in the red. About 53% of stations had  $B \approx 1.2$ , and the rest had greater values. Clearly, then we must expect some variation in the shape of the scattering phase function with wavelength, and the extent to which this occurs will not be the same at all points in the ocean. From the data of Petzold (1972) in Table 4.2 it can be seen that the backscattering ratio at 530 nm was 0.044 for the clear ocean water (Bahama Islands), and 0.019 for the turbid (San Diego) harbour water. In the Oslo Fjord, Aas *et al.* (2005) found, on the basis of a large number of measurements, a backscattering ratio (for the particulate fraction) of 0.018 to 0.022 for wavelengths from 412 to 665 nm. For the turbid waters of Chesapeake Bay (USA) Tzortziou *et al.* (2006) found the backscattering ratio at 530 nm to have an average value of  $0.0128 \pm 0.0032$ . For the turbid, inorganic particle-dominated, waters of Lake Taihu (China), Sun *et al.* (2009) found the backscattering ratio at 532 nm to have an average value of 0.013, but with a range of 0.005 to 0.027.

Since total light scattering in natural waters is dominated by the particulate contribution, it increases broadly in proportion to the concentration of suspended particulate matter. For example, Jones and Wills (1956), using suspensions of kaolin (which would scatter but not significantly absorb light), found a linear relation between the beam attenuation coefficient (approximately equal in this system to the scattering coefficient) for green (550 nm) light and the concentration of suspended matter. Approximately linear relations between scattering coefficient and concentration of suspended matter have been observed for natural aquatic particulates by other workers.<sup>119,1301</sup> The constant of proportionality can, however, vary from one kind of suspended matter to another:<sup>333</sup> the refractive index and the size distribution of the particles both influence the relation between  $b$  and sediment concentration.

The concentration of particulate matter, and therefore the intensity of scattering, in inland and estuarine waters, and to some extent in coastal waters, is strongly influenced, not only by the nature of the physical environment (climate, topography, soil type, etc.) but also by the uses to which the land is put. The more thickly the ground is covered with vegetation, the less erosion and so the less transference of soil particles to surface waters occurs. Erosion is very low under undisturbed forest and is generally not high from permanent grassland. Logging activities and overgrazing of pastures can cause serious erosion even in these environments. Ground that is broken up for crop planting is susceptible to erosion until such time as the crop canopy is established. The extent to which erosion occurs in these different terrestrial systems depends not only on the extent to which the ground is protected by vegetation, but also on the nature of the soil (some types being more easily eroded than others), the average slope (the greater the slope, the greater the erosion) and the intensity of the rainfall (a short torrential downpour causes more erosion than the same amount of rain falling over a longer period). The average lifetime of the soil particles in suspension once they have been transferred into the aquatic sphere is quite variable and depends on their size and mineral chemistry, and on the ionic composition of the water: some fine clay particles for example, particularly in waters of low electrolyte content, can remain in suspension for long periods with drastic consequences for light attenuation in the water bodies that contain them.

It is clear that to understand the underwater light field, we must know not only about the water itself but also about the surrounding land forms, which to a large degree confer upon the aquatic medium the particular optical properties it possesses.

#### 4.4 The scattering properties of phytoplankton

Phytoplankton cells and colonies scatter, as well as absorb, light and can make a significant contribution to the total scattering behaviour of the aquatic medium, but to an extent that varies from one species to another: this has been studied in detail, both experimentally and theoretically, by Morel, Bricaud and coworkers.<sup>160,162,943,948</sup> A convenient parameter in terms of which to compare the scattering propensities of different species is the specific scattering coefficient,  $b_c$ , which is the scattering coefficient that would be exhibited by cells of a given species suspended at a concentration corresponding to 1 mg chlorophyll  $a\text{ m}^{-3}$ ; it has the units  $\text{m}^2\text{ mg chl } a^{-1}$ . Table 4.3 lists values for

Table 4.3 *Specific scattering coefficients for phytoplankton.*

Organism	Wavelength (nm)	$b_c$ ( $\text{m}^2\text{ mg chl } a^{-1}$ )	Reference
<b>Marine</b>			
<i>Tetraselmis maculata</i>	590	0.178	948
<i>Hymenomonas elongata</i>	590	0.078	948
<i>Emiliania huxleyi</i>	590	0.587	948
<i>Platymonas suecica</i>	590	0.185	948
<i>Skeletonema costatum</i>	590	0.535	948
<i>Pavlova lutheri</i>	590	0.378	948
<i>Prymnesium parvum</i>	590	0.220	948
<i>Chaetoceros curvisetum</i>	590	0.262	948
<i>Isochrysis galbana</i>	590	0.066	948
<i>Synechocystis</i> sp.	590	0.230	943
<i>Synechococcus</i>	450	0.40	945
	550	0.30	945
	665	0.180	945
<i>Prochlorococcus</i>	450	0.04	945
	550	0.030	945
	665	0.015	945
<b>Fresh water</b>			
<i>Scenedesmus bijuga</i>	550	0.107	284
<i>Chlamydomonas</i> sp.	550	0.044	284
<i>Nostoc</i> sp.	550	0.113	284
<i>Anabaena oscillarioides</i>	550	0.139	284
<b>Natural (freshwater) populations</b>			
Irondequoit Bay, L. Ontario (USA)			
Av. mixed population	400–700	0.08	1445
Cyanobacterial bloom	400–700	0.12	1445
L. Hume, Murray R., Australia	400–700	0.11	1014
<i>Melosira granulata</i> dominant			
L. Mulwala, Murray R., Australia	400–700	0.22	1014
<i>M. granulata</i> dominant			

$b_c$  measured on laboratory cultures of a range of marine and freshwater phytoplankton species, and on some natural populations. Algae such as diatoms (*S. costatum*) and coccolithophores (*E. huxleyi*) in which a substantial proportion of the total biomass consists of mineralized cell walls, or scales, scatter more light per unit chlorophyll than, for example, naked flagellates (*I. galbana*). Also, blue-green algae with gas vacuoles scatter light much more intensely than those without.<sup>433</sup>

Like the mineral and detrital particles, which carry out the greater part of the scattering in most natural waters, algal cells have a scattering phase function that is strongly peaked at small forward angles,<sup>1308</sup> but the backscattering ratio ( $b_b/b$ , the proportion of the total scattering that is in a backwards direction,  $\theta > 90^\circ$ ) is much lower (0.0001–0.004) for the living cells<sup>162,1308</sup> than for the mineral and detrital particles ( $\sim 0.019$ ). This is a consequence<sup>162</sup> of the low refractive index (relative to water) of the living cells (1.015–1.075)<sup>7,205,943</sup> compared with that of the inorganic particles (1.15–1.20).<sup>636</sup> The backscattering ratio is greater in the small (picoplankton) cells, such as cyanobacteria, than in the larger eukaryotic cells.<sup>1308</sup>

Volten *et al.* (1998) measured the angular distribution of light scattering over the range 20 to 160° by laboratory cultures of 15 phytoplankton species and two types of estuarine sediments. In most of the phytoplankton species, scattering, which was in every case predominantly in the forward direction, declined to a minimum at  $\sim 120^\circ$  and then increased somewhat over the 120 to 160° range. Scattering by the estuarine silt samples, by contrast, remained essentially flat above 120°.

In the ocean, satellite remote sensing shows that blooms of coccolithophores (haptophyte algae with spherical cells covered with circular calcareous plates called *coccoliths*, Fig. 4.10) have a high reflectance, indicating efficient upward, and therefore backward, scattering, which might seem to contradict the generalization that phytoplankton are weak backward scatterers. As coccolithophore cells age the coccoliths become detached and it is thought that the intense upward scattering from these blooms originates mainly from the numerous detached coccoliths, rather than from the living cells themselves.<sup>579,943,65</sup> Balch *et al.* (1996a) found the backscattering ratio in the most turbid parts ( $b = 1\text{--}3\text{ m}^{-1}$ ) of a very large ( $\sim 0.5 \times 10^6\text{ km}^2$ ) bloom of *Emiliania huxleyi* in the North Atlantic to be  $\sim 0.01$  to 0.02 at 440 and 550 nm. For laboratory cultures of *E. huxleyi*, Voss *et al.* (1998) found that the backscattering coefficient varied inversely with wavelength, in accordance with  $\lambda^{-1.4}$  for coccoliths, and  $\lambda^{-1.2}$  for the cells with coccoliths attached. Calculations using anomalous diffraction theory<sup>64</sup> show that for spherical particles, calcite-specific

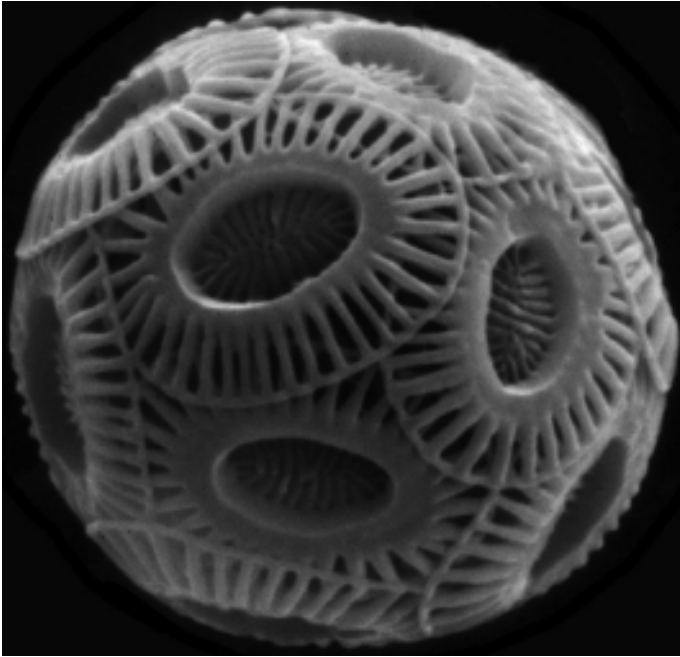


Fig. 4.10 Cell of the common coccolithophore species, *Emiliana huxleyi*, showing the attached circular calcareous plates (coccoliths), which are mainly responsible for the intense scattering properties of this phytoplankter. (Courtesy Dr Susan Blackburn, CSIRO Marine and Atmospheric Research.)

scattering ( $\text{m}^2 \text{ mg calcite C}^{-1}$ ) is at a maximum at 1 to  $3 \mu\text{m}$ , which is about the diameter of the individual coccoliths, but is much lower for spheres of the typical diameter ( $\sim 10 \mu\text{m}$ ) of the coccolithophores themselves. Using an inversion algorithm developed by Gordon and Boynton (1998), Gordon *et al.* (2009) used *in situ* radiance/irradiance profiles measured in an *E. Huxleyi* bloom off the coast of Plymouth, UK, to calculate spectral values of the backscattering coefficient of the scattering particles – predominantly detached coccoliths – present in the water. On the basis of estimates of coccolith numbers obtained by flow cytometry (see below), they calculated a backscattering cross-section (strictly speaking, the upper limit) of individual coccoliths to be  $0.123 \pm 0.039 \mu\text{m}^2/\text{coccolith}$  at 500 nm.

Figure 4.11 shows coccolithophorid blooms in the Atlantic Ocean, west of Ireland and of Cornwall, and also in the Celtic Sea, as observed by the SeaWiFS sensor from space.



Fig. 4.11 Coccolithophorid blooms in the Atlantic Ocean, west of Ireland and of Cornwall, and also in the Celtic Sea, Monday 18 May 1998. Image collected at NERC Satellite Receiving Station, Dundee, Scotland. (Courtesy of the SeaWiFS Project, NASA Goddard Space Flight Center.) See [colour plate](#).

For a single-angle scattering meter measuring backscattering at  $\sim 140^\circ$ , Vaillancourt *et al.* (2004) found the conversion factor ( $\chi(\theta)$ ) for obtaining  $b_b$  from  $\beta(\theta)$  (using  $b_b = 2\pi \chi(\theta) \beta(\theta)$ , see above) averaged 0.82 for cultures of nine phytoplankton species. This may be compared with values in the region of 1.2, which have been found for coastal sea waters.<sup>139,216</sup>

The powerful technique of flow cytometry, which makes use of light scattering from individual cells, has been adapted for the study of phytoplankton populations.<sup>7,224,809,1048,1268,1280,1485</sup> The sample fluid, e.g. ocean water, is injected coaxially into a stream of particle-free sheath fluid. The liquid passes through a capillary flow chamber which is traversed by an intense argon-ion laser beam operating typically at 488 or 514 nm. The dimensions of, and rate of flow through, the flow chamber are such that the individual cells pass through the laser beam one at a time, and as they do so they scatter the incident light, and also exhibit fluorescent emission in response to absorption of light by their

photosynthetic pigments. Light scattered forward (in the range  $1.5\text{--}19^\circ$ ) and at  $\sim 90^\circ$ , and fluorescent emission in the orange (530–590 nm) and/or red ( $>630$  nm) wavebands, are measured. Different sizes and pigment classes of phytoplankton have different combinations of scattering and fluorescence signals, and so the technique can be used for enumerating, characterizing and following the development of natural phytoplankton populations.

# 5

## Characterizing the underwater light field

Having described the nature of the incident radiation flux presented to the aquatic biosphere and the influences to which the light is subject within the water, we shall now consider the kind of light field that results. We shall begin, in this chapter, by examining the ways in which the properties of this light field are studied. The physical definitions of these properties are given in [Chapter 1](#).

### 5.1 Irradiance

#### Irradiance meters

The most frequently and easily measured property of the underwater light field is irradiance. Knowledge of this parameter is valuable, not only because it provides information about how much light is available for photosynthesis, but also because irradiance plays a central role in the theory of radiation transfer in water. An irradiance meter, since it is meant to measure the radiant flux per unit area, must respond equally to all photons that impinge upon its collector, regardless of the angle at which they do so. With any given meter this can be tested by observing the way in which its response to a parallel light stream varies with its angle to that light stream.

As the angle of the radiant flux to the collector changes, the area of the collector projected in the direction of that radiant flux changes, and the proportion of the flux intercepted by the collector changes correspondingly ([Fig. 5.1](#)). Thus, the response of an irradiance meter to parallel radiant flux (wider than the collector) should be proportional to the cosine of the angle ( $\theta$ ) between the normal to the collector surface and

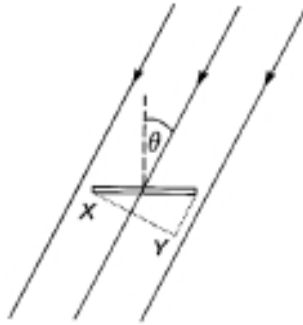


Fig. 5.1 The area that the collector presents to the beam is linearly related to  $XY$ , which is proportional to  $\cos \theta$ .

the direction of the flux. An irradiance collector that meets this criterion is known as a cosine collector. The collector of an irradiance meter usually consists of a flat disc of translucent diffusing plastic, although opal glass may be used when measurements below 400 nm are required.<sup>638</sup> It has been found that a more faithful cosine response to light incident at large values of  $\theta$  is obtained if the disc projects slightly up above the surrounding housing, allowing some collection of light through the edge.<sup>1238</sup> Some of the light that penetrates into the diffusing plastic is scattered backwards and a part of this succeeds in passing up through the diffuser surface again. Because the difference between the refractive indices of plastic and water is less than that between those of plastic and air, there is less internal reflection of this light within the collector and therefore a greater loss of light when the collector is immersed in water than when it is in air: this is known as the immersion effect. To take account of this, if an irradiance meter has been calibrated in air, the underwater readings should be multiplied by the appropriate correction factor for that instrument. This factor is usually in the region of 1.3 to 1.4 in the case of a plastic collector.

Within the irradiance sensor, beneath the collecting disc, there is a photoelectric detector: a silicon photodiode, which has a broad spectral response, is commonly used. If a very narrow waveband of light is measured, as in certain spectroradiometers (see below), then a photomultiplier may be used as the detector to provide the necessary sensitivity. The electrical signal from the photodetector is transmitted by cable to the boat where, after amplification if required, it is displayed on a suitable meter or digital readout.

In all natural waters most of the light at any depth is travelling in a downwards direction. Measurement of the irradiance of the upwelling

flux is nevertheless worthwhile. This is partly because, in some waters, upwelling flux is a significant component (up to  $\sim 20\%$ ) of the total available radiant energy, but even more so because the ratio of upwelling to downwelling flux (irradiance reflectance,  $R = E_u/E_d$ ) can provide information about the inherent optical properties of the water (see §§4.2, 6.4) and because the properties of the upwelling flux are of central importance to the remote sensing of the composition of natural waters. Thus, the more we know about this flux and its relation to other characteristics of the medium the better.

The holder in which the sensor is lowered into the water (Fig. 5.2) should thus be made so that the sensor can be facing upwards to measure downwards irradiance ( $E_d$ ), or downwards to measure upward irradiance  $E_u$ . To minimize shading effects, the sensor is always lowered on the sunny side of the boat. For measurements in rivers, the sensor must be attached to a rigid support.

Measurements made with an uncorrected wide-band detector are unreliable because of the spectral variation of sensitivity: part of the diminution of irradiance with depth could be due to a shift of the wavelength of the predominating light to a part of the spectrum where the detector is less sensitive. It is therefore desirable to confine the measured light to a specific waveband with an appropriate filter in the sensor: narrow-band interference filters are best for this purpose. The alternative, and in the context of photosynthesis the best, solution (short of determining the complete spectral distribution of irradiance), is to use a meter designed to respond equally to all quanta within the photosynthetic range regardless of wavelength, but to be insensitive to quanta outside this range. In this way a measure of the total photosynthetically available radiation (PAR) is obtained.

It is better that the meter should be designed to respond equally to quanta regardless of wavelength rather than to respond equally to a given amount of radiant energy regardless of wavelength, because the usefulness of the prevailing light for photosynthesis is more closely related to the flux of quanta than to the flux of energy. This is because once a quantum has been absorbed by a cell, it makes the same contribution to photosynthesis regardless of its wavelength (see §3.1), although the probability of its being absorbed in the first place does, of course, vary with wavelength. An absorbed red quantum, for example, is just as useful as an absorbed blue quantum even though it may contain only two thirds of the energy.

An irradiance meter designed in this way is commonly referred to as a quanta meter. Since no existing photodetector in its normal state

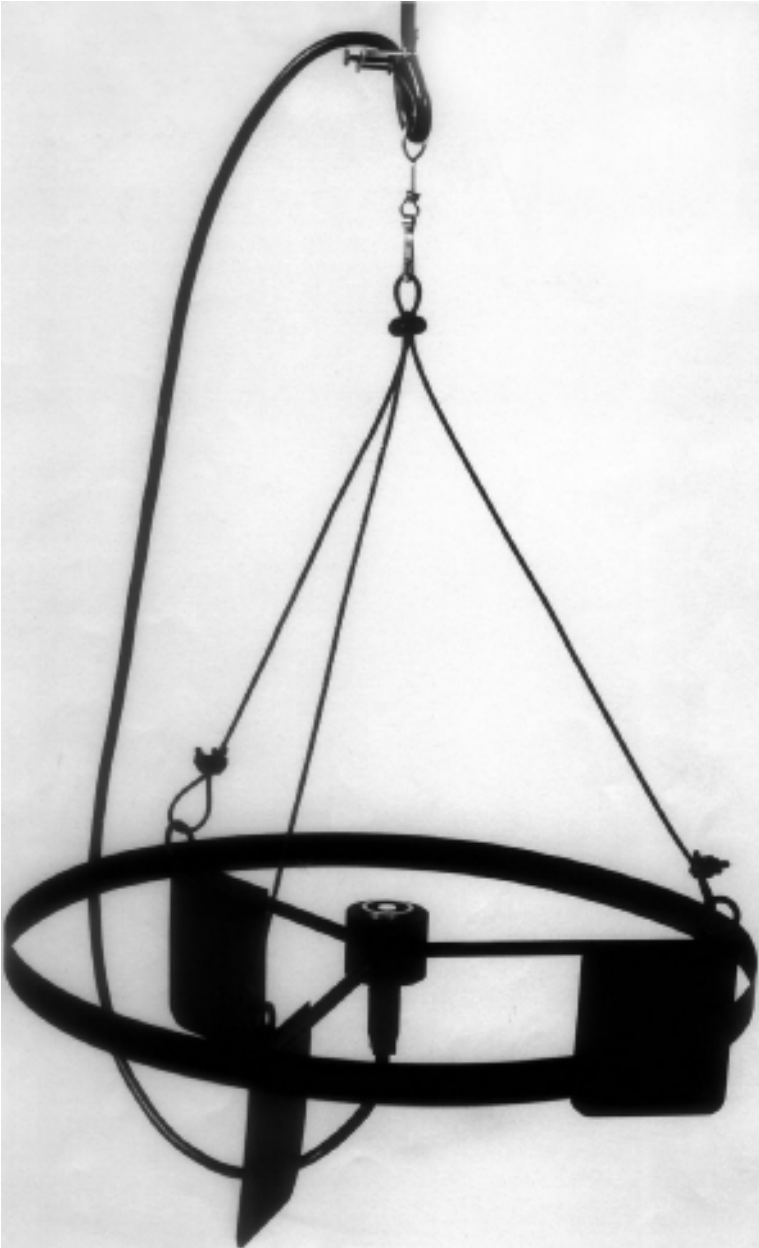


Fig. 5.2 Submersible irradiance sensor (Li-Cor 192S Underwater Quantum Sensor: Li-Cor Inc., Lincoln, Nebraska, USA) in a lowering frame. The sensor can be placed in the frame facing upwards or downwards.

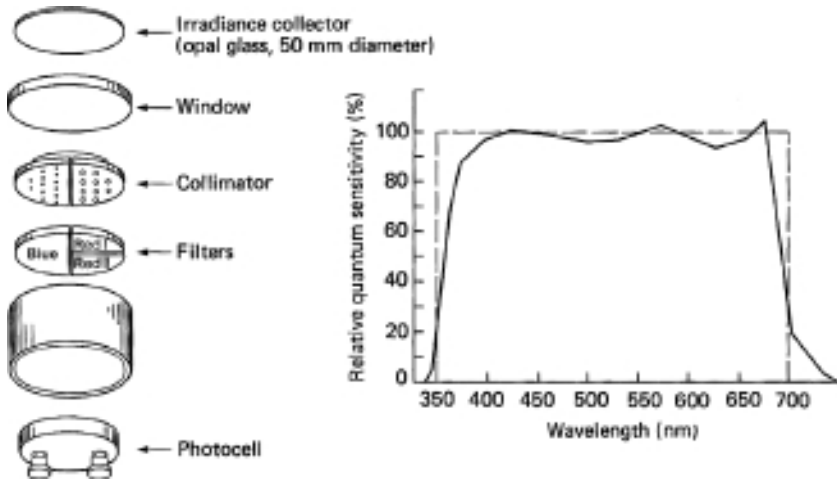


Fig. 5.3 Exploded view of a quanta meter together with its quantum sensitivity curve (after Jerlov and Nygard, 1969).

responds equally to all quanta throughout the photosynthetic range, ways of adjusting the relative response in different parts of the spectrum must be found. Jerlov and Nygard (1969) used a combination of three colour filters, each covering a different part of the photodetector (Fig. 5.3). The filters were covered with an opaque disc with a number of small holes drilled in it: the number, size and position of these holes determined the amount of light reaching each filter. By a suitable combination of this variable attenuation with the differing absorption properties of the filters it was possible to obtain an approximately constant quantum sensitivity throughout the photosynthetic range. Commercial instruments using filter combinations with a silicon photodiode, and measuring the total quantum flux in the range 400 to 700 nm, are readily available.

The photosynthetically available radiation at any depth can be measured with a submersible quanta meter. Smith (1968) suggested that the vertical attenuation coefficient for downwards irradiance of PAR is the best single parameter by means of which different water bodies may be characterized with respect to the availability of photosynthetically useful radiant energy within them. As we shall see in the next chapter,  $K_d$  for PAR is not exactly constant with depth even in a homogeneous water body. Nevertheless the variation is not great and knowledge of, say, the average value of  $K_d(\text{PAR})$  over a certain depth range such as the euphotic depth, is very useful. It is determined by measuring downwelling PAR at a

series of depths within the depth interval of interest and making use of the approximate relation (see §§ 6.1, 6.3)

$$\ln E_d(z) = -K_d z + \ln E_d(0) \quad (5.1)$$

where  $E_d(z)$  and  $E_d(0)$  are the values of downward irradiance at  $z$  m and just below the surface, respectively. The linear regression coefficient of  $\ln E_d(z)$  with respect to depth gives the value of  $K_d$ . Or, less accurately,  $K_d$  may be determined from measurements at just two depths,  $z_1$  and  $z_2$

$$K_d = \frac{1}{z_2 - z_1} \ln \frac{E_d(z_1)}{E_d(z_2)} \quad (5.2)$$

Equations 5.1 and 5.2 can also be used to obtain  $K_d(\lambda)$ , the vertical attenuation for downward irradiance in a narrow waveband centred on  $\lambda$ , when vertical profiles of irradiance have been measured with a spectroradiometer (see below), or a radiometer with a narrow-band interference filter.

To determine the *irradiance-weighted vertical attenuation coefficient*,  ${}^wK(av)$ , (§1.3) we use the irradiance data (downward, upward, net or scalar, as appropriate) for a series of depths at equal intervals down to a depth below which the remaining radiation is a trivial proportion of the total in the water column. For  $N$  depth intervals

$${}^wK(av) = \frac{\sum_{i=1}^N K(z_i, z_{i+2}) E(z_{i+1})}{\sum_{i=1}^N E(z_{i+1})} \quad (5.3)$$

To achieve adequate smoothing of the data, each  $K(z)$  value is calculated from

$$K(z_i, z_{i+2}) = \frac{1}{2\Delta z} \ln \frac{E(z_i)}{E(z_{i+2})} \quad (5.4)$$

i.e. from the diminution in irradiance over two depth intervals. Each  $K(z_i, z_{i+2})$  is then multiplied by  $E(z_{i+1})$ , the irradiance in the depth interval in between, in the numerator of eqn 5.3.

### Measurement problems in the field

There are three main sources of error in the measurement of underwater irradiance in the field: wave action, fluctuations in surface-incident flux due to drifting clouds and perturbation of the light field by the ship. The

convex part of a surface wave acts as a converging lens and will focus the incident light at some depth within the water. As the wave moves along, so this zone of intense light travels with it. This is essentially the same phenomenon as that which produces the well-known moving patterns of bright lines to be seen on the bottom of a swimming pool on a sunny day. A stationary upward-pointing irradiance meter will be subjected to a series of intense pulses of radiation of duration typically of the order of some milliseconds as the waves move past overhead. There are, in addition, rapid negative fluctuations in irradiance caused by the de-focusing effect of the concave part of the wave.

An irradiance meter traversing a series of depths will also be subject to these rapid temporal fluctuations in intensity. Dera and Gordon (1968) showed that the average fractional fluctuation in irradiance for a given surface wave field increased with depth to a maximum and then decreased, eventually to insignificant levels. For example, at a shallow coastal site, where  $K_d(525\text{ nm})$  was  $0.59\text{ m}^{-1}$ , the average fractional fluctuation in  $E_d(525\text{ nm})$  rose to a maximum value of  $\sim 67\%$  at about 0.5 m depth, and then decreased progressively with depth, falling to  $\sim 5\%$  at about 3 m. It was found that the clearer the water, the greater the depth at which significant rapid temporal fluctuation could be detected. The upwelling light field, by contrast, is hardly at all affected by this wave-focusing phenomenon. At the above site, for example, the average fractional fluctuation in  $E_u$  was only  $\sim 5\%$  over the whole depth range. On the basis of a long-term series of measurements at a deep-sea mooring in the Mediterranean Sea, Gernez and Antoine (2009) found that the conditions for maximum fluctuations in downward irradiance (510 nm) at 4 m depth under clear skies are for wave heights of  $\sim 0.5\text{ m}$ , or wind speeds between  $\sim 1$  and  $5\text{ m s}^{-1}$ . Fluctuations under clear skies are reduced for wave heights greater than  $\sim 1.5\text{ m}$  or wind speeds in excess of  $\sim 7\text{ m s}^{-1}$ .

To extract good values for the vertical attenuation coefficient, some kind of smoothing of the data must be carried out. At its simplest, in the case of a manual instrument with a meter readout, the operator can concentrate on taking observations at any given depth, only between the 'blips'. Alternatively, a simple electronic damping circuit can be used to smooth out the fluctuations.<sup>287,699</sup> In the case of sophisticated rapid-profiling instruments, which continuously record irradiance, complete with all the wave-induced rapid fluctuations, as they descend,<sup>1249</sup> a variety of mathematical smoothing procedures can subsequently be applied to the stored data.<sup>1246</sup>

Fluctuations in the light field due to clouds differ from those due to waves first in that they are much slower, and second in that their effects

are manifest throughout the whole illuminated water column and affect the upwelling and downwelling light streams to the same extent. The procedure most commonly used to overcome this problem is to monitor the incident solar flux continuously with a reference irradiance meter on deck, and use the data so obtained to adjust (for purposes of determining vertical attenuation coefficients, or reflectance) the concurrently obtained underwater irradiance values as appropriate. Davies-Colley *et al.* (1984) found that a more satisfactory (less variable) correction for changing ambient light was achieved if the reference meter were placed within the water at some fixed depth, preferably the one at which irradiance was reduced to 10 to 20% of the surface value.

Computer modelling of the light field<sup>476</sup> indicates that the third problem perturbation of the field – by the ship – is relatively unimportant for measurements of downward irradiance made on the sunny side of the vessel under clear skies, but that errors under overcast conditions can be significant, and measurements of upward irradiance are strongly influenced by the ship's presence under either type of illumination. To solve this problem, techniques have been developed for deploying the instrument at some distance from the ship.<sup>1443</sup> Since the seriousness of the problem is a function of the size of the boat, it is of more significance for oceanographers than for limnologists. Calculations by Gordon and Ding (1992) show that in measurement of the upward irradiance (or radiance), self-shading by the instrument itself can cause significant error. The error is greatest in strongly absorbing waters, and under vertical Sun, and increases with the diameter of the instrument and the absorption coefficient of the water.

A measurement problem of a different nature to those discussed above is that of obtaining a representative set of measurements within a realistic time period when, as is invariably the case in the sea, the area of interest is very large. To address this problem, Aiken (1981,1985) and Aiken and Bellan (1990) have developed the undulating oceanographic recorder, an instrument platform which is towed 200 to 500 m behind the ship. It is designed to follow an undulating trajectory within the water: for example, when towed at 4 to 6 m s<sup>-1</sup> (8–12 knots) it moves between near-surface depths and ~70 m with an undulation pitch length of ~1.6 km. The platform is fitted with a suite of sensors measuring a range of oceanographic parameters, including downwelling and upwelling light in a number of wavebands across the photosynthetic range. The distance from the towing vessel is such that ship shadow and wake problems are eliminated. The data can be logged at, for example, 10-s intervals for

durations of 11 h, so that essentially continuous information over long stretches of ocean can be accumulated.

Another approach to the problem of collecting optical data over large areas of ocean is to use autonomous underwater vehicles (AUVs), which have the capability to traverse substantial distances and depth intervals, in a pre-programmed manner. An example is the Seaglider, developed by Eriksen *et al.* (2001) at the University of Washington. This is a slim, low drag, light-weight (52 kg), 1.8 m long vehicle with internal mechanisms and circuitry housed within a pressure hull enclosed by a fibreglass fairing to which wings, a rudder and a trailing antenna are attached. Propulsion is achieved by buoyancy control effected by variation of vehicle-displaced volume. This involves pumping hydraulic oil from an internal to an external reservoir, or letting it flow back, as required. As the vehicle sinks or rises, the wings provide hydrodynamic lift to propel the vehicle forward. It can operate down to a depth of 1000 m. Data can be collected from onboard instruments both as the Seaglider dives and as it rises again to the surface. At the surface, the Seaglider dips its nose to raise its antenna out of the water. It then determines its position using Global Positioning System (GPS), uploads its oceanographic data to the Iridium data telemetry satellite and then downloads a file with any new instructions that may be necessary. While to date this vehicle does not seem to have been fitted with instruments for measuring the underwater light field, this would presumably be possible. Perry *et al.* (2008) have carried out measurements with a Seaglider equipped to record chlorophyll *a* fluorescence and the water backscattering coefficient. The vehicle carried out V-shaped transects, approximately 450 km long, off the coast of Washington State, USA. Each transect took ~30 days with three dives per day, with 5-km spacing between dives.

Wijesekera *et al.* (2005) used an AUV fitted both with a multispectral irradiance meter, operating in seven wavebands, an ac-9 nine-channel optical spectrometer for measuring absorption and beam attenuation coefficients and a scattering sensor. The AUV was used to follow cross-shelf transects extending from 4.34 to 18.47 km from the Oregon coast at depth of 2, 4, 6, 8 and 10 m.

There has been in recent years a major increase in the deployment of unattended instruments *in situ* for prolonged periods to carry out long-term monitoring of the underwater light field or of optical properties of the water. All such instruments are subject to the problem of *biofouling*, the formation of layers of algae, and eventually invertebrate animals, on optical windows. Depending on the environment this can become serious

in as little as a week, and should certainly be expected within about two weeks if no countermeasures are taken. We saw earlier (§3.2) that automatic periodic injection of bromine proved effective to keep a moored absorption meter clear. Wiping mechanisms have been used.<sup>1126</sup> The HydroRad spectroradiometer (see below) is available in a version with a copper anti-fouling shutter that automatically protects the light collector from biofouling between readings.

### Secchi depth

A crude visual method of estimating  $K_d$ , commonly used before the ready availability of photoelectric instruments but not used today, is based on the device known as the Secchi disc. A white disc, of diameter 20 to 30 cm, is lowered into the water and the depth at which it just disappears from view is noted. This is referred to as the *Secchi disc transparency*, or as the *Secchi depth*,  $Z_{SD}$ . On the basis of their measurements in marine waters, Poole and Atkins (1929) made the empirical observation that the Secchi depth is approximately inversely proportional to the vertical attenuation coefficient for downwelling irradiance and pointed out that  $Z_{SD}$  could therefore be used to estimate  $K_d$ : the value obtained will be that applicable to a rather broad waveband corresponding roughly to the spectral sensitivity curve of the human eye. To calculate  $K_d$  the relation  $K_d = 1.44 / Z_{SD}$  may be used.<sup>580</sup>

Using the contrast transmittance theory of Duntley and Preisendorfer, Tyler (1968) concluded that the reciprocal of the Secchi depth is proportional to  $(c + K_d)$ , the sum of the beam attenuation and vertical attenuation coefficients, rather than to  $K_d$  alone. On theoretical grounds, Tyler arrived at the relation  $(c + K_d) = 8.69 / Z_{SD}$ ; from measurements in turbid coastal sea water, Holmes (1970) obtained  $(c + K_d) = 9.42 / Z_{SD}$ . For a number of New Zealand lakes covering a wide range of optical properties, Vant and Davies-Colley (1984, 1988) have also found an approximately linear relationship between the reciprocal of Secchi depth and  $(c + K_d)$ .

Since, in natural waters,  $c$  is usually substantially greater than  $K_d$ , the Secchi depth is determined more by  $c$  than by  $K_d$ . Within some waters, for example in much of the ocean, variations in attenuation and transparency are predominantly due to changes in one component of the system, such as the phytoplankton. As a consequence,  $K_d$  and  $c$  will tend roughly to covary, and this will account for the approximate constancy of the inverse relationship between  $Z_{SD}$  and  $K_d$  that is sometimes observed in such cases. A priori considerations suggest, however, that use of the Secchi disc could

sometimes give highly inaccurate values for  $K_d$ . If, for example, as a consequence of increased levels of particles, light scattering in a water body increased much more than absorption, then  $c$  would increase much more than  $K_d$  and use of the relation  $K_d = 1.44 / Z_{SD}$  would overestimate  $K_d$ . There is, in fact, now ample field evidence that the product,  $K_d Z_{SD}$ , is very far from constant, especially in inland waters: it has been found to vary as much as five-fold in New Zealand lakes,<sup>286</sup> and seven-fold in Alaskan lakes.<sup>736</sup> In agreement with theory, Secchi depth is particularly sensitive to turbidity.

A comprehensive account of the physical and physiological basis of the Secchi disc procedure was given by Preisendorfer (1986a, b), and the subject has also been reviewed by Højerslev (1986). Preisendorfer concluded that the primary function of the Secchi disc, and indeed its only legitimate *raison d'être*, is to provide a simple visual index of water clarity in terms of  $Z_{SD}$ , or the inferred quantity  $(c + K_d)$  (which is  $\sim 9/Z_{SD}$ , and which could reasonably be referred to as the *contrast attenuation coefficient*<sup>707,1403</sup>). In the same vein, Davies-Colley and Vant (1988), on the basis of their own extensive studies on the relationship between Secchi depths and other optical properties in 27 New Zealand lakes, propose that this device should be recognized as measuring image attenuation, as distinct from diffuse light attenuation.

## 5.2 Scalar irradiance

Although some multicellular aquatic plants have their photosynthetic tissue so arranged as to achieve maximum interception of light incident from above, to the randomly oriented cells of the phytoplankton all light, from whatever direction it comes, is equally useful. Scalar irradiance  $E_0$ , as we saw earlier (§1.3), is defined as the integral of radiance distribution at a point over all directions about the point: it is equivalent to the total radiant flux per  $m^2$  from all directions at a given point in the medium. In the context of photosynthesis, information on the scalar irradiance is therefore somewhat to be preferred to data on irradiance.

The technology of measurement of scalar irradiance is essentially the same as that of irradiance with the exception of the collector. Since this must respond equally to light from all directions, it has to be spherical. [Figure 5.4](#) illustrates the principles involved in collectors used for scalar irradiance and for its downwelling and upwelling components. Like the collector of a normal irradiance meter, the spherical collector is made of

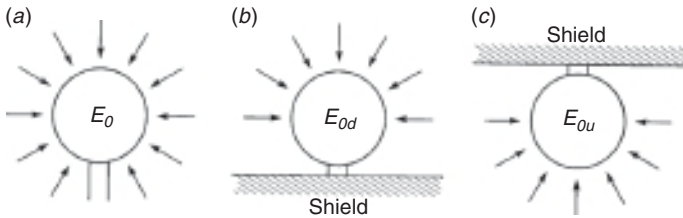


Fig. 5.4 Principles involved in collection of light for determination of (a) scalar irradiance, (b) downward scalar irradiance and (c) upward scalar irradiance. In the cases of downward and upward scalar irradiance, the collector must have a shield wide enough relative to the collector to ensure that very little upward and downward light, respectively, reaches the collector.

diffusing plastic or opal glass so that it collects all incident photons with equal efficiency, regardless of the angle at which they encounter its surface. The light that penetrates the spherical collector can be transmitted to the photodetector via another, flat collector in the bottom of the sphere<sup>570</sup> or, in the case of a solid diffusing sphere, can be transmitted from the centre of the sphere by a fibre-optic bundle or quartz light-conducting rod.<sup>133</sup> Scalar irradiance meters can use a filter to confine the measured light to a narrow waveband,<sup>570</sup> or can be designed as quanta meters covering the whole (400–700 nm) photosynthetic range.<sup>133,1282</sup>

Figure 5.5 shows two commercial quantum (PAR) scalar sensors.

Karelin and Pelevin (1970) developed a meter with three collectors: upward and downward irradiance collectors and a spherical collector for scalar irradiance. Any one of five colour filters could, by remote control, be placed in front of the photodetector. From measurements of  $\vec{E}$  above and below a given depth,  $K_E$ , the vertical attenuation coefficient for net downward irradiance is obtained. The absorption coefficient is then calculated from  $a = K_E \vec{E} / E_0$  (§1.7) using the values of  $\vec{E}$  and  $E_0$  at the depth in question. The data obtained with this meter were used to determine the absorption coefficients of the medium, as well as to characterize the underwater light field.

### 5.3 Spectral distribution of irradiance

Any photon with wavelength from 400 to 700 nm is in principle *available* for photosynthesis; however, the probability of a given photon being captured by the photosynthetic biomass within a water body will vary markedly with wavelength in accordance with the absorption spectrum of

(a)



(b)



Fig. 5.5 Submersible scalar irradiance sensors. (a) Li-Cor Spherical Quantum Sensor LI-193SB, in lowering frame (Li-Cor Inc., Lincoln, Nebraska, USA). (b) Biospherical Quantum Scalar Irradiance Sensor QSP-200, in lowering frame (courtesy of Biospherical Instruments Inc., San Diego, California, USA).

the array of photosynthetic pigments present. It is quite possible for two different light fields to have the same irradiance for PAR but, because of their differing spectral distributions, to differ significantly in their usefulness to a particular type of alga. Thus, a better assessment of the value of a particular light field for photosynthesis can be made if the way in which irradiance or scalar irradiance varies across the spectrum is known. An instrument that measures this is known as a spectroradiometer. A spectroradiometer is an irradiance or scalar irradiance meter in which a variable monochromator, typically a diffraction grating,<sup>79,1386</sup> is interposed between the collector and the photodetector, and such instruments are commercially available. To achieve monochromaticity the spectrum can be dispersed onto a silicon photodiode array, as in the Satlantic HyperOCR instrument<sup>606</sup> or onto the pixels of a charge-coupled device (CCD) as in the HOBI Labs HydroRad-E1.<sup>605</sup> The typical spectral range of such instruments is 300 to 800 or 850 nm.

A highly specialized spectroradiometer has been developed<sup>772,754,755</sup> for measuring scalar irradiance at a very fine vertical scale within microbenthic communities such as microbial mats or coastal sediments. This has a 70  $\mu\text{m}$  diffusing sphere attached to the tip of an optical fibre (125  $\mu\text{m}$  diameter, tapered to 15–20  $\mu\text{m}$  diameter, and coated with opaque enamel<sup>772</sup>). Light from the fibre-optic microprobe is focused onto the entrance slit of a spectrograph, within which a diffraction grating disperses the light (400–880, or 440–920 nm) over a diode array (1024 photodiodes). In another version of this instrument the light probe is an untapered 125  $\mu\text{m}$  fibre with a flat-cut end.<sup>754,755</sup> This acts as a spectral radiance meter with an acceptance half-angle in water of 8.6°. A microprobe for approximate measurements of scalar irradiance of PAR (isolated with a broad-band filter, 420–730 nm) within microbial mats has also been developed.<sup>312</sup>

As we shall discuss later (Chapter 7), in the context of remote sensing, the ratio of nadir radiance,  $L_u$  (the radiance of upwelling light in an angular interval centred on the vertical), to the downward irradiance,  $E_d$ , is of particular significance. The Biospherical PRR-800 Profiling Reflectance Radiometer is an underwater spectroradiometer that measures both quantities simultaneously in 15 wavebands (selectable within the range 305 to 875 nm) achieved with interference filters. To collect reflectance data over large areas of ocean, Robinson *et al.* (1995b) have developed an instrument – the *Lightfish* – which measures near-surface irradiance reflectance simultaneously in six wavebands (410, 443, 490, 520, 550, 670 nm; nominally 20 nm wide) while it is towed from a research vessel at a depth of a few metres. The irradiance sensors are mounted with

six on the upper, and six on the lower, surface of a cylinder which, to minimize the self-shading problem (see below), has a diameter of only 63.5 mm. The appropriate sampling period depends on the speed of the vessel: at 9 knots, for example, a 10 s interval was adopted.

As a result of the world-wide depletion of stratospheric ozone, and the development of a hole in the ozone layer over Antarctica, there is greatly increased interest in the penetration of ultraviolet radiation into the sea, but this is difficult to measure both because of the low levels of energy in the UV under water, and of the very rapid change of irradiance with wavelength in this spectral region. To specifically address this problem, Smith *et al.* (1992) developed an underwater spectroradiometer that measures irradiance from 250 to 350 nm with 0.2 nm resolution, and from 350 to 700 nm with 0.8 nm resolution. A commercially available underwater radiometer, designed for the UV region, measures irradiance in six wavebands from 305 to 395 nm, using interference filters with 10 nm FWHM.<sup>1095</sup>

## 5.4 Radiance distribution

To understand fully the underwater light field we need a detailed knowledge of the angular distribution of radiant flux at all depths. Some information on the angular structure of the field can be derived from the measurements of irradiance discussed above. Irradiance reflectance ( $R = E_u/E_d$ ) is a crude measure of angular structure. More information is contained in the three average cosines:  $\bar{\mu}$  for the total light field,  $\bar{\mu}_d$  for the downwelling stream and  $\bar{\mu}_u$  for the upwelling stream, all of which can be derived from irradiance and scalar irradiance values

$$\bar{\mu} = \vec{E}/E_o, \bar{\mu}_d = E_d/E_{od}, \bar{\mu}_u = E_u/E_{ou}$$

For a complete description, however, we need the value of radiance at all vertical and azimuthal angles, i.e. the radiance distribution. Radiance is a measure of the radiant intensity (per unit projected area) in a specified direction at a particular point in the field, and so should be measured with a meter that can be oriented in that direction and that ideally should have an infinitesimally small acceptance angle. In reality, to ensure that the meter collects enough light to measure with reasonable accuracy, particularly in the dim light fields existing at greater depths, acceptance angles of 4 to 7° may be used. The simplest type of radiance meter is known as a

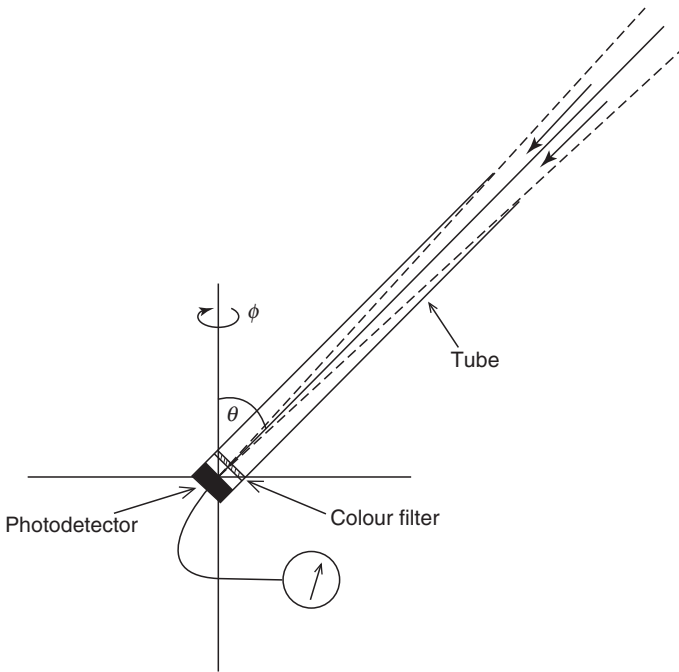


Fig. 5.6 Schematic diagram of a radiance meter.

Gershun tube photometer, after the Russian physicist Gershun, who made notable contributions to our understanding of the structure of light fields in the 1930s. It uses a cylindrical tube to limit the acceptance angle; the photodetector, with a filter in front of it, is at the bottom (Fig. 5.6). To achieve the necessary sensitivity, a photomultiplier would normally be used as the detector.

The most difficult problem encountered in the measurement of underwater radiance is that of accurately controlling the zenith and azimuth angle of the photometer tube: quite complex systems involving built-in compasses, servo mechanisms and propellers to rotate the instrument are required.<sup>636,1172,1380</sup> Another problem is that to determine a complete radiance distribution with a radiance meter is likely to take quite a long time, during which the position of the Sun will change. For example, if radiance is measured at intervals of  $10^\circ$  for the zenith angle ( $0-180^\circ$ ) and  $20^\circ$  for the azimuth angle ( $0-180^\circ$  is sufficient, the distribution being symmetrical about the plane of the Sun) then 190 separate values must be recorded. Smith, Austin and Tyler (1970) developed a photographic technique by means of which radiance distribution data can be recorded

quickly. Their instrument consists of two cameras placed back to back, each equipped with a  $180^\circ$ -field-of-view lens. One camera photographs the upper and the other photographs the lower hemisphere. By densitometry of the film, the relative radiance values over all zenith and azimuth angles can be determined at whatever degree of resolution is required, at a later time. In a further refinement of the same principle, Voss (1989) developed an electro-optic radiance distribution camera system, in which the radiance distribution is recorded, not on film, but with a  $260 \times 253$  pixel electro-optic charge injection device.

Of particular interest in the context of remote sensing of the ocean is the *nadir radiance*. This is the upward radiance ( $L_u$ ) in a small angular interval centred around the vertical, i.e. it is the radiance measured by a radiance meter pointing vertically downward. As noted earlier in the case of irradiance, self-shading by the instrument itself can cause errors. On the basis of Monte Carlo modelling, Gordon and Ding (1992) found that for direct sunlight with the refracted solar beam at a solar zenith angle of  $\theta_w$ , the proportionate error in  $L_u$ , defined by

$$\varepsilon = \frac{L_u^{\text{true}} - L_u^{\text{measured}}}{L_u^{\text{true}}} \quad (5.5)$$

is a function of the product of the absorption coefficient ( $a$ ) and the radius ( $R$ ) of the instrument in accordance with

$$\varepsilon \approx 1 - e^{-kaR} \quad (5.6)$$

where  $k = 2/\tan \theta_w$ . A relationship of the same general form, but with a different  $k$ , is obtained for that part of the incident flux contributed by skylight. Field data obtained with radiometers of varying diameter by Zibordi and Ferrari (1995) in the Lago di Varese (Italy) are in good agreement with the Gordon and Ding predictions, and errors can range from a few per cent to several tens of per cent. Aas and Korsbø (1997) found the relative self-shading error for an instrument radius of 7.5 cm to be in the range 0.04 to 0.18 in average optical conditions in the Oslofjord (Norway).

## 5.5 Modelling the underwater light field

The nature of the underwater light field resulting from a given incident light field is determined by the inherent optical properties of the aquatic medium. In principle, therefore, it should be possible, if we know the

inherent optical properties, to calculate the properties of the underwater light field. Such a calculation procedure could be used, for example, to explore in more detail than would be practicable by measurement, the exact way in which the nature of the light field depends on the inherent optical properties. It could be used as a substitute for *in situ* measurement in environments in which such measurement might be difficult. It could also be used for predicting the effects on the underwater light field of anticipated changes in the optical properties of the water, resulting perhaps from the activities of man, such as, for example, the discharge of wastewater into a water body.

In reality, the complex behaviour of the photon population in the water caused by the combined effects of scattering and absorption precludes the establishment of an explicit analytical relation between the properties of the field and those of the medium. There are, however, computer modelling procedures by means of which it is possible, by making physically realistic assumptions about the ways in which the behaviour of light at any point in a water body is determined by the scattering and absorption properties of the medium, to calculate the nature of the light field that will be set up throughout the whole water column.

The simplest calculation procedure, and the one that has been used most, is the Monte Carlo method. Its application to the behaviour of solar photons in the ocean was pioneered by Plass and Kattawar (1972), and it has also been put to extensive use by Gordon and coworkers.<sup>477,484</sup> The principles are described in some detail in Kirk (2004). A brief account of the principle of the method will be given here.

The behaviour of individual photons within a scattering/absorbing medium is stochastic in nature. The lifetime of, and the geometrical path followed by, any given photon are governed by its random encounters with absorbing molecules or algal cells and with scattering particles. The inherent optical properties of the medium – the absorption and scattering coefficients, the volume scattering function – are not only (in accordance with their definitions) measures of the proportion of an incident flux absorbed, scattered and so on per unit depth by a thin layer of medium, but are also related in simple ways to the probability that any given photon will, within a certain distance, be absorbed, scattered or scattered at a certain angle.

The Monte Carlo method takes advantage of the statistical nature of photon behaviour and uses a computer to follow the fate of a large number of photons, one at a time, passing into an imaginary body of water (corresponding, if desired, to some real body of water) with

specified optical properties. Random numbers are used in conjunction with appropriate cumulative frequency distributions (based on the optical properties) to choose pathlengths between each interaction with the medium, to decide whether the interaction is one of scattering or absorption, to select the scattering angle and so on. Photons are introduced from above the surface, at an angle or a selection of angles appropriate for the lighting conditions (direct Sun, overcast sky, etc.) under consideration. Refraction at the surface is allowed for. If it is wished to take account of waves, then the surface slope/wind frequency distribution data of Cox and Munk (1954) can be used. Each photon is followed, its trajectory being recalculated after each scattering event until it is absorbed or scattered up through the surface again. Within the imaginary water body there is a series of depth markers. For every single trajectory of each photon the computer records which depth markers the photon passes, in what direction (upwards or downwards) and at what angle. When a large number (say  $10^7$ ) of photons has been processed, the computer can calculate from the accumulated data the values at each depth of irradiance and scalar irradiance (upwards and downwards), reflectance, average cosines (downwards, upward, total) and radiance distribution (at a set of azimuth angles or averaged over all azimuth angles). In this way a complete description of the underwater light field is obtained.

It will very often be the case that something much less than a complete description of the light field is required: perhaps just the vertical attenuation coefficient for irradiance in the photosynthetic waveband ( $K_d[\text{PAR}]$ ), or the subsurface reflectance ( $R[0,\lambda]$ ) in certain wavebands, or the visual clarity of the water body expressed in terms of the Secchi depth  $Z_{SD}$ . In such cases, rather than carrying out the full computer simulation, much simpler calculations can be carried out using certain empirical relationships – expressing  $K_d$ , or  $R$ , or  $Z_{SD}$  as approximate functions of the inherent optical properties – that have arisen out of computer simulation of the light field in waters of various optical types (see §6.7).

Mobley (1989, 1994) has developed an alternative numerical modelling procedure for simulating the underwater light field, which uses invariant imbedding techniques to solve the radiative transfer equation. This is computationally quicker than the Monte Carlo method and is available commercially in the *Hydrolight* software package.

As we noted above, one of the practical applications of modelling of the underwater light field is the prediction of the effects of discharge of

wastewater on the optical character of the receiving water body.<sup>709,711</sup> Laboratory measurements of absorption and scattering on the wastewater and the receiving water, together with data on anticipated dilution rates, will make it possible to calculate the values of  $a$  and  $b$  in the water body before and after discharge of the wastewater. With this information, together with an appropriate scattering phase function, the light field that would exist (under some standard meteorological conditions) in the water body with and without the added wastewater can be calculated by Monte Carlo modelling. Alternatively, if it is only certain aspects of the field, such as  $K_d[\text{PAR}]$ ,  $R[0,\lambda]$  or  $Z_{SD}$ , which are required, the empirical relationships referred to above may be used. In this way an industrial water user, for example, can assess what effect its effluent will have on certain key indicators of optical water quality in a surface water body, before that effluent is ever discharged.

## 6

# The nature of the underwater light field

Having in earlier chapters considered the nature of the solar radiation flux incident on the surface of the aquatic ecosystem, and the influences to which the light is subject once it enters the water, we shall now discuss the kind of underwater light field that results.

### 6.1 Downward irradiance – monochromatic

As a result of absorption and scattering of the solar flux, the downward irradiance,  $E_d$ , of the light field diminishes with depth. In Fig. 6.1,  $E_d$  for greenish-yellow light, expressed as a percentage of the value just below the surface, is plotted against depth in a freshwater impoundment. Irradiance diminishes in an approximately exponential manner in accordance with

$$E_d(z) = E_d(0) e^{-K_d z} \quad (6.1)$$

or

$$\ln E_d(z) = -K_d z + \ln E_d(0) \quad (6.2)$$

where  $E_d(z)$  and  $E_d(0)$  are the values of downward irradiance at  $z$  m and just below the surface, respectively, and  $K_d$  is the vertical attenuation coefficient for downward irradiance.

In Fig. 6.2*a-d*, the logarithm of  $E_d$  is plotted against depth for red, green and blue light in one oceanic and three inland waters. The graphs are approximately linear, in accordance with eqn 6.2, but significant divergence from linearity is in some cases apparent. In the oceanic water, for example, it can be seen that the green and the blue light are

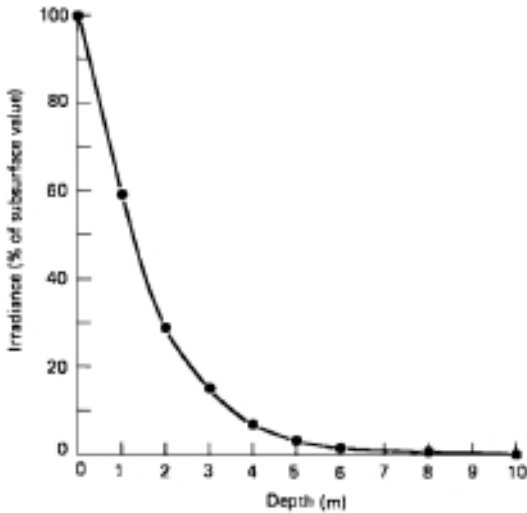


Fig. 6.1 Exponential diminution of downward irradiance of greenish-yellow (580 nm) light with depth in a freshwater body (Burrinjuck Dam, NSW, Australia, 8 December 1977). (Kirk, unpublished data.)

attenuated more rapidly below about 10 m than above. This may be attributed to the downward flux becoming more diffuse, less vertical in its angular distribution with depth, with a consequent increase in attenuation (see §§6.6, 6.7).

The relative rates of attenuation in the different wavebands are determined largely by the absorption spectrum of the aquatic medium. In the tropical Pacific Ocean (Fig. 6.2*a*), and in non-productive oceanic waters generally, where water itself is the main absorber, blue and green light both penetrate deeply and to about the same extent, while red light, which water absorbs quite strongly, is attenuated much more rapidly. In the productive waters of oceanic upwelling areas, blue light is attenuated more strongly than green light, due to absorption by phytoplankton pigments,<sup>942</sup> but still not as strongly as red light. In coastal waters, which contain more yellow substances and phytoplankton than normal oceanic waters, green is again the most penetrating waveband. Only in the most coloured coastal waters, influenced by major river discharge (Jerlov's types 7–9), however, is blue light attenuated as strongly as red light.

In contrast to the sea, in fresh water the blue waveband is usually the most strongly attenuated (Fig. 6.2*b–d*), because of the higher levels of yellow substances that typically occur in inland waters. Green is

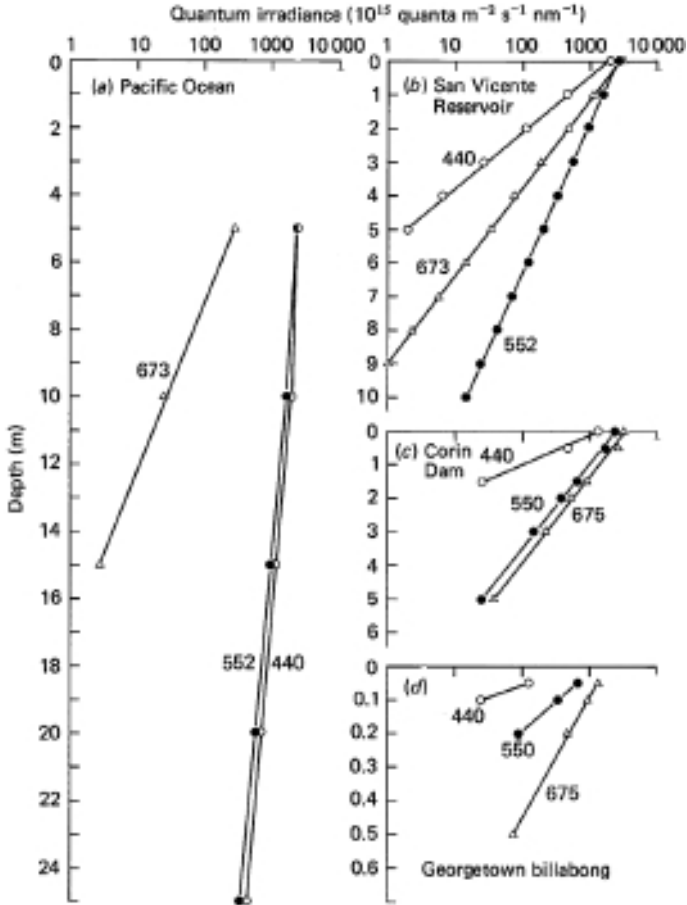


Fig. 6.2 Depth profiles for downward irradiance of blue (○), green (●) and red (△) light in a tropical oceanic and three inland freshwater systems. (a) Pacific Ocean, 100 km off Mexican coast (plotted from data of Tyler and Smith, 1970). (b) San Vicente Reservoir, California, USA (plotted from data of Tyler and Smith, 1970). (c) Corin Dam, ACT, Australia (Kirk, unpublished data). (d) Georgetown billabong, Northern Territory, Australia (plotted from unpublished data of P. A. Tyler). All measurements were taken under sunny conditions. Note the expanded depth scale in (d). The wavelength (nm) at which measurements were made is indicated alongside each graph.

usually the most penetrating waveband in inland waters, followed by red (Fig. 6.2b). When the concentration of yellow materials is high, however, red light may penetrate as far as green (Fig. 6.2c), and in very yellow waters red light penetrates best of all (Fig. 6.2d).

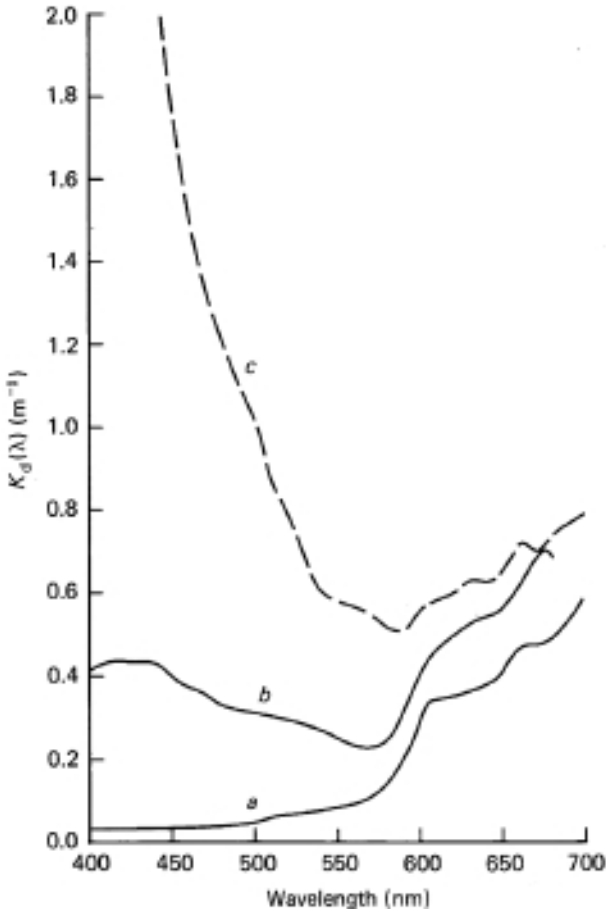


Fig. 6.3 Spectral variation of vertical attenuation coefficient,  $K_d(\lambda)$ , for downward irradiance in (a) the Gulf Stream (Atlantic Ocean) off the Bahama Islands (plotted from data of Tyler and Smith, 1970). (b) The Mauritanian upwelling area ( $8.0\text{--}9.9\text{ mgchl } a\text{ m}^{-3}$ ) off the West African coast (plotted from data of Morel, 1982). (c) Burrinjuck Dam, southern tablelands of NSW, Australia (plotted from data of Kirk, 1979).

Figure 6.3 compares the spectral variations of the vertical attenuation coefficient for irradiance across the photosynthetic range in an unproductive oceanic water, a productive (upwelling) oceanic water and an inland impoundment. Information on the extent to which solar radiation penetrates sea ice is important in global climate modelling. Light *et al.* (2008) measured depth profiles of spectral irradiance in sea ice in the Beaufort Sea (Arctic Ocean) and found that  $K_d(\lambda)$  showed a

broad minimum near 500 nm and a strong increase at near-infrared wavelengths:  $K_d(600 \text{ nm})$  was  $\sim 0.8 \text{ m}^{-1}$  for bare ice and  $\sim 0.6 \text{ m}^{-1}$  for ponded ice.

As the solar altitude decreases, so the pathlength of the unscattered solar beam within the water, per metre depth, increases in proportion to  $(1/\mu_0)$ , where  $\mu_0 = \cos \theta_w$ , the cosine of the zenith angle of the refracted solar beam within the water. We may therefore expect  $K_d$  to increase with diminishing solar altitude. Such an effect is observed but is small:<sup>636</sup> it is only of significance in the upper layer of very clear waters. Baker and Smith (1979) found that in an inland impoundment,  $K_d$  at several wavelengths varied by not more than 5% between solar altitudes of  $80^\circ$  and  $50^\circ$ , and by not more than 18% between  $80^\circ$  and  $10^\circ$ . In the clear water of the Sargasso Sea (Atlantic Ocean), Stramska and Frye (1997) found that  $K_d(\lambda)$  at wavelengths (412, 443, 490, 510 and 555 nm) in the blue to green region of the spectrum decreased by 18 to 30% as solar altitude increased from  $17^\circ$  ( $1/\mu_0 = 1.45$ ) to  $60^\circ$  ( $1/\mu_0 = 1.08$ ).  $K_d(\text{PAR})$  also decreased, by about 25%. At the red end of the spectrum (665 and 683 nm), by contrast,  $K_d(\lambda)$  increased as solar altitude increased. Irradiance reflectance also increased dramatically ( $>100\%$ ) in the red, but changed only slightly at the other wavelengths. The authors attribute the anomalous behaviour of  $R$  and  $K_d$  at the long-wavelength end of the spectrum to the presence in the radiation field of additional red light generated by Raman scattering and chlorophyll fluorescence.

The ultraviolet component ( $\lambda < 400 \text{ nm}$ ) of the solar flux is responsible for a large part of the photoinhibition of photosynthesis that occurs in aquatic ecosystems (see [Chapter 10](#)), and so measurements in this spectral region are highly relevant for an understanding of primary production. For most inland water bodies, because of their high levels of yellow substances, which absorb even more strongly in the UV than in the visible region, this is less important than it is in the ocean. The ultraviolet radiation reaching the Earth's surface is, for convenience, considered as being made up of two spectral regions: UVA 320 to 400 nm, UVB 280 to 320 nm. UVB has a much greater photoinhibitory effect than UVA, and so it is on this waveband that most attention is focused. Very little solar radiation at wavelengths  $< 300 \text{ nm}$  penetrates the Earth's atmosphere, so in fact we need to consider only the 300 to 320 nm band. To characterize UVB penetration, measurements at 310 nm are commonly carried out. [Table 6.1](#) shows a selection of  $K_d(310)$  and  $K_d(305)$  values for a number of marine and inland waters.

Table 6.1 *Vertical attenuation coefficients for downward irradiance of UVB in some marine and fresh waters.*

Water body	$K_d(310 \text{ nm})$	Reference
<b>I. Marine</b>		
Central Equatorial Pacific Ocean	0.150	1242
Sargasso Sea, Atlantic Ocean	0.116	1242
Eastern Mediterranean	0.150	632
Western Mediterranean	0.16–0.43	578
Western Greenland	0.17–0.21	578
Shetland-Faeroe	0.19	578
North Sea (Fladen Ground)	0.37–0.67	578
German Bight	0.53–5.0	578
Baltic Sea proper	3.0–3.5	578
Yellow Sea	31.8–37.3	578
Gulf of Aqaba, Red Sea	0.19	Illuz, D., pers. comm., 1993
Gulf of Mexico, N–S transect across Louisiana Shelf, February 1988		
Depth 14 m	1.35	575
Depth 40 m	0.98	575
Depth 64 m	0.263	575
Depth 184 m	0.123	575
St Lawrence R. System, Canada		
Estuary	4.5	757
Gulf of St Lawrence	0.7	757
Kongsfjord, Spitsbergen	0.34	525
(spring, clearest water conditions)	(280–320 nm)	
<b>II. Inland waters</b>		
Canada, lakes		
Pipit, Alberta	1.26	1201
Snowflake, Alberta	2.91	1201
Silver, Ontario	0.68	1201
Swan, Ontario	4.18	1201
Cromwell, Quebec	27.80	1201
Croche	15.40	1201
L. Ontario, N. Shore station	2.89	1201
L. Ontario, deep (178 m) station	2.30	1201
Pennsylvania, USA, lakes		
Giles	1.38	1201
Lacawac	10.06	1201
$K_d(305 \text{ nm})$		
Mountain lakes, Europe (Alps, Pyrenees)		
Predominantly rock catchments (10 lakes)	0.51 av.	776
Alpine meadow catchments (5 lakes)	1.89 av.	776
Forested catchments (9 lakes)	2.89 av.	776
L. Biwa, Japan		
North Basin, clear station EW6	1.74	95
South Basin, turbid site NS9	8.37	95

## 6.2 Spectral distribution of downward irradiance

The data in Fig. 6.2 show that attenuation of solar radiation in the whole photosynthetic waveband takes place at widely different rates in different parts of the spectrum. As a consequence, the spectral composition of the downwelling flux changes progressively with increasing depth. Figure 6.4a shows the changes down to 25 m depth in the clear oceanic water of the Gulf Stream. Most of the light below about 15 m is confined to the blue-green, 400 to 550 nm, waveband with the peak occurring in the blue region at about 440 to 490 nm. In the coastal/estuarine water of Batemans Bay, Australia, attenuation due to yellow substances in the blue region is comparable to that due to water at the red end of the spectrum, so that at 4 m depth, while there is still substantial radiant flux throughout the photosynthetic range, the distribution peaks markedly at about 570 nm (Fig. 6.4b). In European coastal waters, Halldal (1974) found spectral distributions rather similar to that in Fig. 6.4b, with a marked peak at about 570 nm.

In inland waters with their, usually, higher concentration of yellow substances, the rapid attenuation at the short-wavelength end of the spectrum means a virtually complete removal of blue light within quite shallow depths. In Lake Burley Griffin, Australia, for example, at a time of low water turbidity (Fig. 6.4c) there was essentially no blue light still present below about 2 m depth. In the lower half of the euphotic zone (defined in the following section) in such waters, the photosynthetically available flux typically consists of a broad band extending from the green to the red, often with a peak in the yellow at about 580 nm. Near the surface of the water there are significant levels of blue light available for photosynthesis, but taking the euphotic zone as a whole, the total amount of blue light available for photosynthesis is greatly reduced in such waters (see §6.5).

In those coloured, turbid waters in which there are high levels of humic material in the particulate fraction as well as in the soluble state, green light is also attenuated rapidly (Fig. 6.2d), with the result that the downward flux in the lower part of the, very shallow, euphotic zone consists largely of orange-red (600–700 nm) light. In the spectral distribution for Lake Burley Griffin under turbid conditions, shown in Fig. 6.4d, the peak is right over at the far-red end of the spectrum.

## 6.3 Downward irradiance – PAR

As a broad indication of the availability of light for photosynthesis in an aquatic ecosystem, information on the penetration of the whole

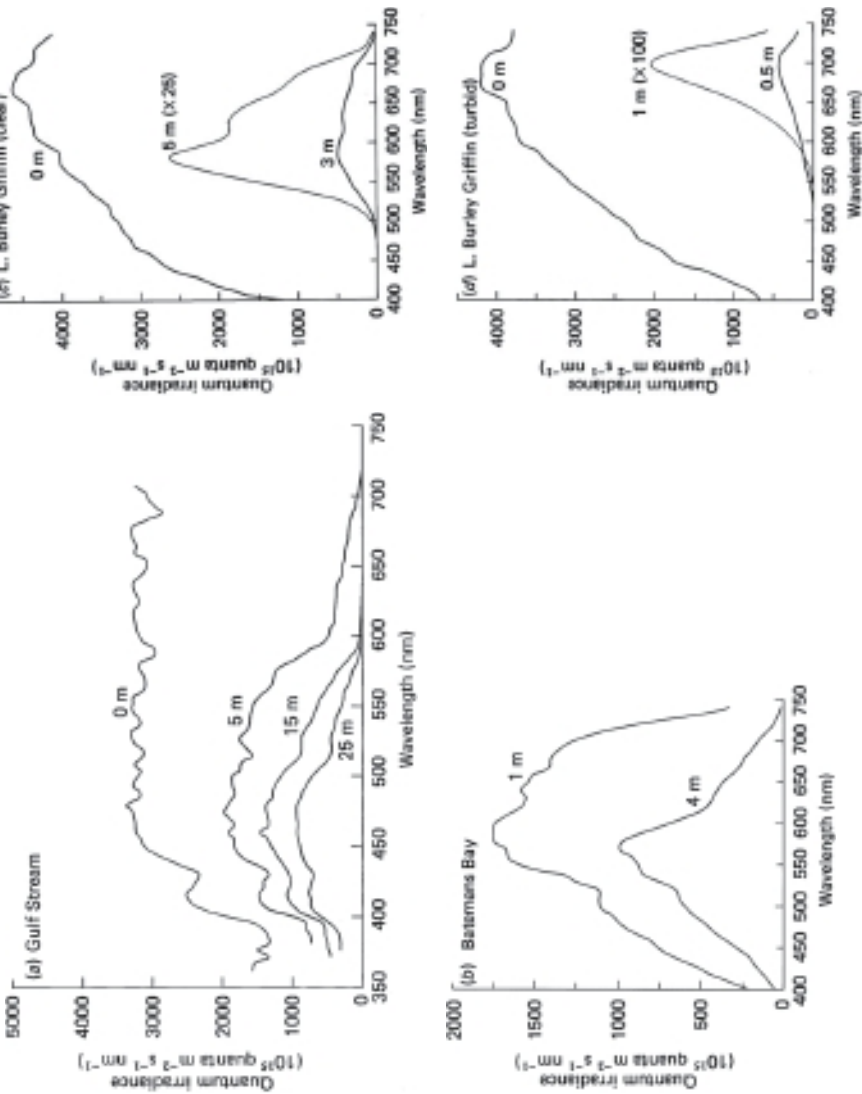


Fig. 6.4 Spectral distribution of downward irradiance in marine and inland waters. (a) The Gulf Stream (Atlantic Ocean) off the Bahama Islands (plotted from data of Tyler and Smith, 1970). (b) Batemans Bay, NSW, Australia (after Kirk, 1979). (c) Lake Burley Griffin, ACT, Australia, 29 September 1977; water comparatively clear (turbidity = 3.7 NTU) (after Kirk, 1979). (d) Lake Burley Griffin, 6 April 1978; water turbid (turbidity = 69 NTU) (after Kirk, 1979).

photosynthetic waveband is of great value. As solar radiation penetrates a water body, it becomes progressively impoverished in those wavelengths which the aquatic medium absorbs strongly and relatively enriched in those wavelengths which are absorbed weakly. We would therefore expect the attenuation coefficient for total PAR to be higher in the upper few metres and to fall to a lower value with increasing depth. This change in the rate of attenuation of PAR with depth can readily be observed in most marine waters and the clearer inland systems: two of the curves in Fig. 6.5 – for the Tasman Sea, and for a relatively clear lake – show the increase in slope of the  $\log E_d$  curve with increasing depth. The curve eventually becomes approximately linear, indicating that the downward flux is now confined to wavebands all with about the same, relatively low, attenuation coefficient. In oceanic waters the light in this region is predominantly blue-green (Fig. 6.2a), whereas in inland waters the penetrating waveband is likely either to be green (Fig. 6.2b), to extend from the green to the red (Fig. 6.2c), or to be predominantly red (Fig. 6.2d).

A countervailing tendency, which exists at all wavelengths, is for attenuation to increase with depth as a result of the downward flux becoming more diffuse, due to scattering. By counteracting the effect of changes in spectral composition, it may partly explain why graphs of  $\log E_d$  against depth for turbid waters are so surprisingly linear (Fig. 6.5, L. Burley Griffin), and lack the biphasic character seen in the clearer waters. However, since high turbidity is commonly associated with increased absorption at the blue end of the spectrum (see §3.3) it is also true that in such waters the blue waveband is removed at even shallower depths than usual and so the change in slope of the curve occurs quite near the surface and is not readily detectable.

Even when, as in the clearer waters, the graph of  $\log E_d$  against depth is noticeably biphasic, the change of slope is usually not very great. Thus, the attenuation of total PAR with depth is nearly always approximately, and often accurately, exponential in agreement with eqns 6.1 and 6.2. Attenuation of PAR in a given water body can therefore generally be characterized by a single value of  $K_d$ , or, at worst, by two values, one above and one below the change in slope. The vertical attenuation coefficient for downward irradiance of PAR provides a convenient and informative parameter in terms of which to compare the light-attenuating properties of different water bodies. Table 6.2 presents a selection of values, including some obtained by summation of spectral distribution data across the photosynthetic range. Oceanic waters have the lowest values of  $K_d(\text{PAR})$  as might be expected from their low absorption and

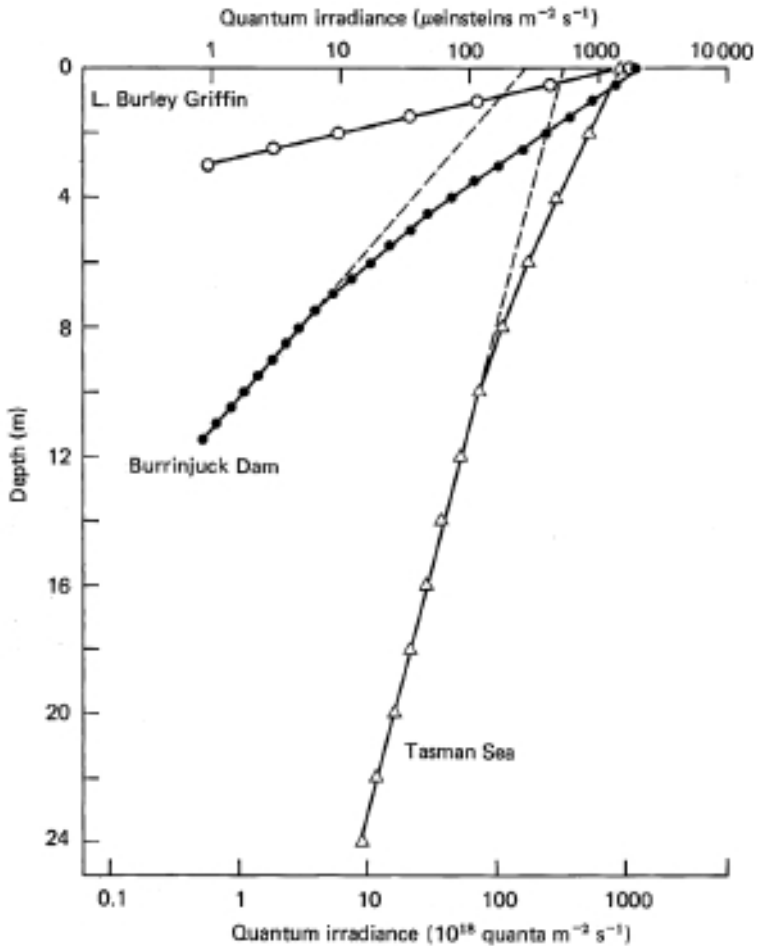


Fig. 6.5 Attenuation of downward quantum irradiance of PAR with depth in a coastal water (Tasman Sea, off Batemans Bay, NSW) and two inland waters (Lake Burley Griffin, ACT; Burrinjuck Dam, NSW) in Australia (Kirk, 1977a, and unpublished). The marked decrease in rate of attenuation in Burrinjuck Dam below about 7 m is particularly noteworthy: spectroradiometric measurements showed that most of the light below this depth was confined to the 540 to 620 nm (green-yellow) waveband.

scattering. Inland waters, with rare exceptions such as Crater Lake in Oregon, USA, have much higher values, with coastal and estuarine waters coming in between. The highest values are found in very turbid waters (e.g. L. George and Georgetown billabong in Australia) in which the suspended tripton strongly absorbs, as well as scatters, the light. High

Table 6.2 *Vertical attenuation coefficients for downward quantum irradiance of PAR in some marine and fresh waters. Where several measurements have been taken, the mean value, the standard deviation, the range and the time period covered are in some cases indicated.*

Water body	$K_d$ (PAR) ( $m^{-1}$ )	Reference
<b>I. Oceanic waters</b>		
<i>Atlantic Ocean</i>		
Sargasso Sea	0.03	1382
Sargasso Sea		
5 m	0.098	1250
35 m	0.073	
75 m	0.046	
Gulf Stream, off Bahamas	0.08	1386
<i>Tropical East Atlantic</i>		
Guinea Dome	0.08–0.096	942
Mauritanian upwelling, offshore	0.16–0.38	942
Mauritanian upwelling, coastal	0.20–0.46	942
<i>Pacific Ocean</i>		
Off Oahu, Hawaii	0.032	112
100 km off Mexico	0.11	1386
Eastern North Pacific (33° N, 142° W)	0.112–0.187	1224
2-week period		
<i>South Pacific, East of New Zealand</i>		
Subtropical convergence zone (41–42° S), av. 5 stns	0.087	721
Sub-antarctic water (46–47° S), av. 4 stns	0.100	721
West Chatham Rise, av. 4 stns	0.104	721
East Chatham Rise	0.126, 0.134	721
East of shelf, ~100 km off Dunedin	0.059, 0.080	721
<b>II. Coastal and estuarine waters</b>		
<i>Europe</i>		
<i>North Sea</i>		
Offshore Netherlands	0.41	1129
Dogger Bank	0.06–0.15	1129
<i>Ems-Dollard Estuary (Netherl./Germany)</i>		
Inner region	~7	254
Outer region	~1	254
Århus Bay, Kattegat, Denmark	0.152–0.557 av. 0.293	834
Bjornafjord, Norway	0.15	638
Kongsfjord, Spitsbergen (spring, clearest water conditions)	0.12	521
<i>Shannon Estuary, Ireland</i>		
Upper	1.8–8.6	892
Middle	1.7–4.5	892
Lower	0.35–1.8	892
Coastal Clyde Sea, Scotland	0.163	148
Clyde R. Estuary		

Table 6.2 (*cont.*)

Water body	$K_d$ (PAR) ( $m^{-1}$ )	Reference
Gare Lough entrance	0.429	148
Upstream (Dumbarton)	1.158	148
Lough Etive, Scotland	0.3–0.4	887
<i>North America</i>		
Gulf of California	0.17	1386
Chesapeake Bay, Rhode R. mouth	1.10–2.05	428
Delaware R. Estuary	0.6–5.0	1317
Hudson R. Estuary, N.Y., 10 stns av., July	2.02	1312
San Francisco Bay		
Shallows, inner estuary	10–13	246
Outer estuary	~1	246
Georgia Embayment		
St Catherine's Sound	2.9	1005
8 km offshore	1.8	1005
30 km offshore	0.27	1005
60 km offshore	0.09	1005
Fraser R., Strait of Georgia (Canada)		
River mouth	0.8	539
Porlier Pass	0.27	539
<i>Australia</i>		
Tasman Sea, coastal New South Wales	0.18	697
Port Hacking Estuary, NSW	0.37	1199
Clyde R. Estuary, NSW	0.71	697
Coastal sea lakes, NSW		
Lake Macquarie	0.55 ± 0.09	1200
Tuggerah Lakes	1.25 ± 0.18	1200
Coastal turbid-zone coral reef, Cleveland Bay (Great Barrier Reef system), Queensland	0.147–0.439	26
Swan R. Estuary, Western Australia		
7 km upstream from mouth	0.40 (0.25–0.69)	749
39 km upstream from mouth	2.19 (0.72–3.69)	749
<i>New Zealand</i>		
9 estuaries, North Island, mouth sites, low water	0.3–1.1	1401
<b>III. Inland waters</b>		
<i>North America</i>		
Great Lakes		
L. Superior	0.1–0.5	639
L. Huron	0.1–0.5	639
L. Erie	0.2–1.2	639, 1285
L. Ontario	0.15–1.2	639
Irondequoit Bay, L. Ontario	1.03 ± 0.11	1445
Finger Lakes, N.Y.		
Otisco	0.564 ± 0.111	346
Seneca	0.468 ± 0.075	346
Skateateales	0.238 ± 0.029	346
Crater L., Oregon	0.06	1386
San Vicente reservoir, California	0.64	1386

Table 6.2 (cont.)

Water body	$K_d(\text{PAR})$ ( $\text{m}^{-1}$ )	Reference
L. Minnetonka, Minnesota	0.7–2.8	896
McConaughy reservoir, Nebraska	1.6 (av.)	1144
Yankee Hill reservoir, Nebraska	2.5 (av.)	1144
Pawnee Hill reservoir, Nebraska	2.9 (av.)	1144
Alaskan lakes		
44 clear lakes, little colour	$0.31 \pm 0.12$	736
21 clear lakes, yellow	$0.70 \pm 0.07$	736
23 turbid lakes, little colour	$1.63 \pm 1.51$	736
<i>Europe</i>		
L. Zurich, 10-month period	0.25–0.65	1182
Esthwaite Water, England	0.8–1.6	536
Loch Croispol, Scotland	0.59	1274
Loch Uanagan, Scotland	2.35	1274
Forest lakes, Finland		
Nimeton	3.45	658
Karkhujarvi	2.49	658
Tavilampi	1.75	658
Mountain lakes (Alps, Pyrenees)		
Predominantly rock catchments (10 lakes)	0.16 av.	776
Alpine meadow catchments (5 lakes)	0.35 av.	776
Forested catchments (10 lakes)	0.40 av.	776
Las Madres L., Spain	0.42–0.88	21
<i>Middle East</i>		
Sea of Galilee (L. Kinneret), Israel	0.5	331
during <i>Peridinium</i> bloom	3.3	331
<i>Africa</i>		
L. Simbi, Kenya	3.0–12.3	897
Saline-alkaline lakes, Kenya		
Bogoria	$12.7 \pm 0.2$	1003
Nakuru	$13.8 \pm 0.3$	1003
Elmentaita	$12.5 \pm 0.3$	1003
L. Tanganyika	$0.16 \pm 0.02$	550
Volcanic lakes, Cameroon		
Barombi Mbo	0.148	733
Oku	0.178	733
Wum	0.305	733
Beme	0.353	733
South African impoundments		
Hartbeespoort	0.67	1431
Rust de Winter	1.70	1431
Bronkhorstspuit	4.23	1431
Hendrik Verwoerd	13.1	1431
<i>Australia</i>		
<i>(a) Southern Tablelands</i>		
Corin Dam, ACT	0.87	720
L. Ginninderra, ACT	$1.46 \pm 0.68$	697, 720
3-year range	0.84–2.74	

Table 6.2 (cont.)

Water body	$K_d(\text{PAR})$ ( $\text{m}^{-1}$ )	Reference
Burrinjuck Dam, NSW	$1.65 \pm 0.81$	697, 720
6-year range	0.71–3.71	
L. Burley Griffin	$2.81 \pm 1.45$	697, 720
6-year range	0.86–6.93	
L. George	$15.1 \pm 9.3$	697, 720
5-year range	5.7–24.9	
<i>(b) Murray-Darling system</i>		
Murrumbidgee R., Gogeldrie Weir, 10 months	1.4–8.0	1014
Murray R. upstream of Darling R. confluence	1.85–2.16	1014
Darling R. upstream of confluence with Murray	2.78–8.6	1014
<i>(c) Snowy Mountains impoundments</i>		
Blowering	0.48	1200
Eucumbene	0.38	1200
Jindabyne	0.49	1200
Talbingo	0.46	1200
<i>(d) Southeast Queensland coastal dune lakes</i>		
Wabby	0.48	151
Boomanjin	1.13	151
Cooloomera	3.15	151
<i>(e) Northern Territory (Magela Creek billabongs)</i>		
Mudginberri	1.24	725
Gulungul	2.21	725
Georgetown	8.50	725
<i>(f) Tasmania (lakes)</i>		
Perry	0.21	152
Ladies Tarn	0.41	152
Barrington	1.23	152
Gordon	1.86	152
Pedder	2.39	152
<i>New Zealand (lakes)</i>		
Taupo	0.14	287
Rotokakahi	0.32	286
Ohakuri	0.40	286
Rotorua	0.90	286
D	2.30	286
Hakanoa	12.1	286
<i>Japan</i>		
L. Biwa		
North Basin, clear station EW6	0.3	95
South Basin, turbid site NS9	1.71	95

values ( $>2.0 \text{ m}^{-1}$ ) may also be associated with dense algal blooms (Sea of Galilee – *Peridinium*), with intense soluble yellow colour but low scattering (L. Pedder, Tasmania), or with a combination of high soluble colour and scattering (L. Burley Griffin, Australia). In shallow lakes, resuspension of

bottom sediments by wind-induced wave action can increase the attenuation coefficient severalfold, and if the sediments contain a substantial proportion of clay particles then the increased attenuation can last for a week or so after the initial storm event.<sup>551</sup> In shallow coastal waters, such as those in and adjoining coral reefs, resuspension of sediments by wave action can greatly reduce light availability for benthic plant life. On the basis of a two-year study in a turbid coastal-zone reef within the Great Barrier Reef Lagoon (Australia), Anthony *et al.* (2004) concluded that the main factor (74 to 79%) limiting availability of PAR for the coral was high turbidity caused by wave-induced resuspension: clouds accounted for only 14 to 17% and tides for 7 to 10% of the variations in benthic irradiance.

In the enormous (68 800 km<sup>2</sup>) tropical African lake, L. Victoria, the factors controlling penetration of PAR vary from place to place. Loiselle *et al.* (2008) observed that in nearshore areas where extensive wetlands are present, dissolved yellow colour plays the dominant role. Attenuation due to tripton was important around a river outflow, and biomass-related attenuation increased in significance towards the open lake. In the Swan River estuary, Western Australia, which has a highly coloured freshwater inflow from coastal wetlands, Kostoglidis *et al.* (2005) found, using multiple regression, that 66% of the variation in  $K_d(\text{PAR})$  was explained by CDOM and an additional 8% by total suspended solids. In the rather turbid waters (average  $b \sim 1.9 \text{ m}^{-1}$ ) of Århus Bay, Kattegat (North Sea-Baltic estuarine transition) Lund-Hansen (2004) estimated that water contributes 9%, CDOM 17%, phytoplankton 32% and suspended particulate matter (inorganic) 42% to total  $K_d(\text{PAR})$ .

At high latitudes for much of the year, PAR has to pass through a layer of sea ice before it can pass into the water column. Ehn *et al.* (2004) measured spectral transmittance through a 28 cm thick layer of landfast sea ice near the entrance to the Gulf of Finland (Baltic Sea). The Baltic Sea has higher levels of yellow substances than most other marine ecosystems, and the sea ice contained higher levels of dissolved and particulate colour than are typical for the Arctic. Spectral albedo values integrated over 400 to 700 nm were commonly between 0.33 and 0.42 and  $K_d(\text{PAR})$  values were in the range 3.2 to 4.7 m<sup>-1</sup>.

A useful, if approximate, rule-of-thumb in aquatic biology is that significant phytoplankton photosynthesis takes place only down to that depth,  $z_{ew}$ , at which the downwelling irradiance of PAR falls to 1% of that just below the surface. That layer within which  $E_d(\text{PAR})$  falls to 1% of the subsurface value is known as the *euphotic zone*. Making the

assumption that  $K_d(\text{PAR})$  is approximately constant with depth, the value of  $z_{eu}$  is given by  $4.6/K_d$ . This, as we have seen, is a reasonable assumption for the more turbid waters and so will give useful estimates of the depth of the euphotic zone in many inland, and some coastal, systems. In the case of those clear marine waters in which there is a significant increase in slope of the  $\log E_d(\text{PAR})$  *versus* depth curve, a value of  $K_d(\text{PAR})$  determined in the upper layer could give rise to a substantial underestimate of the euphotic depth.

Another useful reference depth is  $z_m$ , the mid-point of the euphotic zone. This, by definition, is equal to  $\frac{1}{2} z_{eu}$ : given the approximately exponential nature of the attenuation of PAR with depth, it follows that  $z_m \sim 2.3/K_d$ , and corresponds to that depth at which downward irradiance of PAR is reduced to 10% of the value just below the surface.

## 6.4 Upward irradiance and radiance

As a result of scattering within the water, at any depth where there is a downward flux there is also an upward flux. This is always smaller, usually much smaller, than the downward flux but at high ratios of scattering to absorption can contribute significantly to the total light available for photosynthesis. Furthermore, in any water the upwelling light is of crucial importance for the remote sensing of the aquatic environment (Chapter 7), since it is that fraction of the upward flux which penetrates the surface that is detected by the remote sensors. At any depth, the upward flux can be regarded as that fraction of the downward flux at the same depth which at any point below is scattered upwards and succeeds in penetrating up to that depth again before being absorbed or scattered downwards. Thus we might expect the irradiance of the upward flux to be linked closely to the irradiance of the downward flux; this is found to be the case. Figure 6.6 shows the upward and downward irradiance of PAR diminishing with depth in parallel together in an Australian lake. Changes in downward irradiance associated with variation in solar altitude, or cloud cover, would also be accompanied by corresponding changes in upward irradiance. Given the close dependence of upward irradiance on downward irradiance, it is convenient to consider any effects that the optical properties of the water may have on the upwelling flux in terms of their influence on the ratio of upwelling to downwelling irradiance,  $E_u/E_d$ , i.e. irradiance reflectance,  $R$ .

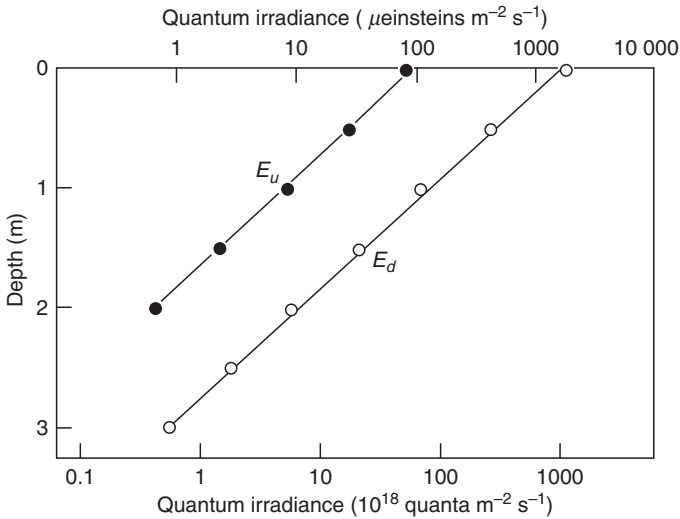


Fig. 6.6 Parallel diminution of upward (●) and downward (○) irradiance of PAR with depth in an Australian lake (Burley Griffin, ACT) (after Kirk, 1977a).

A small proportion of the upward flux originates in forward scattering, at large angles, of downwelling light that is already travelling at some angular distance from the vertical. As solar altitude decreases and the solar beam within the water becomes less vertical, there is an increase in that part of the upward flux which originates in forward scattering. The shape of the volume scattering function is such that this more than counterbalances the fact that an increased proportion of back-scattered flux is now directed downwards. The net result is that irradiance reflectance increases as solar altitude decreases, but the effect is not very large. In the Indian Ocean,  $R$  for 450 nm light at 10 m depth increased from 5.2 to 7.0% as the solar altitude decreased from 80 to 31°.<sup>636</sup> For Lake Burley Griffin in Australia, irradiance reflectance of the whole photosynthetic waveband (400–700 nm) just below the surface increased from 4.6% at a solar altitude of 75° to 7.9% at a solar altitude of 27°. However, at 1 m, by which depth in this turbid water the light field was well on the way to reaching the asymptotic state (see §6.6),  $R$  increased only from 7.4 to 8.6%.<sup>697</sup>

Although, as we have seen, there is a contribution from forward scattering, most of the upwelling flux originates in backscattering. Thus we might expect  $R$  to be approximately proportional to the back-scattering coefficient,  $b_b$ , for the water in question. As the upwards-scattered photons travel up from the point of scattering to the point of

measurement, their numbers are progressively diminished by absorption and – less frequently – by further backscatterings that redirect them downwards again. We may therefore expect that reflectance will vary inversely with the absorption coefficient,  $a$ , of the water. We might also expect that the dominant tendency of reflectance to increase with backscattering will be somewhat lessened by the contribution of backscattering to the diminution of the upward flux.

The actual manner in which irradiance reflectance varies with the inherent optical properties of the medium has been explored by mathematical modelling of the underwater light field. A simplified version of radiative transfer theory<sup>339,956</sup> leads to the conclusion that  $R$  is proportional to  $b_b/(a + b_b)$  for media (such as most natural waters) in which  $b_b \ll a$ . This is the kind of relation that might be anticipated on the qualitative grounds outlined above. In fact, since  $b_b$  is generally very much smaller than  $a$ , we might expect that to a reasonable approximation,  $R$  should be proportional simply to  $b_b/a$ . Numerical modelling of the underwater light field for waters of various optical types, by Monte Carlo and other methods,<sup>484,702,1091</sup> reveals that this is indeed the case and we can write

$$R(0) = C(\mu_0) b_b/a \quad (6.3)$$

where  $R(0)$  is the irradiance reflectance just below the surface. The constant of proportionality,  $C(\mu_0)$ , is itself a function of solar altitude, which we can express in terms of  $\mu_0$ , the cosine of the zenith angle of the refracted solar beam, below the surface. For any given water body it is the case that reflectance increases as solar altitude decreases,<sup>478,484,706,949</sup> i.e.  $C(\mu_0)$  increases as  $\mu_0$  decreases, and indeed can be expressed as an approximately linear function of  $(1 - \mu_0)$ ,<sup>706,712</sup>  $1/\mu_0$ ,<sup>640</sup> or  $[(1/\mu_0) - 1]$ ,<sup>478</sup> in, for example, a relationship such as

$$C(\mu_0) = M(1 - \mu_0) + C(1.0) \quad (6.4)$$

where  $C(1.0)$  is the value of  $C(\mu_0)$  for zenith sun ( $\mu_0 = 1.0$ ) and  $M$  is a coefficient whose value is determined by the shape of the scattering phase function.<sup>478,712</sup> It turns out to be the case for zenith sun that the constant of proportionality in eqn 6.3, i.e.  $C(1.0)$ , is approximately equal to 0.33,<sup>484,702,1091</sup> and this remains true for waters with a wide range of scattering phase functions.<sup>712</sup> In the field of ocean remote sensing,  $C(\mu_0)$ , the constant of proportionality between irradiance reflectance and  $b_b/a$  in eqn 6.3 is usually given the symbol,  $f$ , it being recognized that  $f$  is itself a function of solar altitude and the scattering phase function. Thus

$$R(0) = f \frac{b_b}{a} \quad (6.5)$$

For any given oceanic location, an approximate but realistic estimate of  $f$  ( $\equiv C[\mu_0]$ ) can be obtained from eqn 6.4, using the solar zenith angle, and selecting a plausible value of  $M$  from those previously published for a range of water types.<sup>712</sup> Using radiative transfer theory, and applying certain approximations, Hirata and Højerslev (2008) have shown that for waters and wavebands for which the absorption coefficient is numerically much larger than the backscattering coefficient (i.e. excluding violet-blue wavelengths in clear oceanic waters), the constant of proportionality,  $f$ , is an approximate function of the average downward cosine of the light field below the surface (largely determined by solar angle),  $\bar{\mu}_d$ , and the average cosine of backscattering,  $g_b$ , in accordance with

$$f = \frac{1}{\bar{\mu}_d} \frac{g_b - 0.0849}{g_b + 0.8585} \quad (6.6)$$

Morel and Prieur (1977) compared their measurements of  $R$  across the photosynthetic spectrum with the values calculated using eqn 6.3, for a variety of oceanic and coastal waters. For clear blue oceanic waters, agreement between the observed and the calculated curves of spectral distribution of  $R$  was good. For upwelling oceanic waters with high phytoplankton levels and for turbid coastal waters, agreement was satisfactory from 400 to 600 nm, but in some cases not good at longer wavelengths. Part of the problem in productive waters was a chlorophyll fluorescence emission peak at 685 nm (see §7.5) in the upwelling flux, which increased the observed reflectance over the calculated values in this region. At wavelengths greater than 580 nm, spuriously high reflectance values are also caused by Raman emission.

That part of the upwelling flux just below the surface that is directed approximately vertically upwards is of particular significance for remote sensing. The subsurface radiance in a vertically upward direction we shall refer to as  $L_u$ . The angular distribution of the upwelling flux is such that upward radiance does not change much with nadir angle in the range 0 to 20°. Thus, a measured value of  $L_u(\theta)$  within this range, or an average value over this range, can be taken as a reasonable estimate of  $L_u$ .  $L_u$ , like  $E_u$ , varies for a given water, in parallel with  $E_d$ , and we shall refer to the ratio  $L_u/E_d$  as the *radiance reflectance*. In the context of remote sensing it is often referred to as the *subsurface remote sensing reflectance*,  $r_{rs}$ .

$$r_{rs} = \frac{L_u(0)}{E_d(0)} \quad (6.7)$$

and

$$r_{rs} = \frac{R(0)}{Q} \quad (6.8)$$

where  $Q$  is the ratio of upward irradiance to nadir radiance

$$Q = \frac{E_u}{L_u} \quad (6.9)$$

Some remote sensing radiometers have a very wide field of view: in the SeaWiFS scanner for example (§7.1) it is  $\pm 58.3^\circ$ . While, because of refraction at the surface, the angular range under water is smaller, it is nevertheless the case that some remotely measured radiance values will correspond to underwater radiances well away from the nadir. In recognition of this fact, Morel and Gentili (1993, 1996) define another version of  $Q$ , as a function of zenith solar angle ( $\theta_0$ ), the nadir angle ( $\theta'$ ) of the radiance direction under consideration, and the azimuth difference ( $\phi$ ) between the vertical plane of the radiance and the plane of the Sun.

$$Q(\theta_0, \theta', \Delta\phi) = \frac{E_u(\theta_0)}{L_u(\theta_0, \theta', \Delta\phi)} \quad (6.10)$$

For the subsurface irradiance reflectance, they use the symbol,  $R(\theta_0)$ , to indicate its dependence on solar zenith angle.

The value of radiance reflectance, like that of irradiance, is a function of the inherent optical properties of the water. Given a relation between  $E_u/E_d$  and inherent optical properties, such as that embodied in eqns 6.3 and 6.4, if we know  $Q$ , the ratio of  $E_u$  to  $L_u$ , we can relate  $L_u/E_d$  (i.e.  $r_{rs}$ ), to  $b_b$  and  $a$ . Substituting for  $R(0)$  in eqn 6.8, we obtain

$$r_{rs} = \frac{f b_b}{Q a} \quad (6.11)$$

The simplifying assumption is often made that the radiance distribution of the upwelling flux is identical to that above a Lambertian reflector (same radiance values at all angles). If this were so, then the ratio,  $E_u/L_u$ , would be equal to  $\pi$ . In fact, the radiance distribution is not Lambertian (see §6.6 and Fig. 6.13) and measurements in Lake Pend Oreille at a solar altitude of  $57^\circ$ <sup>1380</sup> showed that  $Q$  was equal to 5.08, near the surface in this water body.<sup>42</sup> Monte Carlo modelling calculations (Kirk, unpublished)

have yielded values of  $Q$ , just below the surface, of about 4.9 for waters with  $b/a$  values in the range 1.0 to 5.0, at a solar altitude of  $45^\circ$ . Thus, for intermediate solar altitudes we may reasonably assume that  $E_u/L_u \approx 5$ . Monte Carlo calculations for waters with  $b/a$  values in the range 1.0 to 5.0 give a value of  $f/Q$  of  $\sim 0.083$ , i.e.

$$r_{rs} = 0.083 b_b/a \quad (6.12)$$

for a solar altitude of  $45^\circ$ .

Aas and Højerslev (1999) present data showing  $Q$  as a function of solar elevation ( $h_s$ ) at 5 m depth, based on measurements of angular radiance distribution at 70 stations in the western Mediterranean.  $Q$  decreased with increasing solar elevation, falling from  $\sim 5.2$  at  $h_s \sim 0^\circ$  to  $\sim 3.4$  at  $h_s \sim 90^\circ$ . The relationship could approximately be represented by

$$Q = (5.33 \pm 0.30) \exp[-(0.45 \pm 0.08) \sin h_s] \quad (6.13)$$

in agreement with one proposed earlier by Siegel (1984)

$$Q = 5.3 \exp(-0.5 \sin h_s) \quad (6.14)$$

for clear water in the central Atlantic Ocean. Aas and Højerslev suggest that this relationship (eqns 6.13 and 6.14 being essentially the same) may be generally valid for clear ocean water, close to the surface.

Loisel and Morel (2001) used computer modelling (Hydrolight) to characterize the extent to which the upward radiance field in Case 2 waters (see §3.4 for an explanation of this term) departs from isotropy. In turbid, sediment-dominated water,  $Q$  increased progressively from 3.53 to 4.09 as solar altitude decreased from  $90^\circ$  to  $15^\circ$ . In clearer, yellow colour-dominated water,  $Q$  increased from 3.69 to 5.02, over the same range of solar angle. For nadir radiance the function,  $f/Q$ , which prescribes (eqns 6.11, 6.12) the dependence of subsurface remote sensing reflectance on  $b_b/a$ , was not markedly dependent on solar angle, remaining fairly close to 0.08 over the angular range in both types of water. For radiance at an extreme nadir angle  $-35^\circ$ , corresponding to  $50^\circ$  above the water, however,  $f/Q$  was dependent on solar angle, increasing, as solar altitude decreased from  $90^\circ$  to  $15^\circ$ , from 0.085 to 0.129 in the turbid water, and from 0.069 to 0.123 in the coloured water.

In oceanic remote sensing it is  $R_{rs}$ , the above-surface radiance reflectance—the vertically upward water-leaving radiance ( $L_w$ ) divided by  $E_d(0^+)$ , the downward irradiance above the surface

$$R_{rs} = \frac{L_w}{E_d(0^+)} \quad (6.15)$$

which is in the first instance determined (we here adopt the convention that  $0^+$  corresponds to any point just above the surface, and  $0^-$  indicates zero depth just beneath the surface). To proceed from this to the subsurface radiance reflectance, we obtain the subsurface radiance from

$$L_u(0^-, \theta', \phi) = \frac{n^2}{[1 - \rho(\theta', \theta)]} L_w(\theta, \phi) \quad (6.16)$$

where  $\theta$  is the above-surface zenith angle of the radiance,  $\theta'$  is the corresponding refracted nadir angle in the water,  $\phi$  is the azimuth angle,  $n$  is the refractive index of sea water and  $[1 - \rho(\theta', \theta)]$  is the Fresnel reflection at the water–air interface for radiance at nadir angle  $\theta'$ <sup>491,951</sup>. Because of surface reflection, the incident solar flux gives rise to a slightly reduced downward irradiance just beneath the surface

$$E_d(0^-)_0 = E_d(0^+)(1 - \bar{\rho}) \quad (6.17)$$

where  $E_d(0^-)_0$  is the downward irradiance at zero depth which is created by that solar radiation which has just penetrated the surface, and  $\bar{\rho}$  is the Fresnel reflection at the water surface for the whole, Sun + sky, incident solar flux.

The total downward irradiance at zero depth,  $E_d(0^-)$ , is slightly greater than  $E_d(0^-)_0$  because to the surface-penetrating flux there is added that part of the upwelling flux which is reflected downwards again at the water–air interface. To arrive at an estimate of this additional irradiance we can consider the initial downward flux giving rise, as the result of upward scattering within the water column, to an upward flux with irradiance  $E_d(0^-)_0 R$ , where  $R$  is irradiance reflectance,  $R = E_u/E_d$ . Part of this upward flux undergoes downward reflection at the water–air interface, giving rise to a new downward flux with irradiance,  $E_d(0)_0 R\bar{r}$ , where  $\bar{r}$  is the water-air Fresnel reflection for the whole diffuse upwelling radiation stream, and has a value of  $\sim 0.48$ .<sup>41</sup> This new downward flux in turn, as a result of upward scattering followed by internal surface reflection, gives rise to a second additional downward flux with irradiance  $E_d(0)_0 (R\bar{r})^2$ . An infinite series of diminishing downward fluxes is generated in this way

$$E_d(0^-) = E_d(0^-)_0 [1 + R\bar{r} + (R\bar{r})^2 + (R\bar{r})^3 + \dots + (R\bar{r})^i + \dots]$$

which, when summed gives us

$$E_d(0^-) = \frac{E_d(0^-)_0}{(1 - R\bar{r})} \quad (6.18)$$

and

$$E_d(0^-) = \frac{E_d(0^+)(1 - \bar{\rho})}{(1 - R\bar{r})} \quad (6.19)$$

For the subsurface remote sensing reflectance,  $L_w(0^-)/E_d(0^-)$ , we can therefore write

$$r_{rs} = \frac{L_w(\theta, \phi) n^2 (1 - R\bar{r})}{E_d(0^+)(1 - \bar{\rho})[1 - \rho(\theta', \phi)]} \quad (6.20)$$

In eqn 6.20, the water-leaving radiance,  $L_w(\theta, \phi)$ , and the surface-incident irradiance,  $E_d(0^+)$ , are the experimentally determined input parameters; refractive index,  $n$ , is known ( $\sim 1.34$ ); the Fresnel reflectances,  $\rho$  and  $\bar{\rho}$ , can be calculated; since  $R$  in ocean waters is usually  $< 0.1$  and  $\bar{r}$  is  $\sim 0.48$ , the  $(1 - R\bar{r})$  term is close to 1.0 anyway, and can be estimated if a plausible value of  $R$  for the oceanic region is inserted. Thus, subsurface remote sensing reflectance,  $r_{rs}$ , a quantity directly related to the inherent optical properties of the water, can be obtained for each pixel of a remotely sensed scene (see Chapter 7).

The spectral distribution of the upwelling flux must depend in part on that of the downwelling flux, but, as eqns 6.3 and 6.5 show, it is also markedly influenced by the variation in the ratio of  $b_b$  to  $a$  across the spectrum. In clear oceanic waters, for example,  $R$  can be as high as 10% at the blue (400 nm) end of the photosynthetic spectrum where pure water absorbs weakly but backscatters relatively strongly (see §4.3), and as low as 0.1% at the red (700 nm) end where water absorbs strongly.<sup>956</sup> Figure 6.7 shows the spectral distributions of upward irradiance and irradiance reflectance in a clear oceanic water and in an inland impoundment. The upwelling flux in the oceanic water consists mainly of blue light in the 400 to 500 nm band. In productive oceanic waters with high levels of phytoplankton, the photosynthetic pigments absorb much of the upwelling blue light and so the peak of the upwelling flux is shifted to 565 to 570 nm in the green.<sup>956</sup> There is also a peak at 685 nm due to fluorescence emission by phytoplankton chlorophyll. In the inland water (Fig. 6.7b), yellow substances and phytoplankton absorb most of the blue light and a broad band, peaking at about 580 nm, with most of the quanta

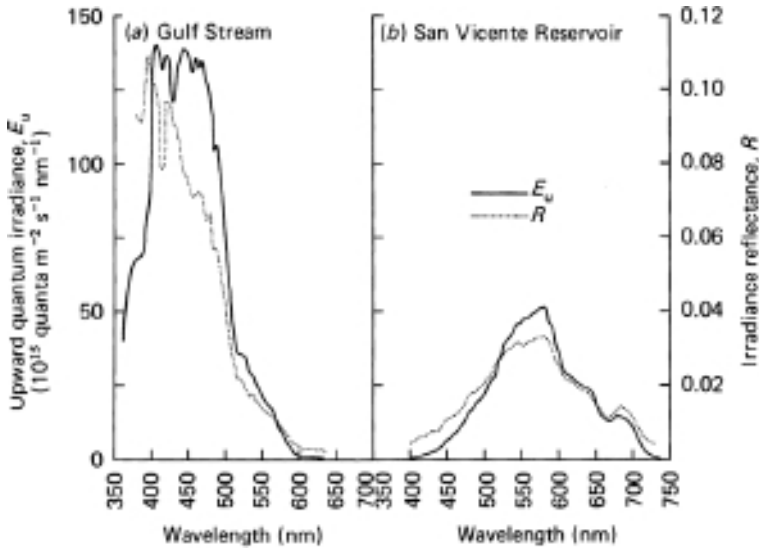


Fig. 6.7 Spectral distribution of upward irradiance and irradiance reflectance in an oceanic and an inland water (plotted from data of Tyler and Smith, 1970). (a) Gulf Stream (Atlantic Ocean) off Bahama Islands, 5 m depth. (b) San Vicente Reservoir, San Diego, California, USA, 1 m depth.

occurring between 480 and 650 nm is observed: the chlorophyll fluorescence emission at about 680 nm can be seen in this curve.

Of the upwelling light flux that reaches the surface, about half is reflected downwards again, and the remainder passes through the water–air interface to give rise to the *emergent flux* (§7.2). It is this flux, combined in varying proportions with incident light reflected at the surface, that is seen by a human observer looking at a water body, and its intensity and spectral distribution largely determine the perceived visual/aesthetic quality of the water body.<sup>289,705,709,711</sup> Figure 6.8 shows the spectral distributions of the subsurface upwelling flux in an Australian lake when it had on one occasion a clear, green appearance, and on another, a turbid, brown appearance. In the first case the spectral distribution peaked in the green-yellow region at about 575 nm, as a consequence of absorption at the blue end of the spectrum by moderate levels of humic substances, and at the red end by water itself. In the second case the upwelling flux had a greater total irradiance, due to intense scattering by suspended soil particles, and a peak in the red region at 675 to 700 nm, resulting from strong absorption in the blue and green regions by high concentrations of soluble and particulate humic substances. Rivers

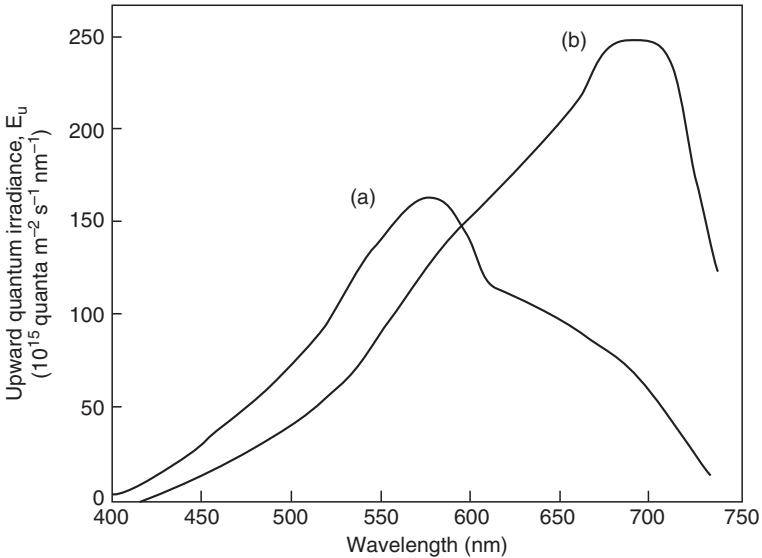


Fig. 6.8 Spectral distribution of subsurface upward irradiance in Lake Gininderra, ACT, Australia. (a) 20 April 1983. Appearance – clear, green.  $b = 3.2 \text{ m}^{-1}$ .  $a_{440} = 1.22 \text{ m}^{-1}$ . (b) 15 August 1984. Appearance – turbid, brown.  $b = 28.2 \text{ m}^{-1}$ .  $a_{440} = 23.1 \text{ m}^{-1}$ .

derived from glaciers are characteristically milky white or grey in appearance, due to the presence of high concentrations of mineral particles ('glacial flour'), but little organic material.

The apparent colour of a water body is determined by the chromaticity coordinates of the flux received by the observer, and these can be calculated from the spectral distribution using the CIE (International Commission on Illumination) standard colorimetric system (see Jerlov, 1976, for further details). Davies-Colley *et al.* (1988) have carried out such calculations using upwelling spectral distribution data, for 14 New Zealand lakes, and suggest that this is a potentially useful tool for water resource managers with a concern for the aesthetic quality of the water bodies for which they are responsible. A comprehensive treatment of colour and clarity in natural water bodies in the context of human use of such waters may be found in the book by Davies-Colley, Vant and Smith (2003).

In the oceanic waters studied by Tyler and Smith (1970), irradiance reflectance for total PAR at 5 m depth varied from about 2 to 5%. For slightly to very turbid inland water bodies in southeast Australia, irradiance reflectance values for PAR just below the surface were usually

between 4 and 10%, but values as low as 2% and as high as 19% were observed, the higher values being associated with higher turbidity.<sup>697,700</sup> The reflectance values increased somewhat with depth (see §6.6), the maximum value observed so far being about 24%. In inland waters with low scattering, but intense colour due to high concentrations of soluble yellow substances, reflectance of PAR can be very low. In a series of lakes of this type in Tasmania, irradiance reflectance for PAR just below the surface ranged from about 1.2% down to 0.14%.<sup>152</sup>

Where there is a bloom of coccolithophores – haptophycean algae whose cells are covered with highly scattering calcareous scales (coccoliths, Fig. 4.10) – the reflectance of the ocean is greatly increased. In a coccolithophore bloom in the Gulf of Maine, Balch *et al.* (1991) measured subsurface reflectance values in the blue-green waveband of 5 to 7% at one station, and 22 to 39% at another. The high reflectance values appeared to be due primarily to large numbers of detached coccoliths suspended in the water, rather than to the whole cells.

In clear ocean waters with little colour, Raman scattering of the predominantly blue-green downwelling light stream gives rise, because of the associated shift to longer wavelengths (see §§4.2, 7.5), to a faint diffuse scattered light field in the 520 to 700 nm range.<sup>869,1291,1321</sup> While this is of little importance for photosynthetic primary production, and makes only a small contribution to the downwelling light field, it can contribute significantly to the upwelling light stream in the lower region of the euphotic zone, and is the probable cause of anomalous increases in reflectance at greater depths, which have sometimes been observed.

In water bodies that are sufficiently shallow for significant light to reach the bottom, then unless the bottom is very dark in colour there is an increase in  $E_u$  near the bottom due to reflection from it.

## 6.5 Scalar irradiance

For randomly oriented phytoplankton cells, photons are equally useful in photosynthesis regardless of the direction from which they come. Scalar irradiance,  $E_0$ , is therefore the best all-round measure of the availability of light for photosynthesis at a given depth. For monochromatic light scalar irradiance, like downward irradiance, typically diminishes with depth in an approximately exponential manner, as the linear graph (Fig. 6.9) of  $\log E_0$  against depth for green light in the Danish Sound<sup>570</sup> shows. When scalar irradiance is measured with a quanta meter that responds to the

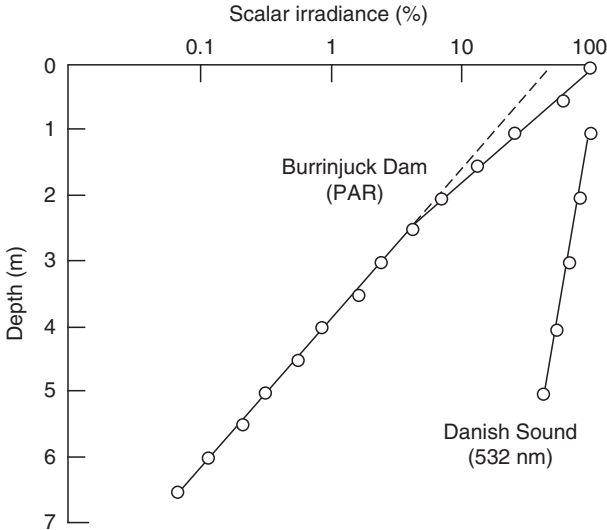


Fig. 6.9 Attenuation of scalar irradiance with depth. The data for Burrinjuck Dam (an Australian inland impoundment) were obtained with a scalar quantum irradiance sensor measuring the full 400 to 700 nm waveband (Kirk, unpublished measurements). The data for the Danish Sound (Baltic Sea) are measurements by Højerslev (1975) at 532 nm.

whole photosynthetic waveband, the variation of  $\log E_0$  with depth in fairly clear water is biphasic, the rate of attenuation being higher near the surface than lower down. This can be seen in the data for Burrinjuck Dam, Australia, in Fig. 6.9. The explanation is the same as that for the analogous phenomenon observed with downward irradiance (Fig. 6.5): the more strongly absorbed wavelengths are being removed in the upper layer, leaving the weakly absorbed wavelengths to penetrate lower down. Using numerical modelling, Leathers and McCormick (1998) have shown that in highly scattering waters (high  $b/a$  ratio) under near-vertically incident light, it is possible for scalar irradiance to at first increase slightly with depth, near the surface, before commencing to decrease. Such behaviour has not yet been described in the field.

Although scalar irradiance is the best parameter in terms of which to express the availability of light for photosynthesis, the most commonly measured parameter is downward irradiance,  $E_d$ . It is of interest to examine the relation between them. As might be expected, since scalar irradiance includes both the upwelling and the downwelling light, and since it represents all angular directions equally (whereas downward irradiance, in accordance with the cosine law, is progressively less affected

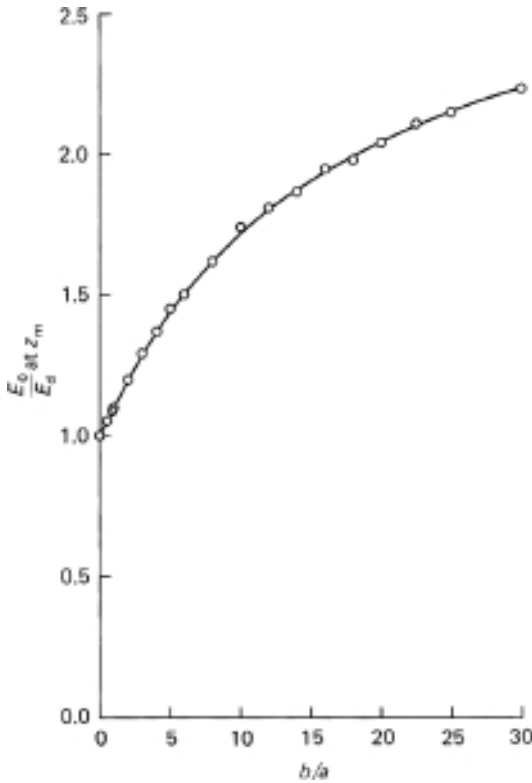


Fig. 6.10 Ratio of scalar to downward irradiance at the mid-point of the euphotic zone as a function of the ratio of scattering to absorption coefficients. Data obtained by Monte Carlo calculation for vertically incident monochromatic light using the method of Kirk (1981a, c).

by light flux as its zenith angle increases), at any point in the water the value of scalar irradiance is always higher than that of downward irradiance.

From the radiance distribution data for Lake Pend Oreille, USA,<sup>1076,1380</sup> it is possible to calculate that in the 480 nm waveband the ratio  $E_0/E_d$  is 1.30 to 1.35 for various depths within the euphotic zone. The higher the ratio of scattering to absorption, the more diffuse the underwater light field becomes, and the greater the difference between  $E_0$  and  $E_d$ . Figure 6.10 shows the way  $E_0/E_d$  at the mid-point of the euphotic zone ( $z_m$ ) increases as the ratio of the scattering coefficient to the absorption coefficient increases:  $E_0/E_d$  is equal to 1.5, 1.75 and 2.0 for  $b/a$  values of 6, 10 and 18, respectively. Since the absorption coefficient of natural

waters can vary markedly with wavelength, the ratios of scalar to downward irradiance will vary across the spectrum. Taking the whole photosynthetic waveband, for clear oceanic waters the average  $b/a$  ratio is low enough to give rise to  $E_0/E_d$  values of up to about 1.2. For typical inland and some coastal waters, however, with  $b/a$  values in the region of 4 to 10, or even up to 20 or 30 in the most extreme cases, we might commonly expect  $E_0/E_d$  to be in the region of 1.4 to 1.8, rising to 2.0 to 2.5 in the very turbid waters.

Thus, if it is wished to determine the absolute amount of light available for photosynthesis at a given depth in a water body, a measurement of downward irradiance may seriously underestimate this, particularly in turbid waters. On the other hand, the vertical attenuation coefficient,  $K_d$ , for downward irradiance is close in value to the vertical attenuation coefficient,  $K_0$ , for scalar irradiance. Monte Carlo calculations (Kirk, unpublished) show that for media with  $b/a$  ranging from 0.3 to 30,  $K_d/K_0$  varies only between about 1.01 and 1.06. The measured value of  $K_d$  can therefore be taken as a reasonable estimate of the value of  $K_0$ , and used to predict the attenuation of scalar irradiance with depth.

It would be useful to have, for any given water body, a measure of the total amount of light available for photosynthesis at a given instant, throughout the whole water column, 1 m square. We shall give this parameter the symbol,  $Q_t$ : it has the units joules or quanta. Assuming that no light reaches the bottom, it can be shown that

$$Q_t = \frac{E_0(0)}{c_w {}^wK_0(av)} \quad (6.21)$$

Where  $E_0(0)$  is the scalar irradiance just below the surface,  $c_w$  is the speed of light in water and  ${}^wK_0(av)$  is the irradiance-weighted vertical attenuation coefficient for scalar irradiance (§1.3). Thus, if one water body has a  ${}^wK_0(av)$  value twice that in another water body, then for a given subsurface scalar irradiance it has about half the total amount of light available for photosynthesis.

## 6.6 Angular distribution of the underwater light field

As sunlight enters a water body, immediately it penetrates the surface its angular distribution begins to change – to become less directional, more diffuse – as a result of scattering of the photons. The greater the depth,

the greater the proportion of photons that have been scattered at least once. The angular distribution produced is not, however, a function of scattering alone: the less vertically a photon is travelling, the greater its pathlength in traversing a given depth, and the greater the probability of its being absorbed within that depth. Thus the more obliquely travelling photons are more intensely removed by absorption and this effect prevents the establishment of a completely isotropic field. The resultant angular distribution is determined by this interaction between the absorption and the scattering processes. Eventually the angular distribution of light intensity takes on a fixed form – referred to as the *asymptotic radiance distribution* – which is symmetrical about the vertical axis and whose shape is determined only by the values of the absorption coefficient, the scattering coefficient and the volume scattering function.<sup>338,636,1076,1092,1368</sup> That such an equilibrium radiance distribution would be established at great depth was predicted on theoretical grounds independently by Whitney (1941) in the USA and Poole (1945) in Ireland, and mathematical proofs of its existence were given by Preisendorfer (1959) and Højerslev and Zaneveld (1977). Early measurements by Jerlov and Liljequist (1938) in the Baltic Sea showed some movement of the radiance distribution towards a symmetrical state with increasing depth. The particularly accurate measurements of Tyler (1960) down to 66 m in Lake Pend Oreille, USA, demonstrated the very close approach of the radiance distribution to the predicted symmetrical state at this near asymptotic depth.

The progression of the angular structure of the underwater light field towards the asymptotic state can be seen from the change in the radiance distribution with increasing depth. This is illustrated in Fig. 6.11, which is based on the measurements of Tyler (1960) in Lake Pend Oreille. Figure 6.11a is for radiance at different vertical angles in the plane of the Sun. Near the surface the light field is highly directional with most of the flux coming from the approximate direction of the Sun. With increasing depth the peak in the radiance distribution becomes broader as its centre shifts towards  $\theta = 0^\circ$ . The final, asymptotic, radiance distribution would be symmetrical about the zenith. It is noticeable that in the plane of the Sun this final state had not quite been reached even at 66 m. Figure 6.11b shows that in a plane almost at right angles to the Sun, the radiance distribution is nearly symmetrical about the vertical even near the surface. At intermediate azimuth angles, radiance distributions intermediate between those in Fig. 6.11a and b exist.

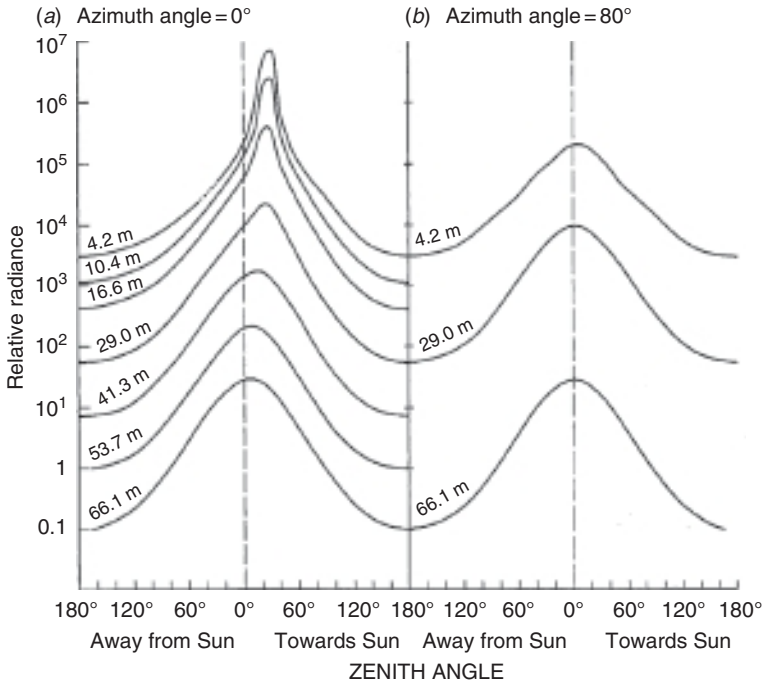


Fig. 6.11 Radiance distribution of underwater light field at different depths. Plotted from measurements at 480 nm made by Tyler (1960) in Lake Pend Oreille, USA, with solar altitude  $56.6^\circ$ , scattering coefficient  $0.285 \text{ m}^{-1}$  and absorption coefficient  $0.117 \text{ m}^{-1}$ . (a) Radiance distribution in the plane of the Sun. (b) Radiance distribution in a plane nearly at right angles to the plane of the Sun.

Figure 6.12 shows the near-asymptotic radiance distribution in Lake Pend Oreille in the form of a polar diagram. If in a natural water the ratio of scattering to absorption increases to high levels, then the shape of such a polar diagram of the asymptotic radiance distribution tends towards a circle (i.e. the light field approaches the completely diffuse state). If, however, scattering decreases to low values relative to absorption, then the polar diagram takes on the form of a narrow, downward pencil.<sup>1075</sup>

Aas and Højerslev (1999) analysed a large data set of underwater angular radiance distributions, 70 from the western Mediterranean and 12 from Lake Pend Oreille, Idaho (USA). They were able to find two simple functions that between them can be used to characterize the angular radiance distribution. The  $\epsilon$  function represents the eccentricity of the ellipse that approximates the azimuthal radiance distribution in

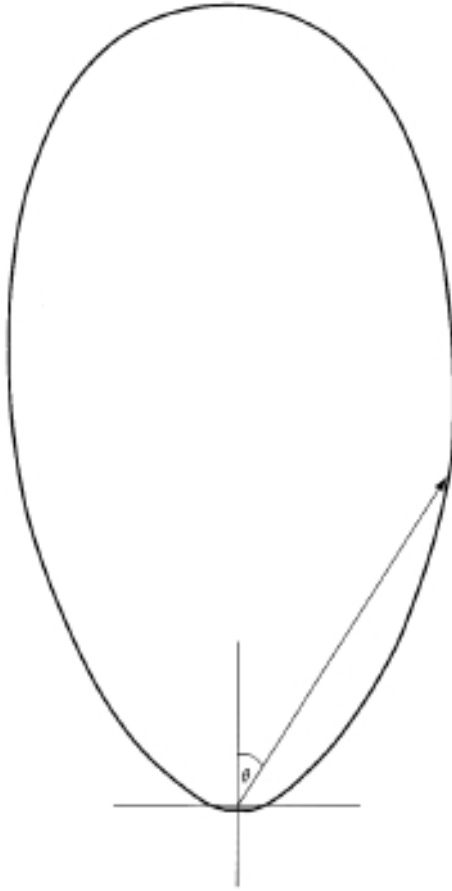


Fig. 6.12 Near-asymptotic radiance in Lake Pend Oreille, USA, plotted as a polar diagram. The data are the same as those in the lowest curve of Fig. 6.11*b*.

polar coordinates: it provides the azimuthal mean of downward radiance at a given depth with an average error  $\leq 7\%$  and of upward radiance with an error of  $\sim 1\%$ . The parameter,  $\alpha$ , plays a similar role for the azimuthal mean of upward radiance. It describes the zenith angle dependence of the azimuthal mean of upward radiance with an average error of  $\leq 7\%$  in clear ocean water, increasing to  $\leq 20\%$  in turbid lake water. Determination of  $\epsilon$  requires measurement of two azimuthal values of radiance:  $\alpha$  is obtained from measurements of any two of the quantities,  $L(180^\circ)$ ,  $E_u$  and  $E_{0u}$ .

In the context of photosynthesis, what is significant about a radiance distribution is its relevance to the rapidity of attenuation of light intensity

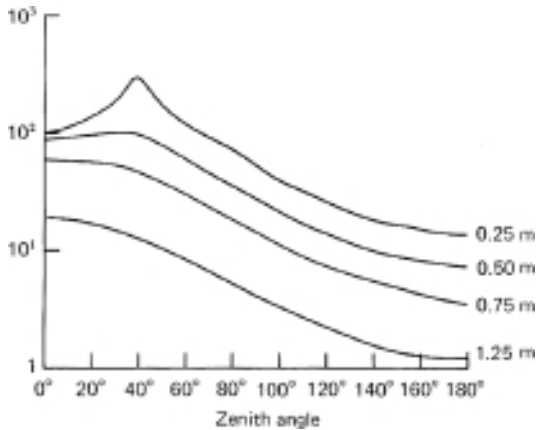


Fig. 6.13 Radiance distribution of underwater light field averaged over all azimuth angles in a turbid lake. Radiance values for total PAR in Lake Burley Griffin, Australia, were obtained by Monte Carlo calculation using the method of Kirk (1981a, c) on the basis of the measured absorption and scattering properties (absorption spectrum, Fig. 3.9b; scattering coefficient,  $15.0 \text{ m}^{-1}$ ; solar elevation,  $32^\circ$ ).

with depth. The azimuthal distribution of radiance at each vertical angle has no bearing on this. It is therefore legitimate, and in the interests of simplicity advantageous, to express the angular distribution of the light field at any depth in terms of the radiance averaged over all azimuth angles at each vertical angle. Figure 6.13 shows a series of such radiance distributions at increasing depth, calculated by the Monte Carlo procedure, for PAR in an Australian lake. The much more rapid approach to a final symmetrical distribution in this case is partly the result of averaging over all azimuth angles, and partly because of the increased scattering relative to absorption in this lake relative to Lake Pend Oreille.

An even simpler way of expressing the angular distribution of the light field is in terms of the three average cosines (see §1.3) and the irradiance reflectance. In Fig. 6.14 the values of these parameters, obtained by Monte Carlo calculation,<sup>702,704</sup> are plotted against the optical depth ( $\zeta = K_d z$ ) in water in which  $b/a = 5.0$ . The average cosine and the average downward cosine initially both diminish sharply in value but then begin to level off as the angular distribution of the light approaches the asymptotic radiance distribution. There is no significant further change in the angular distribution beyond the depth ( $z_{eu}$ ,  $\zeta = 4.6$ ) at which irradiance has been reduced to 1% of the subsurface value, and indeed most of

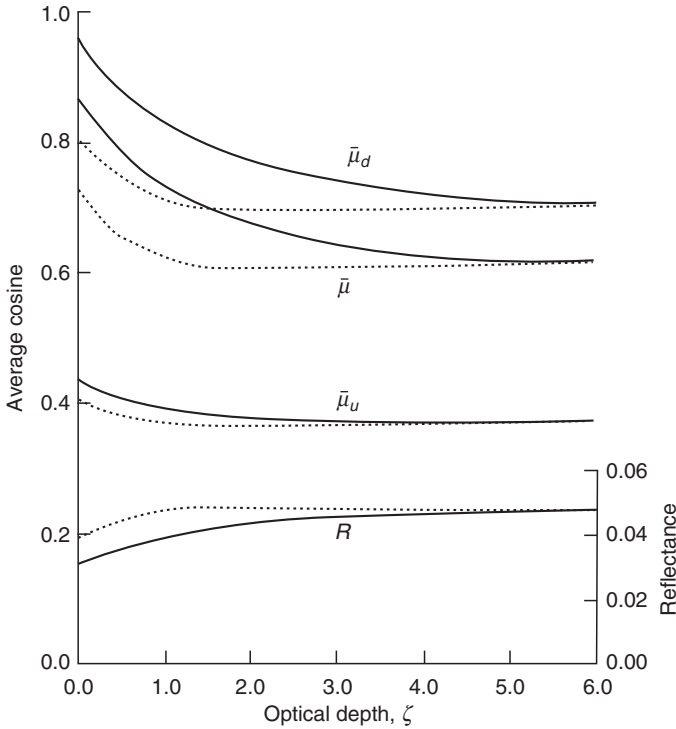


Fig. 6.14 Variation of average cosines for downwelling ( $\bar{\mu}_d$ ) upwelling ( $\bar{\mu}_u$ ) and total ( $\bar{\mu}$ ) flux, and irradiance reflectance ( $R$ ) with optical depth ( $\zeta = K_d z$ ) in water with  $b/a = 5$ . Data obtained by Monte Carlo calculation.<sup>702</sup> (Vertically incident light \_\_\_\_\_ . Light incident at 45° -----.)

the change takes place before  $z_m$  ( $\zeta = 2.3$ ) is reached. The decrease in  $\bar{\mu}$  with depth towards its asymptotic value is approximately exponential.<sup>106</sup>

It will be noted that for vertically incident light  $\bar{\mu}_d$  starts (at  $z = 0$ ) from a value of slightly less than 1.0. This is because the downwelling light just below the surface includes not only those photons that have just passed down through the surface (and these do have  $\bar{\mu}_d = 1.0$ ), but also those photons that were part of the upwelling stream and that have just been reflected downwards from the surface. These latter photons have a  $\bar{\mu}_d$  much less than 1.0 and so, although they constitute only a small proportion of the total, they bring the average value of  $\bar{\mu}_d$  significantly below 1.0.

For light incident on the surface at angles other than the vertical, the behaviour is much the same as for perpendicularly incident light except that  $\bar{\mu}$  and  $\bar{\mu}_d$  just below the surface have lower values, and the light

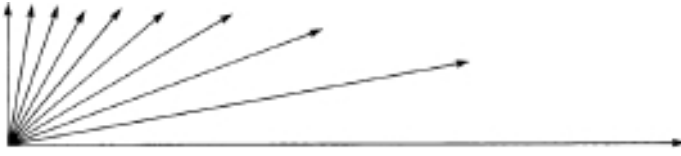


Fig. 6.15 Vector diagram of radiance distribution of upwelling light at 4.24 m depth in Lake Pend Oreille, USA. Radiance measurements of Tyler (1960) averaged over all azimuth angles. Radiance vectors are at nadir angle intervals of  $10^\circ$ .

field reaches its asymptotic state at shallower depths: compare the curves for  $\theta = 0^\circ$  and  $\theta = 45^\circ$ . In the case of a non-perpendicular incident beam it should be realized that although the angular distribution averaged over all azimuths has settled down to almost its final form at  $z_{eu}$ , the downward radiance distribution in the vertical plane of the Sun is still significantly different from the asymptotic distribution: this can be seen in Fig. 6.11a in the curves for 29 m ( $z_{eu} \approx 28$  m).

The angular distribution of the upwelling stream acquires its final form a very short distance below the surface. In Lake Pend Oreille, USA,  $\bar{\mu}_u$  varied only between 0.37 and 0.34 at all depths between 4.2 and 66.1 m.<sup>1383</sup> Monte Carlo calculations<sup>702</sup> indicate that for waters with  $b/a$  values ranging from 0.1 to 20,  $\bar{\mu}_u$  is typically in the range 0.35 to 0.42 throughout the euphotic zone. That the upwelling stream should have these characteristics is not surprising since it consists predominantly of back-scattered light: backscattering does not vary strongly with angle and so rather similar upward radiance distributions are produced whatever the downward radiance distribution.

The radiance distribution of the upwelling light stream near the surface in Lake Pend Oreille is shown in the form of a polar diagram in Fig. 6.15. If, as is sometimes assumed (see §6.4), the upwelling flux has the same radiance distribution as that above a Lambertian reflector (same radiance at all angles), all the radiance vectors in Fig. 6.15 would be the same length. It is clear from the data that the upward radiance distribution is far from Lambertian.

As might be expected from the changes in angular distribution with depth, irradiance reflectance increases with depth but levels off at a final value concurrently with the settling down of  $\bar{\mu}$  and  $\bar{\mu}_d$  to their final values (Fig. 6.14). Thus, in natural water bodies the depth at which the asymptotic radiance distribution (averaged over all azimuth angles) is established can be found by determining at what depth the value of irradiance reflectance ceases to increase.

## 6.7 Dependence of properties of the field on optical properties of the medium

We have noted earlier that the diminution of light intensity with depth is due to a combination of absorption and scattering processes, and also that the angular distribution of light intensity is determined by interaction between absorption and scattering. We shall now examine the quantitative relations that exist between the inherent absorption and scattering properties of the medium, and the angular structure and vertical attenuation of irradiance in the light field that is established.

### Angular structure

The shape of the volume scattering function, as defined by  $\tilde{\beta}(\theta)$ , the normalized volume scattering function (§1.4), can have a major influence on the character of the light field. In the majority of natural waters, however, scattering is particle dominated to such an extent that  $\tilde{\beta}(\theta)$  curves are rather similar in shape from one water to another. To begin with, therefore, we shall not consider the effects of variation in  $\tilde{\beta}(\theta)$ , and shall assume that the waters under consideration have a typical particle-dominated volume scattering function, similar to that measured by Petzold in San Diego harbour (Fig. 4.9).

To give the conclusions as much generality as possible, our analysis will be in terms of optical depth ( $\zeta = K_d z$ ) rather than actual depth. This makes it permissible to confine our attention to the ratio of scattering to absorption coefficients,  $b/a$ , rather than to their absolute values. A convenient optical depth at which to study the effects of changes in  $b/a$  is  $z_m$ , the mid-point of the euphotic zone ( $\zeta = 2.3$ ). Figure 6.16 shows the total and downward average cosines, and reflectance at  $z_m$  as a function of  $b/a$ , determined by Monte Carlo calculation.<sup>702</sup> As scattering increases relative to absorption, so the underwater light field at this depth becomes less vertical, more diffuse, as shown by the decrease in  $\bar{\mu}$  and  $\bar{\mu}_d$ . Reflectance increases almost linearly with  $b/a$  over much of the range, but the curve as a whole has a slightly sigmoid character. If the zenith angle of the incident light is changed from 0 to 45°, it makes very little difference to the reflectance, and not much to the average cosine except at low values of  $b/a$ .

In addition to delineating the quantitative dependence of the angular structure of the light field on  $b/a$ , Fig. 6.16 illustrates a useful general conclusion. Namely, that for water with a given  $\tilde{\beta}(\theta)$ , the relations between  $\bar{\mu}$ ,  $\bar{\mu}_d$ ,  $\bar{\mu}_u$ ,  $R$  at a specified optical depth, and  $b/a$ , are fixed at any given angle of incident light, and indeed are largely independent of

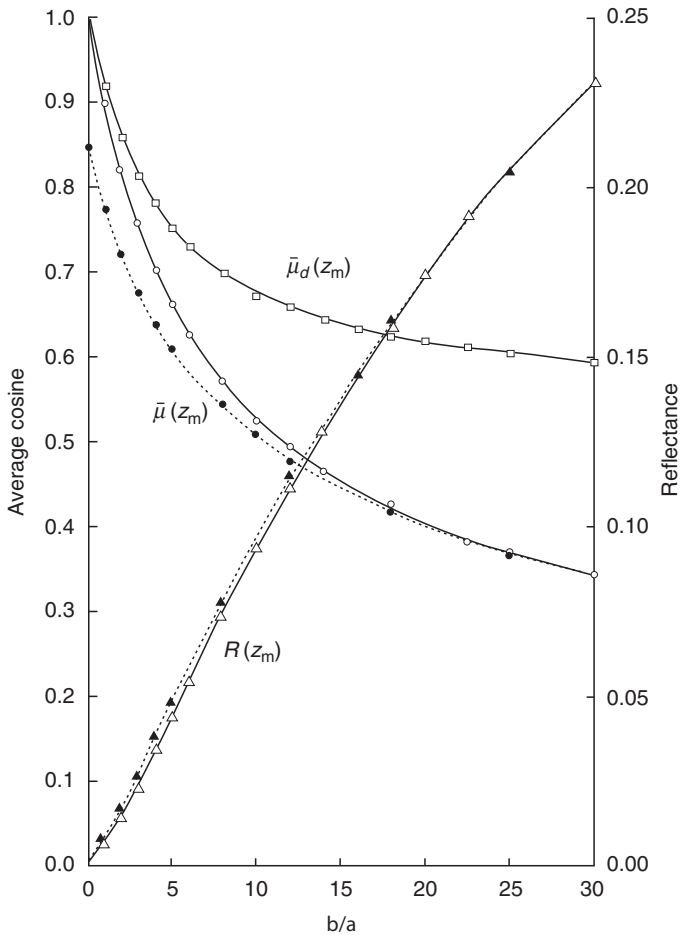


Fig. 6.16 Average cosines and irradiance reflectance at mid-point ( $z_m$ ) of euphotic zone as a function of  $b/a$ . Data obtained by Monte Carlo calculation.<sup>702</sup> (Vertically incident light \_\_\_\_\_ Light incident at  $45^\circ$  -----.)

the angle of incident light. The fixed nature of the relation between  $\bar{\mu}$ ,  $R$  and  $b/a$  provides the basis for a method of estimating the absolute values of both  $b$  and  $a$  for any real water body, using only measurements of underwater irradiance (see §4.2).

### Vertical attenuation of irradiance

In the absence of scattering ( $b = 0$ ),  $K_d$ , the vertical attenuation coefficient for downward irradiance, is determined only by the absorption

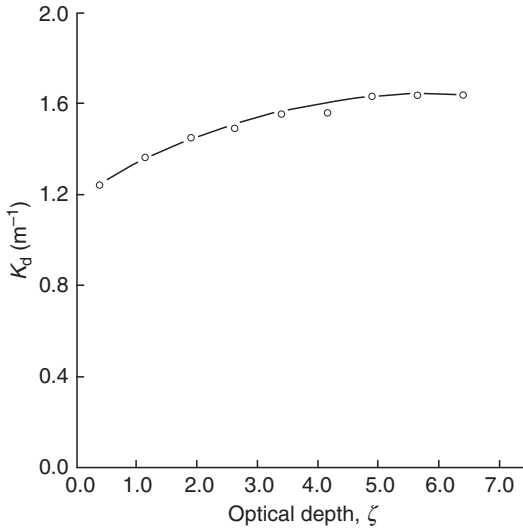


Fig. 6.17 Vertical attenuation coefficient for downward irradiance as a function of optical depth for  $b/a=5$ , and  $a=1.0\text{ m}^{-1}$ . Data obtained by Monte Carlo calculation for vertically incident light.<sup>702</sup>

coefficient and the zenith angle,  $\theta$ , of the light beam within the water, in accordance with  $K_d = a/\cos \theta$ .

In a scattering medium,  $K_d$  is increased, partly because of the altered angular distribution of the downwelling light, and partly because of upward scattering of the downwelling stream. Concurrently with the progressive change in angular distribution with depth, so the value of  $K_d$  increases with depth, levelling off at that optical depth at which the asymptotic radiance distribution becomes established. Figure 6.17 shows  $K_d$  as a function of optical depth for vertically incident light in a medium for which  $b/a=5.0$ .

While  $K_d$  always increases with depth when the incident light is parallel, it is possible that the converse might be true if the incident light were diffuse, e.g. from an overcast sky. If, as could be the case, especially in water with a low value of  $b/a$ , the final asymptotic radiance distribution were more vertical than the initial radiance distribution, then  $K_d$  would decrease with depth.

The relation between  $K_d$  and the absorption and scattering coefficients may, for a given incident light field and a given  $\tilde{\beta}(\theta)$ , be expressed with complete generality by expressing  $K_d/a$  as a function of  $b/a$ . The absolute values of  $a$ ,  $b$  and  $K_d$  do not have to be specified: it is the ratios that are

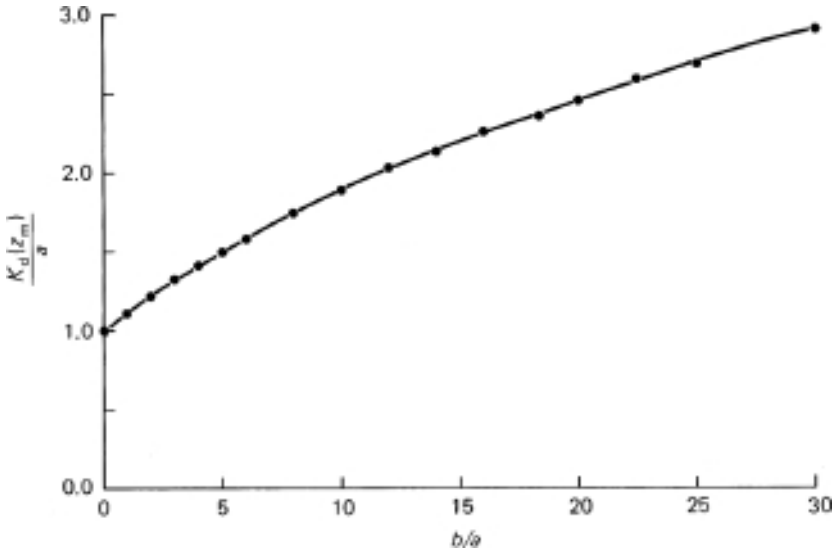


Fig. 6.18. Ratio of vertical attenuation coefficient for downward irradiance (at  $z_m$ ) to absorption coefficient as a function of  $b/a$ . Data obtained by Monte Carlo calculation for vertically incident light.<sup>702</sup>

important. A certain ratio of  $b$  to  $a$  gives rise to a specific ratio of  $K_d$  to  $a$ , regardless of the actual value of any of the coefficients. The calculated value of  $K_d/a$  at  $z_m$  for vertically incident light is plotted against  $b/a$  in Fig. 6.18. The value of  $K_d$  starts off equal to  $a$  when  $b = 0$ , and rises progressively as  $b$  increases, in a linear manner to begin with, but curving over at high ratios of  $b$  to  $a$ . The values of  $K_d(z_m)/a$  over the whole range up to  $b/a = 30$  were found<sup>702</sup> to fit very closely to a curve specified by the equation

$$\frac{K_d(z_m)}{a} = \left[ 1 + \frac{Gb}{a} \right]^{1/2} \quad (6.22)$$

or

$$K_d(z_m) = (a^2 + Gab)^{1/2} \quad (6.23)$$

$G$  is a coefficient that can be regarded as determining the relative contribution of scattering to vertical attenuation of irradiance, and its value is determined by the shape of the scattering phase function. For a water with the San Diego harbour  $\tilde{\beta}(\theta)$ , as in Fig. 6.18,  $G$  has the value 0.256.

Similar equations to 6.22 and 6.23 can be written in which  $K_d(z_m)$  is replaced by  $K_d(av)$ , the average value of  $K_d$  through the zone within which downward irradiance is reduced to 1% of that penetrating the surface: in this case the coefficient,  $G$ , has a slightly different value (0.231). Although  $K_d(z_m)$  is a more precisely defined, and theoretically satisfactory, form of  $K_d$ , we shall nevertheless from here on direct our attention mainly to  $K_d(av)$ , since this is the  $K_d$  most commonly measured in the field.  $K_d(z_m)$  and  $K_d(av)$  are in fact normally close to each other in value, and show the same kinds of dependence on the inherent optical properties of the medium.

The way in which  $K_d$  varies with solar altitude is conveniently expressed in terms of its dependence on  $\mu_0$ , the cosine of the refracted solar beam just beneath the surface. This dependence is due not only to the anticipated change, with angle, in the pathlength of the photons per vertical metre traversed, which gives rise to a dependence of  $K_d$  on  $(1/\mu_0)$ , but in addition to the fact that the coefficient  $G$  also varies with solar angle in accordance with

$$G(\mu_0) = g_1\mu_0 - g_2 \quad (6.24)$$

where  $g_1$  and  $g_2$  are constants for a particular scattering phase function.<sup>706,712</sup> Thus we can write

$$\frac{K_d}{a} = \frac{1}{\mu_0} \left[ 1 + G(\mu_0) \frac{b}{a} \right]^{1/2} \quad (6.25)$$

and

$$K_d = \frac{1}{\mu_0} [a^2 + G(\mu_0)ab]^{1/2} \quad (6.26)$$

or the corresponding forms, such as

$$K_d = \frac{1}{\mu_0} [a^2 + (g_1\mu_0 - g_2)ab]^{1/2} \quad (6.27)$$

in which we substitute for  $G(\mu_0)$ . For water bodies with the San Diego phase function, in the version of eqn 6.27 applicable to  $K_d(av)$ , the constants have the values  $g_1 = 0.425$  and  $g_2 = 0.19$ . In the version for  $K_d(z_m)$ ,  $g_1 = 0.473$  and  $g_2 = 0.218$ . Using these values of  $g_1$  and  $g_2$ , eqn 6.27 can be used to calculate  $K_d$  from  $\mu_0$ ,  $a$  and  $b$  for most of the waters that limnologists and coastal oceanographers deal with, and is of considerable predictive value in relation to the optical water quality of these aquatic ecosystems.<sup>709,711</sup>

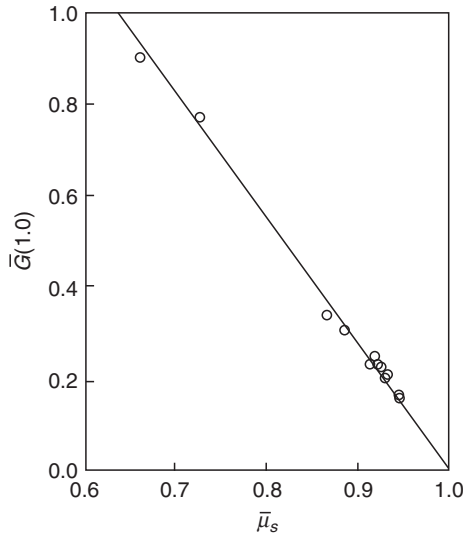


Fig. 6.19 Variation of  $G(1.0)$  with the average cosine of scattering of the water.

In the various regions of the open ocean, the scattering phase function can differ significantly in shape from the phase function of coastal and inland waters. The relationships embodied in eqns 6.22 to 6.27 nevertheless still apply.<sup>712</sup> It is the value of the coefficient  $G(\mu_0)$  that varies with the shape of the phase function. A useful measure of the shape of the scattering phase function is  $\bar{\mu}_s$ , the average cosine of scattering (see §1.4), and we can use this to illustrate the nature of the dependence of  $G(\mu_0)$  on the characteristics of the phase function. It is helpful to bear in mind that  $\bar{\mu}_s = 1.0$  corresponds to all the photons being scattered forward without any change in direction, and that a progressive decrease in  $\bar{\mu}_s$  from 1.0 towards zero corresponds to photons being scattered through wider and wider angles. To simplify matters we can confine our attention initially to  $G(1.0)$ , the value of  $G$  for vertically incident light ( $\mu_0 = 1.0$ ). Monte Carlo calculations of the light field in a wide range of optical water types<sup>712</sup> show (Fig. 6.19), as we might expect, that the dependence of vertical attenuation on scattering, expressed through  $G(1.0)$ , diminishes steeply as the scattering becomes increasingly concentrated within narrow forward angles ( $\bar{\mu}_s$  increases towards 1.0), and disappears altogether when  $\bar{\mu}_s = 1.0$ . Linear regression gives

$$G(1.0) = -2.401\bar{\mu}_s + 2.430 \quad (6.28)$$

With  $r^2 = 0.997$ . To a reasonable approximation this can alternatively be expressed as

$$G(1.0) = 2.4(1 - \bar{\mu}_s) \quad (6.29)$$

The relationships embodied in eqns 6.22–6.27 for  $K_d$  as a function of  $a$  and  $b$  are empirical in nature, derived as they are from analysis of the light fields generated by realistic Monte Carlo modelling of the fate of solar radiation in idealized water bodies having a wide range of optical properties. Maffione (1998) has shown that, at least for highly turbid media, a relationship equivalent to that in eqn 6.23 can be derived on purely theoretical grounds. This equation was found to be useful<sup>851</sup> for interpreting the propagation of light through sea ice, a highly scattering optical medium.

The dependence of the apparent optical property,  $K_d$ , on the inherent optical properties of the water,  $a$  and  $b$ , as expressed in eqn 6.26 or 6.27, can be put to the test in waters where apparent optical properties (AOP) and inherent optical properties (IOP) data are both available. The equation has been found to work well for  $K_d(\text{PAR})$  in a number of inland waters in Australia,<sup>706,433,723</sup> the USA<sup>348,1446</sup> and Japan;<sup>95</sup> also for  $K_d(\lambda)$  in several monochromatic wavebands in the visible region in the Clyde Sea (Scotland).<sup>148,888</sup>

As an indication of the extent to which scattering intensifies vertical attenuation of light it may be noted from Fig. 6.18 that  $b/a$  ratios of about 5 and 12 increase  $K_d$  by 50 and 100%, respectively. Comparable effects can be shown for real water bodies. In Table 6.3, data that show the effect of scattering on attenuation of the whole photosynthetic waveband in four Australian inland waters of varying turbidity are presented. The table compares the values of  $K_d$  for PAR calculated from the total absorption spectrum of the water, assuming no scattering, with those actually measured within the water with an irradiance (PAR) meter. The ratio of the observed to the calculated value of  $K_d$  is a measure of the extent to which scattering intensifies light attenuation. The increase in  $K_d(\text{PAR})$  due to scattering ranged from 16% in Burrinjuck Dam, which was rather clear at the time, to more than three-fold in the very turbid water of Lake George.

In our consideration of the ways in which scattering affects attenuation we can now make use of eqn 1.63, derived from radiative transfer theory by Preisendorfer (1961), which expresses the vertical attenuation coefficient for downward irradiance as a function of the diffuse absorption and backscattering coefficients.

Table 6.3 *Effects of light scattering on vertical attenuation coefficient ( $K_d$ ) for irradiance of PAR (400–700 nm), in four water bodies of differing turbidity, in southeast Australia.  $K_d$  values calculated from the measured absorption spectra are compared with those obtained in situ with a quanta meter.*

Water body	Turbidity (NTU)	$K_d$ (calculated) ( $m^{-1}$ )	$K_d$ (observed) ( $m^{-1}$ )	Effect of scattering $\frac{K_d (obs.)}{K_d (calc.)}$
Burrinjuck Dam	1.8	0.775	0.90	1.16
L. Ginninderra	4.6	0.547	0.90	1.65
L. Burley Griffin	17.4	1.333	2.43	1.82
L. George	49.0	1.742	5.67	3.25

$$K_d(z) = a_d(z) + b_{bd}(z) - b_{bu}(z)R(z)$$

Although this relation is not, in view of the difficulty of measuring the diffuse coefficients, of everyday practical use, it is conceptually valuable in helping us to understand the nature and relative importance of the radiation transfer mechanisms underlying the attenuation process. It tells us that attenuation of downward irradiance is the result of three different processes, represented by the three different terms on the right-hand side of the equation. Absorption from the downwelling stream is accounted for by the diffuse absorption coefficient  $a_d(z)$ , which is equal to  $a/\bar{\mu}_d(z)$ , and so must increase as scattering causes  $\bar{\mu}_d$  to decrease. Light is also removed from the downwelling stream by upward scattering of the photons: this process is represented by the diffuse backscattering coefficient for the downwelling stream,  $b_{bd}(z)$ . Opposing these two processes is the downward scattering of photons from the upwelling stream, which acts to increase the downward flux: this is represented by the term,  $-b_{bu}(z)R(z)$ , where  $b_{bu}(z)$  is the diffuse backscattering coefficient for the upwelling stream and  $R(z)$  is irradiance reflectance.

For any given values of  $a$  and  $b$ , and having specified  $\tilde{\beta}(\theta)$  and the incident light field, then if the radiance distribution at depth  $z$  m is calculated by a Monte Carlo, or other, procedure, it is possible to calculate the diffuse optical properties at that depth.<sup>700</sup> Thus all the terms on the right-hand side of eqn 1.63 may be determined for a series of values of  $b$  and  $a$ , and so the relative importance of the three different processes can be evaluated for different types of water.

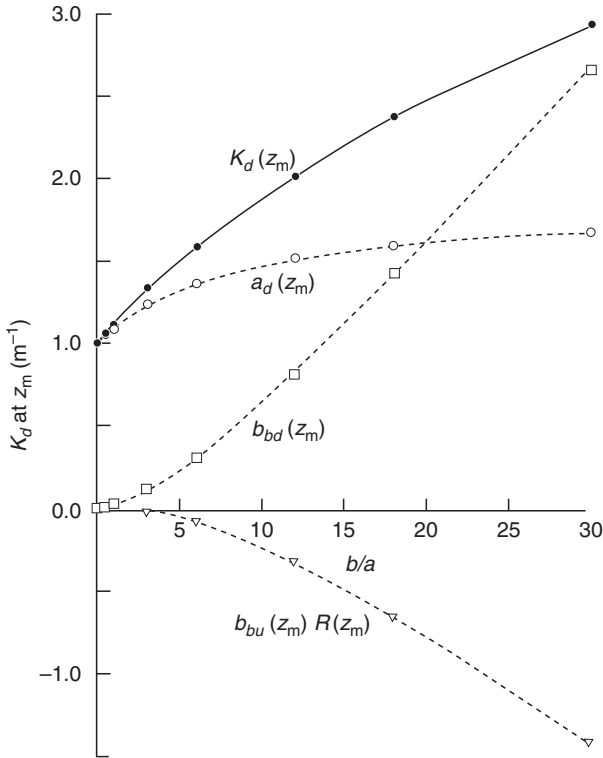


Fig. 6.20 Changes in the different components of the attenuation processes as a function of  $b/a$ . The calculated values of the three right-hand terms in eqn 1.63 are plotted alongside the corresponding values of  $K_d$  at  $z_m$  (data from Kirk, 1981a).

Figure 6.20 shows the change in value of each of these three terms, compared to the value of  $K_d$ , at  $z_m$ , as the ratio of scattering to absorption coefficients increases from 0.0 to 30.0. At low values of scattering, up to  $b/a$  ratios of about three, attenuation is almost entirely due to absorption, and furthermore the scattering-induced increase in attenuation is mainly a consequence of the increase in absorption resulting from the changed angular distribution of the downwelling flux. Upward scattering of the  $b/a$  downwelling stream contributes only slightly to attenuation.

When  $b/a$  has risen to about seven, upward scattering of the downwelling stream accounts for about 25% of all the attenuation and contributes as much to the increase in attenuation as does the increase in absorption of the downwelling light. At  $b/a$  values of about 11 and 20, upward scattering of the downwelling light accounts for 0.5 and 1.0 times

as much attenuation, respectively, as does absorption, and at higher  $b/a$  values it becomes the major mechanism for attenuation. The downward scattering of the upwelling stream, which acts to diminish attenuation, has little effect over the lower part of the range of  $b/a$  values studied, but becomes significant from about  $b/a = 6$  onwards, and counteracts a large part of the attenuation due to the other two processes at  $b/a$  values in the range 12 to 30.

## 6.8 Partial vertical attenuation coefficients

In any medium containing a number of absorbing and scattering components, the contributions of the different components to any one of the absorption and scattering coefficients (normal, diffuse, forward, back) are additive, e.g. if there are  $n$  components, then

$$a_{\text{total}} = a_1 + a_2 + \dots + a_n$$

and similar relations hold for  $b$ ,  $a_d(z)$ ,  $b_{bd}(z)$  etc. Consequently, for an aquatic medium containing  $n$  absorbing/scattering components we can expand eqn 1.63 to

$$\begin{aligned} K_d(z) &= a_d(z)_1 + a_d(z)_2 + \dots + a_d(z)_n \\ &\quad + b_{bd}(z)_1 + b_{bd}(z)_2 + \dots + b_{bd}(z)_n \\ &\quad - b_{bu}(z)_1 R(z) - b_{bu}(z)_2 R(z) - \dots - b_{bu}(z)_n R(z) \end{aligned}$$

Rearranging, we obtain

$$\begin{aligned} K_d(z) &= [a_d(z)_1 + b_{bd}(z)_1 - b_{bu}(z)_1 R(z)] \\ &\quad + [a_d(z)_2 + b_{bd}(z)_2 - b_{bu}(z)_2 R(z)] \\ &\quad + \dots + [a_d(z)_n + b_{bd}(z)_n - b_{bu}(z)_n R(z)] \end{aligned}$$

which can be written in the form

$$K_d(z) = K_d(z)_1 + K_d(z)_2 + \dots + K_d(z)_n \quad (6.30)$$

Thus the vertical attenuation coefficient for downward irradiance in a natural water can be partitioned into a set of partial vertical attenuation coefficients, each corresponding to a different component of the medium. The partial vertical attenuation coefficient for the  $i$ th component is given by

$$K_d(z)_i = a_d(z)_i + b_{bd}(z)_i - b_{bd}(z)_i R(z) \quad (6.31)$$

It is important to remember that although the contributions of the different components of the medium to total attenuation of irradiance can be simply added together in accordance with eqn 6.31, the nature of their contributions to attenuation can vary markedly from one component to another. Consider, for example, a water in which component  $j$  is dissolved yellow colour, and component  $j+1$  consists of suspended mineral particles, scattering intensely but with little intrinsic colour. For the  $j$ th component,  $K_d(z)_j$  will consist mainly of the absorption term,  $a_d(z)_j$ , in eqn 6.31, whereas for the  $(j+1)$ th component,  $K_d(z)_{j+1}$  will consist mainly of the backscattering term,  $b_{bd}(z)_{j+1}$ .

It is also important to remember that the value of  $K_d(z)_i$ , and consequently the contribution of the  $i$ th component to  $K_d(z)$ , is not a linear function of the concentration of that component. Any substantial change in the absorption and/or scattering characteristics of the medium resulting from a change in concentration of one of the components will inevitably affect the radiance distribution at depth  $z$ . The absorption and scattering coefficients on the right-hand side of eqn 6.31, being quasi-inherent rather than inherent optical properties (see §1.5) are functions of the radiance distribution as well as of the concentration of the component in question. Consequently, although their values will increase with the concentration of the component, the increase will not be linear with concentration. Furthermore,  $R$ , being a function of the radiance distribution, will also change as the concentration of any component changes. In short,  $K_d(z)_i$  and  $K_d(z)$  will certainly increase as the amount of any of the components of the medium increases, but except for small increments in concentration, the increases will not be linearly related to the increase in concentration.

## 7

# Remote sensing of the aquatic environment

In any water body some of the light that penetrates the water is caused, by scattering within the water, to pass up through the surface again. Of this emergent flux, 90% originates within the depth (equal to  $1/K_d$ ) in which downward irradiance falls to 37% ( $1/e$ ) of the subsurface value.<sup>490</sup> It can be regarded as a sample derived from the underwater light field, and so by studying it with appropriate detection instruments above the surface, information about that field, and therefore about the optically significant components of the medium, can be obtained. There is not much point in having detection instruments just above the surface: they would be more useful below. If, however, this emerging radiant flux can be studied by remote sensing instruments, located a considerable distance above the surface, in an aeroplane or space satellite, then the considerable advantage is gained that information about the underwater environment over a large area can be obtained in a short time. This makes it possible to acquire a synoptic view of a large aquatic ecosystem, with a fraction of the time and effort that would be involved in carrying out measurements over the same area from a surface vessel.

It will readily be appreciated, however, that a price must be paid. Measurements of the emergent flux, from a great distance, cannot be as accurate, or yield as much information, as measurements carried out within the water itself. We shall now consider the kinds of measurements that can be made, the correction procedures that must be carried out and the nature of the information that may be obtained. We shall then go on to examine some of the studies that have been carried out so far.

### 7.1 The upward flux and its measurement

A photometer in an aeroplane or satellite, pointed down at the ocean or any other water body can receive light originating in four different ways: by scattering from below the surface, by reflection of skylight at the surface, by reflection of the direct solar beam at the surface and by scattering within the atmosphere (Fig. 7.1). Only the first of these four light fluxes, which we shall refer to as the emergent flux, contains information about the underwater light field and the composition of the aquatic medium. The essential problem, therefore, is to quantify the emergent flux in the presence of the other light fluxes.

The photometer used to measure the light flux above the water surface is a radiance meter with a narrow angle of acceptance. To avoid receiving the surface-reflected solar beam, the radiance meter can be directed at a part of the surface well outside the solar glitter pattern. A more difficult problem is that of accounting for that part of the measured radiance which originates within the atmosphere. Depending on wavelength, anything from 80 to 100%, typically ~90%, of the radiance received by a satellite-borne radiance meter, directed at the ocean surface outside the

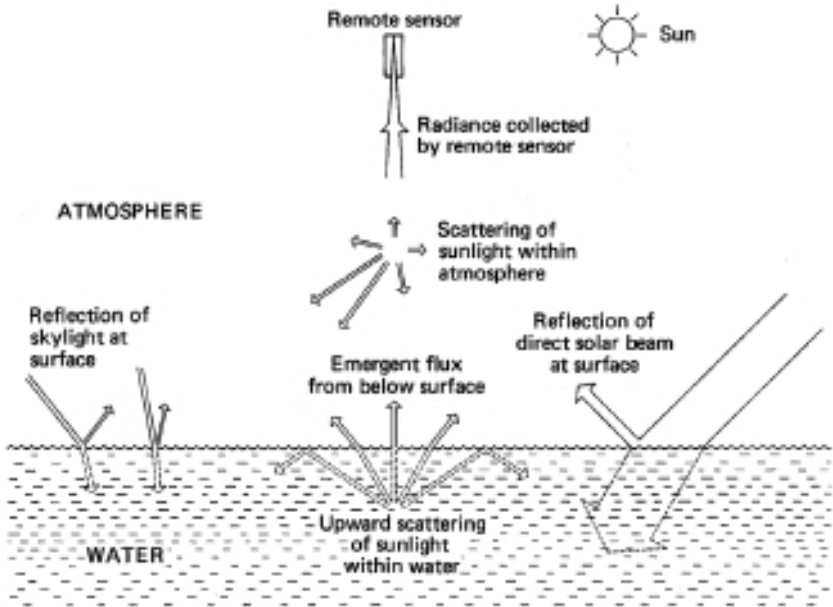


Fig. 7.1 The different origins of the light received by a remote sensor above a water body.

Sun glitter pattern, originates in atmospheric Rayleigh (air molecule) and aerosol (particle) scattering. Ways of correcting for this flux are considered in a later section. This problem is largely eliminated when measurements are taken from low-flying aircraft (see Fig. 7.8a).

Skylight also originates in atmospheric scattering. Correction for the contribution of reflected skylight to the measured upwelling flux can be lumped in with the total atmospheric scattering correction.<sup>485</sup> An alternative procedure is to carry out the measurements at an angle of  $53^\circ$  to the vertical.<sup>234</sup> Light reflected from a plane surface at this angle (Brewster's angle) is polarized and can be eliminated by placing a polarized filter oriented at right angles to the major axis of polarization over the aperture of the radiance meter. A consequence of viewing at this angle, however, is that the effective air mass through which the flux from within the water must travel is increased by a factor of 1.67:<sup>41</sup> this would be a significant disadvantage in the case of a satellite or high-flying aircraft, but not in the case of a low-flying aircraft.

### **Measurement systems – general considerations**

Remote sensing photometers used in low-altitude aircraft normally have a fixed direction of view. They measure upward radiance at a series of points along a linear track determined by the flight path of the aircraft. For two-dimensional mapping, the aircraft must traverse the area of interest many times. The spectral distribution of the radiance at each point is determined using interference filters or a spectroradiometer.

With increasing altitude the area that it is practicable to 'view' increases. To take advantage of this, remote sensing from satellites and higher-altitude aircraft uses spatially scanning photometers, which collect information, not just from the thin line immediately below the trajectory of the satellite or aircraft, but from a broad swath of the Earth's surface, which can be anything from a few kilometres to hundreds of kilometres wide. There are two ways of achieving this, sometimes referred to respectively as 'pushbroom' scanning and 'whiskbroom' scanning.<sup>1231</sup> In a pushbroom scanner the instrument optics form an image of a thin transverse strip of the Earth's surface extending right across the swath at right angles to the line of flight, and present it across a line array of photo-detector elements. Each of these detector elements thus receives radiation from one of the elements of area at the surface, which between them form the strip across the swath.

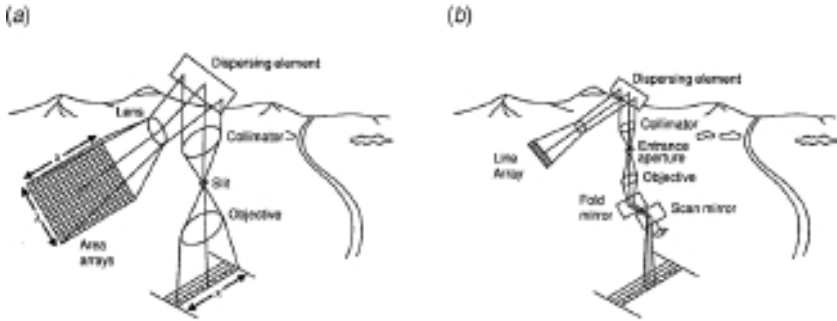


Fig. 7.2 Imaging spectrometry in remote sensing. (a) Pushbroom scanner with two-dimensional array of photodetectors. (b) Whiskbroom scanner with line array of photodetectors. (After HIRIS Instrument Panel Report. NASA, 1987.)

In fact, what is required for each element of area at the surface is a sample not of the total radiation but of the radiant flux in each of some specified set of spectral wavebands. The radiation from the transverse strip at the surface can, by means of dichroic beam splitters (partially reflective mirrors that reflect radiation below a certain wavelength and let the longer wavelength energy through), be subdivided into a number of separate fluxes each of which can be directed through a different spectral filter onto its own line array of photodetector elements. A more radical solution is to spectrally disperse the radiant flux with a prism or grating and form an image on a two-dimensional array of photodetectors, one axis corresponding to position of the individual surface element across the swath, the other to wavelength (Fig. 7.2a). In principle, in this way, a complete spectrum of the flux from each element of area can be obtained.

Remote sensing radiometers of the whiskbroom type scan by means of a rotating or oscillating mirror, which ensures that the direction of viewing is continually moving from one side of the swath to the other, at right angles to the satellite/aircraft trajectory (Fig. 7.2b). The scene reflected in the mirror is viewed through a telescope with a very small acceptance angle ( $0.002\text{--}0.05^\circ$ ) so that at any given instant only a small unit element of the Earth's surface is in view. The flux collected by the telescope can be partitioned into a set of spectral bands using beam splitters and filters, and a corresponding set of photodetectors, or be dispersed with a grating or prism onto a line array of detector elements to provide a more complete spectral distribution.

With either the pushbroom or whiskbroom type of radiometer, a series of contiguous but non-overlapping, square image elements,

corresponding to a linear sequence of elements of area at the surface, extending across the swath, is recorded. By the time the next side-to-side scan begins the satellite or aircraft has moved on so that the next left-to-right sequence of image elements adjoins, but does not overlap, the previous sequence. The accumulated set of image elements constitutes a mosaic corresponding to that strip of the Earth's surface defined by the path of the satellite/aircraft and its maximum lateral angle of view.

For each image element, i.e. for each element of surface, the photometer has recorded a set of radiance values corresponding to the number of spectral bands with which it operates. The radiance values are encoded digitally, and a key parameter for any remote sensing instrument is the number of bits to which digitization is carried out: this can vary from 6 bits giving a measurement range of up to 64 different radiance values, to 16 bits giving 65 536 different values. This information, after being relayed to a receiving station in the case of a satellite, is stored on tape or other medium. The data can then be used, after appropriate computer processing, to prepare a map of any part of the Earth's surface that lay beneath the satellite's orbit, or aircraft's path. The continuous swath covered by a satellite is broken down for mapping purposes into individual sections that might be some hundreds of kilometres long.

Each small element of the map, referred to as a *pixel*, corresponds to one of the square unit elements of surface viewed by the scanning photometer. The intensity, or the colour within a selected colour scale, of each pixel in the final map displayed on the computer screen can be directly related to the radiance value in any one of the spectral bands, or can be determined by the value of some parameter (e.g. chlorophyll concentration) derived by calculation from more than one of the spectral radiance values.

### **Low altitude (0–600 m) line-of-flight, and stationary, systems**

We consider here instruments that measure radiance only along a linear path, i.e. that do not simultaneously scan from side to side.

For completeness we shall deal first here with radiometric sensing of water bodies carried out from boats, even though this is, of course, strictly speaking not 'remote' sensing. As a quantitative measure of ocean colour, Jerlov (1974) defined the *colour index* to be the ratio of nadir radiance (i.e. vertically upwards flux, nadir angle  $\theta_n = 0^\circ$ ) within the water in the blue at 450 nm to that in the green at 520 nm, and developed

a colour meter consisting of a pair of downward pointing Gershun tubes with a blue and a green interference filter, respectively, to measure it. The meter was designed to be lowered manually from shipboard to any depth. Neuymin *et al.* (1982) chose a somewhat different pair of wavelengths in the blue and green for the colour index, namely 440 and 550 nm, which has the advantage that this ratio is particularly sensitive to algal pigments, and consequently this is the pair of wavelengths most favoured for remote sensing of oceanic phytoplankton (see later). As it happens, Neuymin *et al.* chose to define their colour index in terms of the green to blue ratio (in the upwelling flux), rather than vice versa, and so their index *increases* with phytoplankton content. Their instrument was located at 5 to 6 m depth in a shaft running through the vessel, and could provide a continuous record of the colour index of the sea along the ship's track.

Bukata, Jerome and Bruton (1988) developed a shipboard radiometer mounted on a 4.5 m boom from the bow, at 4.5 m above the water surface. Nadir radiance from the lake water surface was measured in four broad wavebands in the blue, green, red and near-infrared regions, together with downward solar irradiance in the same four wavebands. Measurements were taken continually from the moving vessel at half-second intervals.

Deschamps *et al.* (2004) have developed a hand-held radiometer (SIMBAD) for shipboard use, which measures the emergent flux from the ocean in five spectral bands – 443, 490, 560, 670 and 870 nm – with 10 nm bandwidths. To reduce sunglint and skylight-reflection effects, radiance is measured through a vertical polarizer, and the instrument is held at 45° from the nadir (near the Brewster angle) and 135° from the principal plane of the Sun. The field of view is 3°. The instrument incorporates a sun photometer to measure aerosol optical thickness, from which the downward solar irradiance in each waveband can be estimated, and the values of remote-sensing reflectance can thus be calculated. The major advantage of this, and other, above-water systems is that the ship does not need to stop for measurements to be taken.

Wood and Cunningham (2001) constructed an above-surface, ship-borne reflectance radiometer, which by means of a grating and a CCD array carried out near-simultaneous measurements of water-leaving radiance (radiometer acceptance angle, 1°) and downward irradiance over the range 380 to 800 nm. With the instrument mounted high on the ship superstructure, at an angle of 53° to the vertical (the Brewster angle), a point on the surface at a distance of about 30 m from the sunnier side of the vessel was viewed through a polarizing filter. The authors point out

that the movement of the ship, and the presence of waves on the surface, prevent the Brewster angle being achieved exactly, and some reflected light from the sky will therefore pass through the polarizing filter. Even after applying a correction for this problem, there remained a significant discrepancy between the  $L_u$  spectrum obtained with the shipborne instrument, and the true underwater  $L_u$  spectrum. However, if the reflectance spectra ( $L_u[\lambda]/E_d[\lambda]$ ) were normalized to reflectance at 490 nm, there was good agreement between them in the 475 to 750 nm range.

The Atlantic Micro Surface Acquisition System (MicroSAS) is designed for above-water measurements of ocean colour, and is suitable for mounting on ships or on low-flying aircraft. It has a radiance meter pointing at the ocean to measure the water-leaving radiance, another pointed at the sky to provide the information necessary to correct for reflected skylight, and an irradiance sensor pointing upward to measure the downward solar flux so that remote-sensing reflectance can be calculated. In a typical configuration it operates simultaneously in seven wavebands corresponding to those that are used in the spaceborne SeaWiFS scanner (see later).

In an example of innovative use of inexpensive, off-the-shelf instrumentation, Goddijn and White (2006) used the red-green-blue output from a digital camera to characterize water colour in Galway Bay (Ireland). To eliminate reflection from the water surface a tube was fitted around the camera lens to penetrate the water surface, the end of the tube being about 10 cm below the surface. The data were used to study the distribution of CDOM (see later).

The usual aim in ocean remote sensing is to obtain information from a large area of the sea within a short space of time: in effect, a 'snapshot' of the area of interest as it was at one point in time. An alternative approach is to concentrate on one small location of interest and use remote sensing to follow changes with time. For this purpose towers can be used, but for practical reasons have only so far been constructed in shallow coastal waters. The Aqua Alta Oceanographic Tower, built in 1970, is located in the Adriatic Sea, about 15 km SE of the Venice Lagoon, in a water depth of 17 m. The optics platform is 7 m above the sea surface. Hooker *et al.* (2004) carried out above-water radiance measurements in five wavebands in the blue-green – 412, 443, 490, 510 and 555 nm. To avoid sunglint the radiometer was pointed 90° or 135° away from the plane of the Sun. To remove the contribution of reflected skylight they measured downwelling sky radiance at the appropriate angle, in the same plane, and calculated reflected sky radiance assuming Fresnel reflection at the surface.

Zibordi *et al.* (2006) used the Gustaf Dalén Lighthouse Tower, located in the northern Baltic, five nautical miles off the Swedish coast in a water depth of 16 m, from which to monitor water-leaving radiance at regular intervals from June through October 2005. The instrument used was a SeaPRISM radiometer with seven channels (412, 440, 500, 555, 675, 870 and 1020 nm), with  $1.5^\circ$  full angle field of view, placed on top of the tower, 25.5 m above average sea level. The sea-viewing angle was  $40^\circ$ , and the relative azimuth with respect to the Sun was  $90^\circ$ . With this instrument, which operated automatically, they were able to monitor the development and subsequent decay of a cyanobacterial bloom during July.

An advantage of above-water monitoring of the submarine light field is that the radiometers are not subject to the problem of biofouling, which bedevils long-term measurement within the water. From towers, such as described above, only a small area of the sea surface can be observed. For long-term, above-water optical monitoring of important medium-scale aquatic ecosystems, such as certain estuaries, the placement of spatially scanning radiometers in tethered balloons might be worth considering.

Gitelson and Kondratyev (1991) sought to combine both 'remote' and sea level sensing by flying 10 to 15 m above the sea surface in a helicopter from which they simultaneously made radiometric measurements and took water samples. Upward and downward radiance and irradiance, in nine 10-nm spectral channels between 430 and 750 nm were measured with a hand-held spectrometer requiring less than 1 s to complete its readings.

Where a spectroradiometer is being used from an aircraft it is important that the spectral scan is completed quickly to minimize the effects of changes in the emergent flux from point to point along the flight path. Clarke *et al.* (1970) used a spectroradiometer with a  $3^\circ \times 0.5^\circ$  field of view, which scanned from 400 to 700 nm in 12 s. The instrument was operated at the Brewster angle in conjunction with a polarizer, to eliminate reflected skylight. Neville and Gower (1977) used a spectroradiometer<sup>1426</sup> in which the spectrum produced by a diffraction grating was distributed over an array of 256 silicon diodes, each of which continuously detected the radiant flux in its own narrow region of the spectrum. It was possible to read out the complete spectrum, 380 to 1065 nm, at 2 s intervals.<sup>137</sup> This instrument was also operated at the Brewster angle.

At the other extreme, spectrally speaking, useful information can be obtained by airborne remote sensing in two or three wavebands, provided these are carefully chosen. Arvesen, Millard and Weaver (1973) developed a differential radiometer, which carried out simultaneous measurements of upward radiance at 443 and 525 nm, and continuously compared one

with the other (in effect, measuring Jerlov's colour index). This had the advantage that changes in incident light intensity or variations in surface water roughness had similar effects on the flux in both wavebands and so were automatically corrected. Changes in phytoplankton concentration, however, which would be expected specifically to affect the ratio of upward flux in these two wavebands (see §7.5), markedly affected the signal.

To address the need for an affordable aircraft ocean colour instrument, the National Aeronautics and Space Administration (NASA) and the National Oceanic and Atmospheric Administration (NOAA) developed the Ocean Data Acquisition System (ODAS).<sup>526,1448</sup> This measures nadir radiance in three 15-nm bands centred on 460, 490 and 520 nm, these bands being chosen specifically to make possible the use of a previously developed<sup>199</sup> spectral curvature algorithm for remote sensing of phytoplankton. The three radiances are sampled ten times per second and averaged over 1 s. With the aircraft flying at  $50 \text{ ms}^{-1}$  at an altitude of  $\sim 150 \text{ m}$ , the footprint of the instrument is about  $5 \times 50 \text{ m}$ . Position is measured accurately at 20 s intervals with Loran-C navigation.

### Medium/high altitude (2–20 km) spatially scanning systems

The NASA Multichannel Ocean Colour Sensor (MOCS)<sup>199</sup> measures radiance in 20 contiguous 15-nm wide bands between 400 and 700 nm. It has a spatial resolution of  $4 \times 2 \text{ mrad}$ , corresponding to  $20 \times 10 \text{ m}$  at the surface, and a field of view of  $17.1^\circ$ , corresponding to a swath width of  $\sim 1.5 \text{ km}$ , when viewed from a plane at 5 km altitude.

The Daedalus Airborne Thematic Mapper has eleven channels, with five broad, approximately contiguous, bands in the visible region covering the range 420 to 690 nm, and another six bands in the infrared.<sup>1470</sup> It has a particularly wide field of view ( $86^\circ$ ), and an angular resolution of 2.5 mrad, corresponding to a geometric resolution at sea level of 10 m square from a plane at 4 km altitude. An updated version, the AZ-16, is now available with a slightly increased field of view ( $90^\circ$ ) and 16-bit rather than 8-bit resolution.

A great leap forward in airborne remote sensing has been the development of what is known as *hyperspectral* imagers. These use diffraction gratings to spectrally disperse the collected light across linear, or two-dimensional, photodetector arrays containing large numbers of elements. In this way measurement can be carried out in 200 to 300 wavebands, with bandwidth 3 to 10 nm, across the spectrum, thus providing

something very close to a continuous reflectance spectrum. An early and notable example was the NASA Airborne Visible and Infrared Imaging Spectrometer (AVIRIS),<sup>975</sup> which became operational in 1987 and is still in use today. Its optical system is of the whiskbroom type illustrated in Fig. 7.2*b*, using line arrays of silicon and indium alloy detectors to provide 224 contiguous spectral bands covering the visible/infrared region from 0.4 to 2.5  $\mu\text{m}$ , with  $\sim 10$  nm resolution.<sup>46</sup> There are 677 pixels across the swath, and a complete spectrum is obtained for each pixel. Data encoding is 16 bit. AVIRIS is designed primarily to be flown at  $\sim 20$  km in a high altitude ER-2 aircraft: with its angular resolution of 1 mrad, its ground-instantaneous-field-of-view is 20 m. The total field of view is  $34^\circ$ , giving a swath width of 11 km. When flown in the Twin Otter aircraft, at 4 km above the ground, each ground pixel is 4 m square, and the swath is 2 km wide.

Commercial hyperspectral imagers for airborne use are now available. The CASI 1500 (Compact Airborne Spectrographic Imager), for example, is of the pushbroom type, and covers a spectral range of 650 nm, adjustable between 380 and 1050 nm, with up to 288 spectral bands.<sup>613</sup> The total field of view is  $40^\circ$  across-track, over 1500 pixels. Data encoding is 14 bit.

### Satellite systems

Remote sensing of ocean colour from space is carried out by a variety of radiometers on spaceborne satellites launched by a number of nations around the globe. Coordination of these studies is carried out by the International Ocean-Colour Coordinating Group (IOCCG, [www.ioccg.org](http://www.ioccg.org)), established in 1996. There are two types of orbits for Earth observation satellites, polar-orbiting and geostationary. Polar-orbiting satellites typically operate at an altitude of 700 to 800 km, with a revisit time of two to three days, whereas geostationary satellites operate in time scales of hours, which could in principle provide data on the diurnal variation in phytoplankton abundance and productivity.

Of the several Landsat satellites<sup>1219</sup> that have been placed in orbit, the ones most relevant to observing aquatic ecosystems are those that contain the Thematic Mapper scanner. This has broad bands in the blue (450–520 nm), green (520–600 nm), red (630–690 nm) and near-infrared (760–900 nm) plus three infrared bands. The unit element of area viewed is 30 m square. Although primarily designed for prediction of crop production, the Thematic Mapper has received some use for coastal and

inland waters. The most recent version, the Landsat 7 Enhanced Thematic Mapper Plus, achieves its 185 km cross-track ground swath by using an oscillating mirror to traverse a  $15^\circ$  cross-track field of view. Its 705 km altitude orbit is polar sun-synchronous, so that it scans the entire Earth surface. The instantaneous field of view is 0.043 mrad ( $0.00123^\circ$ ). The Advanced Land Imager, on the Earth Observing-1 satellite is a prototype of the next generation of Landsat series satellites, with three additional spectral bands and higher radiometric resolution (16 bit, compared to 8 bit).

Two other spaceborne sensors, not designed for studies on waterbody colour and composition, but which have occasionally been used for this purpose, are the Advanced Very High Resolution Radiometer (AVHRR), and the high resolution radiometer (HRV) in the System Probatoire d'Observation de la Terre (SPOT). The AVHRR, the current version of which is on the NOAA-15 satellite, at an altitude of 807 km, has a band in the red (580–680 nm) and in the near-infrared (725–1000 nm) and four other bands in the near-infrared, three of which are for sea surface temperature measurement. Its resolution at sea level is 1 km, with a 3000 km swath. The HRV on the French SPOT platform (latest version – SPOT 5, launched 2002, 822 km altitude) has a green (500–590 nm), a red (610–680 nm) and a near-infrared (780–890 nm) band, and is distinguished by its high ground-level resolution of 2.5 m (with a 60 km swath), and by being pointable ( $\pm 26^\circ$ ) both across and along track. It has 8-bit digitization.

In October 1978, the Nimbus-7 satellite was launched, carrying the Coastal Zone Colour Scanner (CZCS), which was designed specifically for remote sensing of the marine environment: its optical system is shown in Fig. 7.3. The CZCS had four bands in the visible region, each 20 nm wide, centred on 443, 520, 550 and 670 nm, one band in the near-infrared (700–800 nm) and another band in the infrared (10.5–12.5  $\mu\text{m}$ ) for temperature sensing. To facilitate avoidance of Sun glitter the sensor could be tilted so that it scanned at up to  $20^\circ$  from the nadir, ahead of or behind the spacecraft. It had a mirror at  $45^\circ$  rotating at 8.1 revolutions per second, at which was directed a telescope that gave an instantaneous field of view of 865  $\mu\text{rad}$  ( $0.05^\circ$ ) corresponding, at the satellite altitude of 955 km, to a unit element of area 825 m square at the surface.<sup>588,589</sup> It covered a continuous swath 1636 km wide, which for mapping purposes was broken down into individual sections that might typically be 700 km along the spacecraft's track. The radiometric sensitivity of the CZCS was 60-fold higher than that of the MSS on Landsat and had 8-bit

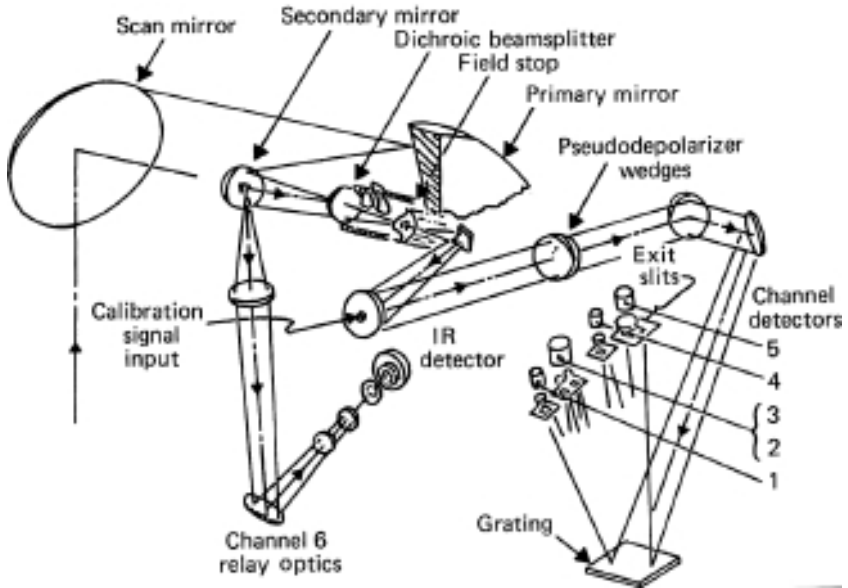


Fig. 7.3 Optical system of the Coastal Zone Colour Scanner in the Nimbus-7 satellite (by permission, from Hovis, 1978).

digitization. A simple threshold, using the high reflectance of clouds and land in the 700 to 800 nm waveband, was used to distinguish these areas from open water: it is only to these latter picture elements that an atmospheric correction procedure was applied.

The CZCS eventually ceased to function in 1986. During its life it revolutionized our knowledge of the global distribution of ocean colour and, more importantly, of those oceanic constituents, particularly phytoplankton, which affect ocean colour. The archived data accumulated from this scanner during its years of operation are still being worked on. The implications of this new synoptic view of the oceanic biosphere are so far-reaching for our understanding of the marine ecosystem, and in particular for the global carbon cycle, in which oceanic primary production plays a crucial role, that the urgent necessity to replace the CZCS so that this crucially important information flow could continue, was clearly apparent. A number of other, more advanced, ocean colour scanners were developed and are now in orbit. Some of these we shall now consider.

The immediate successor to the CZCS was the SeaWiFS (Sea-viewing Wide-field-of-view Sensor), a joint Earth Observation Satellite (EOSAT)/NASA project. It was launched on 1 August 1997, on the relatively

small Pegasus rocket, which was first carried up to the low stratosphere on board a Lockheed L-1011 aircraft and released at an altitude of 12 km. The Pegasus rocket then engaged, and carried the spacecraft up to a low Earth orbit at 278 km. The SeaStar spacecraft was then released from the Pegasus, and using its own hydrazine propulsion system, raised the satellite to its final 705 km circular orbit.

The scanner is of the whiskbroom type with a rotating telescope, and measurement is carried out in eight wavebands isolated with dichroic beam splitters and interference filters. There are six 20-nm spectral bands in the visible region, centred on 412, 443, 490, 510, 555 and 670 nm, and two bands for atmospheric correction in the near-infrared at 745 to 785 nm (blocked between 760 and 770 nm to minimize interference from the atmospheric oxygen absorption band) and 845 to 885 nm. As the name indicates, the SeaWiFS has a very wide field of view,  $\pm 58.3^\circ$  to either side of the track, which, from its orbit height of 705 km, gives a swath width of 2800 km. To avoid Sun glitter, the instrument can be directed at the nadir, or at  $20^\circ$ , along track or behind. The sea level resolution is 1.13 km, and the radiance values are 10-bit digitized. [Figure 7.4](#) shows the instrument design, and in [Fig. 7.5](#) it is shown deployed on the SeaStar spacecraft on which it is in fact (unlike CZCS on Nimbus-7) the only instrument.

The European Space Agency developed the Medium Resolution Imaging Spectrometer (MERIS).<sup>370</sup> This is a programmable, medium-resolution imaging spectrometer operating in the visible and near-infrared range. It is one of the instruments on the ENVISAT satellite, which was launched by an ARIANE 5 rocket on 1 March 2002 into a near-circular, near-polar orbit at 800 km. The optical system, of which there are five identical units within the instrument each with its own diffraction grating, covers the spectral range 390 to 1040 nm, but measurements are confined to 15 spectral bands – which can be selected on command from the ground within this range. For ocean remote sensing, there are eight bands in the visible, centred on 412.5, 442.5, 490, 510, 560, 620, 665 and 681.25 nm, each 10 nm wide except for the 681.25 nm (chlorophyll fluorescence peak) band which is 7.5 nm wide. Of the seven bands in the near-infrared (700–1040 nm) three are used to calculate the atmospheric contribution to the radiance measured in the visible bands above the atmosphere (see §7.3), and the remainder for measurement of water vapour, clouds, vegetation and oxygen absorption. Scanning is of the pushbroom type, and the two-dimensional photodetector arrays are silicon matrix CCDs (charge-coupled devices); the radiance values are 12-bit digitized.

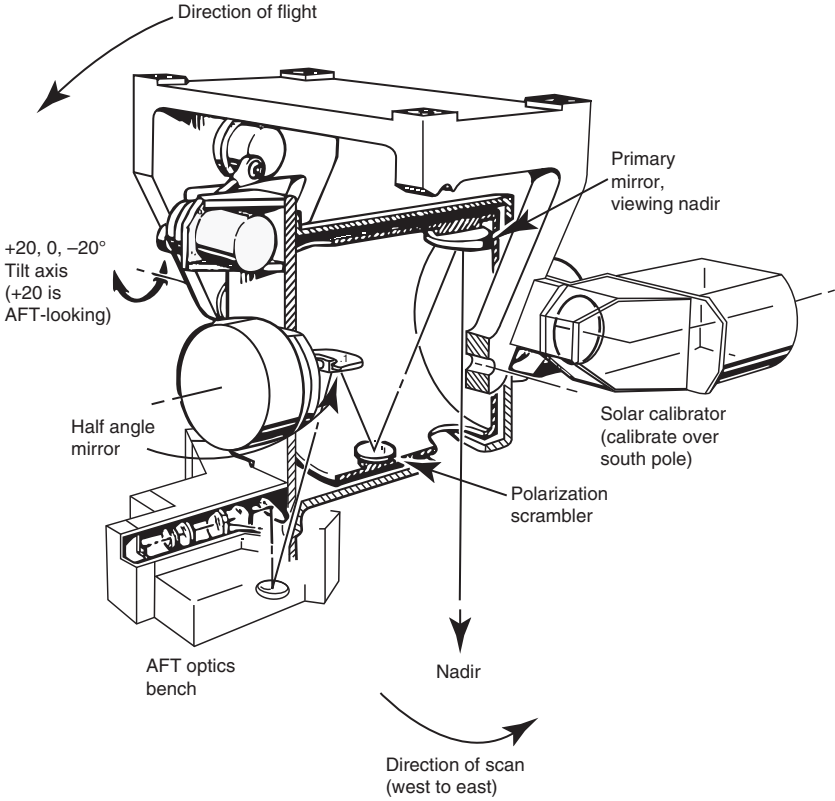


Fig. 7.4 Design of the SeaWiFS instrument for remote sensing of the ocean from space. By permission, Orbital Sciences Corporation, USA.

The instrument field of view is  $68.5^\circ$  centred about the nadir. This wide field of view is shared between the five identical optical modules, each of them receiving  $14^\circ$  of the total field. The spatial resolution at sea level is 300 m when the instrument is operated in full resolution mode (e.g. in coastal waters) and 1200 m in reduced resolution mode (e.g. over the ocean). From the orbit height of  $\sim 800$  km the swath width is 1150 km, and complete coverage of the Earth's surface is carried out every three days.

The *Terra* and *Aqua* satellites, developed by NASA, both carry the Moderate Resolution Imaging Spectrometer (MODIS), which can be used for ocean colour sensing. Both spacecraft are in near-polar, circular orbits at an altitude of 705 km. *Terra* (launched in December 1999) passes from north to south across the equator in the morning, while *Aqua*

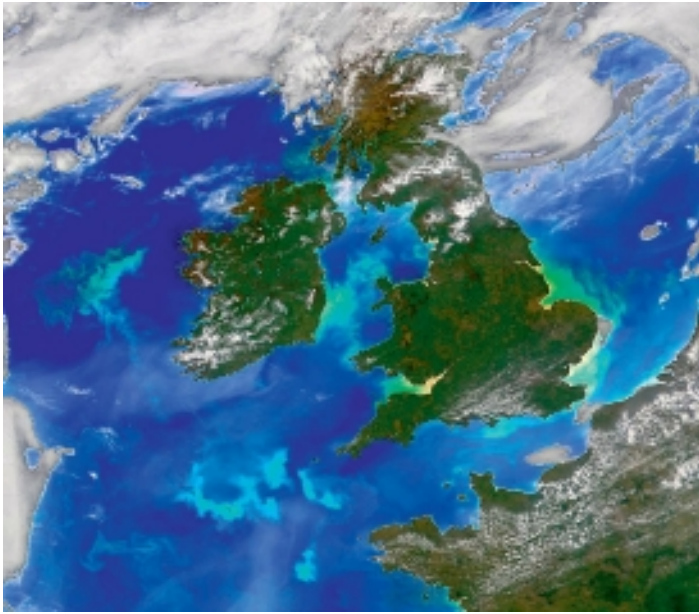


Fig. 4.11 Cocolithophorid blooms in the Atlantic Ocean, west of Ireland and of Cornwall, and also in the Celtic Sea, Monday 18 May 1998. Image collected at NERC Satellite Receiving Station, Dundee, Scotland. (Courtesy of the SeaWiFS Project, NASA Goddard Space Flight Center.)

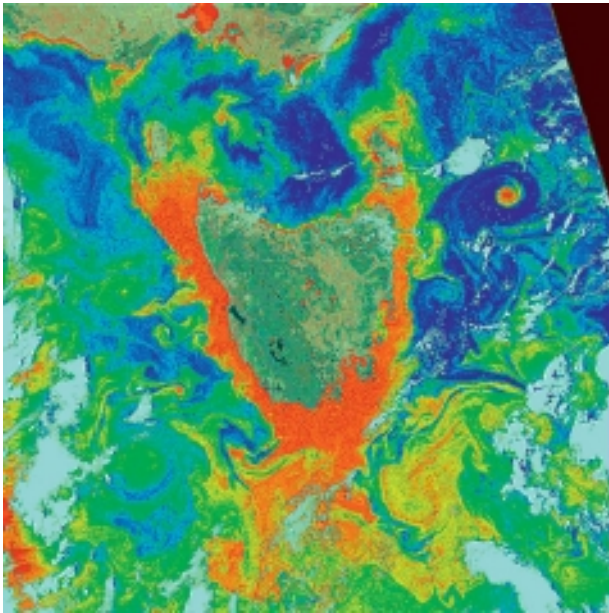


Fig. 7.10 Distribution of phytoplankton in the ocean around Tasmania (Southern Ocean, south of the Australian continent), 27 November 1981, derived from CZCS data. Phytoplankton chlorophyll *a* concentration is colour coded from red (high) to blue (low). Courtesy of the NASA GSFC Earth Sciences Data and Information Services Center (GES DISC).

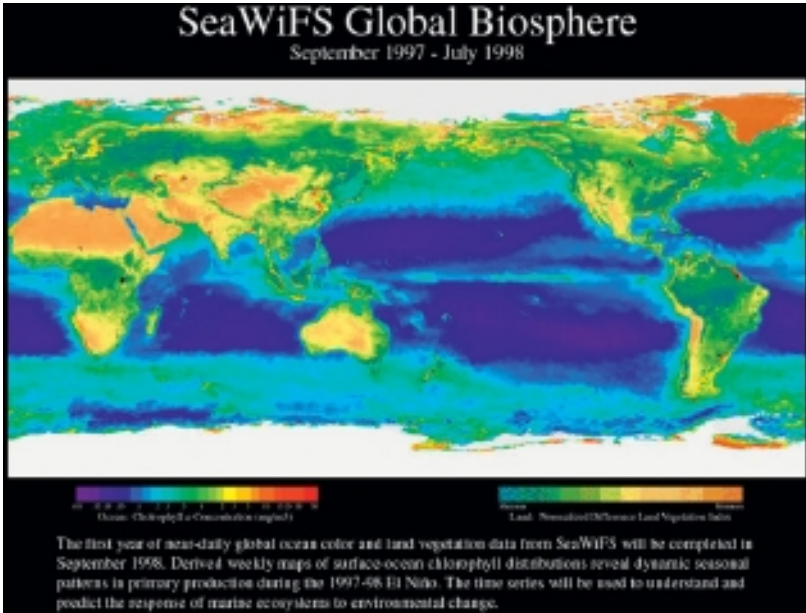


Fig. 7.11 Average distribution of phytoplankton chlorophyll in the global ocean (and also terrestrial vegetation) over an 11-month period in 1997–98, derived from SeaWiFS data. Provided by the SeaWiFS Project, NASA/Goddard Space Flight Center and ORBIMAGE.

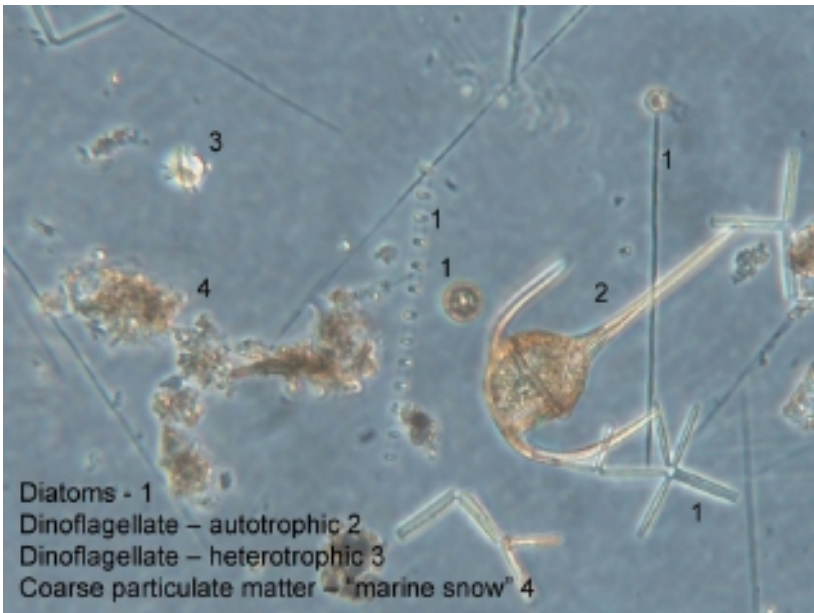


Fig. 9.5 Mixed coastal phytoplankton, Tasmania, Australia. (Courtesy Ian Jameson, CSIRO Marine & Atmospheric Research.)

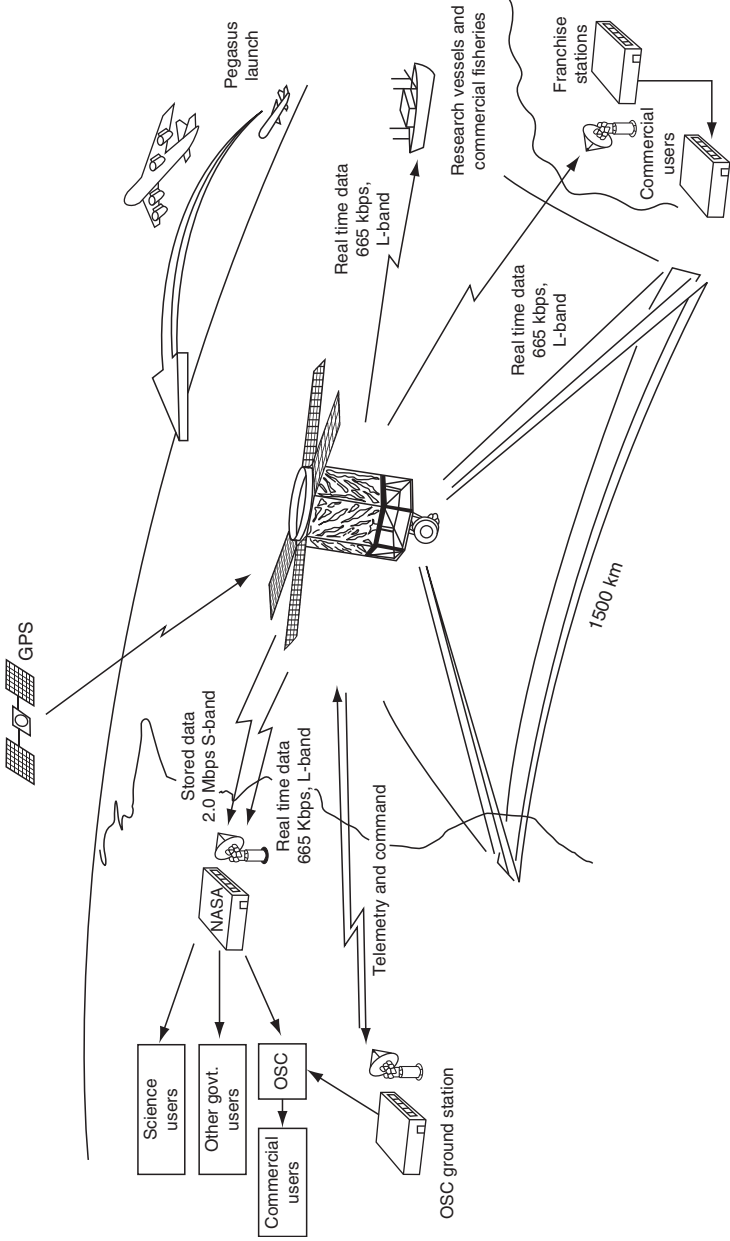


Fig. 7.5 SeaWiFS instrument shown deployed on the SeaStar™ spacecraft. By permission, Orbital Sciences Corporation, USA.

(launched in May 2002) passes south to north across the equator in the afternoon. Between them they view the entire Earth's surface every one to two days, measuring radiance in 36 wavebands in the visible, near-infrared and infrared.<sup>924</sup> For ocean colour, there are seven  $\sim 10$  nm bands in the visible region, centred on 412, 442, 488, 531, 551, 667 and 678 nm, plus two in the near-infrared centred on 748 and 870 nm, for atmospheric correction. The optical system uses a continuously rotating double-sided mirror to scan through  $\pm 55^\circ$ , achieving a cross-track swath width of 2330 km, with 1 km resolution. Radiance values are 12-bit digitized.

The Indian IRS-P4 (*Oceansat*) satellite, launched in 1999, carries the Ocean Colour Monitor (OCM) sensor, which operates in six visible wavebands – 414, 442, 489, 512, 557 and 670 nm, with 20 nm bandwidth. It also has two near-infrared bands – 768 and 867 nm, with 40 nm bandwidth, for atmospheric correction. Digitization is 12 bit. The instrument, which is of the pushbroom type, has separate wide-angle optics and a linear array CCD detector for each of the eight spectral channels: it can be tilted in the along-track direction to avoid sunglint. The cross-track swath width is  $\sim 1420$  km, with a  $360 \times 250$  m instantaneous field of view. *Oceansat* travels in a sun-synchronous polar orbit at 720 km.

China has launched a series of meteorological satellites, all with the name *Feng Yun* ('Wind and Cloud'). *Feng Yun 1C*, launched in 1999, carried the Multichannel Visible and Infrared Scan Radiometer (MVISR), with rather broad bands (50 nm) in the visible centred on 455, 505, 555, 630 and 685 nm. The spacecraft was in sun-synchronous polar orbit at an altitude of 858 km. *Feng Yun 1C* had the dubious distinction of being the first space satellite to be destroyed by an anti-satellite weapon, fired from Xichang (China) on 11 January 2007. It was replaced in orbit by *Feng Yun 1D*, with the same sensor.

In November 2000, NASA launched the Earth Observing 1 (EO-1) satellite, which carries three sensors intended primarily for terrestrial observation, but two of which – *Hyperion* and *Advanced Land Imager* – are of some value also for marine and inland aquatic systems. EO-1 is flying in formation with *Landsat 7* in a sun-synchronous, near-polar orbit at 705 km. The *Hyperion* sensor is a hyperspectral imager that provides 220 contiguous 10-nm bands from 400 to 2500 nm. It has a much higher ground-level resolution (30 m) than the ocean colour sensors described above, but a correspondingly narrower swath (7.7 km). The *Advanced Land Imager* (ALI) is a pushbroom instrument, which has four rather broad bands (433–453, 450–515, 525–605 and 630–690 nm)

in the visible and another five in the near-infrared. The swath width is 37 km with 30 m ground-level resolution.

A number of new ocean colour sensors are scheduled to be launched into space in the next few years. These are listed in [Table 7.1](#), together with their optical, and other, characteristics and the proposed launch dates. An additional instrument currently under development is the Ocean Ecosystem Spectrometer (OES), which will fly as part of the Aerosol, Cloud and Ocean Ecosystem mission (ACE), and will be constructed by NASA with international partners (ACE mission overview report – McClain 2009 (available on Web), and Paula Bontempi, personal communication). It is intended to have 86 hyperspectral bands covering the visible/near-infrared range (350–1000 nm), and three short-wave infrared bands. A resolution of 5 nm is aimed for in the 350 to 755 nm range. Four 10 nm bands (667, 678, 710 and 748 nm) will be assigned to chlorophyll fluorescence measurement, and five bands (at wavelengths from 748 to 1640 nm) will be used for aerosol correction. It will have 58.3° cross-track scanning, a 20° sensor tilt for glint avoidance, and a 1 km spatial resolution at the nadir. The satellite will have a sun-synchronous orbit, permitting two-day global coverage of ocean radiometer measurements. The tentative launch date is 2017/18.

## 7.2 The emergent flux

The particular light flux that is of the greatest interest in the present context is the upwelling light flux just below the surface. However, the flux that, after due correction, is remotely sensed, is the emergent flux – that part of the upwelling flux that succeeds in passing up through the surface. How are the two related?

Although about half the total upwelling light flux is reflected downwards again at the water–air interface, this does not represent a serious loss, since it is mainly the flux at larger angles which undergoes reflection. Remote sensing normally involves measurement of radiance at a specific angle rather than total upward irradiance, this angle being not more than 58° from the nadir. Thus remote sensing is normally concerned with that upwelling flux which, below the surface, is at angles of 0 to 40° to the vertical, and under calm conditions only ~2 to 6% of this is reflected downwards at the water–air boundary. Reflection in this angular range is

Table 7.1 Scheduled Ocean-Colour Sensors.

Sensor Agency	Satellite	Scheduled launch	Swath (km)	Resolution (m)	# of bands	Spectral coverage (nm)	Orbit
HSI DLR (Germany)	EnMAP	2013	30	30	228	420–2450	Polar
GOCI KARI/ KORDI (South Korea)	COMS-1	Early 2010	2500	500	8	400–865	Geostationary
OLCI ESA (Europe)	GMES-Sentinel 3A (ESA/EUMETSAT)	2013	1270	300/1200	21	400–1020	Polar
OLCI ESA (Europe)	GMES-Sentinel 3B (ESA/EUMETSAT)	2017	1265	260	21	390–1040	Polar
S-GLI JAXA (Japan)	GCOM-C (Japan)	2014	1150–1400	250/1000	19	375–12 500	Polar
VIIRS NOAA/NASA	NPP (USA)	2011	3000	370/740	22	402–11 800	Polar
VIIRS NOAA/NASA	JPSS-1 (USA)	2015	3000	370/740	22	402–11 800	Polar

From the IOCCG website ([www.ioccg.org/sensors/scheduled.html](http://www.ioccg.org/sensors/scheduled.html)) 2010.

somewhat increased under rough conditions: at the smaller angles losses remain insignificant but can rise to 16 to 27% for angles at the upper end of this range.<sup>41</sup>

As the light passes through the water–air boundary it undergoes refraction, which in accordance with Snell’s Law (§2.5) increases its angle to the vertical. A further consequence of refraction is that the flux contained within a small solid angle,  $d\omega$ , below the surface spreads out to a larger solid angle,  $n^2 d\omega$  (where  $n$  is the refractive index), above the surface. Because of this effect, the value of emergent radiance at any given angle is about 55% of the corresponding subsurface radiance from which it is derived. Combining this effect with the much smaller effect of internal reflection, Austin (1980) proposed a factor of 0.544 for relating radiance just above the surface,  $L_w(\theta, \phi)$  (the *water-leaving radiance*), to the corresponding radiance just below the surface,  $L_u(\theta', \phi)$

$$L_w(\theta, \phi) = 0.544 L_u(\theta', \phi) \quad (7.1)$$

$\theta'$  being the nadir angle within the water,  $\theta$  the angle in air after refraction at the surface, and  $\phi$  the azimuth angle of the vertical plane containing  $L_w(\theta, \phi)$  and  $L_u(\theta', \phi)$  relative to the plane of the Sun. If  $L_w(\theta, \phi)$  can be determined from remote sensing measurements, then it can be multiplied by 1.84 to give  $L_u(\theta', \phi)$ , and thus provide information about the underwater light field. For water-leaving radiance values at the higher zenith angles,  $L_u(\theta', \phi)$  can be calculated more accurately using eqn 6.16 (see §6.4)

$$L_u(0^-, \theta', \phi) = \frac{n^2}{[1 - \rho(\theta', \theta)]} L_w(\theta, \phi)$$

Gordon (2005) has shown, by modelling the light field, that even at wind speeds as high as  $20 \text{ m s}^{-1}$ , the transmittance of the roughened water–air interface (away from whitecaps) for upward radiance is nearly identical to that for a flat surface.

As we saw earlier (§6.4), it is not the absolute value of upward radiance, but the ratio of upward radiance to downward irradiance, which contains information about the composition of the water, and this can be calculated using eqn 6.20

$$r_{rs} = \frac{L_w(\theta, \phi)n^2(1 - R\bar{r})}{E_d(0^+)(1 - \bar{\rho})[1 - \rho(\theta', \phi)]}$$

from the experimentally determined  $L_w(\theta, \phi)$  and  $E_d(0^+)$  values.

### 7.3 Correction for atmospheric scattering and solar elevation

We have already noted that about 90% of the upward radiance measured by a photometer in a satellite, or in a very high altitude ( $\sim 20$  km) aircraft, above the ocean originates by scattering of the solar beam by air molecules and by aerosol particles (dust, water droplets, salt etc.) within the atmosphere – this is known as the *path radiance*. To arrive at a value of the water-leaving radiance,  $L_w(\theta, \phi)$ , from the measured radiance, the path radiance must be removed, and furthermore the attenuation of the emergent flux during its passage through the turbid atmosphere to the sensor must be allowed for.

Since it is the ratio of the emergent flux to the incident downward flux, rather than the absolute value of emergent flux alone, which is directly related to the optical properties of the aquatic medium, it is desirable to have an estimate of the downward irradiance at the surface of the water: this will be determined by solar elevation and by attenuation of the solar beam through the atmosphere, and so both of these will have to be taken into account.

As we have seen, there are several spaceborne ocean colour scanners now aloft, in addition to various airborne scanners. The detailed procedure for atmospheric correction is not only somewhat technical, but varies from one scanner to another. Here we shall confine our attention to the underlying principles, and to illustrate these we shall use the procedure developed by Gordon and Wang (1994), for SeaWiFS.

The total radiance,  $L_t(\lambda)$ , measured at wavelength  $\lambda$  by the sensor at the top of the atmosphere is the sum of a series of different radiance values originating in various different physical processes, in accordance with

$$L_t(\lambda) = L_r(\lambda) + L_a(\lambda) + L_{ra}(\lambda) + L_g(\lambda) + tL_w(\lambda) \quad (7.2)$$

where

- $L_r(\lambda)$  is the radiance due to multiple Rayleigh scattering by air molecules in the absence of aerosols
- $L_a(\lambda)$  is the radiance due to multiple scattering by aerosols in the absence of air
- $L_{ra}(\lambda)$  is the radiance generated by multiple scattering of photons between the aerosol particles and air molecules<sup>306</sup>
- $L_g(\lambda)$  is the radiance due to sunglint, i.e. photons that have undergone specular reflection from the direct solar beam at the wind-roughened ocean surface

- $tL_w$  is the water-leaving radiance attenuated by the atmospheric transmittance factor  $t$  during its passage from the surface to the satellite.

The atmospheric transmission factor is for diffuse rather than direct transmittance because when the sensor is viewing a given element of area, some of the flux is coming from neighbouring elements, and is given approximately by

$$t(\theta_v, \lambda) = \exp \left[ -\frac{[\tau_r(\lambda)/2] + \tau_{Oz}(\lambda)}{\cos \theta_v} \right] \quad (7.3)$$

where  $\tau_r(\lambda)$  is the optical thickness due to Rayleigh (molecular) scattering,  $\tau_{Oz}(\lambda)$  is the optical thickness of the ozone layer and  $\theta_v$  is the zenith angle of the line between the sensor and any given pixel.

Since it is ultimately the reflectance of the ocean, in the form of  $R_{rs}$  or  $r_{rs}$ , rather than the absolute value of water-leaving radiance, which contains information about water composition it is now normal practice to express the above relationships entirely in terms of reflectance,  $\rho$ . This is defined as

$$\rho = \frac{\pi L(\lambda)}{F_0(\lambda) \cos \theta_0} \quad (7.4)$$

where  $L(\lambda)$  is any one of the individual radiances in eqn 7.2,  $F_0(\lambda)$  is the extraterrestrial (top of atmosphere) solar irradiance at wavelength  $\lambda$  and  $\theta_0$  is the solar zenith angle. Equation 7.2 can thus be rewritten

$$\rho_t(\lambda) = \rho_r(\lambda) + \rho_a(\lambda) + \rho_{ra}(\lambda) + \rho_g(\lambda) + t(\lambda)\rho_w(\lambda) \quad (7.5)$$

The sunglint term,  $\rho_g(\lambda)$ , is usually omitted since most ocean-colour sensors can be tilted away from the specular image of the Sun.

The Rayleigh–aerosol interaction term,  $\rho_{ra}(\lambda)$ , can be ignored in atmospheres with low aerosol and Rayleigh optical thicknesses and a correspondingly small contribution from multiple scattering. Thus, in the simplest situations, eqn 7.2 can be replaced by

$$\rho_t(\lambda) = \rho_r(\lambda) + \rho_{as}(\lambda) + t(\lambda)\rho_w(\lambda) \quad (7.6)$$

where  $\rho_{as}(\lambda)$  is reflectance due to single scattering by aerosol. Since the contribution to scattering by air molecules is essentially constant, the radiance at the sensor's viewing angle due to Rayleigh scattering is a known function of solar elevation, wavelength and surface atmospheric pressure<sup>483</sup> and so  $\rho_r(\lambda)$  can be calculated and is the same for all pixels.

To estimate the aerosol contribution, advantage is taken of the fact that water absorbs light strongly in the red/near-infrared region, and so essentially all the radiance measured at this end of the spectrum can be attributed to scattering within the atmosphere. SeaWiFS bands 7 (765 nm) and 8 (865 nm) are suitable for the purpose. At these wavelengths  $\rho_w(\lambda)$  in eqn 7.6 can be assumed to be zero, Rayleigh scattering can be calculated as we have indicated, the reflectance attributable to aerosol accordingly is

$$\rho_{as}(\lambda) = \rho_t(\lambda) - \rho_r(\lambda) \quad (7.7)$$

and so we obtain the ratio of aerosol reflectance for the two wavebands

$$\varepsilon(\lambda_7, \lambda_8) = \frac{\rho_{as}(\lambda_7)}{\rho_{as}(\lambda_8)} \quad (7.8)$$

The aerosol reflectance ratio, as in eqn 7.8, is a smoothly varying function of wavelength, which usually conforms approximately to

$$\varepsilon(\lambda_i, \lambda_8) = \left( \frac{\lambda_8}{\lambda_i} \right)^{-n} \quad (7.9)$$

where  $n$  is known as the Angström exponent. In the simple situation, envisaged above, in which multiple scattering is small enough to be disregarded,  $\varepsilon(\lambda_7, \lambda_8)$  could be determined from experimental data in accordance with eqn 7.8, and then used to determine the  $n$  exponent in eqn 7.9. With this value of  $n$ ,  $\varepsilon(\lambda_i, \lambda_8)$  could be calculated for the other wavebands of interest, and then in turn the corresponding values of  $\rho_{as}(\lambda)$ .

When, as is more often than not the case, multiple scattering is too significant to be ignored, it is  $[\rho_a(\lambda) + \rho_{ar}(\lambda)]$ , rather than  $\rho_{as}(\lambda)$ , which must be calculated. In the approach used by Gordon and Wang (1994) it is assumed, once again, that  $\rho_w(\lambda)$  is zero at 765 and 865 nm, so for these wavebands we can write

$$\rho_a(\lambda) + \rho_{ar}(\lambda) = \rho_t(\lambda) - \rho_r(\lambda) \quad (7.10)$$

At this long-wavelength end of the spectrum Rayleigh scattering is weak and  $\rho_{ar}(\lambda)$  is very small, and for the 765 and 865 nm wavebands, eqn 7.7 for  $\rho_{as}(\lambda)$  can be considered to apply. Accordingly,  $\varepsilon(\lambda_7, \lambda_8)$  can be estimated from

$$\varepsilon(\lambda_7, \lambda_8) = \frac{\rho_t(\lambda_7) - \rho_r(\lambda_7)}{\rho_t(\lambda_8) - \rho_r(\lambda_8)} \quad (7.11)$$

The next requirement is to determine what kind of spectral variation of scattering might be expected from the aerosol in question. To achieve this, Gordon and Wang calculated – for a range of aerosol types (nine in total), including marine, tropospheric and coastal – scattering as a function of  $\lambda$ , and for each aerosol type  $\varepsilon(\lambda_7, \lambda_8)$  was then obtained using eqn 7.8. The estimated value of  $\varepsilon(\lambda_7, \lambda_8)$  from eqn 7.11 will generally be found to fall between two of the model aerosol values. It is then assumed that the general relationship,  $\varepsilon(\lambda_i, \lambda_8)$  also falls between those for the two selected aerosol models proportionately in the same manner as was found for  $\varepsilon(\lambda_7, \lambda_8)$ . The  $\rho_{as}(\lambda_i)$  values for the set of SeaWiFS bands in the visible region can then be calculated from the measured value of  $\rho_{as}(\lambda_8)$ .

Since we are assuming that in the visible region multiple scattering is significant, what we now need is  $[\rho_a(\lambda) + \rho_{ar}(\lambda)]$  rather than  $\rho_{as}(\lambda)$ . In fact a near-linear relationship exists between  $[\rho_a(\lambda) + \rho_{ar}(\lambda)]$  and  $\rho_{as}(\lambda)$ , but differing from one aerosol type to another. Once again, the two aerosol models that bracket the aerosol under study are used, proportionately, to provide the relationship by which, using lookup tables,  $[\rho_a(\lambda) + \rho_{ar}(\lambda)]$  can be obtained from  $\rho_{as}(\lambda)$ . Thus, for each individual pixel in the scene,  $[\rho_a(\lambda) + \rho_{ar}(\lambda)]$  can be calculated, and with the separately calculated values of  $\rho_r(\lambda)$  and  $t(\lambda)$ , using a rearranged form of eqn 7.5 (omitting sunglint)

$$\rho_w(\lambda) = \{\rho_t(\lambda) - \rho_r(\lambda) - [\rho_a(\lambda) + \rho_{ar}(\lambda)]\}/t(\lambda) \quad (7.12)$$

that component of total measured reflectance that is due to the water-leaving flux is obtained. It should be noted that the calculated values of  $\rho_r(\lambda)$  and  $[\rho_a(\lambda) + \rho_{ar}(\lambda)]$  include the contribution of skylight reflected at the water surface.

All the individual reflectances in eqn 7.12 can be expressed in terms of the corresponding radiance, and the extraterrestrial irradiance, in accordance with eqn 7.4. Applying this to  $\rho_w(\lambda)$  and rearranging, we obtain the water-leaving radiance

$$L_w(\lambda) = \frac{F_0(\lambda) \cos \theta_0}{\pi} \rho_w(\lambda) \quad (7.13)$$

i.e. the atmospheric correction procedure can provide values for  $\rho_w(\lambda)$  or  $L_w(\lambda)$ , as required. The water-leaving radiance is for some purposes converted to the *normalized water-leaving radiance*,  $[L_w(\lambda)]_N$ ,<sup>486,480</sup> which may be defined as the radiance that would exit the ocean in the absence of the atmosphere, with the Sun at the zenith, at the mean Earth–Sun distance. To arrive at  $L_w(\lambda)$ ,  $[L_w(\lambda)]_N$  is first reduced by the factor

$\cos \theta_0$  to allow for non-vertical Sun, and is then further reduced to take account of the attenuation of the downward solar flux through the atmosphere (pathlength  $1/\cos \theta_0$ ) by Rayleigh scattering and ozone absorption (the contribution by aerosol being disregarded). The relationship between the two radiances is given by<sup>480,28</sup>

$$L_w(\lambda) = \varepsilon_c [L_w(\lambda)]_N \cos \theta_0 \exp \left\{ - \left[ \frac{\tau_R(\lambda)}{2} + \tau_{O_3}(\lambda) \right] \left( \frac{1}{\cos \theta_0} \right) \right\} \quad (7.14)$$

where  $\tau_R$  and  $\tau_{O_3}$  are the Rayleigh and ozone optical thicknesses, respectively, and  $\varepsilon_c$  is a correction factor, applied to  $F_0(\lambda)$  and consequently to  $[L_w(\lambda)]_N$ , accounting for changes in the Earth–Sun distance. Equation 7.14 can be written, more simply, as

$$L_w(\lambda) = \varepsilon_c [L_w(\lambda)]_N \cos \theta_0 t(\theta_0, \lambda) \quad (7.15)$$

Where  $t(\theta_0, \lambda)$ , given by

$$t(\theta_0, \lambda) = \exp \left\{ - \left[ \frac{\tau_R(\lambda)}{2} + \tau_{O_3}(\lambda) \right] \left( \frac{1}{\cos \theta_0} \right) \right\} \quad (7.16)$$

is the irradiance transmittance for Sun zenith angle,  $\theta_0$ . The SeaWiFS Data Analysis System (SeaDAS) provides atmospherically corrected ocean colour data at six wavelengths in the visible region in terms of the normalized water-leaving radiance.

The Landsat series of satellites are designed primarily for the remote sensing of the terrestrial surface, and so are not optimized for the much lower reflectance values of the ocean and other surface waters. A standard formulation of the relation between irradiance reflectance at the surface ( $\rho_w(\lambda)$ ), remotely sensed radiance at the top of the atmosphere ( $L_t(\lambda)$ ), and atmospheric conditions, used for the Landsat satellites is

$$\rho_w(\lambda) = \frac{\pi [L_t(\lambda) - L_{path}(\lambda)] / t(\theta_v, \lambda)}{F_0(\lambda) \cos \theta_0 t(\theta_0, \lambda) + {}^{sky}E_d(0^+, \lambda)} \quad (7.17)$$

where  $L_{path}(\lambda)$  is the path radiance due to Rayleigh and aerosol scattering,  $t(\theta_v, \lambda)$  is the atmospheric transmittance along the path from the ground (or sea) surface pixel to the sensor,  $t(\theta_0, \lambda)$  is the atmospheric transmittance along the path from the Sun to the ground (or sea) surface and  ${}^{sky}E_d(0^+, \lambda)$  is the downward irradiance at the surface due to scattered solar flux in the atmosphere.<sup>936</sup> In the case of Landsat studies on aquatic systems, there is as yet no standard method of correcting for these atmospheric effects.

The use of Landsat for remote sensing of water composition has most commonly involved correlating increases in radiance in particular wavebands with increases in concentration of particular types of suspended particles, the increased radiance being due to increased backscattering. In some cases correlations between the uncorrected radiances and concentration of a particular component have been used. The problem in such a case is that on another occasion, when atmospheric conditions have changed, the previously derived relation will no longer apply. In studies on Lake Superior, Canada, for example, the curve of measured radiance against turbidity shifted up and down and changed somewhat in slope on different days, in accordance with changes in atmospheric conditions.<sup>1184</sup>

A simple, but very approximate, procedure for reducing atmospheric effects is the *dark pixel correction method*,<sup>1134,1135,1142</sup> sometimes also referred to as the *dark object subtraction method*. This involves locating the darkest pixel in the scene, and subtracting the radiance value for this from the radiance values for all the other pixels. The rationale is that the darkest pixel will have the same atmospheric contribution as all the other pixels, but must have the smallest contribution from scattering within the water. Subtraction of the darkest pixel radiance from all the other pixel radiances should thus remove their atmospheric contribution, and what is left is a function of the *difference* in particle scattering between the various parts of the water body, and that part with the darkest pixel. To be useful, this method does, however, require that there should exist somewhere in the scene an area of water with a particles content that is at least relatively low: it also assumes constant atmospheric conditions throughout the scene, a reasonable assumption in the case of lakes, the water bodies to which this procedure has usually been applied.

Chavez (1988, 1996) has further developed the dark object subtraction method to take account of the wavelength dependence of scattering. A histogram is prepared of digital number (corresponding to top-of-atmosphere radiance) for all pixels in the scene in selected wavebands. In this way a suitable dark pixel is found to provide the starting dark-object haze value (i.e. path radiance,  $L_{path}$  from atmospheric scattering). The next requirement is to select a spectral scattering model that best represents the atmospheric conditions at the time of data collection, and the amplitude of the starting haze can be used as a guide to identify these atmospheric conditions. Chavez uses five categories – very clear, clear, moderate, hazy and very hazy. It is assumed that in every case scattering is, in agreement with the Angström law, proportional to  $\lambda^{-n}$ . To each type of atmosphere a different value of  $n$  is assigned, these being 4, 2, 1, 0.7 and 0.5,

respectively, for the five atmospheric categories. The selected scattering model is then used to predict the haze values for the other spectral bands, from the starting haze value.  $^{sky}E_d(0^+, \lambda)$  in eqn 7.17 is set to zero, i.e. the contribution to  $E_d$  from sky radiation is ignored. Chavez (1996) found that the cosine of the solar zenith angle could be used as an approximate estimate of the atmospheric transmittance along the path from the Sun to the ground, and so could be substituted for  $t(\theta_0, \lambda)$  in eqn 7.17. The atmospheric transmittance along the path from surface to sensor,  $t(\theta_v, \lambda)$ , is assigned a value of 1.0.

Verdin (1985) attempted to determine the actual reflectance values of a water body from Landsat data, with the help of atmospheric radiative transfer calculations. An essential component of the procedure is that there should be an area within the scene that can confidently be assumed to contain clear oligotrophic water. For each waveband a reflectance value for this area is assumed, on the basis of literature data. A plausible initial assumption concerning the prevailing atmospheric turbidity is made from which, by radiative transfer calculation, a value for path radiance is arrived at and tested to see whether, taken together with the assumed water body reflectance, it accounts for the satellite-measured radiance from the clear water. The calculation is repeated in an iterative manner, progressively altering atmospheric turbidity, until a satisfactory value for path radiance is arrived at, and this is assumed to apply throughout the scene. The radiative transfer calculations also yield values for the transmittance of solar radiation down through the atmosphere, and of radiance from the water surface back to the satellite. Thus, for every pixel in the scene, the value of the water-leaving radiance,  $L_w$ , and of the incident solar irradiance, can be calculated, and from these the reflectance can be determined.

Brivio *et al.* (2001) used the radiative transfer calculation procedure of Gilbert *et al.* (1994) to correct for atmospheric effects in their Landsat Thematic Mapper (TM) study of Lake Garda (Italy). They assumed a horizontally homogeneous atmosphere so that transmittance and path radiance were constant throughout the scene. The path radiance,  $L_{path}(\lambda)$ , was determined from the radiance,  $L_t(\lambda)$ , measured by the sensor in TM wavebands 1 (450–520 nm) and 3 (630–690 nm), over dark areas within the scene. The Rayleigh contribution was calculated and subtracted from the total path radiance to give the aerosol path radiance,  $L_a(\lambda)$ . Through the wavelength dependence of the aerosol path radiance in these two bands an appropriate aerosol model was identified, and used to retrieve the aerosol path radiances in the other spectral bands. The

aerosol optical thickness,  $\tau_a(\lambda)$ , was calculated for each band assuming a linear relationship with  $L_a(\lambda)$ . Rayleigh,  $\tau_R(\lambda)$ , and ozone,  $\tau_{O_2}(\lambda)$ , optical thicknesses were calculated by standard procedures. Atmospheric transmittance was then obtained as an exponential function of total optical thickness. Total downward irradiance at the surface,  $E_d(0^+, \lambda)$ , was obtained by summing both direct and diffuse irradiance, as calculated on the basis of atmospheric scattering. In this way, everything required for calculation of  $\rho_w(\lambda)$ , in eqn 7.17, was obtained.

With six (or seven) narrow wavebands in the visible region, and two in the near-infrared, the SeaWiFS and MODIS (Terra) spaceborne sensors provide much better data for atmospheric correction than the Landsat satellites. Since all three satellites are Sun-synchronous, are at an altitude of  $\sim 705$  km, and have orbits not widely separated in time, it is generally the case that for a given Landsat 7 TM scene, a concurrent SeaWiFS or MODIS scene will be available. Hu *et al.* (2001) propose that for atmospheric correction of Landsat 7 TM radiances over aquatic environments, the Rayleigh and aerosol data estimated with SeaWiFS and/or MODIS should be used. Gong *et al.* (2008) found that vicarious correction with MODIS data worked very well for Landsat TM images of Taihu Lake in China.

## 7.4 Relation between remotely sensed reflectance and the scattering/absorption ratio

While values for water-leaving radiance or reflectance are of some interest in themselves, their main significance lies in what they can tell us about the optical properties of the medium, and thus about the concentrations of the optically significant constituents in the water. A route by which such information may be acquired makes use of the approximate relations, derived from theoretical modelling of the underwater light field (§6.4), that exist between radiance reflectance ( $L_u/E_d$ ), or irradiance reflectance ( $E_u/E_d$ ), and the ratio of backscattering coefficient to absorption coefficient. From eqn 7.4, and explicitly recognizing that  $L_w$  and  $\rho_w$  are functions of solar angle, satellite viewing angle and azimuth, we obtain

$$\rho_w(\lambda, \theta_0, \theta_v, \phi) = \frac{\pi L_w(\lambda, \theta_0, \theta_v, \phi)}{F_0(\lambda) \cos \theta_0} \quad (7.18)$$

The downward irradiance at the surface,  $E_d(0^+, \lambda)$ , is a function of the extraterrestrial irradiance,  $F_0(\lambda)$ , solar zenith angle, and the irradiance transmittance of the atmosphere, in accordance with

$$E_d(0^+, \lambda) = F_0(\lambda) \cos \theta_0 t(\theta_0, \lambda) \quad (7.19)$$

so we can substitute for  $F_0(\lambda) \cos \theta_0$  in eqn 7.18 to obtain

$$\rho_w(\lambda, \theta_0, \theta_v, \phi) = \frac{\pi t(\theta_0, \lambda) L_w(\lambda, \theta_0, \theta_v, \phi)}{E_d(0^+, \lambda)} \quad (7.20)$$

From eqn 6.20, (§6.4) we know that

$$\frac{L_w(\lambda, \theta_0, \theta_v, \phi)}{E_d(0^+, \lambda)} = \frac{(1 - \bar{\rho})[1 - \rho(\theta', \phi)]}{n^2(1 - R\bar{r})} r_{rs} \quad (7.21)$$

To simplify notation, Morel and Gentili (1996) introduced the term,  $\Re(\theta)$ , which combines all the reflection and refraction effects, in accordance with

$$\Re(\theta') = \frac{(1 - \bar{\rho})[1 - \rho(\theta', \phi)]}{n^2(1 - R\bar{r})} \quad (7.22)$$

Using this notation, and substituting also for  $r_{rs}$  (the subsurface remote sensing reflectance) from eqn 6.11, we obtain

$$\rho_w(\lambda, \theta_0, \theta_v, \phi) = \pi t(\theta_0, \lambda) \Re(\theta') \frac{f(\lambda, \theta_0)}{Q(\lambda, \theta_0, \theta', \phi)} \left[ \frac{b_b(\lambda)}{a(\lambda)} \right] \quad (7.23)$$

In eqn 7.23, for each pixel,  $\rho_w(\lambda, \theta_0, \theta_v, \phi)$  is what is measured, and  $\pi t(\theta_0, \lambda) \Re(\theta')$  can be calculated. As we saw in Chapter 6, however, the  $f/Q$  ratio, although it is commonly in the region of 0.08 to 0.09, is a function of solar altitude, solar azimuth and satellite viewing angle, and also varies with the optical character of the water, e.g. colour dominated versus turbidity dominated.<sup>824</sup> We saw earlier (§6.4, eqn 6.4) that  $f$  (indicated by  $C[\mu_0]$ ) can be expressed in terms of the cosine of the refracted solar beam ( $\mu_0$ ), and a coefficient ( $M$ ) determined by the shape of the scattering phase function. For clear ocean water,  $Q$  can be calculated from solar elevation using eqn 6.13 or 6.14. Thus at least an approximate estimate of  $f/Q$  can be arrived at.

Morel and Gentili (1996) have developed a much more detailed procedure, which uses precomputed lookup tables to provide values of the  $f/Q$  ratio in all the necessary conditions. To get the process underway, an approximate initial estimate of the chlorophyll content of the

water is required. It is assumed to begin with that for each of two wavebands (443 and 555 nm),  $f/Q$  is the same for all pixels in the scene, and appropriate average values from the literature are assigned. From eqn 7.23 (in fact from the equivalent expression for  $L_w$ ) the  $(b_b/a)$  values at the two wavelengths are obtained from the remotely sensed  $L_w(\lambda)$  values, and in turn these are used to provide the so-called *blue-to-green ratio*

$$\rho_{443-555} = \frac{a(443)b_b(555)}{a(555)b_b(443)} \quad (7.24)$$

In Case 1 ocean waters, the blue-to-green ratio is mainly determined by the level of phytoplankton. Approximate relationships between the ratio of  $(b_b/a)_\lambda$  values at selected pairs of wavelengths and the chlorophyll concentration can be derived empirically (see below). Morel and Gentili use such a relationship – a polynomial expressing  $\ln \rho_{443-555}$  as a function of  $\ln [\text{Chl}]$  – to arrive at the first estimate of chlorophyll concentration,  $\text{Chl}_1$ , on the basis of the blue-to-green ratio determined as above. With this value of  $[\text{Chl}]$ , appropriate  $f/Q$  values, using  $\theta_0$ ,  $\theta'$ ,  $\phi$ , and  $[\text{Chl}]$  as inputs, are obtained from the precomputed lookup table. With the second set of  $f/Q$  data, a second set of  $(b_b/a)$  values is obtained from remotely sensed  $L_w$  at 443 and 555 nm, and for each pixel a new chlorophyll concentration,  $\text{Chl}_2$ . This is in turn entered into the lookup table, and the iteration is continued in this way until acceptable accuracy is achieved.

Once realistic values for the various terms in eqn 7.23 have been arrived at, then  $b_b/a$ , the ratio of the backscattering coefficient to the absorption coefficient, can be estimated from the remotely sensed  $\rho_w(\lambda)$ . If, on the basis of other information, a plausible value could be selected for  $b_b$ , then an approximate value for  $a$  could be obtained. In the far-red/near-infrared region, absorption is normally almost entirely attributable to water itself, and  $a$  is known, and so for waters turbid enough to exhibit significant water-leaving radiance in this highly absorbing spectral region,  $b_b$  can be estimated. If measurements are made at three wavelengths, and reasonable assumptions are made about the manner in which  $b_b$  and the values of  $a$  for the different absorbing components (water, phytoplankton, non-living colour) vary with wavelength, then the actual concentrations of phytoplankton and non-living pigmented material can be estimated: the theoretical basis for such calculations is given by Morel (1980).

## 7.5 Relation between remotely sensed reflectances and water composition

Most remote sensing studies of water composition have made use, not of the a priori deductive method outlined above, but of an empirical approach in which relations have been sought between remotely measured radiances in particular wavebands, or functions of one or more radiances or reflectances, and the concentrations of specific components such as phytoplankton and suspended solids determined by *in situ* measurements within water bodies. Once such relations are established it should in principle be possible to use them to determine the optical properties and composition of water bodies from remote sensing data alone. This is an active field of research, which has given rise to a very large quantity of published work in recent years. The treatment here will not be encyclopaedic: rather, general principles are outlined and a variety of representative examples are discussed.

A useful concept in this context is that of a *retrieval variable*,<sup>1347</sup> which is any function of the reflectance (or radiance) values in one or more wavebands,  $X[R(\lambda_i)]$ , that is empirically found to be related to the concentration of some component of the water by a simple algorithm. Thus, the problem in remote sensing is usually to identify a suitable  $X$ , and to develop a simple equation, by means of which the concentration of the constituent of interest may be calculated from  $X$ .

### Suspended solids

One of the water quality parameters that has been most extensively studied in this way is the concentration of total suspended solids (TSS). Increases in the amount of suspended particles will, at wavelengths where the particles do not absorb strongly, increase the backscattering coefficient of the water more than the absorption coefficient, and so, in accordance with eqns 6.3 and 6.5, increase the emergent flux.

In the case of reservoirs in Mississippi, it was found that the irradiance reflectance measured above the water surface increased with the concentration of suspended (inorganic) sediment at all wavelengths from 450 to 900 nm (Fig. 7.6).<sup>1136</sup> The best, linear, correlation between reflectance and suspended solids concentration was found between 700 and 800 nm. Correlations between suspended solids or nephelometric turbidity (proportional to suspended solids) and radiances in particular wavebands have been obtained with the Landsat satellites. Klemas *et al.* (1973,

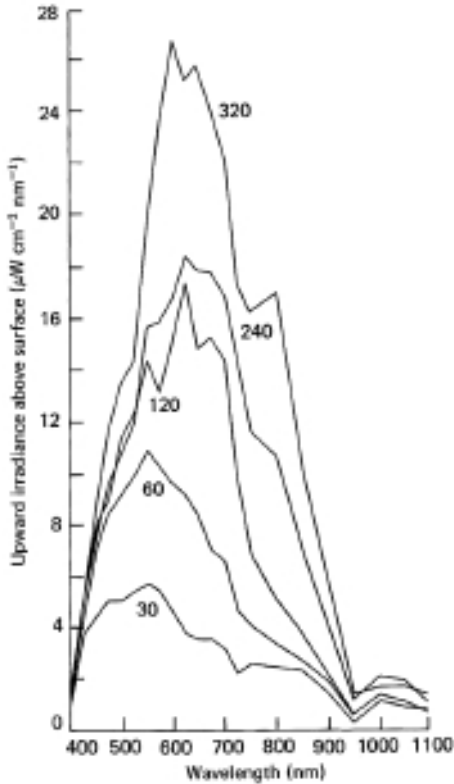


Fig. 7.6 Intensity and spectral distribution of upwelling radiation measured 20 to 50 cm above the surface of freshwater bodies containing various levels of suspended solids (after Ritchie, Schiebe and McHenry, 1976). The concentration of suspended solids in  $\text{mg l}^{-1}$  is indicated next to each curve.

1974) found that in Delaware Bay the distribution of mineral suspended sediments (MSS) 600–700 nm radiance corresponded best with sediment load in the upper 1 m of the water (Fig. 7.7); the 500 to 600 nm radiance was more subject to interference from atmosphere haze while the 700 to 800 nm waveband did not penetrate sufficiently into the water column. Similarly, in Landsat imagery of Kenyan coastal waters, the 700 to 800 nm band revealed only high sediment concentrations near the surface, whereas the 600 to 700 nm and 500 to 600 nm bands were sensitive to lesser concentrations lower in the water column.<sup>156</sup> Suspended solids values for the Bay of Fundy, Nova Scotia, Canada, correlated with particular functions of upward radiance in the 500 to 600, 600 to 700 and 700 to 800 nm bands, but the latter two bands gave the highest

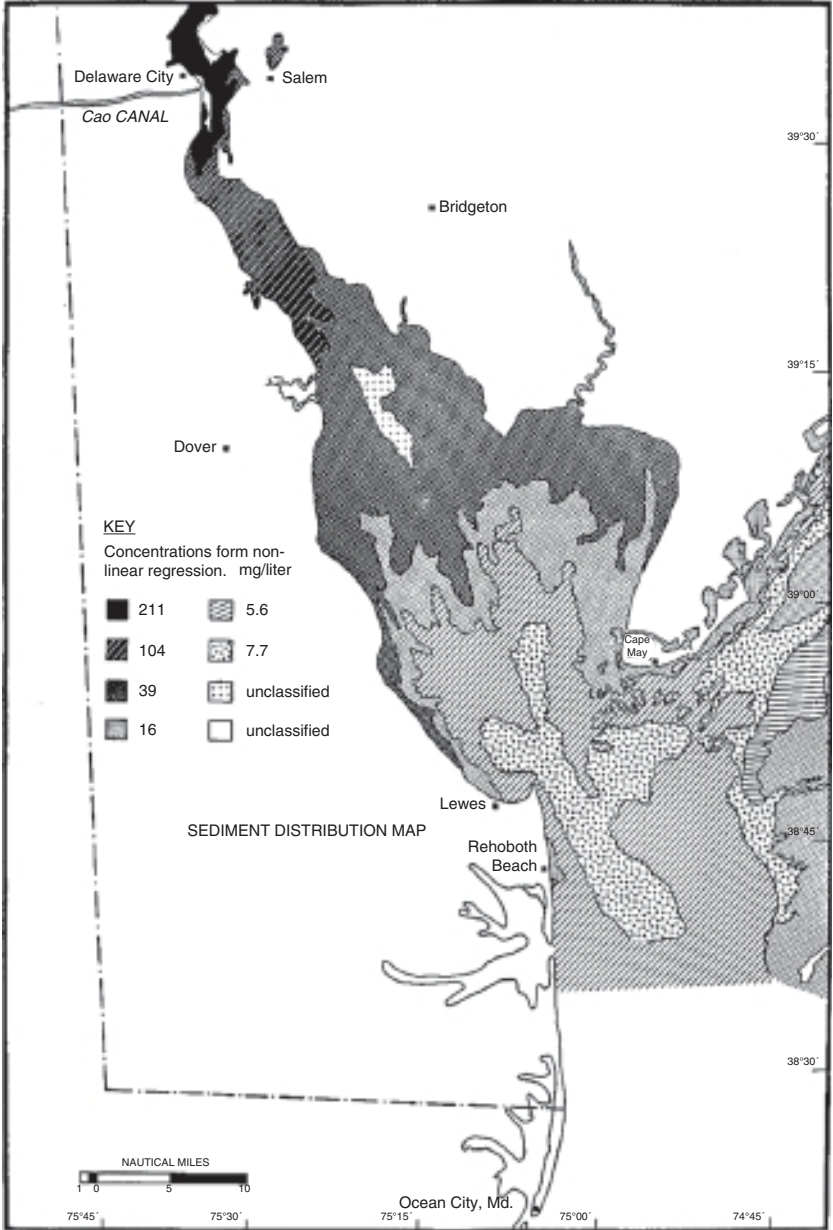


Fig. 7.7 Distribution of suspended solids concentration in Delaware River estuary and Delaware Bay derived from Landsat 600 to 700 nm radiance measurements (by permission, from Klemas *et al.* (1974), *Remote Sensing of Environment*, 3, 153–74).

correlation coefficients.<sup>965</sup> In the case of Lake Ontario, Canada, a good linear relation was observed between radiance reflectance in the 600 to 700 nm band and measured turbidity.<sup>181</sup> For two turbid oxbow lakes of the Mississippi River (USA), Moon Lake (Mississippi) and L. Chicot (Arkansas), it was found that of the four Landsat MSS bands, the 700 to 800 nm band was the best for monitoring suspended sediment loads.<sup>1132,1135,1185</sup>

Munday and Alfoldi (1979) found that Landsat radiance values correlated somewhat better with the logarithm of TSS than with TSS alone, in the Bay of Fundy. Some algorithms for suspended sediments have been developed using combinations of Landsat radiances rather than the radiance values in a single waveband.<sup>683,1132,1133,1371</sup> The quest for a universal algorithm for suspended sediments<sup>582,1133</sup> is, however, never likely to succeed, no matter what combination of bands is used. The main reason is that the scattering efficiency of suspended particles *per unit weight* is very much a function of size (Fig. 4.3), and average particle size of suspended sediments is quite variable, both with time and place. There are additional reasons related to the absorption properties of the surrounding medium and of the particles themselves. Since reflectance varies inversely with  $a$ , at the same time as it increases with  $b_b$ , a reproducible linear relation between emergent radiance and TSS is only to be expected if the total absorption coefficient of the aquatic medium remains constant while the concentration of suspended solids varies. This need not be the case, and variations in absorption coefficient from place to place or over a period of time, within the water body under study, would affect the reproducibility of any empirically derived relation between  $L_w$  and TSS, and so affect the accuracy with which the concentration of suspended solids can be determined from remotely sensed data. In the red and near-infrared wavebands, however, absorption is mainly due to water itself, and so fluctuations in absorption should not be large.

Confirming the advantage of the near-infrared for monitoring suspended particles, Doxaran *et al.* (2002) found, for the highly turbid waters of the Gironde estuary (France), that the (atmospherically corrected) reflectances in the visible-wavelength bands (green, 500–590 nm; red, 610–680 nm) of the HRV sensor on the SPOT satellite correlated poorly with suspended particulate matter (SPM), showing a logarithmic increase up to  $500 \text{ mg l}^{-1}$  and then saturating. Reflectance in the near-infrared (790–890 nm), and also the ratio of near-infrared reflectance to that in either visible band, by contrast, were highly correlated with SPM. On the basis of their *in situ* measurements of spectral reflectance and

concentration of suspended particles they arrived at an algorithm, expressing the ratio of reflectance in the near-infrared ( $R_{790-890}$ ) to that in the green ( $R_{500-590}$ ) as a function of SPM in  $\text{mg l}^{-1}$ .

$$\frac{R_{790-890}}{R_{500-590}} = 0.3193 \ln \text{SPM} - 0.9614$$

Applied to a high-resolution (2.5 m) SPOT image of part of the Gironde, it revealed a detailed picture of sedimentary flow in the estuary.

Binding *et al.* (2005) studied the relationship between concentration of MSS and subsurface irradiance reflectance in six wavebands in the 400 to 700 nm region at a large number of stations in the moderately turbid Irish Sea. The most robust relationship between MSS and reflectance was found in the red (665 nm). These authors attributed the residual variability in the results to variation in the specific scattering coefficient ( $b_{MSS}^*$ ) of the particles, which in fact extended over the range, 0.04 to  $0.57 \text{ m}^2 \text{ g}^{-1}$  for all stations. When their regression model was re-run using the local value for specific scattering coefficient applicable to each station, the agreement was much improved. Their results suggest that the errors in predicted MSS concentration can be reduced from 56% to as little as 12% with prior knowledge of the scattering properties of the sediments under study. Binding *et al.* suggest that in order to obtain quantitative estimates of MSS in moderately turbid waters from space it may be necessary to pre-determine scattering efficiencies ( $b_{MSS}^*$ ) within the area of interest.

The spectral distribution of light reflected by suspended inanimate particulate matter varies in accordance with its own absorption properties, which are determined by its chemical nature. For example, suspensions of white clay and red silt have quite different reflectance spectra.<sup>1000</sup> Sydor (1980), on the basis of his measurements of the spectral distribution of light scattered upwards from suspensions of particular types (red clay, mine tailings) concluded that evidence on the identity as well as concentration of the suspended solids may be derived using the 500 to 600, 600 to 700 and 700 to 800 nm bands of Landsat.

The work that we have discussed so far, and indeed the majority of studies on TSS that have been carried out, have made use of Landsat MSS data, but there have been some studies with other sensors. Ritchie, Cooper and Schiebe (1990) found Thematic Mapper data to be as good as, but no better than, MSS data for estimating suspended sediments in Moon Lake (Mississippi), despite the narrower spectral band width of the former. They consider that the major justification for using Thematic Mapper data for sediment studies would be that its higher

spatial resolution (30 m) would make it possible to monitor smaller lakes. The SPOT multispectral scanner has a ground-level resolution of 20 m. For the turbid waters of Green Bay, L. Michigan, Lathrop and Lillesand (1989) found that for extra-atmospheric reflectance in all three bands (green, red, near-infrared) the best correlation was with the logarithm of suspended sediment concentration: some improvement was obtained by regressing the logarithm of TSS against a combination of the three reflectances.

Stumpf and Pennock (1989) developed a method for determining suspended sediment concentrations in estuaries using the red and near-infrared channels of the AVHRR. They used a correction procedure similar to that developed for CZCS data to remove atmospheric effects, and worked in terms of the calculated values for reflectance. For the turbid waters along the Louisiana (USA) coast, Myint and Walker (2002) compared (atmospherically corrected) reflectances measured in two AVHRR wavebands with concentrations of total suspended solids (TSS) and suspended sediments (SS; SS = TSS after ignition) determined on water samples collected within a few hours of the satellite overpass. For Channel 1 (580–680 nm) TSS and SS as a function of reflectance were satisfactorily represented in the form of cubic equations. For the near-infrared Channel 2 (725–1100 nm), simple linear functions were found to work well.

Using atmospherically corrected reflectance values obtained with AVHRR band 1 (580–680 nm), Bowers *et al.* (1998) produced mean winter and summer maps of MSS concentration in the Irish Sea for the years 1982–88. For the Irish Sea as a whole, concentrations in winter were found to be higher than those in summer by a factor of 2.7. The highest sediment concentrations were found to occur in the more shallow areas and in the regions of strongest tidal currents.

Some, limited, use of SeaWiFS imagery has been made for remote sensing of the distribution of SS. Myint and Walker (2002) compared water-leaving radiance values, atmospherically corrected in accordance with Gordon and Wang (1994), with TSS and SS values from water samples collected off the Louisiana coast within a few hours of the satellite overpass. Correlation coefficients between Channel 5 (555 nm) radiances and TSS/SS were poor, only 0.46 to 0.47. In the case of Channel 6 (670 nm), however, the correlation coefficient was quite high, 0.85. Of various statistical models tried, expressing TSS or SS as a simple power function of  $L(670)$  gave the best results. Binding *et al.* (2003) measured subsurface irradiance reflectance in the SeaWiFS visible wavebands,

together with the concentration of MSS at 124 stations in the Irish Sea. The ratio of reflectance in the red to that in the green, which might have been expected to be strongly correlated with MSS, was found to be a reliable indicator only in those waters where MSS dominated the optical properties: with increasing influence of phytoplankton or yellow substance the relationship broke down. Reflectance in the red region (665 nm) on its own, on the other hand, showed a satisfactory correlation with MSS throughout the region studied, which could be represented by the following algorithm.

$$MSS = 0.0441 R_{665}^2 + 1.1392 R_{665} + 1.7459$$

The application of this algorithm to a SeaWiFS image of the Irish Sea accurately reproduced known regions of high turbidity, with realistic concentrations of MSS.

For turbid waters in the Bay of Biscay, Froidefond *et al.* (2002) found the (atmospherically corrected) SeaWiFS radiance at 555 nm to be strongly correlated with the concentration of suspended particulate matter (SPM) measured at sea level. From the data, the algorithm

$$Y = (0.811 + 0.376 X)^2$$

where  $Y$  is SPM conc. in  $\text{mg l}^{-1}$ , and  $X$  is the normalized water-leaving radiance at 555 nm, was derived.

Warrick *et al.* (2004) used SeaWiFS to map the distribution of SS in the turbid coastal waters of the Santa Barbara Channel (California). For atmospheric correction, the dark pixel method (see above) was used. The reflectance of the darkest single ocean pixel,  $\rho_{atm}$ , was assumed to be contributed entirely from the atmosphere. Reflectance due to water-leaving flux was then obtained from

$$\rho_w(\lambda) = \frac{\rho_t(\lambda) - \rho_{atm}(\lambda)}{t_v(\lambda)}$$

Where  $\rho_t(\lambda)$  is the total reflectance, and  $t_v(\lambda)$  is the diffuse atmospheric transmittance along the line of view of the sensor. Only reflectances in the 555, 670, 765 and 865 nm bands were used: the data from bands in the violet and blue (412, 443, 490 and 510 nm) were omitted because these are the bands most affected by phytoplankton and CDOM. To determine the sediment concentration, spectral mixture analysis was used, the end members for the analysis being provided by laboratory measurements of water-leaving spectral reflectance on sediment suspensions of known

concentration. Images of sediment distribution up to  $60 \text{ mg l}^{-1}$ , in increments of  $10 \text{ mg l}^{-1}$ , were obtained.

The 1 km spatial resolution of SeaWiFS is entirely suitable for the open ocean, but is not optimal for small-scale coastal features such as estuaries and bays. The Landsat and Landsat TM satellites have much better spatial resolution (80 m sq, 30 m sq) but have a revisit time of  $\sim 16$  days, and are therefore not well suited for monitoring dynamic change in coastal ecosystems. Sensors such as SeaWiFS and MODIS, by contrast, achieve near-global coverage every one to two days. The MODIS sensor on the Terra spacecraft, in addition to the nine narrow ( $\sim 10 \text{ nm}$ ) spectral bands in the visible and near-infrared used for ocean colour, which have a spatial resolution of  $\sim 1 \text{ km}$ , has two broader wavebands, Band 1 (620–670 nm) and Band 2 (842–876 nm), with 250 m sq resolution.<sup>924</sup> Miller and McKee (2004) used MODIS Band 1 to map the concentration of total suspended matter in coastal and estuarine waters in the northern Gulf of Mexico. A linear relationship ( $r^2 = 0.89$ ) was found between Band 1 reflectances, atmospherically corrected by the dark pixel subtraction method, and the total suspended matter (TSM) concentration measured on water samples from 52 stations in this region. For determining TSM concentration from Band 1 reflectance, the following algorithm was derived

$$\text{TSM (mg l}^{-1}\text{)} = 1140.25 (\text{Band 1 reflectance, \%}) - 1.91$$

### Phytoplankton – increased reflectance

One empirical approach to the remote sensing of phytoplankton is to treat it as a special case of suspended solids and to use the increased reflectance in the near-infrared associated with the increased biomass. In the Landsat MSS red (600–700 nm) band, high concentrations of algae are associated with decreased radiance because of the chlorophyll absorption in this region. Strong (1974) observed in the case of Landsat pictures of an algal bloom on Utah Lake, USA, that there was a contrast reversal in going from the red to the infrared (700–800 nm or 800–1100 nm) bands: areas dark in the red image showed up as light against a darker background in the infrared images. Bukata *et al.* (1974) found that the reflected radiance in the Landsat 700 to 800 nm band correlated well with the logarithm of the chlorophyll concentration in Lake Ontario, Canada, and some nearby eutrophic water bodies. The sensitivity of this method is, however, comparatively low ( $>10 \text{ mg chl a m}^{-3}$ ) and it is perhaps most applicable to highly productive inland waters that develop algal blooms.

Suspended inorganic particles can also increase reflectance in the 700 to 800 nm band. A comparison of the distribution of 600 to 700 nm waveband reflectance (which correlates better with inorganic turbidity than with biomass) with that of 700 to 800 nm reflectance is necessary to ensure that suspended sediments are not mistaken for phytoplankton.<sup>80</sup>

Reflectance spectra of algal cultures or eutrophic lake waters show, in addition to a dip at 670 to 680 nm, corresponding to the chl *a* absorption peak in the red, a peak in the 700 to 715 nm region.<sup>918,1181</sup> As the phytoplankton concentration increases, the height of this near-infrared peak relative to reflectance at 670 to 680 nm increases, and the peak itself shifts from about 698 nm to 712 nm.<sup>455,1181</sup> With increasing biomass, scattering, and hence reflectance, in the near-infrared must increase. The peak in reflectance at 700 to 715 nm corresponds to that narrow waveband of light which is not absorbed by the intensifying chl *a* band on the short-wavelength side or by the very steep rise in water absorption with wavelength on the other side. The water absorption remains constant, but as the chlorophyll band intensifies it removes increasing amounts of light from the short-wavelength side of the reflectance peak, thus pushing it further towards the infrared.

Dekker *et al.* (1991), using a multispectral scanner (the Programmable Multispectral Imager) from an aircraft at 1000 m over eutrophic lakes in the Netherlands, found a good linear negative correlation between phytoplankton chlorophyll and the ratio of red (673–687 nm) to near-infrared (708–715 nm) radiance values. In an equivalent observation, Mittenzwey *et al.* (1992), using a shipboard spectroradiometer positioned just above the water surface, found for productive (3–350 mg chl *a* m<sup>-3</sup>) lakes and rivers around Berlin, a very clear-cut positive correlation ( $r^2 = 0.98$ ) between phytoplankton chlorophyll concentration and the ratio of a near-infrared (705 nm) to a red (670 nm) reflectance ( $R_{705}/R_{670}$ ). This provided the basis for an algorithm expressing chlorophyll concentration as a function of this reflectance ratio.

$$\text{Chl } a \text{ (mg m}^{-3}\text{)} = 89 (R_{705}/R_{670}) + 10 (R_{705}/R_{670})^2 - 34$$

Gower *et al.* (2005) report that with the MERIS sensor, which has a band (704–714 nm) centred on 709 nm, this near-infrared peak could be detected from space, in an image of a coastal phytoplankton bloom, off Vancouver Island (Canada). They used top-of-atmosphere radiances, uncorrected for the atmospheric contribution, and computed the *Maximum Chlorophyll Index*, which is the radiance in Band 9 (709 nm) above a baseline formed by linear interpolation between the radiances

in Bands 8 (681 nm) and 10 (753 nm). Gower *et al.* suggest that the MERIS 709 nm band provides an important tool for the detection of intense algal blooms, phenomena of great significance – because they are so often toxic – for aquaculture. In a later study, Gower *et al.* (2008) report that with this technique they find an average of about one plankton bloom event somewhere in the world on any given day.

The reflectance of water bodies in the green waveband also increases with phytoplankton concentration (see next section). Lathrop and Lillestrand (1986), using Thematic Mapper data for Lake Michigan, found good linear relationships between the logarithm of chlorophyll concentration and the logarithm of radiance in the green band (520–600 nm), for the central lake (oligotrophic) and Green Bay (eutrophic). The relationships were, however, very different for the two parts of the lake, the central lake showing a much higher green radiance for a given level of phytoplankton than the bay, possibly due to a higher level of yellow humic substances in the latter water body, leading to greater absorption of green light. Clearly there is no prospect for a universal phytoplankton algorithm based on green reflectance, but locally applicable algorithms of this type may be of some use.

A special case of increased reflectance associated with increased phytoplankton concentration is that of coccolithophore blooms. These algae, despite their chloroplast pigments are very highly reflective because of the disc-shaped calcium carbonate coccoliths that cover the cells (Fig. 4.10), and which also become detached to float freely in very large numbers in the water. These show up as large milky-white patches in the ocean. They develop annually in the North Sea<sup>578</sup> and can occur anywhere in the world's oceans. In every case examined so far the species responsible has been *Emiliania huxleyi*. Brown and Podesta (1997) observed, in CZCS images, blooms of this species off the southeastern coast of South America in late spring and summer, which seasonally occupied an area as large as 550 000 km<sup>2</sup>.

Floating macroalgae, such as *Sargassum* spp., or *Enteromorpha prolifera* (massive blooms of which in the Yellow Sea presented problems for the sailing events in the 2008 Olympic Games) have a reflectance peak at ~860 nm in the near-infrared. Hu (2009) has developed an algorithm – the Floating Algae Index (FAI) – for use with the MODIS instrument on the Terra and Aqua satellites, which is defined as the difference between reflectance at 859 nm, and a linear baseline between the red band (645 nm) and the short-wave infrared band (1240 or 1640 nm). This has been found to work well for the detection of floating algae in a number of locations around the world's oceans.

### Phytoplankton – increased absorption

The best approach to the remote sensing of phytoplankton is undoubtedly that which makes use of the increased absorption, and therefore reduced radiance reflectance, at the blue end of the spectrum caused by the photosynthetic pigments. Clarke *et al.* (1970) measured from a low-flying aircraft, the spectral distribution of the emergent flux in different regions of the Northwest Atlantic Ocean with chlorophyll *a* concentrations varying from  $<0.1$  to  $3.0 \text{ mg m}^{-3}$ . The general tendency (Fig. 7.8*b*) was that as the phytoplankton concentration increased, reflectance decreased in the blue (400–515 nm) and increased in the green (515–600 nm). The increased reflectance in the green may be attributed to the

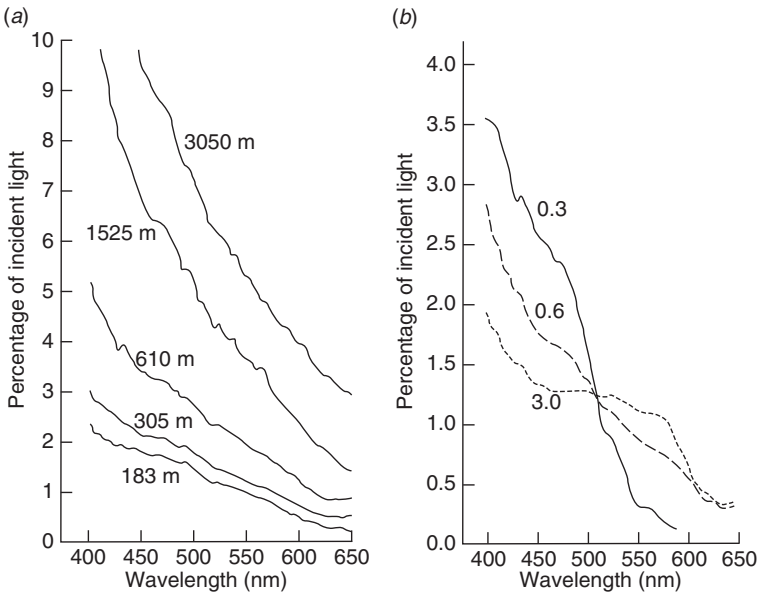


Fig. 7.8 Spectral distribution of reflectance above the Atlantic ocean off New England, USA (after Clarke *et al.*, 1970). Measurements were made at zenith angle of  $53^\circ$ , using a polarizer to eliminate reflected skylight. (a) Dependence of reflectance on altitude: measurements were made at five altitudes over the same location ( $1^\circ$  latitude east of Cape Cod). The large, and increasing, contribution of atmospheric scattering to measured reflectance at altitudes above 305 m is readily apparent. (b) Dependence of reflectance on phytoplankton content. Measurements were made at low altitude (305 m). The phytoplankton chlorophyll level ( $\text{mg chl } a \text{ m}^{-3}$ ) is indicated above each curve. The three curves are for water on the northern edge of the Gulf Stream ( $0.3 \text{ mg chl } a \text{ m}^{-3}$ ), on the edge of the continental shelf ( $0.6 \text{ mg chl } a \text{ m}^{-3}$ ) and over the productive Georges Shoals ( $3.0 \text{ mg chl } a \text{ m}^{-3}$ ).

fact that phytoplankton, being refractive particles, increase scattering at all wavelengths, but in this spectral region absorb only weakly. Empirical methods of remotely estimating phytoplankton concentration generally take advantage of both the decreased reflectance in the blue and the increased reflectance in the green, by working in terms of the ratios or differences between reflectances in these two wavebands.

Morel and Prieur (1977) on the basis of their measurements of the spectral distribution of the upwelling and downwelling light flux in various oceanic waters found that the ratio of underwater irradiance reflectance (related in the manner described previously to the reflectance estimated by remote sensing above the water) at 440 nm to that at 560 nm decreases as the phytoplankton pigment content increases. If data for waters with high scattering coefficients due to suspended sediments are omitted then an approximately linear relation is obtained between the logarithm of  $R_{440}/R_{560}$  and the logarithm of the chlorophyll plus phaeopigment (chlorophyll breakdown products) concentration over the range 0.02 to 20 mg total pigment  $\text{m}^{-3}$ .<sup>941</sup>

Gordon *et al.* (1983) used the effect of phytoplankton on the spectral distribution of the upwelling flux to develop an algorithm by means of which  $L_w$  values obtained from the CZCS in the Nimbus-7 satellite could be used to calculate phytoplankton pigment concentration. They measured the upward nadir radiance within the water (which as we saw earlier is directly related to the emergent flux) at 440, 520 and 550 nm in marine waters with chlorophyll *a* (plus phaeopigment) concentrations ranging from 0.03 to 78  $\text{mg m}^{-3}$ . The data conformed reasonably well to relations of the type

$$\log_{10} C = \log_{10} A + B \log_{10} R_{i,j} \quad (7.25)$$

where  $C$  is the chlorophyll *a* (plus phaeopigment) concentration in  $\text{mg m}^{-3}$ , and  $R_{i,j}$  is the 440/550, 440/520 or 520/550 ratio of radiances. In the case of the 440/550 nm pair, for example, in Case 1 waters,  $\log_{10} A$  is 0.053 and  $B$  is =1.71, i.e. as phytoplankton concentration increases so the ratio of upwelling radiance at 440 nm to that at 550 nm decreases. By substitution of a pair of values of upwelling radiance into the appropriate form of eqn 7.25 the chlorophyll (plus phaeopigment) concentration can be calculated. For chlorophyll concentrations below 0.6  $\text{mg m}^{-3}$  the radiances at 443 and 550 nm are most useful. At higher concentrations, however,  $L_w(443)$  becomes too small for accurate determination by the CZCS, and the radiances at 520 and 550 nm are used instead. Approximate agreement was found between the variation of chlorophyll concentration

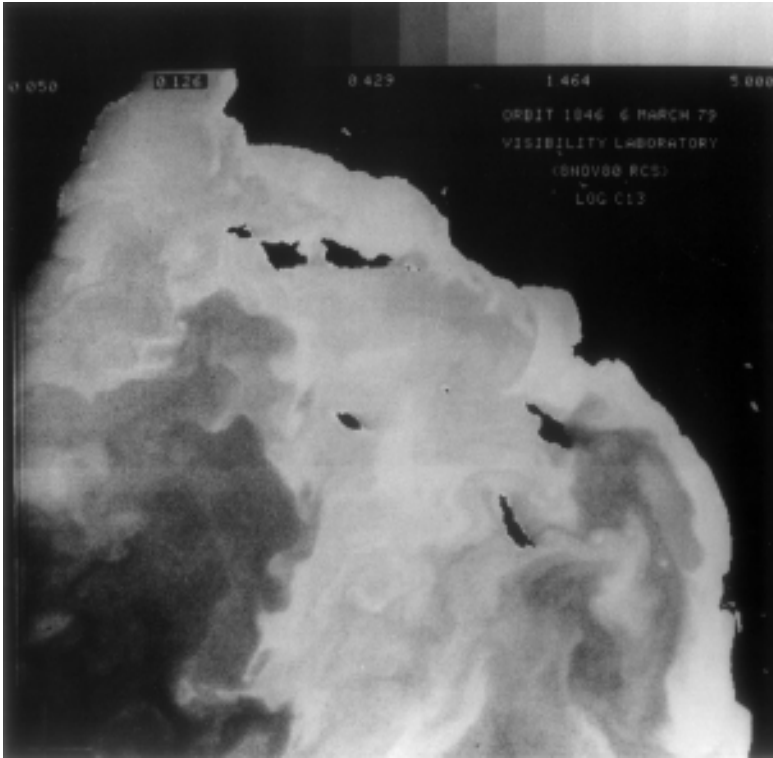


Fig. 7.9 Phytoplankton distribution in the California Bight on 6 March 1979, derived from Coastal Zone Colour Scanner data (by permission, from Smith and Baker (1982), *Marine Biology*, **66**, 269–79). The relation between chlorophyll *a* concentration ( $\text{mg m}^{-3}$ ) and the density of the image is indicated on the scale at the top of the figure.

determined by surface sampling along a ship course of several hundred kilometres in the Gulf of Mexico with that calculated for the same course from CZCS data:<sup>488</sup> similar results were obtained in the Atlantic Bight and Sargasso Sea.<sup>487</sup>

During its operational life from 1978 to 1986, the CZCS accumulated a large amount of data, mapping phytoplankton distribution across the world's oceans, and the results of many such studies can be found in the literature. An early example may be found in Fig. 7.9, which shows the distribution of phytoplankton in the California Bight on a day in March 1979, derived by Smith and Baker (1982) from CZCS data.

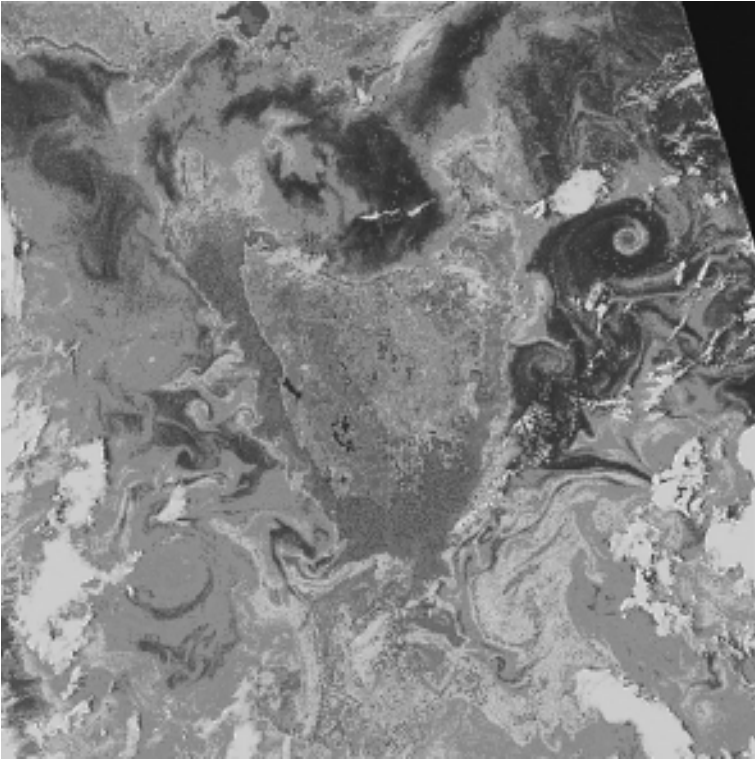


Fig. 7.10 Distribution of phytoplankton in the ocean around Tasmania (Southern Ocean, south of the Australian continent), 27 November 1981, derived from CZCS data. Phytoplankton chlorophyll *a* concentration is colour coded from red (high) to blue (low). Courtesy of the NASA GSFC Earth Sciences Data and Information Services Center (GES DISC). See [colour plate](#).

Figure 7.10 shows the very complex distribution of phytoplankton around Tasmania, in the Southern Ocean, south of the Australian continent, on one November day in 1981.

To arrive at a suitable algorithm for SeaWiFS, O'Reilly *et al.* (1998) analysed a data set consisting of remote-sensing reflectance values ( $R_{rs}[\lambda] = L_w[\lambda]/E_d[0^+, \lambda]$ ) measured in the SeaWiFS wavebands at sea level, together with chlorophyll concentrations (range  $0.02\text{--}32.8\text{ mg m}^{-3}$ ) at 919 oceanic stations. Most of the observations were from Case 1 non-polar waters, but included  $\sim 20$  from more turbid coastal stations. The performance of 17 potentially suitable algorithms, using various combinations of wavebands, was evaluated. Two were identified as performing particularly well: ocean chlorophyll 2 algorithm (OC2), which uses two

wavebands (490 and 555 nm), and ocean chlorophyll 4 algorithm (OC4), which uses four bands (443, 490, 510 and 555 nm). Both are empirical polynomials representing  $C$ , the phytoplankton chlorophyll concentration ( $\text{mg m}^{-3}$ ), as a function of  $R$ , the logarithm of the ratio of reflectance values in two wavebands

$$R = \log_{10} \frac{R_{rs}(\lambda_i)}{R_{rs}(\lambda_j)} \quad (7.26)$$

255 new oceanic stations were subsequently added to the original data set and used to arrive at new versions of the algorithms – OC2v4 and OC4v4.<sup>976</sup> OC2 version 4 is a modified cubic polynomial, which take the form

$$C = 10^{f(R)} - 0.071 \quad (7.27)$$

where

$$f(R) = 0.319 - 2.336R + 0.879R^2 + 0.135R^3 \quad (7.28)$$

OC4 version 4 is a fourth-order polynomial, of the form,  $C = 10^{f(R)}$ , where

$$f(R) = 0.366 - 3.067R + 1.930R^2 + 0.649R^3 - 1.532R^4 \quad (7.29)$$

The difference between the two algorithms is that whereas OC2 uses only the 490 and 555 nm wavebands, OC4 uses whichever of the three ratios –  $R_{rs}(443)/R_{rs}(555)$ ,  $R_{rs}(490)/R_{rs}(555)$  or  $R_{rs}(510)/R_{rs}(555)$ , is the greatest for any given pixel. Algorithms such as OC4, where the reflectance ratio is selectable, are sometimes referred to as ‘switching’ algorithms. Numerous examples of the use of these algorithms for mapping phytoplankton distribution in the world’s oceans from SeaWiFS data can now be found in the remote sensing and oceanographic literature, and also on NASA’s SeaWiFS website ([oceancolor.gsfc.nasa.gov](http://oceancolor.gsfc.nasa.gov)). **Figure 7.11** shows the average distribution of phytoplankton chlorophyll in the global ocean as revealed by SeaWiFS observations for the period September 1997 to July 1998.

The algorithms described above are purely empirical. There are others, however, which seek to make use of the approximate proportionality between the apparent optical property,  $R_{rs}$ , and the ratio of inherent optical properties,  $b_b/a$ . These are known as *semianalytic* algorithms because as well as the analytic function,  $R_{rs} \propto b_b/a$ , they make use of empirically derived relationships between reflectance ratios and optical



Fig. 7.11 Average distribution of phytoplankton chlorophyll in the global ocean (and also terrestrial vegetation) over an 11-month period in 1997–98, derived from SeaWiFS data. Provided by the SeaWiFS Project, NASA/Goddard Space Flight Center and ORBIMAGE. See [colour plate](#).

properties such as the spectral distribution of backscattering, and the wavelength dependence of phytoplankton absorption etc. An example is that developed by Carder *et al.* (1999) for the MODIS instrument on the *Terra* and *Aqua* satellites. This uses  $R_{rs}$  at a number of MODIS wavebands to derive the absorption coefficient of phytoplankton chlorophyll at 675 nm, and the absorption coefficient due to the combined effects of CDOM and detritus at 400 nm. Chl *a* concentration is then calculated assuming an appropriate value for the specific absorption coefficient –  $0.0193 \text{ m}^2 \text{ mg}^{-1}$  for subtropical waters studied by Carder *et al.* Three versions of the algorithm were developed, parameterized for different bio-optical domains: (1) high light tropical/subtropical regions with minimal pigment packaging (see §9.2 for an explanation of this term), (2) upwelling and non-summer high-latitude regions where extensive pigment packaging is to be expected, (3) a transitional or global-average type. The appropriate domain is to be identified from space.

Another semianalytic algorithm in current use is the Garver–Siegel–Maritorea model (GSM01),<sup>440,866</sup> which from measurements of

normalized water-leaving radiance such as those provided by SeaWiFS simultaneously retrieves estimates for chlorophyll concentration, the absorption coefficient at 443 nm for dissolved and detrital colour, and the particulate backscattering coefficient at 443 nm. In tests of the model against a large body of archived data for non-polar Case 1 ocean waters, GSM01 was found to estimate chlorophyll with an accuracy similar to that of the standard SeaWiFS algorithm (OC4v4).

Algorithms such as those embodied in eqns 7.25 to 7.29, with appropriate values of the various coefficients, can be applied to all Case 1 oceanic waters, i.e. waters whose optical properties are almost entirely determined by phytoplankton and its associated debris and breakdown products. In Case 2 waters, whose optical properties are substantially affected by river-borne turbidity and dissolved yellow colour, or by resuspended sediments, relationships of these types still apply,<sup>171,491,917</sup> but the values of the coefficients are different from those for Case 1 waters, and will also differ from one Case 2 water to another. Thus there is no universal Case 2 algorithm, so for these waters algorithms must be sought which are locality specific.

An example is one that Darecki *et al.* (2005) have developed for the southern Baltic Sea, a marine region of shallow depth and with much higher levels of yellow substance than the open ocean. On the basis of 700 simultaneous measurements of (*in situ*) remote sensing reflectance and chlorophyll at a large number of stations they arrived at a two-band algorithm

$$\text{Chl } a \text{ (mg m}^{-3}\text{)} = 10^{(-0.141 - 2.8652R)}$$

where  $R = \log_{10}[R_{rs}(490)/R_{rs}(555)]$ , and a (switching) four-band algorithm

$$\text{Chl } a \text{ (mg m}^{-3}\text{)} = 10^{(-0.028 - 3.9015R)}$$

where, as in OC4v4 above,  $R = R_{rs}(443)/R_{rs}(555)$ ,  $R_{rs}(490)/R_{rs}(555)$  or  $R_{rs}(510)/R_{rs}(555)$ , whichever is the greatest for any given pixel. For the Baltic these algorithms were found to provide more accurate estimates of chlorophyll than OC2 or OC4.

In the Mediterranean Sea, although the waters are mainly Case 1, use of the standard NASA algorithms, OC2v4 and OC4v4, with SeaWiFS leads to a significant overestimation of chlorophyll. Using a large data set of *in situ* measurements of chlorophyll and  $R_{rs}(\lambda)$ , Volpe *et al.* (2007) arrived at a modified version of OC4v4, referred to as 'MedOC4',

implemented in the same way, i.e. switching between the bands, but using a form of eqn 7.29 with a different set of coefficients

$$f(R) = 0.4424 - 3.686R + 1.076R^2 + 1.684R^3 - 1.437R^4$$

where  $R$  is the maximum band ratio. In this region MedOC4 performs better than OC2v4 or OC4v4. They suggest that the poorer performance of the earlier algorithms in deriving chlorophyll concentration from SeaWiFS radiances is due, not to a problem with the atmospheric correction term, but to peculiarities in the optical properties of the water column in the Mediterranean. The presence of Saharan desert dust has been suggested as a possible explanation.<sup>239</sup>

In the Irish Sea, a shallow shelf sea lying between Ireland and Great Britain, McKee and Cunningham (2006) found that in the majority of stations the water could be classified into one or other of two optical types. Using the ratio of particle backscattering ( $b_{bp}$ ) to the (non-water) absorption coefficient at 676 nm ( $a_n$ ), the data fell into two clusters: Group A having  $b_{bp}/a_n > 0.5$  and Group B having  $b_{bp}/a_n < 0.5$ . Particle inherent optical properties (IOPs) were dominated by mineral suspended sediments in Group A waters and by phytoplankton in Group B waters. McKee *et al.* (2007) used *in situ* measurements of optical properties and  $R_{rs}(\lambda)$  to assess the performance of standard SeaWiFS algorithms at 102 stations in the Irish and Celtic Seas. They found that OC4v4 performed poorly for this region, with a strong tendency to overestimate chlorophyll concentration. The mean percentage error was 140%, but estimates for individual stations were up to a factor of six too high. Group A stations could be distinguished from Group B by higher values of normalized water-leaving radiance ( $nL_w[\lambda]$ ) in the green and red wavebands. A threshold value of  $nL_w(665 \text{ nm}) = 0.1 \mu\text{W cm}^{-2} \text{ nm}^{-1} \text{ sr}^{-1}$  was found to be a suitable flag with which to separate the data by optical water type. To develop improved algorithms for these waters, McKee *et al.* retained the form of OC4v4, but used their data to fine tune the coefficients. The modified versions of eqn 7.29 for the new regional chlorophyll algorithms are, for water type A, IS<sub>A</sub>-chl, in which

$$f(R) = -0.2223 - 3.4118R - 3.6683R^2 - 2.6599R^3 - 0.8431R^4$$

and for water type B, IS<sub>B</sub>-chl, in which

$$f(R) = 0.1948 - 2.4851R - 2.4062R^2 - 2.7332R^3 - 1.5733R^4$$

$R$  is the maximum band ratio, selected as in OC4v4.

In Case 2 waters with significant amounts of CDOM, it is impossible with CZCS data to distinguish the lowered reflectance in the blue caused by this soluble yellow colour from that due to phytoplankton. The succeeding generation of ocean-viewing spaceborne radiometers, such as SeaWiFS and MERIS, are designed to carry out measurements at the extreme short-wave end of the visible spectrum, at  $\sim 410$  nm, where phytoplankton absorption has somewhat diminished (relative to that at 440 nm), but CDOM absorption is even higher. It was anticipated that the availability of this short-wavelength band would increase the feasibility of distinguishing phytoplankton from dissolved yellow colour,<sup>203,1175</sup> but this has not yet proved easy to achieve. Gohin *et al.* (2002), using a data set derived from the English Channel and the continental shelf of the Bay of Biscay have created a lookup table that relates the triplet – OC4 maximum band ratio,  $L_w(412 \text{ nm})$ , and  $L_w(555 \text{ nm})$  – to chlorophyll concentration. Application of this table they believe can provide realistic chlorophyll maps for regions such as these.

The Landsat Thematic Mapper has a blue, as well as a green and a red, waveband. The limited amount of data so far available suggests that while it is not likely to be suitable for measuring the low levels of phytoplankton in oligotrophic ocean waters, it might provide useful data on the higher levels occurring in coastal waters, by means of a blue-green algorithm<sup>345,684,690</sup> along the lines of eqn 7.25.

Eutrophic inland lakes very commonly develop blooms of cyanobacteria, which present particular problems to water management agencies because of their frequently toxic nature. Early detection, and monitoring, of such blooms is therefore clearly desirable. A major photosynthetic pigment in these algae is the biliprotein, phycocyanin, which has an absorption peak at  $\sim 620$  nm. Cyanobacterial blooms therefore can give rise to a diminution in reflectance in this waveband. Algorithms for the detection of these blooms, which make use of the phycocyanin absorption band, have been developed for the MERIS spaceborne radiometer,<sup>1229</sup> which has a band at 620 nm, and for hyperspectral radiometers used either *in situ*<sup>1180,1105</sup> or from aircraft.<sup>298,664</sup> Ruiz-Verdu *et al.* (2008) have compared the relative performance of these algorithms using data from lakes and reservoirs in Spain and the Netherlands.

### Phytoplankton – fluorescence

The methods for remote sensing of phytoplankton described above make use of the fact that algal cells absorb light in a certain region of the

spectrum. However, algal cells also emit light: in the laboratory, typically about 1% of the light a photosynthesizing cell absorbs is re-emitted as fluorescence, with a peak at about  $\sim 685$  nm. Fluorescence quantum yield ( $\phi_f$ ) in the sea is calculated on the basis of measurements of the spectral distribution of downwelling irradiance and upwelling radiance underwater, together with measurements of absorption spectra of the particulate and soluble fractions. In the tropical Pacific Ocean, Maritorea *et al.* (2000), for near-surface waters, found an average fluorescence quantum yield of 0.84% in oligotrophic waters of the central Pacific and 1.53% for the productive waters of the Peruvian upwelling.  $\phi_f$  increased with depth, to  $\sim 2\%$  in the *Prochlorococcus*-dominated oligotrophic waters, but to 5 to 6% in the diatom-dominated productive waters. Maximal values were found near 70 m. In the North Sea, off the northeastern coast of the United Kingdom, Morrison (2003) also found  $\phi_f$  to increase with depth, typically from  $\sim 0.5$  to 1% at the surface to 4 to 6% at depths ranging from 5 to 20 m. In the turbid waters of the North China Sea, Xing *et al.* (2008) found  $\phi_f$  near the surface to have an average value of 1.7%. The maximum was 6%, but most values were in the range from 0.1 to 2%. Phytoplankton fluorescence is too feeble to be detected in the downwelling light stream within the water but can show up as a distinct peak in the spectral distribution of the upwelling stream or in the curve of apparent reflectance against wavelength (see Fig. 6.7).<sup>956,1385</sup>

This peak can also be detected in the spectral distribution of the emergent flux. Calculations indicate that the increased fluorescence associated with an increase in phytoplankton chlorophyll of  $1 \text{ mg m}^{-3}$  in the water would lead to an additional upward radiance of  $0.03 \text{ W m}^{-2} \text{ sr}^{-1} \mu\text{m}^{-1}$  above the water.<sup>396,397</sup> Neville and Gower (1977) showed that in the radiance reflectance (upward radiance/downward irradiance) spectra of productive British Columbian coastal waters obtained at the Brewster angle from a low-flying aircraft, a distinct peak at 685 nm was present, the height of which was proportional to chlorophyll concentration in the upper few metres of water. In a coastal inlet the height of the fluorescence peak above the baseline (measured above the water, but from a boat) was linearly correlated ( $r^2 = 0.85$ ) with a weighted average (allowing for vertical distribution) chlorophyll *a* concentration over the range 1 to  $20 \text{ mg m}^{-3}$ .<sup>501</sup> On the basis of the observed height of the peak it seems unlikely that the results would be of acceptable accuracy below about  $1 \text{ mg chlorophyll } a \text{ m}^{-3}$ .

The MERIS spaceborne sensor has a waveband, Band 8, centred on 681.25 nm, on the short-wavelength side of the chlorophyll emission

maximum to avoid the atmospheric oxygen absorption band at 687 nm. Gower and King (2007) extracted the fluorescence signal (as *fluorescence line height, FLH*) from the top-of-atmosphere radiance values using the radiance excess in Band 8 over a linear baseline computed from the radiances in Bands 7 and 9 (665 and 709 nm). By comparing the fluorescence line height from MERIS radiances with *in situ* measurements of chlorophyll on the continental shelf off Vancouver Island and Washington State they were able to express FLH as a function of chlorophyll concentration (*chl*,  $\text{mg m}^{-3}$ ) and solar zenith angle ( $\theta_0$ )

$$FLH = \left[ \frac{0.18chl}{1 + 0.2chl} - 0.24 \right] \cos \theta_0$$

The purpose of the 0.2 *chl* term in the denominator is to take account of the re-absorption of fluorescence by chlorophyll: as might be expected this becomes more significant at higher levels of phytoplankton. This equation can readily be inverted for the calculation of chlorophyll concentration from measured fluorescence.

The MODIS sensor on the *Terra* and *Aqua* satellites is also equipped to measure solar-stimulated fluorescence of phytoplankton, using Bands 13 (665.1 nm), 14 (767.7 nm) and 15 (746.3 nm), all with 10 nm bandwidth. To obtain the FLH, a baseline is formed between the radiances for Bands 13 and 15, and then subtracted from the Band 14 radiance. Hu *et al.* (2005) used MODIS FLH to monitor the development and movement of a 'red tide' of the toxic dinoflagellate, *Karenia brevis*, in coastal waters off southwest Florida. Using the algorithm

$$Chl (\text{mg m}^{-3}) = 1.255 \times (FLH \times 10)^{0.86} \quad (r^2 = 0.92)$$

developed with *in situ* chlorophyll samples collected within a few hours of the satellite overpass, they were able to achieve satisfactory mapping of the red tide. The standard chlorophyll algorithm using reflectance ratios, by contrast, did not work well for this system, consistently overestimating chlorophyll several-fold.

A problem with using Sun-induced chlorophyll fluorescence to measure chlorophyll is that the relationship between the two is not at all constant. For British Columbia coastal waters, Gower *et al.* (1999) found the slope of the approximately linear relationship between FLH and chl concentration to vary through a factor of  $\sim 2.5$  for measurements made in the period 1975 to 1981. The height of the fluorescence peak is markedly affected by the concentrations of CDOM and suspended particles in the water.<sup>502,889</sup> Another problem with the method is that even in the

chlorophyll fluorescence waveband, most of the light in the emergent flux arises from scattering rather than fluorescence. To address this problem, Gilerson *et al.* (2006) have made use of the fact that the elastically scattered component is partially polarized, while the fluorescence signal is unpolarized. With a rotating polarizer in front of the optical probe it was possible, both in algal cultures and two inshore coastal sites, to greatly reduce the proportion of scattered light in the measured radiance. The method does not work well in the presence of very high concentrations of suspended mineral particles, which cause depolarization of the scattered light, but should be generally applicable to open ocean and coastal waters. On the basis of their data the authors conclude that the traditional method of extracting fluorescence height using the baseline method can give significant errors, particularly for coastal waters where it strongly overestimates the fluorescence values.

Phytoplankton chlorophyll can be estimated using the fluorescence excited by light from an airborne laser rather than by sunlight, and the method has certain advantages. A key problem in the use of remotely sensed chlorophyll fluorescence as an indication of phytoplankton biomass is that the proportion of the fluorescent light that succeeds in passing up to the sensor, as well as the proportion of the exciting light (solar or laser) that succeeds in reaching the algae, depends on the optical properties of the water. Two different water bodies with the same phytoplankton content, but different attenuation properties, could give quite different fluorescence signals. To correct for the effects of attenuation by the aquatic medium, Hoge and Swift (1981) and Bristow *et al.* (1981) have made use of the laser-induced Raman emission of water.

When water molecules scatter light, most of the scattered light undergoes no change in wavelength. A small proportion of the scattered photons, however, when they interact with the scattering molecule, lose or gain a small amount of energy corresponding to a vibrational or rotational energy transition within the molecule, and so after scattering are shifted in wavelength. These appear in the scattered light as emission bands at wavelengths other than that of the exciting light, and are referred to as Raman emission lines, after the Indian physicist who discovered this phenomenon. A particularly strong Raman emission in the case of liquid water arises from the O–H vibrational stretching mode: this shows up as an emission band roughly 100 nm on the long-wavelength side of the exciting wavelength (Fig. 7.12). Since the water content of the aquatic medium is essentially constant, the intensity of this Raman emission, when remotely sensed from above the water is, for a given exciting light

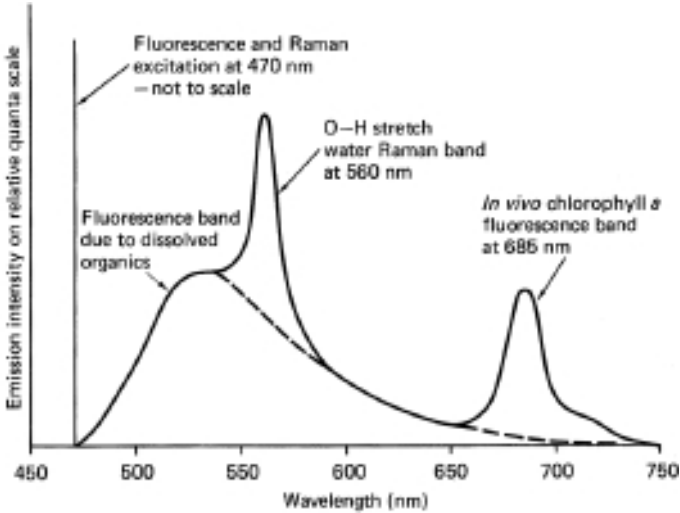


Fig. 7.12 Idealized emission spectrum of natural waters resulting from excitation with a laser at 470 nm (by permission from Bristow *et al.* (1981), *Applied Optics*, **20**, 2889–906).

source, determined entirely by the light-attenuating properties of the water, low Raman signals indicating high attenuation, and vice versa.

Thus to correct for variation in the optical character of the water, the measured chlorophyll fluorescence intensity at each station is divided by the corresponding water Raman emission intensity. Chlorophyll fluorescence values measured from the air, and normalized in this way, have been found to correlate closely with chlorophyll contents determined on water samples.<sup>166</sup>

Bristow *et al.* (1981) used a pumped dye laser, emitting at 470 nm, and exciting Raman emission at 560 nm, operated from a helicopter at 300 m above the water (Fig. 7.13a). The light returning from the water was collected by a telescope with a 30 cm diameter Fresnel lens; a beam splitter, interference filters and separate photomultipliers (Fig. 7.13b) being used to separately detect the chlorophyll fluorescence and Raman emission. Hoge and Swift (1981) used a neodymium-doped yttrium aluminium garnet (Nd:YAG) laser emitting at 532 nm, and exciting a water Raman emission at 645 nm: the equipment was flown in a P-3A aircraft at 150 m above the water surface. With a frequency-tripled Nd:YAG laser emitting at 355 nm there is a Raman emission peak at 402 nm, which can be used together with the CDOM fluorescence at 450 nm to estimate absorption due to yellow substances (see later). Hoge *et al.* (2005) report

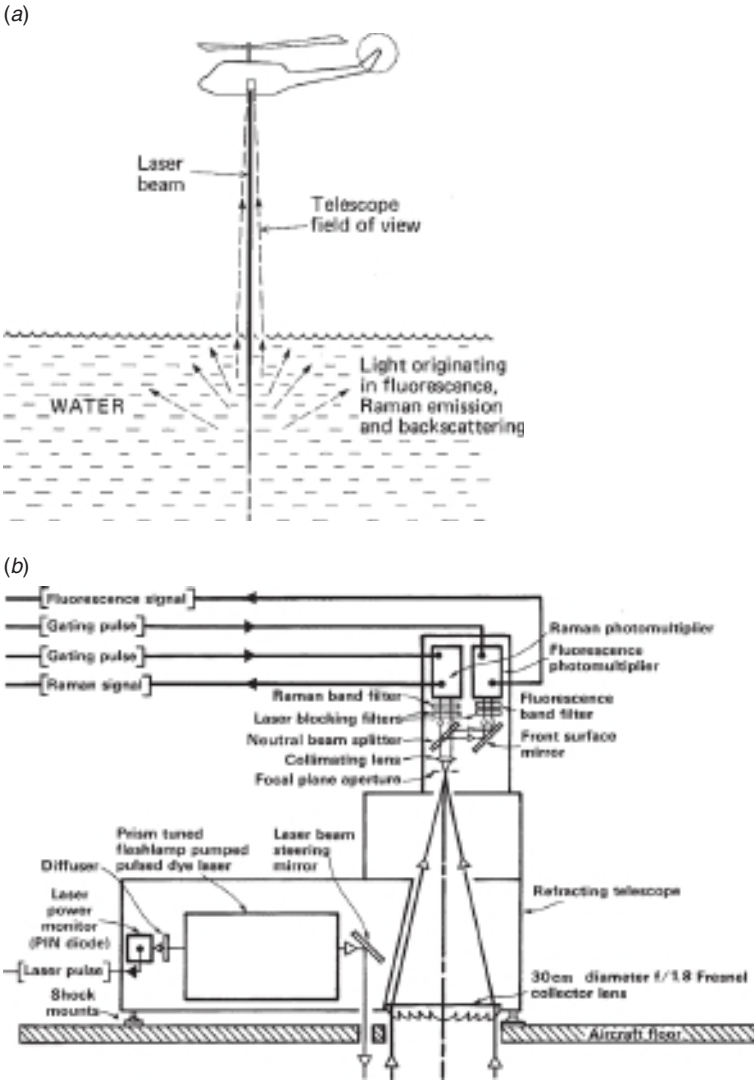


Fig. 7.13 Mode of operation of airborne laser system for detection of chlorophyll fluorescence and water Raman emission. (a) Schematic diagram of light fluxes. (b) Diagram of laser and optical receiver system (by permission, from Bristow *et al.* (1981), *Applied Optics*, **20**, 2889–906).

that combining these data with the chlorophyll 683 nm fluorescence and 645 nm Raman data (from 532 nm laser excitation) leads to improved estimates of phytoplankton chlorophyll content. The 355 nm laser on its own also excites chlorophyll fluorescence at  $\sim 680$  nm, and the

fluorescence to Raman (404 nm) ratio (which they find to be proportional to chlorophyll) has been used by Barbini *et al.* (2004) with a shipborne instrument to continuously measure surface chlorophyll content in transects from Italy to New Zealand and back again.

In waters in which the phytoplankton population includes a significant proportion of cyanophyte and/or cryptophyte algae, the laser-induced fluorescence spectrum includes a substantial peak at  $\sim 580$  nm due to emission from the biliprotein photosynthetic pigment, phycoerythrin,<sup>372,586</sup> and thus can provide some information about the types of algae present.

### **Gilvin (CDOM), and total absorption coefficients**

The dissolved yellow humic substances in surface waters have (Chapter 3) an absorption spectrum rising exponentially into the blue. Where, as in many lakes, rivers and estuaries, CDOM is the dominant contributor to light absorption, there are generally found to be simple relationships between CDOM concentration and the ratio of reflectance in the blue to that at some longer wavelength. Bowers *et al.* (2000) studied the relationship between subsurface radiance reflectance ( $r_{rs}[\lambda]$ ) ratios and CDOM in shallow inshore waters of the Clyde Sea (Scotland), a region receiving a considerable input of fresh water from land run-off. The ratio of reflectance in the red (670 nm) to that in the blue-green/blue at 490, 443 or 412 nm increased linearly with concentration of yellow substance, as expressed through measurement of 440 nm absorption ( $g_{440}$ ) on a filtrate.  $g_{440}$  could thus in principle be obtained from remotely sensed reflectance ratios. In the more turbid waters of the Conwy estuary (North Wales) Bowers *et al.* (2004) again found a linear relationship between  $r_{rs}(670)/r_{rs}(490)$  and  $g_{440}$  but the slope and intercept were different from those previously found for the Clyde Sea. The authors attributed the difference to the fact that in these waters, suspended sediment particles contributed significantly to total light absorption. In Galway Bay (Ireland), Goddijn and White (2006) found a linear relationship between  $g_{440}$  and the red/blue output ratio of a digital camera.

Among the world's major marine ecosystems, the Baltic Sea is unique in the extent to which optical properties are dominated by yellow substances, a consequence of its very high inflow of fresh water from northern European rivers combined with restricted interchange with the North Sea through the Straits of Denmark. Kowalczyk *et al.* (2005) studied the relationship between remote sensing reflectance ( $R_{rs}[\lambda]$ ), measured at sea

level, and CDOM absorption, at a large number of stations in the southern Baltic Sea. Using SeaWiFS wavebands they found the most satisfactory retrieval variable to be the ratio of reflectance at 490 nm to that at 590 nm. For CDOM absorption at 400 nm the data could be represented by the algorithm

$$a_{\text{CDOM}}(400 \text{ nm}) = 10^{f(X)}$$

where

$$f(X) = -0.20 - 0.50 X + 0.65 X^2$$

and  $X = \log_{10}(R_{rs}[490]/R_{rs}[590])$

Schwarz (2005) using a simpler algorithm

$$\ln g_{440} = -0.1123 - 0.8725 \ln[R_{rs}(443)/R_{rs}(510)]$$

based on a limited number of *in situ* measurements, used SeaWiFS data to map dissolved organic carbon concentration in the Baltic Sea.

Kahru and Mitchell (2001) compared *in situ* measurements of CDOM concentration at stations in the California Current (at 300 nm because of low CDOM in these waters) with concurrently collected SeaWiFS radiances. The algorithm for CDOM concentration derived from the data was

$$a_{\text{CDOM}}(300) = 10^{(-0.393 - 0.872 R)}$$

where  $R$  is the ratio of normalized water-leaving radiance at 443 nm to that at 510 nm. D'Sa and Miller (2003) examined the relationships between (sea-level)  $R_{rs}(\lambda)$  values in SeaWiFS wavebands, and CDOM absorption in the Mississippi outflow region of the northern Gulf of Mexico. The reflectance ratios for 412 and 510 nm, 443 and 510 nm, 510 and 555 nm, were all highly correlated with CDOM absorption, the logarithm of the reflectance ratio decreasing linearly with  $\log a_{\text{CDOM}}(412)$ . For the 443/510 pair the relationship was

$$\log_{10} a_{\text{CDOM}}(412) = -0.874 - 2.025 \log_{10}[R_{rs}(443)/R_{rs}(510)]$$

Menon *et al.* (2006) used *in situ* measurements of water-leaving radiance ( $L_w$ ) and CDOM absorption in estuarine waters in Goa, on the west coast of India to develop an algorithm for use with the Ocean Colour Monitor on board the Indian Remote Sensing (IRS) satellite. They found that the diminution of the ratio of radiance at 412 nm to that at 670 nm with increasing CDOM concentration could be expressed as

$$a_{\text{CDOM}}(440) = 2.9393 R^{-2.2486}$$

where  $R = L_w(412)/L_w(670)$ , and they used this algorithm to map the distribution of CDOM in the estuaries and the nearby inshore waters. Kutser *et al.* (2009) made use of the high radiometric (16 bit), and spatial (30 m), resolution of the Advanced Land Imager on the EO-1 satellite, to map the distribution of CDOM in Estonian coastal waters (Baltic Sea), using the algorithm

$$a_{\text{CDOM}}(420 \text{ nm}) = 5.13 \left( \frac{R_4}{R_5} \right)^{-2.67}$$

where  $R_4$  and  $R_5$  are the reflectances (atmospherically corrected by the dark pixel method) in ALI Bands 4 (525–605 nm) and 5 (630–690 nm), respectively. Their data revealed the high local variability of CDOM concentration, and the consequent need for high spatial resolution for mapping it, in coastal waters.

When the optical properties of a surface water are dominated by a single component, such as phytoplankton or CDOM, simple algorithms such as those described above might reasonably be expected to provide a realistic picture of the distribution of the component in question. The greater part of the ocean consists of Case 1 waters in which phytoplankton is the major optically significant component. In humic lakes and in coastal regions receiving substantial outflows of gilvin-rich river water, CDOM is often the major contributor. In most Case 2 waters, however – coastal, typically shallow, often with turbid river inflow – phytoplankton, CDOM and suspended sediments all contribute significantly to the optical character of the water and application of the simple algorithms is likely to give highly misleading results.

A straightforward, and sometimes feasible, way of addressing this problem is to develop simple empirical algorithms that work in a given locality, but have no general application. A more challenging approach is to try to develop algorithms that can, from remotely sensed radiance values, extract the actual inherent optical properties themselves –  $a(\lambda)$  and  $b_b(\lambda)$  – and then apportion these appropriately to the components of the medium. There have been numerous attempts to achieve this: some using purely empirical relationships, and others – referred to as *semianalytical* or *quasi-analytical* – which combine empirical with algebraic relationships arising out of radiative transfer theory. Many such algorithms are now available which give promising results, and they are comprehensively described in IOCCG Report No. 5 – *Remote Sensing of Inherent*

*Optical Properties: Fundamentals, Tests of Algorithms and Applications.*<sup>787</sup>

There is, however, a fundamental problem underlying this approach, namely that of ambiguity. Defoin-Platel and Chami (2007) point out that solutions arrived at may be non-unique since several combinations of IOP can lead to the same reflectance spectrum.

A special case of retrieval of an inherent optical property, which seems to work in both Case 1 and Case 2 waters, is the measurement of yellow substance absorption using airborne lidar. Gilvin, the dissolved yellow humic constituent of natural waters, like chlorophyll, emits fluorescence when excited by the laser beam: its emission spectrum extends through the visible region with a broad peak at  $\sim 530$  nm when excited at 470 nm (Fig. 7.12). It has been monitored in river water in terms of the combined emission at 531 and 603 nm,<sup>165</sup> and in coastal water in terms of the emission at 500 nm.<sup>1187</sup> Hoge *et al.* (1995) used a frequency-tripled Nd:YAG laser at 355 nm flown on a P-3B aircraft to excite CDOM fluorescence over the Middle Atlantic Bight from Delaware Bay to the Sargasso Sea, in Monterey Bay and in the Gulf of Mexico. Using the CDOM fluorescence signal at 450 nm, normalized by the 404 nm water Raman spectral line height to allow for variation in attenuation by the water (see above), and expressed relative to the fluorescence of a quinine sulfate standard, they developed an algorithm for  $a_{CDOM}(355)$ , the absorption coefficient of CDOM at the exciting wavelength. Making a reasonable assumption about the value of the spectral slope parameter,  $S$  (eqn 3.5), the absorption coefficients of CDOM at other wavelengths can then be calculated.

It is worth noting that the Raman signal itself can be used for mapping the attenuation properties of the water: the reciprocal of the signal is proportional to an attenuation coefficient intermediate in value between  $K_d$  and  $c$ .

### Vertical attenuation coefficients for downward irradiance

As well as providing information about levels of phytoplankton, suspended solids and CDOM, remotely sensed radiances can be used to map vertical attenuation coefficients for downward irradiance. Austin and Petzold (1981) derived empirical relationships by means of which  $K_d(490)$  and  $K_d(520)$  could be obtained from the ratio of radiances in the CZCS 443 and 520 nm wavebands. Analysing SeaWiFS data mainly from Case 1 waters, Mueller (2000) arrived at the following algorithm for  $K_d(490)$

$$K_d(490) = 0.016 + 0.15645 \left[ \frac{nL_w(490)}{nL_w(555)} \right]^{-1.5401}$$

where  $nL_w(\lambda)$  is the normalized water-leaving radiance at wavelength  $\lambda$ , and the 0.016 term is the  $K_d(490)$  for pure water. An updated version of this algorithm,<sup>1451</sup> omitting the constant term is

$$K_d(490) = 0.1853 \left[ \frac{nL_w(490)}{nL_w(555)} \right]^{-1.349}$$

This algorithm (SeaWiFS  $K[490]$ ) does not, however, work well in waters where  $K_d(490)$  is greater than  $0.25 \text{ m}^{-1}$ . As referred to earlier, McKee and Cunningham (2006) found that the Irish and Celtic Seas could be classified into one or other of two optical water types: A with higher scattering/absorption and B with lower scattering/absorption ratios. McKee *et al.* (2007), on the basis of *in situ* measurements at 102 stations, found that the SeaWiFS  $K(490)$  algorithm satisfactorily predicted  $K_d(490)$  from water-leaving radiances in the clearer, B, waters but in the more turbid, A, waters an algorithm with altered coefficients

$$K_d(490) = 0.016 + 0.3189 \left[ \frac{nL_w(490)}{nL_w(555)} \right]^{-3.0054}$$

worked better.

An alternative route to  $K_d(490)$ , proposed by Morel *et al.* (2007) is to first use the remotely sensed data to retrieve the chlorophyll concentration and then apply the following algorithm based on [Chl]

$$K_d(490) = 0.0166 + 0.0773 [\text{Chl}]^{0.6715}$$

Lee *et al.* (2005) have devised a more complex, semi-analytical, algorithm for remotely sensing  $K_d(490)$ , which appears to be more widely applicable than the standard empirical algorithms. The first step is to use a previously devised quasi-analytical algorithm<sup>788,787</sup> to estimate  $a$  and  $b_b$  at the wavelength of choice, e.g. 490 nm, from remotely sensed radiances at 440 and 555 nm.  $K_d$  is then calculated using an equation expressing  $K_d$  as a function of  $a$  and  $b_b$ , derived empirically from Hydrolight simulations<sup>790</sup>

$$K_d = (1 + 0.005\theta_a)a + 4.18(1 - 0.52e^{-10.8a})b_b$$

where  $\theta_a$  is the solar zenith angle.

In any given optical water type there should be an approximately constant relationship between  $K_d(490)$ , which can be determined by

remote sensing, and  $K_d(\text{PAR})$ , the coefficient for the whole photosynthetic waveband. To be able to map  $K_d(\text{PAR})$  from remote sensing data would be of great value for studies of ocean productivity, but the relationship between the two coefficients is likely to vary from one water type to another. Pierson *et al.* (2008) used values of inherent optical properties determined at a large number of sites in the Baltic Sea to model the underwater light field. They found that  $K_d(\text{PAR})$  could satisfactorily be expressed in terms of  $K_d(490)$ , either as a linear

$$K_d(\text{PAR}) = 0.6098 K_d(490) + 0.1134 \quad (r^2 = 0.8872)$$

or a power

$$K_d(\text{PAR}) = 0.6677[K_d(490)]^{0.6763} \quad (r^2 = 0.9074)$$

relationship. The Baltic Sea is, as we have noted earlier, untypical because of its high CDOM concentration. Other relationships will therefore need to be found for other parts of the ocean. On the basis of an extensive oceanic data set, primarily but not exclusively in Case 1 waters, Morel *et al.* (2007) propose

$$K_d(\text{PAR}) = 0.0665 + 0.874 K_d(490) - 0.00121[K_d(490)]^{-1}$$

Lee *et al.* (2007) have developed a method using values of IOPs calculated from remotely sensed  $R_s(\lambda)$  data by the quasi-analytical algorithm (above), to determine the euphotic depth ( $z_{\text{eu}}$ ), which is equivalent, since  $K_d(\text{PAR}) \approx 4.6/z_{\text{eu}}$ , to determining  $K_d(\text{PAR})$  itself. The method worked reasonably well for certain coastal, as well as oceanic, waters.

Another broad waveband of major ecological significance is the near-UV, 300 to 400 nm, not only because of its damaging effects on marine life forms, and its contribution to the photoinhibition of photosynthesis (§10.1), but also because of its role in the photochemical breakdown of coloured dissolved organic matter. The incident solar UV flux can now be monitored from space with ozone-mapping satellite-borne spectrometers. Remote sensing of vertical attenuation coefficients in the UV would thus make it possible to assess the underwater UV radiation field in different parts of the ocean. On the basis of *in situ* measurements in the Bering Sea and the Mid-Atlantic Bight, Johannessen *et al.* (2003) derived empirical expressions for  $K_d(\lambda)$  at 323, 338 and 380 nm as simple power law functions of the ratio of radiance reflectance at 412 nm to that at 555 nm. Using SeaWiFS radiances at 412 and 555 nm they were then able to map the distribution of  $K_d(323)$  in the Mid-Atlantic Bight. Starting from a

more wide-ranging *in situ* data set, and using a more complex statistical approach (principal component analysis), Fichot *et al.* (2008) have devised two new algorithms for mapping  $K_d(\lambda)$  in the UV at 320, 340 and 380 nm, which give a somewhat improved performance.

Vasilkov *et al.* (2001) developed an algorithm for calculating UV penetration into Case 1 waters based on the simplifying assumption that the optical properties of such waters are entirely attributable to water and phytoplankton together with a CDOM contribution having an  $a(440\text{ nm})$  corresponding to 20% of the phytoplankton plus water absorption at that wavelength. For the optical properties the starting input data were the standard SeaWiFS estimates of chlorophyll *a* and  $K_d(490)$ . Specific absorption coefficients (absorption per mg chl *a*,  $\text{m}^2\text{mgchl } a^{-1}$ ) for phytoplankton in the UV – where there is substantial absorption by mycosporine-like amino acids (see §3.3) – were taken from literature data for coastal waters of the Antarctic Peninsula. The authors acknowledged that these may not be entirely typical for the ocean at large, but there was a shortage of such data at the time. To estimate the backscattering coefficient, use was made of an approximate relationship developed by Gordon (1989a)

$$\frac{K_d}{D_0} = 1.0395(a + b_b)$$

between the vertical attenuation coefficient for downward irradiance ( $K_d$ ), the distribution function ( $D_0$ , the reciprocal of the average downward cosine) just under the surface, and  $a$  plus  $b_b$ .  $D_0$  is readily obtained as a simple function of solar angle, and the relative amount of direct sunlight and skylight.  $a(490)$  was derived from the SeaWiFS chlorophyll value together with the CDOM assumption and an appropriate CDOM spectrum. The SeaWiFS  $K_d(490)$ , and the calculated  $D_0$  and  $a(490)$  values were then used in the Gordon equation to derive  $b_b(490)$ . The values of  $b_b$  at wavelengths in the UV were calculated from  $b_b(490)$  on the assumption that  $b_b$  is proportional to  $\lambda^{-1}$ . Using the values of  $a(\lambda)$  and  $b_b(\lambda)$  derived as above, together with the appropriate values of solar angle and the proportion of direct and diffuse sunlight, penetration of UV radiation into the water column was calculated using a simple analytical model. Data from the Total Ozone Mapping Spectrometer (TOMS) satellite instrument provided solar UV irradiance values at the ocean surface. The final output data are presented in various ways, including the distribution of the 10% UVB (280–320 nm) penetration depth over the global ocean for the month of July 1998.

### Distribution of seagrass and other macrophytes

Seagrass beds are of great ecological significance in shallow bays, estuaries and coastal lakes but are frequently under threat from dredging, eutrophication and other consequences of human activity. Ocean colour sensors such as SeaWiFS are of little use for monitoring these ecosystems because of their low spatial resolution. Remote sensors such as Landsat Thematic Mapper, although spectrally limited, do have potential for this purpose because of their high ground-level resolution – 30 m in the case of Landsat TM. With the help of *in situ* measurements of reflectance spectra of various seagrass and macroalgal species, and of  $K_d(\lambda)$  spectra at the sampling sites, Dekker *et al.* (2005) were able to use atmospherically corrected Landsat TM images to retrospectively monitor four seagrass species over a 14-year period in Wallis Lake – a shallow coastal tidal lake on the East coast of Australia. A substantial reduction in the area of *Zostera* beds was observed, but little change in the area occupied by *Posidonia*, *Ruppia* and *Halophila*. Sagawa *et al.* (2008), used data from the IKONOS satellite sensor, which has bands in the blue, green, red and infrared, and a resolution of 4 m, to map seagrass beds in Funakoshi Bay, Honshu Island, Japan. Phinn *et al.* (2008) used remote sensing to map seagrass species, cover and biomass in shallow (<3.0 m depth) waters in Moreton Bay (Australia). Ground-truth validation was achieved with underwater photography, and sampling of the benthos, along transects. The airborne CASI hyperspectral sensor was found to perform best, followed by Quickbird 2 (spacecraft at 450 km altitude; blue, green, red, near-infrared bands; 2.4 m ground-level resolution), followed by Landsat TM.

In the narrow shallow perimeter off rocky shores, extensive beds of large brown algae frequently occur, and are of great ecological significance. Simms and Dubois (2001) used satellite images recorded by Landsat TM (blues, green and red bands) and the SPOT HRV sensor (green and red bands), together with scuba diving inventories and *in situ* reflectance data, to follow seasonal variation in kelp (*Laminaria longicruris*) beds in the Baie des Chaleurs (Gulf of St Lawrence, Quebec, Canada).

### Secchi depth

An optical water property important for the fauna and – in coastal regions – for human beings, is the in-water visibility, which can be expressed quantitatively in terms of the Secchi depth ( $Z_{SD}$ , §5.1). Chen

*et al.* (2007) investigated the relationship between *in situ* measured Secchi depth and SeaWiFS radiances in Tampa Bay, Florida. For the 1997 to 2005 period, 80 matching data pairs were recovered. An empirical relationship

$$Z_{SD} = 1.04 K_d(490)^{-0.82}$$

was found between Secchi depth and the value of  $K_d(490)$  calculated from the SeaWiFS radiances using the semi-analytical algorithm of Lee *et al.* (2005) (see above): the authors suggest that this could be used for routine monitoring of this aspect of water quality in coastal and large estuarine waters such as Tampa Bay.

For the Peel–Harvey estuary in Western Australia, Lavery *et al.* (1993) studied the relationship between radiance values in Landsat TM Bands 1 (450–520 nm) and 3 (630–690 nm), atmospherically corrected by the dark-pixel method, and Secchi depth. Using the algorithm

$$Z_{SD} = 0.74 - 0.05L_w(630 - 690) + 1.80 \frac{L_w(450 - 520)}{L_w(630 - 690)} \quad (r^2 = 0.81)$$

they mapped the distribution of  $Z_{SD}$  in this estuarine system. On the basis of *in situ* measurements in a number of lakes in central Spain, Dominguez Gomez *et al.* (2009) arrived at an empirical relationship between Secchi depth and above-surface reflectance in the 520 to 600 nm waveband (corresponding to TM Band 2)

$$Z_{SD} = 4.0098[R_{520-600}]^{-1.3659}$$

With the help of atmospherically corrected Landsat TM images, this relationship was then used to monitor water transparency in lakes in the study area at intervals over the period 1984 to 2000.

We saw earlier that  $Z_{SD}$  is approximately proportional to  $1/(c + K_d)$ , so if  $(c + K_d)^{-1}$  can be estimated from remotely sensed radiances then in-water visibility could be mapped. Doron *et al.* (2007) have developed an algorithm to achieve this, using radiance values only in two wavebands, 490 and 709 nm. At 490 nm, absorption and scattering by all seawater constituents contribute to variability in reflectance, whereas at 709 nm – where water absorbs strongly but other components hardly at all – variations in reflectance are almost solely due to changes in the particle backscattering coefficient. The absorption coefficient at 709 nm ( $a[490]$ ) is assumed to be equal to that of pure water, which is known. The constant of proportionality ( $f$ ) relating irradiance reflectance to  $b_b/a$  in eqn 6.5 is,

on the basis of literature data, given the value 0.335, for both wavebands. From reflectance at 709 nm,  $b_b(709)$  is thus obtained. Using an assumed ratio between particulate backscattering at 490 nm and that at 709 nm, the backscattering coefficient ( $b_{bp}[490]$ ) at 490 nm, due to particles, is obtained. From  $b_{bp}(490)$ , the total particulate scattering coefficient ( $b_p$ ) is obtained with the help of an empirical relationship expressing the total particulate scattering coefficient ( $b_p$ ) as a function of the particulate backscattering coefficient, at 490 nm, derived on the basis of a substantial data set obtained from *in situ* measurements at a large number of stations in Case 1 and Case 2 ocean waters. Addition of scattering due to water (known) to that due to particles gives  $b(490)$ , the total scattering coefficient. The absorption coefficient at 490 nm,  $a(490)$ , is obtained from  $b_b(490)$  and reflectance at 490 nm, using eqn 6.5. The beam attenuation coefficient is then obtained from  $c(490) = a(490) + b(490)$ . Using the Lee *et al.* (2005) algorithm,  $K_d(490)$  can be estimated from reflectance data, so that  $[c(490) + K_d(490)]^{-1}$  can finally be arrived at. Values of  $[c(490) + K_d(490)]^{-1}$  calculated from *in situ* reflectances as described, correlated closely ( $r^2 = 0.90$ ) with those obtained by direct measurement of  $c(490)$  and  $K_d(490)$  within the water.



## PART II

### Photosynthesis in the aquatic environment



## 8

# The photosynthetic apparatus of aquatic plants

In [Part I](#), we considered the underwater light climate: the particular characteristics that it has in different types of natural water bodies, the scattering and absorption processes that take place in the aquatic medium, and the ways that these operate upon the incident light stream to produce the kinds of underwater light field that we observe. Now, in [Part II](#), we turn our attention to the utilization of this underwater light for photosynthesis by aquatic plants. We begin, in this chapter, by asking: with what intracellular structures, from the level of organelles down to that of molecules, do aquatic plants harvest radiant energy from the underwater light field and convert it to chemical energy?

### 8.1 Chloroplasts

In eukaryotic plants, photosynthesis is carried out by the organelles known as *chloroplasts*, the best known members of the great class of related and interconvertible organelles known as *plastids*. Detailed accounts of these organelles may be found in Kirk and Tilney-Bassett (1978), Staehelin (1986) and Falkowski and Raven (2007): we shall here content ourselves with a rather brief treatment.

The chloroplasts contain the pigments that capture the light, the electron carriers that use the absorbed energy to generate reducing power in the form of  $\text{NADPH}_2$  and biochemical energy in the form of ATP, and the enzymes that use the  $\text{NADPH}_2$  and the ATP to convert  $\text{CO}_2$  and water to carbohydrate. The pigments and electron carriers are contained in a specialized type of membrane known as the *thylakoid*. The enzymes of  $\text{CO}_2$  fixation are distributed throughout the rest of the inner volume – the *stroma* – of the chloroplast, although in certain

algal chloroplasts some of the enzymes may be located in a specific structure within the chloroplast known as the *pyrenoid* (see below). In cyanobacteria, the most plentiful photosynthetic enzyme – ribulose-1,5-bisphosphate carboxylase/oxygenase, also known as *carboxydismutase*, or *Rubisco* – is located in an icosahedral crystalline structure known as a *carboxysome*.

Chloroplasts occupy a substantial proportion of the cytoplasmic volume outside the vacuole. There is usually enough chloroplast material per cell to ensure that most of the light incident on the cell passes through one or more chloroplasts. As we shall see in a later chapter, however, the disposition of the chloroplast(s) within the cell, and hence the proportion of the cellular cross-section occupied by chloroplast substance, can vary with light intensity.

In higher plants, including aquatic species, chloroplasts are typically lens-shaped bodies, 4 to 8  $\mu\text{m}$  in diameter and about 2  $\mu\text{m}$  thick in the centre. There are commonly 20 to 400 chloroplasts per mature leaf cell, depending partly on the size of the cell. In terrestrial plants, the chloroplasts occur mainly in the palisade and mesophyll cells of the leaves, whereas the plastids in the epidermal cells usually do not develop into chloroplasts. In submerged aquatic plants, however (the only kind with which we are concerned in this book), the epidermal cells often have well-developed chloroplasts. The palisade layer within the leaf in some cases does not develop at all, being replaced by spongy parenchyma.<sup>603</sup> Stomata are scarce or absent in submerged leaves, the  $\text{CO}_2$  presumably being taken up directly through the epidermal cell walls.

Among the eukaryotic algae, chloroplasts vary greatly in size, number and morphology. Comprehensive accounts may be found in Fritsch (1948), Bold and Wynne (1978), Raymont (1980) and Larkum, Douglas and Raven (2003). In both unicellular and multicellular algae, chloroplasts can occur singly, in pairs or in numbers of up to 100 or more per cell. In many algal species the chloroplasts contain dense bodies, 1 to 5  $\mu\text{m}$  in diameter – the pyrenoids. These are often the site of polysaccharide deposition and are tightly packed with granular or crystalline aggregates of what appears to be ribulose bisphosphate carboxylase.

The chloroplasts may be lens-shaped (*Euglena*, *Coscinodiscus*), helical (*Spirogyra*), star-shaped (*Zygnema*), plate-like (*Pinnularia*), in the form of an irregular network (*Oedogonium*), or various other shapes (Fig. 8.1). Where they occur singly they are usually large as, for example, the flat, approximately rectangular chloroplast of *Mougeotia*, which is commonly 100 to 150  $\mu\text{m}$  long. Where they occur in large numbers

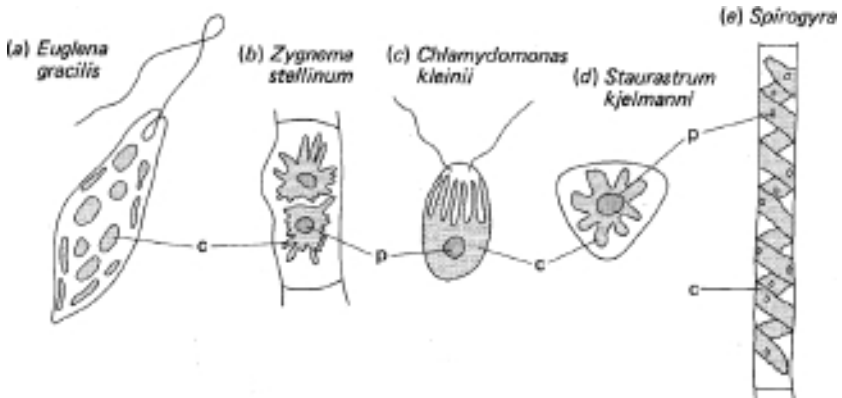


Fig. 8.1 Some algal chloroplasts. c = chloroplast, p = pyrenoid. (b)–(e) after West, G. S. (1904), *The British Freshwater Algae*, Cambridge University Press.

they are usually lens-shaped and of similar size (a few  $\mu\text{m}$  in diameter) to higher plant chloroplasts.

If we direct our attention to individual groups of algae, some useful generalizations are possible. Most of the green algae (Chlorophyta), major components of both the attached and the planktonic flora, contain one chloroplast per cell. This may be a cup-shaped structure as in *Chlamydomonas*, *Chlorella* and other unicellular planktonic species, or it may have a spiral, flat or other shape in the large-celled filamentous forms. Some desmids contain two chloroplasts per cell. Three of the 15 or so orders of green algae, the Caulerpales, Siphonocladales and Dasycladales, have a *coenocytic* construction. As well as having some cells of normal construction they have tubular filaments lacking cross-walls. These tubular structures contain large numbers of, usually lens-shaped, chloroplasts.

The brown algae (Phaeophyta) may contain one, a few or many chloroplasts per cell. The Laminariales and Fucales, two orders of particular importance for coastal primary production, both contain numerous chloroplasts per cell in their large thalli. A characteristic of these brown algal chloroplasts is that when they contain a pyrenoid, this forms a bulbous structure protruding out from the otherwise lens-shaped chloroplast.

In that very diverse division the Chrysophyta (yellow, yellow-green or yellow-brown single cells), also known as Heterokontophyta, we shall consider, on the grounds of their major contribution to planktonic primary production, just one of the classes – the Bacillariophyceae or

diatoms. Diatom species often form the major component of the phytoplankton in both fresh waters and in the cooler higher latitude regions of the ocean. In the centric (circular) diatoms the chloroplasts are commonly small, lens-shaped and numerous. In the pennate (elongated) diatoms, fewer (often only two) and larger (lobed or plate-like) chloroplasts are present.

The class Prymnesiophyceae, in the division Haptophyta, includes the coccolithophorids, major constituents of the marine phytoplankton, particularly in the warmer regions. Members of this class typically have two, but sometimes four or more, lens-shaped chloroplasts.

The division Dinophyta (formerly Pyrrophyta), or dinoflagellates, is a major contributor to aquatic, especially marine, primary production; being comparable in importance to the diatoms. The Pyrrophyta are made up of two classes, the Dinophyceae with numerous small, lens-shaped chloroplasts and the Desmophyceae with few, plate-like chloroplasts.

Members of the Euglenophyta, unicellular flagellates of common occurrence in ponds, have a variety of types of chloroplast structure, ranging from large numbers of lens-shaped plastids (Fig. 8.1) to small numbers of large plate-like or ribbon-like bodies. Another group of unicellular flagellates, the Cryptophyta, occasionally significant components of the phytoplankton in coastal waters, contain usually two, but sometimes one, chloroplast(s) per cell.

The Rhodophyta, or red algae, are predominantly thalloid in form and occur mainly in marine habitats. They are major components of the benthic (growing, attached, on the bottom) flora of coastal waters. They can be divided into two groups: the Bangiophycidae, which usually have a single, stellate, axial chloroplast; and the Florideophycidae, which normally contain numerous small lens-shaped chloroplasts around the periphery of the cell.

## 8.2 Membranes and particles

In electron micrographs of sections, chloroplasts are seen to be bounded by an envelope consisting of two (green algae, red algae, higher plants), three (Euglenophyta, dinoflagellates) or four (brown algae, diatoms, prymnesiophytes, haptophytes) membranes, and to be filled with a granular matrix. This matrix is referred to as the *stroma* and is composed of a concentrated solution or gel of proteins, consisting mainly of the enzymes used in carbon dioxide fixation. Embedded within the stroma there is an

array of flattened, membrane-bounded sacs known as *thylakoids*. These lie approximately parallel to the main plane of the chloroplast and when seen in electron microscope sections at right angles to that plane, they present the appearance of membranes in pairs. There are large numbers of thylakoids in each chloroplast. In the algae most of the thylakoids extend from one end of the chloroplast to the other.

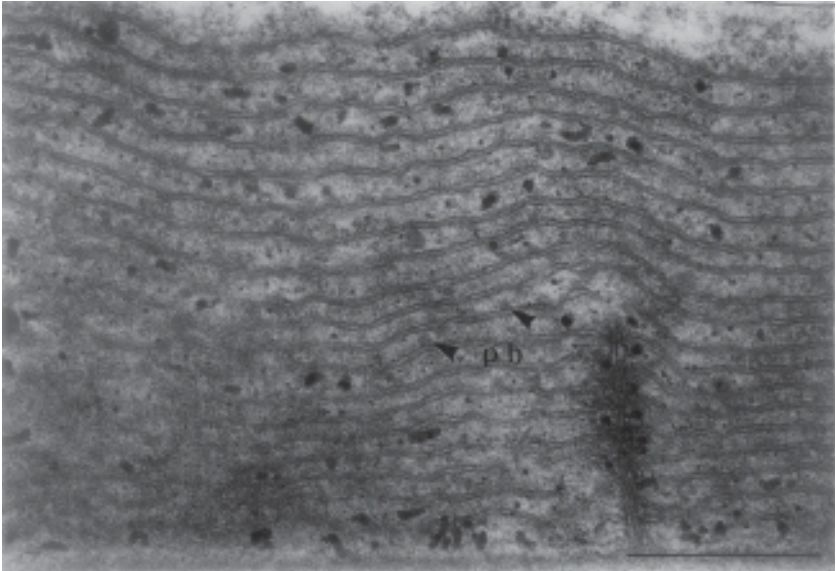
The different classes of algae differ from one another in the way in which the thylakoids are grouped together. The simplest arrangement is that found in the red algae (Fig. 8.2*b*). These have single thylakoids, about 20 nm thick, lying separately in the stroma. Attached to the outer surface of each thylakoid is an array of particles 30 to 40 nm in diameter, known as *phycobilisomes* and consisting mainly of biliprotein molecules.

The next simplest type of thylakoid arrangement is that found in the Cryptophyta, which have thylakoids loosely associated in pairs (Fig. 8.3*a*). They are thicker than the thylakoids of other algae, being 19 to 36 nm across, and their interior space is filled with a finely granular, electron-dense material, which is thought to consist of the biliprotein pigments.

In all other classes of algae, with the exception of some of the Chlorophyta, the thylakoids are grouped, or stacked, in threes (Fig. 8.3*b*). These stacks of thylakoids are referred to as compound lamellae. In aquatic higher plants and in some green algae a more complex arrangement of the thylakoids is found. They occur in much bigger stacks consisting typically of 5 to 20 thylakoids, but the individual thylakoids in the stacks are of much smaller diameter than a typical algal thylakoid. Each such stack is referred to as a *granum*. There may be 40 to 60 *grana* in a typical chloroplast. There are numerous interconnections between the different grana and between the different thylakoids within a stack (Fig. 8.4). In this type of chloroplast the thylakoids can best be regarded as individual compartments in a complex, ramifying system of interconnected compartments that constitutes the photosynthetic membrane system of the chloroplast. The thylakoid system in the chloroplast of a submerged aquatic higher plant may be seen in Fig. 8.4*b*.

Blue-green algae (Cyanophyta) are prokaryotes and so the various cellular functions are not compartmented within separate membrane-bounded organelles. These algae also have thylakoids but these lie free within the cytoplasm (Fig. 8.2*a*). They are similar in type to those of the red algal chloroplasts, occurring as separate, single thylakoids with phycobilisomes on the surface. A type of prokaryotic alga, *Prochloron*, which occurs in symbiotic association with certain marine ascidians, does

(a)



(b)

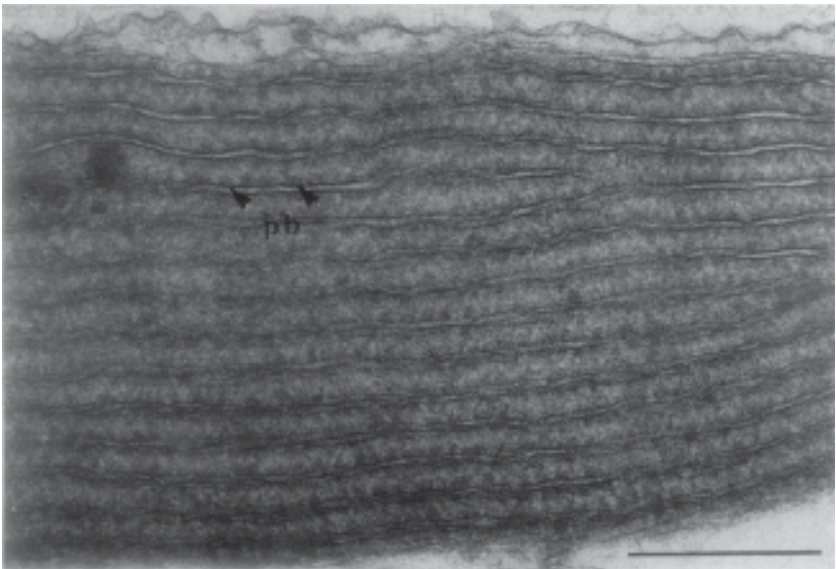
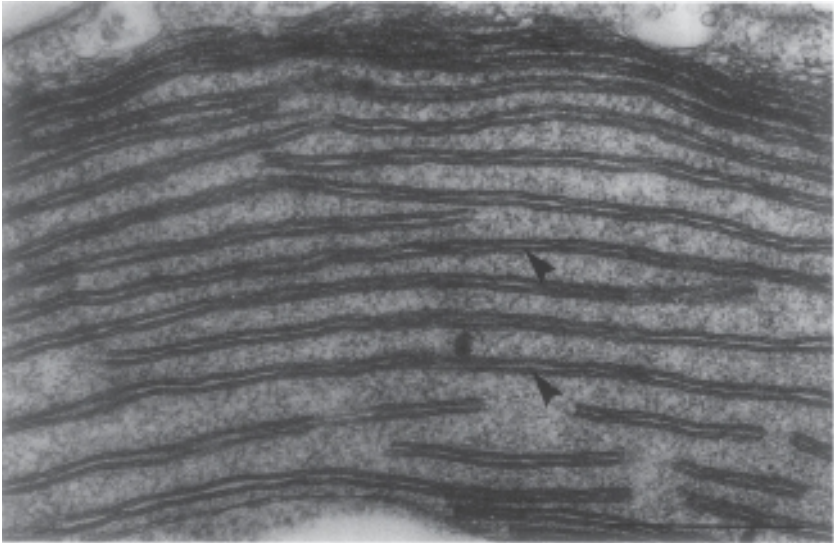


Fig. 8.2 Parallel single thylakoids with adherent phycobilisomes in blue-green and red algae (by courtesy of Dr M. Veski). pb – phycobilisomes. Bar = 0.5  $\mu\text{m}$ . (a) Thylakoids lying free within the cytoplasm of the blue-green alga *Oscillatoria brevis*. (b) Part of a chloroplast in the red alga *Halitilon cuvieri*, showing the regularly spaced single thylakoids.

(a)



(b)

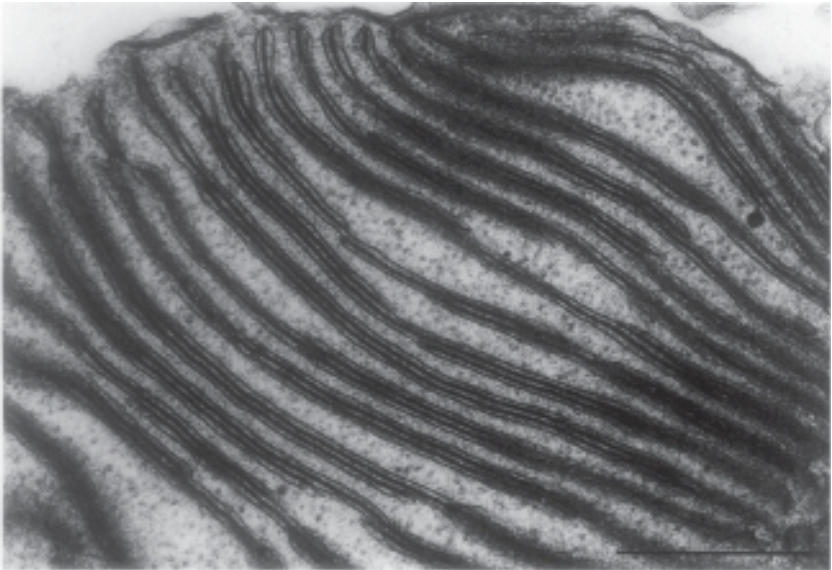
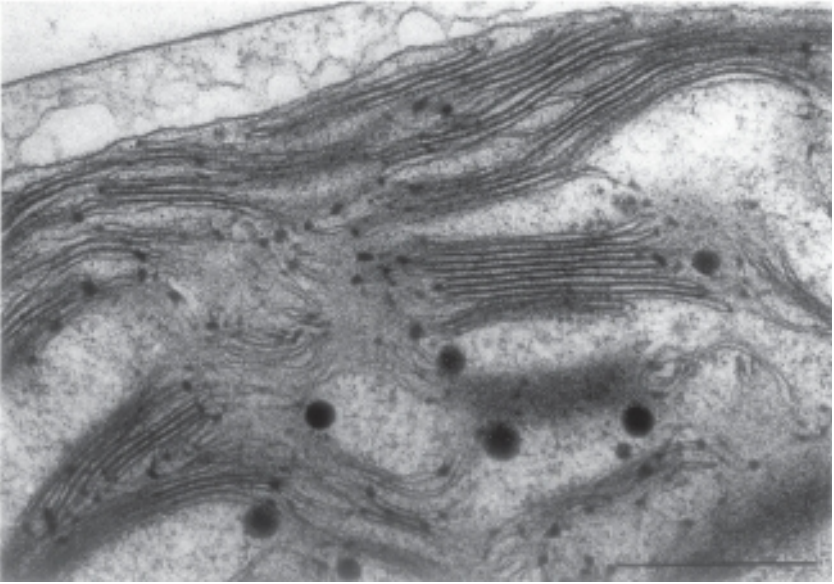


Fig. 8.3 Algal chloroplasts with thylakoids grouped in pairs and triplets (by courtesy of Dr M. Vesik). Bar = 0.5  $\mu\text{m}$ . (a) Part of a chloroplast of the cryptophyte alga *Chroomonas* sp., showing the paired thylakoids (arrows) filled with a phycobiliprotein matrix. (b) Part of a chloroplast of the dinoflagellate *Gymnodinium splendens*, showing the compound lamellae, each consisting of three closely appressed thylakoids.

(a)



(b)

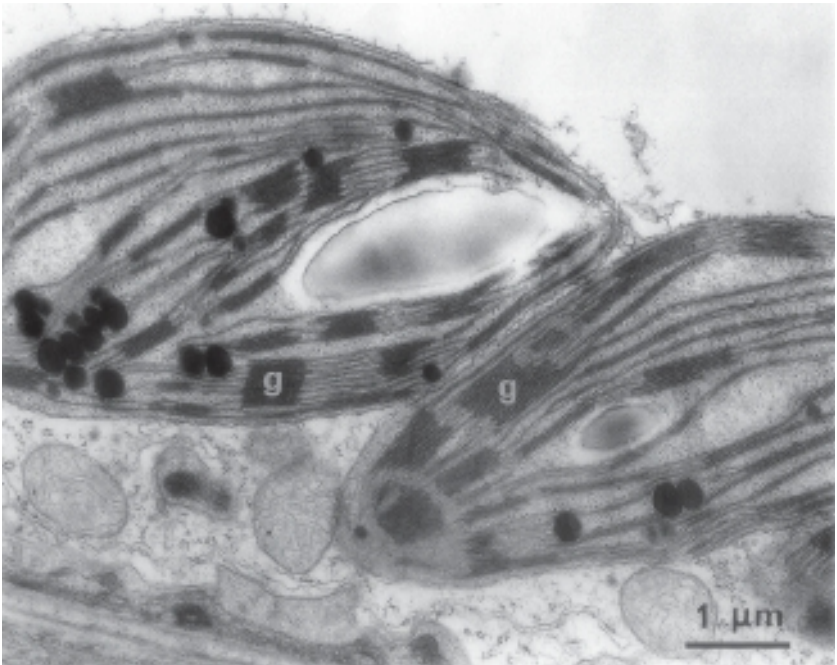


Fig. 8.4 Chloroplast structure in green aquatic plants. (a) Part of a chloroplast of the green unicellular flagellate *Dunaliella tertiolecta* (Chlorophyta) showing the somewhat irregular stacking of thylakoids to form rudimentary grana (by courtesy of Dr M. Veski). Bar = 0.5  $\mu\text{m}$ .

not contain biliproteins and so lacks phycobilisomes. It was proposed by Lewin (1976) that these algae should be placed in a new algal division, the Prochlorophyta, but the counterproposal has been put by Antia (1977) that the criteria defining the Cyanophyta be widened so that the group could include algae such as *Prochloron*. Different isolates of *Prochloron* have thylakoids lying within the cytoplasm singly, in pairs or in stacks of up to 12 thylakoids.<sup>1356,1459</sup> Free-living prochlorophyte species also exist: a filamentous form, *Prochlorothrix*, has been found in a lake, and coccoid forms are abundant in the sea.<sup>187,227</sup> These marine coccoid forms, all currently referred to as *Prochlorococcus marinus*,<sup>225</sup> are now known to be of great ecological importance, contributing substantially to ocean primary productivity, particularly in the lower regions of the euphotic zone. The cells contain two or three thylakoids appressed together, adjacent and closely parallel to the cytoplasmic membrane, and extending most of the way around the cell.<sup>225,810</sup> *Prochlorococcus marinus* does not possess phycobilisomes, although some strains do contain biliproteins.

The thylakoid membrane in all plants consists of a polar lipid bilayer with protein particles embedded within it. The thylakoids of higher plant chloroplasts are made up of about 32% colourless lipid, 9% chlorophyll, 2% carotenoid and 57% protein, and it is likely that algal thylakoids have a broadly similar average chemical composition. The nature of the lipids constituting the bilayer varies from one class of alga to another, but it seems that in every case, major components are the two galactolipids – mono- and digalactosyl diglyceride (Fig. 8.5*a* and *b*), which are polar but uncharged. Functional membranes also need ionized lipids, and in the thylakoid these are present partly in the form of phospholipids, such as phosphatidyl glycerol and phosphatidyl choline, common constituents of most biological membranes. In addition, thylakoid membranes contain a sulfolipid – sulfoquinovosyldiacylglycerol (SQDG, Fig. 8.5*c*) – which is a sulfonic acid and exists in the membrane in its ionized, negatively charged, form. Functionally, the sulfolipid can in some situations substitute for phospholipids. This substitution appears to have been successfully achieved by the important marine prochlorophyte,

Caption for Fig. 8.4 (cont.)

(*b*) Chloroplasts in the leaf of the submerged aquatic plant *Vallisneria spiralis* (by courtesy of Mr D. Price and Dr S. Craig), showing the stacking of thylakoids to form grana (g), and the stroma thylakoids connecting the grana. A large starch grain is evident in the left-hand chloroplast.

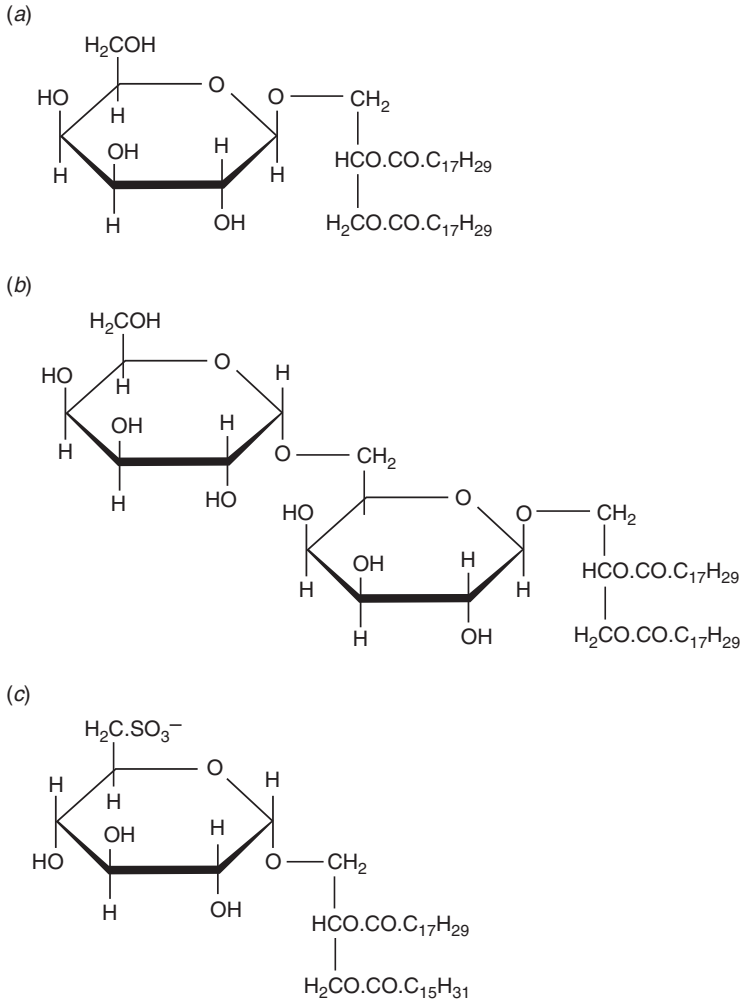


Fig. 8.5 Chloroplast glycolipids. (a) Monogalactosyl diglyceride. (b) Digalactosyl diglyceride. (c) Thylakoid sulfolipid: sulfoquinovosyldiacylglycerol.

*Prochlorococcus*. Van Mooy *et al.* (2006) found that in the oligotrophic North Pacific Subtropical Gyre, the world's largest biome, *Prochlorococcus* – which dominates the phytoplankton – synthesized predominantly SQDG, rather than phospholipids. In cell cultures, the vast majority ( $94 \pm 5\%$ ) of membrane lipids in *Prochlorococcus* and in the related genus, *Synechococcus*, were composed of the sulfolipid

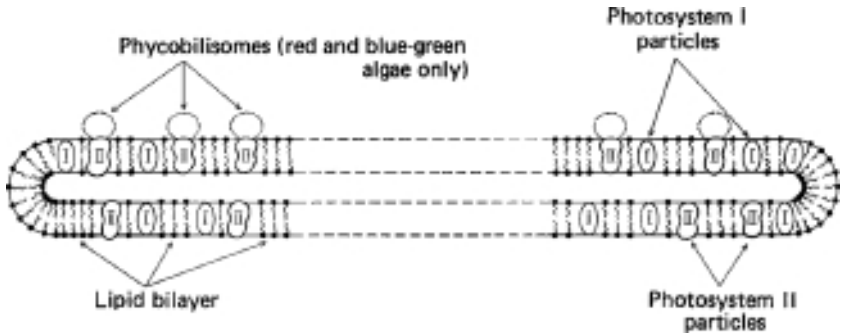


Fig. 8.6 Possible mode of organization of the thylakoid membrane in algae and aquatic higher plants.

(36–66% in axenic cultures) and the two galactolipids. The authors suggest that the evolution of this ‘sulfur for phosphorus’ strategy, taking advantage as it does of the more plentiful supply of sulfate than of phosphate in sea water, may be a large part of the reason for the success of picocyanobacteria in oligotrophic environments.

The light absorption/electron transport system of photosynthesis consists of two subsystems, referred to as photosystem I and photosystem II (see §8.5). It is thought that these exist within the thylakoid membrane as two distinct, but interacting, types of particle, each containing a reaction centre and light-harvesting pigment-proteins, and having specific types of electron transfer components associated with it. The molecular structure of the photosynthetic membrane is likely to vary markedly from one algal class to another, but there are grounds for supposing that the mode of organization is something along the lines indicated in Fig. 8.6.

### 8.3 Photosynthetic pigment composition

The task of collecting light energy from the underwater light field is carried out by the photosynthetic pigments – molecules whose structures are such that they efficiently absorb light in different parts of the 400 to 700 nm range. There are three chemically distinct types of photosynthetic pigment: the chlorophylls, the carotenoids and the biliproteins. All photosynthetic plants contain chlorophyll and carotenoids; the red algae, the blue-green algae and the cryptophytes contain biliproteins as well. A comprehensive account of the photosynthetic pigments of algae has been given by Rowan (1989).

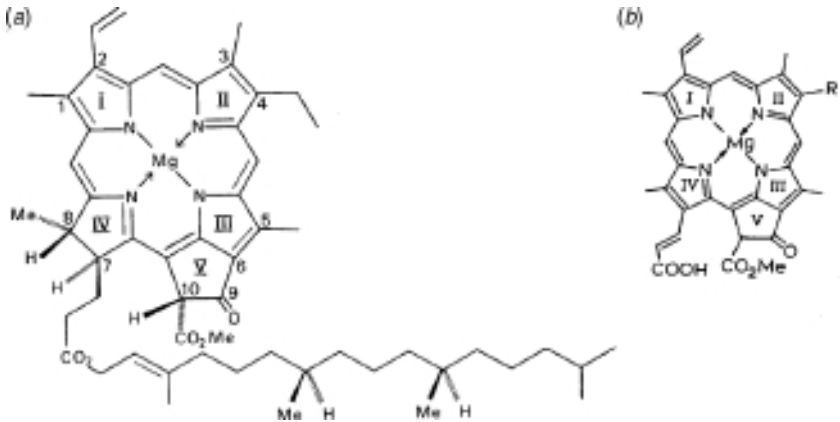


Fig. 8.7 The chlorophylls. (a) *a/b*. In chlorophyll *b* the  $-\text{CH}_3$  on ring II is replaced by a  $-\text{CHO}$ . In chlorophylls  $a_2$  and  $b_2$  the ethyl on ring II is replaced by a vinyl. (b)  $c_1/c_2$ . In  $c_1$  R is  $-\text{C}_2\text{H}_5$ ; in  $c_2$  R is  $-\text{CH}=\text{CH}_2$ .

### The chlorophylls

The chlorophylls are cyclic tetrapyrrole compounds with a magnesium atom chelated at the centre of the ring system. Chlorophylls *a* and *b* are derivatives of dihydroporphyrin: their structures are shown in Fig. 8.7*a*. In the coccoid marine prochlorophyte, *Prochlorococcus marinus*, chlorophylls *a* and *b* are replaced by the divinyl forms,  $a_2$  and  $b_2$ ,<sup>225,467</sup> in which the ethyl group on ring II is replaced by a vinyl group. Chlorophyll *d*, which has so far been found only in cyanobacteria in the genus *Acaryochloris*, has a structure similar to that of chlorophyll *a*, except that the vinyl group on ring I is replaced by a formyl ( $-\text{CHO}$ ) group. Chlorophylls *a*, *b* and *d* are rendered hydrophobic by the presence of a  $\text{C}_{20}$  isoprenoid alcohol, phytol, esterified to the propionic acid residue on ring IV.

Chlorophylls  $c_1$  and  $c_2$  are porphyrins rather than dihydroporphyrins: their structures are shown in Fig. 8.7*b*. In those algae that possess them, the greater part of the *c* chlorophyll lacks the phytol group, but in certain species a small proportion is found to be present in the phytylated form.<sup>981,439,1499</sup> In addition to containing phytylated chlorophyll *c*,<sup>439</sup> the coccolithophorid, *Emiliania huxleyi*, has been shown by Garrido *et al.* (2000) to contain another non-polar form consisting of chlorophyll  $c_2$  to which the chloroplast lipid – monogalactosyldiacylglyceride – is attached, most probably by an ester link through the carboxyl group on ring IV. In the picoplanktonic alga, *Pelagococcus subviridis* (Chrysoophyceae),

isolated from the East Australian Current, Vesk and Jeffrey (1987) found in addition to chlorophylls *a* and *c*<sub>2</sub>, a new chlorophyll, which they referred to as chlorophyll *c*<sub>3</sub>. Jeffrey and Wright (1987) found this pigment also to be present in *Emiliana huxleyi*, in a proportion approximately equal to that of *c*<sub>2</sub>. In chlorophyll *c*<sub>3</sub> the methyl group on ring II of chlorophyll *c*<sub>2</sub> (Fig. 8.7*b*) is replaced by a methylated carboxyl group (-COOCH<sub>3</sub>).<sup>404</sup>

In *Micromonas* and certain other green marine flagellates in the Prasinophyceae, Ricketts (1966) found that 2 to 9% of the total chlorophyll consisted of Mg 2,4-divinylphaeoporphyrin *a*<sub>5</sub> monomethyl ester, an intermediate in the biosynthesis of chlorophyll *a*, with a structure similar to chlorophyll *c*<sub>2</sub>, differing only in that the acrylic acid group attached to ring IV is reduced to a propionic acid residue (-CH<sub>2</sub>CH<sub>2</sub>COOH). Using fluorescence excitation spectra, Brown (1985) was able to show, using one of these algal species, *Mantoniella*, that there is excitation energy transfer from this pigment to chlorophyll *a*, indicating that it is a functional part of the antenna for photosynthesis, rather than merely an accumulating biosynthetic intermediate.

All photosynthetic plants contain chlorophyll *a* (or *a*<sub>2</sub>), and most classes of plant contain, in addition, either chlorophyll *b* (or *b*<sub>2</sub>), or one or more of the chlorophyll *c*s, or (in one known genus so far) chlorophyll *d*. The distribution of the chlorophylls among the different plant groups is summarized in Table 8.1. Chlorophyll *a* normally constitutes most of the chlorophyll present.

Among the algae, the chlorophyll *a* content varies widely. The ranges of concentrations found among the three major pigment classes of the littoral multicellular marine algae off Helgoland were, as a percentage of dry mass: red, 0.09 to 0.44; brown, predominantly 0.17 to 0.55; green, 0.28 to 1.53.<sup>350</sup> The amounts per unit area of thallus, in mg dm<sup>-2</sup>, were: red, 0.5 to 2.8; brown, predominantly 4.3 to 7.6; green, 0.5 to 1.4. So far as the phytoplankton in natural waters are concerned, the chlorophyll *a* content is at its highest in nutrient-rich waters favouring rapid growth. Steele and Baird (1965) found that in the northern North Sea the ratio of carbon to chlorophyll *a* in the mixed phytoplankton population was at its lowest value of 20:1 in the spring, after which it increased to a value of about 100:1 in late summer. Assuming the phytoplankton to contain about 37% carbon, and disregarding the silica of the frustules of the diatoms present, these ratios correspond to chlorophyll *a* contents of about 1.8% and 0.37% of the dry mass, respectively. In the upwelling area off Peru, the average carbon:chlorophyll *a* ratio of the phytoplankton throughout the euphotic zone was 40 (≡ chlorophyll ~0.9% non-SiO<sub>2</sub>

Table 8.1 *Distribution of chlorophylls among different groups of plants.*

Plant group	<i>a</i>	<i>b</i>	<i>c</i> <sub>1</sub>	<i>c</i> <sub>2</sub>	<i>c</i> <sub>3</sub>	<i>d</i>
<b>Angiosperms, Gymnosperms, Pteridophytes, Bryophytes</b>	+	+	-	-	-	-
<b>Algae</b>						
Chlorophyta	+	+	-	-	-	-
Euglenophyta	+	+	-	-	-	-
Heterokontophyta						
Chrysophyceae <sup>a</sup>	+	-	+	+	-	-
Xanthophyceae	+	-	-	-	-	-
Eustigmatophyceae	+	-	-	-	-	-
Bacillariophyceae <sup>b</sup>	+	-	+ (-)	+	- (+)	-
Haptophyta <sup>c</sup>	+	-	+/-	+	+/-	-
Pyrrophyta (Dinophyta) <sup>d</sup>	+	-	- (+)	+	-	-
Phaeophyta	+	-	+	+	-	-
Cryptophyta	+	-	-	+	-	-
Rhodophyta	+	-	-	-	-	-
Cyanophyta	+	-	-	-	-	-
<i>Acaryochloris</i> <sup>e</sup>	+	-	-	-	-	+
Prochlorophyta <sup>f</sup>	+	+	-	-	-	-

<sup>a</sup> Some *c*<sub>2</sub>-containing chrysophytes also contain chlorophyll *c*<sub>3</sub>, where it replaces chlorophyll *c*<sub>1</sub>.<sup>630,1290</sup>

<sup>b</sup> All of 51 diatom species examined by Stauber and Jeffrey (1988) contained chlorophyll *c*<sub>2</sub>, and all except 8 also contained chlorophyll *c*<sub>1</sub>: where *c*<sub>1</sub> was absent it was usually replaced by chlorophyll *c*<sub>3</sub>.

<sup>c</sup> All haptophytes so far studied contain chlorophyll *c*<sub>2</sub> plus either *c*<sub>1</sub> or *c*<sub>3</sub>; some (*Prymnesium*, *Ochrosphaera*) contain all three *c* chlorophylls.<sup>1500</sup>

<sup>d</sup> The majority of dinoflagellates (Pyrrophyta), those containing peridinin as the major carotenoid, with one known exception contain only chlorophyll *c*<sub>2</sub>: those dinoflagellates in which peridinin is replaced by fucoxanthin contain both *c*<sub>1</sub> and *c*<sub>2</sub>.<sup>627</sup>

<sup>e</sup> In the unusual cyanophyte, *Acaryochloris*, discovered by Miyashita *et al.* (1996), not only is chlorophyll *d* present, but it is the major photosynthetic pigment, the cellular content being at least 25 times that of chlorophyll *a*. Previous reports of the presence of small amounts of chlorophyll *d* in some Rhodophyta are now thought to be due to the presence of colonies of *Acaryochloris* growing epiphytically on the red algal thalli.<sup>967</sup>

<sup>f</sup> The coccoid oceanic prochlorophytes contain the divinyl forms, *a*<sub>2</sub> and *b*<sub>2</sub>, instead of the normal forms, of chlorophylls *a* and *b*.<sup>227,467</sup>

dry mass): this population consisted almost entirely of diatoms.<sup>828</sup> In the eastern Pacific Ocean, off La Jolla, California, USA, the carbon:chlorophyll *a* ratio of the phytoplankton average about 90 ( $\equiv$  chlorophyll  $\sim$ 0.4% non-SiO<sub>2</sub> dry mass) in nutrient-depleted surface waters, and about 30 ( $\sim$ 1.2% non-SiO<sub>2</sub> dry mass) in deeper, nutrient-rich waters.<sup>365</sup>

When grown in culture under conditions favouring high pigment content – low light intensity, high nitrogen concentration in the medium – algae usually have chlorophyll levels higher than those observed under natural conditions. Unicellular green algae such as *Chlorella* commonly have chlorophyll contents in the range 2 to 5% of the dry mass and *Euglena gracilis* has been observed to contain 3.5% chlorophyll, when grown under these conditions.

The molar ratio of chlorophyll *a* to chlorophyll *b* is about 3 in higher plants and in freshwater green algae. Marine species of green algae, both multicellular and unicellular, are characterized by low *a:b* ratios, in the range 1.0 to 2.3.<sup>623,973,1494</sup> Outside the Chlorophyta, chlorophyll *b* occurs only in the Euglenophyta and in the prokaryotic Prochlorophyta. In *Euglena gracilis*, *a:b* is commonly about 6, and in the Prochlorophyta values (*a<sub>2</sub>:b<sub>2</sub>*) of 1 to 12 have been reported.<sup>1356,187,227</sup>

In those algae which contain chlorophyll *c*, this pigment constitutes (on a molar basis) about the same proportion of the total chlorophyll as chlorophyll *b* does in the green algae and higher plants. In surveys by Jeffrey (1972, 1976) and Jeffrey *et al.* (1975), the range of values of the molar ratio of *a* to *c* (where  $c = c_1 + c_2$ ) found for different classes of marine algae were: diatoms, 1.5 to 4.0 (mean, 3.0); peridinin-containing dinoflagellates, 1.6 to 4.4 (mean, 2.3); fucoxanthin-containing dinoflagellates, 2.6 to 5.7 (mean, 4.2); chrysomonads, 1.7 to 3.6 (mean, 2.7); cryptophytes, 2.5; and brown algae, 2.0 to 5.5 (mean, 3.6). In the majority of those algae that contained both *c*<sub>1</sub> and *c*<sub>2</sub> they were present in approximately equal amounts: however, ratios (*c*<sub>1</sub>:*c*<sub>2</sub>) from 2:1 to 1:5 were found. Most of the dinoflagellates and cryptomonads were found to lack chlorophyll *c*<sub>1</sub>. The newly defined algal class, Synurophyceae,<sup>23</sup> contains *c*<sub>1</sub> but not *c*<sub>2</sub>.

The light absorption properties of chlorophyll are interpreted in terms of two excited singlet states (see §3.1) – upper and lower – of the electrons. The absorption spectra of chlorophylls *a* and *b* in organic solvent are shown in Fig. 8.8. They each have a strong absorption band (*Q<sub>y</sub>*) in the red (corresponding to the lower singlet state) and another stronger band (the Soret band, corresponding to the upper singlet state) in the blue region, together with a number of satellite bands. The lower the wavelength of an absorption band, the higher the energy of the photons that are absorbed, and so the higher the energy level to which the electrons in the molecule are excited. The chlorophyll *Q<sub>y</sub>* band corresponds to excitation from the ground state to one of the rotational

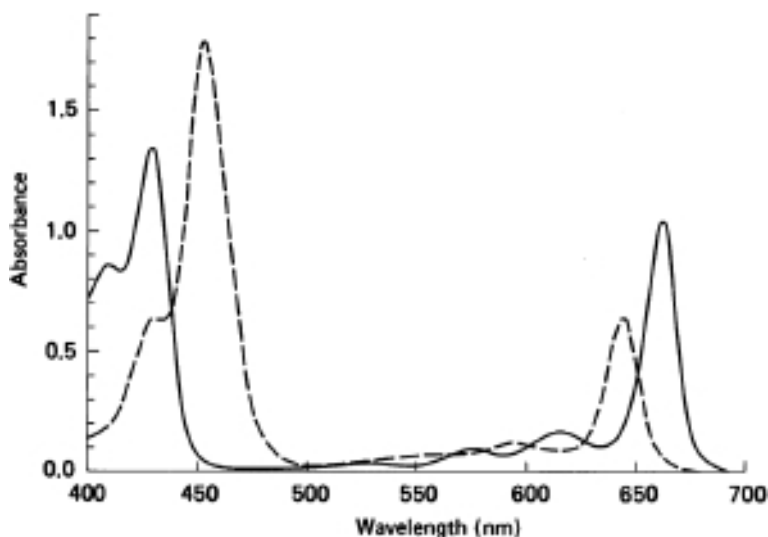


Fig. 8.8 Absorption spectra of chlorophylls *a* and *b* in diethyl ether at a concentration of  $10 \mu\text{g ml}^{-1}$  and 1 cm pathlength. Calculated from data given by French (1960). (Chlorophyll *a* —; chlorophyll *b* -----.)

sublevels in the lowest vibrational sublevel of the lower excited singlet state. The adjoining absorption band ( $Q_x$ ) is at a wavelength about 47 nm shorter than the  $Q_y$  peak, corresponding to an energy difference of about  $14 \text{ kJ mol}^{-1}$ , similar to the energy spacing between vibrational sublevels. This waveband, at  $\sim 615 \text{ nm}$ , can thus plausibly be attributed<sup>994</sup> to excitation to the first excited vibrational sublevel above the lowest sublevel (Fig. 8.9).

The Soret band corresponds to excitation of the chlorophyll *a* molecule to the upper singlet state. This is very unstable and decays to the lower excited singlet state in about  $10^{-12}$  seconds by a radiationless transition (see §3.1). The excited molecule can now revert to the ground state by emission of a photon – the phenomenon of fluorescence (Fig. 8.9). Since the energy change is about the same (give or take some slight difference in rotational energy levels) as that accompanying excitation of a molecule from the ground state to the lower excited singlet state, the main chlorophyll fluorescence peak is in the red (Fig. 8.10), but at a slightly longer wavelength than the  $Q_y$  absorption band – being centred on 666 nm, compared to 662 nm, in diethyl ether, and 671 nm compared to 665 nm in carbon tetrachloride.<sup>174a,1217a</sup> Figure 8.10 shows the fluorescence emission spectrum of chlorophyll *a* in  $\text{CCl}_4$ . There is an additional smaller

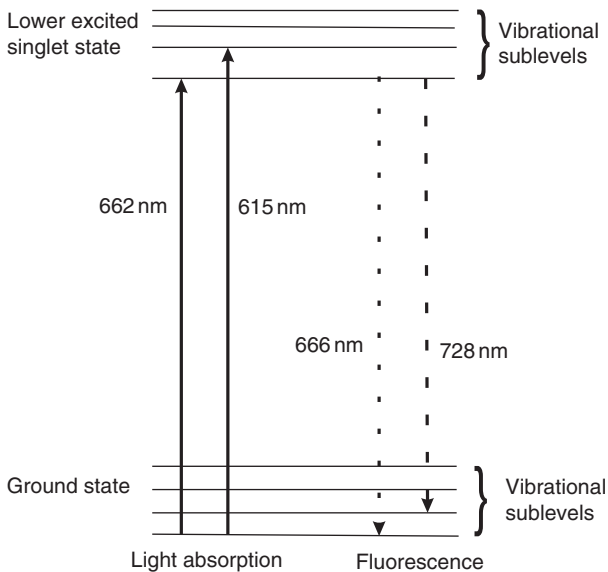


Fig. 8.9 Energy level diagram indicating the vibrational sublevels of the ground state and the lower excited singlet state of chlorophyll *a* (after Nobel, P. S. (1991). *Physicochemical and Environmental Plant Physiology*. San Diego: Academic Press.). Solid vertical lines indicate absorption of a photon by chlorophyll *a* dissolved in diethyl ether; dashed lines represent the transitions corresponding to emission of a photon in fluorescence.

peak in the emission spectrum at about 720 to 730 nm, corresponding to photons emitted as the chlorophyll *a* molecules undergo transition from the lowest vibrational sublevel of the lower excited state to the first excited vibrational sublevel of the ground state<sup>994</sup> (Fig. 8.9). The emitted photons are at longer wavelength because the energy change is somewhat smaller.

Absorption is very low, but not zero, in the middle, green, region of the spectrum, hence the green colour of these pigments. As chlorophylls *c*<sub>1</sub> and *c*<sub>2</sub> are metalloporphyrins rather than metallodihydroporphyrins, they have spectra (Fig. 8.11) in which the Soret band is more intense, and the *Q*<sub>y</sub> band less intense, than the corresponding bands in chlorophylls *a* and *b*. Also, the *Q*<sub>x</sub> band (~580 nm) in the *c* chlorophylls is comparable in intensity to the *Q*<sub>y</sub> band (~630 nm). It can be seen from Figs 8.8 and 8.11 that chlorophyll *a* absorbs only weakly between 450 and 650 nm, and that chlorophylls *b* or *c*, when present, have the effect of increasing absorption within this window, at both the long- and the short-wavelength ends.

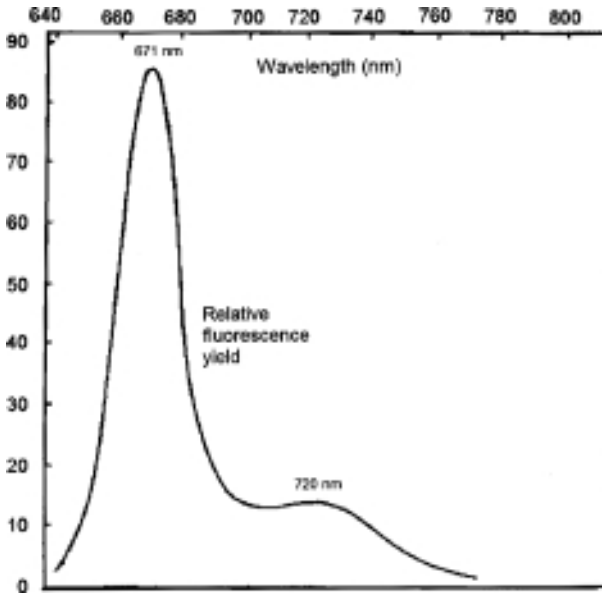


Fig. 8.10 Fluorescence emission spectrum of chlorophyll *a*, dissolved at  $10^{-6}$  M in carbon tetrachloride (redrawn from Fig. 5 in Broyde and Brody, 1967).

### The carotenoids

The carotenoids are another class of photosynthetic pigment, which extend absorption still farther into the 'window', at the short-wavelength end. Chemically they are quite distinct from the chlorophylls, being  $C_{40}$  isoprenoid compounds. There are far more known carotenoids than there are chlorophylls. The distribution of the various chloroplast carotenoids among different plant groups is shown in Table 8.2.  $\beta$ -carotene is present in all except the Cryptophyta. In higher plants and green algae, which rely mainly on chlorophylls for light harvesting, the molar ratio of carotenoid to chlorophyll ( $a + b$ ) is about 1:3. Other classes of algae, apart from those that contain biliproteins, depend to a greater extent on their carotenoids to capture light, and this is evident in the pigment composition. The molar ratio of carotenoid to chlorophyll ( $a + c$ ) is about 1:0.5 in the diatom *Phaeodactylum*,<sup>514</sup> 1:1.4 in the dinoflagellate *Gyrodinium*<sup>627</sup> and among the brown algae is about 1:2 in *Hormosira*<sup>698</sup> and 1:0.5 in *Laminaria*.<sup>16</sup> Even among the red algae, which have biliproteins, the carotenoid:chlorophyll molar ratio varies from 1:2.6 to 1:1.<sup>121</sup>

The structures of some of the most important carotenoids in higher plants and algae are shown in Fig. 8.12. Their ability to absorb visible

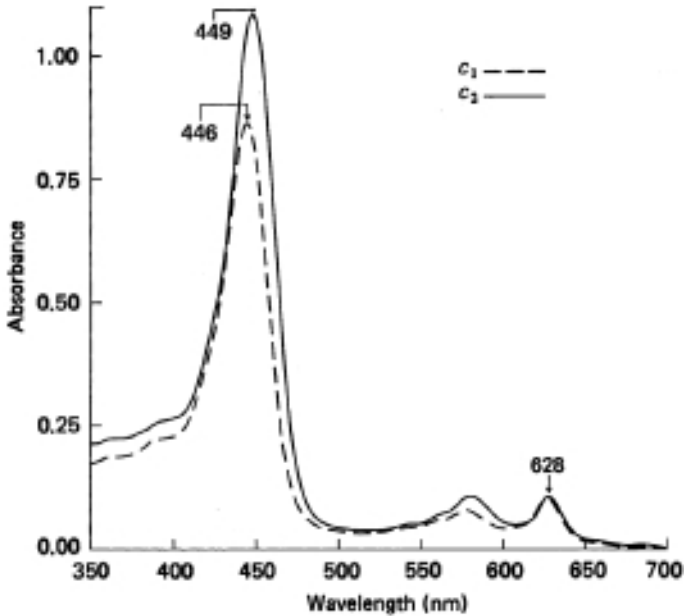


Fig. 8.11 Absorption spectra of chlorophyll *c*<sub>1</sub> and *c*<sub>2</sub> in acetone containing 2% pyridine with a pathlength of 1 cm (Jeffrey, S. W., unpublished data). (Chlorophyll *c*<sub>1</sub> ( $2.68 \mu\text{g ml}^{-1}$ ) -----; chlorophyll *c*<sub>2</sub> ( $2.74 \mu\text{g ml}^{-1}$ ) ——.)

quanta is due to their possessing systems of up to 11 conjugated double bonds. They absorb at the short-wavelength end of the visible range, which is why their characteristic colours are yellow, orange or red. The absorption spectrum of  $\beta$ -carotene is shown in Fig. 8.13.

Of particular importance in aquatic ecosystems is fucoxanthin, which, together with its various derivatives, is the principal carotenoid in the brown algae (Phaeophyta), diatoms (Bacillariophyceae), Haptophyta and Chrysophyceae, and in some dinoflagellate species. While it commonly occurs only in its unmodified form it is frequently accompanied by derivatives with hexanoyl or butanoyl residues esterified to a hydroxyl group on carbon atom 19' and/or with a keto group at position 4 of the left-hand ring.<sup>349</sup>

### Chlorophyll/carotenoid-protein complexes

Essentially all the chlorophyll and most of the carotenoid in chloroplasts occur complexed to protein. There is good reason to suppose that these

Table 8.2 Major chloroplast carotenoids in various algal classes.

Carotenoid	Chloro-phyta <sup>a</sup>	Xantho-phyceae	Eustigmato-phyceae	Bacillario-phyceae	Chryso-phyceae <sup>b</sup>	Hapto-phyta	Eugleno-phyta	Phaeo-phyta	Pyrro-phyta	Crypto-phyta	Rhodo-phyta	Cyano-phyta	Prochloro-phyta
$\alpha$ -Carotene	+	-	-	-	+	-	-	-	-	+	+	-	+ <sup>f</sup>
$\beta$ -Carotene	+	+	+	+	+	+	+	+	+	-	+	+ <sup>c</sup>	+ <sup>f</sup>
Echinenone	-	-	-	-	-	-	-	-	-	-	-	+	-
Lutein	+ <sup>c</sup>	-	-	-	-	-	-	-	-	-	+ <sup>c</sup>	-	-
Zeaxanthin	+	-	-	-	-	-	-	-	-	-	+	+	+
Neoxanthin	+	-	-	-	-	-	+	-	-	-	-	-	-
Vaucherixanthin	-	+	+ <sup>c,d</sup>	-	-	-	-	-	-	-	-	-	-
Violaxanthin	+	-	+ <sup>c</sup>	-	-	-	-	+	-	-	-	-	-
Heteroxanthin	-	+	-	-	-	-	-	-	-	-	-	-	-
Fucoxanthin	-	-	-	+ <sup>c</sup>	+ <sup>c</sup>	+	-	+ <sup>c</sup>	(+) <sup>e</sup>	-	-	-	-
Diatoxanthin	-	+	-	+	+	-	+	-	-	-	-	-	-
Diadinoxanthin	-	+ <sup>c</sup>	-	+	+	+	+ <sup>c</sup>	-	+	-	-	-	-
Peridinin	-	-	-	-	-	-	-	-	+ <sup>c</sup>	-	-	-	-
Alloxanthin	-	-	-	-	-	-	-	-	-	+ <sup>c</sup>	-	-	-
Myxoxanthophyll	-	-	-	-	-	-	-	-	-	-	-	+	-

<sup>a</sup> These data for the Chlorophyta apply to higher plants also. Sublittoral species of green algae usually possess siphonaxanthin or siphonoin instead of, or as well as, lutein.<sup>1012,1493</sup> Some species in the Prasinophyceae contain prasinaxanthin as their major carotenoid.<sup>406,1155</sup>

<sup>b</sup>  $\beta$ -carotene frequently present; Prymnesiophyceae (Haptophyceae) have similar carotenoid composition to Chrysophyceae.

<sup>c</sup> Predominant carotenoid(s) present.

<sup>d</sup> Predominantly esterified.

<sup>e</sup> In some dinoflagellates, fucoxanthin (and/or fucoxanthin derivatives such as 19'-hexanoyloxyfucoxanthin) replaces peridinin as the major carotenoid.<sup>627</sup>

<sup>f</sup> Carotene predominantly  $\alpha$  in *Prochlorococcus* and  $\beta$  in *Prochloron* and *Prochlorothrix*.<sup>187,227,467</sup> In the chlorophyll-*d* containing cyanophyte, *Acaryochloris marina*, the major carotenoids are  $\alpha$ -carotene and zeaxanthin, present in approximately equimolar amounts.<sup>919</sup>

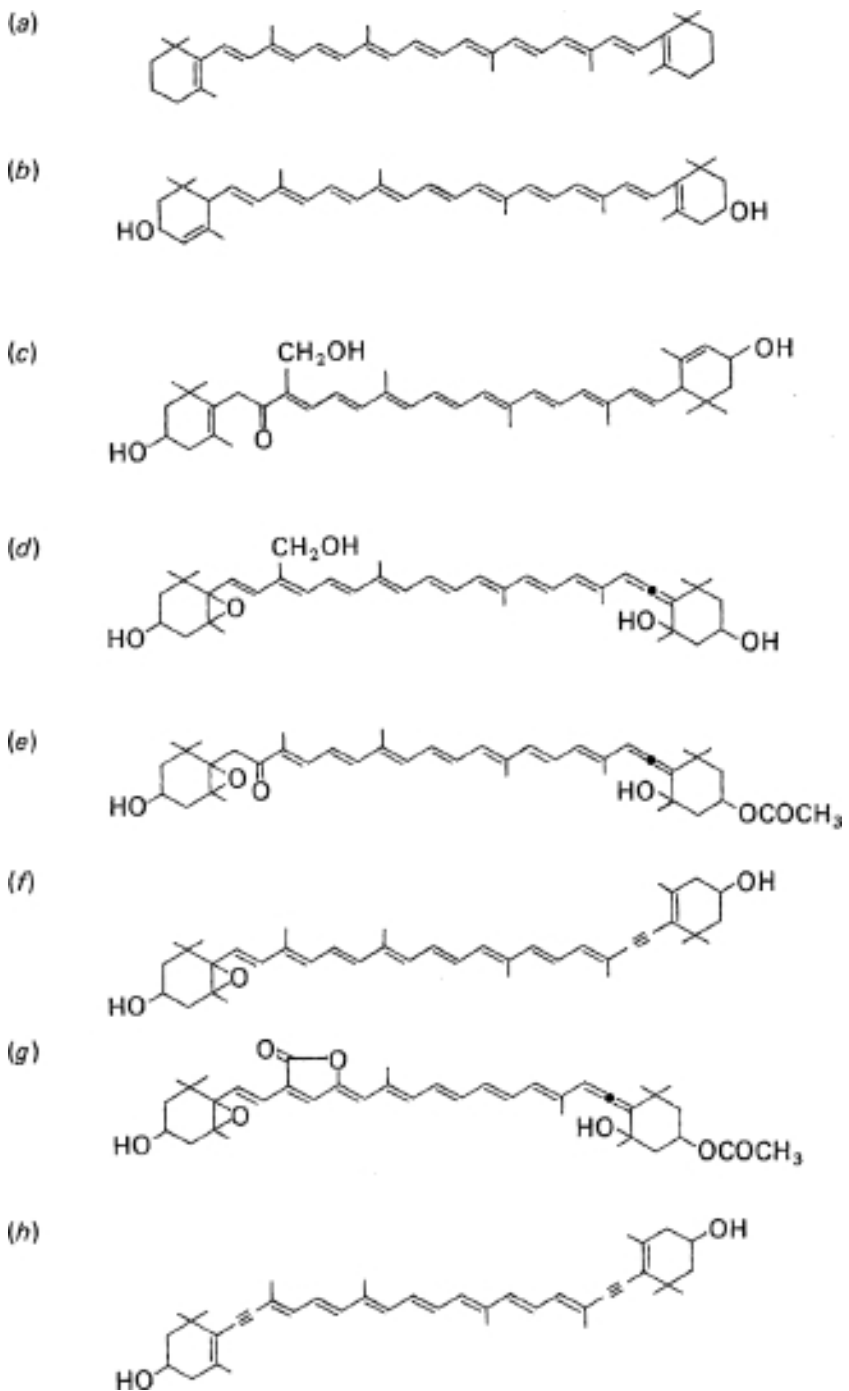


Fig. 8.12 Structures of chloroplast carotenoids. (a)  $\beta$ -carotene. (b) Lutein. (c) Siphonaxanthin. (d) Vaucherixanthin. (e) Fucoxanthin. (f) Diadinoxanthin. (g) Peridinin. (h) Alloxanthin.

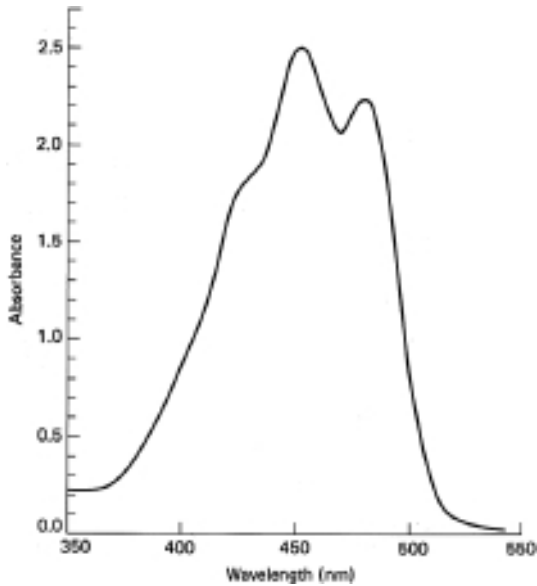


Fig. 8.13 Absorption spectrum of  $\beta$ -carotene in petrol at a concentration of  $10 \mu\text{g ml}^{-1}$  and pathlength 1 cm.

pigments can function in photosynthesis only as components of specific complexes with protein. Many different chlorophyll/carotenoid-proteins from higher plants and algae have been described in recent years. They have in most cases been liberated from the thylakoid membranes, in which they are normally embedded, with the help of detergents. It seems likely that these are variants on a relatively small number of fundamental pigment-protein types, and we shall treat them accordingly. All such photosynthetic complexes that have been examined so far contain chlorophyll *a*: some also contain chlorophyll *b* or *c*. The great majority of these complexes contain one or more carotenoids as well as chlorophyll. There are usually several chlorophyll molecules per polypeptide together with one, or several, carotenoid molecules. The reviews by Larkum and Barrett (1983), Thornber (1986), Anderson and Barrett (1986), Rowan (1989), Wilhelm (1990), Hiller, Anderson and Larkum (1991), Thornber *et al.* (1991) and Green and Durnford (1996) may be consulted for further details.

As is discussed later (§8.5), the light reactions of photosynthesis take place within two distinct pigment-protein/electron carrier systems, referred to as *photosystems I* and *II*, which contain the components required for charge separation and electron transfer, together with chlorophyll/carotenoid

pigment-proteins for collecting light. In addition, associated with each complex there are pigment-proteins that do not carry out any photoreactions, but which function simply to harvest photons from the prevailing field and transfer the absorbed energy to the reaction centres.

By analogy with radio or TV antennae, which collect energy from the long-wavelength radio/TV electromagnetic field, photosynthetic pigment molecules are often referred to as the 'antennae' of the photosystems. For each photosystem we distinguish between the internal antenna, made up of those pigment-protein molecules built into the core complex, and the external antenna composed of the light-harvesting pigment-proteins that are more loosely associated with the complex.

Core complex I consists of two 84 kilodalton (kDa) hydrophobic proteins, which, in addition to incorporating P<sub>700</sub> and the other electron transfer elements of photosystem I (see below), contain, as its internal antenna, 75 to 100 molecules of chlorophyll *a* and 12 to 15 molecules of  $\beta$ -carotene, these pigment molecules being distributed between the two proteins. While the core complex I does itself absorb light (in barley chloroplasts, for example, it contains about 20% of the total chlorophyll), it nevertheless has associated with it a light-harvesting pigment-protein complex to supply it with additional energy. This is referred to as light-harvesting complex I (LHC I). In higher plants it contains chlorophylls *a* and *b* (*a*:*b* ~3.5) and xanthophylls (mainly lutein), bound to at least four protein subunits (24, 21, 17 and 11 kDa): in barley chloroplasts it accounts for about 18% of the total chlorophyll. The green flagellate *Chlamydomonas reinhardtii* also has an LHC I, rather similar to the higher plant complex.<sup>1476</sup>

The siphonalean green alga, *Codium*, has an LHC I, containing chlorophyll *a* and *b*, in which siphonaxanthin is the main carotenoid.<sup>231</sup> In the unicellular red alga, *Porphyridium cruentum*, an LHC I has been found containing chlorophyll *a* and zeaxanthin.<sup>1475</sup> The LHC I from the xanthophyceean alga, *Pleurochloris meiringensis*, was found to contain, in addition to chlorophyll *a*, significant amounts of all the accessory pigments (chlorophyll *c*, diadinoxanthin, vaucherixanthin ester, heteroxanthin and diatoxanthin) that are present in this organism.<sup>178</sup> Excitation spectra of fluorescence indicated that the accessory pigments were transferring energy to chlorophyll *a* in the isolated LHC I. Table 8.3 summarizes the rather limited compositional data available on the photosystem I external antenna pigment-proteins of algae.

Algae and higher plants also contain another essential chlorophyll *a*/ $\beta$ -carotene protein complex, core complex II, which functions in photosystem

Table 8.3 *Algal photosystem I light-harvesting pigment-proteins (LHC Is).*

Number of pigment molecules per 100 molecules of Chlorophyll <sup>a</sup>						
Algal group	Chl <i>a</i>	Chl <i>b</i>	Chl <i>c</i>	Carotenoid	Apoprotein M. Wt. (kDa)	Reference
<b><i>Chlorophyta</i></b>						
Chlorophyceae						
<i>Chlamydomonas</i>	100	~20	–	Xanthophyll + carotene, 6–8	20–31 (10 polypeptides)	76
Bryopsidophyceae						
<i>Codium</i>	100	~60	–	Siphonaxanthin	24.5, 23, 22.5, 20, 19	231
Prasinophyceae						
<i>Mantoniella squamata</i> <sup>a</sup>	100	113	17	Prasinoxanthin 30 Violaxanthin 7 Neoxanthin 15	20, 22	1469,1123
<b><i>Heterokontophyta</i></b>						
Xanthophyceae						
<i>Pleurochloris meiringensis</i>	100	–	3	Diadinoxanthin 18 Heteroxanthin 6 Diatoxanthin 3 Vaucherixanthin ester 9	20.7, 16.7	178
<b><i>Rhodophyta</i></b>						
<i>Porphyridium cruentum</i>	100	–	–	Lutein 75	18–23.5	1475

M. Wt. = molecular weight

<sup>a</sup> This pigment-protein serves as the external antenna for both photosystems in *Mantoniella*.<sup>1186</sup>

II, the absorbed light energy being transferred to the reaction centre known as P<sub>680</sub>, which is part of the total complex. It is estimated that there are about 40 chlorophyll *a* molecules and one P<sub>680</sub> reaction centre for each photosystem II unit. Most of the chlorophyll and  $\beta$ -carotene is present in two non-identical but similarly sized pigment-proteins, CPa-1 and CPa-2, also known as CP47 and CP43. CPa-1 is of molecular weight ~52 kDa and contains 20 to 22 molecules of chlorophyll *a* and 2 to 4 of  $\beta$ -carotene; CPa-2 is ~48 kDa and contains 20 chlorophyll *a* and 5  $\beta$ -carotene molecules.<sup>508</sup> These pigment-proteins function as the internal antenna of photosystem II and together they account (in barley) for about 10% of the total thylakoid chlorophyll. They are closely associated with the reaction centre part of the complex, which consists of a pair of hydrophobic proteins, D1 and D2,

containing four to six chlorophyll *a* and one to two  $\beta$ -carotene molecules, together with two phaeophytin *a*, two plastoquinone and one non-haem iron. About 1% of the total thylakoid chlorophyll is contained in these reaction centres. Cytochrome *b*<sub>559</sub> is also part of the complex.

Like core complex I, core complex II, as well as absorbing light directly, is supplied with additional energy by an associated light-harvesting pigment-protein complex, which is referred to as light-harvesting complex II (LHC II). In higher plants LHC II is made up of at least four individual pigment proteins – LHC IIa, b, c and d – all containing chlorophylls *a* and *b*, and the three chloroplast xanthophylls, lutein, violaxanthin and neoxanthin. Light-harvesting complex IIb is the major component containing as it does 40 to 45% of the total chloroplast chlorophyll: the other three LHC II pigment-proteins between them account for 10 to 15% of the total chlorophyll. The aggregate LHC II has a chlorophyll *a*:*b* ratio of about 1.4; for LHC IIb the ratio is about 1.33. Light-harvesting complex IIb preparations contain three slightly different apoproteins – 28, 27 and 25 kDa – possibly resulting from post-translational modification of a single polypeptide. Each apoprotein molecule is thought to bind about 15 chlorophyll molecules (eight *a*, six to seven *b*), and about three xanthophyll molecules.

Among the various classes of algae, a large number of different light-harvesting pigment-proteins has been found in recent years. Most of these are of the LHC II type, feeding their energy to photosystem II. They all contain chlorophyll *a* together with, in most cases, whatever accessory chlorophyll – *b* or *c* – is present in that particular alga. In addition they contain the major light-harvesting xanthophyll carotenoid(s) characteristic of that algal class. While they all have peaks in the red region of the spectrum, due to chlorophyll(s), their main light absorption, due to a combination of chlorophyll Soret and carotenoid bands, is in the 400 to 550 nm, blue-green waveband. Table 8.4 lists a selection of these putative LHC II algal proteins, with their pigment and polypeptide composition. In *Mantoniella squamata*, a member of the primitive green algal class, Prasinophyceae, it appears that a single pigment-protein serves as the external antenna for both photosystems.<sup>1186</sup>

Katoh and Ehara (1990) have presented evidence that in vivo these light-harvesting proteins are organized into supramolecular assemblies. Using the mild detergent, octyl sucrose, they were able to isolate, from chloroplasts of the brown algae *Petalonia fascia* and *Dictyota dichotoma*, pigment-protein complexes of molecular weight about 700 kDa, containing in each complex about 128 molecules of chlorophyll *a*, 27 of

Table 8.4 Algal light-harvesting pigment-proteins (presumptive LHC II<sub>s</sub>).

Algal group	Chl <i>a</i>	Chl <i>b</i>	Chl <i>c</i>	Carotenoid	Apoprotein M. Wt. (kDa)	Reference
<b>Chlorophyta</b>						
Chlorophyceae						
<i>Chlamydomonas reinhardtii</i>	100	106	–	Lutein 12	29, 25	673
<i>Chlorella fusca</i>	100	88	–	Violaxanthin 11 Neoxanthin 6 $\beta$ -carotene 5 Lutein 12 Violaxanthin 6 Neoxanthin 6 Trihydroxy- $\alpha$ - carotene 12	30.4, 28	1469
Bryopsidophyceae						
<i>Bryopsis</i>	100	116	–	Siphonaxanthin 51 Siphonein 15 Neoxanthin 28		974
<i>Codium</i>	100	58			25–19	231
Prasinophyceae						
<i>Mantoniella squamata</i> <sup>a</sup>	100	113	17	Prasinoxanthin 30	20, 22	1469, 1123
				Violaxanthin 7 Neoxanthin 15		
<b>Euglenophyta</b>						
<i>Euglena gracilis</i>	100	49	–	Diadinoxanthin 31 Neoxanthin 9 $\beta$ -carotene 1	26.5, 28, 26	272
<b>Heterokontophyta</b>						
Xanthophyceae						
<i>Pleurochloris meiringensis</i>	100	–	6	Diadinoxanthin 16	21.9	178
				Heteroxanthin 9 Diatoxanthin 5 Vaucherixanthin ester 13		
Eustigmatophyceae						
<i>Nannochloropsis</i>	100	–	–	Violaxanthin 26–44 Vaucherixanthin 22–25 Neoxanthin 2 $\beta$ -carotene 4	26	173, 1323
Bacillariophyceae						
<i>Phaeodactylum tricornutum</i>	100	–	40	Fucoxanthin 192	18	412

Table 8.4 (cont.)

Algal group	Chl <i>a</i>	Chl <i>b</i>	Chl <i>c</i>	Carotenoid	Apoprotein M. Wt. (kDa)	Reference
<b>Haptophyta</b>						
Prymnesiophyceae						
<i>Pavlova lutherii</i>	100	–	21	Fucoxanthin	21	558
<b>Pyrrophyta</b>						
<b>(Dinophyta)</b>						
<i>Amphidinium carterae</i> <sup>b</sup>	100	–	–	Peridinin 450	32	548
<i>Amphidinium carterae</i>	100	–	57	Peridinin 171	19	559
				Diadinoxanthin 29		
<b>Phaeophyta</b>						
<i>Fucus serratus</i>	100	–	16	Fucoxanthin 70 (predominant)	21.5, 23	206, 207
<b>Cryptophyta</b>						
<i>Chroomonas</i>	100	–	65	Unidentified (Alloxanthin?)	20, 24	610
<b>Prochlorophyta</b>						
<i>Prochloron</i>	100	42	–		34	557
<i>Prochlorothrix</i>	100	25	–		30–33	185

M. Wt. = molecular weight

<sup>a</sup> This pigment-protein serves as the external antenna for both photosystems in *Mantoniella*.<sup>1186,1192</sup>

<sup>b</sup> This is the water-soluble peridinin–chlorophyll *a* complex.

chlorophyll *c*, 69 of fucoxanthin and 8 of violaxanthin. Electron microscopy showed that each complex was discoidal in shape, being 11.2 nm in diameter and 10.2 nm in height, with a small pit at the centre of the disc.

In photosynthetic pigment-proteins the bonding between the pigments and the protein, although highly specific, is not covalent. The molecular structure of the major chlorophyll *a/b* light-harvesting protein of higher plants (LHC II) has been determined to 3.4 Å resolution by Kühlbrandt, Wang and Kuniyoshi (1994) using electron crystallography, and to 2.7 Å resolution by Liu *et al.* (2004) using X-ray crystallography. The chlorophylls (8 chlorophyll *a* and 6 chlorophyll *b* per protein monomer) are attached to the polypeptide by coordination of the central magnesium atom to polar amino acid side chains (histidine, asparagine, glutamine), or to main-chain carbonyls in the hydrophobic interior of the complex. In addition, there must be hydrogen bonding between oxygen-containing ring substituents in the chlorophyll molecules, and appropriate groups in

the polypeptide chains, as well as hydrophobic associations between the phytol chains and the non-polar regions of the protein. Of the 232 amino acid residues of the polypeptide, 36% form transmembrane helices, the remainder being exposed on the inner (luminal) and outer (stromal) membrane surfaces.

There are four carotenoid molecules per LHC II monomer. The major carotenoid is the xanthophyll, lutein, of which there are two molecules located within the monomer. There is also a neoxanthin molecule. In the case of the carotenoids there are hydrophobic associations between the central hydrocarbon chain region of the carotenoid and non-polar amino acid side chains of the polypeptide. The polar groups at each end of the carotenoid molecule presumably participate in hydrogen bonding with polar groups in the polypeptide. In the case of  $\beta$ -carotene, which has no polar groups, all interactions with the protein must be hydrophobic. The lutein molecules are closely associated with chlorophyll *a* molecules, to which they can transfer energy, and the neoxanthin is similarly associated with chlorophyll *b* molecules to which it can transfer its energy. The fourth carotenoid site is at the monomer–monomer interface and is believed to be where one or other of the intermediates of the xanthophyll cycle – violaxanthin, antheraxanthin, zeaxanthin (see §10.2) – is located.

A very important consequence of the interaction between the pigments and the protein is that the absorption spectra of the former are modified. The absorption peaks are, to varying degrees, shifted to longer wavelength, with, in the case of the chlorophylls, some increase in complexity as well. Chlorophyll *a* in living cells or chloroplasts has a rather broad absorption peak in the red at about 676 nm, a shift of 9 to 15 nm relative to its position in organic solvents (usually 661 to 667 nm). Computer deconvolution of the absorption curve indicates that the peak is made up of four major forms of chlorophyll *a* with peaks at 662, 670, 677 and 684 nm, together with two minor forms at 692 and 703 nm.<sup>411</sup> Isolated chlorophyll–protein complexes show similar complexity: this may possibly be due to exciton interaction between the chlorophyll molecules within each pigment–protein complex, leading to splitting of the absorption bands and/or to the presence of different types of chlorophyll–protein binding.

In the case of some chloroplast carotenoids, such as  $\beta$ -carotene, the absorption peaks *in vivo* are shifted, relative to their positions in organic solvents, to longer wavelengths to about the same extent as the chlorophyll peak. However, certain major light-harvesting carotenoids in the algae – fucoxanthin, peridinin, siphonaxanthin – have *in vivo* spectra

shifted by about 40 nm to longer wavelengths relative to their spectra in organic solvents. This has the effect of substantially increasing absorption in the green window between the chlorophyll blue and red peaks. The diatoms and the Phaeophyta, for example, are brown in colour rather than green precisely because of their higher absorption in the green waveband. The shift in absorption to longer wavelengths is a consequence of the specific association between the carotenoid and the protein: if this association is disrupted by, say, heat denaturation, then the carotenoid spectrum reverts to the *in vitro* type. When a piece of brown-algal thallus is dipped in hot water it rapidly turns green. Quite low temperatures will suffice to bring about the change. When chloroplasts, or an isolated pigment-protein (chlorophylls *a* and *c*, fucoxanthin,  $\beta$ -carotene) from the brown alga, *Hormosira sp.*, were subjected to a progressive temperature rise of  $1^{\circ}\text{C min}^{-1}$ , dissociation of the fucoxanthin-protein link (measured in terms of decrease in absorbance at 535 nm) was detectable at  $35^{\circ}\text{C}$  and complete at  $60$  to  $65^{\circ}\text{C}$ , 50% dissociation being achieved at  $44$  to  $48^{\circ}\text{C}$ .<sup>698</sup> One possibility is that the binding between protein and carotenoid is such that the polyene chain of the latter is twisted: apparently this could account for the shift of the absorption band to longer wavelengths.<sup>179</sup>

Fucoxanthin and peridinin are the dominant carotenoids in those algae that contain them, and show up in the *in vivo* spectra as a major shoulder in the 500 to 560 nm region (see Fig. 9.4*b*). Siphonaxanthin does not to the same extent dominate the carotenoid make-up of those algae that possess it, and shows up as a subsidiary peak at about 540 nm in the *in vivo* spectrum.<sup>1493</sup>

### Biliproteins

The biliprotein chloroplast pigments are found only in certain algae: the Rhodophyta, Cryptophyta and Cyanophyta. They are either red (phycoerythrins, phycoerythrocyanin) or blue (phycocyanins, allophycocyanins) in colour. They have been reviewed by Bogorad (1975), Gantt (1975, 1977), O'Carra and O'h Eocha (1976), Glazer (1981, 1985), MacColl and Guard-Friar (1987), Rowan (1989) and Mimuro and Kikuchi (2003).

The biliproteins of the red and blue-green algae are closely related and we shall consider them together. They are divided into four classes on the basis of the position of their absorption bands: these are, in order of increasing wavelength, the phycoerythrins, the phycoerythrocyanins, the

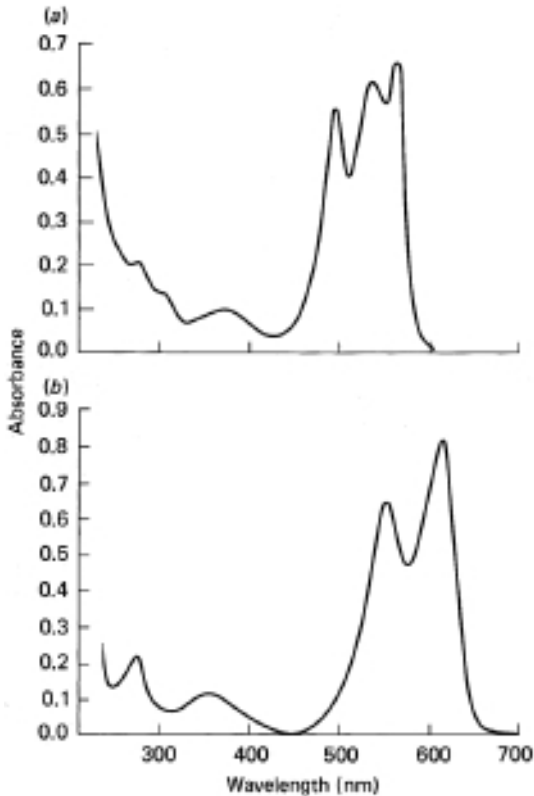


Fig. 8.14 Absorption spectra of biliproteins (after O'h Eocha, 1965). (a) R-phycoerythrin from *Ceramium rubrum*. (b) R-phycoerythrin from *Porphyra laciniata*.

phycoerythrin and the allophycoerythrin. The position of the main absorption peaks are listed in Table 8.4, and absorption spectra of a red-algal phycoerythrin and phycoerythrin are shown in Fig. 8.14.

The general principle governing the distribution of these pigments appears to be that allophycoerythrin and one or other of the phycoerythrin occur in all red and blue-green algal species: a phycoerythrin (or phycoerythrocyanin in some blue-green algae) may or may not, in addition, be present. Phycoerythrin is rarely absent in the red algae but is frequently absent in the blue-green algae. The typical situation is that in the red algae, phycoerythrin constitutes most of the biliprotein present, whereas in the blue-green algae, phycoerythrin or (less commonly) phycoerythrocyanin is the major component: allophycoerythrin is nearly always a minor component.

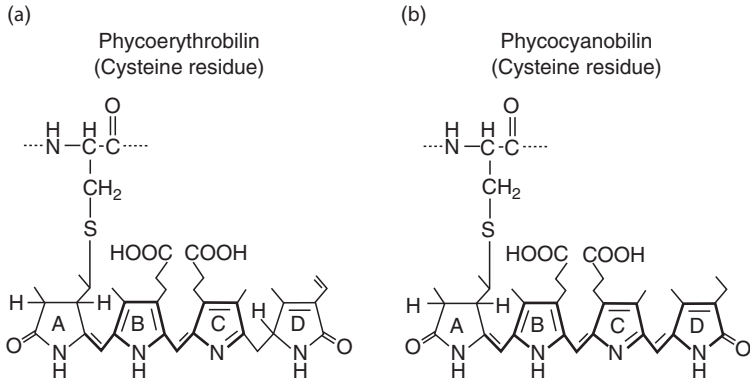


Fig. 8.15 Structures, and probable mode of binding to protein, of the phycobilin chromophores of algal biliproteins.<sup>458,689</sup> The systems of conjugated double bonds, upon which the spectral properties of the chromophores depend, are emphasized by heavy lines. Phycourobilin is likely to have  $\text{CH}_2$  rather than  $\text{CH}$  groups joining rings A to B and C to D. Linkage to protein cysteine can also occur through the vinyl/ethyl group on ring D.<sup>458</sup>

The chromophores to which biliproteins owe their colour are open-chain tetrapyrrole compounds known as phycobilins. There are four main chromophores – phycocyanobilin (blue), phycoerythrobilin (red), phycourobilin (yellow) and phycoviolobilin (purple) – also known as cryptoviolin. Unlike chlorophylls and carotenoids, they are covalently bound to their proteins. Their structures and modes of linkage to the apoproteins are shown in Fig. 8.15.

All the algal biliproteins contain equimolar amounts of two kinds of subunit, referred to as  $\alpha$  and  $\beta$ : some of the phycoerythrins contain in addition much lesser amounts (one molecule for every six of  $\alpha$  or  $\beta$ ) of a third class of subunit,  $\gamma$ . The  $\alpha$  and  $\beta$  subunits have molecular weights of about 17 to 22 kDa but the  $\gamma$  subunit may be larger. Each  $\alpha$  or  $\beta$  subunit in a biliprotein has at least one phycobilin chromophore attached. The  $\alpha$  subunit can have one or two chromophores; the  $\beta$  subunit has one, two or three; and the  $\gamma$  subunit has four. The distribution of chromophores among the subunits in the different proteins is shown in Table 8.5. This distribution may not be immutable. In phycoerythrin from the red alga *Callithamnion roseum* it seems that the proportion of phycoerythrobilin to phycourobilin varies with light intensity during growth:<sup>1495</sup> it is possible that at some sites within the protein, either of these two chromophores may be attached.

Biliproteins occur as aggregates of the basic  $\alpha\beta$  structure. In the isolated, soluble state, various sizes are found of which the most common

Table 8.5 *Spectroscopic properties of the different biliproteins and the distribution of phycobilin chromophores among their subunits.*<sup>457,459,1002,1008,17,1018,1442,458,841,842,844</sup>

Biliprotein	Algal type <sup>a</sup>	Absorption maxima in photosynthetic range <sup>b</sup> (nm)	$\alpha$ -subunit <sup>c</sup>	$\beta$ -subunit <sup>c</sup>	$\gamma$ -subunit <sup>c</sup>
<i>Red and blue-green algae</i>					
Allophycocyanin	R, B	650, (620)	1 PCB	1 PCB	—
Allophycocyanin-B	R, B	671, 618	1 PCB	1 PCB	—
C-Phycocyanin	R, B	620	1 PCB	2 PCB	—
R-Phycocyanin	R	618, 553	1 PCB	1 PCB, 1 PEB	—
Phycocerythrocyanin	B	(590), 568	1 CV	2 PCB	—
C-Phycocerythrin	B	562–565	2 PEB	3 PEB	—
CU-Phycocerythrin	B	490–500, 545–560	2 PEB	3 PEB, 1 PUB	—
b-Phycocerythrin	R	(563), 545	2 PEB	4 PEB	—
B-Phycocerythrin	R	(565), 546, (498)	2 PEB	3 PEB	2 PEB, 2 PUB
R-Phycocerythrin	R	568, 540, 598	2 PEB	2 PEB, 1 PUB	1 PEB, 3 PUB
<i>Cryptophytes</i>					
Phycocyanin-615		615, 585	1 PCB	2 PCB, 1 CV	—
Phycocyanin-630		630, 585	n.d.	n.d.	—
Phycocyanin-645		645, (620), 585	1 U	2 PCB, 1 CV	—
Phycocerythrin-544		(565), 544	2 PEB, 2 CV	PEB	—
Phycocerythrin-555		555	PEB	PEB	—
Phycocerythrin-568		568	PEB	PEB	—

<sup>a</sup> R, red algae; B, blue-green algae.

<sup>b</sup> Minor maxima or shoulders are in brackets.

<sup>c</sup> PCB, phycocyanobilin; PEB, phycocerythrobilin; PUB, phycourobilin; CV, cryptoviolin; U, unknown phycobilin chromophore, distinct from the previous four, with peak at 697 nm. The absence of a number means that the number of chromophores is unknown.

n.d., no data.

appear to be the hexamer  $\alpha_6\beta_6$  and the trimer  $\alpha_3\beta_3$ . Those phycocerythrins that have a  $\gamma$  subunit are likely to occur as  $\alpha_6\beta_6\gamma$  aggregates in the isolated state. In vivo, biliproteins occur as much larger aggregates, the phycobilisomes, particles of diameter 30 to 40 nm attached to the outer surface of the thylakoids (Fig. 8.2). These are ordered, specific structures

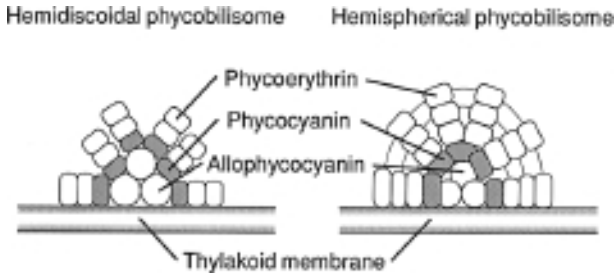


Fig. 8.16 Schematic representation of phycobilisome structure (after Glazer, 1985; Gantt, 1986; Glazer and Melis, 1987).

rather than random aggregates, and it seems likely that the three or so different biliproteins present in the alga are all present in each phycobilisome, together with small amounts of some colourless proteins. Allophycocyanin, which as we shall see later transfers the energy harvested by the phycobilisome to chlorophyll, is believed to be located at the base of the particle, adjoining the membrane: the other, more plentiful proteins form a shell around the allophycocyanin, with the phycocyanin being next to the allophycocyanin and the phycoerythrin or phycoerythrocyanin forming the periphery of the particle. Electron microscope and biochemical studies have given rise to a model of phycobilisome structure along the lines of that shown schematically in Fig. 8.16. In the chlorophyll *d*-containing prokaryote, *Acaryochloris marina*, the biliproteins (phycocyanin and allophycocyanin) exist as rod-shaped structures located on the cytoplasmic side of the thylakoid membrane.<sup>594</sup>

Turning to the Cryptophyta we find some similarities to, as well as marked differences from, the situation in the Rhodophyta and Cyanophyta. The cryptophyten pigments are either red or blue and accordingly are classified either as phycoerythrins or phycocyanins. Each cryptophyte species appears to contain only one biliprotein. No allophycocyanin-like pigments have yet been found in this group. The main absorption peaks are in the 612 to 645 nm range in the case of the phycocyanins, and the 544 to 568 nm range in the case of the phycoerythrins. The chromophores so far detected in these proteins are phycoerythrobin, phycocyanobilin, cryptoviolin (phycoviolobilin) and an unknown phycobilin with an absorption peak (in acid urea) at 697 nm.<sup>580</sup>

The cryptophyte biliproteins appear to be organized on the same  $\alpha\beta$  subunit principle as the red and blue-green algal proteins: in the isolated state they exist predominantly as  $\alpha_2\beta_2$  dimers. The subunits, at 10 and 17.5 kDa, respectively appear, however, to be smaller than those in the

other algae, and there are two types of  $\alpha$  subunit so that the dimer composition is better represented as  $\alpha\alpha'\beta_2$ .<sup>513</sup> Where they differ most strikingly from the corresponding proteins in the other algae is their location in the photosynthetic apparatus: instead of being present as phycobilisomes on the surface of the thylakoids, the cryptophyte biliproteins occur as a dense granular matrix filling the interior of the thylakoid (Fig. 8.3).

## 8.4 Reaction centres and energy transfer

The crucial step within photosystems I and II is the use of the absorbed light energy to transfer an electron from a donor molecule to an acceptor molecule. The particular donor and acceptor molecules are different in the two photosystems. The site in a photosystem at which this event occurs is known as the *reaction centre*. The central role of using the excitation energy to extract an electron from one molecule and transfer it to another is, in each photosystem, carried out by a special form of chlorophyll *a* complexed with a specific protein. When the reaction centre chlorophyll receives excitation energy, it is raised to an excited electronic state. In this excited state it can reduce (transfer an electron to) the acceptor molecule. The oxidized chlorophyll then withdraws an electron from the donor molecule, and so returns to its original state. The loss of an electron is accompanied by a fall in the absorption spectrum of the reaction centre chlorophyll, in the region of its red peak. The spectral change is maximal at about 700 nm in photosystem I and at about 680 nm in photosystem II: accordingly, the specialized forms of chlorophyll are referred to as P<sub>700</sub> and P<sub>680</sub>, respectively. Since the reaction centre chlorophylls constitute only a very small proportion of the total chlorophyll *a* – one P<sub>700</sub> and one P<sub>680</sub> per 500 total chlorophyll molecules in green plants – their spectral changes are insignificant with respect to the total absorption spectrum of the system.

Excitation of reaction centre chlorophyll can be brought about by direct absorption of a photon. Since P<sub>700</sub> and P<sub>680</sub> constitute a tiny proportion of the total pigment, however, this does not take place very often. In fact, virtually all the excitation energy received by the reaction centre is energy initially captured by the vastly more numerous light-harvesting or antenna pigment molecules of that photosystem and transferred to the reaction centre. The mechanism by which this takes place is known as inductive resonance transfer, first postulated by the theoretical chemist T. Förster in 1947.

Absorption of a photon by one molecule is followed by vibrational energy dissipation, bringing the excited electron to its lowest excited state. This can be in a state of resonance with one of the upper vibrational levels of the excited state of another molecule (not, initially, in an excited state). The energy is transferred from the first molecule to the second, i.e. the first molecule reverts to the ground state and the second molecule is raised to an excited electronic state. For efficient transfer the fluorescence emission peak of the donating molecule must overlap the absorption spectrum of the receiving molecule. Since the fluorescence emission spectrum of any molecule is a mirror image on the long-wavelength side of the absorption spectrum, with the peak shifted to longer wavelength, it follows that for efficient energy transfer the absorption peak of the donating molecule should be at a shorter wavelength than that of the receiving molecule. In addition the molecules must not be too far apart: efficient transfer can take place at distances up to about 5 nm.

The light-harvesting, as opposed to reaction centre, pigment molecules are made up of the great majority of the chlorophyll *a* molecules, chlorophylls *b*, *c*<sub>1</sub> (or *c*<sub>3</sub>) and *c*<sub>2</sub>, the various carotenoids and the biliproteins. All these (except carotenoids) fluoresce actively *in vitro* and so the assumption that energy transfer among them takes place by inductive resonance presents no problem. Carotenoids, on the other hand, show virtually no fluorescence *in vitro*, and the view is sometimes expressed that energy transfer from carotenoids to other pigments must involve some other mechanism. It has nevertheless been shown that carotenoid fluorescence does in fact occur, but at very low yield:  $6 \times 10^{-5}$  in  $\beta$ -carotene<sup>453a</sup> and  $5 \times 10^{-5}$  in fucoxanthin.<sup>680a</sup> Absorption of a photon by a carotenoid molecule raises its energy level to the first excited singlet state, indicated by  $1B_u$ . This is followed by a fast non-radiative relaxation to an optically forbidden singlet state,  $2A_g$ , at a lower energy level ('optically forbidden' meaning that the molecule cannot arrive at this state directly by absorption of a photon). In the case of  $\beta$ -carotene, Gillbro and Cogdell (1989) believe that the fluorescence emission is from the  $1B_u$  excited singlet state, and that its very short lifetime excludes the Förster mechanism as a candidate for efficient energy transfer from carotenoids in the light-harvesting antenna. As a possible alternative they suggest a short-range electron exchange interaction. In the case of fucoxanthin, Katoh *et al.* (1991) present evidence that the fluorescence emission originates from the  $2A_g$  state, and suggest that energy transfer takes place by the Förster mechanism to the  $Q_y$  singlet state (corresponding to the  $\sim 670$  nm absorption band) of chlorophyll *a*.

In higher plants and green algae, energy absorbed by chlorophyll *b* is transferred to chlorophyll *a* with about 100% efficiency: energy absorbed by carotenoids is transferred (with lower efficiency), probably first to chlorophyll *b* and then to chlorophyll *a*. In all those algae containing chlorophyll *c*, the energy absorbed by this pigment is transferred efficiently to chlorophyll *a*. In those algae that contain major light-harvesting carotenoids – fucoxanthin, peridinin or siphonaxanthin – with substantial absorption in the 500 to 560 nm region, there is efficient energy transfer directly from the carotenoid to chlorophyll *a*. In red and blue-green algae, the sequence of transfer, 80 to 90% efficient overall, is phycoerythrin (or phycoerythrocyanin) → phycocyanin → allophycocyanin → chlorophyll *a*. In cryptophytes, which usually have only one biliprotein, this sequence is not possible: direct energy transfer from the biliprotein to chlorophyll *a* may occur, with quite high efficiency from phycocyanin, but lower efficiency from phycoerythrin.

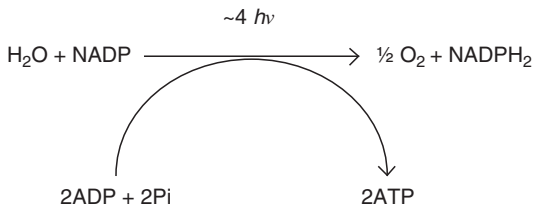
In every case (with the exception of chlorophyll *d*-containing organisms – see below), no matter which pigment first captures the light, the absorbed energy always ends up in chlorophyll *a*. This is to be expected since chlorophyll *a* has its absorption peak at a longer wavelength than any of the other pigments and, as noted earlier, energy migration by this mechanism is in the direction of the molecules absorbing at the greatest wavelength. Among the bulk chlorophyll *a*-protein complexes, the excitation energy moves at random until it reaches a reaction centre, where it is immediately trapped and used for electron transfer.

In the unusual cyanophyte, *Acaryochloris marina*, the major light-absorbing pigment is chlorophyll *d*, with an in vivo  $Q_y$  absorption band at about 715 nm,<sup>920,908</sup> compared to ~676 nm for chlorophyll *a*. The photosystem I reaction centre chlorophyll in this organism appears to be a form of chlorophyll *d*: the spectral change when it is excited and loses an electron is maximal at about 740 nm, and so it is referred to as P<sub>740</sub>.<sup>595</sup> *Acaryochloris marina* does contain a small amount of chlorophyll *a* – about 3% of the chlorophyll *d* content – and there is evidence that the photosystem II reaction centre chlorophyll in this organism is in fact chlorophyll *a*, and that ‘uphill’ transfer of energy from chlorophyll *d* to chlorophyll *a* takes place.<sup>907,908</sup> The biliproteins in *A. marina* provide energy only to photosystem II.<sup>594</sup>

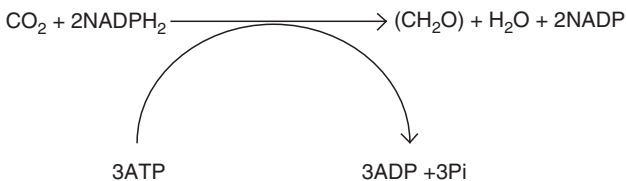
## 8.5 The overall photosynthetic process

The photosynthetic process can be divided into two parts, the light reactions and the dark reactions. In the light reactions, which take place in the

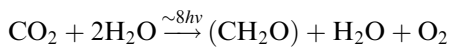
thylakoid membrane system, hydrogen is withdrawn from water and passed along a series of hydrogen carriers to NADP, so that NADPH<sub>2</sub> is formed and oxygen is liberated. Associated with this hydrogen (or electron) transport there is a conversion of ADP (adenosine diphosphate) and inorganic phosphate to ATP (adenosine triphosphate), probably two (or, on average, some fractional number between one and two) ATP molecules being formed for every two electrons transferred or molecule of NADP reduced. These chemical changes are associated with a considerable increase in free energy: this is made possible by the light energy absorbed by the chloroplast pigments. Thus we may summarize the light reactions by the equation



In the dark reactions, which take place in the stroma of the chloroplast, the NADPH<sub>2</sub> produced in the light reactions is used to reduce CO<sub>2</sub> to the level of carbohydrate. This too is associated with an increase in free energy, the energy being supplied by the concomitant breakdown of ATP produced in the light reactions. The dark reactions can be summarized by the equation



Thus, the overall photosynthetic process can be represented by



### The light reactions

It is now generally believed that there are two photochemical reactions, occurring in series in photosynthesis. The subject is comprehensively reviewed in the multi-author work, edited by Staehelin and Arntzen

(1986); see also Mathis and Paillotin (1981), Parson (1991), Chitnis (2001), Nobel (2005) and Nelson and Yocum (2006). Light reaction 1 is associated with the reduction of NADP; light reaction 2 brings about the liberation of oxygen from water. Each of the photoreactions takes place in a reaction centre in association with specialized light-harvesting pigment-proteins and electron transfer agents. The set of specific functional components associated with light reaction 1 is referred to as *photosystem I*; the set associated with light reaction 2 is referred to as *photosystem II*. The functional unit consisting of a single photosystem I and a single photosystem II working together, plus a set of light-harvesting pigment-proteins, is commonly referred to as a *photosynthetic unit*.

Each photosystem has a chlorophyll *a*/carotenoid-protein, which both harvests light and is intimately associated with the reaction centre. This pigment-protein represents a funnel through which all the excitation energy collected by other pigment-proteins must pass before it is delivered to the reaction centre. Core complex I, and core complex II chlorophyll *a*/ $\beta$ -carotene-proteins present in all plants (see §8.3) perform this role for photosystems I and II, respectively.

The extent to which each of the other light-harvesting pigment-proteins of algae and higher plants, described in §8.3, transfers energy specifically to one photosystem or the other, or to both, is uncertain. There is some evidence that the major light-harvesting pigment-proteins, such as the various chlorophyll/carotenoid-containing LHC IIs of higher plants and green algae, and the biliproteins of red algae, transfer most, but not all, of their energy initially to photosystem II. Transfer of some of this energy from photosystem II to photosystem I (referred to as 'spillover', or 'state transition') then takes place, thus making it possible for the two photoreactions to continue at the same rate. The review by Butler (1978) may be consulted for a detailed account of this topic. There is now evidence (discussed in Allen, 2003; Falkowski and Raven, 2007) that spillover involves a phosphorylation of the the major photosystem II light-harvesting protein (e.g. the chl *a/b* LHC II of green algae and higher plants), and that as a consequence of the increase in negative charge, some of the light-harvesting complex becomes detached from photosystem II and migrates to photosystem I.

The marine cyanobacterium, *Synechocystis*, may be an exception to the rule that biliproteins belong to photosystem II, in that both photosystems appear to have their own light-harvesting biliproteins. Kondo *et al.* (2007) present evidence that this alga has two different kinds of phycobilisome. In addition to a 'normal' phycobilisome, containing phycocyanin and

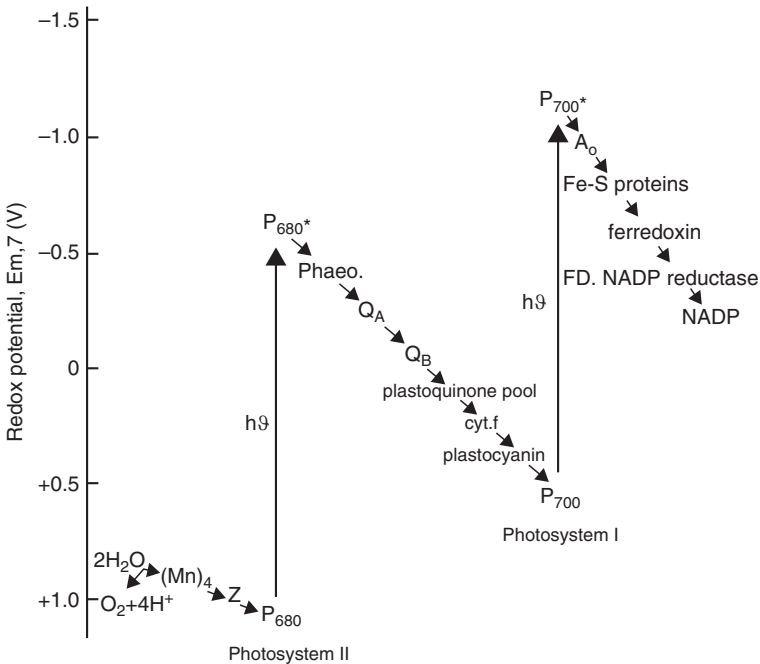


Fig. 8.17 The light phase of photosynthesis. The details are discussed in the text.

allophycocyanin, transferring energy primarily to photosystem II, and loosely attached to the thylakoid membrane, there is another type of phycobilisome, lacking allophycocyanin and firmly attached to the membrane, which transfers energy mainly, but not solely, to photosystem I.

Turning now to what actually happens in the light phase of photosynthesis, the current view of the sequence of events is summarized in Fig. 8.17. In photosystem I the reaction centre, P<sub>700</sub>, consists of a chlorophyll dimer: one of the two molecules is chlorophyll *a*, the other is chlorophyll *a*' , the C13<sup>2-</sup>-epimer of chlorophyll *a*. When P<sub>700</sub> acquires excitation energy it loses an electron to a primary acceptor, A<sub>0</sub>, which is believed to be another chlorophyll *a* dimer. The reduced primary acceptor is then oxidized by a phyloquinone molecule (vitamin K). From the quinone the electron is transferred to F<sub>x</sub>, a 4Fe-4S cluster ligated by protein cysteinyl residues in reaction centre proteins PsaA and PsaB, and then to F<sub>A</sub> and/or F<sub>B</sub>, 4Fe-4S clusters ligated by cysteinyl residues in reaction centre protein PsaC. Electrons are then transferred to the iron-sulfur protein, ferredoxin, and from there, via the flavoprotein ferredoxin-NADP reductase, to NADP, giving NADPH<sub>2</sub>.

Simultaneously with photosystem I, activation of photosystem II takes place. When the reaction centre chlorophyll in photosystem II,  $P_{680}$  – believed to be a chlorophyll *a* dimer – acquires excitation energy it loses an electron first to an associated phaeophytin molecule, which then rapidly reduces a molecule of plastoquinone ( $Q_A$ ), bound to protein. Electrons are then transferred to another specialized plastoquinone molecule ( $Q_B$ ), which, when fully reduced (two electrons), is displaced from its binding pocket in the core complex by another – oxidized – molecule of plastoquinone and diffuses within the thylakoid membrane until it reaches the cytochrome  $b_6/f$  complex where it reduces cytochrome  $b_6$ . Cytochrome  $b_6$  reduces cytochrome  $f$ , which in turn reduces the copper-containing protein, plastocyanin, from which an electron is then transferred to the oxidized photosystem I reaction centre chlorophyll,  $P_{700}^+$ , restoring it to its original (reduced) state.

The oxidized reaction centre chlorophyll,  $P_{680}^+$ , is reduced by transfer of an electron from a tyrosyl residue in a reaction centre protein. Within the complex there is a cluster of four Mn ions together with one  $Ca^{2+}$  and a  $Cl^-$  ion. It is believed that this inorganic ion cluster reduces the tyrosine radical, and the oxidized form of the cluster can then remove electrons from water, leading to the liberation of oxygen. Putting all these processes together, the transfer of hydrogen from water to NADP, giving rise to oxygen and  $NADPH_2$ , is now complete.

Oxidation of a reduced plastoquinone molecule by the cytochrome  $b_6/f$  complex in the electron transfer chain between the two photosystems requires removal of two hydrogen atoms. The electrons are transferred to the cytochromes and two protons are released into the intrathylakoid space (lumen). Also, the removal of electrons from water by photosystem II is accompanied by the transfer of  $H^+$  to the intrathylakoid space. For every oxygen molecule liberated there is a movement of not less than eight protons from outside the thylakoid to the thylakoid lumen. It is believed that the pH gradient and electric potential set up in this way operate, by means of a reversible ATPase in the membrane, working backwards, to bring about ATP synthesis, i.e. *photophosphorylation*.

### **The dark reactions**

The pathway by which, in the stroma of the chloroplast, the  $NADPH_2$  and ATP produced in the light reactions are used to convert  $CO_2$  to carbohydrate was elucidated largely by the work of Calvin and Benson, and is outlined in Fig. 8.18. The cycle is somewhat involved and needs

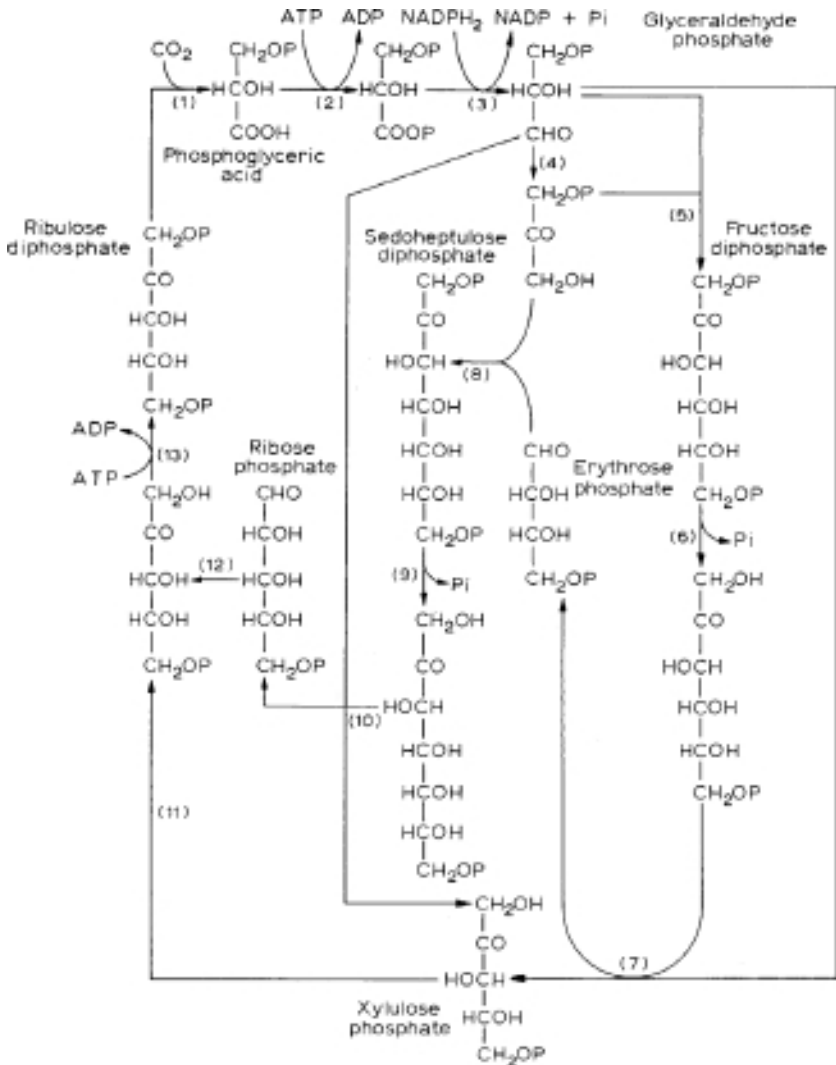
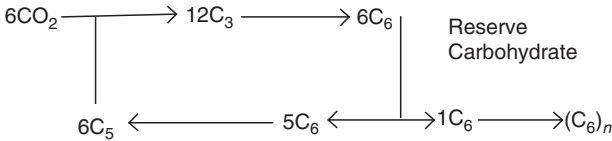


Fig. 8.18 The photosynthetic CO<sub>2</sub> fixation cycle. P = phosphate group; Pi = inorganic phosphate. The enzymes involved in each step are: (1) Rubisco; (2) 3-phosphoglyceric acid kinase; (3) glyceraldehyde-3-phosphate dehydrogenase; (4) triose phosphate isomerase; (5) fructose-diphosphate aldolase; (6) fructose 1,6 diphosphatase; (7) transketolase; (8) aldolase; (9) sedoheptulose 1,7 diphosphatase; (10) transketolase; (11) xylulose-5-phosphate epimerase; (12) ribose-5-phosphate isomerase; (13) ribulose-5-phosphate kinase.

several turns to produce one molecule of hexose. To understand the overall effect of the dark reactions let us consider the fate of six molecules of  $\text{CO}_2$ . These react with six molecules of ribulose biphosphate ( $\text{C}_5$ ) to give 12 molecules of phosphoglyceric acid ( $\text{C}_3$ ). The phosphoglyceric acid is, with the help of ATP and  $\text{NADPH}_2$ , reduced to triose phosphate. For simplicity we can regard these as being converted to six molecules of hexose phosphate ( $\text{C}_6$ ). One of these molecules of hexose can be removed to form starch or other reserve carbohydrate, leaving five hexose phosphate molecules. These are now rearranged to form six pentose phosphate ( $\text{C}_5$ ) molecules which are, with the help of ATP converted to six molecules of ribulose biphosphate. Thus the cycle is completed with six molecules of  $\text{CO}_2$  being converted to one of hexose. The overall process in terms of carbon atoms may be summarized



Some higher plants, known as  $\text{C}_4$  plants, possess a variant of this cycle in which  $\text{CO}_2$  is first fixed in the form of a  $\text{C}_4$  acid, such as malic acid. The  $\text{C}_4$  acid is then translocated to another tissue where  $\text{CO}_2$  is liberated from it again and converted to carbohydrate by the normal cycle. It seems very unlikely that this  $\text{C}_4$  pathway occurs in any alga, and it does not appear to exist in submerged aquatic higher plants, so we may disregard it as a contributor to aquatic photosynthesis within the water column. Some aquatic higher plants do, however, have a simplified form of  $\text{C}_4$  pathway in which a substantial proportion of the  $\text{CO}_2$  fixation is indeed initially into  $\text{C}_4$  acids, from which the  $\text{CO}_2$  is subsequently liberated and used for photosynthesis, but within the same cell.<sup>149,681,1111</sup> The effect of this is to increase the  $\text{CO}_2$  supply to the  $\text{CO}_2$ -fixing enzyme, ribulose biphosphate carboxylase (commonly referred to as *Rubisco*), this being a significant limiting factor in aquatic photosynthesis, as we shall discuss in more detail in a later chapter (see §11.3). In cyanobacteria, *Rubisco* occurs together with carbonic anhydrase in icosahedral crystalline bodies,  $\sim 0.1 \mu\text{m}$  in diameter, referred to as *carboxysomes*, and it seems likely that this is where  $\text{CO}_2$  fixation occurs. In eukaryotic algae most of the *Rubisco* is localized in the pyrenoid.<sup>958,384</sup>

In bright sunlight, photosynthesis produces carbohydrates faster than they can be used in respiration or growth. Accordingly the plant

must store the fixed carbon in some form that it can utilize later, most commonly as grains of polysaccharide. The chemistry of algal storage products was reviewed by Craigie (1974). In higher plants and green algae, fixed carbon is accumulated inside the chloroplast as starch grains in the stroma, or forming a shell around the pyrenoid in those algae that have them. In algal phyla other than the Chlorophyta, the photosynthetic end products accumulate outside the chloroplast. Where a pyrenoid is present the polysaccharide grains are usually found in the cytoplasm but in close contact with the pyrenoid region of the chloroplast.

The Floridean starch of the Rhodophyta is an  $\alpha$ -D-(1 $\rightarrow$ 4)-linked glucan with  $\alpha$ -D-(1 $\rightarrow$ 6)-branch points, and can thus be regarded as an amylopectin, like the major component of higher plant starch. Cryptophytes accumulate a starch of the higher plant type, containing both amylose and amylopectin. Members of the Pyrrophyta accumulate grains of a storage polysaccharide with staining properties similar to starch. Brown algae (Phaeophyta) accumulate the polysaccharide laminaran, a  $\beta$ -D-(1 $\rightarrow$ 3)-linked glucan with 16 to 31 residues per molecule and a mannitol residue at the reducing end of each chain: some of the laminaran molecules are unbranched, some have two to three  $\beta$ -D-(1 $\rightarrow$ 6) branch points per molecule. In addition, these algae accumulate large amounts of free mannitol. In the Euglenophyta, the photosynthetic storage product accumulates as granules of paramylon, a  $\beta$ -D-(1 $\rightarrow$ 3) glucan, with 50 to 150 residues per molecule. The photosynthetic storage product of the Heterokontophyta and Haptophyta is chrysolaminaran (also known as leucosin), a  $\beta$ -D-(1 $\rightarrow$ 3)-linked glucan with possibly two 1 $\rightarrow$ 6 branch points per 34-residue molecule. Diatoms also contain polysaccharides of the chrysolaminaran type. The storage carbohydrate of the cyanophytes and prochlorophytes is an  $\alpha$ -1,4-glucan, similar to starch.

# 9

## Light capture by aquatic plants

The collection of light energy for photosynthesis by aquatic plants is, as we have seen, carried out by the photosynthetic pigments. We have already examined the spectral absorption capabilities of each of the different classes of pigment. We shall now consider the light-harvesting properties of the complete photosynthetic system, with particular reference to the dependence of these on the specific combination of pigments present and, in the case of phytoplankton, on the size and shape of the cells or colonies.

### 9.1 Absorption spectra of photosynthetic systems

We might measure the absorption spectrum of, say, phytoplankton or a multicellular algal thallus, for a number of different reasons. We might seek information on what pigments are present. We might wish to compare the spectral position and shape of an *in vivo* absorption peak with those of the same peak in the isolated pigment with a view to assessing the extent to which the absorption properties are modified by binding to protein. We might want to know to what extent an alga is equipped to efficiently harvest light from the underwater radiation field in which it lives.

An absorption spectrum is the variation of some measure of light absorption by a system with wavelength. Light absorption might be expressed in terms of the absorptance,  $A$ , the per cent absorption (100  $A$ ), the absorption coefficient,  $a$ , the absorbance,  $D$  (where  $D = -\log_{10}(1 - A)$ ), or some other function such as the first derivative of the absorbance. The particular light absorption parameter chosen will depend on the purpose of the absorption spectrum. If, for example, we wish to be able to

estimate the contribution of a planktonic alga to the total absorption coefficient of the aquatic medium at any wavelength, then we would measure the absorbance of a suspension of known concentration of the algae, as a function of wavelength, and (since absorbance is proportional to the absorption coefficient) calculate the specific absorption coefficient per unit algal biomass or pigment at the wavelength of interest. If, on the other hand, we require information on the rate at which an algal thallus is absorbing quanta from a particular incident light field, then the absorbance, or per cent absorption, spectrum of that thallus is what is needed.

Before returning to the absorbance spectra of algae we shall in some detail consider absorbance spectra: these are, in effect, absorption coefficient spectra, linked as they are by simple proportionality (see §3.2). At this point it should be noted that since living cells scatter, as well as absorb, light then all measurements, of whatever absorption parameter, must be carried out with procedures that eliminate the effect of scattering on the absorption spectrum, as described in §3.2. Except where otherwise specified, it should be assumed in the remainder of this chapter that all absorption spectra referred to have been corrected for scattering.

We saw in the previous chapter that what actually carries out the light absorption in aquatic plants, the fundamental light-absorbing system, is the thylakoid. The absorbance spectrum of the thylakoid is determined by the particular kind and quantity of chlorophyll/carotenoid-protein and, in some cases, biliprotein complexes present within, or attached to, the membrane. It might therefore be thought that two species of planktonic algae that have the same array of pigment-proteins, and consequently the same absorbance spectrum at the thylakoid level, must also have the same *in vivo* absorbance spectrum in suspensions of cells or colonies at the same total pigment concentration. This is not the case. While two such algal species would certainly have rather similar spectra with the peaks and the troughs in the same positions, the extent to which the peaks rise above the troughs, and the specific absorption coefficient per unit pigment at any wavelength, can differ markedly between the two species. This is because the *in vivo* absorbance spectrum is, as we shall see, determined by the size and shape of the chloroplasts, cells or colonies, as well as by the pigment composition.

It is not feasible to determine the absorbance spectrum of a single thylakoid directly. However, in many cases it is possible to disperse the chloroplasts, by physical disruption and/or detergents, into particles so small that the effects of size and shape on the spectrum are eliminated, but with the pigment-protein interaction, so important for spectral

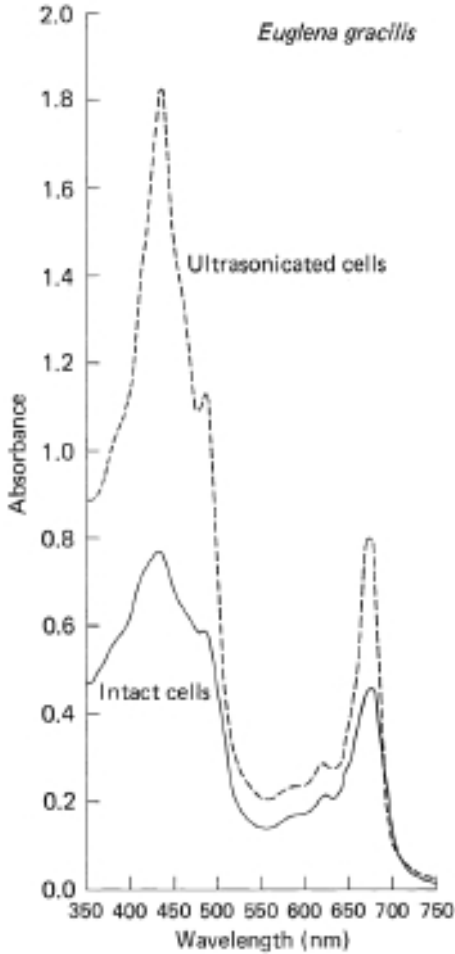


Fig. 9.1 Absorbance spectrum of whole cells of *Euglena gracilis* compared with that of disrupted cells in which absorption is essentially due to thylakoid fragments (Kirk, unpublished). The spectra of intact cells (—) and of cells fragmented by ultrasonication (-----) have been corrected for scattering and in both cases correspond to  $12\mu\text{g chlorophyll } a\text{ ml}^{-1}$  and 1 cm pathlength.

characteristics, being unaffected. Spectra of such preparations may be regarded as being reasonable approximations to the true *in situ* absorbance spectra of the thylakoids. Figure 9.1 shows a spectrum of this type for thylakoid fragments of the green planktonic alga *Euglena gracilis*.

## 9.2 The package effect

The absorbance spectrum of a cell or colony suspension (in the case of unicellular algae) or of a segment of thallus or leaf (in the case of multicellular aquatic plants) will always differ noticeably from that of dispersed thylakoid fragments. The *in vivo* spectra (e.g. *Euglena*, Fig. 9.1) will be found to have peaks that are less pronounced with respect to the valleys, and to have, at all wavelengths, a lower specific absorption per unit pigment. These changes in the spectra are due to what we shall refer to as the *package* effect – sometimes, inappropriately, called the *sieve* effect. It is a consequence of the fact that the pigment molecules, instead of being uniformly distributed, are contained within discrete packages: within chloroplasts, within cells and within cell colonies. This, as one might intuitively suspect, lessens the effectiveness with which they collect light from the prevailing field – hence the lowered specific absorption. It is in the nature of the package effect to be proportionately greatest when absorption is strongest<sup>343</sup> – hence the flattening of the peaks. The influence of the package effect on the absorption spectra of algal suspensions was first studied, experimentally and theoretically, by Duysens (1956), and its implications for the absorption of light by phytoplankton populations have been analysed by Kirk (1975a, b, 1976a) and Morel and Bricaud (1981).

To better understand the package effect, let us compare the absorption properties of a suspension of pigmented particles with those of the same amount of pigment uniformly dispersed – in effect, in solution. We shall for simplicity ignore the effects of scattering, and absorption by the medium. Consider a suspension containing  $N$  particles per  $\text{m}^3$ , illuminated by a parallel beam of monochromatic light through a pathlength of 1.0 m. The  $j$ th particle in the light beam would, in the absence of the other particles, absorb a proportion  $s_j A_j$  of the light in unit area of beam, where  $s_j$  is the projected area of the particle ( $\text{m}^2$ ) in the direction of the beam, and  $A_j$  is the particle absorptance – the fraction of the light incident on it which it absorbs.  $s_j A_j$  has the dimensions of area and is the absorption cross-section of the particle (see §4.1). The absorptance of unit area of the suspension due to the  $j$ th particle is thus  $s_j A_j$ , and so (from eqn 1.36) the absorption coefficient of the suspension due to the  $j$ th particle is  $\ln 1/(1 - s_j A_j)$  which, since  $s_j A_j$  is small, is approximately equal to  $s_j A_j$ . Assuming that Beer's Law applies to a suspension of particles, i.e. that the absorbance (or absorption coefficient) of the suspension is equal to the sum of the absorbances (or absorption coefficients) due to all the individual particles,<sup>343,1302</sup> then the absorption coefficient of the suspension is

$$a_{sus} = \sum_{j=1}^N s_j A_j = N \overline{sA} \quad (9.1)$$

Where  $\overline{sA}$  is the mean value, for all the particles in the suspension, of the product of the projected area and the particle absorptance, i.e. the average absorption cross-section. The absorbance (0.434 *ar*, see §3.2) of the suspension for a 1.0 m pathlength, is given by

$$D_{sus} = 0.434 N \overline{sA} \quad (9.2)$$

If the particles have an average volume of  $\overline{v} \text{ m}^3$ , and the pigment concentration within the particle is  $C \text{ mg m}^{-3}$ , then if the pigment were to be uniformly dispersed throughout the medium, it would be present at a concentration of  $NC\overline{v} \text{ mg m}^{-3}$ . If the specific absorption coefficient of the pigment (the absorption coefficient due to pigment at a concentration of  $1 \text{ mg m}^{-3}$ ) at the wavelength in question is  $\gamma \text{ m}^2 \text{ mg}^{-1}$ , then the absorption coefficient due to the dispersed pigment is given by

$$a_{sol} = NC\overline{v}\gamma \quad (9.3)$$

and the absorbance (1.0 m pathlength) by

$$D_{sol} = 0.434 NC\overline{v}\gamma$$

The extent of the package effect can be characterized by the ratio of the absorption coefficient or absorbance of the suspension to that of the solution. From eqns 9.1 and 9.3, it follows that this ratio is given by

$$\frac{a_{sus}}{a_{sol}} = \frac{D_{sus}}{D_{sol}} = \frac{\overline{sA}}{C\overline{v}\gamma} \quad (9.4)$$

It can be shown<sup>693</sup> that for particles of any shape or orientation,  $a_{sus}/a_{sol}$  is always less than 1.0. However, it can also be shown<sup>695</sup> that if the individual particles absorb only weakly, e.g. because they are small or because the pigment concentration within the particles is low, then

$$\overline{sA} \approx C\overline{v}\gamma$$

and so, for such particles  $a_{sus} \approx a_{sol}$ .

We shall now consider what happens if we make the particles absorb progressively more strongly. For simplicity we shall keep the size and shape of the particles constant, i.e. we shall keep  $s$  and  $\overline{v}$  constant. Both  $C$  and  $\gamma$  can be increased in value almost indefinitely by increasing the pigment concentration within the particles, and by changing to a more

intensely absorbed wavelength, respectively: thus the denominator in eqn 9.4 can be increased in value many-fold. As  $C$  or  $\gamma$  increases, so  $A$  in the numerator also increases, but since this is the *fraction* of the light incident on the particle which is absorbed, it can never exceed 1.0, and cannot increase in proportion to the increase in  $C$  or  $\gamma$ . When  $A$  is very low (weakly absorbing particles) a doubling in  $C$  or  $\gamma$  can bring about an almost commensurate increase in  $A$ , but the closer  $A$  gets to 1.0 the less leeway it has to increase in response to a given increase in  $C$  or  $\gamma$ . This is why the package effect, the discrepancy between the spectrum of the particle suspension, and the corresponding solution, becomes more marked as absorption by the individual particles increases: this in turn explains why the peaks of the spectrum are affected more than the troughs. In short, it is the dependence of the absorption spectrum of a suspension on the *fractional absorption per particle* (particle absorptance) that accounts for the flattening of the spectrum and the lowered specific absorption per unit pigment concentration. A more extensive treatment of this phenomenon can be found elsewhere.<sup>693,694,695</sup> It should be noted that the package effect still affects the absorption spectrum even in suspensions so dense that no photon can avoid traversing a chloroplast while passing through: this is one reason why the term 'sieve effect' is inappropriate.

In the special case of spherical cells or colonies, which present the same cross-section to the light, whatever their orientation, an explicit expression for the particle absorptance was derived by Duysens (1956)

$$A = 1 - \frac{2[1 - (1 + \gamma Cd)e^{-\gamma Cd}]}{(\gamma Cd)^2}$$

where  $d$  is the diameter of the particle. Morel and Bricaud (1981) and Kirk (1975b) have used this relation to carry out an analysis of the package effect and its implications for light absorption for spherical phytoplankton cells.

It is apparent from eqn 9.4 that the extent to which the package effect influences absorbance depends only on the absorption properties of the individual particles. It is therefore just as true for a suspension of particles as it is for a solution, that the *shape* of the absorbance spectrum, and the specific absorbance per unit pigment, are independent of concentration. Measured spectra of suspensions of algal cells might sometimes seem not to conform to this rule: concentrated suspensions may have higher absorbances than anticipated, even when spurious absorbance due to scattering of light away from the detector is eliminated. This is because there is a

residual scattering artifact in dense suspensions that cannot be overcome by instrumental means; namely, that as a result of the multiple scattering that takes place within such suspensions, the pathlength of the photons and hence the number absorbed within the suspension is increased.

We noted at the beginning of this section that the package effect can be observed in the absorbance spectra of multicellular photosynthetic tissues as well as in those of suspensions. This is because within the tissue the pigments are also segregated into packages – the chloroplasts. However, since the chloroplasts are not randomly distributed in space and since, moreover, in many cases they change their position within the cells in response to changes in light intensity, no simple mathematical treatment of the light absorption properties of multicellular systems is possible.

### 9.3 Effects of variation in cell/colony size and shape

We have seen in the previous section that the absorption coefficients and hence the light-harvesting efficiency of the photosynthetic pigments are lower when they are segregated into packages than when they are uniformly dispersed. The kind of packages within which the photosynthetic pigments occur in the aquatic biosphere vary greatly in size, shape and internal pigment concentration, however, and so we need some more general rules to assist our understanding of the light-intercepting capabilities of these different forms.

We already have two rules:

- (i)  $a_{sus} < a_{sol}$
- (ii) Where  $s_p$  is the projected area of the particle (cell or colony) in the direction of the light beam, and  $A_p$  is the particle absorptance, then at constant cell/colony size and shape (constant  $s_p$ ), when  $A_p$  is increased (by raising the intracellular pigment concentration or altering the wavelength),  $a_{sus}/a_{sol}$  decreases.

It is possible also to deduce the following:

- (iii) At constant total pigment and biomass in the system, when both  $s_p$  and  $A_p$  are increased (by decreasing the number and thus increasing the size of the cells or colonies, without changing their shape),  $a_{sus}/a_{sol}$  decreases.
- (iv) At constant total pigment in the system, when biomass is increased (by increasing cell/colony number or volume, without changing the shape),  $a_{sus}/a_{sol}$  increases.

- (v) At constant total pigment and biomass in the system, and constant cell/colony volume, as the shape becomes more extended, e.g. more elongated, so  $a_{sus}/a_{sol}$  increases.

In both (iv) and (v) the diminution in absorptance associated with the dilution of the pigment into more biomass, or the stretching-out of the cells/colonies, is proportionately less than the increase in projected area and so, overall, the absorption cross-section  $s_p A_p$  increases.

Having examined the underlying mechanism, and the general rules governing the expression, of the package effect we shall now consider, in quantitative terms, just how much it can influence the light-harvesting capacity of planktonic algae. A convenient parameter to look at is the absorption cross-section of a given amount of algal biomass organized into packages of different sizes and shapes.<sup>695</sup> Figure 9.2a shows the absorption cross-section at wavelengths from 350 to 700 nm calculated for model randomly oriented blue-green algal colonies of various geometrical forms: the volume of biomass is  $100\,000\ \mu\text{m}^3$  in each case, and the pigment concentration is constant at 2% (of the dry mass) chlorophyll *a*. It can be seen that the least efficient arrangement for light collection is the large, spherical colony,  $58\ \mu\text{m}$  in diameter (lowest curve). Matters are improved somewhat if the spheres are elongated into prolate spheroids,  $230 \times 29\ \mu\text{m}$ . A much greater increase in efficiency is achieved if the spheres are transformed into long, thin, cylindrical filaments,  $3500\ \mu\text{m}$  long and  $6\ \mu\text{m}$  in diameter. Only a marginal further increase in light-harvesting capacity is brought about if the filaments are chopped up into about 900 pieces, each piece being rounded up into a sphere of  $6\ \mu\text{m}$  diameter (uppermost curve). The advantages of the more extended package are much more evident at strongly absorbed, than weakly absorbed, wavelengths. For example, the ratio of the absorption cross-section of the thin cylinder to that of the large sphere is 3.82 at 435 nm but only 1.16 at 695 nm. A given change in shape cannot increase the absorption cross-section by more (proportionately) than it increases the average projected area. As the light absorption by the cell is intensified (i.e. as  $A_p$  approaches 1) so the effect of a given geometrical change on absorption cross-section tends to become identical to the effect on average projected area.

As another quantitative illustration of the significance of the package effect, Fig. 9.2b shows how the specific absorption coefficient per mg chlorophyll *a* present in the form of a suspension of spherical cells or colonies, at its red peak, decreases as the diameter of the cells/colonies increases.

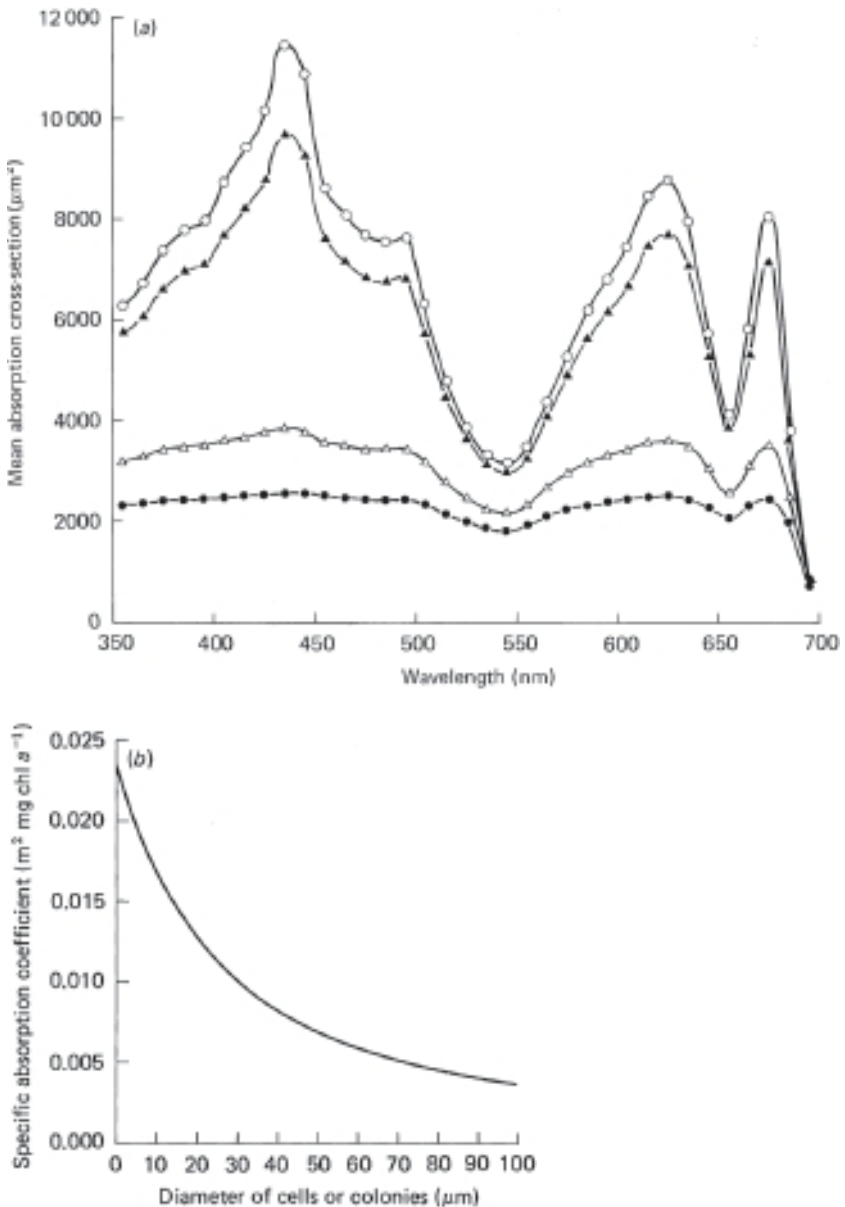


Fig. 9.2 Effect of size and shape on light absorption properties of phytoplankton. (a) The absorption cross-section spectra of randomly oriented blue-green algal colonies of various shapes and sizes (calculated by Kirk (1976a) for idealized colonies containing 2% dry mass, chlorophyll *a*). In every case the data apply to  $100\,000\ \mu\text{m}^{-3}$  of algal volume. This corresponds

That the package effect really does have a major influence on the light-harvesting capability of algal cells has now been demonstrated in numerous experiments comparing different phytoplankton species varying in cellular size and pigment content, or comparing cells of a given species having a range of pigment contents due to variation in growth irradiance.<sup>101,284,379,516,614,947,954,982,1173,1268</sup> A striking example in the field has been described by Robarts and Zohary (1984): in Hartbeespoort Dam (South Africa), as the colony size of the dominant blue-green alga *Microcystis aeruginosa* increased, there was a corresponding increase in euphotic depth resulting from the less efficient light interception of biomass distributed in larger packages. Phytoplankton populations in the coastal waters of the Antarctic Peninsula appeared, on the basis of chlorophyll-specific vertical attenuation coefficients measured at wavelengths through the photosynthetic spectrum, to have a markedly greater package effect than populations from temperate oceans: Mitchell and Holm-Hansen (1991a) attributed this to the presence of larger cells with high cellular pigment concentration resulting from chronic low-light adaptation in nutrient-rich waters. In another Antarctic oceanic region, the southwestern Ross Sea, Arrigo *et al.* (1998) found that a bloom dominated by large-celled cryptophytes had substantially lower chlorophyll-specific absorption values, both in the red and the blue spectral regions, than blooms of the much smaller diatoms or of the prymnesiophyte, *Phaeocystis antarctica*. In the Huon River estuary, Tasmania, Clementson *et al.* (2004) found that the specific absorption coefficients (per mg chlorophyll) of blooms dominated by diatoms were substantially greater than those of blooms dominated by the much larger cells of the dinoflagellate, *Gymnodinium catenatum*, the difference being  $\sim 2\frac{1}{2}$ -fold at the 675 nm chlorophyll *a* peak.

Caption for Fig. 9.2 (cont.)

to one particle in the cases of the 57.6  $\mu\text{m}$  diameter spheres (●), the  $230.4 \times 28.8 \mu\text{m}$  prolate spheroids (Δ) and the  $3537 \times 6 \mu\text{m}$  cylinders (▲); and to 884 particles in the case of the 6  $\mu\text{m}$  diameter spheres (○). (b) Specific absorption coefficient of phytoplankton chlorophyll at the red maximum (670–680 nm) as a function of cell or colony size (Kirk, unpublished). The values were obtained from the particle absorbance values calculated using the equation of Duysens (1956), assuming that the cells/colonies contained 2% dry mass ( $\sim 4 \text{ g l}^{-1}$  cell volume) of chlorophyll *a* and that the (natural logarithm) specific absorption coefficient of chlorophyll *a* in solution at its red peak is about  $0.0233 \text{ m}^2 \text{ mg}^{-1}$ , as it is, for example, in diethyl ether.<sup>410</sup> Similar calculations have been carried out by Morel and Bricaud (1981).

Geider and Osborne (1987) showed that for the relatively small diatom *Thalassiosira* (~5 µm diameter) grown in culture, the package effect reduced light-absorption efficiency by 50% at the blue absorption maximum (435 nm), and by 30% at the chlorophyll *a* red maximum (670 nm), but had no significant effect at the absorption minimum (600 nm): larger diatoms would show an even greater package effect. In the picoplankton (<2 µm diameter), such as the unicellular cyanophytes and prochlorophytes of the ocean, however, the package effect should be of no significance.<sup>708</sup>

It is now recognized that the influence of the package effect on the light-absorption efficiency of oceanic phytoplankton varies in a systematic manner with the nutrient status of the water. In the western North Atlantic, for a large number of stations with chlorophyll *a* concentrations ranging from 0.1 to 8.0 mg m<sup>-3</sup> (Sargasso Sea to Gulf of Maine), Yentsch and Phinney (1989) found that the absorption coefficient due to particles (predominantly phytoplankton) at 670 nm increased with chlorophyll concentration, not linearly but in accordance with [chl]<sup>0.758</sup>, indicating that there was a progressive decrease in the specific absorption coefficient as total phytoplankton chlorophyll increased. They attributed this to an increased package effect associated with the greater proportion of larger cells in the more eutrophic waters. Bricaud *et al.* (1995), using a more wide-ranging oceanic database (815 stations), and correcting the spectra of the particulate matter for the contribution of non-algal material, arrived at an equation of the form

$$a_{\phi}^*(\lambda) = A(\lambda)[\text{Chl}]^{-B(\lambda)}$$

for wavelengths from 400 to 698 nm, where [Chl] is the concentration of phytoplankton chlorophyll *a* in mg m<sup>-3</sup>,  $a_{\phi}^*(\lambda)$  is the specific absorption coefficient of the phytoplankton (m<sup>2</sup> mg chlorophyll *a*<sup>-1</sup>), and  $A(\lambda)$  and  $B(\lambda)$  are coefficients applicable at each wavelength.  $A(\lambda)$  and  $B(\lambda)$  were 0.403 and 0.332, respectively at 440 nm, and 0.0201 and 0.158 at 675 nm. They found that, accompanying an increase in [Chl] from 0.02 to 25 mg m<sup>-3</sup> across this range of oceanic environments, the package effect brought about a three-fold reduction in the height of the red absorption band. In the blue region of the spectrum the reduction was around ten-fold: this, however, was due, not only to the package effect, but also to variations in the proportion of accessory pigments, including an increase in the cellular concentration of photoprotective carotenoids in oligotrophic waters.

For a data set of 465 samples from a range of estuarine, coastal and oceanic stations, Staehr and Markager (2004) calculated  $\hat{a}_{ph}^*$ , the

numerical mean of the chlorophyll-specific phytoplankton absorption coefficient ( $\text{m}^2 \text{mg chlorophyll } a^{-1}$ ), over the 400 to 700 nm range (*not* to be confused with  $\bar{a}_p(z)$ , the effective absorption coefficient of the phytoplankton for PAR at depth  $z$ , see eqn 9.9, below), and found that it decreased with increasing phytoplankton concentration ( $\text{mg m}^{-3}$ ), in accordance with

$$\hat{a}_{ph}^* = 0.025 [\text{Chl } a]^{-0.24}$$

which may be regarded as a measure of the variation in package effect with phytoplankton concentration, for absorption across the whole photosynthetic waveband.

In the southern Beaufort Sea, Canadian Arctic, Matsuoka *et al.* (2009) found that as ambient light levels declined from autumn when open water still existed, to early winter when sea ice cover formed, there was an increase in  $a_{\phi}^*(\lambda)$  across the spectrum, resulting from a biological selection of smaller-sized phytoplankton, more efficient at absorbing light.

In aquatic macrophytes also, the efficiency of light absorption is influenced by the package effect, but because of the complexities imposed by the three-dimensional structure, does not lend itself to mathematical analysis. In two seagrass species sampled at different times of the year, Cummings and Zimmerman (2003) found that a five-fold increase in leaf chlorophyll content (in seasonally low light) was accompanied by only an 18.5% increase in photosynthetic light-harvesting efficiency, a disparity which they attributed to the package effect. In brown, red and green macroalgae, Grzyski *et al.* (1997), by comparing absorption spectra of intact tissue with those of suspensions of sonically disrupted thylakoids, concluded that the package effect was responsible for a significant flattening of the absorption peaks in these species.

## 9.4 Rate of light absorption by aquatic plants

The rate of photosynthesis by an aquatic plant must ultimately be limited by (although it is not always simply proportional to) the rate at which the higher plant leaf, or multicellular algal thallus, or individual phytoplankton cell or colony, is absorbing quanta from the underwater light field. In the case of the leaf or the algal thallus, the rate of absorption of quanta of a given wavelength incident at a particular angle on a particular element of tissue surface is equal to  $E(\lambda, \theta, \phi) \cdot \delta s \cdot A(\lambda, \theta, \phi)$ , the product of the

irradiance at that angle, the area of the element, and the absorptance for that wavelength and that angle. The total rate of absorption of light of that wavelength by the whole leaf or thallus is the sum of this product over all angles of incident light for each element of surface, and over all the elements that constitute the total area of the leaf or thallus.

It is clear that the crucial optical property of the tissue is the *absorptance* (the fraction of incident light absorbed) rather than the *absorbance*. Because of the variation in optical path through the tissue with angle, the absorptance of the leaf or thallus at any point will in fact vary somewhat with the angle of incidence of the light. The effective absorptance of the tissue at a given point for the total light of a given wavelength incident at all angles is a function of the angular distribution of the light field, and so it is not, strictly speaking, possible to attribute a particular absorptance to the tissue for underwater light of a given wavelength independent of the radiance distribution of that light. The absorptance is in fact usually determined with the measuring beam at right angles to the plane of the photosynthetic tissue. This is considered to provide at least an approximate measure of the absorptance that the tissue will present to the light incident on it within the water. Due to variations in thickness, and/or chloroplast number and pigment composition, there can be variation in absorptance from place to place within a leaf or thallus. This is particularly likely to be the case with long algal thalli, different parts of which are normally exposed to different light environments, e.g. because the lower parts are shaded. The increase in photon pathlength resulting from multiple scattering within the tissue can accentuate absorption by multicellular plants.

Figure 9.3 shows the 90° absorptance spectrum for an aquatic higher plant; corresponding spectra for various kinds of multicellular algae are shown in Fig. 10.6*a*, *b* and *c*. The differences between the spectra are in part due to differences in concentration of chloroplast pigments per unit area, and this can of course vary markedly within any algal class as well as from one class to another. Some of the differences in the shape of the spectra are, however, attributable to the different types of pigment present. The relatively greater absorption in the 500 to 560 nm region in the brown alga compared to the green alga and higher plant is due to the presence of fucoxanthin in the former. The broad peak at 520 to 570 nm in the spectrum of the red alga is due to the presence of the biliprotein, phycoerythrin.

In the case of phytoplankton, the rate of absorption by an individual cell or colony of light quanta of a given wavelength coming from a given

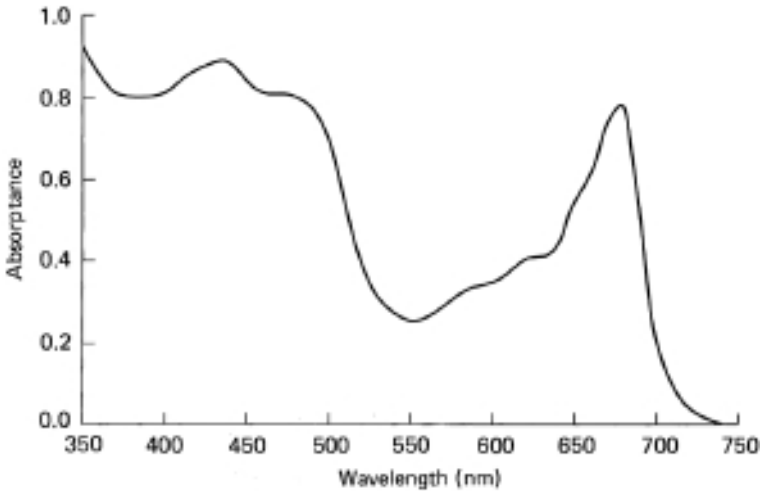


Fig. 9.3 Absorption spectrum of the leaf of a freshwater macrophyte (Kirk, unpublished). The spectrum was measured on a piece of leaf of *Vallisneria spiralis* (Hydrocharitaceae), free of epiphytic growth, from Lake Ginninderra, ACT, Australia, with the sample cell close to the photomultiplier: the spectrum has been corrected for scattering.

direction, is equal to  $E(\lambda, \theta, \phi) \cdot s_p(\theta, \phi) \cdot A_p(\lambda, \theta, \phi)$ , the product of the irradiance in that direction, the cross-sectional area (in the specified direction) of the cell or colony and the absorptance of the particle in its particular orientation with respect to the light stream. Since the cells or colonies are randomly oriented, each will present a somewhat different projected area, and absorptance, to light flowing in the specified direction. The average rate of absorption of this light per particle is  $E(\lambda, \theta, \phi) \cdot \overline{s_p A_p}$ . It will be recalled that  $\overline{s_p A_p}$  is the average absorption cross-section of the particles (§9.2). It follows from the random orientation of the cells or colonies that they have the same average absorption cross-section for light at all directions. We can therefore validly attribute an average absorption cross-section to a phytoplankton population, regardless of the angular distribution of the underwater light field. It is in fact possible to attribute an average absorptance to the individual particles in a plankton population, but this is not a useful thing to do, since it is the product of absorptance and cross-sectional area (which vary together, with orientation) rather than absorptance alone, which determines the rate of collection of quanta from a particular light stream.

What, in the present context, we wish to know about a phytoplankton population is the average absorption cross-section of the cells or colonies

composing the population, at all wavelengths in the photosynthetic range. To carry out measurements on individual cells or colonies, although possible, is technically difficult and does not give results of high accuracy. We must therefore rely on spectroscopic measurements carried out on suspensions of phytoplankton. The concentrations at which phytoplankton normally occur are too low for accurate absorption measurements. It is therefore necessary to prepare more concentrated suspensions by filtration or centrifugation, followed by resuspension in a smaller volume.

Given a reasonably concentrated suspension of phytoplankton, by what sort of measurement can we determine the average absorption cross-section? Despite the importance of absorbance of the individual cell or colony in determining the absorption cross-section, measurements of the absorbance of the whole suspension tell us relatively little about the absorption properties of the individual particles in the suspension. The absorbance spectrum of the suspension changes shape as the phytoplankton concentration changes, and at very high concentrations tends to become a straight line, with  $A_{sus} \approx 1.0$  throughout the spectrum (total absorption of light at all wavelengths). The absorbance spectrum of the suspension, however, is of relevance if, for some reason, we need to know the rate of light absorption by the whole suspension – for example, in laboratory studies of photosynthetic efficiency.

To determine the average cross-section per individual free-floating particle, whether cell or colony, in the suspension, what we in fact measure is the absorbance of the suspension,  $D_{sus}$ . Figure 9.4 shows the absorbance spectra of suspensions of three planktonic algae: *Chlorella* (green), *Navicula* (a diatom) and *Synechocystis* (a blue-green). The absorbance, in a 1 cm pathlength, of a suspension of particles, as we saw earlier (eqn 9.2, §9.2), is equal to  $0.434 n \overline{s_p A_p}$ , where  $n$  is the number of particles per ml, and  $\overline{s_p A_p}$  is the average absorption cross-section per particle. Thus we may obtain the values of  $\overline{s_p A_p}$  throughout the photosynthetic range for any phytoplankton population by preparing a suitably concentrated suspension, measuring the absorbance spectrum and  $n$ , and applying the relation

$$\overline{s_p A_p} = \frac{D_{sus}}{0.434 n} \quad (9.5)$$

at a series of wavelengths from 400 to 700 nm. Since the pathlength is 1 cm then  $n$ , as well as being the number of cells per ml, is also the number of particles per  $\text{cm}^2$  in the path of the measuring beam. Thus, in eqns 9.2 and 9.5,  $N$  or  $n$  can be taken to mean the number of particles per unit area,

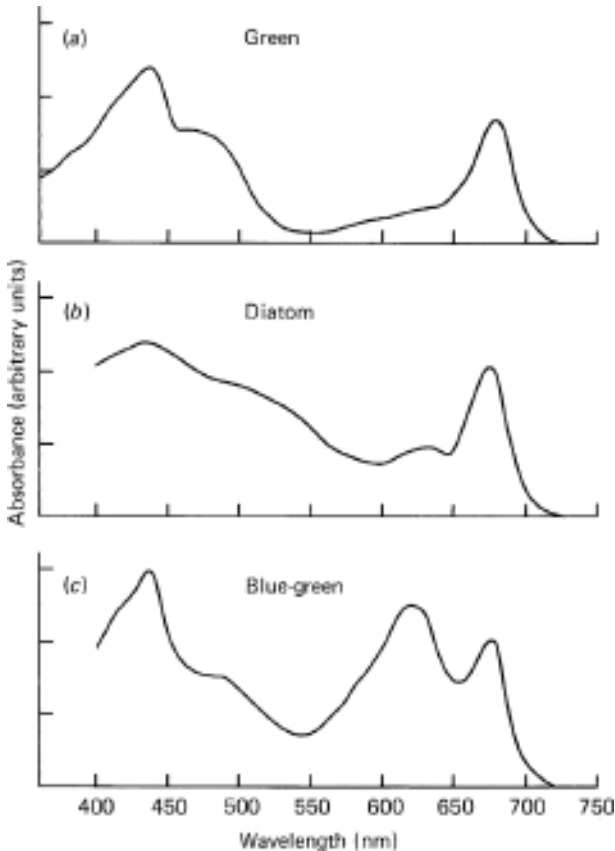


Fig. 9.4 Absorbance spectra of cultured cells of three species of planktonic algae measured using an integrating sphere (after Latimer and Rabinowitch, 1959). (a) *Chlorella pyrenoidosa* (green). (b) *Navicula minima* (diatom). (c) *Synechocystis* sp. (blue-green).

provided only that the units in which area is expressed are the same as those in which absorption cross-section ( $\overline{s_p A_p}$ ) is expressed, i.e. with a given number of particles per unit area, the absorbance is the same no matter through what pathlength they are distributed.

The average rate of absorption of light of wavelength  $\lambda$ , per individual phytoplankton cell or colony at depth  $z$  m, is  $E_0(\lambda, z) \cdot \overline{s_p A_p}(\lambda)$ , where  $E_0(\lambda, z)$  is the scalar irradiance of light of that wavelength at that depth and  $\overline{s_p A_p}(\lambda)$  is the average absorption cross-section in  $\text{m}^2$ . The rate of light absorption (in W, or quanta  $\text{s}^{-1}$ ) per horizontal  $\text{m}^2$  by all the phytoplankton within a thin layer of thickness  $\Delta z$  m, at depth  $z$  m is given by

$$E_p = E_0(\lambda, z) \cdot \overline{s_p A_p(\lambda)} \cdot \Delta z N \quad (9.6)$$

where  $N$  is the number of phytoplankton cells or colonies per  $\text{m}^3$ .

In the field of aquatic primary production, phytoplankton concentration is more commonly expressed in terms of  $\text{mg chlorophyll } a \text{ m}^{-3}$ , than cells or colonies  $\text{m}^{-3}$ . Since, from eqn 9.1

$$\overline{N s_p A_p(\lambda)} = a_p(\lambda)$$

where  $a_p(\lambda)$  is the absorption coefficient due to phytoplankton, we can write

$$E_p = E_0(\lambda, z) \cdot a_p(\lambda) \cdot \Delta z \quad (9.7)$$

and

$$E_p = E_0(\lambda, z) \cdot [\text{Chl}] \cdot a_\phi^*(\lambda) \cdot \Delta z \quad (9.8)$$

where  $[\text{Chl}]$  is the concentration of phytoplankton chlorophyll  $a$  in  $\text{mg m}^{-3}$ , and  $a_\phi^*(\lambda)$  is the specific absorption coefficient of the phytoplankton per  $\text{mg chlorophyll } a \text{ m}^{-3}$ :  $a_\phi^*(\lambda)$  has the units  $\text{m}^2 \text{mg chlorophyll } a^{-1}$ .

In any given waveband, if the total absorption coefficient due to all components of the medium is  $a_t(\lambda)$ , then the proportion of the total absorbed energy which is captured by phytoplankton is  $a_p(\lambda)/a_t(\lambda)$ . A set of values for the specific absorption coefficient of marine phytoplankton across the photosynthesis spectral region may be found in Fig. 3.9 (Chapter 3).

A useful concept when considering light capture by phytoplankton is the effective absorption coefficient of the phytoplankton population existing at a given depth for the light field at that depth, across the whole photosynthetic spectrum.<sup>940</sup> It may be thought of as a weighted average absorption coefficient of the phytoplankton for PAR, taking into account the actual spectral distribution of PAR at the depth in question, and is defined by

$$\bar{a}_p(z) = \frac{\int_{400}^{700} a_p(\lambda) E_0(\lambda, z) d\lambda}{\int_{400}^{700} E_0(\lambda, z) d\lambda} \quad (9.9)$$

where  $E_0(\lambda, z)$  is the scalar irradiance per unit bandwidth ( $\text{nm}^{-1}$ ) at wavelength  $\lambda$  and depth  $z \text{ m}$ . We can also define a specific effective absorption coefficient of the phytoplankton,  $\bar{a}_\phi^*(z)$ , for PAR as the value of  $\bar{a}_p(z)$  for phytoplankton at  $1 \text{ mg chl } a \text{ m}^{-3}$ , and having the units  $\text{m}^2 \text{mg chl } a^{-1}$ .

Even if the concentration and nature of the phytoplankton remain the same, the values of the effective, and specific effective, absorption coefficients for PAR do vary with depth, in accordance with the change in spectral distribution of PAR. In the ocean, where there is generally little dissolved yellow colour, the light field with increasing depth becomes increasingly confined to the blue-green (400–550 nm) spectral region (§6.2, Fig. 6.4). Since this is where phytoplankton have their major absorption peak (Fig. 3.9), the value of  $\bar{a}_{\phi}^*(z)$  in such waters increases with depth, by up to 50 or even 100% within the euphotic zone.<sup>728,940</sup> In the Pacific Ocean southeast of Japan, Kishino *et al.* (1986) found  $\bar{a}_{\phi}^*(z)$  to increase rapidly with depth from 0.022 m<sup>2</sup> mg chl a<sup>-1</sup> at the surface to 0.044 at 30 m. In the green waters of highly productive upwelling regions,  $\bar{a}_{\phi}^*(z)$  can decrease with depth.<sup>940</sup>

The photomicrograph in Fig. 9.5, of a mixed sample from a Tasmanian coastal site, shows what at least some of the phytoplankton cells that absorb energy from the underwater light field actually look like.

## 9.5 Effect of aquatic plants on the underwater light field

We have concerned ourselves so far in this chapter with the ability of phytoplankton and macrophytes to make use of the underwater light field. By harvesting light from the field, however, the plants in turn modify the light climate for any other plants below them in the water column. Within any substantial stand of aquatic macrophytes, such as a kelp forest, or a bed of seagrass or freshwater aquatic higher plants, the intensity of PAR is greatly reduced. Phytoplankton also increase the rapidity of attenuation of light with depth, and in productive waters may do so to such an extent that by self-shading they become a significant factor limiting their own population growth. The contribution of phytoplankton to vertical attenuation of PAR must therefore be taken into account in any consideration of the extent to which light availability limits primary production in the aquatic biosphere.

We saw in §6.8 that the total vertical attenuation coefficient for monochromatic irradiance at a given depth can be regarded as the sum of a set of partial attenuation coefficients, each corresponding to a different component of the medium. This proposition does not, strictly speaking, hold for the average vertical attenuation coefficient throughout the euphotic zone, and even less does it hold for the whole photosynthetic waveband, 400 to 700 nm. Nevertheless, the assumption that the average

$K_d(\text{PAR})$  for the euphotic zone can be partitioned in this way is so useful that, despite its only approximate truth, it is commonly made, and may be given approximate expression through the equation

$$K_d(\text{PAR}) = K_W + K_G + K_{TR} + K_{PH} \quad (9.10)$$

where  $K_W$ ,  $K_G$ ,  $K_{TR}$  and  $K_{PH}$  are the partial attenuation coefficients (for PAR) due to water, gilvin, tripton and phytoplankton, respectively. The contribution of phytoplankton to vertical attenuation of PAR can therefore be expressed in terms of the contribution of  $K_{PH}$  to the value of  $K_d(\text{PAR})$  in eqn 9.10.

To arrive at a quantitative estimate of the contribution of phytoplankton to  $K_d(\text{PAR})$  we must determine  $K_{PH}$ . To do this we make use of a further commonly made assumption, which as we saw in §6.7 is also only approximately valid, namely that the contribution of any component of the medium to  $K_d(\text{PAR})$  is linearly related to the concentration of that component. Applying this to the phytoplankton we assume that

$$K_{PH} = [\text{Chl}]k_c \quad (9.11)$$

Where  $[\text{Chl}]$  is the phytoplankton biomass concentration expressed in terms of mg chlorophyll  $a \text{ m}^{-3}$ , and  $k_c$  is the specific vertical attenuation coefficient (units  $\text{m}^2 \text{ mg chl } a^{-1}$ ) per unit phytoplankton concentration. We may now write

$$K_d(\text{PAR}) = K_W + K_G + K_{TR} + [\text{Chl}]k_c \quad (9.12)$$

If, for any given water body, an estimate of the specific attenuation coefficient,  $k_c$ , is available, then from a measurement of the phytoplankton concentration,  $[\text{Chl}]$ , we obtain a value for  $K_{PH}$ .

The value of  $k_c$  has been calculated for each of the four kinds of blue-green algal colonies to which the data in Fig. 9.2 apply:  $k_c$  was  $0.0063 \text{ m}^2 \text{ mg}^{-1}$  for the  $58 \mu\text{m}$  spheres,  $0.0084 \text{ m}^2 \text{ mg}^{-1}$  for the  $230 \times 29 \mu\text{m}$  prolate spheroids,  $0.0133 \text{ m}^2 \text{ mg}^{-1}$  for the  $3500 \times 6 \mu\text{m}$  cylinders and  $0.0142 \text{ m}^2 \text{ mg}^{-1}$  for the  $6 \mu\text{m}$  spheres.<sup>695</sup> This marked variation of  $k_c$  among the different types of algae confirms the importance of the package effect in light capture by phytoplankton. These values were all obtained by calculation for idealized algae:  $k_c$  can also be determined experimentally for real phytoplankton populations by measuring  $K_d$  for PAR in natural water bodies at different times as the algal population waxes and wanes, and determining the linear regression of  $K_d(\text{PAR})$  with respect to phytoplankton chlorophyll  $a$  concentration. Not many measurements of  $k_c$  covering the whole photosynthetic waveband have in fact

been made. There are, however, other data in the literature, on the effect of varying phytoplankton concentration on the value of  $K_d$  in particular spectral bands within the 400 to 700 nm range, obtained with irradiance meters fitted with broad-band filters. Talling (1957b) found that for various natural waters an approximate value for  $K_d(\text{PAR})$  could be obtained by multiplying the minimum value of  $K_d(\lambda)$  for the water body concerned (usually that in the green waveband in inland waters) by 1.33; for Lough Neagh, N. Ireland, a factor of 1.15 was found to be more suitable.<sup>642</sup> Using this sort of relation, measurements of  $K_d$  in wavebands within the photosynthetic range can be used to provide estimates of  $k_c$ . Table 9.1 lists some values of  $k_c$  determined in various natural water bodies, from measurements either of irradiance for total PAR or for a particular waveband. It can be seen that  $k_c$  varies widely – by a factor of four between the lowest and the highest value – from one alga, one water body, to another.

There are several possible reasons for this variability. One is the influence of cell size and geometry. We noted above that the package effect – within the range that might occur in nature – can vary  $k_c$  by a factor of more than two in blue-green algae of identical pigment composition. We may reasonably attribute the low  $k_c$  values for the large dinoflagellates in Table 9.1 to the low efficiency of light collection by large pigmented particles. The package effect also, as outlined earlier (§9.2), increases the more strongly the particles absorb (at constant size and shape). Thus, even for algae of similar size, shape and pigment type,  $k_c$  will decrease as total pigment content increases. In addition, since  $k_c$  is expressed per unit chlorophyll *a*, there can be marked variation in specific attenuation from one alga to another, due to differences in the type of other photosynthetic pigments present and their ratio to chlorophyll *a*. Calculations for model cells having the same chlorophyll *a* content indicated that  $k_c$  for diatoms would be about 70% higher than that for green algae because of the increased absorption in the 500 to 560 nm region due to fucoxanthin;  $k_c$  for blue-green algae with substantial levels of the biliprotein phycocyanin, absorbing in the 550 to 650 nm region, was calculated to be about twice that for diatoms.<sup>695</sup>

The colour of the aquatic medium in which the cells are suspended can also have a marked influence on the values of  $k_c$ . Green algal cells, for example, absorb strongly in the blue region (Fig. 9.4a). In typical inland waters, however, with high levels of yellow substances, the contribution of the blue spectral region to the underwater light field is greatly diminished, and so in such waters, green cells have a low value of  $k_c$ .<sup>694</sup> The  $k_c$  values we have considered so far have been the average values over some considerable optical depth, i.e. a depth in which the downward irradiance

Table 9.1 Values of specific vertical attenuation coefficient for PAR per mg phytoplankton chlorophyll a, obtained from in situ measurements of irradiance.

Water body	Phytoplankton type	$k_c$ ( $\text{m}^2 \text{mg}^{-1}$ )	Reference
L. Windermere, England	<i>Asterionella</i> (diatom)	0.027 <sup>a</sup>	1335
Esthwaite Water, England	<i>Ceratium</i> (large dinoflagellate)	~0.01 <sup>a</sup>	1337
L. George, Uganda	<i>Microcystis</i> (blue-green)	0.016–0.021 <sup>a</sup>	430
Loch Leven, Scotland	<i>Synechococcus</i> (blue-green)	0.011 <sup>a</sup>	117
L. Vombsjon, Sweden	<i>Microcystis</i> (blue-green)	0.021 <sup>a</sup>	444
Lough Neagh, Ireland	<i>Melosira</i> (diatom)	0.014 <sup>b</sup>	642
	<i>Stephanodiscus</i> (diatom)	0.008 <sup>b</sup>	
	<i>Oscillatoria</i> (blue-green)	0.012–0.013 <sup>b</sup>	
L. Minnetonka, Minn., USA	Mixed blue-green ( <i>Aphanizomenon</i> etc.)	0.022 <sup>c</sup>	896
L. Tahoe, Calif.-Nevada, USA	Small diatoms (mainly <i>Cyclotella</i> )	0.029	1363
Irondequoit Bay, L. Ontario, USA	Mixed blue-green	0.019	1445
L. Constance, Germany	Mixed	0.015 <sup>c</sup>	1361
L. Zurich (0–5 m depth), Switzerland	Mixed	0.012	1182
Sea of Galilee (L. Kinneret), Israel	<i>Peridinium</i> (large dinoflagellate)	0.0067	331
Various oceanic and coastal waters	Mixed	0.016	1240

<sup>a</sup> Obtained by multiplying  $K_d(\lambda)_{min}$  by 1.33.

<sup>b</sup> Obtained by multiplying  $K_d(\lambda)_{min}$  by 1.15.

<sup>c</sup> Derived from measurements of scalar, rather than downward, irradiance of PAR.

falls to some small fraction of that at the surface. In fact, since the spectral distribution of the light changes progressively with depth, so the value of  $k_c$  calculated over a small increment of depth also changes.<sup>38</sup> In the case of blue-green algae which, due to the presence of ample levels of biliprotein, absorb strongly in the green, as well as in the blue and red regions,  $k_c$  does not vary markedly with depth in any water type. In the case of green algae, however, in an inland water absorbing strongly in the blue, calculations by Atlas and Bannister (1980) indicate that  $k_c$  diminishes from about  $0.012 \text{ m}^2 \text{ mg}^{-1}$  in the surface layer to about  $0.005 \text{ m}^2 \text{ mg}^{-1}$  at the

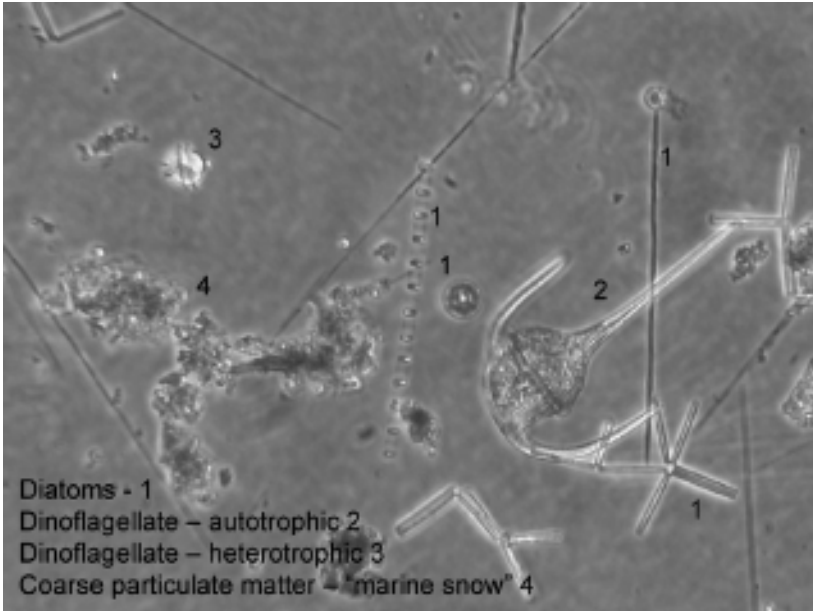


Fig. 9.5 Mixed coastal phytoplankton, Tasmania, Australia. (Courtesy Ian Jameson, CSIRO Marine & Atmospheric Research.) See [colour plate](#).

bottom of the euphotic zone. In the ocean we would expect the same sort of changes in  $k_c$  with depth as are found for the effective specific absorption coefficient,  $\bar{\alpha}^*(z)$  (see previous section).

One further possible cause of variation in the value of  $k_c$  from one kind of phytoplankton to another is variation in their light-scattering properties. Scattering, as we saw earlier (§6.7), contributes in various ways to the vertical attenuation of irradiance. In dense algal blooms the contribution of the algal population to total scattering could significantly increase  $k_c$ . The amount of scattering – especially per unit chlorophyll *a* – can vary markedly from one species to another (see [Table 4.2](#)). Coccolithophores and diatoms, for example, scatter light more intensely than algae enclosed within less refractile integuments.

The effects of macrophytes on the underwater light field vary so much with the growth habit of the plants and the morphology of the leaves or thallus that a general theoretical account is not feasible. According to Westlake (1980c) the specific vertical attenuation coefficient per mg chlorophyll is lower for macrophytes than for phytoplankton. Dense stands of emergent and floating macrophytes can make the whole water column virtually aphotic. Within submerged weed beds the spectral distribution of irradiance is predominantly green.<sup>1457</sup>

# 10

## Photosynthesis as a function of the incident light

The rate of photosynthesis achieved by a phytoplankton cell or aquatic macrophyte depends on the rate of capture of quanta from the light field. This is determined by the light absorption properties of the photosynthetic biomass, which we have considered in some detail, and by the intensity and spectral quality of the field. The rate of photosynthesis is not, however, simply proportional to the rate of capture of photons. The efficiency with which the photosynthetic apparatus can make use of the absorbed energy to fix  $\text{CO}_2$  varies from one plant cell to another and within a given cell as its physiological state changes. Light quanta may be collected by the pigments faster than the electron carriers and enzymes can make use of them. In particularly high light intensities the excess absorbed energy can inactivate the photosynthetic system. The relation between the rate of photosynthesis and the characteristics of the incident light is thus not a simple one: we shall examine it in this chapter.

### 10.1 Measurement of photosynthetic rate in aquatic ecosystems

In order to study the effects of light intensity and spectral quality on photosynthesis, suitable quantitative procedures for determining the photosynthetic rate per unit biomass must be used. Detailed descriptions of such methods for use in the field or the laboratory may be found elsewhere,<sup>1169,1419</sup> and so only the principles will be described here.

#### **Direct measurement: $\text{CO}_2$ fixation and $\text{O}_2$ liberation**

Photosynthesis can be measured in terms of either  $\text{CO}_2$  fixed or  $\text{O}_2$  released. For terrestrial plants the method of choice is direct measurement

of  $\text{CO}_2$  removal from the gas stream by monitoring the infrared absorption by  $\text{CO}_2$ , but for obvious reasons this will not work in an aquatic medium. Because of the stoichiometry of the overall photosynthetic process (§ 8.5), approximately one  $\text{O}_2$  molecule is liberated for every molecule of  $\text{CO}_2$  fixed. However, since the average composition of plant biomass differs somewhat from  $\text{CH}_2\text{O}$  due to the presence of protein, lipid and nucleic acid as well as carbohydrate, the  $\text{O}_2:\text{CO}_2$  ratio (known as the *photosynthetic quotient*) is usually in the range 1.1 to 1.2, rather than exactly 1.0. In the case of the more active photosynthetic systems, it is convenient to measure  $\text{O}_2$  liberation – using chemical analysis, an oxygen electrode or manometry. For field measurements of phytoplankton photosynthesis, however, in all except highly productive waters, the much more sensitive procedure of measuring fixation of  $^{14}\text{CO}_2$  is used: this method was introduced by Steemann Nielsen in 1952. Bottles containing water samples with the natural phytoplankton population present and with small amounts of [ $^{14}\text{C}$ ]-bicarbonate (hydrogen carbonate,  $\text{HCO}_3^-$ ) added, are suspended at a series of depths throughout the euphotic zone, generally for periods of a few hours in the middle of the day. The amount of radioactivity fixed in cells, collected on a filter and treated with acid to remove excess [ $^{14}\text{C}$ ]-bicarbonate, is determined.

Alternatively, the incubations of the phytoplankton samples with [ $^{14}\text{C}$ ]-bicarbonate can be carried out in the laboratory at the same temperature as that in the water body, and at a series of irradiance values designed to correspond to different depths. For marine phytoplankton, Jitts (1963) introduced the technique of carrying out the laboratory incubations under a series of thicknesses of blue glass, to simulate the variation of spectral distribution, as well as total irradiance, with depth. Failure to reproduce, in the laboratory, spectral distributions similar to those found underwater can lead to substantial errors in estimates of primary production.<sup>778</sup>

The rate may be expressed as either *gross* or *net* photosynthesis. Gross photosynthesis is the total rate of carbon dioxide fixation, making no allowance for the fact that some  $\text{CO}_2$  is simultaneously lost in respiration. Net photosynthesis is the total rate of photosynthetic  $\text{CO}_2$  fixation minus the rate of loss of  $\text{CO}_2$  in respiration. The rate of increase in oxygen concentration within an illuminated bottle containing phytoplankton is a measure of net photosynthesis; a value for gross photosynthesis may be obtained by adding to this the rate of respiratory oxygen consumption measured in a darkened bottle incubated in parallel. Whether the  $^{14}\text{CO}_2$  fixation method measures net or gross photosynthesis, or something

between the two, remains a matter of controversy. In short-term incubations, such as are possible in the more productive waters, there are a priori as well as experimental grounds for considering  $^{14}\text{CO}_2$  fixation as an approximate measure of gross photosynthesis.

### Indirect measurement: chlorophyll fluorescence

An alternative to measurement of radiocarbon fixation or oxygen evolution for determining photosynthetic rate is to use measurement of what is referred to as the *variable component of chlorophyll fluorescence*. Since this has become in recent years a commonly used procedure, a simplified outline of what are believed to be the underlying biochemical processes is presented here. More detailed discussions of this complex topic may be found in Butler (1978), Kolber and Falkowski (1993), Schreiber *et al.* (1995), Kromkamp and Forster (2003), Suggett *et al.* (2003) and Falkowski and Raven (2007).

We have already noted that all oxygenic photosynthetic organisms when illuminated, emit some light in the red, with a peak at  $\sim 685$  nm, as fluorescence at low yield ( $\sim 1\%$ ) from chlorophyll *a*. Evidence from fluorescence excitation spectra, and action spectra for  $\text{O}_2$  evolution, together with studies on biochemically fractionated photosynthetic systems, have led to the conclusion that this originates almost entirely from photosystem II. An early indication that fluorescence could be used to measure photosynthesis was the observation by Samuelsson and Öquist (1977) that in cultures of four species of unicellular green algae the fluorescence increase induced by the herbicide, DCMU, which blocks electron flow from photosystem II, correlated closely with the rate of photosynthesis, as measured with  $\text{H}^{14}\text{CO}_3^-$ .

The fluorescence yield of phytoplankton cells, or macrophyte tissue, can be measured using very low levels of activating light, which do not in themselves bring about significant photosynthesis. When the cells or tissue are left for some time in the dark, and then fluorescence is measured in this way, it is found to occur at a low value, commonly indicated with the symbol,  $F_0$ . If the light intensity is now suddenly increased, so that measureable photosynthesis ensues, or if a short-duration high-intensity (saturating) flash is given, then within a very short interval –  $\sim 200$  milliseconds in leaves and isolated chloroplasts but typically much less in phytoplankton suspensions – the fluorescence emission quickly rises and levels off at a higher value in the region of  $\sim 3$  times  $F_0$ . This is often referred to as the *Kautsky effect*, after its 1930s discoverer. The high level

of chlorophyll fluorescence is found to be still present if it is measured, once again with a low-intensity activating beam, immediately after switching off the light. In continued darkness, photosynthetic cells quickly (within a millisecond) revert to the much lower  $F_0$  fluorescence (when measured with a low-intensity measuring beam).

Any process that lessens the intensity of fluorescence from a system is said to *quench* that fluorescence. The rapid return of the cells to the  $F_0$  state in the dark means that during this dark adaptation something is produced that quenches the fluorescence of chlorophyll *a* in photosystem II. Duysens and Sweers (1963) proposed that it is the primary electron acceptor of photosystem II, now believed to be  $Q_A$ , a protein-bound form of plastoquinone, which in its oxidized form is the quencher. The reduced version of  $Q_A$  (which, since it has acquired a single electron, we can indicate by  $Q_A^-$ ), formed by photochemical electron transfer within photosystem II when the light returns, is assumed not to be a quencher, so that fluorescence rises. If, after dark adaptation, the cells are illuminated with continuous light of intensity sufficient to bring about photosynthesis, then the steady-state level of fluorescence ( $F$ ) exhibited increases with increasing irradiance up to a maximum value ( $F_m$ ), which is believed to correspond to essentially all of the  $Q_A$  being in the reduced (non-quenching) form. This maximum increase above the dark-adapted level, ( $F_m - F_0$ ), is a measure of the variable component of chlorophyll fluorescence, and is indicated by  $F_v$ .

If the progressive increase in fluorescence with increasing ambient light does indeed correspond to the increasingly reduced state of  $Q_A$ , then we may plausibly suppose that at any given light intensity the increase in fluorescence above the dark-adapted value ( $F - F_0$ ), divided by the maximum possible (high light) increase above the dark-adapted value ( $F_m - F_0$ ) corresponds approximately to the proportion of photosystem II reaction centres that contain  $Q_A^-$ . Or, if we prefer to think in terms of the extent to which the fluorescence at a given light intensity *falls short* of the maximum possible fluorescence, we can make the equivalent supposition that ( $F_m - F$ ) divided by ( $F_m - F_0$ ) is approximately equal to the proportion of photosystem II centres in which  $Q_A$  still exists in the oxidized (quenching) form: this quantity is usually indicated by  $q_p$ .

$$q_p = \frac{F_m - F}{F_m - F_0} \quad (10.1)$$

Since ( $F_m - F_0$ ) corresponds to the maximum amount by which chlorophyll fluorescence can vary it is, as noted above, indicated by  $F_v$ .

A photosystem II in which the reaction centre chlorophyll is already oxidized (i.e. is in the form  $P_{680}^+$ ), and the protein-bound plastoquinone is already reduced ( $Q_A^-$ ), cannot make use of any subsequent excitation to achieve photochemical charge separation, and is said to be 'closed', i.e. is not currently available for photosynthetic electron transport. As soon as, in the light,  $P_{680}^+$  once again becomes reduced and  $Q_A^-$  is re-oxidized, another photochemical electron transfer can take place, and the reaction centre is said to be 'open'. Thus, as an alternative to discussing the proportion of photosystem II reaction centres in which  $Q_A$  exists in the oxidized or reduced form, we can refer to the proportion that are open or closed, and this is in fact the common terminology in the literature.  $q_P$  is thus the proportion of photosystem II centres that are open.

For cells photosynthesizing at a given light intensity, the overall efficiency with which photosystem II is working at any given time is equal to the steady-state proportion of reaction centres that are open ( $q_P$ ) multiplied by the efficiency of those reaction centres that are open.<sup>445</sup> On the basis of a particular model of energy transfer within the photosystem II photosynthetic unit, Butler and Kitajima (1975) showed that the maximum yield of photochemistry (the number of electrons produced by a single charge separation event in photosystem II, per photon absorbed), i.e. the yield when all photosystem II centres are open, is equal to  $F_v/F_m$ . Genty *et al.* (1989) pointed out that since, when some but not all of the photosystem II centres are open, the quantum yield of photosystem II electron transport ( $\phi_{PS2}$ ) is equal to the maximum yield ( $F_v/F_m$ ) multiplied by the proportion of centres that are open ( $q_P$ ), then we can write

$$\phi_{PS2} = \frac{F_v}{F_m} q_P \quad (10.2)$$

and therefore, from eqn 10.1 and  $F_v = (F_m - F_0)$ , it follows that

$$\phi_{PSII} = \frac{\Delta F}{F_m} \quad (10.3)$$

where  $\Delta F = (F_m - F)$ , the amount by which the steady-state fluorescence falls short of the maximum fluorescence. The advantage of this formulation is that it makes it possible to estimate the photosystem II quantum yield without determining the difficult-to-measure quantity,  $F_0$ . In agreement with the theory, Genty *et al.*, using leaves of a number of terrestrial higher plant species, found that  $\Delta F/F_m$  was linearly related to the quantum efficiency of  $CO_2$  fixation over a range of light intensities.

In continuous light, particularly at high intensity, the maximum fluorescence emission often settles down to a lower value ( $F'_m$ ) than that measured shortly after a long dark period ( $F_m$ ). Similarly, the minimum fluorescence, as measured in the dark, is often at a lower level ( $F_0'$ ) after the cells have been exposed for some time to high irradiance. It is thus apparent that prolonged high irradiance causes some additional quenching, which, since it is believed not to involve the reaction centre quencher,  $Q_A^-$ , is referred to as *non-photochemical quenching*. There are two main kinds of mechanism by which non-photochemical quenching can occur. One is a reduction in the effective absorption cross-section of photosystem II due to a change in its carotenoid composition in the xanthophyll cycle (see later): the reaction centre in this case still functions but has a lower probability of capturing excitation energy. The other is due to reaction centres being rendered non-functional by radiation-induced damage.

Following the approach in the review by Kromkamp and Forster (2003), we can, as a simple initial version of the relationship between photosynthetic rate and fluorescence, write

$$ETR = E \times a^* \times 0.5 \times \Delta F / F_m \quad (10.4)$$

where  $ETR$  is the electron transport rate (mol electrons mg chl  $a^{-1} s^{-1}$ ),  $E$  is irradiance (mol quanta  $m^{-2} s^{-1}$ ),  $a^*$  is the absorption cross-section ( $m^2$  mg chl  $a^{-1}$ , equivalent to the chlorophyll-specific absorption coefficient of the phytoplankton, §9.4), the 0.5 factor arises from the simplifying assumption that the absorbed light is distributed equally between the two photosystems, and  $\Delta F / F_m$  is the quantum efficiency of photosystem II (electrons produced per photon absorbed). To avoid the assumption that photosystem II and photosystem I absorb light at the same rate, we can replace this equation with

$$ETR = E \times a_{PSII}^* \times n_{PSII} \times \Delta F / F_m \quad (10.5)$$

where  $a_{PSII}^*$  is the absorption cross-section of a photosystem II unit ( $m^2$  mol photosystem II reaction centres $^{-1}$ ) and  $n_{PSII}$  is the number of photosystem II units per mg chl  $a$  (mol photosystem II mg chl  $a^{-1}$ ).

If a plausible value for the electron yield of oxygen evolution ( $\Phi_e$ , moles of  $O_2$  produced per mole of electrons removed from water in photosystem II) can be assumed (ideally  $\Phi_e = 0.25$ , 4 electrons per  $O_2$  evolved), then the chlorophyll-specific rate of photosynthetic oxygen evolution (mol  $O_2$  mg chl  $a^{-1} s^{-1}$ ) can be obtained from the fluorescence-derived  $ETR$

$$P^*(O_2) = ETR \times \Phi_e \quad (10.6)$$

For the Kolber and Falkowski (1993) 'pump and probe' fluorescence procedure (see below) the appropriate relationship for  $P^*(O_2)$  is

$$P^*(O_2) = E \times \sigma_{PSII} \times n_{PSII} \times q_p \times \Phi_e \quad (10.7)$$

where  $\sigma_{PSII}$  is the functional absorption cross-section of photosystem II (the  $f$  factor present in the original Kolber and Falkowski equation has been omitted).<sup>753</sup>  $\sigma_{PSII}$  can be determined from the flash-intensity saturation curve of variable fluorescence, on the assumption that this corresponds to a cumulative one-hit Poisson function.<sup>807,739</sup>

Experimentally there are two different approaches to the measurement of photosynthesis rates using fluorescence, the single turnover (ST) and the multiple turnover (MT). In the ST method the cells are exposed to an intense but very short (150–400 microseconds) light flash, which fully reduces  $Q_A$ , the primary electron acceptor of photosystem II, and thus brings about a simultaneous single closure event of all photosystem II reaction centres.<sup>739,1320,753</sup> In the MT method, a flash of lower intensity but much longer duration (50–1200 milliseconds) is given, which fully reduces not only  $Q_A$ , but also  $Q_B$  and the plastoquinone pool. In the Kolber and Falkowski (1993) 'pump and probe' (ST) method, the fluorometer generates a three-flash sequence: a weak 'probe' flash to measure the initial fluorescence signal, followed after a 500 ms delay by an actinic 'pump' flash of  $\sim 200$  times greater intensity to bring about the single turnover event, followed after a 70  $\mu$ s delay by a second 'probe' flash to measure the resultant change in fluorescence. In a further development of this technique, Kolber *et al.* (1998) use fast repetition rate (FRR) fluorometry to achieve the same effect but with greater flexibility. Instead of a single flash the cells are exposed to a sequence of 80 to 120 'flashlets' of 0.125 to 1.0  $\mu$ s duration at 0.5 to 2.0  $\mu$ s intervals.

The MT method makes use of what is referred to as pulse amplitude modulation (PAM) fluorometry, developed by Schreiber *et al.* (1986, 1993, 1995). Fluorescence is monitored continuously with weak  $\sim 1$   $\mu$ s light pulses at a frequency selectable at 1.6 to 100 KHz. Actinic (MT) pulses of longer duration, as above, are given at specified intervals, e.g. 16 Hz. The modulated nature of the light used to activate fluorescence makes it possible to detect the resulting modulated fluorescence signal against a large background of continuous signals from the actinic illumination (stray light and fluorescence). Instruments for studying photosynthesis using FRR or PAM fluorometry are now commercially available, for submersible or laboratory operation. They do not, however,

give identical results since they do not measure precisely the same quantity. The fluorescence measured with an MT flash is, for example, somewhat larger than that achieved with an ST flash. For estimating photosynthetic rate in benthic organisms, Gorbunov *et al.* (2000) have developed an underwater FRR fluorometer, which can be hand held by a scuba diver or permanently moored, and which is pointed at whatever part of the benthos is under study.

Fluorescence-based measurements of photosynthesis are quick and convenient to use, but in aquatic systems do not always show such reliably linear relationships between the fluorescence-derived and the directly measured  $^{14}\text{C}$ ,  $\text{O}_2$ ,  $\text{CO}_2$  values as those obtained by Genty *et al.* (1989) with terrestrial higher plant leaves. In a natural bloom of freshwater cyanobacteria, Masojídek *et al.* (2001), using PAM fluorometry, found that the relationship between fluorescence-derived *ETR* and photosynthetic  $\text{O}_2$  evolution was linear at irradiance values up to  $800 \mu\text{mole quanta m}^{-2} \text{s}^{-1}$ , but non-linear at higher irradiances. Similarly, using cultures of the green alga, *Dunaliella tertiolecta*, Fujiki *et al.* (2007) concluded that FRR fluorometry can be used as a good indicator of photosynthetic rates from low to middle light levels, but becomes increasingly questionable as the maximum photosynthetic rate is approached. In species of green, brown and red macroalgae, Beer and Axelsson (2004) found a clear positive correlation between  $\text{O}_2$  evolution and fluorescence-based *ETR* at low irradiances, but at high irradiance there was a decrease in *ETR* while  $\text{O}_2$  evolution remained relatively constant. Smyth *et al.* (2004) compared FRR fluorometry and  $^{14}\text{C}$  incorporation measurements of phytoplankton photosynthesis in the Celtic Sea. The light-saturated photosynthetic rates estimated by fluorometry were consistent with those measured using radiocarbon, but there were systematic differences when the estimates of the initial slope ( $\alpha$ ) and the saturation onset parameter ( $E_k$ , see below for definitions) of the photosynthesis versus irradiance curve were compared. On the other hand, Kolber and Falkowski (1993) found a linear correlation ( $r = 0.86$ ) between the fluorescence and the  $^{14}\text{C}$  estimates of integral primary production in the western North Atlantic. Suggett *et al.* (2003) express the view that while the PAM and FRR approaches can make a major contribution to understanding variability of photosynthesis in aquatic systems, whether these techniques can improve estimates of primary productivity remains an open question. Until we arrive at a better understanding of the underlying fundamental processes that are controlling fluorescence emission at the molecular level, the data must be interpreted with caution.

In all the work described above, the fluorescence emission studied has been activated by artificial light supplied by the experimenter. Some studies have also been carried out to determine to what extent information on photosynthetic rates can be obtained by *in situ* measurements of the natural, solar-stimulated fluorescence of phytoplankton at  $\sim 683$  nm. On the basis of measurements at 76 stations, from oligotrophic oceanic to productive inshore waters, Chamberlin *et al.* (1990) found that photosynthetic rate ( $^{14}\text{C}$ , *in situ*) was highly correlated with natural fluorescence emission. At higher irradiance values the quantum yield of photosynthesis decreased more rapidly than the quantum yield of fluorescence. In addition, Chamberlin and Marra (1992), using data from the North Atlantic and the Weddell-Scotia Seas (Antarctica) found that at lower temperatures the ratio of quantum yield of photosynthesis to that of fluorescence decreased, there being an approximately linear relationship between the ratio of quantum yields and temperature. On the basis of their measurements they arrived at a relationship expressing photosynthetic rate as a function of the temperature, scalar irradiance of PAR, and fluorescence emission, together with certain empirically determined constants. A log-log plot of measured versus predicted photosynthesis exhibited approximate linearity for stations covering a wide range of productivity. For Mexican coastal waters (California Current and Gulf of Mexico), Garcia-Mendoza and Maske (1996) found natural fluorescence data to be useful as a proxy of primary production ( $r^2 = 0.85$ ) for volumetric rates of photosynthesis up to  $\sim 300$  nmol C m $^{-3}$  s $^{-1}$ .

### Expression of photosynthetic rate

Rates of photosynthesis, whether net or gross, can be expressed per unit biomass (specific photosynthetic rate) or per unit area or volume of the water. Typical units of biomass-specific photosynthetic rate ( $P^*$ ) for a phytoplankton population are  $\mu\text{moles CO}_2$  (or  $\text{O}_2$ ) or mg C (carbon), per mg chlorophyll *a* per h. It is convenient to indicate it as  $P^*(\text{CO}_2)$ ,  $P^*(\text{O}_2)$  or  $P^*(\text{C})$ , in accordance with the units being used. If the rate per m $^3$  of water,  $P_v$ , is summed for every 1 m depth interval from the surface to the bottom of the euphotic zone, then the areal (or integral) photosynthetic rate,  $P_A$ , i.e. the rate of photosynthesis in the whole water column beneath 1 m $^2$  of surface, is obtained: its units are moles (or  $\mu\text{moles}$ )  $\text{CO}_2$  (or  $\text{O}_2$ ), or g (or mg) C, m $^{-2}$

$$P_A = \int_{z_{eu}}^{\text{surface}} P_v dz$$

It may be useful to indicate areal photosynthetic rate as  $P_A(\text{CO}_2)$ ,  $P_A(\text{O}_2)$  or  $P_A(\text{C})$ , in accordance with the units used. Rates of photosynthesis of benthic macrophytes may be expressed per g dry mass of tissue, or per  $\text{m}^2$  of the substrate on which they are growing. Rates of photosynthesis of the microbial benthos – diatoms, cyanobacteria etc. on the surface, or within the interstices, of the sediments – are commonly expressed per  $\text{m}^2$  of the substrate.

## 10.2 Photosynthesis and light intensity

The variation of the photosynthetic rate of a phytoplankton population with incident light intensity can be studied using bottles suspended at a series of depths: in this case the attenuation of light with depth provides the necessary range of irradiance values. Alternatively the measurements can be carried out under artificial light in the laboratory.

### *P* versus $E_d$ curves

In the dark there is of course no photosynthesis and aquatic plants exhibit a net consumption of  $\text{O}_2$  and liberation of  $\text{CO}_2$ , due to cellular respiration. As the light intensity is gradually increased from zero, some photosynthetic  $\text{O}_2$  production and  $\text{CO}_2$  consumption takes place, but at very low intensities shows up as a diminution in the rate of  $\text{O}_2$  consumption rather than a net liberation of  $\text{O}_2$ , i.e. there is significant gross photosynthesis but no net photosynthesis. An irradiance value ( $E_c$ ) is eventually reached at which photosynthetic oxygen liberation just equals respiratory oxygen consumption: this is the *light compensation point*. Beyond this point liberation exceeds consumption and net photosynthesis is achieved. The typical pattern of behaviour from here on is that  $P$  increases linearly with  $E_d$  up to a certain value. The graph then begins to curve over and eventually levels off. In the range of irradiance values where  $P$  does not vary with  $E_d$ , photosynthesis is said to be light saturated,  $P$  now having the value  $P_m$ , the maximum photosynthetic rate. The biomass-specific maximum photosynthetic rate,  $P_m^*$  is sometimes referred to as the *photosynthetic capacity*. With further increase in irradiance,  $P$  begins to decrease again, a phenomenon referred to as *photoinhibition*. Figure 10.1 shows two typical  $P$  versus  $E_d$  curves, one for marine phytoplankton,<sup>1159</sup> the other for a mixed population of freshwater diatoms.<sup>91</sup>  $P$  versus  $E_d$  curves for macrophytes have a similar shape but often do not show

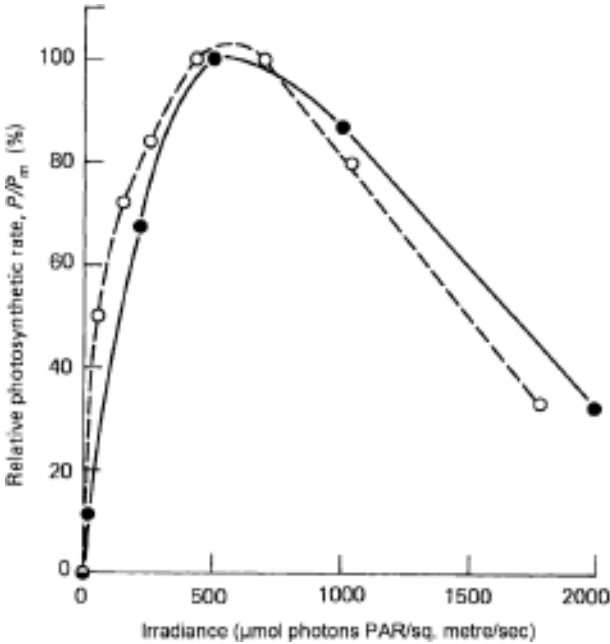
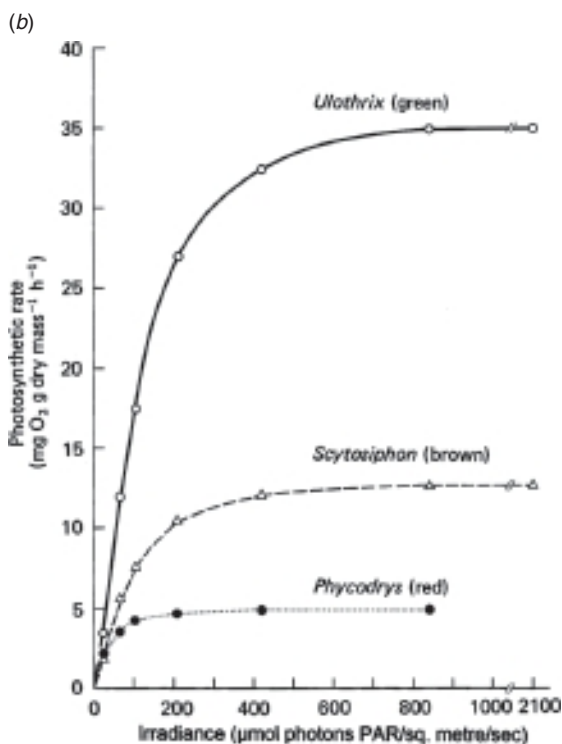
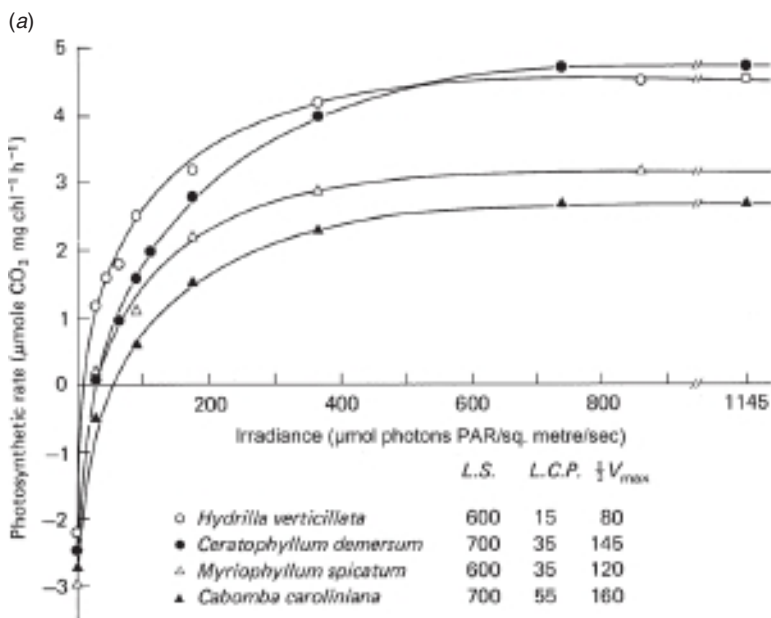


Fig. 10.1 Relative specific photosynthetic rate ( $P/P_m$ ) of phytoplankton as a function of irradiance ( $E_d$ ). Marine phytoplankton from the mid-point of the euphotic zone in the Sargasso Sea (redrawn from data of Ryther and Menzel, 1959) ---●---. Freshwater diatoms (mainly *Asterionella formosa* and *Fragilaria crotonensis*) in Lake Windermere, England (redrawn from data of Belay, 1981) ---○---. Appropriate conversion factors have been used to convert the authors' original  $E_d$  values to  $\mu\text{mol photons PAR m}^{-2} \text{s}^{-1}$

photoinhibition in full sunlight. Figure 10.2 shows the variation of  $P$  with irradiance in four freshwater macrophyte species,<sup>1394</sup> and in green, brown and red marine algal species.<sup>691</sup>

Because of the gradual onset of saturation as  $E_d$  increases, it is difficult to pinpoint the irradiance value at which photosynthesis is just saturated. A more easily measured parameter by means of which the onset of saturation may be characterized<sup>1334</sup> is the irradiance ( $E_k$ ) at which the maximum rate,  $P_m$  would be reached if  $P$  were to continue to increase linearly with  $E_d$ . The value of  $E_k$  is that value of  $E_d$  corresponding to the point of intersection between the extrapolated linear part of the curve and the horizontal line at  $P_m$ . This is illustrated on the idealized  $P$  versus  $E_d$  curve in Fig. 10.3. It can be seen that the slope,  $\alpha$ , of the linear part of the curve is equal to  $P_m/E_k$ :  $\alpha$  is the rate of photosynthesis per unit biomass



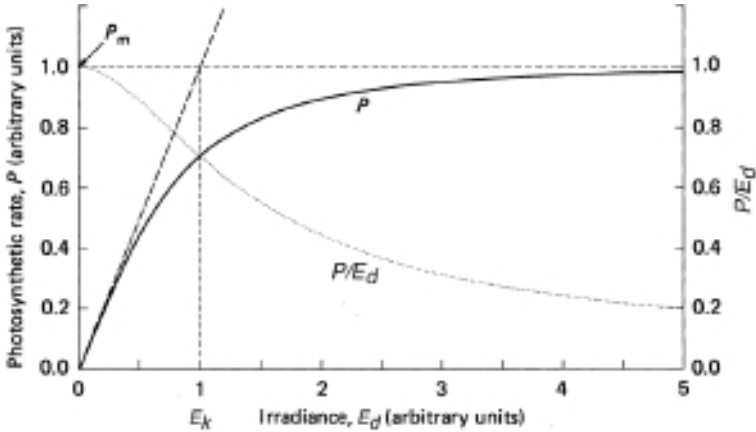


Fig. 10.3 Idealized curve of specific photosynthetic rate ( $P$ ) as a function of irradiance ( $E_d$ ) illustrating the maximum photosynthetic rate,  $P_m$ , and the saturation onset parameter,  $E_k$ . The variation of  $P/E_d$  (a measure of the efficiency of utilization of incident light) with irradiance value is also indicated (.....).

per unit of incident irradiance, and so is a measure of the efficiency with which the biomass utilizes light, at low intensities, to fix  $\text{CO}_2$ .

The light intensity required to saturate photosynthesis, and the compensation point, vary markedly from one species to another. Furthermore, as we shall see in a later section, these parameters also depend on the  $\text{CO}_2$  concentration and the temperature. Thus, if measurements of the photosynthetic response as a function of light are to be ecologically meaningful, they must be measured under conditions approximating those in the aquatic ecosystem. In the case of measurements on phytoplankton the effect of photoinhibition, which develops to a greater extent

Caption for Fig. 10.2 Photosynthetic rates of aquatic macrophytes as a function of irradiance of PAR (a) Freshwater macrophytes from lakes in Florida, USA (by permission, from Van, Haller and Bowes (1976) *Plant Physiology*, 58, 761–8. The rates are limited by low, but typical *in situ*,  $\text{CO}_2$  concentration ( $0.42 \text{ mg l}^{-1}$ ). Temperature is  $30^\circ\text{C}$ . L.S. = irradiance required for light saturation. L.C.P. = irradiance at the light compensation point.  $\frac{1}{2}V_{\text{max}}$  = irradiance required for half-maximal photosynthetic rate. (b) Green, brown and red multicellular algae from the western Baltic Sea (plotted from data of King and Schramm, 1976). The samples of *Ulothrix speciosa* (eulittoral green), *Scytosiphon lomentaria* (eulittoral brown) and *Phycodryx rubens* (sublittoral red) were collected in the spring and the measurements were carried out at  $10^\circ\text{C}$ . The published irradiance values have been converted from  $\text{mW cm}^{-2}$  to  $\mu\text{mol photons PAR m}^{-2} \text{ s}^{-1}$ .

during incubation in stationary bottles than in freely circulating cells (see later), is to lead to underestimation, both of the irradiance required for light saturation and of the maximum photosynthetic rate.<sup>867</sup> Thus, for phytoplankton,  $P$  versus  $E_d$  data obtained in relatively short incubations are to be preferred: there is inevitably considerable uncertainty associated with results obtained from incubations of many hours' duration, such as are required for unproductive oceanic waters. The ability of aquatic plants, including phytoplankton, to utilize light of any given intensity can be highly dependent on the light climate to which they were exposed during growth: it is therefore preferable, for ecological interpretation, if  $P$  versus  $E_d$  curves are measured on naturally occurring, rather than laboratory-grown, plant material. Table 10.1 presents a selection of published data on the irradiance values that have been observed to correspond to light compensation, onset of light saturation and saturation, in a range of naturally occurring aquatic plants. The data do not permit any firm generalization with respect to differences in light saturation values between one algal class and another. This is partly because of the inherent difficulty in identifying the saturation irradiance in a  $P$  versus  $E_d$  curve. Comparisons would be facilitated if the practice of always recording the more easily identified parameter,  $E_k$ , corresponding to onset of saturation, was generally adopted. One permissible generalization is that for any given algal species the light compensation point is lower in the winter or spring than in the summer or autumn: whether this is due simply to the differences in temperature or whether other factors are involved remains uncertain.<sup>691</sup> Within some species the greater the depth from which the sample was taken, the lower the irradiance required to saturate photosynthesis:<sup>1101</sup> this is true of phytoplankton as well as macroalgae.<sup>1297</sup> Adaptation to different ambient light levels is discussed more fully in Chapter 12. Within the phytoplankton there is evidence that the dinoflagellates have higher respiration rates, and therefore higher light compensation points, than the diatoms:<sup>382,1258</sup> this may be due to the energy required to sustain motility in the former group.

In the measurement of  $P$  versus  $E_d$  curves by standard procedures, the photosynthetic system – angiosperm leaves, phytoplankton suspensions, macrophyte thalli – is given enough time, at least some minutes but often much longer, to settle down at each new irradiance value used. With the advent of fluorometric methods of measuring electron transport rates in photosystem II, such as PAM fluorometry, it has become possible to measure photosynthetic response as a function of irradiance very much more rapidly, e.g. carrying out measurements of  $ETR$  at a series of eight

Table 10.1 Irradiance values required for saturation and light compensation of photosynthesis in various aquatic plants. Only data obtained for naturally occurring plant material, measured in natural water or its equivalent, have been used. Irradiance values published in other units have where necessary been converted to mol quanta of PAR  $m^{-2} s^{-1}$  (where  $1.0 \text{ mol quanta} = 6.02 \times 10^{17}$  quanta) with the use of appropriate conversion factors. In many cases saturation onset,  $E_k$ , or compensation irradiance values, where not published, have had to be estimated from authors' data; the uncertainty is particularly great in estimates of the irradiance required to saturate photosynthesis.

Species or plant type	Location, season	Temperature °C	Irradiance, $\mu\text{mol quanta (PAR)} m^{-2} s^{-1}$			Reference
			At saturation	At onset of saturation $E_k$	At compensation point	
<b>Freshwater algae</b>						
<b>Diatoms</b>						
<i>Asterionella formosa</i>	L. Windermere, England. Spring	5 10	– –	28 50	– –	1333 1333
<i>Melosira italica</i>	L. Windermere, England. Winter	5	–	16	–	1333
<b>Blue-green algae</b>						
<i>Microcystis</i> etc.	L. George, Uganda	27–34	–	135–323	–	431
<i>Arthrospira fusiformis</i>	L. Bogoria, Kenya	28	–	41	–	1003
	L. Nakuru, Kenya	24	–	38	–	1003
	L. Elmentaita, Kenya	23	–	128	–	1003
<i>Oscillatoria</i> sp.	L. Neagh, Ireland. Spring	9	14	49	–	641
	L. Neagh, Ireland. Summer	15	203	64	–	641
<b>Green</b>						
<i>Cladophora glomerata</i>	Green Bay, L. Michigan, USA, July–Aug	25–27	345–1125	–	44–104	794

**Freshwater macrophytes**

<i>Hydrilla verticillata</i>	Lakes, Fla., USA	30	600	—	15	1394
<i>Ceratophyllum demersum</i>	Lakes, Fla., USA	30	700	—	35	1394
<i>Myriophyllum spicatum</i>	Lakes, Fla., USA	30	600	—	35	1394
<i>Cabomba caroliniana</i>	Lakes, Fla., USA	30	700	—	55	1394
<i>Myriophyllum brasiliense</i>	Orange L., Fla., USA	30	250–300	—	42–45	1166
<i>Vallisneria americana</i>	Lake, Wisc., USA. Summer	25	140	—	—	1370
<i>Nuphar japonicum</i>	Japan	—	—	—	—	609
Floating leaf		20	400–600	—	3	—
Submerged leaf		21	75	—	3	—
Deep-water characean species	L. Coleridge, New Zealand	—	—	—	—	1267

*Chara fibrosa**Chara globularis**Chara corallina***Marine microalgae**

Oceanic phytoplankton 0 m	Pacific Ocean (3° S)	20–25	600	—	—	645
Oceanic phytoplankton	Pacific Ocean, off Japan. Summer	—	—	—	—	1332
10 m		23	>700	240	—	—
80 m		23	~140	50	—	—
Oceanic picoplankton	Coral Sea, Oct–Nov	—	—	—	—	424
10 m		~27	—	344–818	—	—
100 m		—	—	72–245	—	—
NE Tropical Atlantic Ocean Phytoplankton	Eutrophic site	—	—	150–160	—	50
	Mesotrophic site	—	—	~240	—	—
	Near surface	—	—	150–160	—	—
	Mid-point euphotic	—	—	—	—	—

Table 10.1 (*cont.*)

Species or plant type	Location, season	Temperature °C	Irradiance, $\mu\text{mol quanta (PAR) m}^{-2} \text{s}^{-1}$			Reference
			At saturation	At onset of saturation $E_k$	At compensation point	
	Oligotrophic site	—	—	—	—	
	Near surface	—	—	~400	—	
	Mid-point euphotic	—	—	~320	—	
	Bottom of euphotic	—	—	~60	—	
North Atlantic Ocean	Azores Front, ~34° N	~25	—	206	—	829
	Surface	~17	—	28	—	
	Deep chlorophyll maximum (~100 m)	0–1	50	18	0.5–1.0	581, 915
Continental shelf phytoplankton	Bransfield Strait, Antarctica, Dec–March	0–15	~300	105 (av.)	4 (av.)	1063
Coastal phytoplankton (1–10 m)	Nova Scotia, Canada, all year	0–15	—	—	—	1298
Coastal phytoplankton (0 m)	Baltic, Denmark	1	400	200	—	
3 Feb		17	1200	500	—	
15 July		12	800	300	—	
31 Oct		16	—	254	—	1252
Coastal phytoplankton 1 m	S. California Bight, USA	12	—	42	—	
32 m		15	700	300	—	198
Surf zone phytoplankton	Algoa Bay, Sth Africa	22.5	1000	450	—	

Estuarine phytoplankton	Chesapeake Bay, USA. June				525
<i>Proocentrum mariae-lebouriae</i>		24	—	412	—
Surface mixed layer (0.5 m)					
Subpynocline (15 m)		21	—	67	—
Intertidal benthic diatoms	Cape Cod, USA. Summer	27	57	—	1349
Sea-ice algae (pennate diatoms)	Canadian Arctic. Spring	—1	3–25	0.5–4.3	258
Sea-ice algae (pennate diatoms)	McMurdo Sound, Antarctica. Summer	—2	25	5.4	1033
Platelet ice diatoms	McMurdo Sound, Antarctica.	—2	—	5.9–12.6	1139
Benthic diatoms (26 m)	November	—2	—	1.3–4.5	—
Subtidal microphytobenthos	Port Phillip Bay, Australia. Werribee site, 10 m depth	—	—	12.2	—
	July (winter)	—	—	~320	—
	March (early autumn)	—	—	—	—
<b>Seagrasses</b>					
<i>Cymodocea nodosa</i>	Malta	25	—	158	323
<i>Halophila stipulacea</i>		25	—	83	8
<i>Posidonia oceanica</i>		17	—	108	17
<i>Phyllospadix torreyi</i>	Calif., USA	15	—	149	21
<i>Zostera marina</i>		15	—	208	25
<i>Zostera angustifolia</i>	Scotland	10	—	133	323
<i>Halophila ovalis</i> meadow, 14–16 m depth	South Sulawesi, Indonesia	—	~400	—	367

Table 10.1 (cont.)

Species or plant type	Location, season	Temperature °C	Irradiance, $\mu\text{mol quanta (PAR) m}^{-2} \text{s}^{-1}$			Reference
			At saturation	At onset of saturation $E_k$	At compensation point	
<b>Marine macroalgae</b>						
Chlorophyta						
<i>Enteromorpha intestinalis</i>	W. Baltic. Spring Summer	10 20	450 —	— —	6 15	691
	Calif., USA	21	245	56	6	29
	W. Baltic. Summer	20	700	—	8	691
<i>Cladophora glomerata</i>	Spring	10	200	—	7	
<i>Acrosiphonia centralis</i>	Spring	10	700	—	6	
<i>Ulothrix speciosa</i>	N. Baltic	5	120	—	—	1430
<i>Monostroma grevillei</i>	Woods Hole, Mass. USA. Summer	23	250	160	—	1101
<i>Ulva lactuca</i>						
<i>Ulva lobata</i>	Calif., USA	16	245	76	11	29
<i>Ulva rigida</i>		21	412	50	9	
<i>Codium fragile</i>		21	346	50	9	
<i>Chaetomorpha linum</i>		21	418	82	10	
Phaeophyta						
<i>Fucus serratus</i>	W. Baltic. Winter Autumn	5 15	350 200	— —	5 12	691
<i>Laminaria saccharina</i>	W. Baltic. Winter Autumn	5 15	25 700	— —	4 18	
<i>Scytosiphon lomentaria</i>	W. Baltic. Spring	10	700	—	8	
<i>Ectocarpus confervoides</i>	W. Baltic. Spring	10	200	—	5	

<i>Laminaria saccharina</i>	NE Greenland, Young Sound. New leaf blades. June, 10 m, under ice August, open water	1.8	—	35	2	138
	2.5 m depth	0	—	170	22	
	10 m depth	0	—	17	4.2	
<i>Laminaria solidungula</i>	Alaskan High Arctic. Summer	2	—	38-46	—	340
<i>Dictyosiphon foeniculaceus</i>	N. Baltic	14	300	—	18	1430
<i>Pilayella littoralis</i>	N. Baltic	14	200	—	20	
		4	100	—	—	
<i>Macrocystis integrifolia</i>	Vancouver I., BC, Canada, September	13	80	50	—	1256
<i>M. pyrifera</i>	S. Calif., USA. March-August	16-21	300	140-300	—	446
<i>Nereocystis luetkeana</i>	Vancouver I., BC, Canada.					1463
	February	9.5	—	22	—	
	September	14	—	64	—	
Fucoid-dominated macroalgal community	South Australia	19	642	214	34	223
	Summer	15	447	149	8	
	Winter					
<i>Rhodophyta</i>						
<i>Dumontia incrassata</i>	W. Baltic. Winter	5	100	—	5	691
	Spring	10	500	—	8	
<i>Phycodrys rubens</i>	W. Baltic. Spring	10	200	—	5	

Table 10.1 (cont.)

Species or plant type	Location, season	Temperature °C	Irradiance, $\mu\text{mol quanta (PAR) m}^{-2} \text{ s}^{-1}$			Reference
			At saturation	At onset of saturation $E_k$	At compensation point	
<i>Phycodrydrys rubens</i>	Summer	20	200	—	14	
<i>Polysiphonia nigrescens</i>	W. Baltic, Spring	10	400	—	7	
	Autumn	15	300	—	24	
<i>Ceramium tenuicorne</i>	N. Baltic	11	100	—	—	1430
<i>Rhodobryopsis confervoides</i>	N. Baltic	4, 10	40	—	—	
<i>Chondrus crispus</i>	Woods Hole, Mass., USA.	23	120	60	—	1101
<i>Porphyras umbilicatis</i>	Woods Hole, Mass., USA. Summer	23	250	90	—	
<b>Coral</b>						
<i>Stylophora pistillata</i>	Sinai, Egypt	28	600–2000	—	350	378
High light form		28	200	—	40	
Low light form		28	1400–1800	780–1060	60–105	
Coral reef algal turf	Virgin Islands, Caribbean Sea, Jul, Oct, Nov, Dec					209

different  $E_d$  values at intervals of only 10 to 15 s. *ETR* versus  $E_d$  curves obtained in this way are often referred to as *rapid light curves* (RLC). Although an RLC looks very like a classical  $P$  versus  $E_d$  curve, it is not the same since the cells have not been allowed to adapt to each actinic light intensity before the rate measurement is taken. Hawes *et al.* (2003), using PAM fluorometry to study photosynthesis in submerged meadows of the quillwort, *Isoetes alpinus*, in Lake Wanaka, New Zealand, found that for plants at 7 m depth the  $E_k$  value obtained from an RLC ( $117 \mu\text{mol photons m}^{-2} \text{s}^{-1}$ ) was markedly lower than that obtained ( $164 \mu\text{mol photons m}^{-2} \text{s}^{-1}$ ) from leaves adapted to the varying ambient irradiance during the day. Ralph and Gademann (2005) offer suggestions as to how RLCs may usefully be interpreted.

A number of attempts have been made to find mathematical expressions that give a reasonable fit to the empirical curves relating  $P$  to  $E_d$ . Since it is a fact of observation that for any given phytoplankton population the curve will exhibit a fairly well-defined initial slope and a maximum, asymptotically approached, value of  $P$ , the values of  $\alpha$  and  $P_m$  being characteristic of that population, then we may reasonably anticipate that the relationship we are seeking will express  $P$  as a function of  $\alpha$  and  $P_m$ , as well as  $E_d$ . Furthermore the relationship will be such that  $P = f(\alpha, P_m, E_d)$  reduces to  $P = \alpha E_d$  as  $E_d$  tends to zero, and approaches  $P = P_m$  as  $E_d$  tends to infinity. Jassby and Platt (1976) tested eight different expressions that have at various times been proposed, against 188  $P$  versus  $E_d$  curves measured for marine phytoplankton in coastal Nova Scotia waters. The two that fitted best were

$$P = \frac{P_m \alpha E_d}{(P_m^2 + \alpha^2 E_d^2)^{1/2}} \quad (10.8)$$

originally (in a somewhat different form) proposed by Smith (1936), and

$$P = P_m \tanh(\alpha E_d / P_m) \quad (10.9)$$

proposed by Jassby and Platt (1976), the latter expression giving somewhat the better fit. These two expressions for  $P$  have been chosen simply on the basis of goodness of fit to the observations: they are not based on any assumptions about the mechanisms of photosynthesis.

There is a third, equally simple, equation

$$P = P_m \left[ 1 - e^{-\frac{\alpha E_d}{P_m}} \right] \quad (10.10)$$

originally proposed by Webb *et al.* (1974) to describe photosynthesis in the tree species, *Alnus rubra*, and which Peterson *et al.* (1987) have found

to satisfactorily describe  $P$  versus  $E_d$  curves in a wide range of phytoplankton systems that can be given a plausible rationale in terms of the mechanism of photosynthesis. By application of simple Poisson distribution statistics to the capture of photons by the photosynthetic unit per unit of time  $t$ , where  $t$  is the turnover time, and assuming that excess photons are not utilized, it can be shown that the rate of photosynthesis is proportional to  $(1 - e^{-m})$  where  $m$  is the mean number of incident photons captured by the photosynthetic unit in time  $t$ .<sup>1050</sup> Since  $m$  must be proportional to the incident flux,  $E_d$ , it is clear that eqn 10.10, or its alternative version

$$P = P_m \left[ 1 - e^{-\frac{E_d}{E_k}} \right] \quad (10.11)$$

(since  $P_m/\alpha = E_k$ ), is in accordance with this simple mechanistic model.

Equations 10.8 to 10.11 describe the variation of  $P$  with  $E_d$  only up to the establishment of saturation; they do not encompass the decline in  $P$  at higher values of  $E_d$ . Platt *et al.* (1980) have obtained an empirical equation that describes the photosynthetic rate of phytoplankton as a single continuous function of available light from the initial linear response up to and including photoinhibition.

### Photoinhibition

The inhibition of photosynthesis at high light intensities must be taken into account in ecological studies, since the intensities typically experienced in the surface layer of natural waters in sunny weather are in the range that can produce photoinhibition. Indeed if the depth profile of phytoplankton photosynthetic activity is measured by the suspended bottle method in inland or marine waters, a noticeable diminution in the specific photosynthetic rate or the rate per unit volume is commonly, although not invariably, observed near the surface. Figure 10.4 shows examples of this surface inhibition of photosynthesis in a coastal and an inland water. With increasing depth and diminishing light intensity, photoinhibition lessens and the maximum, light-saturated but not inhibited, photosynthetic rate is achieved. With further increase in depth, irradiance falls to the point at which light intensity becomes limiting and from here on the photosynthetic rate diminishes roughly exponentially with depth approximately in parallel with irradiance.

Many, but not all, macrophyte species also show inhibition of photosynthesis when exposed to light intensities in the range of full sunlight,

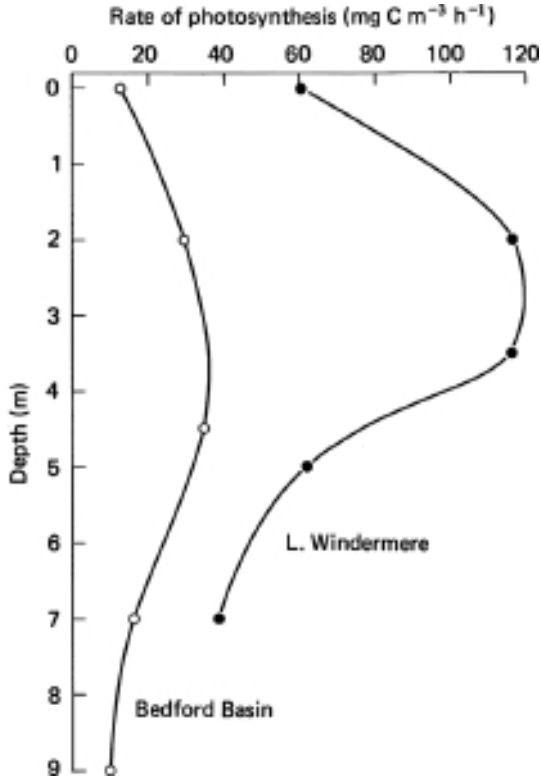


Fig. 10.4 Depth profiles of phytoplankton photosynthetic rate per unit volume of water. The curves are for an inland water (Lake Windermere, England; plotted from data of Belay, 1981, assuming a photosynthetic quotient of 1.15), and a coastal water (Bedford Basin, NS, Canada; plotted from data of Marra, 1978).

and this is especially the case for algae taken from greater depths.<sup>517,1162</sup> Ecologically, however, this phenomenon is of less significance since any given macrophyte species is generally to be found growing at a depth where the light intensity is one to which it is well adapted (Chapter 12), whereas phytoplankton are circulated within a range of depths by water movement. Some photoinhibition nevertheless sometimes occurs in macrophytes in shallow waters in the middle part of the day.<sup>517</sup> Marine macrophytic algae of the intertidal zone are intermittently exposed to very high light intensities. At irradiance values equivalent to full sunlight some of these species show no inhibition, but others are partially inhibited.<sup>691</sup> In the coral, *Stylophora pistillata*, in the Gulf of Aqaba (Red Sea), Winters *et al.* (2003) using *in situ* PAM fluorescence

measurements, found a marked midday depression (63%) of effective quantum yield in coral growing at 2 m depth, but only an 8% depression in coral growing at 11 m.

Inhibition of photosynthesis by high light intensities takes time to develop. In the case of phytoplankton populations from Lake Ontario, Canada, the decline in photosynthetic activity began after about 10 min exposure.<sup>537</sup> Measurements of the time course of photosynthesis by populations of the diatom *Asterionella* in bottles suspended at the surface of a Welsh lake indicated that the inhibitory effect was small during the first hour but became significant during the second hour.<sup>91</sup> The higher the temperature at a given light intensity, the more rapidly inhibition ensues.<sup>537</sup> In the case of laboratory cultures of *Asterionella* grown at 18°C and 200  $\mu\text{mol photons m}^{-2} \text{s}^{-1}$ , exposure to 2000  $\mu\text{mol photons m}^{-2} \text{s}^{-1}$  ( $\sim$  full sunlight) for 1 h at 18° and 25°C reduced the subsequently measured photosynthetic rate by about 10 and 50%, respectively.<sup>92</sup>

Phytoplankton can recover from the inhibitory effects of intense light if they are transferred to a lower light intensity.<sup>470</sup> The longer the exposure to bright light, the longer the recovery takes. In the case of *Asterionella* populations from a Welsh lake, recovery from 2 h exposure to bright sunlight was complete after 4 h in low light intensity: after 6 h bright sunlight, which reduced photosynthetic rate by 70%, recovery took 20 h.<sup>91</sup>

The mechanism of photoinhibition has been studied in most detail in higher plants. Jones and Kok (1966) measured the action spectrum of photoinhibition of electron transport in spinach chloroplasts. The spectrum showed its main activity in the ultraviolet (UV) region with a peak at 250 to 260 nm. Photoinhibition also occurred in the visible region but with a very much lower quantum efficiency. Between 400 and 700 nm, the action spectrum followed the absorption spectrum of chloroplast pigments, with a distinct chlorophyll peak at 670 to 680 nm. The lesion appears primarily to affect the light reactions of photosynthesis by damaging the reaction centre of photosystem II.<sup>265,266,230</sup>

The shape of the action spectrum in the UV region suggests that plastoquinone or some other quinone functional in the reaction centre may be the sensitive molecule so far as UV inhibition is concerned. The primary site of damage to the photosynthetic system by UVB appears to be photosystem II, suggesting that it is  $Q_A$ , the quinonoid primary electron acceptor of photosystem II that is the crucial target. The shape of the action spectrum in the visible region indicates that at very high light intensities some of the energy absorbed by the photosynthetic pigments

themselves is transferred to a sensitive site – not necessarily the same site as that affected by UV – where it causes damage.

Although detailed studies on the basis of photoinhibition of algal photosynthesis have not been carried out, the most plausible and economical hypothesis is that the mechanism is the same as in higher plants. For oceanic phytoplankton, the observed photoinhibition was found to vary linearly with the daily biological dose calculated using the Jones and Kok action spectrum.<sup>1247</sup> In the surface layer of clear ocean waters, 50% of the photoinhibitory dose is at wavelengths less than 390 nm; in moderately productive waters ( $0.5 \text{ mg chl } a \text{ m}^{-3}$ ) at 10 m depth, 50% of the photoinhibitory dose is at wavelengths less than 430 nm.<sup>1243</sup> Thus, for oceanic waters we may attribute about 50% of the photoinhibition to UV and about 50% to visible light. Field measurements by Smith *et al.* (1992) in the Bellingshausen Sea in the austral spring of 1990 indicated that primary production in the Antarctic marginal ice zone was 6 to 12% inhibited by the increased UV flux resulting from ozone depletion. In the giant kelp, *Macrocystis pyrifera*, Clendennen *et al.* (1996) found that doses of UV that reduced photosynthesis by 50% caused a substantial reduction in the number of functional photosystem II centres, and impaired energy transfer from antenna pigments (fucoxanthin, chlorophyll *a*, chlorophyll *c*) to photosystem II, but had no effect on photosystem I, indicating that in this phaeophyte species, as in spinach, photosystem II is the primary site of damage. The 32 kDa D1 protein of photosystem II, which contains the  $Q_B$  plastoquinone-binding site, undergoes continuous rapid turnover in the light, at a rate which increases with light intensity. Greenberg *et al.* (1989) found that the quantum yield for degradation was highest in the UVB region of the spectrum, suggesting that enhanced breakdown of this protein may be involved in the sensitivity of photosystem II to UV.

Glacial lakes at higher latitudes, which were formed following the retreat of the glaciers at the end of the last Ice Age,  $\sim 10\,700$  years ago, did not acquire tree cover in their catchments for many centuries, and consequently lacked the supply of dissolved organic matter, with its associated colour, which tree leaves provide. On the basis of palaeoecological analysis (fossil algal pigments, organic matter content) of the sediments of lakes in British Columbia, Canada, Leavitt *et al.* (2003) concluded that algal abundance was depressed ten-fold by UV radiation in the first millennium of lake existence.

Over the course of evolution, some aquatic plants have acquired a degree of protection against UV in the form of the *mycosporine-like amino*

acids (MAAs, Chapter 3), compounds that absorb in the UV with peaks in the 300 to 360 nm region. Their distribution in marine organisms has been reviewed by Shick and Dunlap (2002). They occur in both prokaryotic and eukaryotic phytoplankton, but not all species possess them. Bloom-forming dinoflagellates have a particularly high capacity to form MAAs, and the cellular concentration is many-fold greater in cells grown at high light than in low light.<sup>978</sup> Some diatom species do not accumulate these compounds. Five species of Antarctic diatom in culture showed little or no ability to synthesize MAAs, even when exposed to high levels of UV, in contrast to the Antarctic prymnesiophyte, *Phaeocystis*, which does form these compounds.<sup>281</sup> The marine cyanobacterium, *Trichodesmium*, which forms extensive surface blooms in oligotrophic tropical and subtropical seas, and which is consequently exposed to intense solar radiation, contains particularly high levels of MAAs, among the highest known for free-living phytoplankton.<sup>1319</sup> Among the macrophytes, MAA synthesis is common among the Rhodophytes, but less so among Chlorophytes. Some deep-water red algal species, which would not normally encounter UVB, lack the ability to make MAAs.<sup>590</sup> Phaeophytes do not synthesize MAAs, but may not need to since brown algae contain UV-absorbing phenolic compounds: in the intertidal brown alga, *Cystoseira tamariscifolia*, in southern Spain, Abdala-Diaz *et al.* (2006) found the level of phenolic compounds in the thallus to increase about four-fold as daily integrated irradiance increased from February to June, and then to decrease by nearly 50% as irradiance decreased from June to November. In those algae that can make MAAs, there is a general tendency for the amounts formed to increase with UV exposure. In coral reefs the concentration of MAAs within the coral colonies decreases with depth.<sup>337</sup>

Aquatic yellow substances absorb strongly in the UV. We may therefore expect photoinhibition to be less apparent in the more coloured waters: this has been observed to be the case in highly productive tropical oceanic waters with high levels of gilvin.<sup>735</sup> By the same token it seems likely that photoinhibition in the more highly coloured (i.e. most inland) waters is caused mainly by the visible (400–700 nm) component of the solar radiation.

In addition to that photoinhibition which is due to direct damage to the reaction centres, and which takes some hours to repair, there is another kind which comes into operation very quickly in intense light, and which is reversed relatively quickly (in a matter of minutes rather than hours) in the dark. This process, which involves reversible changes in

the carotenoid composition of photosystem II, referred to as the *xanthophyll cycle*,<sup>1482,303,1021</sup> can be regarded as a useful adaptive response of the photosynthetic system to excessively intense light rather than a symptom of internal damage. In higher plants and most members of the Chlorophyta, and in the Phaeophyta, one of the antenna pigments feeding energy to the reaction centre of photosystem II is the diepoxide carotenoid, violaxanthin. When the photosystems are absorbing light energy at a rate approaching the maximum at which the photochemically generated electrons can be used for CO<sub>2</sub> reduction, the internal pH of the thylakoid lumen falls markedly. This activates the enzyme, violaxanthin de-epoxidase, which removes first one of the epoxy O atoms, to give the monoepoxide, antheraxanthin, and then removes the other to give the non-epoxide carotenoid, zeaxanthin. Energy absorbed by zeaxanthin is not transferred to the photosystem II reaction centre and is, instead, dissipated as heat. When the cells are transferred to the dark, the intralumenal pH rises and a different enzyme, an epoxidase, is brought into play, which brings about the oxidation of zeaxanthin, by the addition of two epoxy O atoms, reconverting it to violaxanthin. In non-green algae, xanthophyll cycles that make use of other carotenoids occur. For example, in the Bacillariophyceae, Chrysophyceae, Haptophyceae and Euglenophyta, interconversion takes place between the monoepoxide, diadinoxanthin (Fig. 8.12f), and the non-epoxide, diatoxanthin.

In the algae generally, both phytoplankton and benthic, the proportion of total xanthophyll existing in the photosynthetically non-functional, photoprotective form, such as zeaxanthin, increases with the light intensity in their environment, and changes with ambient irradiance during the day. In the case of the floating pelagic phaeophyte, *Sargassum natans*, in the gulf of Mexico, Schofield *et al.* (1998) found that the violaxanthin:zeaxanthin ratio fell from  $\sim 4$  at 04:00 h to  $\sim 1$  at midday, and then rose again to  $\sim 6$  by 22:00 h. The microphytobenthos of tidal mudflats adjusts the state of its xanthophyll pool when it becomes exposed to full sunlight at low tide. In the mudflats of the estuary of the River Barrow (Ireland), where the microphytobenthic community is dominated by diatoms, Van Leeuwe *et al.* (2008) found that whereas diatoxanthin could hardly be detected at 09:00 h immediately after emersion, the diatoxanthin/(diatoxanthin + diadinoxanthin) ratio had risen to  $\sim 0.2$  at 10:00 h, and reached its maximum value of just over 0.3 at midday. In phytoplankton populations from a large number of stations in the Arabian Sea and coastal waters around Vancouver Island (Canada), Stuart *et al.* (1998) found a strong inverse relationship between the proportion of non-photosynthetic

carotenoids, such as zeaxanthin and diatoxanthin, and the chlorophyll concentration, suggesting that the small cells that are characteristic of oligotrophic waters have a higher proportion of photoprotective xanthophyll pigments. In phytoplankton sampled from depths between 5 and 75 m in the NW Atlantic Ocean near the continental shelf break, Prieto *et al.* (2008) found a significant positive correlation between the proportion of photoprotective carotenoids and the irradiance of PAR to which the cells were exposed at the time of collection.

Depth profiles of phytoplankton photosynthesis, such as those in Fig. 10.4, determined by the suspended bottle method, tend to overestimate the extent to which photoinhibition diminishes primary production.<sup>537,867,855</sup> In nature the phytoplankton are not forced to remain at the same depth for prolonged periods. Some, such as dinoflagellates and blue-green algae, can migrate to a depth where the light intensity is more suitable (see §12.6). Even the non-motile algae will only remain at the same depth for extended periods under rather still conditions. Wind blowing across a water surface induces circulatory currents known as Langmuir cells, after the eminent physical chemist, Irving Langmuir, who first studied them.<sup>765</sup> Langmuir cells are horizontal tubes (roll vortices) of rotating water, their axes aligned approximately parallel to the wind direction (Fig. 10.5). Adjacent tubes rotate in opposite directions and tubes of varying diameter can be present at the same time. The simultaneous occurrence of both wind and waves is necessary for the generation of these roll vortices,<sup>386</sup> but even a light wind over small-amplitude waves can set them going. Cells can have diameters ranging from a few centimetres to hundreds of metres: with a wind speed of  $5 \text{ m s}^{-1}$ , a typical cell might have a diameter of 10 m and a surface speed of  $1.5 \text{ cm s}^{-1}$ .<sup>371</sup> Measurements by Weller *et al.* (1985) from the research platform FLIP, drifting off the coast of southern California, showed that with quite moderate wind speeds (mainly  $1\text{--}8 \text{ m s}^{-1}$ ), downwelling flows typically between  $0.05$  and  $0.1 \text{ m s}^{-1}$  were generated. The mixed layer above the seasonal thermocline was at the time about 50 m deep, and the strongest downwelling flows were observed between 10 and 35 m depth, corresponding to the middle region of the mixed layer. Above and below that region, downwelling flows were generally less than  $0.05 \text{ m s}^{-1}$ , and there appeared to be no downwelling flow in or below the seasonal thermocline.

Thus it will very commonly be the case that phytoplankton are not held in the intensely illuminated surface layer but are slowly circulating throughout the mixed layer. Harris and Piccinin (1977) point out that on the Great Lakes of North America the average monthly wind speed

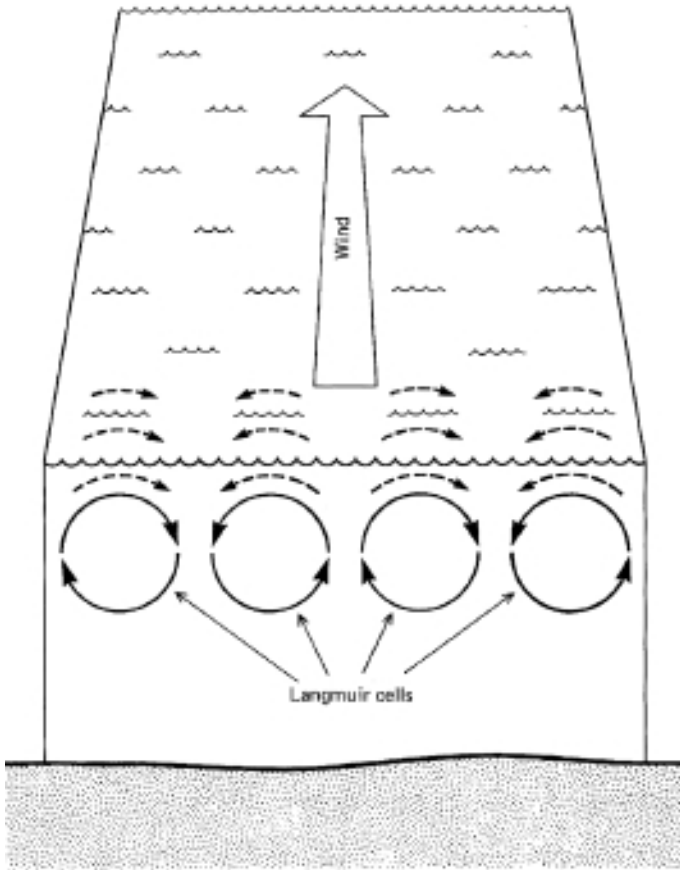


Fig. 10.5 Wind-induced circulatory currents (Langmuir cells) in a water body.

throughout all the winter, and most of the summer period, is sufficient to generate Langmuir cells, and that the residence time at the surface under such conditions will not be long enough for photoinhibition to set in. Within any given month of course, although the average wind speed may be enough to ensure Langmuir circulation, there will be calm periods in which it does not occur. Phytoplankton sampled in winter from the waters of Vineyard Sound (Massachusetts, USA) showed marked photoinhibition in bottles held at surface light intensities, but were in fact well adapted to the average light intensity that they would actually encounter in this well mixed shallow coastal water.<sup>462</sup>

Photoinhibition of phytoplankton is only likely to be of frequent significance in water bodies in which high solar irradiance commonly occurs

together with weak wind activity, leading to the formation of transient shallow temperature/density gradients in the surface layer that impede mixing and thus trap phytoplankton for part of the day in the intense near-surface light field. A well-documented example is the high-altitude (3803 m), low-latitude (16° S) Lake Titicaca (Peru–Bolivia). Vincent, Neale and Richerson (1984) found the typical pattern of thermal behaviour to be that a near-surface thermocline began to form each morning, persisted during the middle part of the day, and was then dissipated by wind mixing and convective cooling towards evening and through the night. While the near-surface stratification persisted, phytoplankton photosynthesis in the upper layer was strongly depressed. That this was not an artifact resulting from phytoplankton immobilization in bottles was shown by the observation that the cellular fluorescence capacity (believed to correlate with the number of functional photosystem II complexes) of phytoplankton samples taken from the water was also greatly reduced. Neale (1987) estimated the diminution of total water column photosynthesis in L. Titicaca on such days to be at least 20%. Elser and Kimmel (1985) have also used measurements of cellular fluorescence capacity to show that in reservoirs in temperate regions (southeastern USA) photoinhibition does occur in the surface layer under calm sunny conditions.

On balance we may reasonably conclude that photoinhibition of photosynthesis in the surface layer, although it exists, is not as frequent a phenomenon as was originally thought. It can significantly reduce areal photosynthesis under sunny, still conditions, but is likely to be of small or no significance when there is even a light wind. Underestimates of primary production resulting from the use of stationary bottles are likely to be more serious in oligotrophic waters requiring long incubation times than in productive waters. It should be noted, however, that circulation does not by any means always increase primary production: as we shall discuss more fully in the next chapter, circulation through too great a depth can diminish total photosynthesis by keeping the cells for significant periods in light intensities too low for photosynthesis.

### **10.3 Efficiency of utilization of incident light energy**

Of the light energy incident on the water surface, only a small fraction is converted to chemical energy in the form of aquatic plant biomass. We shall now consider the reasons why this is so.

The first mode by which energy is lost is reflection at the surface. As we saw earlier (§2.5, Table 2.1), however, such losses are small. For that range of solar angles at which most aquatic primary production takes place, only 2 to 6% of the incident light is lost by surface reflection. Thus the main causes of inefficiency of light utilization are to be found beneath the water surface.

In shallow water bodies (very shallow in coloured and/or turbid waters; moderately shallow in clear waters) substantial amounts of light reach the bottom. Some is absorbed, some reflected, the proportion depending on the optical characteristics of the substrate. Of the bottom-reflected light, a fraction will succeed in passing up through the water column again and escaping through the surface. Thus in shallow waters, bottom absorption and bottom reflection, followed by surface escape, are mechanisms preventing utilization of some of the light in photosynthesis. The light lost can be anything from a trivial proportion up to nearly 100% in, say, very shallow clear water over a white sandy bottom. Our main concern here, however, is with optically deep waters in which the fraction of the incident light that penetrates to the bottom is negligible. In such waters, most of the light that penetrates the surface is absorbed within the aquatic medium. A fraction of the light, however, usually small, is back-scattered upwards within the water (see §6.4) and some of this succeeds in passing up to, and out through, the surface. Combining data for the irradiance reflectance just beneath the surface (§6.4) with the fact that about half the upwelling flux is reflected down again at the water–air boundary,<sup>41</sup> we may conclude that the amount of incident PAR lost in this way is 1 to 2.5% in oceanic waters, 1 to 10% in inland waters of low to high turbidity and as little as 0.1 to 0.6% in waters with intense colour but low scattering.

### **Proportion of incident light captured by phytoplankton**

A major factor limiting conversion of solar energy to chemical energy by phytoplankton is, as was pointed out by Clarke (1939), the competition for radiant energy by all the non-living components of the water. We saw in Chapter 3 that the different components of the aquatic medium – water, soluble colour, tripton and phytoplankton – each account for a proportion of the total light absorbed by the water body. We also saw that to obtain an accurate estimate of the amount of PAR captured by each component separately, calculations should be carried out using the absorption coefficients for a series of narrow wavebands followed by

summation across the photosynthetic spectrum. A useful approximation, however, is to first consider the total PAR and then assume that the relative rates of absorption of light by the different components of the aquatic medium are in proportion to their individual contributions to the total vertical attenuation coefficient for downward irradiance of PAR, in accordance with eqn 9.10

$$K_d(\text{PAR}) = K_w + K_G + K_{TR} + K_{PH}$$

For many, perhaps most, waters of interest to limnologists and marine biologists, this assumption will not be unacceptably far from the truth but it does presuppose that absorption rather than scattering is the dominant contributor to each of the partial attenuation coefficients on the right-hand side of eqn 9.10. For  $K_w$  (water),  $K_G$  (gilvin) and  $K_{PH}$  (phytoplankton) this will be true, and when the tripton fraction is strongly coloured (e.g. by insoluble humic material) it will also be true for  $K_{TR}$ . If, however, the tripton fraction is high in concentration so that  $K_{TR}$  is high, but consists of mineral particles low in intrinsic colour so that  $K_{TR}$  is made up mainly of the scattering contribution (see §6.8, eqn 6.31), then the assumption that relative rates of absorption are proportional to the partial vertical attenuation coefficients will be seriously in error.

Nevertheless, for waters other than the kind we have just described, the fraction of the total absorbed light that is captured by the phytoplankton is, with this approximate treatment, given by

$$\frac{K_{PH}}{K_d(\text{PAR})} = \frac{[Chl]k_c}{K_w + K_G + K_{TR} + [Chl]k_c} = \frac{[Chl]k_c}{K_{NP} + [Chl]k_c} \quad (10.12)$$

where  $K_{NP}$  (which is equal to  $K_w + K_G + K_{TR}$ ) is the vertical attenuation coefficient due to all non-phytoplankton components,  $[Chl]$  is the phytoplankton concentration ( $\text{mg chl } a \text{ m}^{-3}$ ) and  $k_c$  is the specific vertical attenuation coefficient per unit phytoplankton concentration. Thus the extent to which the phytoplankton succeed in competing with other components of the medium for the available quanta depends on the relative size of  $[Chl]k_c$  and  $K_{NP}$ . The range of possibilities is limitless but we shall consider a few specific examples. We shall take  $0.014 \text{ m}^2 \text{ mg}^{-1}$  as a typical mid-range value of  $k_c$  (see Table 9.1). Table 10.2 lists some values for the proportion of absorbed PAR captured by phytoplankton in a number of hypothetical (but typical) water bodies ranging from very pure oceanic water with  $K_{NP}$  not much greater than that due to pure water ( $K_w = 0.03 - 0.06 \text{ m}^{-1}$ ), to a quite highly coloured,

Table 10.2 *Proportion of total absorbed PAR captured by phytoplankton in idealized water bodies of different types. Calculations carried out using eqn 10.12 and assuming  $k_c = 0.014 \text{ m}^2 \text{ mg chl a}^{-1}$ .  $K_{\text{NP}}$  is the vertical attenuation coefficient due to all non-phytoplankton material.*

Type of water body	$K_{\text{NP}}$ ( $\text{m}^{-1}$ )	Phytoplankton ( $\text{mg chl a m}^{-3}$ )	Proportion of absorbed PAR captured by phytoplankton (%)	Proportion of absorbed PAR captured by non-phytoplankton material (%)
Clear oceanic	0.08	0.2	3.4	96.6
		0.5	8.0	92.0
		1.0	14.9	85.1
Coastal	0.15	1.0	8.5	91.5
		2.0	15.7	84.3
		4.0	27.2	72.8
Clear lake, limestone catchment	0.4	4.0	12.3	87.7
		8.0	21.9	78.1
		12.0	29.6	70.4
Productive lake, coloured water	1.0	8.0	10.1	89.9
		16.0	18.3	81.7
		32.0	30.9	69.1
Oligotrophic lake, coloured water	2.0	64.0	47.3	52.7
		1.0	0.7	99.3
		2.0	1.4	98.6
		4.0	2.7	97.3

but productive, inland water. Very approximate though these calculations are, they do show that the share of the available quanta collected by the phytoplankton can vary from a few per cent in the less productive waters, to well over 40% in highly productive systems. They also emphasize the point that quite dilute algal populations can collect a substantial proportion of the quanta, provided the background absorption is low.

Some calculations of this type have been carried out for real water bodies. Dubinsky and Berman (1981) estimated that in the eutrophic Lake Kinneret (Sea of Galilee) the proportion of the absorbed quanta captured by phytoplankton (mainly the dinoflagellate *Ceratium*) varied from about 4 to 60% as the algal concentration rose from about 5 to 100  $\text{mg chl a m}^{-3}$ . For the eutrophic, blue-green-algal-dominated Halsted Bay, Lake Minnetonka, USA, Megard *et al.* (1979) calculated

that the proportion of absorbed PAR collected by the algae rose from about 8 to 80% as the phytoplankton concentration increased from about 3 to 100 mgchl  $a\text{ m}^{-3}$ . From the data of Talling (1960) these workers estimated that for Lake Windermere (*Asterionella*-dominated), England, which has relatively low background absorption, the proportion of absorbed PAR collected by the algae rose from about 5 to 25% over the population density range of 1 to 7 mgchl  $a\text{ m}^{-3}$ . For the eutrophic, shallow (and therefore turbid) Lough Neagh, Ireland, Jewson (1977) estimated that phytoplankton accounted for about 20% of the absorbed light at the lowest population level (26.5 mgchl  $a\text{ m}^{-3}$ ) and 50% at the highest (92 mgchl  $a\text{ m}^{-3}$ ). In mesotrophic Lake Constance (Germany), Tilzer (1983) calculated fractional light absorption by phytoplankton to vary between about 4 and 70% over a two-year period in which chlorophyll  $a$  levels varied between about 1 and 30  $\text{mg m}^{-3}$  (Fig. 11.8).

As we saw in the previous chapter, in the sea, where the waters are deep and usually with little dissolved yellow colour, and the light field with increasing depth becomes increasingly confined to the blue-green (400–550 nm) spectral region, the specific effective absorption coefficient of the phytoplankton for PAR,  $\bar{a}_{\phi}^*(z)$  (§9.4 and below), also increases with depth. Where, as is normally the case in the ocean, there is a layer of increased phytoplankton concentration (the deep chlorophyll maximum, §11.1) near the bottom of the euphotic zone, the combination of increased pigment concentration and enhanced light-harvesting efficiency leads to a great increase in the proportion of the total light absorption that is carried out by the phytoplankton. In the Pacific Ocean, off southeastern Japan, Kishino *et al.* (1986) found the fractional light absorption by phytoplankton to increase from 1.7% at the surface to 40% in the middle of the deep chlorophyll maximum at 75 m.

As we have just discussed, the usefulness of a given light field for photosynthesis is not simply a function of the total intensity of PAR, but is very much determined by how well the spectral distribution of the PAR matches the absorption spectrum of the phytoplankton or other aquatic plants. Morel (1978, 1991) has introduced the concept of *photosynthetically usable radiation*, or PUR, which may be thought of as a modified PAR obtained by weighting the actual PAR across its spectrum for absorbability by the phytoplankton. This can be achieved by multiplying the PAR in each narrow waveband by some dimensionless quantity proportional to phytoplankton absorption in that waveband, and

then summing across the spectrum. As a suitable dimensionless quantity, Morel in fact chose the ratio of the phytoplankton absorption coefficient in any given waveband to the maximum absorption coefficient – which is commonly the value it has at about 440 nm. Photosynthetically usable radiation can thus be defined by

$$PUR(z) = \int_{400}^{700} E_0(\lambda, z) \frac{a_p(\lambda, z)}{a_p(\lambda_{\max}, z)} d\lambda \quad (10.13)$$

where  $a_p(\lambda, z)$  and  $a_p(\lambda_{\max}, z)$  are the absorption coefficients at wavelengths  $\lambda$  and  $\lambda_{\max}$  (wavelength of maximum phytoplankton absorption), respectively, of the phytoplankton population existing at depth  $z$  m, and  $E_0(\lambda, z)$  is the scalar irradiance per unit bandwidth ( $\text{nm}^{-1}$ ) at wavelength  $\lambda$  and depth  $z$  m. From the definition of the effective absorption coefficient,  $\bar{a}_p(z)$ , of the phytoplankton for the whole PAR waveband (eqn 10.16, see below) it follows that we can also write

$$PUR(z) = PAR(z) \frac{\bar{a}_p(z)}{a_p(\lambda_{\max}, z)} \quad (10.14)$$

### Efficiency of conversion of absorbed light

Once the light energy is absorbed by the chloroplast pigments of the phytoplankton or aquatic macrophytes it is used, by means of the photosynthetic fixation of  $\text{CO}_2$ , to generate useful chemical energy in the form of carbohydrate. We shall now consider the efficiency of this conversion of excitation energy to chemical energy.

An upper limit to the efficiency is imposed by the nature of the physical and chemical processes that go on within photosynthesis. We saw in [Chapter 8](#) that the transfer of each hydrogen atom from water down the electron transport chain to NADP requires two photons, each driving a distinct photochemical step. The reduction of one molecule of  $\text{CO}_2$  to the level of carbohydrate uses four hydrogen atoms ( $2 \times \text{NADPH}_2$ ) and so requires eight photons. Putting it another way, to convert one mole of  $\text{CO}_2$  to its carbohydrate equivalent (one sixth of a mole of a glucose unit incorporated in starch) requires not less than eight molar equivalents, i.e. 8 moles of photons. The energy in a photon varies with wavelength ( $\varepsilon = hc/\lambda$ ) and so we shall obtain an average value by taking advantage of the observation by Morel and Smith (1974) that for a wide range of water types  $2.5 \times 10^{18}$  quanta of underwater

PAR = 1 J, with an accuracy of better than 10%. We may thus regard typical underwater light as containing 0.24 MJ (megajoules) of energy per mole photons and so 8 moles of photons is equivalent to 1.92 MJ. The increase in chemical energy associated with the photosynthetic conversion of one mole of CO<sub>2</sub> to its starch equivalent is 0.472 MJ. Thus, of the light energy absorbed and delivered to the reaction centres, about 25% is converted to chemical energy as carbohydrate and this is the maximum possible efficiency.

To equate the plant biomass to carbohydrate is an oversimplification, since the aquatic plants also contain protein, lipids and nucleic acids, none of which conform closely in their overall composition to CH<sub>2</sub>O. The biosynthesis of these substances requires additional photosynthetically generated reducing power and chemical energy in the form of NADPH<sub>2</sub> and ATP, and so requires additional light quanta per CO<sub>2</sub> incorporated. The true minimum quantum requirement per CO<sub>2</sub> for growing cells is likely to be about 10 to 12 rather than 8,<sup>1099</sup> which brings the maximum efficiency down to 16 to 20%. Thus the best efficiency we can hope for in the conversion of absorbed light energy to chemical energy in the form of new aquatic plant biomass is about 18%.

The conversion efficiency or quantum yield actually achieved by a given phytoplankton population or macrophyte can be determined from measurements of the photosynthetic rate and the irradiance, provided that information on the light absorption properties of the plant material is available. Using the absorption spectrum, 400 to 700 nm, rates of light absorption for a series of wavebands can be calculated and summed. For example, the rate of absorption of PAR by phytoplankton per unit volume of medium at any given depth,  $z$ , is

$$\frac{d\Phi_p(z)}{dv} = \int_{400}^{700} a_p(\lambda, z) E_0(\lambda, z) d\lambda \quad (10.15)$$

where  $a_p(\lambda, z)$  is the absorption coefficient at wavelength  $\lambda$  of the phytoplankton population existing at depth  $z$  m, and  $E_0(\lambda, z)$  is the scalar irradiance per unit bandwidth (nm<sup>-1</sup>) at wavelength  $\lambda$  and depth  $z$  m.

A useful concept here is that of the effective absorption coefficient of the phytoplankton for the whole PAR waveband. This is defined by

$$\bar{a}_p(z) = \frac{\int_{400}^{700} a_p(\lambda, z) E_0(\lambda, z) d\lambda}{\int_{400}^{700} E_0(\lambda, z) d\lambda} \quad (10.16)$$

and as an alternative to eqn 10.15 we can therefore write

$$\frac{d\Phi_p(z)}{dv} = \bar{a}_p(z) E_0(\text{PAR}, z) \quad (10.17)$$

The specific absorption coefficient of the phytoplankton for PAR,  $\bar{a}_\phi^*(z)$ , is defined by substituting  $a_\phi^*(\lambda, z)$  for  $a_p(\lambda, z)$  in eqn 10.16: also  $\bar{a}_p(z) = [\text{Chl}] \bar{a}_\phi^*(z)$  so that

$$\frac{d\Phi_p(z)}{dv} = [\text{Chl}] \bar{a}_\phi^*(z) E_0(\text{PAR}, z) \quad (10.18)$$

In any attempt to calculate the rate of energy absorption by phytoplankton (and, by implication, quantum yield – see below) with eqn 10.18, using estimated values of  $\bar{a}_\phi^*(z)$  the fact that, as we saw earlier, the effective specific absorption coefficient of the phytoplankton for PAR can vary markedly with depth must be taken into account.

It is often more convenient to work in terms of downward, rather than scalar, irradiance, but  $E_0$  is always greater than  $E_d$  (see Fig. 6.10, §6.5) by a factor that depends on the angular structure of the light field at that particular depth. Following Morel (1991) we shall indicate this ‘geometrical’ correction factor by  $g$ . This correction is not trivial: for wavelengths in the photosynthetically important 400 to 570 nm region, and for phytoplankton concentrations in the 0.1 to 1.0 mg chl  $a \text{ m}^{-3}$  range, Morel (1991) calculated values of  $g$  varying between 1.1 and 1.5. Using the geometrical correction factor we can now write another expression for the rate of absorption of PAR by phytoplankton per unit volume of medium at depth  $z \text{ m}$ , namely

$$\frac{d\Phi_p(z)}{dv} = \int_{400}^{700} a_p(\lambda, z) E_d(\lambda z) g(\lambda, z) d\lambda \quad (10.19)$$

where  $E_d(\lambda, z)$  is the downward irradiance per unit bandwidth ( $\text{nm}^{-1}$ ) at wavelength  $\lambda$  and depth  $z \text{ m}$ .

An alternative approach starts from the fact that the rate of absorption of radiant energy per unit volume at depth  $z \text{ m}$  is given by

$$\frac{d\Phi(z)}{dv} = K_E \vec{E}(z) \quad (10.20)$$

where  $\vec{E}(z)$  is the *net* downward irradiance at depth  $z \text{ m}$  and  $K_E$  is the vertical attenuation coefficient for net downward irradiance. From this it can readily be shown that

$$\frac{d\Phi(z)}{dv} = K_d E_d(z) \left[ 1 - R(z) \left( \frac{K_u}{K_d} \right) \right] \approx K_d E_d(z) [1 - R(z)] \quad (10.21)$$

where  $K_u$  is the vertical attenuation coefficient for upward irradiance and (as is usually the case)  $K_u \approx K_d$ , and  $R(z)$  is irradiance reflectance ( $E_u[z]/E_d[z]$ ). If we choose to ignore the contribution of the upwelling flux – a reasonable approximation in most marine waters, with reflectance values of only a few per cent, but not in turbid waters – then we can write

$$\frac{d\Phi(z)}{dv} \approx K_d E_d(z) \quad (10.22)$$

for the total rate of absorption of energy per unit volume, as a function of downward irradiance. To calculate the rate of absorption of energy by phytoplankton we make use of the fact that in any given waveband the proportion of the absorbed energy that is captured by the phytoplankton is  $a_p(\lambda, z)/a_t(\lambda, z)$ , the ratio of the absorption coefficient due to phytoplankton to the total absorption coefficient, at that wavelength. The rate of absorption of PAR by phytoplankton per unit volume of medium, as a function of downward irradiance is therefore given by

$$\frac{d\Phi_p(z)}{dv} = \int_{400}^{700} [a_p(\lambda, z)/a_t(\lambda, z)] K_d(\lambda, z) E_d(\lambda, z) d\lambda \quad (10.23)$$

where  $K_d(\lambda, z)$  is the vertical attenuation coefficient for downward irradiance at wavelength  $\lambda$  and depth  $z$  m. In eqns 10.15, 10.16 and 10.19 we can, of course, replace  $a_p(\lambda, z)$  with  $[Chl](z) a_\phi^*(\lambda, z)$ , the product of the phytoplankton concentration ( $\text{mg chl } a \text{ m}^{-3}$ ) and the specific absorption coefficient ( $\text{m}^2 \text{ mg chl } a^{-1}$ ) at wavelength  $\lambda$ , of the phytoplankton population present at depth  $z$  m.

To arrive at an accurate determination of photosynthetic efficiency, the spectral variation both of the light field and of absorption by the biomass should be taken into account, along the lines indicated above, and numerous workers have sought to do this.<sup>111,244,376,727,728,778,940,1190</sup>

Useful information can, however, still be obtained from photosynthesis measurements combined with broad-band irradiance data. Since, as we saw earlier, the fraction of the total absorbed PAR that is captured by the phytoplankton is approximately  $[Chl]k_c/K_d(\text{PAR})$ , then from eqn 10.22 we can write

$$\frac{d\Phi_p(z)}{dv} \approx [Chl]k_c E_d(\text{PAR}, z) \quad (10.24)$$

for the rate of absorption of light energy by phytoplankton per unit volume, at depth  $z$  m. Estimates of energy absorption by phytoplankton (and consequently of quantum yield – see below) made with eqn 10.24

can, however, be grossly inaccurate if the variation of  $k_c$  with the type of phytoplankton present, the background colour of the water and the depth ( $k_c$  varying with depth in a similar manner to  $\bar{a}_\phi^*$ ) are not taken into account.

It is useful in dealing with the present topic to have a specific symbol for the rate of absorption of PAR by phytoplankton per unit volume of medium at a given depth. We here introduce the symbol  $\chi$ , defined by

$$\chi(z) = \frac{d\Phi_p(z)}{dz} \quad (10.25)$$

where  $\chi(z)$  can have the units  $\text{W m}^{-3}$ , or  $\text{MJ m}^{-3} \text{h}^{-1}$ , or quanta (or  $\mu\text{moles photons}) \text{m}^{-3} \text{s}^{-1}$ . We can, in addition, define  $\chi^*(z)$  to be the *specific* rate of absorption of PAR by phytoplankton per unit volume at depth  $z \text{ m}$ , i.e. the rate per unit phytoplankton concentration, expressed in terms of  $\text{mg chl a m}^{-3}$ . Thus  $\chi(z) = [\text{Chl}] \chi^*(z)$ , and  $\chi^*(z)$  has the units  $\text{W mg chl a}^{-1}$ , or quanta (or  $\mu\text{moles photons}) \text{s}^{-1} \text{mg chl a}^{-1}$ . For any given aquatic system,  $\chi(z)$  is determined by using one or other of eqns 10.15, 10.17, 10.23 and 10.24, or some equivalent procedure.

To obtain the energy conversion efficiency at a given depth we divide the rate of accumulation of chemical energy per unit volume at that depth by the rate of absorption of light energy by phytoplankton per unit volume. Given a specific photosynthetic rate of  $P^*(\text{CO}_2)$  moles  $\text{CO}_2$  fixed  $\text{mg chl a}^{-1} \text{h}^{-1}$ , and an increase in chemical energy of 0.472 MJ associated with the fixation of each mole of  $\text{CO}_2$ , then the rate of accumulation of chemical energy per unit volume is  $0.472 [\text{Chl}] P^*(\text{CO}_2) \text{ MJ m}^{-3} \text{h}^{-1}$ . Dividing by  $\chi(z)$  we obtain the conversion efficiency

$$\varepsilon_c = \frac{0.472[\text{Chl}]P^*(\text{CO}_2)}{\chi(z)} = \frac{0.472P^*(\text{CO}_2)}{\chi^*(z)} \quad (10.26)$$

$\chi(z)$  being expressed in  $\text{MJ m}^{-3} \text{h}^{-1}$  (quanta measurements can be converted using  $2.5 \times 10^{24}$  quanta  $\equiv 1 \text{ MJ}$ , see above). Alternatively, if  $P^*$  is expressed in terms of  $\text{mg carbon fixed mg chl a}^{-1} \text{h}^{-1}$ ,  $P^*(\text{C})$ , then, since there is an increase in chemical energy of  $3.93 \times 10^{-5} \text{ MJ}$  associated with the fixation of  $1 \text{ mg C}$ , the conversion efficiency is given by

$$\varepsilon_c = \frac{3.93 \times 10^{-5}[\text{Chl}]P^*(\text{C})}{\chi(z)} = \frac{3.93 \times 10^{-5}P^*(\text{C})}{\chi^*(z)} \quad (10.27)$$

Another way of expressing the efficiency of conversion of absorbed light energy to chemical energy by aquatic plants is the quantum yield,  $\phi$ . This is defined to be the number of  $\text{CO}_2$  molecules fixed in biomass per

quantum of light absorbed by the plant. Given the quantum requirement per  $\text{CO}_2$  fixed, imposed by the mechanism of photosynthesis (see above), it follows that the quantum yield could never be greater than 0.125, and for growing cells, even under ideal conditions, is unlikely to exceed about 0.1. Quantum yield and per cent conversion efficiency are, of course, linearly related. Allowing 0.472 MJ chemical energy per  $\text{CO}_2$  fixed and 0.24 MJ per mole photons of underwater PAR, we arrive at

$$\varepsilon_c = 1.97\phi \quad (10.28)$$

Equations corresponding to 10.26 and 10.27 can be written for the calculation of quantum yield from  $\chi(z)$  or  $\chi^*(z)$  and specific photosynthetic rate

$$\phi = \frac{[Chl]P^*(\text{CO}_2)}{\chi(z)} = \frac{P^*(\text{CO}_2)}{\chi^*(z)} \quad (10.29)$$

$$\phi = \frac{[Chl]P^*(C)}{12\,000 \cdot \chi(z)} = \frac{P^*(C)}{12\,000 \cdot \chi^*(z)} \quad (10.30)$$

$\chi(z)$  in these equations has the units moles photons  $\text{m}^{-3} \text{h}^{-1}$ .

The quantum yield attained by an aquatic plant is a function of the light intensity to which it is exposed. That this is so is apparent from the variation of specific photosynthetic rate with irradiance (Fig. 10.3). Ignoring for the moment any changes in chloroplast shape or position with light intensity, we may assume that the rate of absorption of quanta is proportional to the incident irradiance. Thus, at any point in the photosynthesis versus irradiance curve the value of  $P/E_d$  (see Fig. 10.3) is proportional to the quantum yield.

For a plant to be able to make efficient use of light quanta being absorbed at a given rate, the activity of the electron transfer components in the thylakoid membranes and of the enzymes of  $\text{CO}_2$  fixation in the stroma must both be high enough to ensure that the excitation energy collected by the light-harvesting pigments is utilized as fast as it arrives at the reaction centres. If this situation exists, then a moderate increase in light intensity, causing a proportionate increase in quantum absorption rate, leads to a corresponding increase in the specific rate of photosynthesis. In the initial, linear, region of the  $P$  versus  $E_d$  curve this is what is happening. Over this range of intensity,  $P/E_d$  is constant and has its highest value, indicating that the plants are achieving their highest conversion efficiency and quantum yield. If the absorption characteristics of the plant are known, then this maximum value of  $P/E_d$  can be used to calculate  $\phi_m$ , the maximum quantum yield.

As the incident light intensity is further increased, the rate of absorption of quanta reaches the point at which excitation energy begins to arrive at the reaction centres faster than it can be made use of by the electron transfer components and/or the CO<sub>2</sub> fixation enzymes. At this stage some of the additional absorbed quanta (over and above those the system can readily handle) are utilized for photosynthesis, and some are not, the energy of the latter being eventually dissipated, mainly as heat. For this reason, in this range of light intensity, increments in  $E_d$  are accompanied by less than commensurate increases in  $P$ , i.e. the slope of the curve progressively diminishes, until eventually the point is reached at which  $\Delta P/\Delta E_d$  becomes zero. In this light-saturated state, the electron transfer and/or CO<sub>2</sub> fixation enzymes (most likely, the latter) are working as fast as they are capable, and so any additional absorbed quanta are not used for photosynthesis at all. From the end of the linear region through to the light-saturated region, since photosynthetic rate does not increase in proportion to irradiance ( $P/E_d$  steadily falls – Fig. 10.3) the quantum yield and conversion efficiency necessarily undergo a progressive fall in value. This is accentuated further if, at even higher light intensities, photoinhibition sets in. If the cells contain photoprotective carotenoids, in which absorbed light energy is dissipated as heat rather than being transferred to the reaction centre, then to the extent that these capture the incident light, the quantum yield must be proportionately reduced at any light intensity.

The characteristic manner in which  $P$  varies with  $E_d$  can, as we saw earlier, be represented mathematically in a number of different ways (eqns 10.8, 10.9, 10.10, 10.11). Since quantum yield and  $P/E_d$  are linearly related, then for each particular form of the function,  $P = f(E_d)$ , there will be a corresponding expression for quantum yield as a function of  $E_d$ , i.e.  $\phi = \text{Constant} \cdot E_d^{-1} \cdot f(E_d)$ . Using the tanh form (eqn 10.9) Bidigare *et al.* (1992) arrived at

$$\phi = \phi_m \frac{E_k}{E(PAR, z)} \tanh \left[ \frac{E(PAR, z)}{E_k} \right] \quad (10.31)$$

and using the exponential form (eqn 10.11) we obtain

$$\phi = \phi_m \frac{E_k}{E(PAR, z)} \left[ 1 - e^{-\frac{E_d(PAR, z)}{E_k}} \right] \quad (10.32)$$

The consequence in natural water bodies of the decrease in quantum yield with increasing light intensity is that quantum yield and conversion efficiency vary markedly with depth, the general tendency being, as might

be expected, for  $\phi$  and  $\varepsilon_c$  to increase with depth.<sup>330,940</sup> Quantum yields in the surface layer in the middle period of the day, when irradiance values are generally above the range corresponding to the linear part of the  $P$  versus  $E_d$  curve, are usually below  $\phi_m$ .

Morel (1978) calculated the quantum yield at a series of depths from  $^{14}\text{CO}_2$  fixation, chlorophyll and light data for a variety of oceanic waters from the highly oligotrophic Sargasso Sea to the productive waters of the Mauritanian upwelling area. In most cases  $\phi$  increased with depth, i.e. with decreasing irradiance. On average, the  $\phi$  values for green eutrophic waters were higher than those observed in blue oligotrophic waters. In the surface layers the  $\phi$  values were mainly in the range 0.003 to 0.012 (equivalent to  $\varepsilon_c$  values of 0.6–2.4%). Kishino *et al.* (1986) found, in the Pacific Ocean southeast of Japan, that quantum yields of photosynthesis were 0.005 to 0.013 at the surface, 0.013 to 0.033 at that depth (10–20 m) where photosynthesis reached its maximum rate in the surface mixed layer, and 0.033 to 0.094 in the deep chlorophyll maximum (~70 m). If, as these authors suggest, we reduce all these values by 20%, as an approximate correction factor for the fact that they are based on measured irradiance, rather than scalar irradiance, values then we obtain quantum yields of 0.004 to 0.01, 0.01 to 0.026, and 0.026 to 0.075, respectively.

In oligotrophic Lake Superior, Fahnenstiel *et al.* (1984) found quantum yields to be very low, ~0.003, at the surface, and to increase with depth, reaching maximum values of 0.031 to 0.052 (corrected for scalar irradiance) at 15 to 25 m. Dubinsky and Berman (1981) estimated that during the spring *Peridinium* bloom in Lake Kinneret (Sea of Galilee),  $\varepsilon_c$  rose from about 5% at the surface to 8.5% at 3 m. In late summer, with a much lower population of different (green) algae,  $\varepsilon_c$  was 2.5% at the surface but rose to about 12% at 5 to 7 m.

The maximum quantum yield that a phytoplankton population, or aquatic macrophyte, can exhibit,  $\phi_m$ , is a parameter of considerable theoretical and ecological interest. On the assumption (see above) that in the linear region of the  $P$  versus  $E$  curve the cells are achieving their maximum efficiency, estimates of  $\phi_m$  are normally obtained from the observed slope,  $P/E$ , commonly referred to as  $\alpha$ , in this region of the curve.

From the equations for  $\phi$  it follows that  $\phi_m$  should be proportional to  $\alpha$ . For example, if  $E$  is  $E_0$ , then from eqns 10.29, 10.25 and 10.18 it follows that  $\phi_m = \alpha/\bar{a}_\phi^*$ . If  $E$  is  $E_d$ , then from eqns 10.29, 10.25 and 10.24 it follows that  $\phi_m = \alpha/k_c$ . The photosynthetic process imposes by its

essential nature a maximum value for  $\phi_m$  of  $\sim 0.1$ , for all photosynthetic systems. On the basis of a critical analysis of literature data, Bannister and Weidemann (1984) have concluded that published values of *in situ*  $\phi_m$  in excess of 0.10 are almost certainly in error. The fact that a  $\phi_m$  value  $\sim 0.1$  is one which any plant species might in principle achieve, and also that  $\alpha$  is linearly related to  $\phi_m$  (since  $\alpha = \bar{a}_\phi^* \phi_m$  or  $k_c \phi_m$ ), has aroused expectations that  $\alpha$  should not vary markedly for a given species in different environments, or from one species to another. Such expectations, however, ignore the extent to which the proportionality factor,  $\bar{a}_\phi^*$  or  $k_c$ , can vary. We saw earlier (Chapter 9) how markedly  $\bar{a}_\phi^*$  varies with the size and shape of the cells or colonies, for example decreasing as the absorbing units become larger or more intensely pigmented. Taguchi (1976), from studies on seven species of marine diatom, found, as might be predicted, that  $\alpha$  decreased with increasing size of the cells. Also, since  $\bar{a}_\phi^*$  and  $k_c$  are expressed per unit chlorophyll *a*, then they can vary markedly in value in accordance with variation in the type of accessory photosynthetic pigments present, and their ratio to chlorophyll *a* (§ 9.5): the resulting changes in shape of the absorption spectrum markedly influence the rate of energy capture from the white light fields normally used in the determination of  $\alpha$ . Welschmeyer and Lorenzen (1981), in a comparison of six species of marine phytoplankton growing exponentially under identical conditions, found that there were no significant differences in  $\phi$ , but there were significant differences in  $\alpha$ : these they attributed to differences in the light absorption efficiency per unit of chlorophyll.

Another problem in the determination of  $\alpha$  values, particularly when we wish to compare different data sets from the literature, is that there is no generally accepted standard for the light source to be used in its measurement. Some workers use natural sunlight, others use tungsten-halogen lamps, while some will use lamps fitted with blue filters. The spectral distribution of the incident light will be quite markedly different in all three cases, with the result that for any given phytoplankton population, with a given absorption spectrum,  $\alpha$  will have a different value for each light source because the effective specific absorption coefficient,  $\bar{a}_\phi^*$ , for the incident PAR will be different for each light source.

Thus, even if we did not expect  $\phi_m$  to vary dramatically with species or environment, we should not expect the same constancy of  $\alpha$ , because of the variability of  $\bar{a}_\phi^*$  and  $k_c$ . Unfortunately this variability in  $\bar{a}_\phi^*$  and  $k_c$ , and the consequent uncertainty in their values, makes the determination of  $\phi_m$  in natural populations, from  $\alpha$ , difficult. The best estimates are undoubtedly those based on full spectral data for phytoplankton

absorption and the underwater light field, and combining eqn 10.29 with  $\chi(z)$  values from eqns 10.15, 10.19 or 10.23.

Some typical values of  $\alpha$  for natural phytoplankton populations, in the units  $\text{mg C mg chl } a^{-1} \text{ h}^{-1}$  ( $\mu\text{moles photons m}^{-2} \text{ s}^{-1}$ )<sup>-1</sup>, are: 0.05 (range 0.007–0.15) for Nova Scotia coastal waters,<sup>1063</sup> 0.06 for nanoplankton (<22  $\mu\text{m}$ ) in the lower Hudson estuary, USA,<sup>859</sup> 0.033 to 0.056 for picoplankton in the Celtic Sea,<sup>649</sup> and 0.024 for diatoms and 0.034 for blue-green algae in eutrophic Lough Neagh, N. Ireland.<sup>641</sup> In the Arabian Sea, Johnson *et al.* (2002) found that  $\alpha$  was  $0.025 \pm 0.011$  in the spring and fall intermonsoon seasons, but rose to  $0.040 \pm 0.016$  in the early Southwest Monsoon, when nitrate levels were elevated.

For reasons that are not fully understood, the maximum quantum yield of phytoplankton populations in the ocean is extremely variable. For example, Prezelin *et al.* (1991) found that in a 200 km transect of a hydrographically variable region of the Southern California Bight, the value of  $\phi_m$  varied over the range  $\sim 0.01$  to 0.06, the variation being found both with distance along the transect through different water masses, and with depth at any given station. Some of this spatial variation may have a genetic base, i.e. it may be due to the presence of taxonomically different phytoplankton populations: diatom-dominated communities in the Southern California Bight had  $\phi_m$  values twice as high as the cyanobacterial picoplankton in the deep chlorophyll maximum.<sup>1190</sup> Some of it may have a physiological basis, due to populations differing in nutritional status, or recent light exposure history. For phytoplankton photosynthesis in the Sargasso Sea, Cleveland *et al.* (1989) found an inverse relationship between  $\phi_m$  – which varied from 0.033 to 0.102 – and distance from the top of the nitracline. Similar results were obtained by Kolber, Wyman and Falkowski (1990) in the Gulf of Maine, and in both cases the conclusion was reached that quantum yield was related to nitrogen flux. Also, in the Arabian Sea, Johnson *et al.* (2002) found that  $\phi_m$  was  $0.020 \pm 0.009$  in the spring and fall intermonsoon seasons, and  $0.051 \pm 0.024$  in the early Southwest Monsoon, when nitrate concentrations were higher. The widespread, and successful prymnesiophyte species, *Phaeocystis pouchetii*, appears to be able to achieve quantum yields close to the maximum. Samples from a massive bloom of this phytoplankton in the northern Greenland Sea achieved values of  $\phi_m$  averaging 0.102.<sup>260</sup>

Babin *et al.* (1996) measured phytoplankton carbon fixation at three sites in the northeast tropical Atlantic, representing typical eutrophic, mesotrophic and oligotrophic regimes. In the eutrophic and mesotrophic

sites the mixed layer extended deeper than the euphotic zone, and photosynthetic parameters were nearly constant with depth,  $\phi_m$  averaging 0.05 and 0.03 in the eutrophic and mesotrophic waters, respectively. At the oligotrophic site, there was a deep chlorophyll maximum (DCM), and  $\phi_m$  varied from  $\sim 0.005$  in the upper, nutrient-depleted, mixed layer to 0.063 below the DCM in this stratified water. Across all the sites  $\phi_m$  was found to roughly covary with nitrate concentration, this factor accounting overall for a two-fold variation in quantum yield.  $\phi_m$  varied inversely with increasing relative concentrations of non-photosynthetic carotenoids, to an extent that could give rise to a three-fold variation in quantum yield.

As well as the spatial variation, there is at any given location in the ocean, a diurnal variation in  $\phi_m$ ,<sup>728,1082,1087</sup> often, but not invariably, involving a decrease in the afternoon. In Lake Constance (Germany), Tilzer (1984) found maximum quantum yield at midday to vary over the range 0.022 to 0.092 throughout the year, but on any given day  $\phi_m$  could vary by up to three-fold, the tendency again being for a diminution in the afternoon.

In five biogeochemical ocean provinces extending across the North Atlantic from the east coast of Canada to the Canary Islands, Kyewalyanga *et al.* (1998) found that the maximum quantum yield of photosynthesis ( $\text{mol C} [\text{mol photons}]^{-1}$ ), averaged over all provinces, in the fall of 1992 ( $\phi_m = 0.032 \pm 0.015$ ) was about twice that in the following spring of 1993 ( $\phi_m = 0.017 \pm 0.007$ ). The photosynthetic parameters of the phytoplankton were found to be more variable between seasons than between provinces. The authors attributed the seasonal differences to the different environmental conditions that prevailed.

### Areal and volumetric efficiencies

We have seen that the efficiency of utilization of the light incident on the aquatic ecosystem for primary production is determined by two main factors: the extent to which the aquatic plants succeed in competing with the other components of the system for the quanta in the underwater light field, and the efficiency with which the absorbed light energy is converted to chemical energy. We shall now consider the overall efficiency that results from the simultaneous operation of these two factors.

The most common and generally useful way of expressing the overall efficiency is as the proportion of the light energy (400–700 nm) incident per  $\text{m}^2$  of water surface that is photosynthetically stored as chemical energy in plant biomass throughout the water column. This we shall refer

to as the areal efficiency,  $\varepsilon_A$ : it is obtained by dividing the areal (integral) photosynthetic rate expressed in energy units (MJ equivalent of photosynthetic assimilate) per  $\text{m}^2$  per unit of time (hour or day), by the total PAR (in MJ) incident per  $\text{m}^2$  of water surface in the same time

$$\varepsilon_A = 0.472P_A(\text{CO}_2)/E_d(\text{on surface}) \quad (10.33)$$

For oceanic waters,  $\varepsilon_A$  values vary by a factor of 100 to 300 from the least to the most productive. Koblents-Mishke (1979) reviewing Russian and other work reported that marine  $\varepsilon_A$  values world-wide ranged from 0.02 to 5%. Morel (1978) reported  $\varepsilon_A$  values (calculated on a daily basis) of about 0.02% for the very oligotrophic Sargasso Sea, 0.02 to 0.07% for the Caribbean Sea (oligotrophic), 0.06 to 0.25% for the moderately productive eastern equatorial Pacific, and 0.4 to 1.66% for the eutrophic Mauritanian upwelling area in the eastern tropical Atlantic. Smith *et al.* (1987), studying primary productivity across a coastal front in the Southern California Bight, found  $\varepsilon_A$  to vary from 1.57% on the cold side of the front where phytoplankton concentration was high ( $\sim 2.5 \text{ mg chl } a \text{ m}^{-3}$ ), down to 0.11% on the warm side of the front where phytoplankton levels were much lower (0.1 to  $0.5 \text{ mg chl } a \text{ m}^{-3}$ ).

Brylinsky (1980) analysed the collected International Biological Programme data for lakes and reservoirs throughout the world. The calculated  $\varepsilon_A$  values for the whole growing season ranged from about 0.002 to 1.0%, most of the values being in the range 0.1 to 1.0%. Talling *et al.* (1973) found high efficiencies in two very productive Ethiopian soda lakes dominated by blue-green algae:  $\varepsilon_A$  based on half-hour incubations at high incident irradiances ranged from 0.5 to 1.6% in Lake Kilotes and from 1.2 to 3.3% in Lake Aranguadi. In the Sea of Galilee (Lake Kinneret), Dubinsky and Berman (1981) found  $\varepsilon_A$  (measured 09:00–12:00 h) to vary from 0.3% in August when the phytoplankton consisted mainly of small chlorophytes, to a maximum of 4% in April during the *Peridinium* (dinoflagellate) bloom.

From literature data for eight lakes covering a wide range of latitude and trophic status, Tilzer, Goldman and De Amezaga (1975) calculated values of  $\varepsilon_A$  ranging from 0.035% in the very oligotrophic, high-altitude Lake Tahoe (California, USA) up to 1.76% in the eutrophic Loch Leven (Scotland). Areal efficiency was strongly correlated with the concentration of algal biomass per unit volume: Tilzer *et al.* considered that the key factor responsible for the variation in  $\varepsilon_A$  in these lakes was the proportion of the total incident light captured by the phytoplankton. Areal efficiency tends to decrease with increasing surface irradiance.<sup>898,1087</sup>

In comparing the efficiency of primary production in different aquatic systems, it is interesting to compare not only the daily production per unit area, as expressed through  $\varepsilon_A$ , but also the relative performance of different phytoplankton populations, per unit phytoplankton biomass. As a measure of this Falkowski (1981) and Falkowski and Raven (2007) proposed the *light utilization efficiency function*,  $\Psi$ , defined by

$$\Psi = \frac{\int_0^D \int_0^{z_{eu}} P_v(z, t) dz dt}{\int_0^{z_{eu}} [Chl](z) dz \cdot \int_0^D E_d(0^+, t) dt} \quad (10.34)$$

where  $P_v(z, t)$  is the volumetric rate of photosynthesis at depth  $z$  and time  $t$ , in  $\text{g C m}^{-3} \text{h}^{-1}$ ,  $z_{eu}$  is the euphotic depth,  $D$  is the daylength in hours,  $[Chl](z)$  is the phytoplankton concentration in  $\text{g chl a m}^{-3}$  at depth  $z$ , and  $E_d(0^+, t)$  is the downward irradiance of PAR on the surface at time  $t$ . In simple terms,  $\Psi$  is the total amount of primary production carried out within a  $1 \text{ m}^2$  water column per day ( $\text{g C m}^{-2} \text{day}^{-1}$ ) divided by the total phytoplankton biomass in that water column ( $\text{g chl a m}^{-2}$ ) and by the total light energy in the form of PAR incident upon the top of the water column in one day ( $\text{mol quanta m}^{-2} \text{day}^{-1}$ ): it thus has the units  $\text{g C (g chl a)}^{-1} (\text{mol quanta})^{-1} \text{m}^2$ . An early analysis of the data then available from various parts of the ocean, by Platt (1986) seemed to indicate a clustering of  $\Psi$  values in the range 0.31 to 0.66  $\text{g C (g chl a)}^{-1} (\text{mol quanta})^{-1} \text{m}^2$ . On the basis of an analysis of the much larger data set now available, Falkowski and Raven (2007), however, found a much greater variability to exist, with  $\Psi$  values ranging from  $\sim 0.1$  to  $\sim 1.5 \text{ g C (g chl a)}^{-1} (\text{mol quanta})^{-1} \text{m}^2$ . They found that  $\Psi$  increased as the average daily irradiance decreased, and that it was lower in low-nutrient regions of the ocean. It appears that the highest values in world oceans are those in the subarctic northwestern Pacific, at the times of phytoplankton blooms.<sup>1216</sup>

In an alternative version of the light utilization efficiency function, proposed by Morel (1991), the rate of photosynthesis and the incident radiant flux are both expressed in energy terms (kilojoules).

$$\Psi^* = \frac{39 P_A(C)}{[Chl]_{total} \cdot E_d(PAR, 0^+)} \quad (10.35)$$

$P_A(C)$  is the areal photosynthetic rate, in  $\text{g C m}^{-2} \text{day}^{-1}$ . The factor, 39, converts g C to its energy equivalent in kilojoules.  $[Chl]_{total}$  is the total phytoplankton biomass in  $1 \text{ m}^2$  water column, and  $E_d(PAR, 0^+)$  is the total light energy in the form of PAR incident upon the top of the water

column in one day expressed in kilojoules.  $\Psi^*$  has the units,  $\text{m}^2 (\text{g chl } a)^{-1}$  and may be referred to as the *chlorophyll-specific cross-section for photosynthesis*.  $\Psi^*$  and  $\Psi$  are related by  $\Psi = 6.174 \Psi^*$ . At a coastal Antarctic region, studied over the period 1991 to 1994, Claustre *et al.* (1997) found a six-fold variation in  $\Psi^*$  with time of year, the minimum occurring in the austral summer (Dec–Feb). They also found a taxonomic dependency of  $\Psi^*$ . For identical chlorophyll content and surface irradiance, the mean value of  $\Psi^*$  was  $0.114 \pm 0.051 \text{ m}^2 (\text{g chl } a)^{-1}$  for diatom blooms, and  $0.053 \pm 0.011 \text{ m}^2 (\text{g chl } a)^{-1}$  when cryptophytes dominated, emphasizing the desirability of having taxonomic information when estimating primary production from irradiance and chlorophyll data. In a region (500 km longitude by 750 km latitude, centred on  $41.5^\circ \text{ N}$ ,  $19^\circ \text{ W}$ ) of the northeast Atlantic, Claustre *et al.* (2005) found  $\Psi^*$  to equal  $0.088 \text{ m}^2 (\text{g chl } a)^{-1}$ , which is about 25% higher than the average for the world's oceans. Looking more closely at how this production was distributed among the different size classes of phytoplankton, they found that carbon storage by the water column was more efficient ( $\Psi^* = 0.135 \text{ m}^2 (\text{g chl } a)^{-1}$ ) with microphytoplankton (20–200  $\mu\text{m}$ ) than with nanophytoplankton (2–20  $\mu\text{m}$ ,  $\Psi^* = 0.089 \text{ m}^2 (\text{g chl } a)^{-1}$ ) or picophytoplankton (<2  $\mu\text{m}$ ,  $\Psi^* = 0.064 \text{ m}^2 (\text{g chl } a)^{-1}$ ). Their observations suggest that when large phytoplankton predominate at the expense of smaller ones, the specific absorption coefficient ( $\bar{a}_c$ ) is, as expected, lower, while other photophysiological properties –  $\alpha$ ,  $P_m$ ,  $\phi_m$  – are higher. They conclude that large phytoplankton (essentially diatoms) are potentially more efficient in carbon storage than any other phytoplankton group, on a chlorophyll *a* or light basis.

A way of expressing the overall efficiency of light utilization, which can provide information about its variation with depth through the water column, is the volumetric efficiency,  $\varepsilon_V$ . We may define this as the proportion of the downwelling light energy (400–700 nm) incident upon the upper surface of any unit volume within a water body which is photosynthetically stored as chemical energy in plant biomass within that volume. A more all-embracing definition of  $\varepsilon_V$  should take into account the light incident upon the unit volume from all directions, i.e. scalar irradiance,  $E_0$ , rather than downward irradiance,  $E_d$ . The definition based on  $E_d$  is, however, more convenient and serves the purpose well enough:  $\varepsilon_V$  is given by

$$\varepsilon_V = \frac{0.472 [\text{Chl}] P^*(\text{CO}_2)}{E_d(z)} \quad (10.36)$$

$P^*(\text{CO}_2)$  being expressed in moles  $\text{CO}_2 \text{ mg chl } a^{-1} \text{ h}^{-1}$ , and  $E_d(z)$  in  $\text{MJ m}^{-2} \text{ h}^{-1}$ . Unlike  $\varepsilon_c$  and  $\varepsilon_A$ ,  $\varepsilon_V$  is not dimensionless, since it has the

units  $\text{m}^{-1}$ . Platt (1969) pointed out that volumetric efficiency at a specific depth has the same dimensions,  $\text{m}^{-1}$ , as the vertical attenuation coefficient for irradiance, and that it is in fact equivalent to that part of the total vertical attenuation coefficient for downward irradiance that is due to removal of light by photosynthetic conversion to chemical energy

$$K_d(\text{total}) = K_d(\text{photosynthetic}) + K_d(\text{physical})$$

$K_d(\text{physical})$  being that part of the total vertical attenuation coefficient which is due to removal of light by all processes other than photosynthetic conversion to chemical energy: it thus includes that part of the light absorption by phytoplankton which fails to result in photosynthesis.

$K_d(\text{photosynthetic})$  is equivalent to  $\varepsilon_V$ . Platt's data for St Margaret's Bay, Nova Scotia, Canada, indicate a general tendency for  $\varepsilon_V$  to increase with depth (average  $\varepsilon_V$  was  $0.07\% \text{ m}^{-1}$  at 1 m and  $0.21\% \text{ m}^{-1}$  at 10 m). This is to be expected since, as we have already noted, conversion efficiency,  $\varepsilon_c$ , increases with depth, and  $\varepsilon_V = [\text{Chl}]k_c\varepsilon_c$ .

Having noted the equivalence of  $\varepsilon_V$  with  $K_d(\text{photosynthetic})$ , we can now go on to define one more efficiency parameter, namely, the proportion of the total light energy *absorbed* within unit volume of medium that is photosynthetically stored as biomass chemical energy. This is equal to  $K_d(\text{photosynthetic})/K_d(\text{total})$  and, following Morel (1978), we shall refer to it as the radiation utilization efficiency, and give it the symbol,  $\varepsilon$

$$\varepsilon = \frac{\varepsilon_V}{K_d} \quad (10.37)$$

From the definitions of  $\varepsilon_c$  and  $\varepsilon_V$  it follows that

$$\varepsilon = \frac{[\text{Chl}]k_c}{K_d} \varepsilon_c \quad (10.38)$$

i.e.  $\varepsilon$  is the (dimensionless) product of the fraction of the total absorbed light that is captured by phytoplankton and the energy conversion efficiency of the phytoplankton. Thus,  $\varepsilon$  combines directly the two factors controlling the efficiency with which the aquatic ecosystem utilizes incident light energy for photosynthesis:  $\varepsilon$  varies with depth and the integral of  $\varepsilon(z)$  with respect to depth over the whole euphotic zone gives  $\varepsilon_A$ , the areal efficiency.

Given the tendency of the conversion efficiency,  $\varepsilon_c$ , to increase with depth we might expect  $\varepsilon$  also to increase with depth, and this generally seems to be the case.<sup>940</sup> However, variation in  $\varepsilon$  with depth depends also on the variation of  $k_c$  with depth resulting from changes in the spectral distribution. From one water body to another,  $\varepsilon$  will increase as the

phytoplankton biomass increases ( $[Chl]$  in eqn 10.38) but decrease as the background attenuation due to dissolved colour etc. (increasing  $K_d$  in eqn 10.38) rises. For the oligotrophic Sargasso Sea and Caribbean Sea, Morel (1978) found  $\varepsilon$  to increase with depth from about 0.01 to 0.1%. In the somewhat more productive waters of the equatorial eastern Pacific the range was from about 0.01% near the surface to approaching 1% at low light levels. In the productive waters of the Mauritanian upwelling,  $\varepsilon$  rose from 0.1 to 0.4% near the surface to 2 to 7% near the bottom of the euphotic zone. In Lake Kinneret (Sea of Galilee), Dubinsky and Berman (1981) found that during the *Peridinium* bloom ( $428 \text{ mg chl } a \text{ m}^{-2}$ ),  $\varepsilon$  rose from just under 1% at the surface to 6.5% at 3 m. After the *Peridinium* bloom had collapsed, to be replaced with a much lower biomass ( $50 \text{ mg chl } a \text{ m}^{-2}$ , chlorophytes),  $\varepsilon$  was  $\sim 0.3\%$  at the surface, and rose to about 2% at 10 m.

#### 10.4 Photosynthesis and wavelength of incident light

The spectral composition of underwater light in a given water body varies markedly with depth and at any specified depth it varies with the optical properties of the water (Chapter 6). Thus, in order to assess the suitability of a given underwater light field for photosynthesis by different kinds of aquatic plant, we need to know in what ways the photosynthetic rates of the various plant types depend upon the wavelengths of the light to which they are exposed. Some of the information we need can be provided by an action spectrum of photosynthesis: this is the curve obtained by plotting the photosynthetic response of a plant per unit incident irradiance ( $\text{quanta } \text{m}^{-2} \text{ s}^{-1}$ ) of incident light at a series of wavelengths across the photosynthetic range. Action spectra are normally measured at light intensities low enough to ensure that the response is proportional to the incident irradiance, i.e. they are measured in the initial, linear region of the  $P$  versus  $E_d$  curve. The rate of photosynthesis at any wavelength under these conditions will be equal to the rate of photon absorption times the quantum yield,  $\phi$ . In the case of a macrophyte thallus or leaf, the rate of light absorption at a given wavelength is proportional to the absorbance at that wavelength. Thus the action spectrum will have a shape similar to that of the absorbance spectrum, modified by any variation in quantum yield with wavelength that may occur (see later).

The action spectrum of macrophytes can usually be measured on a single leaf or thallus or piece thereof, and can reasonably be taken as

representative of the ability of the original plant *in situ* to make use of light of different wavelengths. In the case of phytoplankton, however, action spectra must for practical reasons be measured on suspensions containing many cells or colonies: sometimes, if reasonable rates are to be achieved, on concentrated suspensions. How does an action spectrum determined on a suspension relate to the action spectrum we wish to know, namely that of the individual cell or colony? The action spectrum of a cell or colony would be identical to the spectral variation in rate of absorption of quanta, modified as usual by any variation in quantum yield. The average rate of absorption of quanta per individual cell or colony, from a light beam, is the product of the irradiance and the mean absorption cross-section ( $\overline{s_p A_p}$ ) of the cells or colonies (§9.4). Thus the action spectrum of a single cell or colony would have the same shape (allowing for variations in  $\phi$ ) as the spectral variation in  $\overline{s_p A_p}$  and this is fixed, being determined only by the absorption characteristics of the individual cells or colonies.

The action spectrum of the phytoplankton suspension measured in the laboratory will, by contrast, have the same shape (allowing for variations in  $\phi$ ), as the absorbance spectrum of the whole suspension. The shape of this spectrum is not fixed, being a function of the number of cells/colonies per unit area of the illuminating beam. Since absorbance can only approach 1.0 and can never exceed it, the absorbance at weakly absorbed wavelengths (e.g. in the green in the case of chlorophytes, diatoms etc.) progressively approaches absorbance at strongly absorbed wavelengths (e.g. at the chlorophyll red peak) as the concentration of cells or colonies increases.

From its definition (§3.2) it follows that the *absorbance* of the suspension,  $D_{sus}$  is equal to  $-0.434 \ln(1 - A_{sus})$ , where  $A_{sus}$  is the absorbance of the suspension. From this it in turn follows (since  $\ln(1 + x) \approx x$ , when  $x \ll 1$ ) that for low values of  $A_{sus}$ ,  $D_{sus} \approx 0.434 A_{sus}$ . We saw earlier (§9.2) that  $D_{sus} = 0.434 n \overline{s_p A_p}$ , and therefore at low values of  $A_{sus}$ ,  $A_{sus} \approx n \overline{s_p A_p}$  where  $n$  is the number of cells or colonies per ml. The true action spectrum of the individual cells or colonies follows (allowing for variations in  $\phi$ ) the spectral variation in  $\overline{s_p A_p}$  (see above). Therefore, the action spectrum of the suspension will have approximately the same shape as the action spectrum of the individual cells or colonies provided that it is measured on suspensions with low values of absorbance. The discrepancies are about 5, 11 and 19% when  $A_{sus}$  is 0.1, 0.2 and 0.3, respectively. The general effect of the error is that the action spectrum of the suspension will be flattened (i.e. peaks lowered relative to the valleys) compared to the true action spectrum of the cells or colonies.

The earliest measurements of photosynthetic action spectra were those of Engelmann (1884). He illuminated pieces of algal tissue with a spectrum and then observed the migration of oxygen-requiring bacteria to the different parts of the tissue. He used the concentration of bacteria around different parts of the tissue as an indication of the relative ability of different colours of light to elicit O<sub>2</sub> evolution. Approximate though this method was, the results did indicate that other pigments in addition to chlorophyll participated in photosynthesis. Nowadays, laboratory determination of action spectra is most commonly carried out using a high-intensity monochromator as a light source, and a platinum electrode to measure the rate of O<sub>2</sub> evolution.<sup>547</sup> Manometry has also been used,<sup>359,360</sup> as has <sup>14</sup>CO<sub>2</sub> fixation.<sup>617,803</sup>

When the action spectrum is measured by determining the rate at a series of different wavelengths, then the curve of photosynthetic rate per unit irradiance obtained is generally found to be somewhat similar, but not identical, to the curve of absorbance for the tissue or cell suspension. Figure 10.6 shows the action and corresponding absorbance spectra measured on multicellular green, brown and red algae,<sup>547</sup> and on the unicellular green alga *Chlorella*,<sup>360</sup> together with an action spectrum for the marine diatom *Skeletonema*.<sup>617</sup>

It will be observed that the action spectrum falls below the absorption spectrum in certain spectral regions. This means that the amount of photosynthesis achieved per unit light absorbed is lower, i.e. the quantum yield is lower, at these wavelengths than at others. Figure 10.7 shows the quantum yield as a function of wavelength in the blue-green alga *Chroococcus*, the green alga *Chlorella* and the diatom *Navicula*.<sup>359,360,1343</sup> A fall in quantum yield is observed on the long-wavelength side (680–710 nm) of the chlorophyll *a* red absorption peak, and also in the region of carotenoid absorption (440–520 nm), this latter fall being particularly marked in the blue-green alga and significant in the green alga but only slight in the diatom. Such observations led to the belief, initially, that while light absorbed by the carotenoid fucoxanthin in diatoms is efficiently used for photosynthesis, light absorbed by carotenoids in blue-green and green algae is used with much lower efficiency. While there can indeed be some variation in the efficiency with which light absorbed by different pigments is utilized for photosynthesis, it is now thought that this is not the major factor involved in the fall in quantum yield. Furthermore, the explanation originally suggested for the decrease in  $\phi$  in the far-red – namely, that the quanta are insufficiently energetic to bring about photosynthesis – is also incorrect.

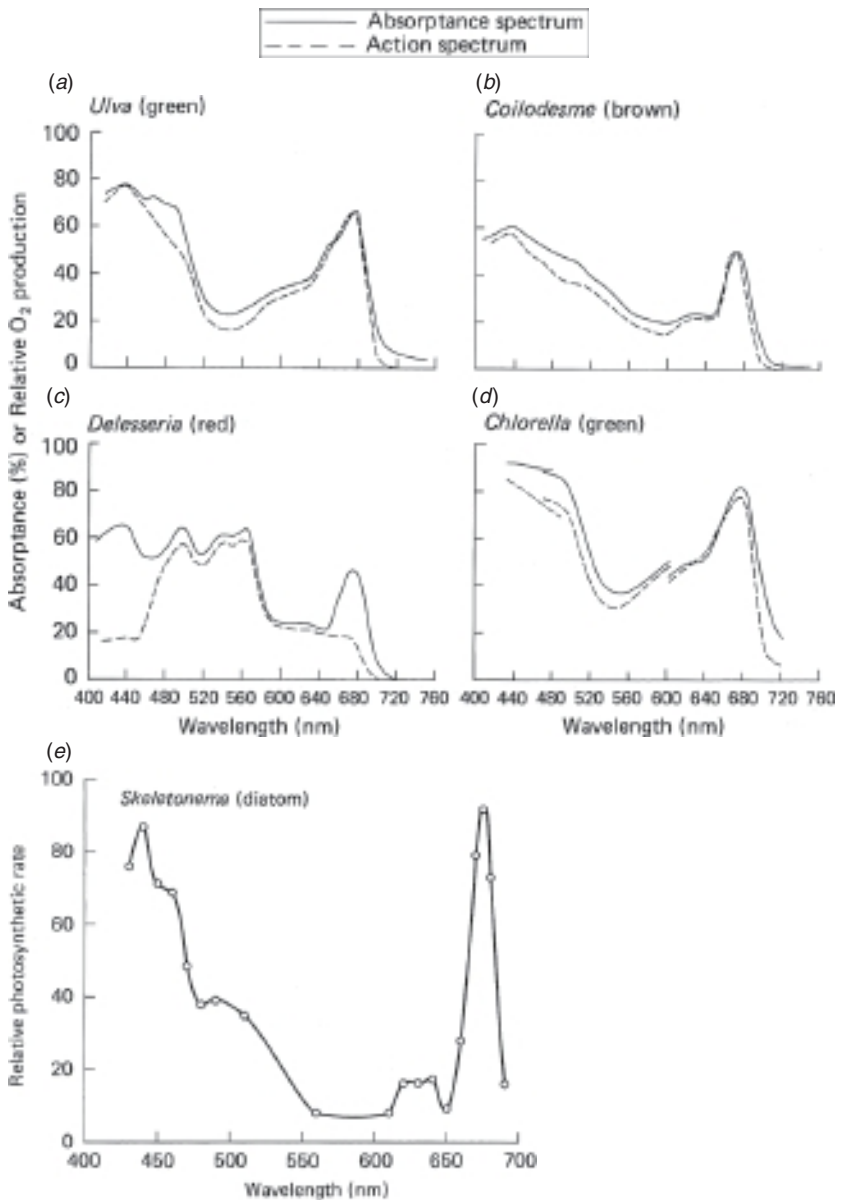


Fig. 10.6 Action spectra of photosynthesis in multicellular and unicellular algae. In (a)–(d) the action spectrum (photosynthetic rate per unit incident irradiance) has been plotted so that it coincides with the absorbance spectrum at some appropriate wavelength. (a), (b) and (c) – bare platinum electrode method (after Haxo and Blinks, 1950). (d) – manometric method (after Emerson and Lewis, 1943); the spectra in this case were obtained with dense suspensions and so do not accurately correspond to the absorption and action spectra of individual cells (see text). (e) –  $^{14}\text{CO}_2$  method (plotted from data of Iverson and Curl, 1973). (a) *Ulva taeniata* (multicellular green). (b) *Coilodesme californica* (multicellular brown). (c) *Delesseria decipiens* (multicellular red, from shaded habitat). (d) *Chlorella pyrenoidosa* (unicellular freshwater chlorophyte). (e) *Skeletonema costatum* (marine diatom).

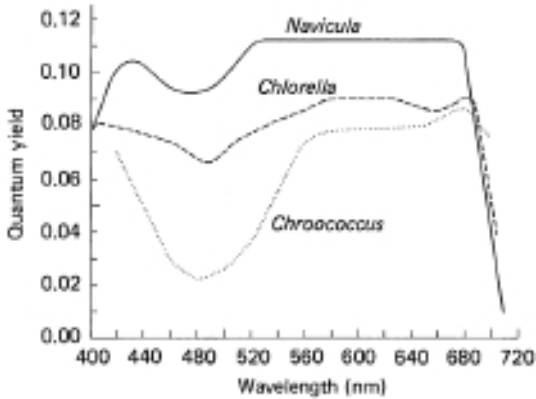


Fig. 10.7 Quantum yield as a function of wavelength in three unicellular algae. (— *Navicula minima*, diatom (after Tanada, 1951); - - - - *Chlorella pyrenoidosa*, green (after Emerson and Lewis, 1943); ..... *Chroococcus* sp., blue-green (after Emerson and Lewis, 1942).)

The variation in quantum yield with wavelength is now considered to be primarily due to the fact that there are two light reactions, both of which must be energized for photosynthesis to occur, and which have – to an extent varying with the algal type – different light-harvesting pigment arrays with differing absorption spectra. Thus, during the measurement of an action spectrum, when the wavelength of the monochromatic light provided is strongly absorbed by one photosystem but weakly by the other, then the two light reactions do not operate at the same rate and so photosynthetic efficiency is low. For example, 680 to 710 nm light is absorbed quite well by photosystem I but poorly by photosystem II. Consequently when cells are illuminated with far-red light, the rate of photosynthesis is low because photosystem II cannot keep up with photosystem I.

Emerson (1958) showed that if *Chlorella* cells illuminated with far-red light were simultaneously exposed to light absorbed by chlorophyll *b* (which transfers most, perhaps all, its energy to photosystem II), then the quantum yield increased above that expected on the basis of the additive contributions of the two kinds of light alone. This phenomenon, of a synergistic effect of two wavebands of light, is referred to as *enhancement* and can plausibly be explained in terms of the existence of the two photosystems. Invoking the photosystems to explain the dependence of quantum yield on wavelength immediately raises problems of its own however. The virtually constant and high value of  $\phi$  between 560 and 680 nm (Fig. 10.7) indicates that both photosystems are working at the

same rate throughout this wavelength range, which is rather surprising in view of the differing pigment complements of the two photosystems. The generally accepted explanation of this phenomenon, originally proposed by Myers and Graham (1963), is that when photosystem II is absorbing light faster than photosystem I, some of its excitation energy is transferred to photosystem I, so that both systems can operate at the same rate. This is known as the 'spillover' hypothesis, and there is now good evidence for its validity:<sup>191</sup> transfer of energy from photosystem I to II does not appear to take place. Put simply, light absorbed by photosystem II can be used to drive both light reactions; light absorbed by photosystem I drives only light reaction I. We may therefore take the fall-off in quantum yield in certain parts of the spectrum as indicating that in those spectral regions absorption is mainly due to photosystem I pigments.

It follows from all this that action spectra measured with monochromatic light are going to be biased heavily in their shape towards the absorption spectrum of photosystem II, and may therefore be a poor guide to the ability of a particular plant to make use of the mixture of wavelengths (however enriched this may be in one spectral region or another) that is invariably present in underwater light fields. A more meaningful action spectrum, for ecological purposes, may be obtained by carrying out the measurements with two simultaneously applied light sources; one with wavelength changing progressively to cover the whole photosynthetic range, the other constant at a wavelength absorbed by photosystem II. In this way, even when the variable source is set to spectral regions where absorption is mainly due to photosystem I, the fixed-wavelength background source ensures that photosystem II continues to operate. [Figure 10.8](#) shows, for a red alga, the difference between action spectra measured<sup>405</sup> in the absence or the presence of background green (546 nm) light, absorbed by phycoerythrin, which is known to supply its energy directly to photosystem II. When photosystem II is energized in this way, there is a great increase in the photosynthetic response to light in the 400 to 480 nm and 600 to 700 nm regions. It appears likely that most of the chlorophyll *a* (400–450 nm, 650–700 nm) and carotenoids (400–500 nm) in this alga are part of photosystem I. The discrepancy between action spectra measured with and without background photosystem II light is particularly great in biliprotein-containing algae, because in such algae it seems to be generally true that the biliproteins, which constitute such a major but spectrally confined part of the light-harvesting apparatus, transfer all their energy directly to photosystem II, whereas the chlorophyll *a* directs most of its energy to

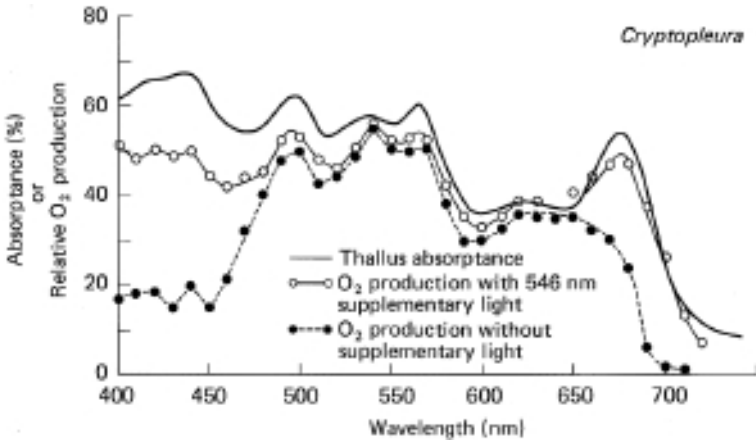


Fig. 10.8 Photosynthetic action spectra of the red alga *Cryptopleura crista* measured with and without background green (546 nm) light, together with the absorbance spectrum (from Fork, 1963). Reproduced from *Photosynthetic Mechanisms in Green Plants*. Washington, DC: National Academy Press (1963).

photosystem I. In algae such as the diatoms, brown algae and green algae, where the pigment arrays of the two photosystems are not so different, the difference between action spectra measured with and without background photosystem II light is not so marked.

It can be observed in Fig. 10.8 that the action spectrum measured with background photosystem II light is fairly close to the absorbance spectrum of the thallus. A similar observation has been made for other red algae.<sup>1128</sup> In the absence of action spectra data measured with background photosystem II light, the absorbance spectrum may be used as an approximate guide to the ability of an aquatic plant not only to capture but also to use light of different wavelengths. The discrepancies between the absorbance spectra and the photosystem II-supplemented action spectra of aquatic plants are nevertheless significant and of interest. It has been observed for a number of red algae,<sup>405,1128</sup> and can be seen in Fig. 10.8, that the green-supplemented action spectrum falls significantly below the absorbance spectrum in the 400 to 520 nm region, indicating that some of the pigment molecules absorbing in this region are not transferring their excitation energy efficiently to the reaction centres. The molecules in question are probably carotenoids. It seems unlikely that the carotenoids in the red algae are completely inactive: if they were inactive we would expect a much greater fall in the green-supplemented action spectrum between 450 and 500 nm. The

photosystem II-supplemented action spectrum of the blue-green alga *Anacystis* also indicates that carotenoids contribute excitation energy for photosynthesis.<sup>654</sup> The photosynthetically inactive carotenoid is in some cases likely to consist mainly of zeaxanthin, which, as we have noted earlier, appears to have the function of protecting the photosynthetic system against excessive light levels.

Thus, in the red and blue-green, and possibly also green and xanthophycean algae<sup>466</sup> the absorption spectrum is likely, because of the inactivity of some of the xanthophyll molecules, partly to overestimate the ability of the cells to utilize light in the blue region of the spectrum. In those algal groups (diatoms, phaeophytes, dinoflagellates, siphonous green algae) that rely heavily on specialized carotenoids (fucoxanthin, peridinin, siphonaxanthin) for light harvesting, however, the major carotenoid species transfer their absorbed energy to the reaction centres as efficiently as does chlorophyll. In these algae we may reasonably assume that the absorption spectrum (absorbance or absorption cross-section, as appropriate) is quite an accurate guide to the ability of the cells to utilize light in all regions of the photosynthetic spectrum, although even in these cases there are minor carotenoids – such as diadinoxanthin in the coccolithophorid, *Emiliana huxleyi*,<sup>546</sup> which are photosynthetically ineffective.

# 11

## Photosynthesis in the aquatic environment

Having considered the photosynthetic response of aquatic plants to light of different intensities and spectral qualities, we shall now examine how the availability of light influences where, when and how much photosynthesis takes place in aquatic ecosystems, and also the extent to which other parameters of the environment can limit photosynthesis. Aquatic production ecology is an enormous field: a comprehensive account will not therefore be attempted. Rather, the broad principles governing the controlling influence of light and other parameters will be outlined and illustrated by examples. More detailed accounts and extensive bibliographies can be found in the books on phytoplankton ecology by Reynolds (1984), Harris (1986), and Fogg and Thake (1987), and the symposium proceedings edited by Platt and Li (1986), and Falkowski and Woodhead (1992). The essay by Fogg (1991) on 'The phytoplanktonic way of life' provides a particularly valuable overview of the multifarious interactions between the phytoplankton and its environment.

### 11.1 Circulation and depth

We saw in the previous chapter that except under very still conditions with virtually no wind or waves, there is always circulation of water in the upper layer. We also saw that this can be an advantage to the phytoplankton in so far as, by ensuring that they are not exposed to the intense light just below the surface for very long, they avoid photoinhibition. This circulation can, however, also be a disadvantage to the phytoplankton if, in the lower reaches of the mixed layer, the light intensity is too low for net photosynthesis to be achieved. As the depth of the mixed layer through which the phytoplankton is circulating increases, so the average

light intensity to which the cells are exposed decreases, and consequently the total rate of photosynthesis by the whole phytoplankton population throughout the water column decreases. The rate of respiration of the whole phytoplankton population, on the other hand, will be essentially constant whatever the mixing depth. Thus, as was first pointed out by Braarud and Klem (1931), there exists a mixed-layer depth – the *critical depth*,  $z_c$  – beyond which respiratory carbon loss by the whole population exceeds photosynthetic carbon gain, and so net phytoplankton growth cannot occur. Even when the critical depth is not exceeded, increases in mixing depth tend to reduce total photosynthesis.

The depth through which circulation can occur is limited either by the depth of the bottom or (from spring to autumn in temperate latitudes and throughout the year in tropical oceans) by the presence of a shallow *thermocline*. A thermocline (temperature gradient) gives rise to a *pycnocline* (density gradient): density gradients within fluids are intrinsically stable, with a significant capacity to resist disruption. Thus, one answer to the question, where does aquatic photosynthesis take place is that it takes place best in shallow waters or in waters in which circulation is confined to a shallow layer by thermal stratification. The converse is that net photosynthesis occurs poorly, or not at all, in waters in which the phytoplankton is circulated through great depths. For a series of Japanese lakes covering a wide range of depths, Sakamoto (1966) found a general tendency for deeper lakes to be less productive than shallow ones. Even when differences in nutrient supply were allowed for, the inhibiting effect of depth remained. Comparing two South African impoundments, of comparable optical and chemical character, Grobbelaar (1989) found the shallow Wuras Dam ( $z_{\max} = 3.4$  m) to be eight times as productive as the deep Hendrik Verwoerd Dam ( $z_{\max} > 60$  m). In the marine environment too, we may plausibly attribute the greater productivity of shallow coastal waters (relative to the deeper waters) in part (i.e. in addition to nutrient differences) to their lesser depth. Isolated shallow areas within the oceans such as the Faroebank (100 m depth) west of the Faroe Islands are also more productive than the surrounding oceanic waters.<sup>1296</sup> In the turbid waters of the San Francisco Bay estuary, phytoplankton biomass is generally higher in the lateral shallows than in the channel.<sup>248</sup>

### Depth distribution of benthic flora

The higher productivity of shallow water applies to the benthic flora also. Any surface within the euphotic zone of a water body is usually found to

support a productive plant community. This applies not only to the more obvious macrophyte communities such as kelp forests, seagrass beds, brown and red algal associations on underwater rocks, but also to seemingly bare sand and mud surfaces, which usually harbour a dense microflora among the grains. This microflora, or *microphytobenthos*, is likely to consist of specialized benthic diatoms in temperate mudflats and sand, or of symbiotic algae within Foraminifera in the sands of tropical lagoons.<sup>1272</sup> Moving in a seawards direction, as depth increases so the standing crop of biomass (macrophytes and microflora) per unit area, and the rate of primary production per unit area, both decrease until eventually a depth is reached beyond which the light intensity is too low to support any plant growth. For the important group of large sublittoral brown algae, loosely referred to as the kelps, the lower limit occurs at depths where the downward irradiance is 0.7 to 1.4% of that penetrating the surface: this depth limit ranges from as little as 8 m in the turbid water around the island of Helgoland (North Sea) to about 95 m in the very clear waters of the central Mediterranean.<sup>833</sup> For the coralline crustose red algae – commonly the most deeply occurring algal type – the lower depth limit occurs where the irradiance is 0.01 to 0.1% of the subsurface value: this corresponds to about 15 m depth off Helgoland but to as much as 175 m in the Caribbean.<sup>833</sup> In the ultra-clear waters east of the Bahamas, Littler *et al.* (1986) using a submersible, observed a zone of crustose coralline red algae between 189 and 268 m depth, on a seamount. Lüning and Dring (1979) found for the sublittoral region off Helgoland that the total downwelling light (400–700 nm) received *per year* was about 15 MJ m<sup>-2</sup> or 70 mol photons m<sup>-2</sup> at the lower kelp limit (8 m) and 1 MJ m<sup>-2</sup> or 6 mol photons m<sup>-2</sup> at the lower red-algal limit (15 m): these may be regarded as the approximate minimum yearly requirements of PAR for growth of these algal types. Much higher annual light requirements (mol photons m<sup>-2</sup> yr<sup>-1</sup>) have been estimated for some freshwater macrophytes by Sand-Jensen and Madsen (1991): 40 to 200 for charophytes (*Nitella* and *Chara*), 416 for a bryophyte (*Fontinalis antipyretica*), 455 for an isoetid angiosperm (*Isoetes lacustris*) and 1760 for the shallow-water angiosperm, *Littorella uniflora*.

The depth distribution of aquatic macrophytes is controlled by a number of environmental factors, but the underwater light climate is frequently the primary one.<sup>1273</sup> An important ecological parameter for any water body is  $z_{\text{col}}$ , the maximum depth to which it is colonized by macrophytes, and this tends to be approximately proportional to the reciprocal of the vertical attenuation coefficient for PAR in the water

body, although the constant of proportionality appears to be a function of latitude.<sup>1404</sup> For nine New Zealand (North Island) lakes at  $\sim 38^\circ$  S, Vant *et al.* (1986) found macrophyte depth limits to vary with the attenuating character of the water in accordance with  $z_{\text{col}} = 4.34/\bar{K}_d$ , where  $\bar{K}_d$  was the vertical attenuation coefficient of the lake for PAR averaged over a year. For 18 lakes in the South Island of New Zealand ( $41\text{--}46^\circ$  S), Schwarz *et al.* (1996) found that  $z_{\text{col}}$  was significantly ( $r^2 = 0.92$ ) related to  $K_d(\text{PAR})$  by the relationship  $z_{\text{col}} = (4.5/K_d[\text{PAR}]) - 2.2$ . Characean algae dominated the deepest communities in 16 of the lakes. For one such species, *Chara corallina*, from measurements of its photosynthetic properties, of the incident solar radiation over the course of a year, and of the values of  $K_d(\text{PAR})$ , Schwarz *et al.* calculated for 17 of the lakes, and for each day of the year, the depth (compensation depth) at which net photosynthesis was equal to zero. This was then averaged for the whole year. They found a linear 1:1 relationship ( $r^2 = 0.86$ ) between the predicted compensation depth and the observed maximum depth of colonization by this alga. For lakes in Scotland and the English Lake District ( $54\text{--}57^\circ$  N), Spence (1976) found the approximate relationship  $z_{\text{col}} = 1.7/K_d(\text{PAR})$ . In the case of *Vallisneria americana*, a common macrophyte in Australian inland waters, Blanch *et al.* (1998) found the maximal depth of colonization to be predicted by  $z_{\text{col}} = (8.89/K_d[\text{PAR}]) - 0.06$ .

For seagrasses Duarte (1991), from a survey of literature data, arrived at the relationship  $z_{\text{col}} = 1.86/K_d$ . In the case of seagrass beds, the depth at the lower edge of the bed is sometimes referred to as the *ecological compensation depth* (ECD), because it is the depth below which the carbon balance for the entire canopy becomes negative and hence unsustainable.<sup>429</sup> For seagrass beds in the Indian River Lagoon, Florida, Gallegos and Kenworthy (1996) found that the depth distribution could satisfactorily be predicted on the basis that the ECD corresponded to  $\sim 20\%$  light penetration. Seagrass growth was inhibited in the vicinity of the outflow of a canal discharging highly coloured water. Estuaries which are significant waterways are routinely dredged to maintain the navigation channels, an activity which, unfortunately, leads to substantial, and frequently persistent, increases in turbidity. Onuf (1994) carried out underwater light measurements in the Laguna Madre, Texas, over a period covering 3 months before to 15 months after a dredging project in 1988, and concluded on the basis of his data that maintenance dredging had been responsible for the loss of seagrass cover that had taken place in this waterway between 1965 and 1974.

### Mixed layer depth and phytoplankton production

It is instructive to consider under what conditions phytoplankton primary production may be prevented altogether as a result of the mixed depth exceeding the critical depth. Using Talling's (1957b) model for calculating integral photosynthesis (see §11.5) we can derive an approximate expression for the critical depth

$$z_c = \frac{N}{24 K_d \rho} \ln \left( \frac{\bar{E}_d(0)}{0.5 E_k} \right) \quad (11.1)$$

where  $\rho$  is the ratio of respiration rate to light-saturated photosynthetic rate in the phytoplankton,  $K_d$  is the vertical attenuation coefficient for downwards irradiance of PAR,  $N$  is daylength in hours (readily calculated from eqn 2.11),  $\bar{E}_d(0)$  is the average value of downward irradiance just below the surface during daylight hours, and  $E_k$  is the irradiance value defining the onset of saturation (§10.2). We can see from eqn 11.1 that the likelihood of the mixed layer depth exceeding the critical depth increases (i.e.  $z_c$  decreases) as respiration rate (relative to photosynthetic rate), attenuation by the water, or the light-saturation parameter, increase: an increase in incident irradiance or in daylength has the opposite effect.

As an example of a temperate-zone lake with relatively low attenuation we shall take Lake Windermere, England, and use the data of Talling (1957a). For a day in late spring (1 May 1953), with  $\bar{E}_d(0) \approx 170 \text{ W m}^{-2}$ , daylength  $\approx 15 \text{ h}$ ,  $K_d = 0.43 \text{ m}^{-1}$ , and the phytoplankton (predominantly the diatom, *Asterionella*) having  $E_k = 6.3 \text{ W m}^{-2}$ , and  $\rho = 0.033$ , we may calculate that the critical depth was about 177 m. Since the lake itself (North basin) has a maximum depth of only about 63 m, there is clearly no possibility of net primary production being prevented altogether. Even if the lake were much deeper, once the spring–summer thermal stratification had set in, the comparatively shallow depth of the *epilimnion* (the layer, commonly 5–20 m deep, above the thermocline, within which wind-induced circulation occurs) would prevent the critical depth being exceeded. For Lake Windermere in midwinter, on the other hand, with daily incident light down to a small fraction of the summer value and circulation through the full depth of the lake, Talling (1971) estimated that phytoplankton growth was impossible. In the much shallower Esthwaite Water ( $z_{\text{max}} = 15 \text{ m}$ ), in contrast, he concluded that phytoplankton growth should be possible throughout the year.

Even in shallow water bodies, if the attenuation is high enough the circulation depth can exceed the critical depth. For turbid Lough Neagh

(N. Ireland), with a mean depth of 8.6 m and  $K_d$  values commonly 1.5 to  $3.5 \text{ m}^{-1}$ , Jewson (1976) estimated that the critical depth would be exceeded in winter, thus precluding growth. In spring, despite the lack of stratification in this well-mixed lake, the increase in illumination was sufficient to ensure that  $z_c$  was not exceeded.

When high attenuation is combined with a requirement for high light intensity for saturation, then the critical depth can be very shallow. In Lake George, Uganda, on the equator, Ganf (1975) observed  $K_d$  values in the region of  $9 \text{ m}^{-1}$ , and the blue-green algal population had a light-saturation onset parameter ( $E_k$ ) of about  $55 \text{ W m}^{-2}$ , on a day (12 April 1968) when the average incident irradiance ( $\bar{E}_d(0)$ ) was  $360 \text{ W m}^{-2}$ . Assuming  $\rho$  to be about 0.1 and the daylength to be 12 h, eqn 11.1 gives a critical depth of 1.4 m. Thus, despite the high irradiance incident on this tropical lake, the mixed depth could often exceed the critical depth. In productive lakes of this type a large part of the attenuation is due to the phytoplankton itself and so the situation is self-correcting. Cessation of growth is likely to be followed by breakdown of the algae, following which attenuation falls and photosynthesis and growth can recommence.

In the marine environment, the relation between the mixed depth and the critical depth is of particular importance, and indeed the first attempt to characterize this relation quantitatively was carried out by Sverdrup (1953) for the Norwegian Sea. In middle and high latitudes the mixed layer is deep at the end of the winter (varying from 100–400 m in March at  $66^\circ \text{ N } 2^\circ \text{ E}$ ), but in the spring a shallow mixed layer (25–100 m) develops due to thermal stratification. For the  $66^\circ \text{ N}$  station that Sverdrup studied, he estimated that until the last week of April the mixed layer was much deeper than the critical depth, thus precluding phytoplankton growth, but that after the middle of May the mixed layer depth was smaller than the critical depth so that growth was possible. Springtime stratification can be established very quickly. At a station in the North Atlantic, south of Iceland, Dickey *et al.* (1994) found that the mixed layer shoaled from  $\sim 550$  to  $\sim 50$  m within a five-day period towards the end of April. This was followed by a major phytoplankton bloom, with a ten-fold increase in near-surface chlorophyll in less than three weeks.

Within any water body, essentially all the infrared component ( $\lambda > 700 \text{ nm}$ ) of incident solar radiation is absorbed within the uppermost 0.5 m by water itself. The depths at which the remainder of the solar flux, the 45 to 50% which is PAR, is absorbed and converted to heat is determined by the inherent optical properties of the water in question. Phytoplankton blooms, by increasing the absorption of solar radiation

near the surface, can significantly increase sea surface temperature, and in this way give rise to stronger near-surface thermal stratification, and shallower mixed layers.<sup>1304</sup>

If, in early spring, with increasing solar irradiance, vertical wind mixing is weak or absent, phytoplankton blooms can develop even before stratification is established.<sup>1373,599</sup> Townsend *et al.* (1992) observed such a phenomenon in the Gulf of Maine, in March 1990. In locations where shallow coastal waters are permanently well mixed by tidal action, such as the coast of Brittany (France) in the western English Channel, a stratification-induced spring bloom does not occur, and the light intensity is such that the euphotic depth becomes comparable to the water depth.<sup>1474</sup>

In some aquatic systems strong prevailing wind, by causing deep mixing, can become the main limiting factor for primary production even after the phytoplankton growing season has commenced. This has been observed for the Atlantic sector of the Southern Ocean<sup>1398</sup> and also for a deep lake, Loch Ness (average depth 132 m), in Scotland.<sup>661</sup>

Density stratification brought about by vertical variation in salt concentration, rather than by solar heating, can also induce a phytoplankton bloom. This has been observed in the case of lower salinity upper layers resulting from freshwater inflow in estuarine and coastal waters,<sup>247,1042,1374</sup> and from melting ice in the marginal ice zones around Antarctica,<sup>915,1259</sup> or from intrusion of dense continental slope water beneath less saline coastal water.<sup>1374</sup> In the Southern Ocean Marginal Ice Zone, Fitch and Moore (2007) found that in the Antarctic summer, phytoplankton blooms were largely suppressed at high wind speeds, due to breakdown of the vertical stratification. At low wind speeds ( $\sim 5 \text{ m s}^{-1}$ ), blooms covered about one third of the Marginal Ice Zone.

Strictly speaking, these various interactions between mixed depth and critical depth apply to non-motile forms such as diatoms. Motile algae such as dinoflagellates can to some degree escape these effects by migrating again up to regions of higher irradiance if the circulating water moves them down. Nevertheless the evidence is clear that for the total phytoplankton population, circulation of water within the mixed layer is a major factor influencing primary production, and frequently determines whether such production takes place at all.

In the sea, the mixed layer, once thermal stratification has been established (spring to autumn in moderate and high latitudes, all year in the tropics), is typically 20 to 100 m deep. Within and below the thermocline there is comparatively little circulation of the water. Since the euphotic zone will frequently be deeper than the mixed layer (for marine waters

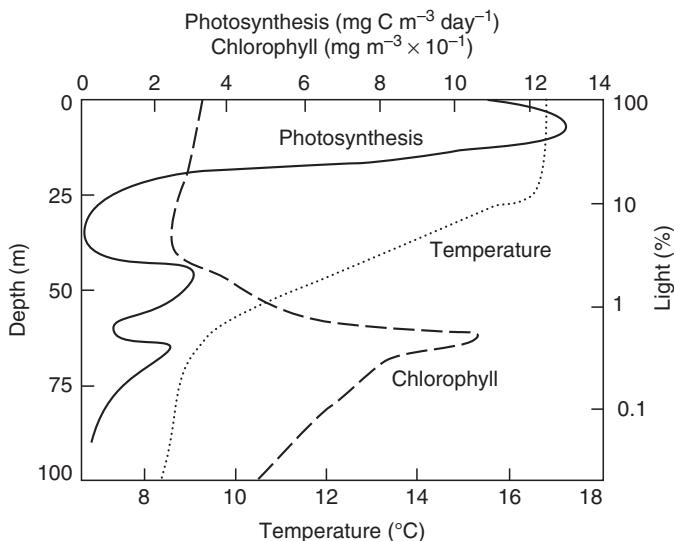


Fig. 11.1 The deep chlorophyll maximum in the Northeast Pacific Ocean (after Anderson, 1969). The temperature profile shows that the mixed layer is about 25 m deep.

with  $K_d$  values of 0.03, 0.05, 0.11, 0.16  $\text{m}^{-1}$  (Table 6.1),  $z_{eu} \approx 153, 92, 42$  and 29 m, respectively), there is, throughout much of the oceans and coastal seas, a substantial layer of water which combines sufficient light intensity to support photosynthesis, with a stable water column.

### Deep chlorophyll maximum

When the vertical profile of phytoplankton chlorophyll is measured in the (stratified) ocean, a distinct peak of chlorophyll concentration is normally found close to the bottom of the (nominal) euphotic zone. An example of this *deep chlorophyll maximum* (DCM) as it is often called, in the northeast Pacific Ocean is shown in Fig. 11.1. The peak of the chlorophyll distribution is either a little above or a little below (as in Fig. 11.1) the depth at which  $E_d$  is 1% of the subsurface value. It will be noted that there is a layer of increased photosynthetic activity in this region indicating that the algal cells are active, not moribund. This layer of deep phytoplankton is very widespread in the world's oceans: it appears, for example, to extend right across the Pacific.<sup>1220</sup> It occurs only where the water column is stabilized by a pycnocline (density gradient).<sup>24,1408</sup> In the Atlantic subtropical gyres, the DCM was found by Perez *et al.* (2006) to extend

on average from 67 to 126 m depth. It seems likely that the increase in chlorophyll concentration in this deep layer, relative to that in the mixed layer, is due to an increase in chlorophyll concentration within the cells as well as to an increased population of phytoplankton.<sup>24,268,687,1022</sup> Kiefer *et al.* (1976) found the chlorophyll per unit biomass in the deep phytoplankton layer to be about twice the value near the surface. At five stations in the eastern subtropical Atlantic, Veldhuis and Kraay (2004) found DCMs at depths (position of maximum chlorophyll) ranging from 80 to 130 m. The small prokaryote, *Prochlorococcus*, dominated the surface waters, but eukaryotic species were the major component of phytoplankton biomass in the DCM. The cellular chlorophyll to carbon ratios increased with depth in both the prokaryotes and the eukaryotes: in the case of *Prochlorococcus* the increase was as much as 20-fold. In the Gulf of Aqaba (Eilat), Red Sea, Stambler (2006) observed that a DCM characterized by high concentrations of *Prochlorococcus* developed at ~80 m after summer stratification was established. There was a marked increase in the chlorophyll content per cell with depth.

The mechanism (apart from shade adaptation) by which the deep chlorophyll maximum becomes established is uncertain. A commonly held view is that it is related to the distribution of nutrients. In the well-illuminated mixed layer the phytoplankton rapidly consumes the nutrients in the spring, and the population then decreases. Below the thermocline nutrient concentrations are much higher. Furthermore, additional nutrients can diffuse upwards from the deep water below. The continued availability of nutrients in this region, possibly combined with a diminution in the sinking rate of the phytoplankton once it reaches these nutrient-rich waters, may account for the establishment and maintenance of this phytoplankton layer.<sup>24,619,1294</sup> At stations in the Adriatic Sea the DCM has been found to form well below the pycnocline, and is associated rather with the nutricline, and close to the depth at which PAR is 1% of that at the surface.<sup>1119,993</sup>

The deep phytoplankton layer makes a significant contribution to total primary production in those waters where it occurs. In the Azores Front (Eastern N. Atlantic), Lorenzo *et al.* (2004) found that photosynthesis in the DCM accounted for  $54 \pm 17\%$  of the total depth-integrated primary production. In the Atlantic subtropical gyres, Pérez *et al.* (2006) found the contribution to be  $46 \pm 2\%$ . On the north slope of the Dogger Bank in the North Sea, which is a highly productive continental shelf sea, Weston *et al.* (2005) found, in a strongly stratified region, that 58% of water column productivity occurred within the thermocline associated with the DCM.

In shallow, tidally energetic shelf seas, there can be two turbulent mixed layers, the surface mixed layer and the bottom mixed layer, separated by a thermocline. At a station in the western English Channel in August 1999, Sharples *et al.* (2001) found such a region with a thermocline at  $\sim 30$  m. In the lower half of the thermocline there was a narrow DCM with a vertical thickness of  $\sim 5$  m. The average chlorophyll *a* concentration was  $26 \text{ mg m}^{-3}$ , but reached a peak of  $80 \text{ mg m}^{-3}$ . The turbulence generated by tidal mixing both aided phytoplankton growth by supplying bottom-layer nutrients into the DCM, and simultaneously depleted phytoplankton numbers by entraining them into the bottom mixed layer.

In most inland waters the euphotic depth is less than the mixed depth, and so the conditions for the development of a deep chlorophyll maximum do not occur. However, Fee (1976) found a very narrow layer with very high phytoplankton chlorophyll concentration in the region of, or below, the thermocline in a series of lakes in northwestern Ontario (Canada), which were both clear and thermally stratified. This layer was found between 4 and 10 m depth (depending on the lake) where the irradiance was 0.3 to 3.5% of the subsurface value. Phytoplankton samples from this layer were always dominated by large colonial chrysophycean flagellates of the genera *Dinobryon*, *Synura*, *Uroglena* and *Chryso-sphaerella*, just one species normally being dominant in the deep chlorophyll layer of any given lake. A curious and interesting feature of these chrysophycean phytoplankton layers is that, as well as photosynthesizing, they derive a substantial proportion of their carbon by phagotrophic ingestion of bacteria.<sup>118</sup> In the very clear, colourless waters of Crater Lake and Lake Tahoe, comparable optically to ocean water, a deep chlorophyll maximum develops at considerable depth ( $\sim 75$  m) in the summer.<sup>769,1364</sup> In Lake Michigan a deep chlorophyll layer develops below the thermocline, after seasonal stratification sets in. This appears to be due to *in situ* growth but also, to a lesser extent, to sedimentation and shade adaptation.<sup>373</sup>

## 11.2 Optical characteristics of the water

We saw in the previous chapter that a major factor in limiting efficiency of utilization of incident light in aquatic ecosystems is the removal of a large proportion of the light energy by the aquatic medium. This occurs in waters in which the vertical attenuation of PAR by non-phytoplanktonic material is high (see Table 10.1). We would therefore expect, for example, brown-water lakes with a high concentration of CDOM to be on average

less productive than lakes with low background colour. There is some evidence that this is the case, although relatively few systematic studies have in fact been carried out. Jackson and Hecky (1980) found, for water bodies in northern Manitoba (Canada), that primary productivity was inversely related to total dissolved organic carbon (which would be linearly related to CDOM). While these authors did suggest that this was due to the humic substances complexing iron, thus making it unavailable to phytoplankton, rather than by increasing light attenuation, competition by CDOM for light is nevertheless a plausible explanation. For lakes in Wisconsin, Carpenter *et al.* (1998) observed a weak negative correlation between phytoplankton concentration, and also primary production rates, and the levels of dissolved organic carbon. In the St Johns River, Florida, Philips *et al.* (2000) found in time series at two locations over a four-year period that periods of high colour corresponded to periods of low phytoplankton concentration, and vice versa. Jones (1992) points out that increased colour, by promoting absorption of solar radiation in the surface layer, can give rise to a more shallow mixed layer when stratification sets in, thus decreasing the mixing depth and increasing the average light intensity to which the phytoplankton are exposed. He suggests, nevertheless, that this effect is only likely to be of significance in small sheltered forest lakes. Larger lakes with wind exposure do not show a correlation between mixing depth and water colour.

It should be noted that a high total vertical attenuation coefficient need not necessarily be associated with low productivity since that high coefficient may be due to a high concentration of phytoplankton: it is high attenuation by non-algal material that we expect to lower the productivity. So far as seagrasses and freshwater macrophytes are concerned, we have already seen (§11.1) that the depth of colonization is inversely proportional to the vertical attenuation coefficient for PAR, indicating that the more highly attenuating the water, the lower the macrophyte productivity of the water body.

Estuaries are often highly attenuating water bodies, due to the presence of high concentrations of suspended sediment particles, which both absorb and scatter light, and to dissolved humic colour in the river inflow. Turbidity, and consequently attenuation, varies longitudinally down the estuary, rising to a peak at the so-called 'turbidity maximum' the position of which varies with the tide, attenuation and turbidity then diminishing in a seaward direction.<sup>246,251,528,650,856,1042</sup>

Cole and Cloern (1984, 1987) have found, for a number of estuaries, that phytoplankton daily productivity can be expressed as a linear

function of  $[\text{Chl}]E_d(0^+)/K_d(\text{PAR})$  or, equivalently, of  $[\text{Chl}]E_d(0^+)z_{eu}$ . To interpret this, we note that in optically deep waters all the daily surface-incident light,  $E_d(0^+)$  (apart from the small fraction which is reflected at, or back-scattered through, the surface), is absorbed in the water column, and also that the proportion of this light which is absorbed by the phytoplankton is  $a_p/a_t$  (see §9.4). Given that  $a_p$  (the phytoplankton absorption coefficient) is linearly related to the phytoplankton concentration,  $[\text{Chl}]$ , and that  $K_d(\text{PAR})$  is very approximately proportional to  $a_t$  (where this is understood as a depth- and spectrally averaged total absorption coefficient for the estuarine water), we can see that  $[\text{Chl}]E_d(0^+)/K_d(\text{PAR})$  is an approximate measure of the daily absorption of light by the phytoplankton population. Light limitation of primary productivity due to high turbidity is common in estuaries: examples are the Hudson River estuary (New York State, USA)<sup>253</sup> and the Gironde estuary in southwest France.<sup>612</sup>

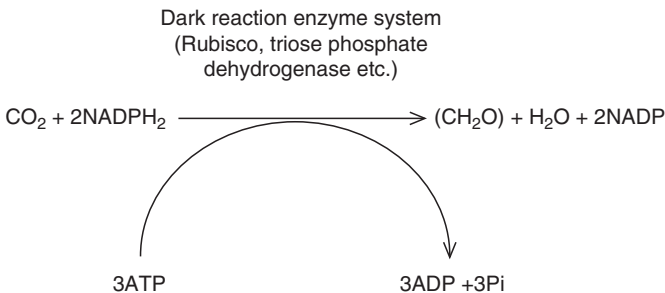
Turbid waters in which the turbidity is due to large numbers of mineral particles which are themselves of low intrinsic colour, and in which dissolved colour is also low – such as lakes with suspended glacier-derived mineral flour – represent a special case. Because of the intense scattering, the total vertical attenuation coefficient,  $K_d(\text{PAR})$ , may be quite high so that the euphotic zone is shallow. This fact alone does limit production by reducing the volume of medium that the phytoplankton can exploit photosynthetically. Nevertheless, within the euphotic zone the relative ability of the phytoplankton to collect light is dependent on its absorption properties compared to the other constituents of the medium ( $a_p/a_t$ ), and since in the present case the rest of the medium does not absorb the light strongly despite its intense scattering, the phytoplankton is well placed to compete for the available photons. In a medium of this type, the assumption, contained in eqn 10.12, that the relative amounts of the absorbed light captured by phytoplankton and by the rest of the medium are in proportion, respectively, to  $[\text{Chl}]k_c$  and  $K_{NP}$ , is no longer even approximately valid. We saw in §10.3 that this assumption can in fact only be made with reasonable accuracy for waters in which vertical attenuation is absorption dominated.

The kind of mechanism we have envisaged, namely effective competition by phytoplankton for the photons within the shallow euphotic zone, may in part account for the surprisingly high productivity of some waters with high inorganic turbidity.<sup>1005</sup> The shallowness of such waters (the turbidity often being due to wind resuspension of bottom sediments) will further promote their productivity by ensuring that the circulating cells

do not for long remain below the illuminated layer. In addition, the ratio of scalar to downward irradiance is high in turbid waters with a high ratio of scattering to absorption (see Fig. 6.10), and so there is substantially more light available for photosynthesis than the values of downward irradiance alone would indicate.

### 11.3 Other limiting factors

To fully understand the extent to which light availability limits primary production it is necessary to be aware of the limitations that are imposed at the same time by other environmental factors. Consider, for example, a diatom population photosynthesizing in lake water at a saturating light intensity of  $\sim 400 \mu\text{mol photons m}^{-2} \text{ s}^{-1}$ , as illustrated in Fig. 10.1. A small increase in light intensity will bring about no change in photosynthetic rate and a large increase will even lead to photoinhibition. What is happening within the cells is that the rate of formation of the products of the light reactions of photosynthesis, namely  $\text{NADPH}_2$  and ATP, is so high that the enzyme system responsible for the dark reactions is saturated so far as  $\text{NADPH}_2$  and ATP are concerned. Any increase in their steady-state concentration resulting from an increase in light intensity is therefore not accompanied by an increase in the rate of  $\text{CO}_2$  fixation. This does not mean, however, that the system is necessarily working at its maximum possible rate. The  $\text{CO}_2$  concentration may be too low to saturate the first enzyme, ribulose biphosphate carboxylase (Rubisco), in the dark reaction sequence so that it is not functioning at its maximum capacity. Alternatively, or in addition, the temperature may be too low for maximum activity: at a higher temperature the enzymes of the whole dark reaction system might operate more rapidly and thus be able to consume the  $\text{NADPH}_2$  and ATP at a faster rate.



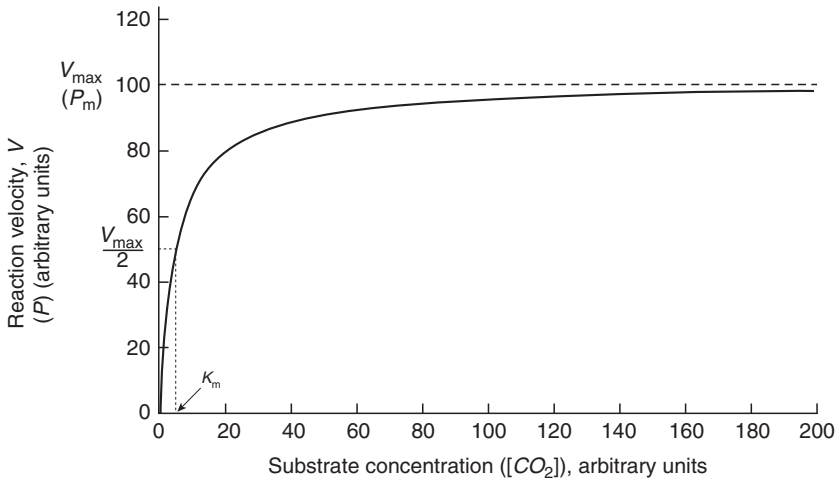


Fig. 11.2 Idealized curve of rate of an enzymic reaction as a function of substrate concentration. Calculated from Michaelis–Menten equation.

### Carbon dioxide

We shall first consider the extent to which CO<sub>2</sub> availability limits the overall rate. Given that CO<sub>2</sub> is a substrate that is used by an enzyme (system), then we may plausibly suppose that the photosynthetic rate at any given light intensity will vary with CO<sub>2</sub> concentration approximately in accordance with the well-known Michaelis–Menten equation for enzyme kinetics

$$v = \frac{V_s s}{K_m + s}$$

where  $v$  is the rate of enzyme reaction at substrate concentration  $s$ ,  $V$  is the maximum rate obtainable at saturating substrate concentrations and  $K_m$  is the dissociation constant of the enzyme–substrate complex, but is also equivalent to the substrate concentration that gives half the maximum rate. Re-expressing the equation in photosynthetic terms we obtain

$$P = \frac{P_m[CO_2]}{K_m(CO_2) + [CO_2]} \quad (11.2)$$

Figure 11.2 shows an idealized curve of rate versus substrate concentration for an enzymic reaction, in accordance with the Michaelis–Menten equation. Observed curves of photosynthetic rate versus CO<sub>2</sub>

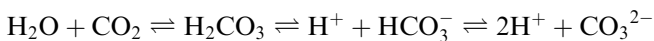
concentration for aquatic plants are approximately of this type, and so by obtaining the  $K_m$  values from such curves and comparing them with the *in situ*  $\text{CO}_2$  concentrations, we may be able to assess to what extent  $\text{CO}_2$  availability limits photosynthesis in natural waters.

In the isolated state, Rubisco from aquatic plants has a  $K_m$  value for  $\text{CO}_2$  of 30 to 70  $\mu\text{M}$ .<sup>1489</sup> The  $K_m(\text{CO}_2)$  values for living plants, however, can be higher because of diffusive resistance to entry of carbon dioxide into the plant, or lower due to active uptake of  $\text{CO}_2$ . Some values for  $K_m(\text{CO}_2)$  determined for phytoplankton and macrophyte species, at pH values low enough ( $\text{pH} < 6$ ) to ensure that essentially all the inorganic carbon (Ci) exists as  $\text{CO}_2$  (or its hydrated form,  $\text{H}_2\text{CO}_3$ ), are listed in Table 11.1: they range from 4 to 185  $\mu\text{M}$ . Fresh water in equilibrium with the atmosphere ( $\sim 0.035$  vol%  $\text{CO}_2$ ) at 15°C contains dissolved  $\text{CO}_2$  at about 14  $\mu\text{M}$  concentration. Calculations for sea water at 26°C indicate a free  $\text{CO}_2$  concentration of about 12  $\mu\text{M}$ .<sup>136</sup> We might therefore expect it commonly to be the case that aquatic plant photosynthesis in natural waters is undersaturated with respect to  $\text{CO}_2$  concentration, and should respond to an increase in  $\text{CO}_2$  concentration with an increase in photosynthetic rate. This need not apply only at saturating light intensity: the assumption that photosynthetic rate depends on  $\text{CO}_2$  concentration in accordance with the Michaelis–Menten relation implies that even at low light intensities an increase in  $\text{CO}_2$  concentration above a typical starting value of 12 to 14  $\mu\text{M}$  would lead to an increase in photosynthetic rate. This means that at subsaturating light intensities, photosynthesis by plants within a water body could be simultaneously limited by availability of both light and  $\text{CO}_2$ . The aquatic moss, *Fontinalis antipyretica*, and the aquatic higher plant, *Cabomba caroliniana*, both show marked increase in photosynthetic rate with increasing  $\text{CO}_2$  concentration in the range 10 to 25  $\mu\text{M}$  at low, subsaturating, as well as at high, light intensities.<sup>523,1235</sup> Figure 11.3 shows Smith's (1938) data for *Cabomba*. These examples are, however, somewhat untypical since most aquatic higher plants and algae, in the particular waters in which they naturally occur, do not show much response to an increase in  $\text{CO}_2$  supply. The reason is that not only can aquatic plants draw on other sources of inorganic carbon, but most of them also have the ability to carry out active transport of Ci, this being commonly referred to as the *carbon-concentrating mechanism*, or CCM. This topic is reviewed by Falkowski and Raven (2007), by Kaplan and Reinhold (1999), and in the proceedings of the *4th International Symposium on Inorganic Carbon Utilization by Aquatic Photosynthetic Organisms*, 2001 (*Functional Plant Biology*, 2002, Vol. 29).

Table 11.1 Apparent half-rate constants ( $K_m$ ) for  $CO_2$  for photosynthesis in certain phytoplankton and macrophyte species.

Plant species	$K_m(CO_2)$ ( $\mu M$ )	Reference
<b>Freshwater phytoplankton</b>		
Chlorophyta		
<i>Pediastrum boryanum</i>	40	19
<i>Cosmarium botrytis</i>	170	19
<i>Chlamydomonas reinhardtii</i>	29	384
<i>Scenedesmus obliquus</i>	38	384
Euglenophyta		
<i>Euglena gracilis</i>	25	384
Cyanophyta		
<i>Anabaena cylindrica</i>	60	19
<i>Aphanizomenon flos-aquae</i>	105	384
<i>Coccochloris peniocystis</i>	121	384
<i>Plectonema boryanum</i>	100	384
<b>Freshwater macrophytes</b>		
<i>Nitella flexilis</i>	100	19
<i>Eurhynchium rusciforme</i>	80	19
<i>Fontinalis antipyretica</i>	170	19
<i>Elodea canadensis</i>	30	19
<i>Potamogeton crispus</i>	20	19
<i>Hydrilla verticillata</i>	170	1394
<i>Myriophyllum spicatum</i>	150	1394
<i>Ceratophyllum demersum</i>	165	1394
<b>Marine phytoplankton</b>		
Chlorophyta		
<i>Stichococcus bacillaris</i>	4	966
Heterokontophyta		
<i>Cylindrotheca fusiformis</i> (diatom)	36	384
<i>Olisthodiscus luteus</i> (raphidophyte)	59	384
Rhodophyta		
<i>Porphyridium cruentum</i>	22	384
Cyanophyta		
<i>Synechococcus</i> sp.	240	384
<b>Marine macrophytes</b>		
<i>Ulva</i> sp.	30	86
<i>Ulva lactuca</i>	185	321

Sea water and most inland waters contain much more inorganic carbon in the form of bicarbonate ion,  $HCO_3^-$  than in the form of  $CO_2$ . The different forms of inorganic carbon are interconverted in accordance with



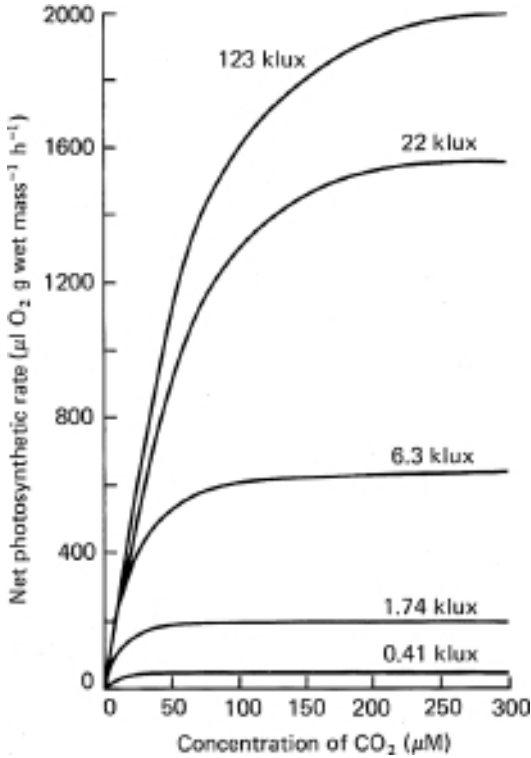


Fig. 11.3 Photosynthetic rate as a function of CO<sub>2</sub> concentration at different light intensities in the aquatic higher plant *Cabomba caroliniana* (after Rabinowitch, 1951, based on data of Smith, 1938).

The higher the pH of the water, the more this equilibrium shifts to the right with HCO<sub>3</sub><sup>-</sup> constituting more than 50% of the total from pH 6.2 to 9.3, and more than 80% between pH 6.7 and 8.8. Given that CO<sub>2</sub> tends, as we have seen, to be present at suboptimal concentration, it would clearly be an advantage in many waters for aquatic plants to be able to use bicarbonate as a carbon source for photosynthesis, and in fact many, but not all, species do. The inorganic carbon species used by the carboxylase enzyme is always CO<sub>2</sub>. In the plants that can utilize bicarbonate, the HCO<sub>3</sub><sup>-</sup> ions are transported into the cell where they give rise to CO<sub>2</sub> by the reversal of the first two of the above interconversion reactions. The reversible dehydration of H<sub>2</sub>CO<sub>3</sub> to give CO<sub>2</sub> is catalyzed by carbonic anhydrase, an enzyme that occurs in the chloroplast, but can also be present within the cytoplasm and on the exterior surface of the

cytoplasmic membrane. The liberated  $\text{CO}_2$  is then used in photosynthesis. In the case of the external enzyme, the liberated  $\text{CO}_2$  diffuses through the cytoplasmic membrane into the cell. The combination of  $\text{HCO}_3^-$  ions with  $\text{H}^+$  to give  $\text{H}_2\text{CO}_3$  leads to a corresponding accumulation of  $\text{OH}^-$  ions (from  $\text{H}_2\text{O} \rightarrow \text{H}^+ + \text{OH}^-$ ) which are excreted from the cells to balance the uptake of  $\text{HCO}_3^-$ .

So far as marine ecosystems are concerned, photosynthetic utilization of bicarbonate has been found in most of the seaweed species – green, brown and red – which have been examined, but is not universally present. Maberly (1990) found that out of 35 species of marine macroalgae, six species – all rhodophytes – were unable to use  $\text{HCO}_3^-$  and five of these occurred in relatively low-light habitats, beneath a canopy of larger Phaeophyta. He suggested that most species growing at depths where light is low will be unable to use  $\text{HCO}_3^-$ . The red macroalga *Chondrus crispus*, although it does not take up bicarbonate directly, nevertheless gains access to this plentiful inorganic carbon pool by dehydrating  $\text{HCO}_3^-$  to  $\text{CO}_2$  with an external carbonic anhydrase.<sup>1254,1255</sup> Out of 29 macroalgal species (13 green, 5 red, 11 brown) studied by Larsson and Axelsson (1999) all except one (*Palmaria palmata*, red) utilized  $\text{HCO}_3^-$  by means of an external carbonic anhydrase.

In addition to being able to utilize  $\text{HCO}_3^-$  via an external carbonic anhydrase, some algae also have the ability to actively transport this anion into the cell. Two common and successful green algal species, *Cladophora glomerata* and *Enteromorpha intestinalis*, both have bicarbonate transporters.<sup>229,771</sup> Some, but not all, green algal species have an inducible bicarbonate transporter, which operates by anion exchange:<sup>770,229</sup> this capacity develops at high pH. It was absent from a number of brown and red algal species tested. The brown alga, *Hizikia fusiforme*, possesses an external carbonic anhydrase, but does not carry out active transport of  $\text{HCO}_3^-$ .<sup>1506</sup> Choo *et al.* (2002) found that in addition to an external carbonic anhydrase and an anion exchange-type bicarbonate transporter, *Cladophora glomerata* can also form a transporter that uses a proton pump of the ATPase type. Protons are electrogenically pumped out of the cell to create an active proton gradient, which then leads to inward transport of  $\text{H}^+$  and  $\text{HCO}_3^-$ . Formation of the proton pump is induced by carbon limitation. An additional mechanism that makes use of the proton gradient is the localized combination of  $\text{H}^+$  and  $\text{HCO}_3^-$  to give  $\text{H}_2\text{CO}_3$  from which  $\text{CO}_2$  is liberated by means of the external carbonic anhydrase. This appears to be present in the charophyte, *Chara corallina*,<sup>393,1088</sup> and in the brown alga, *Laminaria saccharina*.<sup>47</sup> The  $\text{CO}_2$  thus produced is present at locally high concentration, leading to inward

diffusion across the cell membrane. In *Chara*, proton secretion takes place in specialized acidic bands. These are accompanied by separate alkaline bands<sup>1114</sup> where  $\text{CaCO}_3$  incrustation takes place: these may correspond to sites where  $\text{OH}^-$  secretion (or  $\text{H}^+$  uptake) takes place to conserve alkalinity.<sup>85</sup> Even in those macrophytes, such as *Ulva*, which can utilize bicarbonate it seems that photosynthesis in bright light can in some cases be limited by the level of inorganic carbon in sea water.<sup>794a</sup>

Bicarbonate utilization is found in some,<sup>87,847,1092a</sup> but apparently not all,<sup>5</sup> seagrasses. Possession of an external, membrane-bound carbonic anhydrase is common among these marine angiosperms.<sup>85</sup> While this facilitates uptake of inorganic carbon it does not on its own constitute a CCM. It appears likely that those seagrasses that can carry out active transport of bicarbonate do so by means of a proton pump creating an  $\text{H}^+$  gradient. This gradient can be used to bring about bicarbonate transport in two ways. There can be inward cotransport of  $\text{H}^+$  and  $\text{HCO}_3^-$ , or there can be localized combination of  $\text{H}^+$  and  $\text{HCO}_3^-$  to give  $\text{H}_2\text{CO}_3$  from which  $\text{CO}_2$  is liberated by means of the external carbonic anhydrase,<sup>393,1088,85</sup> followed by inward diffusion across the cell membrane as described for *Chara*, above. As with *Chara*, it seems likely that there are spatially separated acid and alkaline zones.<sup>85</sup> This particular mechanism for CCM is not universal among seagrasses: out of eight tropical species studied by Uku *et al.* (2005), it was present in six and absent in two. In *Zostera marina*, which does utilize this mechanism, Carr and Axelsson (2008) found that a major part of the ATP used to generate the acid zones was derived from mitochondrial respiration. Seagrasses do not appear to possess an active transport mechanism of the anion exchange type.

On the basis of isotope disequilibrium experiments, carried out on phytoplankton from the eastern Subtropical and Equatorial Pacific Ocean, Tortell and Morel (2002) concluded that  $\text{HCO}_3^-$  was the principal form of inorganic carbon taken up by all of the *in situ* populations sampled. All eukaryotic phytoplankton species contain internal carbonic anhydrase: the presence of an external carbonic anhydrase is common but not universal. Among the marine phytoplankton,  $\text{HCO}_3^-$  utilization has been shown in the coccolithophorid *Coccolithus huxleyi*;<sup>1028</sup> in a number of diatom, haptophyte and eustigmatophyte species;<sup>256</sup> and in the unicellular red alga *Porphyridium cruentum*;<sup>255</sup> but the green plankter *Stichococcus bacillaris* has a high affinity for  $\text{CO}_2$  (Table 11.1) and a low affinity for bicarbonate,<sup>966</sup> and a number of common marine diatoms appear to be unable to use bicarbonate.<sup>296,1127</sup> Dason *et al.* (2004) found that two

marine dinoflagellates, *Amphidinium carterae* and *Heterocapsa oceanica*, are unable to take up bicarbonate, but appear to have an active transport system for  $\text{CO}_2$  itself. This appears to be also the case for two marine chlorophyte species, *Nannochloris atomus* and *N. maculata*.<sup>598</sup> Symbiotic dinoflagellates (*Symbiodinium* sp., zooxanthellae) in giant clams have a CCM, and preferentially transport  $\text{CO}_2$ .<sup>792</sup> Burkhardt *et al.* (2001) present evidence that two marine diatom species, *Thalassiosira weissflogii* and *Phaeodactylum tricornutum*, possess active transport systems for both  $\text{HCO}_3^-$  and  $\text{CO}_2$ . The rhodophyte, *Porphyridium cruentum*, also actively transports both forms of  $\text{C}_i$ ,<sup>598</sup> as do the freshwater eustigmatophyte, *Eustigmatos vischeri*,<sup>597</sup> and certain marine prymnesiophyte species.<sup>108,596</sup> Inhibitor studies suggest that an anion-exchange type of  $\text{HCO}_3^-$  transport system occurs in some eukaryotic marine phytoplankton species but not others.<sup>992</sup> Maberly *et al.* (2009) tested species from 12 chrysophyte families for their ability to take up inorganic carbon. The results indicated that chrysophytes as a group do not have a CCM, and in addition lack the ability to make use of bicarbonate as an alternative source of inorganic carbon.

Marine cyanobacteria, such as *Synechococcus*, actively transport both  $\text{HCO}_3^-$  and  $\text{CO}_2$  into their cells.<sup>55,1089,56</sup> Within the cell  $\text{C}_i$  exists predominantly as  $\text{HCO}_3^-$ . The bicarbonate ions diffuse into the carboxysome, a semi-crystalline structure consisting mainly of Rubisco, but also containing carbonic anhydrase. The latter enzyme maintains a high localized level of  $\text{CO}_2$  by continuously generating it from  $\text{HCO}_3^-$ , and this is sufficient to saturate the carboxylase, and competitively suppress the oxygenase activity of Rubisco.<sup>384</sup>

In fresh waters, according to Hutchinson's (1975) review, most aquatic higher plants can utilize bicarbonate for photosynthesis. Maberly and Madsen (2002), in their review of carbon uptake mechanisms in freshwater angiosperms, report that use of  $\text{HCO}_3^-$  is present in about half the submerged angiosperm species that have been tested, and is more common in lakes of high alkalinity. The species that cannot utilize bicarbonate typically occur in soft waters in which bicarbonate concentrations are low. Aquatic mosses mainly seem to lack the ability to utilize  $\text{HCO}_3^-$ . Most charophyte species (other than those from soft waters) can utilize  $\text{HCO}_3^-$  as can benthic filamentous algae such as *Cladophora*. Among the freshwater phytoplankton, the ability to utilize  $\text{HCO}_3^-$  for photosynthesis varies widely. *Chlorella emersonii*, *Scenedesmus quadricauda*, *Chlamydomonas reinhardtii* (green), *Ceratium hirundinella* (dinoflagellate), *Fragilaria crotonensis* (diatom), *Microcystis aeruginosa* and *Anabaena*

*cylindrica* (blue-green) can all effectively use  $\text{HCO}_3^-$  but *Chlorella pyrenoidosa* (green), *Asterionella formosa* and *Melosira italica* (diatoms) cannot<sup>19,839,1109,1338,1377</sup> Certain other freshwater *Chlorella* species, and the freshwater diatom, *Navicula pelliculosa*, carry out active transport of both  $\text{HCO}_3^-$  and  $\text{CO}_2$ .<sup>256</sup>

Despite the wide occurrence of ability to utilize bicarbonate in the aquatic plant kingdom, it is generally true that, with the possible exception of phytoplankton species adapted to alkaline waters, free  $\text{CO}_2$  if available is the preferred, i.e. more effectively used, carbon source. For example, the freshwater macrophyte *Myriophyllum spicatum*, which can use bicarbonate, gives a much higher photosynthetic rate with free  $\text{CO}_2$  at its optimum concentration than with  $\text{HCO}_3^-$  at its optimum concentration.<sup>1297</sup> Bodner (1994) found that the pondweed, *Potamogeton natans*, used  $\text{CO}_2$  but was unable to use  $\text{HCO}_3^-$ ; *Ranunculus fluitans* preferentially used  $\text{CO}_2$ , but was able to switch to  $\text{HCO}_3^-$  at pH values of 9.0 and above, when the  $\text{CO}_2$  concentration was close to zero. Steemann Nielsen (1975) suggested that one of the reasons for the less effective use of  $\text{HCO}_3^-$  is that energy must be used for its active transport into the plant, whereas  $\text{CO}_2$  diffuses in freely. The data of Allen and Spence (1981) for freshwater macrophytes in Table 11.1 show that in all cases, including the known bicarbonate users *Elodea canadensis* and *Potamogeton crispus*, the apparent  $K_m$  for  $\text{HCO}_3^-$  is 50- to 100-fold higher (indicating a much lower affinity) than the  $K_m$  for  $\text{CO}_2$ . Furthermore, to give the same photosynthetic rate as a certain concentration of  $\text{CO}_2$  (at pH 5.5),  $\text{HCO}_3^-$  (pH 8.8) at 52 to 132 times the concentration was needed. In the case of the blue-green alga *Anabaena cylindrica*, on the other hand, occurring typically in alkaline eutrophic waters, the  $K_m$  values for  $\text{CO}_2$  and  $\text{HCO}_3^-$  are about the same, and the concentrations of  $\text{CO}_2$  and  $\text{HCO}_3^-$  that produce a certain photosynthetic rate are also about the same. On the basis of their studies, Allen and Spence conclude that despite the ability of most freshwater macrophytes to utilize bicarbonate, they do not in fact obtain much of their carbon from  $\text{HCO}_3^-$  until the pH of the water exceeds 9.0, and at these high pH values their photosynthetic rates are greatly reduced anyway. Allen and Spence suggest that the natural rates of photosynthesis of freshwater macrophytes and some planktonic algae are functions mainly of  $\text{CO}_2$  (as opposed to  $\text{HCO}_3^-$ ) concentration. This conclusion may not, however, apply to the more effective bicarbonate users among the macrophytes, such as *Myriophyllum spicatum*. Adams *et al.* (1978) found that in a series of rather alkaline (pH values mainly 7.5–8.8) Italian lakes, all well supplied with phosphorus, the rate of photosynthesis of *M. spicatum* varied

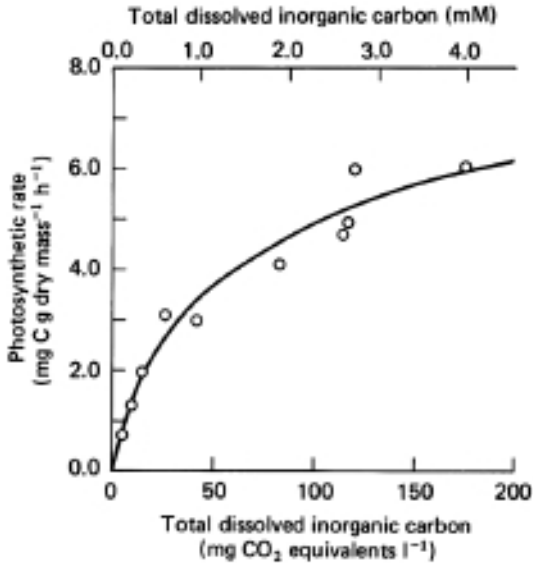


Fig. 11.4 Variation of photosynthetic rate of *Myriophyllum spicatum* with total dissolved inorganic carbon concentration in a series of Italian lakes (plotted from data of Adams *et al.*, 1978). Light intensities were at or near saturation in most cases. Using non-linear regression to the Michaelis–Menten equation, Adams *et al.* calculated a  $K_m$  (half-saturation constant) value of 1.06 mM total dissolved inorganic carbon (46.5 mg CO<sub>2</sub> equivalents l<sup>-1</sup>) and a  $P_m$  value of 7.24 mg C g<sup>-1</sup> dry mass h<sup>-1</sup>.

with the total dissolved inorganic carbon concentration in accordance with a Michaelis–Menten type of relation (Fig. 11.4). From calculations of the amounts of the different forms of inorganic carbon present, it appeared that photosynthetic rate was related primarily to the concentration of HCO<sub>3</sub><sup>-</sup> rather than to the concentration of CO<sub>2</sub>.

Jones (2005) has pointed out that the formation and operation of an active transport system for HCO<sub>3</sub><sup>-</sup> must impose an energy cost on a plant. In experiments with *Elodea nuttallii*, growing in water containing bicarbonate, and bubbled either with normal air or air depleted of CO<sub>2</sub> (which would favour the switch to HCO<sub>3</sub><sup>-</sup> use), he found that after 21 days the bicarbonate-using plants photosynthesized at ~58% higher rate, but had achieved only the same growth as the plants predominantly using CO<sub>2</sub>, suggesting that some of the photosynthetically captured light energy was being used for constructing, maintaining and running the bicarbonate utilization system. Jones estimated that this would correspond in the field to an irradiance of ~80 μmol photons m<sup>-2</sup> s<sup>-1</sup>, below

which  $\text{HCO}_3^-$  use would not be expected in this species. Since this is an irradiance commonly experienced by submerged macrophytes in inland waters,  $\text{HCO}_3^-$  use is likely to be confined to areas where ambient light is above the requisite threshold.

Algae such as *Anabaena cylindrica*, which photosynthesize optimally at pH values in the region of 9.0, make very efficient use of bicarbonate. For these planktonic species and the more effective bicarbonate users among the macrophytes, the natural rate of photosynthesis (as far as carbon supply is concerned) can be regarded as a function of the concentration of  $\text{HCO}_3^-$  plus  $\text{CO}_2$ . The ability of blue-green algae such as *Anabaena*, *Microcystis* and *Spirulina* to continue photosynthesizing in water of high pH, and effectively zero free  $\text{CO}_2$  concentration could be one of the main factors contributing to their frequent domination of eutrophic lakes in late summer and their invariable domination of highly alkaline waters such as the African soda lakes. The ability of some cyanobacteria to form surface blooms gives them an additional advantage: by placing a dense biomass close to the water surface, they are able to intercept a large proportion of the incoming  $\text{CO}_2$  from the atmosphere, as well as the incident light.<sup>607</sup>

Ratray *et al.* (1991) found that two rooted freshwater macrophytes, *Lagarosiphon major* and *Myriophyllum triphyllum*, grew and photosynthesized twice as fast in the water of oligotrophic Lake Taupo (New Zealand) as in the nitrogen- and phosphorus-rich water of eutrophic Lake Rotorua. Ratray *et al.* attributed this to the two-fold higher level of  $\text{CO}_2$  found to be present in the oligotrophic, than in the eutrophic, water. Soft-water oligotrophic lakes are often characterized by the presence of benthic macrophytes with the isoetid growth form: small plants with short stems and rosettes of leaves.<sup>603</sup> Isoetids have solved the problem presented by the low inorganic carbon concentration in these poorly mineralized waters by extracting the  $\text{CO}_2$  from the sediments, where it is formed from decaying organic matter, through their roots.<sup>142,847,1111,846</sup> This  $\text{CO}_2$  diffuses from the roots to the leaves via longitudinal air-filled channels, and in some cases provides virtually all the photosynthetically fixed carbon. The emergent macrophyte, *Cyperus papyrus*, also has large intercellular air cavities (aerenchyma) extending down to its rhizomes in the sediments, and is able to photosynthetically capture  $\text{CO}_2$  coming up from the rhizomes.<sup>808</sup>

The free  $\text{CO}_2$  concentrations of 12 to 14  $\mu\text{M}$  referred to earlier apply only to waters in equilibrium with the atmosphere. Such concentrations might normally be found in the surface layer of the oceans, or of unproductive inland waters, or of most inland waters in the winter. However,

any biologically productive water body is likely not to be in equilibrium with the atmosphere so far as  $\text{CO}_2$  is concerned. The free  $\text{CO}_2$  concentration at any time is likely to differ from the equilibrium value and will vary with time and depth in accordance with where and how fast the processes of consumption (photosynthesis) and production (respiration, decomposition) are taking place. On the basis of model calculations of rates of  $\text{CO}_2$  diffusion to the cell, and of laboratory measurements of growth rates as a function of  $\text{CO}_2$  concentration, Riebesell *et al.* (1993) concluded that during phytoplankton blooms in the ocean, when  $\text{CO}_2$  concentration in the surface layer falls drastically, the growth rate of marine diatoms can be limited by the  $\text{CO}_2$  supply to the cell surface. Vadstrup and Madsen (1995) found in oligotrophic low-alkalinity Lake Hampen (Denmark) that the concentration of free  $\text{CO}_2$  was about five times atmospheric equilibrium concentration in early summer, but had declined virtually to zero by the end of summer.

Free  $\text{CO}_2$  can be even more affected by changes in pH caused by photosynthesis. Talling (1976, 1979) presented data for the changes in free  $\text{CO}_2$  concentration in the eutrophic English lake, Esthwaite Water, from April to July 1971. On 19 April, before thermal stratification, the  $\text{CO}_2$  concentration was the same from the surface down to 10 m depth. By 3 May when the phytoplankton population had begun to increase, and there was some warming of the surface layer,  $\text{CO}_2$  concentration had fallen by about 33% in the upper 4 m but had increased greatly between 6 and 10 m. During July, thermal stratification became established, the phytoplankton population above the thermocline increased substantially and free  $\text{CO}_2$  levels in the epilimnion were reduced virtually to zero, while rising to even higher values than before in the 6 to 10 m layer below the thermocline. The amount of inorganic carbon removed by photosynthesis represented about 50% of the total inorganic carbon in the surface layer. The remainder of the ~1000-fold decrease in free  $\text{CO}_2$  was due to the rise in pH from ~7.0 to above 9.0, resulting from the photosynthetic activity of the dense phytoplankton population. Similar changes are likely to take place in any productive water body. For one of the components of the phytoplankton, the diatom *Asterionella formosa* (not a bicarbonate user), Talling (1979) calculated that on 12 July its photosynthetic rate was virtually zero in the surface layer due to lack of  $\text{CO}_2$ , that it rose between 2 and 3 m due to an increase in  $\text{CO}_2$  accompanied by reasonably high irradiance values, and that it declined again below this depth because of the fall in irradiance. Thus with increasing depth, its photosynthesis was limited first by a  $\text{CO}_2$  supply, then by  $\text{CO}_2$  and light simultaneously, and

then mainly by light availability alone. These changes with depth did not apply to total phytoplankton photosynthesis, however, since when the pH rose and the  $\text{CO}_2$  concentration fell, *Asterionella* was largely replaced by the bicarbonate users *Ceratium* and *Microcystis*.

The sinking rate of diatom cells increases when  $\text{CO}_2$  uptake becomes limited: the  $\text{CO}_2$  depletion associated with summer stratification might lead to an increased sinking rate of diatoms, and this may contribute to the paucity of diatoms frequently observed in productive lakes in the summer.<sup>622</sup>

Immediately next to the surface of any aquatic plant, there is an unstirred layer of water that  $\text{CO}_2$  and/or  $\text{HCO}_3^-$  ions must diffuse across before they can enter the cells and be used for photosynthesis. The thickness of this layer diminishes if the plant is subjected to turbulence or rapid stirring but the layer never disappears completely. Under well-stirred conditions, the unstirred layer might be only about 5  $\mu\text{m}$  thick around a small cell such as *Chlorella* but 30 to 150  $\mu\text{m}$  thick around the surface of a macrophyte such as *Chara*.<sup>1109,1236</sup> In still or slowly moving water the unstirred layer will often be much more than 150  $\mu\text{m}$  thick. Raven (1970), and Smith and Walker (1980), who have reviewed this topic, conclude that diffusion of  $\text{CO}_2$  (and presumably  $\text{HCO}_3^-$ ) across this unstirred layer can be an important rate-limiting step in photosynthesis by aquatic macrophytes. An increase in photosynthetic rate of river plants associated with increased flow velocities in natural waters has in fact been demonstrated by Westlake (1967). Wheeler (1980b) found that the photosynthetic rate of the blade of the great kelp, *Macrocystis pyrifera*, in saturating light, increased about four-fold when the current speed increased from 0 to 5  $\text{cm s}^{-1}$ : in low light, however, the increase was only about 50%. Any morphological adaptation that increases the surface-to-volume ratio will help to overcome the diffusion problem and many aquatic macrophyte species have achieved this by evolving highly dissected leaves.<sup>603</sup> The more dissected the leaf form, the less the stimulation of photosynthesis brought about by increased turbulence.<sup>451</sup> Whether the existence of an unstirred layer around each cell has any significant limiting effect on photosynthesis by phytoplankton remains uncertain.

While the rate of photosynthesis in submerged freshwater macrophytes tends to increase in response to increasing current velocity up to approximately 0.5  $\text{cm s}^{-1}$ , there can be inhibitory effects for water velocities beyond  $\sim 0.5$  to 3  $\text{cm s}^{-1}$ .<sup>845,991</sup> Using autoradiography of  $^{14}\text{CO}_2$ -exposed leaves of *Elodea canadensis*, Nielsen *et al.* (2006) found that at high current velocity the  $\text{CO}_2$  uptake was approximately two-fold higher near

the leaf periphery compared with the midrib section, whereas at low current velocity the area of relatively high  $\text{CO}_2$  uptake expanded from the leaf periphery towards the midrib and basal sections. They propose that slow-moving water creeps around the leaf tips and enters the gaps between the whorls of leaves, delivering  $\text{CO}_2$  to the basal parts of the leaves near the stem. At high water velocity the water does not enter the gaps, but rather skips across, effectively raising the level of the surface. The extent to which this takes place is likely to be very much a function of the plant morphology.

In the majority of terrestrial higher plant species, those which lack the  $\text{C}_4$  pathway, photosynthesis is significantly inhibited by oxygen at the normal atmospheric level (21%), primarily as a result of the direct competition between  $\text{O}_2$  and  $\text{CO}_2$  at the active site of Rubisco. In the oxygenase reaction of Rubisco, the oxygen reacts with ribulose biphosphate to produce phosphoglycollate and phosphoglycerate, and this is the first step in the metabolic pathway known as photorespiration. Photosynthesis by aquatic higher plants and algae, by contrast, in most cases shows relatively little inhibition by oxygen. This appears to be due to the ability of aquatic plants to increase, by one or other of a range of mechanisms, the concentration of  $\text{CO}_2$  in the proximity of the Rubisco molecules within the cell, thus increasing the  $\text{CO}_2/\text{O}_2$  competitive ratio. There is, as we have seen, evidence for active transport of  $\text{CO}_2$ , and in some cases of  $\text{HCO}_3^-$  as well, achieving a many-fold higher internal than external concentration.

As well as the 'biophysical' strategy there are biochemical solutions to the problem of raising the internal  $\text{CO}_2$  concentration. No submerged aquatic plant has yet been found which exhibits  $\text{C}_4$  photosynthesis as it occurs in terrestrial  $\text{C}_4$  species, i.e. with fixation of  $\text{CO}_2$  into a  $\text{C}_4$  acid such as malate in the mesophyll cells, followed by transport of this acid to specialized bundle sheath cells where  $\text{CO}_2$  is released and then re-fixed into carbohydrate by the normal photosynthetic carbon reduction (PCR) cycle. What might, however, be regarded as a structurally abbreviated version of the  $\text{C}_4$  pathway has been found by Salvucci and Bowes (1983) in the freshwater macrophyte *Hydrilla verticillata* (Hydrocharitaceae), where the whole biochemical sequence appears to take place within the same cell. There is also evidence for this kind of  $\text{C}_4$  photosynthesis in certain other members of the Hydrocharitaceae, including *Hydrilla verticillata*<sup>852</sup> and *Egeria densa*.<sup>212</sup> In both cases, formation of the  $\text{C}_4$  cycle enzymes is induced when the plants are grown under conditions (high temperature, high light, long photoperiods) that result in limiting  $\text{CO}_2$  levels in the water. In their review of  $\text{C}_4$  mechanisms in aquatic

angiosperms, Bowes *et al.* (2002) refer to *Hydrilla* as a facultative C<sub>4</sub> that shifts from C<sub>3</sub> to C<sub>4</sub> in low [CO<sub>2</sub>].

It seems likely that most of the initial CO<sub>2</sub> fixation is carried out by phosphoenolpyruvate (PEP) carboxylase in the cytoplasm. The oxaloacetic acid produced is reduced to malic acid. This is transported into the chloroplasts where it is decarboxylated by NADP malic enzyme, and the CO<sub>2</sub> is fixed into carbohydrate by the PCR cycle.<sup>149</sup> Evidence for a C<sub>4</sub> pathway of this type was found in one seagrass species *Cymodocea nodosa*, but not in ten others.<sup>88</sup> There is also evidence for this C<sub>4</sub> pathway, but using PEP carboxykinase as the carboxylating enzyme, in the marine green macro alga *Udotea flabellum*.<sup>118</sup>

Among the phytoplankton, Reinfelder *et al.* (2000) demonstrated short-term labelling of C<sub>4</sub> compounds, and transfer of carbon to sugars, in the marine diatom, *Thalassiosira weissflogii*, which they interpreted as evidence for C<sub>4</sub> photosynthesis in this species. Reinfelder *et al.* (2004) found that a specific inhibitor of PEP carboxylase caused a more than 90% decrease in photosynthesis in cells of *T. weissflogii* acclimated to low [CO<sub>2</sub>], but had little effect on a C<sub>3</sub>-using marine chlorophyte, *Chlamydomonas* sp. On the basis of similar inhibition experiments, McGinn and Morel (2008) propose that C<sub>4</sub>-based CO<sub>2</sub>-concentrating mechanisms are generally distributed in diatoms, and suggest that their possession of a C<sub>4</sub>-based CCM may have contributed to the evolutionary success of this phytoplankton phylum, especially in the low CO<sub>2</sub> concentrations that characterize present-day surface waters.

Another biochemical CO<sub>2</sub>-concentrating mechanism, crassulacean acid metabolism (CAM), occurs in some, but not all, of the isoetid macrophyte species of oligotrophic, soft-water, lakes.<sup>142,681,1111</sup> Their photosynthetic physiology has been reviewed by Madsen *et al.* (2002). These aquatic CAM plants have a rosette of short stiff leaves and large roots that can make up more than 50% of the plant biomass. Through their extensive root system they take up CO<sub>2</sub> from the sediments, where it is present in high concentration. Transport of CO<sub>2</sub> from roots to leaves takes place by diffusion through a system of internal gas spaces (lacunae). Most of the inorganic carbon used in photosynthesis by isoetids comes from sediment CO<sub>2</sub>, and it is taken up during the night as well as during the day. Possession of CAM enables these plants to fix CO<sub>2</sub> during the night by means of PEP carboxylase, in the form of organic acids such as malate, which accumulate in the vacuole. During the day, when light is available, CO<sub>2</sub> is liberated by decarboxylation of the C<sub>4</sub> acids, and fixed into carbohydrate by the PCR cycle.

## Temperature

In considering the effect of temperature on aquatic photosynthesis, it is necessary to distinguish between the effects immediately following a change in temperature and the effects obtained if the plants are allowed to adjust to the new temperature for one to several days. Considering the immediate effects of temperature change first, if the photosynthetic rate of a phytoplankton population or a marine or freshwater macrophyte is measured under saturating light, at a series of temperatures covering the range from just above freezing to temperatures becoming unfavourable for life, say 5 to 40°C, it will be found that photosynthetic rate per unit biomass at first increases with temperature, then levels off, and finally begins to decrease again, i.e. there is a temperature optimum. The temperature optimum determined in the laboratory varies in accordance with the temperature of the normal habitat of the aquatic species. For example, benthic marine algae from tidal pools exposed to high temperatures in the summer have somewhat higher optimum temperatures for photosynthesis than algae, sometimes even of the same species, obtained from the subtidal zone.<sup>921</sup> Figure 11.5

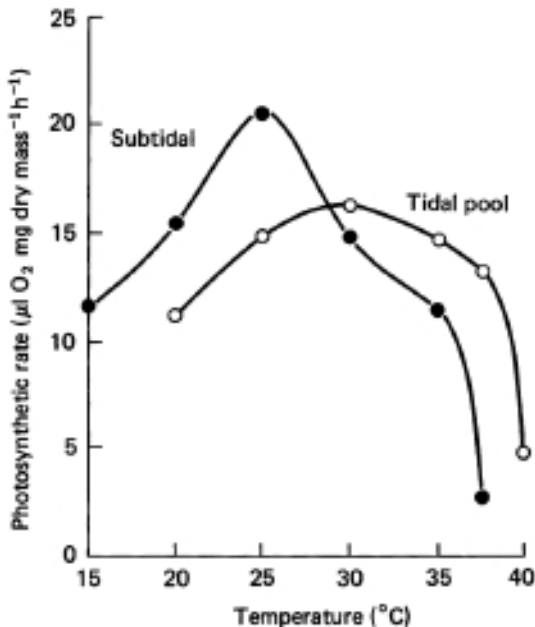


Fig. 11.5 Photosynthetic rate as a function of temperature in samples of the marine benthic alga *Ulva pertusa* (Chlorophyceae) collected from the subtidal zone and from a tidal pool (after Mizusawa *et al.*, 1978).

compares the dependence of photosynthetic rate on temperature for specimens of the green alga *Ulva pertusa* isolated from these two habitats: the temperature optimum for the subtidal sample is about 5°C lower than that for the pool sample. Yokohama (1973) found that for several species of green, brown and red benthic algae collected around the shore of the Izu peninsula, Japan (34°40' N), the temperature optimum was 5 to 10°C higher for material collected in summer than for samples obtained in winter. The reasons for the decrease in photosynthetic rate at temperatures above the optimum are not well understood: denaturation of enzymes, a runaway increase in respiration and other forms of thermal damage are likely to be involved.

If photosynthesis as a function of irradiance is measured at a series of temperatures (not exceeding the optimum), then it is observed that the maximum photosynthetic rate at light saturation increases with temperature: this is shown for the marine diatom *Skeletonema costatum* and the lower-littoral-zone red alga *Gigartina stellata* in Fig. 11.6. It is, however, generally found in experiments of this type (i.e. in which the plants are not given time to adapt to each temperature) that at low light intensities, in the linear part of the  $P$  versus  $E_d$  curve, variation in temperature has little effect on the rate (i.e. the initial slope,  $\alpha$ , is essentially constant over the physiological temperature range. We may reasonably attribute the fall-off in the light-saturated rate ( $P_m$ ) with decreasing temperature to the enzymic reactions of the dark carboxylation system working progressively more slowly as temperature decreases. The irradiance value,  $E_k$ , corresponding to onset of light saturation also decreases together with the temperature: since  $E_k = P_m/\alpha$ , then since  $\alpha$  is unaffected by temperature,  $E_k$  must decrease in parallel with  $P_m$ . When, due to low temperature, the photosynthetic dark reactions are working slowly, less light is required to produce NADPH<sub>2</sub> and ATP fast enough to saturate the dark reaction system. The comparative insensitivity of the photosynthetic rate at low light intensity to temperature is commonly attributed to the fact that photochemical processes are not very sensitive to temperature, and it is mainly the light reactions that determine rate in the light-limited part of the curve. Respiration, however, does increase markedly with temperature. The failure of the light-limited photosynthetic rate to respond means that as temperature increases the light intensity required for photosynthesis to equal respiration, i.e. the light compensation point, also increases.

Although the photosynthetic rate of any individual aquatic plant or phytoplankton population sample is positively correlated with

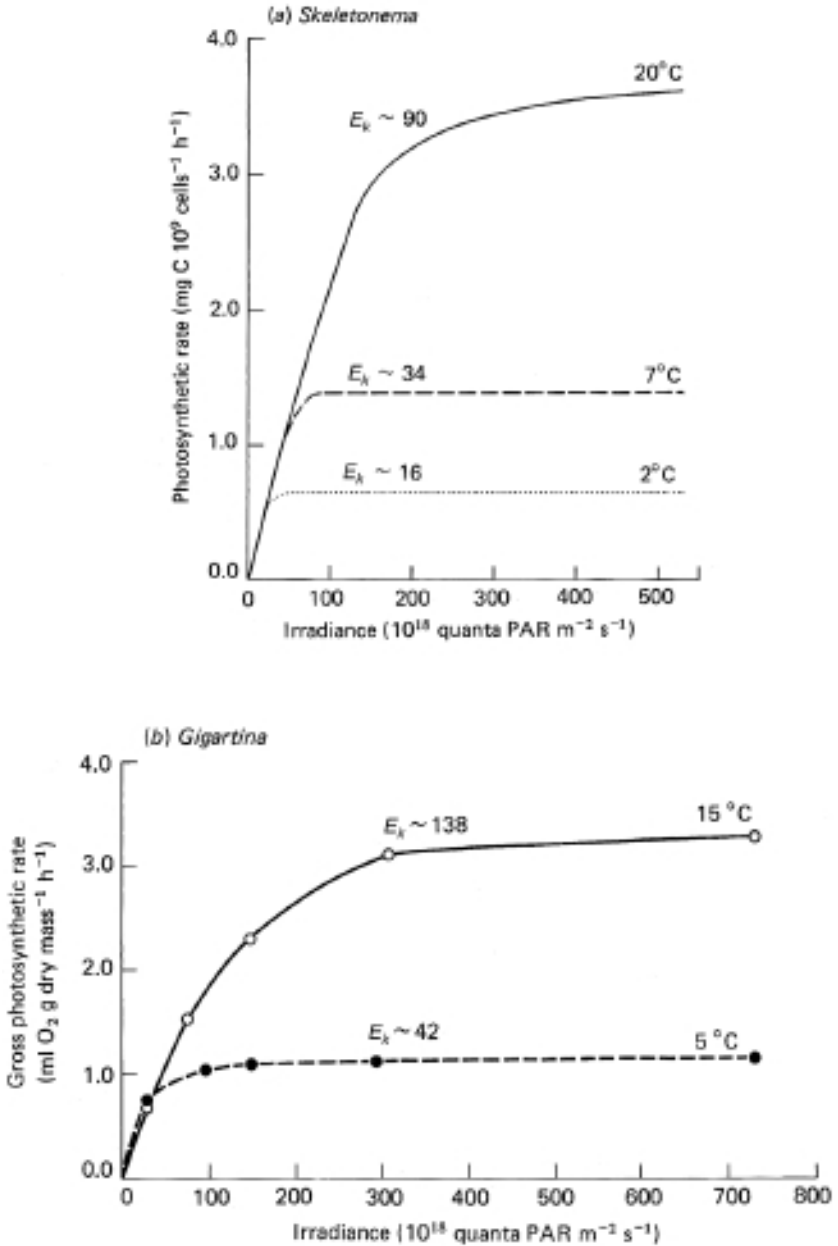


Fig. 11.6 Photosynthetic rate as a function of irradiance at different temperatures. (a) In the marine diatom *Skeletonema costatum* (after Steemann Nielsen and Jørgensen, 1968, and Steemann Nielsen, 1975). The cells were grown under an irradiance of  $75 \times 10^{18}$  quanta m $^{-2}$  s $^{-1}$ , and exposed to the

temperature (up to the optimum) in short-term experiments, in the case of the whole aquatic ecosystem undergoing slow seasonal temperature changes, there is time both for physiological adaptation by any given species, and for changes in the dominant species present. Thus the relation between primary production and temperature may not be so simple at the ecosystem level. Considering adaptation first, if samples of a phytoplankton population are exposed to each new temperature for some days before the  $P$  versus  $E_d$  curve is measured at that temperature, then in the case of some species the cells can adapt and the differences between the light-saturated rates of photosynthesis at the different temperatures is much smaller. For example, Steemann Nielsen and Jørgensen (1968) found that in cells of the diatom *Skeletonema costatum*, grown at 20°C, an immediate transfer to 8°C reduced the light-saturated photosynthetic rate by about two thirds: in contrast, cells grown and measured at 8°C had a light-saturated photosynthetic rate only about 10% lower than that of cells grown and measured at 20°C.

Given that we are interpreting the reduction in light-saturated photosynthetic rate brought about by an immediate temperature lowering as being due to a lowered specific activity of the dark reaction enzyme system, then we might expect the adaptation to lower temperature to consist of an increase in the cellular content of this enzyme system.<sup>1297</sup> Jørgensen (1968) found that the protein content of *S. costatum* per cell was twice as high in cells grown at 7°C as in cells grown at 20°C. In *Dunaliella*, Morris and Farrell (1971) observed that the level of photosynthetic enzymes increased as the growth temperature was lowered.

*Skeletonema costatum* is a ubiquitous diatom, which in nature grows well over a wide range of temperature. It is therefore not surprising that marked adaptive abilities can be demonstrated in the laboratory in this species. Yentsch (1974), however, doubts if most phytoplankton species have this ability. Oceanic measurements from various parts of the world indicate that the photosynthetic rate per unit phytoplankton chlorophyll does not vary in any systematic manner with the water temperature:<sup>1484</sup> in all temperature regions, areas with high and low rates of total primary

Caption for Fig. 11.6 (cont.)

experimental temperature for 30 min before measurements were carried out. (b) In the multicellular red alga *Gigartina stellata* (plotted from data of Mathieson and Burns, 1971). Plants were collected from the lower littoral zone of the coast of New Hampshire, USA. The original irradiance values (in foot-candles) have been converted to quantum units.

production are found.<sup>1297</sup> This could be due to adaptation but more recent studies suggest that there is little temperature adaptation of most oceanic phytoplankton species in nature, and that the lack of a clear dependence of photosynthetic rate on temperature in the oceans is due to the dominance of different (presumably genetically adapted) species in different temperature regimes.<sup>1484</sup> On the Nova Scotian Shelf, Bouman *et al.* (2005) found that the seasonal changes in temperature were closely followed by changes in phytoplankton community structure.

Notwithstanding the apparent lack of a systematic effect of temperature on photosynthesis in the oceans, it is generally found for shallow, productive coastal waters and for inland waters that both the *in situ* photosynthetic capacity (the maximum specific photosynthetic rate per unit phytoplankton or macrophyte) and the integral (areal) rate of photosynthesis are positively correlated with the prevailing temperature. For example, in Nova Scotia (Canada) coastal waters, Platt and Jassby (1976) found that in the period July 1973 to March 1975 (temperature range 0–15°C) the photosynthetic capacity of the phytoplankton was linearly dependent on ambient temperature, with a regression slope of  $0.53 \text{ mg C mg chl } a^{-1} \text{ hr}^{-1} \text{ } ^\circ\text{C}^{-1}$ . For the waters of the Hudson estuary and the New York Bight, through an 11-month period, Malone (1977a, b) found that for both netplankton and nanoplankton, the photosynthetic capacity was an exponential function of ambient temperature from 8 to 20°C, and 8 to 24°C, respectively. The  $Q_{10}$  values (proportionate increase in rate per 10°C rise in temperature) were 2.0 to 2.6 for the nanoplankton and 4.0 for the netplankton. Below 8°C the rates for both fractions were higher than expected on the basis of the exponential dependence on temperature. Above 20°C the photosynthetic capacity of the netplankton declined with temperature. In a number of temperate-zone eutrophic lakes, dominated by blue-green algae, the photosynthetic capacity of the phytoplankton has been found to vary throughout the year in an exponential manner with the prevailing temperature,<sup>117,444,641</sup> the  $Q_{10}$  being about 2 over the approximate range 4 to 20°C. It should be noted that the changes in coastal and inland waters we have just been considering are seasonal changes, which must include changes in the character (species composition, physiological adaptation) of the phytoplankton as well as in the temperature itself, and this may account for the very high seasonal  $Q_{10}$  of 4.0 observed by Malone (1977b) in the New York Bight. If a given phytoplankton population is exposed to a given series of temperatures (i.e. allowing no time for adaptation or species succession), photosynthetic capacity varies exponentially with temperature with a  $Q_{10}$  of about 2.3.<sup>1333</sup>

It is commonly observed in the ocean that the productivity of the phytoplankton population, expressed as specific photosynthetic rate,  $P^*$  ( $\mu\text{moles CO}_2 \text{ mg chl } a^{-1} \text{ hr}^{-1}$ ) tends to decrease as phytoplankton cell size increases. Shiomoto *et al.* (1997), from their measurements in the North Pacific Ocean and the Bering Sea, found that this generalization held in the southern parts of this region, where the *in situ* temperature was  $>10^\circ\text{C}$ . In the northern subarctic region, where the water temperature was  $<10^\circ\text{C}$ , picoplankton ( $<2 \mu\text{m}$ ) productivity was generally about equal to, or lower than that of the larger sized phytoplankton (2–10 and 10–200  $\mu\text{m}$ ). They concluded that picoplankton productivity is more sensitive to *in situ* temperature than is that of larger sized phytoplankton, and that this accounts for the observation that the productivity of picoplankton is not significantly higher than that of the larger phytoplankton in the subarctic region.

We noted earlier that when a given phytoplankton population or macrophyte sample is exposed to different temperatures,  $E_k$ , the irradiance value corresponding to onset of saturation, increases as temperature increases (Fig. 11.6). This also appears to be true on a seasonal basis (i.e. including any changes in the phytoplankton population). In Lough Neagh, N. Ireland, Jewson (1976) found the *in situ*  $E_k$  to be correlated with prevailing temperature throughout a two-year period, rising 2.5- to 4.5-fold between the winter (temperature  $3\text{--}4^\circ\text{C}$ ) and late summer ( $18.5^\circ\text{C}$ ). This rise in  $E_k$  is best seen as being part of the rise in photosynthetic capacity with temperature, than as a separate phenomenon. Given the increase in maximum specific photosynthetic rate, due to the increased rate of operation of the carboxylation system, it simply means that more light is required to produce  $\text{NADPH}_2$  and ATP fast enough to saturate the dark reaction system.

In summary, there is no doubt that in coastal and inland waters temperature, operating mainly through its effect on photosynthetic capacity, is a major limiting factor for photosynthesis. In simple terms we may say that in any optically deep water body at a temperature below the photosynthetic optimum, photosynthesis per unit volume is likely to be limited by light in the lower part of the euphotic zone, by temperature in the upper part of the euphotic zone and by  $\text{CO}_2$  everywhere. In water bodies so shallow that adequate light penetrates to the bottom, temperature (apart from  $\text{CO}_2$ ) can become the dominant factor controlling photosynthesis in the whole system. For a number of stratified lakes with high light penetration in Ontario (Canada), Dale (1986) concluded that depth of colonization by macrophytes was limited by temperature. In the

Beaufort Channel, North Carolina, USA – a shallow estuary of average depth 1 m – Williams and Murdoch (1966) observed a pronounced seasonal cycle in phytoplankton primary production, which appeared to follow the water temperature cycle but not to be related to insolation. They point out that such temperature-driven annual cycles in the productivity of marine phytoplankton are likely to be characteristic of shallow embayments in temperate regions.

### Indirect factors

There are environmental factors other than light, CO<sub>2</sub> and temperature that can have a major influence on the total amount of photosynthesis that takes place (i.e. on primary production in the ecosystem) by their effects on the amount of plant biomass present. Since our concern here is mainly with factors that influence photosynthesis directly we shall touch on these indirect factors only briefly.

Inorganic nutrition – particularly the concentrations of the key elements phosphorus and nitrogen – is the most important indirect factor. The average composition of marine phytoplankton is characterized by the *Redfield ratio*, 106C:16N:1P, originally determined by the marine chemist, Alfred Redfield in the 1930s. If the nutrient concentration is low, then although the existing phytoplankton may be photosynthesizing at a higher rate per unit biomass, they cannot increase their biomass and so the rate of photosynthesis per unit volume or area remains low. When nutrient levels increase, due to agricultural run-off or sewage input in inland waters, or an increase in river outflow in coastal waters caused by increased rainfall, or the commencement of a seasonal upwelling off the west coast of a continental landmass, or a breakdown of stratification in the sea or a lake in the autumn bringing up fresh nutrients from below the thermocline, then the phytoplankton population and therefore total photosynthesis both increase as well. In the sea, rainfall can be a significant, but episodic, source of nitrogen, both in oligotrophic regions of the ocean<sup>1027</sup> and in coastal waters.<sup>143</sup>

When the phytoplankton population has depleted the level of any essential nutrient, then photosynthetic biomass ceases to increase. In the case of nitrogen depletion, however, certain filamentous species of blue-green algae are not prevented from continued growth since they have the ability to fix molecular nitrogen. This ability is present in common bloom-forming genera such as *Anabaena* and *Aphanizomenon* in inland water bodies. In the sea, where nitrogen is usually the limiting mineral

nutrient, the unicellular cyanobacterium *Synechococcus*, a major component of the picoplankton throughout the oceans, cannot fix nitrogen,<sup>1442</sup> but the large colonial filamentous cyanobacterium, *Trichodesmium*, which is often the major component of the phytoplankton in tropical ocean waters, does fix nitrogen. Carpenter and Romans (1991) have concluded that in the tropical North Atlantic Ocean *Trichodesmium* is the most important primary producer, and that its nitrogen fixation contributes about 30 mg of nitrogen per m<sup>2</sup> per day, a value exceeding the estimated upward flux of nitrate from below the thermocline.

In ocean waters, as nutrient availability and total phytoplankton biomass increase, so the contribution of the smaller phytoplankton species decreases as the larger phytoplankton come to dominate. The relative importance of picophytoplankton (cells <2 µm) is greatest in warm oligotrophic waters.<sup>9</sup> From measurements along a north–south transect (48° N to 8° S) in the central Pacific Ocean, Suzuki *et al.* (1995) found that the prochlorophyte, *Prochlorococcus marinus* (0.6–0.8 µm in diameter), although universally present, was most abundant in oceanic environments with higher temperature (15–30°C) and lower nutrient concentrations. The larger surface area to volume ratio of small cells gives them a competitive advantage over large cells where nutrient concentrations are low.

In freshwater lakes, phosphorus is most commonly the limiting mineral nutrient for phytoplankton growth and primary production. Enrichment of inland waters with phosphate from incompletely treated urban wastes, and from fertilizer run-off has, over many decades, led to the phenomenon of *eutrophication*, the excessive growth of phytoplankton and epiphytes, with a variety of undesirable consequences, such as development of toxic blue-green algal blooms, elimination of desirable macrophytes and anaerobiosis due to breakdown of the excessive organic matter leading to fish kills. For many, but not all, lakes in the developed world, steps have been taken in recent years to reduce external phosphorus loading, and Jeppesen *et al.* (2005) report an analysis of long-term data from 35 case studies of lakes in Europe and the USA, of the process of *re-oligotrophication* of these water bodies. The lowering of in-lake phosphorus concentration was accompanied by reductions in chlorophyll *a* concentration and increased water clarity (Secchi depth). Declines in phytoplankton biomass were accompanied by changes in community structure, chrysophytes and dinophytes increasing at the expense of cyanobacteria in deep lakes; diatoms, cryptophytes and chrysophytes becoming more dominant in shallow lakes. Macrophyte abundance increased in some, but not all, lakes.

Anthropogenic eutrophication in coastal waters due to excessive input of nutrients is now a world-wide problem,<sup>22,500</sup> giving rise to harmful algal blooms, loss of seagrass meadows, overgrowth of coral by algae, depletion of deep-water oxygen with consequent loss of benthic fauna and damage to fisheries. To address the problem of eutrophication, the phenomenon must be clearly defined, and linked with appropriate assessment and monitoring systems. As a definition of eutrophication, Andersen *et al.* (2006) propose 'the enrichment of water by nutrients, especially nitrogen and/or phosphorus and organic matter, causing an increased growth of algae and higher forms of plant life to produce an unacceptable deviation in structure, function and stability of organisms present in the water and to the quality of the water concerned, compared to reference conditions'. They go on to propose that measurements of primary production, being a sensitive and accurate indicator of eutrophication, should be mandatory when monitoring and assessing the ecological status of coastal waters. Smith (2007) suggests that the most sensitive and reliable primary productivity parameter to use when evaluating the eutrophication status of coastal marine ecosystems is the light-saturated maximum volumetric rate of photosynthesis ( $\text{mg C m}^{-3} \text{ day}^{-1}$ ) observed in a standard vertical productivity profile. The volumetric expression of primary productivity appears to track changes in nutrient loading and algal biomass more predictably and sensitively than changes in areal (integrated) primary productivity.

For the diatoms, with their external skeleton (frustule) made of silica, silicon is an essential element. Depletion of silica can bring diatom blooms to an end in fresh water.<sup>1120</sup> Leblanc *et al.* (2005) present evidence that the low contribution of diatoms to the spring bloom in the northeast Atlantic is due to the limited availability of silicon. In diatom-dominated ocean ecosystems, silicate is not recycled as quickly as is cellular nitrogen and is thus lost to deep water at a higher rate as diatom cells and diatomaceous faecal pellets sink down through the thermocline.<sup>336</sup> Silicon can also be a limiting element for diatom growth in some very productive coastal upwelling systems.<sup>1115</sup>

The other major environmental factor that limits total phytoplankton photosynthesis by limiting biomass is grazing by the aquatic fauna. The spring bloom of phytoplankton is typically followed by a bloom of zooplankton, which graze upon the phytoplankton cells. It is undoubtedly true that zooplankton grazing can have a major impact on phytoplankton populations and in some cases can be the cause of the decline in phytoplankton numbers following the bloom: the relations, however, are

complex and fluctuations in phytoplankton populations cannot always be interpreted easily in terms of zooplankton grazing. The matter is discussed in more detail for inland waters by Hutchinson (1967) and Reynolds (1984), and for the oceans by Raymont (1980) and Frost (1980). The composition of the phytoplankton population can be affected by selective feeding: the copepod, *Calanus finmarchicus*, for example, in the Norwegian Sea, was found to graze selectively on certain phytoplankton types, such as diatoms, but avoid others, such as cyanobacteria.<sup>900</sup> In addition to those zooplankton large enough to be visible to the naked eye, such as the crustaceans (copepods, krill), single-celled protozoa (ciliates, heterotrophic or mixotrophic flagellates) are also an important part of the food chain, and are thought to be the primary grazers, particularly on the prokaryotic members of the phytoplankton, such as *Synechococcus*. Large colonial phytoplankton forms, such as occur in the Peruvian upwelling, can be grazed directly by herbivorous fish such as the anchovy.<sup>1158</sup>

Benthic filter-feeding fauna, such as shellfish, in shallow coastal or estuarine waters can also make significant inroads into phytoplankton populations. Asmus and Asmus (1991) found that an intertidal mussel (*Mytilus edulis*) bed in the German Wadden Sea (eastern North Sea) reduced phytoplankton biomass by about 37% between the incoming and outgoing tide. Parallel with the uptake of phytoplankton there was, however, a substantial release of nitrogen, as ammonium, from the mussel bed, leading these authors to suggest that the shellfish were simultaneously reducing the standing stock of phytoplankton, and promoting phytoplankton primary production, or to put it another way, the mussel bed was accelerating phytoplankton turnover.

Although throughout most of the world's oceans, phytoplankton biomass appears to be limited by the availability of the major nutrients, there are substantial regions – the Southern Ocean, the equatorial Pacific and the northeast Pacific Ocean – where there is a surplus of phosphate and nitrate in the surface waters, but primary productivity is low. These are sometimes referred to as HNLC (high nitrate, low chlorophyll) regions. A number of plausible hypotheses have been put forward to explain the failure of the phytoplankton in these regions to fully utilize the major nutrients. It has been proposed, for example, notably by Martin and coworkers,<sup>872</sup> that phytoplankton growth in these waters is limited by iron deficiency. Another proposal, specifically for the equatorial Pacific, is that the standing crop of phytoplankton is controlled by closely coupled zooplankton grazing.<sup>270,1434</sup> For the Antarctic Circumpolar Current in the Southern Ocean, Mitchell *et al.* (1991) argue that as a

consequence of the high wind strength, low solar irradiance (persistent clouds) and weak stratification, deep circulation will lead to light limitation of phytoplankton growth to such an extent that they cannot possibly use more than a small fraction of the available nutrients. Another possibility, for the Southern Ocean, is the inhibitory effects of chronic low temperature on nitrate uptake by the phytoplankton.<sup>335</sup> Detailed discussions of these and other possible explanations of ‘What controls phytoplankton production in nutrient-rich areas of the open sea?’ may be found in the special issue of *Limnology and Oceanography* published under this title and edited by Chisholm and Morel (1991).

Notwithstanding the alternative hypotheses, the theory that a deficiency of iron is the factor primarily responsible for the low productivity of HNLC waters has now received direct experimental support. Martin *et al.* (1994) (IronEx I) and Coale *et al.* (1996) (IronEx II) carried out enrichment of substantial patches of ocean (64 and 72 km<sup>2</sup>, respectively) in the equatorial Pacific, using (Martin *et al.*) 450 kg Fe, and (Coale *et al.*) 225 kg (day 1) plus 2 × 112 kg (days 3 and 7), with acidified ferrous sulfate as the iron source. Iron addition triggered a massive phytoplankton bloom, which consumed large quantities of carbon dioxide and nitrate. In the case of IronEx II it was found that during the week following first enrichment there was a dramatic change in the phytoplankton community structure, from one dominated by picoplankton to one dominated by large diatoms.<sup>213</sup>

Boyd *et al.* (2000) carried out a similar experiment at a location, 61° S 140° E, in the Pacific sector of the Southern Ocean. Once again, fertilization was followed by a large algal bloom. Initial increases were due to pico-eukaryotes, but after day 6 there was a shift to large diatoms. Gervais *et al.* (2002) observed several-fold increases in primary productivity and chlorophyll *a*, following iron fertilization in the Atlantic sector (48° S 21° E) of the Southern Ocean. They concluded that iron supply is the central factor controlling phytoplankton primary productivity in the Southern Ocean, even where the mixing depth is >80 m. Lance *et al.* (2007) carried out *in situ* iron-enrichment experiments at two locations along longitude 172° W in the Pacific sector of the Southern Ocean: at 56° S in the Subantarctic Zone, just north of the Subantarctic Front, and at 66° S, just south of the Antarctic Circumpolar Current. In both cases there was a many-fold increase in both chlorophyll and primary productivity. At the northern location there was a population shift from prymnesiophytes towards diatoms, but at the southern site there was no change in the phytoplankton assemblage from its initial composition of ~50% diatoms.

De Baar *et al.* (2005) have reviewed the findings of eight of these iron-addition experiments, carried out in various locations around the world's oceans. They find that the maximum chlorophyll *a*, the maximum dissolved inorganic carbon (DIC) removal and the overall DIC/Fe efficiency (moles carbon removed per mole iron added) all scale inversely with the depth of the wind-mixed layer that defines the light environment. Large diatoms always benefit the most from iron addition.

While it is beginning to look as if iron deficiency is the default explanation for the low productivity of HNLC regions of the ocean, other explanations may apply in certain locations. For example, Goericke (2002) presents evidence that in the HNLC areas of the monsoonal Arabian Sea, where iron is present in abundance, phytoplankton biomass is controlled within tight bounds by microzooplankton grazing.

The impact of zooplankton grazing on phytoplankton populations can be greatly affected by the extent to which the zooplankton themselves are subject to predation by larger animals. The addition of planktivorous fish to a pond in Minnesota was found to lead to an order-of-magnitude increase in total phytoplankton biomass.<sup>835</sup> In addition to the increased levels of those algal species already present, several new species appeared. In a survey of shallow wetlands in northern Alberta (Canada), which tend to be either in a turbid, pea-green (high phytoplankton chlorophyll) or clear, low chlorophyll, state, Norlin *et al.* (2005) found that the two categories corresponded to waters with low, or high, submerged aquatic vegetation coverage, respectively. They suggested that high aquatic vegetation coverage provides protection for efficiently grazing cladocerans (crustacean zooplankton, 'water fleas') from the larger invertebrates that prey on them, leading to effective control of the phytoplankton. In a set of shallow lakes in England, Moss *et al.* (1994) found an inverse correlation between chlorophyll *a* and cladoceran abundance: they suggested that this was due to the dominance of submerged macrophytes and the refuges they provide for these grazing zooplankton.

A limiting factor for one particular group among the phytoplankton, the dinoflagellates, is small-scale turbulence. It appears that turbulence in the water, at levels such as might result from quite moderate winds, can cause the cells to lose their longitudinal flagellum: cell division and growth are also inhibited.<sup>98,1353</sup> In the Sea of Galilee (Lake Kinneret), the absence of the usual winter-spring bloom of the dinoflagellate, *Peridinium*, in 1996 occurred at a time when the dissipation rates of turbulent kinetic energy were extremely high, while record high amounts of dinoflagellates appeared (1994, 1995) when dissipation rates were very

low.<sup>100</sup> The inhibitory effect of turbulence is thought to explain why dinoflagellate red tides only develop in calm weather.

As we have previously noted, in addition to their specific effects on dinoflagellates, high winds are normally inhibitory to primary production because they bring about deep mixing of the phytoplankton so that the average light intensity to which the cells are exposed is too low for net production to occur. In one special case, however, the contrary behaviour is observed. The Sargasso Sea (North Atlantic subtropical gyre) is an oligotrophic, highly unproductive, region of the ocean. Babin *et al.* (2004) used remotely sensed ocean colour data (SeaWiFS) to follow the consequences of the passage of 13 hurricanes through this region in 1998–2001. They observed that in every case there was an increase (5–91%) in surface chlorophyll in the wake of the hurricane. They attributed this to an increased supply of nutrients, mixed in from below, possibly together with entrainment of phytoplankton cells from the deep chlorophyll maximum.

In freshwater bodies, infection of phytoplankton populations by parasitic fungi can, particularly in eutrophic lakes, significantly reduce their numbers, and even terminate blooms.<sup>175,602,1120</sup> In marine waters, pathogenic viruses have been shown to infect a range of phytoplankton types including diatoms, cryptophytes, prasinophytes and cyanobacteria.<sup>1093,1326</sup> Although little quantitative evidence is yet available, preliminary indications are that viral mortality could be another significant factor regulating phytoplankton populations and primary production, in the sea. Cottrell and Suttle (1995) studied the impact of a lytic virus, *MpV*, on populations of the cosmopolitan and abundant prasinophyte phytoplankton species, *Micromonas pusilla*, in Texas coastal waters. The abundance of infective *MpV* was high, and decreased from  $1.3 \times 10^5 \text{ ml}^{-1}$  in January 1993 to  $2.1 \times 10^3 \text{ ml}^{-1}$  at the end of April. Using a laboratory measurement of the adsorption coefficient for *MpV* on *M. pusilla*, they calculated that 2 to 10% (average 4.4%) of the *M. pusilla* population was lysed per day.

Phytoplankton growth can itself limit primary production by the benthic flora. In eutrophic waters interception of light by dense phytoplankton populations can prevent the growth of benthic macrophytes.<sup>663</sup> From their studies on the Norfolk Broads (England), Phillips *et al.* (1978) consider that during progressive eutrophication of water bodies, overgrowth of the macrophyte leaves by epiphytes and mats of filamentous algae, with consequent reduction in light availability, initiates the macrophyte decline even before dense phytoplankton populations have

developed. Overgrowth of leaves by epiphytes has also been implicated in the decline of seagrasses in eutrophicated Cockburn Sound, Western Australia.<sup>197</sup> Eutrophication of shallow estuaries can lead to the proliferation of bloom-forming 'nuisance' macroalgae, typically filamentous (such as *Cladophora*) or sheet-like (such as *Ulva*) forms, usually chlorophytes, that can shade, and eventually displace, seagrasses as the dominant benthic autotrophs.<sup>882</sup>

The density and therefore total photosynthetic rate of the benthic flora is also affected by grazing by invertebrate and vertebrate animals. In the case of macrophytes, snails and other gastropods feed on the photosynthetic tissue, as well as on the attached epiphytes, in both fresh and salt waters: in the sea, limpets and sea urchins are important invertebrate grazers, while in fresh waters insect larvae can be significant consumers. Some specialized species of herbivorous fish such as the grass carp (China) in fresh waters, and the parrot fish, which feeds on seagrasses, eat macrophytes. Higher aquatic grazing animals such as sea turtles and dugongs, as well as ducks and geese, also eat macrophytes. In inland waters, grazing by invertebrates, fish and birds is a significant factor limiting biomass and photosynthesis in some macrophyte communities.<sup>1456</sup> Protection of *Potamogeton filiformis* in Loch Leven (Scotland) from grazing by waterfowl substantially increased its biomass throughout the growing season.<sup>663</sup> Similar observations have been made for three macrophyte species in Lake Stigsholm, Denmark.<sup>1266</sup> Herbivory on freshwater macrophytes has been reviewed by Lodge (1991). In shallow coastal sea waters, grazing by sea urchins can be a major factor limiting the growth of kelps and other seaweeds. Overgrazing in seagrass by sea urchins can cause localized denudation of patches (up to 0.5 km<sup>2</sup>) of meadow, and is thought, for reasons not yet understood, to be on the increase world-wide.<sup>354</sup> Grazing by sea turtles can also have a major impact on seagrass beds.

The biotic relations are complex: whether or not a particular region of the sublittoral zone is colonized by brown algae, and the density at which they grow, are likely to be determined by the abundance of animals such as crabs, lobsters and sea otters (which prey on sea urchins), and the numbers of these animals may in turn be influenced by the activities of man.

The lower limit of *Laminaria hyperborea* at one site in the Isle of Man (UK) was found to be controlled by the sea urchin *Echinus esculentus*, which was present at a density of five animals m<sup>-2</sup>.<sup>667</sup> In a study area in Nova Scotia (Canada), Breen and Mann (1976) found that the lobster

*Homarus americanus*, a major predator of sea urchins, decreased by nearly 50% in 14 years: in the latter six years of this period the sea urchin *Strongylocentrotus* destroyed 70% of the *Laminaria* beds. Areas of bare rock protected from sea urchin grazing were rapidly recolonized by *Laminaria* plants. Similarly, off California, the mass mortality by disease of a localized population of sea urchins on the seaward side of a kelp forest was followed by the rapid seaward expansion of four species of brown algae.<sup>1037</sup> On the basis of archaeological evidence from the Aleutian Islands, Simenstad *et al.* (1978) concluded that when the Aleut people colonized this area and commenced hunting the sea otter, the diminution in otter numbers led to a population explosion of sea urchins, which was in turn followed by the decimation of the abundant kelp beds in the area: since fur hunting in the Aleutians ceased in 1911, both the sea otter and abundant kelp beds have become re-established. In Fiji, extinction of the dugongs and a reduction in sea turtle numbers has caused the seagrasses to increase to the point of becoming a nuisance.<sup>894</sup>

The chloroplasts of some macroalgae can continue to photosynthesize for a limited time after they have been ingested by certain grazing animals. This is the phenomenon of *kleptoplasty*.<sup>1110,1472</sup> This is distinct from the phenomenon of algal symbiosis, common among the marine biota (e.g. coral, tunicates), where intact algal cells live and photosynthesize within their animal host. In *kleptoplasty*, the chloroplasts of the grazed plants are liberated from their cells during ingestion, and survive, and continue to photosynthesize as naked organelles within the cells of the grazer. At the microbial level, *kleptoplasty* on unicellular phytoplankton as the source is carried on by some species of flagellates and ciliates, and also by some dinoflagellates. McManus *et al.* (2004) found that two tide-pool ciliates, *Strombidium oculatum* and *S. stylifer*, are able to ingest ulvaceous green macroalgae (*Enteromorpha* sp.) and retain their chloroplasts. Green algae in the Ulvaceae do not have specialized reproductive structures, and simply convert a large proportion of their vegetative tissue to the reproductive state, in which they release massive numbers of flagellated swarmer zoospore cells. McManus *et al.* observed the ciliates to congregate near the reproductive portion of the *Enteromorpha* tissue, and suggested that they were ingesting the zoospores as they were shed by the thallus. If given a modest supply of food with which to replenish its chloroplasts, *S. stylifer* grew rapidly in the light, but did not survive long in darkness.

The only metazoans that can carry out *kleptoplasty* are the sacoglossans (sea slugs). They feed mainly on green algae, such as species of

*Caulerpa*, and on red algae, such as *Griffithsia*. The algal chloroplasts are retained by the animal in certain specialized cells, and can remain active, supplying the animal with some of its dietary carbon requirements, for days or weeks. The subject is reviewed by Williams and Walker (1999). By comparing  $^{13}\text{C}/^{12}\text{C}$  ratios in sacoglossans with those of the algae on which they were feeding, Raven *et al.* (2001) estimated that up to 60% of the total carbon input to the sacoglossans came from photosynthesis by their kleptoplastids.

### 11.4 Temporal variation in photosynthesis

The short answer to the question 'When does aquatic photosynthesis take place' is that it takes place when and to the extent that the various limiting constraints we have already discussed permit it to take place. Thus, to understand temporal variation in photosynthesis we need to know the manner in which these limiting factors vary with time.

Considering diurnal variation first, there is of course no photosynthesis at night. Photosynthesis begins at dawn and ends at dusk. The total photosynthesis of the whole water column roughly follows the approximately sinusoidal variation of solar irradiance during the day.<sup>535,659,1337</sup> Under still conditions there may be a reduction of photosynthetic rate per unit volume near the surface due to photoinhibition. Also, where dinoflagellates are the dominant organisms, their downward migration to lower light intensities can lower photosynthetic rate per unit volume near the surface in the middle part of the day.<sup>1360</sup> There have been many reports of variation in the photosynthetic capacity (i.e. photosynthesis in samples taken from the water body and exposed to saturating light) of phytoplankton populations and benthic algae during the day (see, for example, the reviews by Sournia (1974), Raymont (1980) and Harris (1980)). This is discussed later (§ 12.6).

In temperate or Arctic/Antarctic latitudes, there is marked seasonal variation in aquatic photosynthesis. This approximately follows, and is also a major contributing factor to, the seasonal variation in plant biomass. For the marine phytoplankton a detailed account has been given by Raymont (1980). In the winter, phytoplankton biomass and total photosynthesis are both very low, partly because of low solar irradiance<sup>1157</sup> but even more because, as a consequence of lowered temperature and winter storms, thermal stratification is lost and the mixed layer through which the phytoplankton are circulated comes to exceed the critical depth for

net column photosynthesis (see §11.1). In the spring, with increased heating of the surface water resulting from increased daily insolation, thermal stratification sets in, circulation below the critical depth is prevented, and this, combined with the increase in incident PAR and the availability of nutrients in the water, leads to a massive increase in phytoplankton biomass, typically of the order of 20-fold, measured as chlorophyll. Riley (1942) found that for a number of stations over the Georges Bank (Gulf of Maine) during the spring bloom the rate of phytoplankton increase (late March to mid-April) was approximately inversely proportional to the depth of the mixed zone. He concluded that the balance between the effects of vertical turbulence and the increasing vernal radiation determines the beginning of the spring bloom (see also § 11.1). When vertical wind mixing is absent or weak, the spring phytoplankton bloom can begin even before thermal stratification is established.<sup>1373</sup>

Typically, the spring bloom is followed by a decline to a lower level of biomass and integral photosynthesis in the summer, caused by zooplankton grazing and possibly also by a loss of nutrients from the mixed layer resulting from the sedimentation of zooplankton faecal pellets down below the thermocline. In the autumn, the fall in temperature and increased wind strength lead to intermittent disruption of thermal stratification with consequent transport of nutrients up from below the thermocline. Thus, in oceanic and continental shelf waters in intermediate and high latitudes, there is typically a second phytoplankton bloom and associated increase in areal photosynthesis in the autumn: this is terminated when disruption of the thermocline becomes so severe that stratification disappears, circulation below the critical depth sets in and productivity declines to the low winter values. Figure 11.7 shows the variation in photosynthetic rate throughout the year in North Pacific coastal water illustrating the large spring, and small autumn, peaks.<sup>734</sup> Broadly speaking, as latitude increases, the growing season becomes progressively shorter and the spring and autumn phytoplankton peaks tend to merge into one.

The pattern of temporal variation for temperate latitudes described above is by no means universal; it can be greatly modified by local conditions. In the Kattegat (Baltic), lowered salinity (and therefore lower density) in the upper layer maintains stratification throughout the year, and so productivity is substantial at all times of the year, diminishing somewhat in the winter due to reduced light availability.<sup>1297</sup> In coastal waters so shallow that the mixed depth rarely or never exceeds the critical depth, production also tends to remain high throughout the year.

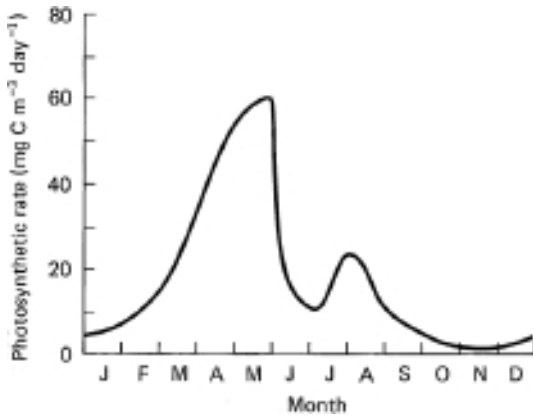


Fig. 11.7 Variation of photosynthetic rate per unit volume throughout the year in North Pacific coastal water (after an average curve derived by Koblenz-Mishke, 1965, from literature data).

Seasonal variation in production may follow the temperature cycle if the water is so shallow that light is non-limiting.<sup>1471</sup>

Data obtained by Dandonneau *et al.* (2006) on the basis of sea-surface sampling along 12 trans-ocean cruises, over the period 1999 to 2002, between France and New Caledonia via New York, Panama and Auckland, confirmed that variability is strongest at high latitudes where the phytoplankton biomass and population structure have large seasonal cycles. The spring bloom in the North Atlantic was marked by chlorophyll concentrations often  $>0.5 \text{ mg m}^{-3}$ , and by high concentrations of fucoxanthin, an indicator of diatoms, while in the summer, chlorophyll was low and populations were dominated by *Prochlorococcus*. Tropical areas had low seasonal variability and were characterized by relatively high divinyl chlorophyll *a* and zeaxanthin (photoprotective carotenoid) concentrations. Barlow *et al.* (2007) used pigment analysis to characterize the seasonal succession of phytoplankton, and the associated changes in chlorophyll *a* and accessory pigments in subtropical waters of the Atlantic, Indian and Pacific Oceans in the southern hemisphere. Under low temperature and irradiance conditions, the photosynthetic carotenoids were prominent, but as temperatures and irradiance increased there was a significant increase in the proportion of photoprotective carotenoids, these eventually becoming the largest component of the pigment pool, exceeding chlorophyll *a*, at the highest temperature and irradiance values.

With the advent of satellite remote sensing of ocean colour, it has now become possible to monitor seasonal phytoplankton changes from space.

Stramska (2005) used SeaWiFS data to examine the year-to-year variability of timing, intensity and spatial distribution of phytoplankton chlorophyll during spring–summer seasons in the north polar region of the Atlantic, over the period, 1998 to 2004. Each year the phytoplankton bloom varied in onset, temporal evolution and intensity to a degree largely controlled by local weather. Timing of the bloom was delayed in years in which there was a high rate of turbulent kinetic energy (TKE) supply to the ocean in March, by wind stirring. In April, phytoplankton chlorophyll and rate of TKE supply were inversely related to one another. Vertical mixing in the ocean increases with the rate of supply of TKE. Pérez *et al.* (2005) analysed the seasonal variability of phytoplankton in the Equatorial Atlantic from 1998 to 2001, using SeaWiFS-derived chlorophyll *a* concentration data. They used the remotely sensed chlorophyll *a* values at monthly intervals to compare phytoplankton changes at locations in the Eastern (10° W) and the Western (25° W) provinces. At both sites chlorophyll *a* levels rose to a maximum around August, but the concentrations achieved were about twice as high at 10° W as they were at 25° W. Romero *et al.* (2006) used SeaWiFS-derived monthly chlorophyll data for the seven-year period, 1998 to 2004, to study seasonal to inter-annual variability of phytoplankton over the Patagonian shelf and shelf break, in the western South Atlantic. North of 45° S, chlorophyll *a* blooms initiated in early austral spring (Sept–Oct), while south of 45° S, blooms began in late spring to early summer (Nov–Jan). Productivity was higher ( $>4$  mg chl  $m^{-3}$ ) than in the open ocean ( $<1.5$  mg  $m^{-3}$ ). Chlorophyll *a* concentrations in the northern mid-shelf sharply decayed in late spring, reaching their lowest values in summer (Feb–March), followed by a secondary maximum in early winter (June). All the high-chlorophyll *a* regions were associated with well-defined fronts.

In the turbid estuarine waters of San Francisco Bay, Cloern (1991) found that the spring phytoplankton bloom each year was associated with the density stratification that resulted from the seasonal increased input of fresh water to the estuary. On a shorter time scale, rapid phytoplankton growth occurred during neap tides (low tidal energy, weak vertical mixing), but populations declined during spring tides (high tidal energy, intense vertical mixing).

In tropical oceanic waters where there is no seasonal variation in the hydrological regime, there is usually no pronounced variation in phytoplankton biomass and photosynthetic production. In regions where there is a seasonal upwelling of nutrient-rich deep water, such as parts of the west coast of Africa, there is an accompanying massive increase in

phytoplankton and photosynthetic production. Seasonal variations in river outflow can also cause seasonal variations in primary production in tropical coastal waters.

Inland waters in intermediate and high latitudes show marked seasonal variation in biomass and total photosynthesis. Both are low in the winter due to a decrease in irradiance (sometimes accentuated by ice or snow cover) and temperature and, in the deeper waters, circulation of the phytoplankton through a depth greater than the critical depth. Increased irradiance and temperature in the spring, together with the availability of nutrients and the onset of thermal stabilization, lead to a phytoplankton bloom and associated increase in areal photosynthesis. The behaviour during the rest of the seasons tends to be both complex and highly variable. Production may remain consistently high, or there may be wide fluctuations in populations and production caused by zooplankton grazing, fluctuations in nutrient content due to influxes of nutrients from the hypolimnion associated with temporary wind-induced disruption of the shallow (by marine standards) thermocline, or major changes in species composition resulting from the seasonal changes in water quality (e.g. higher pH values in late summer tend to favour blue-green algae rather than diatoms).

Discrete spring and autumn blooms separated by a summer minimum are often observed in lakes,<sup>602,1120</sup> but this temporal pattern is more commonly found in eutrophic than in oligotrophic water bodies.<sup>870</sup> Figure 11.8 shows the variation in phytoplankton biomass, and in daily phytoplankton photosynthesis through one-and-a-half years in mesotrophic Lake Constance (Germany–Austria–Switzerland). In some tropical lakes such as Lake George, Uganda, there may be no seasonal variation and primary production and phytoplankton biomass remain high throughout the year.<sup>431</sup> On the other hand, where, as in the case of Lake Chad (Chad, Africa), there are alternating dry and rainy seasons, there can be seasonal variation in temperature, insolation and water level, with associated changes in areal photosynthesis.<sup>795</sup>

Benthic macrophytes, being fixed in position, are not, unlike the phytoplankton, directly affected by the seasonal onset or disappearance of thermal stratification. They do, however, show seasonal variation in photosynthetic production in response to the yearly cycles of irradiance and temperature. Figure 11.9 shows the variation in net photosynthetic rate (per unit area of thallus) of the sublittoral brown alga *Laminaria longicuris* (a kelp) in Nova Scotia, Canada, coastal waters through a 12-month period, together with values of the total amount of PAR

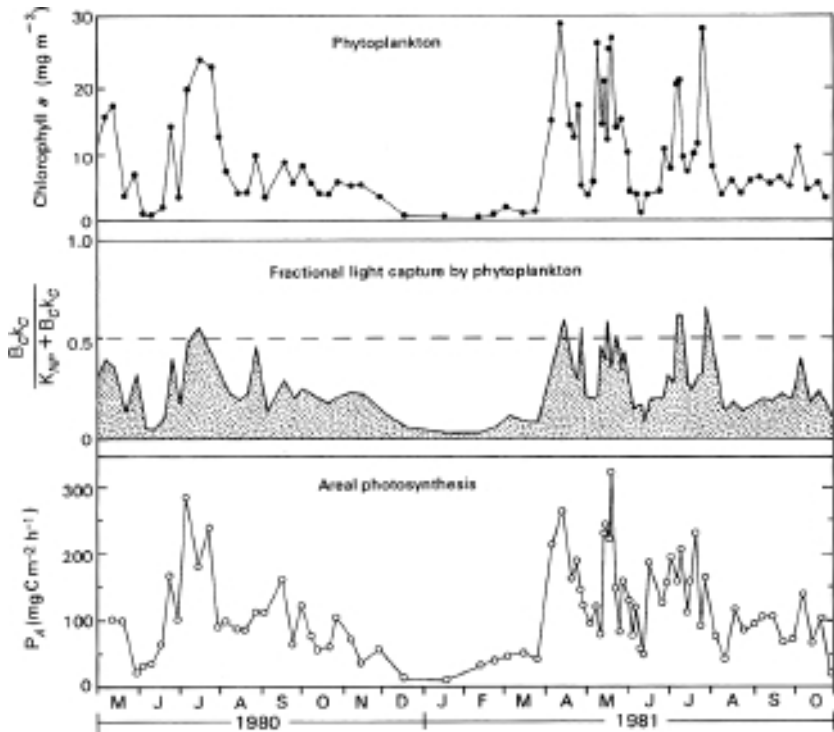


Fig. 11.8 Seasonal variation in phytoplankton biomass and photosynthetic production. Redrawn from data of Tilzer (1983) for the mesotrophic Lake Constance (Germany–Austria–Switzerland). The middle curve represents the estimated proportion of incident PAR that is captured by the phytoplankton. The areal (integral) photosynthetic rate is the hourly average for the middle four hours of the day.

received per day at the sea bottom (10 m depth) on which the algae were growing, and the prevailing water temperature.<sup>543</sup> Photosynthetic rate was highest in summer, declined through the autumn to approximately zero in November–December, became significant once more in late winter and spring, and then rose steeply in early summer. The temporal variation in photosynthesis corresponded roughly to the variation in irradiance. By multiple regression analysis, Hatcher *et al.* (1977) found that 61% of the variance in daily photosynthesis could be accounted for by irradiance. Variation in temperature (from 1.5 to 13°C in these cold waters) did not account for any significant part of the variation in daily photosynthesis. Temperature did account for 56% of the observed variation in light-saturated photosynthetic rate (measured at ambient water temperature,

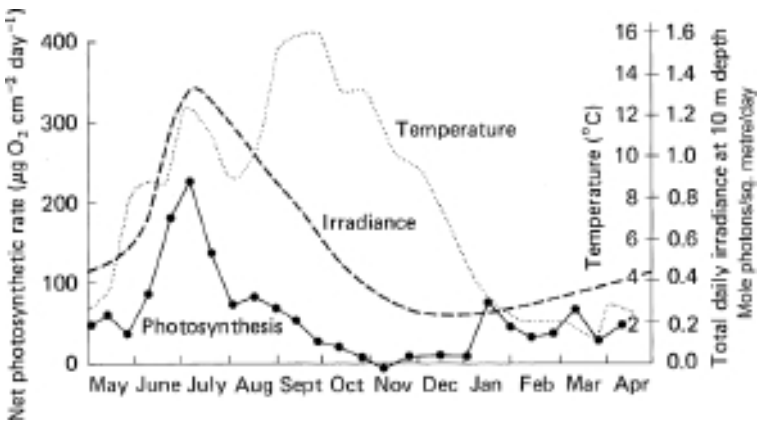


Fig. 11.9 Seasonal variation of the photosynthetic rate of the kelp *Laminaria longicuris* and of total daily irradiance (PAR) and water temperature at 10m depth in a Nova Scotia, Canada, coastal water (St Margaret's Bay) (from data of Hatcher *et al.*, 1977). Photosynthesis measurements were made *in situ* at the prevailing water temperature. The graph of total daily irradiance was obtained by drawing a smoothed curve through the data points of Hatcher *et al.*

back in the laboratory), but since for most of the time the plants *in situ* would be photosynthesizing at subsaturating irradiance values, the effect of temperature on the saturated rate is irrelevant.

Kirkman and Reid (1979) studied the seagrass, *Posidonia australis*, growing in shallow water – from low-water mark to a depth of 3 m below this – at Port Hacking, Australia (34° S). Figure 11.10 shows the variation in relative growth rate ( $\text{mg C g}^{-1} \text{ day}^{-1}$ , which should be closely related to photosynthetic rate), and water temperature during a 12-month period. The growth rate was found to be strongly correlated ( $r = 0.79$ ) with water temperature. In shallow seagrass beds in the northern Gulf of Mexico, also, the seasonal growth cycle of the dominant species, *Thalassia testudinum*, correlates more closely with water temperature than with solar irradiance.<sup>840</sup> It is possible that in these shallow, well-illuminated environments, light intensities were at or near saturation for much of the time, so that temperature became a limiting factor.

Hanisak (1979) carried out a combined field and laboratory study of the growth pattern of the siphonous green alga *Codium fragile*, growing in shallow water (average depth 1.5–2.3 m below mean low-water mark) on the northeastern (41° N) coast of the USA. The main period of growth (as dry matter accumulation, therefore closely related to photosynthesis) was

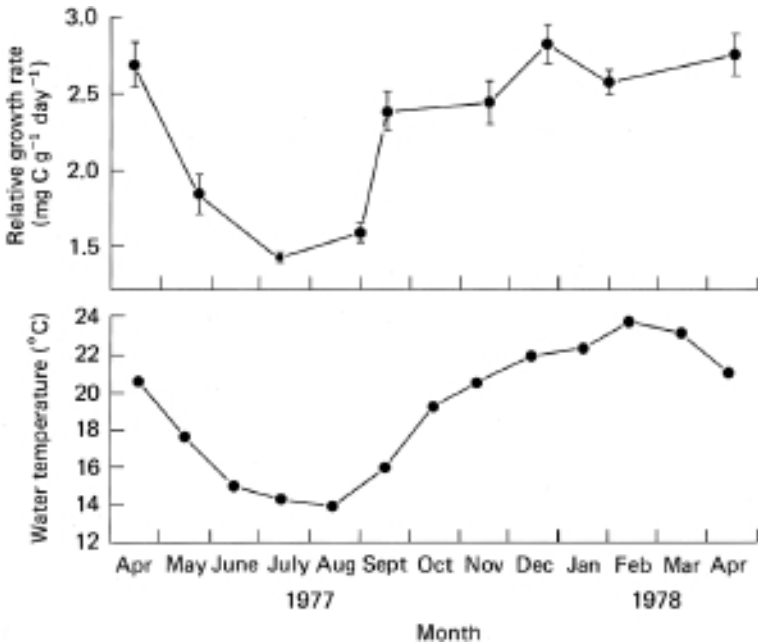


Fig. 11.10 Seasonal variation in relative growth rate of the seagrass *Posidonia australis*, and in surface water temperature, at Port Hacking, NSW, Australia (by permission, from Kirkman and Reid (1979), *Aquatic Botany*, 7, 173–83).

from late spring (April–May) through to early autumn, the maximum rate being in July. It appeared that the total daily irradiance levels were above saturation for growth from April to August/September so that temperature was the major limiting factor, but that in the autumn, when temperatures were still high, the reduced light levels were limiting for growth. In the winter it seemed that both temperature and light were limiting.

In a two-year study of seasonal change in the benthic macroalgae/seagrass community in Puget Sound (Washington, USA), Thom and Albright (1990) found that while water temperature appeared to correlate best overall with standing stock, changes in solar irradiance appeared to trigger the onset of biomass build-up in the spring, and die-back in the autumn. During periods when neither light nor temperature were limiting, nitrate level in the water became the limiting factor for growth.

In some coastal regions the diminution in underwater light availability in the winter due to the lowered solar elevation and shorter days is further

aggravated by a marked increase in the vertical attenuation of light resulting from increased water turbidity caused by the stirring up of sediments in winter storms. At Banyuls-sur-Mer (western Mediterranean),  $K_d$  rose from a minimum value of about  $0.075 \text{ m}^{-1}$  in the summer to a maximum of about  $0.19 \text{ m}^{-1}$  in the winter,<sup>1447</sup> and off Helgoland (North Sea) also, water transparency was much lower from October to March than in the rest of the year.<sup>833</sup>

These data suggest the tentative generalization that primary production of marine macrophytes is limited in deep water by light availability all the year, but in shallow water is usually limited by temperature except that in higher latitudes light becomes limiting in the winter, and that the temporal variation in primary production is in large part a function of the seasonal variation in these two physical parameters. It is likely that macrophyte photosynthesis (other than in deep water) is, in addition, always and everywhere limited by  $\text{CO}_2$  availability, but this does not vary with the seasons. Growth, and therefore photosynthesis, are also determined by the availability of nutrients in the water, particularly nitrate, and in higher latitudes this varies on a seasonal basis being high in the winter but decreasing greatly during the spring phytoplankton bloom. This is less of a limiting factor for many macrophytes than it is for phytoplankton, however. Seagrasses, for example, being rooted plants, can obtain nutrients from the sediments in which they are growing. In the summer, when nitrate concentration in the water is low, the kelps (Phaeophyta) continue to photosynthesize and accumulate carbohydrate reserves for later use, in the winter.<sup>543</sup> In the tropics we might a priori expect relatively little seasonal variation in macrophyte photosynthesis except where there is variation in the hydrological regime, associated for example with seasonal variation in river outflow.

The extent to which seasonal variation in marine macrophyte photosynthesis is influenced by internal, as well as external, changes is unclear. King and Schramm (1976) in their study of many green, brown and red algal species in the Baltic, found, for example, that light compensation points were lower in the winter than at other times of year, and that the light-saturated photosynthetic rates (per g dry mass) varied markedly within any species (but not in the same way in all species) according to the season. However, their measurements were in all cases carried out at the prevailing seasonal water temperature (which, of course, varied during the year) and so they were unable to conclude whether the seasonal adaptation was simply a direct response to temperature change or whether other factors were involved. An example of a seasonal change

in photosynthesis caused by an internal physiological change is, however, provided by the seagrass *Posidonia oceanica*. Drew (1978, 1979) found that in plants of this species growing off Malta the photosynthetic rate (per unit area of leaf) declined markedly in the summer below the spring value, whereas in another seagrass species, *Cymodocea nodosa*, growing nearby, the photosynthetic rate remained high. The decline in *P. oceanica* photosynthesis appeared to be due to senescence (leaf chlorophyll content declined markedly in the summer), possibly triggered by daylength changes.

In fresh waters, the typical pattern of benthic macrophyte primary production in temperate regions is that biomass accumulation does not occur in the winter, that it begins in the spring as a consequence of the increase in solar irradiance and temperature, and rises to its maximum rate (g C or dry matter per m<sup>2</sup> of bottom per day) in the early summer. In the macrophyte-dominated Gryde River (Denmark), Kelly *et al.* (1983) found that the daily primary productivity of the whole plant community throughout one year closely followed the daily insolation. As a consequence, presumably, of light saturation, there was a clear tendency for the *efficiency* of production within a given day to decrease with increasing irradiance during the day. The relative importance of light and temperature in determining the seasonal pattern of freshwater macrophyte photosynthesis is not well understood. We may reasonably suspect that it is largely a matter of depth, temperature being the more important variable in shallow, and light in deeper, water. In the late summer and in the autumn, the rate of accumulation decreases for a number of reasons including a general deterioration in the vigour of the plant due to disease, grazing damage and excessive temperatures.<sup>1456</sup> The rise in pH late in the summer, due to high phytoplankton photosynthesis, can also be inimical to some macrophytes. Since macrophytes can derive nutrients from the sediments in which they are growing, their productivity is not likely to be limited by the seasonal variations in levels of phosphorus and mineral nitrogen in the water. Figure 11.11 shows the seasonal changes in primary production rate in a mixed macrophyte community in a Canadian lake.<sup>830</sup> Internal as well as external changes may influence the seasonal variation in photosynthesis: the photosynthetic capacity of freshwater macrophytes is typically low in the winter and high in the spring.<sup>1455</sup> Variations in photosynthetic capacity could influence the rate of photosynthesis in plants growing at saturating intensities in shallow water but would be of little consequence for plants growing at subsaturating intensities in deep water.

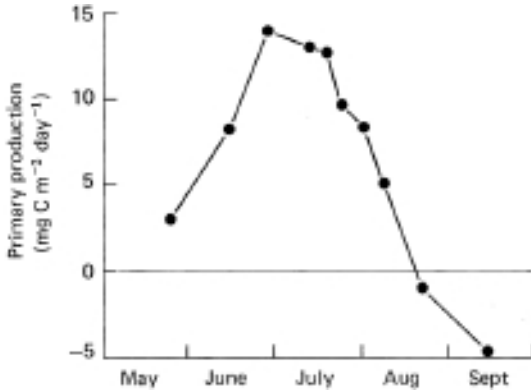


Fig. 11.11 Seasonal variation of the primary production rate of a mixed macrophyte community (predominantly *Chara vulgaris*, *Potamogeton Richardsonii* and *Myriophyllum alterniflorum*) in West Blue Lake, Manit., Canada (after Love and Robinson, 1977).

### 11.5 Photosynthetic yield per unit area

In our consideration of where and when aquatic photosynthesis takes place we have noted that some ecosystems are much more productive per unit area than are others. We shall now look more closely at the basis of this variation in productivity, particularly with respect to the role of light, and shall also examine some of the published data on the primary production rates actually achieved by aquatic ecosystems.

#### Integral photosynthetic rate

Comparisons of phytoplankton productivity in different waters are best carried out in terms of the total phytoplankton production per unit area, i.e. the integral, or areal, photosynthetic rate ( $P_A$ ) for the whole water column beneath 1 m<sup>2</sup> of surface. This can be determined, as we saw earlier, by measuring the depth profile of photosynthesis per unit volume at a given location, and summing through the euphotic zone. This is, however, a very expensive and time-consuming way of determining productivity, and is not feasible if it is wished to map the distribution of productivity within some short time frame, over substantial regions of the ocean. A variety of attempts have therefore been made over the years to find ways of estimating integral photosynthetic rates from smaller amounts of data or more easily measured parameters.<sup>388,1157,1334,1420</sup> In recent times this has been given new impetus by the perceived need to

understand the role of oceanic photosynthesis in the global carbon cycle and therefore the greenhouse effect, and also by the wealth of data on the distribution of phytoplankton biomass through the world's oceans, which has come from remote sensing.

As pointed out by Behrenfeld and Falkowski (1997a) in their review of this topic, depth-integrated productivity models have been appearing in the literature on average once every two years for several decades. No attempt will be made here to describe all these: rather we shall outline just a few representative examples of the many different approaches that have been proposed for the determination of integral productivity. One useful generalization that can be made straight away is that expressions for areal production normally incorporate a  $([Chl]P_m/K_d)$  term. Proportionality of production to the concentration, and to the photosynthetic capacity, of the phytoplankton in the water column is to be expected. Proportionality to  $1/K_d$  is readily understood if we remember that the total amount of light instantaneously available in the water column is proportional to  $l^w K_0(av)$  (see §6.5).

Two of the earliest algorithms were those of Ryther (1956) and Talling (1957b); both of them for vertically homogeneous phytoplankton populations. Ryther arrived, on the basis of measurements of photosynthesis/light intensity curves on cultures of 14 marine phytoplankton species, at a notional average relative light response curve (ratio of photosynthetic rate to maximum photosynthetic rate, as a function of irradiance) for marine phytoplankton populations. Using this curve he was then able to calculate a dimensionless parameter,  $R_s$ , which specified how the daily integral photosynthesis would vary with the daily insolation, and obtained the expression

$$P_A = R_s \frac{P_{sat}}{K_d} \quad (11.3)$$

where  $P_{sat}$  is the light-saturated photosynthetic rate of the population per unit volume of water ( $\text{mg C m}^{-3} \text{ hr}^{-1}$ ), and  $K_d$  is the vertical attenuation coefficient for downward irradiance of PAR.  $P_{sat}$  can be replaced by the product of phytoplankton concentration and the maximum specific photosynthetic rate.

$$P_A = R_s \frac{[Chl]P_m^*}{K_d} \quad (11.4)$$

If a plausible value for the maximum specific photosynthetic rate, or *assimilation number* (units  $\text{mg C mg chl a}^{-1} \text{ hr}^{-1}$ ),  $P_m^*$ , can be assumed

for the phytoplankton in a particular region, and if  $K_d$  can be estimated as a function of phytoplankton concentration ( $[Chl]$ ), then daily integral production can be estimated simply from daily insolation (giving  $R_s$ , using the Ryther empirical curve) and phytoplankton concentration. Ryther and Yentsch (1957), on the basis of their own, and literature, data suggested that  $3.7 \text{ mg C chl } a^{-1} \text{ hr}^{-1}$  was a good estimate of the assimilation number of oceanic phytoplankton, and found that when used in eqn 11.4 it gave estimates of integral production in good agreement with those from *in situ* measurement. Falkowski (1981), however, with the benefit of access to much more oceanographic productivity information than was available in 1957, concluded that phytoplankton assimilation numbers are affected by nutrient levels, temperature, cell size and light history, and in fact vary commonly between 2 and  $10 \text{ mg C mg chl } a^{-1} \text{ hr}^{-1}$ .

It will be noted that Ryther (1956), by adopting a standard relative light curve implicitly assumed a fixed value for the saturation onset parameter,  $E_k$ , of marine phytoplankton. In the Talling (1957b) algorithm for calculating areal production, by contrast,  $E_k$  is included as one of the parameters whose value is selected at each location. On the basis that phytoplankton photosynthesis varies with light intensity in accordance with the equation of Smith (1936) (eqn 10.8), and that irradiance of PAR diminishes exponentially with depth, and ignoring photoinhibition, Talling calculated a standard curve for the photosynthetic rate per unit volume, as a function of depth. By measurement of the area under the curve, and relating it to various parameters of the system, he was able to show that the following relationship approximately holds

$$P_A = \frac{[Chl]P_m^*}{K_d} \ln \left[ \frac{E_d(0)}{0.5E_k} \right] \quad (11.5)$$

where  $E_d(0)$  is the downward irradiance of PAR just below the surface. Talling found that eqn 11.5 gave reasonably accurate estimates of  $P_A$  over a wide range of values of  $E_d(0)/E_k$ , but significant discrepancies did arise for low surface light intensities ( $E_d(0) < E_k$ ). To obtain the daily total of photosynthesis per unit area, Talling found the relationship

$$\text{Areal photosynthesis per day} = \frac{[Chl]P_m^*}{K_d} \left[ 0.9 N \ln \left( \frac{\overline{E_d(0)}}{0.5E_k} \right) \right] \quad (11.6)$$

where  $\overline{E_d(0)}$  is the mean value of subsurface downward irradiance during daylight hours,  $N$  is daylength in hours, and 0.9 is an empirical correction factor, to be satisfactory. The expression in square brackets corresponds

to the  $R_s$  term in the Ryther equation (11.4). As with the Ryther equation, the Talling equation can be used to estimate daily integral production from daily insolation and phytoplankton concentration, with the additional requirement that an appropriate value be assigned to the saturation onset parameter,  $E_k$ . Platt *et al.* (1990) have, by a mathematically sophisticated approach, arrived at an exact but complex analytic solution for the daily integral of photosynthesis by phytoplankton in a vertically homogeneous water column.

Conceptually, one of the simplest solutions to the problem of estimating oceanic primary production from remote sensing data makes use of the parameter,  $\Psi$ , known as the *light utilization efficiency function*,<sup>376,384</sup> discussed earlier (§10.3), which is the total net integral daily primary production in a 1 m<sup>2</sup> water column (g C m<sup>-2</sup> day<sup>-1</sup>), divided by the total amount of phytoplankton chlorophyll *a* in the water column (g chl *a* m<sup>-2</sup>), and by the total light energy in the form of PAR incident upon the top of the water column in one day (mol quanta m<sup>-2</sup> day<sup>-1</sup>). If it proved to be the case that  $\Psi$  (units g C (g chl *a*)<sup>-1</sup> (mol quanta)<sup>-1</sup> m<sup>2</sup>) had, even if only very approximately, the same value everywhere in the ocean, then global marine primary production could be estimated from remotely sensed values of phytoplankton chlorophyll and surface-incident irradiance.

On the basis of a survey of literature data available up to that time, Platt (1986) arrived, as discussed earlier, at the encouraging conclusion that  $\Psi$  varied only over the range 0.31 to 0.66 g C (g chl *a*)<sup>-1</sup> (mol quanta)<sup>-1</sup> m<sup>2</sup>. More recent data, however, indicate that  $\Psi$  is in fact much more variable than this. Campbell and O'Reilly (1988) found, for example, in a wide-ranging study over the oceanographically diverse northwest Atlantic continental shelf, that  $\Psi$  varied about 100-fold, from about 0.1 to 10, and furthermore that its average value was 1.47 g C (g chl *a*)<sup>-1</sup> (mol quanta)<sup>-1</sup> m<sup>2</sup>, much higher than the values reported by Platt.

Even though it does not seem to be quite the 'biogeochemical constant'<sup>944</sup> that it was originally hoped to be,  $\Psi$  is nevertheless a useful unifying concept, and consideration of why in fact it varies so much may be fruitful. Platt (1986) showed that in vertically homogeneous waters,  $\Psi = \alpha/4.6$ , where  $\alpha$  is the initial slope of the photosynthesis versus light intensity curve (§10.1) of the phytoplankton population. Platt *et al.* (1992) found the value of  $\alpha$  to vary about 12-fold with time and place in cruises in the western North Atlantic. Measurements within one water mass during the spring bloom indicated a marked decrease in  $\alpha$  as nitrate levels declined.

Ways of increasing the accuracy with which the geographical distribution of integral primary productivity can be calculated from remote sensing data are under active study in a number of centres. In order to discuss what parameters need to be estimated, we can make use of a general formulation arrived at by Platt and Sathyendranath (1993) using dimensional analysis.

$$P_A \sim \frac{[Chl]P_m^*D}{K_d} f \left[ \frac{E_d(0^+)}{E_k} \right] \quad (11.7)$$

where  $D$  is daylength and  $f[E_d(0^+)/E_k]$  is some function of the surface-incident solar irradiance and the saturation onset parameter of the phytoplankton. An alternative, but essentially equivalent, general formulation is given by Behrenfeld and Falkowski (1997a)

$$P_A = C_{\text{surf}} \times z_{eu} \times P_{\text{opt}}^b \times DL \times F \quad (11.8)$$

where  $C_{\text{surf}}$  is the chlorophyll concentration in the surface layer (e.g. as determined by remote sensing),  $z_{eu}$  is the euphotic depth (which is proportional to  $1/K_d$ ),  $P_{\text{opt}}^b$  is the maximum chlorophyll-specific carbon fixation rate observed within a water column,  $DL$  is the daylength, and  $F$  is the relative fraction of potential photosynthesis lost within the euphotic zone due to light limitation ( $F$  being a function of  $E_d(0^+)/E_k$ ).

Values of  $[Chl]$  can be obtained by remote sensing, but apply only to the surface layer: in the ocean, phytoplankton concentration can vary markedly with depth. Morel and Berthon (1989) and Uitz *et al.* (2006) found that the profile of chlorophyll as a function of optical depth varied in a systematic manner from quasi-uniformity in eutrophic waters to a clear-cut deep chlorophyll maximum in oligotrophic waters. On this basis, statistical relationships were derived by means of which the chlorophyll  $a$  content integrated over the euphotic zone could be estimated from the near-surface chlorophyll  $a$  concentration obtained by remote sensing. To characterize the actual depth distribution of chlorophyll where a DCM is present, Platt *et al.* (1988) proposed a generalized pigment profile consisting of a Gaussian curve (to represent the chlorophyll maximum) superimposed on a constant background level. Millán-Núñez *et al.* (1997) found the Platt *et al.* model to work satisfactorily for chlorophyll profiles in the California Current System between 28° and 37° N. Thus, once the trophic level of the water mass has been identified from the surface chlorophyll concentration, a plausible depth profile can be arrived at. Alternatively, total euphotic zone chlorophyll can be obtained from surface layer

chlorophyll using empirically derived relationships<sup>946,1240</sup> that have been found to apply, between these quantities. Balch *et al.* (1989a) used two standardized profiles, based on accumulated data, of relative chlorophyll concentration versus optical depth, one for nearshore and one for off-shore waters.

Once the phytoplankton chlorophyll has been estimated, an approximate value of  $K_d(\text{PAR})$  can be arrived using an empirical relationship.<sup>62</sup> In the case of the very comprehensive Morel (1991) algorithm, however, the chlorophyll values are used, together with a standard phytoplankton absorption spectrum, to give the actual absorption coefficients in a series of 5 nm wavebands over the 400 to 700 nm interval.

The daily surface-incident solar irradiance,  $E_d(0^+)$ , is determined by the date, latitude and atmospheric conditions: the dependence of irradiance on the first two is readily calculable, but the third is the cause of enormous variation, particularly due to the influence of cloud cover. Kuring *et al.* (1990) have developed a procedure for estimating per cent cloud cover from remotely sensed satellite images and using these values to derive sea-surface irradiance.

There now remains the problem of finding a value for  $P_m^*$ , and it is here that the major uncertainty in the remote sensing of oceanic productivity lies. As we have seen, the photosynthetic characteristics of phytoplankton populations are highly variable both in space and in time, and the reasons are not well understood. One possible cause of variation is temperature. The light-saturated maximum photosynthetic rate,  $P_m^*$ , increases with temperature (Fig. 11.6). Balch *et al.* (1989a, b) obtained, using data from the Southern California Bight, an empirical expression for the dependence of  $P_m^*$  on water temperature, and another empirical expression for mixed-layer depth, and the rate of decline of temperature with depth below that, as a function of surface temperature. Their PTL algorithm (pigments, temperature, light) combines the calculated chlorophyll and  $P_m^*$  depth profiles to calculate photosynthesis as a function of depth through the euphotic zone.<sup>60,61,62</sup> Behrenfeld and Falkowski (1997b), on the basis of a large amount of archived data from many oceanic locations, developed a polynomial expressing  $P^b_{\text{opt}}$  as a function of surface temperature. The Morel (1991) algorithm also takes temperature into account. The significance of algorithms incorporating temperature in this manner is that sea-surface temperature can be mapped from space.

$P_m$  is a linear function of maximum quantum yield,  $\phi_m$  (since  $P_m = \bar{\alpha}_c E_k \phi_m$ ) and  $\phi_m$  appears to be strongly correlated with nitrogen flux<sup>151,512</sup> (see §10.3). The decline of  $\alpha$  as nitrate concentration decreased, in the

western North Atlantic spring bloom referred to earlier, may be attributable to a decline in  $\phi_m$  (since  $\alpha = \bar{\alpha}_\phi^* \phi_m$ ). Variation in  $\phi_m$  due to variation in nitrogen availability is therefore another possible basis for variability in  $P_m$ , but unfortunately, nitrate concentration, or the depth of the nitracline, cannot be measured by remote sensing. Yet another major possible cause of variation in  $\phi_m$  and hence of  $P_m$ , is community composition, which can vary either seasonally at a given location, or from one hydrographically distinct water mass to another along a transect in coastal waters.<sup>110,1252</sup>

$P_m$  is also linearly related to  $\bar{\alpha}_\phi^*$ , the chlorophyll-specific absorption coefficient of the phytoplankton, and this can not only vary for a given phytoplankton species in accordance with its nutritional status, but will vary even more markedly with the taxonomic composition of the phytoplankton community, which as we have just seen is highly variable in both time and space.

All in all, therefore, there are good reasons why we must expect  $P_m$  to be a highly variable, and difficult-to-predict, quantity from one part of the ocean to another. The most feasible approach to the mapping of marine productivity may therefore be to divide the ocean up into regions, within each of which realistic estimates of the relevant physiological parameters can be made.<sup>1068</sup> Platt *et al.* (2008) offer an approach by which this may be achieved. They define *local algorithm* to mean a procedure to convert pigment biomass into primary production, where it is understood that all information essential to implement the procedure is available for the particular space-time point concerned. The minimum information includes the pigment biomass and irradiance at the surface, an equation to describe the photosynthetic response to available light (the photosynthesis–light curve), the local magnitudes of the two parameters for this curve (the photosynthesis parameters), an equation to describe the vertical structure of the pigment biomass and the local magnitudes of the parameters of that equation. The values of the various parameters are assigned on a pixel-by-pixel basis, using archived data for the region in question, in accordance with the remotely sensed chlorophyll concentration and surface temperature. As an example, Platt *et al.* applied their approach to the Northwest Atlantic Ocean, and found it to work satisfactorily.

It will be noted that in all the above discussion of the areal productivity of different parts of the ocean, the light-absorbing biomass has been parameterized in terms of the concentration of phytoplankton chlorophyll  $a$ . An alternative approach is proposed by Marra, Trees and

O'Reilly (2007) who argue that over a range of trophic conditions in the ocean, variations in productivity are more closely related to variations in phytoplankton absorption than in chlorophyll *a* concentration. On the basis of data on primary productivity, phytoplankton pigments and absorption, and ocean optical properties, from the Equatorial Pacific, the Arabian Sea and the Antarctic Southern Ocean, they concluded that productivity normalized to absorption is relatively invariant in the world ocean. The authors acknowledge, however, that since they were unable to include data from the temperate ocean, or from the central ocean gyres, in their analysis, caution in the application of this approach is, for the time being, called for.

As an approach that is at the other extreme to the painstaking, pixel-by-pixel, assessment of biomass and photosynthetic parameters, Berthelot and Deschamps (1994) propose an algorithm that makes use only of the ratio of reflectance in two wavebands, together with incident PAR, using a purely empirical relationship derived by analysis of a large body of *in situ* data. The data consisted of measurements of chlorophyll, primary production, surface-incident solar irradiance, and spectral downward and upward underwater irradiance at stations (all case 1 type) in the West Atlantic (Sargasso Sea, Gulf of Mexico), East Atlantic (Mauritanian upwelling), tropical East Pacific and South Indian Antarctic Oceans. By statistical analysis of the data they arrived at the algorithm

$$\log_{10} P_t = -4.286 - 1.390 \log_{10}(R_{440}/R_{550}) + 0.621 \log_{10} (\text{PAR}) \quad (11.9)$$

where  $P_t$  is daily production in  $\text{g C m}^{-2} \text{ day}^{-1}$ ,  $R_{440}$  and  $R_{550}$  are the irradiance reflectances (subsurface upwelling/above-surface downward) at 440 and 550 nm, and PAR is in  $\text{J m}^{-2} \text{ day}^{-1}$ . Comparing predicted with observed values of primary production, their model had an  $r^2$  of 0.85 to 0.95. The rms accuracy of primary production estimation was 0.17 on a logarithmic scale, corresponding to a factor of 1.5. Berthelot and Deschamps suggest that their model should be applicable for the evaluation of primary production of those oligotrophic and mesotrophic waters that constitute most of the open ocean.

The integral primary production we have discussed above is total primary production. A large part, usually most, of the plant biomass produced is eventually recycled within the euphotic zone as the result of grazing, fungal or viral infection etc., followed by microbial mineralization, but a proportion passes down through the thermocline, in the form of zooplankton faecal pellets and aggregated or dead phytoplankton cells at the end of a bloom, to the deep sea. This downward flux of organic

matter from the euphotic zone is sometimes referred to as *export production*. It brings about a net transfer of carbon from the atmosphere to the deep sea, and is the reason why oceanic photosynthesis is of major importance in the global carbon cycle. In the context of global climate change, the transfer of carbon to the ocean depths by this mechanism is commonly referred to as the *biological pump*. Export production can take place in the much shallower seas of the continental shelf, as well as in the deep ocean, and can involve a mechanism other than passive downward sinking. Sharples *et al.* (2001) observed substantial rates of turbulent entrainment of carbon from the base of the deep chlorophyll maximum into the bottom mixed layer in a well-stratified region in the Western English Channel. They suggest that carbon export into the bottom mixed layer by this mechanism could account for as much as 25% of the gross primary production in stratifying shelf seas.

The downward transport of biomass removes not only carbon (which is continuously replenished by atmospheric CO<sub>2</sub>), but also essential mineral nutrients, especially nitrogen, and if the phytoplankton ecosystem of the euphotic zone is to remain productive, levels of these nutrients must be restored. Nutrients are in fact supplied from outside the euphotic zone in a number of ways: from deep water during seasonal, or temporary wind-induced, breakdown of stratification, from the atmosphere, from nitrogen fixation, and from rivers. Such considerations led Dugdale and Goering (1967) to introduce the concept of *new production*, which is that primary production associated with these nutrient inputs from outside the euphotic zone, as opposed to the primary production associated with the nutrients recycled within the euphotic zone. Clearly, continued export production is only made possible by the existence of new production, and quantitatively the two are approximately equivalent. Eppley and Peterson (1979) defined the *f* ratio as the ratio of new production to total primary production at any given location, and they showed that this varied regionally: *f* increases as total productivity increases, but levels off at about 0.5 for the most productive oceanic regions, such as the Peruvian upwelling. For the oceanic ecosystem as a whole they estimated an *f* ratio of 0.18 to 0.20. In the northeast basin of the Atlantic Ocean (16–22° W, 38–45° N) Fernandez *et al.* (2005) found the seasonal *f* ratio to be ~0.28 in winter, increasing to 0.34 in spring, then decreasing to 0.25 in late summer. In the equatorial Pacific, Le Bouteiller *et al.* (2003) found the *f* ratio to be 0.15 at 3° S, but as high as 0.37 at the equator. In the Southern Ocean, at stations along 141°30' to 143° E, Elskens *et al.* (2002) found low *f* ratios (0.08–0.14) in the Subtropical Convergence

Zone (STCZ, 42° S). South of the STCZ the  $f$  ratio increased to 0.43 to 0.51, and further south (47–55° S) oscillated between 0.22 and 0.44. For the summer-stratified North Sea, Weston *et al.* (2005) estimated that annual new production associated with the deep chlorophyll maximum, supported in part by nutrient flux from the nutrient-rich bottom mixed pool, accounted for 37% of the total new production.

Estimating total primary production by remote sensing, in the manner we have discussed, can provide indirect information about new, or export, production if plausible values of the  $f$  ratio can be assigned, and so is of great potential value for understanding the role of the oceans in the global carbon cycle. Clearly, however, it would be an advantage if some information on the prevailing value of the  $f$  ratio in the region under study could be obtained from remote sensing measurements. Sathyendranath *et al.* (1991) have taken advantage of the fact that nitrate concentration is often negatively correlated with temperature, and that the  $f$  ratio is positively correlated with the nitrate concentration. They combined CZCS-derived phytoplankton estimates with AVHRR sea-surface temperature measurements to estimate not only total primary production, but also the  $f$  ratio and hence new production in the sea over and around Georges Bank, east of Cape Cod (USA).<sup>1174</sup> This method can, of course, only be applied where, as in this case, there is a substantial body of accumulated field data, relating nitrate concentration to temperature.

### Geographical variation of photosynthetic yield

Equations such as 11.4–11.8 predict the amount of phytoplankton photosynthesis per unit area of the ecosystem per day for a specified set of values of the crucial parameters of the system: concentration ( $[Chl]$ ) and photosynthetic characteristics ( $P_m^*$ ,  $E_k$ ) of the phytoplankton, penetration of light into the water ( $K_d$ ), incident radiation ( $E_d(0^+)$ , daylength). All these parameters vary not only throughout the course of the year, but also, taken over the whole year, with geographical location – from one part of the world's oceans to another, from one inland water body to another – because of differences in the average values of the controlling physicochemical parameters of the system such as depth, insolation, nutrient concentration, temperature, optical properties of the water, stability of the water column etc. The consequent geographical variation in annual photosynthetic yield can conveniently be characterized in terms of the total amount of carbon fixed by photosynthesis per m<sup>2</sup> of aquatic ecosystem per year. Data for phytoplankton primary production in

Table 11.2 Annual phytoplankton primary production in the oceans.  
Data from literature surveys by various authors.

	Primary production (g C m <sup>-2</sup> yr <sup>-1</sup> )		Reference
	Continental shelf	Deep ocean	
<i>Ocean</i>			
Indian	259	84	1070
Atlantic	150	102	1070
Northeast Atlantic		203	390
Pacific	190	55	1070
Arctic	50–250	25–55	1164
Southern	184	130	31
<i>Regions within Pacific Ocean</i>			
Tropical deep ocean	28		734
Tropical/temperate transition zone	49		734
Temperate deep ocean	91		734
Continental shelf, temperate	102		734
Inshore coastal, temperate and tropical	237		734
Peruvian upwelling	1350–1570		1435
<i>Various shelf, coastal and estuarine waters</i>			
Irish Sea	101–140		499
Northern Ireland coastal	194		499
Northeast USA coastal	260–505		1210
Chesapeake Bay	347–662		527
Narragansett Bay	323		1026
North Sea	100–300		1504
German Wadden Sea	124–176		1358
Barents Sea	60–80		320
Southern Aegean Sea	25		608
45 estuaries	190		154

various parts of the sea are listed in Table 11.2. Detailed discussions of productivity in various parts of the ocean may be found in Raymond (1980), Cushing (1988) and in the proceedings of the workshop on *Productivity of the Ocean: Present and Past*, edited by Berger, Smetacek and Wefer (1989).

In addition to the rate of carbon fixation per unit area, the productivity of marine ecosystems can be characterized in terms of the total amount of carbon photosynthetically fixed per year in specific defined ocean regions. This is usually expressed in gigatonnes (Gt, 10<sup>9</sup> tonnes) C yr<sup>-1</sup>. Such calculations are carried out using data on the distribution of phytoplankton chlorophyll, sea-surface temperature and incident PAR,

Table 11.3 Total phytoplankton carbon fixation per year in different oceanic regions.

Ocean region	Total carbon fixation (Gt C yr <sup>-1</sup> )	Reference
Arctic	1.1	826
Atlantic	14.8	826
Pacific	19.7	826
Indian	6.5	826
Eastern tropical Atlantic (5° N–10° S, 25° W–10° E)	2.3	927
Subtropical and tropical Northeast Atlantic (5°–40° N, 6°–30° W)	0.82	564
Southern Ocean		
Latitude >30° S	14.2	933
Latitude >50° S	1.95	32
Global ocean		
CZCS data	45–50	826
SeaWiFS data	52–55	1261

obtained by remote sensing, over the area in question, using an algorithm of the type discussed in the previous section. Some of the published estimates are presented in Table 11.3. The total net oceanic primary production of 45 to 55 Gt yr<sup>-1</sup> (Table 11.3) is carried out by an estimated phytoplankton biomass of ~1 Gt C, which is only ~0.2% of the photosynthetically active C biomass on Earth.<sup>377</sup> Agawin *et al.* (2000) estimate that 24% of this phytoplankton biomass consists of picophytoplankton (<2 µm), and that they contribute 39% of the global oceanic production.

The least productive waters are the deep oceans in tropical latitudes. Such waters have a permanent thermocline, which greatly impedes transport of nutrients up from the depths where they are regenerated by mineralization of sedimenting phytoplankton and zooplankton faecal pellets. In the temperate oceans, nutrient levels in the upper layer are restored each winter when thermal stabilization breaks down. The highest rates of production are achieved when the high insolation and temperatures of tropical regions are combined with a plentiful nutrient supply in the form of upwelling water from the depths: the Peruvian upwelling is probably the most productive region of the oceans. Phytoplankton productivity is higher in the shallower waters of the continental shelf, and higher still close inshore, than in the deep oceans, even in tropical latitudes. Nutrient supply from the land, and tidal mixing, are thought to be important factors. Close inshore, recycling of nutrients from the bottom

and the impossibility of deep circulation of the phytoplankton (below the critical depth) are also likely to contribute to the enhanced productivity. In one of the world's oceans – the Arctic – total primary production appears to be increasing, because of the increased area of open water resulting from global warming.<sup>1029</sup>

In the case of inland waters, oligotrophic (nutrient-poor) lakes have phytoplankton primary productivities usually in the 4 to 25 g C m<sup>-2</sup> yr<sup>-1</sup> range whereas eutrophic (nutrient-rich) lakes typically fix 75 to 700 g C m<sup>-2</sup> yr<sup>-1</sup>,<sup>520,1143</sup> although, for the saline Red Rock Tarn in Australia, an annual production of 2200 g C m<sup>-2</sup> has been reported.<sup>520</sup> Hammer presents an extensive compilation of productivity data for inland waters in the 1980 IBP report.<sup>781</sup> Brylinsky's survey of a large number of lakes all over the world for the IBP report indicated that phytoplankton productivity is negatively correlated with latitude. This can reasonably be explained in terms of the diminution of annual solar radiation input with increasing latitude.

We have noted earlier that, by bringing about the transfer of the greenhouse gas, carbon dioxide, from the atmosphere to the deep ocean (the biological pump), marine phytoplankton productivity plays a major role in the regulation of global climate. There is another important mechanism of climate control in which phytoplankton may play a role, namely, cloud formation. Many classes of unicellular marine algae – prymnesiophytes, dinophytes, prasinophytes, some diatoms and chrysophytes<sup>854</sup> – produce large amounts of dimethylsulfoniopropionate (DMSP), which acts as an osmolyte. This is released into the sea, either passively by leakage, or actively by zooplankton grazing or viral lysis, and is then broken down to dimethyl sulfide (DMS) by microbial action. The DMS escapes from the ocean, and is the main biogenic source of reduced sulfur to the atmosphere,<sup>77</sup> where it is oxidized to sulfate in the form of submicron aerosol particles, which act as condensation nuclei for water vapour, thus promoting cloud formation. It was suggested by Charlson *et al.* (1987) that the connection between DMSP-producing algae and clouds represents a climate-regulating mechanism.

# 12

## Ecological strategies

Of the factors that limit the rate of primary production in aquatic ecosystems – light, nutrients, carbon dioxide and temperature – the one that shows the most extreme variation within the aquatic medium is light. As we have seen ([Chapter 6](#)) the irradiance decreases with depth from intensities that are so high as to be damaging down to levels that cannot support photosynthesis, and the spectral distribution of the light also changes markedly. We have also seen that at any given depth the intensity and spectral quality of the light can vary greatly in accordance with the optical properties of the water. Furthermore, to a much greater extent than the other limiting factors, light availability varies with time: both within the day – from darkness to the full noon Sun, and as clouds pass across the Sun and with the seasons during the course of the year.

In this chapter we shall consider the ways in which the aquatic flora is adapted to this variability of the light climate.

### **12.1 Aquatic plant distribution in relation to light quality**

As we saw in [Chapters 8](#) and [9](#), there are major differences between the main taxonomic groups of aquatic plants with respect to the kinds of photosynthetic pigment present and, as a consequence, major differences in the absorption spectra. Given the variation in intensity and spectral quality of the light field in the aquatic environment, we may reasonably suppose that for any given location within a water body there will be certain species that are well equipped to exploit the particular prevailing light field and others that are not. It thus seems

likely that photosynthetic pigment composition could be a major factor determining which species of aquatic plant grow where.

In the case of the benthic algae of marine coastal waters it has been observed that the different major algal groups are not mixed at random. In some parts of the benthic environment browns predominate while in others the reds or the greens predominate, although domination by any type is not usually complete. Furthermore, progressive changes in the proportions of the different algal groups along the depth gradient can often be discerned. It has been a commonly held belief in marine biology since the nineteenth century that the most important factor determining algal zonation is the variation of the light field with depth. This theory has taken two forms, which have, perhaps needlessly, been seen as opposed rather than complementary. According to the *chromatic adaptation* theory of Engelmann (1883) it is the varying colour (spectral distribution) of the light with depth that determines the algal distribution, i.e. as the predominant colour changes due to selective absorption, those algae that have absorption bands corresponding best to the spectral distribution of the surviving light can photosynthesize most effectively and so predominate. Berthold (1882) and Oltmanns (1892), on the other hand, proposed that it is the varying intensity of the light with depth that determines the distribution of the different algal types.

In fact both the colour and the intensity of the light field change simultaneously with depth and the plants must adapt to both. For example, any plant growing near the bottom of the euphotic zone must be able to make use not only of a restricted spectral distribution, but also of a very low total irradiance. One possible form of adaptation to low irradiance is a lowering of the respiration rate; another would be an increase in the concentration of all the photosynthetic pigments present without alteration of the ratios. Harder (1923) suggested that both chromatic and intensity adaptation are involved: it is not in fact easy to disentangle the two. Nevertheless there is persuasive circumstantial evidence that chromatic adaptation plays an important role in determining the distribution of the different plant groups.

Before we examine this evidence, we must make clear the important distinction between *phylogenetic* and *ontogenetic* chromatic adaptation.<sup>1097</sup> Phylogenetic adaptation is adaptation that has taken place during phylogeny, i.e. during the evolution of the species. In the present context it refers to the genetically determined differences in pigment composition between the different taxonomic groups of aquatic plants. Within a given species, while the nature of the pigments formed is fixed,

the proportion of the different pigments can alter, with significant effects on absorption properties, in accordance with the environmental conditions prevailing during growth and development, i.e. during ontogeny. This is ontogenetic chromatic adaptation. We shall consider both kinds of chromatic adaptation.

### **Evidence for phylogenetic chromatic adaptation**

Changes in the pigment category of aquatic plants with depth are striking in sea water but hard to identify in fresh water, and so we shall here consider marine ecosystems. We shall begin by noting that in all marine waters there is ample light in all wavebands near the surface, and so the theory of chromatic adaptation, which is specifically concerned with light-limited situations, has nothing to tell us about the relative success of the different algal groups in this region: resistance to wave action, for example, or, in the case of upper sublittoral forms, to occasional exposure to the atmosphere, are likely to be more important factors.

While in all waters total irradiance diminishes exponentially with depth, the nature of the change of spectral distribution with depth varies in accordance with the absorption properties of the water. In all waters irradiance in the red waveband diminishes quite rapidly due to absorption by water itself. In very clear colourless waters, attenuation is least in the blue region, and with increasing depth the underwater light becomes first blue-green and then predominantly blue in colour (Fig. 6.4*a*). In waters with significant amounts of yellow substances there is rapid attenuation in the blue region as well as the red, so that as depth increases the light becomes increasingly confined to the green waveband (Fig. 6.4*b*). On the basis of chromatic adaptation we might therefore expect somewhat different patterns of algal zonation in the different types of water, and this in fact turns out to be the case.

The depth distribution of the three major eukaryotic algal groups can be expressed in terms of either the biomass, or the number of species, in each group, at a series of depths. Both kinds of information are interesting, the first perhaps more so from our present point of view since it is more directly related to the competitive success through primary production of the different groups: species number, in contrast, can be regarded as a measure of the number of different solutions that the green, brown or red algae have found to the problems of growing at a given depth, or alternatively as a measure of the amount of green, brown or red algal genetic information to be found at that depth. Quantitative distribution

data of either type seem to be rather scarce and unfortunately this is especially true in the case of biomass.

We shall first consider waters of the northern hemisphere temperate zone. For the west coast of Sweden (at the entrance to the Baltic Sea), Levring (1959) reported (although quantitative data were not given) that most members of the Chlorophyta occur in the littoral and upper sublittoral zones, the Phaeophyta occur mainly from the littoral zone down to the middle of the sublittoral zone (~15 m), and the Rhodophyta occur throughout the euphotic zone but are the predominant algal group in the lower sublittoral zone (15–30 m). Distributions described in other northern hemisphere temperate waters are broadly similar to this but clear-cut zonation appears to be absent. Figure 12.1 shows the variation of species number in the three algal groups with depth at three sites in the British Isles and one from northeastern North America. The numbers of green and brown species decreased with depth. The number of red species at some places increased at first with depth but then began to decrease. At all sites green species were much less common than the other two, and brown species were less numerous than red. At the three sites where green algae were found (Chlorophyta apparently being absent or insignificant at the Scilly Isles site) they penetrated well down into the sublittoral – to about the middle or a bit further – but the brown algae penetrated deeper, and the red algae deeper still. In all cases the red algae dominated the lowest region of the sublittoral. Norton, Hiscock and Kitching (1977) measured the depth distribution of biomass of the more abundant seaweeds on a headland in southwest Ireland, and their data are plotted in Fig. 12.2. Green algae were apparently of no quantitative significance at this site. It can be seen that the brown algae constituted nearly all the underwater biomass throughout most of the sublittoral zone. Brown algal biomass consisted almost entirely of the large kelp *Laminaria hyperborea*: it reached its peak between about 6 and 10 m depth but decreased sharply below this, falling virtually to zero biomass at 18 m. Below 18 m the vegetation consisted mainly of a comparatively sparse cover of red algal species. On a deep-water rock pinnacle in the Gulf of Maine (USA), Vadas and Steneck (1988) observed that kelps (mainly *Laminaria* sp.) were dominant from 24 m (pinnacle summit) down to 33 m depth. Foliose red algae were present through the kelp zone but extended further: they were dominant at 37 m and reached a maximum depth of 50 m. Crustose red algae became a significant component at about 37 m, and were the dominant algal type in the lowest region, fleshy crusts extending to 55 m and coralline crusts to 63 m depth. Green algae appeared to be absent from the rock pinnacle.

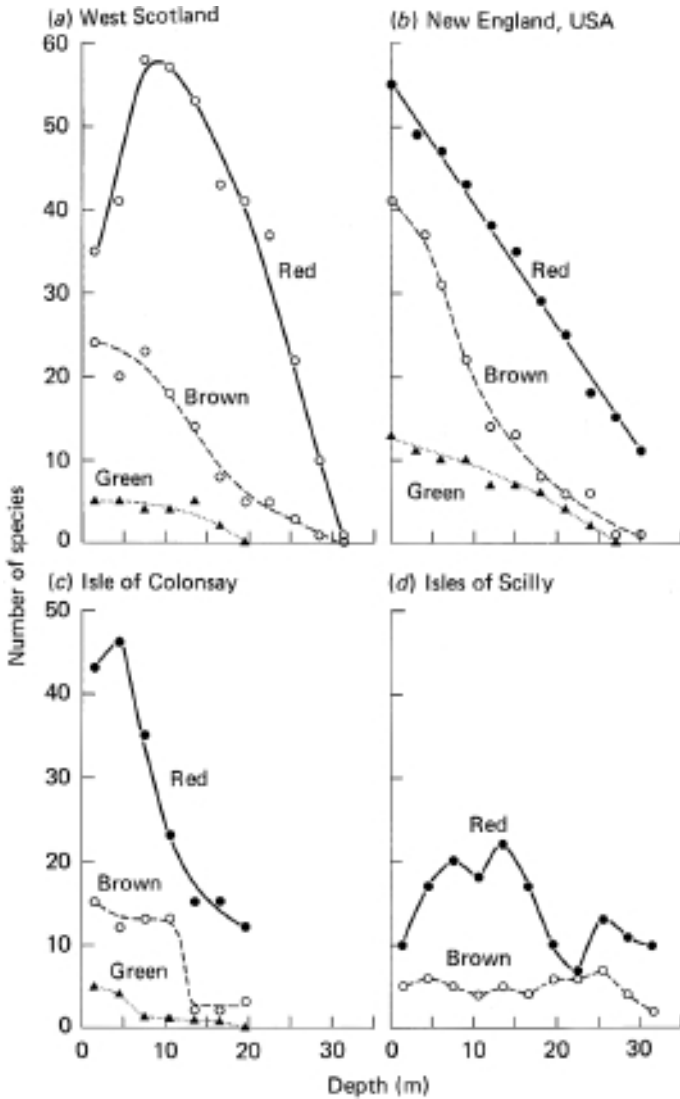


Fig. 12.1 Variation of taxonomic composition of benthic algal flora with depth in northern hemisphere temperate waters. (a) West of Scotland (Argyll and Ayrshire, 56–57° N). Derived from data of McAllister *et al.* (1967). (b) New England, USA (Maine and New Hampshire, 42–43° N). Plotted from data of Mathieson (1979). (c) Isle of Colonsay, Inner Hebrides, Scotland (56° N). Derived from data of Norton *et al.* (1969). (d) Isles of Scilly, England (50° N). Derived from data of Norton (1968). The curves show the number of red (—●—), brown (---○---) and green (. . ▲. .) algal species found at each depth. Curves (a), (c) and (d) were derived from the published depth distribution for each algal species.

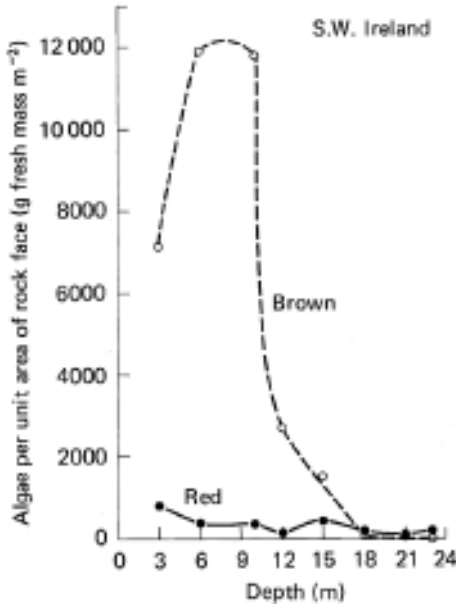


Fig. 12.2 Variation of biomass per unit area of brown and red algae with depth in a northern hemisphere temperate water (Carrigathorna, Lough Ine, southwest Ireland, 51° N). Plotted from data of Norton, Hiscock and Kitching (1977).

Northern European waters contain sufficiently high levels of CDOM to ensure that the underwater light becomes predominantly green in colour,<sup>519,636</sup> and the same is likely to be true of the northeastern American coastal waters. In such waters the rate of assimilation achieved by an alga with increasing depth is going to depend on, among other things, how much absorption it has in the green (500–600 nm) band. The green algae, which show relatively low absorption in this spectral region, are the most disadvantaged, which would explain their small contribution – both in species number and biomass – to the algal community, and the fact that they penetrate least deeply. The brown algae, which show, due to the presence of fucoxanthin, substantial absorption in the 500 to 560 nm region, hold their own through most of the sublittoral euphotic zone. At the lower fringe of the euphotic zone, where the spectral distribution becomes quite narrow, the red algae, whose biliprotein pigments have their absorption peaks within the green region, can compete better for the available light and so come to dominate.

We shall now consider the very different kinds of algal distribution that are observed in coastal waters very low in colour. Taylor (1959) found in

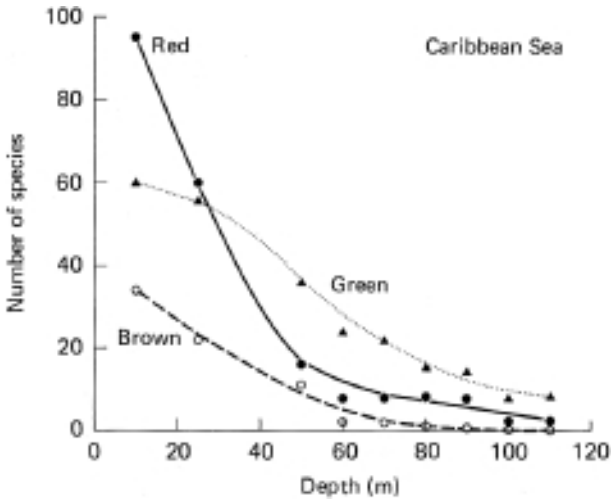


Fig. 12.3 Variation of taxonomic composition of benthic algal flora with depth in a tropical water. Plotted from data of Taylor (1959).

the Caribbean that while red, brown and green species were all well represented in shallow water there was a progressive decrease in species number in all three groups with depth (Fig. 12.3). Proportionately, this decrease was least for the green algae and in the lower 75% of the sublittoral zone there were more green species than either red or brown. Similar distributions have been observed in the Pacific. In Hawaiian coastal waters, green algal species, although overall less numerous, penetrated as deeply as red algal species, and more deeply than the brown.<sup>317</sup> In Eniwetok atoll lagoon, Gilmartin (1960) found that although the numbers of green and red algal species were comparable at depths down to 65 m (both greatly exceeding the number of brown species), the greens appeared (on the basis of visual observation) to be dominant in terms of biomass at all stations down to this depth, at which irradiance was 2 to 4% of that at the surface.

Algal distributions in the Mediterranean show some similarities. On a Corsican headland, Molinier (1960) found that green algae penetrated as deeply as 80 m, being replaced below this by red algae. A particularly valuable quantitative study, of the depth distribution of algal biomass on vertical rock faces off Malta, was carried out by Larkum, Drew and Crossett (1967). They measured the dry mass of algal biomass within the three taxonomic groups per unit area of the cliff face, as a function of depth: the results are shown in Fig. 12.4. Down to about 10 m depth

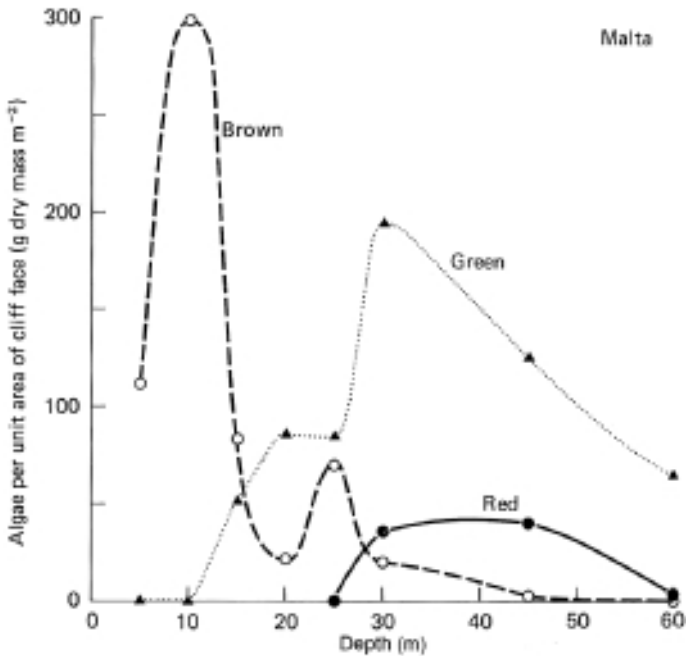


Fig. 12.4 Variation of biomass per unit area of cliff face of green, brown and red algae with depth on vertical rock faces in the Mediterranean Sea (Malta, 36° N). (Plotted from data of Crossett, Drew and Larkum, 1965.)

brown algae were dominant but their contribution to total biomass decreased sharply below this. Green algae became significant at about 15 m and were the major component of the community from 20 to 60 m (the lowest depth studied). Red algae became significant components only at 30 m and decreased again below 45 m, proportionately as well as in absolute terms.

Littler *et al.* (1985,1986) used a submersible to carry out a detailed survey of the depth distribution of algae on the San Salvador Seamount, the top of which forms a  $\sim 1 \text{ km}^2$  flat plateau about 80 m below the ocean surface, 6.5 km north of San Salvador Island (Bahamas). The plateau region and the sides of the seamount down to 90 m depth are dominated (% cover) by the brown alga *Lobophora variegata*, although a wide variety of green, brown and red algae are present. From 90 m down to about 130 m, green and red algae are present but green dominate, the community consisting mainly of four species of the calcareous genus *Halimeda*, especially *H. copiosa*. From 130 down to 189 m the assemblage is

dominated by a crustose red alga, *Peyssonelia*, but two frondose chlorophyte species are also abundant (at least above 157 m). From 189 down to 268 m the dominant species is a crustose coralline red alga, but upwards of 210 m small amounts of the green alga *Ostreobium* appear.

It is clear from these various studies that the most significant difference between the colourless and the slightly yellow coastal waters, so far as algal distribution is concerned, is the very much greater success of green algae in the former. This is just what would be expected on the basis of chromatic adaptation. As we have seen, the underwater light field in such waters becomes particularly rich in that blue waveband in which the green algae carry out most of their light harvesting. Except at the greatest depths there is a high proportion of green as well as blue light. Some species of green algae, in virtue of their containing the carotenoid siphonaxanthin (which when bound to protein in vivo absorbs in the 500–550 nm region), have an enhanced ability to absorb green light. Yokohama *et al.* (1977) and Yokohama (1981), in a survey of green algal species in Japanese waters, found that in three orders (Ulvales, Cladophorales and Siphonocladales) siphonaxanthin is present in deep-water species but absent from those growing in shallow water: a plausible example of chromatic adaptation. In certain other orders (Codiales, Derbesiales and Caulerpales) siphonaxanthin is present in all species, even in those from shallow waters: in the latter, Yokohama suggests that siphonaxanthin may be an evolutionary relic, from deep-water ancestors. Among 14 species of the marine Chaetophoraceae (Chlorophyta), O'Kelly (1982) found five with lutein (the most abundant higher plant/green algal xanthophyll) and no siphonaxanthin, four with siphonaxanthin and no lutein, and five with both. The species having just lutein were found only in the mid- to upper-intertidal habitats, those possessing only siphonaxanthin were confined to the subtidal region, while those containing both pigments occupied intermediate, wide-ranging habitats.

Direct experimental evidence supporting the chromatic adaptation theory has been obtained by Levring (1966, 1968). He measured the photosynthetic rates of samples of green, brown and red algae suspended in bottles at a series of depths in turbid nearshore water (highest transmittance in the green) off the Swedish and North Carolina coasts, and in clear oceanic water (transmittance highest in the blue) in the Gulf Stream. To compare the ways in which photosynthesis and irradiance varied with depth he used a parameter,  $q$ , which may be regarded as the ratio of the vertical attenuation coefficient for photosynthetic rate to the vertical attenuation coefficient for irradiance. If a particular type of alga becomes

increasingly ill-adapted to the spectral distribution of the light with increasing depth, then  $q$  will be greater than 1 (i.e. photosynthesis will decrease faster than irradiance); if the alga is better adapted to the spectral distribution found at great depth, then  $q$  will be less than 1. Below 10 m, for green algae,  $q$  was 1.2 to 1.3 in the turbid/coloured water and  $\sim 0.8$  in the colourless water, indicating that they were better adapted for photosynthesis at depth in the less-coloured water. In the case of red algae,  $q$  was  $\sim 0.8$  in the turbid/coloured water, indicating improved adaptation with depth, and  $\sim 1.0$  in the colourless water, indicating little change in adaptation with depth. For the brown alga, *Fucus*,  $q$  was  $\sim 1.0$  in the coloured/turbid water, but variable (above and below 1.0) in locations with colourless water.

In the case of phytoplankton also there is evidence for phylogenetic chromatic adaptation.<sup>1017,1225</sup> In stratified oligotrophic blue ocean waters, chlorophyll *b*, which is indicative of the presence of green chlorophytes and prochlorophytes, is concentrated near the bottom of the euphotic zone where the light is predominantly blue to blue-green. It is commonly found in these ocean regions that cyanobacteria, such as *Synechococcus*, occur mainly near the surface, their high levels of the photoprotective carotenoid, zeaxanthin, enabling them to tolerate the intense radiation. Prochlorophytes, such as *Prochlorococcus*, congregate mainly in the DCM, at the bottom of the euphotic zone, where the Soret band of their divinyl-chlorophyll *a* enables them to efficiently collect energy from the predominantly blue light field.<sup>237,1213,1412,72</sup> In near-surface, nitrate-rich waters, diatoms predominate: their major accessory pigment, fucoxanthin, efficiently harvests the green light that is abundantly present at these lesser depths. Hickman *et al.* (2009) observed striking vertical gradients in the phytoplankton taxa through the water column across a broad region of the seasonally stratified Celtic Sea. Pigment compositions and the phytoplankton absorption spectra indicated that the different phytoplankton communities were chromatically well adapted to the spectral composition of the light field at the depths where they occurred in the water column. At a mesotrophic and an oligotrophic site in the tropical North Atlantic, Lazzara *et al.* (1996) found, by comparing the spectral distribution of irradiance (500–530 nm and 470–490 nm, respectively) at the bottom of the euphotic zone, with the peaks in the fluorescence excitation curves, evidence for complementary chromatic adaptation in the phytoplankton community to the prevailing spectral irradiance. In the stratified Sargasso Sea, Bidigare *et al.* (1990), by comparing the absorption peaks of accessory

pigments with the spectral irradiance maxima, found evidence for chromatic adaptation of the phytoplankton.

Pick (1991) studied the distribution of different pigment types of picocyanobacteria in 38 lakes of varying optical and trophic status. Some cyanobacterial picoplankton strains contain only phycocyanin and allophycocyanin biliprotein pigments, with absorption peaks at  $\sim 620$  and  $650$  nm, respectively, while other strains also contain phycoerythrin, absorbing in the green at  $\sim 550$  nm. Pick found that as light attenuation among the lakes increased, a trend that would be accompanied by a shift in the underwater spectral distribution from the green towards the red, so the percentage of phycoerythrin-containing picocyanobacteria significantly decreased. In the stratified water of oligotrophic Lake Stechlin (Germany), Gervais *et al.* (1997) found a deep chlorophyll maximum at a depth of 10 to 15 m, where the prevailing light was confined almost exclusively to the 500 to 600 nm waveband. The DCM was dominated, apart from centric diatoms sedimenting through from above, by picocyanobacteria containing phycoerythrin, which absorbs strongly at these wavelengths.

### Evidence against chromatic adaptation

On the basis of the relation between water optical type and algal distribution outlined above, we would predict that in any clear, colourless coastal water, with maximum penetration in the blue waveband, green algae should be certainly a major, and probably a dominant, component of the algal biomass throughout much of the middle and lower sublittoral. The water bathing the coast of South Australia, in the region of the Great Australian Bight and the Gulf of St Vincent, is of a clear, colourless oceanic type: there is little river run-off in this dry region. We might thus expect the depth distribution of benthic algae to be similar to that described above for Caribbean, central Pacific or Mediterranean locations. In fact, a series of thorough studies by Shepherd and Womersley (1970, 1971, 1976), and Shepherd and Sprigg (1976) has shown this not to be so: the distribution is in reality much more similar to that found on northern European coasts, with the mid-sublittoral zone dominated by large brown algal species, giving way in the lower sublittoral to a dense cover of red algae. In calmer waters the brown algae dominate the upper sublittoral too, whereas on rough-water coasts they are replaced in this zone by a short turf of the (presumably) surge-resistant coralline red alga *Corallina*.<sup>1477</sup> In terms of biomass, green algae are generally a minor component of the algal community at all depths. At one site (Pearson

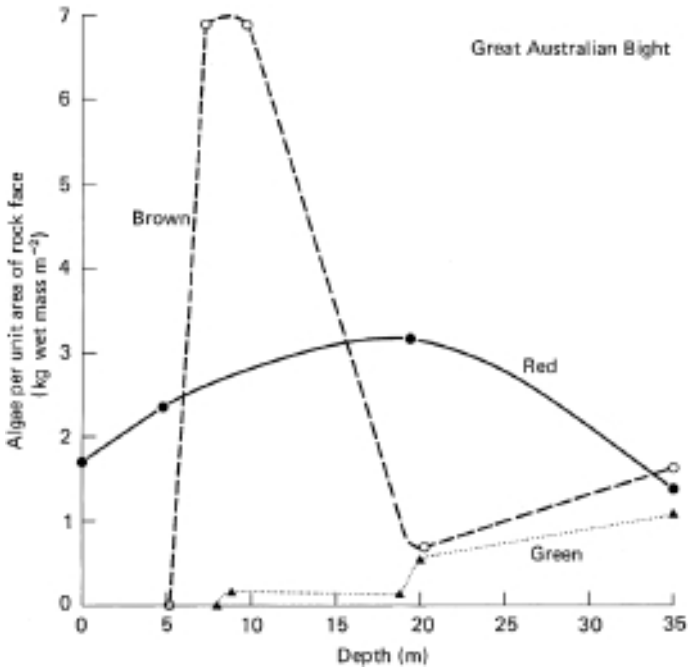


Fig. 12.5 Variation of biomass per unit area of rock face of green, brown and red algae with depth in a clear, colourless southern hemisphere temperate water (Pearson Island, Great Australian Bight, 34° S). Plotted from data of Shepherd and Womersley (1971).

Island, Great Australian Bight), however, where the water was particularly clear and colourless (oceanic water type IA), the Chlorophyta (mainly *Caulerpa* sp.) constituted a significant fraction of the community from 20 to 35 m (Fig. 12.5) but even here never attained the dominant position that green algae occupy in the underwater flora of Malta or Eniwetok atoll. The poor showing of the green algae in these waters cannot be explained on optical grounds.

An alternative possibility is temperature, an environmental parameter that is known to be a major determinant of seaweed geographical distribution. According to Lüning (1990), in his book on *Seaweeds: Their Environment, Biogeography and Ecophysiology*:

the worldwide distribution patterns of seaweeds are mainly determined by global temperature gradients. Deeply imprinted temperature demands, evolved to mirror the geological cycle of cooling and heating of the earth at higher latitudes, keep species of algae apart.

The South Australian waters are comparatively cool, attaining temperatures of 18 to 20°C at the surface in summer. The temperature of the surface water off Malta at the time of the study by Larkum *et al.* was about 27°C.<sup>267</sup> It may be that the siphonaxanthin-containing green algae, being perhaps mainly of tropical origin, require, as a group, higher temperatures for growth than the brown and red algae.

Our consideration of chromatic adaptation has so far been couched in qualitative terms: in terms, for example, of whether a particular pigment absorption band is located within or outside the predominant waveband of light penetrating to a given depth. Dring (1981) has attempted to carry out a quantitative test of the theory by calculating how the amount of photosynthesis per unit irradiance might be expected to change with depth in different kinds of algae in waters of various optical types. The calculations for each alga were carried out using a measured photosynthetic action spectrum for the alga and a series of spectral distributions of irradiance at increasing depth computed for a given water type using the spectral transmission data of Jerlov (1976). In effect, what is being calculated is the extent to which the matching of the active pigment composition to the spectral distribution of available light, i.e. chromatic adaptation, should result in increased or diminished efficiency of utilization of available light with increasing depth, and therefore increased or diminished competitive ability of one algal type compared to another. The results of such calculations can then be compared with observed algal depth distribution data to see if the predictions of the theory correspond to observation.

The findings are somewhat mixed. Some of the predictions accord reasonably well with observation. For example, for coastal waters types 3 and 9 (both of which would have sufficient yellow colour to cause rapid attenuation of the blue waveband) calculations predict that with increasing depth there should be a decrease in photosynthetic effectiveness of green algae such as *Ulva* sp., little change for kelp (brown algae) such as *Laminaria saccharina*, and an increase for red algal species having phycoerythrin as the main biliprotein. This fits in quite well with the algal distributions in such waters on northern European coasts where the maximum depths to which the algae penetrate are generally found to be in the order red > brown > green.

On the other hand, these calculations and earlier ones by Larkum *et al.* (1967) indicate that in colourless oceanic waters, at the deepest limits of algal growth, green algae and thin-bladed brown algae should perform as well as or better than the phycoerythrin-containing red algae. We have in

fact already noted that at least in warm oceanic waters green algae do indeed penetrate deeply and are sometimes dominant throughout most of the sublittoral zone. Nevertheless, at extreme depth in such waters they are eventually replaced by red algae. A problem with these calculations is that the validity of the results is highly dependent on the accuracy of the action spectrum attributed to the alga. Dring used action spectra data measured with just one wavelength at a time. As we saw in a previous chapter (§10.3), such action spectra can be misleading because some wavelengths of light when presented singly are incapable of exciting both photosystems to the same extent. The errors arising in this way are not great in the case of the green and brown algae but can be substantial in the case of the red algae in which photosystems I and II have rather different action spectra. If red algal action spectra are measured with supplementary green light (to ensure that photosystem II is always functioning) then substantially higher relative activity in the blue region is obtained.<sup>405</sup> It may be that if the calculations were carried out again with a corrected red algal action spectrum, the increased activity in the blue might be sufficient to give the red algae a significant advantage over the green algae in the blue-green light field at the bottom of the euphotic zone in oceanic water.

Another objection to the chromatic adaptation theory is based on the fact that if any particular pigment mixture, whether it be that of the green, the brown or the red algae, is raised to a high enough concentration per unit area of thallus, then there is eventually almost complete light absorption at all wavelengths and the algae become virtually black. Absorption by chlorophyll, for example, in the green waveband, although certainly low, is not infinitesimal and at high chlorophyll concentrations becomes substantial. A mature ivy leaf containing about  $60 \mu\text{g cm}^{-2}$  chlorophyll absorbs not only, as we might expect,  $\sim 100\%$  of the red light incident upon it, but also  $\sim 70\%$  of the green (550 nm) light it receives.<sup>722</sup> Ramus *et al.* (1976) argue that if a seaweed is optically thick as are, for example, *Codium fragile* (green) and *Chondrus crispus* (red), then it does not matter what colour it is, and they go on to conclude that the red algae are phylogenetically no better adapted to utilize the ambient light at great depth than are their green counterparts. That optically thick algae have roughly the same light-harvesting capacity (approaching 100% at all wavelengths) whatever the nature of their pigments is certainly true. What must be borne in mind, however, is that if an alga is faced with the problem of absorbing light from an ambient field that is rich in the green waveband, then it is much more efficient in terms of the biochemical

economy of the cell to achieve this with a pigment such as phycoerythrin, which has its absorption peaks in that waveband, than to do it with chlorophyll, which absorbs only weakly. The protein cost (remembering that chlorophyll has to be part of a pigment-protein) of achieving high absorption in the green with chlorophyll will be much greater than the protein cost of achieving it with phycoerythrin. It is true that within each of the three algal groups there are some species that have adopted the strategy of having a thick, deeply coloured, thallus and thus absorbing most of the incident light at all wavelengths, and it would be reasonable to say that algae in this category do not make use of chromatic adaptation: as Ramus *et al.* point out, it does not matter which set of pigments they contain. In most marine algal species, however, absorption is far from complete in parts of, or throughout, the spectrum, and so the degree to which their spectral absorption matches the spectral quality of the field is of great significance for the efficient utilization of the incident radiation.

### **Significance of phylogenetic chromatic adaptation**

The evidence taken together seems to me to lead to the conclusion that chromatic adaptation is a major factor influencing the depth distribution of the three types of benthic marine algae, but that it is not the only one, and in some instances other factors prevail. The fact that all algae that grow at depths where the light is predominantly green or blue-green have pigments, whether specialized carotenoids such as fucoxanthin or siphonaxanthin, or biliproteins such as R-phycoerythrin, which enhance their absorption in that spectral region, cannot in my view be plausibly regarded merely as coincidence. The algae evolved in the sea; this means that they evolved in an environment throughout most of the illuminated part of which, the light field had a predominantly blue-green character. Given the enormous importance of absorption spectra in determining the efficiency of collection of light energy, it is hard to believe that the types of pigment system that evolved would not be influenced by, and thus correspond to, the spectral character of the prevailing light. The argument that the specialized algal pigment systems are merely adaptations to low irradiance I do not find acceptable. That they are adaptations to limiting light levels seems unquestionable, but if the low-intensity light field has a markedly non-uniform distribution across the spectrum, then for efficient utilization of cellular resources it is better to make pigments whose absorption bands are well placed to harvest the dim light. It is in principle possible to achieve any required level of light collection at any depth

with, say, just the green pigment mixture found in surface-dwelling Chlorophyta provided the pigment concentration per unit area is made high enough: the fact that the algae have in the main not chosen that, biochemically expensive, form of adaptation to low irradiance, but have evolved pigments absorbing in the spectral regions where the light actually occurs, indicates that they are adapted not just to low light, but to low light of a particular spectral character.

Thus, the predominance of red algae in the deepest part of the euphotic zone can be plausibly attributed to their possession of phycoerythrin – the most efficient way (in terms of quanta collected per unit of protein invested) of harvesting the dim blue-green light prevailing at those depths. The failure of green algal species lacking siphonaxanthin to penetrate to great depths we may consider to be a consequence of their comparatively poor absorption capacity for the prevailing underwater light field. The greater depth distribution of the siphonaxanthin-containing green species, and the brown algae, we may reasonably regard as being due to the enhanced capacity for absorption in the plentiful 500 to 550 nm waveband, conferred by their specialized carotenoids.

Chromatic adaptation is not, of course, the whole story. We noted early on that there is no reason why it should have anything to do with the relative success of the different algal groups near the surface. The presence of non-siphonaxanthin green species near the surface is not an example of chromatic adaptation, but their failure to penetrate the depths is such an example. The predominance of coralline reds near the surface in rough-water locations in South Australia has everything to do with their resistance to wave movement and nothing to do with their pigment composition. The presence of significant levels of green algae in the 20 to 35 m zone in the clear water of Pearson Island, South Australia (Fig. 12.5), we may regard as an example of chromatic adaptation, but their much poorer performance overall in South Australian than in the optically similar Mediterranean or central Pacific waters indicates that other factors such as, perhaps, temperature can prevail over chromatic adaptation in determining algal depth distribution. Within the deep-water red-alga zone, the transition at the lowest depths from fleshy macroscopic red algae to encrusting coralline red algae<sup>1202</sup> has no obvious explanation in terms of pigment differences. In the very dim light available at those depths, production rates can only be very low, in which case the rates of loss by grazing and respiration become very important. It may be that the encrusting coralline reds are less susceptible to grazing than the fleshy species and/or have a lower respiration rate. The predominance of

seagrasses on sandy bottoms down to great depths in clear colourless water, e.g. to 35 m in the St Vincent Gulf, South Australia<sup>1206</sup> or 50 m in the Red Sea,<sup>814</sup> is not due to their being chromatically better adapted than algae (although they should be reasonably well adapted to the bluish light prevailing in such habitats) but to their ability, by means of their roots and rhizomes, to colonize these unstable substrates.

In short, phylogenetic chromatic adaptation is by no means the only factor responsible for the depth distribution of the different plant groups under water: we should, however, continue to regard it as one important factor in that set of interacting factors that finally determines that distribution.

## 12.2 Ontogenetic adaptation – intensity

Adaptation of the photosynthetic apparatus to changes in light quality (intensity and/or spectral distribution) within a given species can take the form of changes in the total amount of pigment per cell or in the ratio of different pigments, or both.

### Chlorophylls and other pigments

It is generally found (with a few exceptions) among the algae, both unicellular and multicellular, that as the light intensity during growth decreases (even without alteration of spectral composition), the content of their photosynthetic pigments increases: two- to five-fold increases are commonly observed. Many studies of this have now been carried out, in a wide taxonomic range of algal species: reviews may be found in Richardson, Beardall and Raven (1983), and Falkowski and LaRoche (1991). A convenient parameter in terms of which to express this phenomenon is the carbon:chlorophyll *a* ratio of the cells (C:chl *a*). On the basis of an analysis of literature data for eight diatoms, two green algae, one euglenid and two cyanobacteria, Geider (1987) concluded that C:chl *a* increases linearly (i.e. decreasing pigment content) with increased light level at constant temperature, but decreased exponentially (i.e. increasing pigment) with increased temperature at constant light level.

Accessory photosynthetic pigments also increase as the growth light intensity is decreased, and indeed generally do so to a greater extent than chlorophyll *a*.<sup>326</sup> In the higher plants and green algae, the ratio of chlorophyll *b* to *a* increases with diminishing light intensity. For example in the

green flagellate *Dunaliella tertiolecta*, simultaneously with a 2.6-fold rise in chlorophyll *a* content, the *a/b* ratio fell from 5.6 to 2.3 when the growth irradiance was reduced from 400 to 20  $\mu\text{mol photons m}^{-2} \text{s}^{-1}$ .<sup>382</sup> In the marine dinoflagellate *Glenodinium*, as the light intensity during growth was lowered over the range 30 to 2.5  $\text{W m}^{-2}$ , the chlorophyll *a* content per cell rose progressively, by about 80%, but the cellular concentration of the light-harvesting peridinin/chl *a* protein rose seven-fold.<sup>1080</sup> It has been shown with cultures of the cryptomonads *Chroomonas*<sup>387</sup> and *Cryptomonas*,<sup>1351</sup> the cyanobacteria *Anacystis*,<sup>1413</sup> *Oscillatoria*<sup>409</sup> and *Synechococcus*,<sup>674</sup> the unicellular rhodophyte *Porphyridium*<sup>169,313,799</sup> and the red macro alga *Griffithsia*<sup>1425</sup> that the ratio of biliprotein pigment to chlorophyll *a* increases with diminishing light intensity: the increases can be several-fold.

Corresponding changes have been observed in the field. In plants of *Chondrus crispus* growing in sunlit sites at 3 to 4 m depth, the ratio of phycoerythrin to chlorophyll remained high during the winter but underwent a 60% fall in late spring/early summer: in plants in shaded sites at the same depth the ratio remained high during the summer.<sup>1122</sup> When the sunlit plants became shaded due to a dense growth of an epiphytic diatom in August they regained much of their phycoerythrin. In the sublittoral red alga *Gracilaria compressa*, in the Adriatic Sea, the distal portions of the fronds, which received direct illumination, were yellow-green in colour and contained 0.065% (dry mass) chlorophyll and only traces of phycoerythrin. The proximal portions, which were shaded, were purplish-red, and contained 0.085% chlorophyll and 0.82% phycoerythrin.<sup>195</sup> In littoral algal turf communities, there are marked changes in average ambient light exposure within short distances along the thalli, and these are accompanied by marked differences in photosynthetic pigment composition. In the case of two such turf species in the Hawaiian islands, *Ahnfeltiopsis concinna* and *Laurencia mcdermidiae*, Beach and Smith (1996) observed striking pigment alterations within the <10 cm lengths of individual thalli: tissue in the understory region of the turf was red to purple-black in both species, whereas the canopy (exposed) tissue was yellow-orange in *A. concinna* and green in *L. mcdermidiae*. The canopy tissue had lower levels of biliprotein, but increased concentrations of carotenoid and UV-absorbing compounds.

In a brackish eutrophic lake, Veerse Meer, in the Netherlands, a thick mat, consisting of five to seven layers of the green macroalga, *Ulva* spp., forms each year. With increasing depth (diminishing light) within the mat, the layers were found to have increasing absorbance at all wavelengths

over the 400 to 700 nm range, attributable to increases in the concentrations of chlorophylls *a* and *b*, and lutein.<sup>860</sup> In dense stands of the tropical seagrass, *Thalassia testudinum*, in the Mexican Caribbean, Enriquez *et al.* (2002) found that photosynthetic pigment content and leaf absorbance decreased from the basal (more shaded) to the apical (more exposed) regions of the leaves.

An apparent exception to the rule that accessory pigments increase more than chlorophyll *a* as growth light levels decrease is fucoxanthin. In the brown algae *Sphacelaria* and *Laminaria*, and in the diatoms *Nitzschia* and *Phaeodactylum*, fucoxanthin was observed to increase somewhat less than chlorophyll *a* as light intensity diminished.<sup>174,325,1214</sup>

The radiant intensity in full sunlight is so high that, quite apart from causing photoinhibition, it can be quite lethal, in part because of the inability of some plants safely to handle the very high rates of energy absorption by chlorophyll and other pigments, resulting in photo-oxidation of cell material. Carotenoids, however, can as discussed earlier (§10.1) in various ways exert a protective effect against such photo-oxidation,<sup>240</sup> and another adaptive response of algae to high light intensity is, as well as reducing the levels of photosynthetic light-harvesting pigments in the manner we have discussed, to increase the cellular concentration of photoprotective carotenoids. The halophilic unicellular chlorophyte *Dunaliella salina*, which occurs in salt ponds, when grown in full sunlight makes so much photoprotective  $\beta$ -carotene that the cells turn red. This extra  $\beta$ -carotene is not coupled in to the photosynthetic system, and in fact simply acts as a colour filter, with the consequence that the cells show greatly diminished photosynthetic activity in the blue spectral region.<sup>823</sup> In *Dunaliella bardawil*, which also accumulates  $\beta$ -carotene in high light, the pigment is concentrated in oily globules in the interthylakoid spaces of the chloroplast: the  $\beta$ -carotene protects the alga against the photoinhibitory effects of blue light (which it absorbs), but not against the effects of intense red light.<sup>96</sup> Some unicellular algal species, such as those that can give a red tinge to the surface of snow in high mountains, accumulate photoprotective carotenoids outside the chloroplast: these are referred to as *secondary carotenoids*. *Haematococcus lacustris*, an alga of shallow freshwater bodies, accumulates globules of secondary carotenoids, mainly astaxanthin, around the periphery of the cell, when exposed to high light intensities.<sup>518</sup>

Paerl, Tucker and Bland (1983) found that the ratio of carotenoid to chlorophyll in surface blooms of the blue-green alga *Microcystis aeruginosa* rose progressively during the summer, to a high value, and

attributed this to the carotenoids having a protective role. The carotenoid that reached the highest concentration was zeaxanthin, a xanthophyll, which is in fact now thought to exert an important photoprotective function in plants generally, but by mechanisms other than simple interception of the light.<sup>230</sup> In the marine cyanobacterium *Synechococcus*, Kana *et al.* (1988) found that as the light intensity during growth varied from 30 to 2000  $\mu\text{mol photons m}^{-2}\text{s}^{-1}$ , so the cellular content of  $\beta$ -carotene and chlorophyll *a* diminished several-fold in parallel, but the zeaxanthin concentration remained the same. These authors suggested that in this case  $\beta$ -carotene is entirely part of the photosynthetic system, whereas zeaxanthin by contrast has a wholly photoprotective function.

We have discussed earlier (§10.2) the role of the mycosporine-like amino acids in protecting some algae against the damaging effects of the UV component of solar radiation. In an Arctic fjord (Spitsbergen, Norway) Aguilera *et al.* (2002) found that coinciding with the increase in underwater radiation during the sea-ice break-up in June, there was, in two red algal species – *Palmaria palmata* and *Devaleraea ramentacea* – an increase in the concentration of MAAs, in addition to a decrease in the photosynthetic accessory pigments, phycocyanin and phycoerythrin.

### Photosynthetic units

The increases in photosynthetic pigment content that occur in algae as the light intensity at which they are grown is lowered can be due to an increase (per cell, or per unit biomass) in the number of photosynthetic units, or in the average size (as absorption cross-section) of the photosynthetic unit, or both.<sup>381</sup> In most green plants – the algae as well as the angiosperms – it appears that the increase in chlorophyll content during shade adaptation is largely due to an increase in the number of photosynthetic units. This has been shown for higher plants,<sup>128</sup> for the unicellular chlorophytes *Scenedesmus obliquus*<sup>400</sup> and *Dunaliella tertiolecta*,<sup>383</sup> and for the multicellular green species *Ulva lactuca*.<sup>910</sup> In *Chlorella pyrenoidosa* the five-fold increase in chlorophyll during shade adaptation was mainly due to an increased number of photosynthetic units, but there was also a 50% increase in the number of chlorophyll molecules per unit.<sup>971</sup> In *Chlamydomonas reinhardtii*, Neale and Melis (1986) found an actual change in the proportion of photosystem I and photosystem II reaction centres as light intensity during growth was altered. The high-light cells, with half the chlorophyll content of the low-light cells, contained slightly less than half as many photosystem

I centres, but almost as many photosystem II centres, as the low-light cells. The photosystem II/photosystem I ratio shifted from near unity in the low-light cells to greater than two in high-light cells.

In the diatoms *Skeletonema costatum*<sup>383</sup> and *Chaetoceros danicus*<sup>1049</sup> it appears that the increase in cellular chlorophyll during shade adaptation is mainly due to an increase in the number of chlorophyll *a* molecules per photosynthetic unit, and the same appears to be true of the chrysophyte, *Isochrysis galbana*.<sup>1049</sup> The diatom *Phaeodactylum tricoratum*, on the other hand, responds to low light by increasing the number of photosynthetic units per cell, without increasing the unit size.<sup>413</sup>

In the marine dinoflagellate, *Glenodinium*, it does seem likely that the great increase (seven-fold) in the cellular level of the peridinin-chlorophyll *a* protein resulting from a 12-fold decrease in growth irradiance,<sup>1080</sup> especially when compared with the comparatively modest increase in chlorophyll (80%), is associated with a substantial increase in the number of these pigment-protein molecules per photosynthetic unit. Shade adaptation in the symbiotic dinoflagellates (zooxanthellae) of coral is seemingly due to an increase in the size, but not the number, of photosynthetic units per cell.<sup>378,380</sup> In the estuarine dinoflagellate *Prorocentrum mariae-lebouriae*, however, shade adaptation appears to involve increases in both the size and the number of photosynthetic units.<sup>250</sup>

In the unicellular red alga *Porphyridium cruentum*, Levy and Gantt (1988) found that acclimation to low light intensity was accompanied by slightly more than a doubling of biliprotein content, but little change in the amount of chlorophyll or number of photosynthetic units. They concluded that adaptation of this alga to varying light levels involved changes in size of the photosystem II antenna, with little effect on photosystem I. In cases such as *Gracilaria* in the Adriatic Sea referred to above, where shading of macrophytic red algae brings about massive increases in phycoerythrin content, this must be accompanied by increases in the average light-harvesting capacity of the photosynthetic unit. The same is probably true in low-light-grown cultures of the cryptophyte *Cryptomonas*, which show a six-fold increase in phycoerythrin (relative to high-light cultures) compared with only two-fold increases in chlorophylls *a* and *c*.<sup>1351</sup>

Shade adaptation in the cyanobacterium *Anacystis nidulans*, comparing cells grown at  $10 \mu\text{mol photons m}^{-2} \text{s}^{-1}$  to those grown at  $100 \mu\text{mol photons m}^{-2} \text{s}^{-1}$ , was accompanied by a doubling in the number of photosynthetic units per cell, but with no change in the number of chlorophyll molecules per photosynthetic unit: the number of phycocyanin molecules

per cell, however, tripled.<sup>1413</sup> In cultures of the very common bloom-forming cyanobacterium *Microcystis aeruginosa*, shade adaptation led to a 2½-fold increase in the number of photosynthetic units per cell but with little change in the number of chlorophyll molecules per unit.<sup>1107</sup> Raps *et al.* (1985) found the low-light (40  $\mu\text{mol photons m}^{-2} \text{s}^{-1}$ ) cells to have a 2.6-fold greater concentration of phycobilisomes than the high-light (270  $\mu\text{mol photons m}^{-2} \text{s}^{-1}$ ) cells: phycobilisome structure and composition (phycocyanin/allophycocyanin) were the same at both light intensities. In contrast, with a marine *Synechococcus* strain, Kana and Glibert (1987a) found considerable changes in phycobilisome composition as growth irradiance varied. Between 700 and 30  $\mu\text{mol photons m}^{-2} \text{s}^{-1}$ , the phycoerythrin/phycocyanin ratio rose from 3 to 14. The phycoerythrin content of the cells increased 20-fold over this range, while chlorophyll content only doubled, suggesting a major increase in the average absorption cross-section of the photosynthetic units.

### Changes in electron carriers and carboxylase

In higher plant species that are able to adapt to low light conditions, the increase in pigment during shade adaptation is not accompanied by an increase in the content of the photosynthetic electron transfer components – the cytochromes, ferredoxin and plastoquinone. The levels of these per unit mass may remain about the same or may decrease somewhat.<sup>128,1467</sup> The level per unit mass of leaf is markedly lowered in shade-adapted plants.<sup>895</sup> These changes are of adaptive value since at low light intensities the plant will not be able to carry out high rates of electron transfer and carboxylation anyway and so can achieve biosynthetic economies by refraining from increasing, or preferably decreasing, its content of electron transfer components and carboxylase at the same time as it increases its pigment content and photosynthetic unit number. Thus, in shade-adapted higher plants there is an increase in the ratio of pigment assemblies to the pools of electron carriers, and an even bigger increase in the ratio of pigment assemblies to carboxylase.

The same sort of changes have been shown to accompany shade adaptation in some unicellular algae. In the chlorophyte *Scenedesmus obliquus*, while the chlorophyll content per g fresh weight increased by 64% (in the low-light-grown, relative to the high-light-grown cells), the cytochrome *f* content decreased by 33%, and the carboxylase activity also decreased.<sup>400,1203</sup> In shade-adapting *Chlamydomonas reinhardtii*, while the cellular chlorophyll content doubled, the cytochrome *f* level remained

about the same.<sup>979</sup> In another chlorophyte, *Tetraedron minimum*, reduction of growth irradiance from 500 to 50  $\mu\text{mol photons m}^{-2}\text{s}^{-1}$  led to a five-fold increase in cellular chlorophyll and photosynthetic unit number, but the amount of Rubisco per cell remained the same.<sup>398</sup> In partial contrast to some of the above observations, in the marine chlorophyte *Dunaliella tertiolecta*, the cellular cytochrome *f* concentration increased several-fold in parallel with chlorophyll and photosynthetic unit number during shade adaptation, but in this case also Rubisco content per cell remained about the same.<sup>1322</sup> In the marine diatom *Phaeodactylum tricorutum*, grown in continuous culture, while the chlorophyll and carotenoid content rose progressively by about 100% as light intensity was lowered from 12 to 0.5 klux, the Rubisco activity per cell fell to less than 25% of the value present in high-light-grown cells.<sup>82</sup> Thus, in algae the preferred strategy for coping with low light levels appears to be an increase in the number or size (or both) of the pigment assemblies (photosynthetic units) with no increase, or an actual decrease, in the synthesis of carboxylase.

Lin and Carpenter (1997) used epifluorescence microscopy of immunofluorescent-stained cells to study the distribution of Rubisco within the chloroplast of the chlorophyte *Dunaliella tertiolecta*, as a function of light intensity during growth. Over a seven-fold range of intensity the fraction of the cell population that displayed distinct Rubisco staining in the pyrenoid was positively correlated with irradiance. Lin and Carpenter propose that *D. tertiolecta* possesses an adaptive mechanism that brings about the redistribution of Rubisco between the pyrenoid – the probable site of Rubisco activation and  $\text{CO}_2$  fixation – and the stroma (which putatively acts as a reservoir of the enzyme in its inactive form) in response to change in light intensity.

### Photosynthetic consequences of light/shade adaptation

The physiological consequences of these biochemical changes are manifested as changes in the dependence of photosynthetic performance on light intensity. If photosynthetic rate per unit chlorophyll is measured as a function of irradiance then it is in some cases found that rates exhibited by low- and high-light-adapted cells or tissues are much the same at low irradiance, but the low-light-adapted plants level off and reach light saturation first. It is generally the case that high-light-adapted cells require a higher light intensity to reach saturation and achieve a higher light-saturated photosynthetic rate, as is shown for *S. obliquus* in

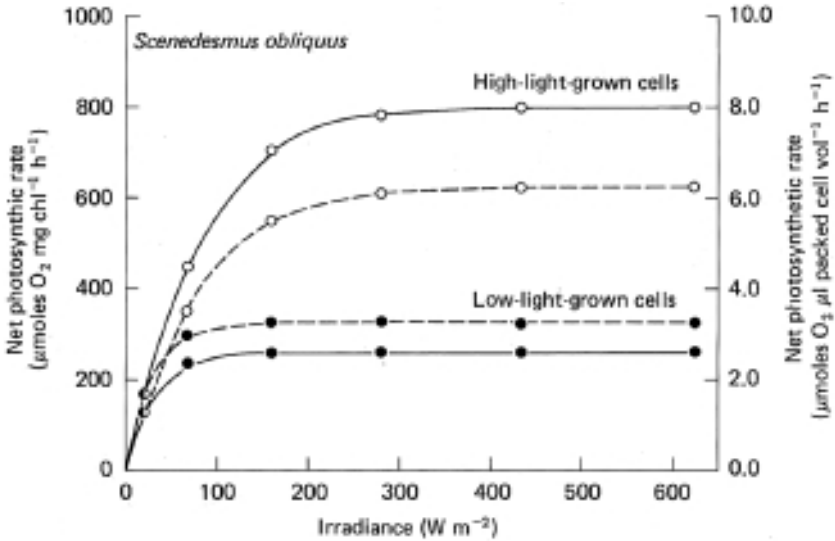


Fig. 12.6 Photosynthetic characteristics ( $P$  versus  $E_d$ ) of cells of *Scenedesmus obliquus* (Chlorophyceae) grown under high (○) or low (●) light intensity. The specific photosynthetic rate is expressed either per mg chlorophyll (—) or per unit cellular biomass (packed cell volume, -----). The cells were grown in continuous culture under high ( $28 \text{ W m}^{-2}$ ) or low ( $5 \text{ W m}^{-2}$ ) irradiance, and contained  $7.8$  and  $12.8 \text{ mg chlorophyll ml}^{-1}$  packed cell volume, respectively. Plotted from data of Senger and Fleischhacker (1978).

Fig. 12.6: the  $E_k$  values were about  $40$  and  $110 \text{ W m}^{-2}$  for the low- and high-light-adapted cells, respectively, in this green alga. Comparable increases in  $E_c$  during high-light adaptation have been observed in a wide range of algal types.

In the case of *S. obliquus*, the high-light-adapted cells also achieve a higher light-saturated photosynthetic rate per unit of cellular biomass (packed cell volume), presumably reflecting the higher cellular content of electron transfer components and carboxylase. This is not observed in all species. In some, such as the dinoflagellate *Glenodinium*,<sup>1080</sup> and the chlorophyte, *Chlamydomonas reinhardtii*,<sup>979</sup> the high-light-adapted forms achieve a higher light-saturated rate per mg chlorophyll but only about the same light-saturated rate per unit cellular biomass as the low-light-adapted forms. It seems likely that in such species the carboxylase content does not change during light adaptation.

We have noted that both high- and low-light-adapted forms of *S. obliquus* and certain other algae have about the same photosynthetic rate per mg chlorophyll at low light intensities: the  $P$  versus  $E_d$  curve has

about the same slope for both types of cells in the light-limited region. This is because at such intensities, electron transfer and carboxylation capacity are present in excess. Photosynthetic rate is determined entirely by the rate of photon capture, and so is determined by the amount of pigment present. Strictly speaking, it is the rate of photosynthesis per unit absorbance rather than per unit chlorophyll that we would expect to be the same for both types of cell in low light, and the ratio of absorbance to chlorophyll can change. The slope,  $\alpha$ , of the  $P$  versus  $E_d$  curve in the light-limited region is equal to  $\bar{\alpha}_\phi^* \phi_m$  where  $\bar{\alpha}_\phi^*$  is the specific absorption coefficient (per mg chlorophyll) for PAR, and  $\phi_m$  is the maximum quantum yield for the algal cells (§10.2). We do not expect  $\phi_m$  to change during shade adaptation; however, we saw earlier (§9.5) that  $\bar{\alpha}_\phi^*$  is a function of the intracellular pigment concentration as well as of cell size and shape. The more concentrated the pigments within the cell, the less efficiently they collect light, and so the lower the value of  $\bar{\alpha}_\phi^*$ . Thus the increase in pigment content that takes place during shade adaptation is likely (assuming no change in the ratio of pigments present) to lead to some reduction in  $\bar{\alpha}_\phi^*$  and therefore in  $\alpha$ : moderate decreases (7–34%) in  $\alpha$  have in fact been observed in certain diatom species during shade adaptation.<sup>1049</sup> In an alga in which there was a substantial increase in the ratio of some other light-harvesting pigment to chlorophyll during shade adaptation, and therefore a diminution in the proportionate contribution of chlorophyll to light absorption, we might expect the shade-adapted cells to show a higher rate of photosynthesis per unit chlorophyll at low irradiance than cells grown at high light intensity. Such an effect is in fact found in, for example, those cyanobacterial and red algal species that increase their biliprotein/chlorophyll ratio during shade adaptation.<sup>408,409,1107,675,799</sup>

When shade-adapted cells achieve about the same photosynthetic rate per unit pigment at low irradiance as high-light-grown cells, but contain more pigment per unit cellular biomass, they consequently have a higher photosynthetic rate per unit biomass than the high-light-grown cells under these conditions. This can be seen for *Scenedesmus obliquus* in Fig. 12.6. The difference becomes more pronounced in accordance with the extent to which pigment content increases and is particularly marked, for example, in the case of *Chlorella vulgaris*.<sup>1297</sup> It is at these low light intensities, when the supply of excitation energy is the limiting factor, that the higher concentrations of light-harvesting pigment within the low-light-grown cells gives them the advantage over the high-light-grown cells.

### Shade adaptation in aquatic angiosperms

All the adaptive changes we have considered so far are in the biochemical composition and consequent functioning of the photosynthetic apparatus. There are also other forms of ontogenetic adaptation, particularly in multicellular species, which can enable plants to cope with variation in the intensity of the light field. In higher plants, both aquatic and terrestrial, adapting to shade, at the same time as chlorophyll content (% of dry mass) increases, the leaves increase in area so as to intercept more light and also become thinner. Because of the increase in specific leaf area (area per unit dry mass of leaf), the chlorophyll content per unit area increases less than content per unit mass during shade adaptation, or may remain the same, or may decrease. Chlorophyll content (per g fresh weight) has been shown to increase not only with shade, but also with growth temperature, in certain submersed freshwater angiosperm species.<sup>71</sup>

Spence and Chrystal (1970) studied light-intensity adaptation in certain species of the freshwater angiosperm genus *Potamogeton* from Scottish lochs. In *P. polygonifolius*, a shallow-water species (occurring from the waters edge to 0.6 m depth), shade plants (grown at 6% of full sunlight) had a specific leaf area three times that of plants grown in full sunlight: the shaded leaves were 0.04 mm and the sunlit leaves 0.12 mm thick. The chlorophyll content in the shaded leaves was about one third higher than that in the sunlit leaves on a dry mass basis. Because of the great increase in area, however, the shade leaves contained only about half as much chlorophyll per unit area as the sunlit leaves. The dark-respiration rate per unit area was 27% lower in the shaded leaves – a greater reduction might have been expected given that leaf thickness was reduced by two thirds. Presumably as a consequence of the diminution in respiration rate, the light compensation point in the shaded leaves was lowered by about the same amount.

*Potamogeton obtusifolius*, a deeper water species (depth range 0.5–3.0 m) appeared to lack the ability to change its specific leaf area in accordance with light intensity, there being little difference in this respect between plants grown at 100% and 6% of full sunlight. There was also little change in the chlorophyll content per unit mass or leaf area. However, the specific leaf area of *P. obtusifolius* ( $\sim 2 \text{ cm}^2 \text{ mg}^{-1}$ ) is already greater than that of *P. polygonifolius* (sunlit leaves,  $0.48 \text{ cm}^2 \text{ mg}^{-1}$ , shaded leaves,  $1.43 \text{ cm}^2 \text{ mg}^{-1}$ ), and so we may suppose that *P. obtusifolius* has already taken this step during evolution, as part of its phylogenetic adaptation to the deeper water, and it may be that further increases in specific leaf area

would not be possible. The respiration rate of *P. obtusifolius* per unit area of leaf was, even in the sunlit leaves, as low as one third, and the light compensation point about half that of the shaded leaves of *P. polygonifolius*, further evidence for the superior phylogenetic adaptation of *P. obtusifolius* to low light. This species still retained some capacity for ontogenetic adaptation, however, since its shaded leaves had a very much lower respiration rate than its sunlit leaves, so much so that its light compensation point was reduced by  $\sim 90\%$ .

The submersed macrophyte *Potamogeton perfoliatus*, a species inhabiting turbid, brackish tidal waters in Chesapeake Bay, responds to a diminution in ambient light by increasing its chlorophyll concentration. Goldsborough and Kemp (1988) found that in plants transferred to a light intensity 11% of ambient, Chl *a*  $\text{cm}^{-2}$  leaf area increased by 20% in 3 days and 50% after 17 days; on returning the plants to normal light intensities, chlorophyll content reverted to normal in about 3 days. The increased pigment content led to a marked increase in the photosynthetic rate per g dry weight of shoot at low light intensity, with a consequent reduction in the light compensation point:  $P_{\text{max}}$  in saturating light did not change during the shade treatment. Shading was accompanied by very marked stem elongation, as well as an increase in specific leaf area.

While *P. perfoliatus* seems to have the capacity to adapt to a reduction in available light, many submersed macrophytes cannot cope so well. Seagrasses, for example, which typically occur in clear, relatively colourless waters, are particularly sensitive to increased turbidity in the water, resulting from human activity such as dredging or effluent disposal.<sup>894,988</sup>

### 12.3 Ontogenetic adaptation – spectral quality

Within the underwater environment the spectral composition of the light varies greatly, both with depth within a given water body and from one water body to another, in accordance with the absorption spectrum of the water. As we saw in the previous section, laboratory studies show that variation in intensity alone can bring about marked changes in pigment composition, photosynthetic characteristics and morphology of aquatic plants. Laboratory studies have also shown that intensity is not the whole story and that the spectral quality of the incident light has, for some plants, a specific role to play.

### Chromatic adaptation within the blue-green algae

The most clear-cut examples are to be found among the blue-green algae (Cyanobacteria), and it was indeed in a blue-green algal species that ontogenetic chromatic adaptation was first described. Gaidukov (1902) observed that *Oscillatoria rubescens* was red in colour when grown in green light, and blue-green when grown in orange light: he attributed these colour changes to the synthesis of different kinds of pigment. Boresch (1921) showed that the colour changes are due to shifts in the types of biliproteins synthesized by the algae: the red cells contain predominantly phycoerythrin, the blue-green cells mainly phycocyanin. This phenomenon was considered by Engelmann and Gaidukov (1902) to be an example of *complementary chromatic adaptation*, the pigment induced by a specific waveband being one which absorbs that waveband (phycoerythrin and phycocyanin have their absorption peaks in the green ( $\sim 565$  nm) and the red ( $\sim 620$  nm), respectively): 'complementary' because the pigment has the complementary colour to that of the light that induces it.

Not all blue-green algal species show chromatic adaptation, and among those that do there are variations in the form that adaptation takes. Tandeau de Marsac (1977) separated cyanobacteria into three groups. In group I strains the biliprotein composition is not affected by the spectral quality of the light in which they are grown, i.e. they lack chromatic adaptation. In group II strains, only the phycoerythrin content of the cells is affected by light quality, being very low in red light and high in green light; phycocyanin content remains high in cells grown under either kind of light. In group III strains, the synthesis of both the major biliproteins is affected by the spectral composition of the light: like the previous group their phycoerythrin content is high in green light and low in red, but their phycocyanin content, while still substantial in green light, is 1.6- to 3.7-fold higher in red light. Of 69 strains examined, 25 were in group I, 13 in group II and 31 in group III.<sup>176,1344</sup>

The phycocyanin formed in group I and group II strains has two polypeptide subunits,  $\alpha$  and  $\beta$ . Bryant (1981) found that in 24 of the 31 group III strains, the phycocyanin formed in green light also contained just two subunits, but the phycocyanin from cells grown in red light contained four subunits,  $\alpha_1$ ,  $\alpha_2$ ,  $\beta_1$  and  $\beta_2$ . The particular subunits present in phycocyanin in the green-light-grown cells were  $\alpha_2$  and  $\beta_1$ . These, being always present, Bryant referred to as constitutive: the other two,  $\alpha_1$  and  $\beta_2$ , formed in red light, he referred to as inducible. Thus, in these 24 strains it

appeared that the increased phycocyanin formation induced in red light consisted of synthesis of different kinds of phycocyanin subunit. It was not possible to determine from the data whether the new phycocyanin subunits associated to form a distinct phycocyanin species,  $(\alpha_1\beta_2)_n$ , or whether they aggregated with the two constitutive subunits,  $\alpha_2$  and  $\beta_1$ , to form a hybrid phycocyanin. In the remaining seven group III strains, no  $\alpha_1$  and  $\beta_2$  phycocyanin subunits were found in red-light-grown cells: the extra phycocyanin in these cases may have consisted just of additional  $\alpha_2$  and  $\beta_1$  subunits. In *Tolypothrix tenuis*, Ohki *et al.* (1985) found that chromatic adaptation in green light resulted in a one for one substitution of phycoerythrin for phycocyanin, so that phycobilisome size remained constant.

Ohki and Fujita (1992) found that cells of the marine cyanophyte *Phormidium* sp. C86 were coloured dark green when grown in red light, and purple-red when grown in green light, this change in colour being due to a massive increase in the cellular content of phycoerythrin. The biliprotein composition (molar basis) in red light was 13% phycoerythrin, 64% phycocyanin and 22% allophycocyanin. In green light this changed to 82%, 10% and 8%, respectively. The phycobilisomes in cells grown in green light were twice as large as those in red-light-grown cells.

The specific nature of the light treatments required to bring about changes in biliprotein composition have been studied in one of the group III strains, *Calothrix* 7101 (formerly *Tolypothrix tenuis*), by Fujita and Hattori (1960, 1962a, b), and Diakoff and Scheibe (1973). It has been found convenient to study the controlling influence of light in *Calothrix* 7101 by first depleting the cells of biliproteins by exposure to intense light for 24 h in the absence of nitrogen, then giving a brief light treatment of the desired spectral quality, and then placing the cells in the dark with a nitrogen source, and following biliprotein synthesis. After a saturating dose of red light the cells synthesize phycocyanin but not phycoerythrin during the subsequent dark incubation: after a saturating dose of green light they continue to make phycocyanin but now also make phycoerythrin. If red and green light treatments are given alternately, the subsequent pattern of biliprotein synthesis is determined by the colour of the last light treatment, i.e. green or red light will each reverse the effect of the other.<sup>423</sup>

The action spectrum for the promotion of phycoerythrin synthesis has a peak in the green at about 550 nm with an additional small peak in the UV at about 350 nm (Fig. 12.7): the action spectrum for inhibition of phycoerythrin synthesis has a peak in the red at about 660 nm, and also

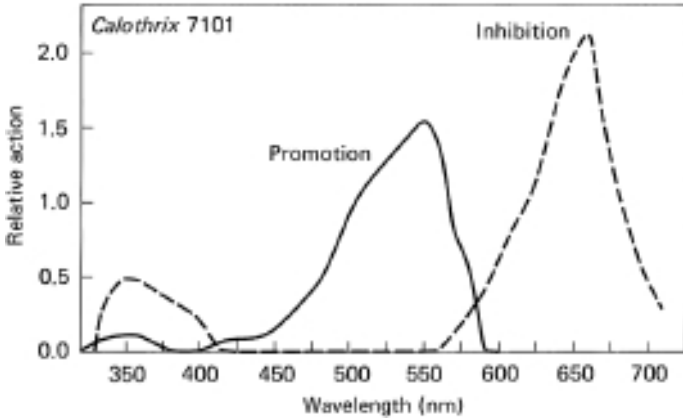
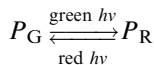


Fig. 12.7 Action spectra for the promotion and inhibition of phycoerythrin synthesis in the blue-green alga *Calothrix* 7101 (*Tolypothrix tenuis*) (after Diakoff and Scheibe, 1973). The reciprocal of the amount of radiant energy ( $J\text{ cm}^{-2}$ ) required to produce a 25% increase (promotion) or decrease (inhibition) in the amount of phycoerythrin (as a proportion of total biliprotein) synthesized in the dark after the light treatment is (after normalization to 500 or 680 nm) plotted against wavelength.

has a subsidiary peak in the UV at about 350 nm.<sup>309,422</sup> The shape of these action spectra are consistent with the photoreceptive pigment system being itself biliprotein in nature. Bogorad (1975) has suggested the term ‘adaptochrome’ for any photoreceptive pigment involved in the regulation of biliprotein synthesis.

Scheibe (1972) has proposed that this controlling pigment is analogous to phytochrome and has two interconvertible forms: one ( $P_G$ ) would have its absorption maximum in the green and on irradiation with green light undergo photoconversion to another form ( $P_R$ ) with an absorption maximum in the red region. On irradiation with red light  $P_R$  would be photoconverted to  $P_G$



Scheibe points out that both forms of the pigment could be biologically active,  $P_G$  promoting phycocyanin and  $P_R$  promoting phycoerythrin formation, or else just one form could be active, its presence or absence determining which of two possible differentiative pathways is to be followed. Oelmüller *et al.* (1988) have shown that in *Fremyella*

*diplosiphon* green light induces the formation of the phycoerythrin messenger RNA and red light induces formation of the phycocyanin mRNA.

Although in light-grown cells the spectral quality of the light influences the pattern of synthesis of biliproteins, light is not essential for the synthesis of these pigments to occur: facultatively heterotrophic cyanobacteria continue to make biliproteins when grown on carbohydrate medium in the dark. When such strains in group III are grown in the dark their biliprotein composition is similar to that of cells grown in red light: high in phycocyanin and low in phycoerythrin.<sup>1344</sup> Bryant (1981) found that the phycocyanin synthesized by *Calothrix* strains 7101 and 7601 in the dark included the inducible subunits,  $\alpha_1$  and  $\beta_2$ , found in red-light-grown but not green-light-grown cells. This was the case whether the inocula used were derived from cultures grown in red or green light. Bryant concluded that it is not exposure to red light, but the absence of green light that turns on the synthesis of the inducible phycocyanin subunits. If there is indeed a photoreversible pigment involved in the control of biliprotein synthesis, then it is presumably the  $P_G$  form, which is synthesized by cells growing in the dark.

### Chromatic adaptation in eukaryotic algae

Red algae do show changes in their pigment composition in response to changes in the spectral quality of the light field in which they are grown. The direction of the pigment change, however, quite apart from its quantitative extent, seems to depend on the intensity of the light. Brody and Emerson (1959) determined the ratio of phycoerythrin to chlorophyll in the unicellular red alga *Porphyridium cruentum* grown in green light (546 nm – absorbed mainly by phycoerythrin) or blue light (436 nm – absorbed mainly by chlorophyll), at low ( $\sim 0.1 \text{ W m}^{-2}$ ) or high ( $25\text{--}62 \text{ W m}^{-2}$ ) intensity. At low irradiance the cells grown in green light had a phycoerythrin/chlorophyll ratio more than twice that of the cells grown in blue light. In three species of red macroalgae – *Corallina elongata*, *Plocamium cartilagineum* and *Porphyra umbilicalis* – collected from a rocky shore on the coast of Malaga (Spain), and incubated in sea water for six hours under different light qualities, Lopez-Figueroa and Niell (1990) found that the synthesis of phycoerythrin was preferentially stimulated by green light, and synthesis of phycocyanin was preferentially promoted by red light. In a *Cryptomonas* species isolated from the deep chlorophyll layer in the western Pacific Ocean, Kamiya and Miyachi

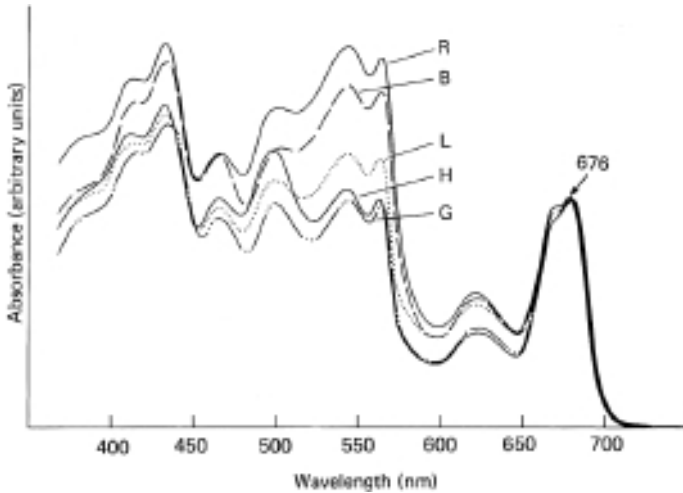


Fig. 12.8 Effect of spectral quality of light field during growth on the photosynthetic pigment composition of the unicellular red alga *Porphyridium cruentum* (by permission, from Ley and Butler (1980), *Plant Physiology*, **65**, 714–22). The spectra are normalized to the same absorbance value at 676 nm. The letter labelling each spectrum indicates the light field in which the cells were grown: R = red, B = blue, L = low-intensity white, H = high-intensity white, G = green.

(1984) found the phycoerythrin/chlorophyll ratio to be much higher in cells grown in green light than in cells grown in blue or red light, the same low irradiance ( $0.8 \text{ W m}^{-2}$ ) being used in each case. We may regard these pigment changes as complementary chromatic adaptation: the cells increased the proportion of that pigment which best absorbed the light to which they were exposed.

In the *Porphyridium* cells grown at high monochromatic irradiance, however, the position was reversed: the phycoerythrin/chlorophyll ratio of cells grown in green light was less than 50% of that in cells grown in blue light. Similarly, Ley and Butler (1980) found that cells of *P. cruentum* grown in high-intensity red ( $112 \mu\text{mol photons m}^{-2} \text{ s}^{-1}$ ) or blue ( $50 \mu\text{mol photons m}^{-2} \text{ s}^{-1}$ ) light have about twice the phycoerythrin/chlorophyll ratio of cells grown in high-intensity green ( $99 \mu\text{mol photons m}^{-2} \text{ s}^{-1}$ ) light (Fig. 12.8). In the multicellular red alga *Porphyra*, Yocum and Blinks (1958) found that plants exposed to high-intensity blue light (436 nm,  $24 \text{ W m}^{-2}$ ) for ten days contained more phycoerythrin and less chlorophyll than plants exposed for the same time to high-intensity green light (546 nm,  $17.5 \text{ W m}^{-2}$ ).

These changes in pigment composition induced by high-intensity monochromatic illumination are accompanied by changes in the photosynthetic characteristics of the plants. Yocum and Blinks (1958) found that marine red algae that had just been collected or had been kept under green light for ten days showed low photosynthetic efficiency in the region of the chlorophyll red absorption band, the action spectrum falling well below the absorption spectrum between 650 and 700 nm. Plants which had been kept for ten days under blue light, however, were highly efficient in the red region (as well as showing some increase in the blue region), the action and absorption spectra now approximately coinciding between 650 and 700 nm. Clearly, what had resulted from the exposure to blue light (itself absorbed by chlorophyll) was an increase in the efficiency of utilization of light absorbed by chlorophyll.

The nature of adaptive changes that take place within the photosynthetic system under these various moderate-to-high intensity, spectrally selective light regimes has been clarified by the detailed study of Ley and Butler (1980) on *Porphyridium cruentum*. By careful analysis of the absorption spectra and the fluorescence behaviour they have been able to arrive at conclusions concerning the absorption characteristics of, and energy transfer between, the two photosystems in cells grown in light of various spectral compositions. In red algae, chlorophyll *a* is the main light-harvesting pigment for photosystem I and phycoerythrin is the main pigment in photosystem II. Cells growing in red or blue light will be receiving much more excitation energy in chlorophyll than in phycoerythrin, which, given a photosynthetic system initially adapted to a broad spread of wavelengths, will lead to a much greater input of energy into photosystem I than photosystem II. To ensure a balanced operation of the photosynthetic system, the cells must increase the absorption cross-section of photosystem II relative to that of photosystem I. This they achieve partly by increasing the ratio of phycoerythrin to chlorophyll, but also by putting a much larger proportion of their chlorophyll into photosystem II. In addition, Ley and Butler found that these red- or blue-light-grown cells have a diminished probability of energy transfer from photosystem II to photosystem I, which helps to keep excitation energy in photosystem II. The increased effectiveness of red light in *Porphyra*, observed by Yocum and Blinks after prolonged exposure of the alga to blue light, we may now plausibly explain in terms of an increased proportion of chlorophyll in photosystem II, and therefore a more balanced functioning of the photosystems in red light. Cells growing in green light will, if they are initially adapted to a mixture of wavelengths, receive far

more excitation energy in photosystem II than I. Their adaptive response is to lower the absorption cross-section of photosystem II relative to that of photosystem I by reducing the phycoerythrin/chlorophyll ratio, and including nearly all their chlorophyll in photosystem I: PS I chlorophyll/PS II chlorophyll is  $\sim 20$  in green-light-grown, compared to  $\sim 1.5$  in red- or blue-light-grown cells.<sup>806</sup> In addition, the green-light-grown cells show a greater probability of energy transfer from photosystem II to I than cells grown in red or blue light.

The red- or blue-light-grown cells have a higher phycoerythrin content than the green-light-grown cells on a per cell basis, as well as in proportion to chlorophyll. It might be argued that although it makes sense to put more chlorophyll into photosystem II, to make more phycoerythrin in red light is not a useful adaptive response since this biliprotein has little absorption above 600 nm and so will not collect the red photons. However, it may be that what the cell 'detects' is not specifically the spectral nature of the incident light, but simply the fact that photosystem I is receiving more energy than photosystem II, and so it responds with a general increase in the pigment complement of photosystem II. Red-dominated light fields do not occur naturally in the marine environment and so we should not expect red algae to show specific adaptation to them.

From the work of Ley and Butler it seems that the general principle on which chromatic adaptation to relatively high intensity, spectrally confined, light fields takes place is adjustment of the composition and properties of the photosystems in such a way as to lead to their being excited at about the same rate, and thus to efficient photosynthesis. The complementary chromatic adaptation observed by Brody and Emerson (1959) in *P. cruentum* exposed to low-intensity blue and green light, since it operates in a contrary fashion so far as pigment changes are concerned, must have a different basis. At low light intensity the total rate of supply of excitation energy rather than imbalance between the photosystems becomes the major constraint on photosynthesis. It may be that the best strategy for the algae growing in dim green or blue-green light is to make whatever pigments will best capture the available light, to incorporate these predominantly into photosystem II (biliproteins are in this photosystem, anyway) and transfer a proportion of the absorbed energy to photosystem I.

The fact that the chromatic adaptation in cyanobacteria, involving changes in the ratio of phycoerythrin to phycocyanin, is entirely of the complementary type is not surprising. Both the pigments involved are biliproteins and both feed their excitation energy to photosystem II, so

the problem of imbalance between the photosystems does not arise. Growth of the blue-green alga *Anacystis nidulans* in red ( $\lambda > 650$  nm) light does lead to a 75% fall in chlorophyll content with little change in phycocyanin content.<sup>655</sup> We may now interpret this as an attempt by the cells to reduce excitation of photosystem I to the point at which it is in balance with photosystem II. In the cyanobacterium *Synechococcus* 6301, the phycocyanin/chlorophyll ratio increases in red light (absorbed by chlorophyll *a*, mainly associated with photosystem I) and decreases in yellow light (absorbed by phycocyanin, associated exclusively with photosystem II). Manodori and Melis (1986) interpreted these changes as representing the achievement of a balanced excitation of the two photosystems by adjustment of photosystem stoichiometry: the actual antenna size of the individual photosystems apparently did not alter.

### The blue-light effect

The underwater light field in oceanic waters becomes, as we have seen earlier, predominantly blue-green and eventually blue with increasing depth. There is evidence for the existence of specific effects of blue light on the development of the photosynthetic apparatus of certain phytoplankton species. Wallen and Geen (1971a, b) found that cells of the marine diatom *Cyclotella nana* grown in blue light ( $0.8 \text{ W m}^{-2}$ ) contained 20% more chlorophyll *a* and had a 70% higher light-saturated photosynthetic rate per cell than cells grown in white light at the same intensity. Jeffrey and Vesik (1977, 1978) observed that in cells of the marine diatom *Stephanopyxis turris* grown in blue-green light ( $4 \text{ W m}^{-2}$ ), the cellular content of all the chloroplast pigments (chlorophylls *a* and *c*, fucoxanthin and other carotenoids) was about twice that in cells grown under the same intensity of white light (Fig. 12.9). Both the number of chloroplasts per cell and the number of three-thylakoid compound lamellae within each chloroplast were higher in the cells grown in blue-green light (Fig. 12.10). Furthermore, the blue-green-light-grown cells were better able to utilize low-intensity (the same irradiance as during growth) blue-green light for photosynthesis than the white-light-grown cells, achieving a 42% higher rate. Vesik and Jeffrey (1977) examined a number of other marine phytoplankton species. Substantial increases in pigment content (55–146%) in blue-green-light-grown cells compared to white-light-grown (both at  $4 \text{ W m}^{-2}$ ) cells were observed in five diatom, one dinoflagellate and one cryptomonad species. Minor increases (17–39%) were found in two diatom, two dinoflagellate, one prymnesiophyte, one chrysophyte and

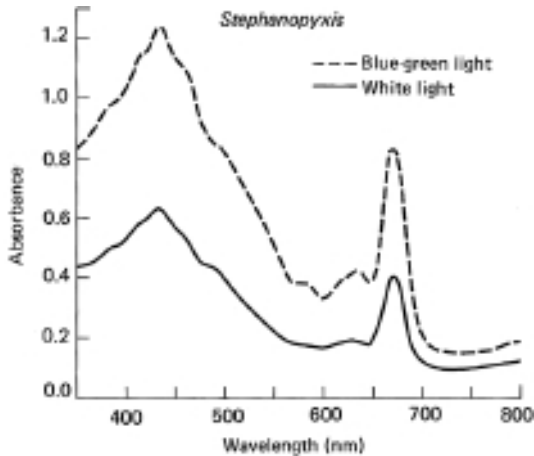


Fig. 12.9 Absorbance spectra of cells of the marine diatom *Stephanopyxis turris* grown in white (—) or blue-green (-----) light ( $4 \text{ W m}^{-2}$ , in each case). (By permission, from Veski and Jeffrey (1977), *Journal of Phycology*, **13**, 280–8.) The cells are suspended at a concentration of  $200\,000 \text{ cells ml}^{-1}$ .

one chlorophyte species. There was no chlorophyll increase in two diatom and one prymnesiophyte species. Thus, the ability to increase pigment content in a blue-green light field is common, but not universal, among marine phytoplankton. There was little alteration in the proportions of the different photosynthetic pigments, and so these blue-light-induced changes are not examples of complementary chromatic adaptation. Evidence that the increases in pigment content were accompanied by increases in the number of thylakoids per chloroplast was obtained in a dinoflagellate and a cryptomonad, as well as certain diatom species: in some diatom species the number of chloroplasts also increased.<sup>626</sup>

## 12.4 Ontogenetic adaptation – depth

We have seen that aquatic plants undergo adaptive changes in response to changes in the intensity and spectral quality of the ambient light. It is not surprising, therefore, that in species that in nature occur over a range of depths, adaptive changes with depth can often be observed. In this section we shall examine some of the changes that have been observed in aquatic plants accompanying increases in depth, and consider to what extent the lowered intensity or the altered spectral composition are responsible.

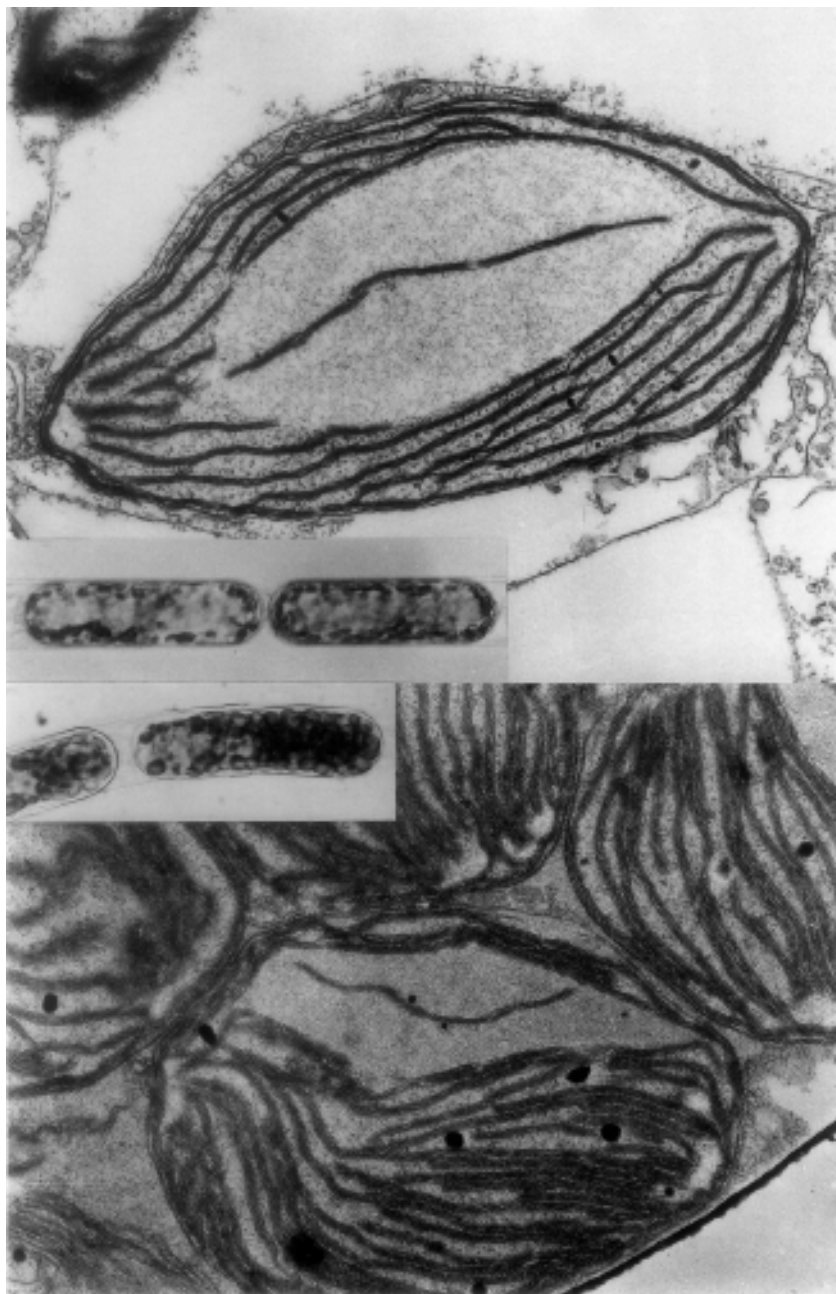


Fig. 12.10 Chloroplast number and structure in cells of the marine diatom *Stephanopyxis turris* grown in white or blue-green light (by permission, from

### Depth variation of pigment composition in macrophytes

Ramus *et al.* (1976) suspended samples of two green (*Ulva lactuca* and *Codium fragile*) and two red algal species (*Chondrus crispus* and *Porphyra umbilicalis*) for seven-day periods at depths of 1 and 10 m in harbour water at Woods Hole, Massachusetts, USA. Pigment compositions were determined. The samples were then reversed in position – the 1 m samples being lowered to 10 m, and vice versa – and after a further seven-day period, further pigment analyses were carried out. In all four species the level of photosynthetic pigments increased in the plants held at 10 m, relative to those held at 1 m, the increase for chlorophyll *a* being about 1.4-fold in the red algae and 2.3- to 3.4-fold in the green. In *U. lactuca*, chlorophyll *b* increased about five-fold, so that the *b/a* ratio rose by 50%, but in *C. fragile* the *b/a* ratio remained the same. In the red algal species the increase in phycoerythrin in the 10 m relative to the 1 m samples was greater than the increase in chlorophyll *a*, so that the phycoerythrin/chlorophyll ratio rose by 50 to 60% with increased depth.

The light field at 10 m depth at this site, being predominantly yellow-green, differed greatly from that at 1 m depth in spectral composition as well as intensity. In an attempt to determine the effects of diminished intensity alone, Ramus *et al.* analysed the pigments from algae taken from sunny and shaded sites in the intertidal region.<sup>1102</sup> Shade increased pigment levels to about the same extent as submersion to 10 m depth. In *U. lactuca* and *P. umbilicalis*, the chlorophyll *b/a* and the phycoerythrin/chlorophyll ratios, respectively, did increase in the shade but to a lesser extent than that induced by increased depth. Ramus *et al.* concluded that the greater shifts in pigment ratio associated with increased depth were indeed a response to the changed spectral composition of the light, not just to the lowered intensity.

Wheeler (1980a) carried out transplantation experiments with the sporophytes of the giant kelp *Macrocystis pyrifera* (Phaeophyta). When plants growing at 12 m depth were moved up to 1 m depth, then over a 10-day period the pigment content per unit area of thallus diminished markedly, the decreases being 52% for chlorophyll *a*, 35% for

Caption for Fig. 12.10 (cont.)

Jeffrey and Vesik (1977), *Journal of Phycology*, **13**, 271–9). Upper: electron micrograph of chloroplast in cell grown in white ( $4 \text{ W m}^{-2}$ ) light. Inset is light micrograph of whole cells. Lower: electron micrograph of chloroplasts in cell grown in blue-green ( $4 \text{ W m}^{-2}$ ) light showing increased number of three-thylakoid compound lamellae. Inset is light micrograph of whole cells showing increased number of chloroplasts.

chlorophyll *c* and 68% for fucoxanthin. When the plants were replaced at 12 m depth pigment levels increased again to their original values in 18 days. Readaptation to increased depth was accompanied by an increase in the molar ratio of fucoxanthin to chlorophyll *a* from 0.50 to 0.77 but by a decrease in the chlorophyll *c/a* ratio from 0.50 to 0.31. When samples of the intertidal brown algae *Ascophyllum nodosum* and *Fucus vesiculosus* were suspended at 4 m depth for seven days, concentrations of fucoxanthin and chlorophylls *a* and *c* per g fresh mass rose 1.5- to three-fold.<sup>1103</sup> However, in these species fucoxanthin increased somewhat less than chlorophyll *a* so that the fucoxanthin/chlorophyll *a* ratio diminished by about 20%: the chlorophyll *c/a* ratio remained the same during depth adaptation.

Interesting though transplantation experiments are, the alternative approach of studying plants of a given species growing naturally at different depths is of greater ecological relevance. Plants of the siphonous green alga *Halimeda tuna* growing in the Adriatic Sea at 5 m had a total chlorophyll content per g dry mass, which was 50% greater than that in plants growing at 2 m depth.<sup>1263</sup> the chlorophyll *a/b* ratio fell only slightly with increased depth, from 2.03 to 1.86. The chlorophyll content of the green benthic alga *Udotea petiolata* growing in Spanish coastal water increased with depth by 50% over the range 5 to 20 m, most of the increase taking place between 5 and 10 m.<sup>1045</sup> the *a/b* ratio did not change with depth. In a high-arctic fjord (Young Sound, NE Greenland), the chlorophyll *a* content of leaf blades of the brown macroalga, *Laminaria saccharina* in August (ice cover absent), increased with depth, being 0.68, 1.13, 1.25 and 2.87  $\mu\text{g mg dry wt}^{-1}$ , at 2.5, 5, 10 and 15 m, respectively.<sup>138</sup> In the case of the giant kelp, *Macrocystis pyrifera*, a single plant can extend through 30 m or more of depth, so that different parts of the same plant are exposed to very different light climates. In plants ~18 m long, growing in a kelp forest in Baja California, Mexico, Colombo-Pallotta *et al.* (2006) found that in tissue sampled from the same plant at seven different depths over the range 0 to 18 m, the concentration (per unit area of blade) of chl *a* increased by 42%, chl *c* by 67%, but fucoxanthin by 110%, so that the fucoxanthin/chl *a* ratio increased by nearly half. Tissue near the surface was well supplied with the photoprotective xanthophyll cycle carotenoids, zeaxanthin and antheraxanthin, but these diminished with depth and were present at negligible levels in tissue collected below 9 m. In addition, the absorption of the tissue in the UV (310 nm), relative to the chlorophyll *a* 675 nm peak, diminished exponentially, by about 50% with depth over the range 0 to 10 m, which we may take as indicative of decreased synthesis of UV-protective pigments.

Wiginton and McMillan (1979) studied a number of seagrass species growing at various depths off the Virgin Islands and the coast of Texas, USA. Three of the species showed no significant increase in chlorophyll content with increasing depth down to their maximum depths of 12 to 18 m. In a fourth species, *Halophila decipiens*, however, which penetrated to 42 m, the chlorophyll content changed only slightly from 7 to 18 m, but approximately doubled between 18 and 42 m. The chlorophyll *a/b* ratio fell from 1.72 at 18 m to 1.49 at 42 m. Plants of this species from a shallow but shaded site had the same chlorophyll content and *a/b* ratio as plants from 42 m depth: this was taken to indicate that the pigment changes associated with increased depth were due to the decrease in total intensity rather than to the change in spectral quality. Plants of the isoetid species *Littorella uniflora* growing at 2.3 m depth (20% of subsurface irradiance) in a Danish lake contained about 65% more chlorophyll (dry weight basis), and had a lower chlorophyll *a/b* ratio (2.6 compared to 3.2) in their leaves than plants growing at 0.2 m depth (70% of subsurface irradiance).<sup>1265</sup>

In the brown alga, *Dictyota dichotoma*, growing in Spanish coastal water, Perez-Bermudez *et al.* (1981) found that the chlorophyll *a* and *c* contents (on a mass basis) increased by 17 and 53%, respectively, between 0 and 20 m depth, the *a/c* ratio decreasing from 2.35 to 1.80: at 10 m depth the values were intermediate. The fucoxanthin content, on the other hand, decreased by 42% between 0 and 10 m depth, and then increased again to its original value between 10 and 20 m depth: the possible functional significance of this is discussed in a later section (§12.5). Plants growing in a shaded site at the surface contained 35% more chlorophyll *a*, 63% more chlorophyll *c* and 20% more fucoxanthin than plants growing in a sunny site. In a study on the red alga *Chondrus crispus* growing from 0 to 20 m depth off Massachusetts, Rhee and Briggs (1977) found that the phycoerythrin/chlorophyll ratio in midsummer remained approximately constant down to about 10 m depth, but approximately doubled between 10 and 13 m, remaining at this value at greater depth. On the basis of the studies that have so far been carried out, it appears that many benthic aquatic species can increase the content and/or alter the proportions of their photosynthetic pigments with increasing depth.

### Depth variation of pigment composition in unicellular algae

The majority of phytoplankton cells are subjected to continually varying irradiance as they circulate through the mixed layer and do not have the time to change their pigment composition in accordance with the

prevailing light field. When, as in some of the clearer, less coloured waters, light penetrates so well that the euphotic zone is deeper than the mixed layer, however, then in the stable water below the thermocline the phytoplankton can remain at approximately the same depth for long periods and there is evidence that they do indeed adapt to the light conditions prevailing at such depths. We noted earlier (§11.1) that phytoplankton isolated from the deep chlorophyll maximum in the oceans have about twice as much chlorophyll per unit biomass as phytoplankton from the surface layer.<sup>687</sup> This is not necessarily adaptation within a species: whether members of the same species are found both in a highly pigmented form in the oceanic deep chlorophyll maximum and in a less-pigmented form near the surface, or whether the taxonomic composition of the phytoplankton population is entirely different at the two depths, is in most cases not known. However, in the cyanophyte, *Prochlorococcus*, which can occur throughout the illuminated water column, there is evidence for a much greater chlorophyll content in the cells in the DCM than in the surface layer.<sup>1289,1407</sup>

In inland waters with their usually more rapid attenuation of light with depth, it is typically the case that the depth of the mixed layer is greater than or equal to that of the euphotic zone, so there is little opportunity for depth adaptation by the phytoplankton. There are, however, some lakes such as Crater Lake, Oregon, USA, and Lake Tahoe, California–Nevada, USA, with water so clear and colourless that the euphotic zone is deeper than the mixed layer and a deep chlorophyll maximum develops at 75 to 100 m depth in the growing season.<sup>769,1364</sup> Even in lakes in which light does not penetrate deeply, if there is for some reason particularly stable thermal stratification so that circulation is restricted to a very shallow layer, then the euphotic depth can exceed the mixed depth. This appears to be the case in Lake Lovojärvi in Finland: in the summer this was found to have an epilimnion about 2.5 m deep but with photosynthesis extending down to about 3.5 m.<sup>659</sup> A chlorophyll maximum, consisting largely of cells of the blue-green alga *Lyngbya limnetica* with a particularly high chlorophyll content, developed at about 3.5 m.

In Lake Tahoe, Tilzer and Goldman (1978) showed that in June and September (particularly the latter) the chlorophyll content of the phytoplankton (mainly diatoms) per unit biomass increased with depth. In September, for example, the chlorophyll *a* content ( $\mu\text{g}$  per mg wet mass) was 0.61, 1.8 and 3.06 at 0, 50 and 105 m depth, respectively. Since one diatom species, *Fragilaria vaucheriae*, constituted about 58% of the total biomass at all three depths, it seems likely that the increase in chlorophyll

content of the total biomass represented true adaptation within this, and perhaps other, species. In June also, when three other species constituted most of the biomass, a doubling of chlorophyll *a* content between 20 and 50 m was accompanied only by comparatively small changes in the population composition, suggesting that chlorophyll content had increased within species. In Lake Lovöjärvi, in contrast, there was a marked change in population composition between the mixed layer and the chlorophyll maximum in the hypolimnion, with *Lyngbya* being unimportant in the former and dominant in the latter: the chlorophyll maximum in this lake we may regard as being due to phylogenetic rather than ontogenetic adaptation. Similarly, in clear-water lakes in northwestern Ontario, Canada,<sup>389</sup> the deep chlorophyll maximum (4–10 m depth) was in each case dominated by a single large, colonial chrysophycean flagellate species (the particular species varying from one lake to another), presumably adapted to this particular niche.

Given the demonstrated *in vitro* pigment adaptation of marine phytoplankton species to blue light, and taking into account also the data for Lake Tahoe (optically similar to ocean water), we may reasonably suspect that the deep chlorophyll maximum in oceanic waters is caused at least in part by increased pigment synthesis promoted by the low intensity and/or the predominantly blue character of the prevailing light, within species that occur over a range of depths. It seems likely that there are present, in addition, specialized, highly pigmented species for which the bottom of the euphotic zone is the preferred niche. Studies of the taxonomic composition of the phytoplankton population as a function of depth in stratified oceanic waters could provide information on the relative importance of phylogenetic and ontogenetic adaptation in the establishment of the deep chlorophyll maximum.

Not all unicellular algae are planktonic. Any species that normally occur attached to, or within, fixed structures, such as the surface of sediments or rocks, or epiphytically upon larger algae, are thereby freed from the continually varying character of the light field experienced by the plankton and so have the opportunity to adapt to the light field prevailing at the depths where they are located. In McMurdo Sound, Antarctica, in the austral spring Robinson *et al.* (1995a) found the molar fucoxanthin/*chl a* ratio of the diatom-dominated algal community in the platelet layer immediately underneath the 2.2 m thick ice layer, and at the benthic surface (26 m depth), to be 1.22 and 1.61, respectively, which may be compared with 0.74 to 0.92 for surface-ice algae, and a literature value of 0.61 to 0.83 from a survey of 51 diatom species.<sup>1290</sup> Robinson *et al.*

interpreted the high fucoxanthin/chl *a* ratios as an adaptive complementary pigmentation response, resulting in enhanced absorption of the predominantly green light. It may be noted that since the surface ice, platelet layer and benthic diatom populations have different taxonomic compositions, these pigment changes should be regarded as essentially phylogenetic, rather than ontogenetic, in nature.

Studies have also been carried out on the symbiotic dinoflagellates (zooxanthellae) that occur within corals. There is a general tendency, but to varying extents in different coral species, for the pigment content of the zooxanthellae to increase with depth. Leletkin *et al.* (1981) compared the zooxanthellae of the coral *Pocillopora verrucosa* growing at 20 and 45 m depth in the Timor Sea. Those from coral at 45 m contained about 1.5 times as much chlorophylls *a* and *c*,  $\beta$ -carotene and diadinoxanthin, and 2.4 times as much peridinin per cell as zooxanthellae from coral at 20 m. The number of chlorophyll molecules per photosynthetic unit was 42% higher in the cells from 45 m than in those from 20 m, but the number of photosynthetic units per cell was about the same. Thus the pigment adaptation to increased depth appears largely to consist of an increase in the pigment complement per photosynthetic unit.<sup>380</sup>

### Depth variation of photosynthetic characteristics in macrophytes

Plants of the subtidal red alga *Ptilota serrata* collected from 24 m depth off northeastern America showed light saturation of photosynthesis at about  $116 \mu\text{mol photons m}^{-2} \text{s}^{-1}$ , whereas plants from 6 m saturated at about  $182 \mu\text{mol photons m}^{-2} \text{s}^{-1}$ .<sup>877</sup> At very low light intensities ( $7\text{--}14 \mu\text{mol photons m}^{-2} \text{s}^{-1}$ ) both kinds of plant achieved the same photosynthetic rate per g dry mass but at higher intensity the deep-water plants levelled off first and achieved a maximum photosynthetic rate only half that of the shallow-water plants (Fig. 12.11). It seems likely that the shallow-water plants contained a more active carboxylation system.

A similar adaptive response has been observed by Glenn and Doty (1981) in the tropical red alga *Eucheuma striatum*. They attached thalli of this alga (grown in shallow water) at a series of points to a line extending from 1 to 9.5 m depth on a Hawaiian reef: irradiance diminished by about a factor of ten over this range. After a month the thalli were recovered for photosynthetic measurements. A progressive decrease in photosynthetic capacity (light-saturated photosynthetic rate per g dry mass) with depth

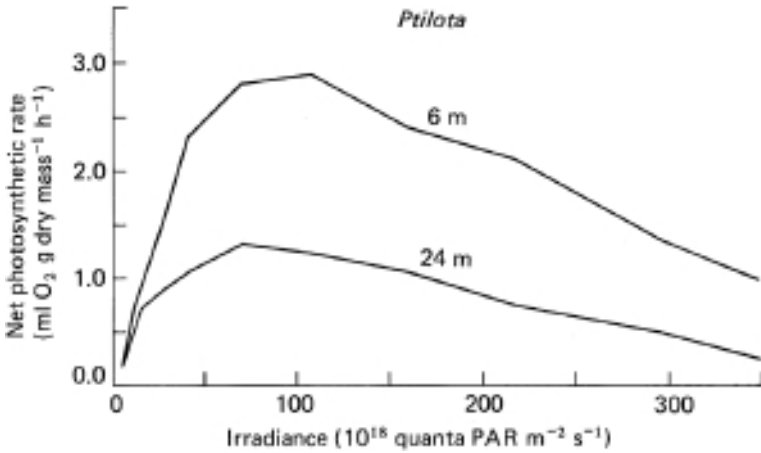


Fig. 12.11 Photosynthesis as a function of irradiance in plants of the subtidal red alga *Ptilota serrata* collected from 6 m and 24 m depth (after Mathieson and Norall, 1975).

was observed, the value in thalli from 9.5 m being about half that in material from 1 m. Thus, *Eucheuma* seems to divest itself of surplus carboxylating capacity as depth increases: a response that should be of benefit to the alga.

Fairhead and Cheshire (2004) studied the seasonal and depth-related variation in the photosynthetic characteristics of the brown macroalga, *Ecklonia radiata*, growing subtidally on a rocky substrate at West Island, South Australia. The light intensity required for saturation decreased with depth. For example, in spring (September)  $E_{\max}$  values were 469, 383, 116 and 77  $\mu\text{mol photons m}^{-2} \text{s}^{-1}$ , respectively, for algae collected from 3, 5, 10 and 12 m depth. In winter, when average irradiance is lower, the photosynthetic efficiency (expressed in terms of  $\alpha$ ) at sub-saturating light increased, and the irradiance required for saturation of photosynthesis, and for light compensation of respiration, both decreased. In a high-arctic fjord (Young Sound, NE Greenland), Borum *et al.* (2002) found that the light saturation onset parameter and the light compensation point of the brown macroalga, *Laminaria saccharina*, in (ice-free) August both decreased with depth:  $E_k$  and  $E_c$  were 170 and 22  $\mu\text{mol photons m}^{-2} \text{s}^{-1}$ , respectively, at 2.5 m depth, and 17 and 4.2  $\mu\text{mol photons m}^{-2} \text{s}^{-1}$  at 10 m depth.

In the case of the giant kelp *Macrocystis pyrifera*, as we noted earlier, a single frond can extend from the holdfast on the sea floor up through as

many as 30 m of water column and thus through a very considerable light gradient. Wheeler (1980a) found that in immature fronds, 12 to 14 m long, growing in 12 m of water in coastal water off Santa Barbara (California), the light-saturated photosynthetic rate per unit area rose progressively with distance from the holdfast, 1.5- to three-fold, reaching a maximum at about 10 to 12 m. Thus, over this part of the frond the photosynthetic capacity per unit area rose with diminishing depth, which we may regard as an adaptive response since it is only at the lesser depths that there is enough light to support a high photosynthetic rate per unit area. In single plants of *M. pyrifera* in Baja California, extending from the holdfast at 18 m depth to the surface, Colombo-Pallotta *et al.* (2006) found the light-saturated photosynthetic rate per unit area of blade to increase progressively with diminishing depth, rising by ~60% between 18 and 0 m. Consistent with the depth variation in the content of xanthophyll cycle photoprotective carotenoids, noted earlier, non-photochemical quenching of chl *a* fluorescence was very marked in tissue from the surface, and still evident in tissue from 3 and 6 m, but virtually absent in tissue from below 9 m depth, confirming that this alga invests in photoprotection of its photosynthetic system only where its fronds encounter it near the surface, and not at greater depth.

In coastal waters of southeastern Florida, two *Halophila* seagrass species, *H. johnsonii* and *H. decipiens*, occur together subtidally, but only the former species is also found in the shallower intertidal waters. Durako *et al.* (2003) found that the onset of photoinhibition occurred at lower irradiances for *H. decipiens* ( $537\text{--}820\ \mu\text{mol photons m}^{-2}\text{ s}^{-1}$ ) than for *H. johnsonii* ( $1141\text{--}2670\ \mu\text{mol photons m}^{-2}\text{ s}^{-1}$ ), and that furthermore, leaves of *H. johnsonii* contained a UV-absorbing (peak, 345 nm), and therefore possibly photoprotective, pigment absent from *H. decipiens*. *Halophila johnsonii* therefore appears to be better adapted to the light stresses of shallow waters than *H. decipiens*. However, since these species, although closely related, are not identical, this should properly be regarded as an example of phylogenetic, rather than ontogenetic, adaptation.

### **Depth variation of photosynthetic characteristics in unicellular algae**

As we have noted earlier, depth adaptation of the photosynthetic system in phytoplankton is only to be expected in waters in which density stratification permits some of the cells to remain for long periods at

depths where circulation is minimal but there is sufficient light for photosynthesis to take place. This situation exists throughout most of the ocean in the lower part of the euphotic zone. By what criteria can we recognize true depth adaptation of the phytoplankton photosynthetic system? The primary criterion is that cells from deep water should achieve a higher photosynthetic rate per unit cellular biomass than cells from the surface, in the light field prevailing in deep water. The deep-water cells would generally achieve this by investing an increased proportion of their cellular substance in light-harvesting pigments, possibly accompanied by lower respiration. A secondary criterion is that the deep-water cells should have a lower photosynthetic rate per unit cellular biomass than the surface cells at saturating light intensity: this would be a consequence of the deep-water cells, in the interests of biochemical economy, synthesizing only as much carboxylase as they can make use of at the low irradiance values existing at the greater depths.

On its own, a reduction in the light saturation parameter,  $E_k$ , is not an entirely satisfactory indication of adaptation to low irradiance.<sup>1486</sup> Since  $E_k = P_m^* / \alpha$  (see §10.2), any environmental factor that reduces the light-saturated photosynthetic rate per mg chlorophyll to a greater extent than it affects the slope of the initial part of the  $P$  (per mg chlorophyll) versus  $E_d$  curve, will reduce  $E_k$ . Yentsch and Lee (1966) showed, by analysing a large amount of published data for both natural and cultured phytoplankton populations, that  $E_k$  tends to be linearly related to  $P_m^*$  and they emphasize the desirability of presenting  $P_m^*$  as well as  $E_k$  values in studies on light adaptation by phytoplankton. Nevertheless if, when measured under standardized conditions, one phytoplankton population is found to have a lower  $E_k$  value (or light saturation value) than another, then while we cannot on this ground alone conclude that its light-harvesting capability has increased, we may reasonably suppose that its ratio of light-harvesting capacity to carboxylation rate has increased, i.e. it has either increased its pigment content or divested itself of some of its surplus carboxylation capacity, or both, all of which can be regarded as forms of shade adaptation. It is generally found in the oceans that once thermal stratification has been established, phytoplankton isolated from the lower part of the euphotic zone have a lower  $E_k$  value than phytoplankton from near the surface.<sup>1297</sup> Phytoplankton from the surface, 50 m and 100 m depth (100%, 10% and 1% of subsurface irradiance) in the Sargasso Sea in October, had  $E_k$  values of about 600, 300 and 60  $\mu\text{mol photons m}^{-2} \text{s}^{-1}$  (Fig. 12.12a).<sup>1159</sup> In the winter when the thermocline breaks down, the algae are circulated rapidly enough to prevent their becoming adapted to

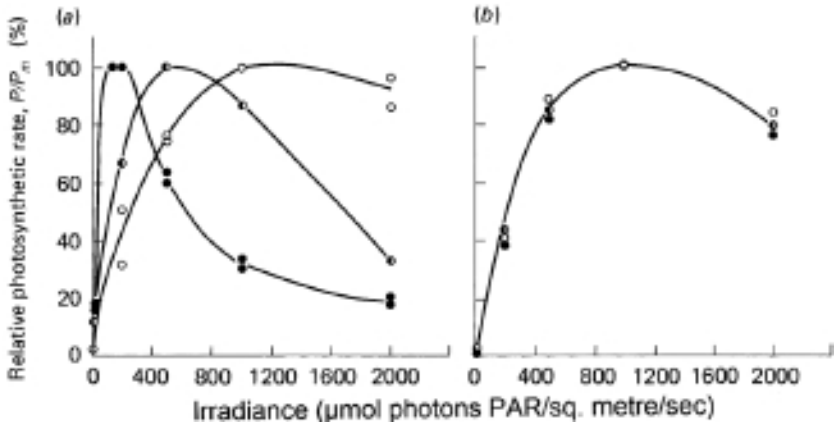


Fig. 12.12 Depth adaptation by marine phytoplankton (after Ryther and Menzel, 1959). These  $P$  versus  $E_d$  curves for Sargasso Sea phytoplankton were determined by the  $^{14}\text{C}$  method at the temperature prevailing at the sea surface. Samples taken from 0 m ( $\circ$ ), 50 m ( $\bullet$ ) and 100 m ( $\bullet$ ) depth. (a) October; water stratified with thermocline at 25 to 50 m. (b) November; water isothermal down to >150 m depth.

the irradiance value at any depth, and it is found that the cells from all depths show the same degree of light adaptation and indeed are rather similar in their properties to summer surface phytoplankton (Fig. 12.12b).<sup>1159,1297</sup> It can be seen from the curves in Fig. 12.12a that the phytoplankton from the lower part of the euphotic zone not only have a lower  $E_k$ , but are much more susceptible to photoinhibition by higher light intensity than are the surface phytoplankton.

Shimura and Ichimura (1973) found that phytoplankton from near the bottom of the euphotic zone in the ocean had a higher photosynthetic activity than surface phytoplankton when both were placed deep in the euphotic zone. In addition the phytoplankton from the deep layer showed a higher ratio of photosynthetic activity in green light to that in red light than surface layer phytoplankton. Thus the phytoplankton growing deep in the euphotic zone of the ocean appeared to be the better adapted to the dim, predominantly blue-green, light prevailing in that region. Similarly, Neori *et al.* (1984) found, for temperate and polar oceanic stations, that both absorption and chlorophyll *a* fluorescence excitation spectra of phytoplankton samples showed enhancement in the blue-to-green part of the spectrum (470–560 nm) relative to that at 440 nm, with increasing depth. They attributed this change to an increase in the concentration of photosynthetic accessory pigments, relative to chlorophyll *a*.

In nature in thermally stratified waters, the cells below the thermocline will be at a lower temperature than those near the surface and as we saw in an earlier section (§11.3), lowering the temperature automatically lowers  $E_k$  (by diminishing  $P_m^*$  without affecting  $\alpha$ ), quite apart from any alterations in the biochemical composition of the depth-adapted cells. That there are nevertheless inherent changes in the light relations of the cells is readily shown (as in the experiments in Fig. 12.12) by comparing the deep- and shallow-water phytoplankton at the same temperature. The *in situ* lowering of the  $E_k$  value of the deep phytoplankton due to lowered temperature is in fact of little ecological significance since the light intensity at that depth will be well below saturation in any case.

As we have noted earlier, the extent to which shade adaptation of the deep phytoplankton in the ocean represents true ontogenetic adaptation (i.e. physiological adaptation within species occurring throughout the illuminated water column) or is phylogenetic adaptation (the predominance in deeper water of particular species genetically adapted to low irradiance values) in most cases remains uncertain. However, Neori *et al.* (1984) believe that the changes in absorption and fluorescence properties with depth that they observed (see above) were predominantly due to shade adaptation within existing species: the depth distribution of species did not seem to account for the spectral changes, and furthermore, similar changes could be detected in phytoplankton samples within one day of transferring them to low light levels.

In the clear, colourless water of Lake Tahoe in which, as in the ocean, the illuminated region extends below the thermocline, Tilzer and Goldman (1978) found that the increase in chlorophyll content of the deep-water cells at the time of maximum thermal stratification (September) was accompanied by a diminution in the light saturation onset parameter: the  $E_k$  values were about 80, 50 and 15 W (PAR)  $m^{-2}$ , for cells from 0, 50 and 105 m depth, respectively. The phytoplankton in this lake satisfied the primary criterion for true depth adaptation of the photosynthetic system. In the light field prevailing in deep water, the deep-water cells achieved a substantially higher photosynthetic rate per unit biomass than cells from the surface (Fig. 12.13). Their light-saturated rate of photosynthesis per unit biomass was not, however, significantly lower than that of the shallow-water cells, suggesting that the deep-water cells in this lake had not adopted the additional shade adaptation strategy of reducing their carboxylase content.

The less turbulent the upper mixed layer of a water body is, the more time the phytoplankton cells have to adapt as they undergo vertical

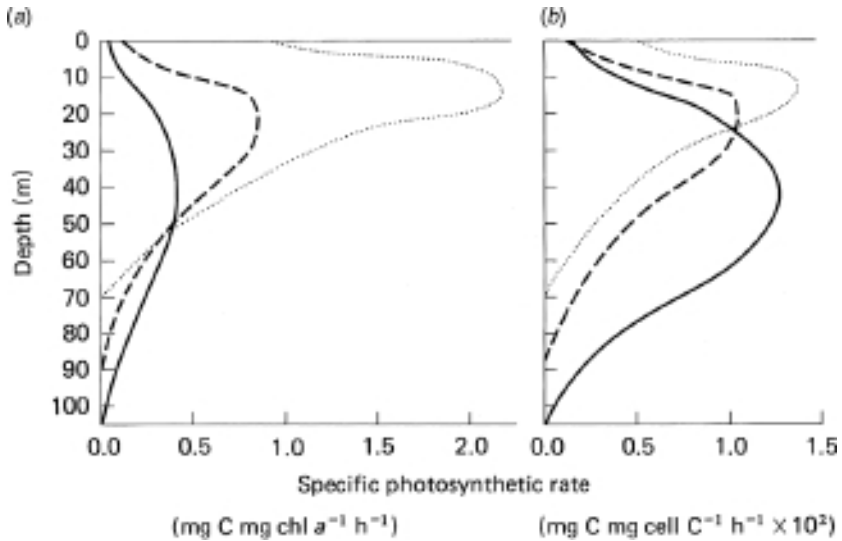


Fig. 12.13 Variation with depth of specific photosynthetic rates of phytoplankton originating from different depths, in Lake Tahoe (California–Nevada, USA) (by permission, from Tilzer and Goldman (1978), *Ecology*, **59**, 810–21. Copyright © 1978, the Ecological Society of America). The phytoplankton were collected from the surface (.....), 50 m (----) and 105 m (—), and incubated with  $^{14}\text{CO}_2$  at a series of depths between the surface and 105 m. (a) Specific photosynthetic rate per unit chlorophyll. (b) Specific rate per unit cellular biomass, expressed as carbon. The lower maximum photosynthetic rate per unit chlorophyll of the deeper water cells is due to their higher pigment content.

circulation. This suggests that even within a mixing layer, photosynthetic differences between the cells at the top and the bottom might develop as turbulence diminishes. Lewis *et al.* (1984) obtained evidence that this can indeed happen. In Bedford Basin (Nova Scotia, Canada) they measured  $\Delta P_m$ , the difference between  $P_m$  (per unit chlorophyll) at the surface and at the base of the mixing region, and also measured the rate of turbulent kinetic energy (TKE) dissipation,  $\varepsilon$  ( $\text{m}^2 \text{s}^{-3}$ ), on 19 occasions over the period of a month. While on many occasions, especially at high rates of TKE dissipation,  $\Delta P_m$  did not differ significantly from zero, on other occasions, as  $\varepsilon$  diminished to low values,  $\Delta P_m$  increased markedly, indicating that photoadaptation had in fact occurred.

In McMurdo Sound, Antarctica, in the austral spring Robinson *et al.* (1995a) found the light saturation onset parameter,  $E_k$ , of the diatom-dominated algal community in the platelet layer immediately underneath the 2.2 m thick ice layer was higher ( $5.9\text{--}12.6 \mu\text{mol photons m}^{-2} \text{s}^{-1}$ ) than

that ( $1.3\text{--}4.5\ \mu\text{mol photons m}^{-2}\text{s}^{-1}$ ) for the diatom community at the benthic surface (26 m depth). The initial slope,  $\alpha$ , of the  $P$  versus  $E_d$  curve was much higher for the benthic algae than for the platelet layer algae –  $0.07\text{--}0.10$  and  $0.003\text{--}0.011$  ( $\text{mg C mg chl } a^{-1}\text{ hr}^{-1} [\mu\text{mol photons m}^{-2}\text{ s}^{-1}]^{-1}$ ), respectively – indicating a higher photosynthetic efficiency at low light levels. As pointed out earlier, strictly speaking, since the two diatom communities are not taxonomically identical, this should be regarded as phylogenetic, rather than ontogenetic, adaptation.

### Morphogenetic adaptation to depth

We have noted earlier that the adaptation of angiosperms to increased shade includes a morphogenetic response: the leaves increase in area while simultaneously becoming thinner. Spence, Campbell and Chrystal (1973) studied five submerged species of *Potamogeton* in several Scottish lochs. They found that specific leaf area (SLA,  $\text{cm}^2\text{mg}^{-1}$  leaf dry mass) increased linearly with water depth. The rate of increase with depth appeared to be typical of the loch (and therefore, presumably, of the water type) rather than of the species, the more rapid rates of increase being observed in the more highly coloured and therefore more attenuating waters. For example, the specific leaf area of *P. perfoliatus* increased from about  $0.6$  to  $1.3\ \text{cm}^2\text{mg}^{-1}$  from near the surface to  $4$  m depth in the brown water of L. Uanagan, but increased only from about  $0.7$  to  $1.1\ \text{cm}^2\text{mg}^{-1}$  from the surface down to  $6$  m depth in the comparatively colourless waters of L. Croispol. It seemed that a given specific leaf area could be achieved in light fields of markedly different spectral quality, and it was thought likely that the total irradiance ( $400\text{--}750$  nm) was of more importance in determining the SLA than any aspect of the spectral quality such as the blue/red or red/far-red ratios. Lipkin (1979) found that in communities of the seagrass *Halophila stipulacea* growing in the northern Red Sea, leaf area increased about 2.5-fold with depth from the surface down to  $30$  m (Fig. 12.14). Although this was at first considered to be an ontogenetic adaptation controlled by light intensity, culture experiments indicated that the differences were genetically controlled and Lipkin concluded that true ecotypes of this seagrass were present in the same locality within short distances, i.e. adaptation was apparently phylogenetic rather than ontogenetic.

The siphonous green alga *Halimeda tuna* growing in the Adriatic Sea shows depth-dependent changes in thallus morphology. Mariani Colombo *et al.* (1976) observed an increase in the total surface number

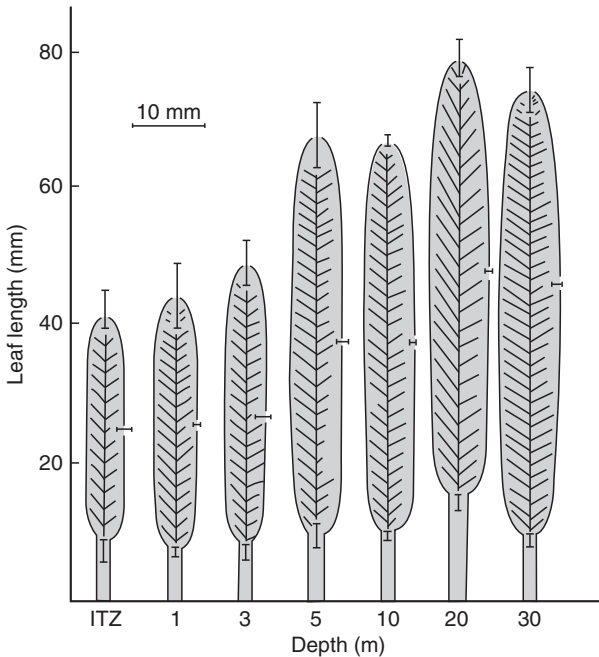


Fig. 12.14 Change in length and area of leaves of the seagrass *Halophila stipulacea* (Sinai, northern Red Sea) with depth (by permission, from Lipkin (1979), *Aquatic Botany*, 7, 119–28). ITZ = intertidal zone.

of branches and number of segments with increasing depth over the range of 7 to 16 m. The overall effect is to increase the photosynthetic surface exposed to light.

## 12.5 Significance of ontogenetic adaptation of the photosynthetic system

From our consideration of this topic so far, it is clear that the ability to adapt the characteristics of their photosynthetic systems to the prevailing light field is widespread among aquatic plants. To what extent is such adaptation of ecological significance?

In broad terms, the significance of ontogenetic adaptation is that it enables a species to exploit a wider range of habitats. Suitability of habitat for aquatic plant photosynthesis varies with depth; with water type, particularly with regard to optical character; with time, as the seasonal cycle progresses; and in the intensity of competition between plants.

The significance of ontogenetic adaptation of the photosynthetic apparatus might therefore be assessed in terms of the extent to which it enables particular species to increase the range of depth and of water types that they can exploit, the proportion of the year in which they can grow and the success with which they withstand competition from other species.

### **Depth and shade adaptation**

Given the demonstrated ability of so many phytoplankton species under laboratory conditions to increase their light-harvesting capability in dim light, especially in dim blue-green light, and given also the observed shade adaptation of natural phytoplankton populations taken from deep in the euphotic zone of stratified waters, we may reasonably conclude that ontogenetic adaptation of the phytoplankton photosynthetic apparatus to the low-intensity light field in these deep layers is a real phenomenon, although it may well coexist with phylogenetic adaptation, certain species being perhaps permanently adapted to the greater depths. We saw earlier (§11.1) that the deep phytoplankton layer makes a significant contribution to total primary production in those waters where it occurs. The shade adaptation of these phytoplankton is therefore not only relevant to our understanding of how that ecological niche comes to be filled, but is also of significance for the total primary production of the oceans. Furthermore, there is evidence for a significant enhancement of zooplankton biomass around the deep chlorophyll maximum; Ortner, Wiebe and Cox (1980) consider that this is a depth zone of particularly intense trophic activity. There is also evidence that turbulent entrainment of carbon from the base of the deep chlorophyll maximum into the bottom mixed layer can make a substantial contribution to new production.<sup>1205</sup> Thus, when all trophic levels are taken into account these shade-adapted phytoplankton may be of even more significance for the ecology of the ocean than their contribution to primary production alone would indicate.

So far as total primary production is concerned, it is true that most of it takes place in the upper region of the euphotic zone and so, as Steemann Nielsen (1975) points out, the most relevant form of adaptation is that of the phytoplankton in the surface layer to the high irradiances prevailing there; for example, their greater ability to withstand photoinhibition. There is evidence that one of the roles of carotenoids, specifically those xanthophylls not involved in light harvesting, is to protect plants against damage by excessive light. There is also evidence that in red algae, for

example, in which carotenoids contribute little to photosynthesis, the ratio of carotenoid to chlorophyll increases if the cells are grown at high light intensity.<sup>313,806</sup> As discussed earlier (§10.2), we may reasonably assume that the acquisition of resistance to photoinhibition by phytoplankton involves increased synthesis of protective carotenoids.

In the case of the multicellular benthic algae and angiosperms, while there is evidence for an increase in light-harvesting capacity as growth irradiance is decreased, it is less well documented than in phytoplankton species, perhaps because of the greater difficulty in culturing these plants under controlled laboratory conditions. Although more studies are required, particularly in the field, we may reasonably conclude on the basis of the information already available that in some species that grow over a range of depth, adaptation in the deeper growing individuals consists in part of an increase in pigment content per unit biomass. An alternative or additional strategy is a reduction in respiration rate; morphological changes that increase light interception by the plants may also occur.

Any adaptive ability that enables an aquatic plant species to cope with the variation in light regime over a range of depth should in principle also enable it to cope with the variation in light quality that will be found within a range of optical water types. The extent to which the ability of particular species to grow in a range of water types is due to ontogenetic adaptation of the photosynthetic apparatus has not been the subject of systematic study.

Given that a common ontogenetic response of aquatic plants to variations in light regime is to vary the light-harvesting capacity of the cells, how important is chromatic adaptation as a component of this? How important, that is, are changes in the shape of the absorption spectra (due to changes in the proportions of the pigments) of the cells, as opposed to changes in absolute absorption across the whole spectrum? In aquatic plants that do not contain biliproteins, i.e. higher plants and algae other than the Rhodophyta, Cryptophyta and Cyanophyta, changes in pigment ratios in response to changes in the ambient light are relatively small, where they occur at all. In certain green species (algae and higher plants) there is some increase in the ratio of chlorophyll *b* to *a*, during shade adaptation: this should somewhat increase the absorption in the 450 to 480 nm waveband relative to other parts of the spectrum. In the dinoflagellate *Glenodinium*, the increase in concentration of the peridinin/chlorophyll *a*-protein associated with growth at low irradiance causes absorption to rise more in the 500 to 550 nm region than elsewhere in the spectrum.<sup>1083</sup> These comparatively subtle changes in the shape of the

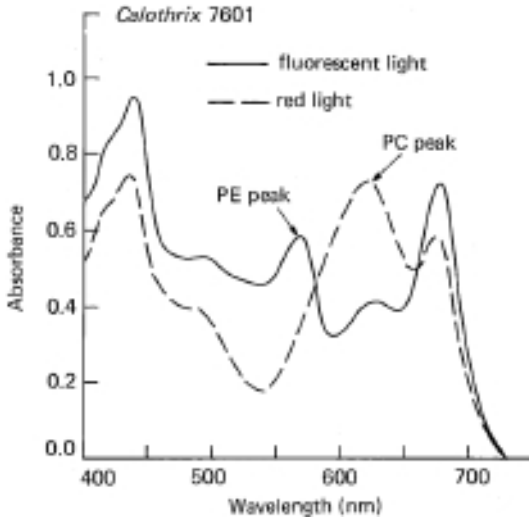


Fig. 12.15 Absorption spectrum of blue-green algae as influenced by spectral quality of light field during growth (after Bennett and Bogorad, 1973). Cultures of *Calothrix* 7601 (formerly *Fremyella diplosiphon*) were grown in red light or in fluorescent light (enriched in the green-yellow waveband), and the absorbance spectra of the whole cells were determined on suspensions containing  $0.68 \text{ mg dry mass ml}^{-1}$ . The presence of high levels of phycoerythrin (PE) in the fluorescent-light-grown cells (—) and of phycocyanin (PC) in the red-light-grown cells (-----) is apparent from the spectra.

absorption spectrum will indeed have the effect of matching the absorption spectrum of the cells better to the spectral distribution of the blue-green light field that prevails at increased depth in many marine waters and so can legitimately be regarded as examples of ecologically useful chromatic adaptation. Nevertheless, the effects of such changes are quantitatively less important for total light capture than the increase in absorption throughout the spectrum resulting from the general increase in pigment concentration. For clear-cut instances of chromatic adaptation we must turn to the biliprotein-containing groups, the Cyanophyta and Rhodophyta.

The changes in the levels of phycoerythrin and phycocyanin in blue-green algae in response to growth in light of differing spectral quality are such as to lead to drastic alterations in the absorption spectra. As shown in Fig. 12.15, the phycocyanin-dominated cells absorb much more strongly in the 600 to 650 nm region than the phycoerythrin-dominated cells, which in turn absorb more strongly in the 500 to 575 nm region. There is no doubt that the former cells would be better

equipped to collect light from an underwater light field of an orange-red character, while the latter cells would harvest more photons from a greenish light field. Underwater light fields with a predominantly orange-red character would almost never be found in marine systems, but do exist in inland waters strongly coloured by soluble and particulate humic materials (see Fig. 6.4*d*). Green light fields are, of course, common in natural waters. Thus, light climates to which these two kinds of cell would be well matched do occur in aquatic ecosystems, but there is a lack of field data on the extent to which adaptation of this type actually happens in nature.

The ratio of biliprotein to chlorophyll can also, as we have seen, change in accordance with the prevailing light. As light intensity diminishes, even when the spectral composition is unaltered, the biliprotein/chlorophyll ratio increases to an extent varying from one blue-green- or red algal species to another. Since this change can be brought about by variation in intensity alone, it could be argued that this is simply 'intensity adaptation' and is not true chromatic adaptation since it does not require a change in spectral composition to bring it about. On the other hand, diminution of light intensity in the underwater environment, as opposed to the laboratory, is most commonly associated with increase in depth in which case it is associated with a change in spectral quality, in particular with a removal of red light. In the course of evolution, therefore, the common association between low irradiance and the virtual absence of red light might well lead to the development of regulatory mechanisms that respond automatically to lowered intensity by increasing the synthesis of pigments, such as phycoerythrin, which absorb in spectral regions other than the red waveband. The plant does not necessarily have to possess a chromatically specific detection system in order to undergo chromatic adaptation. The increase in biliprotein/chlorophyll ratio as light intensity diminishes might reasonably be regarded as both intensity and chromatic adaptation: while it is triggered off by falling intensity, at the same time it makes the cells chromatically better adapted to the particular spectral character that dim underwater light fields usually have.

Little information is presently available on the extent to which this kind of adaptation is of ecological significance. Limited field studies indicating an increase in biliprotein/chlorophyll ratio with depth have been carried out on two red algal species (§12.4).

The non-complementary kind of chromatic adaptation that occurs at relatively high light intensities in red algae, in which the adaptation seems to be directed towards achieving a balanced excitation of the two

photosystems (§12.3) is accompanied by substantial changes in the absorption spectrum (Fig. 12.8). This kind of adaptation has not yet been described in the field. It is most likely to be found among algae growing at relatively shallow depths. On the basis of the laboratory studies and theoretical explanations<sup>169,806,1490</sup> one might predict that with increasing depth and therefore increasing green/red ratio in the underwater light, the phycoerythrin/chlorophyll ratio would at first decrease to ensure equal excitation of the photosystems and then increase again as the need to capture all available quanta became paramount. Although this has not yet been described for a red alga, what could be an analogous phenomenon has been reported for a brown alga. As we noted earlier, in *Dictyota dichotoma* at a Spanish coastal site, the fucoxanthin/chlorophyll ratio decreased by 42% between 0 and 10 m depth, and then increased again to its original value between 10 and 20 m depth.<sup>1045</sup> If, as is likely to be the case, fucoxanthin transfers its excitation energy primarily to photosystem II, then the increasingly blue-green character of the light with increasing depth might lead to greater excitation of photosystem II than photosystem I, and a decrease in the fucoxanthin/chlorophyll ratio could rectify this. At greater depths still, the need to harvest all available quanta becomes of dominating importance and so the fucoxanthin content is increased again.

In the more densely vegetated parts of the aquatic environment, the ability to compete with other plants for light and/or to tolerate shading by other plants is of great importance. On a priori grounds it seems likely that plants that find themselves in dim light, not because of great depth but because of overshadowing by other plants, will undergo similar kinds of shade adaptation to those associated with increased depth, but the topic has received little experimental attention in the case of aquatic ecosystems. An example of shade tolerance enabling a plant to withstand competition for light is the previously mentioned increase in phycoerythrin content in *Chondrus crispus* plants overgrown by epiphytic diatoms.<sup>1122</sup>

A special case of shade adaptation is that of the microalgae living in and under the annual sea ice in North and South polar marine environments. In the Antarctic pack-ice these algae are present at a concentration in the region of  $100 \text{ mg chl } a \text{ m}^{-2}$ , and since the area covered by the annual expansion and contraction of the ice is about 15 million  $\text{km}^2$ , and the algae are released into the water during the summer thaw, it seems likely that these ice algae make a substantial contribution to the productivity of the polar marine ecosystem.<sup>186,1376</sup> The sea-ice algal community is dominated by pennate diatoms, and its photosynthesis saturates

at low incident irradiance values, indicating a high level of shade adaptation.<sup>258,1033,1137</sup> While there is some indication of a modest capacity for ontogenetic shade adaptation within this community,<sup>261,1033</sup> it appears likely that the shade adaptation it exhibits is mainly phylogenetic in nature, i.e. the species present are likely to be genetically adapted to low irradiance.<sup>258</sup>

### Seasonal adaptation – multicellular benthic algae

Away from the tropics the average irradiance during daylight hours changes cyclically with the seasons during the year and we may reasonably suppose that it would be of advantage to the aquatic flora to adapt their photosynthetic systems to the seasonally varying light climate. This should especially be the case for the perennial benthic algae that survive throughout the year and therefore must photosynthesize as best they can at all seasons. However, the seasonal variation in temperature that accompanies the variation in irradiance does itself impose certain changes on the photosynthetic behaviour of aquatic plants. Light compensation and saturation points increase with temperature since the rates of respiration and carboxylation both increase with temperature whereas the rate of the light reactions is relatively unaffected. King and Schramm (1976) in their studies on a large number of benthic algal species from the Baltic found that there was a marked lowering of the compensation point in the winter compared to the summer or autumn. Since their measurements were carried out at the water temperature prevailing at the time, it was impossible to say whether there was any adaptation or whether the lower winter temperatures accounted entirely for the lower compensation points. In most of the species there was no marked seasonal change in the light saturation point but in two *Laminaria* (Phaeophyta) species the irradiance required to achieve saturation was much lower in winter than in autumn. In one of these species, *L. saccharina*, the light-saturated photosynthetic rate per g dry mass was about the same in both seasons suggesting that the reduction in light saturation point in the winter was not merely due to a fall in carboxylation rate caused by the lower temperature.

In the giant kelps *Macrocystis integrifolia* and *Nereocystis luetkeana*, growing off Vancouver Island (BC, Canada), Smith, Wheeler and Srivastava (1983) and Wheeler *et al.* (1984) found that the chlorophyll *a* and fucoxanthin levels (per unit area of blade) were high in winter, declined in spring–summer, and then rose in autumn once again to the

winter level. The seasonal changes in pigment were substantial (two- to three-fold). Although a case might be made that the changes in pigment levels were an adaptive response to seasonally changing insolation, they appeared in fact to correlate best with the nitrate concentration in the water, i.e. perhaps these algae simply make more photosynthetic pigments when they have the nitrogen to do so.

In a number of red algal species it has been shown that the ratio of phycoerythrin to chlorophyll is higher in the winter than in the summer.<sup>194,932,1122</sup> It seems likely in such cases that the irradiance required to achieve saturation would, quite apart from temperature effects, be lower in the winter, but experimental confirmation is required.

In the intertidal red alga *Bostrychia binderi*, growing in a subtropical location (Florida, USA), Davis and Dawes (1981) found little seasonal variation in chlorophyll content, but the light-saturated photosynthetic rate was at its highest in the late summer and autumn and at its lowest in the winter, the summer/autumn values being two- to four-fold greater than the winter values. Since all the measurements were carried out at 30°C, this probably represents a true seasonal variation in carboxylation capacity.

### Seasonal adaptation – phytoplankton

Seasonal temperature changes make interpretation difficult in the case of the phytoplankton also. Steemann Nielsen and Hansen (1961) measured the light saturation onset parameter,  $E_k$ , of phytoplankton in the surface layer in Danish coastal waters at the prevailing temperature at intervals throughout a year. It varied about three-fold, being highest in midsummer and lowest in midwinter. A comparison of the variation in  $E_k$ , daily insolation and water temperature throughout the year (Fig. 12.16) suggests that most of the seasonal change in the light saturation parameter can be attributed to the change in temperature; however, the value of  $E_k$  in the spring seems to be somewhat greater than would be expected on the basis of temperature alone and it may be that the rise in  $E_k$  at this time of year is in part due to adaptation of the photosynthetic system to the higher irradiance.

The values of  $\alpha$  and  $P_m^*$  for the phytoplankton of a Nova Scotia coastal water were found by Platt and Jassby (1976) to vary about five-fold over a period of 2.75 yr. Measurements were carried out at the prevailing water temperature. Values tended to be highest in the summer and early autumn but subsidiary peaks at other times of the year were also sometimes observed. Statistical analysis indicated that photosynthetic capacity

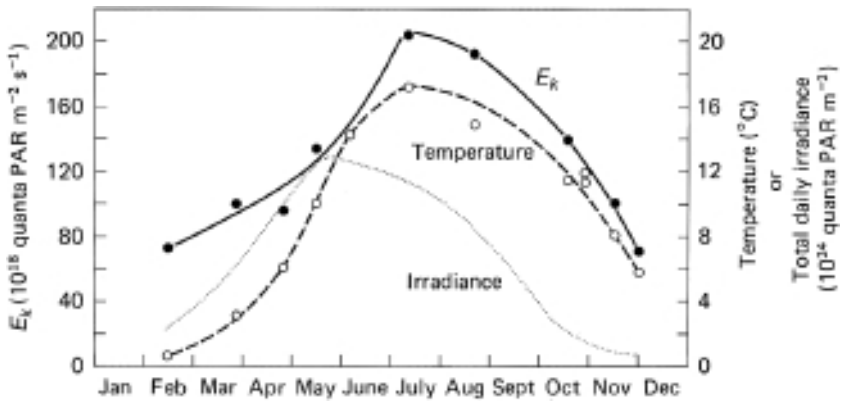


Fig. 12.16 Seasonal variation of saturation onset parameter ( $E_k$ ) of phytoplankton, temperature and total daily irradiance at a Danish coastal station. Plotted from data of Steemann Nielsen and Hansen (1961). The temperature (---○---) and  $E_k$  (—●—) values are for the surface layer and  $E_k$  values were measured at the prevailing temperature. Irradiance values have been converted from lux to quanta  $\text{m}^{-2} \text{s}^{-1}$  using an approximate factor. The values for total daily irradiance (.....) are for days of average cloudiness throughout the year.

( $P_m^*$ , light-saturated photosynthetic rate per mg chlorophyll) was strongly correlated with temperature but that  $\alpha$  (the initial slope of the  $P$  versus  $E_d$  curve) was not. These findings are in accordance with the known insensitivity of the photochemical processes, but sensitivity of carboxylation, to temperature.

The  $E_k$  value of the phytoplankton in a Japanese pond was found to vary about three-fold during the year, rising to a maximum in the summer and falling to a minimum in the winter;<sup>34</sup> however, these measurements were carried out at the prevailing water temperature.

Even when the effects of temperature are allowed for, there is the problem of determining whether any apparent seasonal change in the photosynthetic behaviour of the population is true ontogenetic adaptation within species, or merely represents changes in which species are present, since there are marked successional changes in the taxonomic composition of the phytoplankton population through the year, both in the sea<sup>1115</sup> and in lakes.<sup>1120</sup> A study by Durbin *et al.* (1975) has shown how the relative importance of different types of phytoplankton (separated in terms of size), both as components of total biomass and as contributors to primary production, varied in a northeast American coastal water throughout most of one year (Fig. 12.17). Larger cells (from 20  $\mu\text{m}$  to

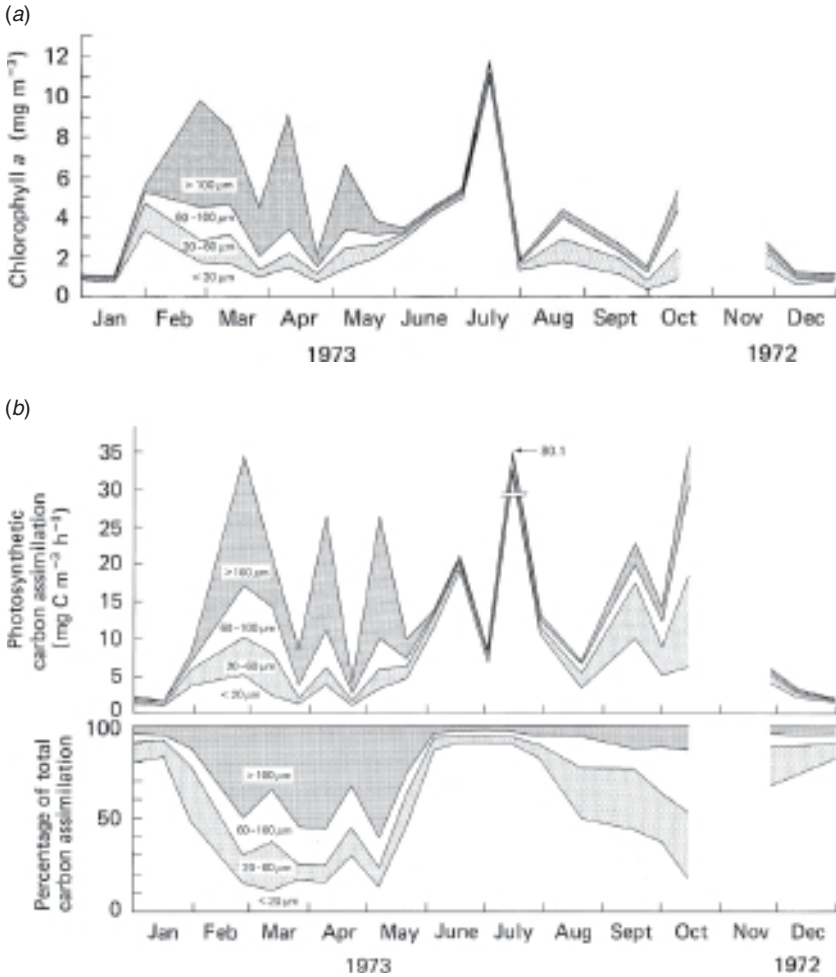


Fig. 12.17 Seasonal variation in the contribution of different size fractions of the phytoplankton to total biomass and to primary production in a north temperate coastal water (by permission, from Durbin, Krawiec and Smayda (1975), *Marine Biology*, **32**, 271–87). The data are for Narragansett Bay, Rhode Island, USA. (a) Cumulative graph of chlorophyll *a* content of the different size fractions. (b) Upper: cumulative graph of photosynthetic carbon assimilation (per unit volume) of the different phytoplankton size fractions. Lower: photosynthetic carbon assimilation by the different size fractions expressed as a percentage of assimilation by the total population.

$>100 \mu\text{m}$ ), mainly diatoms, dominated the winter–spring bloom, while small cells ( $<20 \mu\text{m}$ ), mainly flagellates, dominated the summer population. Even within given size classes the species composition changed with

time: for example, different diatom species were dominant in each of the three abundance peaks during the February to May period.

The photosynthetic capacity of the phytoplankton population in a Canadian Pacific coastal inlet was found by Hobson (1981) to rise rapidly many-fold from a very low value in March to April up to a peak in the June to August period, and then to decrease rapidly in the mid-August to September period, down to a very low value again in October. Although the measurements were carried out at the prevailing water temperature, and although  $P_m^*$  for any given species tends to increase with temperature (§11.3), it seemed that only a small part of the variation ( $\sim 17\%$ ) was accounted for by the changes in temperature. The major changes in  $P_m^*$  in early April and August/September coincided with changes in the taxonomic composition of the phytoplankton, this being dominated by unidentified nanoflagellates at times when photosynthetic capacity was low, and by diatoms (*Chaetoceros*, *Thalassiosira*) or dinoflagellates (*Gymnodinium*, *Peridinium*) when capacity was high. Hobson suggested that the nanoflagellates, which dominated the phytoplankton in the winter, were genetically adapted to conditions of short days and low irradiance.

Situations like these, with a continually varying species composition of the phytoplankton population, are probably the rule rather than the exception in fresh as well as marine waters and so any apparent seasonal adaptation of phytoplankton photosynthetic characteristics (after allowing for temperature effects) is in most cases attributable to changes in the algal species present, i.e. is phylogenetic rather than ontogenetic adaptation. It is possible, of course, that species such as *Skeletonema costatum*, which in many coastal waters are present in significant amounts throughout the year, do indeed adapt to the changing irradiance values, as they are known to do under laboratory conditions, but this is hard to demonstrate in the presence of all the other species. A further complication is that even within the population of a given phytoplankton species at a given geographic location there can be marked genetic heterogeneity, and changes in genetic composition through the seasons. By analysis of isoenzyme patterns and physiological characteristics of individual clones of *S. costatum* isolated from Narragansett Bay (RI, USA), Gallagher (1980, 1982) was able to show that the winter bloom populations of the diatom were on average genetically different from the summer bloom populations, although neither were genetically homogeneous.

In high-latitude and high-altitude lakes, the phytoplankton in the dim light under the ice in winter have a higher cellular chlorophyll content and a lower light-saturation intensity than the phytoplankton present in the

summer.<sup>660,668,1366</sup> In one such case, Lake Pääjärvi, Finland, different algal species were dominant at the different times of the year.<sup>660</sup> In an Austrian alpine lake, however, the species composition did not vary greatly through the year, being mainly dominated by the dinoflagellate species *Gymnodinium uberrimum*,<sup>1360</sup> and Tilzer and Schwarz (1976) attributed the much higher (two- to four-fold) chlorophyll content, and lower  $E_k$  values, of cells under the ice to actual adaptation within the species.

Evidence for comparatively short-term photosynthetic adaptation of phytoplankton, over periods of a few days, has come from a number of field studies.<sup>656,1063,1178</sup> Platt and Jassby (1976) found the value of  $\alpha$  for phytoplankton in Nova Scotia coastal waters to be correlated with the average solar irradiance over the previous three days. In Lough Neagh (N. Ireland) Jones (1978) found that the light saturation onset parameter,  $E_k$ , for the dominating blue-green algal population was positively correlated with the average daily irradiance over the previous five days, i.e. the higher the average irradiance in the previous five days, the higher the light intensity required to achieve saturation. The changes in  $E_k$  appeared to be due more to changes in  $\alpha$  (the initial slope of the  $P$  versus  $E_d$  curve) rather than in the light-saturated rate ( $P_m^*$ ) per mg chlorophyll ( $\alpha = P_m^*/E_k$ ). Since  $\alpha = \bar{\alpha}_\phi^* \phi_m$ , these changes can plausibly be attributed to an increase in the specific average absorption coefficient per unit chlorophyll, associated with a decrease in the cellular chlorophyll content at higher light intensity (§12.2). In view of the short time period during which the changes occurred, we may reasonably assume that they correspond to true ontogenetic adaptation within the species rather than to changes in the population structure.

Thus it may be that while there are substantial seasonal changes in the photosynthetic properties of the phytoplankton population as a whole, due to the succession of species, there are also, on a shorter time scale, adaptive changes in the photosynthetic properties of individual species, during the few weeks that they persist as significant members of the population.

## 12.6 Rapid adaptation of the photosynthetic system

Quite apart from the seasonal cycle in solar irradiance, there are of course extreme changes in the intensity of PAR every day: not only those due to the regular diurnal change in solar altitude, but also the rapid fluctuations in irradiance resulting from variations in cloud cover (Fig. 2.7).

### Flagellate migration

Within the illuminated water column, there is at a given time for any particular species in the phytoplankton population a particular depth at which the light intensity is optimal for photosynthesis: high enough to give the maximum rate without causing photoinhibition. This optimal depth will vary with solar altitude during the day. The ability to move within the water column to whatever depth suits it best would clearly be of advantage to an alga; many groups have this capability.

The possession of flagella is common in all the algal divisions other than the Rhodophyta, Phaeophyta, Bacillariophyceae and Cyanophyta. Vertical migration by flagellated cells has been studied most among the dinoflagellates. In some cases the behaviour pattern is for the cells to migrate downwards away from the surface as the light becomes more intense, towards noon, and then to ascend again during the remainder of the day and the night.<sup>124,1360</sup> Migration appears to be in part phototactic, but can be positive or negative within any given species, the direction of migration being determined by the light intensity at the water surface. For example, Blasco (1978) found that off the coast of Baja California, USA, the marine dinoflagellate *Ceratium furca* migrated towards the sea surface at 07:00 h when the solar irradiance was  $280 \text{ W m}^{-2}$ , but away from the sea surface at 12:00 h when the irradiance was  $900 \text{ W m}^{-2}$ .

Not all dinoflagellate species show a regular up-and-down diurnal migration but instead appear to use their powers of locomotion to move themselves to, and remain at, a particular depth. Heaney and Talling (1980) found that in Esthwaite Water, England, in the spring and summer, *Ceratium hirundinella* showed surface avoidance but not vertical migration. The dinoflagellate cells were found in maximum density at the depth 3 to 4 m, at which irradiance was reduced to about 10% of that penetrating the surface.

Patterns of dinoflagellate movement can be influenced by the availability of nitrate in the water. Cullen and Horrigan (1981) studied the movement of the marine species *Gymnodinium splendens* in a 2 m deep laboratory tank under a 12 h dark/12 h light regime. When nitrate was present throughout the container, the cells spent most of the day near the surface and most of the night at greater depth: they started swimming upwards before the end of the dark period and downwards before the end of the light period. When the nitrate in the water became depleted, the light-saturated photosynthetic rate per unit biomass decreased, and the cells formed a layer at a depth corresponding to the light level at which photosynthesis was saturated. The behaviour pattern of this species was also observed in the sea off the

California coast. During the night (01:10 h) the cells were at 18 m depth, in the region of the nitrocline (the layer in which nitrate concentration is rising from the low value in the upper waters to the high value of deep water). By 10:50 h in the morning the cells had moved up into nitrate-depleted water at 14 m, a depth at which the light intensity was sufficient to saturate photosynthesis. It therefore seems that *G. splendens* moves down at night to a depth where it can accumulate nitrogen and then up during the day to a depth where, although nitrate is lacking, it can photosynthesize at its maximum rate. Its behaviour may be chemotactic as well as phototactic.

Figueroa *et al.* (1998) studied the diel vertical migration of a number of flagellated phytoplanktonic species in a stable, well-stratified estuary, the Ria de Vigo, NW Spain. Each species had its own migration pattern. *Mesodinium rubrum*, which is a marine planktonic ciliate protozoan harbouring a reduced cryptophyte endosymbiont, was highly active: it was present in maximum concentration at the surface during the day, and was able to move down through the pycnocline during the night. A euglenoid flagellate, *Eutreptiella* sp., aggregated at the surface at noon, and migrated down through the pycnocline at night. Cells of the dinoflagellate, *Ceratium furca*, were present throughout the water column during the day, with a tendency to form a subsurface maximum at about 2 m depth in the afternoon, but were located below the pycnocline at dusk. Another dinoflagellate species, *Dinophysis acuminata*, aggregated at the surface at noon, and in the night migrated downward but was unable to cross the pycnocline and so remained mainly above the density gradient.

In lakes, a common (but not universal) flagellate behaviour pattern is for the cells to congregate in the surface water by day and migrate below the thermocline at night. Such behaviour has been described, for example, in the cryptomonad flagellate *Cryptomonas marssonii* in a Finnish brown-water lake,<sup>1165</sup> and in the colonial green flagellate *Volvox* in Lake Cahora Bassa (Mozambique).<sup>1264</sup> In both cases the adaptive significance was considered to be nutrient retrieval (in this case phosphate – generally the limiting nutrient in inland waters) from deep water at night, followed by a return to the illuminated, but nutrient-depleted, upper layer to photosynthesize during the day.

### Vertical movement by blue-green algae

Blue-green algae have a completely different mechanism for moving up and down in the water column, involving the formation and collapse of gas-filled vacuoles within the cells. A comprehensive account of these

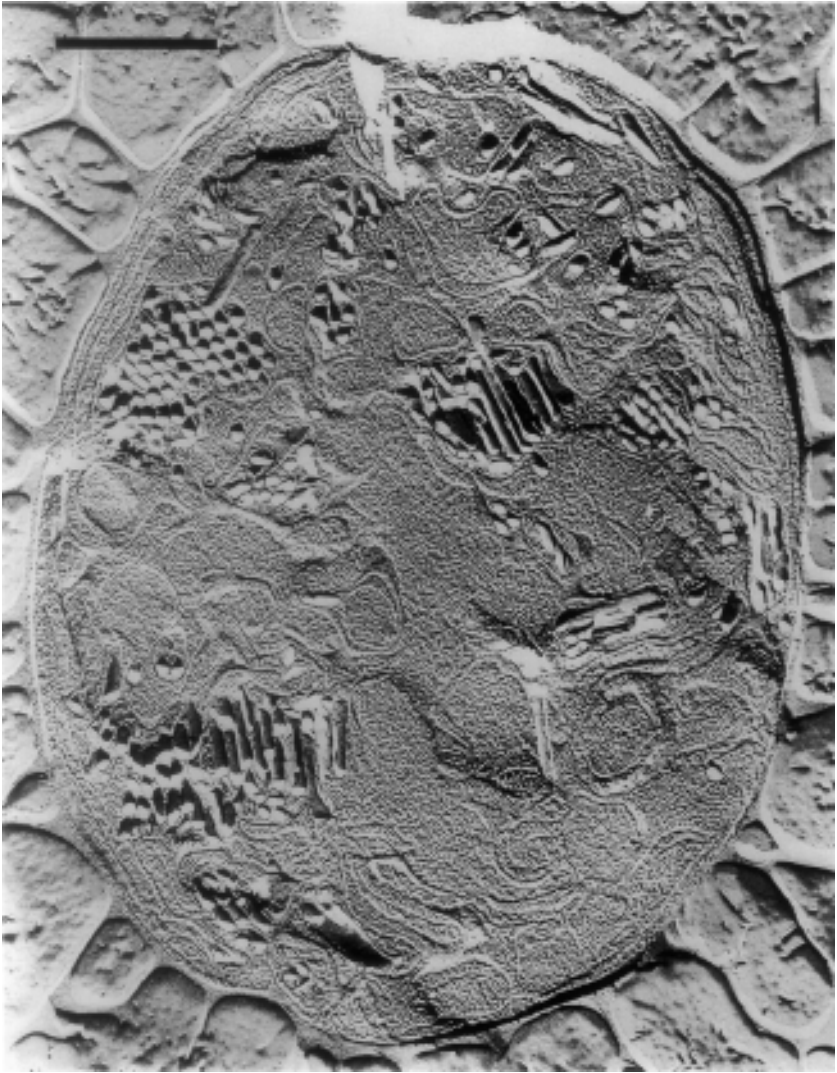


Fig. 12.18 Freeze-fractured cell of *Anabaena flos-aquae* showing cylindrical gas vacuoles longitudinally and in cross-section (by courtesy of Professor D. Branton). The bar corresponds to 1.0  $\mu\text{m}$ .

structures and their likely ecological significance may be found in the monograph on the blue-green algae by Fogg *et al.* (1973) and the reviews by Walsby (1975), Reynolds and Walsby (1975) and Oliver (1994).

The gas vacuoles (Fig. 12.18) are cylindrical structures about 0.07  $\mu\text{m}$  in diameter and of variable length, 0.3 to 0.4  $\mu\text{m}$  being common but up to

2  $\mu\text{m}$  being recorded. There are many in each cell. The membrane by which they are bounded is composed of protein, just one protein species, molecular weight 20.6 kDa, being present.<sup>1427</sup> The gas mixture within the vacuole is the same as that in the surrounding solution and at the same partial pressures. When the turgor pressure within the surrounding cytoplasm rises above a certain critical value, the gas vacuoles collapse. New vacuoles are formed by de novo synthesis rather than by re-inflation of collapsed vacuoles: small vesicles are formed first which then increase in length. Formation of gas vacuoles increases the buoyancy of the blue-green algal cells, making them float towards the surface: collapse of the vacuoles makes the cells sink. It is the gas-vacuole volume/cell volume ratio that determines whether, and how fast, the cells rise or sink, or remain at the same depth.

Vacuole formation is favoured by dim light, by a lack of inorganic carbon ( $\text{CO}_2$ ,  $\text{HCO}_3^-$ ) for photosynthesis, and by a sufficiency of inorganic nitrogen.<sup>402,732,1031,1433</sup> Under these circumstances photosynthesis proceeds rather slowly and the availability of nitrogen both facilitates the synthesis of vacuole membrane and diverts the products of photosynthesis towards the manufacture of cell materials rather than sugar accumulation. Having formed vacuoles, the cells float up towards the surface. With increased light intensity and  $\text{CO}_2$  availability (resulting from diffusion of atmospheric  $\text{CO}_2$ ), the rate of photosynthesis increases. If, as will commonly be the case, mineral nitrogen concentration decreases towards the surface, photosynthesis leads increasingly to sugar accumulation rather than cell growth, turgor pressure within the cell increases and, eventually, the vacuoles begin to collapse. Depending on how far this process goes the cells will either simply slow down in their upward motion and eventually come to a halt at a particular depth, or will begin to actually sink down again towards the deeper layers where nitrogen concentrations are higher. Thus gas-vacuole buoyancy control can be used to enable the blue-green algal population to find a particular depth that suits it and this is what seems to happen to forms such as *Oscillatoria*: these occur as small-diameter single filaments with high resistance to movement through the water, respond slowly to buoyancy changes, and so normally remain in a layer at a particular depth, usually several metres. Species with large colonies, on the other hand, can sink or rise rapidly through the water and since marked buoyancy changes can take place within time periods as short as an hour or so, can respond rapidly to changing conditions during the day. It is in the forms such as *Microcystis* and *Anabaena*, with large colonies, that the algae will frequently rise all

the way up to the surface under still conditions, forming the surface scums so commonly seen on eutrophic lakes in the summer. They are redistributed again from the surface either by collapse of the gas vacuoles or by wind action.

While it appears likely that in most cases the advantage conferred on blue-green algae by buoyancy control resides in the ability of the cells to locate themselves at a depth where light intensity is optimal, there is some evidence that the more rapidly moving forms, such as *Microcystis* and *Anabaena*, can indeed periodically sink down through the thermocline where, like the flagellates referred to earlier, they can take up phosphate before rising up to photosynthesize again in the illuminated, but nutrient-depleted, surface layer.<sup>432</sup> In hypertrophic Hartbeespoort Dam (South Africa), nutrients are always present in excess, but wind speeds and water turbulence are low, and enormous populations of *M. aeruginosa* develop. Zohary and Robarts (1989) attribute the success of this alga to its ability, by means of its strong buoyancy, to maintain itself in the shallow diurnal mixed layer that forms each day under the intense sunlight incident on this subtropical impoundment. Other, non-buoyant, species sediment through the density gradient and are lost. Modelling studies also indicate that the formation of diurnal mixed layers greatly favours positively buoyant algae such as *Microcystis*.<sup>601</sup> Being trapped near the surface in intense sunlight is, of course, a considerable hazard to phytoplankton. The Hartbeespoort *Microcystis*, however, appeared to be well adapted to intense light: it had a low cellular chlorophyll content and a high photosynthetic saturation irradiance ( $E_k$  up to  $1230 \mu\text{mol photons m}^{-2} \text{s}^{-1}$ ).<sup>1505</sup>

### Chloroplast movements

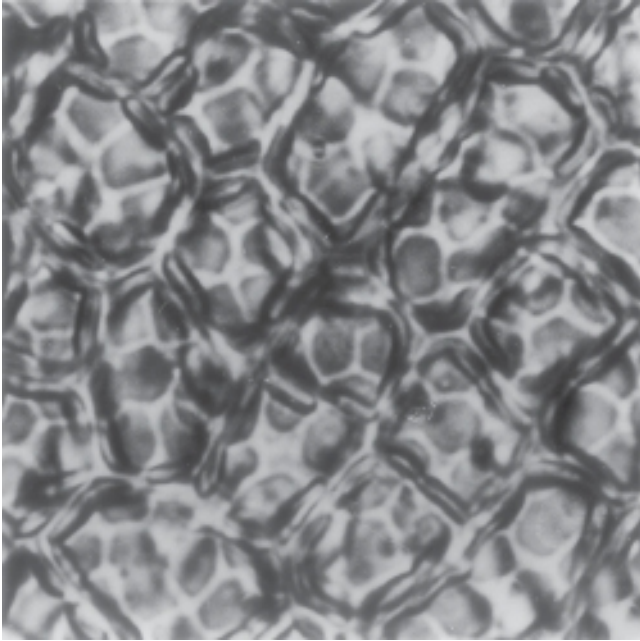
The rate of light collection by chloroplasts depends not only on their pigment complement but also on their position and orientation within the cell. In some aquatic plants this can vary with light intensity. Amongst the higher plants<sup>1415</sup> the general pattern of behaviour is that in low-intensity light the chloroplasts move to a position in the cell such that light absorption is maximized – they spread themselves out adjoining, and parallel to, those cell walls that face the incident light. In high-intensity light (saturating for photosynthesis), the chloroplasts move to a position such that light absorption is minimized, perhaps to reduce photoinhibition: they move away from that cell wall that is directly exposed to the light and align themselves adjoining, and parallel to, those cell walls that are most shaded, typically the side walls so that not only are

they edge-on rather than face-on to the light, but also some are shaded by others. In the case of the aquatic angiosperm *Potamogeton crispus*, growing in a Scottish loch, leaves collected from 0.25 m depth had their chloroplasts around the side walls of the cells, whereas leaves from 2.5 m depth had their chloroplasts distributed over the surface facing the light.<sup>1273</sup> An alternative way of reducing light collection in high-intensity light is for the chloroplasts to assemble in a cluster around the nucleus: this has been observed in leaves of the seagrass *Halophila stipulacea* growing at 0.5 m depth in the Mediterranean.<sup>323</sup> Sharon and Beer (2008) compared *H. stipulacea* plants grown under high light ( $450 \mu\text{mol photons m}^{-2} \text{s}^{-1}$  at midday) or low light ( $150 \mu\text{mol photons m}^{-2} \text{s}^{-1}$  at midday). At 06:00 h, before sunrise, the chloroplasts were evenly dispersed within the cytoplasm of the leaf cell. In the high-light plants, migration of the chloroplasts started at sunrise and the beginning of clumping was observed at 08:00 h. Full clumping had taken place by midday and continued throughout the afternoon. In the late afternoon the chloroplasts began to disperse through the cytoplasm, and full dispersal was achieved a few hours after sunset. In the low-light plants there was no clumping of chloroplasts during the day. In the high-light plants, chloroplast clumping was accompanied by a decrease in leaf absorptance from 0.56 in the early morning to 0.34 at midday, without any accompanying change in chlorophyll content. In plants of *H. stipulacea* in the Gulf of Aqaba (Red Sea), Schwarz and Hellblom (2002) found that chloroplast clumping in plants at 7 m depth reduced leaf absorptance to 55%, compared to 85% in plants at 30 m.

The action spectrum for chloroplast movement in higher plants has a peak in the blue region at about 450 nm: the photoreceptor may be a flavin or a carotenoid.<sup>544</sup> The mechanism may be related to that of cytoplasmic streaming: the chloroplasts appear to move together with the cytoplasm rather than through it.

Nultsch and Pfau (1979) studied chloroplast movements in a large number of littoral and sublittoral marine macroalgae. In most of the brown algal species, the chloroplasts moved to the cell walls facing the light at low irradiance and to the side walls parallel to the light direction at high irradiance (Fig. 12.19): the change from one position to the other took 1 to 2 h. No clear-cut light-induced movements of the chloroplasts were observed in the green or red algal species studied. In the siphonaceous green alga *Caulerpa racemosa*, which grows in tropical shallow water reef areas, Horstmann (1983) observed that in bright sunlight the chloroplasts are retracted from the fronds into the stolon.

(a)



(b)

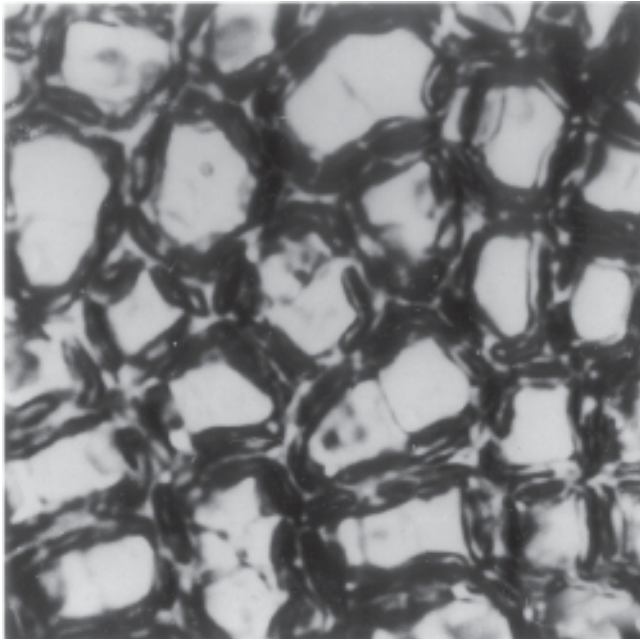


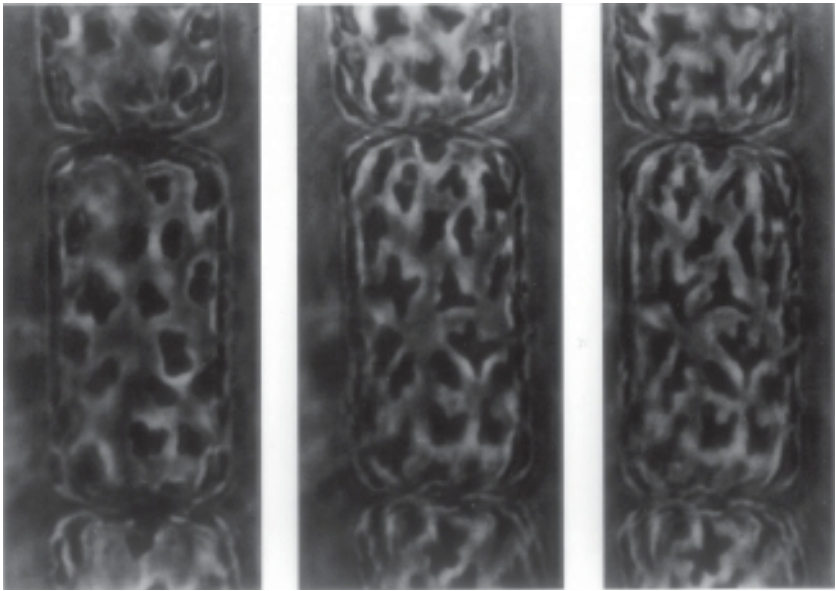
Fig. 12.19 Light-induced movement of the chloroplasts in the brown alga *Laminaria saccharina* (by permission from Nultsch and Pfau (1979), *Marine Biology*, **51**, 77–82). Arrangement of the chloroplasts in (a) low-intensity (1000 lux) and (b) high-intensity (10 000 lux) light. Magnification  $\sim 4000 \times$ .

In the filamentous green algae *Mougeotia* and *Mesotaenium*, which have a single, flat centrally located rectangular chloroplast in each cell, the characteristic movement of the chloroplast in response to a change in the light regime is to turn on its longitudinal axis, rather than to move around the wall. It turns face-on to moderate light, and edge-on to intense light. Haupt (1973) and coworkers have shown that the photoreceptor controlling this movement is phytochrome. In another filamentous, coenocytic alga, *Vaucheria sessilis* (Xanthophyceae), if the filament is illuminated at one point with low-intensity blue light, the chloroplasts and other organelles that are normally carried along by the streaming cytoplasm are caused to aggregate in the illuminated part of the cell.<sup>125</sup> The photosynthetic implications of this are not yet clear.

In the case of floating, planktonic algae, oriented at random with respect to the light, movement alone to one part of the cell or another is not likely – if the cell contains only one or a few chloroplasts – to make much difference to the rate of light collection. In some cases the chloroplast can reduce its absorption cross-section in bright light by shrinking: this has been observed in a dinoflagellate<sup>1329</sup> and in diatoms.<sup>537,686</sup> In the marine centric diatom *Lauderia borealis*, which has about 50 chloroplasts per cell, Kiefer (1973) observed that in the first 2 min of exposure to intense light ( $244 \text{ W m}^{-2}$ ) the chloroplasts contracted in size (Fig. 12.20a). During the following 30 to 60 min the chloroplasts, which in low light were distributed evenly around the periphery, moved to the valvar ends of the cell forming two aggregates of equal size (Fig. 12.20b). The changes in size and position of the chloroplasts were accompanied by a decrease of about 40% in the absorbance of the suspension at 440 nm (probably an underestimate since scattering always contributes some spurious absorbance): thus by a combination of shrinkage and aggregation this diatom is able to substantially reduce its rate of energy collection in bright light.

Stephens (1995) investigated light-induced chloroplast migration, and the associated spectral changes, in the dinoflagellate, *Pyrocystis lunula*, a species abundant in the tropical and subtropical areas of the ocean, which has large crescent-shaped cells. The cells were grown on a 12 h light: 12 h dark cycle. During the dark cycle the chloroplasts were located among cytoplasmic strands in the two distal portions of the cell (the ‘horns’ of the crescent), and were absent from the granular central area of the cell. When cells were removed from the dark and placed in the light beam of the microscope, the chloroplasts began to move and after 2 to 3 min were aggregating in the central area of the cell. The absorption spectrum of the

(a)



(b)

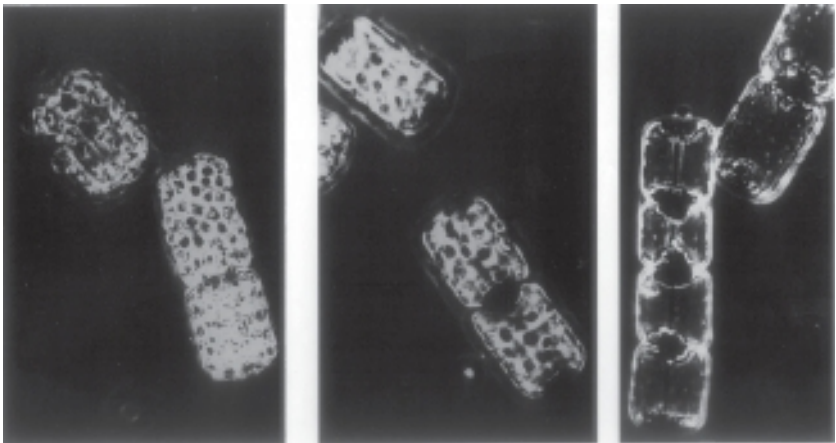


Fig. 12.20 Chloroplast shrinkage and aggregation induced by high light intensity in the marine diatom *Lauderia borealis* (by permission, from Kiefer (1973), *Marine Biology*, **23**, 39–46). In each case the series of micrographs shows increasing light-induced change from left to right. (a) Contraction of chloroplasts. (b) Movement of chloroplasts to valvar ends of the cell, followed by aggregation.

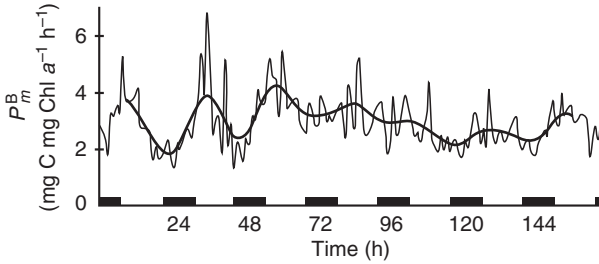


Fig. 12.21 Diurnal rhythm in the photosynthetic capacity ( $P_m$ ) of phytoplankton in the St Lawrence estuary, Canada, over a seven-day period (by permission, from Demers and Legendre (1981), *Marine Biology*, **64**, 243–50).

aggregated chloroplasts in the centre of the cell showed a more marked package effect, i.e. flattening of the peaks, than chloroplasts in the distal regions of the cell. In this case also, chloroplast movement has the effect of reducing the rate of energy collection in bright light.

### Rhythms in the photosynthetic system

Diurnal rhythms in photosynthetic capacity (photosynthetic rate per unit biomass at light saturation) have been described for phytoplankton<sup>318,530,1085,677,858</sup> (reviewed by Sournia, 1974, and Prezelin, 1992) and for multicellular benthic algae.<sup>167,461,665</sup> Photosynthetic capacity rises, often several-fold, during the early part of the day to a maximum that can be reached any time from about mid-morning to mid-afternoon and then declines during the rest of the day and remains low during the night. Figure 12.21 shows the time course of variation in  $P_m^*$  for the phytoplankton in the St Lawrence estuary during the course of a week.<sup>302</sup> In some species, both benthic and planktonic, it has been shown that this diurnal variation is not directly controlled by environmental parameters but is a true circadian rhythm that continues for several cycles in cells kept in the dark.

With cultures, a daily periodicity in  $P_m^*$  has been shown to be present in some, but not all, marine diatom, dinoflagellate and chrysophyte species:<sup>529</sup> the species that showed no day/night differences in  $P_m^*$  were small, rapidly dividing types, whereas larger, slower growing cells almost uniformly showed marked changes. Detailed studies of this rhythm in marine dinoflagellates have been carried out by Sweeney and coworkers. The photosynthetic rate per cell in cultured *Glenodinium* and *Ceratium*

varies two- to six-fold during the cycle, when measured under light-limiting as well as light-saturating conditions.<sup>1084,1086</sup> The fact that the rate variation occurs under light-limited conditions led Prezelin and Sweeney (1977) to conclude that it is variation in the light reactions rather than the dark reactions of photosynthesis that are primarily responsible for the diurnal rhythm: it had previously been shown that carboxylase activity does not vary during the cycle.<sup>190</sup> There is no significant change in the pigment content or the absorption spectrum of the cells during the cycle, but the initial slope ( $\alpha$ ) of the photosynthesis versus irradiance curve varies in parallel with the photosynthetic capacity. This implies that the quantum yield of photosynthesis – the efficiency with which the cells use the quanta that have absorbed – changes in a cyclical manner. For natural phytoplankton populations also, off the Southern California coast, Harding *et al.* (1982a) found that  $\alpha$  and  $P_m^*$  varied (three- to nine-fold) in parallel during the day: this applied to both diatom- and dinoflagellate-dominated assemblages. Changes in chlorophyll content were much smaller and did not correlate with the changes in photosynthetic activity (which was, in any event, expressed per unit chlorophyll). Prezelin and Sweeney suggest that there is a cyclical variation in the proportion of the total photosynthetic units present that are functional.

In the multicellular brown alga *Spatoglossum pacificum* the mechanism may be different. There is evidence that the approximately two-fold daily variation in photosynthetic capacity in this alga is due to variation in the activity of the CO<sub>2</sub>-fixing enzyme system.<sup>1480</sup> In the tropical red macroalga, *Kappaphycus alvarezii*, grown on a 12 h light: 12 h dark cycle, Granbom *et al.* (2001) observed a regular rhythm in photosynthetic activity, consisting of an increase in oxygen evolution rate towards noon, followed by a decrease of about one third in the afternoon. When the plants were transferred to continuous light the circadian rhythm in photosynthetic activity continued, with a period of ~19 to 23 h, for several cycles. Schubert *et al.* (2004) found that the diminution in O<sub>2</sub> evolution in the afternoon was accompanied by decreases in both photosynthetic capacity ( $P_m^*$ ) and  $\alpha$ , and these continued to decrease (when measured in the light) during the 12 h dark period, levelling off at their minimum values about half way through. The troughs in the continued rhythm of photosynthetic activity in continuous light were also accompanied by drastic falls in photosynthetic capacity ( $P_m^*$ ) and  $\alpha$ . The fall in  $\alpha$  was proportionately greater than the fall in  $P_m^*$ , so that the light saturation onset parameter,  $E_k$  (which is equal to  $P_m^*/\alpha$ ), rose to a peak in each trough of the cycle. Since  $\alpha = \bar{\alpha}_\phi^* \phi_m$  (§10.3), the cyclical decrease in  $\alpha$  must

correspond to a cyclical decrease in the quantum yield of photosynthesis or of the specific absorption coefficient of the alga (§9.4) for PAR ( $\text{m}^2 \text{mg chl } a^{-1}$ ). Pigment ratios (chl *a*/phycoerythrin, chl *a*/carotenoid) did not change during the cycle, indicating that it was the quantum yield that was changing. Fluorescence emission spectra of frozen samples indicated that in the troughs of the cycle the phycobilisomes were, proportionately, transferring much more of their energy to photosystem II than to photosystem I. The fundamental mechanism underlying this circadian rhythm remains unclear: changes in the quantum efficiency of photosystem II or I, and/or changes in excitation energy distribution to the reaction centres, are possibilities, but a cyclical change in carboxylase (which was not measured) is also a possibility.

The red alga, *Grateloupia turuturu*, shows a similar circadian rhythm in photosynthetic activity to that described above for *Kappaphycus*. Goulard *et al.* (2004) investigated the concurrent changes in the levels of the gene transcripts (mRNA) encoding the  $\alpha$  and  $\beta$  subunits of phycoerythrin and subunits of Rubisco. Abundance of both transcripts exhibited diurnal and circadian changes, implying control of transcription by the circadian clock. In light–dark cycles the Rubisco transcript peaked around midday, and the phycoerythrin transcript peaked between midday and afternoon. The authors suggest that the correlation of the oscillations of mRNA abundance with the rhythm of photosynthetic oxygen evolution is likely to be of physiological relevance.

What, if any, advantage algae derive from cyclical variations in their photosynthetic capability remains unknown. Conceivably, after the main photosynthetic period is finished each day, certain proteins of the photosynthetic apparatus might be broken down so that their amino acids can be used for other cellular purposes: the proteins would then be resynthesized each morning. These daily variations in photosynthetic properties may affect the amount of primary production that is actually carried out. The effect of variation in light-saturated photosynthetic rate may be, at least in part, offset by the fact that solar irradiance itself varies roughly in parallel. The rate of light-limited photosynthesis also shows diurnal variation, however, and this may reduce the amount of primary production that the cells achieve early and late in the day. Harding *et al.* (1982b) calculated, for Californian coastal phytoplankton, that as a result of the daily periodicity in the parameters of the photosynthesis versus irradiance curves, the primary production achieved would be 19 to 39% less than if the values of  $P_m^*$  and  $\alpha$  remained constant all day at their maximum values.

In calculations of integral daily photosynthesis, although the diurnal variation of solar irradiance is taken into account, it is commonly assumed that the values of  $\alpha$  and  $P_m^*$  observed at midday apply throughout the day. Making this assumption for the Californian phytoplankton yielded values for daily integral photosynthesis ranging from 15% greater to 20% less than values calculated taking account of periodicities in  $\alpha$  and  $P_m^*$ . The variation in size and direction of the discrepancy is caused by variation in the timing of the photosynthetic activity maximum: when this is not at midday, the midday values of  $\alpha$  and  $P_m^*$  come closer to the mean values, and so the errors may not be so great. For phytoplankton in the St Lawrence estuary (Canada), Vandavelde *et al.* (1989) found that calculations of integral daily photosynthesis made using the midday values of  $\alpha$  and  $P_m^*$  gave production estimates 15 to 43% greater than those that took into account the variation in these photosynthetic parameters during the day.

Ramus and Rosenberg (1980) measured the actual photosynthetic rate of five intertidal species (two green, two brown, one red) at hourly intervals during the day in seawater tanks (such that  $E_d$  was 70% of the subsurface value) exposed to ambient sunlight. The most common behaviour pattern on sunny days was for the photosynthetic rate (per unit chlorophyll *a*) to reach its peak in the morning, while solar irradiance was still well below its daily maximum, to decline somewhat during the middle part of the day under the most intense Sun, and then sometimes to show a partial recovery late in the afternoon, before declining again to zero, with falling light levels, towards sunset. Ramus and Rosenberg concluded that an afternoon depression in photosynthesis must be of normal occurrence (on sunny days) in these five species in their intertidal habitat. On cloudy days, when light saturation does not occur, the curve of photosynthetic rate is approximately symmetrical about the time of the Sun's zenith, and in the case of the most light-sensitive species (the rhodophyte *Gracilaria foliifera*) it seemed that total daily production would actually be higher than on sunny days. The characteristic sunny-day diurnal pattern observed in this work is likely to result from the simultaneous operation of a number of independent processes, particularly photoinhibition coming into operation when solar intensities are at their highest, together with the underlying circadian rhythm in photosynthetic capacity with its pre-midday morning peak.<sup>167,665</sup>

Although, as we have seen, no diurnal fluctuation in pigment content was observed in marine dinoflagellates under laboratory conditions, Yentsch and Scigel (1958) have described such a fluctuation in a natural

phytoplankton population dominated by diatoms. In a North American coastal (Pacific) water they found that the chlorophyll content per cell fell by 50 to 60% during late morning, remained approximately constant during the afternoon, and then rose again during the evening. Auclair *et al.* (1982) studied fluctuations in chlorophyll content of estuarine phytoplankton under semi-natural conditions. Water from the St Lawrence estuary was transferred to a 1200 litre tank, exposed to sunlight and the chlorophyll content per litre of water was followed over the next 45 h. Cell numbers showed little change. Chlorophyll content fluctuated up and down in a cyclical manner, through an approximately two-fold range with maxima in chlorophyll content occurring about every 6 h. Auclair *et al.* were able to correlate the variation in pigment content with tidal movements. Assuming the rhythm in the tank was a continuation of that in the estuary, it seemed that the times of maximum chlorophyll content corresponded to the periods of maximum current speed and turbulence and therefore probably, as a result of enforced circulation, to periods of lower average irradiance on the cells. The times of minimum chlorophyll content corresponded to periods of slack water in which a stability gradient was established resulting in a higher irradiance on the cells. It makes sense that the cells should increase their light-harvesting capacity during periods of low light intensity: what is noteworthy about this system is that they do it so rapidly, doubling their chlorophyll content in 2 to 3 h. Regular cyclical changes in phytoplankton pigment content may be more common in nature than we realize. The patchiness of the horizontal distribution of phytoplankton and the additional complicating factor of water movement make it difficult to unequivocally demonstrate such changes in large water bodies.

## 12.7 The microphytobenthos

All benthic sediments – whether in tidal mudflats, surf beaches, coral reef lagoons, shallow coastal waters – which receive significant amounts of light, contain communities of microalgae. This benthic community, in any given aquatic ecosystem, is referred to as the *microphytobenthos*, or sometimes, *epipelon*. A full account of the epipelon is given in Round's (1981) book, *The Ecology of Algae*. The microphytobenthos usually consists predominantly of diatoms, but cyanobacteria, dinoflagellates and euglenophytes can also be prominent components.

Planktonic diatoms are unable to move within the water, although they of course undergo passive movement determined by sinking and turbulence. On surfaces, however, diatoms can move by a mechanism involving secretion of mucilage. Diatoms in sediments, both in fresh and marine waters start to move up to the surface of the sediments before dawn.<sup>196,1152</sup> In the afternoon the cells begin to migrate down into the sediments again, this movement continuing during the first few hours of darkness. In the case of benthic diatoms in a freshwater lake it was found that they would not leave the surface of the sediments for as long as these were illuminated at 750 lux, but migrated downwards again at light intensities of 75 lux or lower.<sup>532</sup> The advantage of moving up onto the illuminated surface during daylight is clear enough: what is less obvious is the benefit the cells derive from burrowing down into the sediments during the hours of darkness – the greater availability of mineral nutrients is a possible explanation.

In turbid estuarine waters, the arrival of the flood tide causes a marked reduction in light intensity. Diatoms in tidal mudflats where the water is turbid can show a tidal rhythm superimposed on the diurnal one. In the River Avon estuary, England, 1 to 2 h before tidal flooding of the sediment at any particular point, the diatoms burrow beneath the surface again: the disappearance of the green or brown film of algae on the surface of the mud moves as a wave along the banks in advance of the tide.<sup>1153</sup> In contrast, in the clear water of the River Eden estuary, Scotland, the movement of the benthic diatoms was found to be strictly diurnal.<sup>1047</sup> In a tropical intertidal mudflat (Goa, India) Mitbavkar and Anil (2004) found the vertical movement of benthic diatoms to be controlled by both light and the tidal cycle, with light being the overriding influence, but continuous darkness under laboratory conditions induced a tidal rhythm. Diurnal movements onto the surface during the day and down into the sediments during darkness occur with benthic euglena and other flagellates, and blue-green algal species, as well as diatoms. Like other plants, benthic microalgae are susceptible to photoinhibition at high light intensities. They can avoid this by downward migration and a midday diminution of cell numbers at the sediment surface has been found both with euglenoids and diatoms.<sup>1153,692</sup>

Light penetrates better into sandy sediments than into mud. In intertidal flats in the submerged Wadden Sea (Germany), Billerbeck *et al.* (2007) found that the depth-integrated scalar irradiance (a measure of the total light available for photosynthesis within the sediment) was 2.04 and 3.45 times as high in fine and coarse sand, respectively, as in mud.

The gross photosynthesis per unit area was about four times as high in the fine sand, and ten times as high in the coarse sand, as in the mud, even though the chlorophyll concentration per unit area was somewhat higher in the mud. Paterson *et al.* (1998) found that PAR consistently declined to <30% of the surface value within 1000  $\mu\text{m}$  of the surface in intertidal mudflats in the Humber estuary (England), and the euphotic zone ( $E_0[\text{PAR}]$  down to 1%) was limited to the upper 1800  $\mu\text{m}$ . Some areas of sediment in this estuary were dark brown in colour, and were dominated by diatoms; others were light or dark green, and were dominated by euglenids. In intertidal sediments in the Tagus estuary (Portugal) in July, Cartaxana *et al.* (2006) found that at muddy sites most of the chlorophyll was found in the top 500  $\mu\text{m}$ , whereas in sandy locations relatively constant concentrations were found throughout the sediment profile, down to at least 3.25 mm. Diatoms were the dominant microalgae, but cyanophytes and euglenophytes were also present. Glud *et al.* (1999) studied a 5 cm thick microbial mat from a hypersaline salt marsh in Egypt. At its surface, a thin layer of diatoms covered a dense 2 mm thick layer of cyanobacteria (*Microcoleus* sp.). In terms of oxygen metabolism, three zones were recognized: the upper, diatom zone with a moderate net  $\text{O}_2$  production; the cyanobacterial zone with a high net  $\text{O}_2$  production; and a lower zone with disintegrating microalgae and cyanobacteria, and a high  $\text{O}_2$  consumption rate.

In estuaries and shallow coastal waters, the microphytobenthos can contribute a substantial proportion of total primary production (reviewed in Cahoon, 1999). Photosynthesis is limited by the extent to which light penetrates to the sediment surface, and this is in turn limited by the depth and the optical properties of the water column. For coastal waters of the northern Adriatic Sea, Blackford (2002) calculated, using numerical modelling, that the microphytobenthos contributed more than 50% of primary production in shallow waters (<5 m depth), but net primary production decreased to zero at 25 m depth. In the eutrophic Gulf of Fos, NE Mediterranean Sea, Barranguet *et al.* (1996) found that although the microphytobenthic biomass per unit area, 27 to 379  $\text{mg chl } a \text{ m}^{-2}$ , exceeded the phytoplanktonic biomass, photosynthetic oxygen production by the microphytobenthos, consisting mainly of pinnate diatoms, exceeded that of the phytoplankton only in waters less than 1 m deep. In shallow (5–15 m) coastal waters of the western Seto Inland Sea, Japan, Yamaguchi *et al.* (2007) found that the increased light attenuation coefficient associated with increased concentration of phytoplankton caused a decrease in the light flux reaching the sea floor, and that the

microphytobenthic biomass ( $1.9\text{--}46.5\text{ mg chl } a\text{ m}^{-2}$ ) within the upper 10 mm of the sediment was inversely correlated with the phytoplanktonic biomass ( $10.9\text{--}65.0\text{ mg chl } a\text{ m}^{-2}$ ) in the overlying water column. They concluded that interception of light by phytoplankton was the main cause of the variation in microphytobenthic biomass. At 17 m depth in the Gulf of Trieste (northern Adriatic Sea), Cibic *et al.* (2008) observed that microphytobenthic primary production was low or negative in the September to December period, and inferred that during these months, associated with low PAR, there was a shift by the benthic microalgae from autotrophic to heterotrophic metabolism. For the shallow (50% <5 m depth) Bay of Brest (France, West coast), Ní Longphuirt *et al.* (2007) estimated average annual production by the microphytobenthos to represent 12 to 20% of total primary production for the ecosystem. In the Ems estuary (Netherlands/Federal Republic of Germany) the microphytobenthos of the tidal flats contributes  $\sim 25\%$  to the total annual primary production.<sup>294</sup>

It is frequently the case in shallow water coral reefs that large areas are occupied by unconsolidated calcareous sediments. The microphytobenthos at Heron Reef (Great Barrier Reef, Australia) was found by Werner *et al.* (2008) to be dominated by diatoms, dinoflagellates and cyanobacteria, and in these permeable, coarse-grained sediments, algal pigments were detectable down to a depth of about 8 cm. Net photosynthesis in the sediments was detectable down to depths of 0.5 to 2.0 cm, depending on the site, and was strongly correlated with chlorophyll *a* content, which varied from 31 to  $84\text{ mg m}^{-2}$ . The authors estimated that the microphytobenthic production for the entire reef was of the same order of magnitude as that of coral.

The algal cells of the microphytobenthos can be suspended into the overlying water column by tidal movement of,<sup>57</sup> or wind-induced turbulence in,<sup>294</sup> the water. In the Ems estuary (Netherlands/Federal Republic of Germany) De Jonge and Van Beusekom (1992) estimated that suspended microphytobenthos (mainly diatoms) made up  $\sim 22\%$  of the total phytoplankton in the lower reaches, and  $\sim 60\%$  in the upper reaches. For the whole estuary they estimated that over 30% of the total chlorophyll *a* in the water column originated as suspended microphytobenthos. In shallow coastal water over mudflats in the Ariake Sea, Japan, Koh *et al.* (2007) found that there was a substantial entrainment of sediment microalgae to the water column during the flood tide, and that as much as  $\sim 66\%$  of the chlorophyll *a* in the water column could be derived from the microphytobenthos.

As is the case with the phytoplankton, a major control of microphytobenthic production is grazing by animals. Gastropods, bivalves and polychaete worms, together with the smaller meiofauna, and also some fish (mullet), consume the microalgae of the sediments. When they are suspended into the water column they become an important food source for calanoid copepods.

An underwater microalgal community with some similarities to the microphytobenthos is the community of epiphytes – typically dominated by diatoms, but with filamentous green algae becoming more prominent in eutrophic waters – growing on the surface of the leaves of seagrasses in estuaries, or of freshwater angiosperms in lakes. Where cover is thick, epiphyte productivity can be as much as 60% of the above-ground productivity of the seagrass itself.<sup>565</sup> A limiting factor on epiphytic production is grazing by gastropod molluscs, and crustaceans such as amphipods, which consume the epiphyte layer but not the leaf tissue underneath.

## 12.8 Highly productive aquatic ecosystems

To achieve a high rate of primary production, an aquatic plant community must achieve a high rate of collection of light energy and an efficient utilization of this absorbed energy by its photosynthetic system, followed by conversion of photosynthate to new cell material. In this section we are concerned with the ways in which some natural and man-made ecosystems manage to do this.

We have discussed earlier (Chapters 3, 9 and 10), the major limitation on aquatic photosynthesis imposed by the fact that the plants have to compete for photons with the other light-absorbing components – water, CDOM, tripton – present in the aquatic medium. The most effective strategy that aquatic plants can follow to minimize the extent to which their photosynthesis is limited by lack of light is to attach themselves to surfaces at depths sufficiently shallow to ensure that for most of the day sufficient light is available to permit active photosynthesis. By ‘choosing’ to be benthic rather than planktonic, plants avoid the problem of being carried by water circulation down to depths where the light is insufficient for growth. Furthermore, the attached benthic flora can, as a consequence of water movement (tides, currents, wind-induced circulation), exploit the nutrients in a much larger volume than that in its immediate vicinity at any moment. The non-motile members of the phytoplankton,

by contrast, are carried around in the moving mass of water and so have less opportunity to find new nutrient supplies. The rooted members of the benthic flora – seagrasses in marine waters and the various kinds of aquatic angiosperms in fresh waters – have the additional advantage that they can derive nutrients from the sediments in which they are growing.

It is thus not surprising that the most productive natural aquatic plant communities are benthic. In marine waters the most productive systems are brown algal beds, seagrass beds and coral reefs. The kelps, brown algae of the genera *Laminaria* and *Macrocystis*, form dense forests in the sublittoral zone of rocky coasts in cool waters. According to Mann and Chapman (1975), these plants achieve annual net production rates in the range 1000 to 2000 g C m<sup>-2</sup>. The intertidal brown seaweeds such as *Fucus* and *Ascophyllum* in temperate and subarctic latitudes have annual net production rates of 500 to 1000 g C m<sup>-2</sup>. Tropical sublittoral seagrass beds dominated by the genus *Thalassia* achieve annual net production rates of 500 to 1500 g C m<sup>-2</sup> and in temperate waters, beds dominated by genera such as *Zostera*, fix in the range of 100 to 1500 g C m<sup>-2</sup>. In *Posidonia oceanica* meadows in the Mediterranean, Pergent *et al.* (1997) estimate that 32 to 36% of the carbon fixed annually is stored in the sediments in the form of rhizomes and attached leaf sheaths. For the globe as a whole, Duarte and Chiscano (1999) calculate, on the basis of literature data for 30 species, an average seagrass annual production of 1012 g dry weight m<sup>-2</sup> yr<sup>-1</sup>, corresponding to ~340 g C m<sup>-2</sup> yr<sup>-1</sup>. They estimate that the average surplus carbon produced by seagrasses globally is about 0.16 Gt per year, which corresponds to 15% of the total excess carbon produced in the global ocean (i.e. the net CO<sub>2</sub> uptake by oceanic biota).

In coral reefs primary production is carried out by multicellular algae and seagrasses, as well as by the symbiotic zooxanthellae living within the cells of the coral. Total annual primary production on coral reefs is typically in the range of 300 to 5000 g C m<sup>-2</sup>.<sup>801.968</sup>

If the immediate products of photosynthesis, which are carbohydrate in nature, are to be used for cell growth and multiplication, proteins, nucleic acids and other cell constituents must be synthesized, for which mineral nutrients are required. A problem faced by aquatic plants is that at the time of year when high solar altitude favours photosynthesis in any one species, it favours it in all so that the period of maximum potential primary production is also a period of low nutrient levels in the water. Certain productive brown algae in the genus *Laminaria* circumvent this problem by separating the period of maximum growth from that of

maximum photosynthesis.<sup>667,831,862</sup> In the summer, the plants accumulate photosynthate in the form of mannitol and laminaran, but grow only slowly. In the winter, although the light intensity is low, the nutrient levels in the water are at their highest and this is when the kelps grow rapidly at the expense of their stored carbohydrate.

Taking the world ocean as a whole, most of the primary production is carried out by phytoplankton. Within coastal embayments and estuaries, however, it is commonly the case that the benthic macrophytes account for most of the primary production. For St Margaret's Bay, Nova Scotia, Canada, Mann (1972) found that seaweed (mainly brown algae) productivity averaged over the whole 138 km<sup>2</sup> of the bay was 603 g C m<sup>-2</sup> yr<sup>-1</sup>, compared to 190 g C m<sup>-2</sup> yr<sup>-1</sup> for phytoplankton. In the Newport River estuary, North Carolina, USA, the contribution of seagrasses to annual primary production was estimated to be 2.5 times that of phytoplankton.<sup>1350</sup>

Beds of submerged macrophytes in inland waters have productivities comparable to those of marine macrophytes. In the temperate zone, values range from below 10 to about 500 g C m<sup>-2</sup> yr<sup>-1</sup>, whereas in tropical regions annual production may exceed 1000 g C m<sup>-2</sup>.<sup>1455</sup>

The major factor responsible for the lower productivity of the phytoplankton, compared to the benthic plants, is, as we have noted, the lower average irradiance they receive as a consequence of vertical circulation. One solution to this problem, adopted by the blue-green algae (§12.6), is the evolution of a flotation mechanism enabling the algae to move vertically within the water to a depth that suits them, without (as in the dinoflagellates) the need for continual expense of energy to drive flagella. This may in part account for the fact that the natural water bodies with the highest phytoplankton productivity are dominated by blue-green algae: annual net yields from such water bodies are commonly in the region of 300 to 1000 g C m<sup>-2</sup> but values in the region of 2000 g C m<sup>-2</sup> have been reported.<sup>520</sup>

The circulation problem is also in some measure solved if the water body is very shallow, so that the cells never get very far away from the light. This is the solution generally adopted in man-made high-yield aquatic ecosystems such as sewage oxidation ponds or algal mass culture systems<sup>1342</sup> in which a high rate of phytoplankton primary production is the aim: depths of 10 to 90 cm are commonly used. It is generally arranged in such systems that mineral nutrients are available in excess, so that the rate of primary production is limited by the rate of supply of PAR, and sometimes also of CO<sub>2</sub>, to the system. Bannister (1974a, b, 1979) has

developed a theoretical treatment of phytoplankton growth under mineral nutrient- and CO<sub>2</sub>-saturated conditions by means of which the steady-state growth rate can be expressed as a function of the incident irradiance and the photosynthetic and respiratory characteristics of the cells. Goldman (1979a, b) has comprehensively reviewed the topic of outdoor mass culture of algae. He concludes that yields in excess of 30 to 40 g dry matter m<sup>-2</sup> day<sup>-1</sup> (equivalent to ~5000 to 7000 g C m<sup>-2</sup> yr<sup>-1</sup>) are unlikely to be exceeded: to date, such rates have been achieved only for short periods (less than a month), and over the long term, yields of 10 to 20 g m<sup>-2</sup> day<sup>-1</sup> are more typical. A crucial limiting factor in such systems is light saturation of photosynthesis. Even in the very dense algal suspensions that develop, the cells near the surface are exposed to irradiances well above their saturation points. Of the three requirements for high productivity listed at the beginning of this section, such cells will have a high rate of collection of light energy, and (given the plentiful nutrient supply) rapid conversion of photosynthate to new cell material: what they will lack is efficient utilization of the absorbed energy in photosynthesis, since their carboxylation system will be unable to keep pace with the high rate of arrival of excitation energy. The inability of algae to increase their photosynthetic rate linearly with irradiance all the way up to full sunlight is likely to remain an insuperable obstacle in the path of increasing yields from outdoor mass culture. To develop, by mutation or genetic engineering, algal types with increased carboxylase and lowered pigment content would not be a solution, because such cells would be poorly adapted to the lower light intensities existing at greater depths. It is essential that the algal suspension should be sufficiently deep and dense to absorb nearly all the light incident upon it. This means that a gradient of irradiance, from full sunlight to near darkness, must exist within the suspension, and no one type of alga can be optimally adapted to all the intensities present. In principle, a laminar arrangement with a range of algal types stacked one above the other in thin layers separated by transparent boundaries, with the most Sun-adapted type at the top and shade-adapted type at the bottom, could increase the yields, but the technical problems and capital cost would be considerable.

Krause-Jensen and Sand-Jensen (1998) have sought, on the basis of a wide-ranging literature review, to determine whether general relationships between chlorophyll concentration, light attenuation and gross photosynthesis, across phytoplankton communities, macrophyte stands and microalgal mats can be arrived at. In the sea, phytoplankton chlorophyll *a* concentrations are typically in the range 0.02 to 0.2 mg m<sup>-3</sup>

in the oligotrophic regions,  $0.5$  to  $10.0 \text{ mg m}^{-3}$  in productive waters (upwelling regions, eutrophic coastal) and somewhere in between in the mesotrophic regions. In eutrophic inland waters, chlorophyll *a* concentrations can rise to  $100 \text{ mg m}^{-3}$  or more. For macrophyte stands, Krause-Jensen and Sand-Jensen estimate the volumetric chlorophyll *a* concentrations to be in the range  $200$  to  $15\,000 \text{ mg m}^{-3}$ . Benthic microalgal mats had the highest chlorophyll *a* concentrations – up to  $700\,000 \text{ mg m}^{-3}$ . Along with increasing chlorophyll concentration, the photic zone diminishes from  $>100$  m in sparse phytoplankton communities, to centimetres/metres in macrophyte stands, down to  $<1$  mm in dense microalgal mats. The compression of the photic zone is accompanied by a corresponding increase in the rate of photosynthesis per unit volume. Integral photosynthesis (photosynthesis per unit area), however, has an upper limit of  $\sim 60 \text{ mmol O}_2 \text{ m}^{-2} \text{ hr}^{-1}$ , at midday, this being achieved by dense macrophyte and phytoplankton communities in which most of the incident light is captured by the plants. Benthic microalgal mats do not appear to be able to attain quite such high rates, being apparently unable to exceed  $\sim 38 \text{ mmol O}_2 \text{ m}^{-2} \text{ hr}^{-1}$ . In the dense phytoplankton and macrophyte communities, maximum integral photosynthesis seems already to be achieved when the plants capture as much as 50% of the incident light, no further benefit being obtained by higher proportional light capture, suggesting that other factors such as  $\text{CO}_2$  exchange limit integral productivity at high plant densities.

A particular type of productive aquatic system that has become more common in recent decades is that referred to as *harmful algal blooms* (HABs), or sometimes as *red tides* or *brown tides*, although not all red or brown tides are harmful. Of the 60 to 80 phytoplankton species that have been reported to be harmful, 90% are flagellates, mainly dinoflagellates.<sup>1233</sup> It is the peridinin or fucoxanthin pigments of the algae that impart the characteristic colour to the water. The topic has been reviewed in a special issue, *The ecology and oceanography of harmful algal blooms*, of *Limnology and Oceanography* (Vol. 42, No. 5, 1997), and in a symposium on *Molecular, Cellular and Ecophysiological Bases of Noxious and Harmful Algal Blooms*, of the Phycological Society of America, 1998, papers from which were published in the *Journal of Phycology* (Vol. 35, No. 6, 1999).

Harmful algal blooms can have a variety of undesirable effects, but the one that causes most concern is the production by some species of toxic metabolites that can kill other marine life forms, including fish, shellfish,

mammals and birds, and can also poison human beings.<sup>1232,906</sup> These blooms have caused major economic losses to aquaculture – farmed fish and cultivated shellfish – in many coastal sites around the world. Increased anthropogenic nutrient enrichment of coastal waters is thought to play a role in the increased occurrence of HABs. In the case of dinoflagellates, the worst offenders, which as we noted earlier (§11.3) are particularly sensitive to turbulence, bloom development is favoured by stratification. Smayda (1997b) suggests that HAB flagellates have evolved four adaptations that assist their bloom-forming propensities. Their ability to carry out vertical migration enables them to retrieve fixed nitrogen from the nitrate-rich layer below the pycnocline. Many flagellates have the ability to take up dissolved and/or particulate organic matter from the water. Some species excrete compounds that inhibit the growth of other members of the phytoplankton (allelochemical interspecific competition). They excrete ichthyotoxins that protect them from grazing by fish larvae and/or toxins that protect them against grazing by copepods (allelopathic defence against predation).

In the case of one particular toxic red tide dinoflagellate, *Karenia brevis* (formerly known as *Gymnodinium breve*) in the Gulf of Mexico, the physical and ecological events that led to it becoming dominant have now been studied in great detail.<sup>1437,1436</sup> Off the west coast of Florida, red tides of *K. brevis*, after sporadic occurrences in the first half of the twentieth century, have occurred virtually every year since 1945. In the western Gulf of Mexico, off Texas, *K. brevis* red tides, formerly rare, are now becoming of annual occurrence.<sup>1436</sup> On the basis of a major research project involving a large number of workers and many institutions, Walsh *et al.* (2006), following earlier work by Walsh and Steidinger (2001), have arrived at a working hypothesis to explain the phenomenon. Wet deposition of iron-rich dust, transported in the wind across the Atlantic Ocean from the Sahara Desert, allows, in these already phosphorus-rich waters, the nitrogen-fixing cyanobacterium, *Trichodesmium*, to bloom in this otherwise nitrogen-poor sea water, thus providing fixed nitrogen for other phytoplankton. Onshore upwelling of seed populations of *K. brevis* takes place into coastal surface waters in which, because of their high levels of CDOM, light inhibition of ichthyotoxic *K. brevis* is alleviated, permitting a small red tide to a level of  $\sim 1 \text{ mg chl } a \text{ m}^{-3}$ . Fish mortality ensues, and the dead fish serve as a supplementary nutrient source, giving rise to large red tides at concentrations  $\sim 10 \text{ mg chl } a \text{ m}^{-3}$ , sufficient to

provide adequate self-shading for this somewhat light-sensitive species. Walsh *et al.* note that *Karenia* spp. have, particularly within the last decade, caused toxic red tides in similar coastal habitats around the world, downwind of the Gobi, Simpson, Great Western and Kalahari Deserts, and suggest that this is a global response to both desertification and eutrophication.

## References and author index

---

The numbers in italic following each item are pages where the author's work is mentioned.

1. Aas, E. & Højerslev, N. K. (1999). Analysis of underwater radiance observations: apparent optical properties and analytic functions describing the angular radiance distribution. *J. Geophys. Res.*, **104**, 8015–24. *173, 183*
2. Aas, E., Høkedal, J. & Sørensen, K. (2005). Spectral backscattering coefficient in coastal waters. *Int. J. Remote Sens.*, **26**, 331–43. *126*
3. Aas, E. & Korsbø, B. (1997). Self-shading effect by radiance meters on upward radiance observed in coastal waters. *Limnol. Oceanogr.*, **42**, 968–74. *149*
4. Abdala-Diaz, R. T., Cabello-Pasini, A., Pérez-Rodríguez, E., Conde Álvarez, R. M. & Figueroa, F. L. (2006). Daily and seasonal variations of optimum quantum yield and phenolic compounds in *Cystoseira tamariscifolia* (Phaeophyta). *Mar. Biol.*, **148**, 459–65. *356*
5. Abel, K. M. (1984). Inorganic carbon source for photosynthesis in the sea-grass *Thalassia hemprichii* (Ehrenb.) Aschers. *Plant Physiol.*, **76**, 776–81. *406*
6. Absorption and Attenuation Meter (ac-9). *User's Guide* (2008). WET Labs Inc. Philomath, Oregon. *60, 105*
7. Ackleson, S. & Spinrad, R. W. (1988). Size and refractive index of individual marine particulates: a flow cytometric approach. *Appl. Opt.*, **27**, 1270–7. *129, 131*
8. Adams, M. S., Guilizzoni, P. & Adams, S. (1978). Relationship of dissolved inorganic carbon to macrophyte photosynthesis in some Italian lakes. *Limnol. Oceanogr.*, **23**, 912–19. *408–9*
9. Agawin, N. S. R., Duarte, C. M & Agustí, S. (2000). Nutrient and temperature control of the contribution of picoplankton to phytoplankton biomass and production. *Limnol. Oceanogr.*, **45**, 591–600. *422, 451*
10. Agrawal, Y. C. (2005). The optical volume scattering function: temporal and vertical variability in the water column off the New Jersey coast. *Limnol. Oceanogr.* **50**, 787–94. *124*
11. Aguilera, J., Bischof, K., Karsten, U., Hanelt, D. & Wiencke, C. (2002). Seasonal variations in ecophysiological patterns in macroalgae from an Arctic

- fjord. II. Pigment accumulation and biochemical defence systems against high light stress. *Marine Biol.*, **140**, 1087–95. 472
12. Aiken, G. R. & Malcolm, R. L. (1987). Molecular weight of aquatic fulvic acids by vapor pressure osmometry. *Geochim. Cosmochim. Acta*, **51**, 2177–84. 69
  13. Aiken, J. (1981). The Undulating Oceanographic Recorder. *J. Plankton Res.*, **3**, 551–60. 140
  14. Aiken, J. (1985). The Undulating Oceanographic Recorder Mark 2. In A. Zirino (ed.), *Mapping Strategies in Chemical Oceanography* (pp. 315–32). ACS Publications. 140
  15. Aiken, J. & Bellan, I. (1990). Optical oceanography: an assessment of a towed method. In P. J. Herring, A. K. Campbell, M. Whitfield & L. Maddock (eds), *Light and Life in the Sea* (pp. 39–58). Cambridge: Cambridge University Press. 140
  16. Alberte, R. S., Friedman, A. L., Gustafson, D. L., Rudnick, M. S. & Lyman, H. (1981). Light-harvesting systems of brown algae and diatoms. *Biochim. Biophys. Acta*, **635**, 304–16. 282
  17. Alberte, R. S., Wood, A. M., Kursar, T. A. & Guillard, R. R. L. (1984). Novel phycoerythrins in marine *Synechococcus* spp. *Plant Physiol.*, **75**, 732–9. 296
  18. Allali, K., Bricaud, A., Babin, M., Morel, A. & Chang, P. (1995). A new method for measuring spectral absorption coefficients of marine particles. *Limnol. Oceanogr.*, **40**, 1526–32. 58, 87
  19. Allen, E. D. & Spence, D. H. N. (1981). The differential ability of aquatic plants to utilize the inorganic carbon supply in fresh waters. *New Phytol.*, **87**, 269–83. 403, 408
  20. Allen, J. F. (2003). State transitions – a question of balance. *Science*, **299**, 1530–2. 302
  21. Alvarez-Cobelas, M., Baltanas, A., Velasco, J. L. & Rojo, C. (2002). Daily variations in the optical properties of a small lake. *Freshwater Biol.*, **47**, 1051–63. 165
  22. Andersen, J. H., Schlüter, L. & Aertebjerg, G. (2006). Coastal eutrophication: recent developments in definitions and implications for monitoring strategies. *J. Plankton Res.*, **28**, 621–8. 423
  23. Andersen, R. A. (1987). Synurophyceae classis nov., a new class of algae. *Amer. J. Bot.*, **74**, 337–53. 279
  24. Anderson, G. C. (1969). Subsurface chlorophyll maximum in the Northeast Pacific Ocean. *Limnol. Oceanogr.*, **14**, 386–91. 395, 396
  25. Anderson, J. M. & Barrett, J. (1986). Light-harvesting pigment-protein complexes of algae. *Encycl. Plant Physiol. (n.s.)*, **19**, 269–85. 286
  26. Anthony, K. R. N., Ridd, P. V., Orpin, A. R., Larcombe, P. & Lough, J. (2004). Temporal variation of light availability in coastal benthic habitats: effects of clouds, turbidity, and tides. *Limnol. Oceanogr.*, **49**, 2201–11. 164, 167
  27. Antia, N. J. (1977). A critical appraisal of Lewin's Prochlorophyta. *Br. Phycol. J.*, **12**, 271–6. 273
  28. Antoine, D. & Morel, A. (1999). A multiple scattering algorithm for atmospheric correction of remotely sensed ocean colour (MERIS instrument): principle and implementation for atmospheres carrying various aerosols including absorbing ones. *Int. J. Remote Sens.*, **20**, 1875–916. 222

29. Arnold, K. E. & Murray, S. N. (1980). Relationships between irradiance and photosynthesis for marine benthic green algae (Chlorophyta) of differing morphologies. *J. Exp. Mar. Biol. Ecol.*, **43**, 183–92. 348
30. Arnone, R. A., Ladner, S., La Violette, P. E., Brock, J. C. & Rochford, P. A. (1998). Seasonal and interannual variability of surface photosynthetically available radiation in the Arabian Sea. *J. Geophys. Res.* **103**, 7735–48. 43, 45
31. Arrigo, K. R., Robinson, D. H., Worthen, D. L., Schieber, B. & Lizotte, M. (1998). Bio-optical properties of the southwestern Ross Sea. *J. Geophys. Res.*, **103**, 21683–95. 450
32. Arrigo, K. R., Van Dijken, G. L. & Bushinsky, S. (2008). Primary production in the Southern Ocean, 1997–2006. *J. Geophys. Res.*, **113**, C08004. 451
33. Arrigo, K. R., Worthen, D., Schnell, A. & Lizotte, M. P. (1998). Primary production in Southern Ocean waters. *J. Geophys. Res.*, **103**, 15587–600. 317
34. Aruga, Y. (1965). Ecological studies of photosynthesis and matter production of phytoplankton. 1. Seasonal changes in photosynthesis of natural phytoplankton. *Biol. Mag. (Tokyo)*, **78**, 280–8. 511
35. Arvesen, J. C., Millard, J. P. & Weaver, E. C. (1973). Remote sensing of chlorophyll and temperature in marine and fresh waters. *Astronaut. Acta*, **18**, 229–39. 206
36. Ashley, L. E. & Cobb, C. M. (1958). *J. Opt. Soc. Amer.*, **48**, 261–8. Quoted by Hodkinson & Greenleaves (1963). 101
37. Asmus, R. M. & Asmus, H. (1991). Mussel beds: limiting or promoting phytoplankton? *J. Exp. Mar. Biol. Ecol.*, **148**, 215–32. 424
38. Atlas, D. & Bannister, T. T. (1980). Dependence of mean spectral extinction coefficient of phytoplankton on depth, water colour and species. *Limnol. Oceanogr.*, **25**, 157–9. 328–9
39. Auclair, J. C., Demers, S., Frechette, M., Legendre, L. & Trump, C. L. (1982). High frequency endogenous periodicities of chlorophyll synthesis in estuarine phytoplankton. *Limnol. Oceanogr.*, **27**, 348–52. 528
40. Aughey, W. H. & Baum, F. J. (1954). Angular-dependence light scattering – a high resolution recording instrument for the angular range 0.05–140°. *J. Opt. Soc. Amer.*, **44**, 833–7. 109
41. Austin, R. W. (1974a). The remote sensing of spectral radiance from below the ocean surface. In N. G. Jerlov & E. S. Nielsen (eds), *Optical Aspects of Oceanography* (pp. 317–44). London: Academic Press. 46, 174, 201, 217, 361
42. Austin, R. W. (1974b). Ocean colour analysis, Part 2. San Diego: Scripps Inst. Oceanogr. 172
43. Austin, R. W. (1980). Gulf of Mexico, ocean-colour surface-truth measurements. *Boundary-layer Meteorol.*, **18**, 269–85. 217
44. Austin, R. W. & Petzold, T. J. (1977). Considerations in the design and evaluation of oceanographic transmissometers. In J. E. Tyler (ed.), *Light in the Sea* (pp. 104–20). Stroudsbury: Dowden Hutchinson Ross. 105
45. Austin, R. W. & Petzold, T. J. (1981). The determination of the diffuse attenuation coefficient of sea water using the Coastal Zone Colour Scanner. In J. F. R. Gower (ed.), *Oceanography from Space* (pp. 239–56). New York: Plenum. 255
46. AVIRIS website (2007). [aviris.jpl.nasa.gov/html/aviris.concept.html](http://aviris.jpl.nasa.gov/html/aviris.concept.html). 208

47. Axelsson, L., Mercado, J. M. & Figueroa, F. L. (2000). Utilization of  $\text{HCO}_3^-$  at high pH by the brown macroalga *Laminaria saccharina*. *Eur. J. Phycol.*, **35**, 53–9. 405
48. Babin, M. & Stramski, D. (2002). Light absorption by aquatic particles in the near-infrared spectral region. *Limnol. Oceanogr.*, **47**, 911–15. 82, 85
49. Babin, M. & Stramski, D. (2004). Variations in the mass-specific absorption coefficient of mineral particles suspended in water. *Limnol. Oceanogr.*, **49**, 756–67. 86
50. Babin, M., Morel, A., Claustre, H. *et al.* (1996). Nitrogen- and irradiance-dependent variations of the maximum quantum yield of carbon fixation in eutrophic, mesotrophic and oligotrophic marine systems. *Deep-Sea Res.*, **43**, 1241–72. 345, 374
51. Babin, M., Morel, A., Fournier-Sicre, V., Fell, F. & Stramski, D. (2003a). Light scattering properties of marine particles in coastal and open ocean waters as related to the particle mass concentration. *Limnol. Oceanogr.*, **48**, 843–59. 125
52. Babin, M., Stramski, D., Ferrari, G. M. *et al.* (2003b). Variations in the light absorption coefficients of phytoplankton, nonalgal particles, and dissolved organic matter in coastal waters around Europe. *J. Geophys. Res.*, **108**, C73211. 73, 84, 86
53. Babin, S. M., Carton, J. A., Dickey, T. D. & Wiggert, J. D. (2004). Satellite evidence of hurricane-induced phytoplankton blooms in an oceanic desert. *J. Geophys. Res.*, **109**, C03043. 427
54. Bader, H. (1970). The hyperbolic distribution of particle sizes. *J. Geophys. Res.*, **75**, 2822–30. 99
55. Badger, M. R. & Andrews, T. J. (1982). Photosynthesis and inorganic carbon usage by the marine cyanobacterium *Synechococcus* sp. *Plant Physiol.*, **70**, 517–23. 407
56. Badger, M. R., Hanson, D. & Price, G. D. (2002). Evolution and diversity of  $\text{CO}_2$  concentrating mechanisms in cyanobacteria. *Funct. Plant Biol.*, **29**, 161–73. 407
57. Baillie, P. W. & Welsh, B. L. (1980). The effect of tidal resuspension on the distribution of intertidal epipelagic algae in an estuary. *Estuar. Coast. Mar. Sci.*, **10**, 165–80. 531
58. Baker, K. S. & Frouin, R. (1987). Relation between photosynthetically available radiation and total insolation at the ocean surface under clear skies. *Limnol. Oceanogr.*, **32**, 1370–7. 33
59. Baker, K. S. & Smith, R. C. (1979). Quasi-inherent characteristics of the diffuse attenuation coefficient for irradiance. *Soc. Photo-opt. Instrum. Eng.*, **208**, 60–3. 21, 157
60. Balch, W. M., Abbott, M. R. & Eppley, R. W. (1989a). Remote sensing of primary production I. A comparison of empirical and semianalytical algorithms. *Deep-Sea Res.*, **36**, 281–95. 445
61. Balch, W. M., Eppley, R. W. & Abbott, M. R. (1989b). Remote sensing of primary production II. A semi-analytical algorithm based on pigments, temperature and light. *Deep-Sea Res.*, **36**, 1201–17. 445
62. Balch, W., Evans, E., Brown, J. *et al.* (1992). The remote sensing of ocean primary productivity: use of a new data compilation to test satellite algorithms. *J. Geophys. Res.*, **97**, 2279–93. 445

63. Balch, W. M., Holligan, P. M., Ackleson, S. G. & Voss, K. J. (1991). Biological and optical properties of mesoscale coccolithophore blooms in the Gulf of Maine. *Limnol. Oceanogr.*, **36**, 629–43. 178
64. Balch, W. M., Kilpatrick, K. A., Holligan, P., Harbour, D. & Fernandez, E. (1996b). The 1991 coccolithophore bloom in the central North Atlantic. 2. Relating optics to coccolith concentration. *Limnol. Oceanogr.*, **41**, 1684–96. 129
65. Balch, W. M., Kilpatrick, K. A. & Trees, C. C. (1996a). The 1991 coccolithophore bloom in the central North Atlantic. 1. Optical properties and factors affecting their distribution. *Limnol. Oceanogr.*, **41**, 1669–83. 117, 129
66. Bannister, T. T. (1974a). Production equation in terms of chlorophyll concentration, quantum yield, and upper limit to production. *Limnol. Oceanogr.*, **19**, 1–12. 534–5
67. Bannister, T. T. (1974b). A general theory of steady state phytoplankton growth in a nutrient-saturated mixed layer. *Limnol. Oceanogr.*, **19**, 13–30. 534–5
68. Bannister, T. T. (1979). Quantitative description of steady state, nutrient-saturated algal growth, including adaptation. *Limnol. Oceanogr.*, **24**, 76–96. 534–5
69. Bannister, T. T. & Weidemann, A. D. (1984). The maximum quantum yield of phytoplankton photosynthesis *in situ*. *J. Plankton Res.*, **6**, 275–94. 373
70. Barbini, R., Colao, F., De Dominicis, L. *et al.* (2004). Analysis of simultaneous chlorophyll measurements by lidar fluorosensor. *Int. J. Remote Sens.*, **25**, 2095–110. 252
71. Barko, J. W. & Filbin, G. J. (1983). Influences of light and temperature on chlorophyll composition in submersed freshwater macrophytes. *Aquat. Bot.*, **15**, 249–55. 478
72. Barlow, R. G., Aiken, J., Holligan, P. M. *et al.* (2002). Phytoplankton pigment and absorption characteristics along meridional transects in the Atlantic Ocean. *Deep-Sea Res.*, **47**, 637–60. 462
73. Barlow, R., Stuart, V., Lutz, V. *et al.* (2007). Seasonal pigment patterns of surface phytoplankton in the subtropical southern hemisphere. *Deep-Sea Res.*, **54**, 1687–703. 432
74. Barranguett, C., Plante-Cuny, M. R. & Alivon, E. (1996). Microphytobenthos production in the Gulf of Fos, French Mediterranean coast. *Hydrobiologia*, **333**, 181–93. 530
75. Bartlett, J. S., Voss, K. J., Sathyendranath, S. & Vodacek, A. (1998). Raman scattering by pure water and seawater. *Appl. Opt.*, **37**, 3324–32. 116
76. Bassi, R., Soen, Y., Frank, G., Zuber, H. & Rochaix, J.-D. (1992). Characterization of chlorophyll a/b proteins from *Chlamydomonas reinhardtii*. *J. Biol. Chem.*, **267**, 25714–21. 288
77. Bates, T. S., Charlson, R. J. & Gammon, R. H. (1987). Evidence for the climatic role of marine biogenic sulphur. *Nature*, **329**, 319–21. 452
78. Bauer, D., Brun-Cottan, J. C. & Saliot, A. (1971). Principe d'une mesure directe dans l'eau de mer du coefficient d'absorption de la lumière. *Cah. Oceanogr.*, **23**, 841–58. 59
79. Bauer, D. & Ivanoff, A. (1970). Spectroradiance-metre. *Cah. Oceanogr.*, **22**, 477–82. 146
80. Bauer, D., & Morel, A. (1967). Etude aux petits angles de l'indicatrice de diffusion de la lumière par les eaux de mer. *Ann. Geophys.*, **23**, 109–23. 107

81. Beach, K. S. & Smith C. M. (1996). Ecophysiology of tropical rhodophytes. I. Microscale acclimation in pigmentation. *J. Phycol.*, **32**, 701–10. 470
82. Beardall, J. & Morris, I. (1976). The concept of light intensity adaptation in marine phytoplankton: some experiments with *Phaeodactylum tricorutum*. *Mar. Biol.*, **37**, 3777–87. 475
83. Beardsley, G. F. (1968). Mueller scattering matrix of sea water. *J. Opt. Soc. Amer.*, **58**, 52–7. 109
84. Beer, S. & Axelsson, L. (2004). Limitations in the use of PAM fluorometry for measuring photosynthetic rates of macroalgae at high irradiances. *Eur. J. Phycol.*, **39**, 1–7. 296, 337
85. Beer, S., Bjork, M., Hellblom, F. & Axelsson, L. (2002). Inorganic carbon utilization in marine angiosperms (seagrasses). *Funct. Plant Biol.*, **29**, 349–54. 406
86. Beer, S. & Eshel, A. (1983). Photosynthesis of *Ulva* sp. II. Utilization of CO<sub>2</sub> and HCO<sub>3</sub><sup>-</sup> when submerged. *J. Exp. Mar. Biol. Ecol.*, **70**, 99–106. 403
87. Beer, S., Eshel, A. & Waisel, Y. (1977). Carbon metabolism in seagrasses I. The utilization of exogenous inorganic carbon species in photosynthesis. *J. Exp. Bot.*, **28**, 1180–9. 406
88. Beer, S. & Wetzel, R. G. (1982). Photosynthetic carbon fixation pathways in *Zostera marina* and three Florida seagrasses. *Aquat. Bot.*, **13**, 141–6. 414
89. Behrenfeld, M. J. & Falkowski, P. G. (1997a). A consumer's guide to phytoplankton primary productivity models. *Limnol. Oceanogr.*, **42**, 1479–91. 441, 444
90. Behrenfeld, M. J. & Falkowski, P. G. (1997b). Photosynthetic rates derived from satellite-based chlorophyll concentration. *Limnol. Oceanogr.*, **42**, 1–20. 445
91. Belay, A. (1981). An experimental investigation of inhibition of phytoplankton photosynthesis at lake surfaces. *New Phytol.*, **89**, 61–74. 339–40, 353, 354
92. Belay, A. & Fogg, G. E. (1978). Photoinhibition of photosynthesis in *Asterionella formosa* (Bacillariophyceae). *J. Phycol.*, **14**, 341–7. 354
93. Belzile, C., Gibson, J. A. E. & Vincent, W. F. (2002). Colored dissolved organic matter and dissolved organic carbon exclusion from lake ice: implications for radiation transmission and carbon cycling. *Limnol. Oceanogr.*, **47**, 1283–93. 67
94. Belzile, C., Roesler, C. S., Christensen, J. P., Shakhova, N. & Semiletov, I. (2006). Fluorescence measured using the WETStar fluorometer as a proxy for dissolved matter absorption. *Estuar. Coast. Shelf Sci.*, **67**, 441–9. 73
95. Belzile, C., Vincent, W. F. & Kumagai, M. (2002a). Contribution of absorption and scattering to the attenuation of UV and photosynthetically available radiation in Lake Biwa. *Limnol. Oceanogr.*, **47**, 95–107. 97, 125, 158, 166, 194
96. Ben-Amotz, A., Shaish, A. & Avron, M. (1989). Mode of action of the massively accumulated  $\beta$ -carotene of *Dunaliella bardawil* in protecting the alga against damage by excess irradiation. *Plant Physiol.*, **91**, 1040–3. 471
97. Bennett, A. & Bogorad, L. (1973). Complementary chromatic adaptation in a filamentous blue-green alga. *J. Cell Biol.*, **58**, 419–35. 506
98. Berdalet, E. (1992). Effects of turbulence on the marine dinoflagellate *Gymnodinium nelsonii*. *J. Phycol.*, **28**, 267–72. 426
99. Berger, W. R., Smetacek, V. S. & Wefer, G. (eds) (1989). *Productivity of the Ocean: Present and Past*. Chichester: Wiley. 450

100. Berman, T. & Shteinmann, B. (1998). Phytoplankton development and turbulent mixing in Lake Kinneret (1992–1996). *J. Plankton Res.*, **20**, 709–26. 426–7
101. Berner, T., Dubinsky, Z., Wyman, K. & Falkowski, P.G. (1989). Photo adaptation and the ‘package’ effect in *Dunaliella tertiolecta* (Chlorophyceae). *J. Phycol.*, **25**, 70–8. 317
102. Berthelot, B. & Deschamps, P.-Y. (1994). Evaluation of bio-optical algorithms to remotely sense primary production from space. *J. Geophys. Res.*, **99**, 7979–89. 447
103. Berthold, G. (1882). Über die Verteilung der Algen im Golf von Neapel nebst einem Verzeichnis der bisher daselbst beobachteten Arten. *Mitt. Zool. Sta Neapol.*, **3**, 393–536. 454
104. Berthon, J.-F., Shybanov, E., Lee, M.E.-G. & Zibordi, G. (2007). Measurements and modeling of the volume scattering function in the coastal northern Adriatic Sea. *Appl. Opt.*, **46**, 5189–203. 108
105. Bertilsson, S. & Tranvik, L.J. (2000). Photochemical transformation of dissolved organic matter in lakes. *Limnol. Oceanogr.*, **45**, 753–62. 80
106. Berwald, J., Stramski, D., Mobley, C.D. & Kiefer, D. (1995). Influences of absorption and scattering on vertical changes in the average cosine of the underwater light field. *Limnol. Oceanogr.*, **40**, 1347–57. 186
107. Bezrukov, L.B., Budnev, N.M., Galperin, M.D. *et al.* (1990). Measurement of the light attenuation coefficient of water in Lake Baikal. *Oceanology*, **30**, 756–9. 59
108. Bhatti, S., Huertas, I.E. & Colman, B. (2002). Acquisition of inorganic carbon by the marine haptophyte *Isochrysis galbana* (Prymnesiophyceae). *J. Phycol.*, **38**, 914–21. 407
109. Bidigare, R.R., Marra, J., Dickey, T.D. *et al.* (1990). Evidence for phytoplankton succession and chromatic adaptation in the Sargasso Sea during spring 1985. *Mar. Ecol. Prog. Ser.*, **60**, 113–22. 462
110. Bidigare, R.R., Prezelin, B.B. & Smith, R.C. (1992). Bio-optical models and the problems of scaling. In P.G. Falkowski & A.D. Woodhead (eds), *Primary Productivity and Biogeochemical Cycles in the Sea* (pp. 175–212). New York: Plenum. 446
111. Bidigare, R.R., Smith, R.C., Baker, K.S. & Marra, J. (1987). Oceanic primary production estimates from measurements of spectral irradiance and pigment concentrations. *Global Biogeochem. Cycles*, **1**, 171–86. 87, 368
112. Bienfang, P.K., Szyper, J.P., Okamoto, M.Y. & Noda, E.K. (1984). Temporal and spatial variability of phytoplankton in a subtropical ecosystem. *Limnol. Oceanogr.*, **29**, 527–39. 163, 236
113. Billerbeck, M., Røy, H., Bosselmann, K. & Huettel, M. (2007). Benthic photosynthesis in submerged Wadden Sea intertidal flats. *Estuar. Coast. Shelf Sci.*, **71**, 704–16. 529
114. Binding, C.E., Bowers, D.G. & Mitchelson-Jacob, E.G. (2003). An algorithm for the retrieval of suspended sediment concentrations in the Irish Sea from SeaWiFS ocean colour satellite imagery. *J. Remote Sens.*, **24**, 3791–806. 233
115. Binding, C.E., Bowers, D.G. & Mitchelson-Jacob, E.G. (2005). Estimating suspended sediment concentrations from ocean colour measurements in

- moderately turbid waters: the impact of variable particle scattering properties. *Remote Sens. Environ.*, **94**, 373–83. [232](#)
116. Binding, C. E., Jerome, J. H., Bukata, R. P. & Booty, W. G. (2008). Spectral absorption properties of dissolved and particulate matter in Lake Erie. *Remote Sens. Environ.*, **112**, 1702–11. [77](#)
117. Bindloss, M. E. (1974). Primary productivity of phytoplankton in Loch Leven, Kinross. *Proc. Roy. Soc. Edin. (B)*, **74**, 157–81. [328](#), [419](#)
118. Bird, D. F. & Kalff, J. (1989). Phagotrophic sustenance of a metalimnetic phytoplankton peak. *Limnol. Oceanogr.*, **34**, 155–62. [397](#)
119. Biscaye, P. E. & Eitrem, S. L. (1973). Variations in benthic boundary layer phenomena: nepheloid layer in the North American basin. In R. J. Gibbs (ed.), *Suspended Solids in Water* (pp. 227–60). New York: Plenum. [127](#)
120. Bishop, J. K. B. & Rossow, W. B. (1991). Spatial and temporal variability of global surface solar irradiance. *J. Geophys. Res.*, **96**, 16839–58. [35](#)
121. Bjornland, T. & Aguilar-Martinez, M. (1976). Carotenoids in red algae. *Phytochem.*, **15**, 291–6. [282](#)
122. Blackford, J. C. (2002). The influence of microphytobenthos on the Northern Adriatic ecosystem: a modelling study. *Estuar. Coast. Shelf Sci.*, **55**, 109–23. [530](#)
123. Blanch, S. J., Ganf, G. G. & Walker, K. F. (1998). Growth and recruitment in *Vallisneria americana* as related to average irradiance in the water column. *Aquat. Bot.*, **61**, 181–205. [391](#)
124. Blasco, D. (1978). Observations on the diel migration of marine dinoflagellates off the Baja California coast. *Mar. Biol.*, **46**, 41–7. [515](#)
125. Blatt, M. R. & Briggs, W. R. (1980). Blue-light-induced cortical fibre reticulation concomitant with chloroplast aggregation in the alga, *Vaucheria sessilis*. *Planta*, **147**, 355–62. [522](#)
126. Blondeau-Patissier, D., Brando, V. E., Oubelkheir, K., Clementson, L. A. & Daniel, P. (2009). Bio-optical variability of the absorption and scattering properties of the Queensland inshore and reef waters. *J. Geophys. Res.*, **114**, C05003. [76](#), [117](#), [125](#), [126](#)
127. Blough, N. V., Zafiriou, O. C. & Bonilla, J. (1993). Optical absorption spectra of waters from the Orinoco River outflow: terrestrial input of colored organic matter to the Caribbean. *J. Geophys. Res.* **98**, 2271–8. [70](#)
128. Boardman, N. K. (1977). Comparative photosynthesis of sun and shade plants. *Ann. Rev. Plant Physiol.*, **28**, 355–77. [472](#), [474](#)
129. Bodner, M. (1994). Inorganic carbon source for photosynthesis in the aquatic macrophytes *Potamogeton natans* and *Ranunculus fluitans*. *Aquat. Bot.*, **48**, 109–20. [408](#)
130. Bogorad, L. (1975). Phycobiliproteins and complementary chromatic adaptation. *Ann. Rev. Plant Physiol.*, **26**, 369–401. [293](#), [482](#)
131. Boivin, L. P., Davidson, W. F., Storey, R. S., Sinclair, D. & Earle, E. D. (1986). Determination of the attenuation coefficients of visible and ultraviolet radiation in heavy water. *Appl. Opt.*, **25**, 877–82. [62](#), [64](#)
132. Bold, H. C. & Wynne, M. J. (1978). *Introduction to the Algae*. Englewood Cliffs, NJ: Prentice-Hall. [266](#)
133. Booth, C. R. (1976). The design and evaluation of a measurement system for photosynthetically active quantum scalar irradiance. *Limnol. Oceanogr.*, **21**, 326–36. [144](#)

134. Boresch, K. (1921). Die komplementäre chromatische Adaptation. *Arch. Protistenkd.*, **44**, 1–70. 480
135. Borgerson, M. J., Bartz, R., Zaneveld, J. R. V. & Kitchen, J. C. (1990). A modern spectral transmissometer. *Proc. Soc. Photo-Opt. Instrum. Eng., Ocean Optics X*, **1302**, 373–85. 105
136. Borowitzka, M. A. & Larkum, A. W. D. (1976). Calcification in the green alga *Halimeda*. *J. Exp. Bot.*, **27**, 879–93. 402
137. Borstad, A., Brown, R. M. & Gower, J. F. R. (1980). Airborne remote sensing of sea surface chlorophyll and temperature along the outer British Columbia coast. *Proc. 6th Can. Symp. Rem. Sens.*, pp. 541–9. 206
138. Borum, J., Pedersen, M. F., Krause-Jensen, D., Christensen, P. B. & Nielsen, K. (2002). Biomass, photosynthesis and growth of *Laminaria saccharina* in a high-arctic fjord, NE Greenland. *Mar. Biol.*, **141**, 11–19. 349, 491, 496
139. Boss, E. & Pegau, W. S. (2001). Relationship of light scattering at an angle in the backward direction to the backscattering coefficient. *Appl. Opt.*, **40**, 5503–7. 110, 131
140. Boss, E., Pegau, W. S., Zaneveld, J. R. V. & Barnard, A. H. (2001). Spatial and temporal variability of absorption by dissolved material at a continental shelf. *J. Geophys. Res.*, **106**, 9499–507. 68
141. Boss, E., Slade, W. H., Behrenfeld, M. & Dall'Olmio, G. (2009). Acceptance angle effects on the beam attenuation in the ocean. *Optics Express*, **17**, 1536–50. 105
142. Boston, H. L. (1986). A discussion of the adaptations for carbon acquisition in relation to the growth strategy of aquatic isoetids. *Aquat. Bot.*, **26**, 259–70. 410, 414
143. Boulart, C., Flament, P., Gentilhomme, V. *et al.* (2006). Atmospherically-promoted photosynthetic activity in a well-mixed ecosystem: significance of wet deposition events of nitrogen compounds. *Estuar. Coast. Shelf Sci.*, **69**, 449–58. 421
144. Bouman, H., Platt, T., Sathyendranath, S. & Stuart, V. (2005). Dependence of light-saturated photosynthesis on temperature and community structure. *Deep-Sea Res.*, **52**, 1284–99. 419
145. Bowers, D. G. & Mitchelson-Jacob, E. G. (1996). Inherent optical properties of the Irish Sea determined from underwater irradiance measurements. *Estuar. Coast. Shelf Sci.*, **43**, 433–47. 61
146. Bowers, D. G., Boudjelas, S. & Harker, G. E. L. (1998). The distribution of fine suspended sediments in the surface waters of the Irish Sea and its relation to tidal stirring. *Int. J. Remote Sens.*, **19**, 2789–805. 233
147. Bowers, D. G., Evans, D., Thomas, D. N. *et al.* (2004). Interpreting the colour of an estuary. *Estuar. Coast. Shelf Sci.*, **59**, 13–20. 252
148. Bowers, D. G., Harker, G. E. L., Smith, P. S. D. & Tett P. (2000). Optical properties of a region of freshwater influence (the Clyde Sea). *Estuar. Coast. Shelf Sci.*, **50**, 717–26. 163, 164, 194, 252
149. Bowes, G. (1987). Aquatic plant photosynthesis: strategies that enhance carbon gain. In R. M. M. Crawford (ed.), *Plant Life in Aquatic and Amphibious Habitats* (pp. 79–98). Oxford: Blackwell. 306, 414
150. Bowes, G., Rao, S. K., Estavillo, G. M. & Reiskind, J. B. (2002). C<sub>4</sub> mechanisms in aquatic angiosperms: comparisons with terrestrial C<sub>4</sub> systems. *Funct. Plant Biol.*, **29**, 379–92. 414

151. Bowling, L. C. (1988). Optical properties, nutrients and phytoplankton of freshwater coastal dune lakes in south-east Queensland. *Aust J. Mar. Freshwater Res.*, **39**, 805–15. 78, 119, 166
152. Bowling, L. C., Steane, M. S. & Tyler, P. A. (1986). The spectral distribution and attenuation of underwater irradiance in Tasmanian inland waters. *Freshwater Biol.*, **16**, 313–35. 78, 119, 166, 178
153. Boyd, P. W., Watson, A. J., Law, C. S. *et al.* (2000). A mesoscale phytoplankton bloom in the polar Southern Ocean stimulated by iron fertilization. *Nature*, **407**, 695–702. 425
154. Boynton, W. R., Kemp, W. M. & Keefe, C. W. (1982). A comparative analysis of nutrients and other factors influencing estuarine phytoplankton productivity. In V. S. Kennedy (ed.), *Estuarine Comparisons*. New York: Academic. 450
155. Braarud, T. & Klem, A. (1931). *Hvalradets Skrift*, **1**, 1–88. Quoted by Steemann Nielsen (1974). 389
156. Brakel, W. H. (1984). Seasonal dynamics of suspended-sediment plumes from the Tana and Sabaki Rivers, Kenya: analysis of Landsat imagery. *Remote Sens. Environ.*, **16**, 165–73. 229
157. Breen, P. A. & Mann, K. H. (1976). Changing lobster abundance and the destruction of kelp beds by sea urchins. *Mar. Biol.*, **34**, 137–42. 428
158. Bréon, F. M. & Henriot, N. (2006). Spaceborne observations of ocean glint reflectance and modeling of wave slope distributions. *J. Geophys. Res.*, **111**, C06005. 49
159. Bricaud, A., Babin, M., More, A. & Claustre, H. (1995). Variability in the chlorophyll-specific absorption coefficients of natural phytoplankton: analysis and parameterization. *J. Geophys. Res.*, **100**, 13321–32. 318
160. Bricaud, A. & Morel, A. (1986). Light attenuation and scattering by phytoplanktonic cells: a theoretical model. *Appl. Opt.*, **25**, 571–80. 128
161. Bricaud, A., Morel, A. & Prieur, L. (1981). Absorption by dissolved organic matter of the sea (yellow substance) in the UV and visible domains. *Limnol. Oceanogr.*, **26**, 43–53. 64, 69, 73, 74, 75
162. Bricaud, A., Morel, A. & Prieur, L. (1983). Optical efficiency factors of some phytoplankters. *Limnol. Oceanogr.*, **28**, 816–32. 128
163. Bricaud, A., Roesler, C. & Zaneveld, J. R. V. (1995). In situ methods for measuring the inherent optical properties of ocean waters. *Limnol. Oceanogr.*, **40**, 393–410. 60, 129, 318
164. Bricaud, A. & Stramski, D. (1990). Spectral absorption coefficients of living phytoplankton and non algal biogenous matter: a comparison between the Peru upwelling and the Sargasso Sea. *Limnol. Oceanogr.*, **35**, 562–82. 84, 86
165. Bristow, M. P. F., Bundy, D. H., Edmonds, C. M. *et al.* (1985). Airborne laser fluorosensor survey of the Columbia and Snake rivers: simultaneous measurements of chlorophyll, dissolved organics and optical attenuation. *Int. J. Remote Sens.*, **6**, 1707–34. 255
166. Bristow, M., Nielsen, D., Bundy, D. & Furtek, R. (1981). Use of water Raman emission to correct airborne laser fluorosensor data for effects of water optical attenuation. *Appl. Opt.*, **20**, 2889–906. 249–52

167. Britz, S. J. & Briggs, W. R. (1976). Circadian rhythms of chloroplast orientation and photosynthetic capacity in *Ulva*. *Plant Physiol.*, **58**, 22–7. 524, 527
168. Brivio, P. A., Giardino, C. & Zilioli, E. (2001). Determination of chlorophyll changes in Lake Garda using an image-based radiative transfer code for Landsat TM images. *Int. J. Remote Sens.*, **22**, 487–502. 224
- 168a. Brock, J., Sathyendranath, S. & Platt, T. (1993). Modeling the seasonality of submarine light and primary production in the Arabian Sea. *Mar. Ecol. Prog. Ser.*, **101**, 209–21. 43
169. Brody, M. & Emerson, R. (1959). The effect of wavelength and intensity of light on the proportion of pigments in *Porphyridium cruentum*. *Amer. J. Bot.*, **46**, 433–40. 470, 483–4, 486, 508
170. Brown, C. W. & Podestá, G. P. (1997). Remote sensing of coccolithophore blooms in the western South Atlantic Ocean. *Remote Sens. Environ.*, **60**, 83–91. 237
171. Brown, J. & Simpson, J. H. (1990). The radiometric determination of total pigment and seston and its potential use in shelf seas. *Estuar. Coast. Shelf Sci.*, **31**, 1–9. 244
172. Brown, J. S. (1985). Three photosynthetic antenna porphyrins in a primitive green alga. *Biochim. Biophys. Acta*, **807**, 143–6. 277
173. Brown, J. S. (1987). Functional organization of chlorophyll a and carotenoids in the alga *Nannochloropsis salina*. *Plant Physiol.*, **83**, 434–7. 290
174. Brown, T. E. & Richardson, F. L. (1968). The effect of growth environment on the physiology of algae: light intensity. *J. Phycol.*, **4**, 38–54. 471
- 174a. Broyde, S. B. & Brody, S. S. (1967). Emission spectra of chlorophyll-a in polar and non-polar solvents. *J. Chem. Phys.*, **46**, 334–40. 280, 282
175. Bruning, K., Lingeman, R. & Ringelberg, J. (1992). Estimating the impact of fungal parasites on phytoplankton populations. *Limnol. Oceanogr.*, **37**, 252–60. 427
176. Bryant, D. A. (1981). The photo regulated expression of multiple phycocyanin genes. *Eur. J. Biochem.*, **119**, 425–9. 480–1, 483
177. Brylinsky, M. (1980). Estimating the productivity of lakes and reservoirs. In E. D. Le Cren & R. H. Lowe-McConnell (eds), *The Functioning of Freshwater Ecosystems*. Cambridge: Cambridge University Press. 376
178. Büchel, C. & Wilhelm, C. (1993). Isolation and characterization of a Photosystem I-associated antenna (LHC I) and a Photosystem I-core complex from the chlorophyll c-containing alga *Pleurochloris meiringensis*. *J. Photochem. Photobiol. B*, **20**, 87–93. 287, 288, 290
179. Buchwald, M. & Jencks, W. P. (1968). Properties of the crustacyanins and the yellow lobster shell pigments. *Biochemistry*, **7**, 844–59. 293
180. Bukata, R. P. & Bruton, J. E. (1974). ERTS-I digital classifications of the water regimes comprising Lake Ontario. *Proc. 2nd Canad. Symp. Rem. Sens.*, pp. 627–34. 236
181. Bukata, R. P., Harris, G. P. & Bruton, J. E. (1974). The detection of suspended solids and chlorophyll a utilizing multispectral ERTS-I data. *Proc. 2nd Canad. Symp. Rem. Sens.*, pp. 551–64. 231, 235
182. Bukata, R. P., Jerome, J. H. & Bruton, J. E. (1988). Particulate concentrations in Lake St Clair as recorded by a shipborne multispectral optical monitoring system. *Remote Sens. Environ.*, **25**, 201–29. 204

183. Bukata, R. P., Jerome, J. H., Bruton, J. E. & Jain, S. C. (1979). Determination of inherent optical properties of Lake Ontario coastal waters. *Appl. Opt.*, **18**, 3926–32. 118
184. Bukaveckas, P. A. & Driscoll, C. T. (1991). Effects of whole-lake base addition on the optical properties of three clearwater acidic lakes. *Can. J. Fish. Aquat. Sci.*, **48**, 1030–40. 118
185. Bullerjahn, G. S., Matthijs, H. C. P., Mur, L. R. & Sherman, L. A. (1987). Chlorophyll-protein composition of the thylakoid membrane from *Prochlorothrix hollandica*, a prokaryote containing chlorophyll *b*. *Eur. J. Biochem.*, **168**, 295–300. 291
186. Bunt, J. S. (1963). Diatoms of Antarctic sea ice as agents of primary production. *Nature*, **199**, 1255–8. 508
187. Burger-Wiersma, T., Veenhuis, M., Korthals, H. J., Van de Wiel, C. C. M. & Mur, L. R. (1986). A new prokaryote containing chlorophylls *a* and *b*. *Nature*, **320**, 262–4. 273, 279, 284
188. Burkhardt, S., Amoroso, G., Riebesell, U. & Sültemeyer, D. (2001). CO<sub>2</sub> and HCO<sub>3</sub><sup>-</sup> uptake in marine diatoms acclimated to different CO<sub>2</sub> concentrations. *Limnol. Oceanogr.*, **46**, 1378–91. 407
189. Burt, W. V. (1958). Selective transmission of light in tropical Pacific waters. *Deep-Sea Res.*, **5**, 51–61. 74
190. Bush, K. J. & Sweeney, B. M. (1972). The activity of ribulose diphosphate carboxylase in extracts of *Gonyaulax polyedra* in the day and night phases of the circadian rhythm of photosynthesis. *Plant Physiol.*, **50**, 446–51. 525
191. Butler, W. L. (1978). Energy distribution in the photochemical apparatus of photosynthesis. *Ann. Rev. Plant Physiol.*, **29**, 345–78. 302, 332, 385
192. Butler, W. L. & Kitajima, M. (1975). Fluorescence quenching in photosystem II of chloroplasts. *Biochim. Biophys. Acta*, **376**, 116–25. 334
193. Cahoon, L. B. (1999). The role of benthic microalgae in neritic ecosystems. *Oceanogr. Mar. Biol. Annu. Rev.*, **37**, 47–86. 530
194. Calabrese, G. (1972). Research on red algal pigments. 2. Pigments of *Petroglossum nicaeense* (Duby) Schotter (Rhodophyceae, Gigartinales) and their seasonal variations at different light intensities. *Phycologia*, **11**, 141–6. 510
195. Calabrese, G. & Felicini, G. P. (1973). Research on red algal pigments. 5. The effect of white and green light on the rate of photosynthesis and its relationship to pigment components in *Gracilaria compressa*. *Phycologia*, **12**, 195–9. 470
196. Callame, B. & Debyser, J. (1954). Observations sur les mouvements des diatomées à la surface des sédiments marins de la zone intercotidale. *Vie milieu*, **5**, 242–9. 529
197. Cambridge, M. L., Chiffings, A. W., Britton, C., Moore, L. & McComb, A. J. (1986). The loss of seagrass in Cockburn Sound, Western Australia II. Possible causes of seagrass decline. *Aquat. Bot.*, **24**, 269–85. 428
198. Campbell, E. E. & Bate, G. C. (1987). Factors influencing the magnitude of phytoplankton primary production in a high-energy surf zone. *Estuar. Coast. Shelf Sci.*, **24**, 741–50. 346
199. Campbell, J. W. & Esaias, W. E. (1983). Basis for spectral curvature algorithms in remote sensing of chlorophyll. *Appl. Opt.*, **22**, 1084–92. 207

200. Campbell, J. W. & O'Reilly, J. E. (1988). Role of satellites in estimating primary productivity on the northwest Atlantic continental shelf. *Cont. Shelf Res.*, **8**, 179–204. 443
201. Cartaxana, P., Mendes, C. R., van Leeuwe, M. A. & Brotas, V. (2006). Comparative study on microphytobenthic pigments of muddy and sandy intertidal sediments of the Tagus estuary. *Estuar. Coast. Shelf Sci.*, **66**, 225–30. 530
202. Carder, K. L., Chen, F. R., Lee, Z. P., Hawes, S. K. & Kamykowski, D. (1999). Semianalytic Moderate-Resolution Imaging Spectrometer algorithms for chlorophyll *a* and absorption with bio-optical domains based on nitrate-depletion temperatures. *J. Geophys. Res.*, **104**, 5403–21. 243
203. Carder, K. L., Hawes, S. K., Baker, K. A. *et al.* (1991). Reflectance model for quantifying chlorophyll *a* in the presence of productivity degradation products. *J. Geophys. Res.*, **96**, 20599–611. 246
204. Carder, K. L., Stewart, R. G., Harvey, G. R. & Ortner, P. B. (1989). Marine humic and fulvic acids: their effects on remote sensing of ocean chlorophyll. *Limnol. Oceanogr.*, **34**, 68–81. 68, 74
205. Carder, K. L., Tomlinson, R. D. & Beardsley, G. F. (1972). A technique for the estimation of indices of refraction of marine phytoplankton. *Limnol. Oceanogr.* **17**, 33–9. 129
206. Caron, L., Dubacq, J. P., Berkaloff, C. & Jupin, H. (1985). Subchloroplast fractions from the brown alga *Fucus serratus*: phosphatidylglycerol contents. *Plant Cell Physiol.*, **26**, 131–9. 291
207. Caron, L., Remy, R. & Berkaloff, C. (1988). Polypeptide composition of light-harvesting complexes from some brown algae and diatoms. *FEBS Lett.*, **229**, 11–15. 291
208. Carpenter, E. J. & Romans, K. (1991). Major role of the cyanobacterium *Trichodesmium* in nutrients cycling in the North Atlantic Ocean. *Science*, **254**, 1356–8. 422
209. Carpenter, R. C. (1985). Relationship between primary production and irradiance in coral reef algal communities. *Limnol. Oceanogr.*, **30**, 784–93. 350
210. Carpenter, S. R., Cole, J. J., Kitchell, J. F. & Pace, M. L. (1998). Impact of dissolved organic carbon, phosphorus, and grazing on phytoplankton biomass and production in experimental lakes. *Limnol. Oceanogr.*, **43**, 73–80. 398
211. Carr, H. & Axelsson, L. (2008). Photosynthetic utilization of bicarbonate in *Zostera marina* is reduced by inhibitors of mitochondrial ATPase and electron transport. *Plant Physiol.*, **147**, 879–85. 406
212. Casati, P., Lara, M. V. & Andreo, C. S. (2000). Induction of a C<sub>4</sub>-like mechanism of CO<sub>2</sub> fixation in *Egeria densa*, a submersed aquatic species. *Plant Physiol.*, **123**, 1611–21. 212
213. Cavender-Bares, K. K., Mann, E. L., Chisholm, S. W., Ondrusek, M. E. & Bidigare, R. R. (1999). Differential response of equatorial Pacific phytoplankton to iron fertilization. *Limnol. Oceanogr.*, **44**, 237–46. 425
214. Chamberlin, S. & Marra, J. (1992). Estimation of photosynthetic rate from measurements of natural fluorescence: analysis of the effects of light and temperature. *Deep-Sea Res.*, **39**, 1695–706. 338
215. Chamberlin, W. S., Booth, C. R., Kiefer, D. A., Morrow, J. H. & Murphy, R. C. (1990). Evidence for a simple relationship between natural fluorescence, photosynthesis and chlorophyll in the sea. *Deep-Sea Res.*, **37**, 951–73. 338

216. Chami, M., Marken, E., Stamnes, J.J., Khomenko, G. & Korotaev, G. (2006a). Variability of the relationship between the particulate backscattering coefficient and the volume scattering function measured at fixed angles. *J. Geophys. Res.*, **111**, C05013. 110, 131
217. Chami, M., Shybanov, E. B., Churilova, T. Y. *et al.* (2005). Optical properties of the particles in the Crimea coastal waters (Black Sea). *J. Geophys. Res.*, **110**, C11020. 121
218. Chami, M., Shybanov, E. B., Khomenko, G. A. *et al.* (2006b). Spectral variation of the volume scattering function measured over the full range of scattering angles in a coastal environment. *Appl. Opt.*, **45**, 3605–19. 126
219. Charlson, R. J., Lovelock, J. E., Andreae, M. O. & Warren, S. G. (1987). Oceanic phytoplankton, atmospheric sulphur, cloud albedo and climate. *Nature*, **326**, 655–61. 452
220. Chavez, P. S. (1988). An improved dark-object subtraction technique for atmospheric scattering of multispectral data. *Remote Sens. Environ.*, **24**, 459–79. 223
221. Chavez, P. S. (1996). Image-based atmospheric corrections – revisited and improved. *Photogramm. Eng. Remote Sens.*, **62**, 1025–36. 223–4
222. Chen, Z., Muller-Karger, F. E. & Hu, C. (2007). Remote sensing of water clarity in Tampa Bay. *Remote Sens. Environ.*, **109**, 249–59. 259–60
223. Cheshire, A. C., Westphalen, G., Wenden, A., Scriven, L. J. & Rowland, B. C. (1996). Photosynthesis and respiration of phaeophycean-dominated macroalgal communities in summer and winter. *Aquat. Bot.*, **55**, 159–70. 349
224. Chisholm, S. W., Armbrust, E. V. & Olson, R. J. (1986). The individual cell in phytoplankton ecology: cell cycles and applications of flow cytometry. In T. Platt & W. K. W. Li (eds), *Photosynthetic picoplankton* (pp. 343–69). *Can. Bull. Fish. Aquat. Sci.*, **214**. 131
225. Chisholm, S. W., Frankel, S. L., Goericke, R. *et al.* (1992). *Prochlorococcus marinus* nov. gen. nov. sp.: an oxytrophic marine prokaryote containing divinyl chlorophyll *a* and *b*. *Arch. Microbiol.*, **157**, 297–300. 273, 276
226. Chisholm, S. W. & Morel, F. M. M. (eds) (1991). What controls phytoplankton production in nutrient-rich areas of the open sea? *Limnol. Oceanogr. (special issue)*, **36** (No. 8). 425
227. Chisholm, S. W., Olson, R. J., Zettler, E. R. *et al.* (1988). A novel free-living prochlorophyte abundant in the oceanic euphotic zone. *Nature*, **334**, 340–3. 273, 278, 279
228. Chitnis, P. R. (2001). Photosystem I: function and physiology. *Ann. Rev. Plant Physiol. Plant Mol. Biol.*, **52**, 593–626. 302
229. Choo, K., Snoeijs, P. & Pedersén, M. (2002). Uptake of inorganic carbon by *Cladophora glomerata* (Chlorophyta) from the Baltic Sea. *J. Phycol.*, **38**, 493–502. 405
230. Chow, W. S. (1993). Photoprotection and photoinhibitory damage. In J. Barber (ed.), *Molecular Processes of Photosynthesis. Adv. Molec. Cell Biol.*, Vol. 7, Greenwich, CT: JAI Press. 354, 472
231. Chu, Z.-X. & Anderson, J. M. (1985). Isolation and characterization of a siphonaxanthin-chlorophyll *a/b* protein complex of Photosystem I from a *Codium* species (Siphonales). *Biochim. Biophys. Acta*, **806**, 154–60. 287, 288, 290
232. Cibic, T., Blasutto, O., Burba, N. & Umani, S. F. (2008). Microphytobenthic primary production as <sup>14</sup>C uptake in sublittoral sediments of the Gulf of

- Trieste (northern Adriatic Sea): methodological aspects and data analyses. *Estuar. Coast. Shelf Sci.*, **77**, 113–22. 531
233. Clarke, G. L. (1939). The utilization of solar energy by aquatic organisms. In F. R. Poulton (ed.), *Problems of Lake Biology* (pp. 27–38). American Association for the Advancement of Science. 361
234. Clarke, G. L., Ewing, G. C. & Lorenzen, C. J. (1970). Spectra of back scattered light from the sea obtained from aircraft as a measure of chlorophyll concentration. *Science*, **167**, 1119–21. 201, 206, 238
235. Clarke, G. L. & James, H. R. (1939). Laboratory analysis of the selective absorption of light by sea water. *J. Opt. Soc. Am.*, **29**, 43–55. 60
236. Claustre, H., Babin, M., Merien, D. *et al.* (2005). Toward a taxon-specific parameterization of bio-optical models of primary production: a case study in the North Atlantic. *J. Geophys. Res.*, **110**, C07512. 378
237. Claustre, H. & Marty, J.-C. (1995). Specific phytoplankton biomasses and their relation to primary production in the tropical North Atlantic. *Deep-Sea Res.*, **42**, 1475–93. 462
238. Claustre, H., Moline, M. A. & Prézelin, B. B. (1997). Sources of variability in the column photosynthetic cross section for Antarctic coastal waters. *J. Geophys. Res.*, **102**, 25047–60. 378
239. Claustre, H., Morel, A., Hooker, S. B. *et al.* (2002). Is desert dust making oligotrophic waters greener? *Geophys. Res. Lett.*, **29**, 10.1029/2001GL014056. 245
240. Clayton, R. K. (1980). *Photosynthesis: Physical Mechanisms and Chemical Patterns*. Cambridge: Cambridge University Press. 471
241. Clementson, L. A., Parslow, J. S., Turnbull, A. R. & Bonham, P. I. (2004). Properties of light absorption in a highly coloured estuarine system in south-east Australia which is prone to blooms of the toxic dinoflagellate *Gymnodinium catenatum*. *Estuar. Coast. Shelf Sci.*, **60**, 101–12. 76, 78, 86, 90, 317
242. Clementson, L. A., Parslow, J. S., Turnbull, A. R., McKenzie, D. C. & Rathbone, C. E. (2001). Optical properties of waters in the Australasian sector of the Southern Ocean. *J. Geophys. Res.*, **106**, 31611–25. 74
243. Clendennen, S. K., Zimmerman, R. C., Powers, D. & Alberte, R. S. (1996). Photosynthetic response of the giant kelp *Macrocystis pyrifera* (Phaeophyceae) to ultraviolet radiation. *J. Phycol.*, **32**, 614–20. 355
244. Cleveland, J. S., Perry, M. J., Kiefer, D. A. & Talbot, M. C. (1989). Maximal yield of photosynthesis in the northwestern Sargasso Sea. *J. Mar. Res.*, **47**, 869–86. 368, 374
245. Cleveland, J. S. & Weidemann, A. D. (1993). Quantifying absorption by aquatic particles: a multiple scattering correction for glass-fiber filters. *Limnol. Oceanogr.*, **38**, 1321–7. 57
246. Cloern, J. E. (1987). Turbidity as a control on phytoplankton biomass and productivity in estuaries. *Continental Shelf Res.*, **7**, 1367–81. 164, 398
247. Cloern, J. E. (1991). Tidal stirring and phytoplankton bloom dynamics in an estuary. *J. Mar. Res.*, **49**, 203–21. 394, 433
248. Cloern, J. E., Alpine, A. E., Cole, B. E. *et al.* (1983). River discharge controls phytoplankton dynamics in the Northern San Francisco Bay estuary. *Estuar. Coast. Shelf Sci.*, **16**, 415–29. 389

249. Coale, K. H., Johnson, K. S., Fitzwater, S. E. *et al.* (1996). A massive phytoplankton bloom induced by an ecosystem-scale iron fertilization experiment in the equatorial Pacific Ocean. *Nature*, **383**, 495–501. 425
250. Coats, D. W. & Harding, L. W. (1988). Effect of light history on the ultrastructure and physiology of *Prorocentrum mariae-lebouriae* (Dinophyceae). *J. Phycol.*, **24**, 67–77. 473
251. Cole, B. E. & Cloern, J. E. (1984). Significance of biomass and light availability to phytoplankton productivity in San Francisco Bay. *Mar. Ecol. Prog. Ser.*, **17**, 15–24. 398
252. Cole, B. E. & Cloern, J. E. (1987). An empirical model for estimating phytoplankton productivity in estuaries. *Mar. Ecol. Prog. Ser.*, **36**, 299–305. 398
253. Cole, J. J., Caraco, N. F. & Peierls, B. L. (1992). Can phytoplankton maintain a positive carbon balance in a turbid, freshwater, tidal estuary? *Limnol. Oceanogr.*, **37**, 1608–17. 399
254. Colijn, F., Admiraal, W., Baretta, J. W. & Ruardij, P. (1987). Primary production in a turbid estuary, the Ems-Dollard: field and model studies. *Continental Shelf Res.*, **7**, 1405–9. 163
255. Colman, B. & Gehl, K. A. (1983). Physiological characteristics of photosynthesis in *Porphyridium cruentum*: evidence for bicarbonate transport in a unicellular red alga. *J. Phycol.*, **19**, 216–19. 406
256. Colman, B., Huertas, I. E., Bhatti, S. & Dason, J. S. (2002). The diversity of inorganic carbon acquisition mechanisms in eukaryotic microalgae. *Funct. Plant Biol.*, **29**, 261–70. 406, 408
257. Colombo-Pallotta, M. F., García-Mendoza, E. & Ladah, L. B. (2006). Photosynthetic performance, light absorption, and pigment composition of *Macrocystis pyrifera* (Laminariales), Phaeophyceae) blades from different depths. *J. Phycol.*, **42**, 1225–34. 491, 497
258. Cota, G. F. (1985). Photoadaptation of high Arctic ice algae. *Nature*, **315**, 219–22. 347, 509
259. Cota, G. F., Harrison, W. G., Platt, T., Sathyendranath, S. & Stuart, V. (2003). Bio-optical properties of the Labrador Sea. *J. Geophys. Res.*, **108**, C73228. 86
260. Cota, G. F., Smith, W. O. & Mitchell, B. G. (1994). Photosynthesis of *Phaeocystis* in the Greenland Sea. *Limnol. Oceanogr.*, **39**, 948–53. 374
261. Cota, G. F. & Sullivan, C. W. (1990). Photoadaptation, growth and production of bottom ice algae in the Antarctic. *J. Phycol.*, **26**, 399–411. 509
262. Cottrell, M. T. & Suttle, C. A. (1995). Dynamics of a lytic virus infecting the photosynthetic marine picoflagellate *Micromonas pusilla*. *Limnol. Oceanogr.*, **40**, 730–9. 427
263. Cox, C. & Munk, W. (1954). Measurement of the roughness of the sea surface from photographs of the sun's glitter. *J. Opt. Soc. Amer.*, **44**, 838–50. 49, 151
264. Craigie, J. S. (1974). Storage products. In W. D. P. Stewart (ed.), *Algal Physiology and Biochemistry* (pp. 206–35). Oxford: Blackwell. 307
265. Critchley, C. (1981). Studies on the mechanism of photoinhibition in higher plants. *Plant Physiol.*, **67**, 1161–5. 354
266. Critchley, C. (1988). The molecular mechanism of photoinhibition facts and fiction. *Aust. J. Plant Physiol.*, **15**, 27–41. 354

267. Crossett, R. N., Drew, E. A. & Larkum, A. W. D. (1965). Chromatic adaptation in benthic marine algae. *Nature*, **207**, 547–8. 460, 465
268. Cullen, J. J. (1982). The deep chlorophyll maximum: comparing vertical profiles of chlorophyll a. *Can. J. Fish. Aquat. Sci.*, **39**, 791–803. 396
269. Cullen, J. J. & Horrigan, S. G. (1981). Effects of nitrate on the diurnal vertical migration, carbon to nitrogen ratio, and the photosynthetic capacity of the dinoflagellate, *Gymnodinium splendens*. *Mar. Biol.*, **62**, 81–9. 515–16
270. Cullen, J. J., Lewis, M. R., Daviss, C. O. & Barber, R. T. (1992). Photosynthetic characteristics and estimated growth rates indicate grazing is the proximate control of primary production in the equatorial Pacific. *J. Geophys. Res.*, **97**, 639–54. 424
271. Cummings, M. E. & Zimmerman, R. C. (2003). Light harvesting and the package effect in the seagrasses *Thalassia testudinum* Banks ex König and *Zostera marina* L.: optical constraints on photoacclimation. *Aquat. Bot.*, **75**, 261–74. 319
272. Cunningham, F. X. & Schiff, J. A. (1986). Chlorophyll-protein complexes from *Euglena gracilis* and mutants deficient in chlorophyll b. *Plant Physiol.*, **80**, 223–38. 290
273. Cushing, D. H. (1988). The flow of energy in marine ecosystems, with special reference to the continental shelf. In H. Postma & J. J. Zijlstra (eds), *Continental Shelves* (pp. 203–30). Amsterdam: Elsevier. 450
274. D'Sa, E. & Miller, R. L. (2003). Bio-optical properties in waters influenced by the Mississippi River during low flow conditions. *Remote Sens. Environ.*, **84**, 538–49. 253
275. D'Sa, E. J., Miller, R. L. & Del Castillo, C. (2006). Bio-optical properties and ocean color algorithms for coastal waters influenced by the Mississippi River during a cold front. *Appl. Opt.*, **45**, 7410–28. 85, 86
276. D'Sa, E. J., Steward, R. G., Vodacek, A., Blough, N. V. & Phinney, D. (1999). Determining optical absorption of colored dissolved organic matter in seawater with a liquid capillary waveguide. *Limnol. Oceanogr.*, **44**, 1142–8. 58
277. Dale, H. M. (1986). Temperature and light: the determining factors in maximum depth distribution of aquatic macrophytes in Ontario, Canada. *Hydrobiologia*, **133**, 73–7. 420
278. Dandonneau, Y., Montel, Y., Blanchot, J., Giraudeau, J. & Neveux, J. (2006). Temporal variability in phytoplankton pigments, picoplankton and coccolithophores along a transect through the North Atlantic and tropical southwestern Pacific. *Deep-Sea Res.*, **53**, 689–712. 432
279. Darecki, M., Kaczmarek, S. & Olszewski, J. (2005). SeaWiFS ocean colour chlorophyll algorithms for the southern Baltic Sea. *Int. J. Remote Sens.*, **26**, 247–60. 244
280. Dason, J. S., Huertas, I. E. & Colman, B. (2004). Source of inorganic carbon for photosynthesis in two marine dinoflagellates. *J. Phycol.*, **40**, 285–92. 406
281. Davidson, A. T., Bramich, D., Marchant, H. J. & McMinn, A. (1994). Effects of UV-B irradiation on growth and survival of Antarctic marine diatoms. *Mar. Biol.*, **119**, 507–15. 356
282. Davies-Colley, R. J. (1987). Optical properties of the Waikato River, New Zealand. *Mitt. Geol.-Paläont. Inst. Univ. Hamburg, SCOPE/ UNEP Sonderbd.*, **64**, 443–60. 79, 85, 114, 119

283. Davies-Colley, R. J. (1992). Yellow substance in coastal and marine waters round the South Island, New Zealand. *N. Z. J. Mar. Freshwater Res.*, **26**, 311–22. 76
284. Davies-Colley, R. J., Pridmore, R. D. & Hewitt, J. E. (1986). Optical properties of some freshwater phytoplanktonic algae. *Hydrobiologia*, **133**, 165–78. 128, 317
285. Davies-Colley, R. J. & Vant, W. N. (1987). Absorption of light by yellow substance in freshwater lakes. *Limnol. Oceanogr.*, **32**, 416–25. 73, 79
286. Davies-Colley, R. J. & Vant, W. N. (1988). Estimates of optical properties of water from Secchi disk depths. *Water Res. Bull.*, **24**, 1329–35. 143, 166, 177
287. Davies-Colley, R. J., Vant, W. N. & Latimer, G. J. (1984). Optical characterization of natural waters by PAR measurement under changeable light conditions. *N. Z. J. Mar. Freshwater Res.*, **18**, 455–60. 139, 140, 166
288. Davies-Colley, R. J., Vant, W. N. & Smith, D. G. (2003). *Colour and Clarity of Natural Waters: Science and Management of Optical Water Quality*, 2nd edn. Blackburn Press, New Jersey. 177
289. Davies-Colley, R. J., Vant, W. N. & Wilcock, R. J. (1988). Lake water colour: comparison of direct observations with underwater spectral irradiance. *Water Res. Bull.*, **24**, 11–18. 176
290. Davis, M. A. & Dawes, C. J. (1981). Seasonal photosynthetic and respiratory responses of the intertidal red alga, *Bostrychia binderi* Harvey (Rhodophyta, Ceramiales) from a mangrove swamp and a salt marsh. *Phycologia*, **20**, 165–73. 510
291. Davis, R. F., Moore, C. C., Zaneveld, J. R. V. & Napp, J. M. (1997). Reducing the effects of fouling on chlorophyll estimates derived from long-term deployments of optical instruments. *J. Geophys. Res.*, **102**, 5851–5. 61
292. Day, H. R. & Felbeck, G. J. (1974). Production and analysis of a humic-acid-like exudate from the aquatic fungus *Aureobasidium pullulans*. *J. Amer. Water Works Ass.*, **66**, 484–8. 66
293. De Baar, H. J. W., Boyd, P. W., Coale, K. H. *et al.* (2005). Synthesis of iron fertilization experiments: from the Iron Age in the Age of Enlightenment. *J. Geophys. Res.*, **110**, C09516. 426
294. De Jonge, V. N. & Van Beusekom, J. E. E. (1992). Contribution of resuspended microphytobenthos to total phytoplankton and its possible role for grazers. *Netherlands J. Sea Res.*, **30**, 91–105. 531
295. Defoin-Platel, M. & Chami, M. (2007). How ambiguous is the inverse problem of ocean color in coastal waters? *J. Geophys. Res.*, **112**, C03004. 255
296. Degens, E. T., Guillard, R. R. L., Sackett, W. M. & Hellebust, J. A. (1968). Metabolic fractionation of carbon isotopes in marine plankton – I. Temperature and respiration experiments. *Deep-Sea Res.*, **15**, 1–9. 406
297. DeGrandpre, M. D., Vodacek, A., Nelson, R. K., Bruce, E. J. & Blough, N. V. (1996). Seasonal seawater optical properties of the U.S. Middle Atlantic Bight. *J. Geophys. Res.*, **101**, 22727–36. 70
298. Dekker, A. G. (1993). Detection of optical water quality parameters for eutrophic waters by high resolution remote sensing. Ph.D. thesis. Amsterdam: Vrije Universiteit. 246
299. Dekker, A. G., Brando, V. E. & Anstee, J. M. (2005). Retrospective seagrass change detection in a shallow coastal tidal lake. *Remote Sens. Environ.*, **97**, 415–33. 259

300. Dekker, A. G., Malthus, T. J. & Seyhan, E. (1991). Quantitative modelling of inland water quality for high-resolution MSS systems. *IEEE Trans. Geosci. Remote Sens.*, **29**, 89–95. 236
301. Del Vecchio, R. & Subramaniam, A. (2004). Influence of the Amazon River on the surface optical properties of the western tropical North Atlantic Ocean. *J. Geophys. Res.*, **109**, C11001. 70, 79
302. Demers, S. & Legendre, L. (1981). Mélange vertical et capacité photosynthétique du phytoplancton estuarien (estuaire du Saint Laurent). *Mar. Biol.*, **64**, 243–50. 524
303. Demmig-Adams, B. & Adams, W. W. (1992). Photoprotection and other responses of plants to high light stress. *Ann. Rev. Plant Physiol. Plant Mol. Biol.*, **43**, 599–626. 357
304. Dera, J. & Gordon, H. R. (1968). Light field fluctuations in the photic zone. *Limnol. Oceanogr.*, **13**, 697–9. 139
305. Deschamps, P.-Y., Fournier, B., Lecomte, P. & Verwaerde, C. (2004). SIMBAD: a field radiometer for satellite ocean-color validation. *Appl. Opt.*, **43**, 4055–66. 204
306. Deschamps, P. Y., Herman, M. & Tanre, D. (1983). Modeling of the atmospheric effects and its application to the remote sensing of ocean color. *Appl. Opt.*, **22**, 3751–8. 218
307. Desiderio, R. (2000). Application of the Raman scattering coefficient of water to calculations in marine optics. *Appl. Opt.*, **39**, 1893–4. 116
308. Di Toro, D. M. (1978). Optics of turbid estuarine water: approximations and applications. *Water Res.*, **12**, 1059–68. 114
309. Diakoff, S. & Scheibe, J. (1973). Action spectra for chromatic adaptation in *Tolypothrix tenuis*. *Plant Physiol.*, **51**, 382–5. 481–2
310. Dickey, T., Marra, J., Stramska, M. *et al.* (1994). Bio-optical and physical variability in the subarctic North Atlantic Ocean during the spring of 1989. *J. Geophys. Res.*, **99**, 22541–56. 393
311. Dmitriev, E. V., Khomenko, G., Chami, M. *et al.* (2009). Parameterization of light absorption by components of seawater in optically complex coastal waters of the Crimea Peninsula. *Appl. Opt.*, **48**, 1249–61. 75
312. Dodds, W. K. (1992). A modified fiber-optic light microprobe to measure spherically integrated photosynthetic photon flux density: characterization of peripheral photosynthesis-irradiance patterns. *Limnol. Oceanogr.*, **37**, 871–8. 146
313. Döhler, G., Bürstell, H. & Jilg-Winter, G. (1976). Pigment composition and photosynthetic CO<sub>2</sub> fixation of *Cyanidium caldarium* and *Porphyridium aeruginosum*. *Biochem. Physiol. Pflanzen*, **170**, 103–10. 470, 505
314. Dokulil, M. (1979). Optical properties, colour and turbidity. In H. Lomer (ed.), *Neusiedlersee: The Limnology of a Shallow Lake in Central Europe* (pp. 15–67). The Hague: Junk. 76
315. Dominguez Gomez, J. A., Chuvieco Salinero, E. & Sastre Merlin, A. (2009). Monitoring transparency in inland waters using multispectral images. *Int. J. Remote Sens.*, **30**, 1567–86. 260
316. Doron, M., Babin, M., Mangin, A. & Hembise, O. (2007). Estimation of light penetration, and horizontal and vertical visibility in oceanic and coastal waters from surface reflectance. *J. Geophys. Res.*, **112**, C06003. 260–1

317. Doty, M. S., Gilbert, W. J. & Abbott, I. A. (1974). Hawaiian marine algae from seaward of the algal ridge. *Phycologia*, **13**, 345–57. 459
318. Doty, M. S. & Oguri, M. (1957). Evidence for a photosynthetic daily periodicity. *Limnol. Oceanogr.*, **2**, 37–40. 524
319. Doxaran, D., Froidefond, J.-M., Lavender, S. & Castaing, P. (2002). Spectral signature of highly turbid waters: application with SPOT data to quantify suspended particulate matter concentrations. *Remote Sens. Environ.*, **81**, 149–61. 231
320. Dragesund, O. & Gjøsaeter, J. (1988). The Barents Sea. In H. Postma & J. J. Zijlstra (eds), *Continental Shelves* (pp. 339–61). Amsterdam: Elsevier. 450
321. Drechsler, Z. & Beer, S. (1991). Utilization of inorganic carbon by *Ulva lactuca*. *Plant Physiol.*, **97**, 1439–44. 403
322. Drew, E. A. (1978). Factors affecting photosynthesis and its seasonal variation in the seagrasses *Cymodocea nodosa* (Ucria) Aschers., and *Posidonia oceanica* (L.) Delile in the Mediterranean. *J. Exp. Mar. Biol. Ecol.*, **31**, 173–94. 439
323. Drew, E. A. (1979). Physiological aspects of primary production in seagrasses. *Aquat. Bot.*, **7**, 139–50. 347, 439, 520
324. Dring, M. J. (1981). Chromatic adaptation of photosynthesis in benthic marine algae: an examination of its ecological significance using a theoretical model. *Limnol. Oceanogr.*, **26**, 271–84. 465–6
325. Dring, M. J. (1986). Pigment composition and photosynthetic action spectra of sporophytes of *Laminaria* (Phaeophyta) grown in different light qualities and irradiances. *Br. Phycol. J.*, **21**, 199–207. 471
326. Dring, M. J. (1990). Light harvesting and pigment composition in marine phytoplankton and macro algae. In P. J. Herring, A. K. Campbell, M. Whitfield & L. Maddock (eds), *Light and Life in the Sea* (pp. 89–103). Cambridge: Cambridge University Press. 469
327. Duarte, C. M. (1991). Seagrass depth limits. *Aquat. Bot.*, **40**, 363–77. 391
328. Duarte, C. M., Agusti, S., Satta, M. P. & Vaqué, D. (1998). Partitioning particulate light absorption: a budget for a Mediterranean bay. *Limnol. Oceanogr.*, **43**, 236–44. 86
329. Duarte, C. M. & Chiscano, C. L. (1999). Seagrass biomass and production: a reassessment. *Aquat. Bot.*, **65**, 159–74. 533
330. Dubinsky, Z. & Berman, T. (1976). Light utilization efficiencies of phytoplankton in Lake Kinneret (Sea of Galilee). *Limnol. Oceanogr.*, **21**, 226–30. 372
331. Dubinsky, Z. & Berman, T. (1979). Seasonal changes in the spectral composition of downwelling irradiance in Lake Kinneret (Israel). *Limnol. Oceanogr.*, **24**, 652–63. 165, 328
332. Dubinsky, Z. & Berman, T. (1981). Light utilization by phytoplankton in Lake Kinneret (Israel). *Limnol. Oceanogr.*, **26**, 660–70. 363, 372, 376, 380
333. Duchrow, R. M. & Everhart, W. H. (1971). Turbidity measurement. *Amer. Fish. Soc. Trans.*, **100**, 682–90. 127
334. Dugdale, R. C. & Goering, J. T. (1967). Uptake of new and regenerated forms of nitrogen in primary productivity. *Limnol. Oceanogr.*, **12**, 196–206. 448
335. Dugdale, R. C. & Wilkerson, F. P. (1991). Low specific nitrate uptake rate: a common feature of high-nutrient low-chlorophyll marine ecosystems. *Limnol. Oceanogr.*, **36**, 1678–88. 425

336. Dugdale, R. C., Wilkerson, F. C. & Minas, H. J. (1995). The role of a silicate pump in driving new production. *Deep-Sea Res.*, **42**, 697–719. 423
337. Dunlap, W. C. & Shick, J. M. (1998). Ultraviolet radiation-absorbing mycosporine-like amino acids in coral reef organisms: a biochemical and environmental perspective. *J. Phycol.*, **34**, 418–30. 356
338. Duntley, S. Q. (1963). Light in the sea. *J. Opt. Soc. Amer.*, **53**, 214–33. 182
339. Duntley, S. Q., Wilson, W. H. & Edgerton, C. F. (1974). *Ocean colour analysis, part 1*. (Ref. 74–10, 1–37). San Diego: Scripps Inst. Oceanogr. 170
340. Dunton, K. H. & Jodwalis, C. M. (1988). Photosynthetic performance of *Laminaria solidungula* measured *in situ* in the Alaskan High Arctic. *Mar. Biol.*, **98**, 277–85. 349
341. Durako, M. J., Kunzelman, J. I., Kenworthy, W. J. & Hammerstrom, K. K. (2003). Depth-related variability in the photobiology of two populations of *Halophila johnsonii* and *Halophila decipiens*. *Mar. Biol.*, **142**, 1219–28. 497
342. Durbin, E. G., Krawiec, R. W. & Smayda, T. J. (1975). Seasonal studies on the relative importance of different size fractions of phytoplankton in Narragansett Bay (U.S.A.). *Mar. Biol.*, **32**, 271–87. 511–13
343. Duysens, L. N. M. (1956). The flattening of the absorption spectrum of suspensions as compared to that of solutions. *Biochim. Biophys. Acta*, **19**, 1–12. 311, 313
344. Duysens, L. N. M. & Sweers, H. E. (1963). *Studies on Microalgae and Photosynthetic Bacteria* (pp. 353–72). Tokyo: Univ. Tokyo Press. 333
345. Dwivedi, R. M. & Narain, A. (1987). Remote sensing of phytoplankton. An attempt from the Landsat Thematic Mapper. *Int. J. Remote Sens.*, **8**, 1563–9. 246
346. Effler, S. W., Brooks, C. M., Perkins, M. G., Meyer, M. & Field, F. D. (1987). Aspects of the underwater light field of eight central New York lakes. *Water Res. Bull.*, **23**, 1193–201. 164
347. Effler, S. W., Roop, R. & Perkins, M. G. (1988). A simple technique for estimating absorption and scattering coefficients. *Water Res. Bull.*, **24**, 397–404. 118
348. Effler, S. W., Wodka, M. C. & Field, S. D. (1984). Scattering and absorption of light in Onondaga Lake. *J. Environ. Eng.*, **110**, 1134–45. 118, 194
349. Egeland, E. S., Garrido, J. L., Zapata, M., Maestro, M. A. & Liaen-Jensen, S. (2000). Algal carotenoids. Part 64. Structure and chemistry of 4-keto-19'-hexanoyloxyfucoxanthin with a novel carotenoid end group. *J. Chem. Soc., Perkin Trans.*, **1**, 1223–30. 283
350. Egle, K. (1960). Menge und Verhältnis der Pigmente. In W. Ruhland (ed.), *Encyclopaedia of Plant Physiology* (pp. 444–96). Berlin: Springer-Verlag. 277
351. Ehn, J., Granskog, M. A., Reinart, A. & Erm, A. (2004). Optical properties of melting landfast sea ice and underlying seawater in Santala Bay, Finland. *J. Geophys. Res.*, **109**, C09003. 167
352. Ehn, J. K., Mundy, C. J. & Barber, D. G. (2008). Bio-optical and structural properties inferred from irradiance measurements within the bottommost layers in an Arctic landfast sea ice cover. *J. Geophys. Res.*, **113**, C03S03. 121
353. Eisner, L. B. & Cowles, T. J. (2005). Spatial variations in phytoplankton pigment ratios, optical properties, and environmental gradients in Oregon coast surface waters. *J. Geophys. Res.*, **110**, C10S14. 86

354. Eklöf, J. S., De la Torre-Castro, M., Gullström, M. *et al.* (2008). Sea urchin overgrazing of seagrasses: a review of current knowledge on causes, consequences and management. *Estuar. Coast. Shelf Sci.*, **79**, 569–80. 428
355. Elser, J. J. & Kimmel, B. L. (1985). Photoinhibition of temperate lake phytoplankton by near-surface irradiance: evidence from vertical profiles and field experiments. *J. Phycol.*, **21**, 419–27. 360
356. Elskens, M., Baeyens, W., Cattaldo, T., Dehairs, F. & Griffiths, B. (2002). N uptake conditions during summer in the Subantarctic and Polar Frontal Zones of the Australian sector of the Southern Ocean. *J. Geophys. Res.*, **107**, C113182. 448–9
357. Elterman, P. (1970). Integrating cavity spectroscopy. *Appl. Opt.*, **9**, 2140–2. 56
358. Emerson, R. (1958). Yield of photosynthesis from simultaneous illumination with pairs of wavelengths. *Science*, **127**, 1059–60. 384
359. Emerson, R. & Lewis, C. M. (1942). The photosynthetic efficiency of phycocyanin in *Chroococcus* and the problem of carotenoid participation in photosynthesis. *J. Gen. Physiol.*, **25**, 579–95. 382, 384
360. Emerson, R. & Lewis, C. M. (1943). The dependence of the quantum yield of *Chlorella* photosynthesis on wave length of light. *Amer. J. Bot.*, **30**, 165–78. 382, 383, 384
361. Engelmann, T. W. (1883). Farbe und Assimilation. *Bot. Zeit.*, **41**, 1–13, 17–29. 454
362. Engelmann, T. W. (1884). Untersuchungen über die quantitativen Beziehungen zwischen Absorption des Lichtes und Assimilation in Pflanzenzellen. *Bot. Zeit.*, **42**, 81–93, 97–108. 382
363. Engelmann, T. W. & Gaidukov, N. I. (1902). Ueber experimentelle Erzeugung zweckmässiger Aenderungen der Färbung pflanzlicher Chromophylle durch farbiges Licht. *Arch. Anat. Physiol. Lpz.:Physiol. Abt.*, 333–5. Quoted by Rabinowitch (1945). 480
364. Enriquez, S., Merino, M. & Iglesias-Prieto, R. (2002). Variations in the photosynthetic performance along the leaves of the tropical seagrass *Thalassia testudinum*. *Mar. Biol.*, **140**, 891–900. 471
365. Eppley, R. W. (1968). An incubation method for estimating the carbon content of phytoplankton in natural samples. *Limnol. Oceanogr.*, **13**, 547–82. 278
366. Eppley, R. W. & Peterson, B. J. (1979). Particulate organic matter flux and planktonic new production in the ocean. *Nature*, **282**, 677–80. 448
367. Erfteimeijer, P. L. A. & Stapel, J. (1999). Primary production of deep-water *Halophila ovalis* meadows. *Aquat. Bot.*, **65**, 71–82. 347
- 367a. Eriksen, C. C., Osse, T. J., Light, R. D. *et al.* (2001). Seaglider: a long-range autonomous underwater vehicle for oceanographic research. *IEEE J. Oceanic Engineering*, **26**, 424–36. 141
368. Ertel, J. R., Hedges, J. I., Devel, A. H., Richey, J. E. & Ribeiro, M. N. G. (1986). Dissolved humic substances of the Amazon River system. *Limnol. Oceanogr.*, **31**, 739–54. 68
369. Ertel, J. R., Hedges, J. I. & Perdue, E. M. (1984). Lignin signature of aquatic humic substances. *Science*, **223**, 485–7. 67
370. ESA (1992). *Medium resolution imaging spectrometer (MERIS). Draft brochure*. Paris: European Space Agency. 211

371. Evans, G. T. & Taylor, F. R. J. (1980). Phytoplankton accumulation in Langmuir cells. *Limnol. Oceanogr.*, **25**, 840–5. 358
372. Exton, R. J., Houghton, W. M., Esaias, W. *et al.* (1983). Laboratory analysis of techniques for remote sensing of estuarine parameters using laser excitation. *Appl. Opt.*, **22**, 54–65. 252
373. Fahnenstiel, G. L. & Scavia, D. (1987). Dynamics of Lake Michigan phytoplankton: the deep chlorophyll layer. *J. Great Lakes Res.*, **13**, 285–95. 397
374. Fahnenstiel, G. L., Schelske, C. L. & Moll, R. A. (1984). In situ quantum efficiency of Lake Superior phytoplankton. *J. Great Lakes Res.*, **10**, 399–406. 372
375. Fairhead, V. A. & Cheshire, A. C. (2004). Rates of primary productivity and growth in *Ecklonia radiata* measured at different depths, over an annual cycle, at West Island, South Australia. *Mar. Biol.*, **145**, 41–50. 496
376. Falkowski, P. G. (1981). Light-shade adaptation and assimilation numbers. *J. Plankton Res.*, **3**, 203–16. 368, 377, 442
377. Falkowski, P. G., Barber, R. T. & Smetacek, V. (1998). Biogeochemical controls and feedback on ocean primary production. *Science*, **281**, 200–6. 451
378. Falkowski, P. G. & Dubinsky, Z. (1981). Light-shade adaptation of *Stylophora pistillata*, a hermatypic coral from the Gulf of Eilat. *Nature*, **289**, 172–4. 350, 473
379. Falkowski, P. G., Dubinsky, Z. & Wyman, K. (1985). Growth irradiance relationships in phytoplankton. *Limnol. Oceanogr.*, **30**, 311–21. 317
380. Falkowski, P. G., Jokiel, P. L. & Kinzie, R. A. (1990). Irradiance and corals. In Z. Dubinsky (ed.), *Coral Reefs* (pp. 89–107). Amsterdam: Elsevier. 473, 495
381. Falkowski, P. G. & LaRoche, J. (1991). Acclimation to spectral irradiance in algae. *J. Phycol.*, **27**, 8–14. 469, 472
382. Falkowski, P. G. & Owens, T. G. (1978). Effects of light intensity on photosynthesis and dark respiration in six species of marine phytoplankton. *Mar. Biol.*, **45**, 289–95. 343, 470
383. Falkowski, P. G. & Owens, T. G. (1980). Light-shade adaptation: two strategies in marine phytoplankton. *Plant Physiol.*, **66**, 592–5. 472, 473
384. Falkowski, P. G. & Raven, J. A. (2007). *Aquatic Photosynthesis*. Princeton, NJ: Princeton University Press. 265, 302, 306, 332, 377, 402, 403, 407
385. Falkowski, P. G. & Woodhead, A. D. (eds) (1992). *Primary Productivity and Biogeochemical Cycles in the Sea*. New York: Plenum. 388
386. Faller, A. J. (1978). Experiments with controlled Langmuir circulations. *Science*, **201**, 618–20. 358
387. Faust, M. A. & Gantt, E. (1973). Effect of light intensity and glycerol on the growth, pigment composition and ultrastructure of *Chroomonas* sp. *J. Phycol.*, **9**, 489–95. 470
388. Fee, E. J. (1969). A numerical model for the estimation of photosynthetic production, integrated over time and depth, in natural waters. *Limnol. Oceanogr.*, **14**, 906–11. 440
389. Fee, E. J. (1976). The vertical and seasonal distribution of chlorophyll in lakes of the Experimental Lakes Area, northwestern Ontario: implication for primary production estimates. *Limnol. Oceanogr.*, **21**, 767–83. 397, 494
390. Fernandez, C., Raimbault, P., Garcia, N., Rimmeli, P. & Caniaux, G. (2005). An estimation of annual new production and carbon fluxes in the northeast Atlantic Ocean during 2001. *J. Geophys. Res.*, **110**, C07S13. 448, 450

391. Ferrari, G. M. & Tassan, S. (1991). On the accuracy of determining light absorption by 'yellow substance' through measurements of induced fluorescence. *Limnol. Oceanogr.*, **36**, 777–86. 75
392. Ferrari, G. M. & Tassan, S. (1999). A method using chemical oxidation to remove light absorption by phytoplankton pigments. *J. Phycol.*, **35**, 1090–8. 84
393. Ferrier, J. M. (1980). Apparent bicarbonate uptake and possible plasma-membrane proton efflux in *Chara corallina*. *Plant Physiol.*, **66**, 1198–9. 405, 406
394. Fichot, C. G., Sathyendranath, S. & Miller, W. L. (2008). SeaUV and SeaUV<sub>C</sub>: algorithms for the retrieval of UV/visible diffuse attenuation coefficients from ocean color. *Remote Sens. Environ.*, **112**, 1584–602. 258
395. Figueroa, F. L., Niell, F. X., Figueiras, F. G. & Villarino, M. L. (1998). Diel migration of phytoplankton and spectral light field in the Ría de Vigo (NW Spain). *Mar. Biol.*, **130**, 491–9. 516
396. Fischer, J. & Kronfeld, U. (1990). Sun-stimulated fluorescence. I: Influence of oceanic properties. *Int. J. Remote Sens.*, **11**, 2125–47. 247
397. Fischer, J. & Schlüssel, P. (1990). Sun-stimulated chlorophyll fluorescence. 2: Impact of atmospheric properties. *Int. J. Remote Sens.*, **11**, 2149–62. 247
398. Fisher, T., Shurtz-Swirski, R., Gepstein, S. & Dubinsky, Z. (1989). Changes in the levels of ribulose-1, 5-bisphosphate carboxylase/oxygenase (Rubisco) in *Tetradron minimum* (Chlorophyta) during light and shade adaptation. *Plant Cell Physiol.*, **30**, 221–8. 475
399. Fitch, D. T. & Moore, J. K. (2007). Wind speed influence on phytoplankton bloom dynamics in the Southern Ocean Marginal Ice Zone. *J. Geophys. Res.*, **112**, C08006. 394
400. Fleischhacker, P. & Senger, H. (1978). Adaptation of the photosynthetic apparatus of *Scenedesmus obliquus* to strong and weak light conditions. *Physiol. Plant.*, **43**, 43–51. 472, 474
401. Fogg, G. E. (1991). The phytoplanktonic way of life. *New Phytol.*, **118**, 191–232. 388
402. Fogg, G. E., Stewart, W. D. P., Fay, P. & Walsby, A. E. (1973). *The Blue-green Algae*. London: Academic Press. 517, 518
403. Fogg, G. E. & Thake, B. (1987). *Algal Cultures and Phytoplankton Ecology*. Madison: University of Wisconsin Press. 388
404. Fookes, C. J. R. & Jeffrey, S. W. (1989). The structure of chlorophyll c<sub>3</sub>, a novel marine photosynthetic pigment. *J. Chem. Soc., Chem. Commun.*, **23**, 1827–8. 277
405. Fork, D. C. (1963). Observations of the function of chlorophyll a and accessory pigments in photosynthesis. In *Photosynthesis Mechanisms in Green Plants* (pp. 352–61). Washington: National Academy of Science-National Research Council. 358–6, 466
406. Foss, P., Guillard, R. R. L. & Liaaen-Jensen, S. (1984). Prasinolanthin – a chemosystematic marker for algae. *Phytochem.*, **23**, 1629–33. 284
407. Fox, L. E. (1983). The removal of dissolved humic acid during estuarine mixing. *Estuar. Coast. Shelf Sci.*, **16**, 431–40. 68
408. Foy, R. H. & Gibson, C. E. (1982a). Photosynthetic characteristics of planktonic blue-green algae: the response of twenty strains grown under high and low light. *Br. Phycol. J.*, **17**, 169–82. 477

409. Foy, R. H. & Gibson, C. E. (1982b). Photosynthetic characteristics of planktonic blue-green algae: changes in photosynthetic capacity and pigmentation of *Oscillatoria redekei* Van Goor under high and low light. *Br. Phycol. J.*, **17**, 183–93. 470, 477
410. French, C. S. (1960). The chlorophylls *in vivo* and *in vitro*. In W. Ruhland (ed.), *Encyclopaedia of Plant Physiology* (pp. 252–97). Berlin: Springer-Verlag. 280
411. French, C. S., Brown, J. S. & Lawrence, M. C. (1972). Four universal forms of chlorophyll *a*. *Plant Physiol.*, **49**, 421–9. 292
412. Friedman, A. L. & Alberte, R. S. (1984). A diatom light-harvesting pigment-protein complex. *Plant Physiol.*, **76**, 483–9. 290
413. Friedman, A. L. & Alberte, R. S. (1986). Biogenesis and light regulation of the major light-harvesting chlorophyll-protein of diatoms. *Plant Physiol.*, **80**, 43–51. 473
414. Friedman, E., Poole, L., Cherdak, A. & Houghton, W. (1980). Absorption coefficient instrument for turbid natural waters. *Appl. Opt.*, **19**, 1688–93. 59
415. Fritsch, F. E. (1948). *The Structure and Reproduction of the Algae*. Cambridge: Cambridge University Press. 266
416. Froidefond, J.-M., Lavender, S., Laborde, P., Herbland, A. & Lafon, V. (2002). SeaWiFS data interpretation in a coastal area in the Bay of Biscay. *Internat. J. Remote Sens.*, **23**, 881–904. 234
417. Frost, B. W. (1980). Grazing. In I. Morris (ed.), *The Physiological Ecology of Phytoplankton* (pp. 465–91). Oxford: Blackwell. 424
418. Fry, E. S. & Kattawar, G. W. (1988). Measurement of the absorption coefficient of ocean water using isotropic illumination. *Proc. Soc. Photo-Opt. Instrum. Eng., Ocean Optics IX*, **925**, 142–8. 56
419. Fry, E. S., Kattawar, G. W. & Pope, R. M. (1992). Integrating cavity absorption meter. *Appl. Opt.*, **31**, 2055–65. 56
420. Fujiki, T., Suzue, T., Kimoto, H. & Saino, T. (2007). Photosynthetic electron transport in *Dunaliella tertiolecta* (Chlorophyceae) measured by fast repetition rate fluorometry: relation to carbon assimilation. *J. Plankton Res.*, **29**, 199–208. 337
421. Fujita, Y. & Hattori, A. (1960). Effect of chromatic lights on phycobilin formation in a blue-green alga, *Tolypothrix tenuis*. *Plant Cell Physiol.*, **1**, 293–303. 481
422. Fujita, Y. & Hattori, A. (1962a). Photochemical interconversion between precursors of phycobilin chromoproteids in *Tolypothrix tenuis*. *Plant Cell Physiol.*, **3**, 209–20. 481–2
423. Fujita, Y. & Hattori, A. (1962b). Changes in composition of cellular material during formation of phycobilin chromoproteids in a bluegreen alga, *Tolypothrix tenuis*. *J. Biochem.*, **52**, 38–42. 481
424. Furnas, M. J. & Mitchell, A. W. (1988). Photosynthetic characteristics of Coral Sea picoplankton (<2 µm size fraction). *Biol. Oceanogr.*, **5**, 163–82. 345
425. Gaidukov, N. (1902). Ueber den Einfluss farbigen Lichts auf die Faerbung levender Oscillarien. *Abh. Preuss Akad. Wiss. Berlin, No. 5*. Quoted by Bogorad (1975). 480
426. Gallagher, J. C. (1980). Population genetics of *Skeletonema costatum* (Bacillariophyceae) in Narragansett Bay. *J. Phycol.*, **16**, 464–74. 513

427. Gallagher, J. C. (1982). Physiological variation and electrophoretic banding patterns of genetically different seasonal populations of *Skeletonema costatum* (Bacillariophyceae). *J. Phycol.*, **18**, 148–62. 513
428. Gallegos, C. L., Correll, D. L. & Pierce, J. W. (1990). Modelling spectral diffuse attenuation, absorption, and scattering coefficients in a turbid estuary. *Limnol. Oceanogr.*, **35**, 1486–502. 74, 75, 117, 164
429. Gallegos, C. L. & Kenworthy, W. J. (1996). Seagrass depth limits in the Indian River Lagoon (Florida, U.S.A.): application of an optical water quality model. *Estuar. Coast. Shelf Sci.*, **42**, 267–88. 391
430. Ganf, G. G. (1974). Incident solar irradiance and underwater light penetration as factors controlling the chlorophyll *a* content of a shallow equatorial lake (Lake George, Uganda). *J. Ecol.*, **62**, 593–609. 328
431. Ganf, G. G. (1975). Photosynthetic production and irradiance-photosynthesis relationships of the phytoplankton from a shallow equatorial lake (Lake George, Uganda). *Oecologia*, **18**, 165–83. 344, 393, 434
432. Ganf, G. G. & Oliver, R. L. (1982). Vertical separation of light and available nutrients as a factor causing replacement of green algae by blue-green algae in the plankton of a stratified lake. *J. Ecol.*, **70**, 829–44. 519
433. Ganf, G. G., Oliver, R. L. & Walsby, A. E. (1989). Optical properties of gas-vacuolate cells and colonies of *Microcystis* in relation to light attenuation in a turbid, stratified reservoir (Mount Bold Reservoir, South Australia). *Aust. J. Mar. Freshwater Res.*, **40**, 595–611. 78, 114, 119, 129, 194
434. Gantt, E. (1975). Phycobilisomes: light-harvesting pigment complexes. *Bioscience*, **25**, 781–8. 293
435. Gantt, E. (1977). Recent contributions in phycobiliproteins and phycobilisomes. *Photochem. Photobiol.*, **26**, 685–9. 293
436. Gantt, E. (1986). Phycobilisomes. *Encycl. Plant Physiol. (n.s.)*, **19**, 260–8. 297
437. Garcia-Mendoza, E. & Maske, H. (1996). The relationship of solar-stimulated natural fluorescence and primary productivity in Mexican Pacific waters. *Limnol. Oceanogr.*, **41**, 1697–710. 338
438. Garrido, J. L., Otero, J., Maestro, M. A. & Zapata, M. (2000). The main nonpolar chlorophyll *c* from *Emiliania huxleyi* (Prymnesiophyceae) is a chlorophyll *c*<sub>2</sub>-monogalactosyldiacylglyceride ester: a mass spectrometry study. *J. Phycol.*, **36**, 497–505. 276
439. Garrido, J. L., Zapata, M. & Muñiz, S. (1995). Spectra characterization of new chlorophyll *c* pigments isolated from *Emiliania huxleyi* (Prymnesiophyceae) by high-performance liquid chromatography. *J. Phycol.*, **31**, 761–8. 276
440. Garver, S. A. & Siegel, D. A. (1997). Inherent optical property of ocean color spectra and its biogeochemical interpretation. 1. Time series from the Sargasso Sea. *J. Geophys. Res.*, **102**, 18607–25. 243
441. Gates, D. M. (1962). *Energy Exchange in the Biosphere*. New York: Harper & Row. 38
442. Geider, R. J. (1987). Light and temperature dependence of the carbon to chlorophyll *a* ratio in microalgae and cyanobacteria: implications for physiology and growth of phytoplankton. *New Phytol.*, **106**, 1–34. 469
443. Geider, R. J. & Osborne, B. A. (1987). Light absorption by a marine diatom: experimental observations and theoretical calculations of the package effect in a small *Thalassiosira* species. *Mar. Biol.*, **96**, 299–308. 318

444. Gelin, C. (1975). Nutrients, biomass and primary productivity of nanoplankton in eutrophic Lake Vombsjön, Sweden. *Oikos*, **26**, 121–39. 328, 419
445. Genty, B., Briantais, J. M. & Baker, N. R. (1989). The relationship between the quantum yield of photosynthetic electron transport and quenching of chlorophyll fluorescence. *Biochim. Biophys. Acta*, **990**, 87–92. 334, 337
446. Gerard, V. A. (1986). Photosynthetic characteristics of giant kelp (*Macrocystis pyrifera*) determined *in situ*. *Mar. Biol.*, **90**, 473–82. 349
447. Gernez, P. & Antoine, D. (2009). Field characterization of wave-induced underwater light field fluctuations. *J. Geophys. Res.*, **114**, C06025. 139
448. Gershun, A. (1936). O fotometrii mutnykh sredin. *Tr. Gos. Okeanogr. Inst.*, **11**, 99. Quoted by Jerlov (1976). 26
449. Gervais, F., Padisák, J. & Koschel, R. (1997). Do light quality and low nutrient concentration favour picocyanobacteria below the thermocline of the oligotrophic Lake Stechlin? *J. Plankton Res.*, **19**, 771–81. 463
450. Gervais, F., Riebesell, U. & Gorbunov, M. Y. (2002). Changes in primary productivity and chlorophyll *a* in response to iron fertilization in the Southern Polar Frontal Zone. *Limnol. Oceanogr.*, **47**, 1324–35. 425
451. Gessner, F. (1937). Untersuchungen über Assimilation und Atmung submerser Wasserpflanzen. *Jahrb. Wiss. Bot.*, **85**, 267–328. 412
452. Gilabert, M. A., Conese, C. & Maselli, F. (1994). An atmospheric correction method for the automatic retrieval of surface reflectance from TM images. *Int. J. Remote Sens.*, **15**, 2065–86. 224
453. Gilerson, A., Zhou, J., Chowdhary, J. *et al.* (2006). Retrieval of chlorophyll fluorescence spectra through polarization discrimination. *Appl. Opt.*, **45**, 5568–81. 249
- 453a. Gillbro, T. & Cogdell, R. J. (1989). Carotenoid fluorescence. *Chem. Phys. Lett.*, **158**, 312–16. 299
454. Gilmartin, M. (1960). The ecological distribution of the deep water algae of Eniwetok atoll. *Ecology*, **41**, 210–21. 459
455. Gitelson, A. (1992). The peak near 700 nm on radiance spectra of algae and water: relationships of its magnitude and position with chlorophyll concentration. *Int. J. Remote Sens.*, **13**, 3367–73. 236
456. Gitelson, A. A. & Kondratyev, K. Y. (1991). Optical models of mesotrophic and eutrophic water bodies. *Int. J. Remote Sens.*, **12**, 375–85. 206
457. Glazer, A. N. (1981). Photosynthetic accessory proteins with bilin prosthetic groups. In M. D. Hatch & N. K. Boardman (eds), *The Biochemistry of Plants* (pp. 51–96). New York: Academic Press. 293, 296
458. Glazer, A. N. (1985). Light harvesting by phycobilisomes. *Ann. Rev. Biophys. Biophys. Chem.*, **14**, 47–77. 293, 295, 296, 297
459. Glazer, A. N. & Cohen-Bazire, G. (1975). A comparison of *Cryptophytan phycocyanins*. *Arch. Mikrobiol.*, **104**, 29–32. 296
460. Glazer, A. N. & Melis, A. (1987). Photochemical reaction centres: structure, organization and function. *Ann. Rev. Plant Physiol.*, **38**, 11–45. 297
461. Glenn, E. P. & Doty, M. S. (1981). Photosynthesis and respiration of the tropical red seaweeds, *Eucheuma striatum* (Tambalang and Elkhorn varieties) and *E. denticulatum*. *Aquat. Biol.*, **10**, 353–64. 495, 524
462. Glibert, P. M., Dennett, M. R. & Goldman, J. C. (1985). Inorganic carbon uptake by phytoplankton in Vineyard Sound, Massachusetts I. Measurements of the

- photosynthesis-irradiance response of winter and early-spring assemblages. *J. Exp. Mar. Biol. Ecol.*, **85**, 21–36. 359
463. Gliwicz, M. Z. (1986). Suspended clay concentration controlled by filter-feeding zooplankton in a tropical reservoir. *Nature*, **323**, 330–2. 121
464. Glud, R. N., Kühl, M., Kohls, O. & Ramsing, N. B. (1999). Heterogeneity of oxygen production and consumption in a photosynthetic microbial mat as studied by planar optodes. *J. Phycol.*, **35**, 270–9. 530
465. Goddijn, L. M. & White, M. (2006). Using a digital camera for water quality measurements in Galway Bay. *Estuar. Coast. Shelf Sci.*, **66**, 429–36. 205, 252
466. Goedheer, J. C. (1969). Energy transfer from carotenoids to chlorophyll in blue-green, red and green algae and greening bean leaves. *Biochim. Biophys. Acta*, **172**, 252–65. 387
467. Goerick, R. & Repeta, D. J. (1992). The pigments of *Prochlorococcus marinus*: the presence of divinyl chlorophyll *a* and *b* in a marine prokaryote. *Limnol. Oceanogr.*, **37**, 425–33. 276, 278, 284
468. Goerick, R. (2002). Top-down control of phytoplankton biomass and community structure in the monsoonal Arabian Sea. *Limnol. Oceanogr.*, **47**, 1307–23. 426
469. Gohin, F., Druon, J. N. & Lampert, L. (2002). A five channel chlorophyll concentration algorithm applied to SeaWiFS data processed by SeaDAS in coastal waters. *Internat. J. Remote Sens.*, **23**, 1639–61. 246
470. Goldman, C. R., Mason, D. T. & Wood, B. J. B. (1963). Light injury and inhibition in Antarctic freshwater plankton. *Limnol. Oceanogr.*, **8**, 313–22. 354
471. Goldman, J. C. (1979a). Outdoor algal mass cultures. I. Applications. *Water Res.*, **13**, 1–19. 535
472. Goldman, J. C. (1979b). Outdoor algal mass cultures. II. Photosynthetic yield limitations. *Water Res.*, **13**, 119–36. 535
473. Goldsborough, W. J. & Kemp, W. M. (1988). Light responses of a submersed macrophyte: implications for survival in turbid tidal waters. *Ecology*, **69**, 1775–86. 479
474. Gong, S., Huang, J., Li, Y. & Wang, H. (2008). Comparison of atmospheric correction algorithms for TM image in inland waters. *Int. J. Remote Sens.*, **29**, 2199–210. 225
475. Gorbunov, M. Y., Falkowski, P. G. & Kolber, Z. S. (2000). Measurement of photosynthetic parameters in benthic organisms in situ using a SCUBA-based fast repetition rate fluorometer. *Limnol. Oceanogr.*, **45**, 242–5. 327
476. Gordon, H. R. (1985). Ship perturbation of irradiance measurements at sea. *Appl. Opt.*, **24**, 4172–82. 140
477. Gordon, H. R. (1989a). Can the Lambert-Beer law be applied to the diffuse attenuation coefficient of ocean water? *Limnol. Oceanogr.*, **34**, 1389–409. 150, 258
478. Gordon, H. R. (1989b). Dependence of the diffuse reflectance of natural waters on the sun angle. *Limnol. Oceanogr.*, **34**, 1484–9. 170
479. Gordon, H. R. (1991). Absorption and scattering estimates from irradiance measurements: Monte Carlo simulations. *Limnol. Oceanogr.*, **36**, 769–77. 106
480. Gordon, H. R. (2005). Normalized water-leaving radiance: revisiting the influence of surface roughness. *Appl. Opt.*, **44**, 241–8. 217, 221, 222
481. Gordon, H. R. & Boynton, G. C. (1998). A radiance-irradiance inversion algorithm for estimating the absorption and backscattering coefficients of natural waters. *Appl. Opt.*, **37**, 3886–96. 130

482. Gordon, H. R. & Brown, O. B. (1973). Irradiance reflectivity of a flat ocean as a function of its optical properties. *Appl. Opt.*, **12**, 1549–51. 150
483. Gordon, H. R., Brown, J. W. & Evans, R. H. (1988). Exact Rayleigh scattering calculations for use with the Nimbus-7 coastal zone color scanner. *Appl. Opt.*, **27**, 862–71. 219
484. Gordon, H. R., Brown, O. B. & Jacobs, M. M. (1975). Computed relationships between the inherent and apparent optical properties of a flat, homogeneous ocean. *Appl. Opt.*, **14**, 417–27. 150, 170
485. Gordon, H. R. & Clark, D. K. (1980). Atmospheric effects in the remote sensing of phytoplankton pigments. *Boundary-layer Meteorol.*, **18**, 299–313. 201
486. Gordon, H. R. & Clark, D. K. (1981). Clear water radiances for atmospheric correction of coastal zone color scanner imagery. *Appl. Opt.*, **20**, 4175–80. 221
487. Gordon, H. R., Clark, D. K., Brown, J. W. *et al.* (1983). Phytoplankton pigment concentrations in the Middle Atlantic Bight: comparison of ship determinations and CZCS estimates. *Appl. Opt.*, **22**, 20–36. 239–40
488. Gordon, H. R., Clark, D. K., Mueller, J. L. & Hovis, W. A. (1980). Phytoplankton pigments from the Nimbus-7 Coastal Zone Scanner: comparison with surface measurements. *Science*, **210**, 63–6. 240
489. Gordon, H. R. & Ding, K. (1992). Self-shading of in-water optical instruments. *Limnol. Oceanogr.*, **37**, 491–500. 140, 149
490. Gordon, H. R. & McLuney, W. R. (1975). Estimation of the depth of sunlight penetration in the sea for remote sensing. *Appl. Opt.*, **14**, 413–16. 199
491. Gordon, H. R. & Morel, A. Y. (1983). *Remote Assessment of Ocean Colour for Interpretation of Satellite Visible Imagery. A Review*. New York: Springer. 94, 174, 244
492. Gordon, H. R. & Wang, M. (1994). Retrieval of water-leaving radiance and aerosol optical thickness over the oceans with SeaWiFS: a preliminary algorithm. *Appl. Opt.*, **33**, 443–52. 218–22, 233
493. Gordon, H. R., Smyth, T. J., Balch, W. M., Boynton, G. C. & Tarran, G. A. (2009). Light scattering by coccoliths detached from *Emiliania huxleyi*. *Appl. Opt.*, **48**, 6059–73. 130
494. Gordon, J. I. (1969). San Diego: Scripps Inst. Oceanogr. Ref. 67–27. Quoted by Austin (1974a). 46
495. Gorham, E. (1957). The chemical composition of lake waters in Halifax County, Nova Scotia. *Limnol. Oceanogr.*, **2**, 12–21. 77
496. Gorham, E., Dean, W. E. & Sanger, J. E. (1983). The chemical composition of lakes in the north-central United States. *Limnol. Oceanogr.*, **28**, 287–301. 80
497. Goulard, F., Lüning, K. & Jacobsen, S. (2004). Circadian rhythm of photosynthesis and concurrent oscillations of transcript abundance of photosynthetic genes in the marine red alga *Grateloupia turuturu*. *Eur. J. Phycol.*, **39**, 431–7. 526
498. Gould, R. W., Arnone, R. A. & Martinolich, P. M. (1999). Spectral dependence of the scattering coefficient in case 1 and case 2 waters. *Appl. Opt.*, **38**, 2377–83. 125
499. Gowen, R. J. & Bloomfield, S. P. (1996). Chlorophyll standing crop and phytoplankton production in the western Irish Sea during 1992 and 1993. *J. Plankton Res.*, **18**, 1735–51. 450
500. Gowen, R. J., Tett, P., Kennington, K. *et al.* (2008). The Irish Sea: is it eutrophic? *Estuar. Coast. Shelf. Sci.*, **76**, 239–54. 423

501. Gower, J. F. R. (1980). Observations of fluorescence of in situ chlorophyll *a* in Saanich Inlet. *Boundary-layer Meteorol.*, **18**, 235–45. 247
502. Gower, J. F. R., Doerffer, R. & Borstad, G. A. (1999). Interpretation of the 685 nm peak in water-leaving radiance spectra in terms of fluorescence, absorption and scattering, and its observation by MERIS. *Int. J. Remote Sens.*, **20**, 1771–86. 248
503. Gower, J. & King, S. (2007). Validation of chlorophyll fluorescence derived from MERIS on the west coast of Canada. *Int. J. Remote Sens.*, **28**, 625–35. 248
504. Gower, J., King, S., Borstad, G. & Brown, L. (2005). Detection of intense plankton blooms using the 709 nm band of the MERIS imaging spectrometer. *Int. J. Remote Sens.*, **26**, 2005–12. 236–7
505. Gower, J., King, S. & Goncalves, P. (2008). Global monitoring of plankton blooms using MERIS MCI. *Int. J. Remote Sens.*, **29**, 6209–16. 237
506. Granbom, M., Pedersén, M., Kadel, P. & Lüning, K. (2001). Circadian rhythm of photosynthetic oxygen evolution in *Kappaphycus alvarezii* (Rhodophyta): dependence on light quality and quantity. *J. Phycol.*, **37**, 1020–5. 525
507. Gray, D. J., Kattawar, G. W. & Fry, E. S. (2006). Design and analysis of a flow-through integrating cavity absorption meter. *Appl. Opt.*, **45**, 8990–8. 60
508. Green, B. R. & Durnford, D. G. (1996). The chlorophyll-carotenoid proteins of oxygenic photosynthesis. *Ann. Rev. Plant Physiol. Plant Mol. Biol.*, **47**, 685–714. 286
509. Green, R. E., Sosik, H. M. & Olson, R. J. (2003). Contributions of phytoplankton and other particles to inherent optical properties in New England continental shelf waters. *Limnol. Oceanogr.*, **48**, 2377–91.
510. Greenberg, B. M., Gaba, V., Canaani, O. *et al.* (1989). Separate photosensitizers mediate degradation of the 32-kDa photosystem II reaction center protein in the visible and UV spectral regions. *Proc. Natl. Acad. Sci. (Wash.)*, **86**, 6617–20. 355
511. Grobbelaar, J. U. (1989). The contribution of phytoplankton productivity in turbid freshwaters to their trophic status. *Hydrobiologia*, **173**, 127–33. 389
512. Grzymiski, J., Johnsen, G. & Sakshaug, E. (1997). The significance of intracellular self-shading on the biooptical properties of brown, red and green macroalgae. *J. Phycol.*, **33**, 408–14. 319
513. Guard-Friar, D. & MacColl, R. (1986). Subunit separation ( $\alpha$ ,  $\alpha'$ ,  $\beta$ ) of cryptomonad biliproteins. *Photochem. Photobiol.*, **43**, 81–5. 297
514. Gugliemelli, L. A., Dutton, H. J., Jursinic, P. A. & Siegelman, H. W. (1981). Energy transfer in a light-harvesting carotenoid-chlorophyll *c*-chlorophyll *a*-protein of *Phaeodactylum tricoratum*. *Photochem. Photobiol.*, **33**, 903–7. 282
515. Gurfink, A. M. (1976). Light field in the surface layers of the sea. *Oceanology*, **15**, 295–9. 49
516. Haardt, H. & Maske, H. (1987). Specific *in vivo* absorption coefficient of chlorophyll *a* at 675 nm. *Limnol. Oceanogr.*, **32**, 608–19. 87, 317
517. Häder, D.-P., Lebert, M., Figueroa, F. L. *et al.* (1998). Photoinhibition in Mediterranean macroalgae by solar radiation measured on site by PAM fluorescence. *Aquat. Bot.*, **61**, 225–36. 353
518. Hagen, C., Braune, W. & Björn, L. O. (1994). Functional aspects of secondary carotenoids in *Haematococcus lacustris* (Volvocales). III. Action as a “sunshade”. *J. Phycol.*, **30**, 241–8. 471

519. Halldal, P. (1974). Light and photosynthesis of different marine algal groups. In N. G. Jerlov & E. S. Nielsen (eds), *Optical Aspects of Oceanography* (pp. 345–60). London: Academic Press. 159, 458
520. Hammer, U. T. (1980). Primary production: geographical variations. In E. D. Le Cren & R. H. Lowe-McConnell (eds), *The Functioning of Freshwater Ecosystems* (pp. 235–46). Cambridge: Cambridge University Press. 452, 534
521. Hanelt, D., Tüg, H., Bischof, K. *et al.* (2001). Light regime in an Arctic fjord: a study related to stratospheric ozone depletion as a basis for determination of UV effects on algal growth. *Mar. Biol.*, **138**, 649–58. 163
522. Hanisak, M. D. (1979). Growth patterns of *Codium fragile* ssp. *tomentosoides* in response to temperature, irradiance, salinity and nitrogen source. *Mar. Biol.*, **50**, 319–22. 436–7
523. Harder, R. (1921). *Jahrb. Wiss. Botan.*, **60**, 531. Quoted by Rabinowitch (1971). 402
524. Harder, R. (1923). Über die Bedeutung von Lichtintensität und Wellenlänge für die Assimilation Färbiger Algen. *Z. Bot.*, **15**, 305–55. 454
525. Harding, L. W. & Coats, D. W. (1988). Photosynthetic physiology of *Prorocentrum mariae-lebouriae* (Dinophyceae) during its subpycnocline transport in Chesapeake Bay. *J. Phycol.*, **24**, 77–89. 158, 347
526. Harding, L. W., Itsweire, E. C. & Esaias, W. E. (1992). Determination of phytoplankton chlorophyll concentrations in the Chesapeake Bay with aircraft remote sensing. *Remote Sens. Environ.*, **40**, 79–100. 207
527. Harding, L. W., Mallonee, M. E. & Perry, E. S. (2002). Toward a predictive understanding of primary productivity in a temperate, partially stratified estuary. *Estuar. Coast. Shelf Sci.*, **55**, 437–63. 450
528. Harding, L. W., Meeson, B. W. & Fisher, T. R. (1986). Phytoplankton production in two East coast estuaries: photosynthesis-light functions and patterns of carbon assimilation in Chesapeake and Delaware Bays. *Estuar. Coast. Shelf Sci.*, **23**, 773–806. 398
529. Harding, L. W., Meeson, B. W., Prezelin, B. B. & Sweeney, B. M. (1981). Diel periodicity of photosynthesis in marine phytoplankton. *Mar. Biol.*, **61**, 95–105. 524
530. Harding, L. W., Prezelin, B. B., Sweeney, B. M. & Cox, J. L. (1982a). Diel oscillations of the photosynthesis-irradiance (*P-I*) relationship in natural assemblages of phytoplankton. *Mar. Biol.*, **67**, 167–78. 524, 525
531. Harding, L. W., Prezelin, B. B., Sweeney, B. M. & Cox, J. L. (1982b). Primary production as influenced by diel periodicity of phytoplankton photosynthesis. *Mar. Biol.*, **67**, 179–86. 526
532. Harper, M. A. (1969). Movement and migration of diatoms on sand grains. *Br. Phycol. J.*, **4**, 97–103. 529
533. Harrington, J. A., Schiebe, F. R. & Nix, J. F. (1992). Remote sensing of Lake Chicot, Arkansas: monitoring suspended sediments, turbidity, and Secchi depth with Landsat data. *Remote Sens. Environ.*, **39**, 15–27.
534. Harris, G. P. (1980). The measurement of photosynthesis in natural populations of phytoplankton. In I. Morris (ed.), *The Physiological Ecology of Phytoplankton* (pp. 129–87). Oxford: Blackwell. 430
535. Harris, G. P. (1986). *Phytoplankton Ecology: Structure, Function and Fluctuation*. London: Chapman & Hall. 388, 430

536. Harris, G. P., Heaney, S. I. & Talling, J. F. (1979). Physiological and environmental constraints in the ecology of the planktonic dinoflagellate *Ceratium hirundinella*. *Freshwater Biol.*, **9**, 413–28. 165
537. Harris, G. P. & Piccinin, B. B. (1977). Photosynthesis by natural phytoplankton populations. *Arch. Hydrobiol.*, **80**, 405–57. 354, 358, 522
538. Harrison, A. W. & Coombes, C. A. (1988). Angular distribution of clear sky short wavelength radiance. *Solar Energy*, **40**, 57–63. 37
539. Harrison, P. J., Fulton, J. D., Taylor, F. J. R. & Parsons, T. R. (1983). Review of the biological oceanography of the Strait of Georgia: pelagic environment. *Can. J. Fish. Aquat. Sci.*, **40**, 1064–94. 164
540. Harron, J. W., Hollinger, A. B., Jain, S. C., Kemenade, C. V. & Buxton, R. A. H. (1983). Presentation. *Annual Meeting, Optical Society of America*.
541. Harvey, G. R., Boran, D. A., Chesal, L. A. & Tokar, J. M. (1983). The structure of marine fulvic and humic acids. *Marine Chem.*, **12**, 119–32. 67
542. Harvey, G. R., Boran, D. A., Piotrowicz, S. R. & Weisel, C. P. (1984). Synthesis of marine humic substances from unsaturated lipids. *Nature*, **309**, 244–6. 67
543. Hatcher, B. G., Chapman, A. R. O. & Mann, K. H. (1977). An annual carbon budget for the kelp *Laminaria longicuris*. *Mar. Biol.*, **44**, 85–96. 434–6, 438
544. Haupt, W. (1973). Role of light in chloroplast movement. *BioScience*, **23**, 289–96. 520, 522
545. Hawes, I., Sutherland, D. & Hanelt, D. (2003). The use of pulse amplitude modulated fluorometry to determine fine-scale temporal and spatial variation of in situ photosynthetic activity within an *Isoetes*-dominated canopy. *Aquat. Bot.*, **77**, 1–15. 351
546. Haxo, F. T. (1985). Photosynthetic action spectrum of the coccolithophorid, *Emiliania huxleyi* (Haptophyceae): 19<sup>l</sup> hexanoyloxyfucoxanthin as antenna pigment. *J. Phycol.*, **21**, 282–7. 387
547. Haxo, F. T. & Blinks, L. R. (1950). Photosynthetic action spectra of marine algae. *J. Gen. Physiol.*, **33**, 389–422. 382, 383
548. Haxo, F. T., Kycia, J. H., Somers, G. F., Bennett, A. & Siegelman, H. W. (1976). Peridinin-chlorophyll *a* proteins of the dinoflagellate *Amphidinium carterae* (Plymouth 450). *Plant Physiol.*, **57**, 297–303. 291
549. Heaney, S. I. & Talling, J. F. (1980). Dynamic aspects of dinoflagellate distribution patterns in a small productive lake. *J. Ecol.*, **68**, 75–94. 515
550. Heckey, R. E. & Fee, E. J. (1981). Primary production and rates of algal growth in Lake Tanganyika. *Limnol. Oceanogr.*, **26**, 532–47. 165
551. Hellström, T. (1991). The effect of resuspension on algal production in a shallow lake. *Hydrobiologia*, **213**, 183–90. 167
552. Hernes, P. J. & Benner, R. (2003). Photochemical and microbial degradation of dissolved lignin phenols: implications for the fate of terrigenous dissolved organic matter in marine environments. *J. Geophys. Res.*, **108**, C93291. 81
553. Hickey, J. R., Alton, B. M., Griffith, F. J. *et al.* (1982). Extraterrestrial solar irradiance variability. Two and one-half years of measurement from Nimbus 7. *Solar Energy*, **29**, 125–7. 29
554. Hickman, A. E., Holligan, P. M., Moore, C. M. *et al.* (2009). Distribution and chromatic adaptation of phytoplankton within a shelf sea thermocline. *Limnol. Oceanogr.*, **54**, 525–36. 462

555. Hill, V. J. (2008). Impacts of chromophoric dissolved organic material on surface ocean heating in the Chukchi Sea. *J. Geophys. Res.*, **113**, C07024. 69
556. Hiller, R. G., Anderson, J. M. & Larkum, A. W. D. (1991). The chlorophyll-protein complexes of algae. In H. Scheer (ed.), *Chlorophylls* (pp. 529–47). Boca Raton: CRC Press. 286
557. Hiller, R. G. & Larkum, A. W. D. (1985). The chlorophyll-protein complexes of *Prochloron* sp. (Prochlorophyta). *Biochim. Biophys. Acta*, **806**, 107–15. 291
558. Hiller, R. G., Larkum, A. W. D. & Wrench, P. W. (1988). Chlorophyll proteins of the prymnesiophyte *Pavlova lutherii* (Droop) comb. nov.: identification of the major light-harvesting complex. *Biochim. Biophys. Acta*, **932**, 223–31. 291
559. Hiller, R. G., Wrench, P. M., Gooley, A. P., Shoebridge, G. & Breton, J. (1993). The major intrinsic light-harvesting protein of *Amphidinium*: characterization and relation to other lightharvesting proteins. *Photochem. Photobiol.*, **57**, 125–31. 291
560. Hirata, T. & Højerslev, N. K. (2008). Relationship between the irradiance reflectance and inherent optical properties of seawater. *J. Geophys. Res.*, **113**, C03030. 171
561. Hobson, L. A. (1981). Seasonal variations in maximum photosynthetic rates of phytoplankton in Saanich Inlet, Vancouver Island, British Columbia. *J. Exp. Mar. Biol. Ecol.*, **52**, 1–13. 513
562. Hodgkinson, J. R. & Greenleaves, J. I. (1963). Computations of lightscattering and extinction by spheres according to diffraction and geometrical optics and some comparisons with the Mie theory. *J. Opt. Soc. Amer.*, **53**, 577–88. 101
563. Hoepffner, N. & Sathyendranath, S. (1993). Determination of the major groups of phytoplankton pigments from the absorption spectra of total particulate matter. *J. Geophys. Res.*, **98**, 22789–803. 86
564. Hoepffner, N., Sturm, B., Finenko, Z. & Larkin, D. (1999). Depth-integrated primary production in the eastern tropical and subtropical North Atlantic basin from ocean colour imagery. *Int. J. Remote Sens.*, **20**, 1435–56. 451
565. Hogarth, P. J. (2007). *The Biology of Mangroves and Seagrasses*, 2nd edn. Oxford: Oxford University Press. 451, 532
566. Hoge, F. R., Lyon, P. E., Wright, C. W., Swift, R. N. & Yungel, J. K. (2005). Chlorophyll biomass in the global oceans: airborne lidar retrieval using fluorescence of both chlorophyll and chromophoric dissolved organic matter. *Appl. Opt.*, **44**, 2857–62. 250–2
567. Hoge, F. E. & Swift, R. N. (1981). Airborne simultaneous spectroscopic detection of laser-induced water Raman backscatter and fluorescence from chlorophyll *a* and other naturally occurring pigments. *Appl. Opt.*, **20**, 3197–205. 249–52
568. Hoge, F. E., Vodacek, A., Swift, R. N., Yungel, J. K. & Blough, N. V. (1995). Inherent optical properties of the ocean: retrieval of the absorption coefficient of chromophoric dissolved organic matter from airborne laser spectral fluorescence measurements. *Appl. Opt.*, **34**, 7032–8. 255
569. Højerslev, N. K. (1973). Inherent and apparent optical properties of the western Mediterranean and the Hårdangerfjord. *Univ. Copenhagen, Inst. Phys. Oceanogr. Rep.*, **21**, 1–70. 118
570. Højerslev, N. K. (1975). A spectral light absorption meter for measurements in the sea. *Limnol. Oceanogr.*, **20**, 1024–34. 61, 144, 178, 179

571. Højerslev, N.K. (1977). Inherent and apparent optical properties of the North Sea. Fladen Ground experiment – Flex 75. *Univ. Copenhagen, Inst. Phys. Oceanogr. Rep.*, **32**, 1–68. [118](#)
572. Højerslev, N.K. (1979). On the origin of yellow substance in the marine environment. In *17th General Assembly of I.A.P.S.O. (Canberra, 1979)* (pp. Abstracts, 71). [68](#)
573. Højerslev, N.K. (1986). Variability of the sea with special reference to the Secchi disc. *Proc. Soc. Photo-Opt. Instrum. Eng., Ocean Optics VIII*, **637**, 294–305. [74](#), [143](#)
574. Højerslev, N. K. (1988). Natural occurrences and optical effects of gelbstoff. *Univ. Copenhagen, Inst. Phys. Oceanogr. Rep.*, **50**, 1–30. [75](#), [76](#)
575. Højerslev, N. K. & Aarup, T. (2002). Optical measurements on the Louisiana Shelf off the Mississippi River. *Estuar. Coast. Shelf Sci.*, **55**, 599–611. [158](#)
576. Højerslev, N. & Lundgren, B. (1977). Inherent and apparent optical properties of Icelandic waters. ‘Bjarni Saemundsson Overflow 73’. *Univ. Copenhagen, Inst. Phys. Oceanogr. Rep.*, **33**, 1–63. [117](#)
577. Højerslev, N.K. & Zaneveld, J.R.V. (1977). A theoretical proof of the existence of the submarine asymptotic daylight field. *Univ. Copenhagen, Inst. Phys. Oceanogr. Rep.*, **34**, 1–16. [182](#)
578. Holligan, P. M., Aarup, T. & Groom, S. B. (1989). The North Sea: satellite colour atlas. *Continental Shelf Res.*, **9**, 667–765. [158](#), [237](#)
579. Holligan, P. M., Viollier, M., Harbour, D. S., Camus, P. & Champagne-Philippe, M. (1983). Satellite and ship studies of coccolithophore production along a continental shelf edge. *Nature*, **304**, 339–42. [129](#)
580. Holmes, R.W. (1970). The Secchi disk in turbid coastal zones. *Limnol. Oceanogr.*, **15**, 688–94. [142](#), [297](#)
581. Holm-Hansen, O. & Mitchell, B.G. (1991). Spatial and temporal distribution of phytoplankton and primary production in the western Bransfield Strait region. *Deep-Sea Res.*, **38**, 961–80. [346](#)
582. Holyer, R. J. (1978). Toward universal multispectral suspended sediment algorithms. *Remote Sens. Environ.*, **7**, 323–38. [231](#)
583. Hommersom, A., Peters, S., Wernand, M. R. & De Boer, J. (2009). Spatial and temporal variability in bio-optical properties of the Wadden Sea. *Estuar. Coast. Shelf Sci.*, **83**, 360–70. [75](#)
584. Hooker, S. B., Zibordi, G., Berthon, J.-F. & Brown, J. W. (2004). Above-water radiometry in shallow coastal waters. *Appl. Opt.*, **43**, 4254–68. [205](#)
585. Horstmann, U. (1983). Cultivation of the green alga *Caulerpa racemosa*, in tropical waters and some aspects of its physiological ecology. *Aquaculture*, **32**, 361–71. [521](#)
586. Houghton, W. M., Exton, R. J. & Gregory, R. W. (1983). Field investigation of techniques for remote laser sensing of oceanographic parameters. *Remote Sens. Environ.*, **13**, 17–32. [252](#)
587. Hovis, W. (1978). The Coastal Zone Colour Scanner (CZCS) experiment. In C. R. Madrid (ed.), *The Nimbus 7 Users' Guide*. Beltsville: Management & Technical Services Co. [210](#)
588. Hovis, W. A., Clark, D. K., Anderson, F. *et al.* (1980). Nimbus-7 Coastal Zone Colour Scanner: system description and initial imagery. *Science*, **210**, 60–3. [209](#)

589. Hovis, W. A. & Leung, K. C. (1977). Remote sensing of ocean colour. *Opt. Eng.*, **16**, 158–66. 209
590. Hoyer, K., Karsten, U. & Wiencke, C. (2002). Induction of sunscreen compounds in Antarctic macroalgae by different radiation conditions. *Mar. Biol.*, **141**, 619–27. 356
591. Hu, C. (2009). A novel ocean color index to detect floating algae in the global oceans. *Remote Sens. Environ.*, **113**, 2118–29. 237
592. Hu, C., Muller-Karger, F. E., Andrefouet, S. & Carder, K. L. (2001). Atmospheric correction and cross-calibration of LANDSAT-7/ETM+ imagery over aquatic environments: a multiplatform approach using SeaWiFS/MODIS. *Remote Sens. Environ.*, **78**, 99–107. 225
593. Hu, C., Muller-Karger, F. E., Taylor, C. (2005). Red tide detection and tracing using MODIS fluorescence data: a regional example in SW Florida coastal waters. *Remote Sens. Environ.*, **97**, 311–21. 248
594. Hu, Q., Marquardt, J. and Iwasaki, I. (1999). Molecular structure, localization and function of biliproteins in the chlorophyll *a/d* containing photosynthetic prokaryote, *Acaryochloris marina*. *Biochim. Biophys. Acta*, **112**, 250–61. 297, 300
595. Hu, Q., Miyashita, H., Iwasaki, I. *et al.* (1998). A photosystem I reaction center driven by chlorophyll *d* in oxygenic photosynthesis. *Proc. Natl. Acad. Sci. (Wash.)*, **95**, 13319–23. 300
596. Huertas, I. E., Bhatti, S. & Colman, B. (2003). Inorganic carbon acquisition in two species of marine prymnesiophytes. *Eur. J. Phycol.*, **38**, 181–9. 407
597. Huertas, I. E., Bhatti, S. & Colman, B. (2005). Characterization of the CO<sub>2</sub>-concentrating mechanism in the unicellular alga *Eustigmatos vischeri*. *Eur. J. Phycol.*, **40**, 409–15. 407
598. Huertas, I. E., Colman, C., Espie, G. S. & Lubian, L. M. (2000). Active transport of CO<sub>2</sub> by three species of marine microalgae. *J. Phycol.*, **36**, 314–20. 407
599. Huisman, J., Van Oostveen, P. & Weissing, F. J. (1999). Critical depth and critical turbulence: two different mechanisms for the development of phytoplankton blooms. *Limnol. Oceanogr.*, **44**, 1781–7. 394
600. Hulatt, C. J., Thomas, D. N., Bowers, D. J., Norman, L. & Zhang, C. (2009). Exudation and decomposition of chromophoric dissolved organic matter (CDOM) from some temperate macroalgae. *Estuar. Coast. Shelf Sci.*, **84**, 147–53. 68
601. Humphries, S. E. & Lyne, V. D. (1988). Cyanophyte blooms: the role of cell buoyancy. *Limnol. Oceanogr.*, **33**, 79–91. 519
602. Hutchinson, G. E. (1967). *A Treatise on Limnology, Vol. 2*. New York: Wiley. 424, 427, 434
603. Hutchinson, G. E. (1975). *A Treatise on Limnology, Vol. 3*. New York: Wiley-Interscience. 266, 407, 410, 412
604. HydroRad multi-channel hyperspectral radiometers. Users Manual (2007). HOBI Labs Inc., Tucson, Arizona. 111
605. HydroScat-2 Backscattering Sensor Fluorometer. Manual (2008). HOBI Labs Inc., Tucson, Arizona. 111, 146
606. Hyperspectral ocean colour radiometer. Operation Manual (2008). Satlantic Inc. Halifax, Nova Scotia. 146

607. Ibelings, B. W. & Maberly, S. C. (1998). Photoinhibition and the availability of inorganic carbon restrict photosynthesis by surface blooms of cyanobacteria. *Limnol. Oceanogr.*, **43**, 408–19. 410
608. Ignatiades, L. (1998). The productive and optical status of the oligotrophic waters of the Southern Aegean Sea (Cretan Sea), Eastern Mediterranean. *J. Plankton Res.*, **20**, 985–95. 450
609. Ikusima, I. (1970). Ecological studies on the productivity of aquatic plant communities. *Bot. Mag. (Tokyo)*, **83**, 330–41. 345
610. Ingram, K. & Hiller, R. G. (1983). Isolation and characterization of a major chlorophyll *a/c*<sub>2</sub> light-harvesting protein from a *Chroomonas* species (Cryptophyceae). *Biochim. Biophys. Acta*, **772**, 310–19. 291
611. International Association for the Physical Sciences of the Ocean (1979). *Sun Report (Report of the working group on symbols, units and nomenclature in physical oceanography)*. Paris. 6
612. Irigoien, X. & Castel, J. (1997). Light limitation and distribution of chlorophyll pigments in a highly turbid estuary: the Gironde (SW France). *Estuar. Coast. Shelf Sci.*, **44**, 507–17. 399
613. Itres Research Ltd. (2007). *Calgary*, Alberta, Canada. 208
614. Iturriaga, R., Mitchell, B. G. & Kiefer, D. A. (1988). Microphotometric analysis of individual particle absorption spectra. *Limnol. Oceanogr.*, **33**, 128–35. 317
615. Iturriaga, R. & Siegel, D. A. (1989). Microphotometric characterization of phytoplankton and detrital absorption properties in the Sargasso Sea. *Limnol. Oceanogr.*, **34**, 1706–26. 58, 84, 87
616. Ivanoff, A., Jerlov, N. & Waterman, T. H. (1961). A comparative study of irradiance, beam transmittance and scattering in the sea near Bermuda. *Limnol. Oceanogr.*, **6**, 129–48. 74
617. Iverson, R. L. & Curl, H. (1973). Action spectrum of photosynthesis for *Skeletonema costatum* obtained with carbon-14. *Physiol. Plant.*, **28**, 498–502. 382, 383
618. Jackson, T. A. & Hecky, R. E. (1980). Depression of primary productivity by humic matter in lake and reservoir waters of the boreal forest zone. *Can. J. Fish. Aquat. Sci.*, **37**, 2300–17. 398
619. Jamart, B. M., Winter, D. F., Banse, K., Anderson, G. C. & Lam, R. K. (1977). A theoretical study of phytoplankton growth and nutrient distribution in the Pacific Ocean off the northwestern U.S. coast. *Deep-Sea Res.*, **24**, 753–73. 396
620. James, H. R. & Birge, E. A. (1938). A laboratory study of the absorption of light by lake waters. *Trans. Wisc. Acad. Sci. Arts Lett.*, **31**, 1–154. 70, 77
621. Jassby, A. T. & Platt, T. (1976). Mathematical formulation of the relationship between photosynthesis and light for phytoplankton. *Limnol. Oceanogr.*, **21**, 540–7. 351
622. Jaworski, G. H. M., Talling, J. F. & Heaney, S. I. (1981). The influence of carbon dioxide depletion on growth and sinking rate of two planktonic diatoms in culture. *Br. Phycol. J.*, **16**, 395–410. 412
623. Jeffrey, S. W. (1961). Paper chromatographic separation of chlorophylls and carotenoids in marine algae. *Biochem. J.*, **80**, 336–42. 279
624. Jeffrey, S. W. (1972). Preparation and some properties of crystalline chlorophyll *c*<sub>1</sub> and *c*<sub>2</sub> from marine algae. *Biochim. Biophys. Acta*, **279**, 15–33. 279

625. Jeffrey, S. W. (1976). The occurrence of chlorophyll  $c_1$  and  $c_2$  in algae. *J. Phycol.*, **12**, 349–54. 279
626. Jeffrey, S. W. (1984). Responses of unicellular marine plants to natural blue-green light environments. In H. Senger (ed.), *Blue Light Effects in Biological Systems* (pp. 497–508). Berlin: Springer. 488
627. Jeffrey, S. W., Sielicki, M. & Haxo, F. T. (1975). Chloroplast pigment patterns in dinoflagellates. *J. Phycol.*, **11**, 374–84. 275, 278, 282, 284
628. Jeffrey, S. W. & Vesk, M. (1977). Effect of blue-green light on photosynthetic pigments and chloroplast structure in the marine diatom *Stephanopyxis turris*. *J. Phycol.*, **13**, 271–9. 487, 489–90
629. Jeffrey, S. W. & Vesk, M. (1978). Chloroplast structural changes induced by white light in the marine diatom *Stephanopyxis turris*. *J. Phycol.*, **14**, 238–40. 487
630. Jeffrey, S. W. & Wright, S. W. (1987). A new spectrally distinct component in preparations of chlorophyll  $c$  from the micro-alga *Emiliania huxleyi* (Prymnesiophyceae). *Biochim. Biophys. Acta*, **894**, 180–8. 277, 278
631. Jeppesen, E., Søndergaard, M., Jensen, J. P. *et al.* (2005). Lake responses to reduced nutrient loading: an analysis of contemporary long-term data from 35 case studies. *Freshwater Biol.*, **50**, 1747–71. 422
632. Jerlov, N. G. (1950). Ultra-violet radiation in the sea. *Nature*, **166**, 111–12. 64, 158
633. Jerlov, N. G. (1951). Optical studies of ocean water. *Rep. Swedish Deep-Sea Exped.*, **3**, 1–59. 92
634. Jerlov, N. G. (1961). Optical measurements in the eastern North Atlantic. *Medd. Oceanogr. Inst. Goteborg, Ser. B*, **8**, 1–40. 108
635. Jerlov, N. G. (1974). Significant relationships between optical properties of the sea. In N. G. Jerlov & E. S. Nielsen (eds), *Optical Aspects of Oceanography* (pp. 77–94). London: Academic Press. 203
636. Jerlov, N. G. (1976). *Marine Optics*. Amsterdam: Elsevier. 48, 67–8, 74–5, 92–3, 99, 109, 117–8, 129, 148, 157, 169, 176, 182, 438, 465
637. Jerlov, (Johnson) N. G. & Liljequist, G. (1938). On the angular distribution of submarine daylight and the total submarine illumination. *Sven. Hydrogr.-Biol. Komm. Skr., Ny Ser. Hydrogr.*, **14**, 1–15. Quoted by Jerlov (1976). 182
638. Jerlov, N. G. & Nygard, K. (1969). A quanta and energy meter for photosynthetic studies. *Univ. Copenhagen Inst. Phys. Oceanogr. Rep.*, **10**, 1–29. 134, 137, 163
639. Jerome, J. H., Bukata, R. P. & Bruton, J. E. (1983). Spectral attenuation and irradiance in the Laurentian Great Lakes. *J. Great Lakes Res.*, **9**, 60–8. 164
640. Jerome, J. H., Bukata, R. P. & Bruton, J. E. (1988). Utilizing the components of vector irradiance to estimate the scalar irradiance in natural waters. *Appl. Opt.*, **27**, 4012–18. 170
641. Jewson, D. H. (1976). The interactions of components controlling net phytoplankton photosynthesis in a well-mixed lake (Lough Neagh, Northern Ireland). *Freshwater Biol.*, **6**, 551–76. 344, 374, 393, 419, 420
642. Jewson, D. H. (1977). Light penetration in relation to phytoplankton content of the euphotic zone of Lough Neagh, N. Ireland. *Oikos*, **28**, 74–83. 327, 328, 364
643. Jewson, D. H. & Taylor, J. A. (1978). The influence of turbidity on net phytoplankton photosynthesis in some Irish lakes. *Freshwater Biol.*, **8**, 573–84. 76, 77

644. Jitts, H. R. (1963). The simulated *in situ* measurement of oceanic primary production. *Aust. J. Mar. Freshwater Res.*, **14**, 139–47. 331
645. Jitts, H. R., Morel, A. & Saijo, Y. (1976). The relation of oceanic primary production to available photosynthetic irradiance. *Aust. J. Mar. Freshwater Res.*, **27**, 441–54. 345
646. Johannessen, S. C., Miller, W. L. & Cullen, J. J. (2003). Calculation of UV attenuation and colored dissolved organic matter absorption spectra from measurements of ocean color. *J. Geophys. Res.*, **108**, C93301. 257
647. Johnson, D. R., Miller, J. & Schofield, O. (2003). Dynamics and optics of the Hudson River outflow plume. *J. Geophys. Res.*, **108**, C103323. 70
648. Johnson, Z., Bidigare, R. R., Goericke, R. *et al.* (2002). Photosynthetic physiology and physicochemical forcing in the Arabian Sea, 1995. *Deep-Sea Res.*, **49**, 415–36. 374
649. Joint, I. R. (1986). Physiological ecology of picoplankton in various oceanographic provinces. In T. Platt & W. K. W. Li (eds), *Photosynthetic picoplankton* (pp. 287–309). 374
650. Joint, I. R. & Pomroy, A. J. (1981). Primary production in a turbid estuary. *Estuar. Coast. Shelf Sci.*, **13**, 303–16. 398
651. Jones, D. & Wills, M. S. (1956). The attenuation of light in sea and estuarine waters in relation to the concentration of suspended solid matter. *J. Mar. Biol. Ass. U.K.*, **35**, 431–44. 127
652. Jones, J. I. (2005). The metabolic cost of bicarbonate use in the submerged plant *Elodea nuttallii*. *Aquat. Bot.*, **83**, 71–81. 409
653. Jones, L. W. & Kok, B. (1966). Photoinhibition of chloroplast reactions. *Plant Physiol.*, **41**, 1037–43. 354
654. Jones, L. W. & Myers, J. (1964). Enhancement in the blue-green alga, *Anacystis nidulans*. *Plant Physiol.*, **39**, 938–46. 387
655. Jones, L. W. & Myers, J. (1965). Pigment variations in *Anacystis nidulans* induced by light of selected wavelengths. *J. Phycol.*, **1**, 6–13. 487
656. Jones, R. I. (1978). Adaptations to fluctuating irradiance by natural phytoplankton communities. *Limnol. Oceanogr.*, **23**, 920–6. 514
657. Jones, R. I. (1992). The influence of humic substances on lacustrine planktonic food chains. *Hydrobiologia*, **229**, 73–91. 398
658. Jones, R. I. & Arvola, L. (1984). Light penetration and some related characteristics in small forest lakes in Southern Finland. *Verh. Internat. Verein. Limnol.*, **22**, 811–16. 165
659. Jones, R. I. & Ilmavirta, V. (1978a). A diurnal study of the phytoplankton in the eutrophic lake Lovojärvi, Southern Finland. *Arch. Hydrobiol.*, **83**, 494–514. 430, 493
660. Jones, R. I. & Ilmavirta, V. (1978b). Vertical and seasonal variation of phytoplankton photosynthesis in a brown-water lake with winter ice cover. *Freshwater Biol.*, **8**, 561–72. 514
661. Jones, R. I., Young, J. M., Hartley, A. M. & Bailey-Watts, A. E. (1996). Light limitation of phytoplankton development in an oligotrophic lake – Loch Ness, Scotland. *Freshwater Biol.*, **35**, 533–43. 394
662. Jørgensen, E. G. (1968). The adaptation of plankton algae. II. Aspects of the temperature adaptation of *Skeletonema costatum*. *Physiol. Plant.*, **21**, 423–7. 418

663. Jupp, B. P. & Spence, D. H. N. (1977). Limitations on macrophytes in a eutrophic lake, Loch Leven. *J. Ecol.*, **65**, 175–86, 431–6. [427](#), [428](#)
664. Jupp, D. L. B., Kirk, J. T. O. & Harris, G. P. (1994). Detection, identification and mapping of cyanobacteria – using remote sensing to measure the optical quality of inland waters. *Aust. J. Mar. Freshwater Res.*, **45**, 801–28. [246](#)
665. Kageyama, A., Yokohama, Y. & Nisizawa, K. (1979). Diurnal rhythms of apparent photosynthesis of a brown alga, *Spatoglossum pacificum*. *Botanica Marina*, **22**, 199–201. [524](#), [527](#)
666. Kahru, M. & Mitchell, B. G. (2001). Seasonal and non-seasonal variability of satellite-derived chlorophyll and coloured dissolved organic matter concentration in the California Current. *J. Geophys. Res.*, **106**, 2517–29. [253](#)
667. Kain, J. M. (1979). A view of the genus *Laminaria*. *Oceanogr. Mar. Biol. Ann. Rev.*, **17**, 101–61. [428](#), [534](#)
668. Kalf, J., Welch, H. E. & Holmgren, S. K. (1972). Pigment cycles in two high-arctic Canadian lakes. *Ver. Internat. Verein Limnol.*, **18**, 250–6. [514](#)
669. Kalle, K. (1937). *Annln. Hydrogr. Berl.*, **65**, 276–82. Quoted by Kalle (1966). [71](#)
670. Kalle, K. (1961). What do we know about the ‘Gelbstoff’? *Union Geod. Geophys. Int. Monogr.*, **10**, 59–62. Quoted by Jerlov (1976). [75](#)
671. Kalle, K. (1966). The problem of the gelbstoff in the sea. *Oceanogr. Mar. Biol. Ann. Rev.*, **4**, 91–104. [71](#)
672. Kamiya, A. & Miyachi, S. (1984). Blue-green and green light adaptations on photosynthetic activity in some algae collected from the sub-surface layer in the western Pacific Ocean. In H. Senger (ed.), *Blue Light Effects in Biological Systems* (pp. 517–28). Berlin: Springer. [483–4](#)
673. Kan, K. S. & Thornber, J. P. (1976). The light-harvesting chlorophyll *a/b*-protein complex of *Chlamydomonas reinhardtii*. *Plant Physiol.*, **57**, 47–52. [290](#)
674. Kana, T. M. & Glibert, P. M. (1987a). Effect of irradiances up to 2000  $\mu\text{E m}^{-2} \text{s}^{-1}$  on marine *Synechococcus* WH7803 – I. Growth, pigmentation and cell composition. *Deep-Sea Res.*, **34**, 479–95. [470](#), [474](#)
675. Kana, T. M. & Glibert, P. M. (1987b). Effect of irradiances up to 2000  $\mu\text{E m}^{-2} \text{s}^{-1}$  on marine *Synechococcus* WH7803 – II. Photosynthetic responses and mechanisms. *Deep-Sea Res.*, **34**, 499–516. [477](#)
676. Kana, T. M., Glibert, P. M., Goericke, R. & Welschmeyer, N. A. (1988). Zeaxanthin and  $\beta$ -carotene in *Synechococcus* WH7803 respond differently to irradiance. *Limnol. Oceanogr.*, **33**, 1623–7. [472](#)
677. Kana, T. M., Watts, J. L. & Glibert, P. M. (1985). Diel periodicity in the photosynthetic capacity of coastal and offshore phytoplankton assemblages. *Mar. Ecol. Prog. Ser.*, **25**, 131–9. [524](#)
678. Kaplan, A. & Reinhold, L. (1999). CO<sub>2</sub> concentrating mechanisms in photosynthetic microorganisms. *Ann. Rev. Plant Physiol. Plant Mol. Biol.*, **50**, 539–70. [402](#)
679. Karelin, A. K. & Pelevin, V. N. (1970). The FMPO-64 marine underwater irradiance meter and its application in hydro-optical studies. *Oceanology*, **10**, 282–5. [144](#)
680. Katoh, T. & Ehara, T. (1990). Supramolecular assembly of fucoxanthin-chlorophyll-protein complexes isolated from a brown alga, *Petalonia fascia*. Electron microscope studies. *Plant Cell Physiol.*, **31**, 439–47. [289](#)
- 680a. Katoh, T., Nagashima, U. & Mimuro, M. (1991). Fluorescence properties of the allenic carotenoid fucoxanthin: implication for energy transfer in photosynthetic pigment systems. *Photosynthesis Res.*, **27**, 221–6. [299](#)

681. Keeley, J. E. (1990). Photosynthetic pathways in freshwater aquatic plants. *Trends Ecol. Evol.*, **5**, 330–3. 306, 414
682. Kelly, M. G., Thyssen, N. & Moeslund, B. (1983). Light and the annual variation of oxygen- and carbon-based measurements of productivity in a macrophyte-dominated river. *Limnol. Oceanogr.*, **28**, 503–15. 439
683. Khorram, S. (1981). Water quality mapping from Landsat digital data. *Int. J. Rem. Sens.*, **2**, 145–53. 231
684. Khorram, S., Cheshire, H., Geraci, A. L. & Rosa, G. L. (1991). Water quality mapping of Augusta Bay, Italy from Landsat-TM data. *Int. J. Remote Sens.*, **12**, 803–8. 246
685. Kieber, R. J., Xianling, Z. & Mopper, K. (1990). Formation of carbonyl compounds from UV-induced photo degradation of humic substances in natural waters: fate of riverine carbon in the sea. *Limnol. Oceanogr.*, **35**, 1503–15. 80, 81
686. Kiefer, D. A. (1973). Chlorophyll *a* and fluorescence in marine centric diatoms: responses of chloroplasts to light and nutrient stress. *Mar. Biol.*, **23**, 39–46. 522–3
687. Kiefer, D. A., Olson, R. J. & Holm-Hansen, O. (1976). Another look at the nitrite and chlorophyll maxima in the central North Pacific. *Deep-Sea Res.*, **23**, 1199–208. 396, 493
688. Kiefer, D. A. & SooHoo, J. B. (1982). Spectral absorption by marine particles of coastal waters of Baja California. *Limnol. Oceanogr.*, **27**, 492–9. 86
689. Killilea, S. D., O'Carra, P. & Murphy, R. F. (1980). Structures and apoprotein linkages of phycoerythrobilin and phycocyanobilin. *Biochem. J.*, **187**, 311–20. 295
690. Kim, H. H. & Linebaugh, G. (1985). Early evaluation of thematic mapper data for coastal process studies. *Adv. Space Res.*, **5**, 21–9. 246
691. King, R. J. & Schramm, W. (1976). Photosynthetic rates of benthic marine algae in relation to light intensity and seasonal variations. *Mar. Biol.*, **37**, 215–22. 340–1, 343, 348, 349, 353, 438, 509
692. Kingston, M. B. (1999). Effect of light on vertical migration and photosynthesis of *Euglena proxima* (Euglenophyta). *J. Phycol.*, **35**, 245–53. 529
693. Kirk, J. T. O. (1975a). A theoretical analysis of the contribution of algal cells to the attenuation of light within natural waters. I. General treatment of suspensions of pigmented cells. *New Phytol.*, **75**, 11–20. 311–16
694. Kirk, J. T. O. (1975b). A theoretical analysis of the contributions of algal cells to the attenuation of light within natural waters. II. Spherical cells. *New Phytol.*, **75**, 21–36. 311–16, 327
695. Kirk, J. T. O. (1976a). A theoretical analysis of the contribution of algal cells to the attenuation of light within natural waters. III. Cylindrical and spheroidal cells. *New Phytol.*, **77**, 341–58. 311–16, 326, 327
696. Kirk, J. T. O. (1976b). Yellow substance (gelbstoff) and its contribution to the attenuation of photosynthetically active radiation in some inland and coastal southeastern Australian waters. *Aust. J. Mar. Freshwater Res.*, **27**, 61–71. 71, 72, 76, 77, 78, 96
697. Kirk, J. T. O. (1977a). Use of a quanta meter to measure attenuation and underwater reflectance of photosynthetically active radiation in some inland

- and coastal southeastern Australian waters. *Aust. J. Mar. Freshwater Res.*, **28**, 9–21. 76–8, 162, 164–6, 169, 178
698. Kirk, J. T. O. (1977b). Thermal dissociation of fucoxanthin-protein binding in pigment complexes from chloroplasts of *Hormosira* (Phaeophyta). *Plant Sci. Lett.*, **9**, 373–80. 282, 293
699. Kirk, J. T. O. (1979). Spectral distribution of photosynthetically active radiation in some south-eastern Australian waters. *Aust. J. Mar. Freshwater Res.*, **30**, 81–91. 139, 156, 160
700. Kirk, J. T. O. (1980a). Relationship between nephelometric turbidity and scattering coefficients in certain Australian waters. *Aust. J. Mar. Freshwater Res.*, **31**, 1–12. 115, 178, 195
701. Kirk, J. T. O. (1980b). Spectral absorption properties of natural waters: contribution of the soluble and particulate fractions to light absorption in some inland waters of southeastern Australia. *Aust. J. Mar. Freshwater Res.*, **31**, 287–96. 56, 77–8, 82–3, 87, 94, 96
702. Kirk, J. T. O. (1981a). A Monte Carlo study of the nature of the underwater light field in, and the relationships between optical properties of, turbid yellow waters. *Aust. J. Mar. Freshwater Res.*, **32**, 517–32. 91, 113, 170, 180, 185, 187–91, 196–7
703. Kirk, J. T. O. (1981b). Estimation of the scattering coefficient of natural waters using underwater irradiance measurements. *Aust. J. Mar. Freshwater Res.*, **32**, 533–9. 113, 114, 118, 119
704. Kirk, J. T. O. (1981c). *A Monte Carlo procedure for simulating the penetration of light into natural waters*. CSIRO Division of Plant Industry, Technical Paper No. 36, 1–18. 180, 185
705. Kirk, J. T. O. (1982). Prediction of optical water quality. In E. M. O'Loughlin & P. Cullen (eds), *Prediction in Water Quality* (pp. 307–26). Canberra: Australian Academy of Science. 176
706. Kirk, J. T. O. (1984). Dependence of relationship between inherent and apparent optical properties of water on solar altitude. *Limnol. Oceanogr.*, **29**, 350–6. 170, 192, 194
707. Kirk, J. T. O. (1985). Effect of suspensoids (turbidity) on penetration of solar radiation in aquatic ecosystems. *Hydrobiologia*, **125**, 195–208. 104, 143
708. Kirk, J. T. O. (1986). Optical properties of picoplankton suspensions. In T. Platt & W. K. W. Li (eds), *Photosynthetic picoplankton* (pp. 501–20). *Can. Bull. Fish Aquat. Sci.*, **214**. 318
709. Kirk, J. T. O. (1988). Optical water quality – what does it mean and how should we measure it? *J. Water Pollut. Control Fed.*, **60**, 194–7. 152, 176, 192
710. Kirk, J. T. O. (1989a). The upwelling light stream in natural waters. *Limnol. Oceanogr.*, **34**, 1410–25. 23, 115
711. Kirk, J. T. O. (1989b). The assessment and prediction of optical water quality. In *13th Fed. Conv. Aust. Water Wastewater Assoc.*, 89/2 (pp. 504–7). Canberra: Institution of Engineers. 152, 176, 192
712. Kirk, J. T. O. (1991). Volume scattering function, average cosines and the underwater light field. *Limnol. Oceanogr.*, **36**, 455–67. 21, 170–1, 192–4
713. Kirk, J. T. O. (1992). Monte Carlo modelling of the performance of a reflective tube absorption meter. *Appl. Opt.*, **31**, 6463–8. 60

714. Kirk, J. T. O. (1994). Estimation of the absorption and scattering coefficients of natural waters by use of underwater irradiance measurements. *Appl. Opt.*, **33**, 3276–8. 61, 114
715. Kirk, J. T. O. (1997). Point-source integrating cavity absorption meter: theoretical principles and numerical modeling. *Appl. Opt.*, **36**, 6123–8. 57
716. Kirk, J. T. O. (1999). Multiple scattering of a photon flux: implications for the integral average cosine of the underwater light field. *Appl. Opt.*, **38**, 3134–40. 12
717. Kirk, J. T. O. (2003). The vertical attenuation of irradiance as a function of the optical properties of the water. *Limnol. Oceanogr.*, **48**, 9–17. 14, 27
718. Kirk, J. T. O. (2004). *Notes for course on Monte Carlo modelling of radiative transfer in the ocean*, Ocean Optics Conference XVII, Fremantle, Western Australia. Available on [www.kirkmarineoptics.com](http://www.kirkmarineoptics.com). 150
719. Kirk, J. T. O. (2006). Light field around a point source in the ocean. *J. Geophys. Res.*, **111**, C07008. 59
720. Kirk, J. T. O. Unpublished data. 73, 75, 76–8, 165–6
721. Kirk, J. T. O., Davies-Colley, R. J., Shooter, D. & Schwarz, A.-M. (1998). Optical properties of ocean waters in the vicinity of the Chatham Rise, South Pacific Ocean. *Mar. Freshwater Res.*, **49**, 1–6. 163
722. Kirk, J. T. O. & Goodchild, D. J. (1972). Relationship of photosynthetic effectiveness of different kinds of light to chlorophyll content and chloroplast structure in greening wheat and in ivy leaves. *Aust. J. Biol. Sci.*, **25**, 215–41. 466
723. Kirk, J. T. O. & Oliver, R. L. (1995). Optical closure in an ultraturbid lake. *J. Geophys. Res.*, **100**, 13221–5. 194
724. Kirk, J. T. O. & Tilney-Bassett, R. A. E. (1978). *The Plastids*, 2nd edn. Amsterdam: Elsevier. 265
725. Kirk, J. T. O. & Tyler, P. A. (1986). The spectral absorption and scattering properties of dissolved and particulate components in relation to the underwater light yield of some tropical Australian freshwaters. *Freshwater Biol.*, **16**, 573–83. 78, 96, 119, 166
726. Kirkman, H. & Reid, D. D. (1979). A study of the seagrass *Posidonia australis* in the carbon budget of an estuary. *Aquat. Bot.*, **7**, 173–83. 436–7
727. Kishino, M., Booth, C. R. & Okami, N. (1984). Underwater radiant energy absorbed by phytoplankton, detritus, dissolved organic matter, and pure water. *Limnol. Oceanogr.*, **29**, 340–9. 76, 77, 368
728. Kishino, M., Okami, N., Takahashi, M. & Ichimura, S. (1986). Light utilization efficiency and quantum yield of phytoplankton in a thermally stratified sea. *Limnol. Oceanogr.*, **31**, 557–66. 325, 364, 368, 372
729. Kishino, M., Takahashi, M., Okami, N. & Ichimura, S. (1985). Estimation of the spectral absorption coefficients of phytoplankton in the sea. *Bull. Marine Sci.*, **37**, 634–42. 82, 86
730. Klemas, V., Bartlett, D., Philpot, W., Rogers, R. & Reed, L. (1974). Coastal and estuarine studies with ERTS-I and Skylab. *Remote Sens. Env.*, **3**, 153–74. 228–30
731. Klemas, V., Borchardt, J. F. & Treasure, W. M. (1973). Suspended sediments observations from ERTS-1. *Remote Sens. Env.*, **2**, 205–21. 228–9
732. Klemer, A. R., Feuillade, J. & Feuillade, M. (1982). Cyanobacterial blooms: carbon and nitrogen limitations have opposite effects on the buoyancy of *Oscillatoria*. *Science*, **215**, 1629–31. 518

733. Kling, G. W. (1988). Comparative transparency, depth of mixing and stability of stratification in lakes of Cameroon, West Africa. *Limnol. Oceanogr.*, **33**, 27–40. 165
734. Koblents-Mishke, O. I. (1965). Primary production in the Pacific. *Oceanology*, **5**, 104–16. 431–2, 450
735. Koblents-Mishke, O. I. (1979). Photosynthesis of marine phytoplankton as a function of underwater irradiance. *Soviet Plant Physiol.*, **26**, 737–46. 356, 376
736. Koenings, J. P. & Edmundson, J. A. (1991). Secchi disk and photometer estimates of light regimes in Alaskan lakes: effects of yellow colour and turbidity. *Limnol. Oceanogr.*, **36**, 91–105. 143, 165
737. Koepke, P. (1984). Effective reflectance of oceanic whitecaps. *Appl. Opt.*, **23**, 1816–24. 47
738. Koh, C.-H., Khim, J. S., Araki, H., Yamanishi, H. & Koga, K. (2007). Within-day and seasonal patterns of microphytobenthos biomass determined by co-measurement of sediment and water column chlorophylls in the intertidal mudflat of Nanura Saga, Ariake Sea, Japan. *Estuar. Coast. Shelf Sci.*, **72**, 42–52. 531
739. Kolber, Z. & Falkowski, P. G. (1993). Use of active fluorescence to estimate phytoplankton photosynthesis in situ. *Limnol. Oceanogr.*, **38**, 1646–65. 332, 336–7
740. Kolber, Z. S., Prášil, O. & Falkowski, P. G. (1998). Measurements of variable chlorophyll fluorescence using fast repetition rate techniques: defining methodology and experimental protocols. *Biochim. Biophys. Acta*, **1367**, 88–106. 336
741. Kolber, Z., Wyman, K. D. & Falkowski, P. G. (1990). Natural variation in photosynthetic energy conversion efficiency: a field study in the Gulf of Maine. *Limnol. Oceanogr.*, **35**, 72–9. 374
742. Kondo, K., Ochiai, Y., Katayama, M. & Ikeuchi, M. (2007). The membrane-associated CpcG2-phycobilisome in *Synechocystis*: a new photosystem I antenna. *Plant Physiol.*, **144**, 1200–10. 302
743. Kondratyev, K. Y. (1954). *Radiant Solar Energy*. Leningrad. Quoted by Robinson (1966). 44
744. Kondratyev, K. Y. & Pozdniakov, D. V. (1990). Passive and active optical remote sensing of the inland water phytoplankton. *ISPRS J. Photogramm. Remote Sens.*, **44**, 257–94.
745. Kopelevich, O. V. (1982). The ‘yellow substance’ in the ocean according to optical data. *Oceanology*, **22**, 152–6. 75
746. Kopelevich, O. V. (1984). On the influence of river and eolian suspended matter on the optical properties of sea water. *Oceanology*, **24**, 331–4. 120
747. Kopelevich, O. V. & Burenkov, V. I. (1971). The nephelometric method for determining the total scattering coefficient of light in sea water. *Izv. Atmos. Oceanic Phys.*, **7**, 835–40. 109, 117, 118
748. Kopelevich, O. V. & Burenkov, V. I. (1977). Relation between the spectral values of the light absorption coefficients of sea water, phytoplanktonic pigments, and the yellow substance. *Oceanology*, **17**, 278–82. 69, 74, 75
749. Kostoglidis, A., Pattiaratchi, C. B. & Hamilton, D. P. (2005). CDOM and its contribution to the underwater light climate of a shallow, microtidal estuary in south-western Australia. *Estuar. Coast. Shelf Sci.*, **63**, 469–77. 76, 164, 167
750. Kowalczyk, P., Olszewski, J., Darecki, M. & Kaczmarek, S. (2005). Empirical relationship between coloured dissolved organic matter (CDOM) absorption and apparent optical properties in Baltic Sea waters. *Int. J. Remote Sens.*, **26**, 345–70. 252–3

751. Kramer, C. J. M. (1979). Degradation by sunlight of dissolved fluorescing substances in the upper layers of the eastern Atlantic Ocean. *Neth. J. Sea Res.*, **13**, 325–9. [80](#)
752. Krause-Jensen, D. & Sand-Jensen, K. (1998). Light attenuation and photosynthesis of aquatic plant communities. *Limnol. Oceanogr.*, **43**, 396–407. [535–6](#)
753. Kromkamp, J. C. & Forster, R. M. (2003). The use of variable fluorescence measurements in aquatic ecosystems: differences between multiple and single turnover measuring protocols and suggested terminology. *Eur. J. Phycol.*, **38**, 103–12. [332](#), [335–6](#)
754. Kühl, M. & Jørgensen, B. B. (1992). Spectral light measurements in microbenthic phototrophic communities with a fiber-optic microprobe coupled to a sensitive diode array detector. *Limnol. Oceanogr.*, **37**, 1813–23. [146](#)
755. Kühl, M. & Jørgensen, B. B. (1994). The light field of microbenthic communities: radiance distribution and microscale optics of sandy coastal sediments. *Limnol. Oceanogr.*, **39**, 1368–98. [146](#)
756. Kühlbrandt, W., Wang, D. N. & Fujiyoshi, Y. (1994). Atomic model of plant light-harvesting complex by electron crystallography. *Nature*, **367**, 614–21. [291](#)
757. Kuhn, P., Brawman, H., McArthur, B. & St-Pierre, J.-F. (1999). Penetration of ultraviolet radiation in the waters of the estuary and Gulf of St. Lawrence. *Limnol. Oceanogr.*, **44**, 710–16. [158](#)
758. Kullenberg, G. (1968). Scattering of light by Sargasso Sea water. *Deep-Sea Res.*, **15**, 423–32. [107](#), [117](#), [124](#)
759. Kullenberg, G. (1984). Observations of light scattering functions in two oceanic areas. *Deep-Sea Res.*, **31**, 295–316. [108](#)
760. Kullenberg, G., Lundgren, B., Malmberg, S. A., Nygard, K. & Højerslev, N. K. (1970). Inherent optical properties of the Sargasso Sea. *Univ. Copenhagen Inst. Phys. Oceanogr. Rep.*, **11**, 1–18. Quoted by Jerlov (1976). [74](#)
761. Kuring, N., Lewis, M. R., Platt, T. & O'Reilly, J. E. (1990). Satellite-derived estimates of primary production on the northwest Atlantic continental shelf. *Continental Shelf Res.*, **10**, 461–84. [445](#)
762. Kutser, T., Paavel, B., Metsamaa, L. & Vahtmäe, E. (2009). Mapping coloured dissolved organic matter concentration in coastal waters. *Int. J. Remote. Sens.*, **30**, 5843–9. [254](#)
763. Kyewalyanga, M. N., Platt, T., Sathyendranath, S., Lutz, V. A. & Stuart, V. (1998). Seasonal variation in physiological parameters of phytoplankton across the North Atlantic. *J. Plankton Res.*, **20**, 17–42. [375](#)
764. Lance, V. P., Hiscock, M. R., Hilting, A. K. *et al.* (2007). Primary productivity, differential size fraction and pigment composition responses in two Southern Ocean in situ iron enrichments. *Deep-Sea Res.*, **54**, 747–73. [425](#)
765. Langmuir, I. (1938). Surface motion of water induced by wind. *Science*, **87**, 1119–23. [358](#)
766. Larkum, A. W. D. & Barrett, J. (1983). Light-harvesting processes in algae. *Adv. Botan. Res.*, **10**, 3–219. [286](#)
767. Larkum, A. W. D., Douglas, S. E. & Raven, J. A. (2003). *Photosynthesis in Algae*. Springer: Dordrecht. [266](#)
768. Larkum, A. W. D., Drew, E. A. & Crossett, R. N. (1967). The vertical distribution of attached marine algae in Malta. *J. Ecol.*, **55**, 361–71. [459–60](#), [465](#)

769. Larson, D.W. (1972). Temperature, transparency, and phytoplankton productivity in Crater Lake, Oregon. *Limnol. Oceanogr.*, **17**, 410–17. 397, 493
770. Larsson, C. & Axelsson, L. (1999). Bicarbonate uptake and utilization in marine macroalgae. *Eur. J. Phycol.*, **34**, 79–86. 405
771. Larsson, C., Axelsson, L., Ryberg, H. & Beer, S. (1997). Photosynthetic carbon utilization by *Enteromorpha intestinalis* (Chlorophyta) from a Swedish rockpool. *Eur. J. Phycol.*, **32**, 49–54. 405
772. Lassen, C., Ploug, H. & Jørgensen, B. B. (1992). Microalgal photosynthesis and spectral scalar irradiance in coastal marine sediments of Limfjorden, Denmark. *Limnol. Oceanogr.*, **37**, 760–72. 146
773. Lathrop, R. G. & Lillesand, T. M. (1986). Use of Thematic Mapper data to assess water quality in Green Bay and central Lake Michigan. *Photogramm. Eng. Remote Sens.*, **52**, 671–80. 237
774. Lathrop, R. G. & Lillesand, T. M. (1989). Monitoring water quality and river plume transport in Green Bay, Lake Michigan with SPOT-1 imagery. *Photogramm. Eng. Remote Sens.*, **55**, 349–54. 233
775. Latimer, P. & Rabinowitch, E. (1959). Selective scattering of light by pigments *in vivo*. *Arch. Biochem. Biophys.*, **84**, 428–41. 323
776. Laurion, I., Ventura, M., Catalan, J., Psenner, R. & Sommaruga, R. (2000). Attenuation of ultraviolet radiation in mountain lakes: factors controlling the among- and within-lake variability. *Limnol. Oceanogr.*, **45**, 1274–88. 77, 82, 158, 165
777. Lavery, P., Pattiaratchi, C., Wyllie, A. & Hick, P. (1993). Water quality monitoring in estuarine waters using the Landsat Thematic Mapper. *Remote Sens. Environ.*, **46**, 268–80. 260
778. Laws, E. A., Tullio, G. R. D., Carder, K. L., Betzer, P. R. & Hawes, S. (1990). Primary production in the deep blue sea. *Deep-Sea Res.*, **37**, 715–30. 331, 368
779. Lazzara, L., Bricaud, A. & Claustre, H. (1996). Spectral absorption and fluorescence excitation properties of phytoplanktonic populations at a mesotrophic and an oligotrophic site in the tropical North Atlantic (EUMELI program). *Deep-Sea Res.*, **43**, 1215–40. 462
780. Le Bouteiller, A., Leynaert, A., Landry, M. R. *et al.* (2003). Primary production, new production, and growth rate in the equatorial Pacific: changes from mesotrophic to oligotrophic regime. *J. Geophys. Res.*, **108**, C128141. 448
781. Le Cren, E. D. & Lowe-McConnell, R. H. (eds) (1980). *The Functioning of Freshwater Ecosystems*. Cambridge: Cambridge University Press. 452
782. Leathers, R. A. & McCormick, N. J. (1998). Ocean scalar irradiance near-surface maxima. *Limnol. Oceanogr.*, **43**, 982–6. 179
783. Leathers, R. A., Downes, T. V. & Davis, C. O. (2000). Analysis of a point-source integrating-cavity absorption meter. *Appl. Opt.*, **39**, 6118–27. 57
784. Leavitt, P. R., Cumming, B. F., Smol, J. P. *et al.* (2003). Climatic control of ultraviolet radiation effects on lakes. *Limnol. Oceanogr.*, **48**, 2062–9. 355
785. Leblanc, K., Leynaert, A., Fernandez, C. *et al.* (2005). A seasonal study of diatom dynamics in the North Atlantic during the POMME experiment (2001): evidence for Si limitation of the spring bloom. *J. Geophys. Res.*, **110**, C07S14. 423

786. Lee, M. E. & Lewis, M. R. (2003). A new method for the measurement of the optical volume scattering coefficient in the upper ocean. *J. Atmos. Ocean. Technol.*, **20**, 563–71. 108
787. Lee, Z.-P. (ed.) (2006). *Remote Sensing of Inherent Optical Properties: Fundamental Testing of Algorithms and Applications*. IOCCG Report No. 5. IOCCG. Dartmouth, Nova Scotia. 254–6
788. Lee, Z.-P., Carder, K. L. & Arnone, R. A. (2002). Deriving inherent optical properties from water color: a multiband quasi-analytical algorithm for optically deep waters. *Appl. Opt.*, **41**, 5755–72. 256
789. Lee, Z.-P., Darecki, M., Carder, K. L. *et al.* (2005). Diffuse attenuation coefficient of downwelling irradiance: an evaluation of remote sensing methods. *J. Geophys. Res.*, **110**, C02017. 256, 260, 261
790. Lee, Z.-P., Du, K.-P. & Arnone, R. (2005). A model for the diffuse attenuation coefficient of downwelling irradiance. *J. Geophys. Res.*, **110**, C02016. 256
791. Lee, Z.-P., Weidemann, A., Kindle, J. *et al.* (2007). Euphotic zone depth: its derivation and implication to ocean-color remote sensing. *J. Geophys. Res.*, **112**, C03009. 257
792. Leggat, W., Mareudy, E. M., Baillie, B. *et al.* (2002). Dinoflagellate symbioses: strategies and adaptations for the acquisition and fixation of inorganic carbon. *Funct. Plant Biol.*, **29**, 309–22. 407
793. Leletkin, V. A., Zvalinskii, V. I. & Titlyanov, E. A. (1981). Photosynthesis of zooxanthellae in corals of different depths. *Soviet Plant Physiol.*, **27**, 863–70. 495
794. Lester, W. W., Adams, M. S. & Farmer, A. M. (1988). Effects of light and temperature on photosynthesis of the nuisance alga *Cladophora glomerata* (L.). Kutz from Green Bay, Michigan. *New Phytol.*, **109**, 53–8. 344
- 794a. Levavasseur, G., Edwards, G. E., Osmond, G. B. & Ramus, J. (1991). Inorganic carbon limitation of photosynthesis in *Ulva rotundata* (Chlorophyta). *J. Phycol.*, **27**, 667–72. 406
795. Leveque, C. Quoted in Le Cren & Lowe-McConnell (1980). 434
796. Levring, T. (1959). Submarine illumination and vertical distribution of algal vegetation. In *Proc. 9th Int. Bot. Congr.* (pp. 183–93). Canada: University of Toronto Press. 456
797. Levring, T. (1966). Submarine light and algal shore zonation. In R. Bainbridge, G. C. Evans & O. Rackham (eds), *Light as an Ecological Factor* (pp. 305–18). Oxford: Blackwell. 461–2
798. Levring, T. (1968). Photosynthesis of some marine algae in clear, tropical oceanic water. *Bot. Mar.*, **11**, 72–80. 461–2
799. Levy, I. & Gantt, E. (1988). Light acclimation in *Porphyridium purpureum* (Rhodophyta): growth, photosynthesis and phycobilisomes. *J. Phycol.*, **24**, 452–8. 470, 473, 477
800. Lewin, R. A. (1976). Prochlorophyta as a proposed new division of algae. *Nature.*, **261**, 697–8. 273
801. Lewis, J. B. (1977). Processes of organic production on coral reefs. *Biol. Rev.*, **52**, 305–47. 533
802. Lewis, M. R., Horne, E. P. W., Cullen, J. J., Oakey, N. S. & Platt, T. (1984). Turbulent motions may control phytoplankton photosynthesis in the upper ocean. *Nature*, **311**, 49–50. 501

803. Lewis, M. R., Warnock, R. E., Irwin, B. & Platt, T. (1985). Measuring photosynthetic action spectra of natural phytoplankton populations. *J. Phycol.*, **21**, 310–15. 382
804. Lewis, M. R., Warnock, R. E. & Platt, T. (1985). Absorption and photosynthetic action spectra for natural phytoplankton populations: implications for production in the open sea. *Limnol. Oceanogr.*, **30**, 794–806. 86
805. Lewis, W. M. & Canfield, D. (1977). Dissolved organic carbon in some dark Venezuelan waters and a revised equation for spectrophotometric determination of dissolved organic carbon. *Arch. Hydrobiol.*, **79**, 441–5. 77, 80
806. Ley, A. C. & Butler, W. L. (1980). Effects of chromatic adaptation on the photochemical apparatus of photosynthesis in *Porphyridium cruentum*. *Plant Physiol.*, **65**, 714–22. 484–6, 505, 508
807. Ley, A. C. & Mauzerall, D. C. (1982). Absolute absorption cross-sections for photosystem II and the minimum quantum requirement for photosynthesis in *Chlorella vulgaris*. *Biochim. Biophys. Acta*, **680**, 95–106. 336
808. Li, M. & Jones, M. B. (1995). CO<sub>2</sub> and O<sub>2</sub> transport in the aerenchyma of *Cyperus papyrus* L. *Aquat. Bot.*, **52**, 93–106. 410
809. Li, W. K. W. (1986). Experimental approaches to field measurements: methods and interpretation. In T. Platt & W. K. W. Li (eds), Photosynthetic picoplankton (pp. 251–86). *Can. Bull. Fish Aquat. Sci.*, **214**. 131
810. Lichtlé, C., Thomas, J. C., Spilar, A. & Partensky, F. (1995). Immunological and ultrastructural characterization of the photosynthetic complexes of the prochlorophyte *Prochlorococcus* (Oxychlorobacteria). *J. Phycol.*, **31**, 934–41. 273
811. Light, B. R. & Beardall, J. (2001). Photosynthetic characteristics of sub-tidal benthic microalgal populations from a temperate, shallow water marine ecosystem. *Aquat. Bot.*, **70**, 9–27. 347
812. Light, B., Grenfell, T. C. & Perovich, D. K. (2008). Transmission and absorption of solar radiation by Arctic sea ice during the melt season. *J. Geophys. Res.*, **113**, C03023. 121
813. Lin, S. & Carpenter, E. J. (1997). Rubisco of *Dunaliella tertiolecta* is redistributed between the pyrenoid and the stroma as a light/shade response. *Mar. Biol.*, **127**, 521–9. 475
814. Lipkin, Y. (1977). Seagrass vegetation of Sinai and Israel. In C. P. McRoy & C. Helfferich (eds), *Seagrass Ecosystems* (pp. 263–93). New York: Marcel Dekker. 469
815. Lipkin, Y. (1979). Quantitative aspects of sea grass communities particularly of those dominated by *Halophila stipulacea*, in Sinai (northern Red Sea). *Aquat. Bot.*, **7**, 119–28. 502–3
816. LISST-100X Particle Size Analyzer. User's Manual, Version 4.60. Sequoia Scientific. Bellevue, Washington. 108
817. Litjens, R. A. J., Quickenden, T. I. & Freeman, C. G. (1999). Visible and near-ultraviolet absorption spectrum of liquid water. *Appl. Opt.*, **38**, 1216–23. 62
818. Littler, M. M., Littler, D. S., Blair, S. M. & Norris, J. N. (1985). Deepest known plant life discovered on an uncharted seamount. *Science*, **227**, 57–9. 460–1
819. Littler, M. M., Littler, D. S., Blair, S. M. & Norris, J. N. (1986). Deepwater plant communities from an uncharted seamount off San Salvador Island, Bahamas: distribution, abundance, and primary productivity. *Deep-Sea Res.*, **33**, 881–92. 390, 460–1

820. Liu, Z., Yan, H., Wang, K. *et al.* (2004). Crystal structure of spinach major light-harvesting complex at 2.72 Å resolution. *Nature*, **428**, 287–92. 291
821. Llewellyn, C. A. & Harbour, D. S. (2003). A temporal study of mycosporine-like amino acids in surface water phytoplankton from the English channel and correlation with solar irradiation. *J. Mar. Biol. Ass. U.K.*, **83**, 1–9. 89
822. Lodge, D. M. (1991). Herbivory on freshwater macrophytes. *Aquat. Bot.*, **41**, 195–224. 428
823. Loeblich, L. A. (1982). Photosynthesis and pigments influenced by light intensity and salinity in the halophile *Dunaliella salina* (Chlorophyta). *J. Mar. Biol. Ass. U.K.*, **62**, 493–508. 471
824. Loisel, H. & Morel, A. (2001). Non-isotropy of the upward radiance field in typical coastal (Case 2) waters. *Int. J. Remote Sens.*, **22**, 275–95. 173, 226
825. Loiseau, S. A., Azza, N., Cózar, A. *et al.* (2008). Variability in factors causing light attenuation in Lake Victoria. *Freshwater Biol.*, **53**, 535–45. 167
826. Longhurst, A., Sathyendranath, S., Platt, T. & Caverhill, C. (1995). An estimate of global primary production from satellite radiometer data. *J. Plankton Res.*, **17**, 1245–71. 451
827. Lopez-Figueroa, F. & Niell, F. X. (1990). Effects of light quality on chlorophyll and biliprotein accumulation in seaweeds. *Mar. Biol.*, **104**, 321–7. 483
828. Lorenzen, C. J. (1968). Carbon/chlorophyll relationships in an upwelling area. *Limnol. Oceanogr.*, **13**, 202–4. 278
829. Lorenzo, L. M., Figueiras, F. G., Tilstone, G. H., Arbones, B. & Miron, I. (2004). Photosynthesis and light regime in the Azores Front region during summer: are light-saturated computations of primary production sufficient? *Deep-Sea Res.*, **51**, 1229–44. 346, 396
830. Love, R. J. R. & Robinson, G. G. C. (1977). The primary productivity of submerged macrophytes in West Blue Lake, Manitoba. *Can. J. Bot.*, **55**, 118–27. 439–40
831. Lüning, K. (1971). Seasonal growth of *Laminaria hyperborea* under recorded underwater light conditions near Heligoland. In D. J. Crisp (ed.), *Fourth European Mar. Biology Symposium* (pp. 347–61). Cambridge: Cambridge University Press. 534
832. Lüning, K. (1990). *Seaweeds: Their Environment, Biogeography and Ecophysiology*. New York: Wiley. 64, 464
833. Lüning, K. & Dring, M. J. (1979). Continuous underwater light measurement near Heligoland (North Sea) and its significance for characteristic light limits in the sublittoral region. *Helgoländer Wiss. Meeresunters.*, **32**, 403–24. 390, 438
834. Lund-Hansen, L. C. (2004). Diffuse attenuation coefficients  $K_d(\text{PAR})$  at the estuarine North Sea-Baltic Sea transition: time-series, partitioning, absorption and scattering. *Estuar. Coast. Shelf Sci.*, **61**, 251–9. 75, 163, 167
835. Lynch, M. & Shapiro, J. (1981). Predation, enrichment and phytoplankton community structure. *Limnol. Oceanogr.*, **26**, 86–102. 426
836. Maberly, S. C. (1990). Exogenous sources of inorganic carbon for photosynthesis by marine macroalgae. *J. Phycol.*, **26**, 439–49. 405
837. Maberly, S. C., Ball, L. A., Raven, J. A. & Sültemeyer, D. (2009). Inorganic carbon acquisition by chrysophytes. *J. Phycol.*, **45**, 1052–61. 407

838. Maberly, S. C. & Madsen, T. V. (2002). Freshwater angiosperm carbon concentrating mechanisms: processes and patterns. *Funct. Plant Biol.*, **29**, 393–405. 407
839. Maberly, S. C. & Spence, D. H. N. (1983). Photosynthetic inorganic carbon use by freshwater plants. *J. Ecol.*, **71**, 705–24. 408
840. Macauley, J. M., Clark, J. R. & Price, W. A. (1988). Seasonal changes in the standing crop and chlorophyll content of *Thalassia testudinum* Banks ex König and its epiphytes in the northern Gulf of Mexico. *Aquat. Bot.*, **31**, 277–87. 436
841. MacColl, R. & Guard-Friar, D. (1983a). Phycocyanin 612: a biochemical and photo physical study. *Biochemistry*, **22**, 5568–72. 296
842. MacColl, R. & Guard-Friar, D. (1983b). Phycocyanin 645: the chromophore assay of phycocyanin 645 from the cryptomonad *Chroomonas* species. *J. Biol. Chem.*, **258**, 14327–9. 296
843. MacColl, R. & Guard-Friar, D. (1987). *Phycobiliproteins*. Boca Raton: CRC Press. 293
844. MacColl, R., Guard-Friar, D. & Csatorday, K. (1983). Chromatographic and spectroscopic analysis of phycoerythrin 545 and its subunits. *Arch. Mikrobiol.*, **135**, 194–8. 296
845. Madsen, T. V., Enevoldsen, H. O. & Jørgensen, T. B. (1993). Effects of water velocity on photosynthesis and dark respiration in submerged stream macrophytes. *Plant Cell Environ.*, **16**, 317–22. 412
846. Madsen, T. V., Olesen, B. & Bagger, J. (2002). Carbon acquisition and carbon dynamics by aquatic isoetids. *Aquat. Bot.*, **73**, 351–71. 410, 414
847. Madsen, T. V. & Sand-Jensen, K. (1991). Photosynthetic carbon assimilation in aquatic macrophytes. *Aquat. Bot.*, **41**, 5–40. 406, 410
848. Maffione, R. A. (1998). Theoretical developments on the optical properties of highly turbid waters and sea ice. *Limnol. Oceanogr.*, **43**, 29–33. 194
849. Maffione, R. A. & Dana, D. R. (1997). Instruments and methods for measuring the backward-scattering coefficient of ocean waters. *Appl. Opt.*, **36**, 6057–67. 110, 111
850. Maffione, R. A., Voss, K. J. & Honey, R. C. (1993). The average cosine due to an isotropic light source in the ocean. *J. Geophys. Res.*, **100**, 13179–92. 59
851. Maffione, R. A., Voss, J. M. & Mobley, C. D. (1998). Theory and measurements of the complete beam spread function of sea ice. *Limnol. Oceanogr.*, **43**, 36–43. 194
852. Magnin, N. C., Cooley, B. A., Reiskind, J. B. & Bowes, G. (1997). Regulation and localization of key enzymes during the induction of Kranz-less, C<sub>4</sub>-type photosynthesis in *Hydrilla verticillata*. *Plant Physiol.*, **115**, 1681–9. 413
853. Malcolm, R. I. (1990). The uniqueness of humic substances in each of soil, stream and marine environments. *Analyt. Chim. Acta*, **232**, 19–30. 67, 69
854. Malin, G. & Kirst, G. O. (1997). Algal production of dimethyl sulfide and its atmospheric role. *J. Phycol.*, **33**, 889–96. 452
855. Mallin, M. A. & Paerl, H. W. (1992). Effects of variable irradiance on phytoplankton productivity in shallow estuaries. *Limnol. Oceanogr.*, **37**, 54–62. 358
856. Malone, T. C. (1977a). Environmental regulation of phytoplankton productivity in the lower Hudson estuary. *Estuar. Coast. Mar. Sci.*, **5**, 157–71. 398, 419
857. Malone, T. C. (1977b). Light-saturated photosynthesis by phytoplankton size fractions in the New York Bight, U.S.A. *Mar. Biol.*, **42**, 281–92. 419

858. Malone, T. C. (1982). Phytoplankton photosynthesis and carbon specific growth: light-saturated rates in a nutrient-rich environment. *Limnol. Oceanogr.*, **27**, 226–35. 524
859. Malone, T. C. & Neale, P. J. (1981). Parameters of light-dependent photosynthesis for phytoplankton size fractions in temperate estuarine and coastal environments. *Mar. Biol.*, **61**, 289–97. 374
860. Malta, E., Rijstenbil, J. W., Brouwer, P. E. M. & Kromkamp, J. C. (2003). Vertical heterogeneity in physiological characteristics of *Ulva* spp. mats. *Mar. Biol.*, **143**, 1029–38. 470–1
861. Mann, K. H. (1972). Ecological energetics of the seaweed zone in a marine bay on the Atlantic coast of Canada. II. Productivity of the seaweeds. *Mar. Biol.*, **14**, 199–209. 534
862. Mann, K. H. & Chapman, A. R. O. (1975). Primary production of marine macrophytes. In J. P. Cooper (ed.), *Photosynthesis and Productivity in Different Environments* (pp. 207–23). Cambridge: Cambridge University Press. 533, 534
863. Manodori, A. & Melis, A. (1986). Cyanobacterial acclimation to Photosystem I or Photosystem II light. *Plant Physiol.*, **82**, 185–9. 487
864. Mariani Colombo, P., Orsenigo, M., Solazzi, A. & Tolomio, C. (1976). Sea depth effects on the algal photosynthetic apparatus. IV. Observations on the photosynthetic apparatus of *Halimeda tuna* (Siphonales) at sea depths between 7 and 16 m. *Mem. Biol. Mar. Ocean.*, **6**, 197–208. 502–3
865. Maritorena, S., Morel, A. & Gentili, B. (2000). Determination of the fluorescence quantum yield by oceanic phytoplankton in their natural habitat. *Appl. Opt.*, **39**, 6275–37. 247
866. Maritorena, S., Siegel, D. A. & Peterson, A. R. (2002). Optimization of a semianalytical ocean color model for global-scale applications. *Appl. Opt.*, **41**, 2705–14. 243
867. Marra, J. (1978). Phytoplankton photosynthetic response to vertical movement in a mixed layer. *Mar. Biol.*, **46**, 203–8. 343, 353, 358
868. Marra, J., Trees, C. C. & O'Reilly, J. E. (2007). Phytoplankton pigment absorption: a strong predictor of primary productivity in the surface ocean. *Deep-Sea Res.*, **54**, 155–63. 446–7
869. Marshall, B. R. & Smith, R. C. (1990). Raman scattering and in-water ocean optical properties. *Appl. Opt.*, **29**, 71–84. 178
870. Marshall, C. T. & Peters, R. H. (1989). General patterns in the seasonal development of chlorophyll *a* for temperate lakes. *Limnol. Oceanogr.*, **34**, 856–67. 434
871. Martin, J. H., Coale, K. H., Johnson, K. S. *et al.* (1994). Testing the iron hypothesis in ecosystems of the equatorial Pacific Ocean. *Nature*, **371**, 123–9. 425
872. Martin, J. H., Gordon, R. M. & Fitzwater, S. E. (1991). The case for iron. *Limnol. Oceanogr.*, **36**, 1793–802. 424
873. Maske, H. & Haardt, H. (1987). Quantitative in vivo absorption spectra of phytoplankton: detrital absorption and comparison with fluorescence excitation spectra. *Limnol. Oceanogr.*, **32**, 620–33. 87
874. Masojidek, J., Grobbelaar, J. U., Pechar, L. & Kobizek, M. (2001). Photosystem II electron transport rates and oxygen production in natural waterblooms of freshwater cyanobacteria during a diel cycle. *J. Plankton Res.*, **23**, 57–66. 337

875. Mathieson, A. C. (1979). Vertical distribution and longevity of subtidal seaweeds in northern New England, U.S.A. *Bot. Mar.*, **30**, 511–20. 457
876. Mathieson, A. C. & Burns, R. L. (1971). Ecological studies of economic red algae. *J. Exp. Mar. Biol. Ecol.*, **7**, 197–206. 417–18
877. Mathieson, A. C. & Norall, T. L. (1975). Physiological studies of subtidal red algae. *J. Exp. Mar. Biol. Ecol.*, **20**, 237–47. 495–6
878. Mathis, P. & Paillotin, G. (1981). Primary processes of photosynthesis. In M. D. Hatch & N. K. Boardman (eds), *The Biochemistry of Plants* (pp. 97–161). New York: Academic Press. 302
879. Matsuoka, A., Larouche, P., Poulin, M., Vincent, W. & Hattori, H. (2009). Phytoplankton community adaptation to changing light levels in the southern Beaufort Sea, Canadian Arctic. *Estuar. Coast. Shelf Sci.*, **82**, 537–46. 319
880. McAllister, H. A., Norton, T. A. & Conway, E. (1967). A preliminary list of sublittoral marine algae from the west of Scotland. *Br. Phycol. Bull.*, **3**, 175–84. 457
881. McGinn, P. J. & Morel, F. M. M. (2008). Expression and inhibition of the carboxylating and decarboxylating enzymes in the photosynthetic C<sub>4</sub> pathway of marine diatoms. *Plant Physiol.*, **146**, 300–9. 414
882. McGlathery, K. J. (2001). Macroalgal blooms contribute to the decline of seagrass in nutrient-enriched coastal waters. *J. Phycol.*, **37**, 453–6. 428
883. McKee, D. & Cunningham, A. (2005). Evidence for wavelength dependence of the scattering phase function and its implication for modeling radiance transfer in shelf seas. *Appl. Opt.*, **44**, 126–35. 126
884. McKee, D. & Cunningham, A. (2006). Identification and characterisation of two optical water types in the Irish Sea from in situ inherent optical properties and seawater constituents. *Estuar. Coast. Shelf Sci.*, **68**, 305–16. 245, 256
885. McKee, D., Cunningham, A. & Craig, S. (2003). Estimation of absorption and backscattering coefficients from in situ radiometric measurements: theory and validation in case II waters. *Appl. Opt.*, **42**, 2804–10. 61
886. McKee, D., Cunningham, A. & Dudek, A. (2007). Optical water type discrimination and tuning remote sensing band-ratio algorithms: application to retrieval of chlorophyll and K<sub>d</sub>(490) in the Irish and Celtic Seas. *Estuar. Coast. Shelf Sci.*, **73**, 827–34. 256
887. McKee, D., Cunningham, A. & Jones, K. J. (2002). Optical and hydrographic consequences of freshwater run-off during spring phytoplankton growth in a Scottish fjord. *J. Plankton Res.*, **24**, 1163–71. 75, 97, 164
888. McKee, D., Cunningham, A., Slater, J., Jones, K. J. & Griffiths, C. R. (2003). Inherent and apparent optical properties in coastal waters: a study of the Clyde Sea in early summer. *Estuar. Coast. Shelf Sci.*, **56**, 369–76. 194
889. McKee, D., Cunningham, A., Wright, D. & Hay, L. (2007). Potential impacts of nonalgal materials on water-leaving Sun-induced chlorophyll fluorescence signals in coastal waters. *Appl. Opt.*, **46**, 7720–9. 245, 248
890. McKnight, D. M., Boyer, E. W., Westerhoff, P. K. *et al.* (2001). Spectrofluorometric characterization of dissolved organic matter for indication of precursor organic material and aromaticity. *Limnol. Oceanogr.*, **46**, 38–48. 66
891. McLachlan, A. J. & McLachlan, S. M. (1975). The physical environment and bottom fauna of a bog lake. *Arch. Hydrobiol.*, **76**, 198–217. 76

892. McMahon, T. G., Raine, R. C. T., Fast, T., Kies, L. & Patching, J. W. (1992). Phytoplankton biomass, light attenuation and mixing in the Shannon estuary. *J. Mar. Biol. Ass. U.K.*, **72**, 709–20. 163
893. McManus, G. B., Zhang, H. & Lin, S. (2004). Marine planktonic ciliates that prey on macroalgae and enslave their chloroplasts. *Limnol. Oceanogr.*, **49**, 308–13. 429
894. McRoy, C. P. & Helfferich, C. (1980). Applied aspects of seagrasses. In R. C. Phillips & C. P. McRoy (eds), *Handbook of Seagrass Biology* (pp. 297–343). New York: Garland STPM Press. 429, 479
895. Medina, E. (1971). Effect of nitrogen supply and light intensity during growth on the photosynthetic capacity and carboxydismutase activity of leaves of *Atriplex patula* spp. *hastata*. *Carnegie Inst. Wash. Yearbook*, **70**, 551–9. 474
896. Megard, R. O., Combs, W. S., Smith, P. D. & Knoll, A. S. (1979). Attenuation of light and daily integral rates of photosynthesis attained by planktonic algae. *Limnol. Oceanogr.*, **24**, 1038–50. 165, 328, 364
897. Melack, J. M. (1979). Photosynthesis and growth of *Spirulina platensis* (Cyanophyta) in an equatorial lake (Lake Simbi, Kenya). *Limnol. Oceanogr.*, **24**, 753–60. 165
898. Melack, J. M. (1981). Photosynthetic activity of phytoplankton in tropical African soda lakes. *Hydrobiologia*, **81**, 71–85. 376
899. Menon, H. B., Lotliker, A. A. & Nayak, S. R. (2006). Analysis of estuarine colour components during non-monsoon period through Ocean Colour Monitor. *Estuar. Coast. Shelf Sci.*, **66**, 523–31. 253
900. Meyer-Harms, B., Irigoien, X., Head, R. & Harris, R. (1999). Selective feeding on natural phytoplankton by *Calanus finmarchicus* before, during and after the 1997 spring bloom in the Norwegian Sea. *Limnol. Oceanogr.*, **44**, 154–65. 424
901. Meyers-Schulte, K. J. & Hedges, J. I. (1986). Molecular evidence for a terrestrial component of organic matter dissolved in ocean water. *Nature*, **321**, 61–3. 67, 69
902. Mie, G. (1908). Beiträge zur Optik trüber Medien, speziell kolloidalen Metalllosungen. *Ann. Phys.*, **25**, 377–445. 100
903. Millán-Núñez, R., Alvarez-Borrego, S. & Trees, C. T. (1997). Modeling the vertical distribution of chlorophyll in the California Current System. *J. Geophys. Res.*, **102**, 8587–95. 444
904. Miller, R. L. & McKee, B. A. (2004). Using MODIS Terra 250 m imagery to map concentrations of total suspended matter in coastal waters. *Remote Sens. Environ.*, **93**, 259–66. 235
905. Miller, W. L., Moran, M. A., Sheldon, W. M., Zepp, R. G. & Opsahl, S. (2002). Determination of apparent quantum yield spectra for the formation of biologically labile products. *Limnol. Oceanogr.*, **47**, 343–52. 81
906. Millie, D. F., Dionigi, C. P., Schofield, O., Kirkpatrick, G. J. & Tester, P. A. (1999). The importance of understanding the molecular, cellular, and ecophysiological bases of harmful algal blooms. *J. Phycol.*, **35**, 1353–5. 537
907. Mimuro, M., Akimoto, S., Yamazaki, I., Miyashita, H. & Miyachi, S. (1999). Fluorescence properties of chlorophyll *d*-dominating prokaryotic alga,

- Acaryochloris marina*: studies using time-resolved fluorescence spectroscopy on intact cells. *Biochim. Biophys. Acta*, **1412**, 37–46. 300
908. Mimuro, M., Hirayama, K., Uezono, K., Miyashita, H. & Miyachi, S. (2000). Uphill energy transfer in a chlorophyll *d*-dominating oxygenic photosynthetic prokaryote, *Acaryochloris marina*. *Biochim. Biophys. Acta*, **1456**, 27–34. 300
909. Mimuro, M. & Kikuchi, H. (2003). Antenna systems and energy transfer in Cyanophyta and Rhodophyta. In, Green, B. R. & Parsons, W. W. (eds). *Light-Harvesting Antennas in Photosynthesis. Advances in Photosynthesis and Respiration. Vol. 13*. pp. 281–306. Springer, Dordrecht. 293
910. Mishkind, M. & Mauzerall, D. (1980). Kinetic evidence for a common photosynthetic step in diverse seaweeds. *Mar. Biol.*, **58**, 89–96. 472
911. Mitbavkar, S. & Anil, A. C. (2004). Vertical migratory rhythms of benthic diatoms in a tropical intertidal sand flat: influence of irradiance and tides. *Mar. Biol.*, **145**, 9–20. 529
912. Mitchell, B. G. (1990). Algorithms for determining the absorption coefficients of aquatic particulates using the quantitative fiber technique (QFT). *SPIE Ocean Optics X*, **1302**, 137–48. 57
913. Mitchell, B. G., Brody, E. A., Holm-Hansen, O., McClain, C. & Bishop, J. (1991). Light limitation of phytoplankton biomass and macronutrient utilization in the Southern Ocean. *Limnol. Oceanogr.*, **36**, 1662–77. 424
914. Mitchell, B. G. & Holm-Hansen, O. (1991a). Bio-optical properties of Antarctic Peninsula waters: differentiation from temperate ocean models. *Deep-Sea Res.*, **38**, 1009–28. 317
915. Mitchell, B. G. & Holm-Hansen, O. (1991b). Observations and modelling of the Antarctic phytoplankton crop in relation to mixing depth. *Deep-Sea Res.*, **38**, 981–1007. 346, 394
916. Mitchell, B. G. & Kiefer, D. A. (1988). Chlorophyll *a* specific absorption and fluorescence excitation spectra for light-limited phytoplankton. *Deep-Sea Res.*, **35**, 639–63. 86
917. Mitchelson, E. G., Jacob, N. J. & Simpson, J. H. (1986). Ocean colour algorithms from the Case 2 waters of the Irish Sea in comparison to algorithms from Case 1 waters. *Continental Shelf Res.*, **5**, 403–15. 244
918. Mittenzwey, K.-H., Ullrich, S., Gitelson, A. A. & Kondratiev, K. Y. (1992). Determination of chlorophyll *a* of inland waters on the basis of spectral reflectance. *Limnol. Oceanogr.*, **37**, 147–9. 236
919. Miyashita, H., Adachi, K., Kurano, N. *et al.* (1997). Pigment composition of a novel oxygenic photosynthetic prokaryote containing chlorophyll *d* as the major chlorophyll. *Plant Cell Physiol.*, **38**, 274–81. 284
920. Miyashita, H., Ikemoto, H., Kurano, N. *et al.* (1996). Chlorophyll *d* as a major pigment. *Nature*, **383**, 402. 278, 300
921. Mizusawa, M., Kageyama, A. & Yokohama, Y. (1978). Physiology of benthic algae in tide pools. *Jap. J. Phycol.*, **26**, 109–14. 415–16
922. Mobley, C. D. (1989). A numerical model for the computation of radiance distribution in natural waters with wind-roughened surfaces. *Limnol. Oceanogr.*, **34**, 1473–83. 151
923. Mobley, C. D. (1994). *Light in Water: Radiative Transfer in Natural Waters*. San Diego: Academic. 6, 151

924. <http://modis.gsfc.nasa.gov>. 214, 235
925. Molinier, R. (1960). Etudes des biocénoses marines du Cap Corse. *Vegetatio*, **9**, 121–92, 219–312. 459
926. Monahan, E. C. & Pybus, M. J. (1978). Colour, ultraviolet absorbance and salinity of the surface waters off the west coast of Ireland. *Nature*, **274**, 782–4. 67
927. Monger, B., McClain, C. & Murtugudde, R. (1997). Seasonal phytoplankton dynamics in the eastern tropical Atlantic. *J. Geophys. Res.*, **102**, 12389–411. 451
928. Monteith, J. L. (1973). *Principles of Environmental Physics*. London: Edward Arnold. 32–8, 41
929. Monteith, J. L. & Unsworth, M. H. (1990). *Principles of Environmental Physics*. London: Edward Arnold. 37
930. Moon, P. (1940). *J. Franklin Inst.*, **230**, 583. Quoted by Monteith (1973). 33
931. Moon, P. (1961). *The Scientific Basis of Illuminating Engineering*. New York: Dover. 30
932. Moon, R. E. & Dawes, C. J. (1976). Pigment changes and photosynthetic rates under selected wavelengths in the growing tips of *Euchaema isiforme* (C. Agardh) J. Agardh var *denudatum* Cheney during vegetative growth. *Br. Phycol. J.*, **11**, 165–74. 510
933. Moore, J. K. & Abbott, M. R. (2000). Phytoplankton chlorophyll distributions and primary production in the Southern Ocean. *J. Geophys. Res.*, **105**, 28709–22. 451
934. Mopper, K., Xianling, Z., Kieber, R. J., *et al.* (1991). Photochemical degradation of dissolved organic carbon and its impact on the oceanic carbon cycle. *Nature*, **353**, 60–2. 80
935. Moran, M. A. & Hodson, R. E. (1994). Dissolved humic substances of vascular plant origin in a coastal marine environment. *Limnol. Oceanogr.*, **39**, 762–71. 67
936. Moran, M. S., Jackson, R. D., Slater, P. N. & Teillet, P. M. (1992). Evaluation of simplified procedures for retrieval of land surface reflectance factors from satellite sensor output. *Remote Sens. Environ.*, **41**, 169–84. 222
937. Morel, A. (1966). Etude expérimentale de la diffusion de la lumière par l'eau, les solutions de chlorure de sodium et leau de mer optiquement pures. *J. Chim. Phys.*, **10**, 1359–66. 109
938. Morel, A. (1973). Diffusion de la lumière par les eaux de mer. Resultats expérimentaux et approche théorique. In *Optics of the Sea* (pp. 3.1–1 to 3.1–76). Neuilly-sur-Seine: NATO. 118, 120
939. Morel, A. (1974). Optical properties of pure water and pure seawater. In N. G. Jerlov & E. S. Nielsen (eds), *Optical Aspects of Oceanography* (pp. 1–24). London: Academic Press. 116, 117, 120
940. Morel, A. (1978). Available, usable and stored radiant energy in relation to marine photosynthesis. *Deep-Sea Res.*, **25**, 673–88. 324, 325, 364, 368, 372, 376, 379–80
941. Morel, A. (1980). In-water and remote measurement of ocean colour. *Boundary-layer Meteorol.*, **18**, 177–201. 227, 239
942. Morel, A. (1982). Optical properties and radiant energy in the waters of the Guinea dome and of the Mauritanian upwelling area: relation to primary production. *Rapp. P. V. Reun. Cons. Int. Explor. Mer.*, **180**, 94–107. 117, 120, 154, 156, 163

943. Morel, A. (1987). Chlorophyll-specific scattering coefficient of phytoplankton. A simplified theoretical approach. *Deep-Sea Res.*, **34**, 1093–105. [128](#), [129](#)
944. Morel, A. (1991). Light and marine photosynthesis: a spectral model with geochemical and climatological implications. *Prog. Oceanog.*, **26**, 263–306. [364](#), [367](#), [377](#), [443](#), [445](#)
945. Morel, A., Ahn, Y.-H., Partensky, F., Vaultot, D. & Claustre, H. (1993). *Prochlorococcus* and *Synechococcus*: a comparative study of their optical properties in relation to their size and pigmentation. *J. Mar. Res.*, **51**, 617–49. [128](#)
946. Morel, A. & Berthon, J.-F. (1989). Surface pigments, algal biomass profiles, and potential production of the euphotic layer: relationships reinvestigated in view of remote-sensing applications. *Limnol. Oceanogr.*, **34**, 1545–62. [444–5](#)
947. Morel, A. & Bricaud, A. (1981). Theoretical results concerning light absorption in a discrete medium, and application to specific absorption of phytoplankton. *Deep-Sea Res.*, **28**, 1375–93. [311](#), [313](#), [317](#)
948. Morel, A. & Bricaud, A. (1986). Inherent optical properties of algal cells including picoplankton: theoretical and experimental results. In T. Platt & W. K. W. Li (eds), *Photosynthetic picoplankton* (pp. 521–59). *Can. Bull. Fish. Aquat. Sci.*, **214**. [128](#)
949. Morel, A. & Gentili, B. (1991). Diffuse reflectance of oceanic waters: its dependence on sun angle as influenced by the molecular scattering contribution. *Appl. Opt.*, **30**, 4427–38. [170](#)
950. Morel, A. & Gentili, B. (1993). Diffuse reflectance of oceanic waters. II. Bidirectional aspects. *Appl. Opt.*, **32**, 6864–79. [172](#)
951. Morel, A. & Gentili, B. (1996). Diffuse reflectance of oceanic waters. III. Implication of bidirectionality for the remote-sensing problem. *Appl. Opt.*, **35**, 4850–62. [172](#), [174](#), [226–7](#)
952. Morel, A., Gentili, B., Chami, M. & Ras, J. (2006). Bio-optical properties of high chlorophyll Case 1 waters and of yellow-substance-dominated Case 2 waters. *Deep-Sea Res.*, **53**, 1439–59. [86](#)
953. Morel, A., Huot, Y., Gentili, B. *et al.* (2007). Examining the consistency of products derived from various ocean color sensors in open ocean (Case 1) waters in the perspective of a multi-sensor approach. *Remote Sens. Environ.*, **111**, 69–88. [256](#), [257](#)
954. Morel, A., Lazzara, L. & Gostan, J. (1987). Growth rate and quantum yield time response for a diatom to changing irradiances (energy and colour). *Limnol. Oceanogr.*, **32**, 1066–84. [317](#)
955. Morel, A. & Prieur, L. (1975). *Analyse spectrale des coefficients d'attenuation diffuse, de reflection diffuse, d'absorption et de retrodiffusion pour diverses regions marines*. Rep. No. 17. Laboratoire d'Océanographie Physique, Villefranche-sur-Mer. Quoted by Jerlov (1976). [95](#)
956. Morel, A. & Prieur, L. (1977). Analysis of variations in ocean colour. *Limnol. Oceanogr.*, **22**, 709–22. [88–9](#), [94](#), [124](#), [170–1](#), [175](#), [239](#), [247](#)
957. Morel, A. & Smith, R. C. (1974). Relation between total quanta and total energy for aquatic photosynthesis. *Limnol. Oceanogr.*, **19**, 591–600. [5](#), [365](#)
958. Morita, E., Abe, T., Tsuzuki, M. *et al.* (1999). Role of pyrenoids in the CO<sub>2</sub>-concentrating mechanism: comparative morphology, physiology and molecular phylogenetic analysis of closely related strains of *Chlamydomonas* and *Chloromonas* (Volvocales). *Planta*, **208**, 365–72. [306](#)

959. Morris, I. & Farrell, K. (1971). Photosynthetic rates, gross patterns of carbon dioxide assimilation and activities of ribulose diphosphate carboxylase in marine algae grown at different temperatures. *Physiol. Plant*, **25**, 372–7. 418
960. Morrison, J. R. & Nelson, N. B. (2004). Seasonal cycle of phytoplankton UV absorption at the Bermuda Atlantic Time-series Study (BATS) site. *Limnol. Oceanogr.*, **49**, 215–24. 90
961. Morrison, R. (2003). In situ determination of the quantum yield of phytoplankton chlorophyll *a* fluorescence: a simple algorithm, observations, and a model. *Limnol. Oceanogr.*, **48**, 618–31. 247
962. Morrow, J. H., Chamberlin, W. S. & Kiefer, D. A. (1989). A two-component description of spectral absorption by marine particles. *Limnol. Oceanogr.*, **34**, 1500–9. 84, 86
963. Moss, B., McGowan, S. & Carvalho, L. (1994). Determination of phytoplankton crops by top-down and bottom-up mechanisms in a group of English lakes, the West Midland meres. *Limnol. Oceanogr.*, **39**, 1020–9. 426
964. Mueller, J. L. (2000). SeaWiFS algorithm for the diffuse attenuation coefficient, *K*(490), using water-leaving radiances at 490 and 555 nm. In O'Reilly, J. E. and co-authors: SeaWiFS Postlaunch Calibration and Validation Analyses, Part 3. S. B. Hooker & E. R. Firestone (eds), NASA/TM-2000-206892, **11**, NASA Goddard Space Flight Center, Greenbelt, Maryland, 24–7. 255–6
965. Munday, J. C. & Alfoldi, T. T. (1979). Landsat test of diffuse reflectance models for aquatic suspended solids measurement. *Remote Sens. Env.*, **8**, 169–83. 231
966. Muñoz, J. & Merrett, M. J. (1988). Inorganic carbon uptake by a small-celled strain of *Stichococcus bacillaris*. *Planta*, **175**, 460–4. 403, 406
967. Murakami, A., Miyashita, H., Iseki, M., Adachi, K. & Mimuro, M. (2004). Chlorophyll *d* in an epiphytic cyanobacterium of red algae. *Science*, **303**, 1633. 278
968. Muscatine, L. (1990). The role of symbiotic algae in carbon and energy flux in reef corals. In Z. Dubinsky (ed.), *Coral Reefs* (pp. 75–87). Amsterdam: Elsevier. 533
969. Musser, J. A., Fry, E. S. & Gray, D. J. (2009). Flow-through integrating cavity absorption meter: experimental results. *Appl. Opt.*, **48**, 3596–602. 60
970. Myers, J. & Graham, J.-R. (1963). Enhancement in *Chlorella*. *Plant Physiol.*, **38**, 105–9. 385
971. Myers, J. & Graham, J.-R. (1971). The photosynthetic unit in *Chlorella* measured by repetitive short flashes. *Plant Physiol.*, **48**, 282–6. 472
972. Myint, S. W. & Walker, N. D. (2002). Quantification of surface suspended sediments along a river dominated coast with NOAA AVHRR and SeaWiFS measurements: Louisiana, USA. *Int. J. Remote Sens.*, **23**, 3229–49. 233
973. Nakamura, K., Ogawa, T. & Shibata, K. (1976). Chlorophyll and peptide compositions in the two photosystems of marine green algae. *Biochim. Biophys. Acta*, **423**, 227–36. 279
974. Nakayama, N., Itagaki, T. & Okada, M. (1986). Pigment composition of chlorophyll-protein complexes isolated from the green alga *Bryopsis maxima*. *Plant Cell Physiol.*, **27**, 311–17. 290
975. NASA (1987). *HIRIS Instrument Panel Report*. 208

976. NASA (2000). *SeaWiFS Postlaunch Technical Report Series*. Vol. **11**, Part 3. 242
977. Neale, P. J. (1987). Algal photo inhibition and photosynthesis in the aquatic environment. In D. J. Kyle, C. B. Osmond & C. J. Arntzen (eds), *Photoinhibition* (pp. 39–65). Amsterdam: Elsevier. 360
978. Neale, P. J., Banaszak, A. T. & Jarriel, C. R. (1998). Ultraviolet sunscreens in *Gymnodinium sanguineum* (Dinophyceae): mycosporine-like amino acids protect against inhibition of photosynthesis. *J. Phycol.*, **34**, 928–38. 356
979. Neale, P. J. & Melis, A. (1986). Algal photosynthetic membrane complexes and the photosynthesis-irradiance curve: a comparison of light-adaptation responses in *Chlamydomonas reinhardtii* (Chlorophyta). *J. Phycol.*, **22**, 531–8. 472, 474–5, 476
980. Nelson, J. R. & Guarda, S. (1995). Particulate and dissolved spectral absorption on the continental shelf of the southeastern United States. *J. Geophys. Res.*, **100**, 8715–32. 70, 74
981. Nelson, J. R. & Wakeham, S. G. (1989). A phytol-substituted chlorophyll *c* from *Emiliania huxleyi* (Prymnesiophyceae). *J. Phycol.*, **25**, 761–6. 276
982. Nelson, N. B. & Prezelin, B. B. (1990). Chromatic light effects and physiological modelling of absorption properties of *Heterocapsa pygmaea* (= *Glenodinium* sp.). *Mar. Ecol. Prog. Ser.*, **63**, 37–46. 317
983. Nelson, N. B., Siegel, D. A., Carlson, C. A. *et al.* (2007). Hydrography of chromophoric dissolved organic matter in the North Atlantic. *Deep-Sea Res.*, **54**, 710–31. 70
984. Nelson, N. & Yocum, C. F. (2006). Structure and function of photosystems I and II. *Ann. Rev. Plant Biol.*, **57**, 521–65. 302
985. Neori, A., Holm-Hansen, O., Mitchell, B. G. & Kiefer, D. A. (1984). Photoadaptation in marine phytoplankton. *Plant Physiol.*, **76**, 518–24. 499–500
986. Neumüller, M., Cunningham, C. & McKee, D. (2002). Assessment of a microscopic photobleaching technique for measuring the spectral absorption efficiency of individual phytoplankton cells. *J. Plankton Res.*, **24**, 741–6. 87
987. Neuymin, G. G., Zemlyanya, L. A., Martynov, O. V. & Solov'yev, M. V. (1982). Estimation of the chlorophyll concentration from measurements of the colour index in different regions of the ocean. *Oceanology*, **22**, 280–3. 204
988. Neverauskas, V. P. (1988). Response of a *Posidonia* community to prolonged reduction in light. *Aquat. Bot.*, **31**, 361–6. 479
989. Neville, R. A. & Gower, J. F. R. (1977). Passive remote sensing of phytoplankton via chlorophyll *a* fluorescence. *J. Geophys. Res.*, **82**, 3487–93. 206, 247
990. Ní Longphuirt, S., Clavier, J., Grall, J. *et al.* (2007). Primary production and spatial distribution of subtidal microphytobenthos in a temperate coastal system, the Bay of Brest, France. *Estuar. Coast. Shelf Sci.*, **74**, 367–80. 531
991. Nielsen, H. D., Nielsen, S. L. & Madsen, T. V. (2006). CO<sub>2</sub> uptake patterns depend on water current velocity and shoot morphology in submerged stream macrophytes. *Freshwater Biol.*, **51**, 1331–40. 412
992. Nimer, N. A., Iglesias-Rodriguez, M. D. & Merrett, M. J. (1997). Bicarbonate utilization by marine phytoplankton species. *J. Phycol.*, **33**, 625–31. 407
993. Ninčević, Ž., Marasović, I. & Kušpilić, G. (2002). Deep chlorophyll-*a* maximum at one station in the middle Adriatic Sea. *J. Mar. Biol. Ass. U.K.*, **82**, 9–19. 396

994. Nobel, P. S. (2005). *Physicochemical and Environmental Plant Physiology*. New York: Academic Press. 281, 302
995. Nolen, S. L., Wilhm, J. & Howick, G. (1985). Factors influencing inorganic turbidity in a Great Plains reservoir. *Hydrobiologia*, **123**, 109–17. 121
996. Norlin, J. I., Bayley, S. E. & Ross, L. C. M. (2005). Submerged macrophytes, zooplankton and the predominance of low- over high-chlorophyll states in western boreal, shallow-water wetlands. *Freshwater Biol.*, **50**, 868–81. 426
997. Norton, T. A. (1968). Underwater observations on the vertical distribution of algae at St. Mary's, Isles of Scilly. *Br. Phycol. Bull.*, **3**, 585–8. 457
998. Norton, T. A., Hiscock, K. & Kitching, J. A. (1977). The ecology of Lough Ine. XX. The Laminaria forest at Carrigathorna. *J. Ecol.*, **65**, 919–41. 456, 458
999. Norton, T. A., McAllister, H. A., Conway, E. & Irvine, L. M. (1969). The marine algae of the Hebridean island of Colonsay. *Br. Phycol. J.*, **4**, 125–36. 457
1000. Novo, E. M. M., Hanson, J. D. & Curran, P. J. (1989). The effect of sediment type on the relationship between reflectance and suspended sediment concentration. *Int. J. Remote Sens.* **10**, 1283–9. 232
1001. Nultsch, W. & Pfau, J. (1979). Occurrence and biological role of light-induced chromatophore displacements in seaweeds. *Mar. Biol.*, **51**, 77–82. 520–1
1002. O'Carra, C. & O'h Eocha, C. (1976). Algal biliproteins and phycobilins. In T. W. Goodwin (ed.), *Chemistry and Biochemistry of Plant Pigments* (pp. 328–76). London: Academic Press. 293, 296
1003. Oduor, S. O. & Schagerl, M. (2007). Phytoplankton primary productivity characteristics in response to photosynthetically active radiation in three Kenyan Rift Valley saline-alkaline lakes. *J. Plankton Res.*, **29**, 1041–50. 165, 344
1004. Oelmüller, R., Coxley, P. B., Federspiel, N., Briggs, W. R. & Grossman, A. R. (1988). Changes in accumulation and synthesis of transcripts encoding phycobilisome components during acclimation of *Fremyella diplosiphon* to different light qualities. *Plant Physiol.*, **88**, 1077–83. 482
1005. Oertel, G. F. & Dunstan, W. M. (1981). Suspended-sediment distribution and certain aspects of phytoplankton production off Georgia, U.S.A. *Mar. Geol.*, **40**, 171–97. 164, 399
1006. Ogura, N. & Hanya, T. (1966). Nature of ultraviolet absorption of sea water. *Nature*, **212**, 758. 64
1007. O'h Eocha, C. (1965). Phycobilins. In T. W. Goodwin (ed.), *Chemistry and Biochemistry of Plant Pigments* (pp. 175–96). London: Academic Press. 294
1008. O'h Eocha, C. (1966). Biliproteins. In T. W. Goodwin (ed.), *Biochemistry of Chloroplasts* (pp. 407–21). London: Academic Press. 296
1009. Ohki, K. & Fujita, Y. (1992). Photoregulation of phycobilisome structure during complementary chromatic adaptation in the marine cyanophyte *Phormidium* sp. C86. *J. Phycol.*, **28**, 803–8. 481
1010. Ohki, K., Gantt, E., Lipschultz, C. A. & Ernst, M. C. (1985). Constant phycobilisome size in chromatically adapted cells of the cyanobacterium *Tolypothrix tenuis*, and variation in *Nostoc* sp. *Plant Physiol.*, **79**, 943–8. 481
1011. Oishi, T. (1990). Significant relationship between the backward scattering coefficient of sea water and the scatterance at 120°. *Appl. Opt.*, **29**, 4658–65. 64, 110

1012. O'Kelly, C. J. (1982). Chloroplast pigments in selected marine Chaetophoraceae and Chaetosiphonaceae (Chlorophyta): the occurrence and significance of siphonaxanthin. *Bot. Mar.*, **25**, 133–7. [284](#), [461](#)
1013. Okullo, W., Ssenyonga, T. and Hamre, B. (2007). Parameterization of the inherent optical properties of Murchison Bay, Lake Victoria. *Appl. Opt.*, **46**, 8553–61. [77](#)
1014. Oliver, R. L. (1990). Optical properties of waters in the Murray-Darling basin, South-eastern Australia. *Aust. J. Mar. Freshwater Res.*, **41**, 581–601. [78](#), [113–14](#), [119](#), [128](#), [166](#)
1015. Oliver, R. L. (1994). Floating and sinking in gas-vacuolate cyanobacteria. *J. Phycol.*, **30**, 161–73. [517](#)
1016. Oltmanns, F. (1892). Über die Kultur und Lebensbedingungen der Meer-salgen. *Jb. Wiss. Bot.*, **23**, 349–440. [454](#)
1017. Ondrusek, M. E., Bidigare, R. R., Sweet, S. T., Defreitas, D. A. & Brooks, J. M. (1991). Distribution of phytoplankton pigments in the North Pacific Ocean in relation to physical and optical variability. *Deep-Sea Res.*, **38**, 243–66. [462](#)
1018. Ong, L. J., Glazer, A. N. & Waterbury, J. B. (1984). An unusual phycoerythrin from a marine cyanobacterium. *Science*, **224**, 80–3. [296](#)
1019. Onuf, C. P. (1994). Seagrasses, dredging and light in Laguna Madre, Texas, U.S.A. *Estuar. Coast. Shelf Sci.*, **39**, 75–91. [391](#)
1020. O'Reilly, J. E., Maritorena, S., Mitchell, B. G. *et al.* (1998). Ocean color chlorophyll algorithms for SeaWiFS. *J. Geophys. Res.*, **103**, 24937–53. [241–2](#)
1021. Ort, D. (2001). When there is too much light. *Plant Physiol.*, **125**, 29–32. [357](#)
1022. Ortner, P. B., Wiebe, P. H. & Cox, J. L. (1980). Relationships between oceanic epizooplankton distribution and the seasonal deep chlorophyll maximum in the northwestern Atlantic Ocean. *J. Mar. Res.*, **3**, 507–31. [396](#), [504](#)
1023. Osburn, C. L., O'Sullivan, D. W. & Boyd, T. J. (2009). Increases in the longwave photobleaching of chromophoric dissolved organic matter in coastal waters. *Limnol. Oceanogr.*, **54**, 145–59. [81](#)
1024. Osburn, C. L., Zagarese, H. E., Morris, D. P., Hargreaves, B. R. & Cravero, W. E. (2001). Calculation of spectral weighting functions for the solar photobleaching of chromophoric dissolved organic matter in temperate lakes. *Limnol. Oceanogr.*, **46**, 1455–67. [81](#)
1025. Oubelkheir, K., Clementson, L. A., Webster, I. T. *et al.* (2006). Using inherent optical properties to investigate biogeochemical dynamics in a tropical macrotidal coastal system. *J. Geophys. Res.*, **111**, C07021. [76](#), [117](#)
1026. Oviatt, C., Keller, A. & Reed, L. (2002). Annual primary production in Narragansett Bay with no Bay-wide winter–spring phytoplankton bloom. *Estuar. Coast. Shelf Sci.*, **54**, 1013–26. [450](#)
1027. Owens, N. J. P., Galloway, J. N. & Duce, R. A. (1992). Episodic atmospheric nitrogen deposition to oligotrophic oceans. *Nature*, **357**, 397–9. [421](#)
1028. Paasche, E. (1964). A tracer study of the inorganic carbon uptake during coccolith formation and photosynthesis in the coccolithophorid *Coccolithus huxleyi*. *Physiol. Plant.*, **3** (suppl.), 1–82. [406](#)
1029. Pabi, S., Van Dijken, G. L. & Arrigo, K. R. (2008). Primary production in the Arctic Ocean, 1998–2006. *J. Geophys. Res.*, **113**, C08005. [452](#)

1030. Paerl, H. W., Tucker, J. & Bland, P. T. (1983). Carotenoid enhancement and its role in maintaining blue-green algal (*Microcystis aeruginosa*) surface blooms. *Limnol. Oceanogr.*, **28**, 847–57. [471](#)
1031. Paerl, H. W. & Ustach, J. F. (1982). Blue-green algal scums: an explanation for their occurrence during freshwater blooms. *Limnol. Oceanogr.*, **27**, 212–17. [518](#)
1032. Palmer, K. F. & Williams, D. (1974). Optical properties of water in the near infrared. *J. Opt. Soc. Amer.*, **64**, 1107–10. [63](#)
1033. Palmisano, A. C., SooHoo, J. B. & Sullivan, C. W. (1985). Photosynthesis-irradiance relationships in sea ice microalgae from McMurdo Sound, Antarctica. *J. Phycol.*, **21**, 341–6. [347](#), [509](#)
1034. Parson, W. W. (1991). Reaction centres. In H. Scheer (ed.), *Chlorophylls* (pp. 1153–80). Boca Raton: CRC Press. [302](#)
1035. Patel, B. N. & Merrett, M. J. (1986). Inorganic carbon uptake by the marine diatom *Phaeodactylum tricornutum*. *Planta*, **169**, 222–7.
1036. Paterson, D. M., Wiltshire, K. H., Miles, A. *et al.* (1998). Microbiological mediation of spectral reflectance from intertidal cohesive sediments. *Limnol. Oceanogr.*, **43**, 1207–21. [530](#)
1037. Pearse, J. F. & Hines, A. H. (1979). Expansion of a Central California kelp forest following the mass mortality of sea urchins. *Mar. Biol.*, **51**, 83–91. [429](#)
1038. Pegau, W. S. & Zaneveld, J. R. V. (1993). Temperature-dependent absorption of water in the red and near-infrared portions of the spectrum. *Limnol. Oceanogr.*, **38**, 188–92. [63](#)
1039. Pelaez, J. & McGowan, J. A. (1986). Phytoplankton pigment patterns in the California Current as determined by satellite. *Limnol. Oceanogr.*, **31**, 927–50.
1040. Pelevin, V. N. (1978). Estimation of the concentration of suspension and chlorophyll in the sea from the spectrum of outgoing radiation measured from a helicopter. *Oceanology*, **18**, 278–82.
1041. Pelevin, V. N. & Rutkovskaya, V. A. (1977). On the optical classification of ocean waters from the spectral attenuation of solar radiation. *Oceanology*, **17**, 28–32. [92–3](#)
1042. Pennock, J. R. (1985). Chlorophyll distribution in the Delaware estuary: regulation by light limitation. *Estuar. Coast. Shelf Sci.*, **21**, 711–25. [394](#), [398](#)
1043. Pérez, V., Fernández, E., Marañón, E., Morán, X. A. G. & Zubkov, M. V. (2006). Vertical distribution of phytoplankton biomass, production and growth in the Atlantic subtropical gyres. *Deep-Sea Res.*, **53**, 1616–34. [395](#), [396](#)
1044. Pérez, V., Fernández, E., Marañón, E., Serret, P. & García-Soto, C. (2005). Seasonal and inter-annual variability of chlorophyll *a* and primary production in the Equatorial Atlantic: in situ and remote sensing observations. *J. Plankton Res.*, **27**, 189–97. [433](#)
1045. Perez-Bermudez, P., Garcia-Carrascosa, M., Cornejo, M. J. & Segura, J. (1981). Water-depth effects in photosynthetic pigment content of the benthic algae *Dictyota dichotoma* and *Udotea petiolata*. *Aquat. Bot.*, **11**, 373–7. [491](#), [492](#), [508](#)
1046. Pergent, G., Rico-Raimondino, V. & Pergent-Martini, C. (1997). Fate of primary production in *Posidonia* oceanic meadows of the Mediterranean. *Aquat. Bot.*, **59**, 307–21. [533](#)

1047. Perkins, E. J. (1960). The diurnal rhythm of the littoral diatoms of the river Eden estuary. *Fife. J. Ecol.*, **48**, 725–8. 529
1048. Perry, M. J. & Porter, S. M. (1989). Determination of the cross-section absorption coefficient of individual phytoplankton cells by analytical flow cytometry. *Limnol. Oceanogr.*, **34**, 1727–38. 131
- 1048a. Perry, M. J., Sackmann, B. S., Eriksen, C. C. & Lee, C. M. (2008). Seaglider observations of blooms and subsurface chlorophyll maxima off the Washington coast. *Limnol. Oceanogr.*, **53**, 2169–79. 141
1049. Perry, M. J., Talbot, M. C. & Alberte, R. S. (1981). Photoadaptation in marine phytoplankton: response of the photosynthetic unit. *Mar. Biol.* **62**, 91–101. 473, 477
1050. Peterson, D. H., Perry, M. J., Bencala, K. E. & Talbot, M. C. (1987). Phytoplankton productivity in relation to light intensity: a simple equation. *Estuar. Coast. Shelf Sci.*, **24**, 813–32. 351–2
1051. Petzold, T. J. (1972). *Volume Scattering Functions for Selected Ocean Waters* (pp. 72–8). Scripps Inst. Oceanogr. 107–8, 113, 117, 118, 121–3, 126
1052. Pfannkuche, J. (2002). Optical properties of Otago Shelf waters: South Island New Zealand. *Estuar. Coast. Shelf Sci.*, **55**, 613–27. 97
1053. Phillips, D. M. & Kirk, J. T. O. (1984). Study of the spectral variation of absorption and scattering in some Australian coastal waters. *Aust. J. Mar. Freshwater Res.*, **35**, 635–44. 106, 118, 125
1054. Phillips, G. L., Eminson, D. & Moss, B. (1978). A mechanism to account for macrophyte decline in progressively eutrophicated freshwaters. *Aquat. Bot.*, **4**, 103–26. 427
1055. Phinn, S., Roelfsema, C., Dekker, A., Brando, V. & Anstee, J. (2008). Mapping seagrass species, cover and biomass in shallow waters: an assessment of satellite multi-spectral and airborne hyper-spectral imaging systems in Moreton Bay (Australia). *Remote Sens. Environ.*, **112**, 3413–25. 259
1056. Phlips, E. J., Cichra, M., Aldridge, F. J. *et al.* (2000). Light availability and variations in phytoplankton standing crops in a nutrient-rich blackwater river. *Limnol. Oceanogr.*, **45**, 916–29. 398
1057. Pick, F. R. (1991). The abundance and composition of freshwater picocyanobacteria in relation to light penetration. *Limnol. Oceanogr.*, **36**, 1457–62. 463
1058. Pierson, D. C., Kratzer, S., Strömbeck, N. & Håkansson, B. (2008). Relationship between the attenuation of downwelling irradiance at 490 nm with the attenuation of PAR (400 nm–700 nm) in the Baltic Sea. *Remote Sens. Environ.*, **112**, 668–80. 257
1059. Plass, G. N. & Kattawar, G. W. (1972). Monte Carlo calculations of radiative transfer in the Earth's atmosphere–ocean system. 1. Flux in the atmosphere and ocean. *J. Phys. Oceanogr.*, **2**, 139–45. 150
1060. Platt, T. (1969). The concept of energy efficiency in primary production. *Limnol. Oceanogr.*, **14**, 653–9. 379
1061. Platt, T. (1986). Primary production of the ocean water column as a function of surface light intensity: algorithm for remote sensing. *Deep-Sea Res.*, **33**, 149–63. 377, 443
1062. Platt, T., Gallegos, C. L. & Harrison, W. G. (1980). The relationship between photosynthesis and light for natural assemblages of coastal marine phytoplankton. *J. Mar. Res.*, **38**, 687–701. 352

1063. Platt, T. & Jassby, A. D. (1976). The relationship between photosynthesis and light for natural assemblages of coastal marine phytoplankton. *J. Phycol.*, **12**, 421–30. 346, 374, 419, 510–11, 514
1064. Platt, T. & Li, W. K. W. (eds) (1986). Photosynthetic picoplankton. *Can. Bull. Fish. Aquat. Sci.*, **214**. 388
1065. Platt, T. & Sathyendranath, S. (1993). Estimators of primary production for interpretation of remotely sensed data on ocean color. *J. Geophys. Res.*, **98**, 14561–76. 444
1066. Platt, T., Sathyendranath, S., Caverhill, C. M. & Lewis, M. R. (1988). Ocean primary production and available light: further algorithms for remote sensing. *Deep-Sea Res.*, **35**, 855–79. 444
1067. Platt, T., Sathyendranath, S., Forget, M.-H. *et al.* (2008). Operational estimation of primary production at large geographical scales. *Remote Sens. Environ.*, **112**, 3437–48. 446
1068. Platt, T., Sathyendranath, S. & Ravindran, P. (1990). Primary production by phytoplankton: analytic solutions for daily rates per unit area of water surface. *Proc. R. Soc. Lond. B*, **241**, 101–11. 443, 446
1069. Platt, T., Sathyendranath, S., Ulloa, O. *et al.* (1992). Nutrient control of phytoplankton photosynthesis in the western North Atlantic. *Nature*, **356**, 229–31. 443
1070. Platt, T. & Subba Rao, D. V. (1975). Primary production of marine microphytes. In J. P. Cooper (ed.), *Photosynthesis and Productivity in Different Environments* (pp. 249–80). Cambridge: Cambridge University Press. 450
1071. Poole, H. H. (1945). The angular distribution of submarine daylight in deep water. *Sci. Proc. R. Dublin Soc.*, **24**, 29–42. 182
1072. Poole, H. H. & Atkins, W. R. G. (1929). Photoelectric measurements of submarine illumination throughout the year. *J. Mar. Biol. Ass. U.K.*, **16**, 297–324. 142
1073. Pope, R. M. & Fry, E. S. (1997). Absorption spectrum (380–700 nm) of pure water. II. Integrating cavity measurements. *Appl. Opt.*, **36**, 8710–23. 62, 64
1074. Preisendorfer, R. W. (1957). Exact reflectance under a cardioidal luminance distribution. *Q. J. Roy. Meteorol. Soc.*, **83**, 540. Quoted by Jerlov (1976). 48
1075. Preisendorfer, R. W. (1959). Theoretical proof of the existence of characteristic diffuse light in natural waters. *J. Mar. Res.*, **18**, 1–9. 182
1076. Preisendorfer, R. W. (1961). Application of radiative transfer theory to light measurements in the sea. *Union Geod. Geophys. Inst. Monogr.*, **10**, 11–30. 11, 14, 22–3, 113, 118, 180, 182, 194
1077. Preisendorfer, R. W. (1976). *Hydrologic Optics*. Washington: US Department of Commerce. 4
1078. Preisendorfer, R. W. (1986a). *Eyeball Optics of Natural Waters: Secchi Disk Science* (Tech. Memo. ERL PMEL-67). NOAA. 143
1079. Preisendorfer, R. W. (1986b). Secchi disk science: visual optics of natural waters. *Limnol. Oceanogr.*, **31**, 909–26. 143
1080. Prezelin, B. B. (1976). The role of peridinin-chlorophyll *a* proteins in the photosynthetic light adaptation of the marine dinoflagellate, *Glenodinium* sp. *Planta*, **130**, 225–33. 470, 473, 476
1081. Prezelin, B. B. (1992). Diel periodicity in phytoplankton productivity. *Hydrobiologia*, **238**, 1–35. 524

1082. Prezelin, B. B., Bidigare, R. R., Matlick, H. A., Putt, M. & Hoven, B. V. (1987). Diurnal patterns of size-fractioned primary productivity across a coastal front. *Mar. Biol.*, **96**, 563–74. 375
1083. Prezelin, B. B., Ley, A. C. & Haxo, F. T. (1976). Effects of growth irradiance on the photosynthetic action spectra of the marine dinoflagellate, *Glenodinium* sp. *Planta*, **130**, 251–6. 505
1084. Prezelin, B. B., Meeson, B. W. & Sweeney, B. M. (1977). Characterization of photosynthetic rhythms in marine dinoflagellates. I. Pigmentation, photosynthetic capacity and respiration. *Plant Physiol.*, **60**, 384–7. 584–5
1085. Prezelin, B. B., Putt, M. & Glover, H. E. (1986). Diurnal patterns in photosynthetic capacity and depth-dependent photosynthesis irradiance relationships in *Synechococcus* spp. and larger phytoplankton in three water masses in the Northwest Atlantic Ocean. *Mar. Biol.*, **91**, 205–17. 524
1086. Prezelin, B. B. & Sweeney, B. M. (1977). Characterization of photosynthetic rhythms in marine dinoflagellates. II. Photosynthesis-irradiance curves and in vivo chlorophyll fluorescence. *Plant Physiol.*, **60**, 388–92. 584–5
1087. Prezelin, B. B., Tilzer, M. M., Schofield, O. & Haese, C. (1991). The control of the production process of phytoplankton by the physical structure of the aquatic environment with special reference to its optical properties. *Aquatic Sciences*, **53**, 136–86. 375, 376
1088. Price, G. D. & Badger, M. R. (1985). Inhibition by proton buffers of photosynthetic utilization of bicarbonate in *Chara corallina*. *Aust. J. Plant Physiol.*, **12**, 257–67. 405, 406
1089. Price, G. D., Maeda, S., Omata, T. & Badger, M. R. (2002). Modes of inorganic carbon uptake in the cyanobacterium, *Synechococcus* sp. PCC 7942. *Funct. Plant Biol.*, **29**, 131–49. 407
1090. Prieto, L., Vaillancourt, R. D., Hales, B. & Marra, J. (2008). On the relationship between carbon fixation efficiency and bio-optical characteristics of phytoplankton. *J. Plankton Res.*, **30**, 43–56. 358
1091. Prieur, L. (1976). *Transfer radiatif dans les eaux de mer*. D.Sc., Univ. Pierre et Marie Curie, Paris. 170
1092. Prieur, L. & Morel, A. (1971). Etude theorique du regime asymptotique: relations entre caracteristiques optiques et coefficient d'extinction relative à la penetration de la lumiere du jour. *Cah. Oceanogr.*, **23**, 35–47. 182
- 1092a. Prins, H. B. A. & Elzenga, J. T. M. (1989). Bicarbonate utilization: function and mechanism. *Aquat. Bot.*, **34**, 59–83. 406
1093. Proctor, L. M. & Fuhrman, J. A. (1990). Viral mortality of marine bacteria and cyanobacteria. *Nature*, **343**, 60–2. 427
1094. PRR-800 Profiling Reflectance Radiometer (2009). Biospherical Instruments Inc. San Diego, California. 146
1095. PUV-2500 Ultraviolet Radiometer (2009). Biospherical Instruments Inc. San Diego, California. 147
1096. Quickenden, T. I. & Irvin, J. A. (1980). The ultraviolet absorption spectrum of liquid water. *J. Chem. Phys.*, **72**, 4416–28. 62, 64
1097. Rabinowitch, E. I. (1945). *Photosynthesis, Vol. I*. New York: Interscience. 454
1098. Rabinowitch, E. I. (1951). *Photosynthesis, Vol. II*. New York: Interscience. 404

1099. Radmer, R. & Kok, B. (1977). Photosynthesis: limited yields, unlimited dreams. *BioScience*, **27**, 599–605. 366
1100. Ralph, P. J. & Gademann, R. (2005). Rapid light curves: a powerful tool to assess photosynthetic activity. *Aquat. Bot.*, **82**, 222–37. 351
1101. Ramus, J., Beale, S. I. & Mauzerall, D. (1976). Correlation of changes in pigment content with photosynthetic capacity of seaweeds as a function of depth. *Mar. Biol.*, **37**, 231–8. 343, 348, 350, 466–7, 490
1102. Ramus, J., Beale, S. I., Mauzerall, D. & Howard, K. L. (1977). Changes in photosynthetic pigment concentration in seaweeds as a function of depth. *Mar. Biol.*, **37**, 223–9. 490
1103. Ramus, J., Lemons, F. & Zimmerman, C. (1977). Adaptation of light-harvesting pigments to downwelling light and the consequent photosynthetic performance of the eulittoral rockweeds *Ascophyllum nodosum* and *Fucus vesiculosus*. *Mar. Biol.*, **42**, 293–303. 491
1104. Ramus, J. & Rosenberg, G. (1980). Diurnal photosynthetic performance of seaweeds measured under natural conditions. *Mar. Biol.*, **56**, 21–8. 527
1105. Randolph, K., Wilson, J., Tedesco, L. *et al.* (2008). Hyperspectral remote sensing of cyanobacteria in turbid productive waters using optically active pigments, chlorophyll *a* and phycocyanin. *Remote Sens. Environ.*, **112**, 4009–19. 246
1106. Raps, S., Kycia, J. H., Ledbetter, M. C. & Siegelman, H. W. (1985). Light intensity adaptation and phycobilisome composition of *Microcystis aeruginosa*. *Plant Physiol.*, **79**, 983–7. 474
1107. Raps, S., Wyman, K., Siegelman, H. W. & Falkowski, P. G. (1983). Adaptation of the cyanobacterium *Microcystis aeruginosa* to light intensity. *Plant Physiol.*, **72**, 829–32. 474, 477
1108. Rattray, M. R., Howard-Williams, C. & Brown, J. M. A. (1991). The photosynthetic and growth rate responses of two freshwater angiosperms in lakes of different trophic status: responses to light and dissolved inorganic carbon. *Freshwater Biol.*, **25**, 399–407. 410
1109. Raven, J. A. (1970). Endogenous inorganic carbon sources in plant photosynthesis. *Biol. Rev.*, **45**, 167–221. 408, 412
1110. Raven, J. A. (1997). Phagotrophy in phototrophs. *Limnol. Oceanogr.*, **42**, 198–205. 429
1111. Raven, J. A., Osborne, B. A. & Johnston, A. M. (1985). Uptake of CO<sub>2</sub> by aquatic vegetation. *Plant Cell Environ.*, **8**, 417–25. 306, 410, 414
1112. Raven, J. A., Walker, D. I., Jensen, K. R. *et al.* (2001). What fraction of the organic carbon in sacoglossans is obtained from photosynthesis by kleptoplastids? An investigation using the natural abundance of stable carbon isotopes. *Mar. Biol.*, **138**, 537–45. 430
1113. Ravisankar, M., Reghunath, A. T., Sathindanan, K. & Nampoori, V. P. N. (1988). Effect of dissolved NaCl, MgCl<sub>2</sub> and Na<sub>2</sub>SO<sub>4</sub> in seawater on the optical attenuation in the region from 430 to 630 nm. *Appl. Opt.*, **27**, 3387–94. 64, 75
1114. Ray, S., Klenell, M., Choo, K.-S., Pedersen, M. & Snoeijs, P. (2003). Carbon acquisition mechanisms in *Chara tomentosa*. *Aquat. Bot.*, **76**, 141–54. 406

1115. Raymont, J. E. (1980). *Plankton and Productivity in the Oceans, Vol. 1. Phytoplankton*, 2nd edn. Oxford: Pergamon. 266, 423–4, 430, 450, 511
1116. Reinfelder, J. R., Kraepiel, A. M. L. & Morel, F. M. M. (2000). Unicellular C<sub>4</sub> photosynthesis in a marine diatom. *Nature*, **407**, 996–9. 414
1117. Reinfelder, J. R., Milligan, A. J. & Morel, F. M. M. (2004). The role of the C<sub>4</sub> pathway in carbon accumulation and fixation in a marine diatom. *Plant Physiol.*, **135**, 2106–11. 414
1118. Reiskind, J. B., Seamon, P. T. & Bowes, G. (1988). Alternative methods of photosynthetic carbon assimilation in marine macroalgae. *Plant Physiol.*, **87**, 686–92. 414
1119. Revelante, N. & Gilmartin, M. (1995). The relative increase of larger phytoplankton in a subsurface chlorophyll maximum of the northern Adriatic Sea. *J. Plankton Res.*, **17**, 1535–62. 396
1120. Reynolds, C. S. (1984). *The Ecology of Freshwater Phytoplankton*. Cambridge: Cambridge University Press. 388, 423–4, 427, 434
1121. Reynolds, C. S. & Walsby, A. E. (1975). Water blooms. *Biol. Rev.*, **50**, 437–81. 517
1122. Rhee, C. & Briggs, W. R. (1977). Some responses of *Chondrus crispus* to light. 1. Pigmentation changes in the natural habitat. *Bot. Gaz.*, **138**, 123–8. 470, 492, 508, 510
1123. Rhiel, E., Lange, W. & Mörschel, E. (1993). The unusual light-harvesting complex of *Mantoniella squamata*: supramolecular composition and assembly. *Biochim. Biophys. Acta*, **1143**, 163–72. 288, 290
1124. Richardson, K., Beardall, J. & Raven, J. A. (1983). Adaptation of unicellular algae to irradiance: an analysis of strategies. *New Phytol.*, **93**, 157–91. 469
1125. Ricketts, T. R. (1966). Magnesium 2,4-divinylphaeoporphyrin a<sub>5</sub> mono-methyl ester, a protochlorophyll-like pigment present in some unicellular flagellates. *Phytochem.*, **5**, 223–9. 277
1126. Ridd, P. V. & Larcombe, P. (1994). Biofouling control for optical backscatter sediment sensors. *Mar. Geol.*, **116**, 255–8. 142
1127. Riebesell, U., Wolf-Gladrow, D. A. & Smetacek, V. (1993). Carbon dioxide limitation of marine phytoplankton growth rates. *Nature*, **361**, 249–51. 406, 411
1128. Ried, A., Hessenberg, B., Metzler, H. & Ziegler, R. (1977). Distribution of excitation energy amongst Photosystem I and Photosystem II in red algae. *Biochim. Biophys. Acta*, **459**, 175–86. 386
1129. Riegmann, F. & Colijn, F. (1991). Evaluation of measurements and calculation of primary production in the Dogger Bank area (North Sea) in summer 1988. *Mar. Ecol. Prog. Ser.*, **69**, 125–32. 163
1130. Riley, G. A. (1942). The relationship of vertical turbulence and spring diatom flowerings. *J. Mar. Res.*, **5**, 67–87. 431
1131. Rimmer, J. C., Collins, M. B. & Pattiaratchi, C. B. (1987). Mapping of water quality in coastal waters using Airborne Thematic Mapper data. *Int. J. Remote Sens.*, **8**, 85–102.
1132. Ritchie, J. C. & Cooper, C. M. (1988). Comparison of measured suspended sediment concentrations with suspended sediment concentrations estimated from Landsat MSS data. *Int. J. Remote Sens.*, **9**, 379–87. 231
1133. Ritchie, J. C. & Cooper, C. M. (1991). An algorithm for estimating surface suspended sediment concentrations with Landsat MSS digital data. *Water Res. Bull.*, **27**, 373–9. 231

1134. Ritchie, J. C., Cooper, C. M. & Schiebe, F. R. (1990). The relationship of MSS and TM digital data with suspended sediments, chlorophyll and temperature in Moon Lake, Mississippi. *Remote Sens. Environ.*, **33**, 137–48. [223](#), [232](#)
1135. Ritchie, J. C., Cooper, C. M. & Yongqing, J. (1987). Using Landsat multi-spectral scanner data to estimate suspended sediments in Moon Lake, Mississippi. *Remote Sens. Environ.*, **23**, 65–81. [223](#), [231](#)
1136. Ritchie, J. C., Schiebe, F. R. & McHenry, J. R. (1976). Remote sensing of suspended sediments in surface waters. *Photogramm. Eng. Rem. Sens.*, **42**, 1539–45. [228](#), [229](#)
1137. Rivkin, R. B. & Putt, M. (1987). Photosynthesis and cell division by Antarctic microalgae: comparison of benthic, planktonic and ice algae. *J. Phycol.*, **23**, 233–9. [509](#)
1138. Robarts, R. D. & Zohary, T. (1984). *Microcystis aeruginosa* and underwater light attenuation in a hypertrophic lake (Hartbeespoort Dam, South Africa). *J. Ecol.*, **72**, 1001–17. [317](#)
1139. Robinson, D. H., Arrigo, K. R., Iturriaga, R. & Sullivan, C. W. (1995a). Microalgal light-harvesting in extreme low-light environments in McMurdo Sound, Antarctica. *J. Phycol.*, **31**, 508–20. [347](#), [494–5](#), [501–2](#)
1140. Robinson, I. S., Weeks, A. R. & Booty, B. A. (1995b). A towed near-surface optical reflectance meter for measuring ocean colour in support of remote sensing. *Deep-Sea Res.*, **42**, 2093–111. [146](#)
1141. Robinson, N. (1966). *Solar Radiation*. Amsterdam: Elsevier. [31](#)
1142. Rochon, G. & Langham, E. J. (1974). Teledetection par satellite dans l'évaluation de la qualité de l'eau. *Verh. Int. Verein. Limnol.*, **19**, 189–96. [223](#)
1143. Rodhe, W. (1969). Crystallization of eutrophication concepts in Northern Europe. In *Eutrophication: Causes, Consequences, Correctives* (pp. 50–64). Washington: National Academy of Science. [452](#)
1144. Roemer, S. C. & Hoagland, K. D. (1979). Seasonal attenuation of quantum irradiance (400–700 nm) in three Nebraska reservoirs. *Hydrobiologia*, **63**, 81–92. [165](#)
1145. Roesler, C. S. (1998). Theoretical and experimental approaches to improve the accuracy of particulate absorption coefficients derived from the quantitative filter technique. *Limnol. Oceanogr.*, **43**, 1649–60. [58](#)
1146. Roesler, C. S., Perry, M. J. & Carder, K. L. (1989). Modelling *in situ* phytoplankton absorption from total absorption spectra in productive inland marine waters. *Limnol. Oceanogr.*, **34**, 1510–23. [84](#)
1147. Roesler, C. S. & Zaneveld, J. R. V. (1994). High resolution vertical profiles of spectral absorption, attenuation and scattering coefficients in highly stratified waters. *Ocean Optics XII. Proc. SPIE.*, **2258**, 309–19. [125](#)
1148. Romero, S. I., Piola, A. R., Charo, M. & Eiras Garcia, C. A. (2006). Chlorophyll-*a* variability off Patagonia based on SeaWiFS data. *J. Geophys. Res.*, **111**, C05021. [433](#)
1149. Rotatore, C. & Colman, B. (1992). Active uptake of CO<sub>2</sub> by the diatom *Navicula pelliculosa*. *J. Exp. Bot.*, **43**, 571–6.
1150. Röttgers, R., Schönfeld, W., Kipp, P.-R. & Doerfer, R. (2005). Practical test of a point-source integrating cavity absorption meter: the performance of different collector assemblies. *Appl. Opt.*, **44**, 5549–60. [57](#)

1151. Round, F. E. (1981). *The Ecology of Algae*. Cambridge: Cambridge University Press. 528
1152. Round, F. E. & Happey, C. M. (1965). Persistent vertical-migration rhythms in benthic microflora. IV. A diurnal rhythm of the epipellic diatom association in non-tidal flowing water. *Br. Phycol. Bull.*, **2**, 465–71. 529
1153. Round, F. E. & Palmer, J. D. (1966). Persistent vertical-migration rhythms in benthic microflora. II. Field and laboratory studies on diatoms from the banks of the River Avon. *J. Mar. Biol. Ass. U.K.*, **46**, 191–214. 529
1154. Rouse, L. J. & Coleman, J. M. (1976). Circulation observations in the Louisiana Bight using Landsat imagery. *Remote Sens. Env.*, **5**, 55–66.
1155. Rowan, K. S. (1989). *Photosynthetic Pigments of Algae*. Cambridge: Cambridge University Press. 275, 284, 286, 293
1156. Ruiz-Verdu, A., Simis, S. G. H., De Hoyos, C., Gons, H. J. & Peña-Martinez, R. (2008). An evaluation of algorithms for the remote sensing of cyanobacterial biomass. *Remote Sens. Environ.*, **112**, 3996–4008. 246
1157. Ryther, J. H. (1956). Photosynthesis in the ocean as a function of light intensity. *Limnol. Oceanogr.*, **1**, 61–70. 430, 440, 441–3
1158. Ryther, J. H. (1969). Photosynthesis and fish production in the sea. *Science*, **166**, 72–6. 424
1159. Ryther, J. H. & Menzel, D. (1959). Light adaptation by marine phytoplankton. *Limnol. Oceanogr.*, **4**, 492–7. 339–40, 498–9
1160. Ryther, J. H. & Yentsch, C. S. (1957). The estimation of phytoplankton production in the ocean from chlorophyll and light data. *Limnol. Oceanogr.*, **2**, 281–6. 442
1161. Sagawa, T., Mikami, A., Komatsu, T. *et al.* (2008). Mapping seagrass beds using IKONOS satellite image and side scan sonar measurements: a Japanese case study. *Int. J. Remote Sens.*, **29**, 281–91. 259
1162. Sagert, S., Forster, R. M., Feuerpfeil, P. & Schubert, H. (1997). Daily course of photosynthesis and photoinhibition in *Chondrus crispus* (Rhodophyta) from different shore levels. *Eur. J. Phycol.*, **32**, 363–71. 353
1163. Sakamoto, M. (1966). Primary production by phytoplankton community in some Japanese lakes and its dependence on lake depth. *Arch. Hydrobiol.*, **62**, 1–28. 389
1164. Sakshaug, E. & Holm-Hansen, O. (1984). Factors governing pelagic production in polar seas. In O. Holm-Hansen, L. Bolis & R. Gilles (eds). *Marine Phytoplankton and Productivity* (pp. 1–18). New York: Springer. 450
1165. Salonen, K., Jones, R. I. & Arvola, L. (1984). Hypolimnetic phosphorus retrieval by diel vertical migrations of lake phytoplankton. *Freshwater Biol.*, **14**, 431–8. 516
1166. Salvucci, M. E. & Bowes, G. (1982). Photosynthetic and photo respiratory responses of the aerial and submerged leaves of *Miriophyllum brasiliense*. *Aquat. Bot.*, **13**, 147–64. 345
1167. Salvucci, M. E. & Bowes, G. (1983). Two photosynthetic mechanisms mediating the low photorespiratory state in submersed aquatic angiosperms. *Plant Physiol.*, **73**, 488–96. 413
1168. Samuelsson, G. & Öquist, G. (1977). A method for studying photosynthetic capacities of unicellular algae based on in vivo chlorophyll fluorescence. *Physiol. Plant.*, **40**, 315–19. 332

1169. San Pietro, A. (1971, 1972, 1980). *Methods in Enzymology*. New York: Academic Press. 330
1170. Sand-Jensen, K. & Madsen, T. V. (1991). Minimum light requirements of submerged freshwater macrophytes in laboratory growth experiments. *J. Ecol.*, **79**, 749–64. 390
1171. Sasaki, H., Miyamura, T., Saitoh, S. & Ishizaka, J. (2005). Seasonal variation of absorption by particles and colored dissolved organic matter (CDOM) in Funka Bay, southwestern Hokkaido, Japan. *Estuar. Coast. Shelf Sci.*, **64**, 447–58. 76, 86
1172. Sasaki, T., Watanabe, S., Oshiba, G., Okami, N. & Kajihara, M. (1962). On the instrument for measuring angular distribution of underwater radiance. *Bull. Jap. Soc. Sci. Fish.*, **28**, 489–96. 148
1173. Sathyendranath, S., Lazzara, L. & Prieur, L. (1987). Variations in the spectral values of specific absorption of phytoplankton. *Limnol. Oceanogr.*, **32**, 403–15. 317
1174. Sathyendranath, S., Platt, T., Horne, E. P. W. *et al.* (1991). Estimation of new production in the ocean by compound remote sensing. *Nature*, **353**, 129–33. 449
1175. Sathyendranath, S., Prieur, L. & Morel, A. (1989). A three-component model of ocean colour and its application to remote sensing of phytoplankton pigments in coastal waters. *Int. J. Remote Sens.*, **10**, 1373–94. 246
1176. Sauberer, F. (1945). Beiträge zur Kenntnis der optischen Eigenschaften der Karntner Seen. *Arch. Hydrobiol.*, **41**, 259–314. 70
1177. Sauberer, F. (1950). Die spektrale Strahlungsdurchlässigkeit des Eises. *Wetter Leben*, **2**, 193–7. 65
1178. Savidge, G. (1988). Influence of inter- and intra-daily light-field variability on photosynthesis by coastal phytoplankton. *Mar. Biol.*, **100**, 127–33. 514
1179. Scattering meter, ECO BB. Users Guide (2008). WET Labs Inc. Philomath, Oregon. 110
1180. Schalles, J. F. & Yacobi, Y. Z. (2000). Remote sensing and seasonal patterns of phycocyanin, carotenoid and chlorophyll pigments in eutrophic waters. *Archiv. Für Hydrobiologie: Advances in Limnology.*, **55**, 153–68. 246
1181. Schalles, J. F., Gitelson, A., Yacobi, Y. Z. & Kroenke, A. E. (1998). Estimation of chlorophyll *a* from time series measurements of high spectral resolution reflectance in an eutrophic lake. *J. Phycol.*, **34**, 383–90. 236
1182. Schanz, F. (1986). Depth distribution of phytoplankton and associated spectral changes in downward irradiance in Lake Zurich (1980/81). *Hydrobiologia*, **134**, 183–92. 165, 328
1183. Scheibe, J. (1972). Photoreversible pigment: occurrence in a blue-green alga. *Science*, **176**, 1037–9. 482
1184. Scherz, J. P., van Domelen, J. F., Holtje, K. & Johnson, W. (1974). Lake eutrophication as indicated by ERTS satellite imagery. In *Symposium on Remote Sensing and Photo Interpretation* (pp. 247–58). Canada: International Society for Photogrammetry. 223
1185. Schiebe, F. R., Harrington, J. A. & Ritchie, J. C. (1992). Remote sensing of suspended sediments: the Lake Chicot, Arkansas project. *Int. J. Remote Sens.*, **13**, 1487–509. 231

1186. Schmitt, A., Herold, A., Welte, C., Wild, A. & Wilhelm, C. (1993). The light-harvesting system of the unicellular alga *Mantoniella squamata* (Prasinophyceae): evidence for the lack of a photosystem I-specific antenna complex. *Photochem. Photobiol.*, **57**, 132–8. 288, 289
1187. Schmitz-Peiffer, A., Viehoff, T. & Grassl, H. (1990). Remote sensing of coastal waters by airborne lidar and satellite radiometer. Part 2: Measurements. *Int. J. Remote Sens.*, **11**, 2185–204. 255
1188. Schnitzer, M. (1978). Humic substances: chemistry and reactions. In M. Schnitzer & S. U. Khan (eds), *Soil Organic Matter* (pp. 1–64). Amsterdam: Elsevier. 65
1189. Schofield, O., Evens, T. J. & Millie, D. F. (1998). Photosystem II quantum yields and xanthophyll-cycle pigments of the macroalga *Sargassum natans* (Phaeophyceae): responses under natural sunlight. *J. Phycol.*, **34**, 104–12. 357
1190. Schofield, O., Prezelin, B. B., Smith, R. C. *et al.* (1991). Variability in spectral and non spectral measurements of photosynthetic light utilization efficiencies. *Mar. Ecol. Prog. Ser.*, **78**, 253–71. 368, 374
1191. Schreiber, U., Hormann, H., Neubauer, C. & Klughammer, C. (1995). Assessment of Photosystem II photochemical quantum yield by chlorophyll fluorescence quenching analysis. *Aust. J. Plant Physiol.*, **22**, 209–20. 332, 336
1192. Schreiber, U., Neubauer, C. & Schliwa, U. (1993). PAM fluorometer based on medium-frequency pulsed Xe flash measuring light: a highly sensitive new tool in basic and applied photosynthesis research. *Photosynthesis Res.*, **36**, 65–72. 336
1193. Schreiber, U., Schliwa, U. & Bilger, W. (1986). Continuous recording of photochemical and non-photochemical chlorophyll fluorescence quenching with a new type of modulation fluorometer. *Photosynthesis Res.*, **10**, 51–62. 336
1194. Schubert, H., Gerbersdorf, S., Titlyanov, T. *et al.* (2004). Circadian rhythm of photosynthesis in *Kappaphycus alvarezii* (Rhodophyta): independence of the cell cycle and possible photosynthetic clock targets. *Eur. J. Phycol.*, **39**, 423–30. 525–6
1195. Schulten, H.-R., Plage, B. & Schnitzer, M. (1991). A chemical structure for humic substances. *Naturwiss.*, **78**, 311–12. 65
1196. Schwarz, A.-M. & Hellblom, F. (2002). The photosynthetic light response of *Halophila stipulacea* growing along a depth gradient in the Gulf of Aqaba, the Red Sea. *Aquat. Bot.*, **74**, 263–72. 520
1197. Schwarz, A.-M., Hawes, I. & Howard-Williams, C. (1996). The role of photosynthesis/light relationships in determining lower depth limits of Characeae in South Island, New Zealand lakes. *Freshwater Biol.*, **35**, 69–80. 391
1198. Schwarz, J. N. (2005). Derivation of dissolved organic carbon concentrations from SeaWiFS data. *Int. J. Remote Sens.*, **26**, 283–93. 253
1199. Scott, B. D. (1978). Phytoplankton distribution and light attenuation in Port Hacking estuary. *Aust. J. Mar. Freshwater Res.*, **29**, 31–44. 164
1200. Scribner, E. A. (1985). Unpublished data (personal communication). 164, 166
1201. Scully, N. M. & Lean, D. R. S. (1994). The attenuation of ultraviolet radiation in temperate lakes. *Arch. Hydrobiol., Ergebn. Limnol.*, **43**, 135–44. 158
1202. Sears, J. R. & Cooper, R. A. (1978). Descriptive ecology of offshore, deep-water, benthic algae in the temperate western North Atlantic Ocean. *Mar. Biol.*, **44**, 309–14. 468

1203. Senger, H. & Fleischhacker, P. (1978). Adaptation of the photosynthetic apparatus of *Scenedesmus obliquus* to strong and weak light conditions. *Physiol. Plant.*, **43**, 35–42. 474, 476
1204. Sharon, Y. & Beer, S. (2008). Diurnal movement of chloroplasts in *Halophila stipulacea* and their effect on PAM fluorometric measurements of photosynthetic rates. *Aquat. Bot.*, **88**, 273–6. 520
1205. Sharples, J., Moore, C. M., Rippeth, T. M. *et al.* (2001). Phytoplankton distribution and survival in the thermocline. *Limnol. Oceanogr.*, **46**, 486–96. 397, 448, 504
1206. Shepherd, S. A. & Sprigg, R. C. (1976). Substrate sediments and subtidal ecology of Gulf St. Vincent and Investigator Strait. In C. R. Twidale, M. J. Tyler & B. P. Webb (eds), *Natural History of the Adelaide Region* (pp. 161–74). Adelaide: Royal Society of South Australia. 463–4, 469
1207. Shepherd, S. A. & Womersley, H. B. S. (1970). The sublittoral ecology of West Island, South Australia: environmental features and algal ecology. *Trans. R. Soc. South Aust.*, **94**, 105–38. 463–4
1208. Shepherd, S. A. & Womersley, H. B. S. (1971). Pearson Island Expedition 1969. 7. The subtidal ecology of benthic algae. *Trans. R. Soc. South Aust.*, **94**, 155–67. 463–4
1209. Shepherd, S. A. & Womersley, H. B. S. (1976). The subtidal algal and seagrass ecology of St. Francis Island, South Australia. *Trans. R. Soc. South Aust.*, **100**, 177–91. 463–4
1210. Sherman, K., Grasslein, M., Mountain, D. *et al.* (1988). The continental shelf ecosystem off the northeast coast of the United States. In H. Postma & J. J. Zijlstra (eds), *Continental Shelves* (pp. 279–337). Amsterdam: Elsevier. 450
1211. Shibata, K. (1959). Spectrophotometry of translucent biological materials – opal glass transmission method. *Meth. Biochem. Anal.*, **7**, 77–109. 56
1212. Shick, J. M. & Dunlap, W. C. (2002). Mycosporine-like amino acids and related gadusols: biosynthesis, accumulation, and UV-protective function in aquatic organisms. *Ann. Rev. Physiol.*, **64**, 223–62. 356
1213. Shimada, A., Maruyama, T. & Miyachi, S. (1996). Vertical distributions and photosynthetic action spectra of two oceanic picophytoplankters, *Prochlorococcus marinus* and *Synechococcus* sp. *Mar. Biol.*, **127**, 15–23. 462
1214. Shimura, S. & Fujita, Y. (1975). Changes in the activity of fucoxanthin-excited photosynthesis in the marine diatom *Phaeodactylum tricorutum* grown under different culture conditions. *Mar. Biol.*, **33**, 185–94. 471
1215. Shimura, S. & Ichimura, S. (1973). Selective transmission of light in the ocean waters and its relation to phytoplankton photosynthesis. *J. Oceanogr. Soc. Japan.*, **29**, 257–66. Quoted by Shimura & Fujita (1975). 499
1216. Shiimoto, A. (2000). Efficiency of water-column light utilization in the subarctic northwestern Pacific. *Limnol. Oceanogr.*, **45**, 982–7. 377
1217. Shiimoto, A., Tadokoro, K., Monaka, K. & Nanba, M. (1997). Productivity of picoplankton compared with that of larger phytoplankton in the subarctic region. *J. Plankton Res.*, **19**, 907–16. 420
- 1217a. Shipman, L. L., Cotton, T. M., Norris, J. R. & Katz, J. J. (1976). An analysis of the visible absorption spectrum of chlorophyll *a* monomer, dimers and oligomers in solution. *J. Amer. Chem. Soc.*, **98**, 8222–30. 280

1218. Shooter, D., Davies-Colley, R. J. & Kirk, J. T. O. (1998). Light absorption and scattering by ocean waters in the vicinity of the Chatham Rise, South Pacific Ocean. *Mar. Freshwater Res.*, **49**, 455–61. [75](#), [86](#), [90](#), [118](#)
1219. Short, N. M. (1976). *Mission to Earth: Landsat Views the World*. Washington: NASA. [208](#)
1220. Shulenberger, E. (1978). The deep chlorophyll maximum and mesoscale environmental heterogeneity in the western half of the North Pacific central gyre. *Deep-Sea Res.*, **25**, 1193–208. [395](#)
1221. Sieburth, J. M. & Jensen, A. (1968). Studies on algal substances in the sea. I. Gelbstoff (humic material) in terrestrial and marine waters. *J. Exp. Mar. Biol. Ecol.*, **2**, 174–89. [67](#)
1222. Sieburth, J. M. & Jensen, A. (1969). Studies on algal substances in the sea. II. The formation of gelbstoff (humic material) by exudates of Phaeophyta. *J. Exp. Mar. Biol. Ecol.*, **3**, 279–89. [68](#)
1223. Siegel, H. (1984). Some remarks on the ratio between the upward irradiance and nadir radiance just beneath the sea surface. *Beitr. Meeresk.*, **51**, 75. Quoted by Aas & Højerslev (1999). [173](#)
1224. Siegel, D. A. & Dickey, T. D. (1987). On the parameterization of irradiance for open sea photoprocesses. *J. Geophys. Res.*, **92**, 14648–62. [163](#)
1225. Siegel, D. A., Iturriaga, R., Bidigare, R. R. *et al.* (1990). Meridional variations of the springtime phytoplankton community in the Sargasso Sea. *J. Mar. Res.*, **48**, 379–412. [462](#)
1226. Siegel, D. A., Maritorena, S., Nelson, N. B. & Behrenfeld, M. J. (2005). Independence and interdependencies among global ocean color properties: reassessing the bio-optical assumption. *J. Geophys. Res.*, **110**, C07011. [97](#)
1227. Siegel, D. A., Maritorena, S., Nelson, N. B., Hansell, D. A. & Lorenzi-Kayser, M. (2002). Global distribution and dynamics of colored dissolved and detrital organic materials. *J. Geophys. Res.*, **107** (C12), 3228. [97](#)
1228. Simenstad, C. A., Estes, J. A. & Kenyon, K. W. (1978). Aleuts, sea otters, and alternative stable-state communities. *Science*, **200**, 403–11. [429](#)
1229. Simis, S. G. H., Peters, S. W. M. & Gons, H. J. (2005). Remote sensing of the cyanobacterial pigment phycocyanin in turbid inland water. *Limnol. Oceanogr.*, **50**, 237–45. [246](#)
1230. Simms, E. L. & Dubois, J.-M. M. (2001). Satellite remote sensing of submerged kelp beds on the Atlantic coast of Canada. *Internat. J. Remote Sens.*, **22**, 2083–94. [259](#)
1231. Slater, P. N. (1980). *Remote Sensing: Optics and Optical Systems*. Reading: Addison-Wesley. [201](#)
1232. Smayda, T. J. (1997a). What is a bloom? A commentary. *Limnol. Oceanogr.*, **42**, 1132–6. [537](#)
1233. Smayda, T. J. (1997b). Harmful algal blooms: their ecophysiology and general relevance to phytoplankton blooms in the sea. *Limnol. Oceanogr.*, **42**, 1137–53. [536](#)
1234. Smith, E. L. (1936). Photosynthesis in relation to light and carbon dioxide. *Proc. Natl. Acad. Sci. (Wash.)*, **22**, 504–11. [351](#), [442](#)
1235. Smith, E. L. (1938). Limiting factors in photosynthesis: light and carbon dioxide. *J. Gen. Physiol.*, **22**, 21–35. [402](#), [403](#)

1236. Smith, F. A. & Walker, N. A. (1980). Photosynthesis by aquatic plants: effects of unstirred layers in relation to assimilation of  $\text{CO}_2$  and  $\text{HCO}_3^-$ ; and to carbon isotopic discrimination. *New Phytol.*, **86**, 245–59. [412](#)
1237. Smith, R. C. (1968). The optical characterization of natural waters by means of an ‘extinction coefficient’. *Limnol. Oceanogr.*, **13**, 423–9. [137](#)
1238. Smith, R. C. (1969). An underwater spectral irradiance collector. *J. Mar. Res.*, **27**, 341–51. [134](#)
1239. Smith, R. C., Austin, R. W. & Tyler, J. E. (1970). An oceanographic radiance distribution camera system. *Appl. Opt.*, **9**, 2015–22. [148](#)
1240. Smith, R. C. & Baker, K. S. (1978a). The bio-optical state of ocean waters and remote sensing. *Limnol. Oceanogr.*, **23**, 247–59. [328](#), [445](#)
1241. Smith, R. C. & Baker, K. S. (1978b). Optical classification of natural waters. *Limnol. Oceanogr.*, **23**, 260–7. [93](#)
1242. Smith, R. C. & Baker, K. S. (1979). Penetration of UV-B and biologically effective dose rates in natural waters. *Photochem. Photobiol.*, **29**, 311–23. [158](#)
1243. Smith, R. C. & Baker, K. S. (1980). Biologically effective dose transmitted by culture bottles in  $^{14}\text{C}$  productivity measurements. *Limnol. Oceanogr.*, **25**, 364–6. [355](#)
1244. Smith, R. C. & Baker, K. S. (1981). Optical properties of the clearest natural waters (200–800 nm). *Appl. Opt.*, **20**, 177–84. [64](#)
1245. Smith, R. C. & Baker, K. S. (1982). Oceanic chlorophyll concentrations as determined by satellite (Nimbus-7 Coastal Zone Colour Scanner). *Mar. Biol.*, **66**, 269–79. [240](#)
1246. Smith, R. C. & Baker, K. S. (1984). The analysis of ocean optical data. *SPIE, Ocean Optics VII*, **489**, 119–26. [139](#)
1247. Smith, R. C., Baker, K. S., Holm-Hansen, O. & Olson, R. (1980). Photo-inhibition of photosynthesis in natural waters. *Photochem. Photobiol.*, **31**, 585–92. [355](#)
1248. Smith, R. C., Bidigare, R. R., Prezelin, B. B., Baker, K. S. & Brooks, J. M. (1987). Optical characterization of primary productivity across a coastal front. *Mar. Biol.*, **96**, 575–91. [376](#)
1249. Smith, R. C., Booth, C. R. & Star, J. L. (1984). Oceanographic biooptical profiling system. *Appl. Opt.*, **23**, 2791–7. [139](#)
1250. Smith, R. C., Marra, J., Perry, M. J. *et al.* (1989). Estimation of a photon budget for the upper ocean in the Sargasso Sea. *Limnol. Oceanogr.*, **34**, 1673–93. [163](#)
1251. Smith, R. C., Prezelin, B. B., Baker, K. S. *et al.* (1992). Ozone depletion: ultraviolet radiation and phytoplankton biology in Antarctic waters. *Science*, **255**, 952–9. [355](#)
1252. Smith, R. C., Prezelin, B. B., Bidigare, R. R. & Baker, K. S. (1989). Bio-optical modelling of photosynthetic production in coastal waters. *Limnol. Oceanogr.*, **34**, 1524–44. [346](#), [446](#)
1253. Smith, R. C. & Tyler, J. E. (1967). Optical properties of clear natural water. *J. Opt. Soc. Amer.*, **57**, 289–95. [95](#)
1254. Smith, R. G. & Bidwell, R. G. S. (1987). Carbonic anhydrase-dependent inorganic carbon uptake by the red macroalga *Chondrus crispus*. *Plant Physiol.*, **83**, 735–8. [405](#)

1255. Smith, R. G. & Bidwell, R. G. S. (1989). Mechanism of photosynthetic carbon dioxide uptake by the red macroalga, *Chondrus crispus*. *Plant Physiol.*, **89**, 93–9. 405
1256. Smith, R. G., Wheeler, W. N. & Srivastava, L. M. (1983). Seasonal photosynthetic performance of *Macrocystis integrifolia* (Phaeophyceae). *J. Phycol.*, **19**, 352–9. 349, 509
1257. Smith, V. H. (2007). Using primary productivity as an index of coastal eutrophication: the units of measurement matter. *J. Plankton Res.*, **29**, 1–6. 423
1258. Smith, W. O. (1977). The respiration of photosynthetic carbon in eutrophic areas of the ocean. *J. Mar. Res.*, **35**, 557–65. 343
1259. Smith, W. O. & Nelson, D. M. (1986). Importance of ice edge phytoplankton production in the Southern Ocean. *BioScience*, **36**, 251–7. 394
1260. Smyth, T. J., Pemberton, K. L., Aiken, J. & Geider, R. J. (2004). A methodology to determine primary production and phytoplankton photosynthetic parameters from Fast Repetition Rate Fluorometry. *J. Plankton Res.*, **26**, 1337–50. 337
1261. Smyth, T. J., Tilstone, G. H. & Groom, S. B. (2005). Integration of radiative transfer into satellite models of ocean primary production. *J. Geophys. Res.*, **110**, C10014. 451
1262. Snyder, W. A., Arnone, R. A., Davis, C. O. *et al.* (2008). Optical scattering and backscattering by organic and inorganic particulates in U.S. coastal waters. *Appl. Opt.*, **47**, 666–77. 117, 126
1263. Solazzi, A. & Tolomio, C. (1976). Sea depth effects on the algal photosynthetic apparatus: 1. Chlorophyll pigments of *Halimeda tuna* Lam. (Chlorophyceae, Siphonales). *Mem. Biol. Mar. Ocean*, **6**, 21–7. 491
1264. Sommer, U. & Gliwicz, Z. M. (1986). Long range vertical migration of *Volvox* in tropical Lake Cahora Bassa (Mozambique). *Limnol. Oceanogr.*, **31**, 650–3. 516
1265. Søndergaard, M. & Bonde, G. (1988). Photosynthetic characteristics and pigment content and composition in *Littorella uniflora* (L.) Aschers in a depth gradient. *Aquat. Bot.*, **32**, 307–19. 492
1266. Søndergaard, M., Bruun, L., Lauridsen, T., Jeppesen, E. & Madsen, T. V. (1996). The impact of grazing waterfowl on submerged macrophytes: in situ experiments in a shallow eutrophic lake. *Aquat. Bot.* **53**, 73–84. 428
1267. Sorrell, B. K., Hawes, I., Schwarz, A.-M. & Sutherland, D. (2001). Interspecific differences in photosynthetic carbon uptake, photosynthate partitioning and extracellular organic carbon release by deep-water characean algae. *Freshwater Biol.*, **46**, 453–64. 345
1268. Sosik, H. M., Chisholm, S. W. & Olson, R. J. (1989). Chlorophyll fluorescence from single cells: interpretation of flow cytometric signals. *Limnol. Oceanogr.*, **34**, 1749–61. 131, 317
1269. Sosik, H. M., Green, R. E., Pegau, W. S. & Roesler, C. S. (2001). Temporal and vertical variability in optical properties of New England shelf waters during late summer and spring. *J. Geophys. Res.*, **106**, 9455–72. 74, 117
1270. Sosik, H. M. & Mitchell, B. G. (1995). Light absorption by phytoplankton, photosynthetic pigments and detritus in the California Current System. *Deep-Sea Res.*, **42**, 171–48. 86

1271. Sournia, A. (1974). Circadian periodicities in natural populations of marine phytoplankton. *Adv. Mar. Biol.*, **12**, 325–89. 430, 524
1272. Sournia, A. (1976). Primary production of sands in the lagoon of an atoll and the role of Foraminiferan symbionts. *Mar. Biol.*, **37**, 29–32. 390
1273. Spence, D. H. N. (1976). Light and plant response in fresh water. In G. C. Evans, R. Bainbridge & O. Rackham (eds), *Light as an Ecological Factor* (pp. 93–133). Oxford: Blackwell. 390, 391, 520
1274. Spence, D. H. N., Campbell, R. M. & Chrystal, J. (1971). Spectral intensity in some Scottish freshwater lochs. *Freshwater Biol.*, **1**, 321–37. 165
1275. Spence, D. H. N., Campbell, R. M. & Chrystal, J. (1973). Specific leaf areas and zonation of freshwater macrophytes. *J. Ecol.*, **61**, 317–28. 502
1276. Spence, D. H. N. & Chrystal, J. (1970). Photosynthesis and zonation of freshwater macrophytes. I. Depth distribution and shade tolerance. II. Adaptability of species of deep and shallow water. *New Phytol.*, **69**, 205–15, 217–27. 478–9
1277. Spencer, J. W. (1971). Fourier series representation of the position of the sun. *Search*, **2**, 172. 39
1278. Spilhaus, A. F. (1968). Observations of light scattering in seawater. *Limnol. Oceanogr.*, **13**, 418–22. 109
1279. Spillane, M. C. & Doyle, D. M. (1983). Final results for STREX and JASIN photoanalyses with preliminary search for whitecap algorithm. In *Whitecaps and the Marine Atmosphere, Report 5* (pp. 8–27). Galway, Ireland: University College. 47
1280. Spinrad, R. W. & Brown, J. W. (1986). Relative real refractive index of marine microorganisms: a technique for flow cytometric estimation. *Appl. Opt.*, **25**, 1930–4. 131
1281. Spinrad, R. W., Zaneveld, J. R. V. & Pak, H. (1978). Volume scattering function of suspended particulate matter at near-forward angles: a comparison of experimental and theoretical values. *Appl. Opt.*, **17**, 1125–30. 109
1282. Spitzer, D. & Wernand, M. R. (1979a). Photon scalar irradiance meter. *Appl. Opt.*, **18**, 1698–700. 144
1283. Spitzer, D. & Wernand, M. R. (1979b). Irradiance and absorption spectra measurements in the tropical East Atlantic. In *17th General Assembly of IAPSO* (Canberra, 1979) (Abstracts p. 73). San Diego: International Association for the Physical Sciences of the Ocean. 61
1284. Stabeno, P. J. & Monahan, E. C. (1983). The influence of whitecaps on the albedo of the sea surface. In *Whitecaps and the Marine Atmosphere, Report 5* (pp. 78–93). Galway, Ireland: University College. 47
1285. Stadelmann, P., Moore, J. E. & Pickett, E. (1974). Primary production in relation to temperature structure, biomass concentration, and light conditions at an inshore and offshore station in Lake Ontario. *J. Fish. Res. Bd. Canada*, **31**, 1215–32. 164
1286. Staehelin, L. A. (1986). Chloroplast structure and supramolecular organization of photosynthetic membranes. *Encycl. Plant Physiol. (n.s.)*, **19**, 1–84. 265
1287. Staehelin, L. A. & Arntzen, C. J. (1986). Photosynthesis III: photosynthetic membranes and light harvesting systems. *Encycl. Plant Physiol. (n.s.)*, **19**. 301

1288. Staehr, P. A. & Markager, S. (2004). Parameterization of the chlorophyll *a*-specific in vivo light absorption coefficient covering estuarine, coastal and oceanic waters. *Int. J. Remote Sens.*, **25**, 5117–30. 318
1289. Stambler, N. (2006). Light and picophytoplankton in the Gulf of Eilat (Aqaba). *J. Geophys. Res.*, **111**, C11009. 396, 493
1290. Stauber, J. L. & Jeffrey, S. W. (1988). Photosynthetic pigments in fifty-one species of marine diatoms. *J. Phycol.*, **24**, 158–72. 278, 494
1291. Stavn, R. H. & Weidemann, A. D. (1988). Optical modeling of clear ocean light fields: Raman scattering effects. *Appl. Opt.*, **27**, 4002–11. 178
1292. Stedmon, C. A., Markager, S. & Kaas, H. (2000). Optical properties and signatures of chromophoric dissolved organic matter (CDOM) in Danish coastal waters. *Estuar. Coast. Shelf Sci.*, **51**, 267–78. 81
1293. Steele, J. H. & Baird, I. E. (1965). The chlorophyll *a* content of particulate organic matter in the northern North Sea. *Limnol. Oceanogr.*, **10**, 261–7. 277
1294. Steele, J. H. & Yentsch, C. S. (1960). The vertical distribution of chlorophyll. *J. Mar. Biol. Ass. U.K.*, **39**, 217–26. 396
1295. Steemann Nielsen, E. (1952). The use of radioactive carbon (<sup>14</sup>C) for measuring organic production in the sea. *J. Cons. Perm. Int. Explor. Mer.*, **18**, 117–40. 331
1296. Steemann Nielsen, E. (1974). Light and primary production. In N. G. Jerlov & E. S. Nielsen (eds), *Optical Aspects of Oceanography* (pp. 361–88). London: Academic Press. 389
1297. Steemann Nielsen, E. (1975). *Marine Photosynthesis*. Amsterdam: Elsevier. 343, 408, 417–18, 419, 431, 477, 498, 499, 504
1298. Steemann Nielsen, E. & Hansen, V. K. (1961). Influence of surface illumination on plankton photosynthesis in Danish waters (56° N) throughout the year. *Physiol. Plant.*, **14**, 595–613. 346, 510–11
1299. Steemann Nielsen, E. & Jørgensen, E. G. (1968). The adaptation of plankton algae. *Physiol. Plant.*, **21**, 401–13. 417–18
1300. Stephens, F. C. (1995). Variability of spectral absorption efficiency within living cells of *Pyrocystis lunula* (Dinophyta). *Mar. Biol.*, **122**, 325–31. 522
1301. Sternberg, R. W., Baker, E. T., McManus, D. A., Smith, S. & Morrison, D. R. (1974). An integrating nephelometer for measuring particle concentration in the deep sea. *Deep-Sea Res.*, **21**, 887–92. 127
1302. Stokes, A. N. (1975). Proof of a law for calculating absorption of light by cellular suspensions. *Arch. Biochem. Biophys.*, **167**, 393–4. 311
1303. Stramska, M. (2005). Interannual variability of seasonal phytoplankton blooms in the north polar Atlantic in response to atmospheric forcing. *J. Geophys. Res.*, **110**, C05016. 433
1304. Stramska, M. & Dickey, T. D. (1993). Phytoplankton bloom and the vertical thermal structure of the upper ocean. *J. Mar. Res.*, **51**, 819–42. 394
1305. Stramska, M. & Frye, D. (1997). Dependence of apparent optical properties on solar altitude: experimental results based on mooring data collected in the Sargasso Sea. *J. Geophys. Res.*, **102**, 15679–91. 157
1306. Stramska, M., Stramski, D., Kaczmarek, S., Allison, D. & Schwarz, J. (2006). Seasonal and regional differentiation of bio-optical properties within the north polar Atlantic. *J. Geophys. Res.*, **111**, C08003. 86

1307. Stramska, M., Stramski, D., Mitchell, B.G. & Mobley, C.D. (2000). Estimation of the absorption and backscattering coefficients from in-water radiometric measurements. *Limnol. Oceanogr.*, **45**, 628–41. 61
1308. Stramski, D. & Morel, A. (1990). Optical properties of photosynthetic picoplankton in different physiological states as affected by growth irradiance. *Deep-Sea Res.*, **37**, 245–66. 129
1309. Stramski, D., Woźniak, S. B. & Flatau, P.J. (2004). Optical properties of Asian mineral dust suspended in water. *Limnol. Oceanogr.*, **49**, 749–55. 85
1310. Strong, A.E. (1974). Remote sensing of algal blooms by aircraft and satellite in Lake Erie and Utah Lake. *Remote Sens. Environ.*, **3**, 99–107. 235
1311. Strong, A.E. (1978). Chemical whittings and chlorophyll distributions in the Great Lakes as viewed by Landsat. *Remote Sens. Environ.*, **7**, 61–72.
1312. Stross, R.G. & Sokol, R.C. (1989). Runoff and flocculation modify underwater light environment of the Hudson River Estuary. *Estuar. Coast. Shelf Sci.*, **29**, 305–16. 164
1313. Stuart, V., Sathendranath, S., Platt, T., Maass, H. & Irwin, B.D. (1998). Pigments and species composition of natural phytoplankton populations: effect on the absorption spectra. *J. Plankton Res.*, **20**, 187–217. 357
1314. Stuermer, D.H. & Harvey, G.R. (1978). Structural studies on marine humus. *Mar. Chem.*, **6**, 55–70. 71
1315. Stuermer, D.H. & Payne, J.R. (1976). Investigation of seawater and terrestrial humic substances with carbon-13 and proton nuclear magnetic resonance. *Geochim. Cosmochim. Acta*, **40**, 1109–14. 71
1316. Stumpf, R.P. & Pennock, J.R. (1989). Calibration of a general optical equation for remote sensing of suspended sediments in a moderately turbid estuary. *J. Geophys. Res.*, **94**, 14363–71. 233
1317. Stumpf, R.P. & Pennock, J.R. (1991). Remote estimation of the diffuse attenuation coefficient in a moderately turbid estuary. *Remote Sens. Environ.*, **38**, 183–91. 164
1318. Stumpf, R.P. & Tyler, M.A. (1988). Satellite detection of bloom and pigment distributions in estuaries. *Remote Sens. Environ.*, **24**, 385–404.
1319. Subramaniam, A., Carpenter, E.J., Karentz, D. & Falkowski, P.G. (1999). Bio-optical properties of the marine diazotrophic cyanobacteria *Trichodesmium* spp. I. Absorption and photosynthetic action spectra. *Limnol. Oceanogr.*, **44**, 608–17. 356
1320. Suggett, D.J., Oxborough, K., Baker, N.R. *et al.* (2003). Fast repetition rate and pulse amplitude modulation chlorophyll a fluorescence measurements for assessment of photosynthetic electron transport in marine phytoplankton. *Eur. J. Phycol.*, **38**, 371–84. 332, 336, 337
1321. Sugihara, S., Kishino, M. & Okami, N. (1984). Contribution of Raman scattering to upward irradiance in the sea. *J. Oceanogr. Soc. Jap.*, **40**, 397–404. 178
1322. Sukenik, A., Bennett, J. & Falkowski, P. (1987). Light-saturated photosynthesis – limitation by electron transport or carbon fixation? *Biochim. Biophys. Acta*, **891**, 205–15. 475
1323. Sukenik, A., Livne, A., Neori, A., Yacobi, Y.Z. & Katcoff, D. (1992). Purification and characterization of a light-harvesting chlorophyll-protein

- complex from the marine eustigmatophyte *Nannochloropsis* sp. *Plant Cell Physiol.*, **33**, 1041–8. 290
1324. Sullivan, J. M., Twardowski, M. S., Zaneveld, J. R. V. *et al.* (2006). Hyper-spectral temperature and salt dependencies of absorption by water and heavy water in the 400–750 nm spectral range. *Appl. Opt.*, **45**, 5294–309. 63
1325. Sun, D., Li, Y., Wang, Q. *et al.* (2009). Light scattering properties and their relation to the biogeochemical composition of turbid productive waters: a case study of Lake Taihu. *Appl. Opt.*, **48**, 1979–89. 118, 125, 126
1326. Suttle, C. A., Chan, A. M. & Cottrell, M. T. (1990). Infection of phytoplankton by viruses and reduction of primary productivity. *Nature*, **347**, 467–9. 427
1327. Suzuki, K., Handa, N., Kiyosawa, H. & Ishizaka, J. (1995). Distribution of the prochlorophyte *Prochlorococcus* in the central Pacific Ocean as measured by HPLC. *Limnol. Oceanogr.* **40**, 983–9. 422
1328. Sverdrup, H. U. (1953). On conditions for the vernal blooming of phytoplankton. *J. Cons. Int. Explor. Mer.*, **18**, 287–95. 393
1329. Swift, E. & Taylor, W. R. (1967). Bioluminescence and chloroplast movement in the dinoflagellate *Pyrocystis lunula*. *J. Phycol.*, **3**, 77–81. 522
1330. Sydor, M. (1980). Remote sensing of particulate concentrations in water. *Appl. Opt.*, **19**, 2794–800. 232
1331. Taguchi, S. (1976). Relationship between photosynthesis and cell size of marine diatoms. *J. Phycol.*, **12**, 185–9. 373
1332. Takahashi, M., Ichimura, S., Kishino, M. & Okami, N. (1989). Shade and chromatic adaptation of phytoplankton photosynthesis in a thermally stratified sea. *Mar. Biol.*, **100**, 401–9. 345
1333. Talling, J. F. (1957a). Photosynthetic characteristics of some freshwater plankton diatoms in relation to underwater radiation. *New Phytol.*, **56**, 29–50. 344, 392, 419
1334. Talling, J. F. (1957b). The phytoplankton population as a compound photosynthetic system. *New Phytol.*, **56**, 133–49. 327, 340, 392, 440, 441–3
1335. Talling, J. F. (1960). Self-shading effects in natural populations of a planktonic diatom. *Wett. Leben*, **12**, 235–42. 328, 364
1336. Talling, J. F. (1970). Generalized and specialized features of phytoplankton as a form of photosynthetic cover. In *Prediction and Measurement of Photosynthetic Productivity* (pp. 431–45). Wageningen: Pudoc. 77, 94
1337. Talling, J. F. (1971). The underwater light climate as a controlling factor in the production ecology of freshwater phytoplankton. *Mitt. Int. Verein. Limnol.*, **19**, 214–43. 328, 392, 430
1338. Talling, J. F. (1976). The depletion of carbon dioxide from lake water by phytoplankton. *J. Ecol.*, **64**, 79–121. 408, 411
1339. Talling, J. F. (1979). Factor interactions and implications for the prediction of lake metabolism. *Arch. Hydrobiol. Beih. Ergebn. Limnol.*, **13**, 96–109. 411
1340. Talling, J. F., Wood, R. B., Prosser, M. V. & Baxter, R. M. (1973). The upper limit of photosynthetic productivity by phytoplankton: evidence from Ethiopian soda lakes. *Freshwater Biol.*, **3**, 53–76. 376
1341. Tam, C. K. N. & Patel, A. C. (1979). Optical absorption coefficients of water. *Nature*, **280**, 302–4. 63

1342. Tamiya, H. (1957). Mass culture of algae. *Ann. Rev. Plant Physiol.*, **8**, 309–34. 534
1343. Tanada, T. (1951). The photosynthetic efficiency of carotenoid pigments in *Navicula minima*. *Amer. J. Bot.*, **38**, 276–83. 382, 384
1344. Tandeau de Marsac, N. (1977). Occurrence and nature of chromatic adaptation in cyanobacteria. *J. Bacteriol.*, **130**, 82–91. 480, 483
1345. Tassan, S. & Ferrari, G. M. (1995). An alternative approach to absorption measurements of aquatic particles retained on filters. *Limnol. Oceanogr.*, **40**, 1358–68. 57, 84
1346. Tassan, S., Ferrari, G. M., Bricaud, A. & Babin, M. (2000). Variability of the amplification factor of light absorption by filter-retained aquatic particles in the coastal environment. *J. Plankton Res.*, **22**, 659–68. 57
1347. Tassan, S. & Sturm, B. (1986). An algorithm for the retrieval of sediment content in turbid coastal waters from CZCS data. *Int. J. Remote Sens.*, **7**, 643–55. 228
1348. Taylor, W. R. (1959). Distribution in depth of marine algae in the Caribbean and adjacent seas. In *Proc. 9th Int. Bot. Congr.* (pp. 193–7). Canada: University of Toronto Press. 458–9
1349. Taylor, W. R. (1964). Light and photosynthesis in intertidal benthic diatoms. *Helgoländer Wiss. Meeresunters*, **10**, 29–37. 347
1350. Thayer, G. W., Wolfe, D. A. & Williams, R. B. (1975). The impact of man on seagrass ecosystems. *Amer. Scientist*, **63**, 288–95. 534
1351. Thinh, L.-V. (1983). Effect of irradiance on the physiology and ultrastructure of the marine cryptomonad, *Cryptomonas* strain Lis (Cryptophyceae). *Phycologia*, **22**, 7–11. 470, 473
1352. Thom, R. M. & Albright, R. G. (1990). Dynamics of benthic vegetation standing-stock, irradiance and water properties in central Puget Sound. *Mar. Biol.*, **104**, 129–41. 437
1353. Thomas, W. H. & Gibson, C. H. (1990). Quantified small-scale turbulence inhibits a red tide dinoflagellate *Gonyaulax polyedra* Stein. *Deep-Sea Res.*, **37**, 1583–93. 426
1354. Thornber, J. P. (1986). Biochemical characterization and structure of pigment-proteins of photosynthetic organisms. *Encycl. Plant Physiol. (n.s.)*, **19**, 98–142. 286
1355. Thornber, J. P., Morishige, D. T., Anandan, S. & Peter, G. F. (1991). Chlorophyll~Carotenoid proteins of higher plant thylakoids. In H. Scheer (ed.), *Chlorophylls* (pp. 549–85). Boca Raton: CRC Press. 286
1356. Thorne, S. W., Newcomb, E. H. & Osmond, C. B. (1977). Identification of chlorophyll *b* in extracts of prokaryotic algae by fluorescence spectroscopy. *Proc. Natl. Acad. Sci. Wash.*, **74**, 575–8. 273, 279
1357. Thurman, E. M. Quoted by Josephson, J. (1982). In Humic substances. *Environ. Sci. Technol.*, **16**, 20A–4A. 65
1358. Tillmann, U., Hesse, K. -J. & Colijn, F. (2000). Planktonic primary production in the German Wadden Sea. *J. Plankton Res.*, **22**, 1253–76. 450
1359. Tilstone, G. H., Smyth, T. J., Gowen, R. J., Martinez-Vicente, V. & Groom, S. B. (2005). Inherent optical properties of the Irish Sea and their effect on satellite primary production algorithms. *J. Plankton Res.*, **27**, 1127–48. 86

1360. Tilzer, M. M. (1973). Diurnal periodicity in the phytoplankton assemblage of a high mountain lake. *Limnol. Oceanogr.*, **18**, 15–30. [430](#), [514](#), [515](#)
1361. Tilzer, M. M. (1983). The importance of fractional light absorption by photosynthetic pigments for phytoplankton productivity in Lake Constance. *Limnol. Oceanogr.*, **28**, 833–46. [328](#), [364](#), [435](#)
1362. Tilzer, M. M. (1984). Seasonal and diurnal shifts of photosynthetic quantum yields in the phytoplankton of Lake Constance. *Verh. Internat. Verein. Limnol.*, **22**, 958–62. [375](#)
1363. Tilzer, M. M. (1987). Prediction of productivity changes in Lake Tahoe at increasing phytoplankton biomass. *Int. Ver. Theor. Angew. Limnol. Verh.*, **20**, 407–13. [328](#)
1364. Tilzer, M. M. & Goldman, C. R. (1978). Importance of mixing, thermal stratification and light adaptation for phytoplankton productivity in Lake Tahoe (California-Nevada). *Ecology*, **59**, 810–21. [397](#), [493–4](#), [500–01](#)
1365. Tilzer, M. M., Goldman, C. R. & De Amezaga, E. D. (1975). The efficiency of photosynthetic light energy utilization by lake phytoplankton. *Verh. Int. Verein. Limnol.*, **19**, 800–7. [376](#)
1366. Tilzer, M. M. & Schwarz, K. (1976). Seasonal and vertical patterns of phytoplankton light adaptation in a high mountain lake. *Arch. Hydrobiol.*, **77**, 488–504. [514](#)
1367. Timofeeva, V. A. (1971). Optical characteristics of turbid media of the sea-water type. *Izv. Atmos. Oceanic Phys.*, **7**, 863–5. [122](#)
1368. Timofeeva, V. A. (1974). Optics of turbid water. In N. G. Jerlov & E. S. Nielsen (eds), *Optical Aspects of Oceanography* (pp. 177–219). London: Academic Press. [182](#)
1369. Timofeeva, V. A. & Gorobets, F. I. (1967). On the relationship between the attenuation coefficients of collimated and diffuse light fluxes. *Izv. Atmos. Oceanic Phys.*, **3**, 166–9. [106](#)
1370. Titus, J. E. & Adams, M. S. (1979). Coexistence and the comparative light relations of the submersed macrophytes *Myriophyllum spicatum* L. and *Vallisneria americana* Michx. *Oecologia*, **40**, 273–86. [345](#)
1371. Topliss, B. J., Amos, C. L. & Hill, P. R. (1990). Algorithms for remote sensing of high concentration, inorganic suspended sediment. *Int. J. Remote Sens.*, **11**, 947–66. [231](#)
1372. Tortell, P. D. & Morel, F. M. M. (2002). Sources of inorganic carbon for phytoplankton in the eastern Subtropical and Equatorial Pacific Ocean. *Limnol. Oceanogr.*, **47**, 1012–22. [406](#)
1373. Townsend, D. W., Keller, M. D., Sieracki, M. E. & Ackleson, S. G. (1992). Spring phytoplankton blooms in the absence of vertical water column stratification. *Nature*, **360**, 59–62. [394](#), [431](#)
1374. Townsend, D. W. & Spinrad, R. W. (1986). Early spring phytoplankton blooms in the Gulf of Maine. *Continental Shelf Res.*, **6**, 515–29. [394](#)
1375. Townsend, S. A., Luong-Van, J. T. & Boland, K. T. (1996). Retention time as a primary determinant of colour and light attenuation in two tropical Australian reservoirs. *Freshwater Biol.*, **36**, 57–69. [81](#)
1376. Tranter, D. J. (1982). Interlinking of physical and biological processes in the Antarctic Ocean. *Oceanogr. Mar. Biol. Ann. Rev.*, **20**, 11–35. [508](#)

1377. Tsuzuki, M. (1983). Mode of  $\text{HCO}_3^-$  utilization by the cells of *Chlamydomonas reinhardtii* grown under ordinary air. *Z. Pflanzenphysiol.*, **110**, 29–37. 408
1378. Twardowski, M. S. & Donaghay, P. L. (2002). Photobleaching of aquatic dissolved materials: absorption removal, spectral alteration, and their inter-relationship. *J. Geophys. Res.*, **107**, C83091. 73
1379. Twardowski, M. S. & Donaghay, P. L. (2001). Separating in situ and terrigenous sources of absorption by dissolved materials in coastal waters. *J. Geophys. Res.*, **106**, 2545–60. 68
1380. Tyler, J. E. (1960). Radiance distribution as a function of depth in an underwater environment. *Bull. Scripps Inst. Oceanogr.*, **7**, 363–411. 148, 180, 182–4, 187
1381. Tyler, J. E. (1968). The Secchi disc. *Limnol. Oceanogr.*, **13**, 1–6. 142
1382. Tyler, J. E. (1975). The in situ quantum efficiency of natural phytoplankton populations. *Limnol. Oceanogr.*, **20**, 976–80. 163
1383. Tyler, J. E. (1978). Optical properties of water. In W. G. Driscoll & W. Vaughan (eds), *Handbook of Optics* (pp. 15–1 to 15–38). New York: McGraw-Hill. 187
1384. Tyler, J. E. & Richardson, W. H. (1958). Nephelometer for the measurement of volume scattering function *in situ*. *J. Opt. Soc. Amer.*, **48**, 354–7. 108
1385. Tyler, J. E. & Smith, R. C. (1967). Spectroradiometric characteristics of natural light under water. *J. Opt. Soc. Amer.*, **57**, 595–601. 247
1386. Tyler, J. E. & Smith, R. C. (1970). *Measurements of Spectral Irradiance Underwater*. New York: Gordon & Breach. 34, 146, 155–6, 160, 163–4, 176–7
1387. Tzortziou, M., Herman, J. R., Gallegos, C. L. *et al.* (2006). Bio-optics of the Chesapeake Bay from measurements and radiative transfer closure. *Estuar. Coast. Shelf Sci.*, **68**, 348–62. 126
1388. Uitz, J., Claustre, H., Morel, A. & Hooker, S. B. (2006). Vertical distribution of phytoplankton communities in open ocean: an assessment based on surface chlorophyll. *J. Geophys. Res.*, **111**, C08005. 444
1389. Uku, J., Beer, S. & Björk, M. (2005). Buffer sensitivity of photosynthetic carbon utilization in eight tropical seagrasses. *Mar. Biol.*, **147**, 1085–90. 406
1390. Vadas, R. L. & Steneck, R. S. (1988). Zonation of deep water benthic algae in the Gulf of Maine. *J. Phycol.*, **24**, 338–46. 456
1391. Vadstrup, M. & Madsen, T. V. (1995). Growth limitation of submerged aquatic macrophytes by inorganic carbon. *Freshwater Biol.*, **34**, 411–19. 411
1392. Vähätalo, A. V., Salkinoja-Salonen, M., Taalas, P. & Salonen, K. (2000). Spectrum of the quantum yield for photochemical mineralization of dissolved organic carbon in a humic lake. *Limnol. Oceanogr.*, **45**, 664–76. 81
1393. Vaillancourt, R. D., Brown, C. W., Guillard, R. R. L. & Balch, W. M. (2004). Light backscattering properties of marine phytoplankton: relationships to cell size, chemical composition and taxonomy. *J. Plankton Res.*, **26**, 191–212. 131
1394. Van, T. K., Haller, W. T. & Bowes, G. (1976). Comparison of the photosynthetic characteristics of three submersed aquatic plants. *Plant Physiol.*, **58**, 761–8. 340–1, 345, 403
1395. Van de Hulst, H. C. (1957). *Light Scattering by Small Particles*. New York: Wiley. 102–3, 126
1396. Van Leeuwe, M. A., Brotas, V., Consalvey, M. *et al.* (2008). Photoacclimation in microphytobenthos and the role of xanthophyll pigments. *Eur. J. Phycol.*, **43**, 123–32. 357

1397. Van Mooy, B. A. S., Rocap, G., Fredricks, H. F., Evans, C. T. & Devol, A. H. (2006). Sulfolipids dramatically decrease phosphorus demand by picocyanobacteria in oligotrophic marine environments. *Proc. Natl. Acad. Sci. (Wash.)*, **103**, 8607–12. [274](#)
1398. Van Oijen, T., Van Leeuwe, M. A., Granum, E. (2004). Light rather than iron controls photosynthate production and allocation in Southern Ocean phytoplankton populations during austral autumn. *J. Plankton Res.*, **26**, 885–900. [394](#)
1399. Van Wijk, W. R. & Ubing, D. W. S. (1963). In W. R. Van Wijk (ed.), *Physics of Plant Environment*. Amsterdam: North Holland. Quoted by Monteith (1973). [41](#)
1400. Vandevelde, T., Legendre, L., Demers, S. & Therriault, J. C. (1989). Circadian variations in photosynthetic assimilation and estimation of daily phytoplankton production. *Mar. Biol.*, **100**, 525–31. [527](#)
1401. Vant, W. N. (1990). Causes of light attenuation in nine New Zealand estuaries. *Estuar. Coast. Shelf Sci.*, **31**, 125–37. [76](#), [114](#), [118](#), [164](#)
1402. Vant, W. N. & Davies-Colley, R. J. (1984). Factors affecting clarity of New Zealand lakes. *N.Z. J. Mar. Freshwater Res.*, **18**, 363–77. [114](#), [119](#), [142](#)
1403. Vant, W. N. & Davies-Colley, R. J. (1988). Water appearance and recreational use of 10 lakes of the North Island (New Zealand). *Verh. Int. Verein. Limnol.*, **23**, 611–15. [142](#), [143](#)
1404. Vant, W. N., Davies-Colley, R. J., Clayton, J. S. & Coffey, B. T. (1986). Macrophyte depth limits on North Island (New Zealand) lakes of differing clarity. *Hydrobiologia*, **137**, 55–60. [391](#)
1405. Vantrepotte, V., Brunet, C., Mériaux, X. *et al.* (2007). Bio-optical properties of coastal waters in the Eastern English Channel. *Estuar. Coast. Shelf Sci.*, **72**, 201–12. [86](#)
1406. Vasilkov, A., Krotkov, N., Herman, J. *et al.* (2001). Global mapping of underwater UV irradiances and DNA-weighted exposures using Total Ozone Mapping Spectrometer and Sea-viewing Wide Field-of-View Sensor data products. *J. Geophys. Res.*, **106**, 27205–19. [258](#)
1407. Veldhuis, M. J. W. & Kraay, G. W. (2004). Phytoplankton in the subtropical Atlantic ocean: towards a better assessment of biomass and composition. *Deep-Sea Res.*, **51**, 507–30. [396](#), [493](#)
1408. Venrick, E. L. (1984). Winter mixing and the vertical stratification of phytoplankton – another look. *Limnol. Oceanogr.*, **29**, 636–40. [395](#)
1409. Verdin, J. P. (1985). Monitoring water quality conditions in a large Western reservoir with Landsat imagery. *Photogramm. Eng. Remote Sens.*, **51**, 343–53. [224](#)
1410. Vesk, M. & Jeffrey, S. W. (1977). Effect of blue-green light on photosynthetic pigments and chloroplast structure in unicellular marine algae from six classes. *J. Phycol.*, **13**, 280–8. [487–8](#)
1411. Vesk, M. & Jeffrey, S. W. (1987). Ultrastructure and pigments of two strains of the picoplanktonic alga, *Pelagococcus subviridis* (Chrysothecae). *J. Phycol.*, **23**, 322–6. [277](#)
1412. Vidussi, F., Marty, J.-C. & Chiavérini, J. (2000). Phytoplankton pigment variations during the transition from spring bloom to oligotrophy in the northwestern Mediterranean Sea. *Deep-Sea Res.*, **47**, 423–45. [462](#)

1413. Vierling, E. & Alberte, R. S. (1980). Functional organization and plasticity of the photosynthetic unit of the cyanobacterium *Anacystis nidulans*. *Physiol. Plant.*, **50**, 93–8. 470, 473–4
1414. Vincent, W. F., Neale, P. J. & Richerson, P. J. (1984). Photoinhibition: algal responses to bright light during diel stratification and mixing in a tropical alpine lake. *J. Phycol.*, **20**, 201–11. 360
1415. Virgin, H. I. (1964). Some effects of light on chloroplasts and plant protoplasm. In A. C. Giese (ed.), *Photophysiology* (pp. 273–303). New York: Academic Press. 519
1416. Visser, S. A. (1984). Seasonal changes in the concentration and colour of humic substances in some aquatic environments. *Freshwater Biol.*, **14**, 79–87. 70
1417. Vodacek, A., Blough, N. V., DeGrandpre, M. D., Peltzer, E. T. & Nelson, R. K. (1997). Seasonal variation of CDOM and DOC in the Middle Atlantic Bight: terrestrial inputs and photooxidation. *Limnol. Oceanogr.*, **42**, 647–86. 70, 73
1418. Vodacek, A., Hoge, F. E., Swift, R. N. *et al.* (1995). The use of in situ and airborne fluorescence measurements to determine UV absorption coefficients and DOC concentrations in surface waters. *Limnol. Oceanogr.*, **40**, 411–15. 73
1419. Vollenweider, R. A. (ed.) (1969). *A Manual on Methods for Measuring Primary Production in Aquatic Environments*. Oxford: Blackwell. 330
1420. Vollenweider, R. A. (1970). Models for calculating integral photosynthesis and some implications regarding structural properties of the community metabolism of aquatic systems. In *Prediction and Measurement of Photosynthetic Productivity* (pp. 455–72). Wageningen: Pudoc. 440
1421. Volpe, G., Santoleri, R., Vellucci, V. *et al.* (2007). The colour of the Mediterranean Sea: global versus regional bio-optical algorithms evaluation and implication for satellite chlorophyll estimates. *Remote Sens. Environ.*, **107**, 625–38. 244–5
1422. Volten, H., de Haan, J. F., Hovenier, J. W. *et al.* (1998). Laboratory measurements of angular distributions of light scattered by phytoplankton. *Limnol. Oceanogr.*, **43**, 1180–97. 129
1423. Voss, K. J. (1989). Electro-optic camera system for measurement of the underwater radiance distribution. *Optical Engineering*, **28**, 241–7. 149
1424. Voss, K. J., Balch, W. M. & Kilpatrick, K. A. (1998). Scattering and attenuation properties of *Emiliania huxleyi* cells and their detached coccoliths. *Limnol. Oceanogr.*, **43**, 870–6. 70, 129
1425. Waaland, J. R., Waaland, S. D. & Bates, G. (1974). Chloroplast structure and pigment composition in the red alga *Griffithsia pacifica*: regulation by light intensity. *J. Phycol.*, **10**, 193–9. 470
1426. Walker, G. A. H., Buchholz, V. L., Camp, D. *et al.* (1974). A compact multi-channel spectrometer for field use. *Rev. Sci. Instrum.*, **45**, 1349–52. 206
1427. Walker, J. E. & Walsby, A. E. (1983). Molecular weight of gas-vesicle protein from the planktonic cyanobacterium *Anabaena flos-aquae* and implications for structure of the vesicle. *Biochem. J.*, **209**, 809–15. 518
1428. Wallen, D. G. & Geen, G. H. (1971a). Light quality in relation to growth, photosynthetic rates and carbon metabolism in two species of marine plankton algae. *Mar. Biol.*, **10**, 34–43. 487

1429. Wallen, D. G. & Geen, G. H. (1971b). Light quality and concentrations of protein, RNA, DNA and photosynthetic pigments in two species of marine plankton algae. *Mar. Biol.*, **10**, 44–51. [487](#)
1430. Wallentinus, I. (1978). Productivity studies on Baltic macroalgae. *Bot. Mar.*, **21**, 365–80. [348](#), [349](#), [350](#)
1431. Walmsley, R. D. & Bruwer, C. A. (1980). Water transparency characteristics of South African impoundments. *J. Limnol. Soc. Sth Afr.*, **6**, 69–76. [165](#)
1432. Walsby, A. E. (1975). Gas vesicles. *Ann. Rev. Plant Physiol.*, **26**, 427–39. [517](#)
1433. Walsby, A. E. & Booker, M. J. (1976). The physiology of water-bloom formation by planktonic blue-green algae. *Br. Phycol. J.*, **11**, 200. [518](#)
1434. Walsh, J. J. (1976). Herbivory as a factor in patterns of nutrient utilization in the sea. *Limnol. Oceanogr.*, **21**, 1–13. [424](#)
1435. Walsh, J. J. (1981). A carbon budget for overfishing off Peru. *Nature*, **290**, 300–4. [450](#)
1436. Walsh, J. J., Jolliff, J. K., Darrow, B. P. *et al.* (2006). Red tides in the Gulf of Mexico: where, when and why? *J. Geophys. Res.*, **111**, C11003. [537–8](#)
1437. Walsh, J. J. & Steidinger, K. A. (2001). Saharan dust and Florida red tides: the cyanophyte connection. *J. Geophys. Res.*, **106**, 11597–612. [537–8](#)
1438. Wang, G., Cao, W., Yang, D. & Zhao, J. (2008). Partitioning particulate absorption coefficient into contributions of phytoplankton and nonalgal particles: a case study in the northern South China Sea. *Estuar. Coast. Shelf Sci.*, **78**, 513–20. [86](#)
1439. Wang, J., Cota, G. F. & Ruble, D. (2005). Absorption and backscattering in the Beaufort and Chukchi Seas. *J. Geophys. Res.*, **110**, C0414. [74](#), [86](#)
1440. Warren, S. G., Brandt, R. E. & Grenfell, T. C. (2006). Visible and near-ultraviolet absorption spectrum of ice from transmission of solar radiation into snow. *Appl. Opt.*, **45**, 5320–34. [65](#)
1441. Warrick, J. A., Mertes, L. A. K., Siegel, D. A. & Mackenzie, C. (2004). Estimating suspended sediment concentrations in turbid coastal waters of the Santa Barbara Channel with SeaWiFS. *Int. J. Remote Sens.*, **25**, 1995–2002. [234](#)
1442. Waterbury, J. B., Watson, S. W., Valois, F. W. & Franks, D. G. (1986). Biological and ecological characterization of the marine unicellular cyanobacterium *Synechococcus*. In T. Platt & W. K. W. Li (eds), Photosynthetic picoplankton (pp. 71–120). *Can. Bull. Fish. Aquat. Sci.*, **214**. [296](#), [422](#)
1443. Waters, K. J., Smith, R. C. & Lewis, M. R. (1990). Avoiding ship-induced light-field perturbation in the determination of oceanic optical properties. *Oceanography*, **3**, 18–21. [140](#)
1444. Webb, W. L., Newton, M. & Starr, D. (1974). Carbon dioxide exchange of *Alnus rubra*: a mathematical model. *Oecologia*, **17**, 281–91. [351](#)
1445. Weidemann, A. D. & Bannister, T. T. (1986). Absorption and scattering coefficients in Irondequoit Bay. *Limnol. Oceanogr.*, **31**, 567–83. [77](#), [113–14](#), [118](#), [128](#), [164](#), [328](#)
1446. Weidemann, A. D., Bannister, T. T., Effler, S. W. & Johnson, D. L. (1985). Particulate and optical properties during CaCO<sub>3</sub> precipitation in Otisco Lake. *Limnol. Oceanogr.*, **30**, 1078–83. [77](#), [114](#), [118](#), [194](#)
1447. Weinberg, S. (1975). Ecologie des Octocoralliaires communs du substrat dur dans la region de Banyuls-sur-Mer. *Bijdr. Dierk.*, **45**, 50–70. [438](#)

1448. Weiss, G. M., Harding, L. W., Itsweire, E. C. & Campbell, J. W. (1997). Characterizing lateral variability of phytoplankton chlorophyll in Chesapeake Bay with aircraft ocean color data. *Mar. Ecol. Prog. Ser.*, **149**, 183–99. 207
1449. Weller, R. A., Dean, J. P., Marra, J. *et al.* (1985). Three-dimensional flow in the upper ocean. *Science*, **227**, 1552–6. 358
1450. Welschmeyer, N. A. & Lorenzen, C. J. (1981). Chlorophyll-specific photosynthesis and quantum efficiency at subsaturating light intensities. *J. Phycol.*, **17**, 283–93. 373
1451. Werdell, P. J. (2005). OceanColor K490 algorithm evaluation. <http://oceancolor.gsfc.nasa.gov/REPROCESSING/SeaWiFS/R5.1/k490-update.html>. 256
1452. Werner, U., Blazejak, A., Bird, P. *et al.* (2008). Microbial photosynthesis in coral reef sediments (Heron Reef), Australia. *Estuar. Coast. Shelf Sci.*, **76**, 876–88. 531
1453. West, G. S. (1904). *The British Freshwater Algae*. Cambridge: Cambridge University Press. 267
1454. Westlake, D. F. (1967). Some effects of low-velocity currents on the metabolism of aquatic macrophytes. *J. Exp. Bot.*, **18**, 187–205. 412
1455. Westlake, D. F. (1980a). Photosynthesis: macrophytes. In E. D. Le Cren & R. H. Lowe-McConnell (eds), *The Functioning of Freshwater Ecosystems* (pp. 177–82). Cambridge: Cambridge University Press. 439, 534
1456. Westlake, D. F. (1980b). Biomass changes: macrophytes. In E. D. Le Cren & R. H. Lowe-McConnell (eds), *The Functioning of Freshwater Ecosystems* (pp. 203–6). Cambridge: Cambridge University Press. 428, 439
1457. Westlake, D. F. (1980c). Effects of macrophytes. In E. D. Le Cren & R. H. Lowe-McConnell (eds), *The Functioning of Freshwater Ecosystems* (pp. 161–2). Cambridge: Cambridge University Press. 328
1458. Weston, K. R., Fernand, L., Mills, D. K., Delahunty, R. & Brown, J. (2005). Primary production in the deep chlorophyll maximum of the central North Sea. *J. Plankton Res.*, **27**, 909–22. 396, 449
1459. Whatley, J. M. (1977). The fine structure of *Prochloron*. *New Phytol.*, **79**, 309–13. 273
1460. Wheeler, J. R. (1976). Fractionation by molecular weight of organic substances in Georgia coastal water. *Limnol. Oceanogr.*, **21**, 846–52. 75
1461. Wheeler, W. N. (1980a). Pigment content and photosynthetic rate of the fronds of *Macrocystis pyrifera*. *Mar. Biol.*, **56**, 97–102. 490, 497
1462. Wheeler, W. N. (1980b). Effect of boundary layer transport on the fixation of carbon by the giant kelp *M. acrocystis pyrifera*. *Mar. Biol.*, **56**, 103–10. 412
1463. Wheeler, W. N., Smith, R. G. & Srivastava, L. M. (1984). Seasonal photosynthetic performance of *Nereocystis luetkeana*. *Can. J. Bot.*, **62**, 664–70. 349, 509
1464. Whitlock, C. H., Bartlett, D. S. & Gurganus, E. A. (1982). Sea foam reflectance and influence on optimum wavelength for remote sensing of ocean aerosols. *Geophys. Res. Lett.*, **9**, 719–22. 47
1465. Whitney, L. V. (1941). The angular distribution of characteristic diffuse light in natural waters. *J. Mar. Res.*, **4**, 122–31. 182
1466. Wiginton, J. R. & McMillan, C. (1979). Chlorophyll composition under controlled light conditions as related to the distribution of seagrasses in Texas and the U.S. Virgin Islands. *Aquat. Bot.*, **6**, 171–84. 492

- 1466a. Wijesekera, H. W., Pegau, W. S. & Boyd, T. J. (2005). Effect of surface waves on the irradiance distribution in the upper ocean. *Optics Express*, **13**, 9257–64. [141](#)
1467. Wild, A., Ke, B. & Shaw, E. R. (1973). The effect of light intensity during growth of *Sinapis alba* on the electron-transport components. *Z. Pflanzenphysiol.*, **69**, 344–50. [474](#)
1468. Wilhelm, C. (1990). The biochemistry and physiology of light-harvesting processes in chlorophyll *b*- and chlorophyll *c*-containing algae. *Plant Physiol. Biochem.*, **28**, 293–306. [286](#)
1469. Wilhelm, C., Wiedemann, I. & May, M. (1990). Comparative analysis of the composition of two chlorophyll-*b*-containing light-harvesting complexes. *Planta*, **180**, 456–7. [288](#), [290](#)
1470. Williams, D. F. (1984). Overview of the NERC airborne thematic mapper campaign of September 1982. *Int. J. Remote Sens.*, **5**, 631–4. [207](#)
1471. Williams, R. B. & Murdoch, M. B. (1966). Phytoplankton production and chlorophyll concentration in the Beaufort Channel, North Carolina. *Limnol. Oceanogr.*, **11**, 73–82. [421](#)
1472. Williams, S. I. & Walker, D. I. (1999). Mesoherbivore–macroalgal interactions: feeding ecology of sacoglossan sea slugs (Mollusca, Opisthobranchia) and their effects on their food algae. *Oceanogr. Mar. Biol. Ann. Rev.*, **37**, 87–128. [429](#), [430](#)
1473. Winters, G., Loya, Y., Röttgers, R. & Beer, S. (2003). Photoinhibition in shallow-water colonies of the coral *Stylophora pistillata* as measured in situ. *Limnol. Oceanogr.*, **48**, 1388–93. [353–4](#)
1474. Wofar, M. V. M., Corre, P. L. & Birrien, J. L. (1983). Nutrients and primary production in permanently well-mixed temperate coastal waters. *Estuar. Coast. Shelf Sci.*, **17**, 431–46. [394](#)
1475. Wolfe, G. R., Cunningham, F. X., Durnford, D., Green, B. R. & Gantt, E. (1994). Evidence for a common origin of chloroplasts with light-harvesting complexes of different pigmentation. *Nature*, **367**, 566–8. [287](#), [288](#)
1476. Wollman, F.-A. (1986). Photosystem I proteins. *Encycl. Plant Physiol. (n.s.)*, **19**, 487–95. [287](#)
1477. Womersley, H. B. S. (1981). Marine ecology and zonation of temperate coasts. In M. N. Clayton & R. J. King (eds), *Marine Botany: an Australian Perspective* (pp. 211–40). Melbourne: Longman Cheshire. [463](#)
1478. Wood, P. & Cunningham, A. (2001). Ship-borne measurements of ocean colour: development of a CCD-based reflectance radiometer and trials on a longitudinal transect of the Atlantic ocean. *Int. J. Remote Sens.*, **22**, 99–111. [204](#)
1479. Xing, X., Zhao, D., Liu, Y., Yang, J. & Wang, L. (2008). In situ determination of sun-induced chlorophyll a fluorescence quantum yield in the North China Sea. *Int. J. Remote Sens.*, **23**, 851–65. [247](#)
1480. Yamada, T., Ikawa, T. & Nisizawa, K. (1979). Circadian rhythm of the enzymes participating in the CO<sub>2</sub>-photoassimilation of a brown alga, *Spatoglossum pacificum*. *Bot. Mar.*, **22**, 203–9. [525](#)
1481. Yamaguchi, H., Montani, S., Tsutumi, H. *et al.* (2007). Dynamics of microphytobenthic biomass in a coastal area of western Seto Inland Sea, Japan. *Estuar. Coast. Shelf Sci.*, **75**, 423–32. [530–1](#)

1482. Yamamoto, H. Y. (1979). Biochemistry of the violaxanthin cycle in higher plants. *Pure & Applied Chem.*, **51**, 639–48. 357
1483. Yentsch, C. S. (1960). The influence of phytoplankton pigments on the colour of sea water. *Deep-Sea Res.*, **7**, 1–9. 57
1484. Yentsch, C. S. (1974). Some aspects of the environmental physiology of marine phytoplankton: a second look. *Oceanogr. Mar. Biol. Ann. Rev.*, **12**, 41–75. 418, 419
1485. Yentsch, C. M., Horan, P. K., Muirhead, K. *et al.* (1983). Flow cytometry and cell sorting: a technique for analysis and sorting of aquatic particles. *Limnol. Oceanogr.*, **28**, 1275–80. 131
1486. Yentsch, C. S. & Lee, R. W. (1966). A study of photosynthetic light reactions, and a new interpretation of sun and shade phytoplankton. *J. Mar. Res.*, **24**, 319–37. 498
1487. Yentsch, C. S. & Phinney, D. A. (1989). A bridge between ocean optics and microbial ecology. *Limnol. Oceanogr.*, **34**, 1694–705. 86, 318
1488. Yentsch, C. S. & Scagel, R. F. (1958). Diurnal study of phytoplankton pigments. An in situ study in East Sound, Washington. *J. Mar. Res.*, **17**, 567–83. 527
1489. Yeoh, H.-H., Badger, M. R. & Watson, L. (1981). Variation in kinetic properties of ribulose-1,5-bisphosphate carboxylases among plants. *Plant Physiol.*, **67**, 1151–5. 402
1490. Yocum, C. S. & Blinks, L. R. (1958). Light-induced efficiency and pigment alterations in red algae. *J. Gen. Physiol.*, **41**, 1113–17. 484–5, 508
1491. Yokohama, Y. (1973). A comparative study on photosynthesis-temperature relationships and their seasonal changes in marine benthic algae. *Int. Rev. Ges. Hydrobiol.*, **58**, 463–72. 416
1492. Yokohama, Y. (1981). Distribution of the green light-absorbing pigments siphonaxanthin and siphonein in marine green algae. *Bot. Mar.*, **24**, 637–40. 461
1493. Yokohama, Y., Kageyama, A., Ikawa, T. & Shimura, S. (1977). A carotenoid characteristic of Chlorophyceae seaweeds living in deep coastal waters. *Bot. Mar.*, **20**, 433–6. 284, 293, 461
1494. Yokohama, Y. & Misonou, T. (1980). Chlorophyll *a:b* ratios in marine benthic green algae. *Jap. J. Phycol.*, **28**, 219–23. 279
1495. Yu, M., Glazer, A. N., Spencer, K. G. & West, J. A. (1981). Phycoerythrins of the red alga *Callithamnion*. *Plant Physiol.*, **68**, 482–8. 295
1496. Zaneveld, J. R. V., Bartz, R. & Kitchen, J. C. (1990). A reflective-tube absorption meter. *Proc. Soc. Photo-Opt. Instrum. Eng., Ocean Optics X*, **1302**, 124–36. 60
1497. Zaneveld, J. R. V., Kitchen, J. C. & Moore, C. (1994). Scattering error correction of reflecting tube absorption meters. *Ocean Optics XII*. S. Ackleson, ed. Proc. SPIE, 2258, 44–55. 60
1498. Zaneveld, J. R. V., Moore, C., Barnard, A. H. *et al.* (2004). Correction and analysis of spectral absorption data taken with the WET Labs ac-s. *Proceedings Ocean Optics XVII Conference*. Fremantle, Western Australia. 106
1499. Zapata, M. & Garrido, J. L. (1997). Occurrence of phytylated chlorophyll *c* in *Isochrysis galbana* and *Isochrysis* sp. (clone T-iso) (Prymnesiophyceae). *J. Phycol.*, **33**, 209–14. 276

1500. Zapata, M., Jeffrey, S.W., Wright, S.W. *et al.* (2004). Photosynthetic pigments in 37 species (65 strains) of Haptophyta: implications for oceanography and chemotaxonomy. *Mar. Ecol. Progress Ser.*, **270**, 83–102. 278
1501. Zhang, Y.L., Liu, M.L., Wang, X., Zhu, G.W. & Chen, W.M. (2009). Bio-optical properties and estimation of the optically active substances in Lake Tianmuhu in summer. *Int. J. Rem. Sens.*, **30**, 2837–57. 77
1502. Zibordi, G. & Ferrari, G.M. (1995). Instrument self-shading in underwater optical measurements: experimental data. *Appl. Opt.*, **34**, 2750–4. 149
1503. Zibordi, G., Strömbeck, N., Mélin, F. & Berthon, J.-F. (2006). Tower-based radiometric observations at a coastal site in the Baltic Proper. *Estuar. Coast. Shelf Sci.*, **69**, 649–54. 206
1504. Zijlstra, J.J. (1988). The North Sea ecosystem. In H. Postma & J.J. Zijlstra (eds), *Continental Shelves* (pp. 231–77). Amsterdam: Elsevier. 450
1505. Zohary, T. & Robarts, R.D. (1989). Diurnal mixed layers and the longterm dominance of *Microcystis aeruginosa*. *J. Plankton Res.*, **11**, 25–48. 519
1506. Zou, D., Gao, K. & Xia, J. (2003). Photosynthetic utilization of inorganic carbon in the economic brown alga, *Hizikia fusiforme* (Sargassaceae) from the South China Sea. *J. Phycol.*, **39**, 1095–100. 405

# Index to symbols

---

Listed below are the numbers of the pages where each of the more commonly used symbols is first introduced and defined.

<p><math>a</math>, 15  <math>A</math>, 15  <math>a_{\phi}^*(\lambda)</math>, 318  <math>\bar{a}_{\phi}^*(z)</math>, 324  <math>a_d(z)</math>, 22  <math>A_j</math>, 311  <math>\bar{a}_p(z)</math>, 324  <math>a_p(\lambda)</math>, 324  <math>a_p(\lambda, z)</math>, 366  <math>a_{sol}</math>, 312  <math>a_{sus}</math>, 312  <math>a(\lambda)</math>, 324  <math>a_u(z)</math>, 22</p> <p><math>b</math>, 15  <math>B</math>, 15  <math>b_b</math>, 20  <math>b_b/b</math>, 126  <math>b_{bd}(z)</math>, 22  <math>b_{bu}(z)</math>, 23  <math>b_f</math>, 20  <math>\bar{b}_p</math>, 123  <math>\bar{b}_b</math>, 20  <math>\bar{b}_f</math>, 20</p> <p><math>c</math>, 16  <math>C</math>, 15  <math>C(\mu_0)</math>, 170  <math>[Chl]</math>, 318</p> <p><math>D_d</math>, 11  <math>D_{sol}</math>, 312</p>	<p><math>D_{sus}</math>, 312  <math>D_u</math>, 11</p> <p><math>E</math>, 8  <math>\bar{E}</math>, 9  <math>E_{0d}</math>, 10  <math>E_{0d}</math>, 10  <math>E_{0u}</math>, 10  <math>E_c</math>, 339  <math>E_d</math>, 9  <math>E_d(0)</math>, 153  <math>\bar{E}_d(0)</math>, 392  <math>E_d(0^+)</math>, 173  <math>E_k</math>, 340  <math>E_u</math>, 9</p> <p><math>f</math> (ratio, new production), 448  <math>f</math> (relating reflectance to IOP), 170  <math>F_0(\lambda)</math> (extraterrestrial irradiance), 204  <math>F_0, F_m, F_v</math> (fluorescence), 332–334  <math>FLH</math>, 248</p> <p><math>G</math>, 191  <math>G(\mu_0)</math>, 192</p> <p><math>I</math>, 6</p> <p><math>K_0</math>, 13  <math>k_c</math>, 326  <math>K_d</math>, 13  <math>K_d(av)</math>, 192  <math>K_d(PAR)</math>, 137</p>
---	--

- $K_d(\lambda)$ , 156  
 $K_E$ , 13  
 $K_m$  (Michaelis-Menten), 401  
 $K_u$ , 13  
 $K_W, K_G, K_{TR}, K_{PH}$ , 326  
  
 $L$ , 7  
 $L(\theta, \phi)$ , 7  
 $L_u$ , 149  
 $L_{ii}(\theta', \phi)$ , 217  
 $L_w$ , 173  
 $[L_w(\lambda)]_N$ , 221  
 $L_w(\theta, \Phi)$ , 175  
 $L_w(\lambda)$ , 221  
  
 $n$  (Angström exponent), 220  
 $n_w$ , 48  
  
 $P^*$  (C), 338  
 $P^*$  (CO<sub>2</sub>), 338  
 $P^*$  (O<sub>2</sub>), 335, 338  
 $P_A$ , 338  
 $P_A(C)$ , 339  
 $P_A(\text{CO}_2)$ , 339  
 $P_A(\text{O}_2)$ , 339  
 $\text{PAR}$ , 30  
 $P_m$ , 340  
 $P_m^*$  (assimilation number), 441  
 $P_v$ , 338  
  
 $Q$  (ratio  $E_{ii}/L_u$ ), 172  
 $Q_{\text{abs}}$ , 102  
 $Q_{\text{att}}$ , 102  
 $q_p$ , 333  
 $Q_{\text{scatt}}$ , 102  
 $Q_y, Q_x$  (chl absorption bands), 279–280  
  
 $R$ , 13  
 $\bar{r}$ , 174  
 $\Re(\theta)$ , 226  
 $\bar{\rho}$  (Fresnel reflectance), 174  
 $r_{rs}$ , 171  
 $R_{rs}$ , 173  
  
 $s_j$ , 311  
  
 $t$ , 219  
 $t(\theta_0, \lambda)$ , 222  
 $T_n$ , 113  
  
 $U(z)$ , 12  
  
 ${}^wK(av)$ , 14  
  
 $z_c$ , 389  
 $z_{eu}$ , 185  
 $Z_{\text{SD}}$ , 142  
 $\alpha$ , 340  
 $\beta(\theta)$ , 18  
 $\tilde{\beta}(\theta)$ , 20  
 $\beta_p(\theta)$ , 123  
 $\gamma$ , 312  
 $\gamma_b$ , 125  
 $\gamma_{bb}$ , 126  
 $\delta$ , 38  
 $\varepsilon$ , 379  
 $\varepsilon(\lambda_7, \lambda_8)$ , 220  
 $\varepsilon_A$ , 376  
 $\varepsilon_c$ , 369  
 $\varepsilon_V$ , 378  
 $\zeta$ , 24  
 $\theta$  (zenith angle), 6  
 $\kappa(z)$ , 23  
 $\lambda$ , 4  
 $\bar{\mu}$ , 11  
 $\bar{\mu}_0$ , 157  
 $\bar{\mu}_c$ , 12  
 $\bar{\mu}_{db}$ , 11  
 $\bar{\mu}_s$ , 21  
 $\bar{\mu}_u$ , 11  
 $\rho$  (Fresnel reflectance), 175  
 $\rho$  (respiration), 392  
 $\rho$  (top of atmosphere reflectance), 219  
 $\sigma_{PSII}$ , 336  
 $\tau$ , 24  
 $\tau_{O_2}(\lambda)$ , 219  
 $\tau_r(\lambda)$ , 199  
 $\phi$  (azimuth angle), 6  
 $\phi$  (quantum yield), 369  
 $\phi_f$  (fluorescence), 247  
 $\phi_m$ , 370  
 $\phi_{PS2}$ , 334  
 $\phi$ , 6  
 $\chi(z)$ , 369  
 $\chi(\theta)$ , 110  
 $\chi^*(z)$ , 369  
 $\Psi$  (light utilization efficiency function), 377  
 $\Psi^*$  (chl specific cross-section for photosynthesis), 378

# Index to organisms

---

- Acaryochloris*, 276, 278, 284, 297, 300  
*Ahnfeltiopsis*, 470  
*Alnus*, 351  
*Amphidinium*, 291, 407  
amphipods, 532  
*Anabaena*, 128, 403, 408, 410, 421, 517, 518  
*Anacystis*, 87, 387, 470, 473, 487  
anchovy, 424  
angiosperms, 67, 278, 390, 472, 478–479,  
502, 505, 520, 533  
*Aphanizomenon*, 328, 403, 421  
*Arthrospira*, 344  
*Ascophyllum*, 491, 533  
*Asterionella*, 328, 340, 344, 354, 364,  
408, 411
- Bacillariophyceae, 267, 284, 290, 357, 515,  
529–530  
Bangiophycidae, 268  
bivalves, 532  
blue-green algae (Cyanophyta), 129, 275,  
296, 315, 323, 328, 344, 358, 363, 376,  
382, 387, 408, 410, 419, 421, 482,  
506, 534  
*Bostrychia*, 510  
brown algae (Phaeophyta), 68, 176, 268,  
277, 279, 289, 320, 337, 340, 356, 390, 405,  
429, 471, 492, 508, 521  
bryophytes, 278, 390  
Bryopsidophyceae, 288, 290  
*Bryopsis*, 290
- Cabomba*, 345, 402, 404  
*Calanus*, 424  
*Callithamnion*, 295  
*Calothrix*, 481, 482, 483, 506
- Caulerpa*, 429, 464, 520  
Caulerpales, 267, 461  
*Ceramium*, 294, 350  
*Ceratium*, 328, 363, 407, 412, 515, 516, 525  
*Ceratophyllum*, 345, 403  
*Chaetoceros*, 128, 473, 513  
*Chaetomorpha*, 348  
Chaetophoraceae, 461  
*Chara*, 345, 390, 391, 405, 406, 412, 440  
Characeae, 345  
Charophyta, 390, 391, 405, 407  
*Chlamydomonas*, 128, 267, 287, 288, 290,  
403, 414, 472, 474, 476  
*Chlorella*, 267, 279, 290, 322, 323, 382, 383,  
384, 407, 412, 472, 477  
Chlorophyceae, 288, 290, 415, 476  
Chlorophyta, 269, 278, 284, 290, 307, 348,  
356, 357, 380, 381, 403, 407, 455–462,  
463–469, 472–473, 527  
*Chondrus*, 350, 405, 466, 470, 490, 492, 508  
*Chroococcus*, 382, 384  
*Chroomonas*, 271, 291, 470  
chrysomonads, 279  
Chrysophyceae, 283, 284, 357, 397  
Chrysophyta, 267, 452, 487  
*Chrysophaerella*, 397  
ciliates, 424, 429  
cladocerans, 426  
*Cladophora*, 344, 348, 405, 407, 428  
Cladophorales, 461  
*Coccochloris*, 403  
coccolithophores, 129, 131, 178, 268, 329,  
387, 406  
*Coccolithus*, 406  
Codiales, 461  
*Codium*, 287, 288, 290, 348, 436, 466, 490

- Coilodesme*, 383  
 coniferous forests, 70  
 copepods, 424, 537  
 coral, 350, 353, 356, 423, 495, 533  
*Corallina*, 463, 483  
 coralline red algae, 390, 456, 468  
*Coscinodiscus*, 266  
*Cosmarium*, 403  
 crabs, 428  
 crustaceans, 424, 532  
*Cryptomonas*, 470, 473, 483, 516  
 Cryptophyta, 268, 269, 278, 282, 284, 291, 293, 296, 317, 427, 487, 505  
 cryptophytes, 275, 279, 307, 378  
*Cryptopleura*, 386  
 cyanobacteria, 531  
 Cyanophyta, 269, 278, 284, 293, 307, 337, 339, 356, 403, 407, 462, 463, 469, 473, 480–483, 486, 505, 506, 515, 516–519, 530  
*Cyclotella*, 328, 487  
*Cylindrotheca*, 403  
*Cymodocea*, 347, 414, 439  
*Cyperus*, 410  
*Cystoseira*, 356
- Dasycladales, 267  
*Delesseria*, 383  
 Derbesiales, 461  
 desmids, 267  
 Desmophyceae, 268  
*Devaleraea*, 472  
 diatoms (Bacillariophyceae), 268, 318, 328, 344, 347, 354, 373, 374, 378, 381, 382, 387, 390, 394, 406, 407, 412, 414, 417, 423, 425, 427, 432, 434, 452, 471, 473, 488, 494, 512, 522, 523, 531  
*Dictyosiphon*, 349  
*Dictyota*, 289, 492, 508  
*Dinobryon*, 397  
 dinoflagellates, 268, 279, 284, 317, 328, 343, 358, 363, 387, 394, 407, 426, 430, 473, 487, 513, 515, 522, 524, 531, 536  
 Dinophyceae, 268  
*Dinophysis*, 516  
 Dinophyta, 268, 291, 452  
 ducks, 428  
 dugongs, 428, 429  
*Dumontia*, 349  
*Dunaliella*, 272, 337, 418, 470, 471, 472, 475
- Echinus*, 428  
*Ectocarpus*, 348  
*Egeria*, 413  
*Elodea*, 403, 408, 409, 412  
*Emiliania*, 128, 129, 130, 276, 387  
*Enteromorpha*, 237, 348, 405, 429  
*Eucheuma*, 495  
*Euglena*, 266, 279, 290, 310, 403  
 Euglenophyta, 268, 278, 284, 290, 307, 357, 403, 469, 529, 530  
*Eurhynchium*, 403  
 Eustigmatophyceae, 278, 284, 290  
 Eustigmatophyta, 406, 407  
*Eustigmatos*, 407  
*Eutreptiella*, 516
- flagellates, 515–516, 536  
 Florideophycidae, 268  
*Fontinalis*, 390, 402, 403  
*Fragilaria*, 340, 407, 493  
*Fremyella*, 483, 506  
 Fucales, 267  
*Fucus*, 291, 348, 462, 491, 533
- gastropods, 428, 532  
 geese, 428  
*Gigartina*, 416, 418  
*Glenodinium*, 470, 473, 476, 505, 524  
*Gracilaria*, 470, 473, 527  
 grass carp, 428  
*Grateloupia*, 526  
 green algae (Chlorophyta), 68, 267, 277, 282, 302, 320, 332, 337, 340, 342, 344, 382, 405, 429, 469  
*Griffithsia*, 470  
*Gymnodinium*, 90, 271, 317, 513, 514, 515, 537  
 gymnosperms, 67, 278  
*Gyrodinium*, 282
- Haematococcus*, 471  
*Halimeda*, 460, 491, 502  
*Haliptilon*, 270  
*Halophila*, 259, 347, 492, 497, 502, 503, 520  
 Haptophyceae, 284, 357  
 Haptophyta, 268, 283, 284, 291, 307, 406  
 haptophytes, 268  
*Heterocapsa*, 397  
 Heterokontophyta, 267, 278, 288, 290, 307, 403

- Hizikia*, 405  
*Homarus*, 429  
*Hormosira*, 282, 293  
*Hydrilla*, 345, 403, 413  
 Hydrocharitaceae, 321, 413  
*Hymenomonas*, 128  
  
*Isochrysis*, 128, 129, 473  
*Isoetes*, 351, 390  
 isoetids, 390, 410, 414, 492  
  
*Kappaphycus*, 525, 526  
*Karenia*, 537, 538  
 kelp, 436, 533  
 kelp forest, 491  
 krill, 424  
  
*Lagarosiphon*, 410  
*Laminaria*, 282, 348, 349, 405, 428, 434, 436,  
 456, 465, 471, 491, 496, 509, 521, 533  
 Laminariales, 267  
*Lauderia*, 522, 523  
*Laurencia*, 470  
 limpets, 428  
*Littorella*, 390, 492  
*Lobophora*, 460  
 lobster, 429  
*Lyngbya*, 493, 494  
  
*Macrocystis*, 349, 355, 412, 490, 496,  
 509, 533  
*Mantoniella*, 277, 288, 289, 290, 291  
*Melosira*, 87, 128, 328, 344, 408  
*Mesotaenium*, 522  
 metazoans, 429  
*Microcoleus*, 530  
*Microcystis*, 317, 328, 344, 410, 412, 471,  
 474, 518  
*Micromonas*, 277, 427  
*Monostroma*, 348  
*Mougeotia*, 266, 522  
 mullet, 532  
 mussel, 424  
*Myriophyllum*, 345, 403, 408, 409, 410, 440  
*Mytilus*, 424  
  
*Nannochloris*, 407  
*Nannochloropsis*, 290  
 nanoflagellates, 513  
*Navicula*, 322, 323, 382, 384, 408  
*Nereocystis*, 349, 509  
  
*Nitella*, 390, 403  
*Nitschia*, 471  
*Nostoc*, 128  
*Nuphar*, 345  
  
*Ochrosphaera*, 278  
*Oedogonium*, 266  
*Olisthodiscus*, 403  
*Oscillatoria*, 270, 328, 344, 470, 480, 518  
*Ostreobium*, 461  
  
*Palmaria*, 405, 472  
*Pavlova*, 128, 291  
*Pediastrum*, 403  
*Pelagococcus*, 276  
*Peridinium*, 165, 166, 328, 372, 376, 380,  
 426, 513  
*Petalonia*, 289  
*Peyssonelia*, 461  
*Phaeocystis*, 317, 356, 374  
*Phaeodactylum*, 282, 290, 407, 471, 473, 475  
 Phaeophyta, 267, 278, 283, 284, 291, 293,  
 307, 348, 357, 387, 405, 438, 455–462,  
 463–469, 490, 496, 509, 515, 520, 527, 533  
*Phormidium*, 481  
*Phycodrys*, 342, 349  
*Phyllospadix*, 347  
*Pilayella*, 349  
*Pinnularia*, 266  
*Platymonas*, 128  
*Plectonema*, 403  
*Pleurochloris*, 287, 288, 290  
*Plocamium*, 483  
*Pocillopora*, 495  
 polychaete worms, 532  
*Polysiphonia*, 350  
*Porphyra*, 294, 350, 483, 484, 485, 490  
*Porphyridium*, 287, 288, 403, 406, 470, 473,  
 483, 484, 485  
*Posidonia*, 259, 347, 436, 437, 439, 533  
*Potamogeton*, 403, 408, 428, 440, 478, 479,  
 502, 520  
 Prasinophyceae, 277, 284, 288, 289, 290,  
 427, 452  
*Prochlorococcus*, 128, 247, 273, 274, 276,  
 284, 396, 422, 432, 462, 493  
*Prochloron*, 269, 284, 291  
 Prochlorophyta, 273, 279, 284, 291,  
 307, 462  
*Prochlorothrix*, 273, 284, 291  
*Prorocentrum*, 347, 473

- prymnesiophyceae, 452  
 Prymnesiophyceae, 268, 284, 291, 356,  
   374, 425  
 Prymnesiophyta, 317, 407, 487  
 prymnesiophytes, 268  
*Prymnesium*, 128, 278  
 pteridophytes, 278  
*Ptilota*, 495, 496  
*Pyrocystis*, 522  
 Pyrrophyta, 268, 278, 284, 291, 307  
  
 quillwort, 351  
  
*Ranunculus*, 408  
 red algae (Rhodophyta), 68, 269, 275, 277,  
   296, 302, 337, 340, 342, 385, 386, 390, 406,  
   430, 484  
*Rhodomela*, 350  
 Rhodophyta, 268, 278, 284, 288, 293, 307,  
   349, 356, 403, 405, 455–462, 463–469, 470,  
   472, 473, 483–486, 495, 505, 506–508, 510,  
   515, 527  
*Ruppia*, 259  
  
 sacoglossans, 429  
*Sargassum*, 237, 357  
*Scenedesmus*, 128, 403, 407, 472, 474, 476, 477  
*Scytosiphon*, 342, 348  
 sea otter, 429  
 sea otters, 428  
 sea turtle, 429  
 sea turtles, 428  
 sea urchins, 428, 429  
 seagrasses, 390, 391, 406, 414, 423, 428, 429,  
   436, 437, 438, 439, 492, 497, 502, 503, 520,  
   533, 534  
 seagrasses, 347  
 Siphonocladales, 267, 461  
*Skeletonema*, 128, 129, 383, 416, 417, 418,  
   473, 513  
 snails, 428  
*Spatoglossum*, 525  
*Sphacelaria*, 471  
  
*Spirogyra*, 266  
*Spirulina*, 410  
*Stephanodiscus*, 328  
*Stephanopyxis*, 487, 488  
*Stichococcus*, 403, 406  
*Strombidium*, 429  
*Strongylocentrotus*, 429  
*Stylophora*, 350, 353  
*Symbiodinium*, 407  
*Synechococcus*, 95, 128, 274, 328, 403, 407,  
   422, 424, 470, 472, 474, 487  
*Synechocystis*, 128, 302, 322  
*Synura*, 397  
 Synurophyceae, 279  
  
*Tetraedron*, 475  
*Tetraselmis*, 128  
*Thalassia*, 436, 471, 533  
*Thalassiosira*, 318, 407, 414, 513  
*Tolypothrix*, 481, 482  
*Trichodesmium*, 356, 422, 537  
  
*Udotea*, 414, 491  
*Ulothrix*, 342  
*Ulva*, 348, 383, 403, 406, 415, 416, 428, 465,  
   470, 472, 490  
 Ulvaceae, 429  
 Ulvales, 461  
*Uroglena*, 397  
  
*Vallisneria*, 273, 321, 345, 391  
*Vaucheria*, 522  
*Volvox*, 516  
  
 waterfowl, 428  
  
 Xanthophyceae, 278, 284, 287, 288, 290,  
   387, 522  
  
 zooplankton, 423, 426, 452, 504  
 zooxanthellae, 495  
*Zostera*, 347, 406  
*Zygnema*, 266

# Index to water bodies

---

(L. = Lake, Lough (Ireland) or Loch (Scotland); R. = River)

- Adelaide, L., 77  
Adriatic Sea, 73, 75, 396, 470, 473, 491, 502, 530, 531  
Aegean Sea, Southern, 450  
Aleutian Islands, 429  
Algoa Bay, 346  
Amazon R., 69, 79  
Antarctic Circumpolar Current, 424, 425  
Antarctic marginal ice zone, 355  
Antarctic pack-ice, 508  
Antarctic Peninsula, coastal, 258, 317  
Arabian Sea, 44, 45, 75, 125, 357, 374, 426, 447  
Aranguadi, L., 376  
Arctic fjord, Spitsbergen, 472  
Arctic Ocean, 64, 74, 121, 156, 201, 450, 451  
Arctic Ocean, Canadian, 347  
Argentine Basin, 35  
Århus Bay, 75, 163, 167  
Ariake Sea, 531  
Atlantic Bight, 240  
Atlantic continental shelf, 443  
Atlantic Ocean, 34, 35, 74, 75, 88, 123, 130, 131, 156, 157, 163, 176, 238, 450, 451, 537  
Atlantic Ocean, central, 173  
Atlantic Ocean, Eastern, 447  
Atlantic Ocean, Eastern subtropical, 396  
Atlantic Ocean, Eastern tropical, 451  
Atlantic Ocean, Equatorial, 433  
Atlantic Ocean, North, 44, 68, 70, 79, 129, 422, 432, 446  
Atlantic Ocean, North polar, 433  
Atlantic Ocean, North Subtropical Gyre, 427  
Atlantic Ocean, North tropical, 462  
Atlantic Ocean, Northeast basin, 448  
Atlantic Ocean, Northeast tropical, 374  
Atlantic Ocean, Northeastern, 396, 423, 450  
Atlantic Ocean, Northwest, 238  
Atlantic Ocean, Northwestern, 358, 443, 446  
Atlantic Ocean, Southwestern, 433  
Atlantic Ocean, Subtropical, 432  
Atlantic Ocean, Subtropical and tropical Northeast, 451  
Atlantic Ocean, Subtropical Gyres, 395  
Atlantic Ocean, Tropical East, 163  
Atlantic Ocean, Tropical North, 90  
Atlantic Ocean, Western, 447  
Avon River estuary, 529  
Azores Front, 346, 396  
  
Bahama Islands, 117, 123, 126, 390  
Baie des Chaleurs, 259  
Baikal, L., 59  
Baja California, 491, 497, 515  
Baltic Sea, 68, 73, 75, 79, 118, 158, 167, 179, 182, 206, 244, 253, 254, 257, 342, 346, 431, 438, 456, 509  
Baltic Sea, North, 349, 350  
Baltic Sea, West, 348, 349  
Banyuls-sur-Mer, 438  
Barents Sea, 450  
Barombi Mbo, L., 165  
Barren Box Swamp, 78  
Barrington, L., 78, 119, 166

- Barrow R., 357  
 Basin, L., 119  
 Batemans Bay, 72, 76, 79, 159  
 Bay of Biscay, 199, 234  
 Bay of Brest, 531  
 Bay of Campeche, 74  
 Bay of Villefranche, 118  
 Beaufort Channel, 421  
 Beaufort Sea, 74, 121, 156, 319  
 Bedford Basin, 353, 501  
 Bellingshausen Sea, 355  
 Beme, L., 165  
 Bering Sea, 199, 420  
 Biwa, L., 158, 166  
 Bjornafjord, 163  
 Black Sea, 75, 109, 110, 118, 121  
 Blaxter L., 76  
 Blowering Dam, 166  
 Bluff, L., 77  
 Bogoria, L., 165, 344  
 Boomanjin, L., 119, 166  
 Bothnian Gulf, 75, 79, 118  
 Bradan, L., 77  
 Bransfield Strait, 346  
 British Columbian coastal, 247  
 Bronkhorstspuit Dam, 165  
 Burley Griffin, L., 83, 96, 119, 159, 160, 161, 162, 166, 169, 185, 195  
 Burrinjuck Dam, 78, 83, 87, 96, 119, 154, 162, 166, 179, 194, 195  
  
 Cahora Bassa, L., 516  
 California Bight, 209, 240  
 California coastal, 516  
 California Current, 253, 338, 444  
 California, Southern coastal, 525  
 Cape Cod, 238, 347, 449  
 Cape San Blas, 74  
 Caribbean Sea, 70, 74, 117, 350, 376, 380, 459, 463, 471  
 Carmean Quarry, 76  
 Carrao R., 77  
 Carrigathorna, Lough Ine, 458  
 Celtic Sea, 131, 245, 256, 374, 462  
 Chad, L., 434  
 Chatham Rise, 75, 89, 90, 118, 163  
 Chesapeake Bay, 75, 81, 117, 126, 164, 347, 450, 479  
 Chicot, L., 231  
 China Sea, North, 247  
 Chukchi Sea, 69, 74  
  
 Cleveland Bay (Great Barrier Reef system), 164  
 Clyde R., 76, 79  
 Clyde R. Estuary, NSW, 164  
 Clyde, R., NSW, 72  
 Clyde Sea, 163, 194, 252  
 Cockburn Sound, 428  
 Coleridge, L., 345  
 Constance, L., 328, 364, 375, 434, 435  
 Conwy estuary, 252  
 Cooloomera, L., 166  
 Coral Sea, 345  
 Corin Dam, 77, 83, 96, 118, 155, 165  
 Cotter Dam, 77, 83, 96  
 Crater, L., 34, 95, 164, 397, 493  
 Crimean coastal, 126  
 Crimean Peninsula, 75  
 Croche, L., 158  
 Croispol, L., 165, 502  
 Cromwell, L., 158  
 Crystal L., 77  
  
 D, L., 79, 119, 166  
 Danish Sound, 178, 179  
 Darling R., 78, 166  
 Dart's, L., 118  
 Darwin River Reservoir, 81  
 Delaware Bay, 70, 205, 229, 255  
 Delaware River estuary, 230  
 Dogger Bank, 163, 396  
  
 East Australian Current, 277  
 East Sound estuary, 68  
 East Sound, Washington, 125  
 Eden River estuary, 529  
 Elmentaita, L., 165, 344  
 Ems estuary, 531  
 Ems-Dollard estuary, 163  
 English Channel, 73, 89, 118, 246, 394, 397, 448  
 Eniwetok atoll, 464  
 Erie, L., 164  
 Erne, L., 77  
 Esthwaite Water, 165, 328, 392, 411, 515  
 Estonian coastal, 254  
 Etive, L., 164  
 Eucumbene, L., 166  
  
 Faroebank, 389  
 Fea, L., 77  
 Finger Lakes, N.Y., 164

- Fitzroy R., 76, 117  
 Fladen Ground, 75, 118, 158  
 Florida, Southeastern coastal, 497  
 Franklin Bay, 121  
 Fraser R., Strait of Georgia, 164  
 Fukami-ike, L., 77  
 Funakoshi Bay, 259  
 Fundy, Bay of, 229, 231  
  
 Galapagos Islands, 117  
 Galway Bay, 205, 252  
 Ganges R., 75  
 Garda, L., 224  
 Gare Lough, 164  
 George, L., NSW, 83, 96, 119, 162, 166, 194, 195  
 George, L., Uganda, 328, 344, 393, 434  
 Georges Bank, 431, 449  
 Georges Shoals, 201  
 Georgetown billabong, 78, 96, 119, 155, 162, 166  
 Georgia Embayment, 164  
 Georgia salt marsh, 75  
 German Bight, 158  
 German Wadden Sea, 450  
 Gilbert Is., 117  
 Giles, L., 158  
 Ginninderra, L., 83, 96, 119, 165, 177, 195, 321  
 Gippsland Lakes, 79, 87  
 Gironde estuary, 231, 399  
 Gogeldrie Weir, 78, 166  
 Googong Dam, 78, 83, 96  
 Gordon, L., 78, 119, 166  
 Great Australian Bight, 463, 464  
 Great Barrier Reef, 76, 117, 125, 126, 531  
 Great Barrier Reef Lagoon, 167  
 Great Bay estuary, 117  
 Green Bay, L. Michigan, 233, 237, 344  
 Greenland Sea, 374  
 Greenland (Western), 158  
 Griffith Reservoir, 78  
 Gryde R., 439  
 Guinea Dome, 163  
 Gulf of Aqaba, 158, 353, 396, 520  
 Gulf of California, 164  
 Gulf of Finland, 167  
 Gulf of Fos, 530  
 Gulf of Guinea, 74  
 Gulf of Maine, 178, 318, 374, 394, 431, 456  
  
 Gulf of Mexico, 74, 85, 117, 125, 158, 201, 235, 253, 255, 338, 357, 436, 447, 537  
 Gulf of Naples, 75  
 Gulf of St Lawrence, 158, 259  
 Gulf of St Vincent, 463  
 Gulf of Trieste, 531  
 Gulf Stream, 34, 156, 159, 176, 235, 461  
 Gulf Stream, off Bahamas, 163  
 Gulungul billabong, 78, 96, 119, 166  
 Guri Reservoir, 77  
  
 Hakanoa, L., 79, 166  
 Halsted Bay, 363  
 Hartbeespoort Dam, 165, 317, 519  
 Hawaiian coastal, 459  
 Hawaiian reef, 495  
 Helgoland, 390, 438  
 Hendrik Verwoerd Dam, 165, 389  
 Heron Reef, 531  
 Hudson estuary, 374  
 Hudson River, 69  
 Hudson River estuary, 399, 419  
 Humber estuary, 530  
 Hume, L., 128  
 Huon estuary, 90  
 Huon R., 76, 78  
 Huon River estuary, 317  
 Huron, L., 164  
  
 Iceland, 75  
 Iceland coastal, 117  
 Indian Ocean, 74, 109, 118, 450, 451  
 Indian Ocean, subtropical, 432  
 Indian River Lagoon, 391  
 Irish Sea, 126, 232, 233, 234, 245, 256, 450  
 Irondequoit Bay, 118, 164  
 Irondequoit Bay, L. Ontario, 77, 113, 128, 328  
 Isle of Colonsay, 457  
 Isles of Scilly, 457  
 Izu peninsula, 416  
  
 Jervis Bay, 75, 91, 118, 125  
 Jindabyne, L., 166  
  
 Karkhujarvi, L., 165  
 Kattogat, 75, 81, 118, 163, 167, 431  
 Keppel Bay, 76, 117  
 Kieta Bay (Solomon Is.), 117  
 Killea Reservoir, 76

- Kilotes, L., 376  
 King, L., 88, 96  
 Kinneret, L., 165, 328, 363, 372, 376,  
     380, 426  
 Kizaki, L., 77  
 Kongsfjord, Spitsbergen, 158, 163  
  
 Lacawac, L., 158  
 Ladies Tarn, 78, 166  
 Lago di Varese, 149  
 Laguna Madre, 391  
 Las Madres, L., 165  
 Latrobe R., 76, 79, 96  
 Leven, L., 328, 428  
 Loughnagay, 77  
 Lovojärvi, L., 493  
  
 Macquarie, L., 164  
 Magela Creek, 166  
 Malaga, coast, 483  
 Malta, 439  
 Malta, coastal, 459, 460, 464, 465  
 Manton River Reservoir, 81  
 Mauritanian coastal, 117  
 Mauritanian upwelling, 117, 120, 156,  
     163, 447  
 McConaughy reservoir, 165  
 McMurdo Sound, 347, 494  
 Mediterranean Sea, 73, 74, 85, 118, 173, 183,  
     244, 459, 460, 463, 468, 520, 533  
 Mediterranean Sea, Eastern, 158  
 Mediterranean Sea, Northeast, 530  
 Mediterranean Sea, (Western), 158  
 Michigan, L., 237, 397  
 Mid-Atlantic Bight, 68, 257  
 Middle Atlantic Bight, 70, 255  
 Minnetonka, L., 165, 328, 363  
 Mississippi outflow, 253  
 Mississippi plume, 74  
 Mississippi R., 81, 85, 231  
 Molonglo R., 78  
 Monterey Bay, 117, 255  
 Moon, L., 231, 232  
 Moreton Bay, 259  
 Mossman-Daintree, 76, 117  
 Mount Bold Reservoir, 78, 119  
 Mudginberri billabong, 78, 119, 166  
 Mulwala, L., 128  
 Murray R., 78, 119, 128  
 Murrumbidgee Irrigation Area, 85  
 Murrumbidgee R., 119, 166  
  
 Nabeta Bay, 76  
 Nakuru, L., 165, 344  
 Napeast, L., 77  
 Narragansett Bay, 450, 512, 513  
 Neagh, L., 327, 328, 344, 364, 374, 393,  
     420, 514  
 Ness, L., 394  
 Neusiedlersee, 76  
 New England shelf, 74, 117  
 New England, coastal, 457  
 New Jersey coast, 69, 124  
 New Jersey offshore, 117  
 New York Bight, 419  
 Newport River estuary, 534  
 Nimeton, L., 165  
 Norfolk Broads, 427  
 North Carolina coastal, 125  
 North Carolina, coast, 461  
 North Pacific coastal, 431  
 North Sea, 73, 75, 118, 158, 163, 167, 237,  
     247, 252, 277, 390, 396, 438, 449, 450  
 North Sea, Eastern, 424  
 Northeast USA coastal, 450  
 Northern Ireland coastal, 450  
 Norwegian Sea, 393, 424  
 Nova Scotia, coastal, 351, 510, 514  
 Nova Scotian Shelf, 419  
  
 Ohakuri, L., 166  
 Okefenokee Swamp, 65  
 Oku, L., 165  
 Onondaga, L., 118  
 Ontario, L., 118, 158, 164, 231, 235, 354  
 Opouri, L., 79  
 Orange, L., 345  
 Orinoco R., 70  
 Orkney-Shetland, 75  
 Oslofjord, 126, 149  
 Otago Shelf, 97  
 Otisco, L., 77  
 Otisco, L., 118, 164  
 Owasco, L., 118  
  
 Pääjärvi, L., 514  
 Pacific Ocean, 74, 89, 109, 117, 155, 163,  
     325, 345, 364, 372, 450, 451, 459  
 Pacific Ocean, Canadian coastal, 513  
 Pacific Ocean, Central, 422, 463  
 Pacific Ocean, Central Equatorial, 158  
 Pacific Ocean, Eastern, 278  
 Pacific Ocean, Eastern equatorial, 69, 376

- Pacific Ocean, Eastern North, 163  
 Pacific Ocean, Eastern Subtropical, 406  
 Pacific Ocean, Equatorial, 35, 406, 424, 425, 447, 448  
 Pacific Ocean, North, 420  
 Pacific Ocean, North Subtropical Gyre, 274  
 Pacific Ocean, Northeastern, 424  
 Pacific Ocean, South, 90, 154  
 Pacific Ocean, Subarctic northwestern, 377  
 Pacific Ocean, subtropical, 432  
 Pacific Ocean, Tropical, 154  
 Pacific Ocean, Tropical Eastern, 447  
 Pacific Ocean, Western, 483  
 Patagonian shelf, 433  
 Pawnee Hill reservoir, 165  
 Pearson Island, 464, 468  
 Pedder, L., 119, 166  
 Peel-Harvey estuary, 232  
 Pend Oreille, L., 118, 180, 181–187  
 Perry, L., 119, 166  
 Persian Gulf, 45  
 Peruvian upwelling, 247, 277, 424, 448, 450, 451  
 Pipit, L., 158  
 Po R., 75  
 Port Hacking, 436, 437  
 Port Hacking estuary, 164  
 Port Phillip Bay, 347  
 Puget Sound, 437  
 Punch Bowl, 77  
  
 Queanbeyan R., 78  
  
 Red Rock Tarn, 452  
 Red Sea, 45, 158, 353, 396, 469, 502, 503, 520  
 Rhine R., 76  
 Rhode R., 74, 117  
 Rhone R., 75  
 Ria de Vigo, 516  
 Risdon Brook, L., 78  
 Romanche Deep, 74  
 Ross Sea, 317  
 Rotokakahi, L., 79, 119, 166  
 Rotorua, L., 79, 119, 166, 410  
 Rust de Winter reservoir, 165  
  
 Sacca di Goro, 75  
 San Diego Harbour, 118, 122, 123  
 San Francisco Bay, 114, 164, 389, 433  
 San Salvador Island (Bahamas), 460  
 San Salvador Seamount, 460  
 San Vicente Reservoir, 155, 176  
 Santa Barbara Channel, 234  
 Sargasso Sea, 70, 74, 84, 87, 117, 124, 157, 158, 163, 205, 240, 318, 340, 372, 374, 376, 380, 427, 447, 462, 498  
 Scilly Isles, 456  
 Sea of Galilee, 165, 166, 328, 363, 372, 376, 380, 426  
 Seneca, L., 118, 164  
 Seto Inland Sea, 530  
 Shannon estuary, 163  
 Shetland-Faeroe, 158  
 Silver, L., 158  
 Simbi, L., 165, 166  
 Sinai, 350  
 Skagerrak, 75, 81  
 Skanateales, L., 164  
 Snowflake, L., 158  
 South Atlantic Bight, 70, 81  
 South Australia, coast, 463, 465, 468  
 South Indian Antarctic Oceans, 447  
 Southern California Bight, 346, 374, 376, 445  
 Southern Ocean, 74, 214, 241, 394, 424, 425, 447, 448, 450, 451  
 Southern Ocean Marginal Ice Zone, 394  
 St Catherine's Sound, 164  
 St Johns R., 398  
 St Lawrence estuary, 524, 527  
 St Lawrence R., 158  
 St Margaret's Bay, 379, 436, 534  
 St Vincent Gulf, 469  
 Stechlin, L., 463  
 Stigsholm, L., 428  
 Straits of Denmark, 232  
 Subantarctic Front, 425  
 Subtropical Convergence Zone, 449  
 Superior, L., 164, 223  
 Swan, L., 76  
 Swan River Estuary, 167  
 Sweden, coast, 461  
 Sweden, West coast, 456  
  
 Tagus River estuary, 530  
 Tahoe, L., 328, 376, 397, 493, 494, 500, 501, 617  
 Taihu, L., 118, 125, 126, 225  
 Talbingo Dam, 166  
 Tampa Bay, 260  
 Tanganyika, L., 165

- Tarawa atoll lagoon, 117  
Tasman Sea, 76, 85, 91, 118, 161, 162, 164  
Taupo, L., 79, 119, 166, 410  
Tavilampi, L., 165  
Texas coastal, 427  
Tianmuhu, L., 77  
Timor Sea, 495  
Titicaca, L., 360  
Tongue-of-the-Ocean, Bahama Islands, 122  
Tuggerah Lakes, 164  
Tyrrhenian Sea, 118, 120  
  
Uanagan, L., 165  
Utah, L., 235  
  
Vancouver Island, 248, 349, 509  
Vancouver Island, coastal, 357  
Var R., 75  
Veerse Meer, 470  
Venice Lagoon, 75  
Victoria, L., 76  
Victoria, L., Africa, 167  
Victoria, L., Uganda, 77  
Villefranche Bay, 75  
Vineyard Sound, 359  
  
Virgin Islands, 350  
Vombsjon, L., 328  
  
Wabby, L., 119, 166  
Wadden Sea, 75, 424, 529  
Waikato R., 79, 85, 119  
Wallis Lake, 259  
Wanaka, L., 351  
Weddell-Scotia Sea, 338  
Wellington, L., 76  
West Blue, L., 440  
West Island, South Australia, 496  
Windermere, L., 328, 340, 344, 364, 392  
Woods Hole, 348, 350, 490  
Woods, L., 118  
Wum, L., 165  
Wuras Dam, 389  
Wyangan, L. 78  
  
Yankee Hill reservoir, 165  
Ybbs R., 76  
Yellow Sea, 75, 158, 237  
Young Sound, 349, 491, 496  
Yucatan Shelf, 74  
  
Zurich, L., 165, 328

# Subject index

---

- absorbance (optical density), 53
- absorptance, 15, 53, 308
  - and action spectra, 382
  - of leaf or thallus, 320
  - of particle, 311
- absorption coefficient, 22, 25, 308
  - defined, 15
  - diffuse, 22, 27, 194
  - effective, for PAR, 324, 366
  - measurement, 17, 53–55
    - in situ*, 60
    - in situ* from irradiance, scalar irradiance, 61
    - of particles, on filter, 86
  - of suspension, 311
  - specific
    - and package effect, 315, 317
    - and shade adaptation, 477
    - of phytoplankton, 324
    - phytoplankton, 446
    - specific for PAR, 373, 526
- absorption cross-section, 102
  - defined, 311
  - of phytoplankton, 321
- absorption meters, 53
  - integrating cavity, 57, 60
  - reflective tube, 60
- absorption spectra, 308–310
  - of planktonic algae, 322
  - total, 91
- accessory pigments, 318
- aerosol optical thickness, 219
- algae
  - beneath ice, 494
  - chloroplast movement in, 520
  - depth distribution, 453–469
    - and temperature, 464
    - mass culture, 534
  - allophycocyanin, 293
  - amylose and amylopectin, 307
  - angiosperms
    - chloroplasts, 269
  - Angström exponent, 220
  - anomalous diffraction, 102, 103
  - apparent optical properties, 21–24
  - assimilation number, 441
  - astaxanthin, 471
  - asymmetry factor, 21
  - asymptotic radiance distribution, 182, 187, 190
  - atmospheric correction, 218–225
    - aerosol, 221, 222, 224
    - dark pixel method, 223, 235
    - ozone layer, 219, 222
    - Rayleigh, 222
    - Rayleigh scattering, 219
  - attenuance, 15
  - attenuation length, 24
  - autonomous underwater vehicles, 141
  - average cosine, 25
  - average cosine of scattering, 21, 193
  - average cosines, 11, 147
    - as a function of  $b/a$ , 188
    - as measure of angular distribution, 185
  - AVIRIS, 208
  - azimuth angle, 6, 148, 151, 182, 185, 187
  - $\beta$ -carotene, 282
    - absorption spectrum, 283
    - fluorescence, 299
    - in Core Complex I, 287

- in Core Complex II, 288
- interaction with protein, 292
- photoprotective, 471
- Bacillariophyceae, 267
- backscattering
  - variation with wavelength, 125
- backscattering coefficient, 20, 23
  - diffuse, 22, 194
  - measurement, 106, 109
    - at fixed angle, 110
- backscattering ratio, 121, 126, 129
  - of phytoplankton, 129
- beam attenuation coefficient, 24
  - and equation of transfer for radiance, 25
  - defined, 16
  - measurement, 104–106
- Beer's Law, 311
- benthic flora
  - and depth, 389
- bicarbonate ions, 403
  - active transport, 405
    - proton pump, 405, 406
  - as carbon source, 403–410
- C source for ocean phytoplankton, 406
  - energy cost of transport, 409
  - use by freshwater angiosperms, 407
- biliproteins, 273, 298, 458
  - absorption spectra, 293
  - and chromatic adaptation, 463, 467
  - and photosystem II, 302
  - chromophores, 295, 297
  - distribution, 294
  - in chromatic adaptation, 480
  - in Cryptophyta, 269
  - ratio to chlorophyll, 507
  - spectroscopic properties, 296
- billabongs, 94
- biofouling, 60, 141
- biological pump, 448
- blue light effect, 487
- blue-green algae. *See* Cyanophyta
  - and vertical attenuation, 327
  - production rates, 534
  - surface scums, 518
  - vertical movement, 516–519
- bog lakes, 95
- Brewster angle, 201, 204
- brown algae, 283
  - absorption spectrum, 320
  - chloroplasts, 267
  - depth limit, 390
  - remote sensing, 259
- carbon dioxide
  - as limiting factor in photosynthesis, 401–414
    - concentration, effect of pH, 411
    - uptake, and current velocity, 412
  - carbon-concentrating mechanism, 402
- carbonic anhydrase, 404
  - in seagrasses, 406
- carboxydismutase. *See* Rubisco
- carboxysomes
  - and CO<sub>2</sub> fixation, 407
- carotenoids, 283
  - distribution, 284
  - in thylakoids, 273
  - photoprotective, 318, 358, 471, 491, 504
    - in kelp, 497
  - photosynthetically inactive, 386, 387
  - ratio to chlorophyll, 282
  - secondary, 471
- Case 1 and Case 2 waters, 94, 254, 261
- CASI, 208
- CDOM (gilvin, yellow substance), 65–82, 154
  - absorption coefficients in natural waters, 74
  - and algal depth distribution, 458
  - and lake productivity, 397
  - and reflectance of PAR, 178
  - and river outflow, 69, 154
  - chemistry and origin, 65–70
  - contribution to absorption of PAR, 96, 97
  - fluorescence, 73, 255
  - from phytoplankton, 68
  - from seaweeds, 68
  - light absorption, 70–79
  - photobleaching, 73, 80
  - remote sensing, 252–255
  - specific absorption coefficient, 81
  - spectral slope, 73
- chlorophyll
  - absorption bands, 52
  - depth profile, 444
  - energy levels, 52
  - fluorescence, 53, 157, 171, 176
    - and remote sensing, 246–252
    - quantum yield, 247, 332
  - in thylakoids, 273
  - singlet state, 52

- chlorophyll *a*  
   energy transfer  
     from allophycocyanin, 297  
   excitation, 298  
   fluorescence  
     excitation, 287  
     fluorescence  
       mechanism, 280  
   in reaction centres, 298
- chlorophyll algorithms  
   Case 2 waters, 244, 246  
   CZCS, 239  
   GSM, 243  
   MODIS, 243  
   SeaWiFS, 241, 244  
   semianalytic, 242
- chlorophyll *d*, 276  
   in *Acaryochloris* reaction centres, 300
- chlorophyll fluorescence  
   fast repetition rate, 336  
   PAM fluorometry, 336  
   pump and probe, 336  
   quenching, 332  
     non-photochemical, 335  
   solar-stimulated, 338  
   variable component, 332
- chlorophyll/carotenoid-protein  
   complexes, 293  
   molecular structure, 291–292
- chlorophylls, 276–281  
   absorption spectra, 281  
     Soret band, 279, 289  
   cellular concentration, 277  
     diurnal fluctuation, 527  
   distribution, 278  
   ratios, 279
- chlorophylls  $c_1$ ,  $c_2$  and  $c_3$ , 276
- Chlorophyta, 267  
   depth distribution, 456
- chloroplasts, 265–268  
   and carbohydrate storage, 307  
   envelope, 268  
   movement  
     action spectrum, 520  
   movements, 519–522  
   shrinkage, 522  
   stroma, 265, 268  
   survival, after ingestion, 429
- chromatic adaptation, 454–469  
   complementary, 480  
   ecological significance, 506  
   in eukaryotic algae, 483–486  
   in macrophyte algae, 459  
   in phytoplankton, 462–463  
   phylogenetic and ontogenetic, 454, 500  
   within blue-green algae, 480
- chrysolaminaran, 307
- Chrysophyta, 267  
   lack of carbon-concentrating mechanism, 407
- circadian rhythms, 524–528
- circulation  
   and photoinhibition, 388  
   and photosynthesis, 396
- cloud, 33, 41
- CO<sub>2</sub> fixation  
    $K_m$  values for, 401–407  
   mechanism, 304–306
- coccolithophores, 276  
   chloroplasts, 268
- colour, 177
- Colour Index (Jerlov), 207
- coral reefs  
   production rates, 533
- Core Complex I, 302
- Core Complex II, 287, 289, 302
- cosine collector, 134
- Cosine Law, 10, 40, 133
- Cox and Munk equations, 49, 151
- crassulacean acid metabolism, 414
- critical depth, 389, 431
- Cryptophyta  
   biliproteins, 297  
   chloroplasts, 268, 269
- cyanobacteria  
   depth distribution, 462  
   in microphytobenthos, 528
- Cyanophyta, 269, 273
- cytochrome  $b_{559}$ , 289
- cytochrome  $f$ , 474
- Daedalus, 207
- daily insolation, 41
- dark pixel correction method, 223
- daylength, 42
- DCM. *See* deep chlorophyll maximum
- deep chlorophyll maximum, 364, 375, 395–397, 493  
   and zooplankton, 504  
   contribution to primary production, 396  
   in inland waters, 397, 493  
   phytoplankton composition, 396

- depth
- morphogenetic adaptation, 502
  - ontogenetic adaptation, 488–503
    - ecological significance, 504
  - variation of photosynthetic characteristics
    - macrophytes, 495–497
    - phytoplankton, 497–502
- detritus, 91, 93, 94
- diatoms, 283
- and silica, 423
  - and vertical attenuation, 327
  - C<sub>4</sub> photosynthesis in, 414
  - chloroplasts, 265–268
  - colour, 293
  - epiphytic, 470, 508
  - in microphytobenthos, 528
  - movement, on surfaces, 529
  - sinking rate, 412
  - underneath ice, 494, 508
- diatoxanthin
- in xanthophyll cycle, 357
- diffraction, 100
- dimethyl sulfide, 452
- dimethylsulfoniopropionate, 452
- dinoflagellates, 283
- and vertical attenuation, 327
  - chloroplasts, 268
  - effects of turbulence, 426
  - in microphytobenthos, 528
  - in red tides, 537
  - migration, 394
  - respiration rates, 343
  - symbiotic, within corals, 495
  - vertical migration, 515
- Dinophyta, 268
- distribution function, 11
- downwelling light, 140
- ecological compensation depth, 391
- efficiency factors, 102
- Einstein-Smoluchowski theory, 99
- electrons
- energy levels, 51
  - excited state, 51
- emergent flux, 176, 199, 215–218
- energy
- quanta/watts ratio, 5
  - spectral distribution, 5
- energy transfer, 298–300
- chlorophyll *b* to chlorophyll *a*, 300
  - chlorophyll *c* to chlorophyll *a*, 300
  - Förster mechanism, 298
  - from biliproteins, 300
  - from carotenoids, 300, 387
- enhancement, 384
- epilimnion, 392
- CO<sub>2</sub> concentration in, 411
- epipelon, 528
- epiphytes, 427, 532
- equation of transfer for radiance, 25
- erosion, 127
- Euglenophyta
- chloroplasts, 268
  - in microphytobenthos, 528
- euphotic zone, 14, 24, 159, 273, 364, 379, 493
- and benthic flora, 389
  - chlorophyll content, 444
  - definition, 167
  - in turbid waters, 399
  - nutrient supply, 448
  - recycling within, 447
- eutrophic water bodies, 123, 452, 470
- blue-green algal blooms, 518
  - remote sensing, 236, 246
- eutrophic waters, 94
- eutrophication, 423, 427
- and photosynthetic rate, 423
- export production, 448
- f* ratio, 448
- ferredoxin, 303, 474
- flagellates
- vertical migration, 515, 516
- Floridean starch, 307
- flow cytometry, 131
- fluorescence, 53
- and energy transfer, 299
- Förster mechanism, 299
- forward scattering coefficient, 20
- measurement, 106, 109
- Fresnel reflection, 174
- Fresnel's equation, 46
- fucoxanthin, 283, 387, 471
- and brown algal absorption spectrum, 320
  - and chromatic adaptation, 458, 467
  - and depth, 491
  - energy transfer from, 508
  - fluorescence, 299
  - in vivo spectral shift, 292

- fucoxanthin (cont.)  
 seasonal variation in kelp, 509  
 fucoxanthin, 293  
 fulvic acid, 66, 67, 68, 69, 71
- galactolipids, 273  
 gas vacuoles, 129, 517  
 gelbstoff, 71  
 Gershun equation, 26  
 Gershun tube, 204  
 Gershun tube photometer, 148  
 gilvin, 71, 91, *See* CDOM  
 glaciers, 177  
 global carbon cycle, 441, 448  
 global warming, 452  
 green algae  
 and vertical attenuation, 327  
 chloroplasts, 267, 269  
 greenhouse effect, 441
- Haptophyta, 268  
 harmful algal blooms, 536  
 Heterokontophyta, 267  
 humic acid, 66, 67, 68, 69, 71  
 humic material, 69, 70, 84, 159  
 humic substances, 65, 67  
 hybrid optical properties, 23  
 Hydrolight, 151  
 hydrologic optics, 3–4  
 hyperspectral imager, 207–208  
 hypolimnion  
 as nutrient source, 434
- ICAM, 56, 73, 82  
 ice and snow  
 diatoms underneath, 494, 501  
 $K_d$ , 156  
 $K_d$  as function of  $a$  and  $b$ , 194  
 light absorption, 64  
 PAR transmission, 167  
 phytoplankton under, 513  
 scattering, 65, 121  
 inductive resonance transfer, 298  
 infrared, 51, 57, 62  
 absorption in upper layer, 393  
 reflectance, 231  
 phytoplankton, 236  
 infrared radiation, 32  
 inherent optical properties, 14–21, 22, 135, 150, 198  
 integral average cosine, 12, 27  
 integral photosynthesis, 392, 527  
 integrating cavity absorption meter, 56, 87  
 integrating sphere, 55, 56, 82, 87  
 IOCCG, 208, 216  
 iron  
 as limiting nutrient, 424–426  
 irradiance  
 definition, 8  
 downward/upward, defined, 9  
 measurement, 133–142  
 problems, 138–142  
 shading effects, 135, 140, 147  
 meters, 133–137  
 immersion effect, 134  
 net downward, defined, 9  
 scalar, defined, 10  
 spectral distribution, 10  
 measurement, 144–147  
 upward, 168–178  
 upward/downward scalar, defined, 10  
 irradiance-weighted vertical attenuation  
 coefficients, 27  
 isoetids  
 CO<sub>2</sub> utilization, 410  
 crassulacean acid metabolism, 414  
 depth adaptation, 492
- Kautsky effect, 332  
 kelp forest, 491  
 kelps, 438  
 depth adaptation, 496  
 effects of grazing, 428  
 production rates, 533  
 kleptoplasty, 429
- Lambertian reflector, 172, 187  
 laminarian, 307, 534  
 Langmuir cells, 358  
 LIDAR, 255  
 and CDOM, 255  
 and phytoplankton, 249  
 light  
 properties, 3  
 light absorption  
 measurement, 56–57  
 light utilization efficiency function, 377, 443  
 Lightfish, 146  
 Light-Harvesting Complex I, 287  
 Light-Harvesting Complex II, 289  
 light-saturation onset parameter, 340, 393  
 lignin, 66, 67, 69

- lutein  
   and chromatic adaptation, 461  
   in Light Harvesting Complex II, 292
- MAAs, 89  
   in phytoplankton, 89
- macrophytes, 61  
   algal, seasonal adaptation, 509–510  
   and eutrophication, 422  
   and vertical attenuation, 329  
   depth distribution, 390, 398  
   effects of grazing, 428–430  
   limitations on production, 438  
   seasonal variation in production, 438–439
- mannitol, 307, 534
- Maximum Chlorophyll Index, 236
- Michaelis–Menten equation, 401
- microalgal mats, 536
- microphytobenthos, 146, 357, 390, 528–532  
   in coral reefs, 531  
   resuspension of, 531
- Mie scattering, 31
- mixed layer, 388  
   and critical depth, 393  
   and wind, 394  
   depth, and production, 392–395
- MOCS, 207
- monsoonal climates, 43
- Monte Carlo method, 150
- Monte Carlo modelling, 170, 172, 185, 187,  
 188, 193, 195
- mycosporine-like amino acids, 89, 472  
   and protection against photoinhibition,  
 356
- nadir angle, 6, 172, 217
- nadir radiance, 149, 172, 173, 204
- neoxanthin  
   in Light Harvesting Complex II, 292
- nephelometric turbidity, 112–114
- new production, 448
- nitracline, 374, 446
- nitrogen fixation, 421
- nutricline, 396
- Ocean colour sensors. *See* satellite remote  
   sensing systems  
   scheduled, 216
- ODAS, 207
- oligotrophic water bodies, 410
- optical classification, 95
- Jerlov classification, 92
- turbid waters, 94
- optical depth, 24, 185, 188
- ozone, 31, 32
- P<sub>680</sub>, 288, 298
- P<sub>700</sub>, 287, 298
- P<sub>740</sub>, 300
- package effect, 311–319  
   and euphotic depth, 317  
   and nutrient status of water, 318  
   and vertical attenuation, 326  
   effects of size and shape, 314–319  
   in macrophytes, 319
- PAR, 32  
   absorption  
   as proportion of solar radiation, 32  
   absorption  
     by different components, 95–97  
     by phytoplankton, 363, 368  
     by water, 64  
   downward irradiance, 159–168  
   measurement, 135  
   minimum yearly requirements, 390  
   penetration into sediments, 529
- paramylon, 307
- partial vertical attenuation coefficients,  
 197–198
- particle size distribution, 99
- path radiance, 218
- peridinin, 293, 387, 470  
   and shade adaptation, 505  
   in zooxanthellae, 495
- Phaeophyta, 267  
   colour, 293  
   depth distribution, 456
- phaeophytin, 289
- phase function, 124, 170, 191, 193
- phosphoenolpyruvate carboxylase, 414
- phospholipids, 273
- photoinhibition, 339, 352–360, 442,  
 499, 515  
   and chloroplast movement, 519  
   and MAAs, 89  
   and quantum yield, 371  
   and stratification, 360  
   in seagrasses, 497  
   mechanism, 354  
   of benthic microalgae, 529
- photon  
   energy, 4

- photons,
  - capture by molecules, 50
  - mol. 8
- photophosphorylation, 301
  - mechanism, 304
- photoprotective carotenoids, 432
- photosynthesis
  - action spectra, 380–387
  - and wavelength, 387
  - as a function of incident light, 330
  - C<sub>4</sub> pathway, 306, 413
    - in aquatic plants, 413–414
  - chlorophyll-specific cross-section for, 378
  - dark reactions, 304–307
  - efficiency, 380
    - maximum possible value, 366
    - per unit area and volume, 380
  - electron transfer, 301
  - in sediments, 530
  - liberation of oxygen, 304
  - light compensation point, 339, 344, 416, 496
  - light reactions, 304
  - NADP reduction, 300, 302, 303
  - overall process, 300–278
  - photosystems, 275, 286
    - antennae, 287
  - pigments, 275–283
  - quantum requirement, 366
  - quantum yield, 366, 368, 369, 370–375, 445
    - and depth, 371
    - and nutrient status, 374
    - as function of wavelength, 382
    - cyclical changes, 525
    - diurnal variation, 375
  - radiation utilization efficiency, 379
  - saturation onset, 340, 344, 442, 444, 475, 496
    - and temperature, 416, 420
  - saturation onset parameter, 500, 525
    - adaptation to low irradiance, 498
    - seasonal variation, 510
    - short-term variation, 514
  - spillover hypothesis, 385
  - yield per unit area, 440–452
- photosynthetic capacity, 339
  - and temperature, 419
  - diurnal rhythm, 524
- photosynthetic pigments
  - accessory, 469
  - and depth, 490–495
  - and light intensity, 469–474
- photosynthetic quotient, 331
- photosynthetic rate
  - and faunal grazing, 424, 426
  - and inorganic nutrition, 421
  - and light intensity, 339–352
  - and temperature, 439
  - diurnal variation, 430
  - expression (units), 338
  - integral, 419, 440–449
    - algorithms for, 441
  - measurement, 330–338
    - by chlorophyll fluorescence, 332–338
    - CO<sub>2</sub> fixation, O<sub>2</sub> liberation, 330–332
  - specific, 420, 441
    - maximum value, 445
  - temporal variation, 430–439
- photosynthetic system
  - adaptation to light field
    - ecological significance, 503
  - rapid adaptation, 514–528
  - rhythms in, 524–528
- photosynthetic systems
  - highly productive, 532–538
- photosynthetic units, 302
  - and light adaptation, 472–474
- photosynthetically available radiation.
  - See* PAR
- photosynthetically usable radiation, 364
- photosystem I, 275, 287, 302
  - and chromatic adaptation, 485
  - cytochrome *b<sub>6</sub>/f* complex, 304
  - electron transfer within, 303
  - phaeophytin in, 304
  - pigment-proteins, 287
    - distribution, 288
  - plastoquinone in, 304
- photosystem II, 275, 302
  - absorption cross-section, 335
  - and chromatic adaptation, 485
  - electron transfer within, 333–336
  - pigment-proteins, 287
    - distribution, 288
  - quantum efficiency, 335
  - reaction centre
    - damage in photoinhibition, 354
- photosystems, 298
- phycobilin chromophores
  - distribution, 296
- phycobilins, 295

- phycobilisomes, 269, 273, 296, 526  
 phycocyanin, 293, 327, 463, 480–483  
 phycoerythrin, 293, 470  
   and chromatic adaptation, 468, 480–483  
   and photosystem II, 385  
   and red algal absorption spectrum, 320  
   seasonal variation in red algae, 510  
   synthesis  
     action spectrum, 481  
     transcript, 526  
 phycoerythrocyanin, 293  
 phytochrome, 522  
 phytoplankton, 61, 84  
   absorption, 82, 154  
   absorption spectra, 86–89  
   and cloud formation, 452  
   cell size  
     and specific photosynthetic rate, 420  
   cell size  
     and nutrient availability, 422  
   contribution to absorption of PAR, 97  
   decomposition, 68, 84  
   depth adaptation, 492, 497–502  
   effects on light field, 325  
   effects on macrophytes, 427  
   infection by pathogens, 427  
   light capture by, 361–365, 399  
   photosynthetic capacity, seasonal  
     variation, 513  
   remote sensing, 238–252  
   scattering by, 128–132  
   seasonal adaptation, 510–514  
   spring bloom, 431, 434  
   taxonomic composition, seasonal  
     variation, 511  
   UV absorption, 88  
 pixel, 203  
 Planck's constant, 4  
 plastids, 265  
 plastocyanin, 304  
 plastoquinone, 289, 474  
   as quencher, 333  
   oxidation, 304  
 point source integrating cavity absorption  
   meter, 56  
 primary production  
   and seasonal upwelling, 433  
   and temperature, 432  
   and upwelling, 451  
   and wind, 427  
   from remote sensing data, 443–447, 450  
   in microphytobenthos, 530  
   in oceans, 450  
   oceanic, geographical variation, 449–452  
   total, different ocean regions, 451  
 Prochlorophyta, 273  
 prochlorophytes, 273, 276  
   in DCM, 462  
 prokaryotes, 269  
 proton pump, 405  
 Prymnesiophyceae, 268  
 PSICAM, 56–57, 73, 82  
 pushbroom and whiskbroom scanning,  
   201–203  
 pushbroom scanner, 214  
 pycnocline, 389, 396, 516  
   and DCM, 395  
 pyrenoid, 266, 267, 307, 475  
   and CO<sub>2</sub> fixation, 306  
 Pyrrophyta, 268  
  
 quanta, 3, 52  
 quanta (PAR) meter, 135  
 quantum yield, 380  
   defined, 369  
   maximum, 370  
 quasi-inherent optical properties, 21, 23, 198  
  
 radiance, 37  
   definition, 7  
   measurement  
     shading effects, 149  
   meters, 147–149  
   nadir, 146, 149  
 radiance distribution, 11, 182, 198  
   as function of depth, 182, 185  
   measurement, 147–149  
 radiance reflectance, 171  
   above-surface, 173  
   as function of IOP, 172  
   subsurface, 174  
 radiant flux, 6, 54  
 radiant intensity, 6  
 radiative transfer theory, 24–27, 194  
 radiometers  
   in low-flying aircraft, 206–207  
   in medium/high altitude aircraft, 207–208  
   in satellites, 208–215  
   on towers, 205  
   shipborne, 203–205  
 Raman emission, 171, 249–252  
 Raman emission line, 116

- Rayleigh's Law, 30
- reaction centre, 287, 288, 298–300, 302  
and quantum yield, 371  
open, closed, 334
- red algae  
absorption spectrum, 320  
chloroplasts, 268, 269  
depth limit, 390
- red tides, 248, 536  
causes of, 537
- Redfield ratio, 421
- reflectance, 13, 22, 23, 146, 147,  
168–178, 195  
and solar altitude, 157, 169, 170–171  
and suspended solids, 228–235  
as function of IOP, 169–171  
from modelling, 151  
measurement, 135  
of PAR, 177  
spectral distributions, 176  
variation with depth, 187
- reflection  
at surface, 174, 215, 361  
from bottom, 178, 361
- reflective tube absorption meter, 87
- refractive index  
of particles, 103, 123, 127  
of phytoplankton, 129  
water, 5, 48, 174
- remote-sensing reflectance  
and CDOM, 252  
and floating macroalgae, 237  
and phytoplankton, 226  
fluorescence, 246–252  
increased absorption, 238–246  
increased reflectance, 237  
and scattering/absorption ratio, 225–228  
and suspended solids, 228–235  
and water composition, 228–255  
atmospheric correction, 218–225  
CDOM  
algorithms, 253–254  
semianalytical algorithms, 254, 256  
subsurface, 171, 173, 175, 226
- remotely sensed reflectance  
and IOP, 254
- remote-sensing reflectance, 171–175
- respiration  
and temperature, 416  
in shade adaptation, 478
- retrieval variable, 228
- Rhodophyta, 268  
depth distribution, 456
- Rubisco, 266, 306  
and light saturation, 400  
in carboxysome, 407  
in pyrenoids, 266  
in shade adaptation, 474–475  
 $K_m$  for carbon dioxide, 402  
oxygenase activity, 407, 413  
transcript, 526
- satellite remote sensing systems  
Advanced Land Imager, 209, 254  
AVHRR, 209, 233  
CASI, 208  
chlorophyll fluorescence, 211  
CZCS, 209, 233, 449  
 $K_d$  values, 255  
phytoplankton, 239  
Earth Observing-1, 209, 214  
Hyperion and Advanced Land  
Imager, 214  
Feng Yun MVISR, 214  
geostationary, 208  
IKONOS, 259  
IRS-P4 Ocean Colour Monitor, 214, 253  
Landsat, 224, 228, 232  
atmospheric correction, 222  
phytoplankton, 235  
MERIS, 211, 246  
chlorophyll fluorescence, 247  
phycocyanin, 246  
MODIS, 212, 225, 235, 237  
chlorophyll fluorescence, 248  
Nimbus-7, 209  
Ocean Ecosystem Spectrometer, 215  
polar-orbiting, 208, 211, 212, 214  
SeaDAS, 222  
SeaWiFS, 210–211, 220, 225, 433  
and Secchi depth, 259  
and suspended sediments, 233  
and UV penetration, 258  
CDOM, 253  
 $K_d$  values, 255  
phytoplankton, 241  
seasonal phytoplankton variability, 433  
spatial resolution, 235  
suspended solids, 234  
SPOT, 209, 231, 233  
kelp distribution, 259  
sunglint, 211, 214, 215

- Terra and Aqua, 212, 237
- Thematic Mapper, 208, 232
  - and Secchi depth, 260
  - atmospheric correction, 224, 225
  - kelp distribution, 259
  - phytoplankton, 246
- scalar irradiance, 146, 178–181
  - and light capture, 365
  - and measurement of  $a$ , 144
  - and rate of light absorption, 323
- collector, 143
- in sediments, 529
- measurement, 144
- ratio to downward irradiance, 400
- scatterance, 15
- scattering
  - aerosol, 201
  - contribution to attenuation of irradiance, 191
  - density fluctuation, 98–116, 124
  - effects on absorption measurement, 55, 57, 60, 82, 309, 313
  - elastic and inelastic, 116
  - measurement, 104–114
  - Mie theory, 100
  - particle, 99–104, 124
    - variation with wavelength, 124
  - phytoplankton, 128–132
  - Raman, 116, 157, 178
  - Rayleigh, 98, 100, 201
  - within atmosphere, 200
- scattering coefficient
  - and volume scattering function, 20
  - defined, 15
  - diffuse, 22, 27
    - measurement, 115
  - measurement, 17
    - at fixed angle, 109–111
    - from *in situ* irradiance, 112–114
  - natural waters, 117
  - of natural waters, 116
  - specific, for phytoplankton, 128
- scattering/absorption ratio, 188
- Seaglider, 141
- seagrasses
  - and depth, 492
  - and eutrophication, 428
  - bicarbonate utilization, 406
  - chloroplast movement in, 520
  - depth adaptation, 502
  - nutrient supply, 533
  - production rates, 533
  - remote sensing, 259
  - seasonal variation, 436
- seamount, 460
- SeaWiFS, 97, 172
- Secchi depth, 142–143
  - and image attenuation, 143
  - and  $K_d$ , 142–143
  - remote sensing, 259–261
- sediment resuspension
  - effect on attenuation, 167
- sewage oxidation ponds, 534
- shade adaptation, 469–479
  - ecological significance, 504
  - in aquatic angiosperms, 478–479
  - photosynthetic consequences, 475–477
- silica
  - as limiting nutrient, 423
- SIMBAD, 204
- siphonaxanthin, 293, 387
  - and chromatic adaptation, 461, 467
- sky radiance, 37
- skylight, 32, 33, 36, 201, 204–205
  - surface reflection, 47, 205
- Snell's Law, 48, 217
- soil erosion, 95
- solar constant, 29
- solar declination, 38
- solar elevation, 173
  - and  $K_d$ , 157
  - and time of day, 39
- solar irradiance
  - daily total, 445
  - diurnal variation, 38–41
  - variation with latitude, 38–41, 42–43
  - variation with time of year, 42–44
- solar radiation, 140
  - and cloud, 33–35
  - and solar elevation, 32, 33
  - angular distribution, 36–38
  - atmospheric transmission, 38
  - atmospheric transmittance, 226
  - extraterrestrial, 28–30, 219, 221
  - scattering, 30
  - spectral distribution, 32, 33
  - surface reflection, 45
  - transmission across air water-interface, 44–47
  - transmission through atmosphere, 30–35
- Soret band, 462

- spectral distribution
  - of reflectance, 232
- spectral distributions, 159
  - change with depth, 455
- spectroradiometers, 134, 142, 146
  - UV, 147
- spillover, 302
- spillover (state transition), 302
- Standard Overcast Sky, 37
- starch grains, 307
- storage carbohydrates, 307
- stratification, 393–395, 431
  - and salinity, 394
  - in spring, 393
- sulfolipid, 273
- Sun
  - as black body, 28
  - nuclear fusion within, 28
  - spectral energy distribution, 29
- sunlint term, 204, 209, 211
- surface reflection, 174
  
- temperature
  - and photosynthetic rate, 415–421
  - seasonal changes, 419
- thermal stratification, 493, 500
- thermocline, 389, 397, 411, 493
  - algal migration through, 516, 519
  - and nutrients, 421
  - permanent, in tropics, 451
- thylakoid, 269
  - absorbance spectrum, 309
  - chemical composition, 273
  - intrathylakoid space, 304
  - membranes and particles, 268–275
- thylakoids, 296
- tripton, 61, 82–86, 95, 162
  - absorption spectra, 84
  - composition, 84
  - contribution to absorption of PAR, 97
  - spectral slope, 84
  - wind-blown dust, 85
- turbidimeters, 111
- turbidity, 111, 122, 159, 161, 167
  - and photosynthesis, 399
  - in estuaries, 398
  
- underwater light field, 153–198
  - angular distribution, 181–188
  - characterizing, 133–152
  - dependence on IOP, 188–197
  - effect of aquatic plants on, 325–328
  - modelling, 152
  - spectral distribution
    - and photosynthesis, 380
- Undulating Oceanographic Recorder, 140
- upwelling light, 124, 140, 168
  - radiance distribution, 187
- UV
  - $K_d$  values, 157, 158
  - photoinhibition, 157, 354
  
- vertical attenuation coefficients
  - and scattering/absorption ratio, 194, 196
  - as function of IOP, 189–197
  - calculation, 14
  - dependence on scattering, 193
  - dependence on solar altitude, 192
  - for downward irradiance, 27, 153–157
  - from modelling, 151
  - from remote sensing, 255
  - irradiance-weighted, 14
  - irradiance-weighted
    - measurement, 138
- PAR, 159–168, 194, 362, 441
  - and integral photosynthesis, 392
  - as function of chlorophyll, 445
  - contribution of phytoplankton, 326, 328
  - effect of light scattering, 161–162, 167
  - from remote sensing, 256
  - natural waters, 163–166
  - specific, for phytoplankton, 326, 362
- UV
  - from remote sensing, 257
- vitamin K, 303
- volume scattering function, 123, 188
  - and equation of transfer for radiance, 25
  - definition, 18
  - measurement, 106–109
  - normalized, 20, 121
  
- wastewater, 150
- water
  - absorption coefficients, 62
  - absorption spectrum, 61–63
    - effects of temperature, salt, 63
  - scattering coefficients, 116

- water-leaving radiance, 173, 175, 217,  
219, 221
  - normalized, 222
- watts, 5
- wave slope, 49
- wavelength, 4
- whiskbroom scanner, 201–202
- whitecaps, 47
- wind
  - and primary production, 426,  
427, 433
  - and surface reflection, 46
  - speed and surface slopes, 49
- xanthophyll cycle, 292, 335
  - mechanism, 357
- zeaxanthin
  - in xanthophyll cycle, 357
  - photoprotective effect, 462, 472
  - photoprotective function, 387
- zenith angle, 25, 148
  - defined, 6
  - solar, 37
- zooplankton, 121
  - grazing by, 423, 431
- zooxanthellae, 495